WL-TR-96-4030

PROCEEDINGS OF THE 1994 USAF STRUCTURAL INTEGRITY PROGRAM CONFERENCE



EDITORS:

Thomas D. Cooper
WL/Materials Directorate
Wright-Patterson AFB, Ohio

John W. Lincoln
ASC/Deputy for Engineering
Wright-Patterson AFB, Ohio

James L. Rudd
WL/Flight Dynamics Directorate
Wright-Patterson AFB, Ohio

USAF Structural Integrity Program Conference
Hyatt Regency
San Antonio, Texas

Final Report for Period 6 - 8 December 1994

FEBRUARY 1996

Approved for public release; distribution is unlimited

19960711 012

MATERIALS DIRECTORATE
WRIGHT LABORATORY
AIR FORCE MATERIEL COMMAND
WRIGHT-PATTERSON AFB, OHIO 45433-7734

DTIC QUALITY INSPECTED 1

NOTICE

When government drawings, specifications, or other data are used for any purpose other than in connection with a definitely related government procurement operation, the United States Government thereby incurs no responsibility or any obligation whatsoever; and the fact that the government may have formulated, furnished, or in any way supplied the said drawings, specifications, or other data, is not to be regarded by implication or otherwise as in any manner licensing the holder or any other person or corporation, or conveying any rights or permission to manufacture use, or sell any patented invention that may in any way be related thereto.

This report has been reviewed by the Office of Public Affairs (ASC/PA) and is releasable to the National Technical Information Service (NTIS). At NTIS, it will be available to the general public, including foreign nationals.

This technical report has been reviewed and is approved for publication.

Gary K. Waggoner

GARY K. WAGGONER
Chief
Systems Support Division

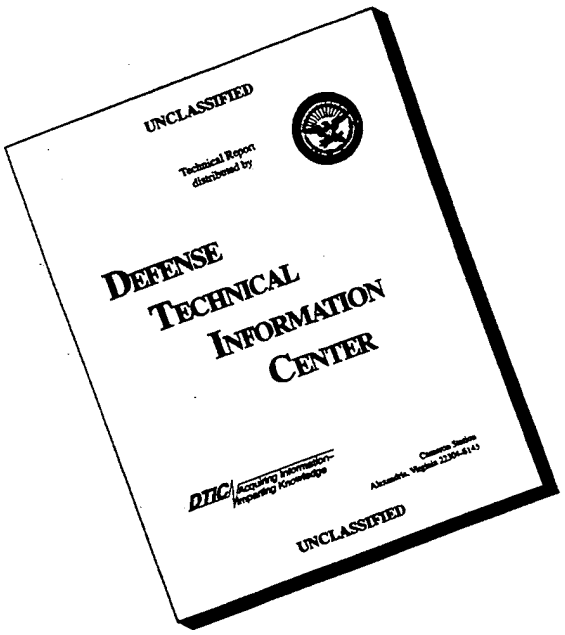
Vincent J. Russo

VINCENT J. RUSSO
Director
Materials Directorate

If your address has changed, if you wish to be removed from our mailing list, or if the addressee is no longer employed by your organization, please notify WL/MLS Bldg 652, 2179 Twelfth St Ste 1, Wright-Patterson AFB, Ohio 45433-7718 to help us maintain a current mailing list.

Copies of this report should not be returned unless return is required by security considerations, contractual obligations, or notice on a specific document.

DISCLAIMER NOTICE



THIS DOCUMENT IS BEST QUALITY AVAILABLE. THE COPY FURNISHED TO DTIC CONTAINED A SIGNIFICANT NUMBER OF PAGES WHICH DO NOT REPRODUCE LEGIBLY.

REPORT DOCUMENTATION PAGE

Form Approved
OMB No. 0704-0188

Public reporting burden for this collection of information is estimated to average 1 hour per response, including the time for reviewing instructions, searching existing data sources, gathering and maintaining the data needed, and completing and reviewing the collection of information. Send comments regarding this burden estimate or any other aspect of this collection of information, including suggestions for reducing this burden, to Washington Headquarters Services, Directorate for Information Operations and Reports, 1215 Jefferson Davis Highway, Suite 1204, Arlington, VA 22202-4302, and to the Office of Management and Budget, Paperwork Reduction Project (0704-0188), Washington, DC 20503.

1. AGENCY USE ONLY (Leave blank)	2. REPORT DATE	3. REPORT TYPE AND DATES COVERED
	FEB 1996	FINAL 12/6/94--12/8/94

4. TITLE AND SUBTITLE

Proceedings of the 1994 USAF Structural Integrity Program Conference

5. FUNDING NUMBERS

PE 62102F
PR 2418
TA 07
WU 04

6. AUTHOR(S)

Thomas D. Cooper, John W. Lincoln, James L. Rudd

7. PERFORMING ORGANIZATION NAME(S) AND ADDRESS(ES)

Materials Directorate
Wright Laboratory
Air Force Materiel Command
Wright Patterson Air Force Base, Ohio 45433-7734

8. PERFORMING ORGANIZATION REPORT NUMBER

WL-TR-96-4030

9. SPONSORING/MONITORING AGENCY NAME(S) AND ADDRESS(ES)

Materials Directorate
Wright Laboratory
Air Force Materiel Command
Wright Patterson Air Force Base, Ohio 45433-7734

10. SPONSORING/MONITORING AGENCY REPORT NUMBER

WL-TR-96-4030

11. SUPPLEMENTARY NOTES

12a. DISTRIBUTION/AVAILABILITY STATEMENT

Approved for Public Release; Distribution is Unlimited

12b. DISTRIBUTION CODE

13. ABSTRACT (Maximum 200 words)

This report contains the proceedings of the 1994 USAF Structural Integrity Program Conference held at the Hyatt Regency Hotel in San Antonio, Texas from 6-8 December 1994. The conference, which was sponsored by the Aeronautical Systems Center's Engineering Directorate and the Wright Laboratory's Flight Dynamics and Materials Directorates, was hosted by the San Antonio Air Logistics Center Aircraft Directorate, Aircraft Structural Integrity Branch (SA-ALC/LADD). This conference, as in previous years, was held to permit experts in the field of structural integrity to communicate with each other and to exchange views on how to improve the structural integrity of military weapon systems. Sessions were primarily focused on analysis and testing, engine structural integrity, structural materials and inspections, structural repair, and force management. This year, as in previous years, our friends from outside the U.S. borders provided the audience with outstanding presentations on activities within their countries. It is anticipated that this conference will include their contributions in the agenda of future meetings. This year eighteen countries were represented in the audience.

14. SUBJECT TERMS

15. NUMBER OF PAGES
892

16. PRICE CODE

17. SECURITY CLASSIFICATION OF REPORT	18. SECURITY CLASSIFICATION OF THIS PAGE	19. SECURITY CLASSIFICATION OF ABSTRACT	20. LIMITATION OF ABSTRACT
UNCLASSIFIED	UNCLASSIFIED	UNCLASSIFIED	SAR

TABLE OF CONTENTS

Page

FOREWORD vii

AGENDA ix

INTRODUCTION xv

SESSION I - OVERVIEWS

C-17 Full Scale Durability Test 3
R. Eastin

ASIP Initiatives for the T-38 Aircraft 41
H. Burnside and J. Dubke

The USCG/AANC HU-25 Project - An Overview 65
CDR J. Moukawsher, LDCR J. Mihelic, P. Walter and C. Jones

A Perspective to Determining the Structural Integrity of USAF Aging Aircraft 87
Capt Karl A. Hart

Optimizing T/AV-8B Harriers for Long Service Lives 137
M. Foster, P. Paul, D. Rich and T. Hullander

C-141 Starlifter: ASIP Methodology in an Aging Aircraft Environment 171
J. Cochran and R. Alford

SESSION II - ANALYSIS AND TESTING

Probabilistic Inspection Strategies — A Key to Controlling Multi-Site Damage 191
A. Brot

Multiple Site Damage (MSD) in a Pressurized Fuselage Rivited Lap Joint 207
Capt S.A. Fawaz and J. Schijve

A Global-Local Fracture Criterion for Ductile Materials 219
T. Weng and C. Sun

Acoustic Emission Monitoring of Full Scale Fatigue Tests on Canadian Forces Aerospace Structures 239
S. McBride, G. Déziel and S. Le Guellec

Effect of Mechanical Paint Removal Processes on the Fatigue Lives of Aircraft 255
Clare A. Paul

Progress Towards a Comprehensive Fatigue Analysis Program for Rotary and Fixed-Wing Aging Aircraft 271
P. Bates

The C-141 Weep Hole Problem Revisited 305
D. Register

Composite Repair Durability/Damage Tolerance Test of C/KC-135 F.S. 880 Floor Beam 353
J. Chung, A. Arrieta and J. Beard

SESSION III - ENGINE STRUCTURAL INTEGRITY

Applying Probabilistic Concepts to Gas Turbine Engine Management 377
Squadron Leader C. Pomfret

Effects of Multiple Blade Impact on Aircraft Engine Containment Structures During a Rotor Burst Failure 411
S. Sankar and S. Atluri

Validation of a Probabilistic Rotor Design System -- Status of the USAF PRDS Contract 427
Dr. P.G. Roth

A New Approach to Tracking Turbine Engine Life 447
J. Hansen and M. Paquet

SESSION IV - STRUCTURAL MATERIALS/INSPECTION

Effect of Test Parameters on the Corrosion Fatigue Crack Growth of Aircraft Structural Materials 489
D. Hoeppner and T. Goswami

The Role of Fretting Corrosion and Fretting Fatigue in Aircraft Rivet Hole Cracking - December 1994 Status Report on FAA Grant Program 509
D. Hoeppner, C. Elliott III, M. Moesser and T. Flournoy

An Evaluation of Fatigue Properties of Aging Aircraft Materials 515
J. Scheuring and A. Grandt, Jr.

Handbook of Nondestructive Evaluation (NDE) Capability and Reliability 541
Ward D. Rummel and George A. Matzkanin

Eddy Current Inspection Reliability at Airline Inspection Facilities 547
F. Spencer

Exfoliation Corrosion Located by Search Peening 563
J. Harrison and R. Thompson

SESSION V - STRUCTURAL REPAIR

Residual Life Analysis and a Novel Repair Method for Cracks in F-16 Center Fuselage Bulkhead 589
S. Jiny, G. Davidi, E. Makevet and D. Shur

Structural Durability of Damaged Metallic Panel Repaired with Composite Patches 609
L. Minnetyen and C. Chamis

An Enhanced Method of Stop Drill Repair with Sleeveless Coldworking 623
M. Creager, M. Weigel and A. Leon

Bonded Repair of Multiple Site Damage with GLARE Fiber Metal Laminate Patches 633
Maj R. Fredell, Capt L. Butkus, R. Muller and C. Borsboom

Interference Fit Bushing Installation and Hole Repair/Resizing Using an Expanded Bushing 647
L. Reid

Ultrasonic Techniques for Repair of Aircraft Structures with Bonded Composites Patches 655
S. Smith, N. Senapati and R. Francini

Aircraft Structural Integrity Management in the Royal Australian Air Force 673
Squadron Leader T. Saunder

Fatigue Crack Initiation, Growth and Residual Strength Characteristics of Revited Fibre Metal Laminate Lap Joints 689
R. Miller and C. Borsboom

SESSION VI - FORCE MANAGEMENT

Embedded Optical Fiber Sensors for Airframe Repair Health Monitoring 705
W. Sproat, D. Szalwinski, J. Sirkis and C. Chang

Aircraft Usage Monitoring: The Structural Data Recording Set, ASH-37, Solution for Optimization of Flight Data Processing 721
J. Mohammadi and D. Crocker

A Fiber-Optic Loads Monitoring System for the CL-600 Challenger Aircraft 733
F. Blaha and Capt L. Grenier

Improving Predictions for Helicopter Usage Monitoring 743
M. Hoffman and W. Carpenter

Development of an Automated Procedure for Correlation of Two Sets of Range Mean Pair Fatigue Sensor Data 767
K. Walker

Aircraft Structural Integrity Program for the Aero Vodochody L 139 Jet Trainer 785
M. Trabert and J. Fidransky

A Simplified Approach to Repeated Loads Development 795
J. Abel and C. Manders

ATTENDEES LIST 837

FOREWORD

This report was compiled by the Systems Support Division, Materials Directorate, Wright Laboratory, Wright-Patterson Air Force Base, Ohio. It was initiated under Task 24180704 "Corrosion Control & Failure Analysis" with Thomas D. Cooper as the Project Engineer.

This technical report was submitted by the editors.

The purpose of this 1994 Conference was to bring together technical personnel in DoD and the aerospace industry who are involved in the various technologies required to ensure the structural integrity of aircraft gas turbine engines, airframes and other mechanical systems. It provided a forum to exchange ideas and share new information relating to the critical aspects of durability and damage tolerance technology for aircraft systems. The conference was sponsored by the Air Force Materiel Command (AFMC), Aeronautical Systems Center, Deputy for Engineering and Materials and Flight Dynamics Directorates of the Wright Laboratory, Wright-Patterson Air Force Base, Ohio. It was hosted by the Aircraft Structural Integrity Branch, Aircraft Directorate of AFMC's San Antonio Air Logistics Center, Kelly Air Force Base, Texas.

FINAL AGENDA

1994 USAF STRUCTURAL INTEGRITY PROGRAM CONFERENCE

6-8 December 1994

THE HYATT REGENCY SAN ANTONIO
SAN ANTONIO, TEXAS

MONDAY, 5 DECEMBER 1994

1700-1900 PRE-REGISTRATION

TUESDAY, 6 DECEMBER 1994

0730-0815 REGISTRATION/CONTINENTAL BREAKFAST

0815-0830 Opening Comments
J. Lincoln, ASC/ENF

Session I - Overviews
Chairman - K. Leikach, NAVAIR

0830-0900 C-17 Full Scale Durability Test
R. Eastin, McDonnell Douglas Aerospace

0900-0930 ASIP Initiatives for the T-38 Aircraft
H. Burnside, Southwest Research Institute
J. Dubke, San Antonio Air Logistics Center

0930-1000 A Review of the USCG/FAA AANC HU25 NDI Project
CDR E. J. Moukawsher and LCDR J. Mihelic, USCG Aircraft Repair & Supply Center
P. Walter and C. Jones, Sandia National Laboratories

1000-1030 REFRESHMENT BREAK

1030-1100 Principles, Procedures, and Outcome of the Damage Tolerance Test Verification of JAS39 Gripen Airframe
H. Ansell, Saab-Scania, Saab Military Aircraft

1100-1130 A Perspective to Determining the Structural Integrity of Aging Aircraft
Capt K. Hart, USAF, WL/FIBEC

1130-1200 Optimizing T/AV-8B Harrier's For Long Service Lives
M. Foster, P. Paul, and D. Rich, T. Hullander, McDonnell Douglas Aerospace

1200-1330 LUNCH and PRESENTATION
C-141 Starlifter: ASIP Methodology in an Aging Aircraft Environment
R. Alford, WR-ALC/LJLE, Robins Air Force Base, GA
J. Cochran, Lockheed Aeronautical Systems Co., - Georgia

Session II - Analysis and Testing
Chairman - J. Rudd, WL/FIB

1330-1400 Probabilistic Inspection Strategies — A Key to Controlling Multi-Site Damage
A. Brot, IAI Tashan Engineering Center, Aircraft Division/Israeli Aircraft Industires LTD

1400-1430 Fatigue Crack Growth and Residual Strength Characteristics of Riveted Fiber Metal Laminate Lap Joints
R. Miller, M. Heerschap, and J. Schijve, Delft University of Technology, The Netherlands

1430-1500 A Global-Local Fracture Criterion for Ductile Materials
T. Weng and C. Sun, Purdue University

1500-1530 REFRESHMENT BREAK

1530-1600 Acoustic Emission Monitoring of Full Scale Fatigue Tests on Canadian Forces Aerospace Structures
S. McBride, Royal Military College of Canada, Kingston, Ontario
G. Déziel and S. Le Guellec, National Defense Headquarters, Ottawa, Ontario, Canada

1600-1630 Determination of External Loads on a Manoeuvring F-18 in View of a Full Scale Fatigue Test
C. Perron, Bombardier/Canadier, Mirabel, Quebec, Canada
G. Déziel, Department of National Defense, Ottawa, Canada

1630-1700 Effect of Mechanical Paint Removal Processes on the Fatigue Life of Aircraft
C. Paul, WL/FIBEC

1700-1730 Progress Towards A Comprehensive Fatigue Analysis Program for Rotary and Fixed-Wing Aging Aircraft
Preston R. Bates, Georgia Tech Research Institute, Smyrna, GA

1800-1930 RECEPTION

WEDNESDAY, 7 DECEMBER 1994

0730-0800 REGISTRATION/CONTINENTAL BREAKFAST

Session II - Analysis and Testing (Continued)

0800-0830 Damage Tolerance Analysis of C-141 Weep Hole Cracks with Boron Composite Repairs
Capt D. Lee, D. Register, and Flt Lt K. Buhler, WR-ALC/TIEDD
D. Pipkins, Knowledge Systems, Inc.

0830-0900 Composite Repair Durability/Damage Tolerance Test of C/KC-135 F.S. 880 Floor Beam
J. Chung, E-Systems
A. Arrieta, OC-ALC/TIESM
J. Beard, OC-ALC/LACRA

Session III - Engine Structural Integrity

Chairman - W. Taylor, ASC/ENFP

0900-0930 Probabilistics in Gas Turbine Engines: Not a Gamble but a Goodie
Squadron Leader Chris Pomfret, WL/POTC

0930-1000 Effects of Multiple Blade Impact on Aircraft Engine Containment Structures During a Rotor Burst Failure
S. Sankar and S. Atluri, Georgia Institute of Technology

1000-1030 REFRESHMENT BREAK

1030-1100 How Valid Was Your Validation
D. Day and D. Painter, Capt, USAF, ASC/SMZF

1100-1130 Validation of Probabilistic Rotor Design Systems — Status of the USAF PRDS Contract
P. Roth, GE Aircraft Engines

1130-1200 A New Approach to Tracking Turbine Engine Life
J. Hansen and M. Paquet, United Technologies, Pratt & Whitney

1200-1330 LUNCH and PRESENTATION
Active Vibration Control
S. McBurnett, ARPA

Session IV - Structural Materials/Inspection
Chairman - T. Cooper, WL/MLS

1330-1400 Improved Aluminum Body Skin (C188-T3) and Extruded Stiffener (7150-T77) Alloys to Increase Safety and Affordability of Fuselage Structure
R. Bucci, M. Kulak, R. Rolf, G. Bray, J. Yeh, and J. Witters, Aluminum Company of America

1400-1430 Effect of Test Parameters on the Corrosion Fatigue Crack Growth of Aircraft Structural Materials
D. Hoeppner and T. Goswami, University of Utah

1430-1500 The Role of Fretting Corrosion and Fretting Fatigue in Aircraft Rivet Hole Cracking - December 1994 Status Report on FAA Grant Program
D. Hoeppner, C. Elliott III, and M. Moesser, University of Utah
T. Flournoy, FAA Technical Center

1500-1530 REFRESHMENT BREAK

1530-1600 An Evaluation of Fatigue Properties of Aging Aircraft Materials
A. Grandt, Jr., Purdue University

1600-1630 Nondestructive Inspection Capabilities Reference Handbook
W. Rummel, Martin Marietta Astronautics
G. Matzkanin, Texas Research Institute, Austin, TX

1630-1700 Eddy Current Inspection Reliability at Airline Inspection Facilities
F. Spencer, Sandia National Laboratories

1700-1730 Exfoliation Corrosion Located by Search Peening
J. Harrison, Metal Improvement Company

1900-2100 NASA/FAA/USAF NASGRO Meeting
Chairman - *R. Forman*

THURSDAY, 8 DECEMBER 1994

0730-0800 REGISTRATION/CONTINENTAL BREAKFAST

Session V - Structural Repair
Chairman - Lt Col J. Rogacki, WL/FIB

0800-0830 Residual Life Analysis and a Novel Repair Method for Cracks in F-16 Center Fuselage Bulkhead
S. Jiny, G. Davidi, E. Makevet, and D. Schur, Israeli Air Force

0830-0900 Str ictural Durability of Damaged Metallic Panel Repaired with Composite Patches
L. Minnetyen, Clarkson University
C. Chamis, NASA Lewis Research Center

0900-0930 C-5 Galaxy: Two Severely Burned Aircraft are Structurally Repaired and Returned to Active Service with USAF AMC
C. Hitchings, San Antonio Air Logistics Center
J. Jobson and K. Hall, Lockheed Aeronautical Systems Co. - Georgia

0930-1000 An Enhanced Method of Stop Drill Repair with Sleeveless Coldworking
M. Creager, Structural Integrity Engineering
M. Weigel and A. Leon, West Coast Industries

1000-1030 REFRESHMENT BREAK

1030-1100 Bonded Repair of Multiple Site Damage with GLARE Fiber Metal Laminate Patches
R. Fredell, Capt, USAF, USAF Academy

1100-1130 Interference Fit Bushing Installation and Hole Repair/Resizing Using an Expanded Bushing
L. Reid, Fatigue Technology Inc.

1130-1200 Ultrasonic Techniques for Repair of Aircraft Structures with Bonded Composites Patches
S. Smith, N. Senapati, and R. Francini, Battelle, Columbus, OH

1200-1330 LUNCH and PRESENTATION
Structural Integrity Management in the Royal Australian Air Force
Squadron Leader T. Saunder, Melbourne, Victoria, Australia

Session VI - Force Management
Chairman - J. Turner, SA-ALC/LADD

1330-1400 Embedded Optical Fiber Sensors for Airframe Repair Health Monitoring
W. Sproat and D. Szalwinski, Lockheed Aeronautical Systems Co. - Georgia
J. Sirkis, University of Maryland

1400-1430 Aircraft Usage Monitoring: The ASH-37 Solution for Optimization of Flight Data Processing
J. Mohammadi, Systems and Electronics, Inc.
D. Crocker, Aerostats, Ontario, Canada

1430-1500 A Fiber-Optic Loads Monitoring System for the CL-600 Challenger Aircraft
F. Blaha, Canadian Marconi Company, Montreal, Canada
Capt L. Grenier, National Defense Headquarters, Ottawa, Canada

1500-1530 REFRESHMENT BREAK

1530-1600 Improving Dynamic Load Prediction for Helicopter Monitoring
M. Hoffman, Naval Air Warfare Center, Warminster, PA
W. Carpenter, University of South Florida, Tampa, FL

1600-1630 Development of an Automated Procedure for Correlation of Two Sets of Range Mean Pair Fatigue Sensor Data
K. Walker and L. Molent, DSTO, Aeronautical and Maritime Research Laboratory, Victoria, Australia

1630-1700	Aircraft Structural Integrity Program for the Aero Vodochody L 139 Jet Trainer *M. Trabert and A. Ghannadan*, ESPRIT Technology *J. Fidransky*, Aero Vodochody *L. Pellum*, Kaman Aerospace Corp.
1700-1730	An ASIP Update - FAA Flight Inspection Fleet of Beech Model 300's *J. Smith*, Beech Aircraft Corporation
1730	Conference Adjourned

EXHIBITORS

- CANADIAN MARCONI COMPANY
- CELERIS AEROSPACE CANADA INC.
- CHRYSLER TECHNOLOGIES AIRBORNE SYSTEMS INC.
- DEVICE TECHNOLOGIES INC.
- FAA TECHNICAL CENTER
- FATIGUE CONCEPTS
- FATIGUE TECHNOLOGY INC.
- GENERAL ELECTRODYNAMICS CORP.
- METAL IMPROVEMENT COMPANY
- MOOG ESPRIT
- MTS SYSTEMS
- NONDESTRUCTIVE TESTING INFORMATION ANALYSIS CENTER
- SMITHS INDUSTRIES AEROSPACE
- SOUTHWEST RESEARCH INSTITUTE
- SYSTEMS ELECTRONICS INC.
- TEXTRON SPECIALTY MATERIALS
- USAF OKLAHOMA CITY AIR LOGISTICS CENTER

INTRODUCTION

This report contains the proceedings of the 1994 USAF Structural Integrity Program Conference held at the Hyatt Regency Hotel in San Antonio, Texas from 6-8 December 1994. The conference, which was sponsored by the Aeronautical Systems Center's Engineering Directorate and the Wright Laboratory's Flight Dynamics and Materials Directorates, was hosted by the San Antonio Air Logistics Center Aircraft Directorate, Aircraft Structural Integrity Branch (SA-ALC/LADD). This conference, as in previous years, was held to permit experts in the field of structural integrity to communicate with each other and to exchange views on how to improve the structural integrity of military weapon systems. Sessions were primarily focused on analysis and testing, engine structural integrity, structural materials and inspections, structural repair, and force management. This year, as in previous years, our friends from outside the U.S. borders provided the audience with outstanding presentations on activities within their countries. It is anticipated that this conference will include their contributions in the agenda of future meetings. This year eighteen countries were represented in the audience.

The sponsors are indebted to their hosts for their support of the conference. The sponsors are also indebted to the speakers for their contributions. In particular, thanks are due to the three luncheon speakers for their informative presentations, Mr. Joe Cochran from Lockheed Aeronautical Systems Company and Mr. Russ Alford from Warner Robins Air Logistics Center provided and excellent presentation on ASIP Methodology for the C-141. Mr. Steve McBurnett of ARPA gave an interesting and informative presentation on active vibration control. Squadron Leader T.J. Saunder provided an inspiring view of Structural Integrity Management in the Royal Australian Air Force.

As usual, much of the success of the conference is due to the efforts of Jill Jennewine and her staff, including Lori Mantia and Tracy Tapia, from Universal Technology Corporation. Their cooperation is greatly appreciated. We are also grateful to Rita Scholes of WL/MLS for her continuing support to the success of this conference.

James L. Rudd
WL/FIB

Thomas D. Cooper
WL/MLS

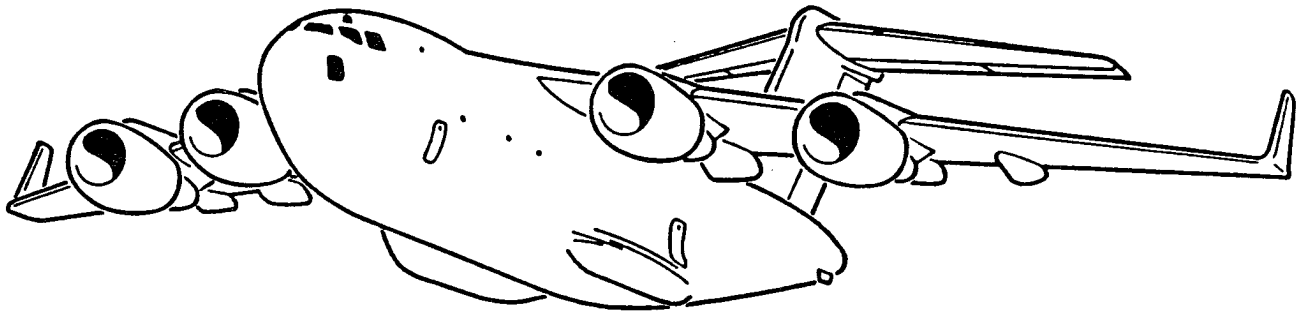
John W. Lincoln
ASC/ENF

SESSION I

OVERVIEWS

Chairman: *K. Leikach*, NAVAIR

C-17
FULL SCALE DURABILITY TEST PROGRAM



1994 USAF ASIP CONFERENCE
DECEMBER 6-8, 1994
SAN ANTONIO, TEXAS

R. G. EASTIN
MCDONNELL DOUGLAS AEROSPACE
TRANSPORT AIRCRAFT
LONG BEACH, CA.

C-17 FULL SCALE DURABILITY TEST PROGRAM

This presentation provides an overview of the durability testing being performed on the C-17 durability test article "D1". Some of the topics which are discussed include design usage, life verification requirements, test article description, test setup, test article loading, spectrum development and characteristics, inspection program, results obtained to date, and lessons learned/relearned.

C-17 DESIGN USAGE

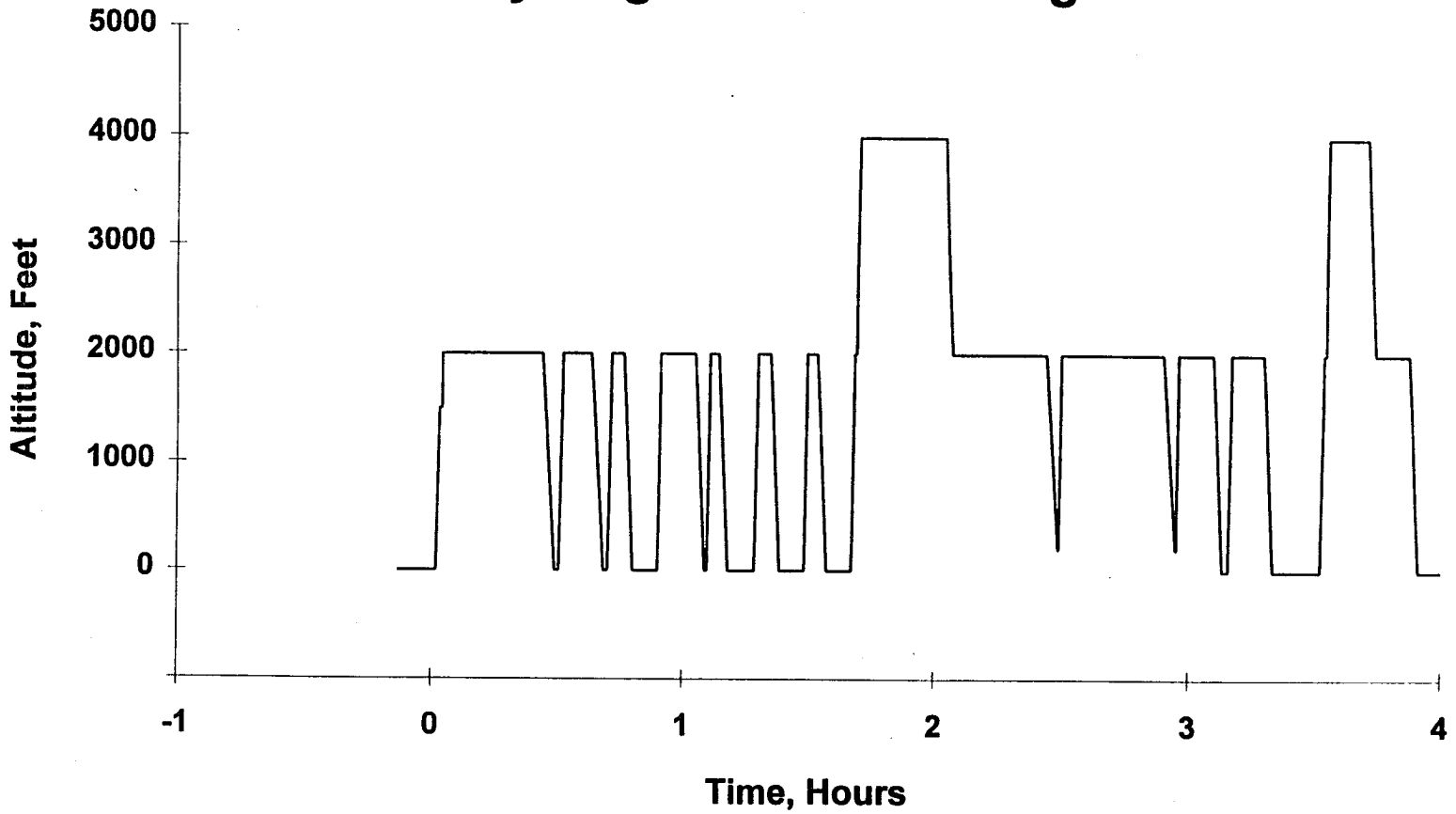
- DESIGN USAGE SPECIFIED IN TERMS OF 25 MISSION PROFILES (35 UNIQUE FLIGHT TYPES) AND CORRESPONDING MISSION MIX.
- MISSION TYPES VARY FROM SIMPLE LOGISTICS MISSIONS TO COMPLEX TRAINING MISSIONS.
- ONE LIFETIME INCLUDES:

8564	FLIGHTS
30000	FLIGHT HOURS
18950	LANDINGS (INCLUDING T&Gs)
4020	FULL PRESSURE CYCLES
3200	HOURS @ V $\geq$ 300 KEAS & h $\leq$ 2000 FEET
6050	HOURS @ V $<$ 300 KEAS & h $\leq$ 2000 FEET

C-17 DESIGN USAGE

Design usage is specified in terms of 25 basic mission profiles. Variations on some of these result in 35 unique flight types which must be addressed for both analysis and test. These vary from logistics flights, with the majority of time spent cruising at altitude and one ground-air-ground (GAG) cycle, to complex training flights, with the majority of time spent at low altitude and as many as eleven GAG cycles. One lifetime consists of 8564 flights, 30000 flight hours, and 18950 landings (including touch and gos). There are approximately 4020 full cabin pressure cycles with many lesser cycles associated with numerous moderate altitude transitions. The specified mission profiles also contain a significant amount of operation at 2000 feet and below. Approximately 30% of the total flight time is spent in this environment with about one third of that spent cruising at 300 KEAS or greater. Also present in many of the missions are special events such as low level high speed cruise, airdrops, aerial refueling and missed approaches.

Flight Type #32
Heavyweight Local Training



FLIGHT TYPE #32

This is an example of one of the 35 design flight profiles. Flight type #32 is one of the more complex flights and represents a training mission to practice heavyweight small austere airfield operations. The payload is 93000 pounds and the flight is four hours in duration. There are 308 of these flights in one lifetime. Present in this profile are ten ground-air-ground cycles and the entire flight is at or below 4000 feet. Much of the cruise time is spent at 250 knots.

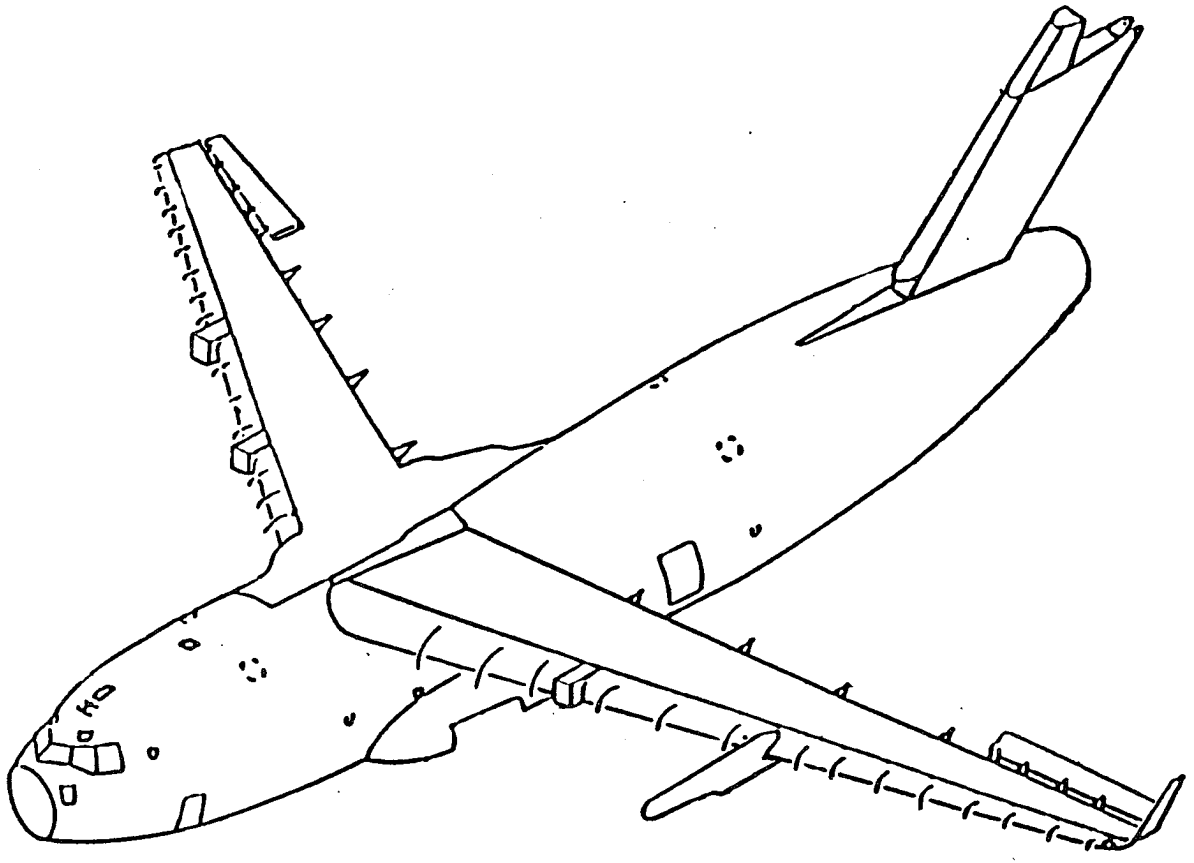
C-17 LIFE VERIFICATION

- ANALYSIS AND TEST
- DURABILITY AND DAMAGE TOLERANCE LIFE VERIFIED BY ANALYSIS:
  - 2 LIFETIMES FROM .01" FLAW TO FUNCTIONAL IMPAIRMENT FOR DURABILITY (LANDING GEAR EXCLUDED),
  - 2 LIFETIMES FROM INITIAL MANUFACTURING DEFECT (E.G. .05" FLAW AT HOLE) TO CRITICAL FOR DAMAGE TOLERANCE.
- DAMAGE TOLERANCE TESTING PERFORMED AT COUPON AND COMPONENT LEVEL ONLY.
- DURABILITY VERIFICATION BY FULL SCALE TESTING FOR TWO LIFETIMES.

LIFE VERIFICATION

The contract requires verification of life by analysis and test. For durability, analyses must be performed to show two lifetimes from an initial .01" flaw to functional impairment. For damage tolerance, analyses must be performed for all safety-of-flight structure to show two lifetimes from an initial manufacturing defect (e.g. .05" flaw at a hole) to critical. Damage tolerance verification testing was performed at the coupon and component level with no testing planned on the full scale article. Durability verification testing is being performed by testing a full scale test article for two design lifetimes.

C-17 DURABILITY AIRFRAME



C-17 DURABILITY AIRFRAME

C-17 airframe durability is being verified by testing of the fifth airframe to be assembled. The test article is designated D1 and consists of the fuselage (including main landing gear pods and right hand side wing-fuselage fairings), wing (including fixed leading edge), wing pylon stubs, left hand outboard pylon, and vertical stabilizer. Production slat tracks, upper landing gear assemblies, left hand winglet, and ailerons are also included to provide realistic loading of the article.

EDERER

TEST SETUP

The D1 test is being conducted in Long Beach, California in a fixture that is located outside. The systems have been weather proofed and weather conditions have made only a minor impact on running the test even though the article and systems are completely exposed. The article was finished with exterior epoxy primer prior to delivery to the test site. The article is surrounded by a super structure which provides support to the article as well as anchor points for tension actuators. This super structure also facilitates access to the article for inspections and repairs. The fuselage is pressurized without any volume reduction. This facilitates access to the interior for inspection and repair.

TEST ARTICLE LOADING

- TENSION PAD ARRAYS BONDED TO UPPER AND LOWER WING COVERS AND LEFT AND RIGHT VERTICAL STABILIZER COVERS LOADED BY TENSION WHIFFLE TREES.
- WING LOADING ALSO INTRODUCED VIA SLAT TRACKS, FLAP HINGES AILERONS AND WINGLETS.
- NOSE AND MAIN LANDING GEAR FIXTURES PROVIDE LOADING TO GEAR ATTACH POINTS.
- DUMMY HORIZONTAL LOADS VERTICAL AT TOP.
- CARGO FLOOR AND RAMP LOADED.
- FUSELAGE SHELL LOADED VIA BONDED ON STRAPS.
- FUSELAGE PRESSURIZED WITH AIR WITHOUT ANY VOLUME REDUCTION.
- OVER 260 HYDRAULIC ACTUATORS DRIVEN BY CLOSED LOOP CONTROL SYSTEM.
- RATES OF 5-8 CYCLES (10-16 END CONDITIONS) PER MINUTE HAVE BEEN ROUTINELY ACHIEVED WITH ACCEPTABLE ACCURACY.

TEST ARTICLE LOADING

Loading is applied to the article in a number of ways. Every effort has been made to introduce loads into the structure as realistically as possible. Extensive use is made of bonded on tension pads. Virtually the entire wing upper and lower covers and vertical stabilizer left and right hand covers are covered with pads to provide distributed loading. Production upper nose and main landing gear assemblies are used to load gear attach points. A dummy horizontal, attached to the vertical stabilizer pivot points and pitch trim actuator support structure, is used to input horizontal stabilizer loads. Loading fixtures are provided inside the article to apply loads to the cargo floor and ramp. The fuselage shell is loaded with bonded on straps to apply inertia loads and is fully pressurized without any volume reduction. Production slat tracks, flap hinges, ailerons and winglets are used to additionally load the wing. There are over 260 hydraulic actuators driven by a closed loop system which are used to load the article. Loading rates of five to eight cycles (10-16 end conditions) per minute have been routinely achieved with acceptable accuracy.

TEST SPECTRA DEVELOPMENT

- OBJECTIVE - CONTROL POINT ANALYSIS SPECTRA AND TEST SPECTRA EQUIVALENCE.
- MAINTAINED COMMONALITY BETWEEN ANALYSIS AND TEST SPECTRA DEVELOPMENT APPROACH WHENEVER POSSIBLE.
- ALL 35 FLIGHT TYPES INCLUDED - TOO UNIQUE TO COMBINE.
- EACH FLIGHT IS ASSEMBLED SEPARATELY SO EVEN FLIGHTS OF THE SAME TYPE ARE UNIQUE.
- LOAD LEVELS OCCURRING LESS THAN 10 TIMES PER LIFE ARE EXCLUDED.

The primary objective was to develop a full scale test spectrum which would result in damage throughout the article which would be equivalent to the damage from the spectra used for design. In order to help insure this goal was met every effort was made to use the same data, ground rules, assumptions, etc. as was used to develop the analysis spectra. Deviations were made when there was no alternative. To this end all 35 flight types were included with each assembled separately the same as for the analysis spectra. All load levels occurring less than 10 times per life were excluded consistent with the analysis spectra.

TEST SPECTRA DEVELOPMENT(continued)

- CABIN PRESSURE SCHEDULE FOLLOWED TO DEFINE FUSELAGE PRESSURE CYCLES. (MAXIMUM CABIN PRESSURE IS 7.8 PSIG).
- RAMP AND CARGO DOOR CYCLES CORRESPOND TO AIRDROP EVENTS.
- TRUNCATION AT GLOBAL LEVEL (E.G. C.G. LOAD FACTOR AND PROBABILITY OF OCCURRENCE).
- GUST AND TAXI LOADING GENERATED USING METHODOLOGY DEVELOPED FOR C-17 TO DEAL WITH PHASING PROBLEM (REFERENCE 1991 ASIP PRESENTATION).
- FINAL SPECTRUM VALIDATED BASED ON COMPARISON OF CRACK GROWTH FROM AN INITIAL .01" FLAW.

TEST SPECTRUM DEVELOPMENT(continued)

The cabin pressure schedule was followed to define cabin pressure throughout each flight with the maximum being 7.8 psig. Ramp and cargo door cycles are included and correspond to airdrop events. One of the major deviations between analysis and test is truncation. For analysis, control point spectra were truncated at a stress range of 2000 psi. Individual control point truncation level compatability cannot be achieved on a large full scale test. Truncation must be performed at the global level. For example, maneuver loads are truncated using a C.G. incremental load factor threshold of 0.30g while gust loads were truncated at an equal probability of occurrence level. Phasing is automatically taken care of when developing individual control point analytical gust spectra but when a sequence of balanced aircraft loads due to gust is required phasing becomes a major dilemma. This also hold true for taxi loads. In order to deal with this problem methodology was specially developed for the C-17 to generate sequences of phased load sets for gust and taxi. This methodology was presented at the 1991 ASIP Conference. Once the test spectrum was developed it had to be validated. The criteria used was growth of a .01" initial flaw. Growth due to the analysis spectra and test spectra were compared at key control points in the structure and test spectra adjustments made until acceptable correlation was obtained.

TEST SPECTRUM CHARACTERISTICS

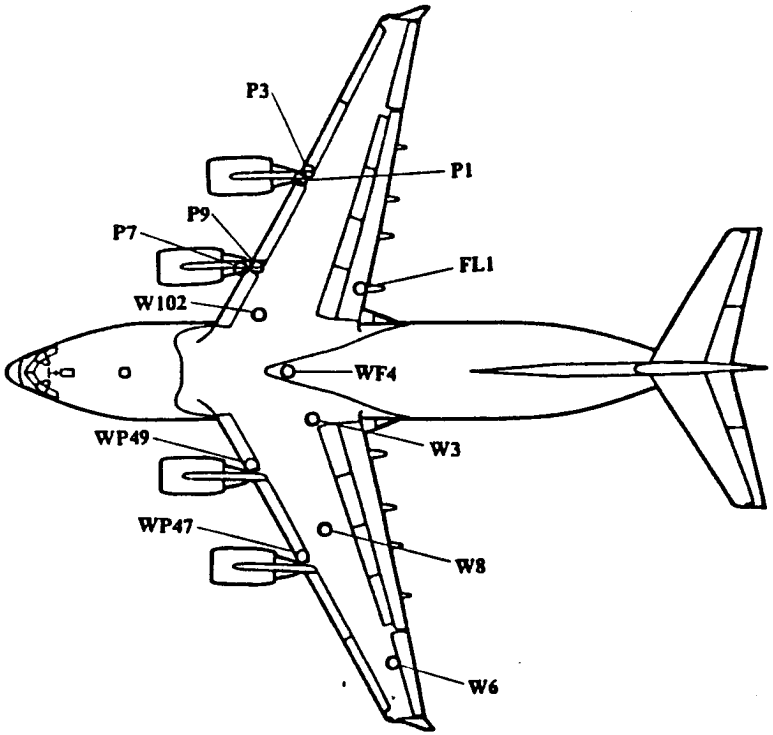
- 1/10 LIFETIME REPEATABLE SEQUENCE CONTAINING 856 FLIGHTS.
- FLIGHTS RANDOMLY ORDERED EXCEPT FOR SPECIAL GROUPING IN MIDDLE AND END TO FACILITATE MARKING.
- 3,670,190 END CONDITIONS PER LIFETIME.
- MAXIMUM ONCE PER 1/10TH LIFETIME WING ROOT BENDING IS DUE TO GUST AND IS 76% OF DESIGN LIMIT LOAD.
- AVERAGE ONCE PER FLIGHT WING ROOT BENDING IS 55% OF DESIGN LIMIT LOAD.

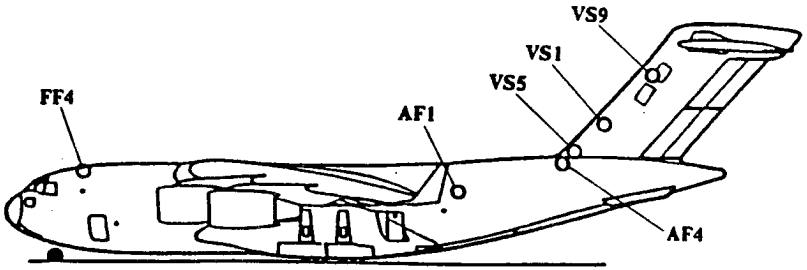
TEST SPECTRUM CHARACTERISTICS

The test spectrum represents one tenth of a lifetime of usage (i.e. 3000 flight hours) and contains 856 flights. The sequence is repeated 20 times to accumulate two lifetimes of usage. The ordering of flights within the sequence is random except for grouping of some of the more damaging flights in the middle and end of the sequence to facilitate marking. This is based on a coupon test program which investigated marking techniques. There are 3,670,190 end conditions which must be applied to accomplish one lifetime. Each end condition is a fully balanced set of actuator loads. The highest wing root upbending that occurs for any end condition in the sequence is due to a gust point and is 76% of design limit root upbending. The average once per flight level is 55% of design limit load.

DAMAGE TRACKING

- CRACK GROWTH TRACKED AT 18 KEY CONTROL POINTS.
- EACH 1/10 LIFETIME PROCESSED AND CRACK GROWTH FROM .01" FLAW PREDICTED USING ACTUAL TEST LOADS (LOAD CELL OUTPUT).
- ACTUAL TEST CRACK GROWTH COMPARED TO DESIRED TEST CRACK GROWTH.
- CONTROL POINT STRESS SPECTRA STATISTICS ALSO COMPARED.





DAMAGE TRACKING

Damage tracking is performed to assess the effect of the actual test loads on damage. Crack growth from an initial .01" flaw is computed at 18 key control points in the structure. Each 1/10 lifetime actual test loads are processed and crack growth predictions are made using the control point spectra generated. This crack growth is compared to growth predicted using the desired test loads. Differences may be cause for adjustments to the test loading system. In addition to crack growth control point stress spectra statistics are also compared (e.g. peak exceedances, range distributions, etc.)

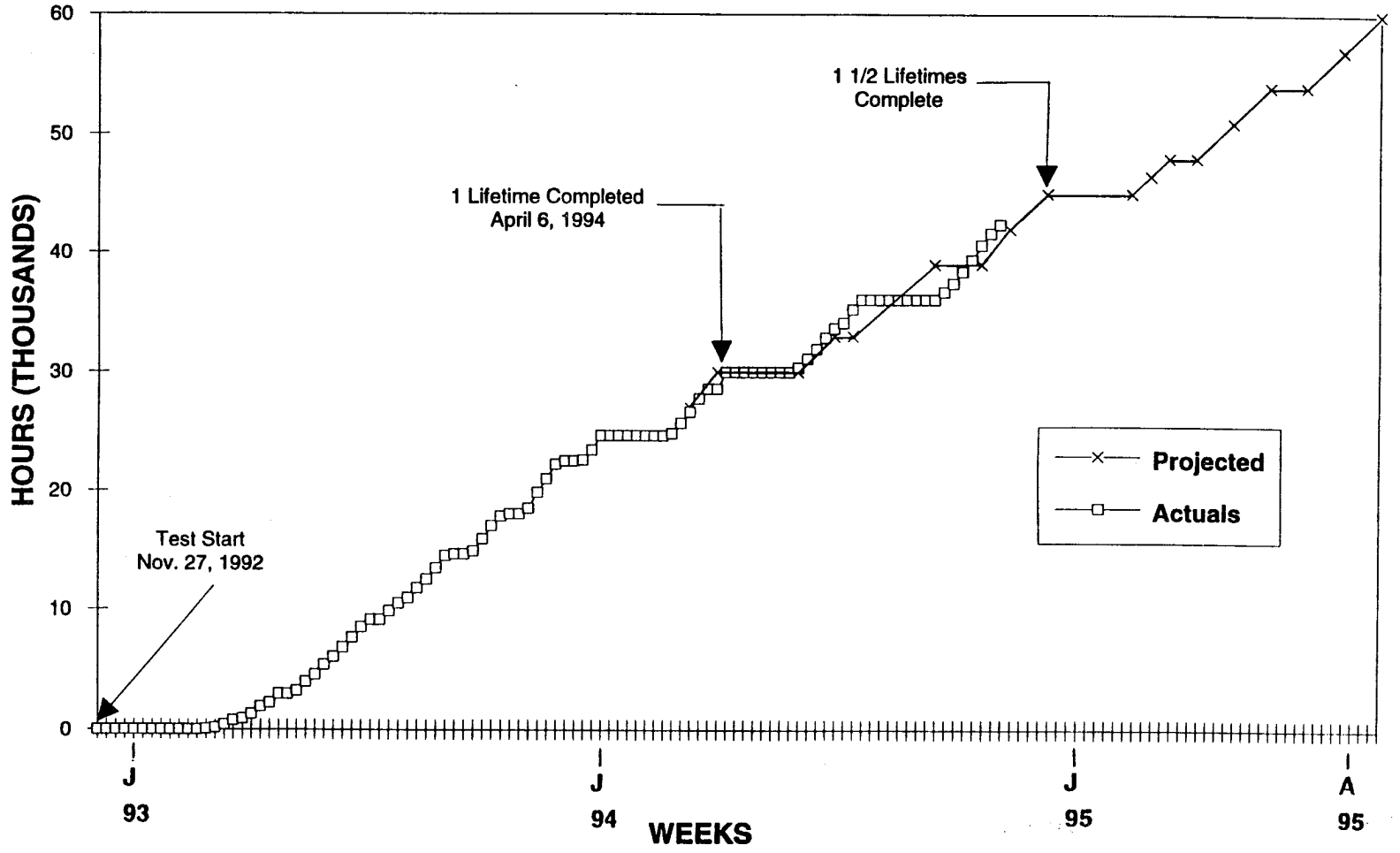
INSPECTION PROGRAM
(MDC-K5091)

- INSPECTION PROGRAM REQUIREMENTS DEVELOPED BY ENGINEERING WITH PRIMARY INPUT FROM DURABILITY AND DAMAGE TOLERANCE ORGANIZATION.
- D1 ARTICLE DIVIDED INTO 7 SECTIONS.
- DETAIL INSPECTION AREAS IDENTIFIED FOR EACH SECTION.
- 200 INSPECTION AREAS IDENTIFIED AT START OF TEST. 20 AREAS ADDED DURING FIRST 1.2 LIFETIMES.
- INITIAL INSPECTION PLAN REQUIRED ONLY VISUAL OR CLOSE VISUAL WITH THE EXCEPTION OF ONE AREA. CURRENT PLAN INCLUDES DYE PENETRANT, EDDY CURRENT AND ULTRASONIC INSPECTIONS.
- ALL AREAS INSPECTED AT 0, .1, 1.0, 1.5 AND 2.0 LIFETIMES.
- AREAS ALSO INSPECTED AT "NOT TO EXCEED" INTERVALS RANGING FROM 300 FLIGHTS TO .5 LIFETIMES.

INSPECTION PROGRAM

The inspection program is documented in report MDC-K5091. The requirements (i.e. where, when and how) were developed by engineering with primary input from the Durability and Damage Tolerance organization. The D1 article is divided into 7 sections and detail inspection requirements are specified for areas in each section. At the beginning of the test there were 200 areas identified which required inspection. Over the course of the first 1.2 lifetimes 20 areas have been added. With the exception of one area the initial inspection plan required visual or close visual inspection only. Currently dye penetrant, eddy current and ultrasonic inspections are also required for some areas. The inspection program is structured such that all areas are inspected at 0, .1, 1.0, 1.5 and 2.0 lifetimes. In addition, to this areas are inspected at "not to exceed" intervals which vary from area to area depending on criticality. Intervals vary from as frequent as 300 test flight hours to .5 lifetimes with .3 test lifetimes being typical.

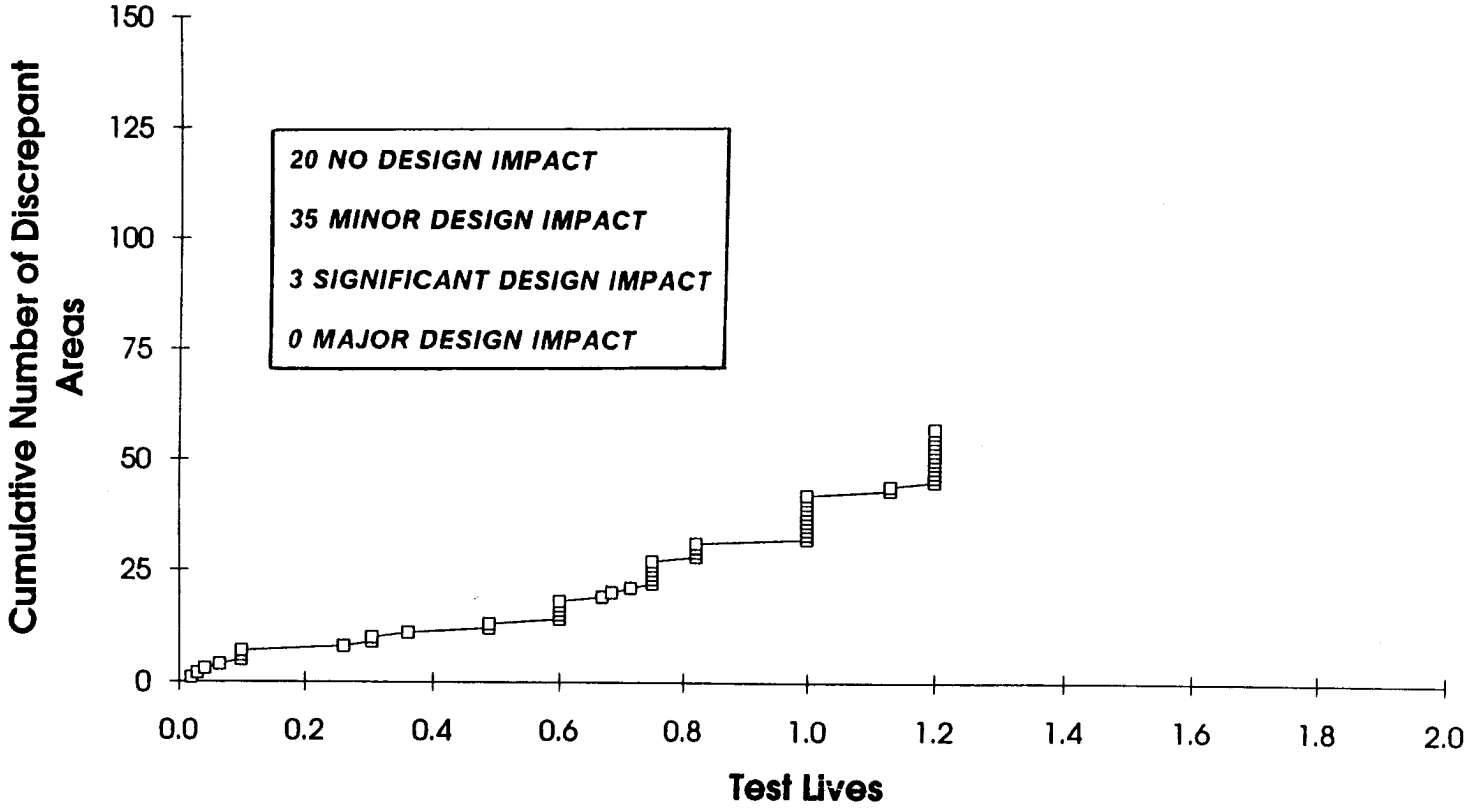
C-17 FULL SCALE DURABILITY TEST SCHEDULE



C-17 FULL SCALE DURABILITY TEST SCHEDULE

Full scale testing started on November 27, 1992, however, full rate cycling did not start until around March 7, 1993. This was due to typical learning curve problems and the impact of the static article wing failure which occurred on October 1, 1992. Once full rate cycling started testing progressed relatively rapidly to completion of one lifetime on April 6, 1994. There were several periods when testing was halted to accomplish various repairs. The completion of 1.5 lifetimes is expected by the end of 1994 with completion of 2 lifetimes expected prior to September 1995. This will complete Full Scale Engineering Development (FSED) testing. A third lifetime of testing is currently in the proposal stage and is expected to follow directly after the second lifetime is complete.

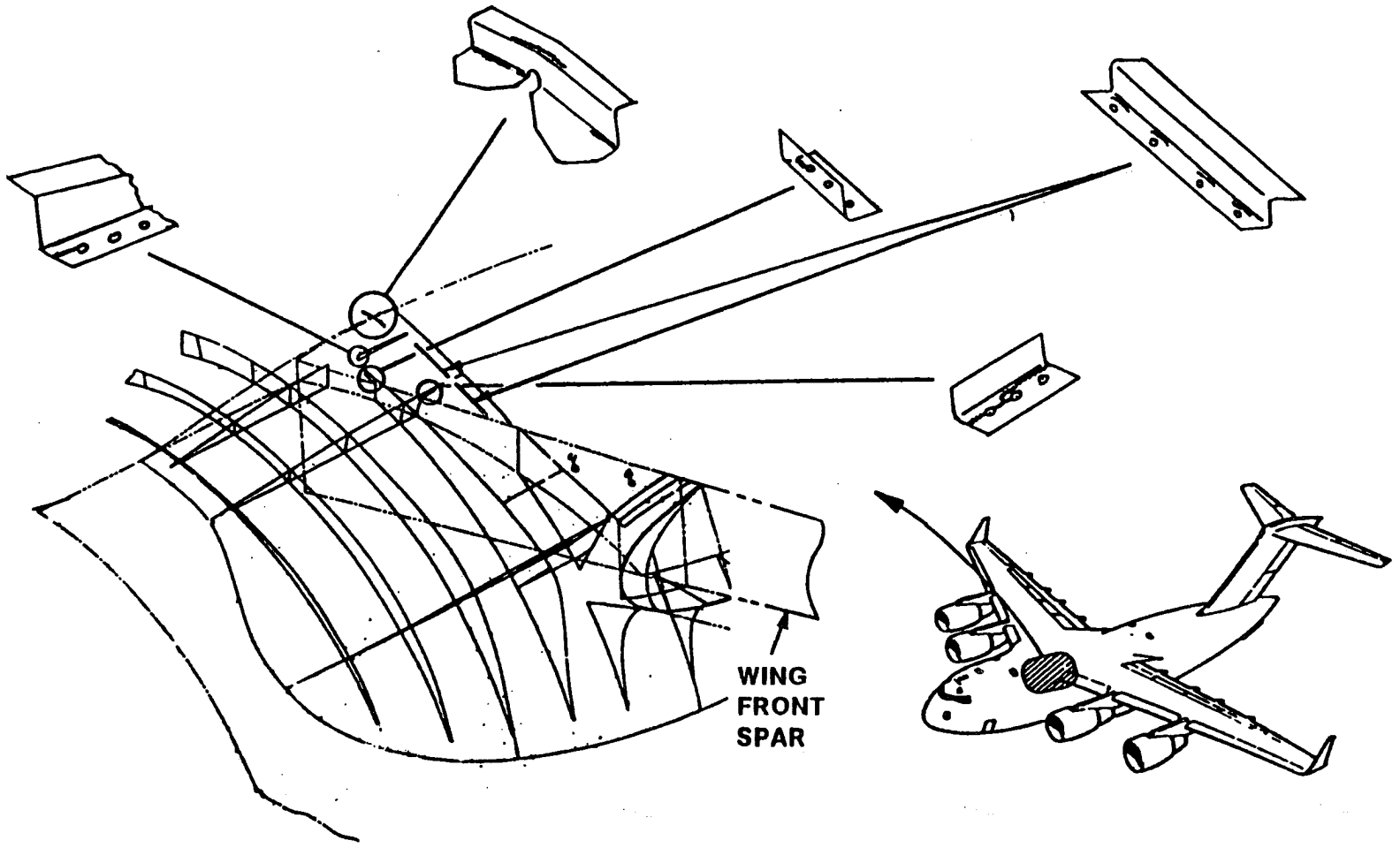
C-17 Full Scale Durability Test History



C-17A FULL SCALE DURABILITY TEST HISTORY

Fifty eight discrepant areas were identified over the course of the first 1.2 lifetimes. Twenty of these did not impact the design and included problems attributed to manufacturing problems (e.g. excessive preload, omission of fastener, workmanship) or a prior failure. Thirty five items required minor redesign/upgrade of discrete parts such as shear clips, spring clips, fairing support structure, fasteners, etc. Three items required significant redesign of local details in primary load path structure. There were no items which were considered major design impact items.

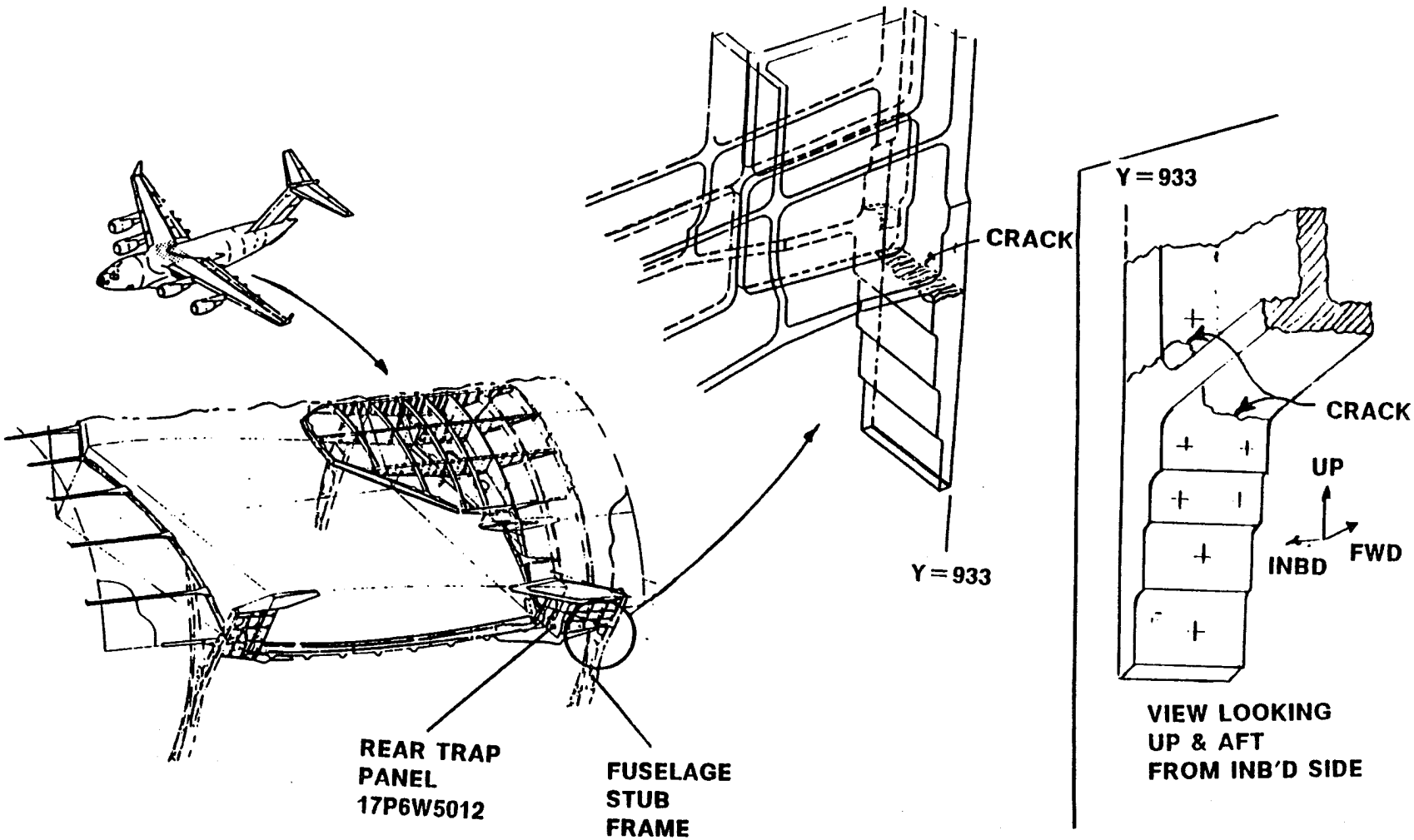
D16 CENTER FUSELAGE OVERWING FAIRING FORMER CLIPS



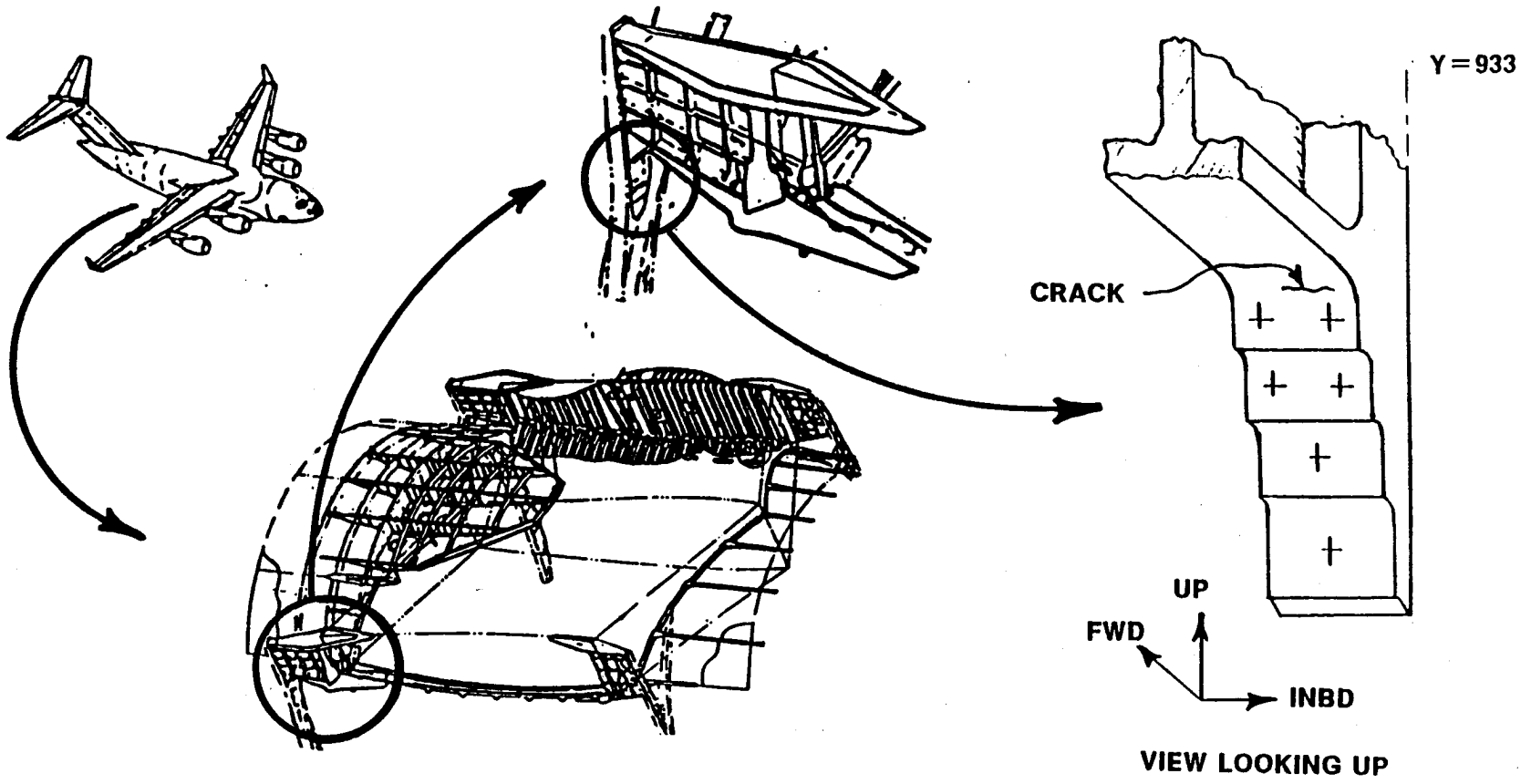
D16 CENTER FUSELAGE OVERWING FAIRING FORMER CLIPS

D16 is an example of one of the discrepancies which is considered to be minor with respect to design impact. This discrepancy involves cracking of various formers and clips that support and attach the overwing fairing to the wing. The first cracks were found at 18000 test flight hours during close visual inspections with additional cracking discovered during subsequent inspections. This is non-safety-of-flight structure with cracking being caused by forced deflections. Design changes involve modification of clip configurations and use of sliding joints.

D28a. LEFT HAND REAR TRAPEZOID PANEL



D28b. RIGHT HAND REAR TRAPEZOID PANEL



D28 REAR TRAPEZOIDAL PANEL

D28 is an example of one of the few discrepancies which is considered to be relatively significant with respect to design impact. It was discovered at 24658 test flight hours (.82 lifetimes) during a close visual inspection on the left hand side. The crack extended completely thru the part severing the vertical tang provided to help distribute the shear load transfer between the trapezoidal panel and wing support frame stub. Inspection of the right side found an identical crack but in a much earlier stage of growth. The left side was cut out and repaired while the left side crack was blended out and the planned production retrofit installed. Multiple crack initiation sites were found in the surface at the radius transition between the tang and horizontal flange of the trapezoidal panel. The aircraft has full 100% design limit load capability with the failure. The fix involves a change to the local design details (e.g. transition radius being increased).

LESSONS LEARNED/RELEARNED

- USE REPEATABLE SEQUENCE REPRESENTING SOME FRACTION OF A LIFETIME.
- ACQUIRE AND RECORD ALL DATA AT EACH END CONDITION.
- TRACK DAMAGE AT KEY CONTROL POINTS IN STRUCTURE USING ACTUAL TEST LOADS.
- HAVE FORMAL INSPECTION PROGRAM WITH Q/A INSPECTORS BUT AUGMENT WITH COGNIZANT ENGINEERS.

LESSONS LEARNED/RELEARNED

There have been many lessons learned to date worth noting. Some of these are discussed below.

1. **The use of a repeatable sequence representing some fraction of a lifetime is highly recommended. This approach has provided an invaluable benchmark which we are always using for reference especially with respect to test loading accuracy. It also helps to minimize the impact on computing resources.**

2. **All data should be acquired and recorded at each end condition for subsequent processing and analysis. External loading is never exact and must be assessed periodically and mid course corrections made. This requires actual loads applied. Additionally, when discrepancies are identified, being able to recover the past strain history in an area is invaluable.**

3. **Damage should be tracked at key locations in the structure using actual test loading for comparison to desired damage. This provides a mechanism to quantity test loading accuracy. Any other way of looking at net accuracy is too subjective.**

4. **A formal inspection program should be implemented using Quality Assurance inspectors however this should be augmented with inspections by motivated cognizant engineers. They will be more successful in finding discrepancies than the typical hourly inspector.**

LESSONS LEARNED/RELEARNED (CONTINUED)

- MINIMIZE INITIAL NUMBER OF STRAIN GAGES AND PROVIDE SYSTEM CAPABILITY AND RESOURCES TO ADD SIGNIFICANT NUMBER AS TEST PROGRESSES.
- EMPHASIZE STRAIN GAGE COMMONALITY WITH AIRLOADS AND STATIC ARTICLES.
- PROVIDE FOR PERIODIC STRAIN SURVEY CONDITIONS.
- PLAN FOR FAILURES.
- PROVIDE FOR 3rd LIFETIME.

LESSONS LEARNED / RELEARNED (CONTINUED)

5. The number of gages at the start of the test should be limited to those required for overall sanity checks of the test and verification of gross internal loads. Nevertheless, the data acquisition system should be structured and resources made available such that a significant number can be added at the test progresses and discrepancies are identified. For the C-17 we should have started with no more than several hundred with capability to go up to at least 1000.

6. Strain gage commonality between the Durability, Static Strength and Air Loads test articles should be stressed. There should be a subset of gages on each article that are common. Commonality on the C-17 was more coincidental than planned. Commonality is invaluable for trouble shooting and can build confidence and/or help identify problems.

7. A set of strain survey cases should be identified and run periodically over the course of the test as a quality check. Additionally as gages are added to investigate discrepant areas these provide a pre-existing baseline for strain surveys.

8. Schedules and allocated resources should reflect the very high probability that failures will occur.

9. The basic FSED package should include a third lifetime of durability testing. Value added with respect to additional information gained to support fleet management, life extension and addressing multiple site damage issues support this approach rather than making it a questionable added on at some later date.

SUMMARY

- C-17 STRUCTURAL DURABILITY BEING VERIFIED BY TESTING THE FIFTH AIRFRAME ASSEMBLED TO TWO DESIGN SERVICE LIFETIMES (I.E. 60000 FLIGHT HOURS).
- TEST SPECTRUM IS A RANDOM CYCLE-BY-CYCLE, FLIGHT-BY-FLIGHT 1/10 LIFETIME REPEATABLE SEQUENCE CONTAINING 856 FLIGHTS.
- 3,670,190 END CONDITIONS APPLIED PER LIFETIME.
- TESTING STARTED ON MARCH 7, 1993 WITH ONE LIFETIME COMPLETED ON APRIL 6, 1994 AND TWO LIFETIMES EXPECTED PRIOR TO SEPTEMBER 1995. A THIRD LIFETIME IS BEING PLANNED.
- 58 DISCREPANT AREAS IDENTIFIED DURING FIRST 1.2 LIFETIMES WITH NONE RESULTING IN MAJOR DESIGN IMPACT.
- TEST CONSIDERED VERY SUCCESSFUL TO DATE.

SUMMARY

C-17 structural durability is being verified by testing the fifth airframe assembled to two design service lifetimes (i.e. 60000 flight hours). The test spectrum being used is a random cycle-by-cycle, flight-by-flight tenth of a lifetime repeatable sequence. In order to represent one lifetime 3,670,190 end conditions must be applied. Testing started on March 7, 1993 with one lifetime completed on April 6, 1994. Completion of two lifetimes is expected prior to September 1995. A third lifetime is currently in the planning stages. Over the course of the first 1.2 lifetimes there were 58 discrepant areas identified. Out of these 58 there were none that resulted in a major design impact. All aspects of the test have gone relatively well and the test is considered very successful to date.

ASIP INITIATIVES FOR THE T-38 AIRCRAFT

by
Hal Burnside, Southwest Research Institute
and
Jon Dubke, San Antonio Air Logistics Center

Presented at the 1994 USAF Structural Integrity Program Conference
San Antonio, Texas, December 6-8, 1994

INTRODUCTION

For almost 34 years the T-38 has been used by the United States Air Force (USAF) as an advanced fighter trainer. No other aircraft in aviation history has fulfilled this mission over such a long period of time. More remarkably, the USAF would like to fly the T-38 until the year 2020, and possibly beyond, which would make the T-38 sixty years old at retirement. Not only is the service time much longer than originally expected, but the current and future training environments represent fighter missions that are more severe than that for which the T-38 was originally designed. This has required that the USAF maintain an active structural integrity program for the T-38. This paper will review the development and evolution of the T-38 structure over the past 34 years and address present initiatives being undertaken by the USAF to ensure structural integrity over its remaining life.

BACKGROUND

The T-38 is a supersonic twin-jet fighter-trainer developed and produced by Northrop Aircraft. Its development started in 1956 with the goal of producing an affordable, low operating and maintenance cost aircraft that would represent the flying characteristics of a supersonic fighter. The first T-38 flew in April 1959, and the first production T-38As became operational at Randolph Air Force Base in March 1961. Fig. 1 shows the timeline of the structural development, evaluations and modifications that have occurred over the T-38's service life. This paper will discuss how these events have contributed to its structural integrity and long life.

Over 1,100 aircraft were manufactured from 1961 to 1972. The T-38 has been used as the USAF's high performance supersonic fighter trainer for the past 34 years and is the mainstay of the USAF's Air Education and Training Command (AETC) Undergraduate Pilot Training (UPT). The size of this training fleet is approximately 400 aircraft. These aircraft are used in various roles, such as the Basic Fighter and Air Combat Maneuver Training. NASA uses the T-38 as flight readiness trainers for its astronauts and as Space Shuttle Orbiter chase aircraft. The U.S. Navy uses the aircraft for test pilot training, and the T-38 also serves for pilot training by several NATO countries. In addition, about 2300 F-5 aircraft, sister to the T-38, were produced from 1963 to 1987, and about 1,600 F-5s are currently flown by foreign air forces.

The development of the T-38 came at a time of rapid advances in transonic aerodynamics, structures and engine technologies and their insertion into design. These advances included, for example in aerodynamics, the use of the area rule for fuselage design to reduce transonic drag, with the resulting increase in transonic acceleration. The T-38 wing structure employs chemical milling and tapered machined skins, and the horizontal stabilizer uses honeycomb bonding to thin aluminum skins. The gross weight of the T-38 was also kept to a minimum by 1950s technological developments in small, high thrust-to-weight ratio engines. Each of the two General Electric J85-GE-5 eight stage, axial flow turbojets have static thrusts of 2,680 lb and 3,850 lb (afterburner) under sea level, standard day conditions. Table 1 summarizes the T-38's major original design characteristics.

Table 1. Summary of Original Design Characteristics

Wing Span	25 ft 3 in
Wing Area	170 sq ft
Length Overall	46 ft 4½ in
Height Overall	12 ft 10½ in
Tailplane Span	14 ft 2 in
Tailplane Area	59 sq ft
Max takeoff and landing weight	12,050 lb
Empty weight	7,663 lb
Max level speed	above Mach 1.23
Max cruising speed at 36,000 ft	above Mach 0.95
External Stores	Centerline Fuselage (LIF)
Maximum Load Factor	7.33 g's at 50% Fuel

STRUCTURAL DESCRIPTION

Wing

Fig. 2 shows a skeleton view of the T-38. The cantilever wing (Fig. 3) is a multi-spar structure manufactured as a one-piece assembly. The wing section is a NACA 65A004.8 (modified), with a 4.8 percent thickness-to-chord ratio and is all aluminum, except for the steel rib supporting the landing gear, and a few magnesium intercostals. The leading edge and wing tip are removable honeycomb assemblies.

The main structural elements of the wing are its one-piece upper and lower skins, spars, ribs, and full depth honeycomb panels in the wing's aft portion. The wing is attached to the fuselage by four primary trunnions, and a secondary support for vertical shear at the intersection of the 66 percent spar and wing station (W.S.) 25.1. Spars outboard of the root rib are identified by their location in percent of chord; spars inboard of the root rib are identified by their location with respect to fuselage station. The upper and lower skins extend across the span bounded by wing station 125.

All wing spars except the 15 and 66.6 percent spars are discontinuous at each rib. The 15 and 66.6 percent spars are I-sections, while all other spars are channel sections. The lands in the wing skin provide a common plane for the spars and ribs and load paths for the bending loads in the spars where they are discontinuous at each rib. The lands in the wing skins are also flared at the spar and rib intersections to reduce stress concentrations. The spars and ribs are manufactured from 7000-series aluminum extrusions or forgings.

The main skins of the wings were initially machined from 7075-T651 aluminum plate. The most current design, called the -29 wing (Part Number 2-23000-29), has a thicker lower skin machined from a single

7075-T7351 plate. This -29 wing is a part of the evolution of the structure to increase the wing's fatigue life and corrosion resistance and will be discussed later in this paper.

Fuselage

The fuselage is a predominately aluminum semi-monocoque structure, with steel, magnesium and titanium used in certain areas. The bending loads in the fuselage are carried by upper and lower longerons, connected by multiple frames and chemical-milled skins. As shown in Fig. 4, the major sections of the fuselage are:

Nose section (F.S. 52.50 to F.S. 144): accommodates equipment and houses the nose wheel landing gear.

Forward fuselage (F.S. 144 to F.S. 284): contains the pressurized cockpit region and the air conditioning unit. The pressurized cockpit region extends from the F.S. 144 bulkhead to the F.S. 264 canted bulkhead.

Center fuselage (F.S. 284 to F.S. 505): The portion from F.S. 284 to F.S. 445 contains the fuel compartments flanked by the engine air intake ducts. The wing primary structural box and the speed brake package are located below the fuel floor and intake ducts. The wing is attached to the fuselage at six points. The primary attachments are at F.S. 328 and F.S. 362, with secondary attachments at F.S. 388. The main landing gear wheels are stowed between F.S. 362 and F.S. 388 immediately behind the wing box. The section from F.S. 445 to F.S. 505 (cant) contains the engines and related accessories. The main engine trunnion supports are at F.S. 508, with a third support at F.S. 478.

Tailcone (F.S. 505 cant and aft): serves as an engine fairing and contains the horizontal tail truss and operating mechanism. The truss and tail cone are attached to the center fuselage at F.S. 505.

Empennage

The horizontal stabilizer's structure is a single, all-moveable surface composed of an aluminum honeycomb core, covered with 7075-T6 chemical milled skins, and attached to a single center spar. The spar transitions to a steel torque tube that is driven by two actuators located in the aft fuselage. The vertical stabilizer is a single spar, multi-rib type structure with integrally stiffened machined skins. The main spar is swept back 12.4 degrees and extends below the exposed surface of the fin and into the fuselage. Fig. 5 shows the horizontal and vertical stabilizers.

DESIGN CRITERIA AND EARLY FATIGUE LIFE EVALUATION

The T-38 structural design criteria were prepared in accordance with MIL-S-5700 [Ref. 1], and as such it was designed under a safe-life fatigue criteria. The service life was initially estimated to be 15,000 flight hours and 37,500 landings [Ref. 2]. Refs. 3 and 4 are the Northrop Aircraft documents related to the structural design and flight criteria, and the initial fatigue certification program is contained in Ref. 5. As shown in Fig. 1, the basic design and analysis were performed during the three and one-half years from December 1956 to June 1960, and a full-scale static test of the complete airframe was completed in January 1960 [Ref. 6]. The results from this static test were used to validate the later NASTRAN finite element models of the wing and fuselage.

The T-38 was initially designed for use by the USAF Air Training Command (ATC) as a student pilot supersonic trainer and instructor pilot proficiency aircraft. Frequency of occurrence data for aircraft usage was projected in 1958 before the first flight [Ref. 7]. This data, supplemented by flight test modified loads recorded during the T-38 flights load program, was used to develop a fatigue spectrum for analysis and

test [Ref. 8]. The spectrum was developed in 100, 200, and 400 flight hour blocks, each containing 55 discrete randomly sequenced loading conditions. This spectrum was applied to full-scale fatigue testing of the wing, control surfaces, and main and nose landing gears [Ref. 9]. Results from the full-scale tests, as well as from small specimens representing critical locations on the wing and fuselage are contained in Ref. 10. A total of 30,000 flight hours of appropriate spectrum loading were applied to the test articles in 100, 200 and 400 hour blocks.

In the early to mid 1960s, a usage survey was initiated to collect VGH (Airspeed [V], normal (Nz) and lateral (Ny) load factor [G] and altitude [H]) data on ATC aircraft. The resulting spectrum, based upon 15,825 hours of VGH recorded data, was compared to the spectrum applied to the full-scale test articles. The comparison given in Ref. 11, indicated that the test article had endured the equivalent of 60,000 hours of ATC usage without a scatter factor included. Using a scatter factor of four, the anticipated 15,000 flight hour service life mentioned earlier for the ATC usage was obtained.

CHANGES IN USAGE

As mentioned in the previous section, the fatigue safe-life of the T-38 was originally estimated to be 15,000 flight hours based upon the ATC usage. However, the T-38 began to be employed in more severe maneuver environments than the ATC, and these missions included: Lead-in-Fighter (LIF), Dissimilar Air Combat Training (DACT) and the Thunderbird Demonstration Team. VGH data were collected at various ATC bases and LIF aircraft at Holloman AFB. Table 2 summarizes the various USAF usages and their major flight characteristics. The usage designated as IFF (Introduction to Fighter Fundamentals) is essentially the old LIF usage and is now being flown at Randolph and Columbus Air Force Bases instead of Holloman AFB.

Table 2. Summary of USAF T-38 Usages

Usage	Purpose
Air Training Command (ATC) • Undergraduate Pilot Training (UPT) • Speciality Undergraduate Pilot Training (SUPT) • Instructor Pilot Training (IPT) • EURO-NATO Joint Jet Pilot Training (ENJJPT)	Develop aircraft flying skills (Formation, Aerobatics, Navigation).
Lead-in Fighter (LIF) Introduction to Fighter Fundamentals (IFF)	Develop air combat and ground attack fighter skills.
Dissimilar Air Combat Training (DACT) (No longer flown)	Develop air combat skills against dissimilar aggressor aircraft.
Air Force Systems Command (AFSC)	• Maintain flying proficiency. • Test Pilot School at Edwards AFB • Flight test chase aircraft.

Starting in the mid 1970s, the USAF started to collect usage information to assess the impact of expanded mission roles on T-38 structural life. This was done with MXU-553 or VGH recorders installed on selected aircraft. Measured flight parameters typically included: airspeed, load factor, altitude, surface deflections, aircraft rigid-body rates and strain gages. The Nz spectra for the ATC, LIF, DACT and Thunderbird usages are shown in Fig. 6, which clearly shows the increased severity of these usages based on Nz spectra. These spectra were used for the original damage tolerance assessment completed in 1979.

It is no surprise that these more severe usages substantially reduced the fatigue life of the lower wing skin and fuselage, which resulted in a series of fatigue life improvements that were incorporated on subsequent wing replacements and fuselage modifications. These will be discussed later.

Over the years the USAF has initiated a number of flight data recorder programs to track the usage changes and the resulting effect on structural integrity. These programs are summarized in Table 3. For example, Fig. 7 shows how the Nz spectra for the ATC usage has changed over the years.

NASTRAN MODELS AND UPDATES

The first NASTRAN idealization of the T-38 was completed in 1977 [Ref. 14] with the development of three separate models: the forward fuselage (F.S. 144 - F.S. 284); the center fuselage (F.S. 284 - F.S. 388); and the wing. Validation [Ref. 15] of the NASTRAN models was completed the following year using experimental results from the full-scale static test of the complete airframe conducted in 1960 [Ref. 6].

The models included both coarse grid representations of the wing and fuselage, as well as local fine mesh models of the wing root radius at W.S. 26 and a typical canopy hook cutout on the longeron. These models were used to obtain far-field and local stresses for the first damage tolerance analysis completed in 1979 [Ref. 16].

For the damage tolerance update of the wing [Ref. 17] completed in 1984, several modifications were made to the initial NASTRAN finite element model (FEM). These included: (1) updating the -27 wing coarse and fine grid model to the -29 wing configuration and (2) coupling the wing and fuselage models together instead of having the wing pedestal mounted as was done for the original wing analysis.

The San Antonio Air Logistics Center (SA-ALC) has two ongoing programs (see Table 4) for the development of NASTRAN models for the forward fuselage and avionics bay door. A new MSC/NASTRAN finite element model of the USAF T-38 forward fuselage, incorporating the recent structural modifications of the upper cockpit longeron, will be developed. This new FEM is to employ the latest MSC/NASTRAN modeling techniques and will be validated using recently obtained USAF flight test data (Table 4). The new forward fuselage model, from F.S. 136 to F.S. 325, will double the number of degrees-of-freedom by explicitly representing structurally significant parts that were previously idealized as lumped elements. Detailed, explicit models of T-38 fatigue critical locations (FCLs) will be imbedded in the model using superelements.

Although not considered in the original and updated damage tolerance analyses, the upper cockpit longeron at the avionics bay door has become an area of interest because of fatigue problems in similar structure on F-5E/F aircraft. Fatigue critical locations were identified in the F-5E/F fleet as a result of a F-5F crash and subsequent fleet inspections and damage tolerance analyses. SA-ALC has initiated a program to perform a damage tolerance analysis and coupon spectrum testing of one fatigue critical location on the T-38 cockpit longeron in the area of the avionics bay door (see Table 7). To analyze this location, a MSC/NASTRAN superelement model of the USAF T-38 forward fuselage in the area of the avionics bay door will be developed. This new superelement will be used as part of the forward fuselage coarse grid finite element model discussed above.

Table 3. Summary of T-38 Usage Surveys

Usage/Base	Period	Hours Collected	Source	Application
ATC/Various	Early to Mid 1960s	15,825	VGH/USAF	Fatigue Certification
ATC/Various	Early to Mid 1960s	4,265 (part of above hours)	VGH/USAF	Original DTA (NOR 77-18)
LIF/Holloman	1975-1976	1,265	VGH/USAF	
DACT	Mid 1970s	95	MXU-553/USAF	
Thunderbird Solo	1974-1975	78	MXU-553/USAF	
ATC/Laughlin	1980	503	Contractor VGH	1984 Update DTA (NOR 83-107) (NOR 84-50)
AFSC/Edwards	1980-1981	503	Contractor VGH	
LIF/Holloman	1978-1980	410	MXU-553/USAF	
AFSC/Edwards, Eglin	1987-1991	951	MXU-553/USAF	Spectra Comparison
ATC/Sheppard	1986-1987	174	MXU-553/USAF	Spectra Comparison
EURO-NATO/ Sheppard	1988-1991	944	MXU-553/USAF	Spectra Comparison
LIF/Holloman	1978-1979	460	MXU-553/USAF	Spectra Comparison
LIF/Holloman	1982-1987	1,638	MXU-553/USAF	Spectra Comparison
LIF/Holloman	1988-1992	570	MXU-553/USAF	1994 Update DTA (SwRI 07-5041)
ATC/Laughlin, Reese, Williams	1988-1990	2,228	Contractor VGH	
SAC/Beale	1988-1991	775	MXU-553/USAF	Spectra Comparison
ATC-SUPT/Reese	1993-1994	504	Contractor VGH	Spectra Comparison
IFF/Randolph and Columbus	1995-1996 (In Progress)	500	Contractor VGH	----

Table 4. Summary of T-38 NASTRAN Analyses

Component	Validated	Reference
Wing, Forward and Center Fuselage	With static test article, see NOR 77-14	NOR 77-13
Update of -29 Wing	None	NOR 83-107
Update of Forward Fuselage FEM Model (F.S. 136- F.S. 325) (In Progress)	With flight test data, see "T-38 Strain Flight Test Plan," SA-ALC/2873TS Flight Test Directive 90-02, May 1991.	SwRI 07-6611
Avionics Bay Door FEM Model (F.S. 264 to F.S. 284) (In Progress)	See above.	SwRI 07-6612

DAMAGE TOLERANCE ANALYSES

As previously mentioned, the T-38 fatigue life was initially established under the safe-life approach. In 1972 the USAF implemented its damage tolerance requirements under MIL-A-83444 [Ref. 18] for new aircraft designs and began retroactively applying damage tolerance to its aircraft already in service. In the mid-1970s fatigue cracking began to be discovered in the lower skins of the -23 and earlier wings. To evaluate this problem, the SA-ALC conducted several destructive teardown inspections of wings removed from service and a laboratory fatigue test wing [Refs. 19-21]. The locations, sizes and types of cracks found in these teardown inspections greatly aided the identification of fatigue critical locations (FCL) and initial flaw sizes for the damage tolerance analyses.

The initial damage tolerance analysis (DTA) was started in 1976 and completed in 1979 [Ref. 16]. That report defined the inspection procedures and inspection intervals required to maintain and to protect structural safety of flight until the economic life limit is attained. The economic life limit was defined as the time to grow an equivalent initial flaw to an assumed detectable flaw size of 0.100 inches. This equivalent initial flaw size (0.001 inch), assumed as a corner crack at the most critical fastener hole in the wing lower skin, was determined from crack growth regression analyses of cracks found in the destructive teardown inspections of ATC wings [Ref. 20]. The analysis indicated a wing economic life of approximately 10,000 flight hours for the ATC usage [Ref. 16]. Damage tolerance analyses were performed for the Lead-in-Fighter (LIF), Air Training Command (ATC), Dissimilar Air Combat Training (DACT) and Thunderbird Solo usages.

The stress spectra used in the analyses and coupon spectrum crack growth testing were developed from Ref. 22 and are based on a random cycle-by-cycle stress sequencing history. Crack growth spectrum testing was also performed [Ref. 23] on preflawed dog-bone coupons representing selected critical locations. Test results were compared with fracture mechanics crack growth analyses to define retardation models and parameters. The original T-38 damage tolerance analysis has been updated a number of times to account for changes in usage, structural modifications and the identification of new fatigue critical locations. These are shown in Table 5.

Table 5. Summary of T-38 Damage Tolerance Analyses

Type	Date/Ref. No.	Component	Spectrum/Ref. No.
Original DTA	1979/NOR 77-18	Wing, Fuselage, Empennage	ATC, LIF, DACT, Thunderbird NOR 77-12
DTA Update	1984/NOR 83-107	-29 Wing Vertical Tail	ATC/Laughlin LIF/Holloman AFSC/Edwards
DTA Update	1984/NOR 84-50	Fuselage and Empennage	NOR 81-142 NOR 83-107 NOR 84-50
DTA Update	1994/SwRI 07-5041	Wing, Fuselage, Empennage	ATC/Laughlin, Reese, Williams LIF/Holloman SwRI 06-1951

One fatigue critical area of greatest concern was the wing lower skin radius at the wing root. This is designated as FCL A-4 in Fig. 8 which also shows other current FCLs and inspection zones on the lower skin. Originally this radius was 0.50 inches for the -19 thru -25 wing designs (see Table 9) but was later increased to 3.0 inches to reduce the stress concentration. Table 6 shows the very short initial and recurring inspections intervals, in flight hours, at FCL A-4 for the early wing designs as determined by the damage tolerance analysis. This and similar results at other FCLs on the lower skin, combined with service experience, prompted the USAF to make a series of fatigue life enhancements that resulted in the current -29 wing. These modifications are discussed later in this paper.

Table 6. Summary of Initial/Recurring Inspection Intervals at W.S. 26.6 Root Radius

Wing Type	ATC	LIF	DACT	Ref.
-23 (0.5 inch radius)	1800/1800	110/110	90/90	NOR 77-19
-27 (3.0 inch radius)	7750/7750	690/690	800/800	NOR 77-19
-29 (3.0 inch radius)	4235/4235 7140/7140 (AFSC)	1685/1685	----	NOR 83-107
-29 (3.0 inch radius)	3275/3275	638/638	----	SwRI 07-5041

The damage tolerance analysis completed in 1979 [Ref. 9] gave unanticipated results with respect to the dorsal longeron. The initial and recurring inspection intervals shown in Table 7 are not particularly short, although the results again show the severity of the LIF and DACT usages. The main problem in applying these results to the aluminum dorsal longeron is that the leg of the longeron next to the fuselage skin, shown in Fig. 9a, is essentially an uninspectable structure. This prompted the USAF to modify the dorsal longeron by removing the vertical leg of the aluminum longeron and replacing it with a steel reinforcement (Fig. 9b) as part of the Pacer Classic Program. The vertical leg of the steel longeron is inspectable.

The damage tolerance analysis also identified several fatigue critical locations on the upper cockpit longeron. Location of concern included the cutouts for the canopy hooks, as illustrated in Fig. 10. Damage tolerance results for the canopy hookslot at F.S. 267 are shown in Table 7. There were also

occurrences of stress corrosion cracking in the 7075-T6 aluminum extrusion material used for original production longerons. The USAF has initiated a cockpit modernization program that replaces the upper longerons with an 7075-T7351 extrusion for improved resistance to stress corrosion and geometry changes in the canopy hookslots and at other locations to increase the fatigue life. The dorsal and cockpit longeron modifications are part of the Pacer Classic I and II Programs.

Initial and recurring inspection results shown in Table 7 for the latest damage tolerance analysis [Ref. 24] do not include retardation effects. Coupon spectrum tests are in progress to evaluate retardation, and the damage tolerance analyses will be updated to reflect the coupon tests results.

Table 7. Summary of Initial/Recurring Inspection Intervals at FCLs on Cockpit and Dorsal Longeron

Location	ATC	LIF	DACT	Ref./Date
Aluminum Dorsal Longeron at F.S. 352	8800/6450	600/420	850/620	NOR 77-19 1979
Steel Mod. Dorsal Longeron at F.S. 352	6490/6490 9020/9020 (AFSC)	1710/1710	----	NOR 84-50 1984
Steel Mod. Dorsal Longeron at F.S. 352	3887/3887 (Unretarded)	902/902 (Unretarded)	----	SwRI 07-5041 1994
Canopy Hookslot on Upper Cockpit Longeron at F.S. 267	6100/6100	2300/2300	1900/1900	NOR 77-19 1979
Canopy Hookslot on Upper Cockpit Longeron at F.S. 267	2920/2920 3825/3825 (AFSC)	----	----	NOR 84-50 1984
Canopy Hookslot on Upper Cockpit Longeron at F.S. 267	7587/7587 (Unretarded) (New Longeron)	5650/5650 (Unretarded) (New Longeron)	----	SwRI 07-5041 1994
Avionics Bay Access Door	In progress (AETC)	In progress (IFF)	----	SwRI 07-6612

DEVELOPMENT OF SUPPLEMENTAL ANALYSIS TOOLS

As indicated in Table 3, a considerable amount of aircraft usage data has been collected for the T-38 fleet over the past twenty years. The source of this data has been both USAF MXU-553 and contractor-supplied flight data recorders. This data is not only voluminous, but it must be checked for reasonableness and completeness before it can be used for spectra comparisons or damage tolerance analyses. Over the last ten years the SA-ALC has invested considerable effort to develop computer algorithms and programs to rapidly and accurately process flight usage data collected for the T-38 fleet. The programs described below are able to take advantage of dramatic advances in microprocessor and personal computer technology for the processing and analysis of that data.

Revision of T-38 MXU Fatigue Damage (FATDAM) Computer Program

The FATDAM (Fatigue Damage) program [Ref. 25] was originally written and modified by the Northrop Corporation. The FATDAM program read tape data collected from onboard MXU-553 recorders and produced both maneuver spectra tables and cycle-by-cycle stress data. The Northrop Individual Aircraft Tracking Program [Ref. 26] used the stress data to perform crack growth analyses at specific critical locations on the T-38. A revision to FATDAM was necessary to account for updated damage tolerance analyses and to add options for improved tabular spectra output.

The code revisions [Ref. 27] exploited the good features and structure of the existing code while simplifying and modularizing where possible. New analysis data and techniques from the updated 1984 damage tolerance analysis [Refs. 17 and 28] were incorporated and the number of fatigue critical locations analyzed increased from six to nineteen. Several options were also added to the program included skipping of invalid flight data during magnetic tape input and user selected spectral printout features. New users' manuals were written for both programs.

The program was used to analyze MXU-553 flight data for the T-38 [Ref. 29]. This served the purposes of program checkout and elimination of backlog flight data for this aircraft. Approximately 2500 valid hours from a span of nine years were analyzed using both programs. The results were graphically compared to previous analyses to assess any changes in usage for the T-38.

Aircraft Spectra and Operational Usage Profiles Development and Analysis

In the mid-1980s the SA-ALC initiated work to develop a series of software programs that would be used to analyze the MXU-553 time history data from T-38, F-5E/F, T-37, and OA-37 aircraft supported by SA-ALC. Several thousand hours of flight data was processed to effectively test the integrity of the programs and to provide updated results to SA-ALC on the usage of each fleet. Southwest Research Institute (SwRI) worked together with Alamo Technology, Inc. (ATI) to write the computer programs and process the Air Force's backlog of MXU-553 recorder data.

The software development consisted of three major modules: a data reduction program (REDUCT); an edit/pre-analysis program (EPRE); and a spectra operational usage profiles program (SOUP). Summaries of these programs were presented at the 1987 USAF ASIP Conference [Refs. 30 and 31].

The REDUCT program is used for the reduction of MXU-553 time history data. This program retains only significant data records, reducing reels of magnetic tape data to a fraction of the original size. The output of REDUCT is used in EPRE for further analysis or data correction. EPRE program allows the user to change any data item in the flight as well as mark the major mission segments of the flight using a graphics screen and a cross-hair cursor. Fig. 11 illustrates the EPRE graphical output for a flight's time history. The last program, SOUP, provides summary information from the data after it has been reduced and edited. A database is generated from which the user may display a variety of tables and plots. These programs have provided useful and flexible tools for the continuing task of assessing fleet usage and can accommodate microprocessor-based recorder system data proposed for future Air Force aircraft.

T-38 Stress Sequence Development Program

The primary objective of this program [Ref. 32] was to develop an in-house engineering analysis capability for cycle-by-cycle stress sequence development for engineers at the SA-ALC Damage Tolerance Analysis Laboratory. As a secondary objective, flight data collected on USAF MXU-553 recording systems for three different usages were evaluated for data validity and mission and phase marking. The flight data were

then processed through the newly developed software to produce stress sequences for each usage for all known fatigue critical locations for the T-38.

Methodology exists to calculate internal stresses at selected locations based on the normal load factor, gross weight, altitude, and Mach for each maneuver of the T-38. This methodology was established by Northrop and used the concept of representative flight conditions for which distributed net loads have been defined. From extensive testing and analysis, Northrop developed relationships between these external net loads and internal stresses. In the past, sequencing these calculated stresses for use with standard crack growth programs has been performed using computer programs that were limited in scope and difficult to use.

To provide a more flexible and user-friendly package, a graphical user interface computer program was written in Visual Basic for the 486-class personal computer running in the Windows™ operating environment. This program solicits input from the user through the use of visual displays and mouse movements and provides several options for stress sequence development. Example program screens are shown in Fig. 12. Because of the Windows compatibility, the program can operate in a multi-tasking environment. The program was written to allow for easy updating when additional FCLs are identified in the future.

This computer program brings together a great deal of published data for the T-38 into a single source that is versatile, fast, and visually striking. The program also incorporates accepted methods for calculating stresses at specific locations and developing sequences for use in analytical crack growth analyses and testing.

T-38 Force Structural Maintenance Plan

The weapon system Aircraft Structural Integrity Program (ASIP) manager is required by AFR 80-13 to develop, implement and maintain a Force Structural Maintenance Plan (FSMP). The FSMP is an engineering document containing the structural integrity related data required to ensure the planned operational life of the fleet. The FSMP will be used by the System Program Manger (SPM) to identify structural inspection, modification, and component replacement schedules, to plan force structure, and to make budget estimates. Periodic updates are required to compensate for deviations from the plan.

The T-38 FSMP database has recently been developed by Southwest Research Institute and delivered to SA-ALC [Ref. 33]. This database contains the following individual aircraft information available for making force planning decisions:

- aircraft and wing serial numbers
- aircraft base and command
- aircraft and wing total flight hours
- aircraft and wing flight hours by base and usage
- major component replacements and airframe hours
- major component repairs/modifications and airframe hours
- accomplished structural inspection hours and results
- projected structural inspection hours
- projected component modification or replacement hours

The User's Guide for the FSMP database [Ref. 34] describes the utilization of the database software for information retrieval, graphical presentation of fleet data and report development. Information on modifications and additions to the database are also described in the User's Guide. Much of the FSMP

database information is common with and accessed by the Individual Aircraft Tracking Program (IATP) database discussed below. Figs. 13-14 illustrate the graphical output from the FSMP database and show the distribution of flight hours for the wing and the number of aircraft assigned to the various commands.

T-38 Individual Aircraft Tracking Program (IATP)

The previous T-38 IATP was developed in 1981 by Northrop [Ref. 26] and utilized mechanical strain recorder (MSR) data and mission mix information to predict crack growth, safety limits, economic lives and inspection intervals at known FCLs. Although this original T-38 IATP employed state-of-the-art technology at the time it was originally developed, it is now outdated and inefficient considering the database management software and computer hardware currently available. In addition, the cancellation of the T-38 MSR program has generated a requirement for an IATP based solely on mission mix data. Furthermore, the T-38 usages have changed since 1981 and the active fleet now is fitted with the -29 wing, whereas the 1981 IATP performed crack growth calculations for the -23 and -27 wings. For these reasons, SA-ALC initiated a program [Ref. 35] to develop an improved, PC-based, T-38 IATP. This IATP will be capable of interfacing with the new T-38 FSMP software mentioned above and have the ability to automatically input stress factor reports (mission mix data) from the USAF REMIS (Reliability and Maintainability Information System) database as shown in Table 8.

Table 8. Summary of T-38 Individual Aircraft Tracking Program (IATP)

Features	• Interfaces with New T-38 FSMP Database • Automatically Inputs Mission Mix Data from the USAF REMIS Database
Enhancements from Previous T-38 IATP	• Contains Revised Usages (AFSC, TAC-LIF, ATC-UPT, ATC-Euro, SAC) • Contains Updated FCLs and DTAs • Includes -29 Wing
Capabilities	• Computes Current Crack Length for Individual Aircraft Using Mission Mix Data • Compares Crack Growth Computed from Mission Mix Data with that from the DTA • Performs Crack Growth Predictions for Projected Future Mission Mixes • Track Inspections at FCLs • Accounts for Wing Swapping • Provides Data for Risk Analysis

STRUCTURAL MODIFICATION PROGRAMS

Wing

Over the past 20 years there have been three major wing changes to the T-38 to increase the fatigue life and enhance its resistance to stress corrosion cracking. The major wing designs (-23, -27 and -29) and their characteristics are shown in the table below. In wing designs prior to the -27, 7075-T651 aluminum

plate was used for the lower skin, but the lower skin material was changed to 7075-T7351 for the -27 and later designs to increase the resistance to stress corrosion cracking.

As Table 9 [Ref. 9] shows, a number of other changes were made during the evolution of the wing to increase its fatigue life. These included: a thicker lower skin to reduce the overall stress levels, an increased radius to reduce the stress concentration factor at the critical wing root, and cold working of fastener holes to increase their life. For the -25, -26 and -27 wings, the 353 coldworked holes included those lower wing skin holes to W.S. 64.8, between the 39 and 44 percent spars, while coldworking of holes at the 27 and 33 percent spars were added for the -29 wing. For the -27 and -29 wing, substructure changes were made to the 39 and 44 percent spars and root rib, and additional changes were made to the forward and outboard spars in the -29 wing.

Table 9. Evolution of the Wing Structure (Part Number 2-23000-29)

	Original Production		Wing Replacements				
	-19 & PRIOR	-23	-23	-25	-26	-27	-29
Material - 7075	T651	T651	T651	T651	T651	T7351	T7351
Thickness at Root/44% Spar	0.420	0.420	0.420	0.420	0.420	0.520	0.600
Critical Root Radius	0.5	0.5	0.5	0.5	3.0	3.0	3.0
Number of Cold Worked Holes	0	0	0	353	353	353	673
Number of Wings	491	696	93	13	22	80	Approx. 640
When Delivered	To 11/64	11/65-1/72	To 5/76	5/76-9/76	9/76-4/77	5/77-5/79	5/79 On

Dorsal and Cockpit Longerons

In 1985 the USAF started modernization programs to assure the continued airworthiness of the T-38 into the twenty-first century. In the first program, called Pacer Classic I, the original design aluminum dorsal longerons (Fig. 9a) were modified with steel replacements (Fig. 9b) to solve the problem of inspectability. In addition, magnesium flight control components on the USAF T-38s were replaced with aluminum.

In 1991 Pacer Classic II was started and will replace both upper cockpit longerons and the 325 bulkhead to improve their resistance to stress corrosion cracking and fatigue. This program, currently ongoing at Kelly and Randolph Air Force Bases. also includes a complete rewire of the forward and aft cockpits. Fig. 15 shows a typical modification line.

CURRENT ASIP INITIATIVES

-29 Wing Durability Test

In 1993 the San Antonio Air Logistics Center initiated a fatigue durability test program for the -29 wing. The purpose of the program was to assess the wing's long-term fatigue behavior in meeting anticipated future fleet usage requirements. A new -29 wing was mounted in a test frame at Southwest Research Institute using the standard fuselage attachment points. Sixteen load jacks per side, controlled by a single computer utilizing servo-valves in a closed-loop, feedback system, were connected to a whiffletree system

that provide the 341 unique load distributions of shear, moment, and torque to the wing. Transducer data (loads, deflections, strain gages) were recorded at each load event in the test sequence. The test represented the EURO-NATO usage (1988-1991), and each 1,000 flight-hour test block represented a spectrum of 48,766 discrete load events to the hydraulic jack system. Reports related to the test setup and execution are given in Refs. 36 and 37. After the initial inspection times were reached, the wing was subjected to extensive periodic nondestructive inspections every 500 simulated flight hours, that included ultrasonic rotoscan, eddy-current and dye penetrant examinations per USAF Technical Orders.

Fig. 16 highlights the test results, with the majority of the NDI indications at fastener holes outboard of W.S. 64.8 as shown in the figure. Few indications were found inboard of W.S. 64.8, where the holes in the lower wing skin were cold worked. For the approximately 60 NDI confirmed indications found during the test, the holes were reamed and oversized fasteners replaced. No indications were found at the root radius at W.S. 26.6. The test also evaluated a reinforcement strap on the 66 percent spar in the area spanning the aileron. At 14,000 flight hours a skin crack was found at the 15 percent left spar at about W.S. 64.8, and a reinforcement was installed before continuing the test. At 22,000 hours a crack found in the right D panel, shown as location A-20 in Fig. 16, was stop-drilled, and was later reinforced with a graphite epoxy patch. At 24,500 hours the skin at the 15 percent right spar at W.S. 64.8 and both 66 percent spar reinforcement straps were found to be cracked. These were replaced and the test continued to 26,500 flight hours. At this time it was decided to stop the test after an approximately 5-inch crack was found running beneath the reinforcement on the left wing's 15 percent spar. The wing will be subjected to a destructive teardown inspection consisting of extensive visual, NDI, microscopic and metallurgical examination of individual fastener holes and surfaces.

Validation of T-38 Horizontal Stabilizer Fatigue Critical Locations

The purpose of this program is to develop and validate new stress-to-load ratios for the USAF T-38 horizontal stabilizer at butt line (B.L.) 5.08. A new stress-to-load ratio is needed since recent flight data recorder programs have shown that stresses measured directly on the horizontal stabilizer are occurring at rates of two to five times those predicted by the methodology based solely on Nz occurrences. In addition to the new stress-to-load ratio at B.L. 5.08, the stress transfer functions for the taper pin holes and the F-5 B.L. 26 transition area will be validated by static test.

Analysis of T-38 Wing Substructure

Current damage tolerance methodology for the F-5A/B/E/F and T-38 differ in that the wing lower skin analyses are performed using spar-intact and spar-failed conditions for the F-5, but only spar-intact conditions for the T-38. Since the two aircraft have similar wing structure, it may be that the T- 38 fleet is flying at greater-than-analyzed risk. It is the purpose of this program to conduct a static test of the T-38 wing, using the -29 wing durability test article, under both spar-intact and spar-failed conditions, and compare the results with current methodologies.

FUTURE ASIP INITIATIVES

Loads/Environment Stress Survey (L/ESS)

As part of Air Education and Training Command's attempt to reduce the T-38's cost per flying hour, SA-ALC is considering ways to reduce the cost of maintaining the current flight loads data recorder, the MXU-553. One alternative is to eliminate the MXU-553 and measure flight data, when required, with a contractor-furnished recorder. Usage surveys would be done every three years or when changes in

training syllabus occur. Contractor-furnished recorders would also be used in lieu of the Standard Flight Data Recorder (SFDR) system, which has been planned for the T-38 fleet.

Coldworking of Lower Wing Skin Fastener Holes

The -29 wing durability test has provided an indication of where fatigue cracking is likely to occur in the future. Many of the fastener holes at or outboard of W.S. 64.8 experienced fatigue cracking during the test. SA-ALC will be implementing a coldworking program to enhance the fatigue life of these fastener holes, thus extending the life of the wing.

Avionics Upgrade

The Air Education and Training Command is considering an avionics upgrade for the T-38. This would permit pilots to be trained in a cockpit environment similar to today's mainstream fighters like the F-15 and F-16. For such a program to be economically attractive, it must be shown that the structure will last until the planned retirement of the T-38. Structural modifications must be planned if analysis shows that such modifications are needed to accommodate T-38's life requirements with new avionics.

SUMMARY

This paper has reviewed the development and implementation of the T-38 structural integrity program. Even though the T-38 was designed under a safe-life criteria and for a comparatively mild training usage, the Air Force's structural integrity initiatives over the past 34 years have been aimed at facilitating the aircraft's long-term usage in much more severe environments than originally intended. This paper has discussed those initiatives that include: implementation of damage tolerance program to protect safety of flight; periodic usage assessments to evaluate the effects of mission changes on structure; development of computer tools for more accurate and efficient structural analysis and evaluation of aircraft usage; and the implementation of structure modification and modernization programs to keep the fleet flying. These initiatives are not cheap to perform, nor can they be undertaken once and then forgotten. They must be constantly applied so that all efforts work together to provide an airframe for training Air Force pilots well into the future.

REFERENCES

(Note: NOR, NAI = Northrop Corporation; SwRI = Southwest Research Institute)

1. MIL-S-5700, "Military Specification Structural Criteria, Piloted Airplanes," December 1954.
2. Stuart, William G., *Northrop F-5 Case Study in Aircraft Design*, AIAA Professional Study Series, September 1978.
3. NAI-56-757, "Structural Design Criteria for the YT-38 and T-38A Supersonic Basic Trainer," September 1956.
4. NAI-57-40, "T-38A Basic Flight Criteria," November 1958.
5. NOR 59-165, "Proposed Fatigue Certification Program for the T-38," March 1959.
6. NOR 60-6, "Static Test of Complete Airframe for the T-38 Airframe," March 1960.
7. NOR 57-64, "T-38A Spectrum for Fatigue Life Studies, September 1958.
8. NOR 60-208, "T-38 Fatigue Spectrum Data for Analysis and Test," October 1960.
9. NOR 77-19, "Summary Report, T-38 Damage Tolerance Assessment Program NPN 3347," February 1979.

10. NOR 60-209, "T-38 Structural Fatigue Test Program," Revision B, August 1965.
11. NOR 60-210, "T-38 Airframe Fatigue Analysis and Service Life Estimate," December 1964.
12. NOR 81-142, "T-38 Lead-In-Fighter and Thunderbird Spectra Update," August 1981.
13. SwRI 06-1951, "Update of ATC Maneuver Spectra," July 1990.
14. NOR 77-13, "T-38 Damage Tolerance Assessment Program 'NASTRAN' Model Idealization Report, T-38 Forward, Center Fuselage and Wing Structure," September 1977.
15. NOR 77-14, T-38 Damage Tolerance Assessment Program "NASTRAN Model Validation Report Forward, Center Fuselage and Wing Structure," March 1978.
16. NOR 77-18, "NPN 3347, T-38 Damage Tolerance Assessment," January 1979.
17. NOR 83-107, "-29 Wing Damage Tolerance Assessment," June 1984.
18. MIL-A-83444, "Air Force Damage Tolerance Requirements," Department of the Air Force, 1974.
19. SwRI 03-4661, "Analytical Condition Inspection (ACI) on T-38 Wing Assembly P/N 2-23000-23," July 1977.
20. SwRI 03-4661, "Teardown Inspection of High Time Air Training Command T-38 Wings," March 1978.
21. NOR 74-325, "Inspection and Evaluation of the Lower Wing Skin from the T-38 Fatigue Test Specimen," Revision A, February 1975.
22. NOR 77-12, "T-38 Damage Tolerance Assessment Program External Loads and Spectra," Revision A, September 1977.
23. NOR 77-17, "T-38 Damage Tolerance Assessment Program NPN 3347 Crack Growth Testing Summary Report," November 1978.
24. SwRI 07-5041, "T-38 Durability and Damage Tolerance Analysis," Draft Final Report, June 1984.
25. NOR 74-52, "T-38 Fatigue Damage Computer Program User's Manual," June 1980.
26. NOR 81-159, "T-38 Force Management Computer Program," September 1981.
27. SwRI 06-8550, "T-38 Fatigue Damage Computer Program (FATDAM) -- User's Manual," April 1987.
28. NOR 84-50, "Update of T-38 Fuselage and Empennage Durability and Damage Tolerance Analysis NPN 6216R1," July 1984.
29. Alamo Technology Incorporated (ATI) 88-0934, "Analysis of T-38 MXU-553 Data," September 1988.
30. Schrader, K.H., "Automated Analysis of MXU-553 Flight Data," *Proceedings of the 1987 Aircraft/Engine Structural Program Conference*, AFWAL-TR-88-4128, pages 793-818.
31. Butts, D., "The Edit/Pre-Analysis Program," *Proceedings of the 1987 Aircraft/Engine Structural Program Conference*, AFWAL-TR-88-4128, pages 845-866.
32. SwRI 07-4426, "T-38 Stress Sequence Development Program -- User/Program Logic Manual," May 1993.
33. SwRI 07-4471, "T-38 Force Structural Maintenance Plan," July 1994.
34. SwRI 07-4471, "T-38 Force Structural Maintenance Plan Database User's Guide," June 1994.
35. SwRI 07-4972, "T-38 Individual Aircraft Tracking Program," December 1994.
36. SwRI 07-5781, "T-38 Full-Scale Wing Durability Test -- Test Procedures," August 1993.
37. SwRI 07-5781, "T-38 -29 Wing Full-Scale Wing Durability Test Loads and Loading Spectra," May 1994.

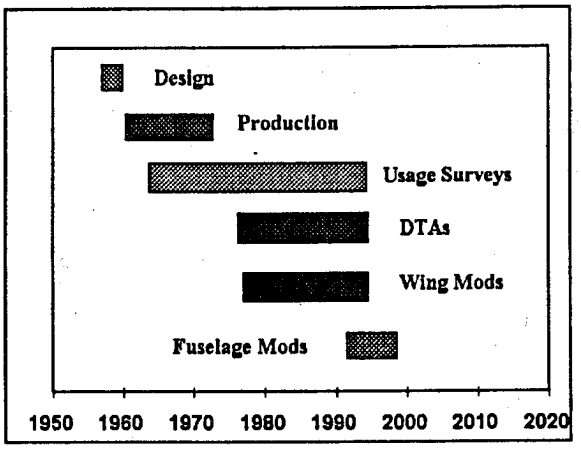


Figure 1. Structural Development, Evaluation and Modification Timeline

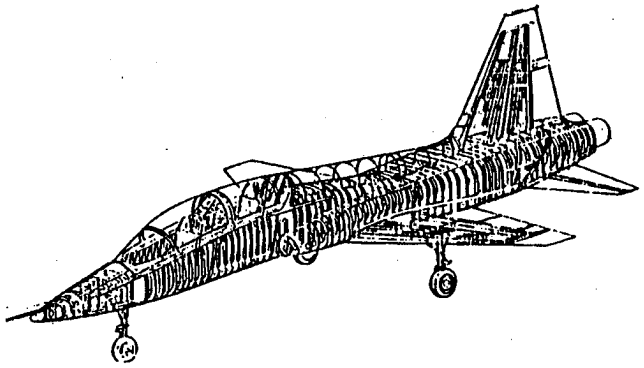


Figure 2. T-38 Structure

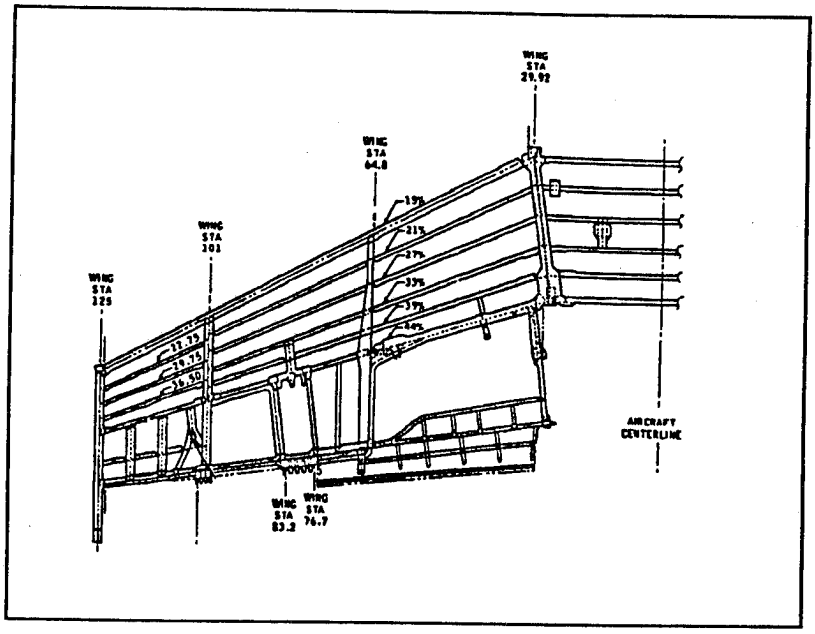


Figure 3. Wing Structure

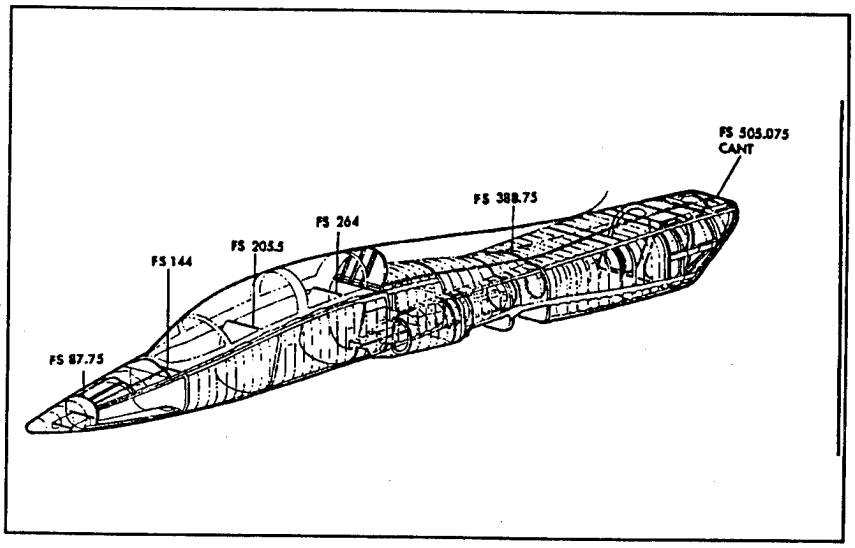


Figure 4. Fuselage Structure

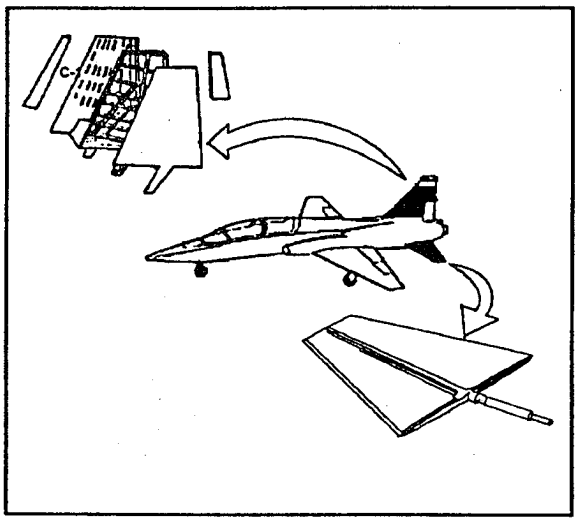


Figure 5. Horizontal Stabilizer and Vertical Fin Structure

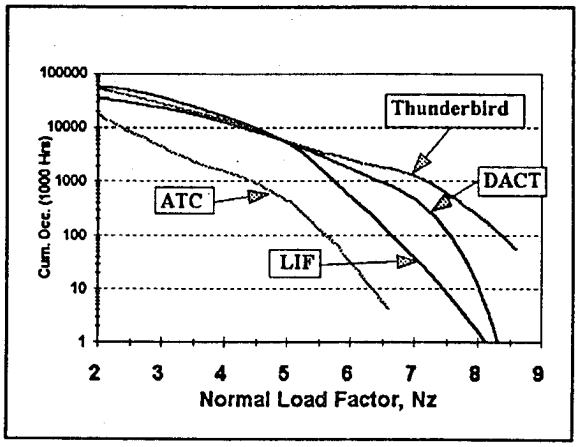


Figure 6. Nz Spectra Comparison for Original DTA Usages

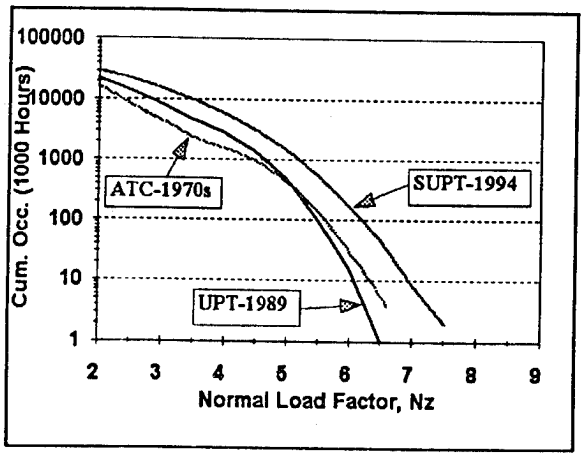


Figure 7. Nz Spectra Comparison for ATC, SUP and SUPT Usages

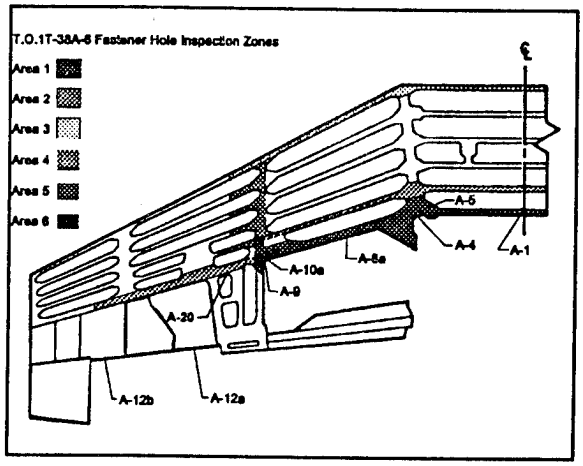


Figure 8. Wing Lower Skin Fatigue Critical Locations

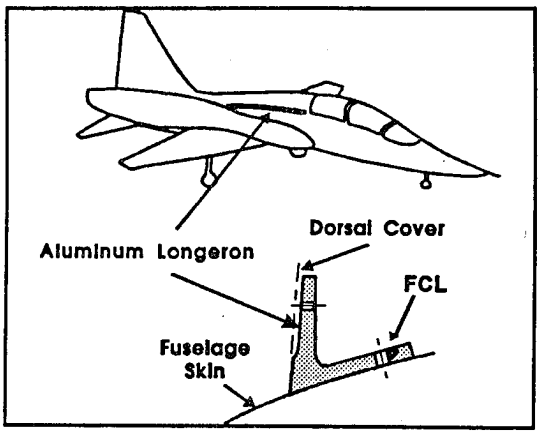


Figure 9a. Dorsal Longeron FCL
(Original Design)

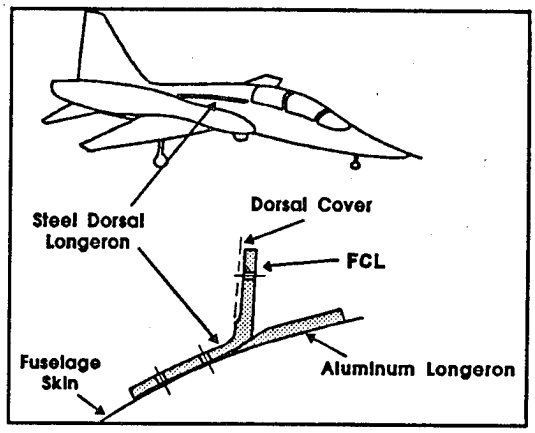


Figure 9b. Dorsal Longeron FCL
(Modified Design)

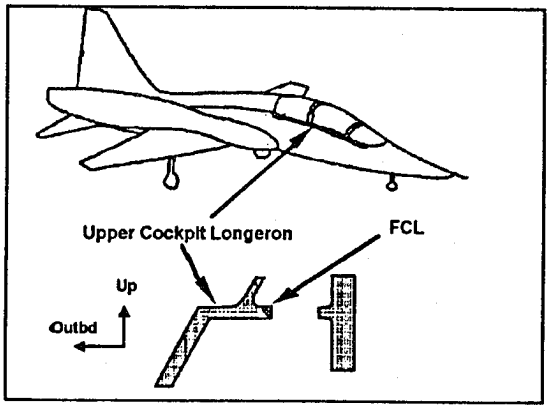


Figure 10. Cockpit Longeron FCL

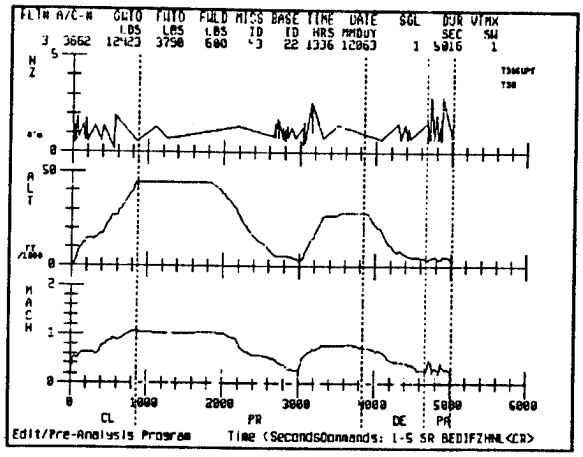


Figure 11. EPRE Graphical Output

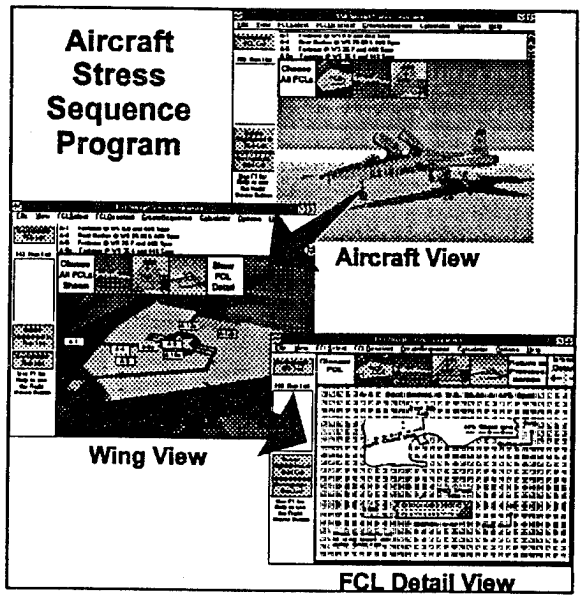


Figure 12. Aircraft Stress Sequence Program Screen

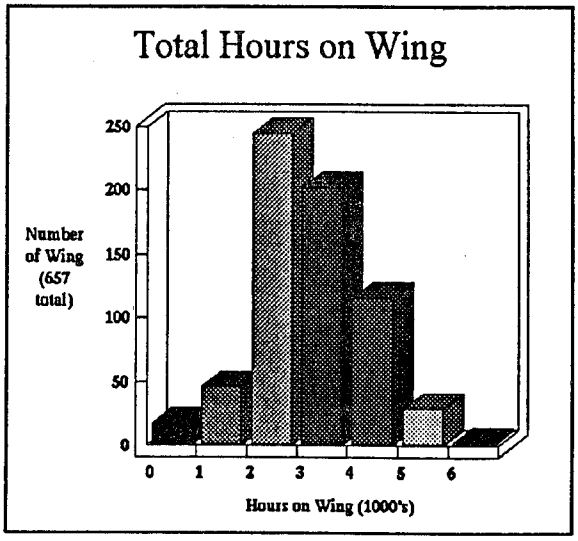


Figure 13. Distribution of Wing Usage by Flight Hours

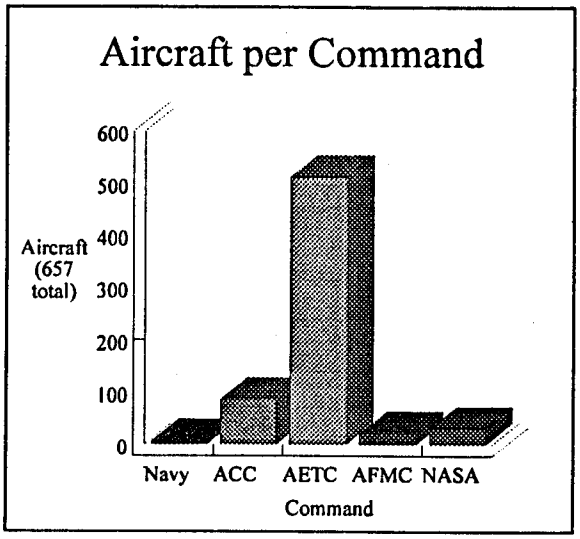


Figure 14. Distribution of Aircraft by Commands

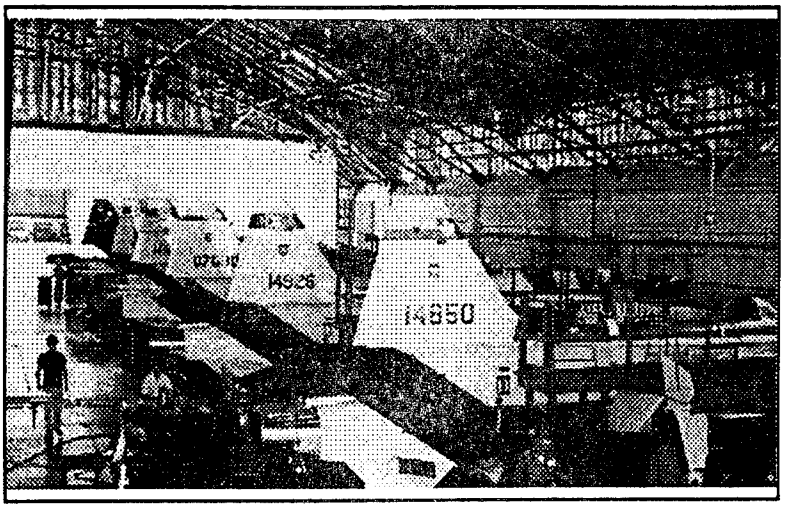


Figure 15. Pacer Classic Modification Line

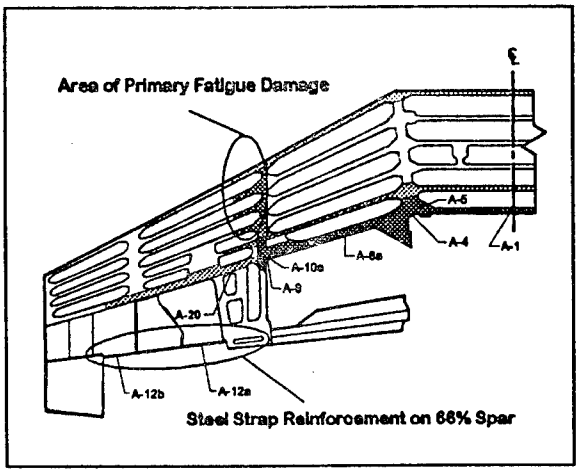


Figure 16. Wing Durability Test Damage

The
USCG / AANC
HU-25 Project

-- An Overview --

U.S. COAST GUARD
2117

Project Managers

- CDR Jim Moukawsher--USCG ARSC
- LCDR Joe Mihelic--USCG ARSC
- Mr. Pat Walter--AANC
- Mr. Craig Jones--AANC

ARSC--Aircraft Repair & Supply Ctr (919) 335-6240

AANC--Aging Aircraft NDI Validation Ctr (505) 844-5226

Purpose

- A cooperative project to focus advanced, state-of-the art NDI techniques on an HU-25.
- Enables the Coast Guard to better understand, monitor and manage the structural condition of HU-25's.
- Technology will be applied to all CG aircraft.

Project Phases

- Phase I -- *By June '95:* **Receive & prepare HU-25. Perform initial inspections, deliver initial report with recommendations that will payoff quickly.**
- Phase II -- *By February '96:* **Continue technique development. Interim reports.**
- Phase III -- *By September '96:* **Further testing. Final reports.**

Milestones / History

■ Initial Discussions	3 Feb 94
■ Approval to Use HU-25	24 Mar 94
■ Draft Agreement	7 Jun 94
■ Delivery of HU-25	14 Jun 94
■ Agreement Formalized	15 Sep 94
■ Initial Results / Reports	Jun 95

Goal -- Reduce PDM Costs

- Now: Visual Predominates.
- Corrosion and fatigue cracks occur in locations that are difficult and expensive to access.
- Present NDI techniques (e.g. x-rays) might be improved upon.

Goal--Improve PDM Management

- Ability to scan aircraft for corrosion, fatigue and disbonds will permit adustments to PDM induction.
- Aging assessments will be done in field or at depot. Improved databases will document aging processes.
- PDM's will be deferred on slowly aging aircraft, postponing $1.1 million dollar costs per aircraft.

Goal -- Modify SSIP / Avoid MCI

- HU-25 service life is not certain.
- Current plan for SSIP requires new load & fatigue analyses, maintenance & service history reviews to establish new Major Corrosion & Fatigue Inspections.
- Using advanced NDI will provide assurance of structural integrity of critical elements. MCI probably unnecessary for all aircraft.

Goal -- Transfer Technologies

- All CG aircraft, particularly the HC-130H, have aging issues similar to the HU-25.
- HU-25 program and techniques will be models for use on other aircraft.
- Participation at AANC makes an HU-25 (a modified business jet) available as a resource for the National Aging Aircraft Research Program.

Approach

- Select problem areas where significant cost & time savings are promising.
- Test candidate techniques at AANC. Will be performed by Sandia personnel and those from other agencies (CASR, NASA, Universities, Private Industry).
- Conduct on-site tests at ARSC or CG Air Stations.
- Write reports and technical packages.

Initial Results -- Windshield Posts

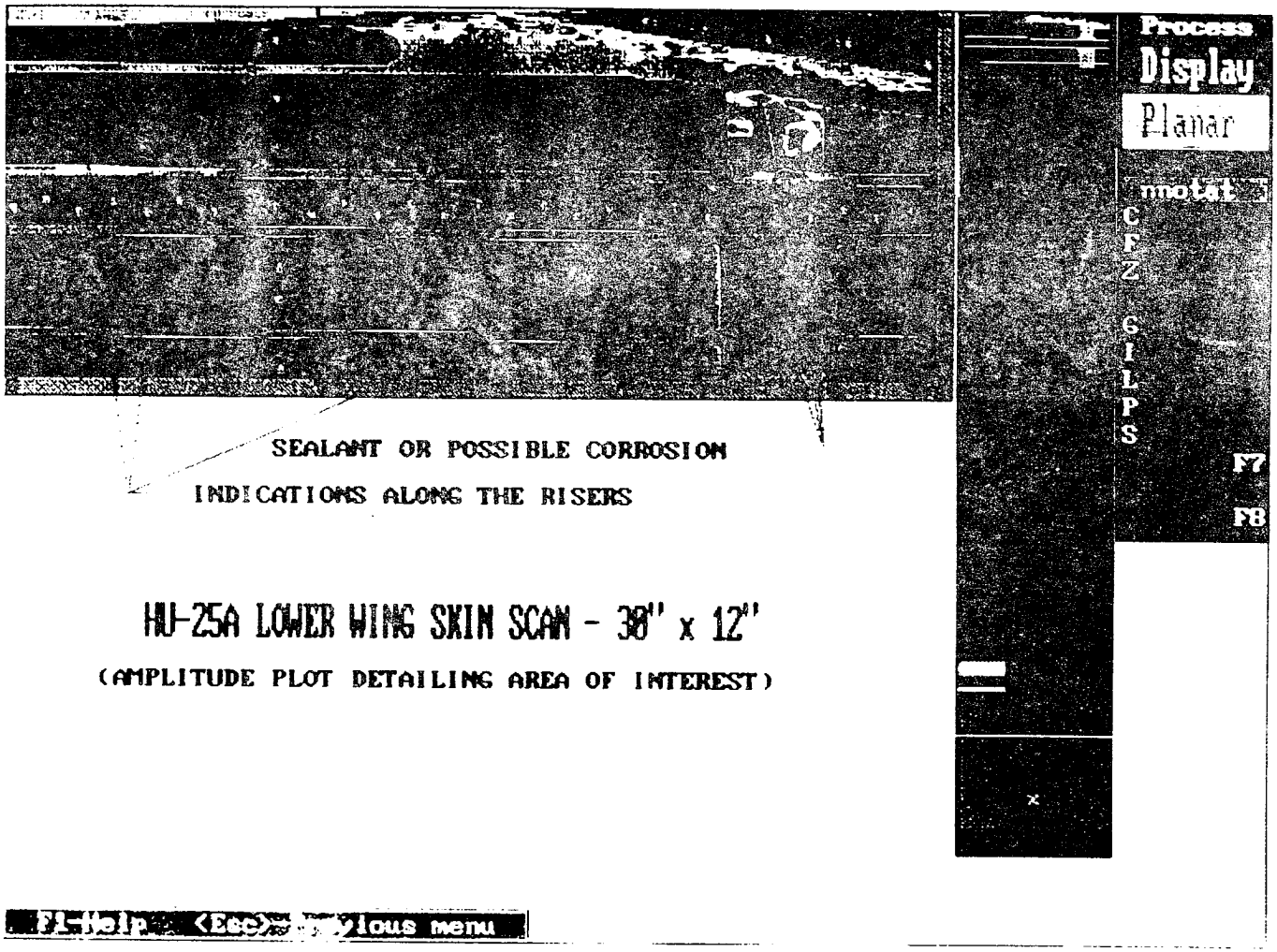
- Cracks in posts at internal fastener holes. Now: Windshields must be removed to inspect with X-rays.
- Solution: Advanced ultrasonic imaging and signal processing techniques will be applied to enable crack detection, documentation and characterization.

Initial Results -- Wing Planks

- Lower wing planks have been removed routinely at PDM to gain access to wing fuel cells to inspect for corrosion. Very little has been found on CG Falcons, but common on civilian version. Hundreds of labor hours to access.
- Advanced ultrasonic scanning has found suspected corrosion on CG2117.

AST GUARD

SAIC
Ultra Image International



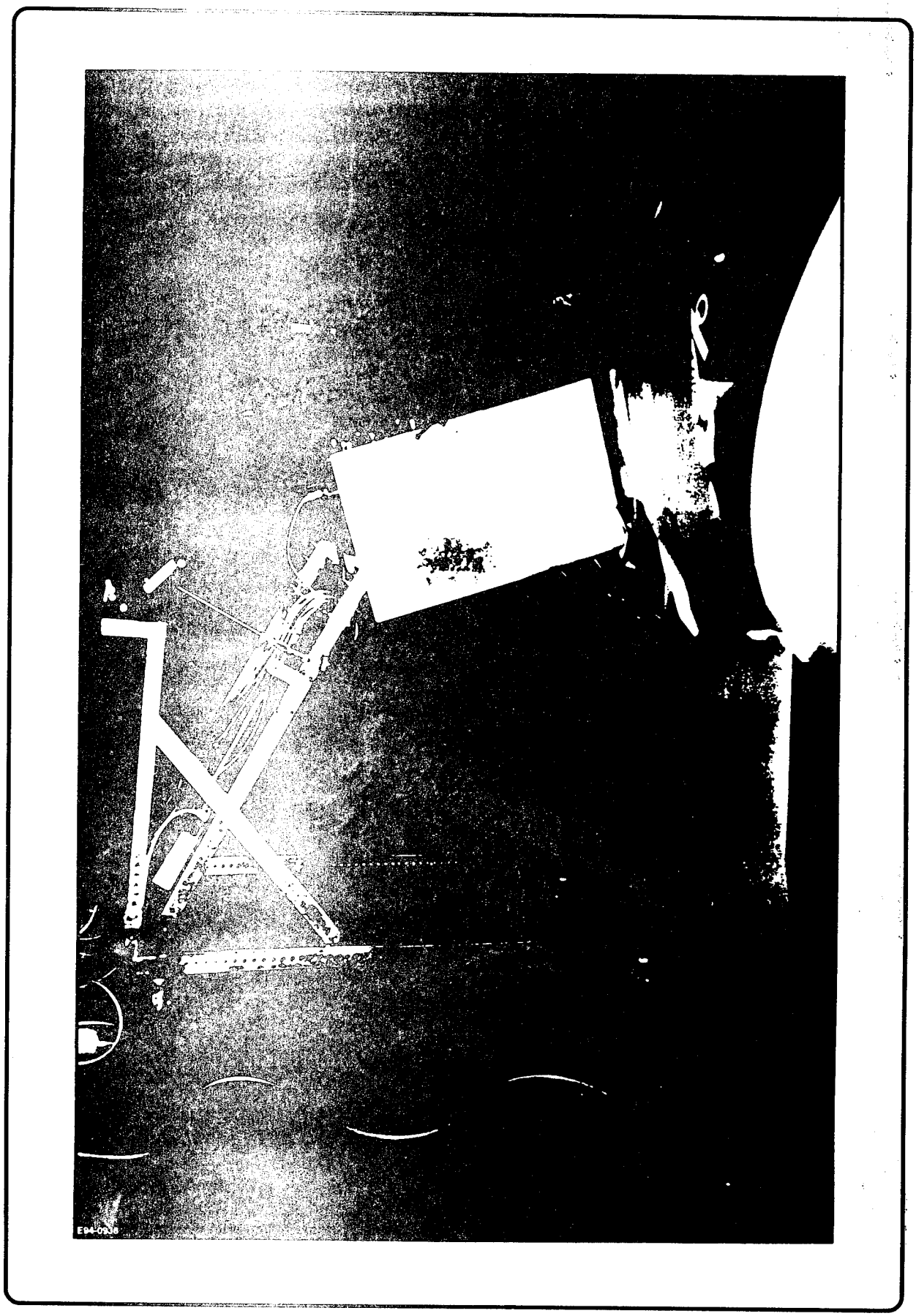
SEALANT OR POSSIBLE CORROSION
INDICATIONS ALONG THE RISERS

HU-25A LOWER WING SKIN SCAN - 36" x 12"

(AMPLITUDE PLOT DETAILING AREA OF INTEREST)

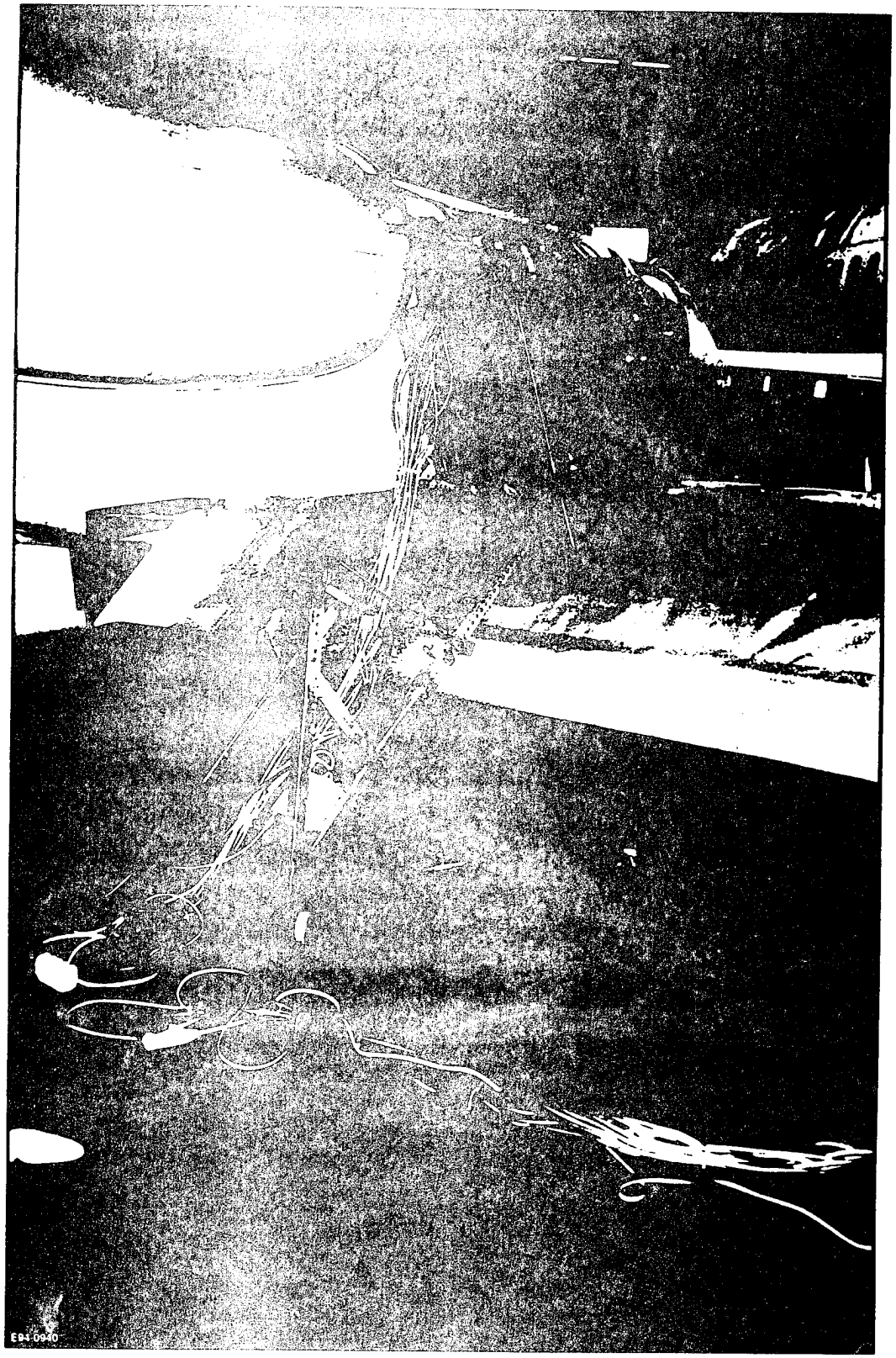
Initial Results -- Window Doubler

- **Search and Rescue Window Doublers are modifications to Falcon 20 design. Effect on fatigue life not determined. No inspection developed to detect disbonds, corrosion, fatigue.**
- **Various Techniques providing assurance of integrity. Thermal Wave Imaging appears to verify absence of corrosion, disbonds. MOI did not detect cracks.**



Initial Results -- Fuselage

- **Verification of fuselage integrity (hidden corrosion, fastener cracks, disbonds of lap joints) will provide high confidence without disassembly while providing valuable data for new service life determination.**
- **MOI has been applied to fasteners. D-Sight will be investigated. Thermal Wave Imaging has been applied, providing initial scan of fuselage & wings.**

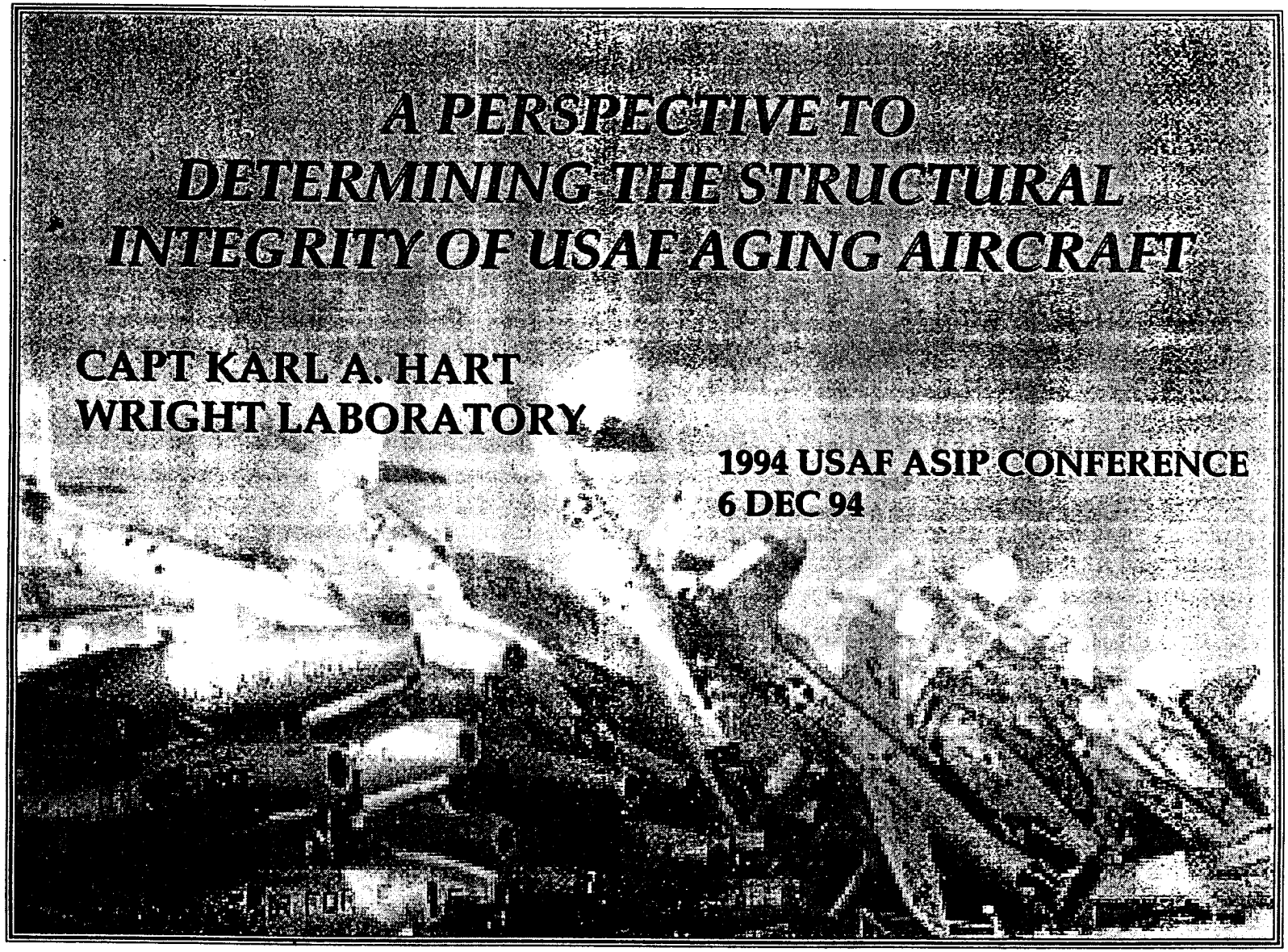

E84-0040

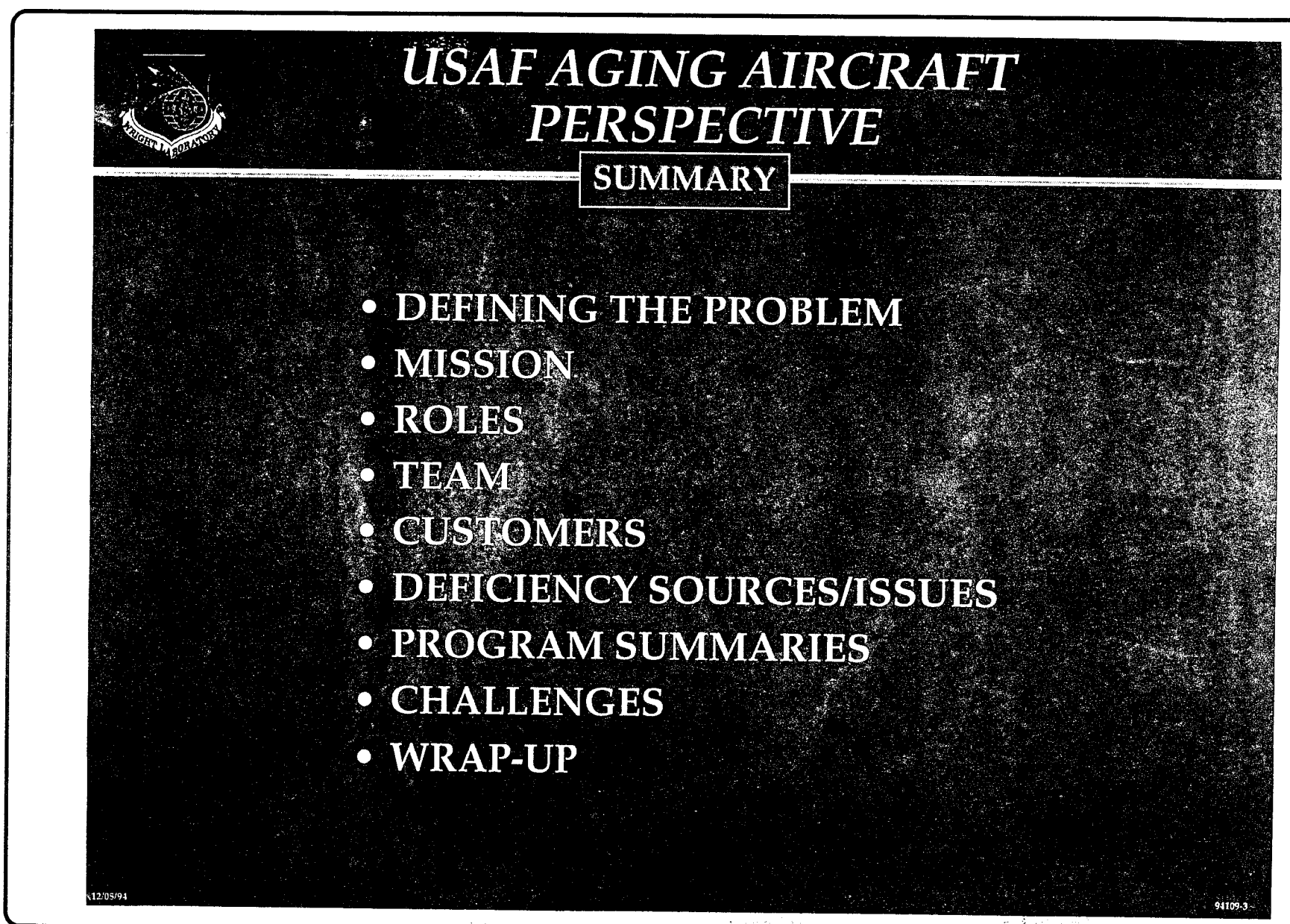
Areas of Emphasis -- Phase II

- Dassault (OEM) engineers supporting project. They are identifying critical structural elements with requirements for inspection. Will inspect at intervals.
- Some other areas: Flap rail attach points. SLAR mounts. Hidden corrosion in horizontal stabilizer. Wing spars. Wing center section joints & splices.

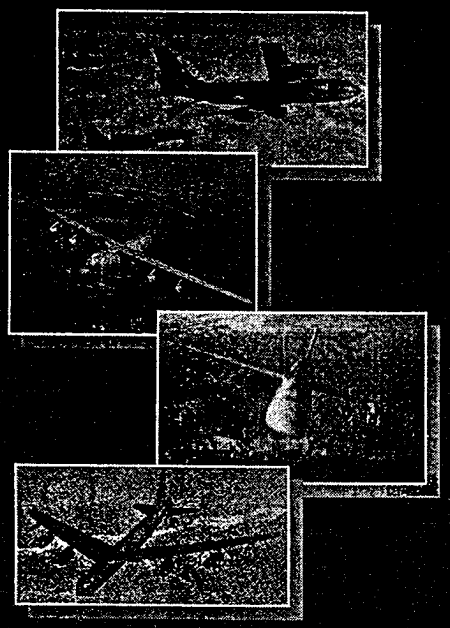
Future Plans

- Complete Phases I - III.
- Implement recommendations as they develop, especially for PDM.
- Re-visit proposed SSIP.
- Cooperate and share information with other similar efforts.
- Transfer approach to other CG aircraft.


A PERSPECTIVE TO
DETERMINING THE STRUCTURAL
INTEGRITY OF USAF AGING AIRCRAFT
CAPT KARL A. HART
WRIGHT LABORATORY
1994 USAF ASIP CONFERENCE
6 DEC 94


USAF AGING AIRCRAFT PERSPECTIVE
SUMMARY
• DEFINING THE PROBLEM
• MISSION
• ROLES
• TEAM
• CUSTOMERS
• DEFICIENCY SOURCES/ISSUES
• PROGRAM SUMMARIES
• CHALLENGES
• WRAP-UP
12/05/94
94109-3

AF AGING FLEET



	ENTRY DATE	PROJECTED RET. DATE	AGE AT RETIREMENT
KC-135	1957	2007	50
		2040*	83
C-141	1965	2003	38
C-5	1969	2038	69
B-52	1961	2030	69

AS OF 1993, 51% OF USAF FLEET WAS OVER 15 YEARS OLD, 44% WAS OVER 20 YEARS OLD.

* DOES NOT INCLUDE EFFECTS OF CORROSION

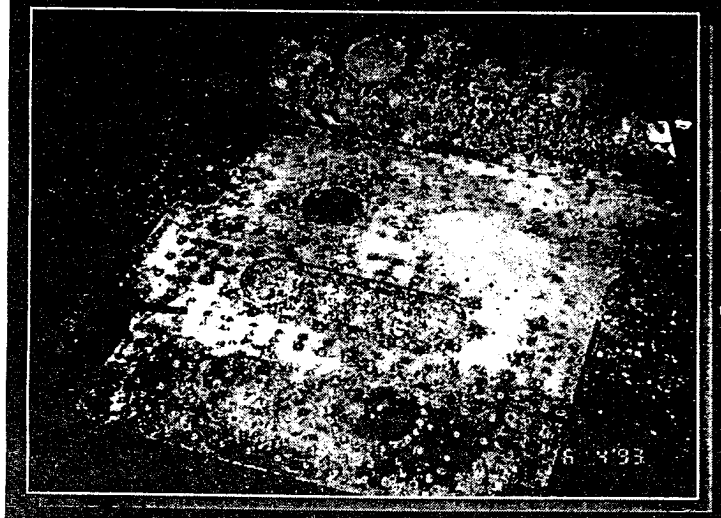
12/08/94

94109-8

OUR CHALLENGE

AMC EQUIPMENT PRIORITY

1995 AIR MOBILITY MASTER PLAN



"BY 2000, BE ABLE TO PREDICT AIRCRAFT ECONOMIC SERVICE LIFE INCLUDING THE EFFECTS OF CORROSION"

12/08/93

94109-5

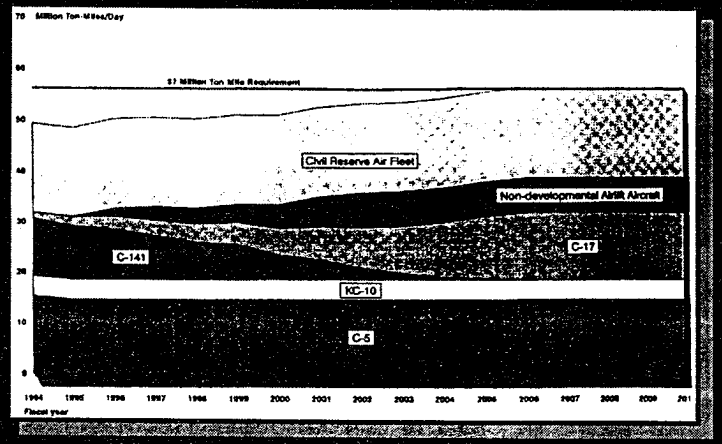
AGING AIRCRAFT RESEARCH

MISSION

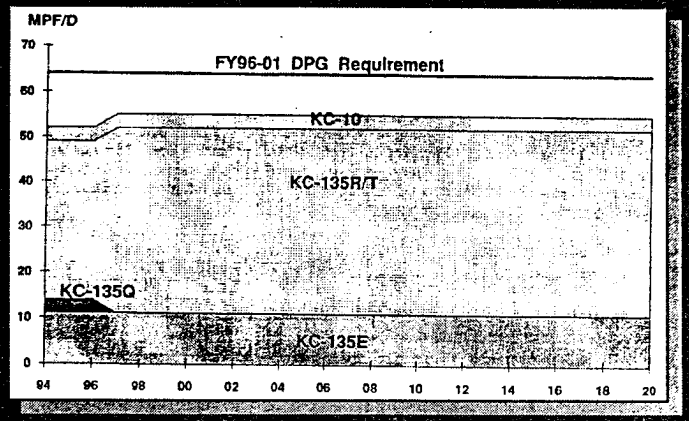
MARCHING ORDERS

DETERMINE TRUE USABLE STRUCTURAL LIFE OF USAF AIRCRAFT EXPERIENCING AGE-RELATED PROBLEMS

AMC MISSION CAPABILITY



STRATEGIC AIRLIFT CAPABILITY
(MILLION TON-MILES/DAY)



AIR REFUELING CAPABILITY
(MILLION POUNDS FUEL/DAY)

QUANTIFYING REQUIREMENTS AND ASSESSING CAPABILITY IS THE FIRST STEP IN EVALUATING FORCE STRUCTURE

12/08/94

94109-4

Quote

1995 ASIP Briefing

Aging Aircraft Research, Roles:

What is the pool of CRAF and NDAA like?

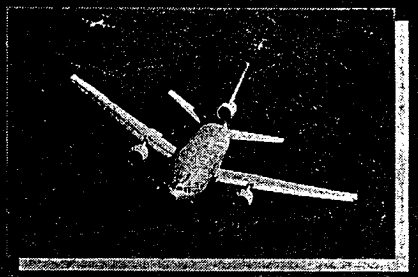
According to an article in the Wall Street Journal, titled, "Jurassic Jets, Airlines Are Keeping Aging Planes Aloft, Testing Repair Rules,

"1,500 jetliners are more than 15 years old, over 1,000 are more than 20 years old, and 550 are more than 25 years old. Among major carriers, TWA is the oldest with an average age of more than 18 years, followed by Northwest at 16 years, and Continental Airlines at almost 15 years of average age."

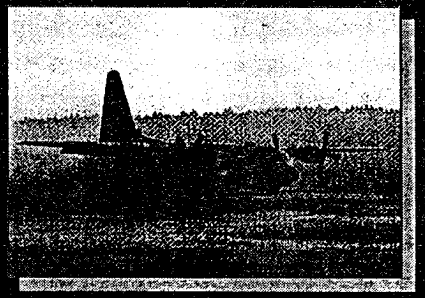
AGING AIRCRAFT RESEARCH

ROLES

- COMMERCIAL SECTOR:
  - FAA - NATIONAL AGING AIRCRAFT RESEARCH PROGRAM
    - » MR CHRIS SEHER - PROGRAM MANAGER
  - NASA - AIRFRAME STRUCTURAL INTEGRITY PROGRAM
    - » DR. CHARLIE HARRIS - IMPLEMENTATION TEAM LEADER



- USAF
  - AFOSR - AGING AIRCRAFT PROGRAM
    - » DR. JIM CHANG, DIRECTOR
    - » LEAD-IN RESEARCH (6.1)
  - WL - AGING SYSTEMS
    - » MR. JIM RUDD - TEAM CHIEF
    - » TRANSITION BASIC RESEARCH INTO USABLE TECHNOLOGY TO MEET AF NEEDS



12/08/94

94109-9

WL AGING AIRCRAFT RESEARCH



Unique Role

- To serve AF customers and act as integrator for ALCs, Airframers, SPOs, AFOSR, FAA/NASA, and others

- To account for differences in:
  - Usage
  - Design Philosophies
  - Maintenance Practices
  - Inspection Methods, Intervals



WL AGING AIRCRAFT TEAM

CUSTOMERS

ALC'S
- ASIP MANAGERS

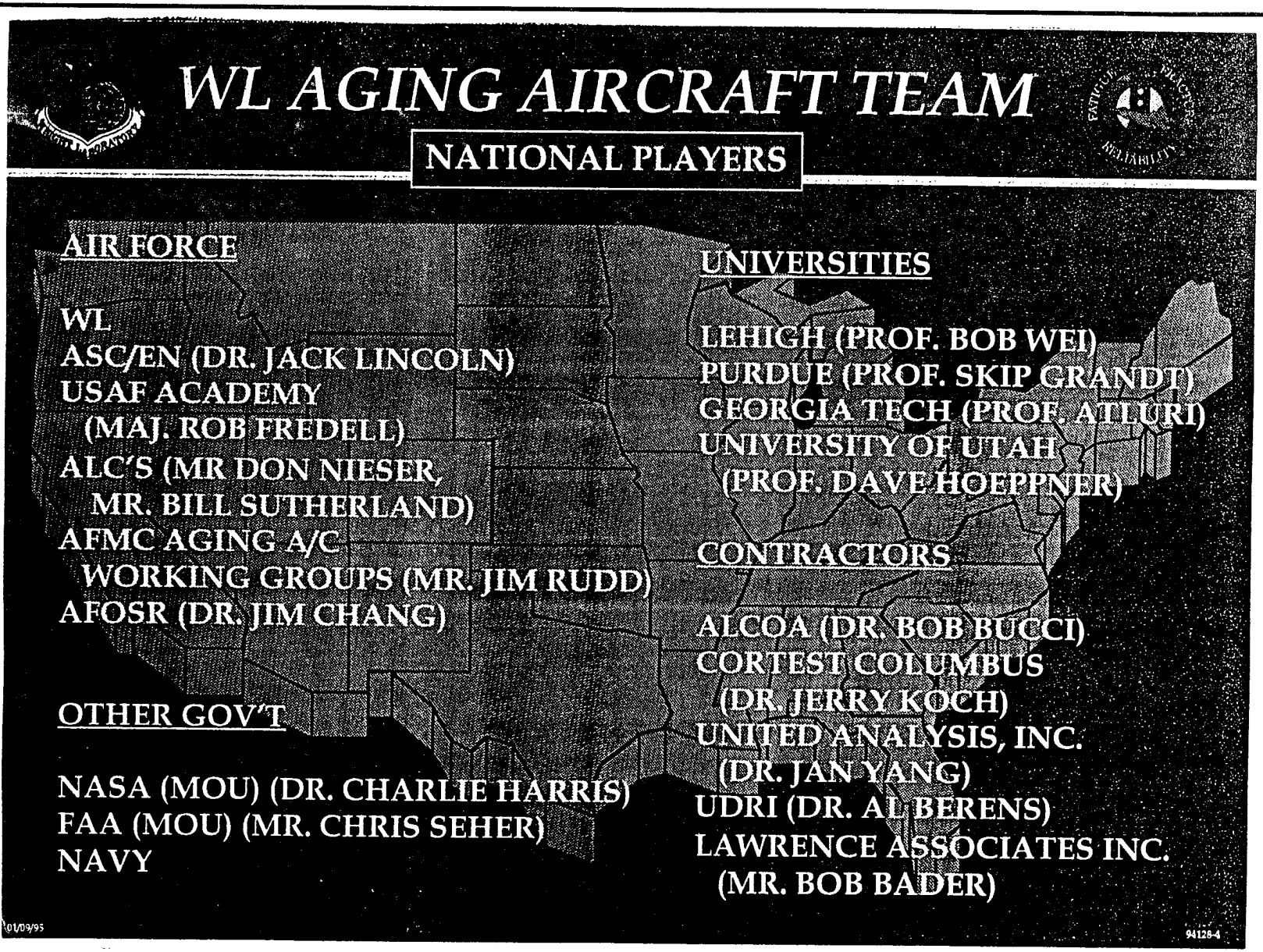
MAJCOM'S
- MISSION PLANNERS

SPO'S
- ASIP MANAGERS

DUAL USE (INDUSTRY)
- AIRFRAMERS
- AIRLINES
- FAA
- NASA

12/08/94

94109-14


WL AGING AIRCRAFT TEAM
NATIONAL PLAYERS
AIR FORCE
WL
ASC/EN (DR. JACK LINCOLN)
USAF ACADEMY
(MAJ. ROB FREDELL)
ALC'S (MR DON NIESER,
MR. BILL SUTHERLAND)
AFMC AGING A/C
WORKING GROUPS (MR. JIM RUDD)
AFOSR (DR. JIM CHANG)
OTHER GOV'T
NASA (MOU) (DR. CHARLIE HARRIS)
FAA (MOU) (MR. CHRIS SEHER)
NAVY
UNIVERSITIES
LEHIGH (PROF. BOB WEI)
PURDUE (PROF. SKIP GRANDT)
GEORGIA TECH (PROF. ATLURI)
UNIVERSITY OF UTAH
(PROF. DAVE HOEPPNER)
CONTRACTORS
ALCOA (DR. BOB BUCCI)
CORTEST COLUMBUS
(DR. JERRY KOCH)
UNITED ANALYSIS, INC.
(DR. JAN YANG)
UDRI (DR. AL BERENS)
LAWRENCE ASSOCIATES INC.
(MR. BOB BADER)
01/09/95
94128-4


WL AGING AIRCRAFT TEAM
INTERNATIONAL PLAYERS
• SWEDEN
• FRANCE
• GERMANY
• NETHERLANDS
• AUSTRALIA
• CANADA
• UNITED KINGDOM
01/19/95
94128-TMC-31

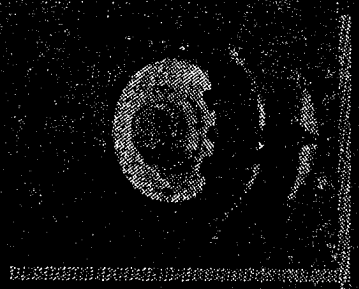
LET'S SOLVE THE PROBLEM

DEFICIENCIES

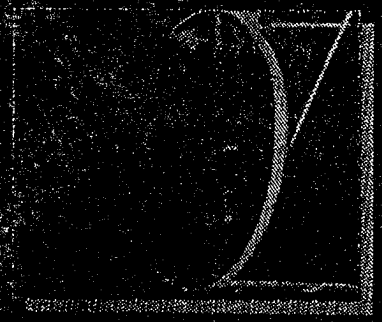
SOURCES

- WL IPT'S
  - AGING SYSTEMS (JIM RUDD)
  - STRUCTURES (LT COL ROGACKI)
  - TRANSPORTS
  - FIGHTERS
  - SYSTEMS & OPERATIONS SUPPORT
- AFMC AGING AIRCRAFT WORKING GROUPS
  - STRUCTURAL INTEGRITY ASSESSMENT & LIFE EXTENSION METHODOLOGY DEVELOPMENT
  - NDE/I
  - MATERIAL DAMAGE BEHAVIOR
  - CORROSION CHEMISTRY

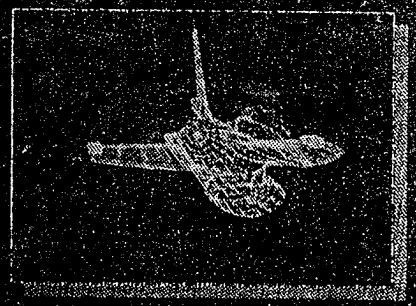
WL AGING SYSTEMS CFIPT



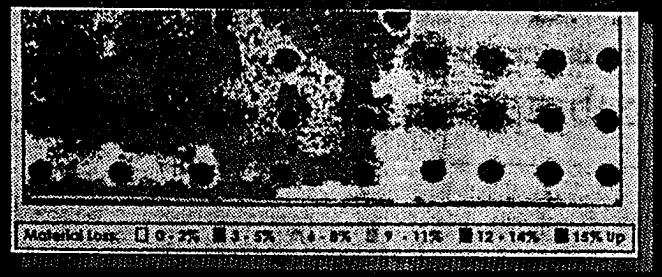
PROPULSION



AVIONICS



STRUCTURES



NDE/I



SUBSYSTEMS

DEFICIENCIES

SOURCES

- ASC/EN (DR. LINCOLN)
- SAB AGING AIRCRAFT SUMMER STUDY - 1994
- INTEGRITY ADVISORY GROUP (0-6)
- TECHNOLOGY NEEDS
- SPO'S
- MAJCOMS
  - MAP'S
  - 95 AMMP

12/08/94

94109-19

EQUIPMENT DEFICIENCIES

1995 AIR MOBILITY MASTER PLAN

1. AMC CAPABILITY IS LIMITED BY INSUFFICIENT AIRLIFT CAPACITY DUE TO:
   - C-141 STRUCTURAL/SERVICE LIFE PROBLEMS
   - AGING C-5 FLEET

2. OLDER SYSTEMS CANNOT BE ECONOMICALLY MAINTAINED DUE TO:
   - LOW RELIABILITY & MAINTAINABILITY OF C-141 AND C-5 AIRCRAFT
   - KC-135 HIGH OPERATING COST

3. AMC CANNOT ADEQUATELY DETERMINE THE ECONOMIC SERVICE LIFE TO ACCOUNT FOR THE EFFECT OF CORROSION.
   - AGING AND CORROSION OF C-5 AND KC-135 FLEETS

01/05/95

94128-3

INFRASTURE TECHNOLOGY NEEDS

CUSTOMER NEEDS

1. #95A0021. ANALYSIS METHODS TO ESTABLISH CRITERIA FOR PREDICTING MULITPLE SITE DAMAGE (MSD). REQUESTED BY DAN REGISTER, WR-ALC

2. #95A0014. OPTIMIZATION OF ADVANCED COMPOSITE REPAIRS OF CRACKED METALLIC STRUCTURES. REQUESTED BY BILL SCWEINBERG, WR-ALC

3. #95A0028. PREDICTIVE CORROSION MODELING. REQUESTED BY DICK KINZIE, WR-ALC

01/05/95

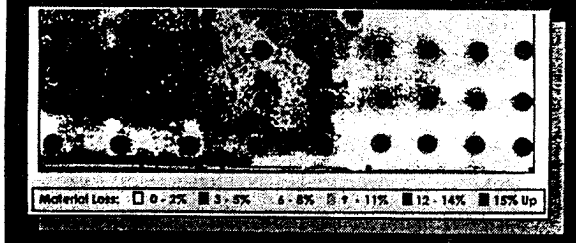
94128-26

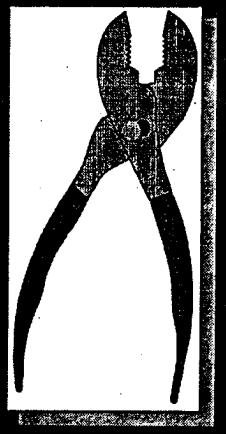
WL AGING AIRCRAFT TEAM

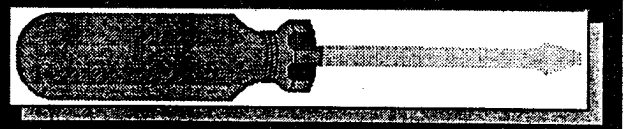
GOAL

- PROVIDE AIR FORCE WITH TECHNOLOGY TO EXTEND USABLE STRUCTURAL LIVES AND/OR REDUCE COSTS OF ITS AGING FLEET

- TECHNOLOGY FOCUSED ON PROVIDING OPTIMAL SCHEDULE FOR:







INSPECTIONS

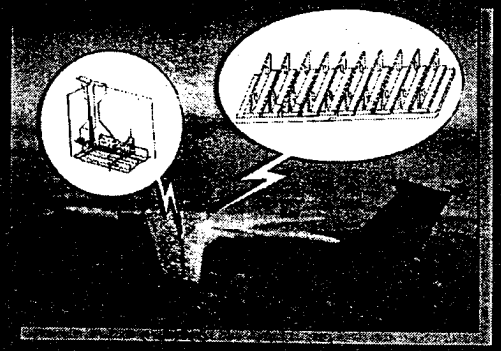
MAINTENANCE

MODIFICATIONS/ REPLACEMENTS

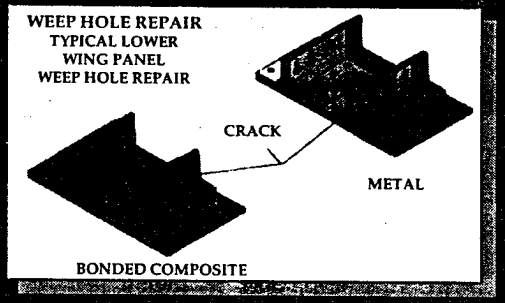
12/08/94

94109-11

PROGRAM SUMMARIES



WFD



REPAIR INTEGRITY



CORROSION FATIGUE

- PROBLEM
- GOALS/RISKS/IMPACT
- APPROACH
- ROADMAP

12/08/94

94109-15

WIDESPREAD FATIGUE DAMAGE

PROBLEM

- NEED TOOLS TO PROPERLY ASSESS STRUCTURES WITH MULTIPLE FATIGUE CRACKS

- NEED TO KNOW EFFECT ON:
  - RESIDUAL STRENGTH
  - CRITICAL CRACK SIZE
  - FAIL SAFETY (MULTIPLE LOAD PATHS)
  - ABILITY TO DETECT MULTIPLE SMALL CRACKS

12/08/94

94109-23

WIDESPREAD FATIGUE DAMAGE

GOAL: PREDICT ONSET AND DETERMINE EFFECTS OF WFD ON STRUCTURAL INTEGRITY OF AIRCRAFT

TODAY'S RISKS:

1. FLIGHT RESTRICTIONS (LOADS)
2. GROUNDED FLEET (C-141, WEEP HOLES)
3. CATASTROPHIC FAILURE (USAF ALOHA)

IMPACT: DECREASED MISSION CAPABILITY

- LOWER TON MILES/DAY FOR CARGO ACFT (C-141)
- LESS POUNDS FUEL/DAY FOR TANKER ACFT (KC-135)

12/05/94

94109-24

WIDESPREAD FATIGUE DAMAGE

APPROACH

1. COLLECT IN-SERVICE/EXPERIMENTAL DATA (DATABASE)

2. QUANTIFY FORMS & DEGREES OF DAMAGE
   - EQUIVALENT INITIAL FLAW SIZE
   - CORROSION (PITS)
   - WFD (MULTIPLE CRACKS)

3. DEVELOP ANALYSIS METHODS
   - UPGRADE DETERMINISTIC LIFE PREDICTION CODES
   - UPGRADE PROBABILISTIC RISK ANALYSIS CODE

4. CONDUCT VALIDATION TESTS

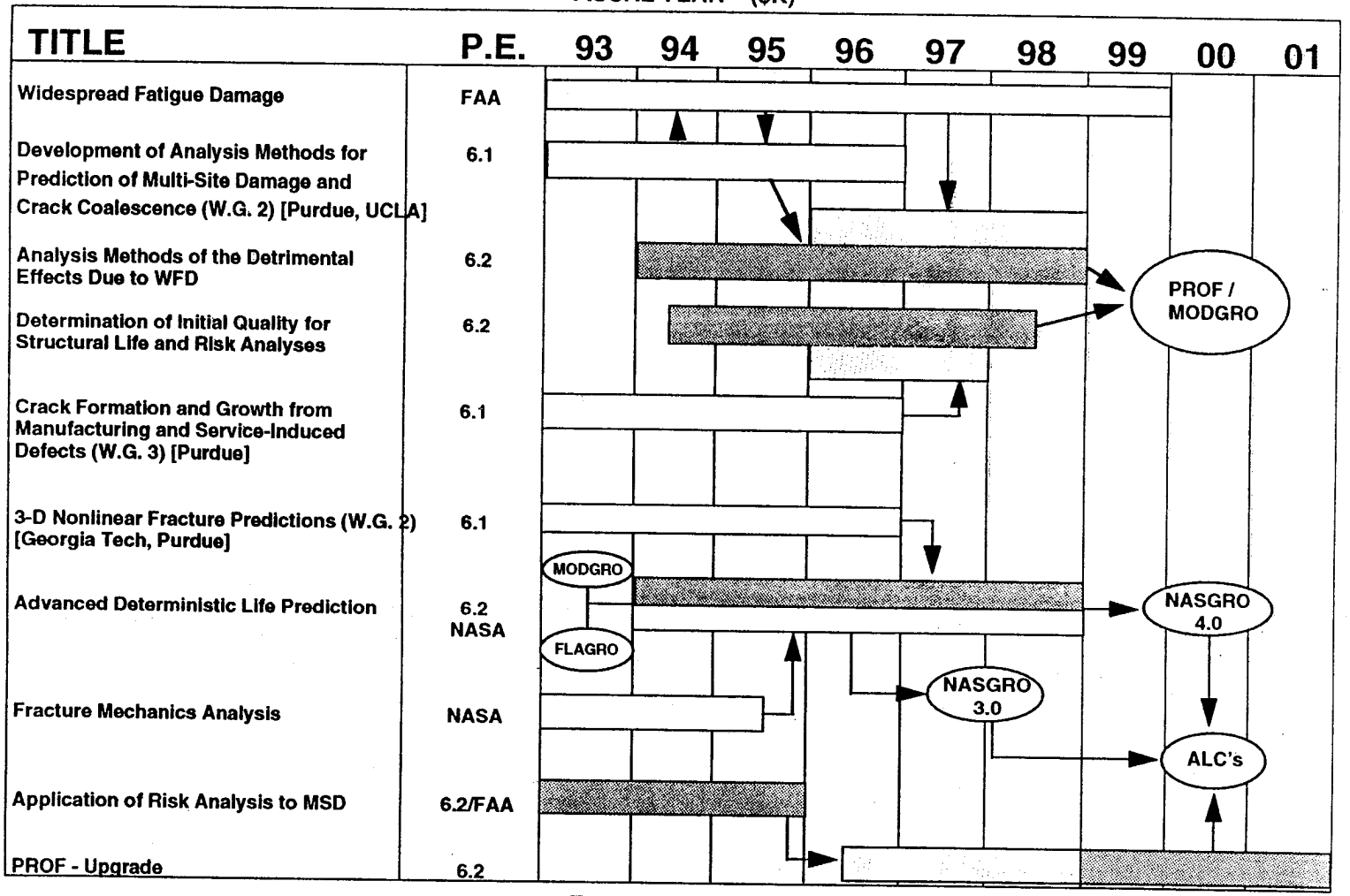
5. UPGRADE USAF DAMAGE TOLERANT DESIGN HANDBOOK (AFWAL-TR-82-3073)

6. LARGE SCALE STRUCTURES DEMO

WFD / MSD / MED

STRUCTURES

FISCAL YEAR ($K)



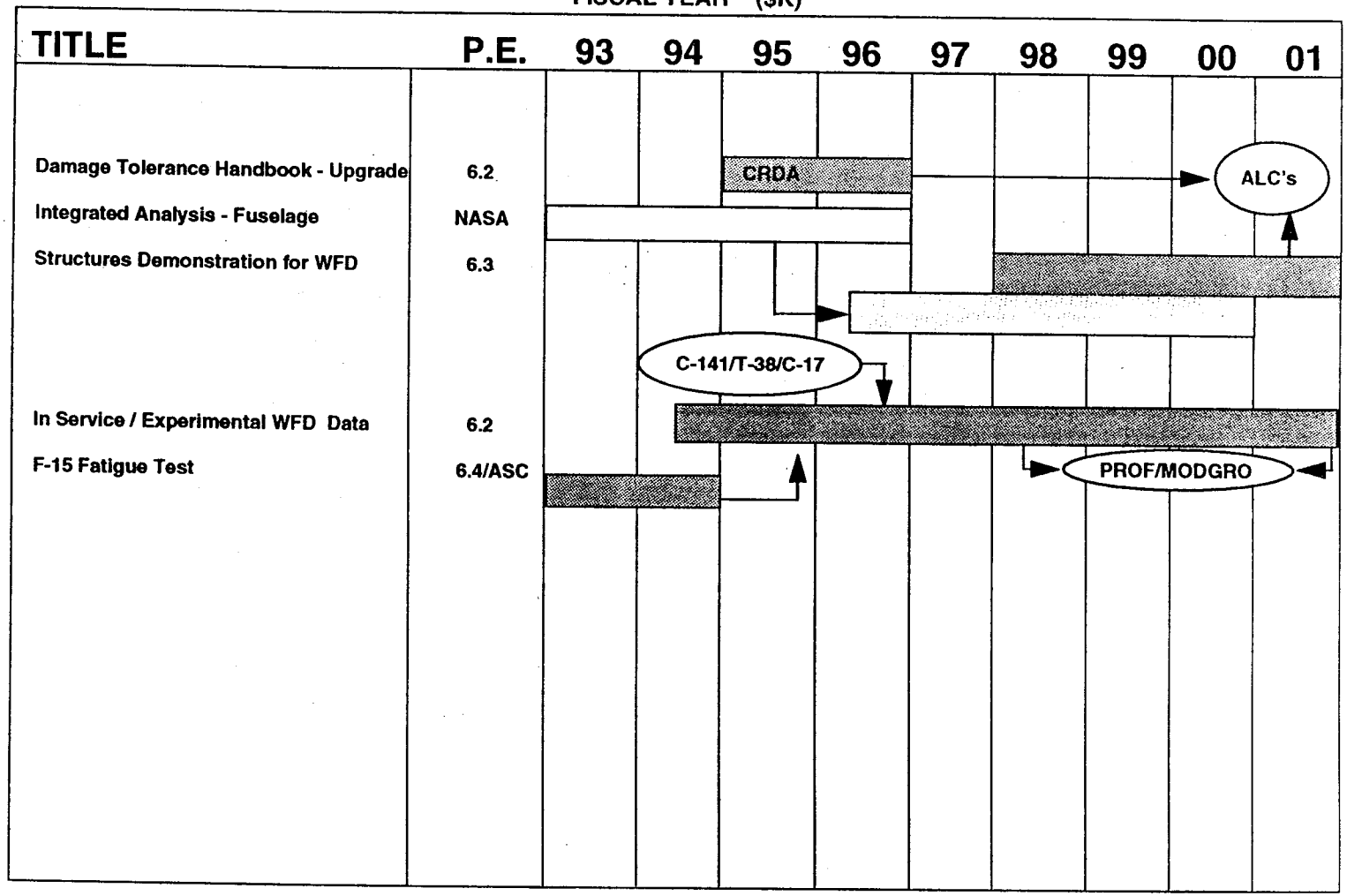
10/24/94

94031D-3

WFD /MSD / MED

STRUCTURES

FISCAL YEAR ($K)



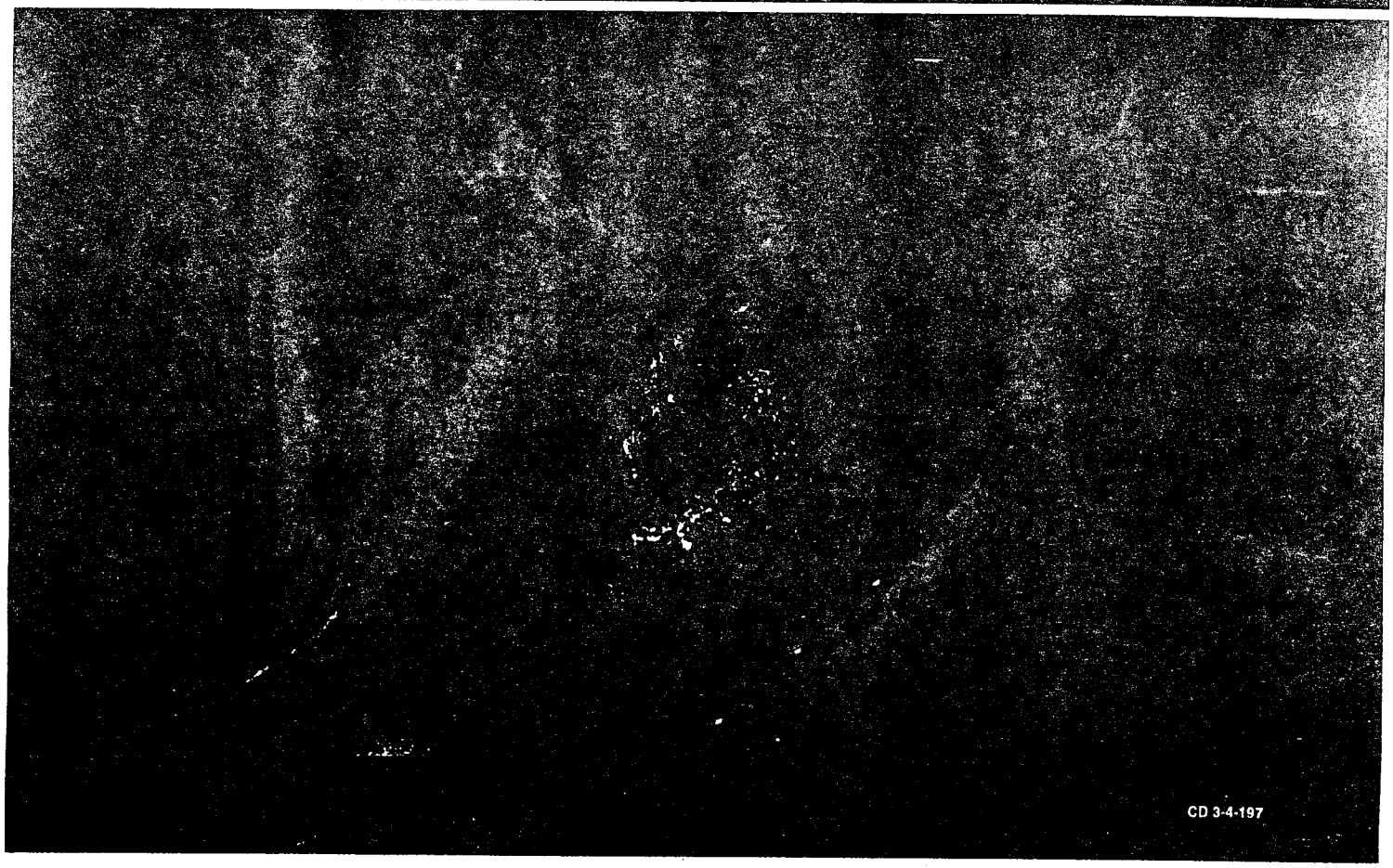
LEGEND:

- Wright Lab Funding
- Supplemental Funding
- Over-Ceiling Requirements
- Outside Activities

10/24/94

94031D-8

DAMAGE / LIFE / RISK ASSESSMENT
CORROSION / FATIGUE



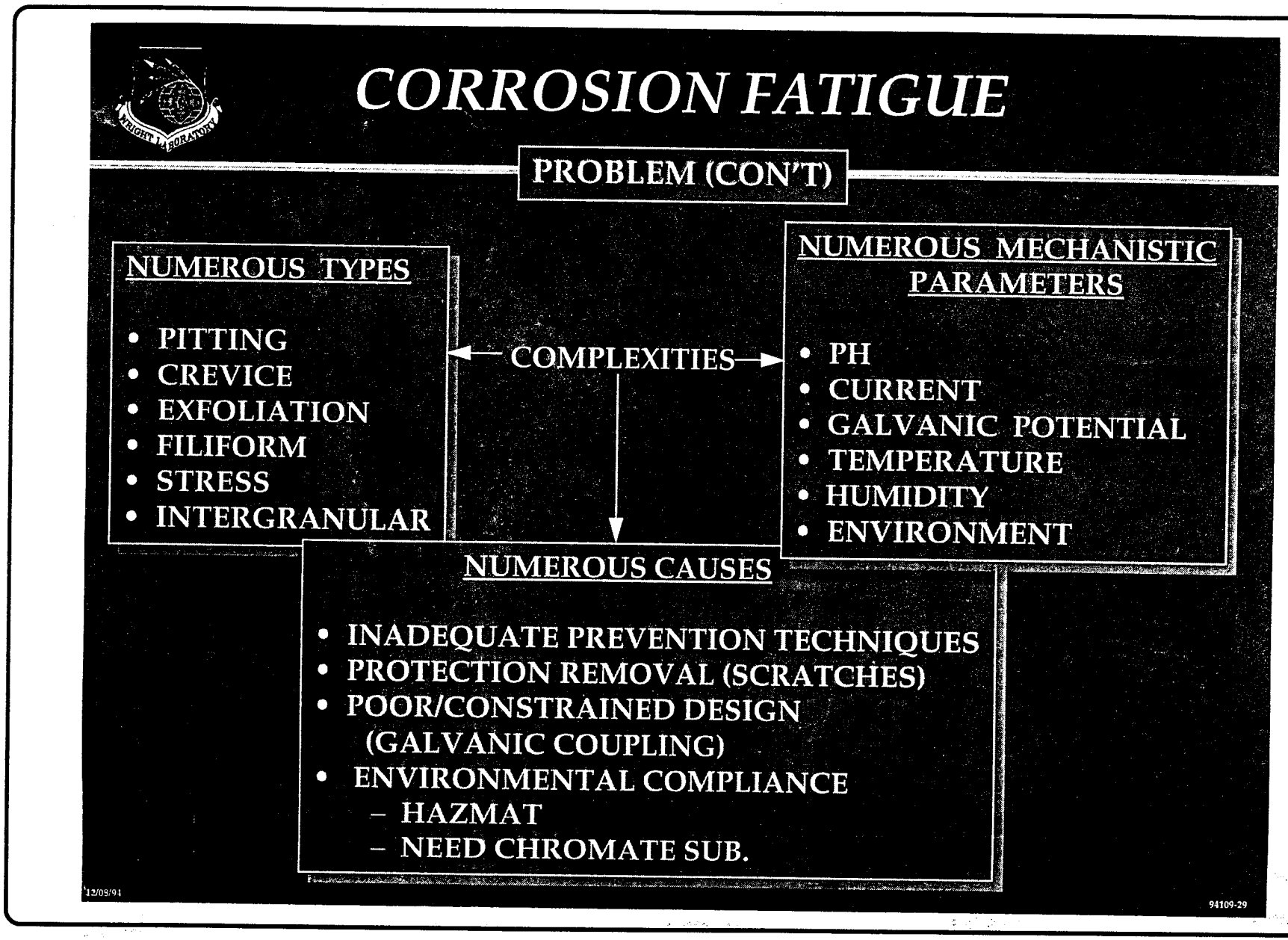
CORROSION FATIGUE

PROBLEM

- CORROSION IS SINGLE MOST EXPENSIVE MAINTENANCE ISSUE FOR USAF
  - $720M IN 1990 FOR DETECTION & REPAIRS
- UNKNOWN EFFECTS TO FATIGUE & FRACTURE CHARACTERISTICS:
  - TIME FOR CRACK NUCLEATION
  - TIME FOR ONSET OF WFD
  - NUMBER OF CRACKS
  - CRACK GROWTH RATES

12/09/94

94109-28


CORROSION FATIGUE
PROBLEM (CON'T)
NUMEROUS TYPES
• PITTING
• CREVICE
• EXFOLIATION
• FILIFORM
• STRESS
• INTERGRANULAR
COMPLEXITIES
NUMEROUS MECHANISTIC PARAMETERS
• PH
• CURRENT
• GALVANIC POTENTIAL
• TEMPERATURE
• HUMIDITY
• ENVIRONMENT
NUMEROUS CAUSES
• INADEQUATE PREVENTION TECHNIQUES
• PROTECTION REMOVAL (SCRATCHES)
• POOR/CONSTRAINED DESIGN (GALVANIC COUPLING)
• ENVIRONMENTAL COMPLIANCE
– HAZMAT
– NEED CHROMATE SUB.
12/09/91
94109-29

CORROSION FATIGUE

GOAL: DETERMINE AND ACCOUNT FOR EFFECTS OF CORROSION/FATIGUE ON STRUCTURAL INTEGRITY OF ACFT

TODAY'S RISK:

1. HIGHER MAINTENANCE COSTS
2. CATASTROPHIC FAILURE (DUE TO HIDDEN DAMAGE)

IMPACT:

1. DECREASED MISSION CAPABILITY
   - » MORE FREQUENT MAINTENANCE ACTIONS
   - » LOWER MISSION RATES
2. SHORTENED FLEET LIVES
   - » EARLIER FLEET REPLACEMENTS

12/08/94

94109-30

CORROSION FATIGUE

APPROACH

1. COLLECT IN-SERVICE/EXPERIMENTAL DATA

2. DEVELOP CORROSION SENSORS
   - BY-PRODUCTS
   - ENVIRONMENT

3. DEVELOP ANALYSIS METHODS
   - TEST TECHNIQUES (PROTOCOL)
   - EFFECTS OF CORROSION ON FATIGUE CRACK PROPAGATION
   - UPGRADE DETERMINISTIC LIFE PREDICTION CODE
   - UPGRADE RISK ANALYSIS CODE

4. CONDUCT VALIDATION TESTS

5. UPGRADE USAF DURABILITY DESIGN HANDBOOK (AFWAL-TR-88-3119)

6. FRETTING FATIGUE AND FRETTING CORROSION

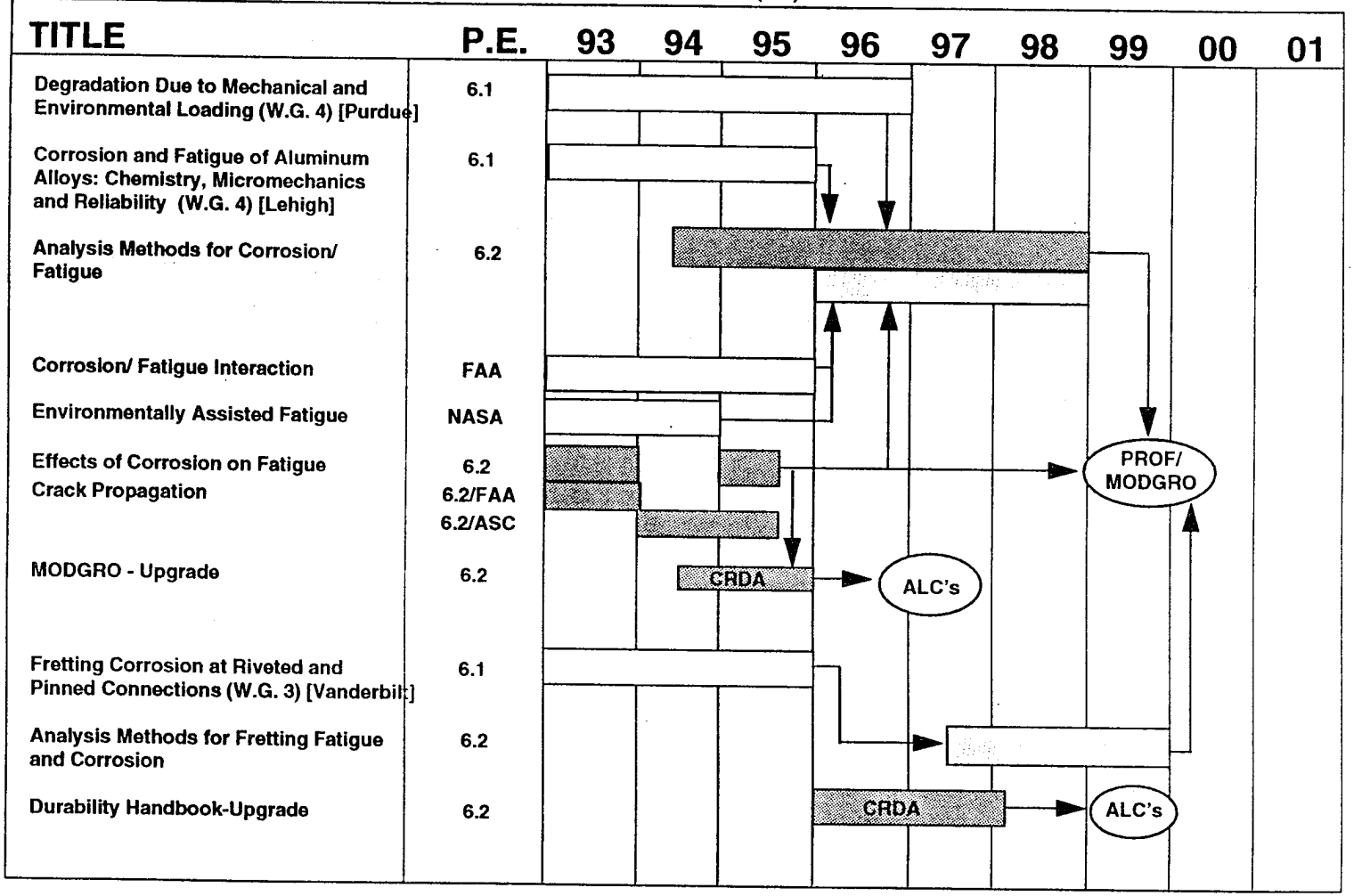
12/08/93

94109-31

CORROSION / FATIGUE

STRUCTURES

FISCAL YEAR ($K)



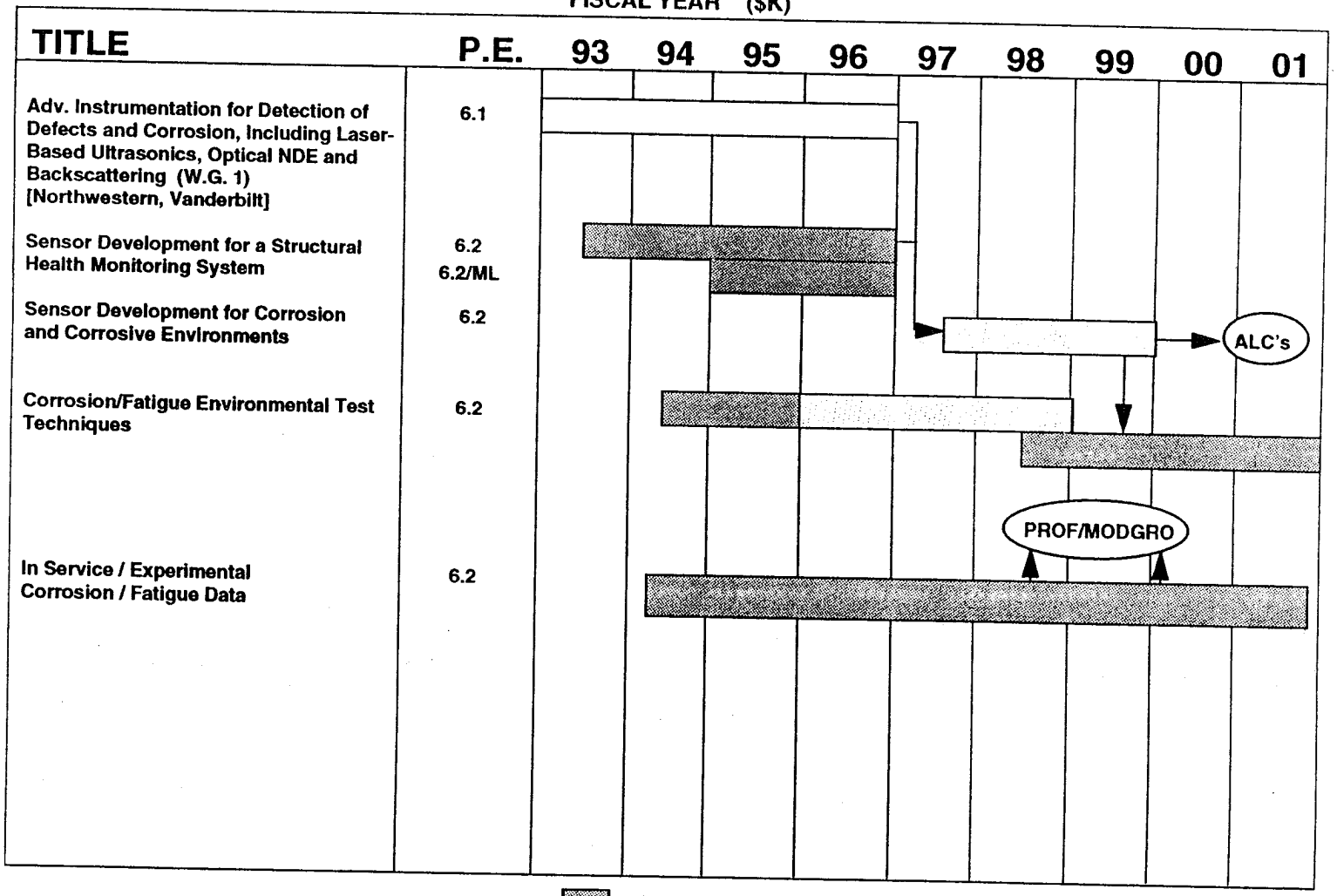
10/24/94

94031D-1

CORROSION / FATIGUE

STRUCTURES

FISCAL YEAR ($K)



11/1/94

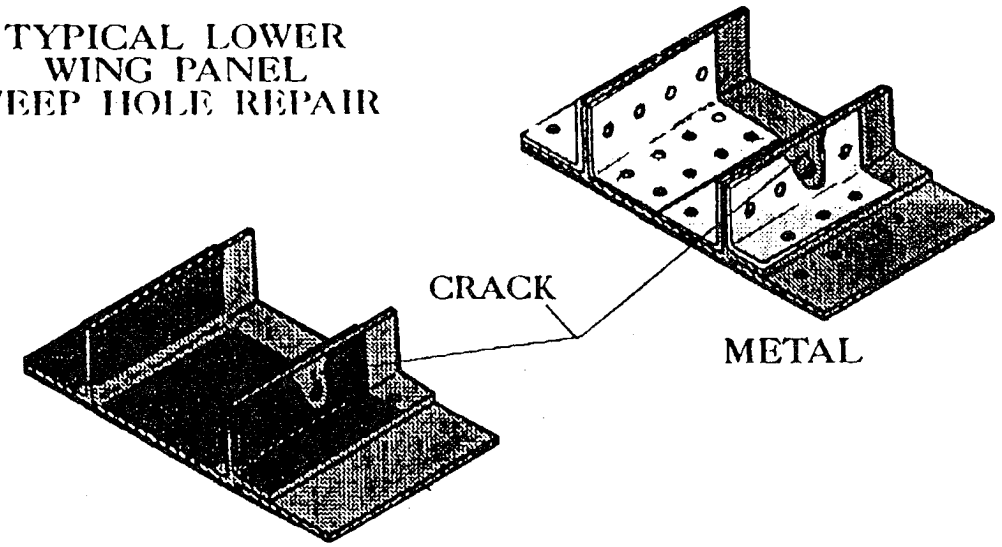
94031D-2

REPAIRS & LIFE ENHANCEMENT TECHNIQUES

REPAIR INTEGRITY ANALYSIS & AIRWORTHINESS VERIFICATION

WEEP HOLE REPAIR

TYPICAL LOWER
WING PANEL
WEEP HOLE REPAIR



REPAIR INTEGRITY

PROBLEM

- LACK OF CLEAR, USER FRIENDLY AND ACCURATE SOFTWARE AND WRITTEN INFORMATION TO:
  - DESIGN
  - ANALYZE
  - INSTALL REPAIRS, MODIFICATIONS
- REPAIR TECHNOLOGY NOT FULLY DEVELOPED
  - BONDED COMPOSITES ON METALLIC STRUCTURE
    - » BORON EPOXY
    - » GLARE
    - » GRAPHITE EPOXY

12/08/94

94109-11

REPAIR INTEGRITY

GOAL: DETERMINE HOW TO EFFECTIVELY ANALYZE REPAIRED ACFT STRUCTURE AND VERIFY ITS FLIGHT WORTHINESS

TODAY'S RISK:

1. FLIGHT RESTRICTIONS
2. GROUND FLEET
3. FAILURE OF REPAIRED STRUCTURE

IMPACT: DECREASED MISSION CAPABILITY

- INCREASED AIRCRAFT DOWNTIME
  - » STRUCTURAL REPLACEMENT VS. REPAIR
- PREMATURE RETIREMENT

94109-34

REPAIR INTEGRITY

APPROACH

1. COLLECT IN-SERVICE/EXPERIMENTAL DATA (DATABASE)

2. DEVELOP REPAIR ANALYSIS CODE
   - DESIGN REPAIR
   - ANALYZE REPAIR
     - » DURABILITY
     - » DAMAGE TOLERANCE

3. CONDUCT VALIDATION TESTS

4. ASSEMBLE REPAIR TECHNOLOGY HANDBOOK

5. ASSEMBLE EXTERNAL & INTERNAL LOADS HANDBOOK

6. UPGRADE USAF HANDBOOK OF FORCE MANAGEMENT METHODS (AFWAL-TR-81-3079)

7. COMPOSITE REPAIR DEMO

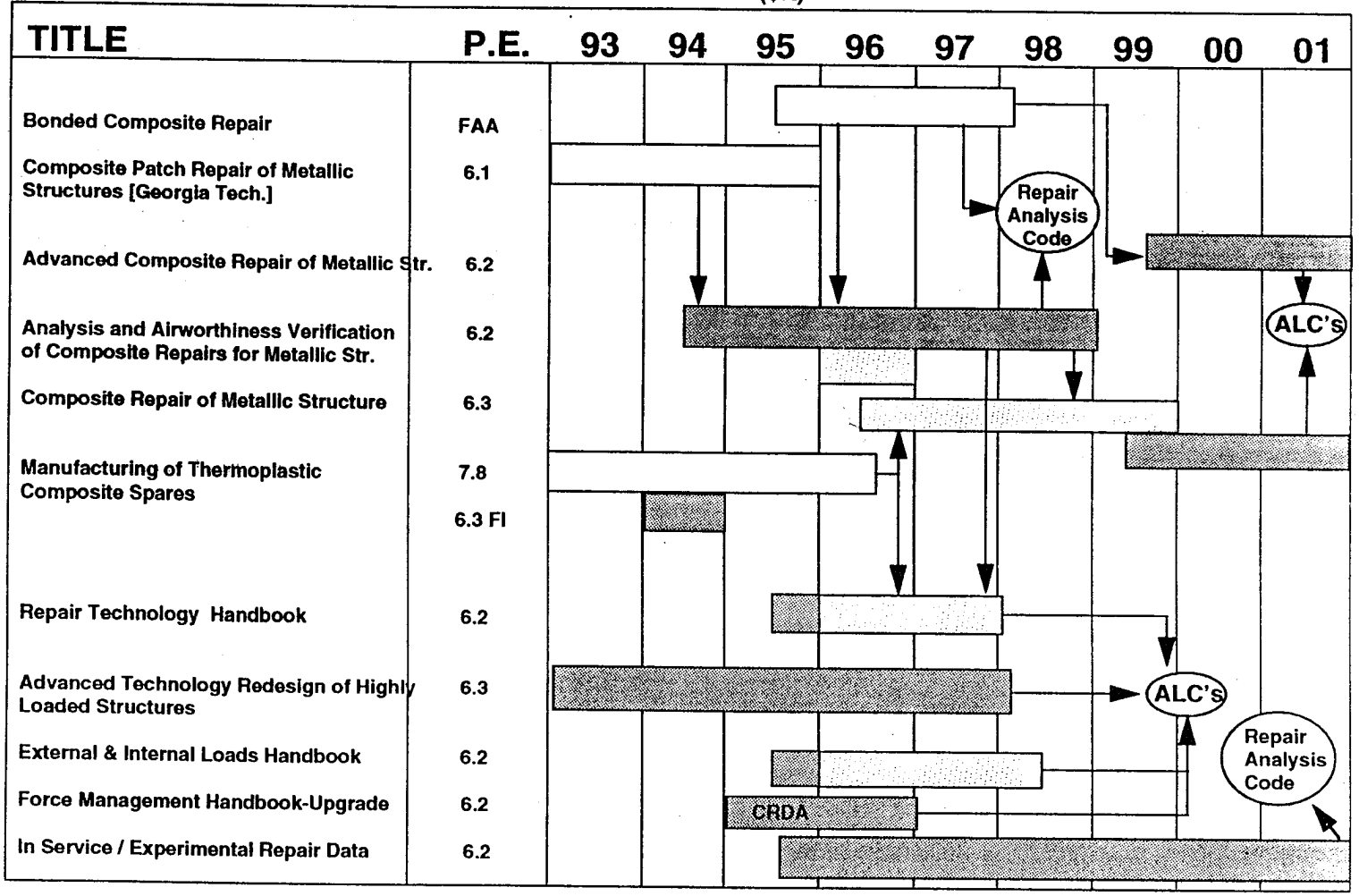
12/05/94

93109-35

REPAIR INTEGRITY ANALYSIS AND AIRWORTHINESS VERIFICATION

STRUCTURES

FISCAL YEAR ($K)



10/24/94

94031D-6



AGING AIRCRAFT RESEARCH

CHALLENGES

- BUDGETARY/MANPOWER
- MODELING
  - CORROSION GROWTH RATES
  - SYNERGY OF WFD AND CORROSION FATIGUE
- TESTING
  - LARGE FIXTURES FOR LARGE PANELS (WFD)
  - ACCELERATED CORROSION TECHNIQUES (PROTOCOL)
  - REPAIR AIRWORTHINESS PROCEDURES
- COORDINATION OF USAF, NASA, FAA, INDUSTRY, OTHERS
- MEETING USERS' NEEDS
  - MARKETING

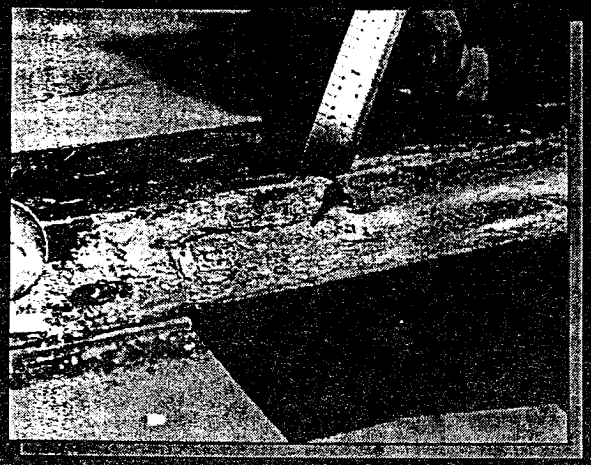
12/05/94

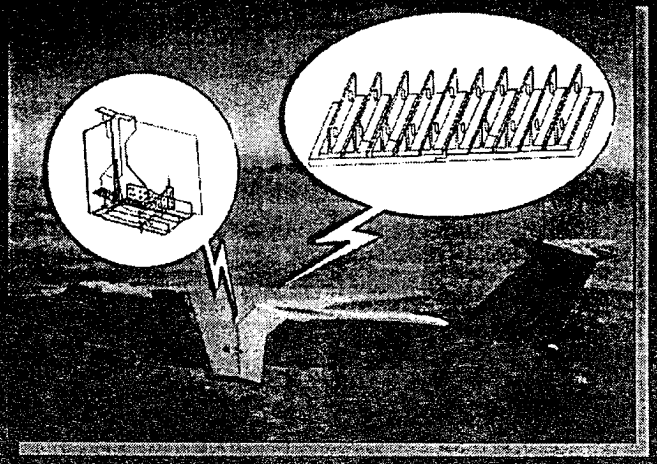
94109-38

AGING AIRCRAFT RESEARCH

CHALLENGES

NDI-NDE





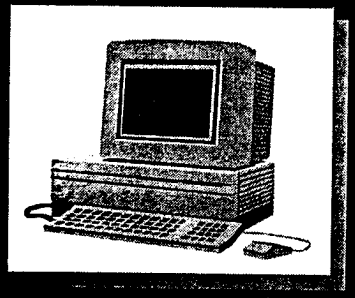
- FIND HIDDEN DAMAGE
- QUANTIFY DAMAGE

12/08/94

94109-39

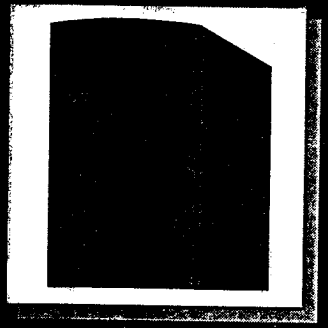
AGING AIRCRAFT PROGRAM

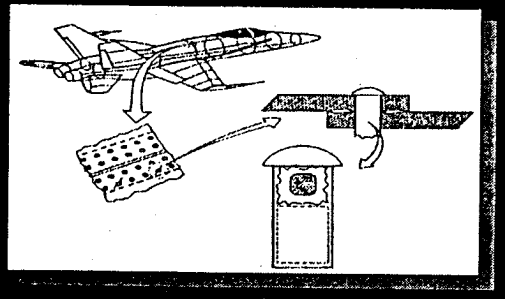
PRODUCTS



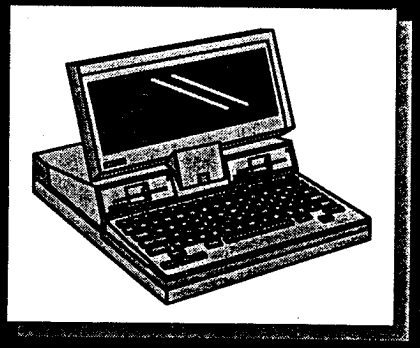
ANALYSIS TOOLS
- DETERMINISTIC
- PROBABILISTIC

HANDBOOKS/GUIDELINES
- REPAIR
- LOADS
- FORCE MGMT
- DURABILITY
- DAMAGE TOLERANCE





CORROSION SENSOR



REPAIR DESIGN/ANALYSIS

94109-45

AGING AIRCRAFT RESEARCH

PRODUCTS



MODGRO

- DETERMINISTIC CRACK GROWTH ANALYSIS
- PC BASED, MENU DRIVEN
- DEVELOPED IN-HOUSE
- REAL TIME CRACK GROWTH GRAPHICS

SUCCESS:

- TASK - DETERMINE WHETHER AGING AEDC WIND TUNNEL COMPRESSOR COMPONENTS SHOULD BE REPAIRED OR REPLACED..
- SOLUTION - REPAIR

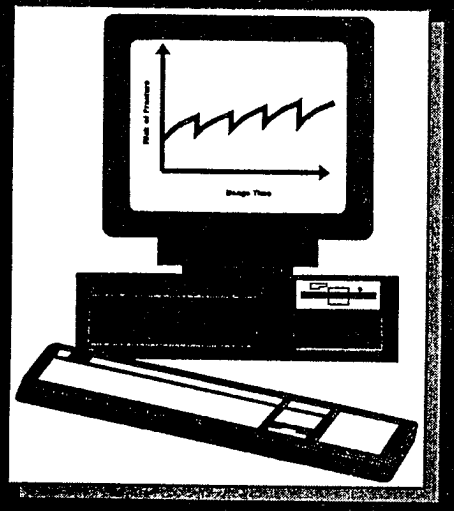
⇒ **SAVED AIR FORCE OVER $4 MILLION**

12/09/94

94109-43

AGING AIRCRAFT RESEARCH

PRODUCTS



PROF

- PROBABILISTIC RISK ANALYSIS
- PC BASED, WINDOWS VERSION
- DEVELOPED BY UDRI
- ACCOUNTS FOR VARIABILITY IN:
  - USAGE
  - INSPECTION METHOD INTERVALS
  - CALCULATES PROBABILITY OF FRACTURE

SUCCESS:

- TASK - QUANTIFY RISK OF FLYING C-141 FLEET WITH WEEP HOLE CRACKS IN LOWER WING SKINS
- SOLUTION - LOCKHEED USED PROF

PROF USED BECAUSE OF EASE OF USE AND ACCURACY

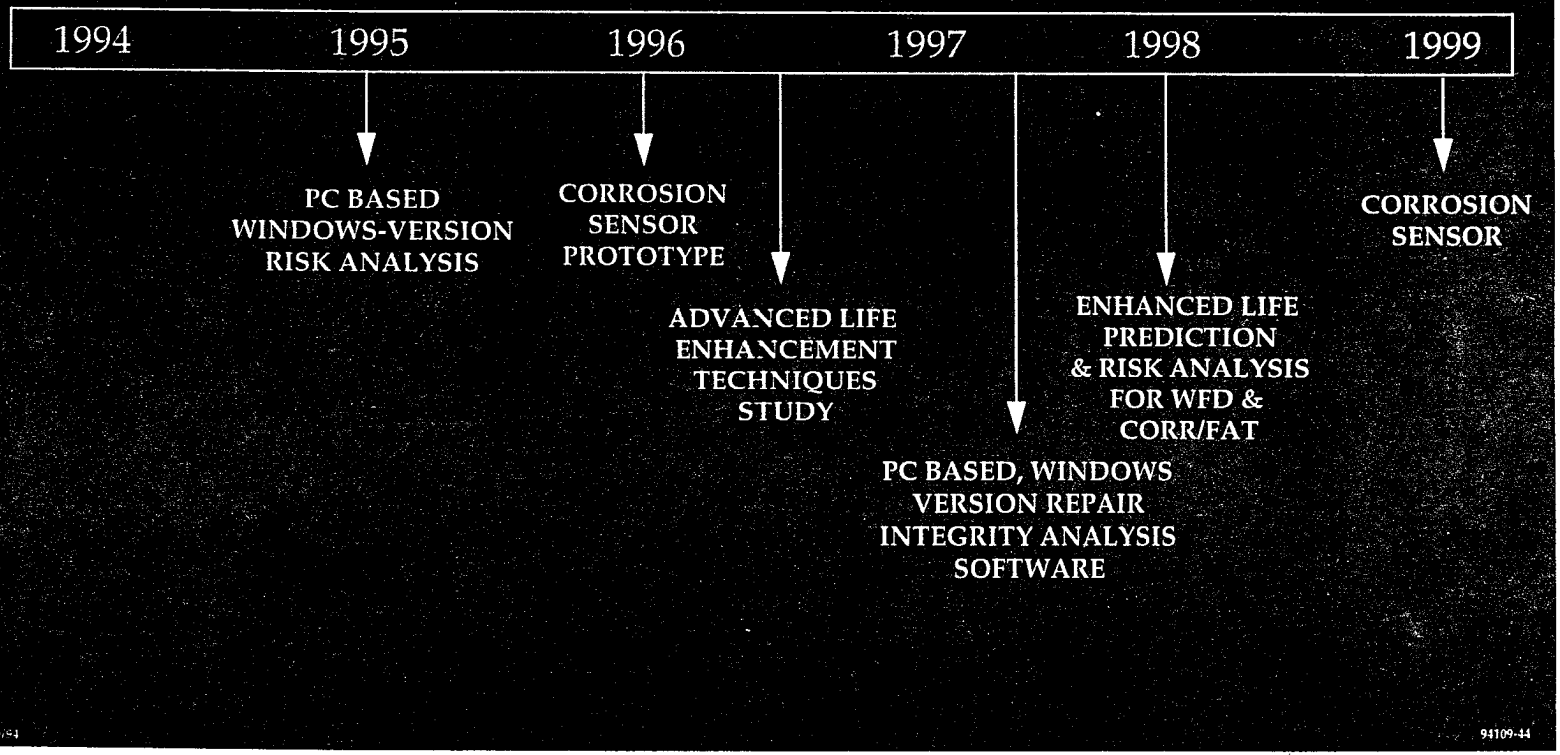
12/09/94

94109-42

AGING AIRCRAFT RESEARCH

MILESTONES

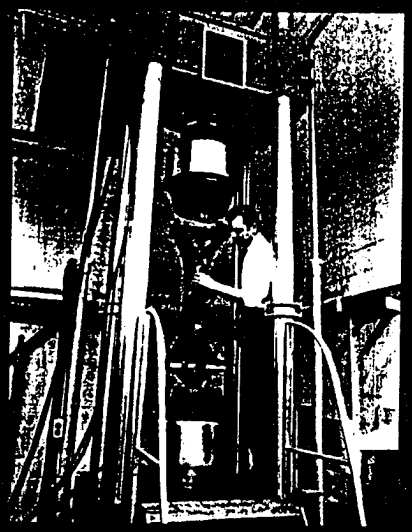
BY FY:

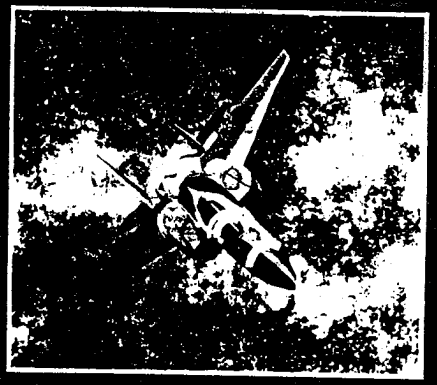


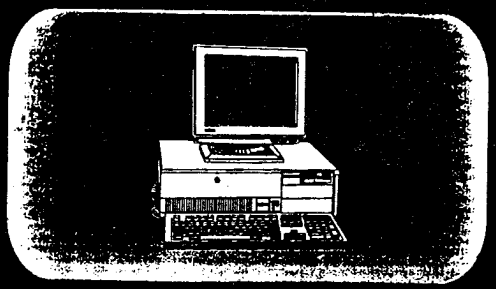
94109-44

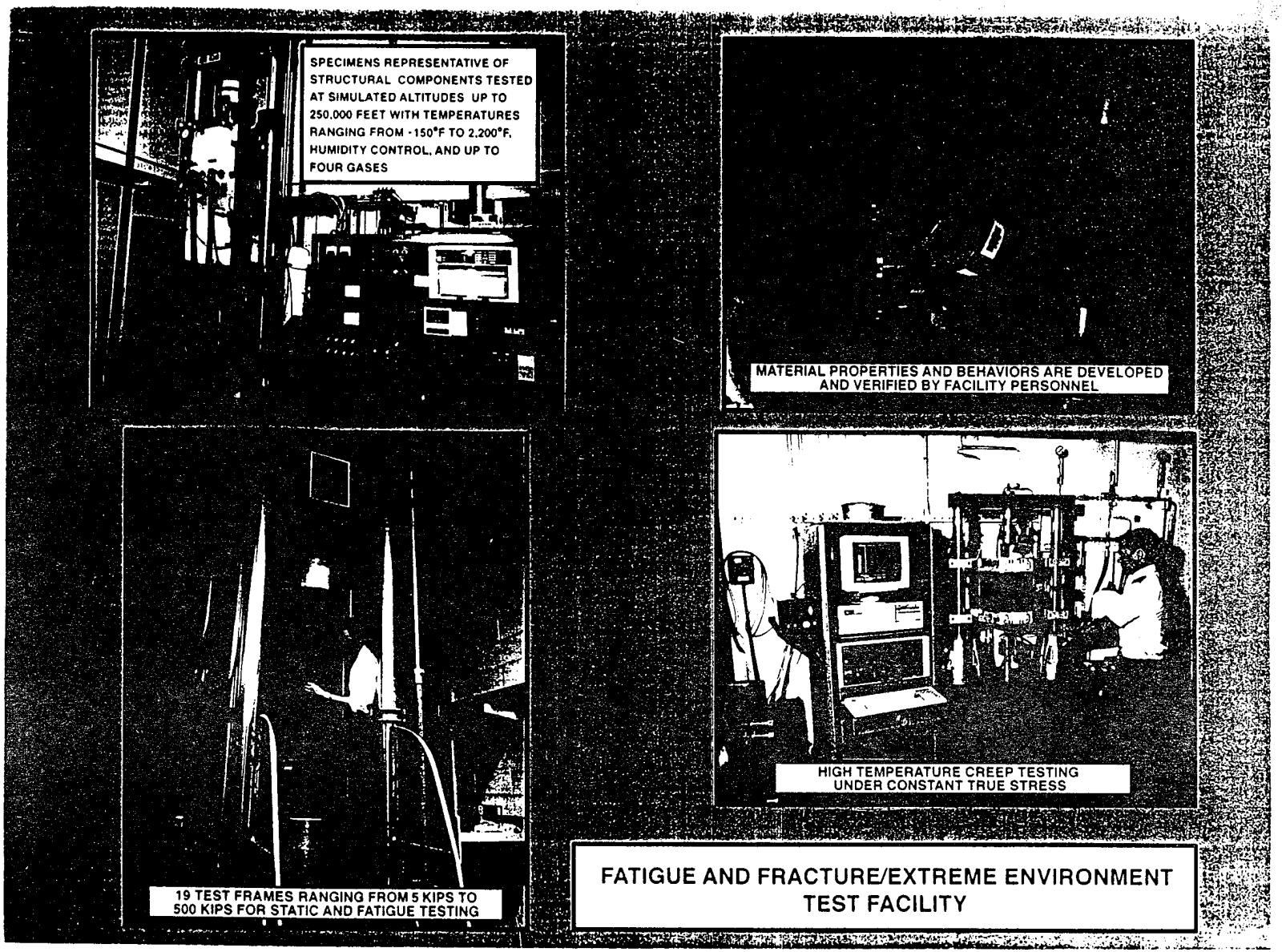
FATIGUE AND FRACTURE TEST FACILITY

PURPOSE: To Validate Structural Integrity Analysis Methods and Design Criteria for Predicting Aircraft Structural Life, and Aid in Solving Flight Safety Problems in Military and Commercial Aircraft








SPECIMENS REPRESENTATIVE OF STRUCTURAL COMPONENTS TESTED AT SIMULATED ALTITUDES UP TO 250,000 FEET WITH TEMPERATURES RANGING FROM -150°F TO 2,200°F, HUMIDITY CONTROL, AND UP TO FOUR GASES
MATERIAL PROPERTIES AND BEHAVIORS ARE DEVELOPED AND VERIFIED BY FACILITY PERSONNEL
19 TEST FRAMES RANGING FROM 5 KIPS TO 500 KIPS FOR STATIC AND FATIGUE TESTING
HIGH TEMPERATURE CREEP TESTING UNDER CONSTANT TRUE STRESS
FATIGUE AND FRACTURE/EXTREME ENVIRONMENT TEST FACILITY

TEST FACILITY'S CAPABILITY

- Structural Fatigue (5-500 Kip)
- Static Loading / Bending (20-100 Kip)
- Real-Time Crack Growth Measurement
- Optical Fiber Based Strain Measurement & Manufacturing
- Corrosive Environment Chamber
- Complex Geometry
- Flight Environment Simulation
  - ➤ -200 to 2200 Degrees F
  - ➤ Sea Level to 25,000 Ft Atmospheric Pressure
  - ➤ Simultaneous Mixing of Four Separate Gases
  - ➤ Variable Humidity Control
- Redundant Load Monitoring / Verification
- Computerized Self-Monitoring Control and Data Acquisition (256 Channels)



WL AGING AIRCRAFT PAYOFFS

Increased Structural Safety

Want to prevent an AF Aloha

Reduced Acquisition Costs

Extend structural life
Delay replacement of fleet

Reduced Operational Costs

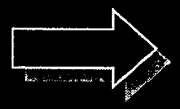
Early detection/repair vs. late detection/replace

Bonus! Increase Operational Readiness

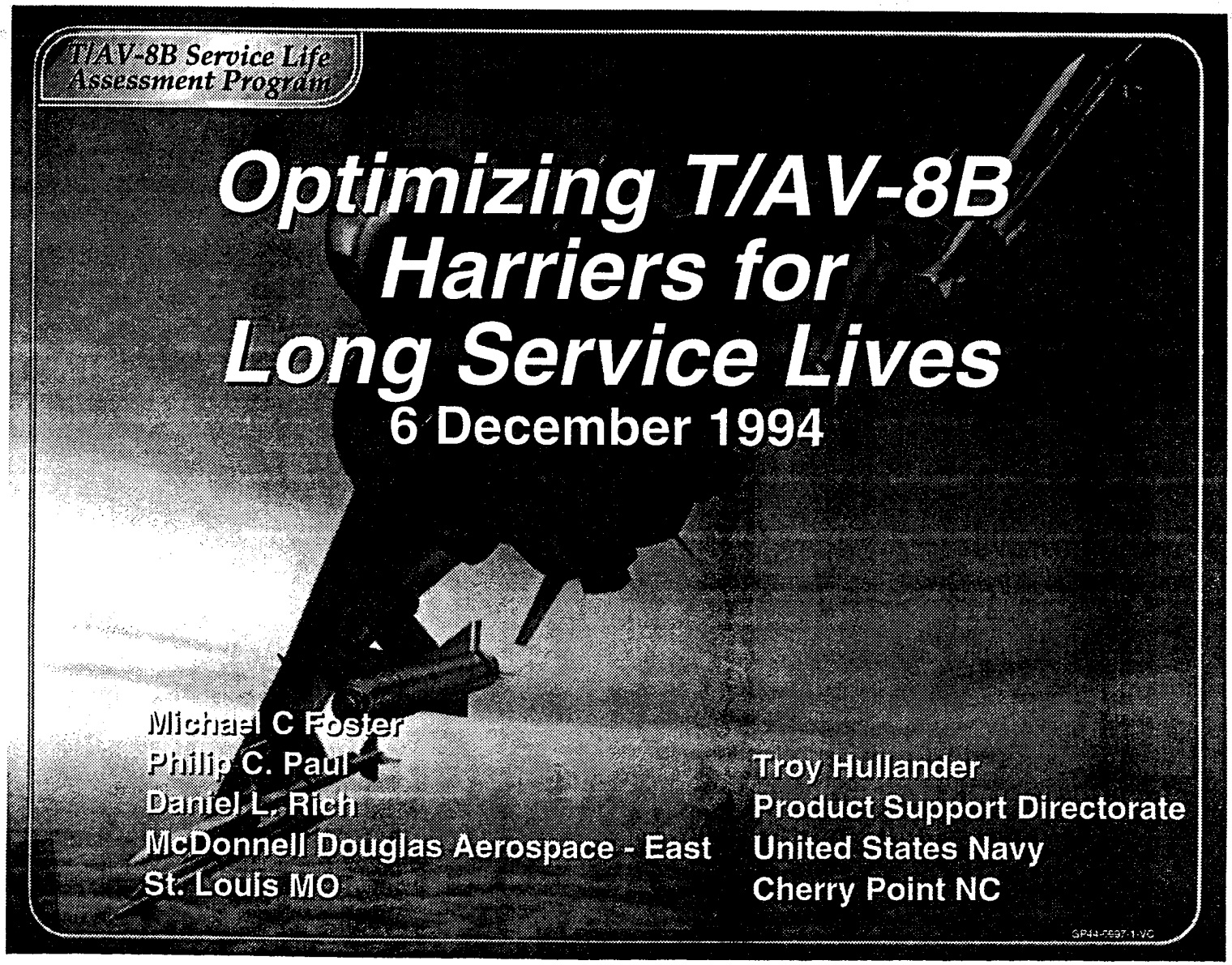
HG7-3-53

CONCLUSIONS

- THE ECONOMIC SERVICE LIFE WILL DEPEND ON OUR ABILITY TO MODERNIZE THE FLEET WITH TECHNOLOGY THAT:
  - IMPROVES STRUCTURAL INTEGRITY
  - RESTORES AVAILABILITY
  - REDUCES COST OF OWNERSHIP
  - MAINTAINS READINESS



TODAY'S AIRCRAFT, FLYING TOMORROW

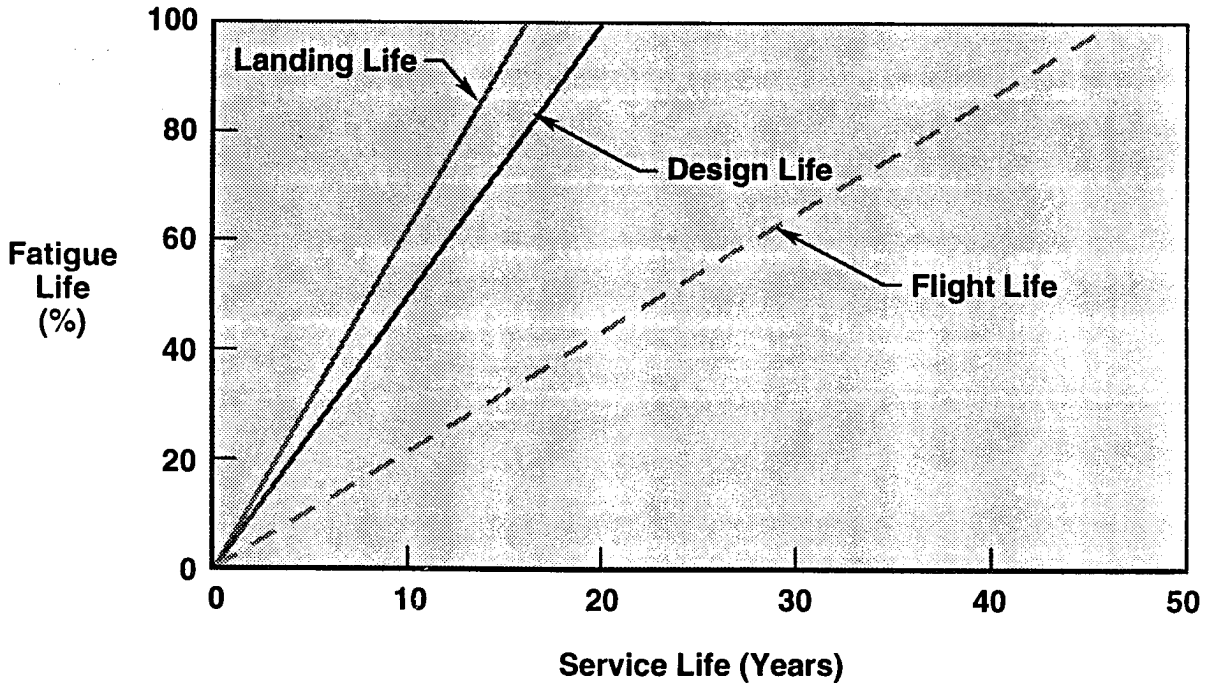

T/AV-8B Service Life Assessment Program
Optimizing T/AV-8B Harriers for Long Service Lives
6 December 1994
Michael C Foster
Philip C. Paul
Daniel L. Rich
McDonnell Douglas Aerospace - East
St. Louis MO
Troy Hullander
Product Support Directorate
United States Navy
Cherry Point NC

Statement of Problem

In 1992, the U.S. Navy initiated the Health of Naval Aviation (HONA) effort. The goal of HONA was for each aircraft program to determine the health of its aircraft and to develop programs to extend the aircraft life to the year 2015. The T/AV-8B was designed for a service life of approximately 20 years, at a usage rate of 25 flight hours per month. Based on vertical load factor exceedances, the NAVAIR Aircraft Structural Life Surveillance Group determined the fuselage and wing should have a substantially longer life than its design requirement. Unfortunately, this could not be utilized to meet the HONA objective, as the fleet aircraft were landing more frequently than anticipated, thus limiting the life of the landing gear, and more importantly the landing gear back-up structure. This study was performed to provide a more accurate (and less conservative) life estimate.

Statement of Problem

Fleet Service Lives



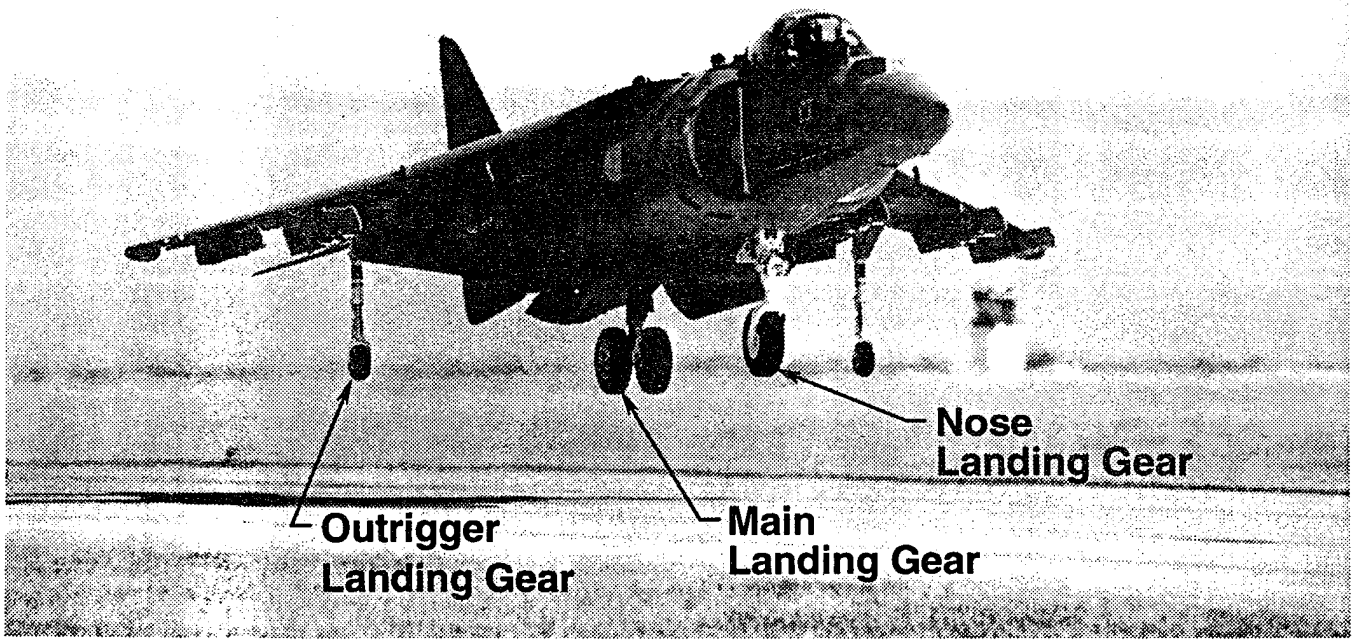
GP44-0997-3-VC

T/AV-8B Landing Gear Systems

The T/AV-8B aircraft have a quadracycle type landing gear consisting of a main landing gear, a nose landing gear, and two outrigger landing gear on the wing. The main and outrigger landing gear have cantilever geometries and utilize oleopneumatic shock absorbers. The nose landing gear has a semi-lever geometry and utilizes a nitrogen supplemented liquid spring shock absorber.

GP44-0997-20-V

T/AV-8B Landing Gear Systems



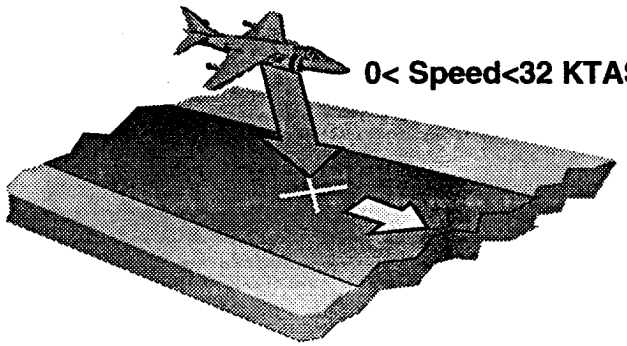
GP44-0997-6-VC

T/AV-8B Landing Types

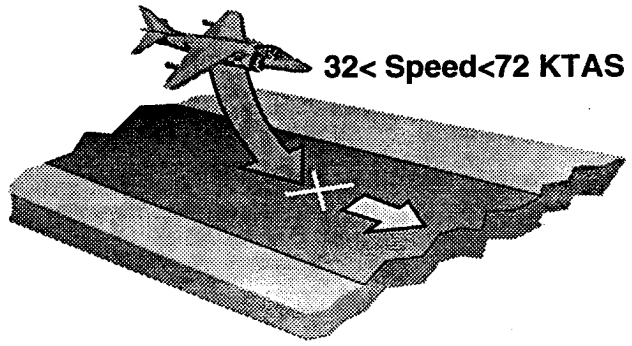
The T/AV-8B has the unique capability to take off and land vertically, in addition to more conventional take offs and landings using vectored thrust. The landings are classified by four different landing types, based on the aircraft's touchdown speed. The types of landings are vertical landings, rolling vertical landings, slow landings, and conventional landings.

GP44-0997-21-V.

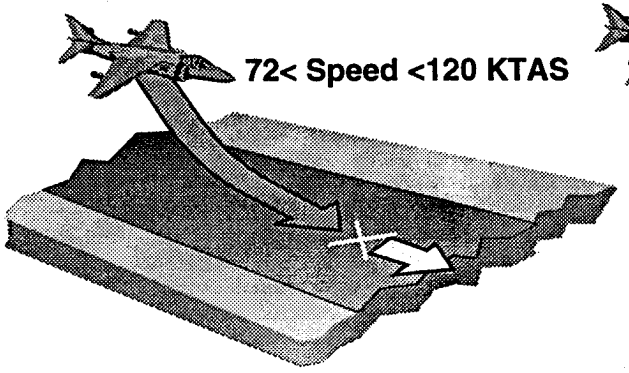
T/AV-8B Landing Types



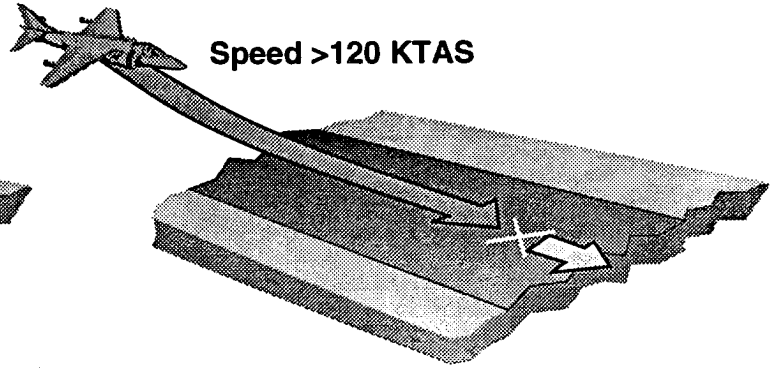
Vertical Landing (VL)



Rolling Vertical Landing (RVL)



Slow Landing (SL)



Conventional Landing (CL)

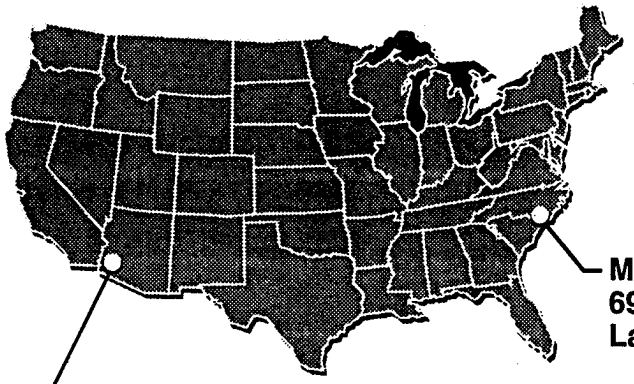
GP44-0997-5-VC

T/AV-8B Fleet Landing Survey

A fleet landing survey was conducted by NAVAIR at MCAS Yuma and MCAS Cherry Point on T/AV-8B aircraft. The survey data were obtained from one of the Fatigue Tracking Files, which contain time histories of flight parameter data and are recorded on the T/AV-8B Data Storage Unit (DSU). This Fatigue Tracking File stores landing parameters, including sink speed, ground speed, vertical load factor, attitude, weight, and aircraft configuration data, for the two seconds prior to weight on wheels at a rate of 20 Hz. Data from over 2000 landings were collected.

GP44-0997-23-V

T/AV-8B Fleet Landing Survey



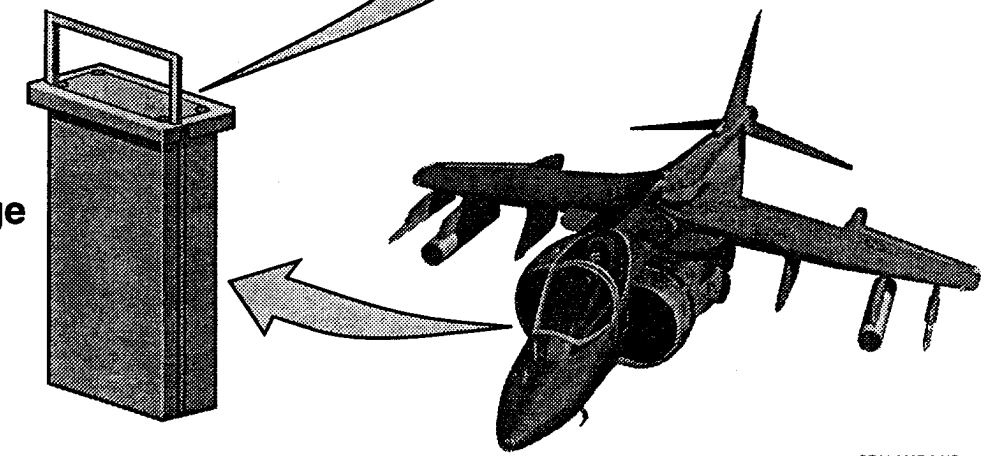
MCAS Cherry Point, NC
694 T/AV-8B Fleet Landings

MCAS Yuma, AZ
1,427 AV-8B Fleet Landings

T/AV-8B Fatigue Tracking Landing File

- Sink Speed
- Ground Speed
- Weight
- N_z
- Attitude

Data Storage Unit (DSU)

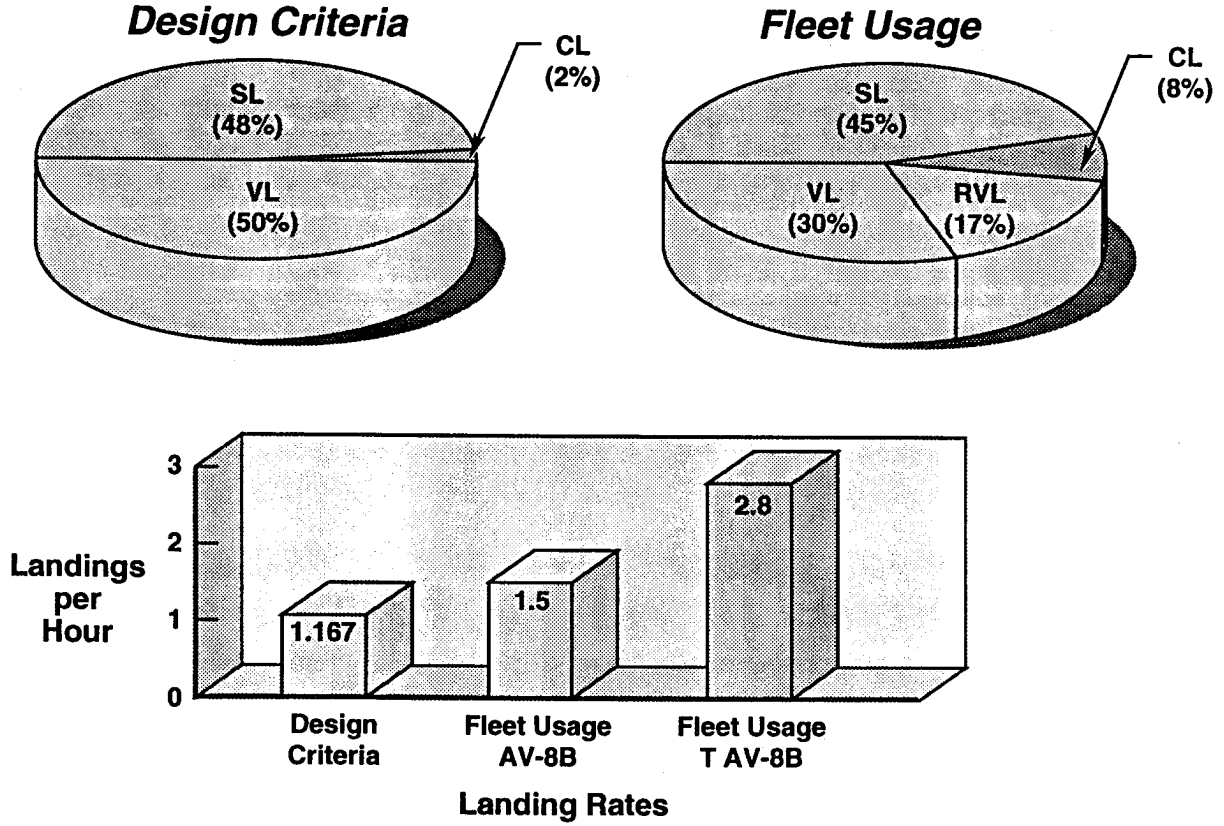


GP44-0997-8-VC

T/AV-8B Fleet Landing Survey Results

Landing type distributions and landing rates were determined as a part of the fleet survey. Unlike the design criteria, the fleet survey included the rolling vertical landing type. If vertical landings and rolling vertical landings are added together in the fleet usage data, then the design and fleet usage distributions compare favorably. However, the fleet landing rates differ significantly from the design criteria. T/AV-8B aircraft are designed for 7000 landings in 6000 hours. The AV-8B's are landing at a rate of 1.5 landings per flight hour, (i.e. 9000 landings in 6000 flight hours). The TAV-8B's are landing at a rate of 2.8 landings per flight hour, (i.e. 16800 landings in 6000 hours). These data indicate the life of the landing gear systems would be expended before the 6000 hour airframe life.

T/AV-8B Fleet Landing Survey Results



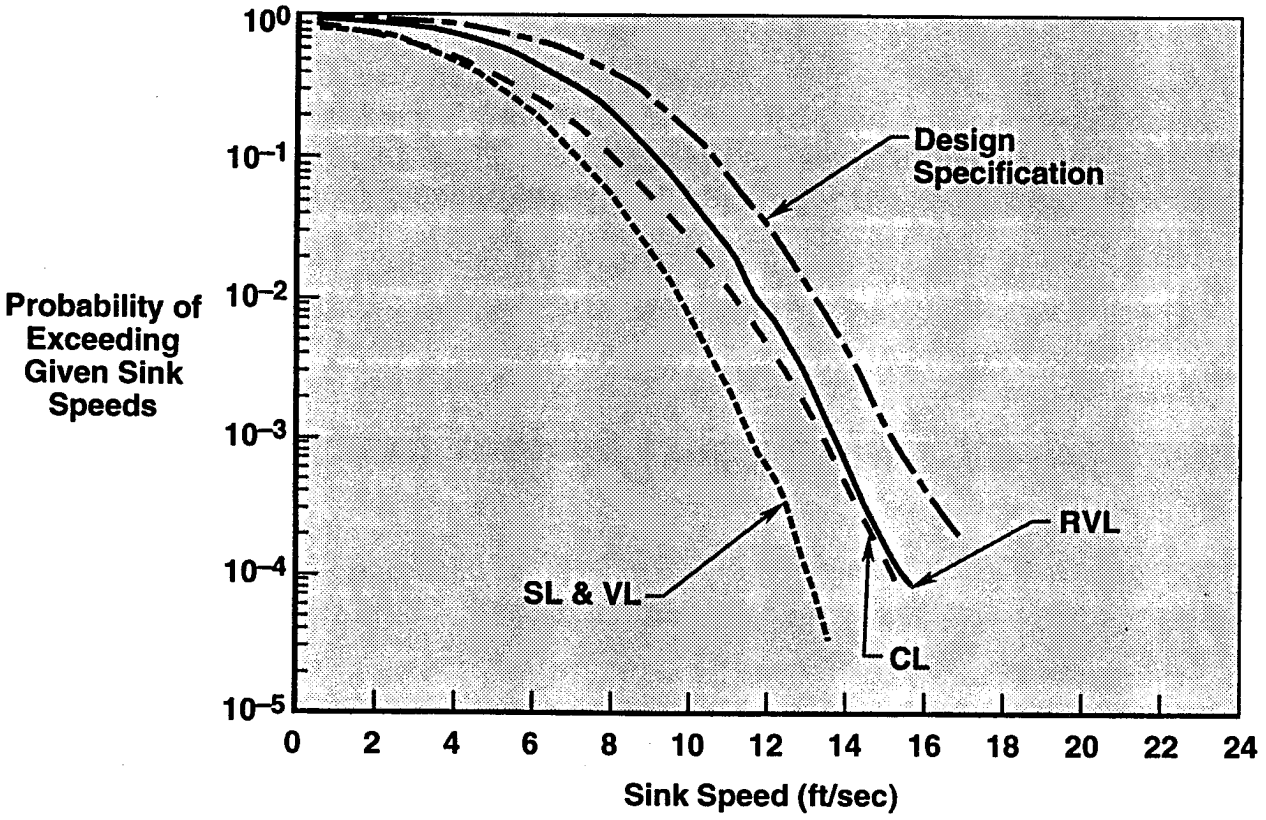
GP44-0997-9-VC

T/AV-8B Fleet Landing Survey Sink Speed Results

Fleet survey data also revealed the aircraft are landing at sink speeds lower than the design criteria. Lower sink speed landings result in decreased loads, and create an improvement in landing gear system life.

GP44-0997-25-V

T/AV8B Fleet Landing Survey Sink Speed Results



GP44-0997-10-VC

Objective

Because the aircraft's landing gear components and support structures determine its life limit, a Structural Life Assessment Program (SLAP) was conducted jointly by NAVAIR and McDonnell Douglas. Its objective was to determine the life limiting component of each gear and back-up structure, and to estimate their fatigue lives based on actual fleet usage. These new life estimates are to be used to optimize future operations and maintenance plans for the T/AV-8B.

GP44-0997-19-V

Objective

- Determine the Life Limiting Component for Each Landing Gear and its Respective Back-Up Structure
- Compute the Estimated Fatigue Life of Each, Based on Actual Fleet Usage
- Optimize Future Operations and Maintenance Plan for the T/AV-8B

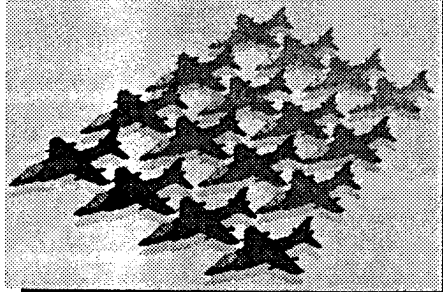
GP44-0997-4-VC

Approach

The approach for this study was as follows. First, a fleet landing survey was conducted. Second, the fleet landing survey data were used to develop fleet usage spectra. Third, the fatigue test article (FTV1) was assessed. Fourth, the fleet fatigue lives were predicted and compared to test predicted lives. Fifth, an Individual Aircraft Tracking method was developed to predict the fatigue service lives of each gear and back-up structure location. Finally, the advantages for the fleet aircraft were determined.

Approach

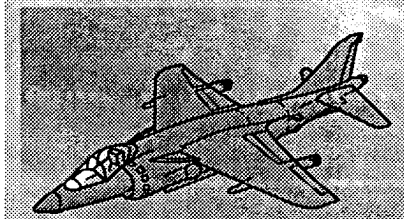
Conduct a Fleet Landing Survey



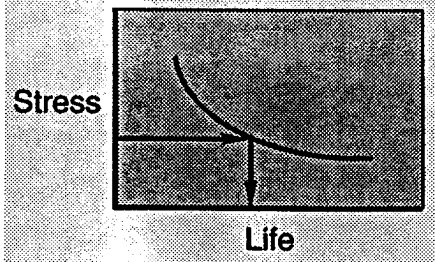
Develop Fleet Usage Spectra

- Landing Type Distribution
- Sink Speed Distribution
- Statistically Established

Assessment of Fatigue Test Article



Predict Fleet Fatigue Lives



Develop Individual Aircraft Tracking (IAT) Method

Life = f(CL, VL, RVL, SL)

Advantages Realized by the Fleet

- More Accurate Fatigue Life Predictions
- Method for Managing Gear Replacement
- Method for Establishing Inspection Intervals

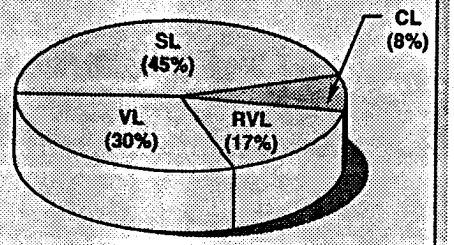
GP44-0997-7-VC

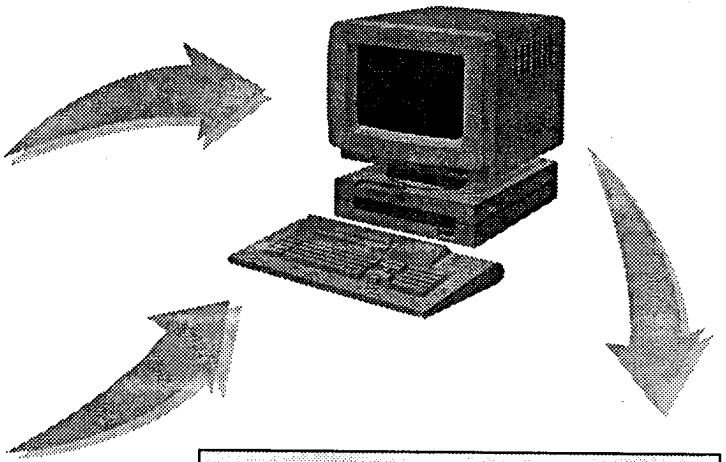
Fleet Usage Spectrum Development

From the survey data, a master event spectrum was developed to represent fleet usage. The spectrum consisted of a repeatable 1000 landings and their corresponding pre-flight and post-flight ground conditions. Stress spectra for each of the critical locations were developed using the master event spectrum.

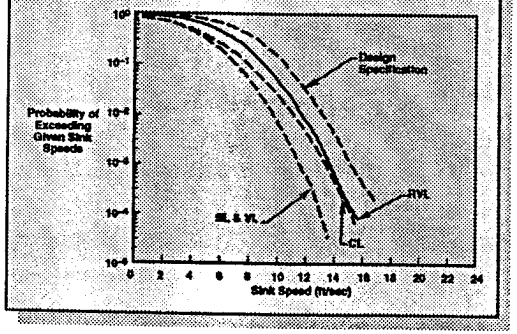
Fleet Usage Spectrum Development

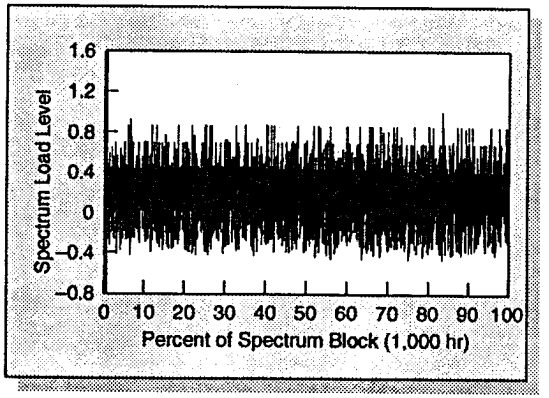
Landing Distibution





Sink Speed Distribution





GP44-0997-11-VC

TIAV-8B Service Life Assessment Program

Test Article Teardown Inspections and Evaluation

The AV-8B fatigue test article (FTV1) was tested for two lifetimes (14000 landings). Additional test phases were conducted to evaluate higher taxi weights, different gear servicing, and growth potential. Periodic inspections were performed during the test to document fatigue cracks.

As part of this study, the back-up structure was subjected to detailed inspections and a teardown evaluation. Fractographic analysis was performed to document crack growth characteristics.

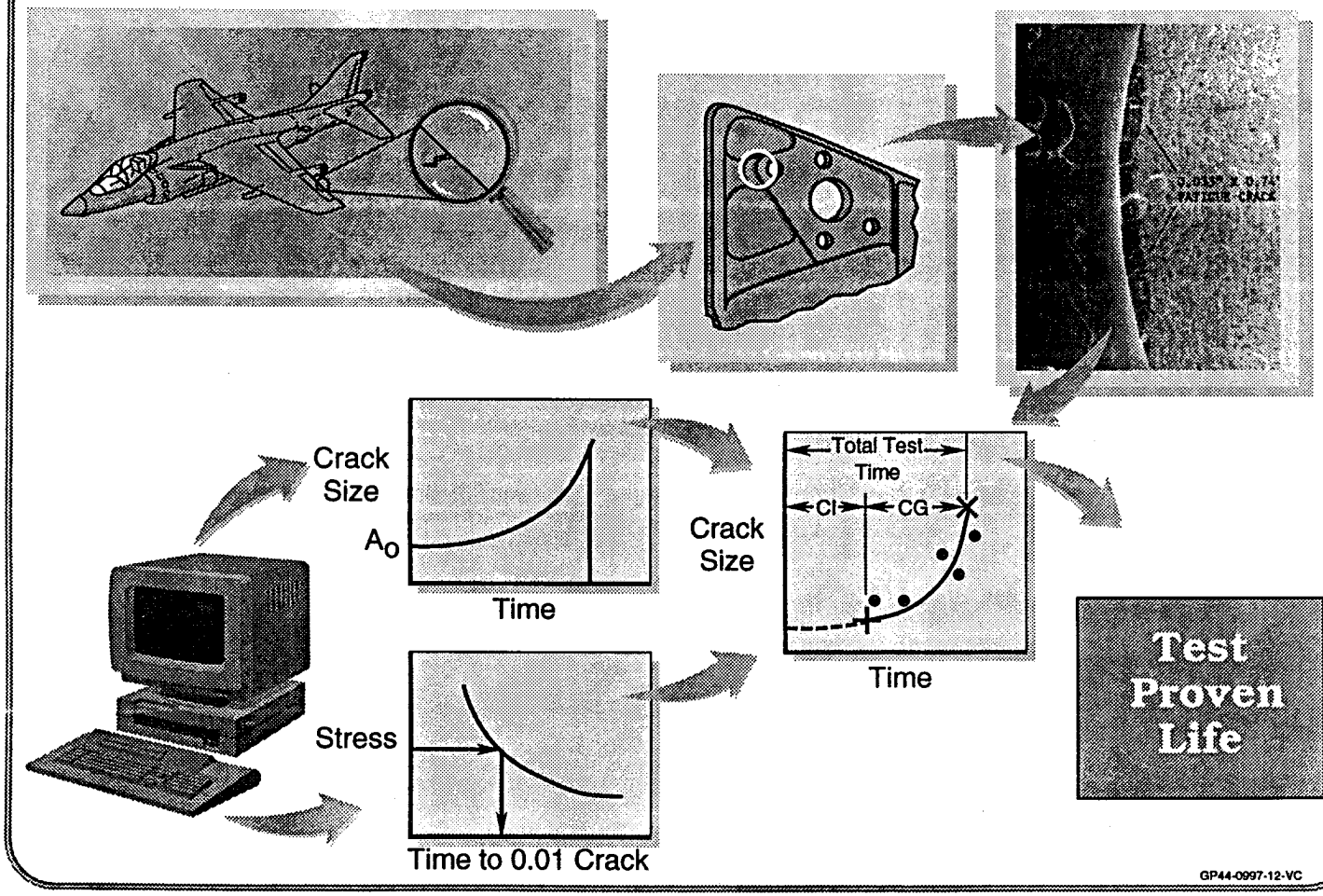
The critical locations of the back-up structure were analyzed to predict the fatigue crack behavior of each location during the test. Specifically, the time to crack initiation and the time to final crack length were identified. This information allowed the test proven life to be determined for each location.

A similar process was used in evaluating each of the landing gear.

GP44-0097-27-V

TAV-8B Service Life Assessment Program

Test Article Teardown Inspections and Evaluation

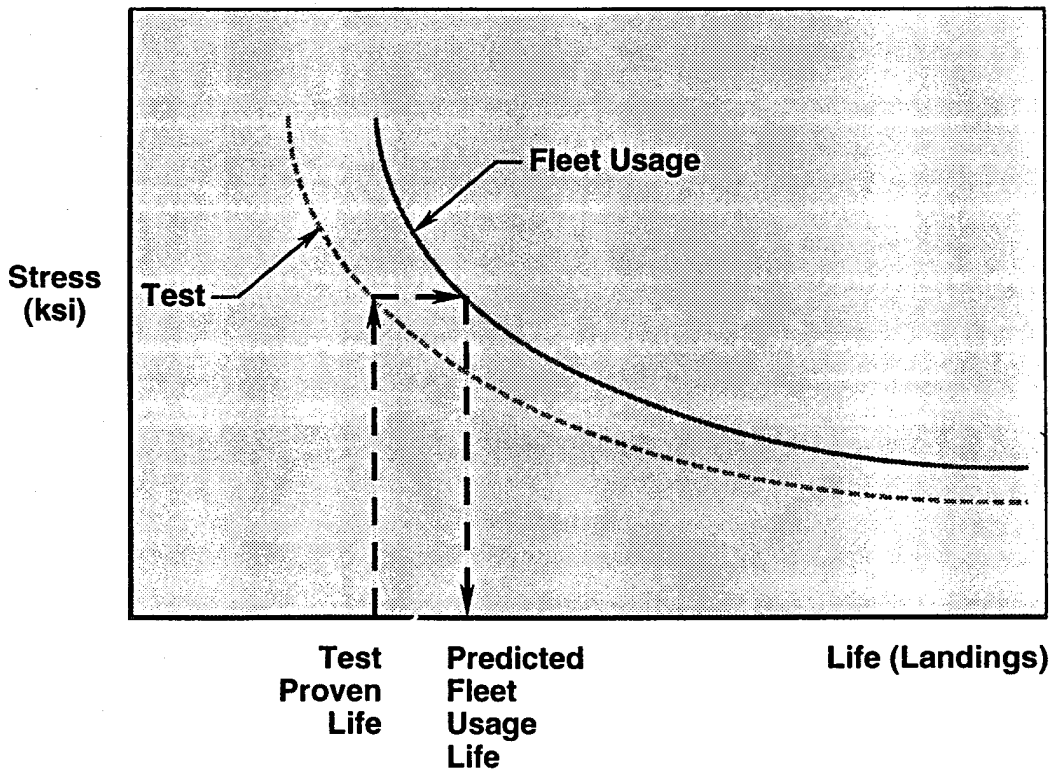


Fatigue Life Predictions

Fatigue life predictions were made for the fleet landing gear and back-up structure. The crack initiation lives (as a function of stress level) were determined at each location for the test spectrum and the fleet usage spectrum. Knowing the test proven lives, the stress levels and the subsequent fleet usage lives were determined.

GP44-0997-28-V

Fatigue Life Predictions



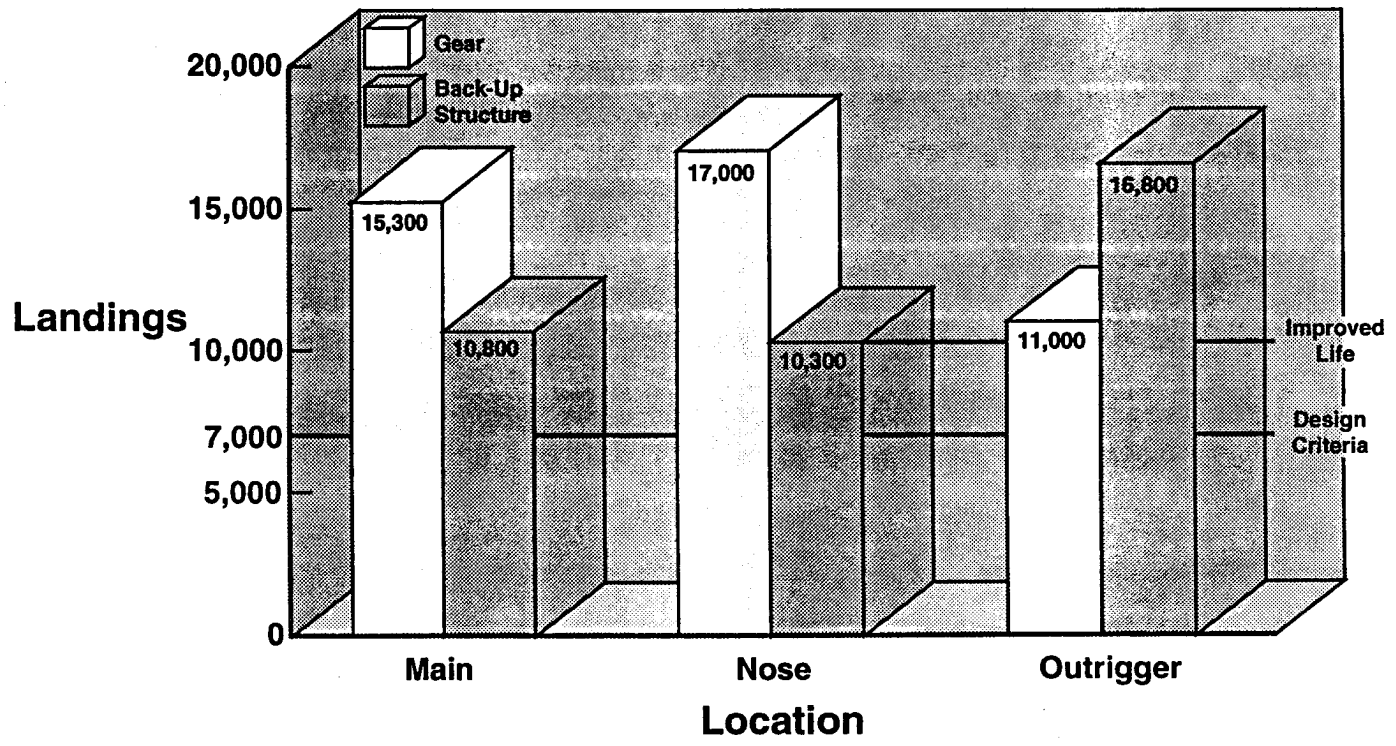
GP44-0997-13-VC

T/AV-8B Fleet Usage Service Lives

A fleet usage service life was determined for each critical location of the landing gear and back-up structure. The fleet usage service lives showed an improvement over the design service lives at all locations.

GP44-0997-29-V

T/AV-8B Fleet Usage Service Lives



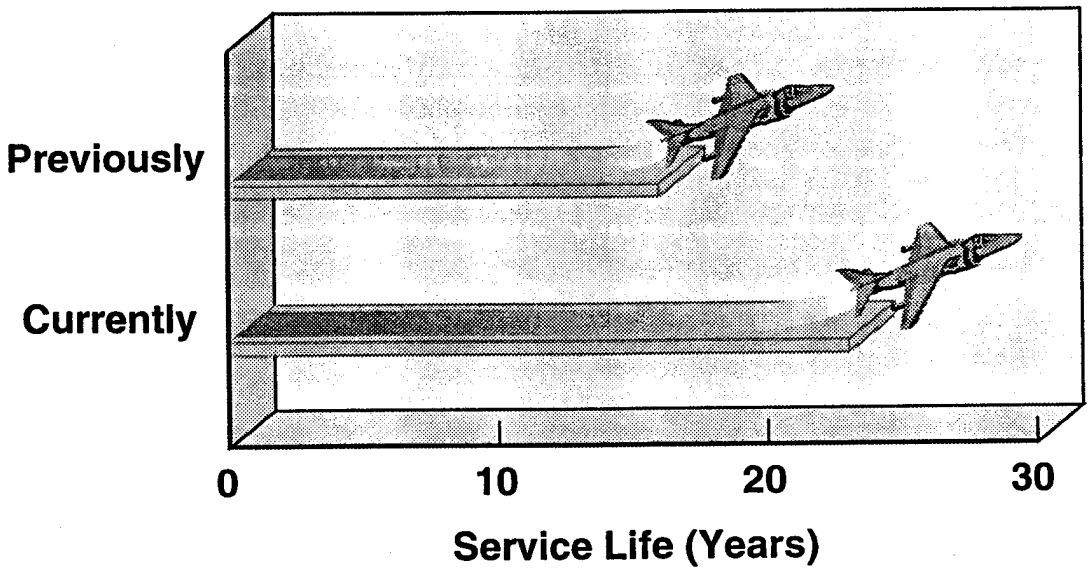
GP44-0997-14-VC

Improved Aircraft Service Lives

Previously, the average fleet aircraft would have used up its landing fatigue life (7000 landings) in 16 years of service. As a result of this study, the expected fleet service life now exceeds 23 years.

GP44-0997-30-V

Improved Aircraft Service Lives



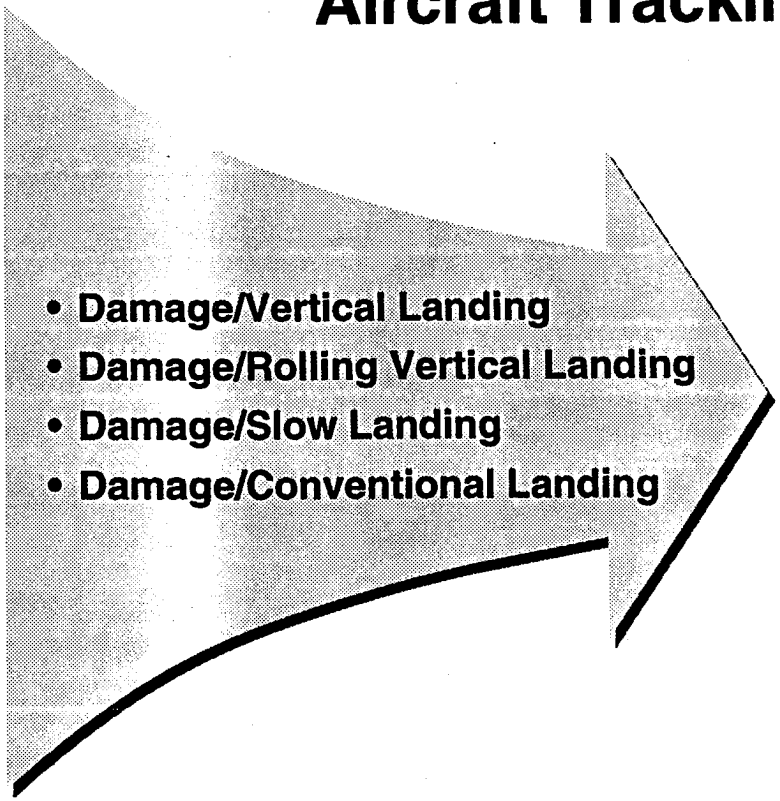
GP44-0997-15-VC

Development of Individual Aircraft Tracking (IAT)

An Individual Aircraft Tracking (IAT) method was developed for the fleet landing gear and back-up structure. The test verified analytical predictions were used in conjunction with fleet usage spectra to determine the amount of damage caused by each of the four landing types. In turn, this information was used to develop Fatigue Life Expended (FLE) equations for each landing gear and back-up structure location. These equations are simply functions of the number of each of the four landing types.

GP44-0997-31-V

Development of Individual Aircraft Tracking (IAT)



- Damage/Vertical Landing
- Damage/Rolling Vertical Landing
- Damage/Slow Landing
- Damage/Conventional Landing

Fatigue Life Expended (FLE) Equations

FLE = f(VL,RVL,SL,CL)

GP44-0997-16-VC

Implementation of Individual Aircraft Tracking

Previously for the T/AV-8B, the number landings was not differentiated by landing type for determining gear and back-up structure fatigue life. The aircraft fuselage and/or landing gear were to be retired at 7000 landings.

As a result of this study, the number landings are differentiated by type. Thus, the Fatigue Life Expended (FLE) equations can be used to ascertain the amount of life remaining. In addition, inspection intervals and gear replacement criteria can be established, based on the FLE calculations.

GP44-0997-32-V

Implementation of Individual Aircraft Tracking

Previously...

- Landings Were Not Differentiated by Type
- Aircraft/Gear Were to Be Retired at 7,000 Landings

Now...

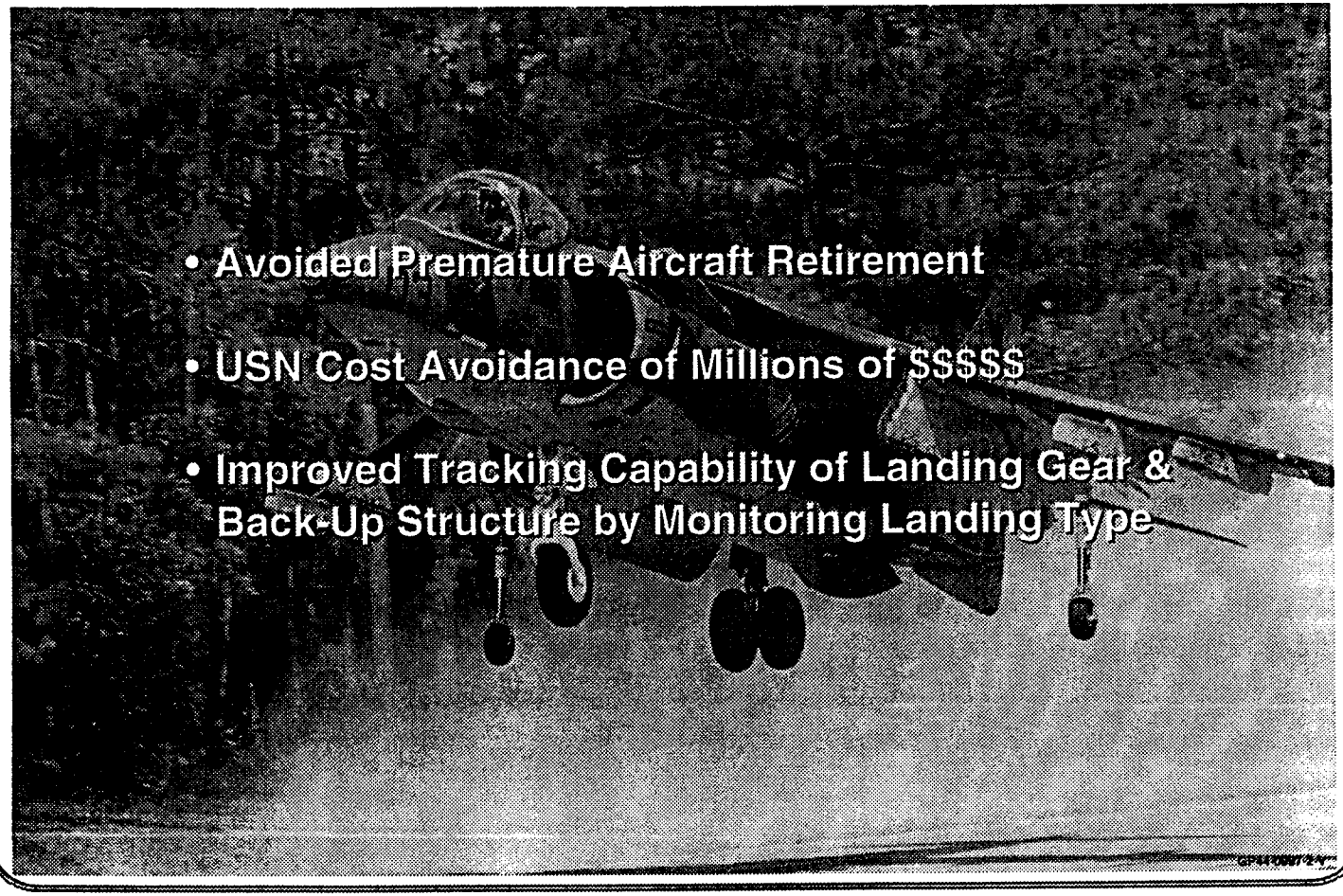
- Landings Are Differentiated by Type
- FLE = f(VL, RVL, SL, CL)
- Inspection Intervals Can Be Established
- Gear Replacement Criteria Can Be Established Based on FLE Calculations

GP44-0997-17-VC

Customer Impact

The results of this study has allowed the U.S. Navy to avoid premature aircraft retirement, and to realize a cost avoidance of millions of dollars. Also, this study provides an improved fatigue tracking capability for the landing gear and back-up structure.

Customer Impact



C-141 Starlifter: ASIP Methodology In An Aging Aircraft Environment

1994 USAF ASIP Conference

San Antonio, Texas

December 6-8, 1994

Joe Cochran
Lockheed Aeronautical Systems Company

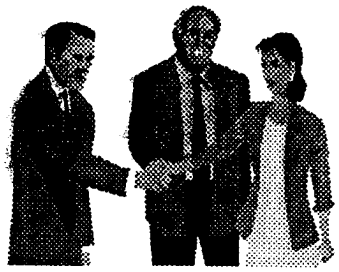
Russ Alford
Warner Robins Air Logistics Center

The C-141 Starlifter is a successful story for ASIP in an Aging Aircraft Environment. From its beginnings in 1968 until the present hour, the C-141 has a remarkable history of structural integrity even though the first 20,000 hours of its service life was based on Miner's Fatigue Methodology. At the 20,000 hour mark, the C-141 underwent a "Stretch" Program to lengthen its fuselage and add aerial refueling capability. At the same time, Fracture Mechanics Methodology became the basis for Service Life Management. From the very outset, a complete and thorough database of service experience was initiated and maintained throughout its service life. Today, the C-141 ASIP Program has evolved into an Individual Aircraft Management System that is operated on a current time database that is near 100% electronic using PC's and Work Station computers. Today's presentation will take the viewer through the C-141 ASIP trail and how today's Aircraft Management Program has evolved.

Preface

Using Command

Prime Manufacturer



Air Logistics Center

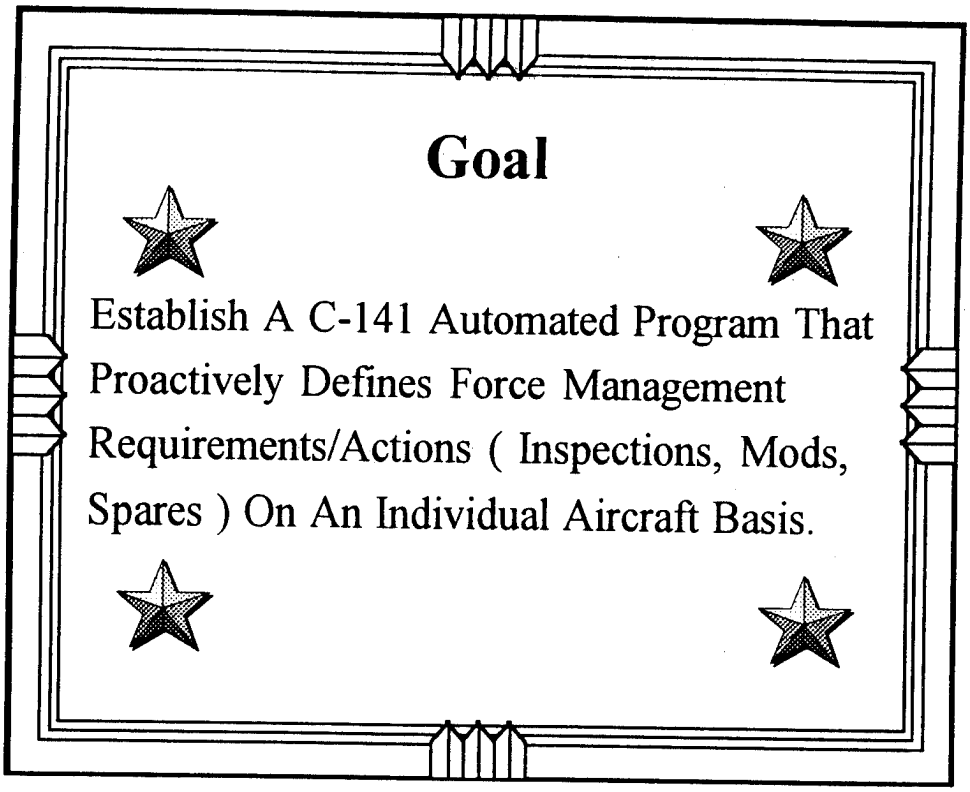
Spirit Of Cooperation

One of the major elements in the success of the C-141 ASIP Program is the spirit or level of cooperation that has been achieved and maintained by the engineering communities of the prime contractor, Air Logistics Center and the using command throughout the history of the C-141. A high level of engineering expertise and credibility was established during the development and production phases and has continued at that level until this present day. Without question, this spirit of cooperation has greatly contributed to the progressive development of an ASIP Program that we feel is at the forefront of related technologies today. Presently, the C-141 community, ASIP Manager and counterparts are expanding and applying the principles of Aircraft **Structural** Integrity to an overall Aircraft **System** Integrity Program. As we continue through this presentation, you will see how this foundation of cooperativeness has played a major role in determining ASIP Methodology in an aging aircraft environment.

Vision

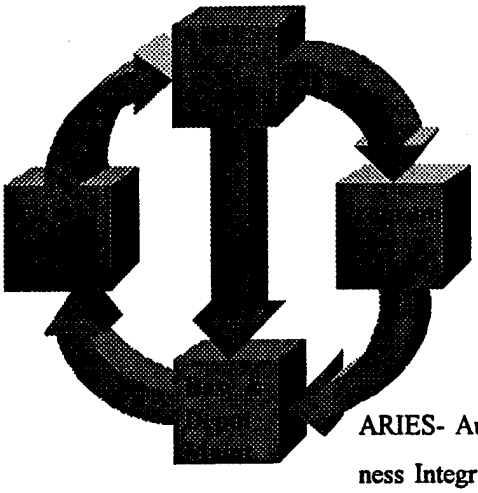
An Automated Engineering Approach To Managing An Aging Aircraft Weapon System, Postured To Respond To The Using Command's Needs Through An All Encompassing Force Management Plan.

During the late 1970s and early 1980s, the C-141 was undergoing a "stretch" modification program as well as a WS 77 mod program for fatigue life extension. As these programs progressed, it became apparent to Engineering that configuration control could become a major problem with regard to the many repairs and inspection requirements that were being generated. It rapidly became apparent that an automated process would be required if force management on the individual aircraft level was to be accurate and pro-active. In the following years, force management from the ASIP Manager's viewpoint was becoming more and more a bookkeeping nightmare with all the various interface requirements between multiple databases. As a result, an Automated Readiness Integrated Engineering System (ARIES) was envisioned and the concept presented to C-141 management for approval.



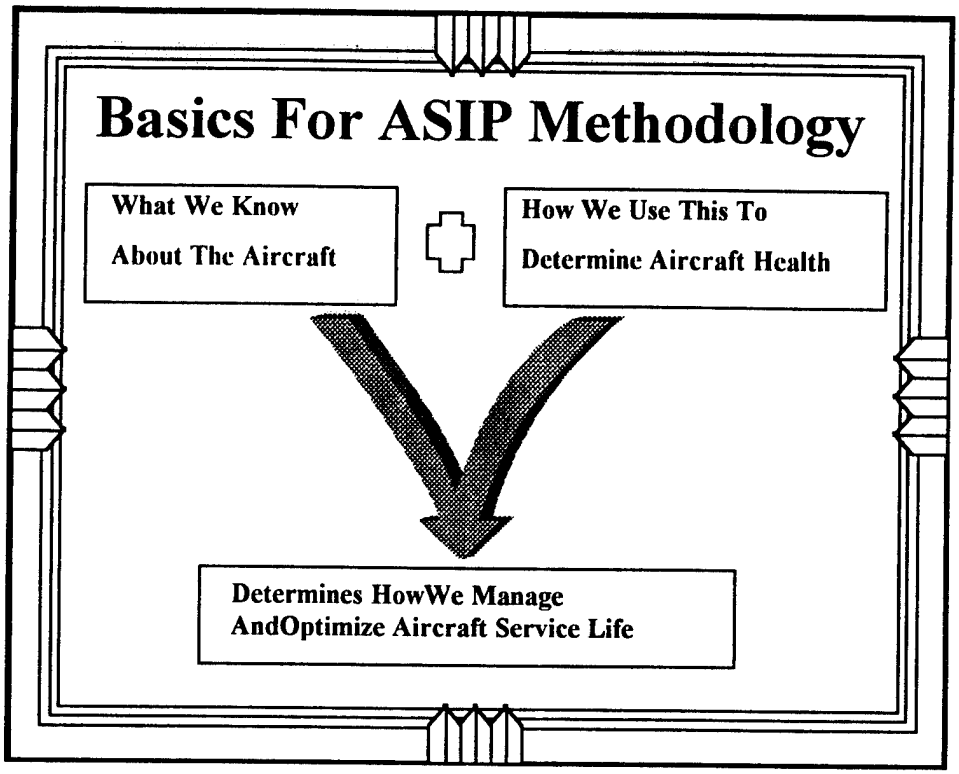
Having received approval all the way through the Logistics Command, goals were established and a time table set up to accomplish development and implementation of the ARIES Program. Scheduled as a five-year development program, ARIES would become a database management tool whereby the ASIP Manager would be able to address force management issues ranging from engineering to production, including spares and cost of repairs/maintenance actions. The basic program goal was to tap into Air Force data systems such as GO81 and other remote data sources, bring into the ARIES control center, and process the data into meaningful reports on an almost real time basis. The entire system works interchangeably with VAX, Workstations, and personal computers.

Objective

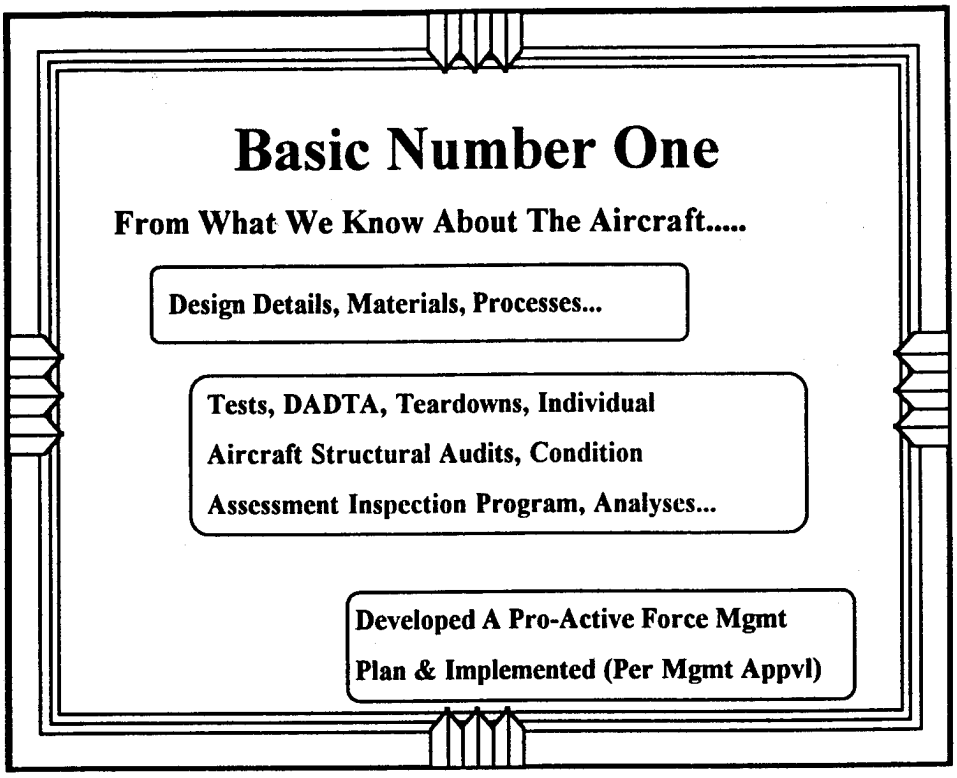


ARIES- Automated Readiness Integrated Engr. System

Overall objective of ARIES is to provide the ASIP Manager with a tool whereby he can readily, on a daily basis (if required), manage the C-141 force or individual tail numbers by using information as current as the raw G081 data and/or base/depot maintenance data to keep Program Management statused on a near real time basis.

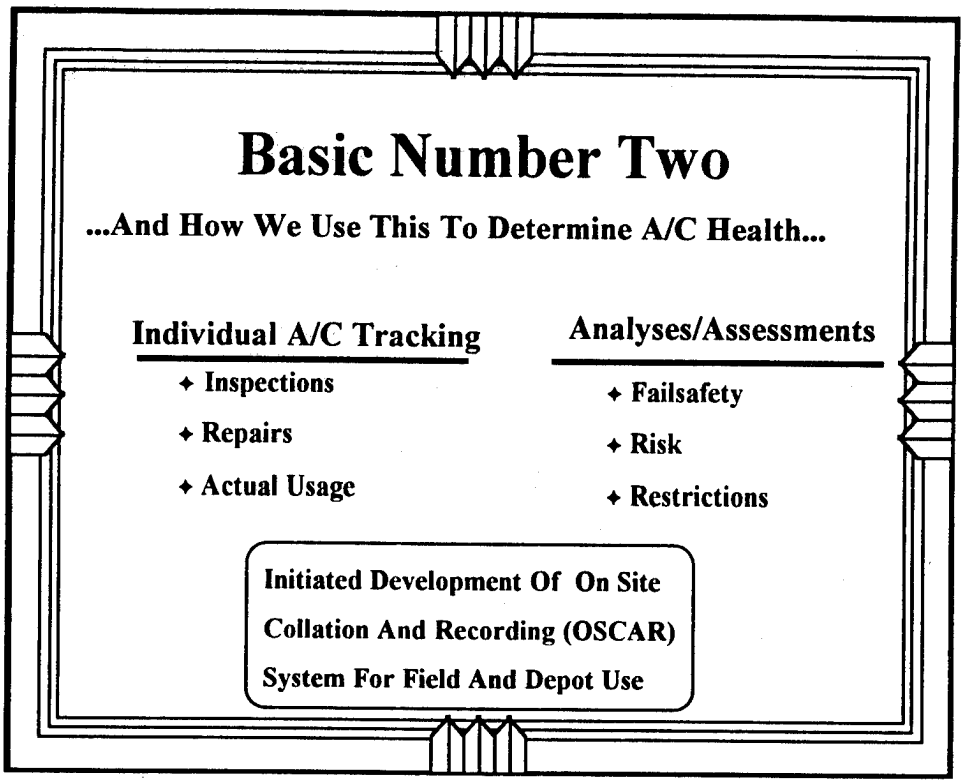


According to MIL-STD-1530A, there are five tasks that define the basics for any Aircraft Structural Integrity Program (ASIP). Actually, these five tasks are the ingredients of any integrity program. A broader scope of ASIP methodology can be defined by (1) what we know about aircraft, plus (2) how we use this knowledge to determine aircraft health for the purpose of (3) deciding how we manage the aircraft for optimized service life. These three basics are a continuing process on the C-141 that has evolved into an overall Aircraft System Integrity Program (ASIP). Time does not permit a full discussion of these basics, but the next three slides should give us a knowledgeable insight to how we have gotten to where we are today on the C-141.



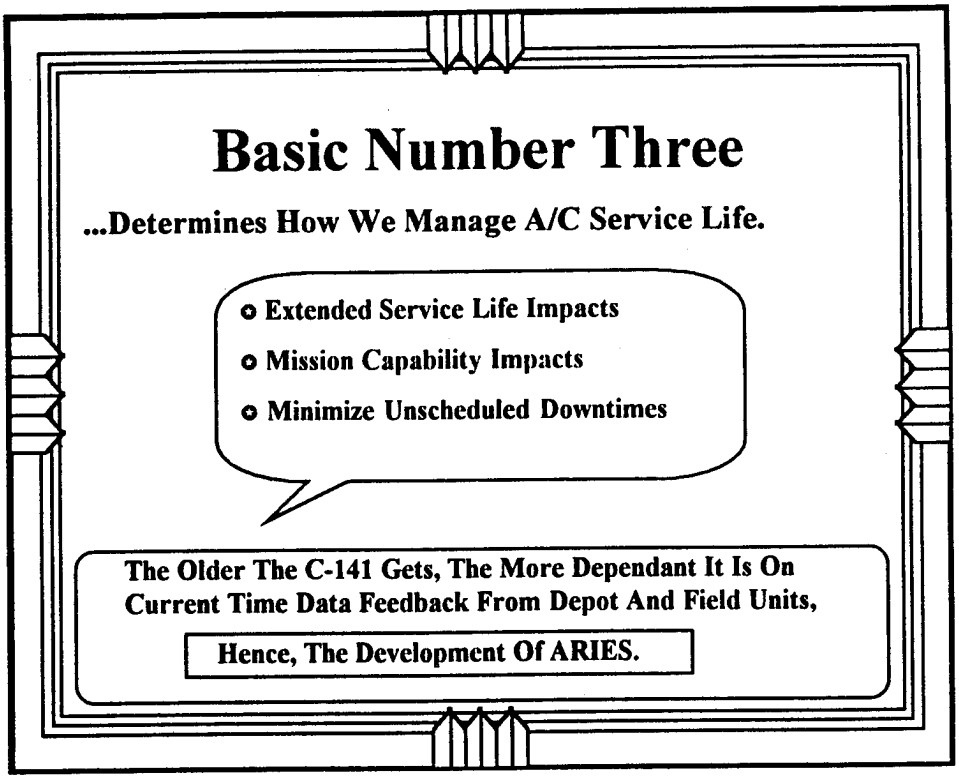
Understanding the aircraft is essential to any successful ASIP program. Original design details, materials and their properties, and manufacturing processes are key elements to a good, manageable corrosion control plan as well as an effective individual aircraft tracking program.

Throughout the life of the C-141, a wealth of data (that continually enhances our knowledge about the aircraft) has accumulated through tests, assessments, teardowns, and audits (structural and functional) from which the ASIP Manager is able to develop (and continuously update) a pro-active force management plan. The tools that enable him to do this leads us to the next chart.



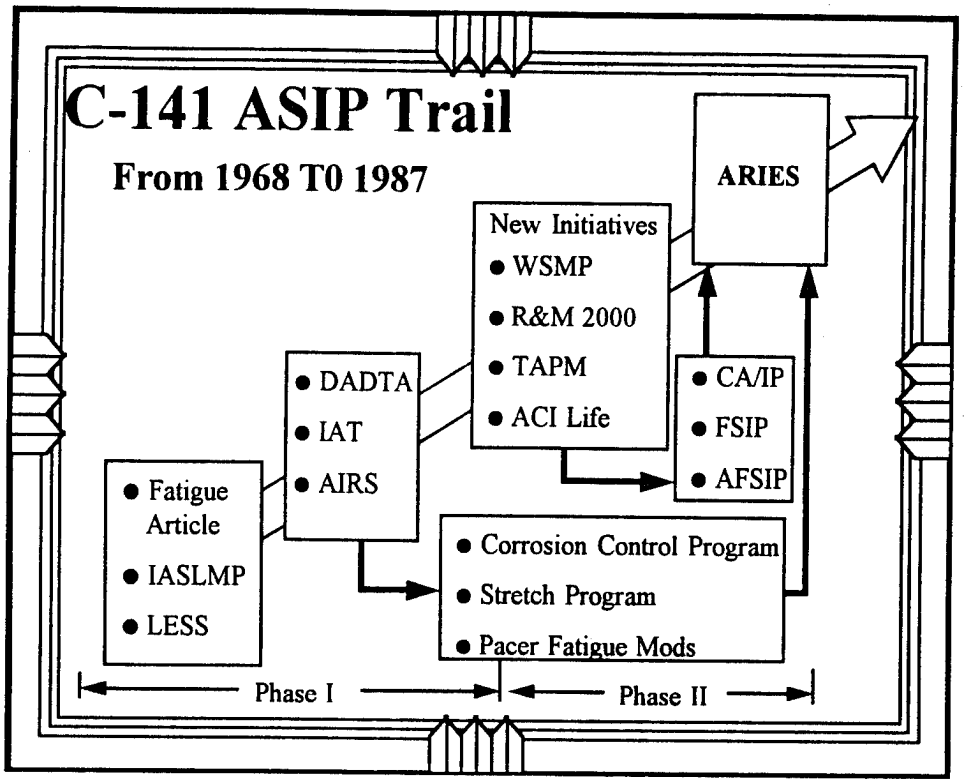
With such a large database at the ASIP Manager's disposal and with the incorporation of an Individual Aircraft Tracking Program (IATP), timely inspections are performed to insure that the aircraft is structurally safe. In a broadening of the IATP, the C-141 now includes corrosion tracking, repair tracking and will soon incorporate systems tracking under its Functional Systems Integrity Program (FSIP).

Through the years, the C-141 ASIP Manager has systematically updated the loads environment programs based on actual usage including severe operational environments. This has further enhanced the accuracy and predictability of the analyses and assessments that on occasion may result in risks determination and/or operational restrictions. But even with all this capability, the ASIP Manager must depend on accurate data feedback from field and depot. To provide this feedback, a data collection system known as On Site Collation And Recording (OSCAR) is being developed.



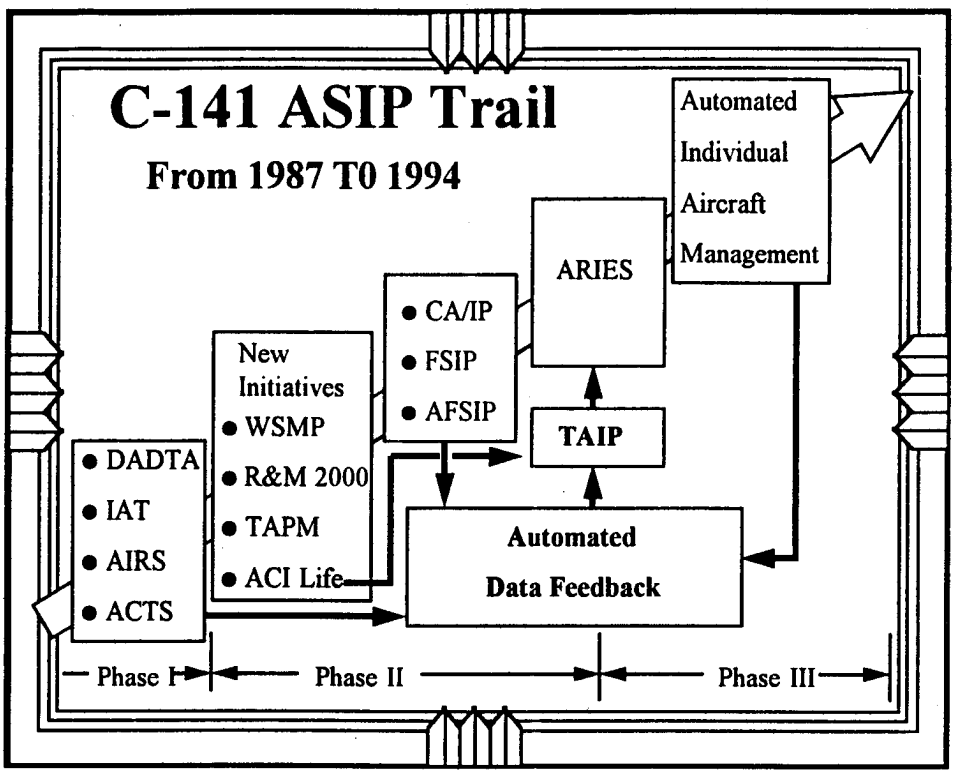
Having the required data and knowing how to use the data through effective tracking programs, the ASIP Manager is adequately equipped to determine the course of action needed for an optimized aircraft service life. The more accurate and the more readily available the data, the easier it is to determine various impacts that affect service life and the way the aircraft is managed. One of the most significant benefits is the minimization of unscheduled downtimes.

However, the more data you acquire the more analyses and dissemination you have to accomplish. The solution that the C-141 has undertaken to handle such a large spectrum of data is an Automated Readiness Integrated Engineering System (ARIES). With this computerized system in place, the C-141 database is as near to real time as data is current.



The C-141 ASIP trail has been a continuous, highly active series of activities aimed at developing a program of data collection, dissemination, and force management. These next two charts graphically depict the major activities that have contributed to the ASIP development from 1968 until the present. Many of these activities are continuous in action and application.

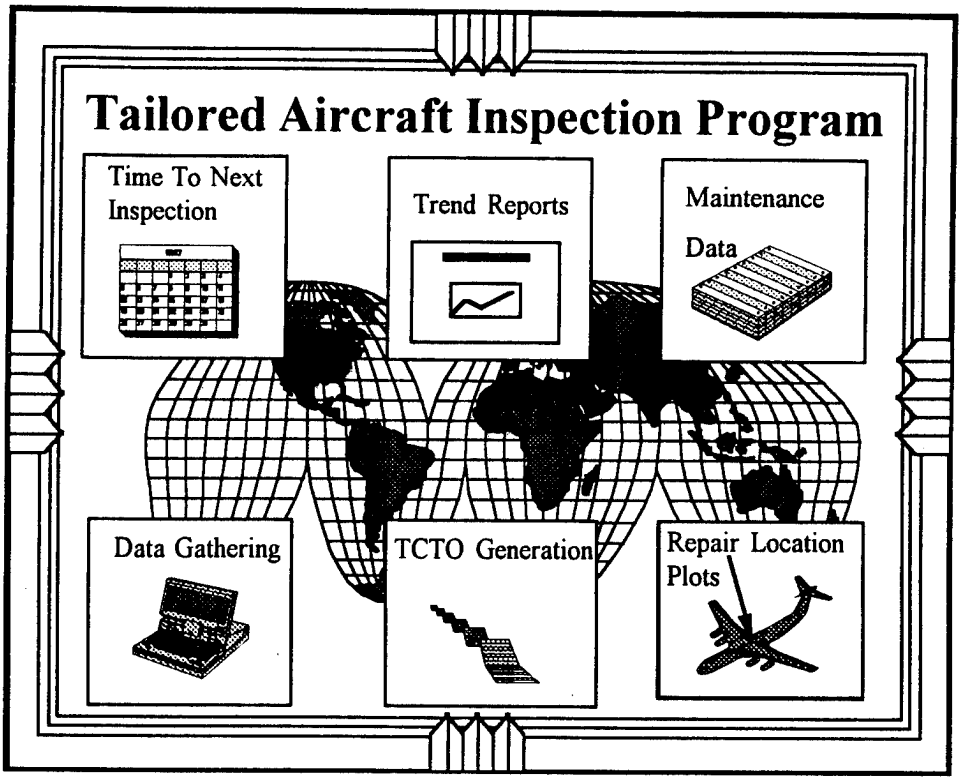
From day one, data collection has been high on the priority list beginning with the fatigue test article, Individual Aircraft Safe Life Monitoring Program (IASLMP) and the Loads Environment Spectra Survey (LESS) programs. A Durability and Damage Tolerance Assessment (DADTA) conducted during the 1970s led into an Individual Aircraft Tracking (IAT) program which in turn necessitated the development and implementation of an Aircraft Information Retrieval System (AIRS) to provide for massive data storage and dissemination.



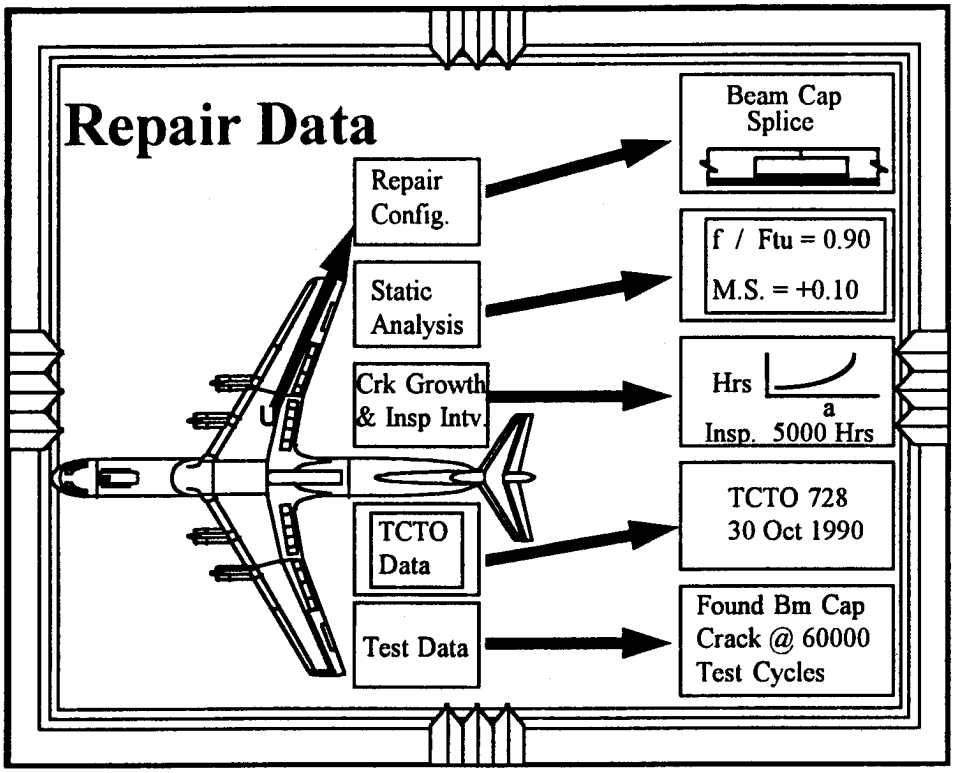
Another by-product of the DADTA was the development of an Aircraft Corrosion Tracking System (ACTS) to specifically gather corrosion data that could be converted into an indexed prediction of corrosion susceptability of part, component, or system.

With the introduction of new Air Force initiatives, the C-141 initiated a Functional System Integrity Program (FSIP) to parallel the ASIP program. Baseline data was obtained by the teardown of ten aircraft systems on sixteen aircraft through a Condition Assessment/Inspection Program (CA/IP). Evaluation of the data led to the establishment of an Aircraft Functional System Instrumentation Program (AFSIP). Today A/C 66-0202 is instrumented with sensors and other measurement devices to provide actual usage data for aircraft systems.

Combining both ASIP and FSIP data has prompted the development of a Tailored Aircraft Inspection Program (TAIP) that can be fed into ARIES, which in turn provides the ASIP Manager with automated aircraft management capability.

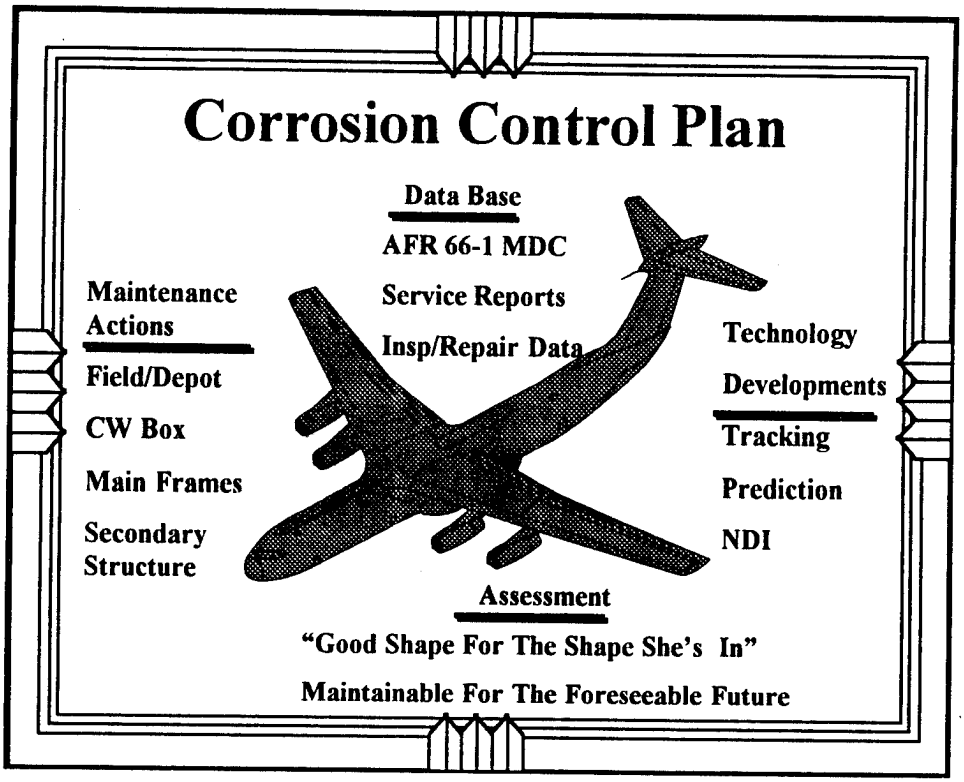


The TAIP is a powerful tool for the ASIP Manager. As depicted in this chart, the tremendous amount of data now available can be used to optimize inspection frequencies (even to PDM scheduling), perform trending analyses (i.e., spares forecasting), provide requirements for TCTO generation, and provide repair location plots (probably the most useful aspect of all). With over 30,000 repairs documented on the C-141 force, the ability to see where they are located by tail number at the push of a button provides the ASIP Manager with an heretofore non-available capability. A further extension of this unique capability is depicted on the next chart.

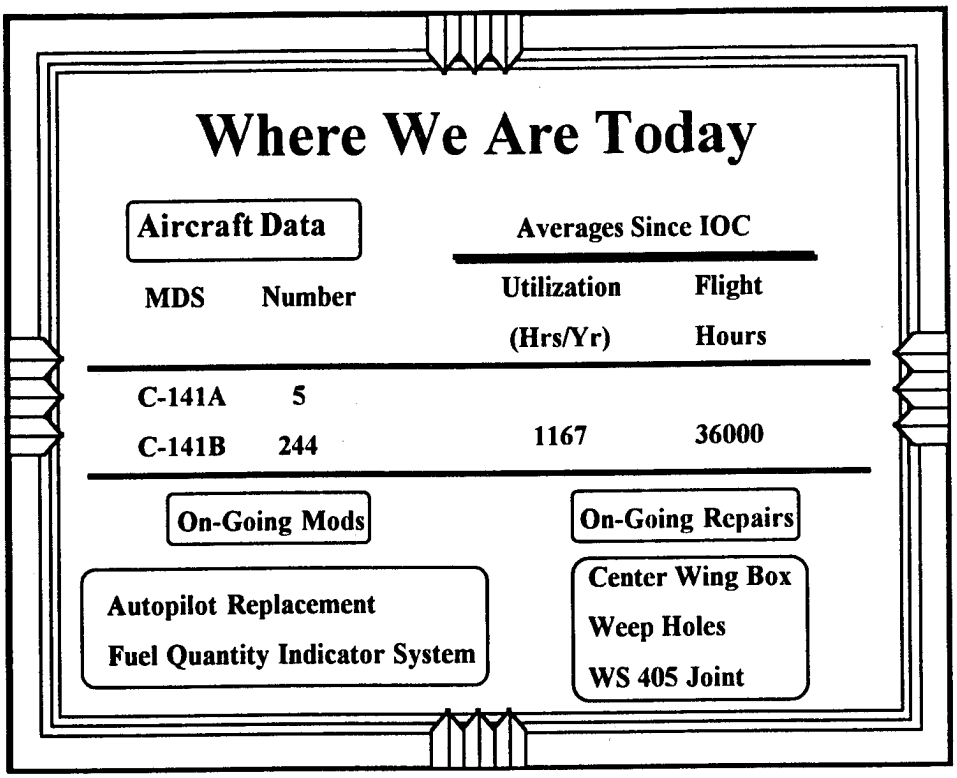


The TAIP tool on repairs provides more than just location. The Repair Data element of TAIP is a fully automated interactive data base that can be viewed on personal computers through very user-friendly ICONS and dialog box selections. Not only can the user see where the repair is located, but configuration, analysis data, inspection information, TCTO data, and related test data can be displayed if required and/or applicable. In today's environment of aging aircraft, a tool such as TAIP is imperative for optimal force management as the aircraft approaches the end of its service life.

The C-141 TAIP is not limited to structural repairs, but steps are already being taken to incorporate systems repairs/replacements as the FSIP matures in the footsteps of ASIP.



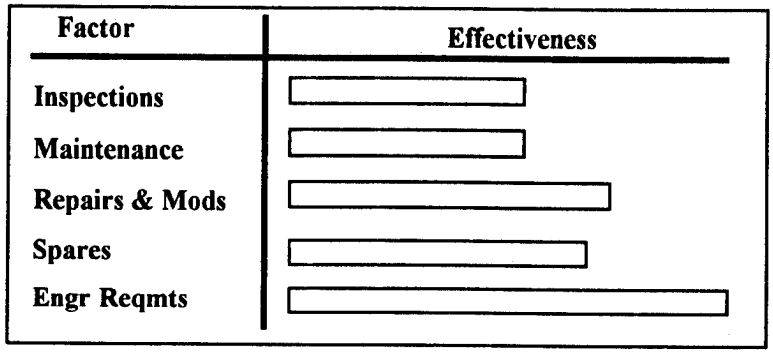
The C-141 has had a corrosion control plan in place since entering service. The plan was based on then known technologies. As processes change or are influenced by "in use" findings, the corrosion control actions are altered to compensate. The corrosion data base is mostly found in documentation such as AFR 66-1, service reports, and inspection/repair data. Corrosion is continuously addressed in the field and at depot. As the C-141 ages, corrosion begins to demand more time in inspection and corrective actions. As a tool for the ASIP Manager, Lockheed was tasked by WR-ALC to develop and implement a corrosion tracking and prediction program. This program is active today on the C-141, but like any tracking program, is heavily dependent on feedback of actions taken in inspections and/or repairs. One of the real challenges today is the development of reliable NDI techniques for corrosion detection in hidden areas. Considering her age, the C-141 is in good condition in regards to corrosion.



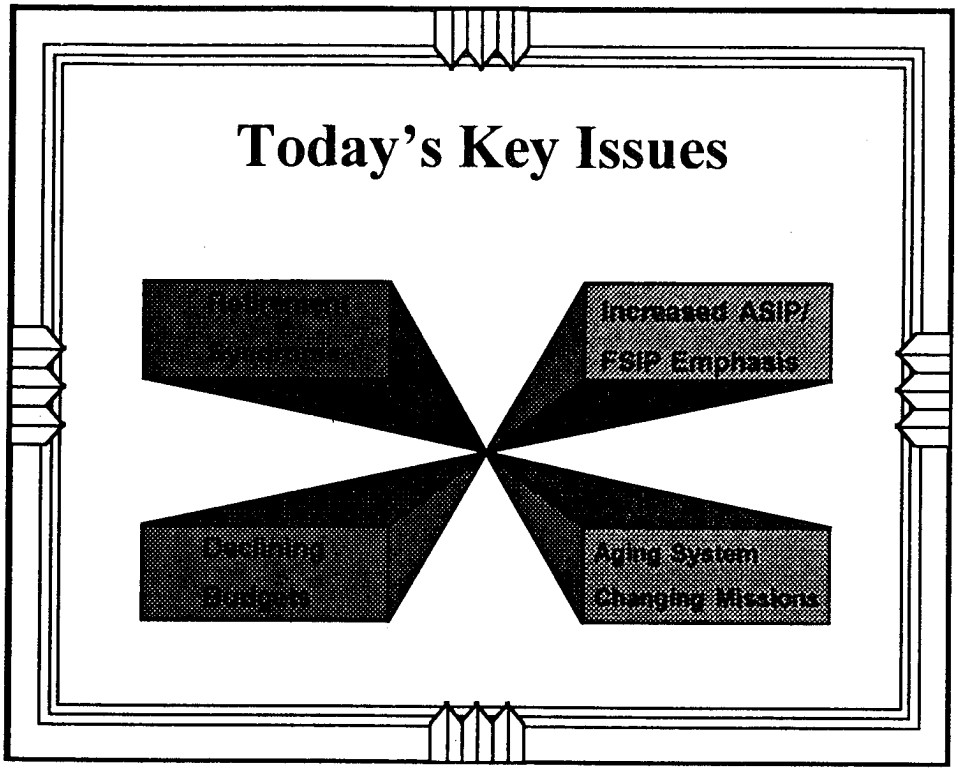
The C-141 original force structure was 285 aircraft. Today there remains 5 C-141A models and 244 C-141B models. The B models have averaged approximately 1,200 flight hours per year utilization, accumulating an approximate total of 36,000 flight hours. The high time aircraft still in service has 41,315 flight hours, the low time aircraft 17,270 flight hours. Drawdown of the force has started with 20 aircraft retired over the last two years. Current drawdown schedules show the aircraft in service into the year 2006. Because the C-141 is the current workhorse (core) airlifter of the Air Mobility Command (AMC), repair programs and modification programs are an active part of the daily force management.

C-141 Score Card

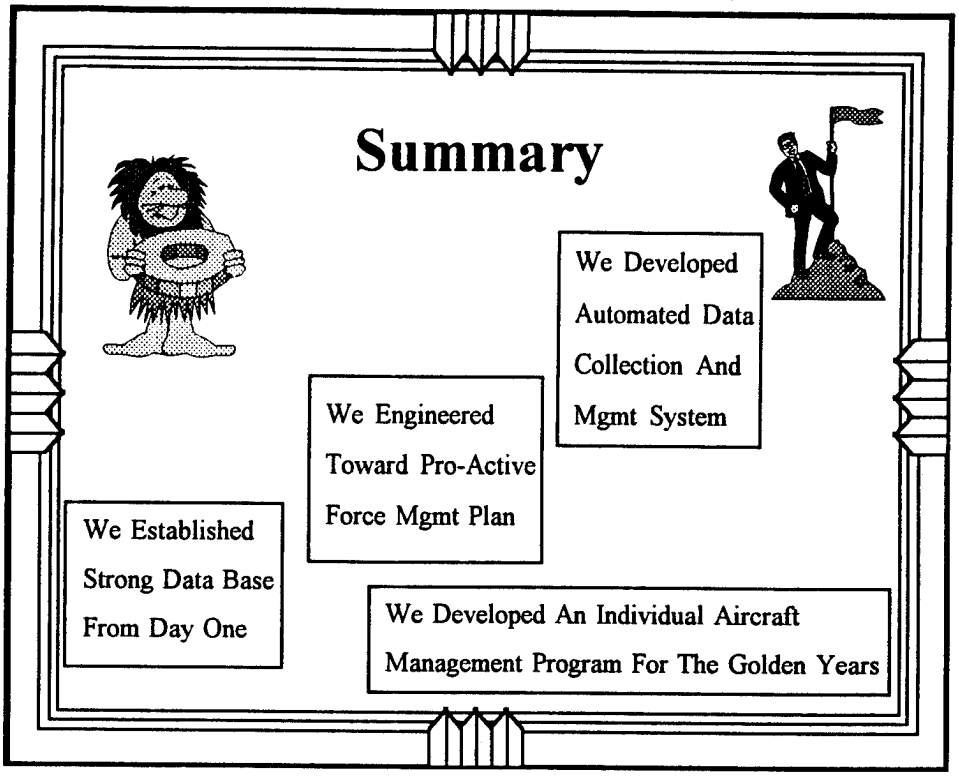
In Light Of The Foregoing, Is The C-141 A Success Story In Aging Aircraft Force Management?



As the C-141 nears the end of its service life, one might question the effectiveness of ASIP and the role it has played in life of the aircraft. This chart is presented only in a relative sense in that the factors shown here are not all that could be evaluated. However, there is no reason why such an effectiveness could not be determined as a means to answer the primary question of success. The C-141 ASIP Manager and his supporting engineering community are probably the ones to "score" ASIP effectiveness in that they have access to the required data, and providing that they have armed themselves with said data as described in the foregoing charts of this presentation.



The issues depicted on this chart are real for any aging aircraft. The retirement syndrome has a negative influence on the need to continue sound maintenance actions as long as the aircraft is in service. Declining budgets also have a negative impact on force sustainment. As the system ages, there is greater need for emphasis on ASIP and FSIP in order to maintain the operational capability and to address the impacts/effects of changing mission requirements.



In summary, the C-141 has a success story in ASIP applications. From day one, a strong and comprehensive data base was established (and continuously updated) from which it was possible to develop and implement a pro-active force management plan. As the data base grew and the force management activities increased, automation in data collection and dissemination was developed to such a high level that it is possible today to individually manage each C-141 to its day of retirement. As a closing statement, the C-141 ASIP Manager has had to learn to broaden his responsibilities to include the systems in the integrity process. In doing so, he has postured himself to provide the user with a more cost effective aircraft system capability that even may result in additional years of safe usage.

SESSION II

ANALYSIS AND TESTING

Chairman: *J. Rudd*, WL/FIB

PROBABILISTIC INSPECTION STRATEGIES -- A KEY TO CONTROLLING MULTI-SITE DAMAGE

Abraham Brot
Engineering Division
Israel Aircraft Industries
Ben-Gurion Airport, Israel

SUMMARY

A simulation method is described which provides strategies for optimum scheduling of structural inspections. The aim of the method used is to simulate the aircraft service life and to determine the probability of failure for various NDI methods and schedules. The simulation method studies the effects of mean service life, damage-tolerance methodology, inspection thresholds and customized inspections on the probability of failure. The multi-site damage phenomenon is studied in detail and the simulation method is used to recommend strategies for controlling failures.

1. INTRODUCTION

Cracks will eventually develop at critical locations of aircraft structures. These cracks propagate and, unless detected and repaired, will eventually result in a failure. There are three, mutually exclusive, possible outcomes of the fatigue process:

(1) The aircraft may reach the end of its operational life and be retired from service. The retired aircraft *may or may not have* undetected cracks at critical locations.

(2) A crack may be detected during maintenance operations. The affected part is usually repaired or replaced.

(3) A crack reaches its critical size undetected and the structure fails in service.

It is the goal of the fatigue engineer to minimize the probability of failure during the service life. Damage-tolerance methodology serves this purpose by requiring or encouraging the following:

(1) Moderate stress levels resulting in long crack initiation and propagation lives and large critical crack lengths;

(2) rationally determined NDI methods and intervals;

(3) fail-safe or crack-arrest design features to avoid catastrophic failures.

However, over the past 10-15 years, a trend has developed in which aircraft are being operated much longer before retirement. For many aircraft models, high-time aircraft greatly exceed original design life goals (Reference 1). With increased service usage, the NDI methods and intervals originally specified, may prove to be inadequate for avoiding failures, and new strategies must be developed in order to minimize failures in service.

2. SIMULATION OF THE FATIGUE PROCESS AND ITS DETECTION

A recent paper (Reference 2) described the **INSIM** (**IN**spection **SIM**ulation) computer program that is used to simulate the fatigue environment. Using **INSIM**, various inspection methods and intervals can be evaluated, based on selected parameters, and the resulting probability of failure can be determined.

INSIM contains five built-in probabilistic simulations:

(1) Service life variation is provided by a normal distribution defined by a mean and high-time ($+3\sigma$) expected service life.

(2) Service load severity is given by a normal distribution defined by a mean spectrum and an extreme ($\pm3\sigma$) variation in stress level.

(3) Crack initiation life is described by a two-parameter (shape factor and characteristic life) Weibull distribution.

(4) Crack growth variation is characterized by a normal distribution defined by a mean rate and an extreme ($\pm3\sigma$) variation.

(5) NDI probability of detection is modeled by a three-parameter (shape factor, characteristic length and minimum detectable length) Weibull distribution.

INSIM performs a simulation of a single critical location in an entire fleet of aircraft. Cracks initiate at various times and grow at variable rates in each aircraft. Inspections

are performed according to a predetermined schedule, using as many as six different NDI methods. Cracks are detected during these inspections according to the statistical expectation of detection. As the simulation proceeds from aircraft to aircraft, cracks are detected, aircraft are retired from service or failures occur. The computer acts as a scorekeeper, amasses the statistics and summarizes the results. In order to provide statistically significant results, a large number of simulations must be performed. In a typical simulation, 300,000 inspections will be performed for a fleet of 100,000 aircraft, taking approximately five minutes on a 486 computer.

The program determines, for the parameters selected:

(1) The probability of an aircraft reaching retirement uncracked.

(2) The probability of an aircraft retiring with an undetected crack.

(3) The probability of detecting a crack before it reaches the size dictated by the damage-tolerance regulations.

(4) The probability of detecting a crack larger than the above, but less than the size required for failure.

(5) The probability of a failure occurring during the service life.

Based on these results, optimum NDI methods and intervals can be selected to provide a required level of safety and cost effectiveness. A typical **INSIM** output is shown in Table 1.

Table 1: A Typical Example of INSIM Results

SUMMARY & STATISTICS			
Fleet Size: 100000	**Threshold: 10000**	**Interval(s):**	**3000**
Mean Service Life:	**20008**	**High-Time Aircraft:**	**30309**
Min. Crack Initiation:	**2059**	**Max. Crack Initiation:**	**69372**
Min. Crack Growth:	**9359**	**Max. Crack Growth:**	**24641**
Inspections Performed:	**382704**	**Inspections Per Aircraft:**	**3.83**
		Number of Aircraft	**Percent**
Aircraft Retired Uncracked:		**78821**	**78.82%**
Aircraft Retired Cracked:		**19396**	**19.39%**
Cracks < Ap Detected:		**1646**	**1.65%**
Cracks > Ap Detected:		**7**	**0.01%**
Failures		**130**	**0.13%**

INSIM has been recently upgraded to account for multi-site damage (MSD) configurations. This will be discussed in the Section 4 of this paper.

3. SELECTING INSPECTION STRATEGIES USING INSIM

The **INSIM** computer program can be used to select inspection strategies that minimize the probability of failure in service. Several examples will be shown to demonstrate this feature.

3.1 The Primary Strategy -- Damage-Tolerance Methodology

The damage-tolerance regulations implicitly require the use of moderate stress levels and rationally determined NDI methods and intervals. This results in several benefits such as: long crack initiation lives, long crack growth lives, relatively large critical crack sizes and ample opportunities to detect cracks. Thus, damage tolerance methodology can be considered to be the primary strategy for minimizing service failures.

Figure 1 compares the probability of failure for a typical location designed to damage-tolerance requirements compared to one designed to safe-life requirements.

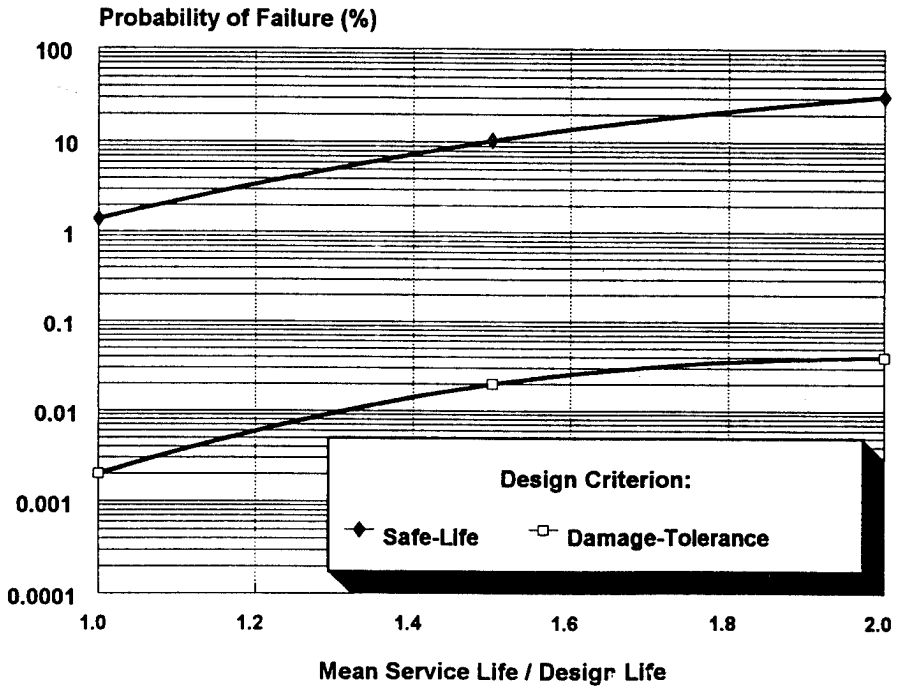


Figure 1: Effect of Mean Service Life on the Probability of Failure

The safe-life requirements assume a mean crack initiation life of two design lifetimes and an inspection interval of half the design lifetime. Implementation of the damage-tolerance requirements resulted, in this case, in a 21% reduction in allowable stress level and set an inspection interval of 20% of the design lifetime.

Figure 1 shows that the probability of failure, for a mean service life equal to the design life, is 1.4% for the safe-life design while it is only 0.002% for the location designed according to the damage-tolerance criterion. As the mean service life of the fleet increases, so does the probability of failure increase. Figure 1 indicates, for a mean service life equal to twice the design life, the probability of failure is 31% for the location designed to the safe-life criterion. The corresponding value for the location designed to be damage-tolerant is only 0.04%.

There is a commonly expressed belief that a structure, designed to the damage-tolerance requirements, is not affected by an extension in service life, since the assumed fatigue damage reverts to a predetermined value after each inspection that did not detect a crack. If this is true, there need not be any limitations on the acceptable service life of an aircraft. Even without considering corrosion damage, which is time dependent, the total life view of **INSIM** shows that this premise is not true, and the probability of failure increases with increased service life. This is obviously due to the fact that, typically, more than 99% of the aircraft can be expected to retire from service without any cracks being detected, as is shown in Table 2. As the service life increases with respect to the design life, less aircraft retire without cracks being detected. Most of the difference is reflected by the number of cracks detected by NDI. However, it is inevitable that some of the difference is accounted for by unsuccessful inspections which lead to service failures. Therefore, it is clear that the probability of failure increases with service usage -- even in locations designed according to the damage-tolerance criteria.

TABLE 2: Typical Distribution of Possible Outcome at a Location

Possible Outcome at a Location	Mean Life / Service Life		
	1.0	1.5	2.0
Retired From Service	99.97%	99.73%	99.06%
Crack Detected by NDI	0.03%	0.25%	0.90%
Failure in Service	0.00%	0.02%	0.04%
Total:	100.00%	100.00%	100.00%

These studies, assisted by the **INSIM** program, demonstrate that the damage-tolerance methodology can be considered to be the primary strategy for minimizing service failures. As is shown in Figures 1, even under adverse conditions of extended service life reasonable probabilities of failures can still be achieved.

3.2 The Inspection Threshold -- Friend or Foe?

It is FAA practice to permit commercial aircraft, designed to be damage-tolerant, to delay the initial inspection to 50% of the design life (See Reference 3). This initial inspection is often called the "inspection threshold".

The concept of an inspection threshold obviously appeals to the manufacturer and operator, who can delay maintenance to a later date. It is assumed that there is only a very small probability that cracks will be detected early in an aircraft designed to be damage-tolerant. Therefore, the initial inspection can be safely delayed until 50% of the design life has been reached.

This premise has been studied, using the **INSIM** computer program, and the results are shown in Figure 2. The parameters used are typical results for a location designed to be damage-tolerant. The mean service life was taken to be equal to the design life. Inspections are performed, after the inspection threshold, at intervals of 15% of the design life.

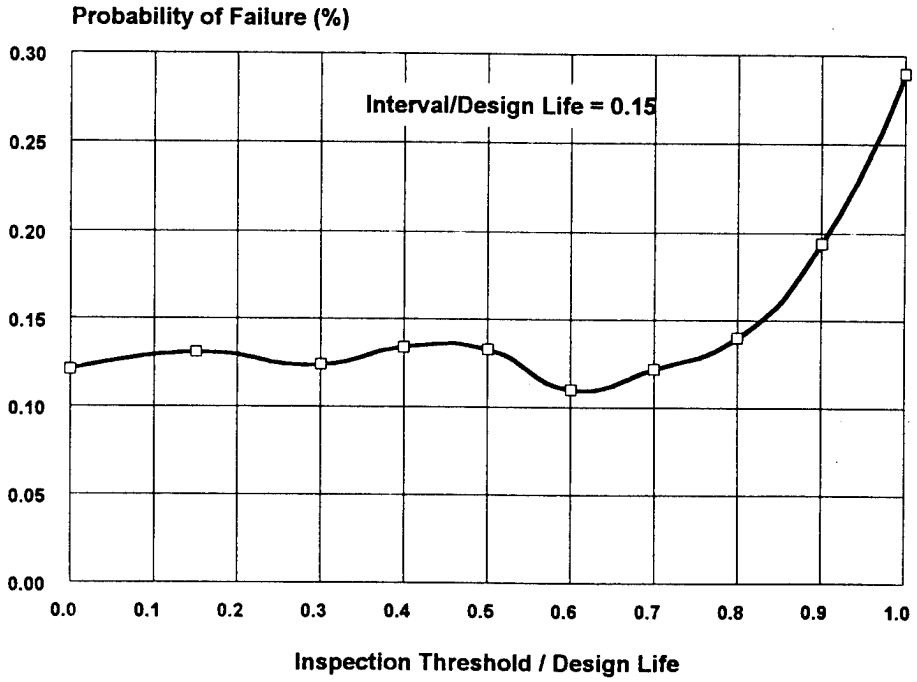


Figure 2: Effect of an Inspection Threshold on the Probability of Failure

Figure 2 indicates that the probability of failure remains nearly constant for conditions ranging from no inspection threshold up to delaying the inspection threshold to 75% of the design life. Only when the inspection threshold is scheduled for after 75% of the design life, does the probability of failure begin to rise rapidly.

As a result of this study, and similar studies performed using **INSIM** over a wide range of parameters, it can be concluded that there is no adverse effect in scheduling the inspection threshold at 50% of the design life for aircraft that have been designed to damage-tolerance requirements.

3.3 Customized Inspections for Minimizing the Probability of Failure

In spite of the virtues of the damage-tolerance methodology in minimizing the probability of failure, adverse situations exist in which conventional inspection intervals are insufficient. In such a case, **INSIM** can be used to select a customized inspection schedule which will reduce the probability of failure to an acceptable level. This will be demonstrated with an actual example.

The example deals with a 2024-T3 plate having several fastener holes. A crack will develop at one fastener hole, eventually severing the ligament and then continue to grow from the opposite side of the hole. The crack continues to grow until it reaches a size critical under service loads, and then failure occurs. Using conventional damage tolerance criteria, the inspection threshold was selected to be 50% of the design life and subsequent inspection intervals were selected to be 20% of the design life, using a liquid penetrant NDI method. Figure 3 indicates the probability of failure for this location.

When the mean service life equals the design life, Figure 3 indicates that the probability of failure would be 0.05% without any inspections. This is due to the relatively large mean crack initiation life of nearly four design lifetimes. When the inspections prescribed by the damage-tolerance criteria are applied, the probability of failure drops to 0.01%.

As the mean service life increases, the probability of failure likewise increases, as is illustrated in Figure 3. When the mean service life reaches twice the design life, the probability of failure is 0.55%, even though the inspections are performed in accordance with the damage-tolerance requirements. This probability of failure is excessive, and should be reduced. Several customized inspection schedules were studied with the assistance of **INSIM**. Table 3 describes the customized inspection schedule which seemed to be the most cost-effective.

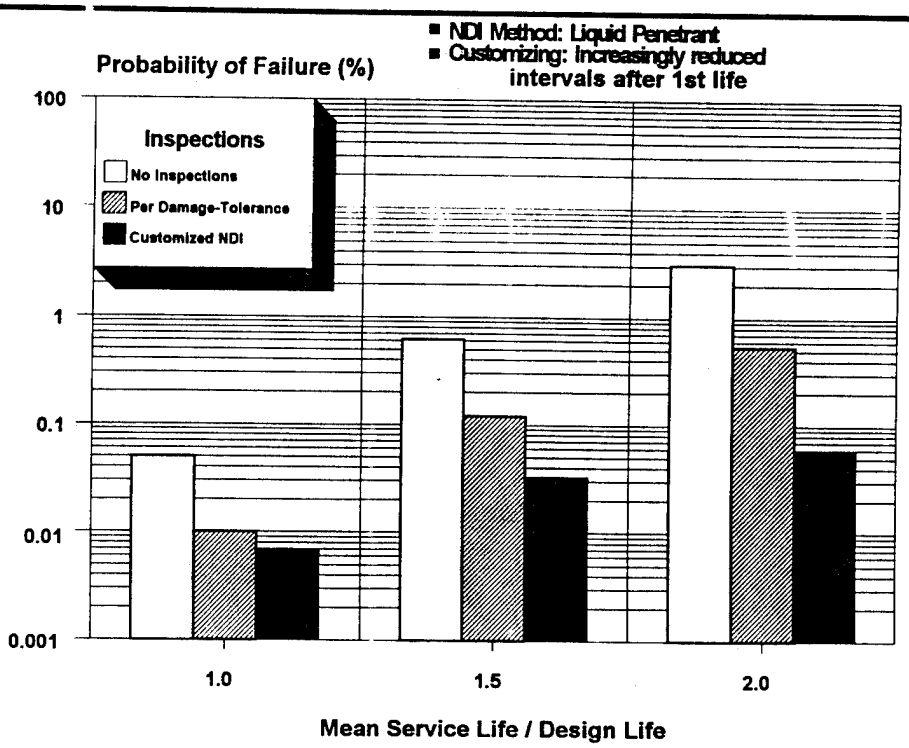


Figure 3: Effect of Customized Inspections on the Probability of Failure

TABLE 3: Customized Inspection Schedule

(All inspections are performed using liquid penetrant)

Service Life / Design Life	Inspection Interval / Design Life
0.50	Inspection Threshold
0.50 -- 1.00	0.20
1.00 -- 1.50	0.15
1.50 -- 2.00	0.10
2.00 --	0.05

The customized inspection begins with the conventional threshold and inspection interval, as dictated by damage-tolerance requirements. With each extension in service life, the interval is reduced, as is shown in Table 3. Figure 3 describes the effect of the customized inspection schedule on the probability of failure. When the mean service life equals the design life, the customized schedule has no real effect. However, when the mean service life reaches 1.5 times the design life, the probability of failure is reduced from 0.12% to 0.033%, as is shown in Figure 3. When the mean service life reaches twice the design life, the customized inspections reduce the probability of

failure from 0.55% to 0.06%. This is a very significant reduction in the probability of failure. This example demonstrates how a specific inspection strategy, of reducing the inspection interval as service life is extended, can be selected to minimize the probability of failure.

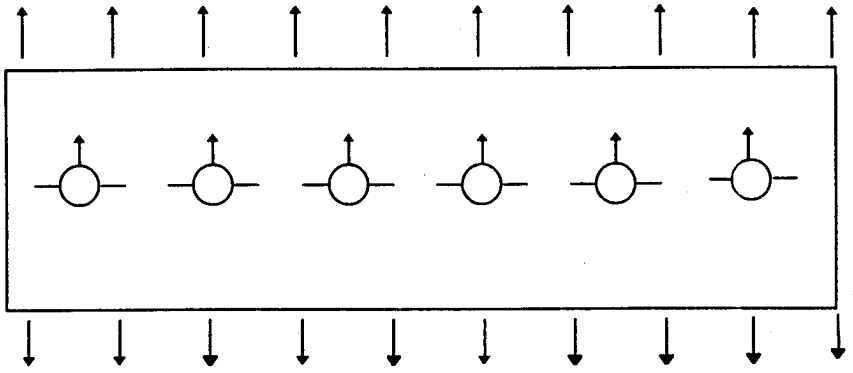
In other situations it was found, by running **INSIM**, that the addition of a supplementary ultrasonic inspection, at the end of each design life, would reduce the probability of failure significantly. This is another example of a customized inspection. In both cases the **INSIM** computer program was used to evaluate the improvement to the probability of failure.

4. CONTROLLING MULTI-SITE DAMAGE USING PROBABILISTIC INSPECTION STRATEGIES

Multi-site damage (MSD) represents a particularly dangerous configuration from the standpoint of structural integrity. Small cracks can initiate at several sites and will grow simultaneously. Eventually the cracks will link-up and failure will occur shortly afterwards.

4.1 Analysis of a Typical Multi-Site Damage Location

Figure 4 describes a typical MSD configuration containing six loaded holes with a total of twelve damage sites. The plate material is 0.25 inch thick 2024-T3 aluminum alloy.



Material: 2024-T3 Aluminum Alloy
Hole Diameter: 0.25 inches
Hole Pitch: 1.0 inches
Edge Distance: 0.5 inches
Remote Stress: 16 KSI
Bearing Stress: 16 KSI

Figure 4: A Typical Multi-Site Damage Configuration

Figure 5 compares the crack growth characteristics of a single hole and the multi-site configuration described in Figure 4. The single hole configuration represents the identical configuration to that shown in Figure 4, but with only one hole, with the identical edge distance.

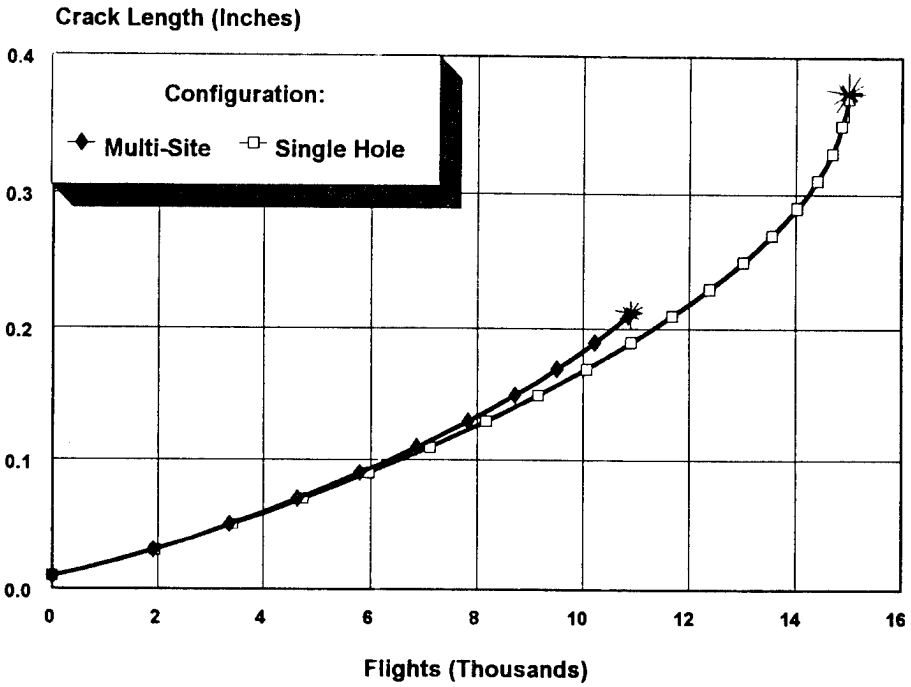


Figure 5: Crack Growth Curves for Multi-Site and Single Hole Configurations

Figure 5, which was calculated using the methods shown in Reference 4, indicates that the multi-site configuration is much more dangerous than the single hole. Not only is the crack growth life considerably shorter than for the single hole, but the critical crack length is also much smaller. This arises from the net-section yield failures that characterize multi-site damage, as opposed to the crack instability type failure that characterizes single hole configurations. As a result of the short crack growth life and small critical crack size, it is very difficult to detect and control multi-site damage before failure.

Crack detectability is often modeled by the three-parameter Weibull distribution,

$$P(a) = 1 - e^{-\left(\frac{(a-a_0)}{(\lambda-a_0)}\right)^{\alpha}} \qquad (1)$$

where P(a) is the probability of detecting a crack of length "a". α, λ and a_0 are the three Weibull parameters that characterize the statistical distribution and are a function of the

NDI method used as well as the characteristics of the cracked location. Figure 6 describes this distribution (curve corresponding to one crack) for a liquid penetrant inspection method under average field conditions.

When several cracks are present, the laws of probability state that the probability of detecting at least one crack is given by,

$$P = 1 - (Q_1 \times Q_2 \times Q_3 \times \ldots \times Q_n) \qquad (2)$$

where P is the probability of detecting at least one crack and Q_n is the probability of not detecting any of the n cracks.

If all the cracks are of equal length, Equation (2) reduces to

$$P = 1 - Q^n \qquad (3)$$

where Q is the probability of not detecting any one crack. Figure 6 is based on Equation (3).

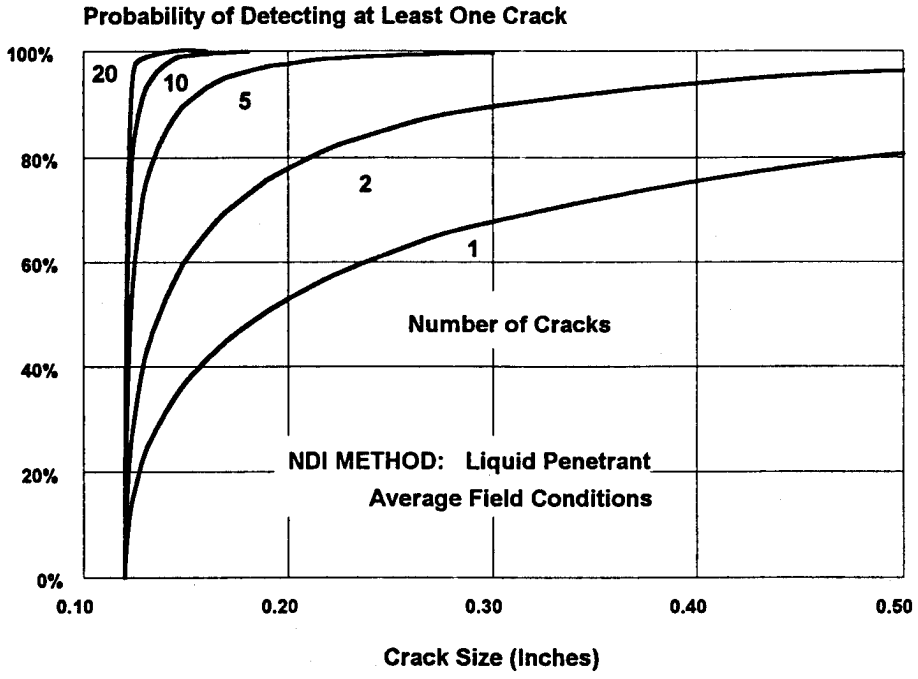


Figure 6: Probability of Detecting at Least One Crack

Figure 6 indicates that as the number of cracks increase, the probability of detecting at least one crack improves dramatically. For example, a single 0.15 inch crack has only about a 40% probability of detection under typical field conditions. However, the probability of detecting at least one of ten such cracks is nearly 100%. Thus, the multitude of cracks, which are so dangerous from the standpoint of structural integrity, makes it possible to achieve very high probabilities of detection.

The **INSIM** computer program has been modified in accordance with Equation (3) in order to model crack detectability in an MSD configuration. It allows the study of the interplay between the relatively short critical crack length and the enhanced crack detectability of the MSD configuration.

INSIM deals with the MSD problem under the assumption that all of the damage sites have equal size cracks. If this were not the case, the net-section yield failure would be delayed until further crack growth takes place, thereby increasing the crack growth life. Hence, it is conservatively assumed that all the crack sizes are equal. This assumption greatly speeds-up the computing, simplifies the analysis, and is considered to be compatible with the typical characteristics of multi-site damage. (See Reference 5.)

The MSD configuration shown in Figure 4, having crack growth characteristics shown in Figure 5, has been studied using **INSIM**. For comparison purposes, the single hole configuration has also been analyzed. Figure 7 describes the probability of failure, for both configurations, as a function of the inspection interval. In both cases, a liquid penetrant NDI method is used, with probabilities of detection as defined in Figure 6. In both cases it is assumed that the fleet mean service life has reached 100% of the design life and the high-time aircraft has reached 150% of the design life, thus representing an aging fleet.

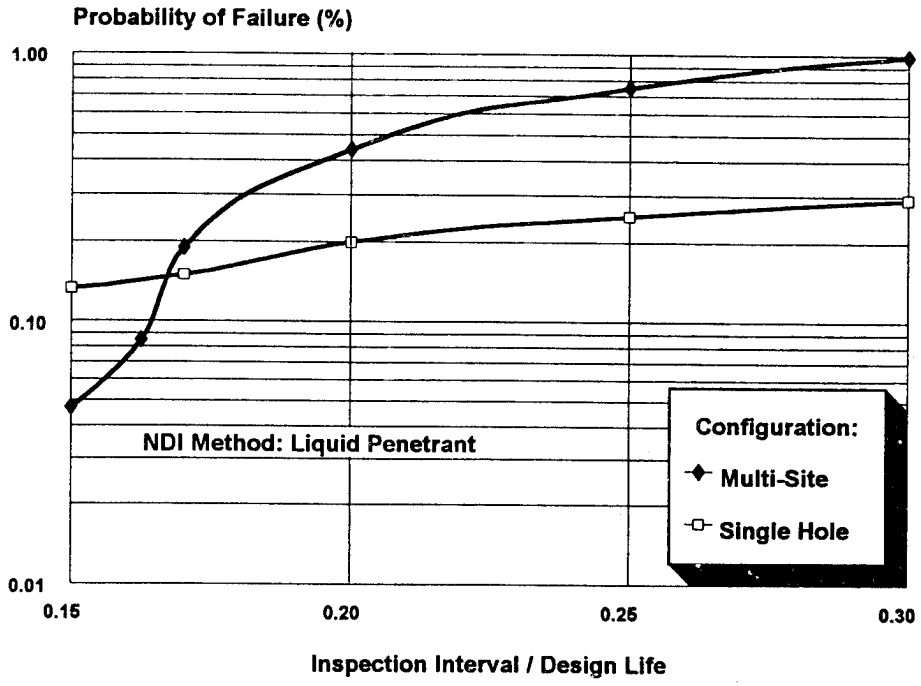


Figure 7: Effect of the Inspection Interval for a Multi-Site and Single Hole Configuration

Figure 7 indicates that, for most of the range, the MSD configuration has the higher probability of failure, as expected. However, when the inspection interval is reduced to below 17% of the design life, the MSD configuration will *actually have a lower probability of failure* than the single hole configuration. This unexpected result is due to the increased opportunity for crack detection that is offered by the twelve cracks that are growing in the MSD configuration. However, this benefit for the MSD configuration can only be realized with relatively short inspection intervals, as is shown in Figure 7.

The effect of an inspection threshold has also been studied, for both configurations, with the help of **INSIM**. An inspection interval of 15% of the design life has been assumed, in accordance with the results shown in Figure 7. The results of this study are shown in Figure 8.

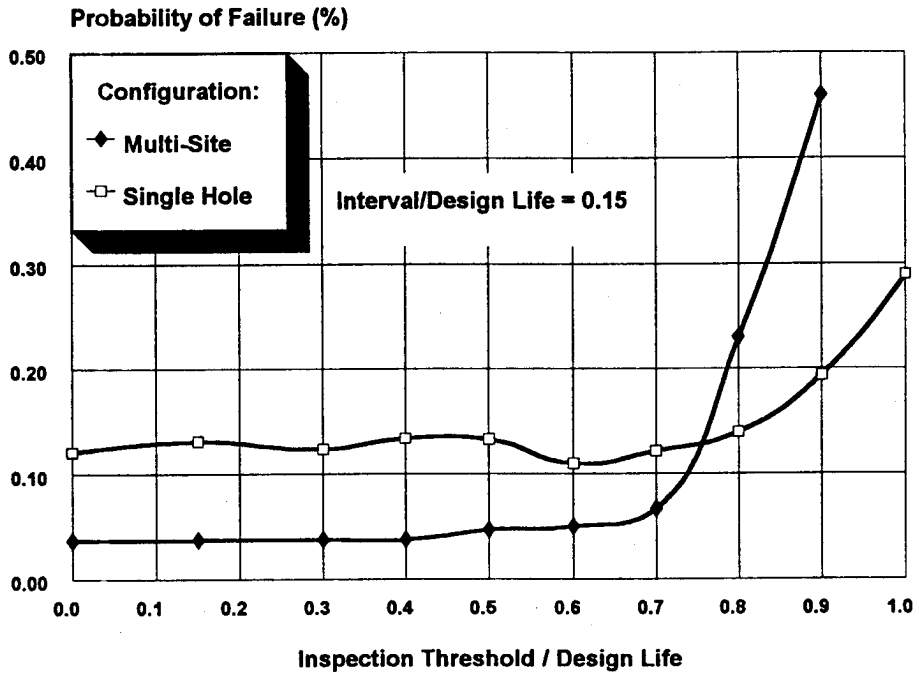


Figure 8: Effect of an Inspection Threshold for a Multi-Site and Single Hole Configuration

Figure 8 indicates that the probability of failure is relatively insensitive to the presence of an inspection threshold for both configurations. However, when the inspection threshold is scheduled for after 60% of the design life, the probability of failure for the MSD configuration begins to increase rapidly. For the single hole configuration, the probability of failure is less sensitive to the threshold location, and only increases significantly when the inspection threshold is scheduled for after 75% of the design life. Since it is FAA practice, for commercial aircraft, to limit the inspection threshold to 50%

of the design life (Reference 3), this **INSIM** study concludes that there are no adverse effects, in allowing the threshold to reach 50% of the design life, for multi-site damage configurations that have been designed to damage-tolerance requirements.

A summary of the **INSIM** study of the aging fleet, multi-site and single hole configurations, is shown in Figure 9. Liquid penetrant inspections are assumed to begin at the inspection threshold of 50% of the design life, and then proceed at 15% intervals of the design life, for both configurations. The results show that the probability of failure will be reduced from 2.1% to 0.047%, for the MSD configuration, by following the above inspection program. For the single hole configuration, the improvement is less dramatic, and the probability of failure is reduced from 0.58% to 0.13% by introducing the inspection program. In both cases, eliminating the inspection threshold will result in only a marginal improvement, as is shown in Figure 9.

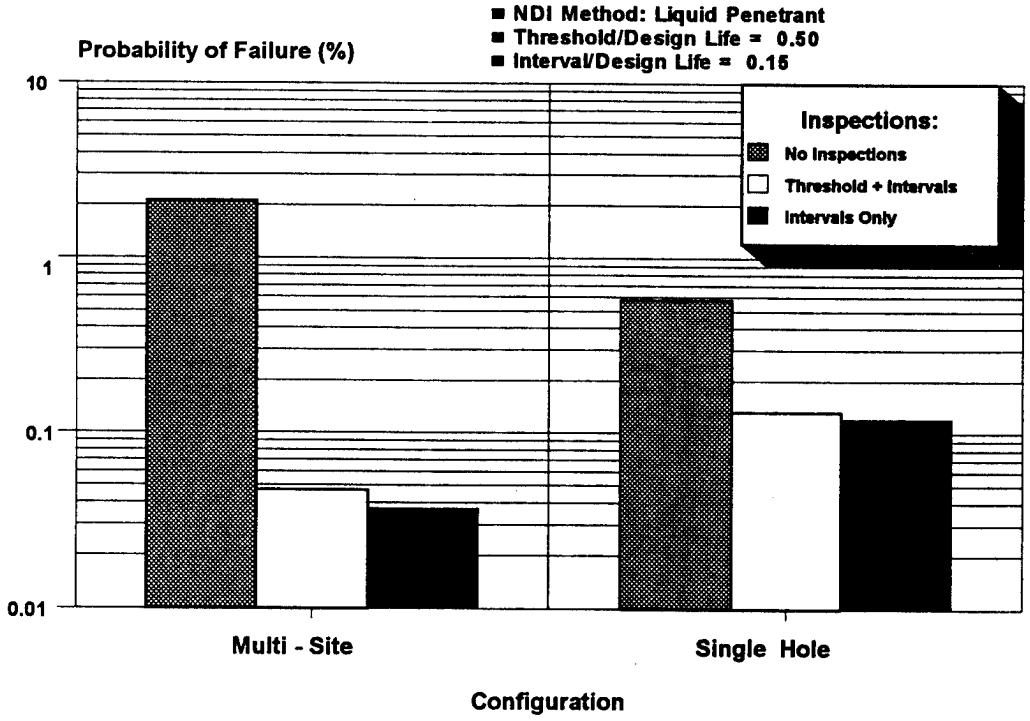


Figure 9: Probability of Failure for a Multi-Site and Single Hole Configuration

4.1 Controlling Multi-Site Damage

Based on the above reported study, and similar analyses that were performed using **INSIM**, it can be concluded that probabilistic inspection strategies can be used to control multi-site damage. The key principles are:

(1) Design the MSD structure so that the critical crack length, under the net-section yield condition, is "detectable" using the selected NDI method. Even if the probability of detection of the individual crack is low, the multitude of cracks in the MSD configuration will insure a relatively large overall probability of detection, as was shown in Figure 6. (For example, the MSD configuration of Figure 4 has a critical crack length of 0.21 inch, as is shown in Figure 5. Figure 6 indicates that, under typical field conditions, the probability of detection of the near critical crack is only about 55%, using liquid penetrant NDI. Nevertheless, this is sufficient to achieve a probability of failure of only 0.047% for an aging fleet, as was shown in Figure 9.)

(2) Evaluate the probability of failure using probabilistic tools such as **INSIM.** Tailor the NDI program, including supplementary inspections if necessary, in order to achieve an acceptable probability of failure.

5. SUMMARY

It was shown that **INSIM** can be used to simulate the entire fatigue environment including operating conditions, crack initiation, crack growth and crack detection. **INSIM** has been used to study the effects of mean service life, damage-tolerance methodology, inspection thresholds, customized inspections and multi-site damage.

It was shown that probabilistic inspection strategies can be used to control multi-site damage, even in an aging fleet.

6. REFERENCES

1 Whittaker, I. C., et al, "Fleet Fatigue Cracking Threshold Prediction", Proceedings of the 16th Symposium of the International Committee on Aeronautical Fatigue (ICAF), Tokyo, Japan, 1991.

2. Brot, A., "Probabilistic Inspection Strategies for Minimizing Service Failures", Proceedings of the FAA/NASA International Symposium on Advanced Structural Integrity Methods for Airframe Durability and Damage Tolerance, Hampton, VA, USA, 1994.

3. Swift, T., "Verification of Methods for Damage Tolerance Evaluation of Aircraft Structures to FAA Requirements", Proceedings of the 12th Symposium of the International Committee on Aeronautical Fatigue (ICAF), Toulouse, France, 1983.

4. Nathan, A. and Brot, A. "An Analytical Approach to Multi-Site Damage", Proceedings of the 17th Symposium of the International Committee on Aeronautical Fatigue (ICAF), Stockholm, Sweden, 1993.

5. Horst, P. and Schmidt, H. J., "On the Significance of Probabilistic Parameters for the Assessment of MSD in the Case of Aging Aircraft", Proceedings of the 19th Congress of the International Council of the Aeronautical Sciences (ICAS), Anaheim, CA, USA, 1994.

Multiple Site Damage (MSD) in a Pressurized Fuselage Riveted Lap Joint

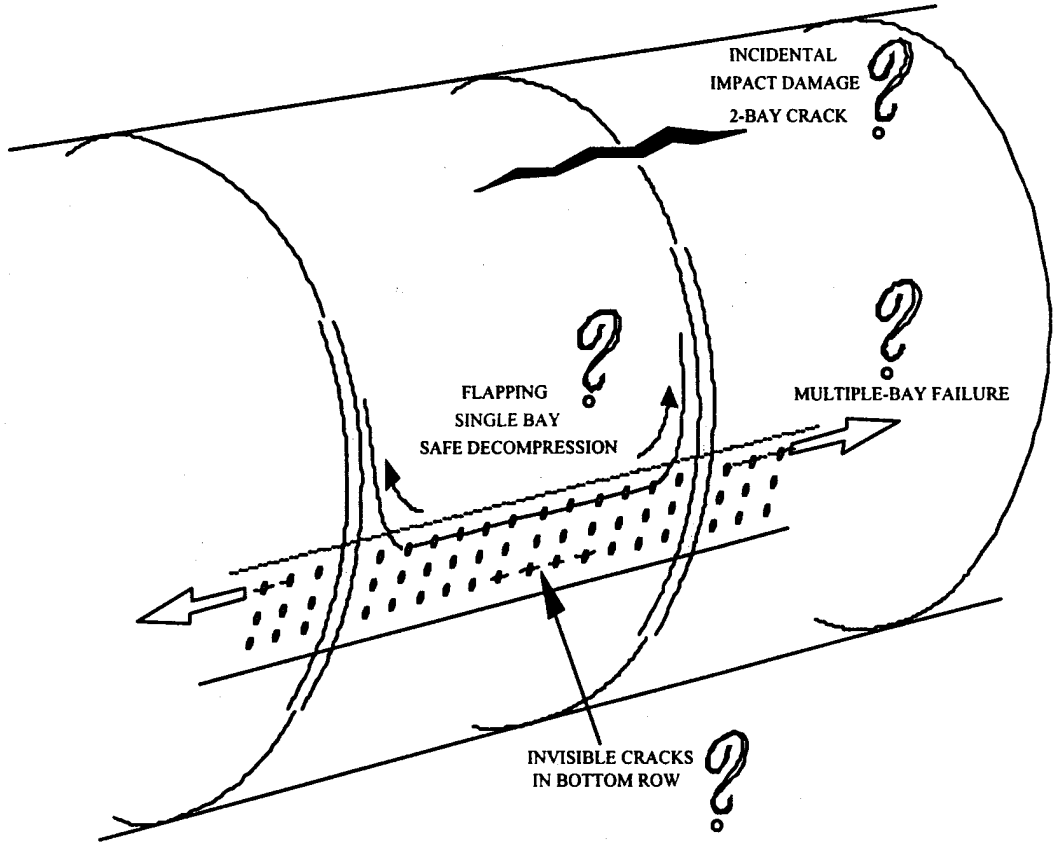
Capt. S. A. Fawaz
United States Air Force

J. Schijve
Faculty of Aerospace Engineering
Delft University of Technology

Introduction

- Multiple Site Damage
- Comparison of Al 2024-T3 & Glare 3
- Current Research Effort
- Conclusions

Multiple Site Damage Concerns



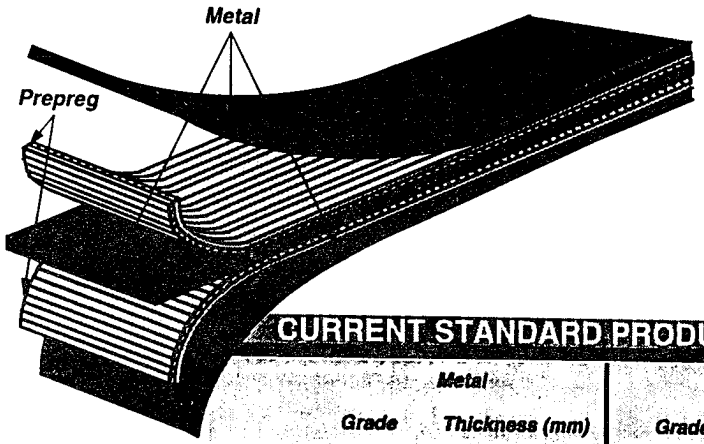
Multiple Site Damage

- **Why all the attention?**
  - **Aloha Airlines Boeing 737, 1988**
  - **Large Number of Aging Civil & Military Aircraft**
- **Unknowns?**
  - **Small Crack Growth Behavior**
  - **Fully Developed Stress Intensity Factor Solutions (SIFs) for a Riveted Lap Joint**

Stress Intensity Factor Solution	AL 2024-T3	Glare 3
Part-Through Crack	Yes	No
Pin Loaded Holes	Yes	No
Biaxial Loading + Secondary Bending	No	No
Crack Interaction	Yes	No

  - **Fibre Metal Laminates, FML (Glare 3)**
    - **Effect of MSD on Residual Strength**
    - **Effect of Layers on SIF in FMLs**
  - **General Failure Criterion for MSD**

Fibre Metal Laminates



CURRENT STANDARD PRODUCT FORMS

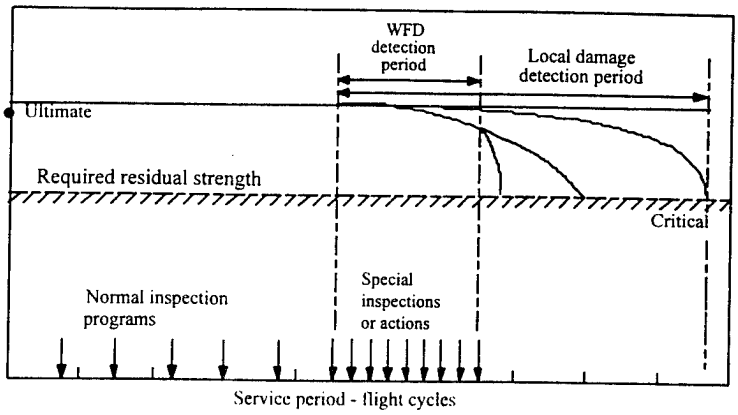
	Metal		Prepreg	
	Grade	Thickness (mm)	Grade	Thickness (mm)
GLARE 1	7475-T761	0.3 - 0.4	U.D. glass	0.25
GLARE 2	2024-T3	0.2 - 0.3 - 0.4	U.D. glass	0.25
GLARE 3	2024-T3	0.2 - 0.3 - 0.4	C.P. glass 50/50	0.25
GLARE 4	2024-T3	0.2 - 0.3 - 0.4	C.P. glass 67/33	0.375
GLARE 5	2024-T3	0.2 - 0.3 - 0.4	C.P. glass 50/50	0.5

U.D. = unidirectional; C.P. = cross-ply;

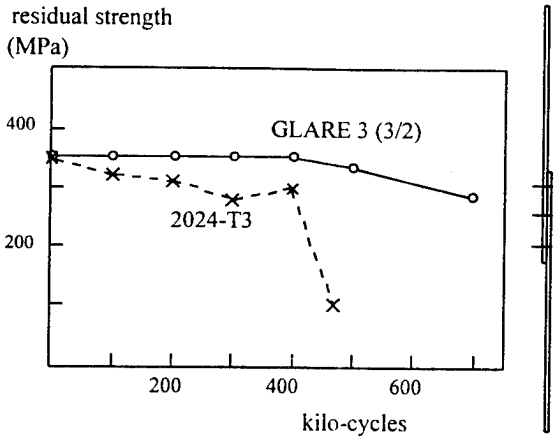
50/50 = 50 % of fibres in longitudinal direction and 50 % in long-transverse direction;

67/33 = 67 % of fibres in longitudinal direction and 33 % in long-transverse direction.

Comparison of Al 2024-T3 and Glare 3



Strength degradation of aging aircraft



S_{max} = 100 MPa

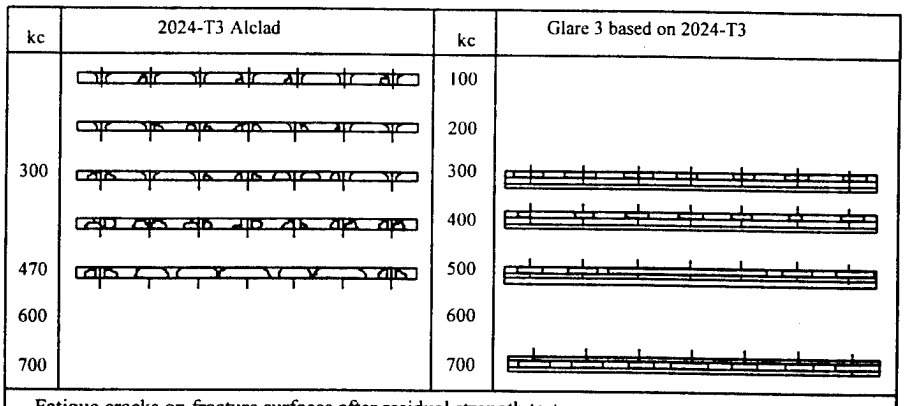
riveted lap joint with
3 rows of 7 rivets

d = 4.8 mm (NAS 1097)

p = 24 mm

W = 168 mm

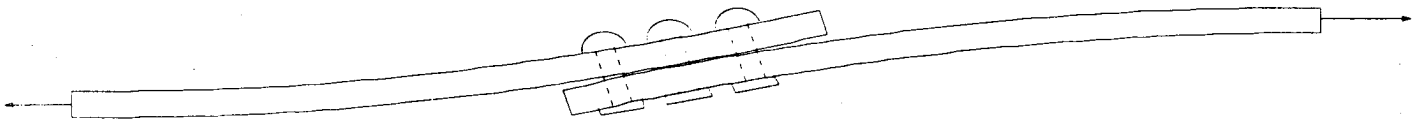
Degrading strength of a riveted lap joint due to fatigue.
Results of Roebroeks (SLC).



Fatigue cracks on fracture surfaces after residual strength tests.

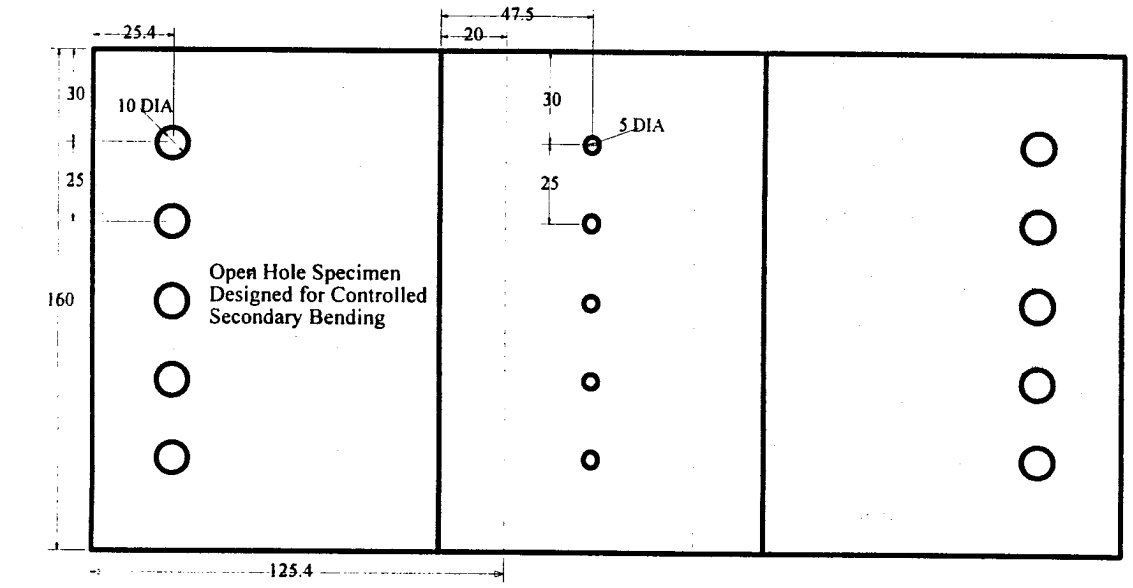
Current Research Effort

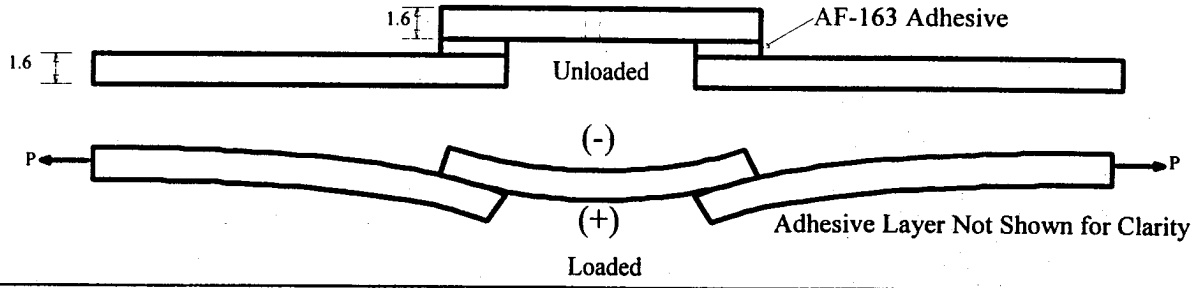
- **Determine Effect of Tension and Secondary Bending on Small Crack Growth**
  - **All fuselage lap joints experience secondary bending due to eccentricity of the joint**
  - **The magnitude of the stress caused by secondary bending can be as large as that created by the hoop stress**



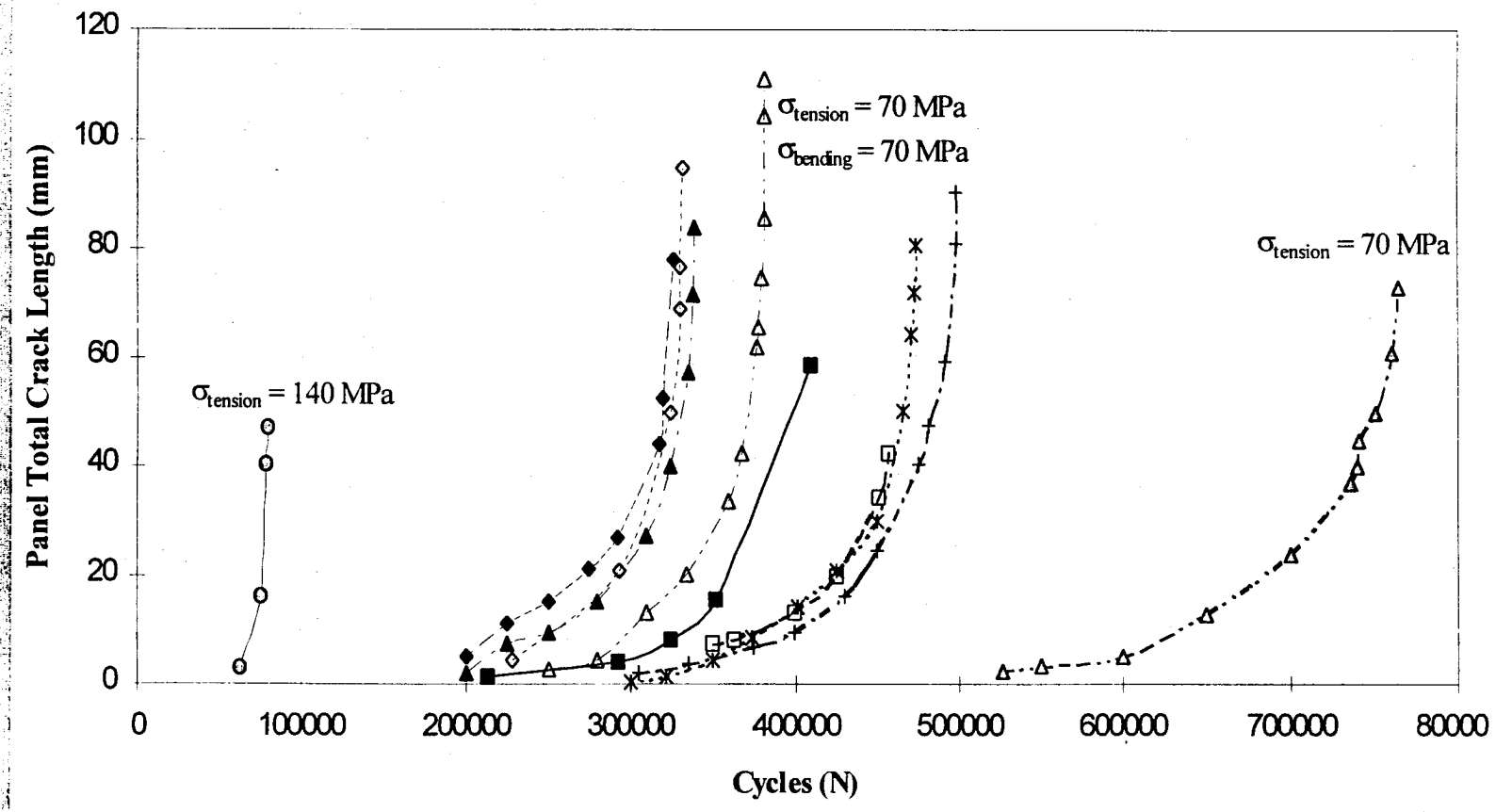
Secondary Bending Experiments

All Dimensions in mm



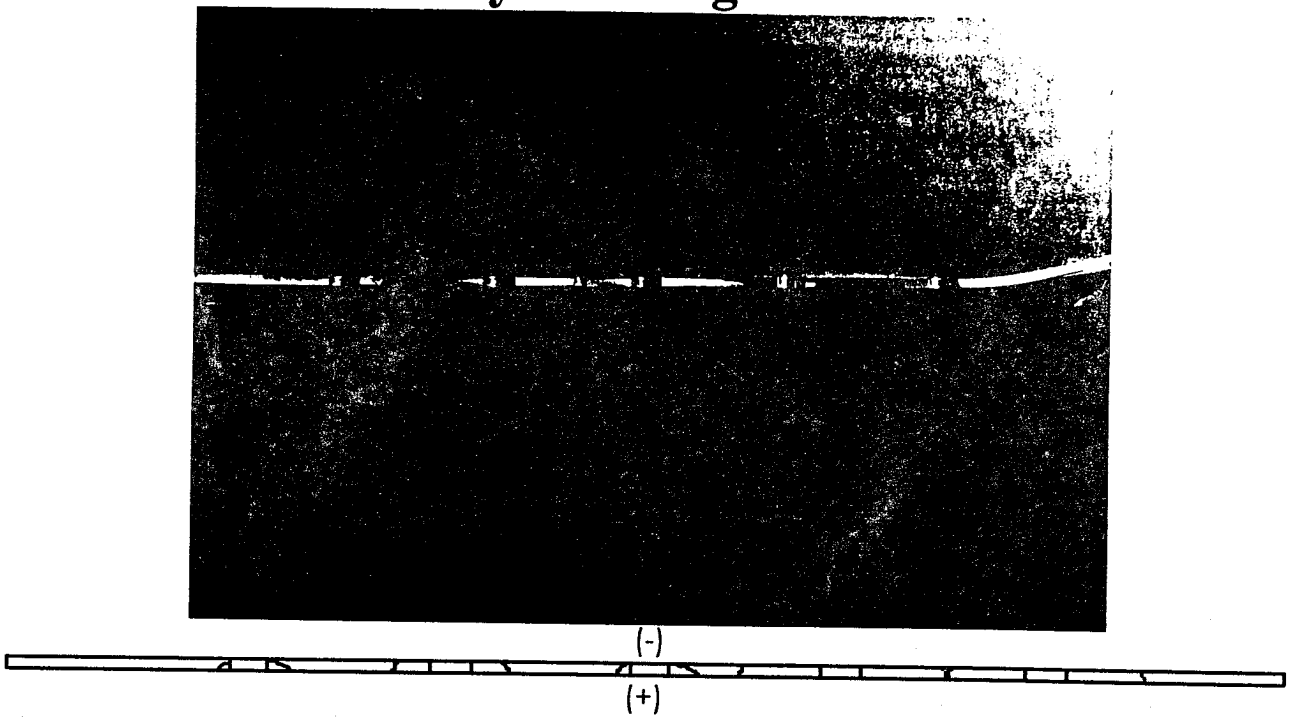


Effect of Tension and Secondary Bending on Crack Growth of a Double Corner Crack at an Open Hole

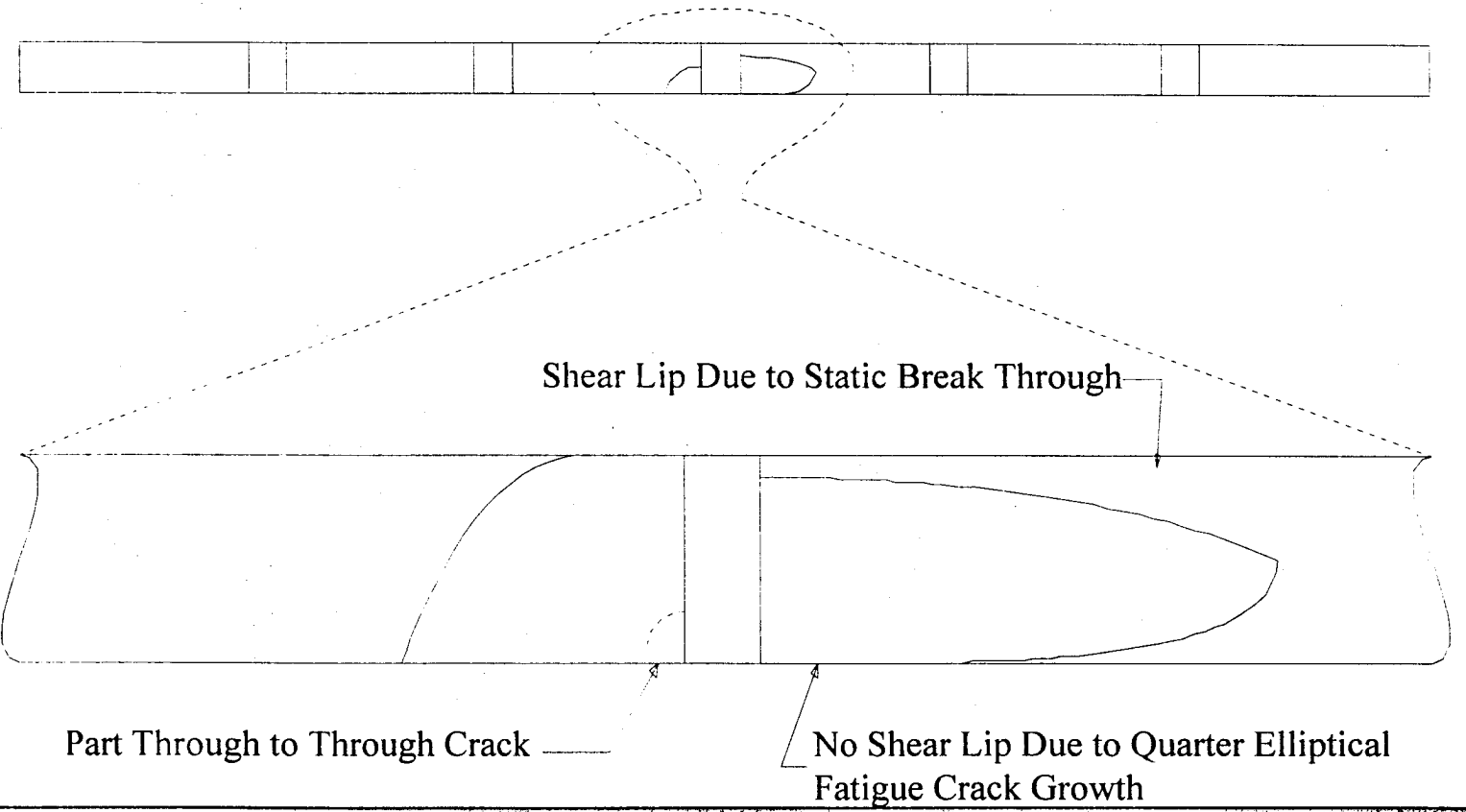


Fractography

- **Tension and Secondary Bending**



Examination of Crack Surface



MSD in a Pressurized Fuselage Lap Joint

- **Conclusions**
  - Cracks emanating from a open hole under tension and secondary bending develop as *part through* cracks
  - Part through cracks can not easily penetrate the full thickness of Glare 3
  - Glare 3 exhibits a greater residual strength under fatigue loading than Al 2024-T3
  - Secondary Bending *decreases* the fatigue life of the open hole specimen
- **Future Work**
  - Investigate the effect of secondary bending on small crack growth
  - Expand simple secondary bending specimen to full riveted lap joint
  - Develop general failure criterion for MSD
  - Explore additional SIF solutions for Glare

A Global-Local Fracture Criterion for Ductile Materials

T. L. Weng and C. T. Sun

School of Aeronautics and Astronautics
Purdue University
West Lafayette, IN 47907-1282

Abstract

Fracture behavior for ductile materials is quite different from that of brittle materials. Ductile materials generally exhibit slow stable crack growth accompanied by considerable plastic deformation. In other words, there is crack growth resistance during crack extension. In such cases, LEFM tends to yield overly conservative predictions. A number of fracture parameters have been studied over the years. In summary, these fracture parameters can be classified into two groups. One group is based on local parameters which characterize the near tip fields, such as stress or strain at the tip, the crack tip opening displacements (COD), the crack opening angle (COA) and the crack tip force. The other group of criteria is based on global parameters which usually represent some type of energy, such as J-integral, plastic energy dissipation rates and crack separation work.

From the physical perspective, the local crack tip state should control the crack growth. Thus, local fracture criteria may have the potential to be more accurate in predicting fracture behavior. Such criteria are expected to be independent of specimen size and geometry, loading configuration, and the amount of crack extension. However, the measurements of these local parameters are very difficult to perform experimentally. As a result, their application is restricted. On the other hand, global parameters are easier to measure but geometrically dependent.

The objective of the present study was to provide a numerical analysis in conjunction with the experimental results to identify suitable fracture parameters characterizing fracture behavior during crack extension in ductile materials. To achieve this goal, several experiments conducted by other authors were re-examined.

From their experimental results, the measured relationships of load line displacement (LLD) versus crack extension (Δa) were selected as the basic input of the FEM analysis to simulate crack growth. During the finite element simulation, various energy rates, crack growth resistance and local parameters were generated and investigated. Based on the observed results, a Global-Local Fracture Criterion (GLFC) was proposed.

In the Global-Local Fracture Criterion, a global parameter (the J-integral) is used to characterize the initial stage of crack extension. In the subsequent steady state crack growth, the fracture criterion is switched to one that is characterized by a local parameter (the effective stress or effective plastic strain). The amount of crack growth wherein the J-integral can be used as a material characteristic is not well defined. However, the existence of a J-controlled crack growth region is quite evident. In the verification of the proposed criterion, the J-Δa curve for the initial amount of crack growth of 5% of the original uncracked ligament of the tested specimen was tentatively assigned as the point for switching.

An advantage in applying the proposed GLFC is that pre-determination of the critical value of the parameter in the local criterion is not necessary in the analysis. The critical value of the selected local parameter is "self-generated" during the analysis and used as the criterion for the subsequent analysis at the instant of switching from global criterion control to local criterion control when the crack growth becomes steady state.

OBJECTIVE

- To identify suitable fracture parameters for a fracture criterion for ductile materials
- To numerically simulate crack growth and verify with experimental data

APPROACH

- Use the J-integral (the global parameter) to characterize the initial stage of crack growth
- Use a local parameter such as effective plastic strain to predict the steady state crack growth
- Validate the Global-Local Fracture Criterion by comparing with experimental data

HRR Field-J-Dominant Region

$$\bar{\varepsilon}^p = \alpha(\bar{\sigma})^n$$

- Deformation Theory

$$\varepsilon_{ij}^p = \frac{3}{2}\alpha(\bar{\sigma})^{n-1} s_{ij}$$

$$J = \int_\Gamma (wn_1 - t_i \frac{\partial u_i}{\partial x_1})\, ds$$

$$\sigma_{ij}(r,\theta) = (\frac{J}{cr})^{\frac{1}{n+1}} \tilde{\sigma}_{ij}(\theta)$$

Fracture criterion $J = J_c$

- Incremental Theory

$$d\varepsilon_{ij}^p = \frac{3}{2}\frac{d\bar{\varepsilon}^p}{\bar{\sigma}} s_{ij}$$

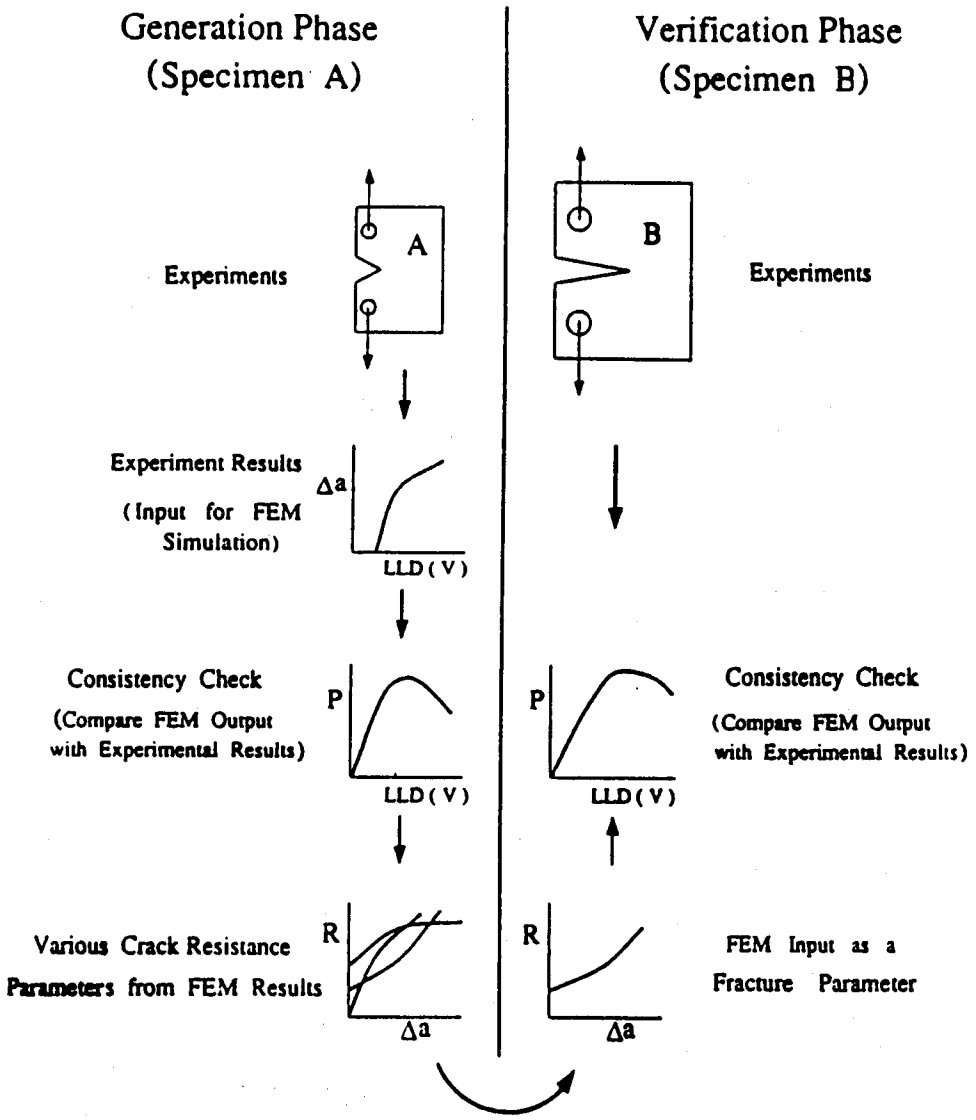
$$w = \int_0^{\varepsilon_{ij}} \sigma_{ij}\, d\varepsilon_{ij}$$

$$\Delta J = \int_\Gamma [\Delta wn_1 - (t_i + \Delta t_i)\frac{\partial \Delta u_i}{\partial x_1} - \Delta t_i \frac{\partial u_i}{\partial x_1}]\, ds$$

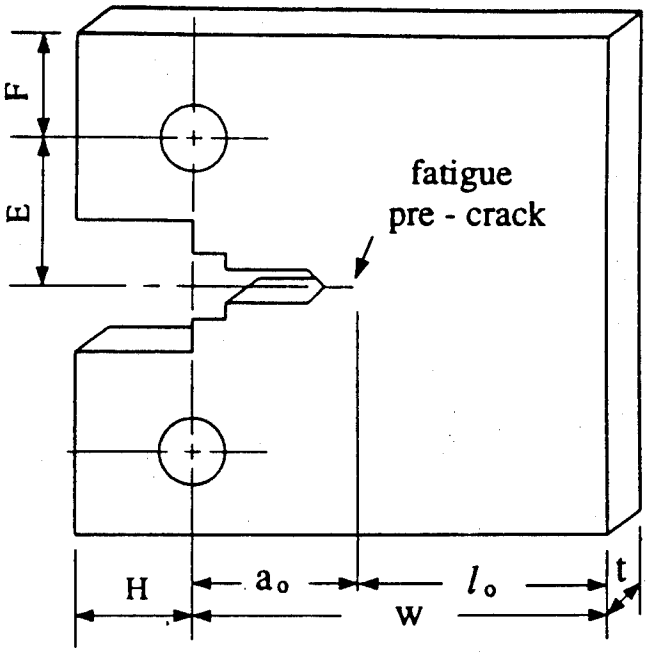
$$J = \Sigma \Delta J$$

CONCLUSIONS

- J-integral is a valid material parameter for characterizing initial crack growth -- HRR field exists; a unique J.
- During steady state crack growth, local stresses ($\bar{\sigma}_1$) or strain ($\bar{\varepsilon}^p$) or plastic work (w^p) near the crack can be used to characterize crack growth.
- The present global-local fracture criterion is capable of predicting ductile fracture behavior of metals.
- The transition from global criterion to local criterion requires additional refinement.
- The thickness effect can be accounted for by modifying the J–Δa curve into a J–$\frac{\Delta a}{t}$ curve.
- Plane stress is suitable for flat-sided specimens, and plain strain, for grooved specimens.



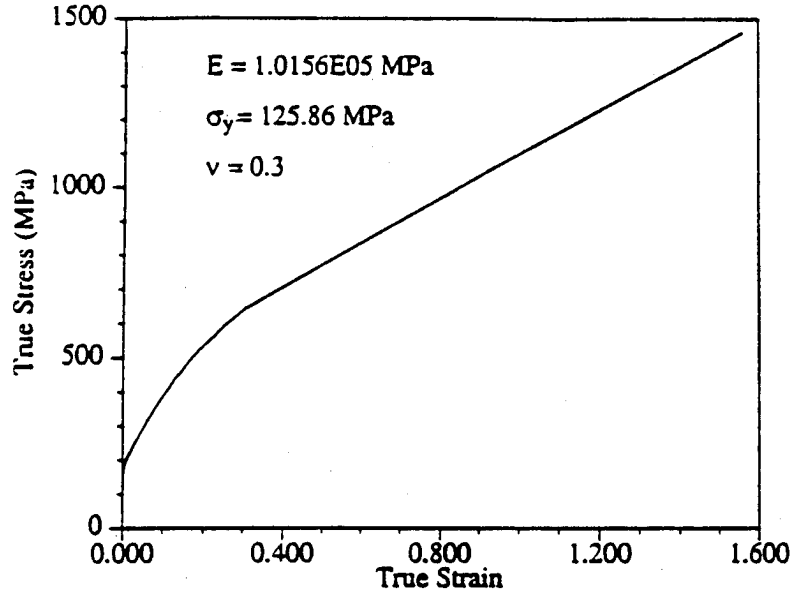
Schematic of the methodology for developing the ductile fracture parameters.



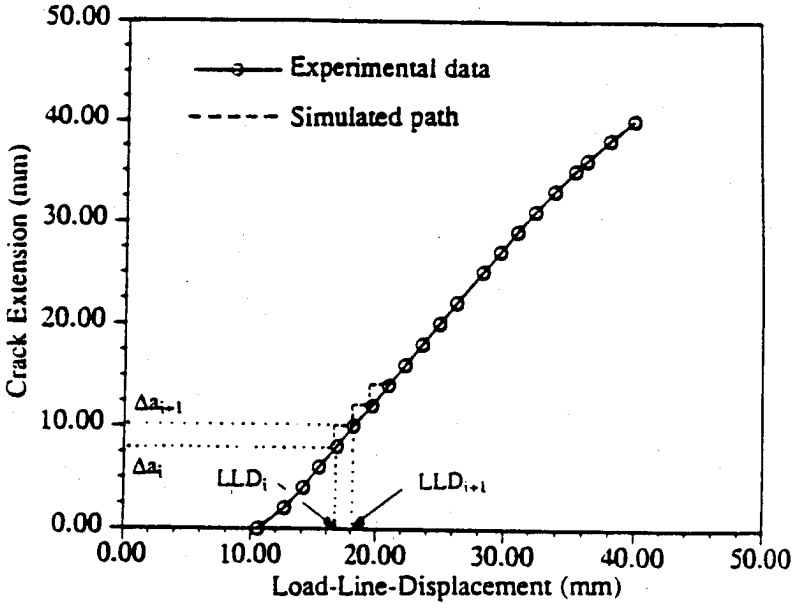
(mm)

specimen size	t	a_o	w	H	E	F
1 T	25.4	27.08	50.80	12.70	13.97	16.51
3 T	25.4	77.29	152.40	38.10	41.49	49.53
10 T	25.4	256.80	508.00	127.00	139.70	165.10

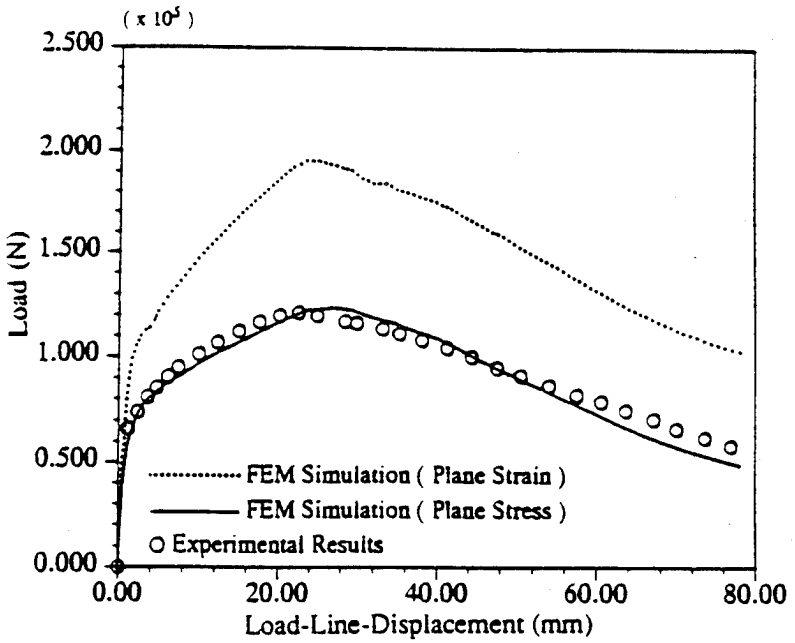
The modified compact tension specimens.



Uniaxial stress-strain curve for type 304 stainless steel at 550°F (288°C).

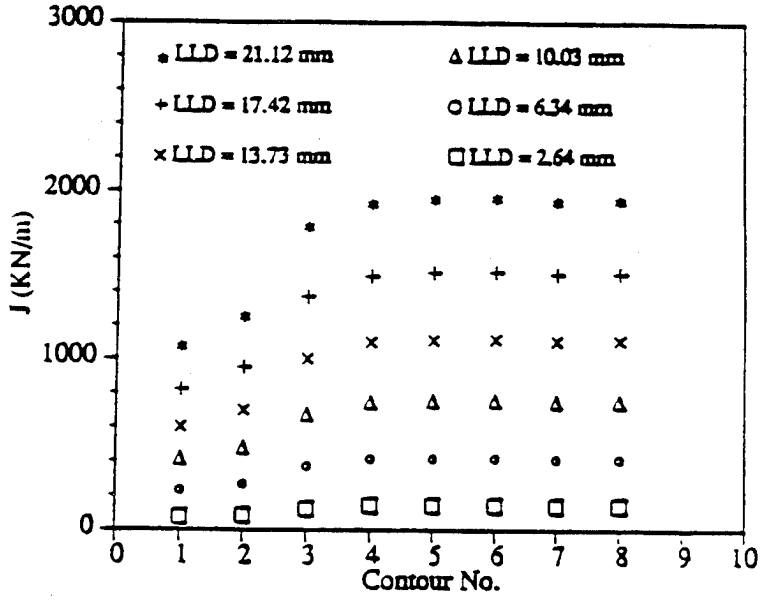


Experimental load-line-displacement versus crack extension (LLD - Δa) for 3T modified CT specimen.

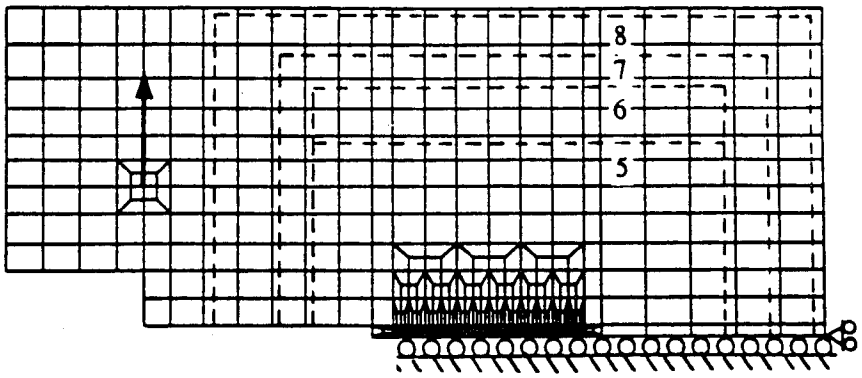


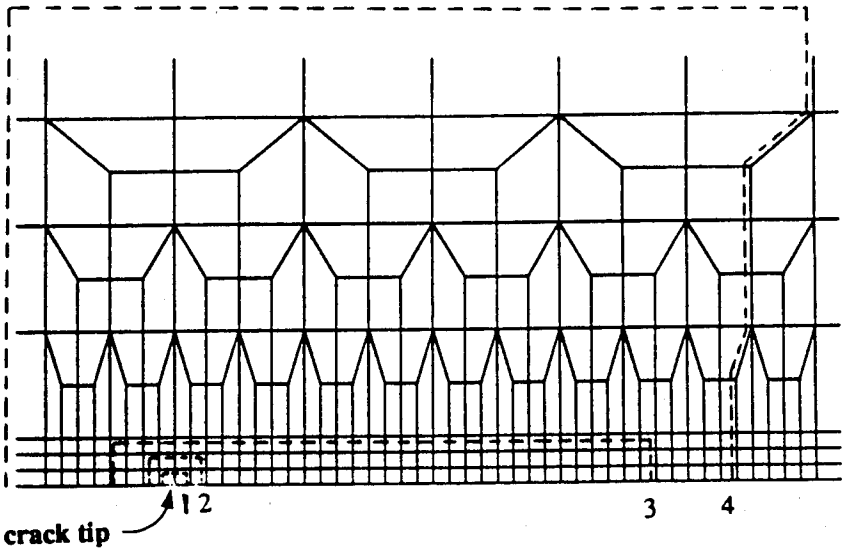
Simulated load versus load-line-displacement for 3T modified CT specimen.

Before Crack Extension

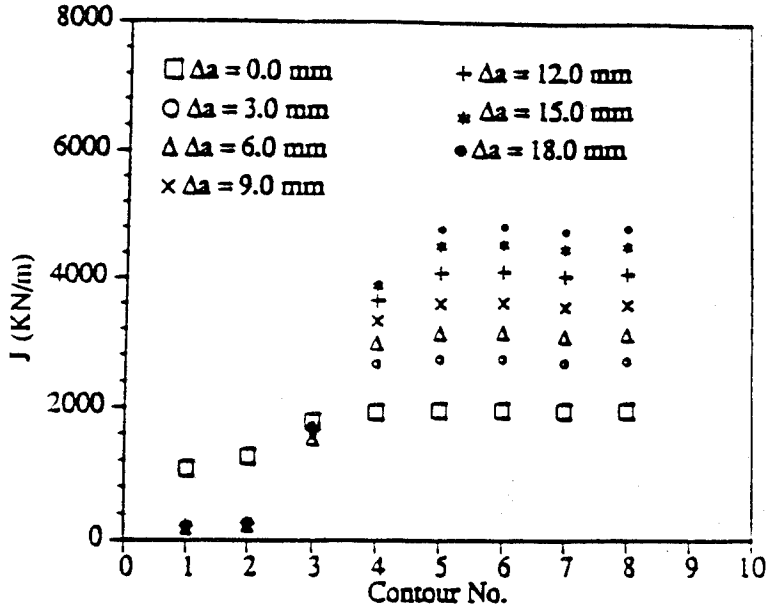


J calculated along different contours at different loading stages before crack growth initiation.

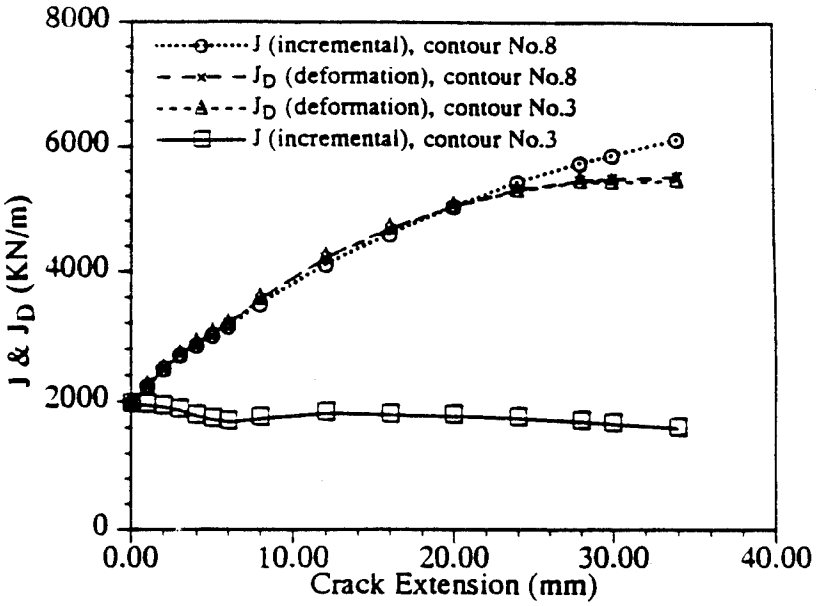




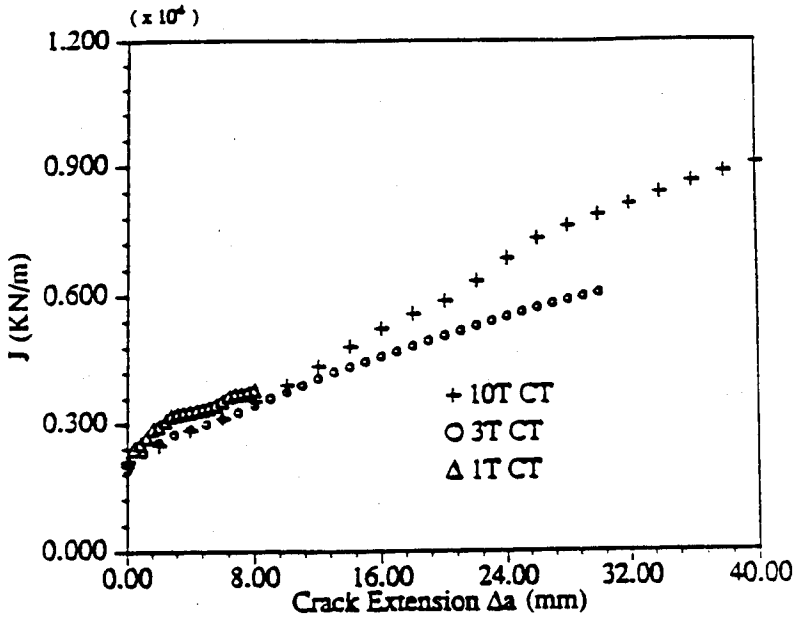
Eight different contours in calculations of J-integral for (modified) compact tension specimen.



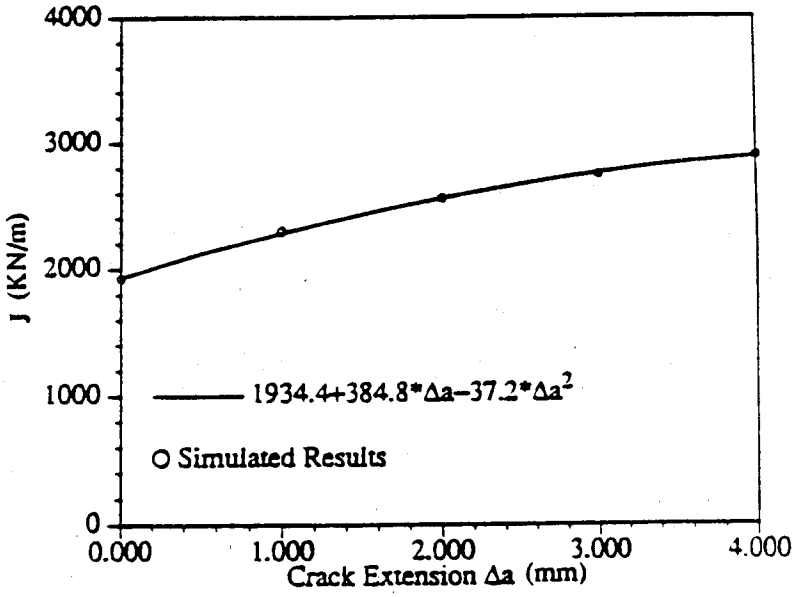
J calculated along different contours under crack extension.



J calculated by using incremental and deformation plasticity, respectively, during crack extension.



J versus Δa for different modified compact tension specimens.



Initial portion of J - Δa curve generated from 3T modified CT specimen.

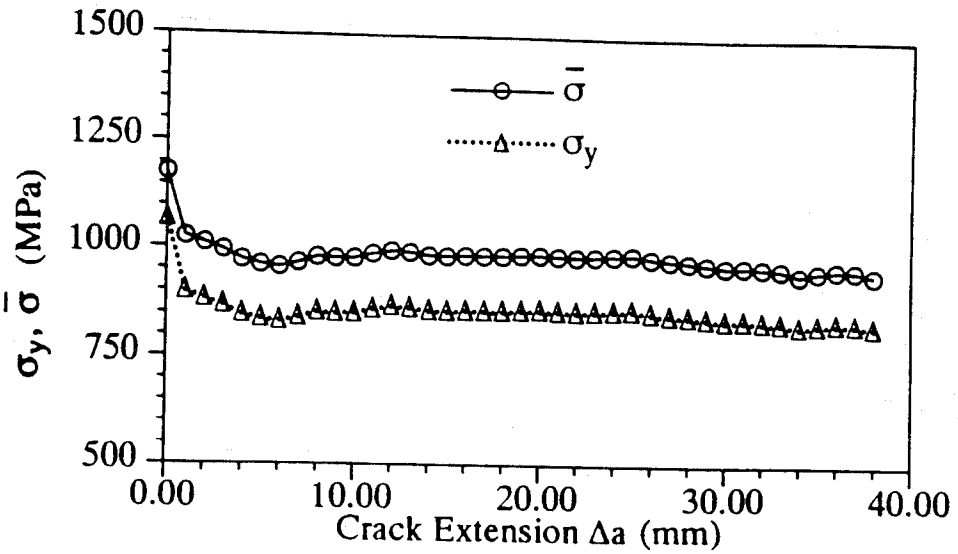
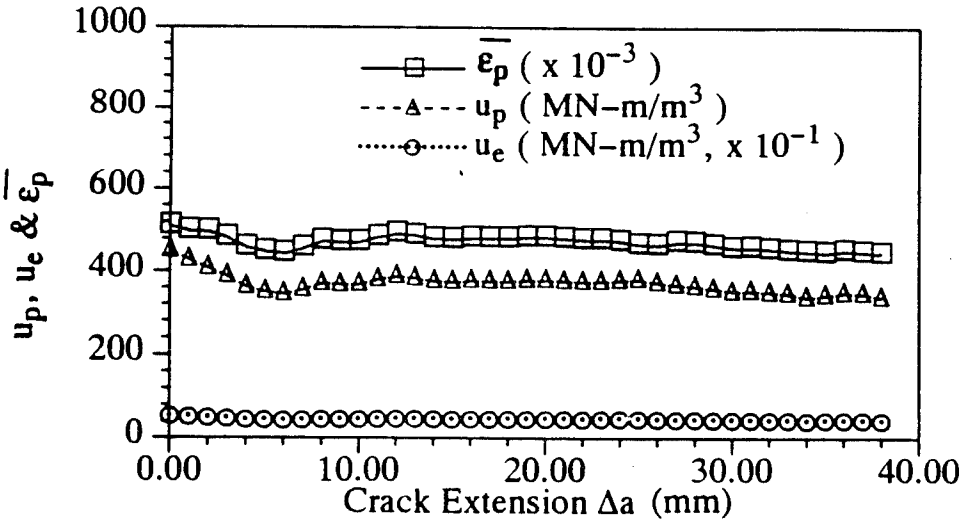
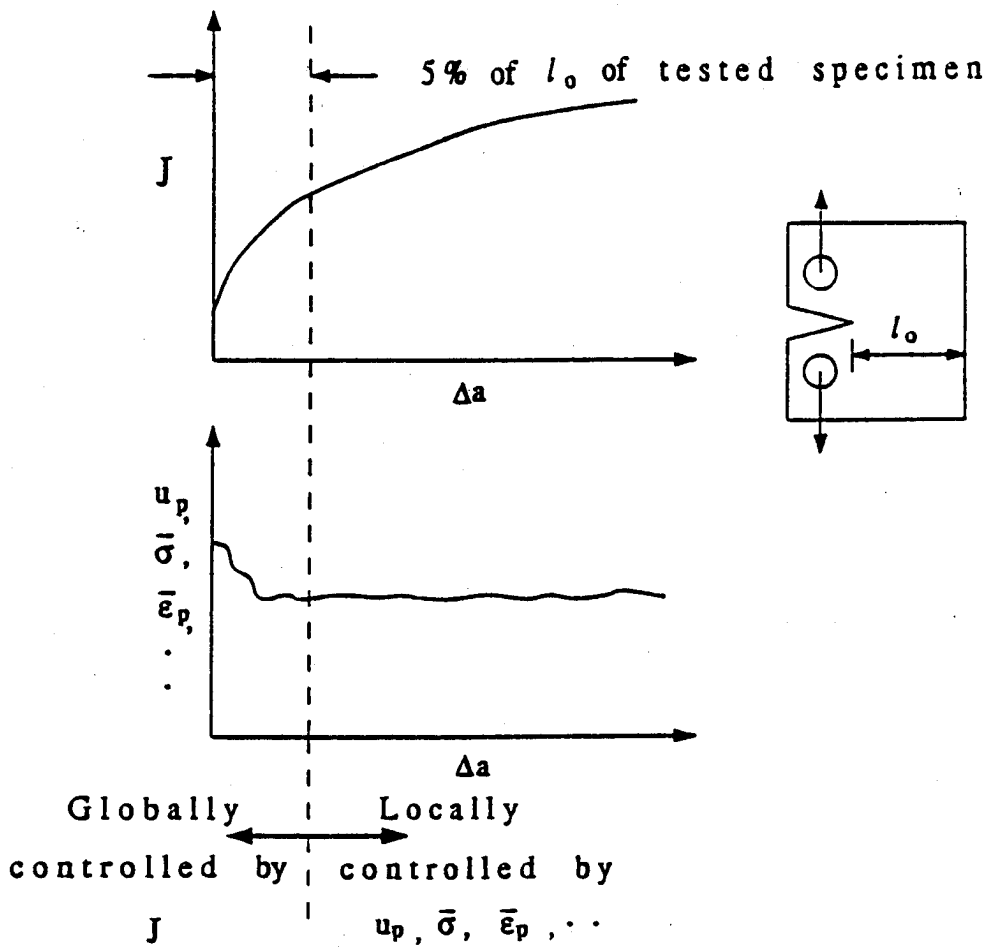


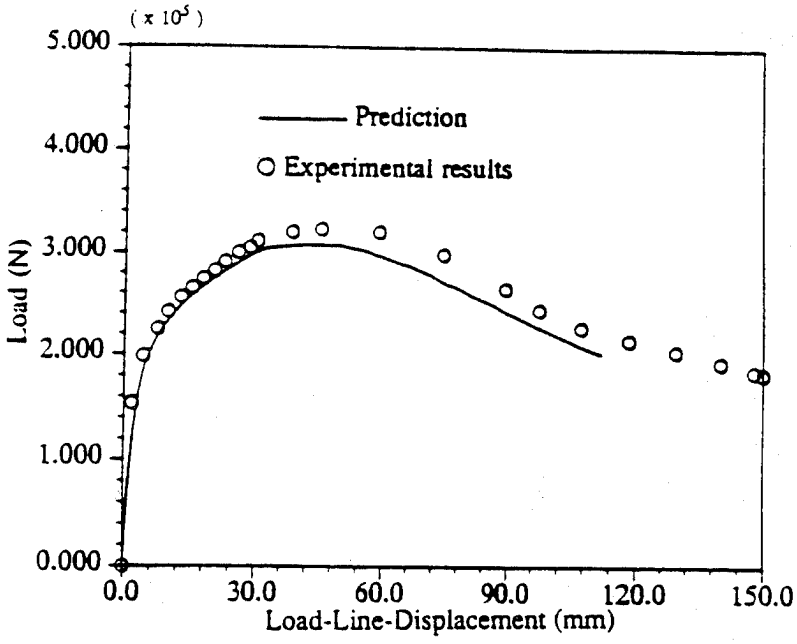
Figure 4.24 σ_y and $\bar{\sigma}$ versus Δa during crack extension.



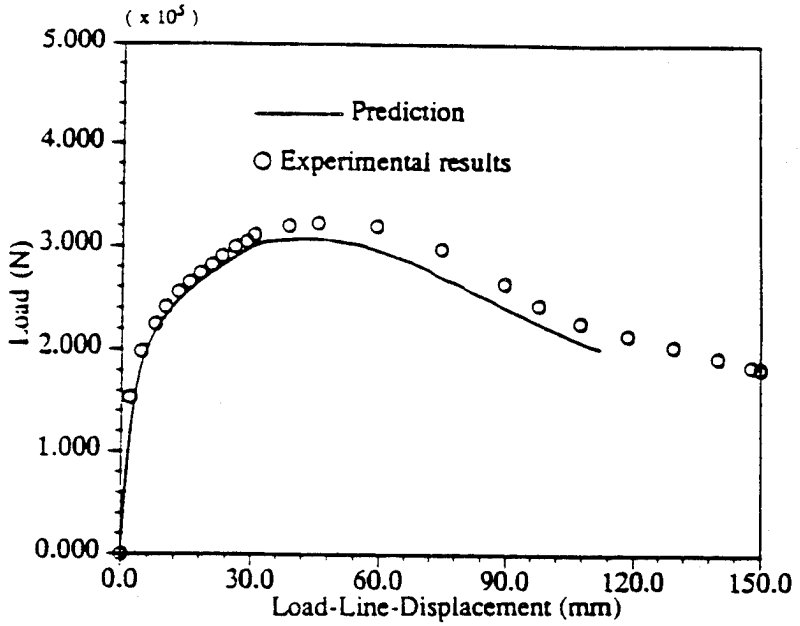
u_p, u_e and $\bar{\varepsilon}_p$ versus Δa during crack extension.



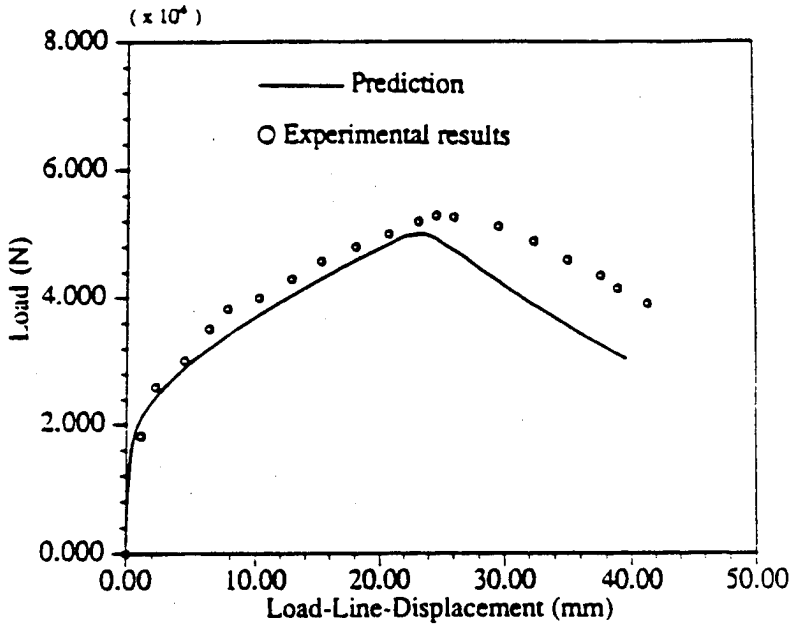
Schematic of GLFC methodology.



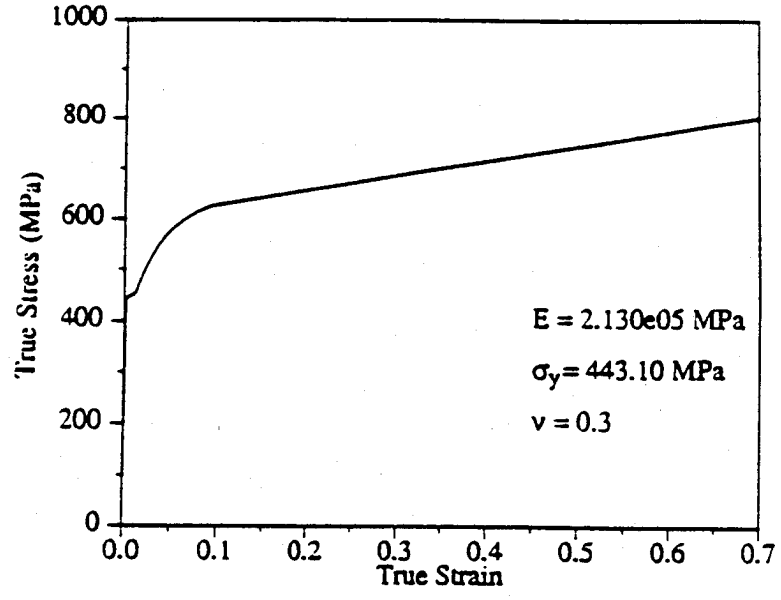
Load versus displacement prediction of 10T modified CT specimen from 3T modified CT specimen. (u_p was used as the local criterion)



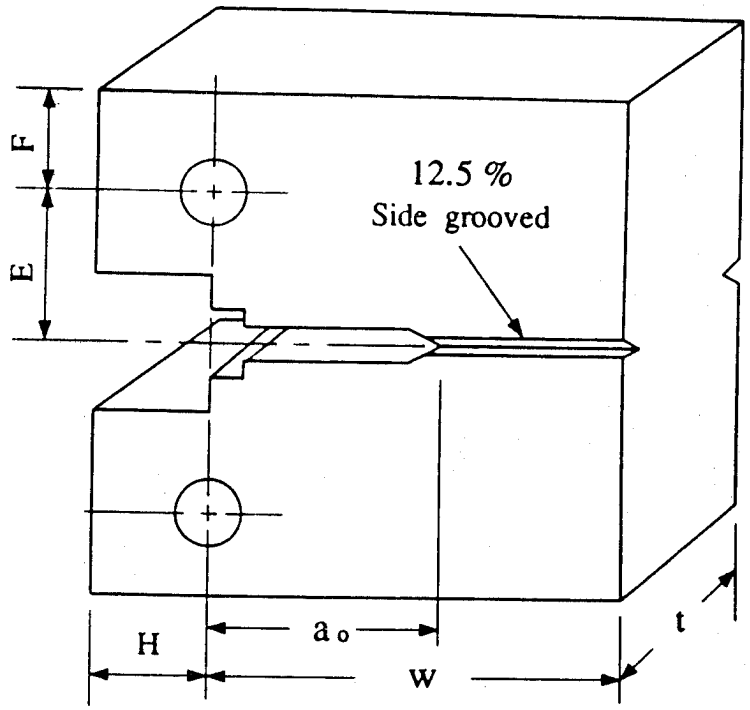
Load versus displacement prediction of 10T modified CT specimen from 3T modified CT specimen. ($\bar{\varepsilon}_p$ was used as the local criterion)



Load versus displacement prediction of 1T modified CT specimen from 3T modified CT specimen. (u_p was used as the local criterion)



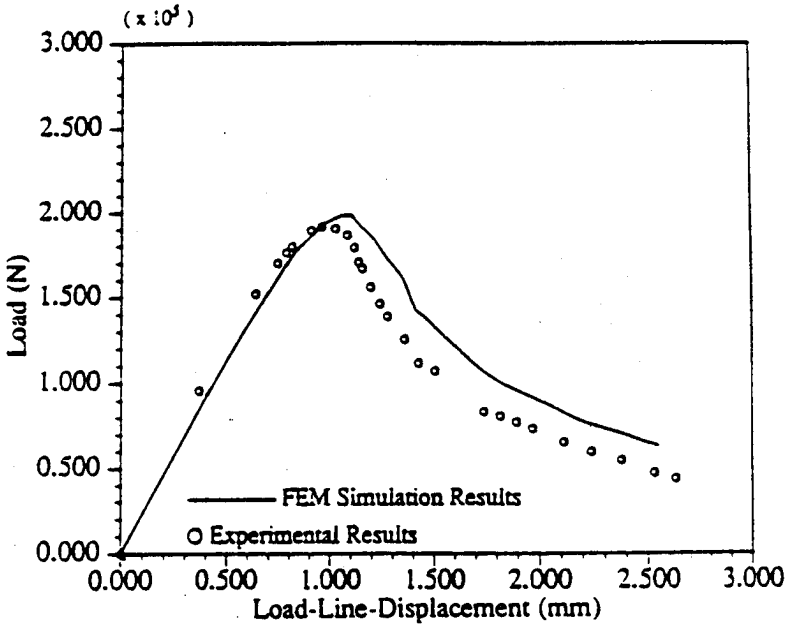
Uniaxial stress-strain data of ASTM A302B steel.



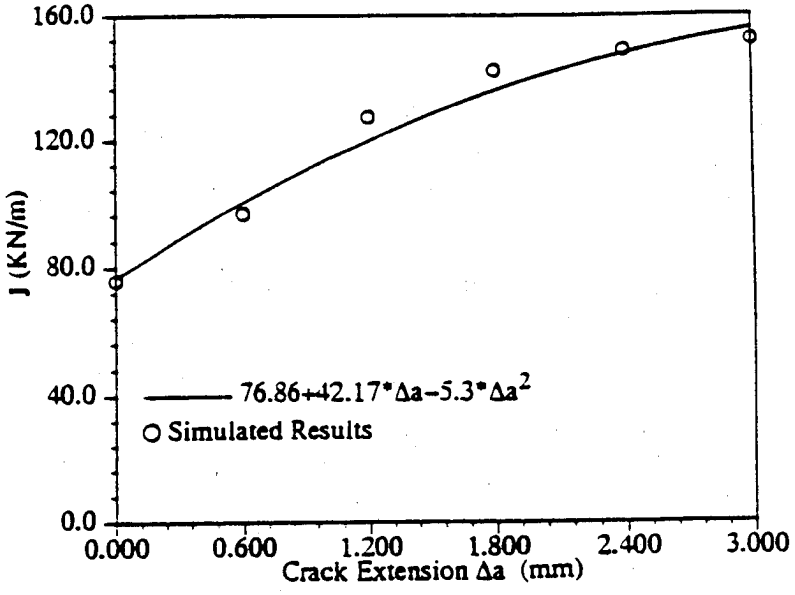
(mm)

specimen size	t	a	w	E	F	H
1 / 2 T	12.70	13.07	25.40	9.53	5.72	6.35
1 T	25.40	26.98	50.80	16.61	13.87	12.70
2 T	50.80	52.39	101.60	27.94	33.02	25.40
4 T	101.60	103.93	203.20	55.88	66.04	50.80

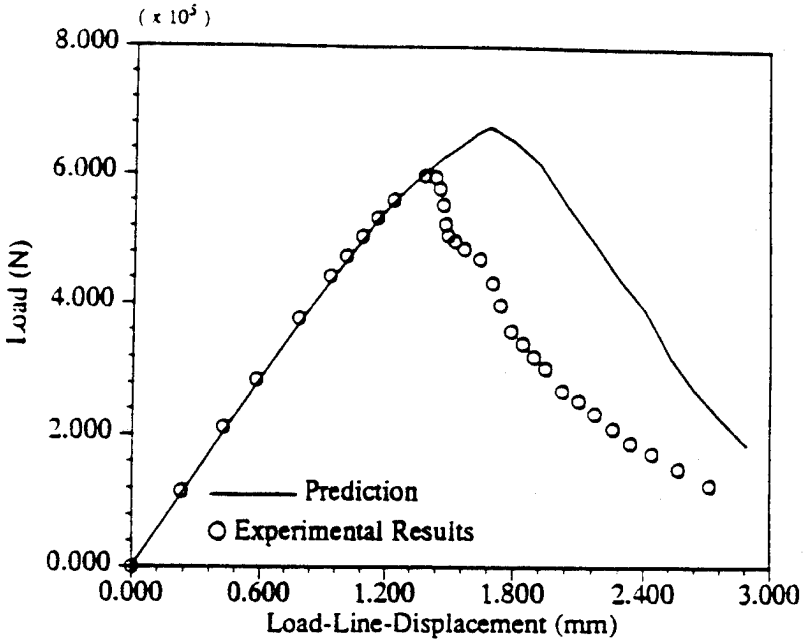
Standard compact tension specimens.



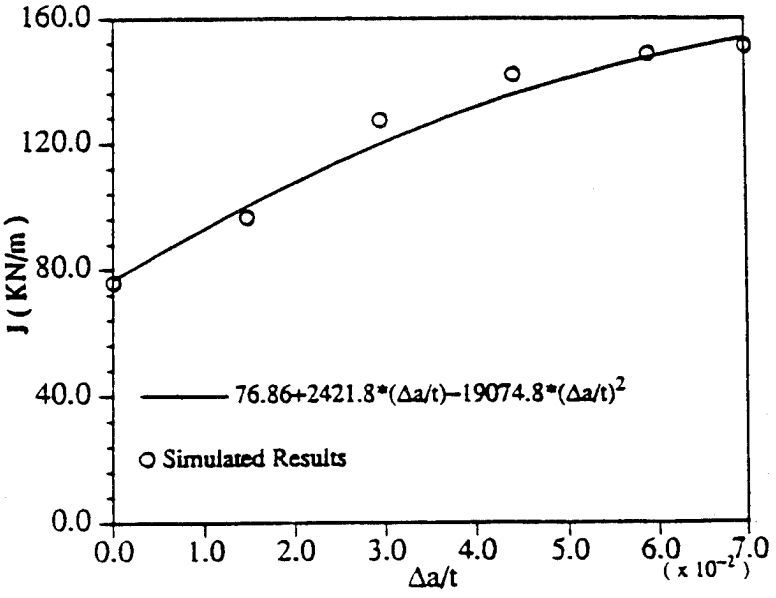
Simulated load versus load-line-displacement for 2T CT specimen.



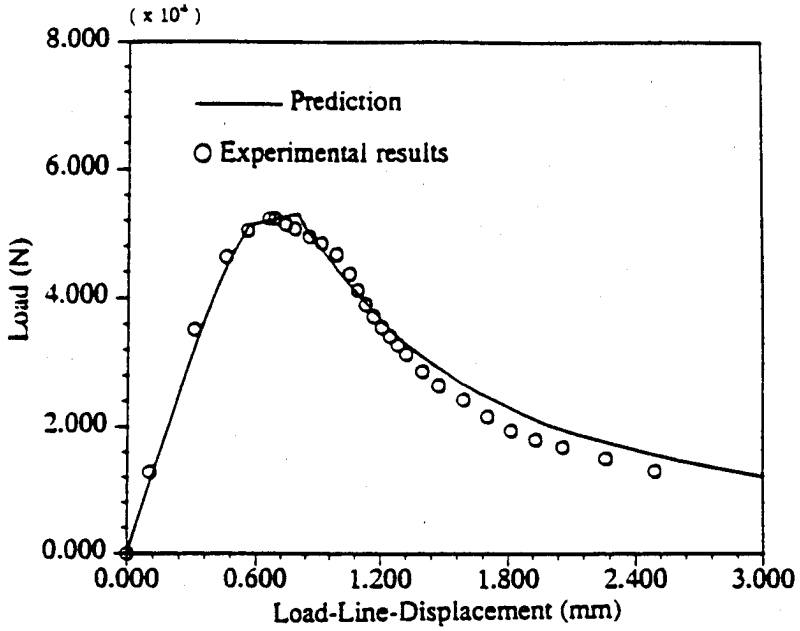
Initial portion of the J - Δa curve generated from 2T CT specimen.



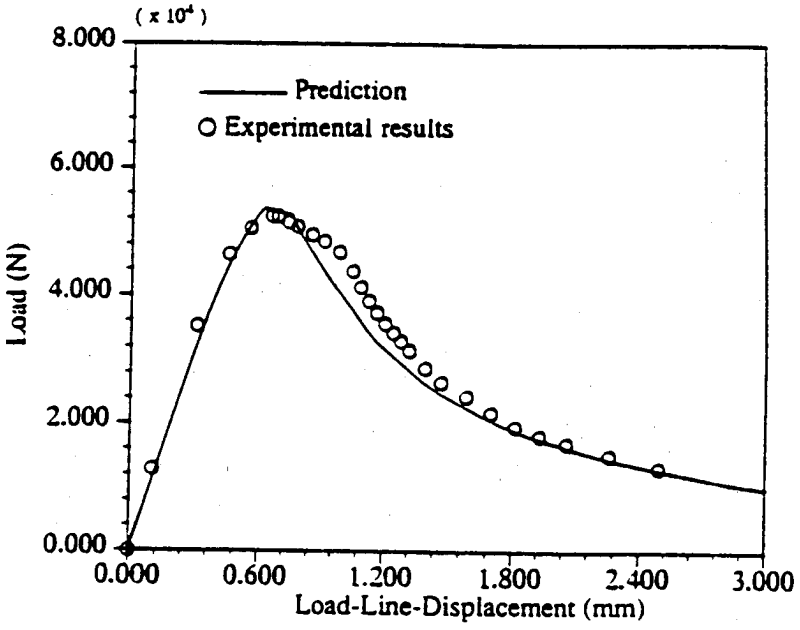
Load versus load-line-displacement prediction for 4T CT specimen without consideration of thickness effects. (2T CT was used as the "characterizing specimen")



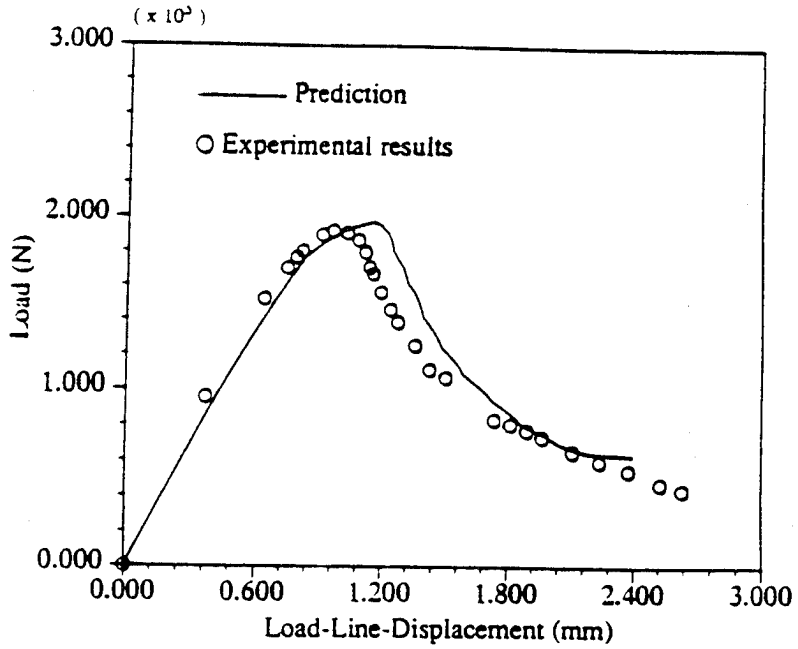
Initial portion of the J - $\Delta a/t$ curve generated from 2T CT specimen.



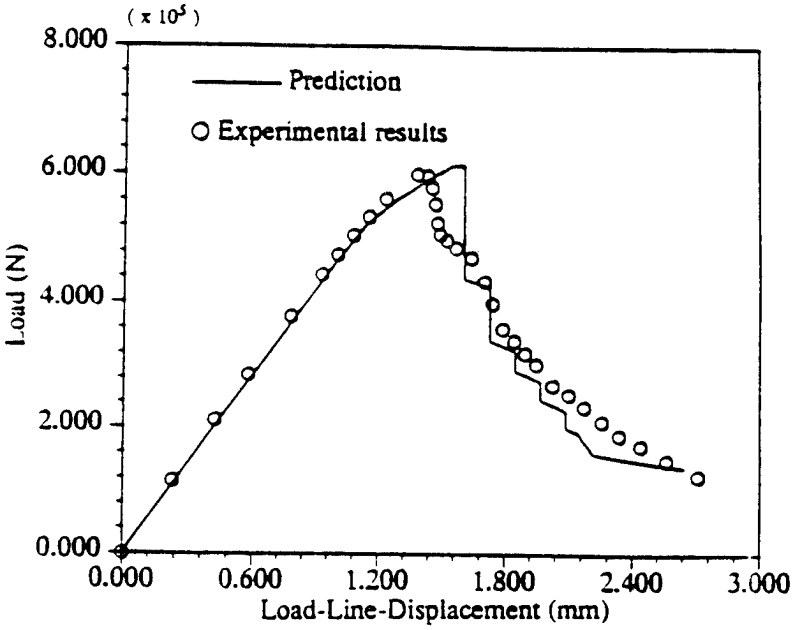
Predicted load versus load-line-displacement for 1T CT specimen by applying the GLC fracture criterion with consideration of thickness effects. (2T CT was used as the "characterizing specimen")



Predicted load versus load-line-displacement for 1T CT specimen by applying the GLC fracture criterion with consideration of thickness effects. (1/2T CT was used as the "characterizing specimen")



Predicted load versus load-line-displacement for 2T CT specimen by applying the GLC fracture criterion with consideration of thickness effects. (1/2T CT was used as the "characterizing specimen")



Predicted load versus load-line-displacement for 4T CT specimen by applying the GLC fracture criterion with consideration of thickness effects. (1/2T CT was used as the "characterizing specimen")

ACOUSTIC EMISSION MONITORING OF FULL-SCALE FATIGUE TESTS ON CANADIAN FORCES AEROSPACE STRUCTURES

Stuart McBride[1,2], Gerald Deziel[3] and Serge Le Guellec[3]

[1]Royal Military College of Canada
Materials Evaluation Laboratory
Kingston, Ontario, Canada, K7K 5L0

[2]AEMS Acoustic Emission Monitoring Services Inc.
4 Cataraqui Street, Suite #306
Kingston, Ontario, Canada, K7K 1Z7

[3]National Defence Headquarters
Department of National Defence
Directorate Aerospace Support Engineering
MGen George R. Pearkes Bldg
Ottawa, Ontario, Canada, K1A 0K2

INTRODUCTION

Acoustic emission monitoring of materials and structures has been the subject of considerable work since the 1960s [1, 2]. The principle of the method is that an incremental change in a defect as the result of an applied stress radiates an acoustic wave through the surrounding material. This stress wave can be detected by a piezoelectric sensor to become a measure of the incremental change in the defect. The accumulation of many such signals over many strain cycles in a structural test can provide a measure of the increase in crack face area for fatigue cracks during the monitoring period [3, 4].

The acoustic emission method has been investigated extensively in Canada for application to structures both in the laboratory [3, 4] and during fight [5-13]. This paper summarizes the recent use of acoustic emission in the CF116 (CF5) full-scale durability and damage tolerance test (FSDDTT) during 15,500 equivalent flying hours (EFH) of continuous monitoring of 16 separate structural areas. The implementation of acoustic emission monitoring for the CF188 International Follow-On Structural Test Project (IFOSTP) centre fuselage test is also described.

ACOUSTIC EMISSION MONITORING EQUIPMENT

Equipment Operation

Figure 1 illustrates the application of acoustic emission to the location of fatigue cracks which propagate under an applied load. The source (fatigue crack increment) radiates in all directions although it's strength may vary with direction or geometry of the structure through which it is propagating. The effect of the structure is to reduce the signal amplitude and to change the form of the signal as shown in figure 2. The arrival time at each of the detecting sensors will also depend on the distance from the source to the sensor and hence the difference in arrival time of signals from a source event at each of the sensors can be related to the source location.

The strain gauge shown in figure 1 provides a measure of the strain in the structure at the time of detection of the acoustic emission event by the sensors. This parameter is very important for the removal of structural noise, such as fretting, from the recorded data since incremental crack advance takes place at or near the maximum load while structural noise occurs predominantly at lower loads.

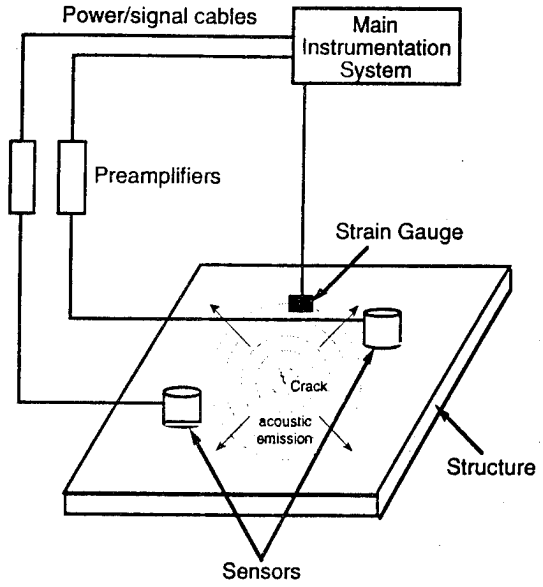


Figure 1 Schematic diagram of an acoustic emission test setup.

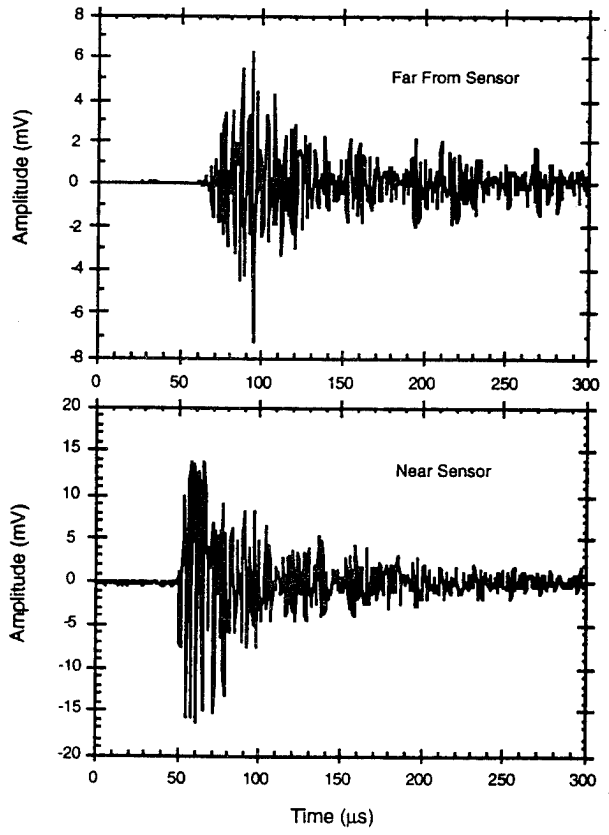


Figure 2 An example of acoustic emission signals close to a sensor and at a distance from the sensor in a dispersive structure. The signals which occur at different times, have different amplitudes and shapes.

The AEMS-1001 data acquisition system (figure 3) is designed to use difference in arrival time to locate acoustic emission sources which have predetermined characteristics (signal risetime, pulse length, amplitude) and which occur under structural loading conditions which may cause crack initiation and growth. The actual range of each characteristic parameter is empirically based on data obtained from monitoring fatigue tests in the laboratory (signal amplitude range and loading conditions for fatigue crack growth) together with the calibration of each structural location using a simulation source (amplitude, risetime, location via difference in arrival time).

To optimize sensitivity, location capability and EMI protection, the AEMS-DS1 sensors were developed. These sensors are much smaller in diameter (10 mm) than those normally used in acoustic emission tests and have a low profile (3 mm) for future in-flight applications. The small diameter is necessary for the CF188 IFOSTP application since many of the locations (particularly in the upper dorsal longeron) do not have sufficiently large, flat surfaces to permit attachment of conventional sensors. Also, the high sensitivity of the AEMS-DS1 sensor permits up to 40 dB detection range for acoustic emission signals resulting from fatigue crack growth in the CF188 metallic components of interest here under full-scale testing conditions.

The output of each of the piezoelectric sensor elements is amplified by a preamplifier with nominal gain of 40 dB. The resulting signal is buffered, logarithmically amplified and envelope followed (figure 4a). The output of each envelope follower is separately fed into the digital data acquisition system where the times of pre-selected amplitude threshold crossings (6 dB apart) are recorded and the digitized peak amplitude detected by a sample and hold technique (figure 4b). The amplified strain gauge values are digitized by an A/D converter, as required, and stored in memory. For the full-scale fatigue test described here, the number of cycles is the number of strain exceedances above a preselected threshold. This provides a numerical label which can be used to directly relate each detected signal to the load spectrum and load cycle position. All of the above data are compressed into an event record as shown in table 1.

The resulting data set is then extracted from the data acquisition system via an RS-422 interface, transferred by modem to the data analysis centre and stored on disk on an external computer. By using a data multiplexer, several 2-channel systems are operated in parallel to achieve multi-channel capability. Since each 2-channel system has a CPU there is no decrease in data acquisition rate as the number of channels is increased. Extensive screening of data, field analysis and interpretation can be carried out immediately on the remote host monitoring computer which is also used for remote control of all features of the multiplexed data acquisition systems. Final analysis and interpretation are accomplished using spreadsheet software. Table 2 lists the general specifications of the apparatus.

The AEMS-1001 loading parameter inputs have fixed ranges of 0-10 volts. In the CF188 IFOSTP application, strain gauge outputs are fed into these parametric inputs and digitized by an 8-bit A/D converter within the AEMS-1001. This strain gauge input is used to define the occurrence of loading conditions during which crack growth is most likely during programme loading such as that illustrated in figure 5. While each case must be considered separately such conditions would normally occur for strains within the top 20% of the strain spectrum. The AEMS-DA1 distribution amplifier is used to amplify and bias this strain range to the input range of the AEMS-1001 (0-10 V). Two such signal conditioning channels are provided and used for strain gauges symmetrically located on the test article. This facility takes into account asymmetries in the structural loading and provides back-up data for use in the event of a strain gauge malfunction.

The AEMS-DA1 distribution amplifier also provides an exceedance counter TTL pulse which provides a count of the number of times a given strain level has been exceeded. These pulses, which are sent to the cycle counter input, identify the location in the loading spectrum block at which the acoustic emission signals are detected. Since the counter in the AEMS-1001 is a hardware circuit, provision is also made in the distribution amplifier for setting the number of exceedances to a selected value should this be necessary.

To facilitate the control of several data acquisition systems a digital multiplexer is used to switch directly between systems and control several AEMS-1001 2-channel systems using a single monitoring computer. A modem is used to provide communication with each of the systems via the multiplexer when data transmission over a telephone line to a remote location is required. The communications system is operated directly from a menu in the AEMS software which takes into account the various possible configurations involving direct connection to a computer, modem transmission and operation with a multiplexer.

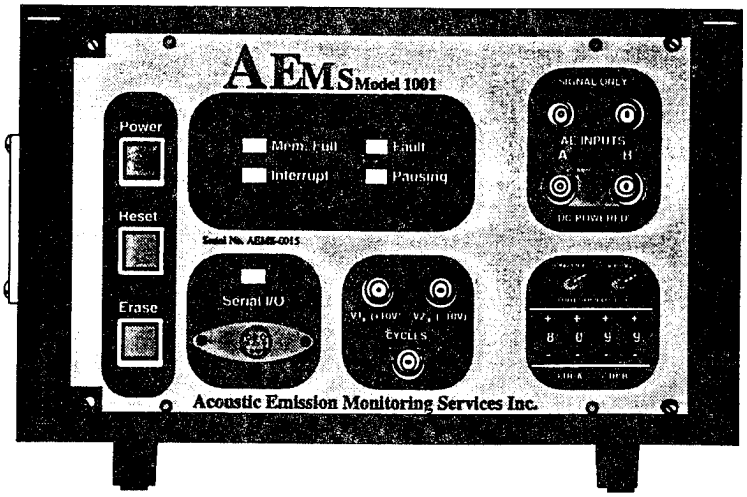


Figure 3 Diagram of the AEMS-1001 2-channel acoustic emission data acquisition system.

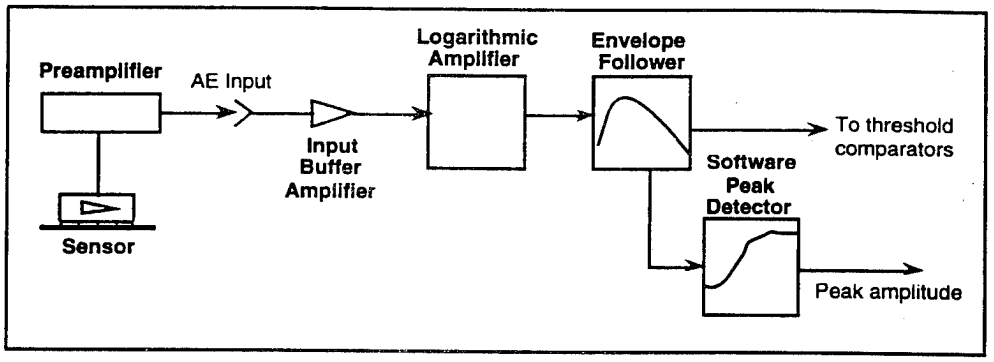


Figure 4a Schematic diagram of the AEMS-1001 acoustic emission signal conditioning.

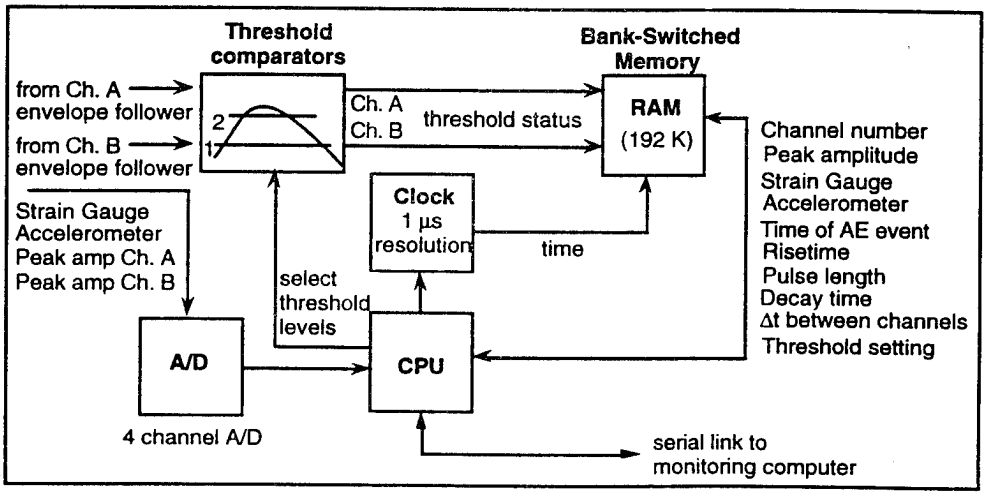


Figure 4b Schematic diagram of the AEMS-1001 acoustic emission data acquisition computer.

Cycles	Channel	AE Peak	Load 1	Risetime µs	Duration µs	Δt µs	Time µs	Time s
61592	0	52	99	4	559	255	59584217895	59584.2
61592	1	48	99	8	462	-16	59584217911	59584.2
61601	0	62	99.5	2	875	255	59603033331	59603
61601	1	56	99.5	4	740	-14	59603033345	59603
61630	0	52.3	99.5	4	456	255	59663804864	59663.8
61630	1	48.7	99.5	29	424	-16	59663804880	59663.8
61654	0	51	95.3	4	565	255	59716189148	59716.2
61654	1	51.7	95.3	7	600	-16	59716189164	59716.2
61845	0	50	97.4	4	560	255	60113147387	60113.1
61845	1	49.3	97.4	8	467	-16	60113147403	60113.1
61866	0	47	98.4	7	488	255	60156491320	60156.5
61866	1	46.7	98.4	7	208	-19	60156491339	60156.5

Table 1 Typical data file of acoustic emission parameters as recorded by the AEMS-1001 data acquisition system. Each row lists the data recorded when a sensor detects a signal.

2 Channels AE	60 dB Dynamic Range
2 Analog Channels	10 V Full-Scale
Power Supply	115/230 V, 47-440 Hz or Battery Powered
Power Consumption	10 Watts Maximum
Data Storage Capacity	384 Kbyte RAM with Battery Back-Up
Dimensions	23 cm x 13.5 cm x 25 cm
Weight	2 kg
Mass Data Storage	External Computer via RS-232 Interface
Windowing on all Recorded Parameters	Available On-Line and During Post Analysis

Table 2 General specifications of the AEMS-1001 digital data acquisition system for in-flight acoustic emission monitoring applications.

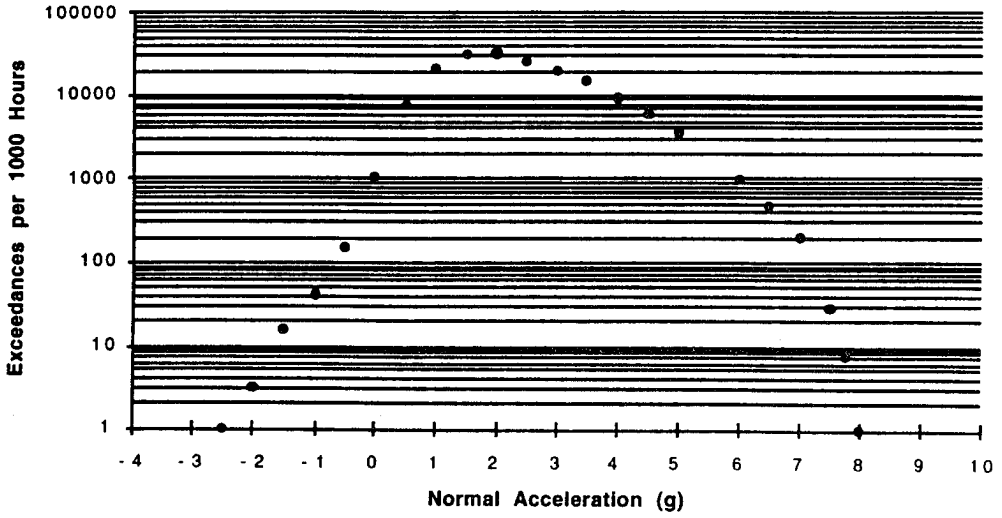


Figure 5 An example of an exceedance diagram derived from recorded in-flight data.

RESULTS AND DISCUSSION

Lower Wing Skin (8,540 EFH to 12,960 EFH)

Figure 6 shows the acoustic emission and nondestructive testing (NDT) defect observations for the wing (referred to here as wing #1) which was monitored from 8,540 EFH to 12,960 EFH. Typical fatigue crack sizes confirmed by NDT applied to fastener holes range from about 0.5 mm (20 thou) to about 1.5 mm (60 thou). These results have been previously reported [12]. The most important finding is that there are many examples for which acoustic emission was able to detect, locate and monitor fatigue cracks up to 3,000 EFH before NDT confirmation was possible. In many of these instances several periodic NDT inspections had been carried out on the structural area identified by acoustic emission before confirmation was achieved. These null results are believed to be the result of the effect of out-of-round fastener holes with damage, corrosion or rough surfaces on the efficacy of the NDT measurements although some of the locations were on the edge of the wing skin. Due to the substantial damage in wing #1, it was removed from the test article at 12,960 EFH and replaced by wing #2. The teardown inspection of wing #1, including the substructure, has been completed. The results were not available, however, for inclusion here but are being examined to take into account the effect of possible buried defects in internal components.

Lower Wing Skin (12,960 EFH to 20,000 EFH)

Based on the results of monitoring wing #1, the inspection and maintenance strategy was modified to rely more heavily on the acoustic emission monitoring results. Potential damage sites within zones identified by acoustic emission were inspected and repaired whether or not NDT confirmed the existence of fatigue damage. This strategy was used to accelerate the test and permitted wing #2 to be tested without mishap for 7,000 EFH. Retirement of the wing was for logistical reasons and was not because of impending failure. Also, acoustic emission data is used to produce estimates of defect size (crack face area) which are in agreement with the NDT results when NDT measurements are able to locate and size the defects provided the crack face geometry is assumed.

Figure 7 and table 3 summarize the acoustic emission and NDT results for wing #2. It should be noted that acoustic emission measures the increase in crack face area during the monitoring period while NDT provides principally the linear measurement of cracks at the surface. The extent to which acoustic emission and NDT measurements are in agreement can be estimated, however, by comparison with the crack face area calculated from the NDT measurements. Table 3 provides a comparison between the acoustic emission and NDT results in those cases where crack face area could be calculated from the NDT measurements. It is also seen that there are a number of cases in figure 7 and table 3 where NDT confirmation data is not given. Those locations for which fatigue damage was identified by acoustic emission but could not be confirmed by NDT are classified as "No Indication". Those for which a detailed inspection was not attempted due to impending wing replacement at 20,000 EFH are classified as "No Assessment".

Vertical Stabilizer Critical Radii (9,000 EFH to 24,000 EFH)

The vertical stabilizer critical radii were monitored using acoustic emission from 9,000 EFH to 24,000 EFH. The monitored region and sensor array are shown in figure 8. Prior to 13,000 EFH, cracks in the horizontal fuselage/vertical stabilizer attach angle bracket were located, monitored, confirmed by NDT and repaired. No significant activity occurred from the critical radii until 19,000 EFH. Acoustic emission detected crack growth from the zone shown in figure 8 for both sides of the vertical stabilizer. The acoustic emission estimate of the crack face area for the left and right sides are 2 mm^2 and 0.5 mm^2 respectively. Neither of these defects could be confirmed by NDT. Note, however, that these defects could be only 2 thou deep if they are through cracks in the skin. Metallographic analysis will be required to resolve this apparent contradiction. Another possible explanation is the existence of substructure defects in the vicinity of the critical radii. This is being investigated.

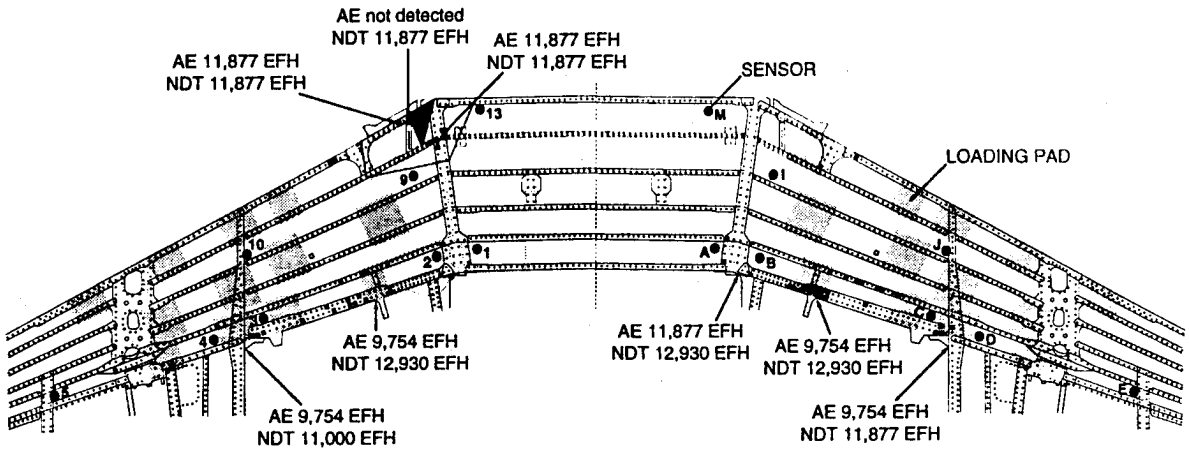


Figure 6 Summary of acoustic emission and NDT results for wing #1 (8,540 EFH - 12,960 EFH). The squares indicate the fastener holes in which fatigue cracks were confirmed using eddy current and LPI.

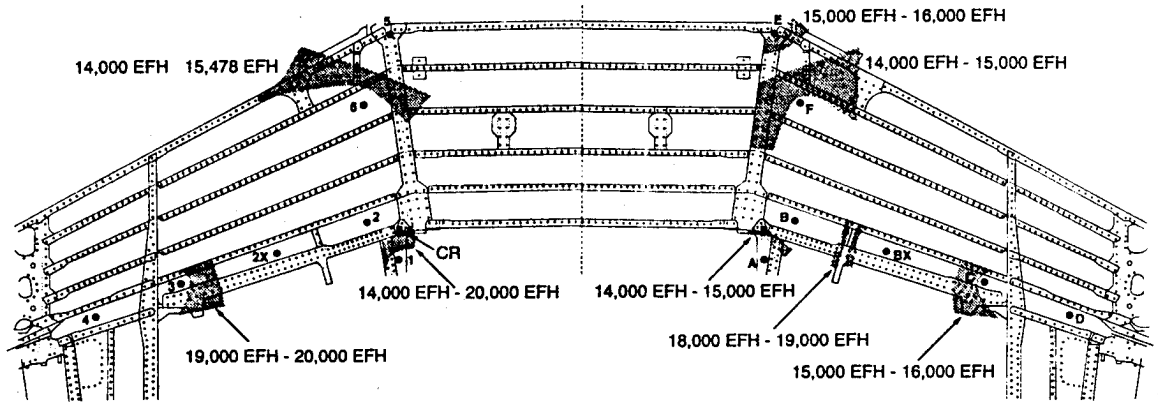


Figure 7 Acoustic emission fatigue crack growth zones (shaded areas) for wing #2 (12,960 EFH - 20,000 EFH). The squares indicate the fastener holes in which fatigue cracks were confirmed using eddy current and LPI.

Sensors	Location	Active EFH	Defect Area	NDT	Defect Location
1 & 2	Critical Radius (WS26L)	13 K-20 K	AE 10 mm^2 NDT 12 mm^2	1. 0.2 " D, 0.06" L 2. 0.05 " D, 0.6" L 3. 0.3 " D	CR, 15 K EFH
1 & 2	44% Spar (WS27L)	14 K-16 K	AE 1 mm^2 NDT 0.8 mm^2	0.020" (hole) 0.062" (countersink)	Hole #24, 15 K EFH
2X & 3	44% Spar (WS57L)	19 K-20 K	AE 1.1 mm^2	No Assessment	
5 & 6	15%/21% Spars (WS34L)	14 K-15,478	AE 5 mm^2 NDT Area Estimate Uncertain	0.5" to 0.7" D 0.04" L 0.02" L	Holes 149, 151, 191 at 15,478 EFH Holes 200, 209, 210 at 16 K EFH
A & B	44% Spar (WS27R)	14 K-15 K	AE 0.4 mm^2	0.06" L	Hole #24, 15 K EFH
B & C	44% Spar (WS57R)	15 K-16 K	AE 0.4 mm^2	No Assessment	
B & BX	44% Spar (WS34R)	18 K-19 K	AE 1 mm^2	No Indication	
E & F	15%/21% Spars (WS34R)	14 K-15 K 15 K-16 K	AE 0.6 mm^2 AE 0.6 mm^2	No Indication No Indication	
11 & 12	V-Stabilizer Critical Radius (Left)	19 K-20 K	AE 0.5 mm^2	No Indication up to 24 K EFH	
K & L	V-Stabilizer Critical Radius (Right)	19 K-24 K	AE 2 mm^2	No Indication	

Table 3 Summary of acoustic emission and NDT results for wing #2 and the vertical stabilizer critical radii. Wing #2 was monitored by acoustic emission from 12,960 EFH to 20,000 EFH. The vertical stabilizer critical radii were monitored from 9,000 EFH to 24,000 EFH.

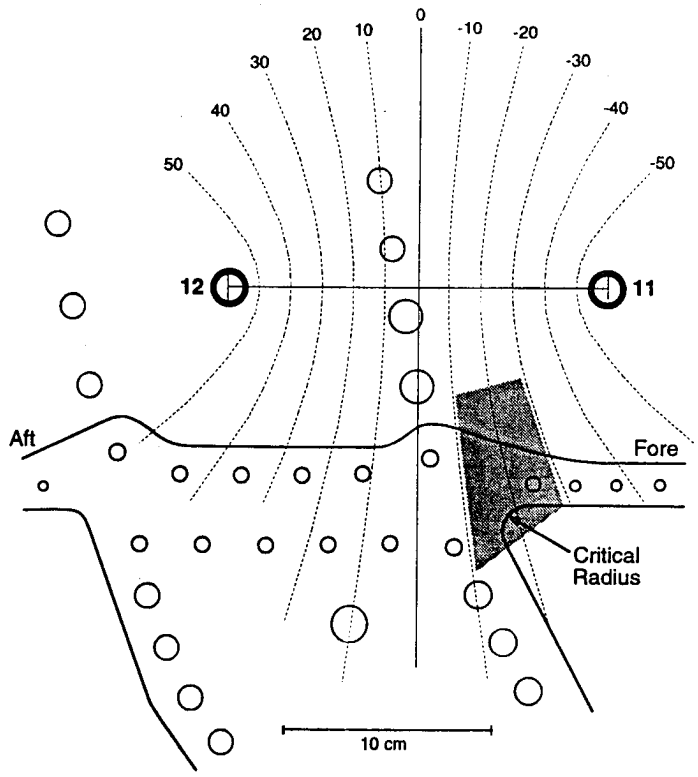
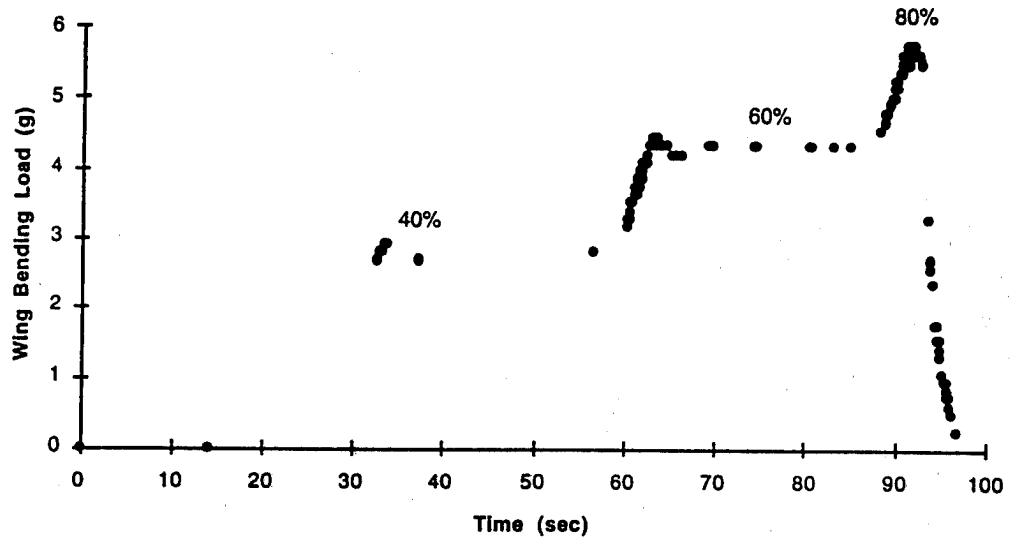


Figure 8 Acoustic emission monitored area on the vertical stabilizer (left-hand side). The contours define lines of constant difference in arrival time at sensors 11 and 12. These are used to locate the acoustic emission source zone.

Upper Wing Skin Boron-Epoxy Repair Patch (12,960 EFH to 20,000 EFH)

Cracks were found in-service at upper wing skin fastener holes. These fastener holes form the golden triangle, above the wing root rib (WS27). A unidirectional boron-epoxy repair patch was designed to alleviate this problem. It was decided to assess the effectiveness of this repair as part of the full-scale test. One fastener was oversized and had an EDM notch parallel to the axis of the fuselage in the aft location. This notch was intended to enhance the probability of crack initiation and therefore provide an optimal test of the effect of the repair patch. After the repair patch was installed, acoustic emission sensors were bonded to the upper surface of the repair patch a few inches inboard and outboard of the three fasteners as shown in figure 9.

Figure 9 shows the occurrence of acoustic emission signals as a function of upper wing skin strain up to 80% of 7 g loading for the first repair patch. Acoustic emission signals result from degradation of the patch and the adhesive bond. Figure 9 also shows the location of the initially detected damage at 40% of maximum loading and the spatial extent of the damage at the highest maximum applied step load (80% of 7 g). Examination of the repair patch by the National Research Council of Canada (NRC), Institute for Aerospace Research (IAR) showed damage and decohesion consistent with the acoustic emission results. The condition of the patch and bond were such that it was replaced by a second patch which was tested and fatigued for 7,000 EFH. Acoustic emission monitoring of the initial static loading of the second boron-epoxy repair patch was much more comprehensive than for the first repair patch due to the success of acoustic emission at identifying the damage area and the precise loading conditions at which damage occurred. Figure 10 shows the acoustic emission sensor array used to monitor the integrity of the entire second repair patch during the initial step loading. Sensor pairs were used to monitor the edges of the patch and the group of three fasteners. Figure 10 also shows the acoustic emission activity as a function of upper wing skin strain for the edge of the patch. No significant activity was detected from the vicinity of the three fasteners which is the location of primary concern. Figure 11 shows the area of degradation during subsequent fatiguing for 3,000 EFH. Examination of the repair patch by NRC/IAR showed damage and decohesion consistent with the acoustic emission results [14, 15]. The wing, with installed repair patch, was monitored continuously for a total of 7,000 EFH without incident. Metallographic analysis of the EDM notch has not been carried out at this time.



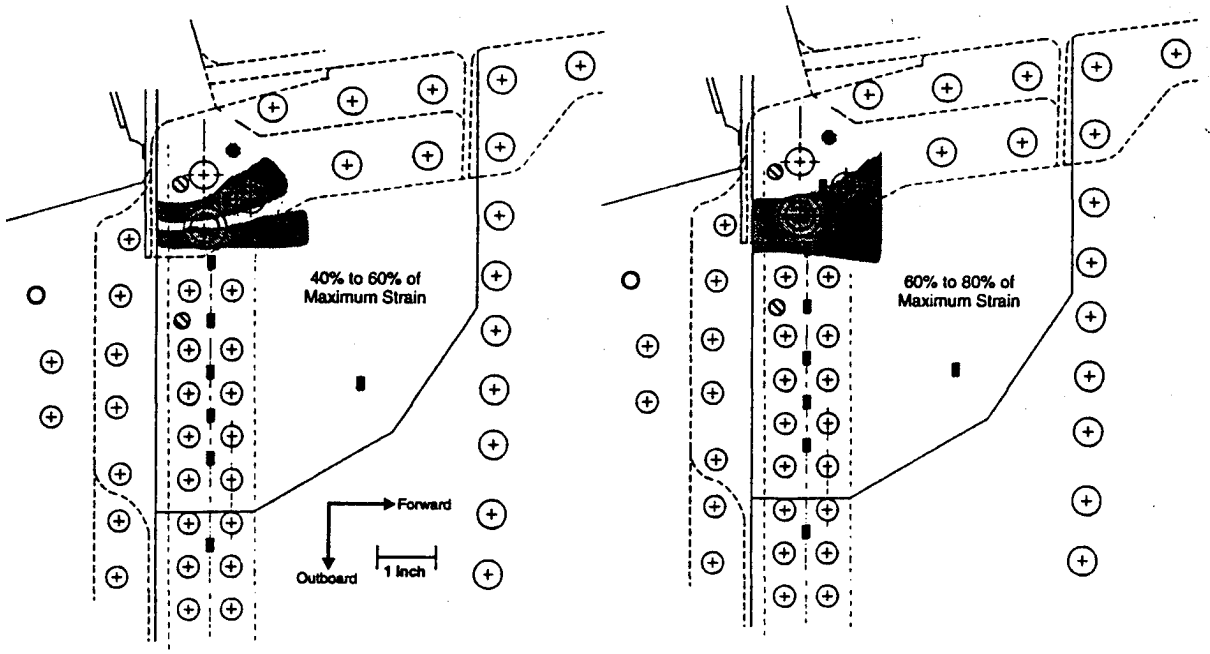
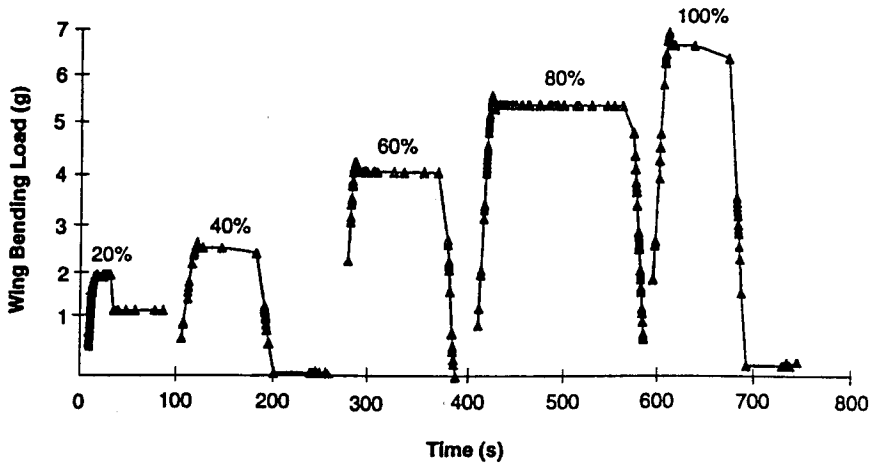
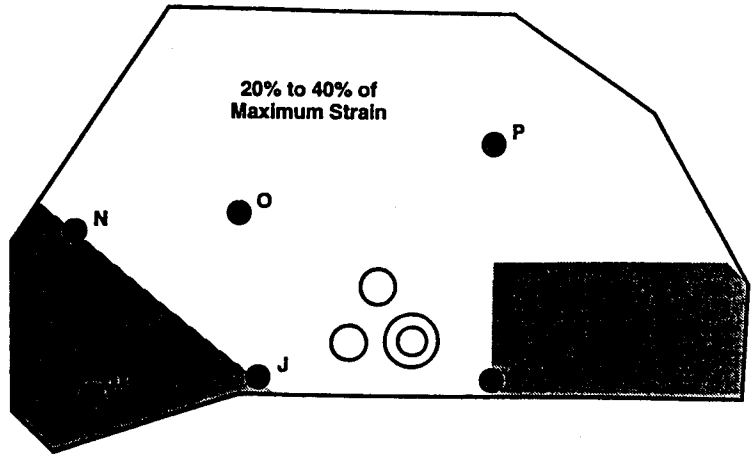


Figure 9 Degradation of the first boron-epoxy repair patch during step loading. The shaded areas indicate the acoustically active zones which are interpreted as the degradation zones.





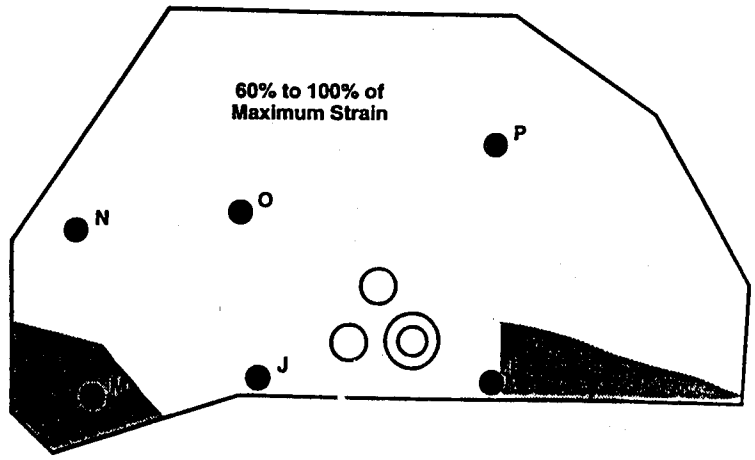


Figure 10 Degradation of the second boron-epoxy repair patch during step loading. The shaded areas indicate the acoustically active zones which are interpreted as the degradation zones.

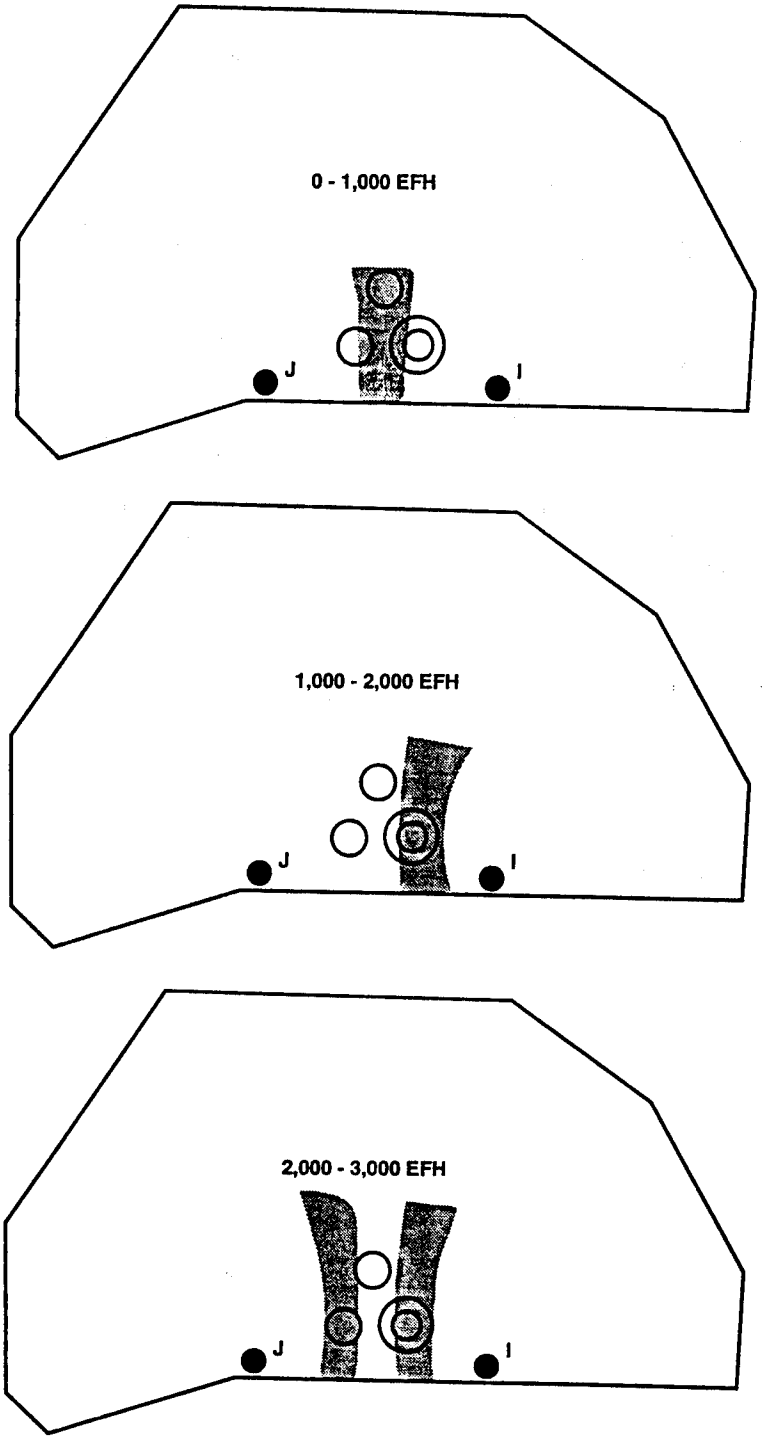


Figure 11 Acoustic emission detection of degradation zones for the second boron-epoxy repair patch during 3,000 EFH of testing

CF188 IFOSTP (Centre Fuselage Test)

Acoustic emission sensors and instrumentation have been installed on the CF188 IFOSTP centre fuselage test article at Canadair Defence Systems Division, Mirabel. Figure 12 is a schematic diagram illustrating the centre fuselage structure. At the commencement of the test 22 locations will be monitored. These are listed in table 4 and include 14 locations on the three main bulkheads, 3 locations on the upper dorsal longerons and 2 locations on the inner wing front spar lower flange A sensor pair has been installed for each location listed in table 4 and a detailed calibration of each sensor array carried out. The calibration is sufficiently comprehensive to permit the location of acoustic emission sources and estimate the amount of crack growth corresponding to each source. Figure 13 is a schematic diagram of the acoustic emission instrumentation.

Acoustic emission monitoring of the CF188 centre fuselage locations will be carried out by both AEMS Inc. and Canadian Forces NDT personnel at CFB Trenton. Parallel analyses of data will be used to train the service personnel on acoustic emission monitoring of aircraft structures to assess the feasibility of introducing acoustic emission to the Canadian Armed Forces for future in-service use.

SUMMARY AND CONCLUSIONS

The CF116 full-scale test has served to demonstrate the efficacy of acoustic emission monitoring in aircraft structures. In the course of 15,500 EFH of full-scale test monitoring it has improved in capability and reputation from a method that "might be able to detect defects in aircraft structures" to a quantitative method for locating and estimating fatigue crack growth in metallics and determining the loading conditions under which they propagate. Acoustic emission has also been shown to be useful for locating and monitoring degraded zones in boron-epoxy composite repair patches and to determine, in detail, the loading conditions under which the degradation advances.

With this background, acoustic emission is now sufficiently proven to be considered a candidate technique for assessing and monitoring the integrity of airframes and airframe components. The future application of the technique to the CF188 centre fuselage test is expected to have a substantial impact on the downtime required for structural inspection, to improve the reliability of inspection particularly in remote inaccessible locations and to minimize structural disassembly for NDT inspections. Minimizing structural disassembly is very important due to the high cost and also the possible effect of reassembly on the validity of the entire test.

ACKNOWLEDGEMENTS

The data acquisition and crack source location were carried out by AEMS Acoustic Emission Monitoring Services Inc., 4 Cataraqui Street, Suite #306, Kingston, Ontario, K7K 1Z7 under contract to Directorate Aerospace Support Engineering via Supply and Services Canada. Supporting funds for the subsequent data analysis was provided to the Royal Military College of Canada by the Department of National Defence, Canada (Academic Research Program FUHDU and CRAD funding from Defence Research Establishment - Pacific 144690RMC01). The CF116 full-scale ground durability and damage tolerance test and NDI measurements were conducted by Canadair, Montreal, under the supervision of M. Beaulieu and Y. Beauvais. The CF188 IFOSTP centre fuselage test is conducted by Canadair (J. Roussel). The National Research Council of Canada, Institute for Aerospace Research (D. Simpson) provided load spectrum development and validity testing expertise. The project is managed by G. Deziel, DAS Eng 6-3-5, of National Defence Headquarters. The project was monitored by Major M. Brassard, DAS Eng 6-2, National Defence Headquarters, Ottawa, Ontario and W. R. Sturrock of the Materials Section, Defence Research Establishment - Pacific, Victoria, British Columbia.

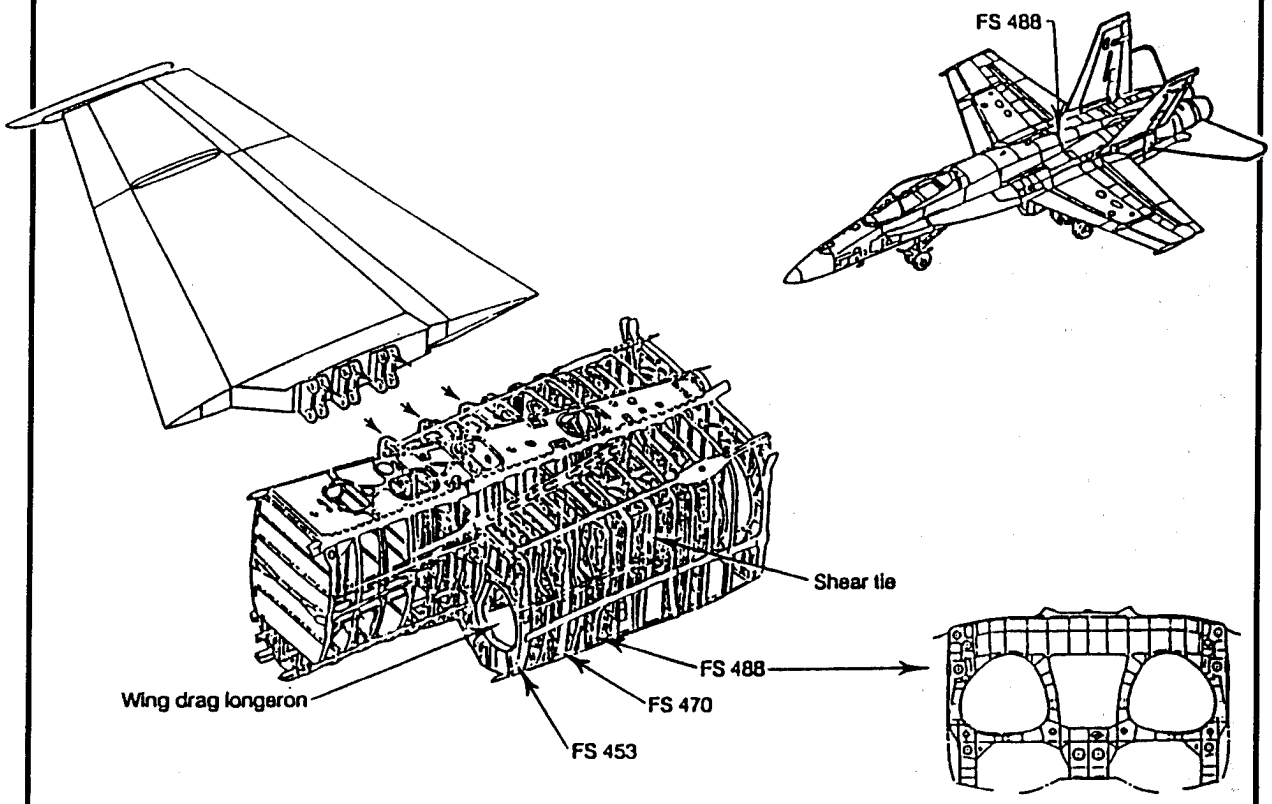


Figure 12 Schematic diagram showing the CF188 centre fuselage structure. This structure includes the three main bulkheads and upper dorsal longerons.

Box No.	Locations	Location Description	Continuous Monitoring	Alternately Monitored	Strain Gauge
1	1	488 bulkhead LH lower lug area	X		Bulkhead
2	2	488 bulkhead RH lower lug area	X		Bulkhead
3	3	488 bulkhead LH upper flange at crease area	X		Bulkhead
4	4	488 bulkhead RH upper flange at crease area	X		Bulkhead
5	5	470.5 bulkhead LH lower lug area	X		Bulkhead
6	6	470.5 bulkhead RH lower lug area	X		Bulkhead
7	7/8	470.5 bulkhd LH/RH MLG retract actuator area		X	MLG R.A.
8	11	453 bulkhead LH lower lug area	X		Bulkhead
9	12	453 bulkhead RH lower lug area	X		Bulkhead
10	13/14	453 bulkhead LH/RH fuel hole area		X	Bulkhead
11	15/16	453 bulkhead LH/RH upper flange at crease area		X	Bulkhead
12	17/18	Dorsal longeron LH/RH FS 455 to FS 460.5		X	Longeron
13	19/20	Dorsal longeron LH/RH FS 484.5 to FS 498		X	Longeron
14	21/22	Dorsal longeron LH/RH FS 543 to FS 548		X	Longeron
15	23/24	Inner wing LH/RH front spar lower flange LEF transmission hinge area		X	Bulkhead

Table 4 Summary of locations selected to be monitored by acoustic emission at the commencement of the CF188 IFOSTP centre fuselage test.

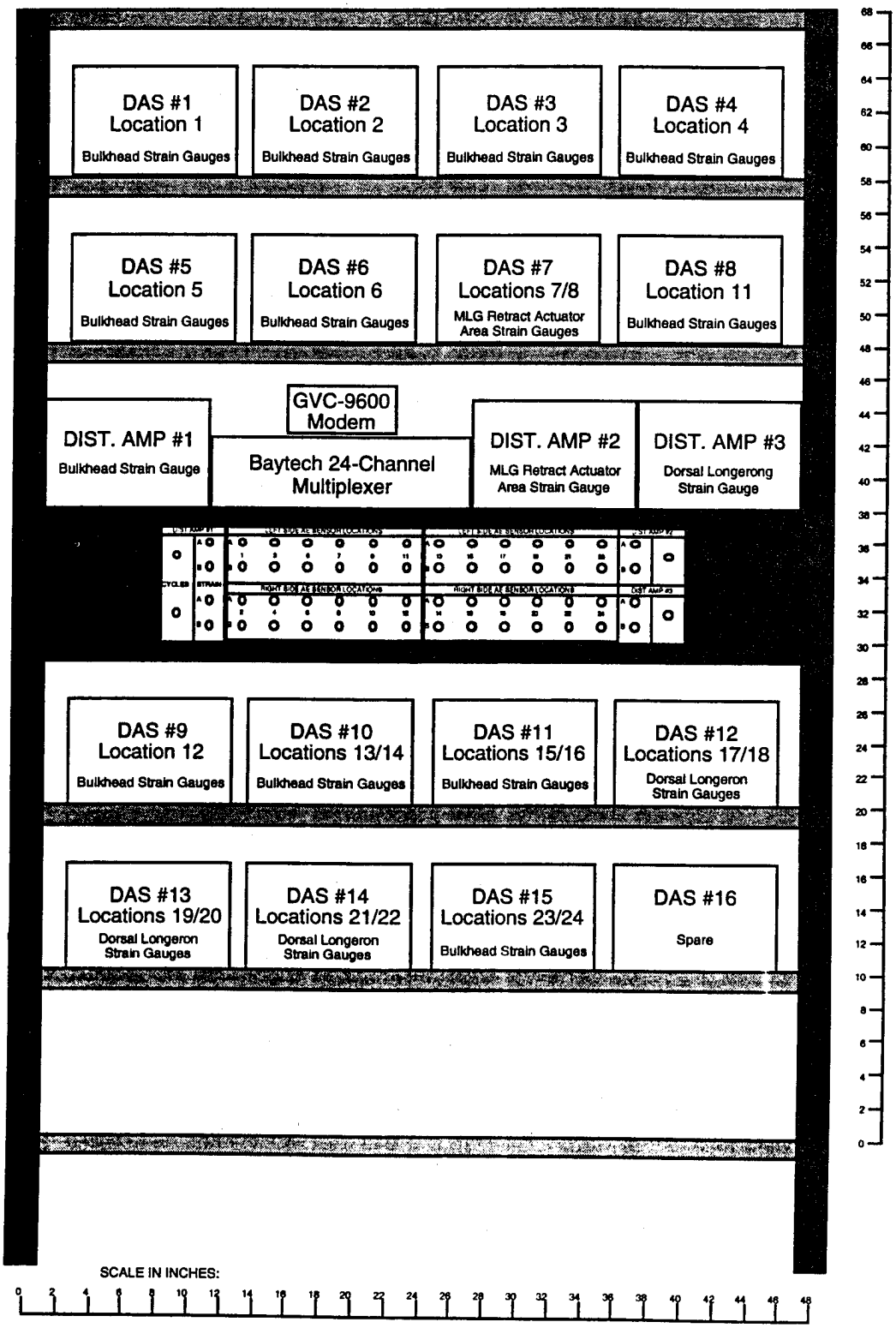


Figure 13 Schematic diagram of the acoustic emission instrumentation used to monitor 22 locations in the CF188 IFOSTP centre fuselage test.

REFERENCES

1. T. F. Drouillard, *Acoustic Emission, A Bibliography with Abstracts* (Plenum Data Co., New York, 1979).
2. T. F. Drouillard, *Bibliography Update* (J. Acoust. Emis., 1982-92).
3. S. L. McBride and Y. Hong, Review of Progress in Quantitative NDE, Vol. 12, edited by D. O. Thompson and D. E. Chimenti (Plenum Press, New York, 1993), p. 2199.
4. S. L. McBride, P. Bowman and K. I. McRae, Progress in Acous. Emis. IV, pp. 528-535, Yamaguchi et al, eds. Japan Society of NDI (1989).
5. S. L. McBride, M. D. Pollard and Y. Hong, Review of Progress in Quantitative NDE, Vol. 12, edited by D. O. Thompson and D. E. Chimenti (Plenum Press, New York, 1993), p. 2191.
6. S. L. McBride, M. R. Viner and M. D. Pollard, Review of Progress in Quantitative NDE, Vol. 11B, edited by D. O. Thompson and D. E. Chimenti (Plenum Press, New York, 1992), p. 2275.
7. S. L. McBride, M. R. Viner and M. D. Pollard, Review of Progress in Quantitative NDE, Vol. 10B, edited by D. O. Thompson and D. E. Chimenti (Plenum Press, New York, 1991), p. 1913.
8. S. L. McBride and J. W. Maclachlan, J. Acoust. Emis. 1, p. 223 (1982).
9. S. L. McBride and J. W. Maclachlan, J. Acoust. Emis. 1, p. 229 (1982).
10. S. L. McBride and J. W. Maclachlan, J. Acoust. Emis. 3, p. 1 (1984).
11. S. L. McBride, M. D. Pollard, J. D. MacPhail, P. Bowman, and D. T. Peters, J. Acoust. Emis. 8, p. 4 (1989).
12. S. L. McBride and G. Deziel, 1992 USAF Structural Integrity Program, WL-TR-93-4080, pp. 496-506 (1993).
13. S. L. McBride, Proceedings of the "Composite Repair of Metallic Aircraft Structures", NRC, Ottawa (Sep 93).
14. D. Raizenne, Proceedings of the "Composite Repair of Metallic Aircraft Structures", NRC, Ottawa (Sep 93).
15. P. Gaudert, M. D. Raizenne, N. C. Bellinger and J. B. R. Heath, IAR/NRC Report # LTR-ST-1973 (1994).

Effect of Mechanical Paint Removal Processes on the Fatigue Lives of Aircraft

CLARE A. PAUL

Wright Laboratory
Flight Dynamics Directorate
Structures Division

WL/FIBE Bldg 45
2130 Eighth St Ste 1
Wright-Patterson AFB OH 45433-7542

Voice: 513-255-6104
Fax: 513-476-4999

8/29/95

Environmental Compliance Requirements

Coating Removal

Non-environmentally compliant chemical strippers will not be allowed to be used for stripping paint



Federal Facility Compliance Act of 1992

"The United States hereby expressly waives any immunity...as well as any other nondiscriminitory charges that are assessed in connection with a Federal, State, Interstate, or Local solid waste or hazardous regulatory program."

Legislative and Executive Order

"The proposed rule would limit this use of organic HAP-containing chemical stripper to an average of 26 gallons per aircraft for commercial aircraft and 50 gallons per aircraft for military aircraft, calculated on an annual basis."

Federal Register, Vol 59, No 107, June 6, 1994, Proposed Rules

Types of Paint Removal Processes

Coating Removal

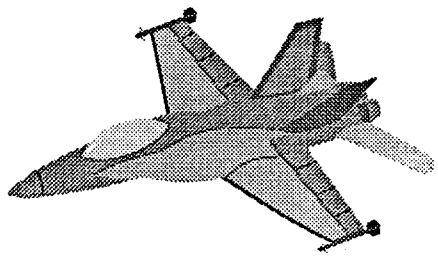
Action Memorandum Signed by Gen Yates 17 Feb 94 directs focus on several stripping removal processes*

- Plastic Media Blast
- Water Jet Technology
  - High Pressure Water
  - Medium Pressure Water
- Environmentally Compliant Chemicals

Backshop (Components)
- Wheat Starch
- Bicarbonate of Soda

However, other processes continue to be developed

- $C0_2$ Blasting
- Flash-lamp
- Laser
- Hybrid Processes
- Others



* - Capt. Carolyn Westmark, Wright Laboratory Paint/Coating Wrokshop, 12-13 May 94

Removal Methods by Organization

Coating Removal

Aircraft	E-3	B-1	B-52	C-135	F-4	F-16	C-5	OV-10	T-37	T-38	A-7	A-10	F-111	F-15	C-130	C-141	KC-10	CF-18	Hawk, Hunter	F-16	F-4	A-310	Small Corporate
Organization	OC	OC	OC	OC	OO	OO	SA	SA	SA	SA	SM	SM	SM	WR	WR	WR		CAF	RAF	RNethAF	GAF		Hunting Aircraft Inc.
Chemical Stripper	X		X	X												X							
Plastic Media Blasting					X	X	X	P	X	X	X	X	X	X				X	Trial	X	X		
Flashjet														P									
High Pressure Water		P		P																			
Scuff Sanding		X																					
Aqua Miser/BOSS															X	P							
Aqua Miser	P		P																		Trial		
Wheat Starch																							X

X - Current
P - Planned

8/29/95

Impact of Paint Removal Processes on Fatigue Life of Metallic Structure

Coating Removal

- Does the mechanical stripping process reduce the fatigue life of an aircraft?
- If it does, how much is the fatigue life reduced in aircraft?

We need to develop the least expensive tests possible which will accurately infer the impact (degradation, no-change, enhancement) of mechanical stripping processes on aircraft fatigue life

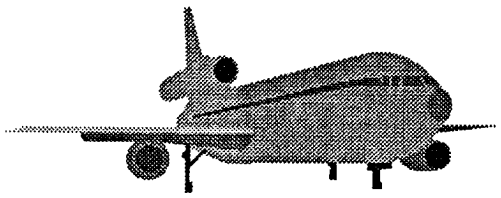
- AFMC Paint/Depaint Technology Screening Committee (IPT) (Mar 1993)
  - Engineering Qualification Test Plan
- IATA Task Force (Dec 1990)
  - IATA Guidelines --> SAE Standard
- NASA/EPA - (MOU Oct 1992)
  - Cooperative test program to assess depaint/cleaning process technology (Draft SOW Oct 93)

Potential Degrading Effects

Coating Removal

Crack Nucleation

- Dense Particle Embedment
- Backside Tensile Residual Stresses
- Loads Induced by the Stripping Process
- Surface Roughness



Crack Growth Rate

- Backside Tensile Residual Stresses

Other

- Anodize Cracking
- Alclad Removal
- Skin Deformation
- Crack Detection
- Mositure Entrapment
- Cadmium Plating Loss

8/29/95

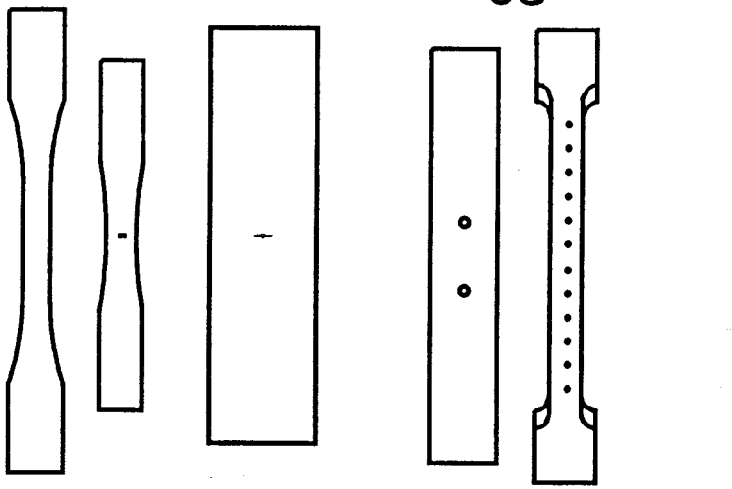
Structural Integrity Test Programs for Aluminum Sheet

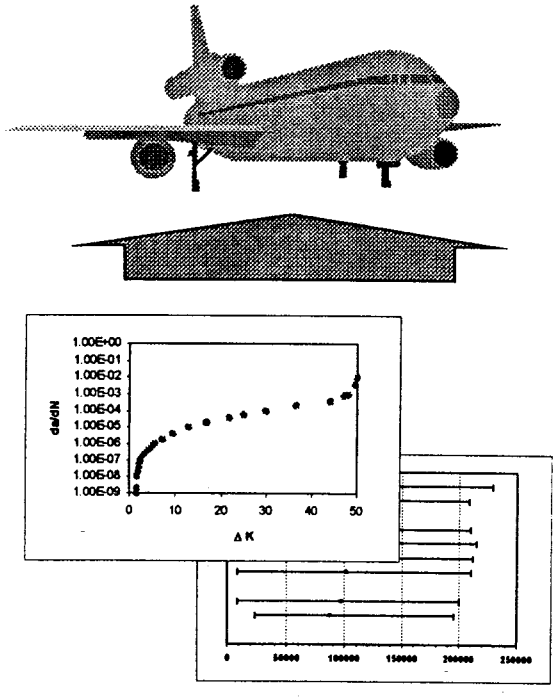
Coating Removal

Organization	Media	Start Date	End Date
SwRI for SA-ALC	PMB		'94
Battelle for WR-ALC	Aqua Miser BOSS		'94
DASA Manching	PMB, Wheat Starch		'94
Boeing	Wheat Starch		'93
Galaxy Scientific for FAA	PMB+	'91	Nov '93
Unitied Technologies, USBI Co. for WL/MT	High Pressure Water	Jul '91	Apr '93+
Boeing Commericial	PMB	'86	'91 (?)
Battelle-Dupont	PMB		Jan' 90
OC-ALC	PMB		Jul '89
Schlick/MBB for Canadian F-18	PMB		Oct '89
MBB	PMB	'86	'88
University of Utah for Ogden ALC	PMB		'88
Grumman for NASC	PMB+	May '83	May '87
Battelle for WR-ALC	PMB	Oct '85	Jul '86
AFWAL/MLSA	PMB	Oct '84	Aug '85

Inferences of Impact of Mechanical Stripping on Aircraft Fatigue Life Using Simple Specimens

Coating Removal





8/29/95

Fatigue Test Results for PMB

Coating Removal

Organization	Media Type	Report Year	Effect on Fatigue Life
NAVAIR	Poly-Plus	1984	Not documented
WRDC/MLSA	II	1985	No reduction
Battelle	II	1986	Significant loss for thin skin, No loss for fatigue specimens with fasteners installed
Grumman	I, II	1987	No reduction
Battelle	I, II, III	1987	No reduction
WL/FIBE	I, II	1988	Reduction
University of Utah	II	1988	No reduction
OC-ALC	I	1989	Substantial reductions
Battelle	I, II	1989	Substantial reductions
General Dynamics	I, II	1989	Increase using 3.5 MOH; indeterminate using 3.0 MOH; decrease noted for specimens with Kt=2.4
Boeing	I, II	1990	No reduction

Surface Roughness Test Results for PMB

Coating Removal

Organization	Media Type	Report Year	Effect on Surface Roughness	Material	Thickness
NAVAIR	Poly-Plus	1984	115 µin - 255 µin (different media sizes)	7075-T6, Clad	Unknown
WRDC/ML	II	1985	47-330 µin for 1st to 56-98 µin for 4th	7075-T6, Clad	0.016 in
Battelle	II	1986	238 µin for 1st to 80 µin for 4th for clad, Bare material had a max. of 18 µin	7075-T6	0.071 in
Grumman	3.0 and 3.5 MOHS	1987	20 µin to 270 µin (2024-T3 clad)	See Grumman Effort	
Boeing	I, II	1990	190 - 400 µin	2024-T3, Clad	0.040 in

Typically, the surface roughness will be less than 20 µin for the Alclad sheet material.

8/29/95

Crack Growth Rate Test Results for PMB

Coating Removal

Organization	Media Type	Report Year	Effect on CGR
Battelle	II	1986	Increase
Battelle	I, II	1987	Substantial increase
General Dynamics	I, II	1989	Increase
OC-ALC	I	1989	Substantial increase
Battelle and duPont	I, II, III, V_X, V_L	1989	Slight increase with Types II, III and V_X; Inclusive results with Types I and V_L
Boeing	I, II	1990	No change
Galaxy Scientific	II	1993	Substantial increase

PMB Process Restrictions

Coating Removal

Restrictions	US Air Force T.O. 1-1-8 1989 Sep 1 Change 6 1991 Sep 30	US Navy PMB Spec Rev A 1991 Jun 19	Boeing D6-54705 1988 Nov 14	Douglas CSD #4 1988 Oct 19	Airbus SIL 51-007 1989 Sep 6 AIPS 02-100 1990 Jan 30
No of PMB Cycles	No limit	No limit	One	Four	No Limit
Min Thick Al	0.016-in	0.016-in	0.036-in	0.050-in	0.047-in
Anodize Parts OK PMB	Yes	Yes	No	Yes	Yes

Source: Charles C.T. Chen, Mark Muller and John W. Reinhardt, "Effects of Plastic Media Blasting on Aircraft Skins," DOT/FAA/CT-91/27, AD-A274 817, November 1993

8/29/95

Current Overall Data Collection and Assessment Studies

Coating Removal

Independent Agency Needs to Collect, Collate, Compare and Assess Past Studies

A good start...

Universal Technology Corporation through WL/MLS

- Assessed past studies and discussed many factors associated with chemical and PMB stripping. Structural Integrity was of one of the factors addressed.

Also...

Joint Depot Maintenance Analysis Group (JDMAG)

- PMB - Report Finished
- Sodium Bicarbonate - Draft Report
- CO_2 - In-progress
- Laser - In-progress
- Water - Start Jan 95

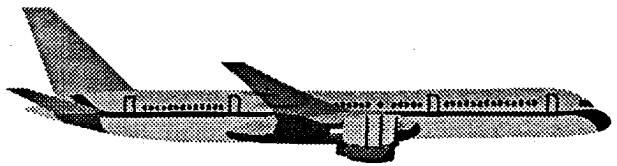
- Need to include foreign as well as domestic sources for data
- Data comparisons needed for all data

Collect, Assess and Recommend (Phase I)

Coating Removal

More needed...

- High Pressure Water
- Medium Pressure Water
- Bicarbonate of Soda
- Wheat Starch?
- Environmentally Compliant Chemical?



Other factors which impact fatigue life

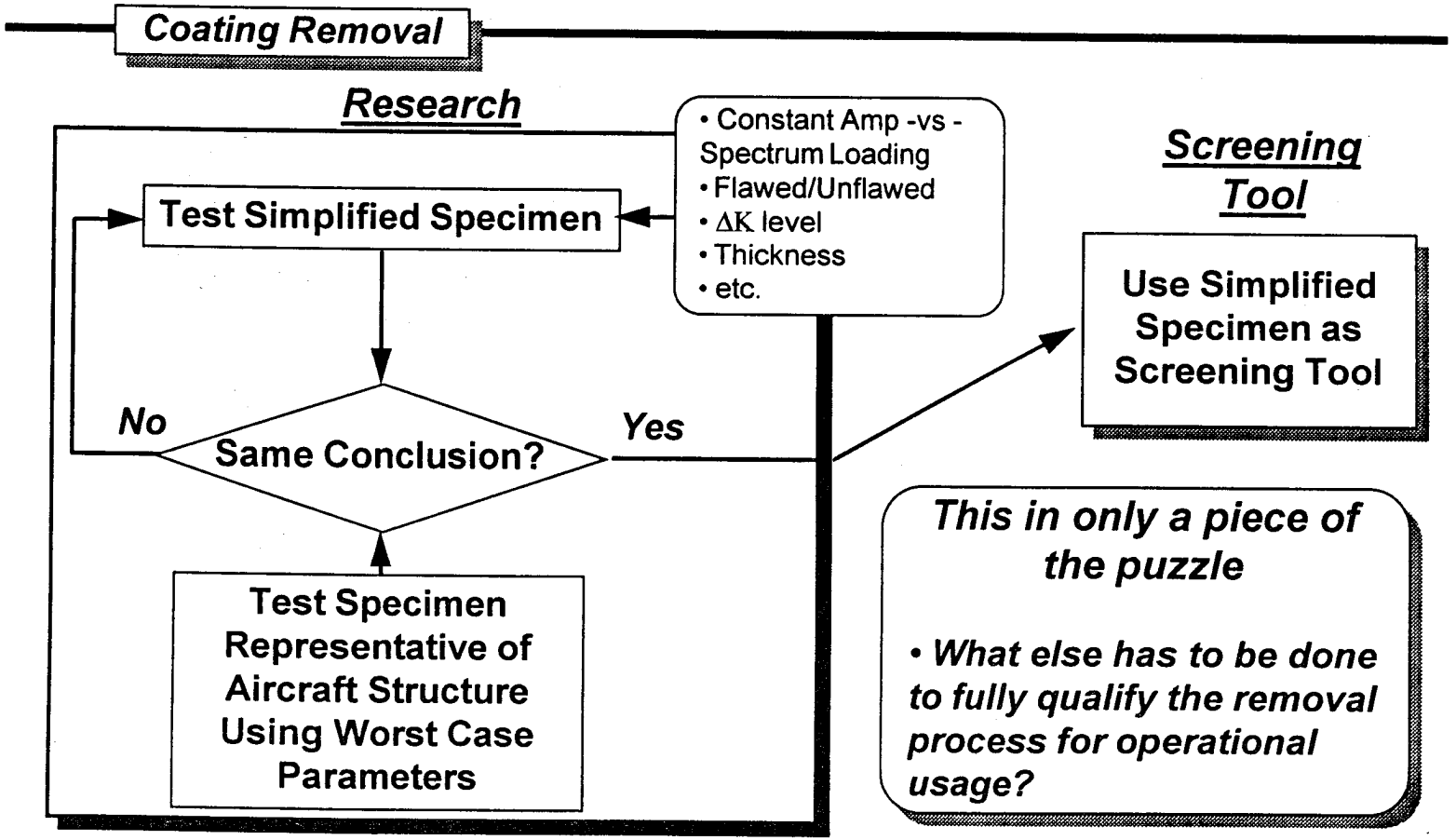
- Clad erosion
- Cadmium plating loss
- Anodic layer cracking
- Moisture entrapment
- Corrosive chemicals

Output of Phase I Effort

- Assessment of all Collected Data
- Data Handbook
- General Recommendations
- Aircraft Skins/Geometry Diagrams
- Design of Phase II Test Plan

8/29/95

Generalized Research Plan and Testing (Phase II)



PROGRESS TOWARDS A COMPREHENSIVE FATIGUE ANALYSIS PROGRAM FOR ROTARY AND FIXED-WING AIRCRAFT

by

Preston R. Bates, Research Engineer, Georgia Tech Research Institute

Gary Chamberlain, Aerospace Engineer, Warner Robins Air Logistics Center

1994 USAF Structural Integrity Program Conference

December 6-8, 1994

Hyatt Regency San Antonio

San Antonio, Texas

PROGRESS TOWARDS A COMPREHENSIVE FATIGUE ANALYSIS PROGRAM FOR ROTARY AND FIXED-WING AIRCRAFT

by
Preston R. Bates, Research Engineer, Georgia Tech Research Institute
Gary Chamberlain, Aerospace Engineer, Warner Robins Air Logistics Center

1.0 INTRODUCTION

Successful mature weapons systems employed by the military services are always called upon to fly faster, higher, stealthier, for longer ranges, with greater maneuverability, and usually with heavier payloads. Very often, missions involve frequent low level nap-of-the-earth or terrain following flight, even in adverse weather. In order to ensure the structural integrity of aging weapons systems under their ever-increasing mission severity, the U.S. Air Force (USAF), through the Warner Robins Air Logistics Center (WR-ALC), has spearheaded a developmental integrity and force management concept applied to helicopters based on the success of their fixed wing counterparts. The specific goals of the program are to:

a) enhance aircraft safety,
b) improve maintenance procedures,
c) increase mission capability, and
d) lower life cycle cost.

Over the past several years, Georgia Tech and Sikorsky Aircraft have supported structural integrity efforts for USAF helicopters. It has been found that while rotorcraft fuselage structural integrity is similar to that for fixed wing aircraft as defined in MIL-STD-1530A (Reference 1), many issues are peculiar to rotorcraft applications particularly with regard to dynamic components, which makes the effort much more complicated. This paper documents work completed as part of a series of tasks required to develop a Structural Integrity Computer Program (SICP) for use by WR-ALC, Georgia Tech, and Sikorsky in support of the H-53 (Figure 1) Aircraft Structural Integrity Program (ASIP), and other aging aircraft in the fleet. After a general description of the SICP, this paper details the results of a task comparing available linear elastic fracture mechanics techniques with emphasis on stress intensity factor solutions, and recommends specific crack growth technology to use for further SICP development.

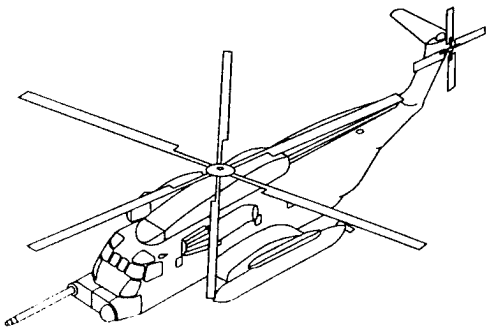


Figure 1. USAF H-53 Helicopter.

Damage tolerance criteria was never specified for the H-53 (originally fielded in the mid 1960s) or any aircraft of that vintage. Consequently, trying to solely apply damage tolerance based fleet management in accordance with design criteria outlined MIL-A-87221 (Reference 2) to such vehicles does not appear practical. Recent American Helicopter Society (AHS) Fatigue and Damage Tolerance Subcommittee studies have shown that there seems to be little correlation between crack initiation time and crack growth time for a given component. Some hybrid form of damage tolerance and safe-life procedures must therefore likely be adopted. Therefore it becomes apparent that a tool such as the SICP to evaluate both crack initiation and crack growth has distinct advantages and utility to the ASIP manager.

In general, dynamic components are particularly difficult to manage using damage tolerance because of relatively rapid crack growth, and may therefore be better suited to safe-life or a hybrid program. The technology and analysis requirements of the Engine Structural Integrity Program are considered to be the most appropriate guideline for future dynamic component design (Reference 3). However, based on experience gained in prior contracted Sikorsky and Georgia Tech crack growth studies for the USAF, force management for helicopters based on damage tolerance analysis may still be possible in a significant amount of helicopter structures. It is necessary to develop more realistic stress spectra, crack models, and material data (Reference 4), which can be achieved by using a combination of flight tests, ground tests, and analytical/computational procedures.

2.0 STRUCTURAL INTEGRITY COMPUTER PROGRAM

A key element of the overall effort is a structural integrity computer program (SICP) which will perform comprehensive fatigue analysis of airframe and rotor system components to determine inspection intervals and component retirement times on an ongoing basis. It is intended to function either in a stand-alone mode or with other logistical software and hardware that track parts and aircraft usage. The SICP provides the ASIP manager with the capability to rapidly make decisions under changing weapon system mission requirements. Once in place, this tool can be used in any helicopter application, and even for fixed-wing aircraft, because the basic architecture and elements of the processor are the same for all applications, and only require data bases specific to a particular weapons system.

Figure 2 illustrates how the computer program will function. All tasks are brought together graphically to provide a clear picture of their interactions. There are six basic steps to the processor, as labeled by the dark shaded boxes. First, usage spectrum generation is either based on a generalized spectrum for the entire fleet, or tailored for an individual aircraft through the use of an individual aircraft tracking program (IATP). For the selected components, accurate stress spectra will be developed utilizing cycle counted flight test measurements or stress analysis. To permit the calculation of stress spectra for mission segments not included in flight tests, a CAMRAD rotor/fuselage loads model is being correlated to flight test measurements to

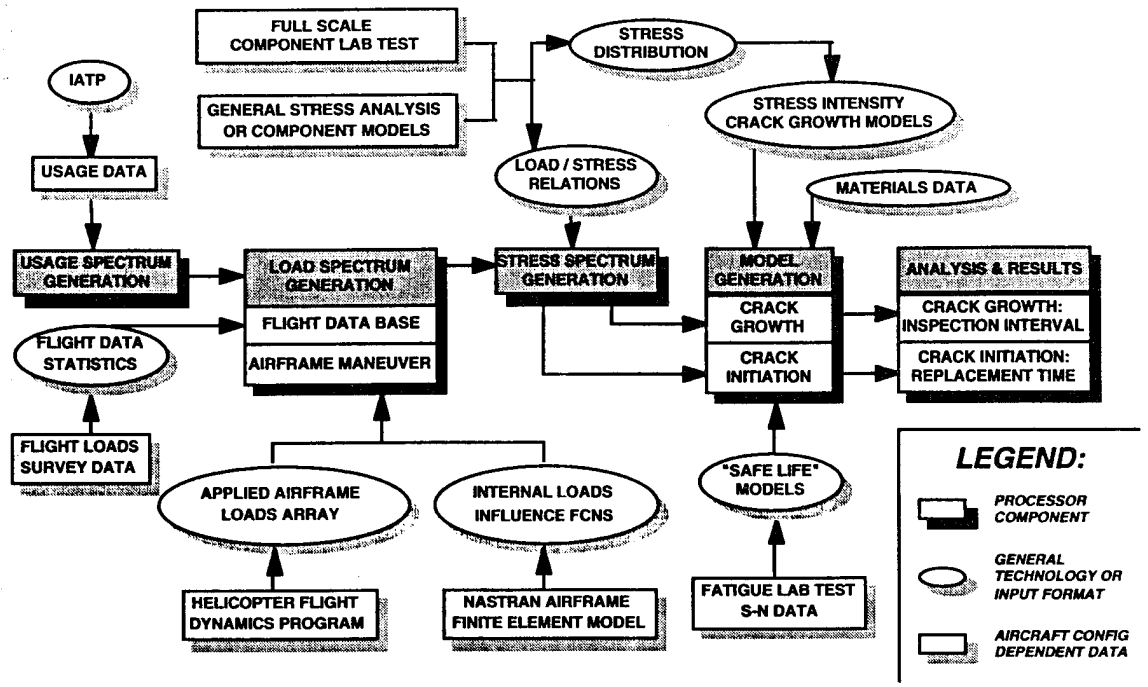


Figure 2. Structural Integrity Computer Program Architecture.

provide steady and transient loads (Reference 5). Crack initiation/growth analyses consider two-dimensional cracks, short crack and closure effects, mixed mode loading, sensitivity to applied stress levels, geometric effects, and variable amplitude loading. Fatigue analysis results for components will be validated by correlation with full scale tests. The results will be used to determine appropriate inspection intervals and component replacement times.

The diagram is further detailed by general technology and aircraft specific modules. General technology & input format modules (light shadowed ovals) include the necessary analytical tools or data processing to perform a primary task (dark shadowed box). The stress intensity factor assessment as detailed in this paper is an example of such a technology. Aircraft specific information modules (light shadowed boxes) are usually in the form of a database, and include such data as flight loads, component and airframe finite element models, or laboratory test results for the user's particular aircraft configuration.

3.0 ASSESSMENT OF HELICOPTER CRACK GEOMETRIES

In previous Georgia Tech and Sikorsky studies, it was recognized that standard available stress intensity factors were not applicable to the more complex 2-D crack fronts found in most helicopter rotor system parts. To define the differences among rotary and fixed wing fatigue failures, a survey of H-53 fatigue test reports and field failure data to determine the variety of cracks found in rotorcraft structures. Full details of the study are given in the final contract report (Reference 6), which is summarized in this paper. USAF H-53 helicopters were originally manufactured between 1964 and 1973. It is assumed that these crack geometries are indicative of those found in most all current U.S. military helicopters, which were typically designed before 1980.

In fixed wing aircraft, critical components include chordwise and spanwise wing splices, stringer-reinforced skin panels, and two bay wing panels. For helicopters, these components may include the rotor hub, blade attachment hardware, pushrods, swashplates, and airframe structure, usually at folding areas and primary fittings. In a separate but related task (Reference 7), the potential failure locations are further examined to define a numerical priority ranking number based on more criteria in addition to crack initiation and growth. Other ranking criteria include margin of safety, fail safe aspects, load path details, stress corrosion cracking, corrosion, accidental damage, and inspectability. For development and validation of the SICP, the most critical of these ranked potential failure locations will be used for detailed analysis and laboratory tests.

Table 1 and Figures 3 through 5 present the result of the crack geometry investigation distinguished by dynamic and airframe components. These results were used to shape the investigation of available stress intensity factor solutions discussed in the next section. Because many failures go unreported in depot facilities, no precise statistics are applicable to the results, and their relative order may change. However, these results do represent as a group the most frequently encountered failures for the H-53 helicopter. A few odd geometries difficult to characterize were also present but not included in this summary.

The dominant crack geometries are part-through cracks, i.e. two-dimensional cracks with a characteristic surface length and through the thickness depth. In general, these flaws are classified as surface or corner cracks. As the flaws grow, the thickness is penetrated and a through crack is formed. For cylindrical components, the crack orientation is given as either axial (along the center line) or circumferential (perpendicular to the center line).

TABLE 1. SUMMARY OF MOST FREQUENT H-53 CRACK GEOMETRIES

DYNAMIC COMPONENTS
A1. Corner Cracks in Lugs
A2. Circumferential Surface (ID & OD) and Through Cracks in Hollow Cylinders
A3. Corner Cracks in Plates (including Nonuniform Stress Fields)
A4. Surface Cracks in Thread Roots
A5. Surface Cracks in Fillets, Counterbores, Loaded/Open Holes (with Nonuniform Stress Fields and Mixed Mode I and II)
AIRFRAME COMPONENTS
B1. Corner Cracks in Loaded and Open Holes
B2. Through Cracks in a Plate in a Row of Rivets
B3. Surface Cracks in Angle Bends and Plates
B4. Corner Cracks in Plates (including Nonuniform Stress Fields)
B5. Tearing Cracks (Mode III)
DYNAMIC AND AIRFRAME GROUPS COMBINED
C1. Corner Cracks in Loaded and Open Holes
C2. Through Cracks in a Plate in a Row of Rivets
C3. Surface Cracks in Plates, Fillets, Counterbores, Holes (with Nonuniform Fields and Mixed Mode I and II)
C4. Corner Cracks in Plates (including Nonuniform Stress Fields)
C5. Corner Cracks in Lugs
C6. Circumferential Surface (ID & OD) and Through Cracks in Hollow Cylinders
C7. Surface Cracks in Thread Roots

While many of these crack geometries are found in fixed wing aircraft, the most noteworthy difference for helicopters is that cracks are found more on rotating mechanical system components (i.e. rotor systems) which occur near structural details (e.g. fillets) and on cylindrical parts. These failures require more specialized investigation since the large body of fracture research on mechanical systems involves mostly pressurized cylinders or cracks near welded joints in thick non-weight critical structure under nearly constant periodic loading conditions. Helicopter mechanical systems experience highly variable periodic loading and have lower safety margins because of their low weight requirements, and therefore demand more accurate analytical solutions.

In addition to the high variability of applied loading, mixed mode cracking and propagation through severe nonlinear stress fields were also present. Mixed mode conditions result near structural details like shoulders and risers. Growth of short cracks under dominant Mode I (tensile) loading can be influenced by Mode II (sliding) if the crack flank surfaces are particularly rough. Through the thickness of cylinders and plates loaded in bending and tension, stresses often go from compression on the free surface to tension on the interior or faying surface. Accurate prediction of fatigue life requires a knowledge of crack growth through these stress gradients.

Many non-redundant thick walled cylindrical members are present in the rotor system to permit complicated rotor blade degrees of freedom via elastomeric or stack bearings. The tail rotor spindle shown in Figure 3 is typical of this design. The cylinders are not loaded in torsion or pressurized where most past research has focused. Three dimensional surface and corner cracks with curved fronts were noted in complexly loaded components like the main rotor swashplate (Figure 4). Cracks in fillet radii and thread roots are often encountered in components like push rods, spindles, and shafts. Lugs are the dominant method of connecting rotor system components and under go significant transverse as well as axial loading. Most fracture work has been done for axially loaded lugs. Other rotorcraft cracks are also found at loaded and unloaded holes in plates, many times with multi-site damage typical of their fixed wing counterparts. Bolt failures under tension, bending, and torsion are commonplace.

The results verify that much of the research done for fixed-wing airframes applies to helicopters, especially for item C2 which pertains to multiple site damage. Figure 5 shows a typical airframe failure location at a backup longeron in the aft fuselage section of the H-53. The aft fuselage and tail sections are highly loaded and comparatively very soft compared to the rest of the airframe. Several failures were noted in splices, lap joints, and along rivet lines of stringer reinforced panels.

4.0 COMPARISON OF COMPUTER PROGRAMS

Standard stress intensity models available in existing computer codes and in the literature are not directly applicable to many of the surface crack geometries in rotor parts without major simplification (see Table 1). It is, therefore, necessary to investigate some of the newly developed methodology, and to define a consistent approach for stress intensity solutions to be incorporated into the SICP. This section focuses on modeling material crack growth properties, critical stress intensity factors, and the distribution of local stresses at the crack location. The capabilities of several widely used computer programs (References 8 through 14) are compared to determine the most appropriate existing Mode I stress intensity solutions. Many of the programs can trace their origin back to the same computer code or person and therefore maintain much similarity. A study was performed to determine where most of the differences in predicted crack growth times come from. The computer codes selected for evaluation were those with which WR-ALC, Georgia Tech, and Sikorsky were most familiar. The codes are listed in Table 2 along with the organizations that developed them.

TABLE 2. SELECTED COMMONLY USED FRACTURE CODES

COMPUTER CODE	DEVELOPER
FLAGRO Version 1 (March 1989) Version 2 (August 1994)	NASA Johnson Space Center (JSC)
MODGRO Version 1.3 (1988) Version 2.3 (1990)	ASD, Wright Patterson AFB
GTCRACK	Georgia Tech
SACGAP	Sikorsky Aircraft Company
SURCK	Pratt & Whitney Company

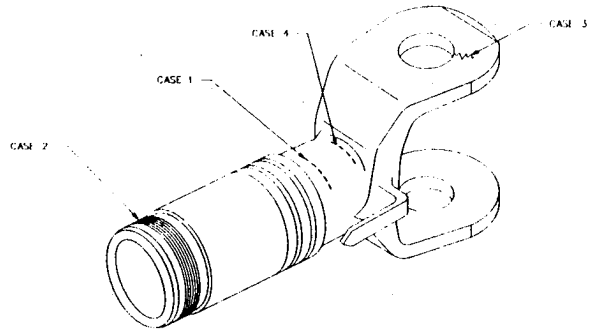
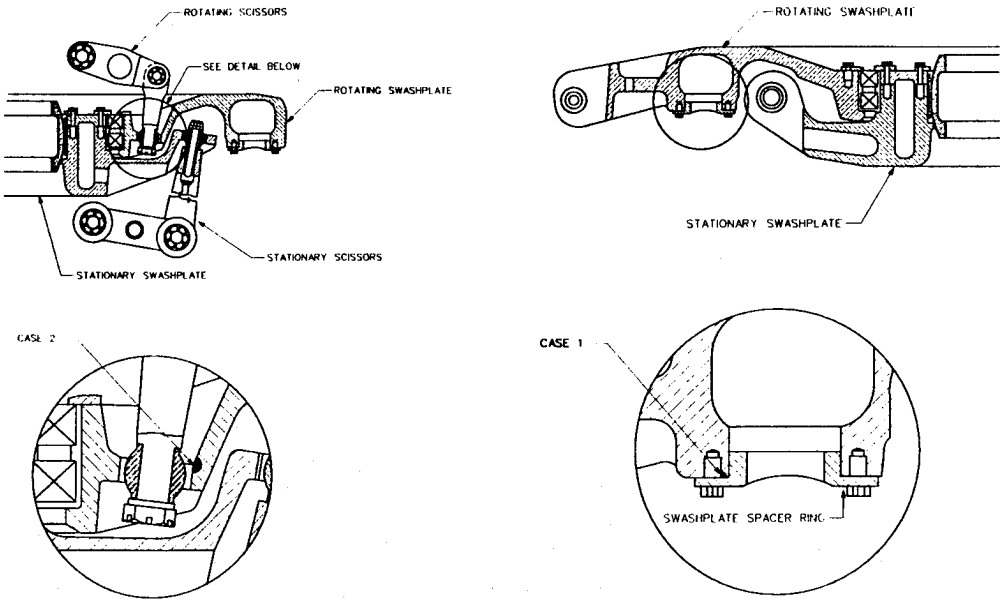


Figure 3. Tail rotor spindle crack geometries.



Case 1: Crack from Threaded Hole

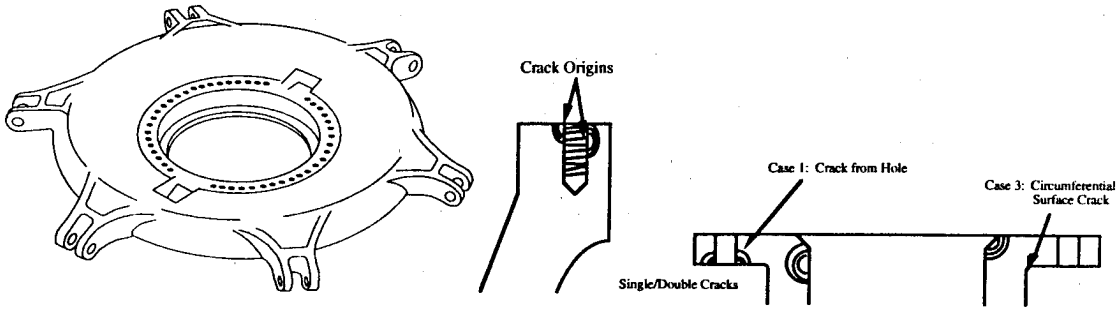


Figure 4. Swashplate crack geometries.

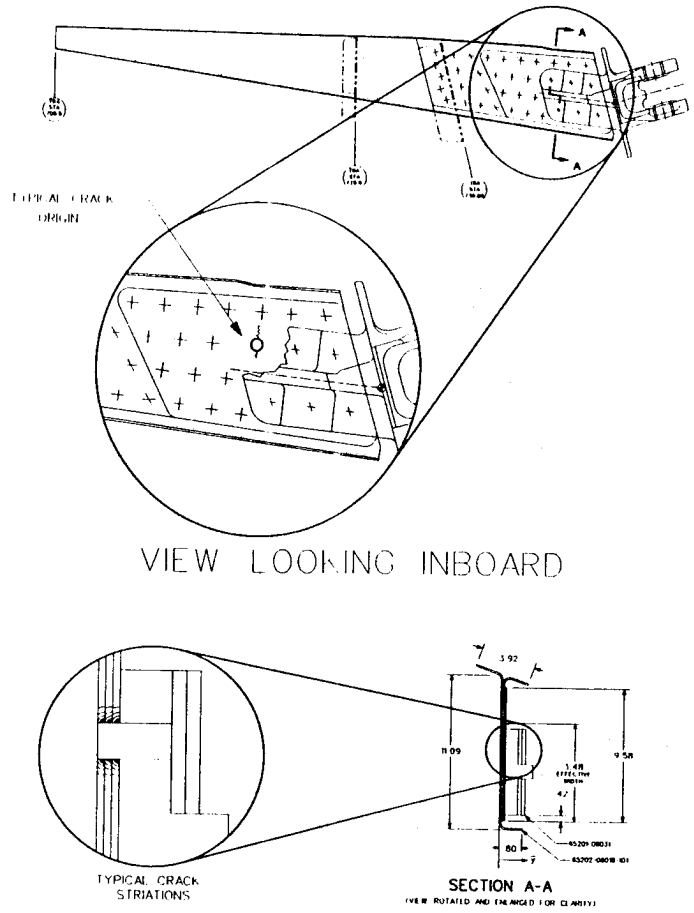


Figure 5. Aft fuselage longeron crack geometry.

The representation of crack growth rate data is the most important variable for the prediction of propagation times. Most all computer codes have several options available to choose from, which are either in tabular or closed form. Table 3 provides program details for material representation and other crack growth parameters.

FLAGRO version 1 utilizes the modified Forman equation, which also converts to other equations such as Paris, Walker, or Forman, when specific values are given for certain variables. The NASGRO 2.0 equation found in FLAGRO version 2 is an even more generalized extension of the modified Forman equation that incorporates a function for crack closure modeling. MODGRO and GTCrack incorporate the Walker equation for crack growth rate data. The user can specify a five-piece curve or give a 25-point tabular representation of the equation. The program linearly interpolates on a logarithmic scale between the piecewise segments or tabular points to calculate the values of da/dN for a given ΔK.

Figure 6 displays the default material data curves for R=0 that exist in the computer codes for the 4340 180 ksi tempered steel. The plot tells a typical story in that the crack growth rate data is extremely different in each program, especially in the near-threshold ΔK region, where most of the crack growth time is spent for short cracks. Depending on the source of data, there is a large amount of variability present. This ultimately leads to unacceptably large differences in predicted growth times.

To model the effect of stress ratio, R, an extensive amount of test data is required to accurately determine how much the da/dN curve shifts with the application of a steady stress in addition to vibratory stress (R-shift). Very often available test data only has a single value of R and so the

shift exponent must be determined another way. FLAGRO incorporates a crack closure analysis based on Newman's equation to calculate the shift parameter for limited actual test data. Typical values of a three dimensional constraint factor, α, were found for different material classes by fitting available test data that had variable R values. Version 2 of FLAGRO makes significant improvements by analyzing more available experimental data. Furthermore, a constant amplitude closure correction function, f, is incorporated into the NASGRO 2.0 crack growth equation to accurately model closure effects. In the modified Forman equation, f=R.

MODGRO utilizes a somewhat different scheme to handle R-shifts. When the 25 tabular data points are used to model the da/dN curve, a separate value of the shift exponent is given for each individual data point. This allows a very controlled placement of data in all ranges of the curve since there is typically more spread in the extremities than in the midrange for various R values. In addition, MODGRO version 2.3 also incorporates a crack closure model.

An R-shift model based on a single exponent, as in FLAGRO, will produce a parallel shift in the basic R=0 curve. A multiple exponent representation, as in MODGRO, shifts each segment of the curve individually to capture the larger spread in the extremities of the da/dN curves. It is very important to accurately model R-shifts since the threshold value, ΔK_{th}, is highly dependent on the stress ratio, and erroneous crack propagation times can result.

The determination of long crack thresholds is important because most of the total crack growth is spent in the threshold or mid-range portion of the da/dN curve, ~~and even~~ small errors here result in large errors of prediction. Most methods modeling the crack growth rate are not very accurate in the threshold region because the crack growth rate is extremely small and difficult to measure experimentally, and because significant test data is often lacking to define this point confidently. Instead the mid-range of the crack growth rate is most accurately modeled.

If a closed form crack growth equation representation is used, the long crack threshold dependency on stress ratio is given in FLAGRO version 1 as

$$\Delta K_{th} = \left(1 - C_0 R\right)^d \Delta K_0$$

where C_0, ΔK_0, and d are material constants. If a tabular material representation is used, the fatigue threshold is the smallest ΔK in the data deck. For very small crack cases of embedded, surface, or corner flaws (either a or c $\leq$ .025 inches), FLAGRO assumes ΔK_{th}=0. Version 2 of FLAGRO has an improved threshold model using the arctan rule for small cracks. A finite value of ΔK_{th} is predicted that duplicates experimental data for crack lengths $\leq$ .025 inches.

The geometries investigated considered not only stress intensity factors and material crack growth curves, but many other techniques involved in crack growth analysis shown in Table 3. These include definition of critical stress intensity factor, failure/transition criteria, retardation models, and nonuniform stress field models.

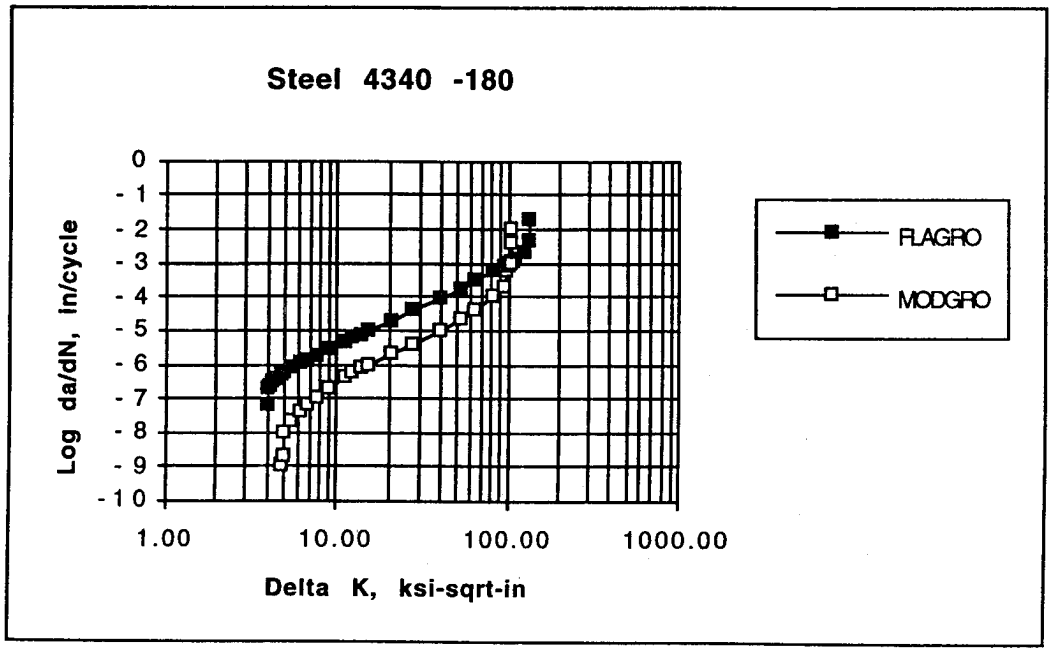


Figure 6. Steel crack growth rate data comparison.

TABLE 3. SIGNIFICANT FEATURES OF FRACTURE COMPUTER PROGRAMS

FEATURE	MODGRO, SACGAP	FLAGRO	GTCrack	SURCK
Program Specs	2K lines of BASIC, PC.	30K lines FORTRAN, Vax	3K lines FORTRAN, PC.	FORTRAN
Geometry Input	Stored in files and edited using preprocessor.	Interactive input only.	Interactive input only.	Stored in files and edited using preprocessor.
Spectrum Input	File must be created or modified externally.	External or internal input; viewed/edited in program.	Entered interactively within program.	File entered externally. Stress-time-temperature histories. Opt process simplifies spectra.
Crack Growth Equation $\frac{da}{dN} =$	Walker (straight line in log-log da/dN vs. ΔK plot) with up to 5 segments to model sigmoidal shape. $C\Delta K^n(1-R)^{n(m-1)}$	Modified Forman eqn. Optional Paris, Walker and Forman equations. $\frac{C\Delta K^n(1-R)^m(\Delta K-\Delta K_{th})^p}{[(1-R)K_c-\Delta K]^q}$ Version 2 uses NASGRO 2.0 eqn. Less influence of ΔK_{th} & K_c on linear part of curve. $\frac{C(1-f)^n\Delta K^n\left(1-\frac{\Delta K_{th}}{\Delta K}\right)^p}{(1-R)^n\left(1-\frac{\Delta K}{(1-R)K_c}\right)^q}$	Walker. Optional Paris, Paris Short Crack, Forman, and Modified Forman. $C\Delta K^n(1-R)^{n(m-1)}$	Hyperbolic sine equation. Optional Paris and double hyperbolic sine equations.
Interpolation of Tabular Material Data	Walker equation between 25 data points (24 line segments on log-log scale).	Piece wise cubic Hermite polynomial on log-log scale.	Walker equation between 25 data points (24 straight line segments on log-log scale).	Pseudo model interpolates between hyperbolic sine and double hyperbolic sine.
Stress Intensity Factor Library	10 models, all flat plates with or without holes.	28 to 31 models including flat plates w/ & w/out holes, lugs, cylinders, threaded rods and standard test specimens. K specified with crack length either in tabular form or polynomial (up to six terms)	10 models, all flat plates with or without holes.	7 models, all flat plates with or without holes.
Uniform Stresses	Uniaxial tension only.	Biaxial forces and moments, internal pressure.	Uniaxial tension only.	Uniaxial Only.
Nonuniform Stresses	MODGRO: Tensile stress profile for width and thickness entered into a Green's function technique SACGAP: Improved for steeper gradients in thickness direction.	Combinations of linear tension and bending for both uniaxial and biaxial loading. Non-linear solution (v 2) available only for surface cracks & limited to variation in thickness direction.	None available.	Sixth order polynomial stress distribution or tabular definition of stress gradient for either width or thickness.
Integration Step (Δa)	User specified at run time.	Fixed at 1% increment.	User specified at run time. Fractional cycles.	User specified at run time.
Retardation Effects (optional)	Generalized Willenborg model for variable amplitude loading. Ver 2.3 has crack closure model.	Newman crack closure model, constant amplitude loading only. Surface and corner cracks apply additional closure factor.	Generalized Willenborg and Wheeler models for variable amplitude loading.	Generalized Willenborg model for variable amplitude loading. Newman crack closure model.
Miscellaneous	Ver 2.3 has on-screen plotting capability.	Arbitrarily proof stress can be applied to check for failure. Crack growth data can be converted to da/dN vs. ΔK. Growth equations can be fitted to tabular data. Stress corrosion cracking check. On-screen plotting (Ver 2).	Forman and Paris equations can be fitted to tabular data.	Stress redistribution due to local plasticity.

Because of the variation between the plane stress and plane strain, different values of the Mode I stress intensity factor, K_I, exist through the thickness. This variation is sigmoidal in shape. K_C is the stress intensity value where unstable crack propagation occurs for a given geometry, causing complete part failure. Because it is conservative, most all sources of experimental crack growth data provide the Mode I plane strain critical stress intensity, K_{IC}, which is lowest possible value for K_C. If the component being analyzed is particularly thin, it is necessary to estimate the proper value of K_C to use for the failure criterion, because the plane strain condition is not present anywhere in the thickness. FLAGRO uses a modified Vroman equation to replicate the sigmoidal shape whereas MODGRO simplifies the variation with a linear fit between plane stress and plane strain. As long as the magnitude of stress intensities is similar, there is only minor variation between the linear and sigmoidal data fits.

Other failure criteria are used to determine fracture or crack transition. These criteria typically have only a minor effect when compared to material differences because the crack is fairly large and has used up much of its total lifetime. The simplest criteria directly compare the crack length to the thickness or width dimensions whereas the more complex methods employ ligament yielding, sustained stress corrosion cracking, and sophisticated residual strength calculations in multi-element structures.

The use of crack retardation models has a significant impact on growth times. FLAGRO incorporates closure techniques to adjust growth rates. MODGRO and GTCrack use Willenborg or Wheeler models. In most cases, crack growth analysis with retardation can only be used for trend studies, since the available models require parameters which, without experimental data to calibrate their accuracy, are no more than arbitrary estimates which result in nonconservative crack propagation times.

5.0 STRESS INTENSITY FACTORS AND CRACK GROWTH

After examining available stress intensity factor solutions found in these computer codes and comparing them with the results of common H-53 failure modes (Table 1), the following three geometries were selected to perform a benchmark crack growth analysis. Corresponding through crack cases were also considered by default in order to capture the transition from the 2-D corner or surface cracks to 1-D through cracks during the course of crack growth.

1. Corner Crack in an Open Hole,
2. Corner Crack in a 40% Loaded Hole, and
3. Corner Crack in a Plate.

The baseline geometry is shown in Figure 7 for the first two cases. The third geometry (corner crack in a plate) has the same dimensions without the hole. The selected material is a 4340 (180 ksi) steel. This particular problem was also used by the American Helicopter Society (AHS) Fatigue and Damage Tolerance Subcommittee as part of a recent damage tolerance 'round robin' effort, where several industry and government participants worked the sample problem to compare differences in crack initiation and crack growth.

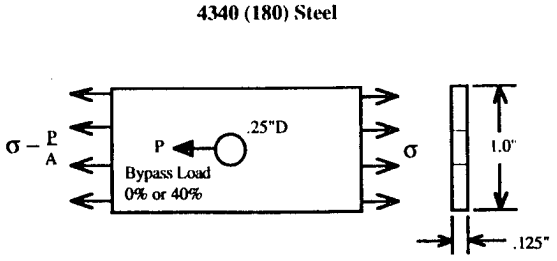


Figure 7. Baseline crack problem geometry.

For the study, a matrix of conditions was generated to obtain comparisons. Several ranges of initial flaw size, constant amplitude loading and allowable crack growth increments, Δa were used to examine major differences in predicted crack growth times using the first three of the five selected computer programs shown in Table 2. In a cycle by cycle representation, stress intensity values are computed for each cycle of growth. Δa specifies the amount of crack extension as a percentage of crack length where stress intensity factors must be recalculated in a blocked spectrum with multiple cycles of a given applied stress level. The values used for the test conditions were:

1) circular initial flaw size .005, .010, .030 ins
2) vibratory stress level 20, 40, 60, 80 ksi
3) allowable crack growth 1, 5, 10 %

Initial results showed that the size of the spectrum block impacts predicted growth time, so a standard block size of 10,000 cycles was selected, using the following general procedure for crack growth analysis.

1. Compare stress intensity factors in each code.
2. Assess growth using various allowable growth levels (Δa) under constant amplitude loading.
3. Compare growth using the same material crack growth rate equations (da/dN vs. ΔK).

In addition to the three geometries, models for a surface crack in a plate and corner crack in a lug were also compared in Step 1, because they were available in the programs. In Step 3 the material crack growth rate data was adjusted to the modified Forman equation representation. Table 4 shows the resulting maximum variations in stress intensity factor and crack growth. For more details of the comparison, the reader is referred to the final contract report (Reference 6).

TABLE 4. RESULTS OF COMPARISON

GEOMETRY	MAX K DIFF	MAX GROWTH DIFF
Open Hole	15%	17% / 97%
Loaded Hole	63%	43% / 65%
Edge Crack	5%	86% / 120%*

Note: Results are with/without same material da/dN data.
* For finite crack growth times only.

For most geometries and crack lengths, typical differences in stress intensity factor values were on the order of 15% or less. The surface crack solutions compared the best, with deviations within 1%. However, worse case conditions showing maximum variations of 63% to 130% were present in the loaded hole and lug models. Lugs are modeled as loaded holes with a full fastener bypass load.

Scatter due to the selected allowable crack extension was on the order of Δa, i.e. a 10% value results in a 10% *nonconservative* difference in growth time. This parameter is typically used to ease the computational burden of the computer, but with the power of modern desktop computers, essentially no difference in speed was noted for 1% versus 10%. Therefore, a value greater than 1% should never be used, so that unnecessary errors in analysis can be avoided.

The different stress intensity factors, failure criteria, and other techniques applied in the codes led to large differences in predicted crack growth times. When the different crack growth data of Figure 6 was used initially, variations in crack growth predictions were greater than when the same material data representation was used. Once the material data was adjusted, differences among the predictions were usually on the order of 15% for larger crack sizes and applied stress levels. Low stress levels (20 ksi) and flaw sizes (.005 in) produced the most variation.

The highest variation in growth times occurred for the edge crack model. Even though the stress intensity factors differed only by a few percent, erratic behavior resulted because the initial flaws and applied stress levels were close to the threshold for crack growth. While one computer code predicted an infinite crack growth time, another gave finite results. FLAGRO automatically changes ΔK_{th} to a value of 0 for elliptical flaw sizes below .025 inches, while the other codes use a single threshold value for all crack sizes. More accurate analytical technology is needed to consistently model the behavior of long cracks near the threshold as well as short cracks which exhibit growth even below the threshold.

The next highest scatter in crack growth times was for the loaded hole. Because adjusting the material data had a moderate effect on scatter, the variation in stress intensity values was the primary cause of the growth time discrepancies. MODGRO incorporates a solution based on a finite element study, while FLAGRO uses a completely different theoretically based approach coupled with finite element results for corner cracks. Both loaded hole and lug stress intensity factors use the same basic technique where a lug is modeled as a loaded fastener hole with full load transfer. The validity of this technique should be further investigated to potentially define a separate more generalized solution for lugs of various shapes.

Even with the same material data, variations as high as 86% were still encountered. In order to examine the specific effect of varying single parameters which generally model material crack growth data and stress intensity factor, an error analysis was conducted for sample problem where an exact solution for crack growth could be determined in closed form. The sample problem consisted of the simple case of a center through crack in an infinite plate, using the Paris equation for crack growth rate. The closed form derivation is as follows.

$$\Delta K = \Delta\sigma\sqrt{\pi a}$$

$$\frac{da}{dN} = C\Delta K^n$$

$$\int_{a_i}^{a_f} a^{-n/2}da = \int_0^N C\left(\Delta\sigma\sqrt{\pi}\right)^n dN$$

$$a_f = \left(\left(1-\frac{n}{2}\right)C\left(\Delta\sigma\sqrt{\pi}\right)^n N + a_i^{(1-n/2)}\right)^{\left(\frac{1}{1-n/2}\right)}$$

$$\text{and } N = \frac{a_f^{(1-n/2)} - a_i^{(1-n/2)}}{\left(1-\frac{n}{2}\right)C\left(\Delta\sigma\sqrt{\pi}\right)^n}$$

Figures 8 graphs the variation in the major parameters. The plot considers the number of cycles it takes to grow a crack from an initial size of .005 inches to a final size of .100 inches. The number of cycles, N, is determined from the exact solution derived above. Material constants C and n were derived from the midrange crack growth rate curves for steel in Figure 6. Selected values of $C=1.0 \times 10^{-8}$ and n=2.5 were used with a cyclic spectrum of 100 ksi.

It can be seen in that the effect of varying the stress intensity solution displays a near quadratic behavior, since the value of n is around 2. Stress intensity factor values for the loaded hole case typically varied by about 25% with differences as high as 63% for larger crack lengths. In our simplified example, a variation of 25% gave an error of 100% (a factor of 2) in predicted crack growth cycles. The stress intensity factor term in the general closed form equation is exponentially dependent on the material constant n, and therefore has a large effect on crack growth time. The material constant C effectively shifts the placement of the da/dN curve (a line for the Paris equation) up or down on the logarithmic scale, resulting in larger or smaller growth rates for the same ΔK. It can be seen that the effect of a perturbation in this constant is very nearly linear and has much less of an effect than the stress intensity factor. The exponent n is simply the slope of the da/dN curve on the logarithmic scale. As expected, this parameter has a direct exponential effect on crack growth time and produces a much larger error than the other parameters.

The AHS Fatigue and Damage Tolerance Subcommittee in a recent round robin effort examined the scatter obtained when several industry and government participants were asked to analyze the same baseline open hole problem. MODGRO tabular rate data was given to all participants who were free to use the computer program of their choice for the analysis. The resulting scatter among four organizations participating was on the order of 300%, or a factor of 4. This was not considered a very discouraging result for crack growth, since a prior round robin effort analyzing crack initiation revealed a scatter factor of 10 among the predicted times. In a similar way, the exercise here has revealed that regardless of the computer program employed, results varied at most by less than 100%, a factor of 2, *when the same material crack growth rate curve is used in a constant amplitude spectrum.* More typically, scatter was on the order of 25% to 50% for three different geometries and three separate computer codes.

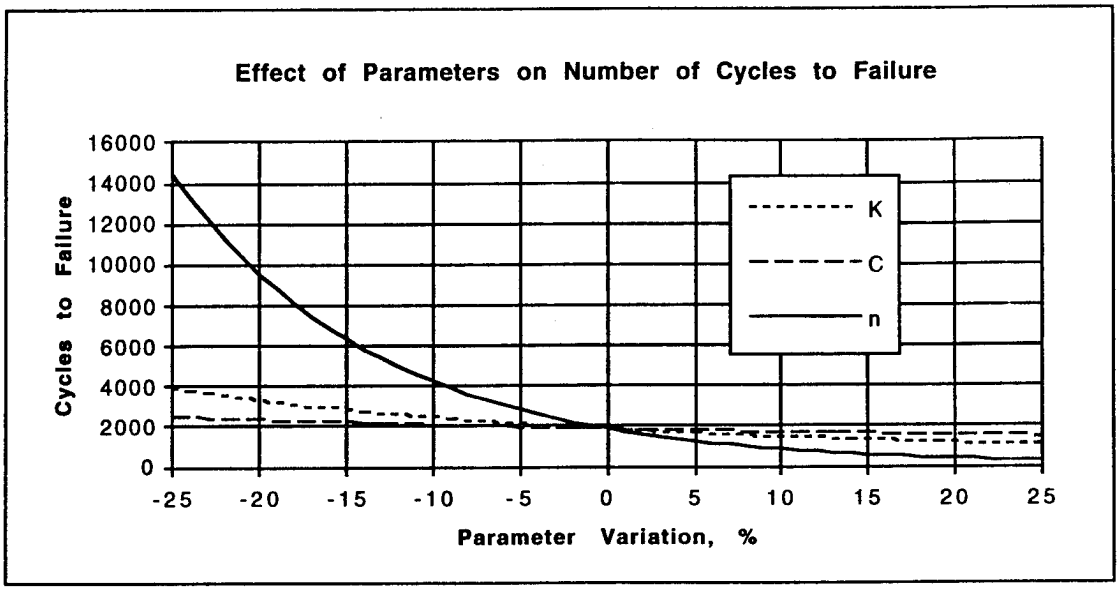


Figure 8. Impact of variation of crack growth constants.

6.0 NONUNIFORM STRESS FIELD TECHNIQUES

The investigation of H-53 helicopter crack geometries determined that part-through cracks were the most common. In addition, these cracks were subjected to a nonuniform stress distribution. The available fracture and fatigue codes FLAGRO version 2, SURCK, SACGAP, and MODGRO were investigated with respect to the part-through crack geometry. Although all programs have the capability to model cracks in nonuniform stresses, each technique has limitations.

The uniform and linear (bending) stress intensity solutions are based upon finite element analysis results of Newman and Raju (References 15 through 18), and are reasonably accurate. However, the stress intensity solutions for general non-uniform stress fields are based upon different solution techniques, and involve various levels of approximation and accuracy, but two basic methods were generally used.

SACGAP and MODGRO account for the non-linear stress distributions for surface and corner cracks with a method developed by Davidson and Grimesly (Reference 19) that corrects the uniform stress intensity factor by an additional correction factor β_{NL}, i.e.,

$$K_{NL} = \beta_{NL} K_U$$

The non-linear correction factor β_{NL} is determined as the ratio of the stress intensity factors *of an embedded circular crack* subjected to nonuniform and uniform distributions.

$$\beta_{NL} = \frac{K_N^*}{K_U^*}$$

SACGAP incorporates a method by DiNicola (Reference 20) which improves the correction factor approach by increasing the number of terms in the series expansion of the nonuniform stress field, resulting in a more accurate representation of the stress gradient. Due to increased mathematical computation requirements, the stress distribution is currently limited to a single direction, but may be modified for a bivariant stress distribution.

Overall, the β correction factor method provides accurate answers for circular cracks, i.e. a/c = 1, but as the crack becomes more elliptical the accuracy decreases. This is because the non-linear correction factor β_{NL} is always determined from the solution of a circular embedded crack.

Both FLAGRO and SURCK utilize the weight function method which is based upon the concept presented by Bueckner (Reference 21) and Rice (Reference 22) that the stress intensity factor K_N for a particular crack type, loaded by an arbitrary stress distribution $\sigma_N(x)$ may be determined according to

$$K_N = \frac{H}{K_R} \int_0^{\xi} \sigma_N(x) \frac{\partial u_R(x,\xi)}{\partial \xi} dx$$

where K_R and u_R are the stress intensity factor and crack opening displacement for the reference problem respectively. Also, ξ is the crack length and H is equal to E for plane stress and $E/(1-\nu^2)$ for plane strain. In general, the reference stress intensity factor and crack opening displacement are determined from simple load configurations such as uniform tension. Using the above approach, the stress intensity factor K_N for a non-linear stress distribution $\sigma_N(x)$ may be calculated. The difficulty of this methodology is due to the complexity in determining the gradient of the crack opening displacement with respect to the crack length, i.e. $\partial u_R/\partial \xi$.

SURCK uses the method of Petroski and Achenbach (Reference 23) which represents the crack opening displacement u_R using a correction factor that accounts for the geometry of a particular crack type. In a similar approach, FLAGRO version 2 uses the weight function methodology developed by Raju et. al. (Reference 24) to find the crack opening displacement gradient in conjunction with the finite element results of Newman and Raju (Reference 17). However, in both programs, a stress distribution is allowed in one direction only.

A literature review was conducted to investigate alternative stress intensity factor calculation methodologies. Theoretical elasticity solutions are cumbersome to use and are usually applied to infinitely sized geometries. Finite element analysis allows finite sized geometries to be investigated, but the method becomes prohibitive in view of the many non-linear loading applications and crack geometries. Furthermore, in view of the integration with a fatigue analysis, the finite element method is not easily implemented and would be computationally expensive. While alternative methods exist, the weight function methodology has been widely accepted and applied as an efficient technique for calculating the stress intensity factor. Of the methods which utilize the weight function methodology, the slice synthesis technique (SST) developed by Fujimoto (Reference 25) was chosen because of its flexibility to model a variety of part-through crack geometries including surface and corner cracks subjected to a non-linear stress distribution.

Applying the SST breaks the cracked body into a system of horizontal and vertical slices, as shown in Figure 9. For a corner crack at a hole, the horizontal slices correspond to radial cracks emanating from a 2-D hole in a plate. Similarly, the vertical slices correspond to 2-D through thickness edge cracks. The underlying principle of the slice synthesis technique is that the 3-D surface crack problem can be approximated by these individual 2-D slices. The shear stresses between the slices which restrict crack opening, can be approximated as a pressure distribution $p^*(x,z)$ along the crack face, represented by idealized springs bridging the crack flanks. Their strength is determined by the compatibility condition that the displacement of a point (x,z) on the original crack surface at the intersection of a particular set of a horizontal and vertical slices, must be equivalent for the radial crack slice and the edge crack slice. A computer program was written which coded the SST using the above procedure to calculate the crack opening displacement function. Numerical integration was performed using Gauss-Legendre quadrature, and the displacements at nine points on the crack flanks were computed.

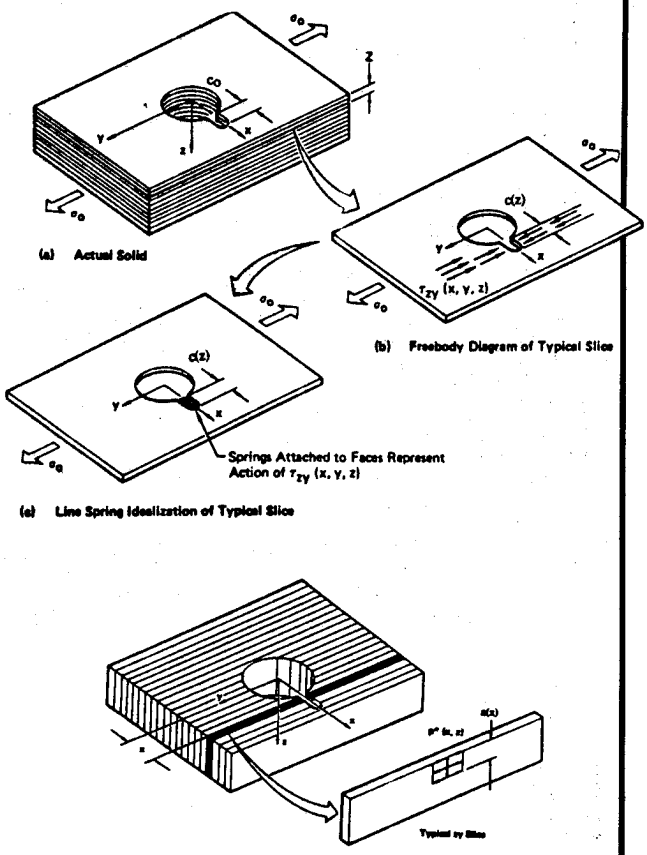


Figure 9. Slice idealization.

Geometries for a corner crack at an open hole in a plate and a corner crack at the edge of a plate were numerically investigated. The plate dimensions were hole radius r = 0.38 inches, thickness t = 0.72 inches, and width W = 100 inches. Two different values of a/c were selected to exercise the stress intensity factor solutions found in the computer programs. The ratio a/c = 1.43 was chosen to compare with experimental studies. A ratio of 1.00 was selected to maximize the accuracy of the beta correction factor technique. The two different values of a/c also require the computer programs to use different equations for stress intensity, which provides a more robust comparison.

Four different nonuniform fields that varied in the thickness direction z were used to evaluate the stress intensity factor calculation methodologies. These fields consisted of uniform (n=0), linear (n=1), quadratic (n=2), and cubic (n=3) distributions according to the following formula.

$$\sigma(z) = \frac{\sigma_0}{2}\left[1+\left(1-\frac{z}{t}\right)^n\right]$$

Figures 10 and 11 show the non-linear beta correction factor, β_{NL}, as a function of crack length in both the surface and depth directions Distributions are presented for the SACGAP and MODGRO codes for the sample problem mentioned above. The uniform tension stress intensity factors are simply multiplied by these correction factors to calculate the non-linear stress intensity factor values.

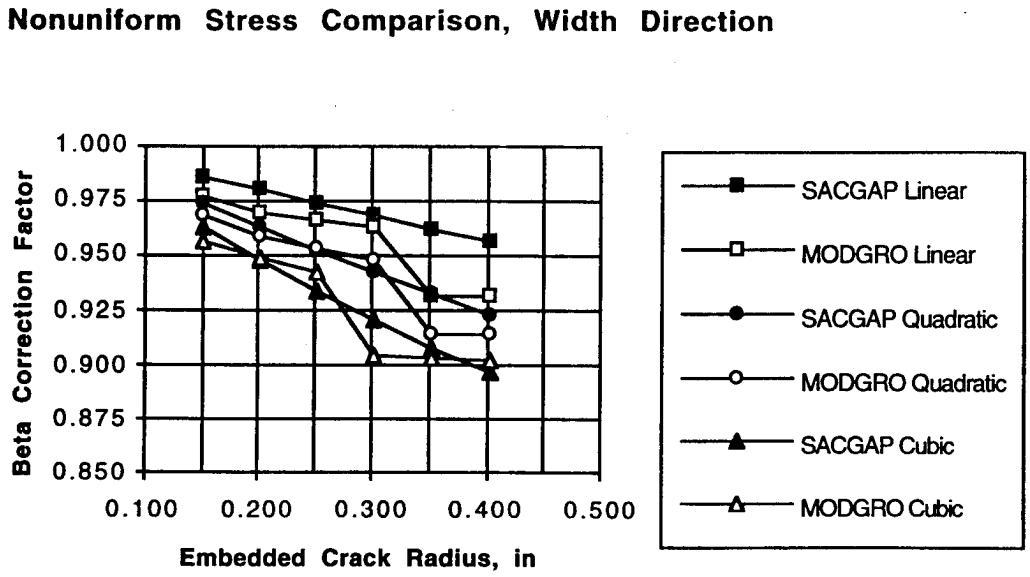


Figure 10. SACGAP and MODGRO stress intensity corrections, width direction.

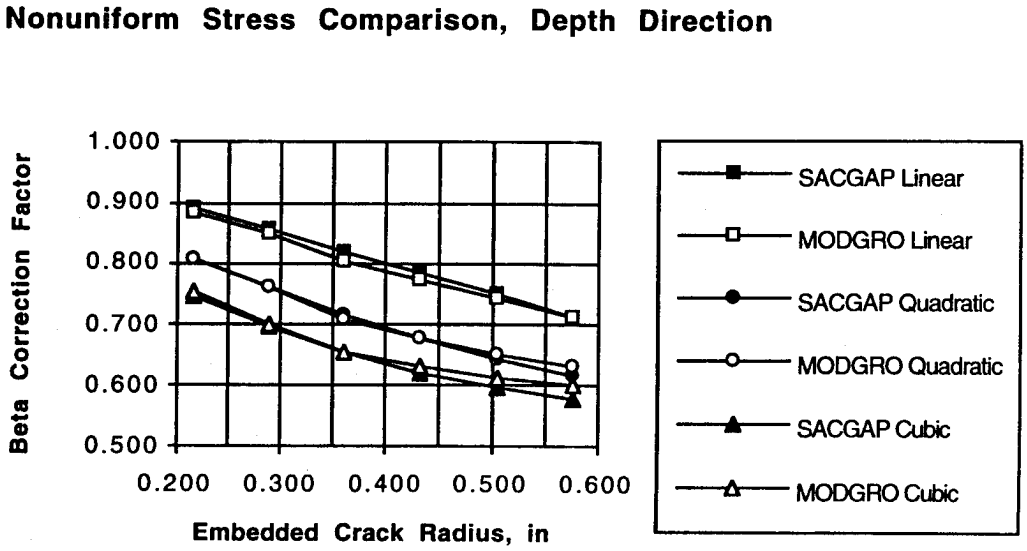


Figure 11. SACGAP and MODGRO stress intensity corrections, depth direction.

The difference due to the higher order terms of the SACGAP technique developed by DiNicola is apparent in the width direction. The discontinuities shown in the MODGRO curves result possibly from the lack of higher order terms or numerical stability difficulties in the Gauss-Legendre integration technique employed to obtain convergence of the correction factor. The depth corrections show excellent agreement. In general, the higher order terms result in smaller values for very steep stress gradients (quadratic and cubic distributions), but larger values for the linear gradient.

The investigation for a/c = 1.43 is presented in Figures 12 and 13. Beta factor values for the uniform stress case is compared to the results of the theoretical work of Shah (Reference 26) and experimental work of Snow (Reference 27) for a corner crack at an open hole in a plate. The Shah results are based on a more detailed analysis where the radial crack is approximated by an elliptical flaw under nonuniform loading on the faces. Snow conducted experimental crack growth studies of PMMA, a transparent polymer. Overall, the methods provide good correspondence, generally falling within the range of the values reported by Shah and Snow.

On the plate surface, the SST provides excellent agreement with the experimental results of Snow. All codes are consistently higher than Shaw when a/t > .4. The SST provides the highest values (5% to 12% higher than SACGAP), followed by FLAGRO. Both SACGAP and MODGRO show essentially the same values with SACGAP being slightly lower.

In the depth direction all codes are in general agreement with each other and with the results of Shah and Snow. It is noted that the curvature of the SST results is opposite to that of the other programs. The reason for this trend is not presently known, but was consistently followed for all cases of stress distribution and even for the edge crack geometry. SST values for a/t ≤ .6 are higher than the experimental values by 10% and lower for the larger flaw sizes by 15%. Snow reported difficulty in achieving stabilized growth for the small flaws at the edge of the hole and hence the accuracy of these values is uncertain. SST values are greater than other codes by at most 16% for a/t = .3 and improve for the larger flaw sizes.

Results for the remaining comparisons with steeper stress gradients are given in Table 5. For these distributions, values for selected computer programs fell within a tight scatter band (usually less than 5%) compared to the SST, which consistently produced larger beta factors. Results are also given for circular cracks with a/c=1.00, for which the beta correction technique is more accurate. For more details of the comparison, the reader is referred to the final contract report (Reference 6).

The investigation for the edge crack (a/c=1.43) is presented in Figures 14 and 15. No experimental results were available for comparison. SACGAP and MODGRO results were essentially identical, and FLAGRO values were slightly higher, within a scatter band of about 5%. Trends are different from the open hole in that the beta factors increase with increasing crack length for both the width and depth directions. SST values are always larger, except for a = .576 (a/t = .8) in the depth direction, indicative of the opposite nature of the SST line curvature mentioned previously. Table 6 presents the results for all stress fields examined.

TABLE 5. OPEN HOLE CRACK COMPARISON

STRESS FIELD	MAX SST DIFF Width	MAX SST DIFF Depth
Uniform	12% / 13%	16% / 21%
Linear	11% / 14%	17% / 25%
Quadratic	18% / 13%	55% / 20%
Cubic	23% / 11%	74% / 19%

Note: Results are given for a/c ratio = 1.43 / 1.00.

TABLE 6. EDGE CRACK COMPARISON

STRESS FIELD	MAX SST DIFF Width	MAX SST DIFF Depth
Uniform	22% / 25%	21% / 27%
Linear	22% / 25%	26% / 33%
Quadratic	22% / 19%	23% / 31%
Cubic	17% / 17%	20% / 28%

Note: Results are given for a/c ratio = 1.43 / 1.00.

As shown, the SST provides β factor values which were consistently higher than those calculated by the other codes. This characteristic trend is most likely attributed to the idealized springs bridging the crack faces being too compliant. As a result, the crack faces have an overly large relative displacement. This indicates that the current method of calculating the spring modulus E_s needs to be improved. Fujimoto has suggested that the spring modulus could be calibrated by using the finite element results of Newman and Raju (Reference 18). Additional insight may be gained from the work of Zhao et al. (Reference 28), who used the SST for finding stress intensity factors for embedded surface cracks at holes. An additional recommendation is to include and/or increase the number of terms in the polynomial expansion for the pressure distribution. Finally, the number of sampling points could be increased. In view of these potential improvements, and the fact that the β correction factor routines in MODGRO and SACGAP are limited to cracks which maintain a circular aspect ratio, the SST is a viable method for calculating stress intensity factor values.

7.0 CONCLUSIONS

A major long term engineering effort has recently been launched to investigate aspects of damage tolerance based fleet management for rotorcraft in accordance with ASIP guidelines. The specific goals of the USAF program are to enhance aircraft safety, improve maintenance procedures, increase mission capability, and lower life cycle cost. Georgia Tech and Sikorsky Aircraft are developing a structural integrity computer program (SICP) to assist the ASIP manager in determining component retirement times and crack growth times of critical structure under changing mission requirements. The SICP technology required for helicopters incorporates improvements over existing fatigue and fracture techniques used for fixed wing aircraft, and the program architecture is general enough to be applied to both types of air vehicles.

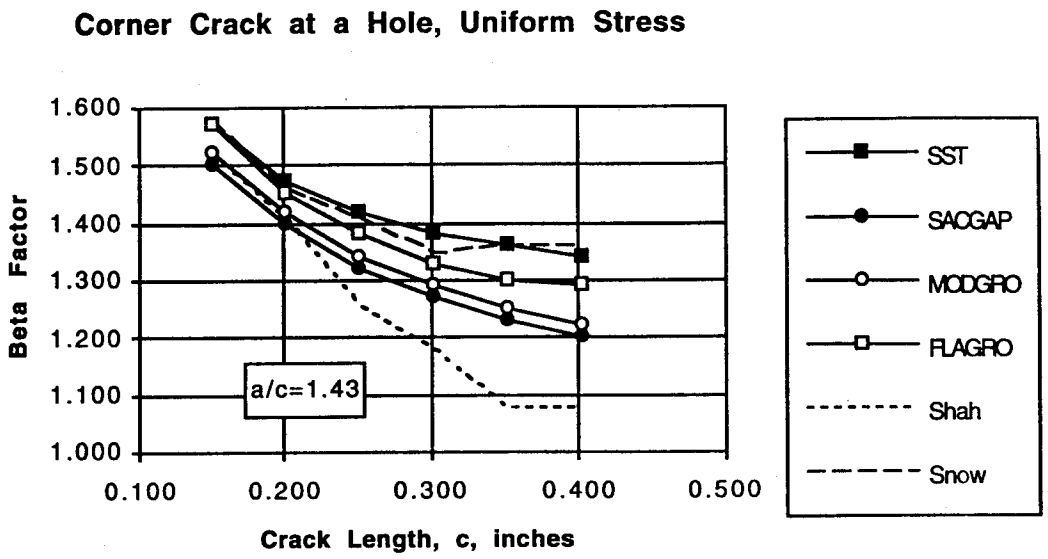


Figure 12. Crack at an open hole beta factors, uniform stress, width direction, a/c=1.43.

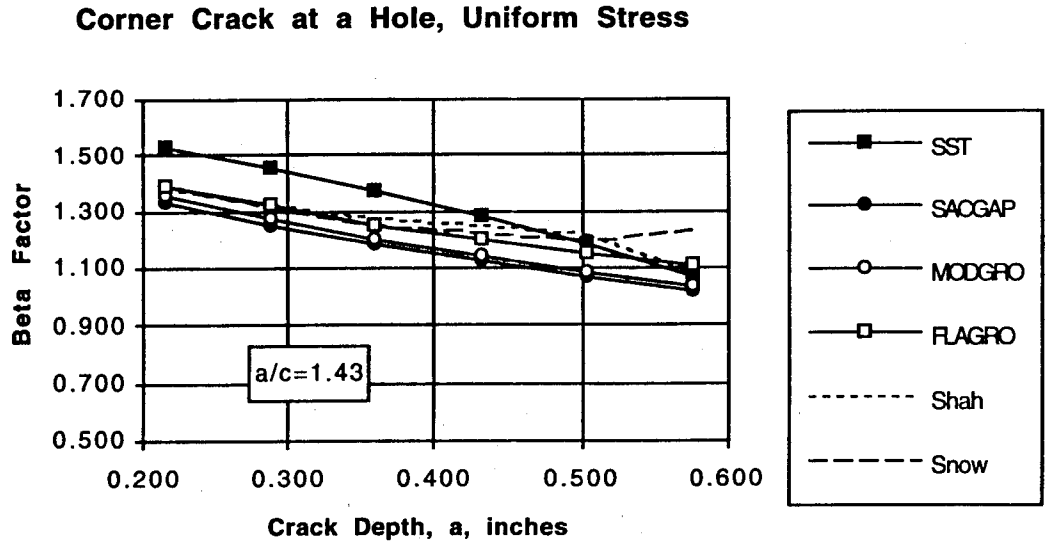


Figure 13. Crack at an open hole beta factors, uniform stress, depth direction, a/c=1.43.

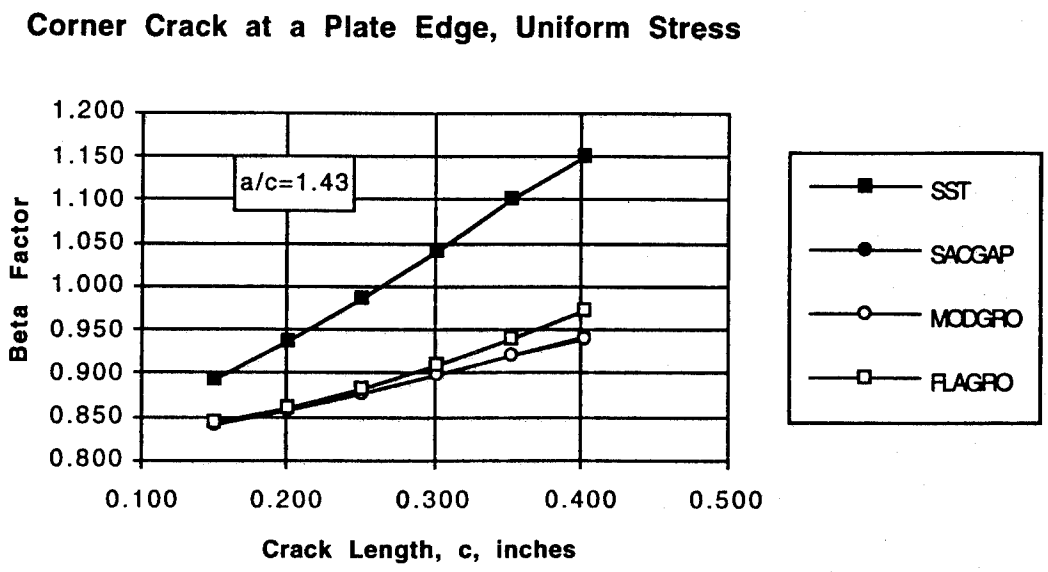


Figure 14. Crack at a plate edge beta factors, uniform stress, width direction, a/c=1.43.

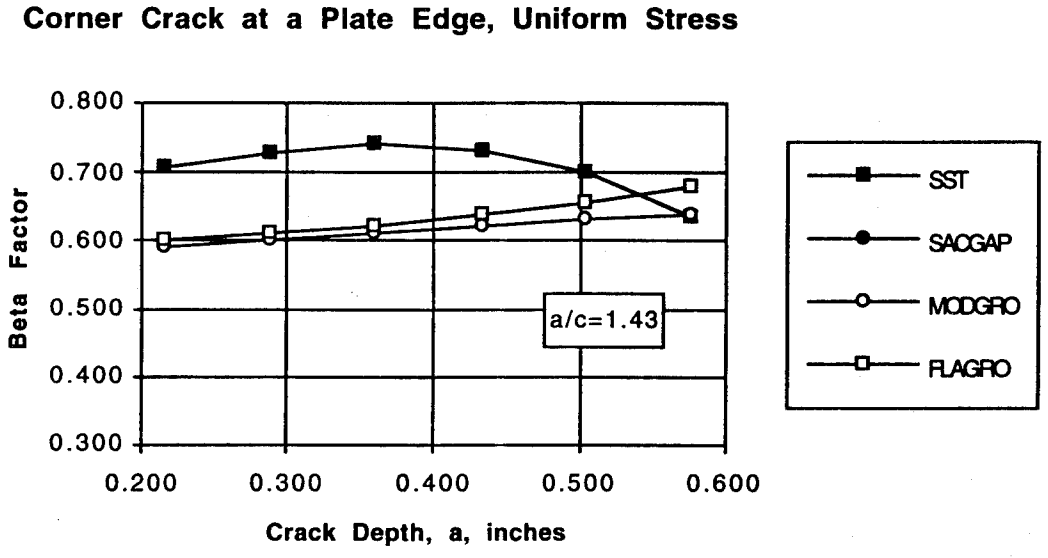


Figure 15. Crack at a plate edge beta factors, uniform stress, depth direction, a/c=1.43.

A review of failure for the H-53 helicopter revealed the following most frequently encountered crack geometries representative of aging helicopter structure in general:

1) corner cracks from loaded and open holes
2) multiple thru-cracks along rivet lines
3) surface cracks in plates under nonuniform and mixed mode loading
4) corner cracks in plates under nonuniform stresses
5) corner cracks in lugs
6) circumferential surface cracks in hollow cylinders
7) surface cracks in thread roots

It can be seen that most all of the geometries are three dimensional problems, requiring more sophisticated stress intensity factor solution techniques. Nonuniform stress fields and mixed modes of crack growth are also frequent. An investigation of capabilities found in several available crack growth programs revealed the following most significant conclusions for helicopter structure.

Stress intensity factor solutions are extremely inconsistent for the loaded hole and lug geometries, showing differences of as much as 130%. The preponderance of safety critical lugs used in rotor components dictates the requirement for further study. Prior research efforts in lug cracks have focused primarily on axial loads, and the effects of important transverse loads have been neglected in most models. Furthermore, for elliptical cracks, lugs are simply modeled as loaded holes with a 100% fastener load. The validity of this technique should be further investigated to potentially define a separate more generalized solution for lugs of various shapes.

Models for general nonuniform stress fields are limited. Severe stress gradients must be defined to accurately use the plate solutions found in the computer codes. FLAGRO version 2 incorporates a nonuniform stress method based on the weight function technique for surface cracks in plates and cylinders, but not for corner cracks. MODGRO and SACGAP have a first order robust technique to model nonuniform gradients, but its accuracy for a wide range of crack shapes has not been well defined. This investigation further examined an approximate higher order solution, the slice synthesis technique (SST), based on the weight function method. SST comparisons with MODGRO and FLAGRO were made for some corner crack geometries with steep stress gradients, with results that were generally 5% to 20% higher than the other codes. Further research should compare these easily programmed methods with the more elaborate alternating method and finite element applications for complex geometries and threaded parts.

Threshold effects and material data variation account for the largest differences in crack growth predictions. In the investigation for a corner crack at the edge of a plate, some programs predicted infinite life while others gave finite crack growth results. The stress intensity solutions varied by only a few percent, but an 86% difference in finite crack growth times was present due to erratic behavior near the long crack threshold. Material crack propagation data should be standardized and used in a tabular format to allow more control and accuracy of data fitting. Consistent small crack models are still lacking. Because helicopters experience higher cycle loading rates (typically 3 to 50 Hz) than their fixed-wing counterparts, cracks grow rapidly, necessitating more accurate life prediction from small flaws. Obtaining the required material data and assessing the applicability of micromechanical and other mechanical models for small cracks is crucial to aging rotorcraft structural integrity.

ACKNOWLEDGMENT

This work was performed under WR-ALC contract F09603-91-G-0096-0017. The following individuals are recognized for their cooperation in this effort: Mr. George Schneider and Dr. Stuart Harbert of Sikorsky Aircraft; Dr. Nagesh Gummaddi, Mr. David Steadman, and Dr. Sathyanaraya Hanagud of Georgia Tech.

REFERENCES

1. MIL-STD-1530A, Aircraft Structural Integrity; Airplane Requirements, Dec. 1975.
2. MIL-A-87221 (USAF), General Specification for Aircraft Structures, Apr. 1986.
3. Lincoln, J., "Damage Tolerance for Helicopters," 1989.
4. Bates, P., Crawford, C., and Chamberlain, G., "Recent Developments in Damage Tolerance Analysis for Rotorcraft," 19th European Rotorcraft Forum, Cernobbio (Como), Italy, 1993.
5. Wasikowski, M., Heiges, M., and Bright, J., "Coupled Rotor Fuselage Load Analysis: a Comparative Evaluation and Correlation," 19th European Rotorcraft Forum, Cernobbio (Como), Italy, 1993.
6. Bates, P., "MH-53J Stress Intensity Factor Models and Solutions," Final Report, GTRI Project A-9311, 1994.
7. Foster, M., "Critical Parts Screening, Roadmap for Future ASIP Requirements," Air Force Mechanical Integrity Workshop, Dayton, Ohio, June 7-8, 1994.
8. JSC-22267, "Fatigue Crack Growth Computer Program, NASA/FLAGRO," NASA Johnson Space Center, Materials Branch, Structures and Mechanics Division, March 1989.
9. JSC-22267A (DRAFT), "Fatigue Crack Growth Computer Program, NASA/FLAGRO Version 2.0," NASA Johnson Space Center, Materials Branch, Structures and Mechanics Division, January 1993.
10. Harter, J. A., AFWAL TM-157-FIBE, "MODGRO User's Manual Version 1.2," Flight Dynamics Laboratory, Air Force Wright Aeronautical Laboratories, Wright-Patterson AFB, January 1988.
11. Harter, J. A., "MODGRO Version 2.3," Flight Dynamics Laboratory, Air Force Wright Aeronautical Laboratories, Wright-Patterson AFB, 1992.
12. "GTCrack User's and Theoretical Manual," School of Aerospace Engineering, Georgia Tech, January 1994.
13. SACGAP Computer Program, Structures Research Division, Sikorsky Aircraft, 1988.
14. "SURCK Fracture Mechanics Mission Life Prediction System, Computer Program Applications Manual, Version 3.2.1," United Technologies Corporation, Pratt & Whitney May 1993.
15. Newman, J. C. Jr. and Raju, I. S., "Analysis of Surface Cracks in a Finite Plate Under Tension and Bending Loads," NASA-TP-1518, 1979.
16. Newman, J. C. Jr. and Raju, I. S., "Stress-Intensity Factor Equations for Cracks in Three Dimensional Finite Bodies," NASA-TM-83200, 1981.
17. Newman, J. C. Jr. and Raju, I.S., "Stress Intensity Factor Equations for Cracks in Three-Dimensional Finite Bodies Subjected to Tension and Bending Loads," NASA-TM-85793, 1984.
18. Raju, I. S. and Newman, J. C., "Stress-Intensity Factors for Corner Cracks in Rectangular Bars," Fracture Mechanics: Nineteenth Symposium, ASTM STP 969, T. A. Cruse, Ed., ASTM, Philadelphia, pp. 43-55, 1988.
19. Davidson and Grimsley, Unpublished work, AFSD0238, 1985.
20. Di Nicola, A. and Schneider, G., Unpublished work, Structures Research Division, Sikorsky Aircraft, 1987.
21. Bueckner, H.F., "A Novel Principle for the Computation of Stress Intensity Factors," *Z. Agnew. Math. Mech.*, Vol. 50, pp. 529-540, 1970.
22. Rice, J. R., "Some Remarks on Elastic Crack-Tip Stress Fields," *International Journal of Solids and Structures*, Vol. 8, pp. 751-758, 1972.
23. Petroski, H. J. and Achenbach, J. D., "Computation of the Weight Function from a Stress Intensity Factor," *Engineering Fracture Mechanics*, Vol. 10, pp. 257-266, 1978.
24. Raju, I. S., Mettu, S. R. and Shivakumar, V., "Stress Intensity Factor Solutions for Surface Cracks in Flat Plates Subjected to Nonuniform Stresses," 24th National Symposium on Fracture Mechanics, Gatlinburg, TN, 1992.
25. Fujimoto, W., "Determination of Crack Growth and Fracture Toughness Parameters for Surface Flaws Emanating from Fastener Holes," McDonnell Douglas Report, MDC A4093, 1976.
26. Shah, R. C., "Stress Intensity Factors for Through and Part-Through Cracks Originating at Fastener Holes," Eighth National Symposium on Fracture Mechanics, Providence RI, 1974.
27. Snow, J. R., "A Stress Intensity Factor Calibration for Corner Flaws at an Open Hole," AFML-TR-74-282, Wright-Patterson AFB, 1975.
28. Zhao, W., Wu, X. R., and Yan, M. G., "Weight Function Method for Three Dimensional Crack Problems-II. Application to Surface Cracks at a Hole in Finite Thickness Plates Under Stress Gradients," *Engineering Fracture Mechanics*, Vol. 34, pp. 609-634, 1989.

Damage Tolerance Analysis of C−141 Weep Hole Cracks with Boron Composite Repairs

Captain David R. Lee and Daniel C. Register
Structures Branch
Technology and Industrial Support Directorate
Warner Robins Air Logistic Center
Robins Air Force Base, Georgia 31098

ABSTRACT

The design of the C−141 wing incorporates integrally stiffened wing skin panels. The integral stiffeners, or risers of the lower inner wing skin panels, have weep holes drilled near their base to facilitate fuel flow through the risers. There are over 1,500 weep holes per aircraft. Weep hole cracks were first discovered after 96,000 cyclic test hours on a full scale fatigue test specimen in 1977. More weep hole cracks were discovered throughout the remainder of the test, until at least 25 different weep hole cracks were found. Lockheed made recommendations for the inspection and coldworking of weep holes to prolong the life of the wing skins. Ultimately, some weep holes were coldworked, and some were not. By the early 1990's, weep hole cracks had become a serious structural problem for the majority of the C−141 fleet. This analysis focused on the ability of boron composite patches to extend the life of the wing skins by reducing the rate at which weep hole cracks grow. The Finite Element Alternating Method was used along with the crack closure method to determine the stress intensities for the different phases of crack growth. The stress intensity information was converted to geometric correction (beta) factors to perform the damage tolerance analysis. Both patched and unpatched weep hole crack configurations were analyzed. For a lower weep hole crack, the patches increase the safety limit by 33 times over the unpatched configuration. For an upper weep hole crack, the safety limit is extended 60 times over the unpatched configuration. This damage tolerance analysis shows that composite patches can be an extremely effective method of repairing cracked metallic structure.

1.0 INTRODUCTION

1.1 The purpose of this report is to document the damage tolerance analysis of weep hole cracks in the wings of the C−141 Starlifter and to document the effectiveness of boron composite patches used to repair the cracks. These analyses were performed by the Structures Branch of the Technology and Industrial Support Directorate, Warner Robins Air Logistics Center (WR−ALC/TIED).

1.2 Figure 1.1 shows the location of the weep holes in the C−141 lower wing skin. There are roughly 760 weep holes in each wing. The weep holes were drilled primarily to facilitate the flow of fuel between the integrally machined risers. In most cases, the weep holes were line drilled through all of the risers of a particular wing panel.

1.3 The first weep hole cracks were discovered in July 1977 by Lockheed during a full scale fatigue test. The cracks were found during pass 32, after 96,000 cyclic test hours. Three cracks were found with a visual inspection, while eleven more were discovered using a bolt hole eddy current inspection. Because of those cracks, the weep holes of four operational aircraft were inspected in July 1978 during depot maintenance. No cracks were found during those inspections. In May 1979, three more cracks were found in the fatigue test specimen's weep holes. Inspection requirements and guidelines were recommended by Lockheed. Further weep hole inspections of operational aircraft were performed that year, but no cracks were discovered.

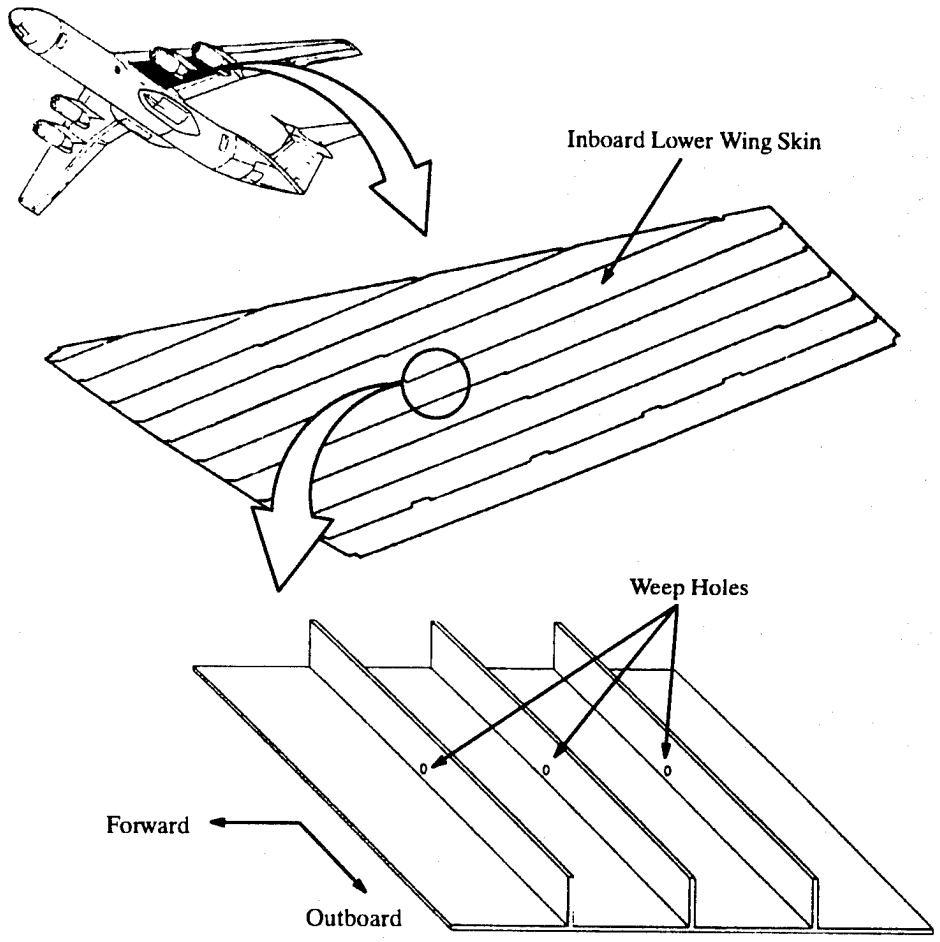


FIGURE 1.1: LOCATION OF THE WEEP HOLES ON THE C-141

1.4 The number of weep hole cracks continued to increase in Lockheed's fatigue specimen, with 25 different cracks being discovered by pass 37. Lockheed recommended coldworking weep holes by 30,000 flight hours. WR-ALC had programmed to start the work in 1986. Ultimately, some weep holes were cold worked, and some were not. By the early 1990's, weep hole cracks had become a serious structural problem for the majority of the C-141 fleet.

1.5 Weep hole cracks are repaired using three possible techniques. The first is to remove the crack by oversizing and then coldworking the weep holes. The initial diameter of a weep hole is typically 0.250 inches, with the maximum oversize being 0.390 inches. If the crack cannot be removed by oversizing the weep hole, the weep holes are plugged with aluminum plugs and repaired using boron composite patches bonded to the riser and the outer skin. Wing panel replacement is the final repair option for multiple weep hole cracks clustered together.

1.6 This analysis focused on the ability of the boron composite patches to extend the life of the wing skins by reducing the rate at which the repaired weep hole cracks grow. Separate analyses not included in this report examined the effects of the repair patches on nearby, unpatched holes -- both weep holes and fastener holes.

Figure 1.2 shows the size and placement of the different patches. The patches are manufactured using uni−directional boron plys designed to have the equivalent strength of the aluminum structure being patched. The intent of the design is for the patches to carry the full load in the event of a complete fracture of the riser and the width of wing skin covered by the exterior patch. In general, three separate patches were used for each weep hole crack repair. One patch is placed on the outer wing skin with the other two patches on both sides of the riser. At spanwise panel splices, the exterior patches are applied as two patches, for a total of four patches. All patches are centered on the weep hole. The wing skin patch has either 13 or 15 plys of boron. Those placed over the spanwise splices have the greater number of plys. All plys are oriented in the zero direction except for two that are at ± 20 degrees. The riser patches are made with 8 plys of boron; two of these plys are also oriented ± 20 degrees with the remainder in the zero direction. Conservatively, only the general case involving the single 13 ply exterior patch was analyzed.

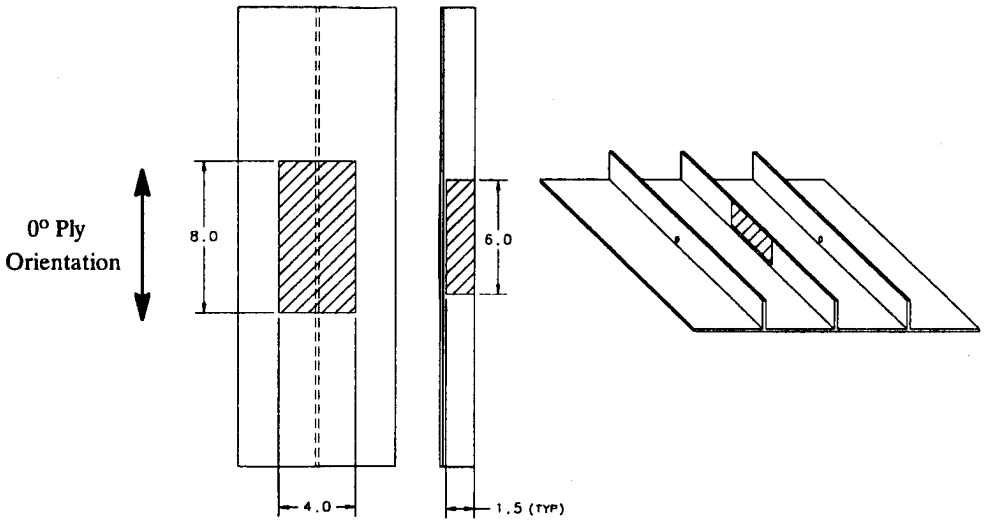


FIGURE 1.2: DIMENSIONS AND PLACEMENT OF BORON COMPOSITE PATCHES

2.0 ANALYSIS

2.1 Baseline Weep Hole Configuration

Each C−141 has over 1,500 weep holes drilled into the risers of the lower wing skin panels. Each riser is continuously tapered in height and thickness along the length of the panels. The skin is also continuously tapered, independent from the taper in the risers. The variable geometry of the wing skin panels creates a large number of possible weep hole configurations. For this analysis, it was assumed that the riser geometry would have the greatest effect upon the length of time it would take a weep hole crack to become critical. Based upon this assumption, the smallest riser with a weep hole in the region of highest tensile stress was chosen as the baseline weep hole configuration for the damage tolerance analysis. This configuration was selected based upon the design limit tensile stress contours on the lower wing skin in Lockheed report ER6423 Vol. V. (see reference 2). Figure 2.1 shows the geometry of the baseline configuration. The baseline configuration represents the middle of a wing skin panel, not a section along the spanwise splices. This configuration was selected to focus the analysis on the weep hole cracks and the benefits provided by the boron patches. Coldworked or oversized weep holes were not considered. We also assumed that there were no other weep hole cracks close enough to the baseline configuration to have an effect upon the results. The patched configuration maintained the existing geometry of the baseline configuration, adding only the three boron composite patches that comprise the weep hole repair.

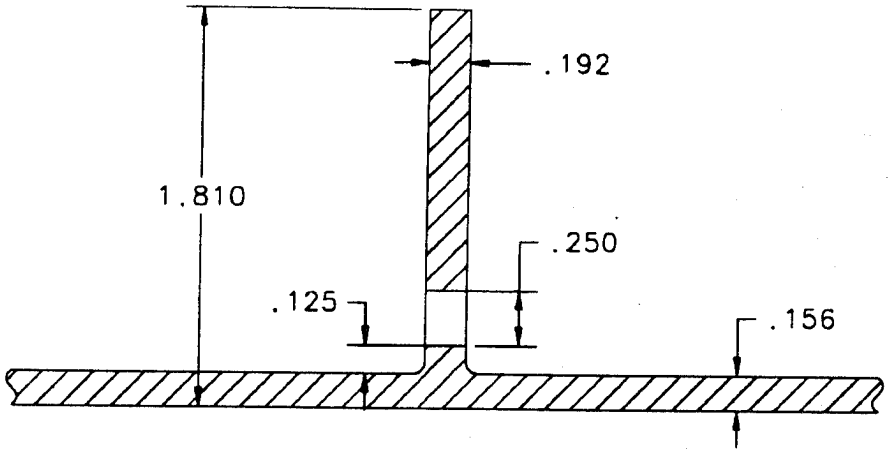


FIGURE 2.1: BASELINE WEEP HOLE CONFIGURATION

2.2 Crack Growth Profiles

2.2.1 Two different crack growth profiles were used in this damage tolerance analysis. The first profile was referred to as Crack Profile A. In this profile, the crack initiated on the lower side of the weep hole, growing into the skin of the wing panel, as illustrated in figure 2.2. The second profile was referred to as Crack Profile B. This profile consisted of a crack that initiated on the upper side of the weep hole and grew until the upper section of riser completely severed. The crack then continued to grow on the lower side of the weep hole, eventually growing into the skin of the wing panel. This profile is illustrated in figure 2.3. The different phases of the profiles were differentiated based upon the type of crack in the wing skin (i.e. part–through or full–through crack). The same crack growth profiles were used for the patched configuration.

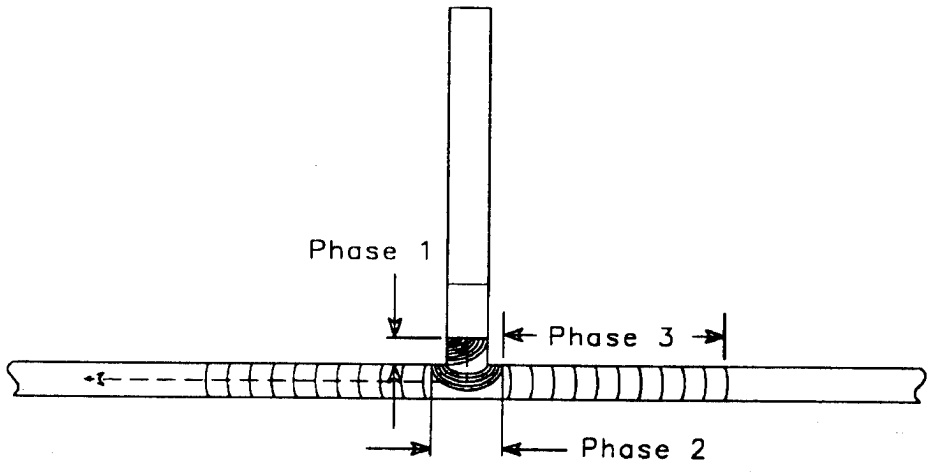


FIGURE 2.2: CRACK PROFILE A

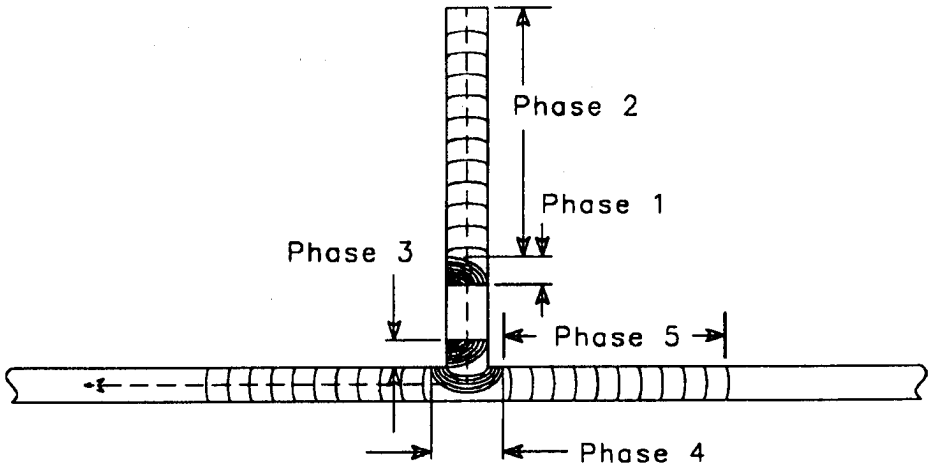


FIGURE 2.3: CRACK PROFILE B

2.2.2 For Crack Profile A, crack length measurements were started at the crack initiation point. It was assumed that once the crack reached the skin it would continue to grow symmetrically with respect to the riser centerline. Because of this assumption, cracks extending into the skin were measured by adding half of the crack length in the skin to the crack length in the riser. This same methodology was used for Crack Profile B. The dashed lines in figures 2.2 and 2.3 represent the lines used to measure crack length.

2.2.3 The focus of this damage tolerance analysis was on crack growth in the aluminum wing skin and the benefits derived by patching the cracks. Flaw growth in the patch or the adhesive layer was primarily ignored. The only flaw in the patch repair modeled in this analysis was a disbond between the patches and the aluminum skin centered around the crack. A single size disbond was used for all patched configuration crack growth calculations. No analysis of disbond growth was performed. The size and location of the assumed disbond is shown in figure 2.4.

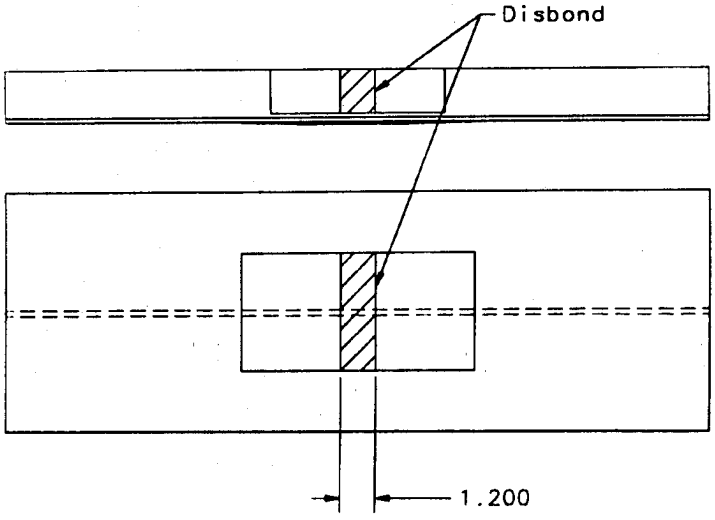


FIGURE 2.4: SIZE AND LOCATION OF THE DISBOND USED IN THE ANALYSIS

2.3 Finite Element Models

2.3.1 Finite element models were used with the Finite Element Alternating Method (FEAM) and the crack closure method to calculate the stress intensity factors used for this damage tolerance analysis. All models, laminates, and results were processed using SDRC's software products I–DEAS and Master Series. Models were solved using CSA/NASTRAN.

2.3.2 The model of the baseline configuration utilized thin shell linear quadrilateral elements having the material properties of 7075–T6511 aluminum. The model was constructed and restrained accounting for quarter symmetry. Springs were placed on the edge of the model to simulate the characteristics of a sheet of continuous skin. Loading of the model was accomplished using enforced displacements. Figure 2.5 shows the baseline finite element model.

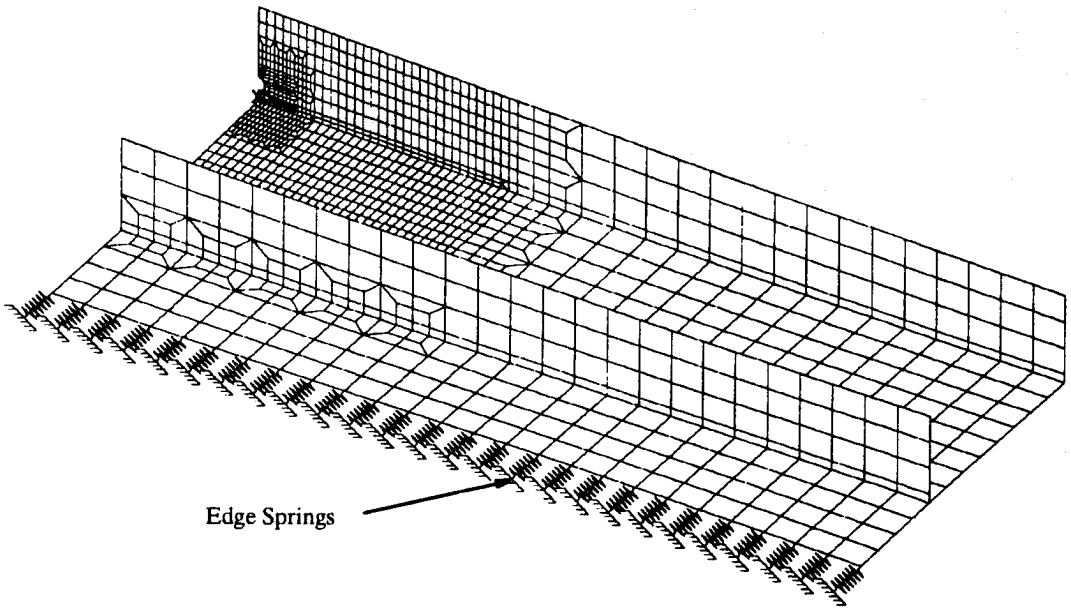


FIGURE 2.5: QUARTER–SYMMETRIC FEM OF THE BASELINE CONFIGURATION

2.3.3 The model of the patched configuration incorporated models of the boron patches with the finite element model of the baseline configuration. The boron patches were modeled using thin shell linear quadrilateral elements. The adhesive elements between the patches and the aluminum were modeled using solid linear brick elements. The adhesive layer was assumed to be 0.010 inches thick and the material properties were assumed linear and isotropic. The nonlinear behavior of the adhesive was ignored since it would not significantly affect the results in the aluminum elements near the crack because of the assumed disbond. Only the stresses and displacements of the aluminum elements were used to calculate stress intensity factors.

2.3.4 The disbond between the composite patches and the aluminum panel was modeled by removing the adhesive elements in the region of the crack. This simulates the disbonding that would likely occur during crack growth and facilitates the use of detailed weep hole models required by the FEAM for calculating stress intensity factors.

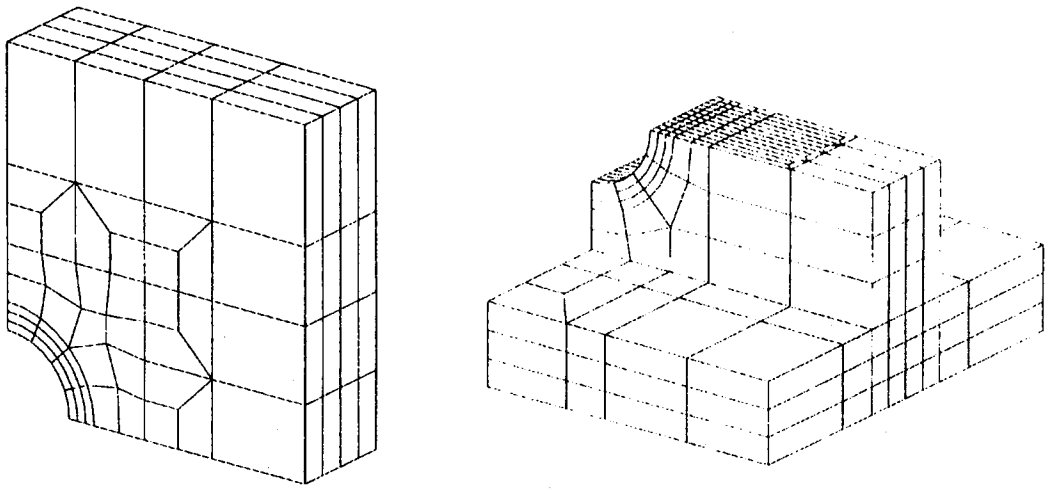
2.4 Stress Intensities

2.4.1 Full–through crack stress intensities, such as for phase 2 growth in Crack Profile B, were calculated for both the baseline and patched configurations using the crack closure method. Part–through crack stress

intensities were calculated with the FEAM. The FEAM was also used to calculate the stress intensities for cracks in phase 4 of Crack Profile B. Stress intensities for the baseline configurations calculated by WR–ALC/TIEDD were compared with those calculated by Lockheed Georgia to verify our FEAM and crack closure methods. Plots showing the stress intensities used in this analysis are shown in appendix A.

2.4.2 The FEAM calculations were performed using a computer program written by the Georgia Institute of Technology under contract number F09603–89–G–0077. The program employed the Schwartz–Neumann alternating method. This approach required the solution of a finite element model of the uncracked geometry. Explicit modeling of the crack was not required. The program performed iterations of the finite element model solution, eliminating all residual stresses on the crack face. The stress intensities were calculated at each iteration, with the overall stress intensity being the summation of all the previously calculated stress intensities. The results included the stress intensity factors along the entire crack front. The program was written for embedded elliptical cracks, semi–elliptical cracks and quarter–elliptical cracks. This method was used primarily to calculate the quarter–elliptical crack stress intensities in the two crack profiles used in this analysis. For further information regarding the FEAM, see reference 3.

2.4.3 The FEAM required the use of 20 noded brick elements. Detailed models of the upper weep hole and the lower weep hole geometry were constructed for use with the FEAM. These models are shown in figure 2.6. The boundary conditions for these models were derived from the larger baseline and patched models. Because the adhesive elements had been removed from the region near the crack, only the surrounding aluminum elements contributed to the boundary conditions of the detailed models. This simplified the development of boundary conditions for the detailed models from the full size models by eliminating the need to specify surface tractions due to the adhesive.



Upper Weep Hole Model

Lower Weep Hole Model

FIGURE 2.6: DETAILED FINITE ELEMENT MODELS USED WITH THE FEAM

2.4.4 The FEAM was also used to calculate the stress intensities for the non–elliptical crack in phase 2 of Crack Profile A and phase 4 of Crack Profile B. The finite element model used to model these phases for the FEAM explicitly modeled the crack in the riser by releasing the riser restraints. A semi–elliptical crack was used to model the crack front which extended into the skin. Figure 2.7 shows the details of how this crack was modeled. The FEAM was not intended to solve this particular crack configuration. Inaccuracies introduced by this technique were minimized due to the limited amount of time that crack growth occurred in these phases.

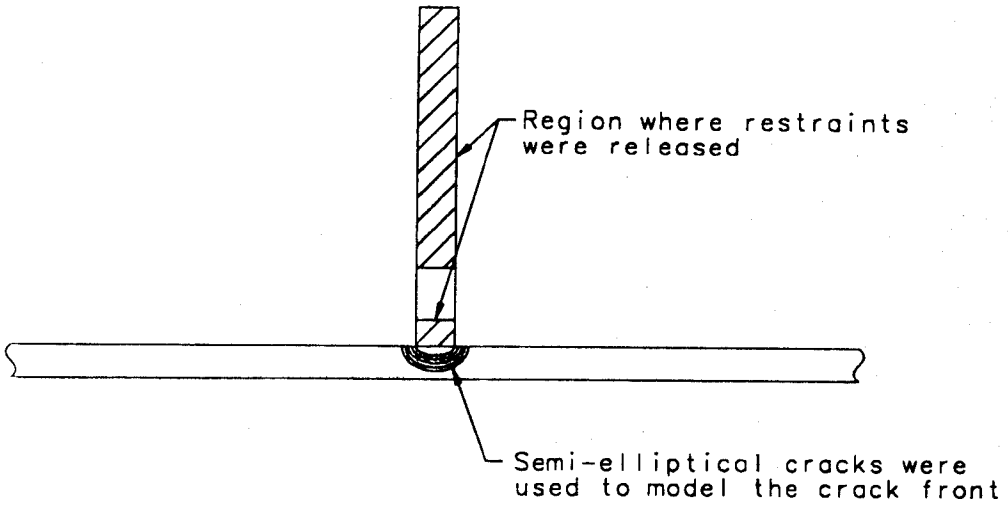


FIGURE 2.7: METHOD USED TO MODEL PHASE 4 CRACKS IN CRACK PROFILE B FOR THE FEAM

2.4.5 For each crack geometry, the FEAM computes nineteen stress intensities at equal angular intervals between the major and minor axes of the ellipse that describes the crack front. As the crack size increases, we lengthen the major and minor axes of the ellipse with respect to the magnitude of the stress intensities at these axes. This allows the quarter or semi-elliptical crack to change its aspect ratio in response to different stress intensities at the two axes. Crack growth simulations were performed using the Durability and Damage Tolerance Analysis (DADTA) Runstream computer software for C-141 crack growth problems, obtained under contract from Lockheed Georgia. This crack growth software is capable of growing a crack in one dimension. Two dimensional crack growth, such as a quarter-elliptical crack, is accomplished by using only the stress intensity at one axis of the crack front. Stress intensities at the minor axis were used in this analysis. The minor axis was oriented vertically with the riser in all crack growth phases where the FEAM was used.

2.5 Crack Growth Calculations

2.5.1 Lockheed's DADTA program for the C-141, referred to as the C-141 Runstream, uses Forman's equation and the Hsu retardation model. The primary user inputs are the range of crack sizes to investigate, material data and geometry effects. The flight-by-flight stress spectra was developed using accessory programs which accounted for aircraft loads, load-to-stress conversion, mission profiles and sequencing.

2.5.2 The geometry effects are described using geometric correction (beta) factors. Beta factors were determined from the stress intensities calculated with the FEAM and crack closure methods. Appendix A outlines how the beta factors were computed from the stress intensity factors.

2.5.3 The Runstream produces stress spectra based upon a single, six degree of freedom set of stress-to-load ratios, which are themselves a function of location on the airframe. Stress-to-load ratios have been determined by Lockheed for various analysis locations on the C-141 structure. This damage tolerance analysis used the stress-to-load ratios for analysis location W-36E, an inner wing lower spanwise splice. The location was chosen due to its proximity to the high design limit tensile stress region of the lower wing skin. Appendix B further discusses the method used to select the stress-to-load ratios.

2.5.4 The mission sequence is a listing of all the mission profiles the aircraft structure is expected to experience, in the order and proper proportion that they are expected to occur. Mission profiles represent the various maneuvers that comprise a mission. The results using the baseline, 122 mission sequence with nineteen mission profiles are shown in this report.

2.5.5 Four analysis cases were considered. Table 1 identifies the elements of each analysis case. Lockheed performed a crack growth analysis with a similar configuration to Analysis Case 1. WR–ALC's and Lockheed's results were compared to identify the differences caused by the stress intensities that were calculated using the FEAM.

Table 1

ANALYSIS CASE DEFINITIONS			
ANALYSIS CASE #	**CONFIGURATION**	**CRACK PROFILE**	**# OF MISSION PROFILES**
Analysis Case 1	Baseline (unpatched)	Profile A	19 Mission Profiles
Analysis Case 2	Baseline (unpatched)	Profile B	19 Mission Profiles
Analysis Case 3	Patched	Profile A	19 Mission Profiles
Analysis Case 4	Patched	Profile B	19 Mission Profiles

3.0 RESULTS

3.1 All of the crack growth results are shown in Figures 3.1 through 3.4 at the end of this section. Figure 3.1 shows the crack length as a function of representative baseline flight hours for Analysis Case 1 and the results from Lockheed's analysis of a similar weep hole configuration. Both cases were for profile A cracks.

3.2 Representative baseline flight hours are a measure of flight time used in the C–141 Runstream program. Baseline analysis represents the flight hours, mission profiles, and mission sequencing of an average C–141 in the fleet. The results must be scaled to compensate for the higher loading of aircraft that are known to operate in a more severe environment. Scaling of the crack growth results in one of the functions of the Aircraft Structural Integrity Program (ASIP).

3.3 The first two phases of crack growth in Analysis Case 1 was performed using the FEAM. Figure 3.1 shows that crack growth based upon stress intensities calculated with the FEAM was slower than crack growth based upon stress intensities used in Lockheed's analysis. Once the crack had grown into phase 3, the stress intensities were nearly identical for Analysis Case 1 and Lockheed's analysis. The significant difference between WR–ALC's and Lockheed's results was caused by jumps in WR–ALC's crack growth curve. These jumps represent fast fracture between crack growth phases, and was assumed to occur by WR–ALC.

3.4 Figure 3.2 shows the crack growth results for Analysis Case 2. These results represented the crack growth of an upper weep hole crack that severed the riser and then continued to grow into the wing skin. The initial smooth portion of the curves were phases 1 and 2. A significant jump occurred between phases 2 and 5, with almost no flight time in phases 3 and 4. This indicated that once the riser became completely severed, there was little time before the crack extended through the skin.

3.5 The patched configuration of Analysis Case 1 was referred to as Analysis Case 3. The results from the crack growth of Analysis Case 3 are shown in Figure 3.3. There was little difference in the overall shape of the crack growth curves between Analysis Case 3 and Analysis Case 1. The significant difference was in the amount of flight hours required to grow the crack. Analysis Case 3 took over 600,000 flight hours to grow the crack to a nearly critical length of 4.0 inches, representing a 3,242 percent improvement in life. This level of improvement was not unexpected. A ten percent decrease in the stress intensities, used as input for the C–141 Runstream program, produces roughly a hundred percent improvement in the number of flight hours until a crack becomes critical. The boron composite patch creates a fifty percent reduction in the stress intensity (see appendix A). Based upon the reduction in stress intensity, the boron patches are expected to produce flight times to critical crack length 32 times longer than a similar unpatched configuration. The expected results nearly matched the results of Analysis Case 3, in which a crack required 33 times the number of flight hours in Analysis Case 1 to become critical

3.6 The results for Analysis Case 4 are shown in Figure 3.4. Unlike Analysis Case 3, there were major differences in the shape of the Analysis Case 4 crack growth curve when compared with the unpatched configuration. Analysis Case 4 showed that a large portion of flight time occurred during phases 3 and 4 of the crack growth. This was caused by the additional structural integrity provided by the patched riser. In Analysis Case 2, significant bending stresses were developed once the upper riser was severed. This lead to the extremely short life in phases 3 and 4. In Analysis Case 4, the riser patch continued to provide a loadpath once the riser became completely severed. Large bending forces were not developed once the upper riser split, resulting in a greater than 50 percent decrease in the stress intensities during crack phases 3 and 4. The benefit of the significant stress intensity reductions caused by the reduced bending stresses, resulted in Analysis Case 4 requiring the largest number of flight hours for the weep hole crack to become critical. Table 2 summarizes all of the WR–ALC's and Lockheed's results.

Table 2

DAMAGE TOLERANCE ANALYSIS RESULTS		
ANALYSIS CASE #	**CRITICAL CRACK LENGTH (inches)**	**SAFETY LIMIT (flight hours)**
Lockheed's Results	1.693	22,977
1	1.683	18,195
2	2.570	17,679
3	≈ 4.00	608,141
4	≈ 4.00	1,058,901

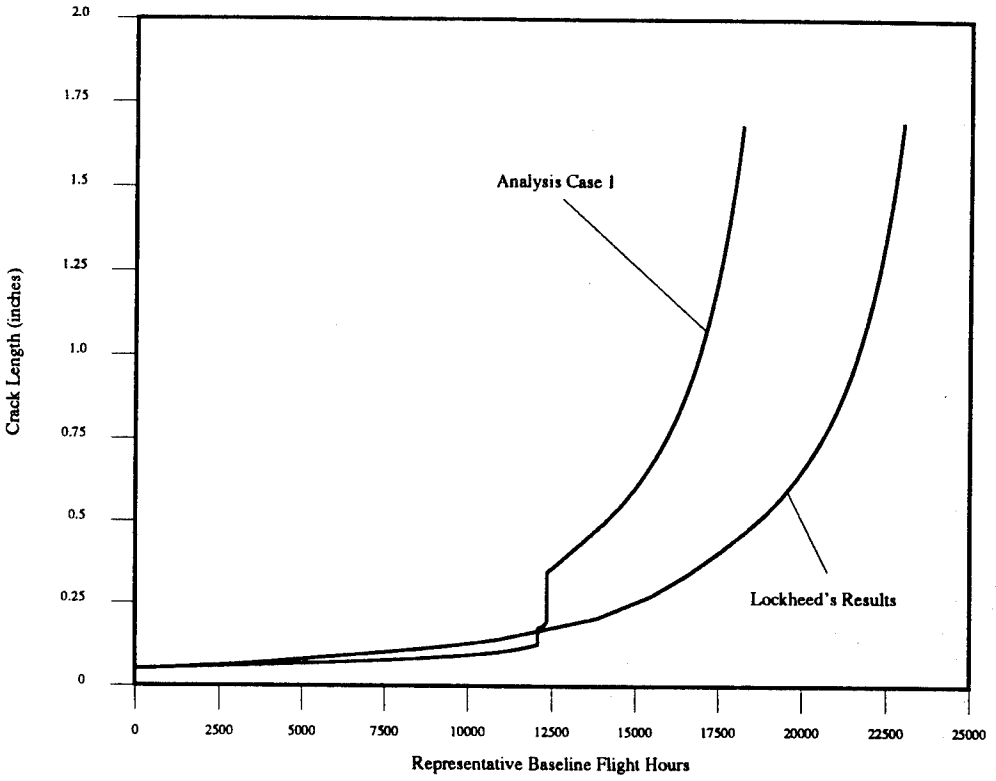


Figure 3.1: Crack Growth Curve for Analysis Case 1 and Lockheed's Results

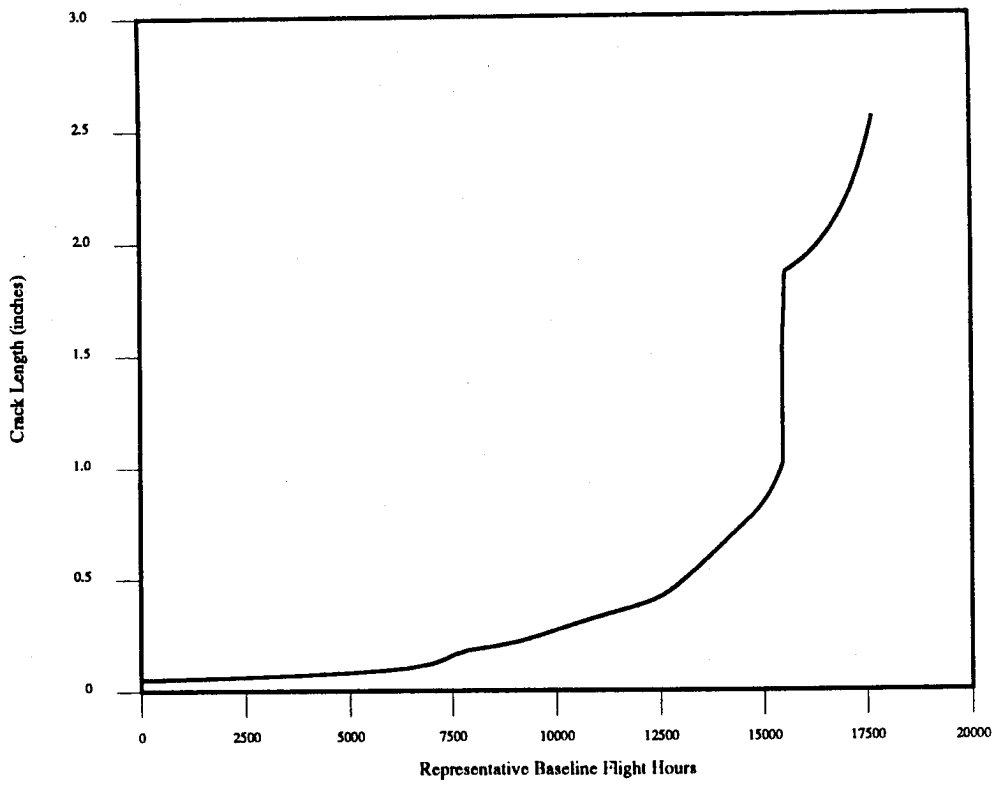


Figure 3.2: Crack Growth Curve for Analysis Case 2

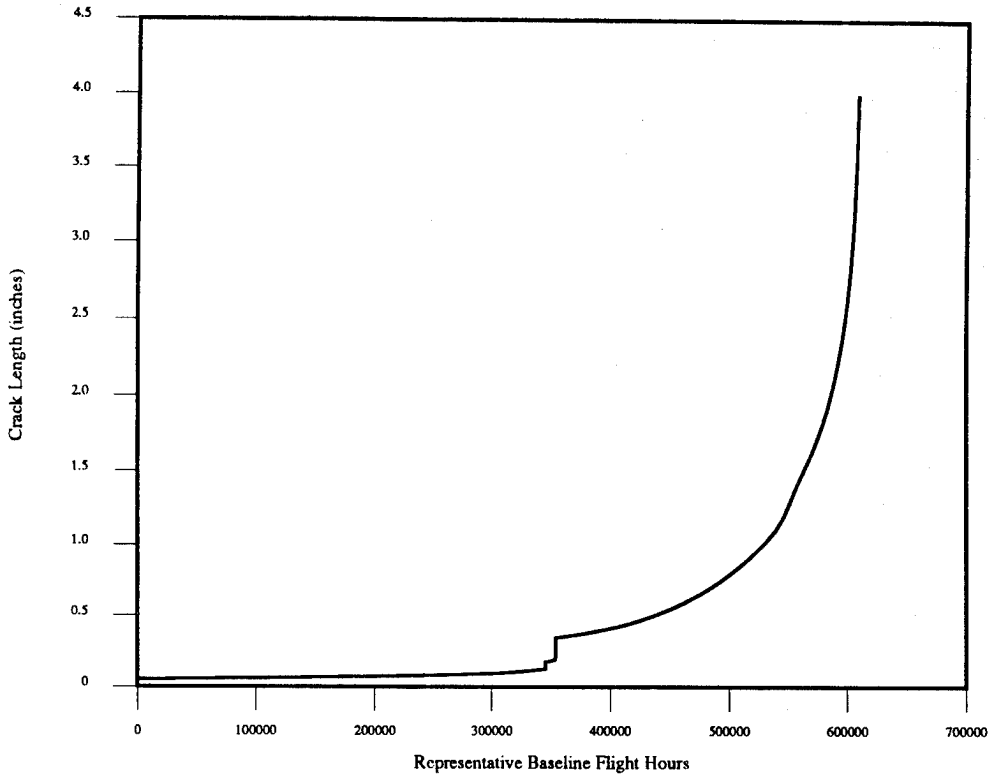


Figure 3.3: Crack Growth Curve for Analysis Case 3

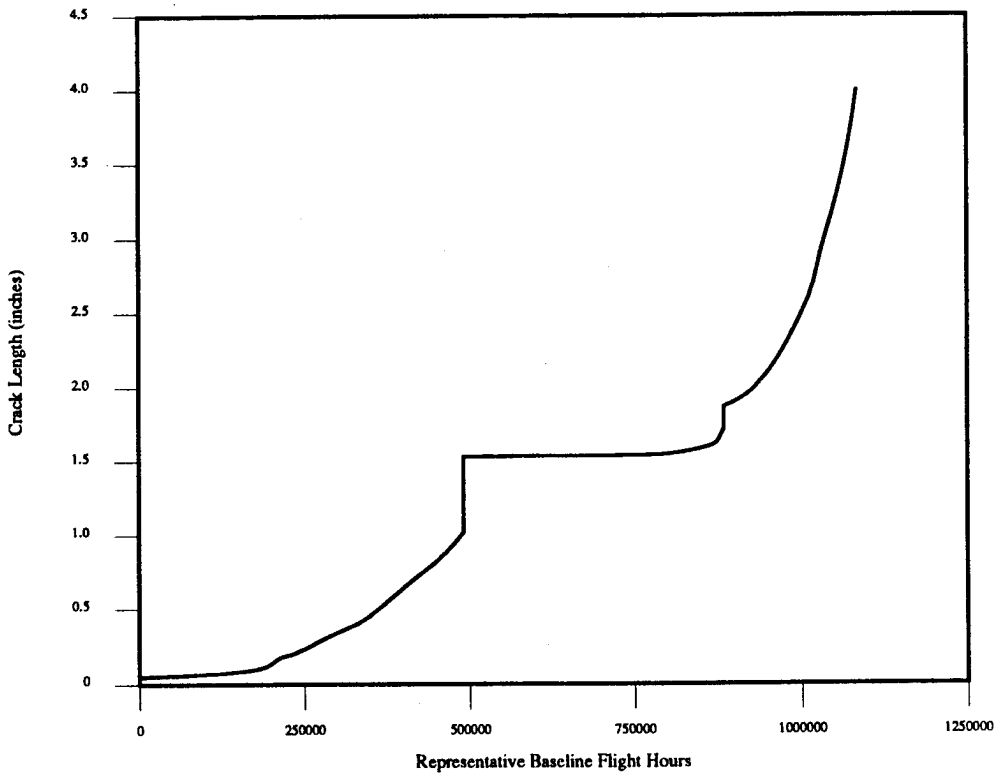


Figure 3.4: Crack Growth Curve for Analysis Case 4

4.0 CONCLUSIONS AND RECOMMENDATIONS

4.1 The boron composite patches were extremely effective as a means of preventing weep hole cracks from growing on C−141 lower wing skin panels. The patches performed so well, that crack growth should be virtually stopped for the remainder of the operational life of the aircraft.

4.2 Fatigue tests of patched specimens have been performed up to 30,000 representative baseline flight hours with no significant crack growth. Based upon the amount of time required for a patched weep hole crack to become critical, it is certain that the integrity of the bondline will be more important for the long term performance of the repair. Bondline failure modes of the patches have been the focus of many tests. Thermal cycle tests have been performed to determine the integrity of the bondline. Fuel soak tests have also been done to ensure that the patches remain bonded to the risers in the wing tanks. Failure of the bondline could potentially have catastrophic results. A sub−critical crack may exist underneath a patch, only to become critical should a patch completely disbond, causing a structural failure.

4.3 Another subject of concern regarded the structure surrounding the patch. While the aluminum underneath the patch saw reduced stresses, there were severe, localized stress concentrations developed at the ends of the patches. Multiple patches in close proximity caused even higher stress concentrations due to their interaction. These negative effects of patching would significantly reduce the life of a crack within the localized stress concentrations. Of particular interest were the Taper−Lok fastener holes along the spanwise splice. If patches were located with the patch edges intersecting a spanwise splice fastener hole, a significant reduction in time−to−failure was expected for cracks growing from these holes. To avoid this, all patches were located so that the edges of the patches were no closer than one inch from the edge of a spanwise splice fastener. The one inch spacing provided the required distance to allow the Taper−Lok fastener holes to only see a modest increase in stress.

4.4 One of the reasons for the large increase in stress at the end of the patch was due to the methodology used to design the patch. During the early stages of the program, patches were designed making conservative assumptions because the beneficial effects were not quantified. Now that this damage tolerance analysis has shown the patches to be extremely effective at lengthening the time to failure of weep hole cracks, thinner patches could be designed to reduce the localized stress concentrations and still meet the present and future operational requirements.

4.5 The use of composite patches to repair aircraft structure has far−reaching benefits for not only the United States Air Force, but also the commercial fleets. This technique can provide a safe means to extend the operating life of an aircraft's structure. This report documents one method of calculating the effects composite patches have on the cracks they are meant to repair. Based upon this analysis, the boron composite patches were highly effective at reducing the crack growth rate for weep hole cracks in the lower wing skins of C−141 Starlifters.

5.0 REFERENCES

1. Lockheed Staff. "C−141 Damage and Repairs − Weep Holes." C−141 Structural Assessment by USAF Scientific Advisory Board, Lockheed Aeronautical Systems Company, Marietta GA. 28−30 April 1993.
2. Lockheed Staff. ER 6423 Volume V, C−141A Correlation of Fatigue Airplane Test Results to Aircraft Service Life, Volume V, Wing−Fuselage Specimen A Test. 30 September 1974.
3. Georgia Institute of Technology. ALTERFEM3D, ALTFGEN3D & ARIVGEN Software Manuals.
4. Bell, R. P. and Chapman, J. W. C−141B Damage Tolerance Analysis (DTA) Update. Lockheed−Georgia Company, Marietta GA. March 1989.
5. Lockheed Staff. LG82ER0040, Volume III, C−141 Weep Hole and Riser Rib Clip Models, Appendix Q. April 1993.
6. Lockheed Staff. SMN 366, Revision C, Fracture Mechanics Methodology and Analytical Procedures. May 1982.
7. Bell, R. P. Fax to D. Register, WR−ALC/TIEDD. May 1993.

APPENDIX A

A.1 The stress intensities for part through cracks were calculated using the Finite Element Alternating Method (FEAM). The full through cracks were calculated with the crack closure method. Figure A1 shows the stress intensities as a function of crack length for a lower weep hole crack (Crack Profile A). Figure A2 shows the same information for an upper weep hole crack (Crack Profile B). The stress intensities are shown in psi(in)$^{0.5}$. Both the patched and unpatched configurations are shown in the figures.

A.2 Lockheed had calculated stress intensities for the unpatched lower weep hole crack configuration, listed in reference 5. The results of Lockheed's stress intensity calculations are shown with the WR−ALC data in figure A1. All of the stress intensity data has been calculated using a 10,000 psi applied stress.

A.3 Beta factors were calculated using the stress intensity data and crack length as the inputs according to the following equation:

$$\beta = \frac{K_I}{\sigma\sqrt{\pi a}}$$

where: K_I = Mode 1 Stress Intensity Factor (psi(in)$^{0.5}$)
σ = Applied Stress (10,000 psi)
a = Crack Length (inches)

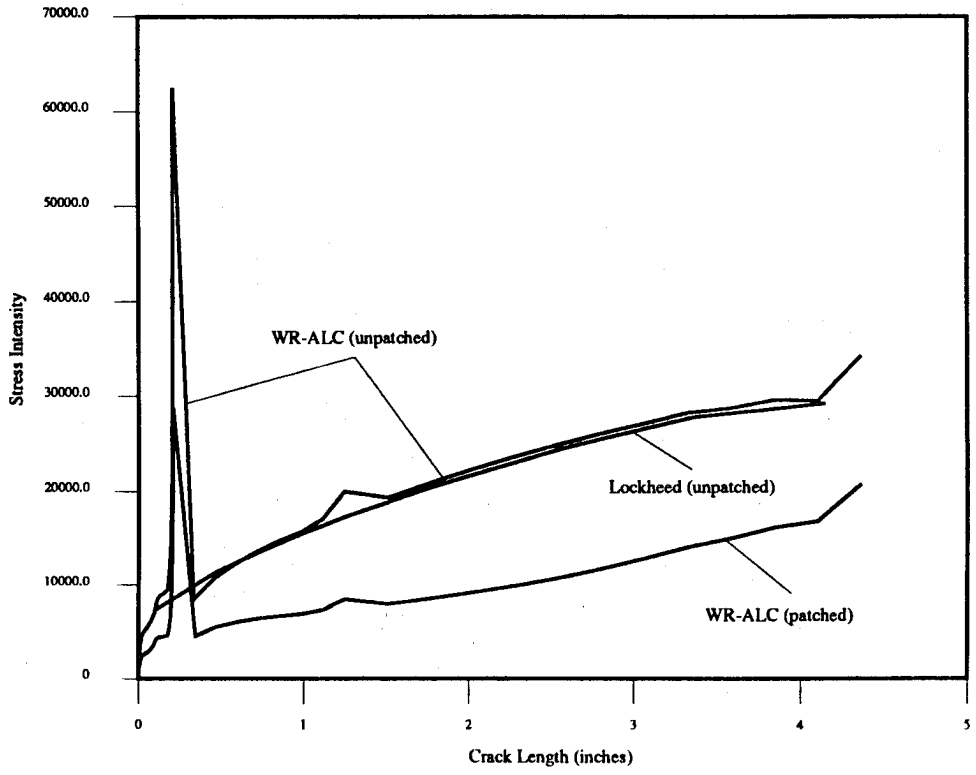


Figure A1: Crack Profile A Stress Intensities

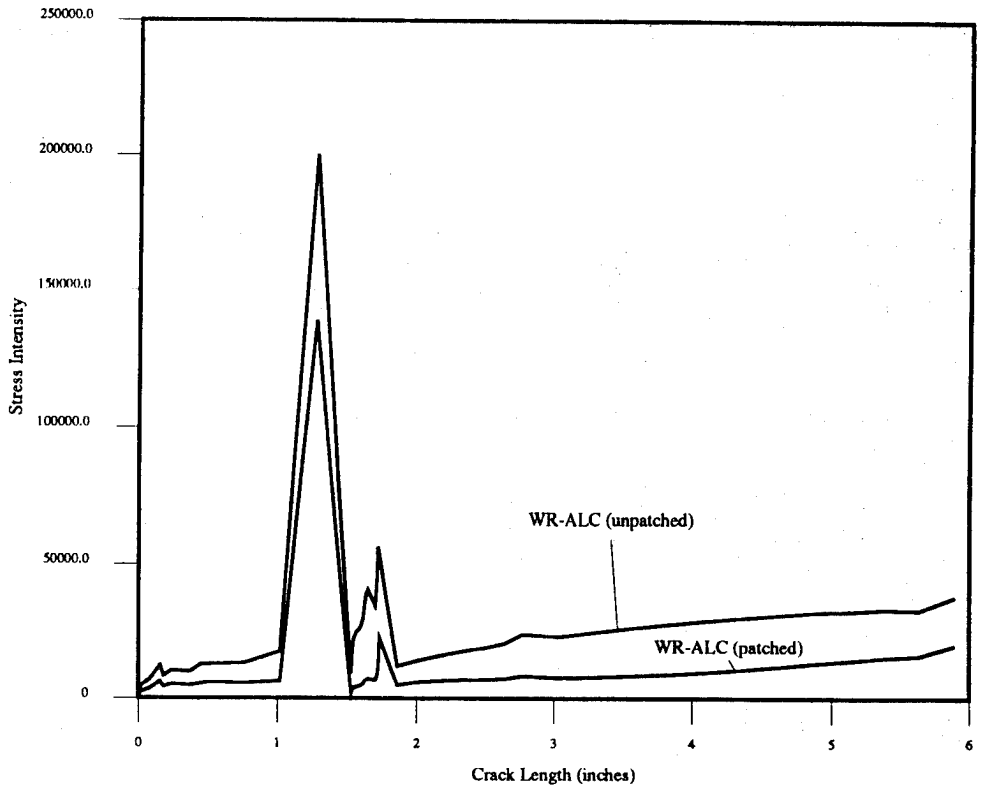


Figure A2: Crack Profile B Stress Intensities

APPENDIX B

Stress−to−load ratios were used by the C−141 Runstream to develop the internal stresses at a given location from a system of unit loads applied in a NASTRAN model. Lockheed has performed a damage tolerance analysis for a variety of locations on the aircraft structure. Analysis point W−36E, the inner wing lower spanwise splice between panels 4 and 5 at IWBRS 191.6, was located close to the region of highest design limit tensile stress. This allowed the use of Lockheed's stress−to−load ratios, as documented on page 147, reference 4. Both axial and shear stress−to−load ratios were developed by Lockheed; however, only the axial ratios were used in this analysis. Shear loads were unimportant for weep hole crack growth calculations because they had little affect upon the stresses in the riser. The following table lists the stress−to−load ratios.

Applied Unit Load Component	Stress−to−Load Ratio (psi/unit load)
	Axial
P_x = 1.0 lb.	−0.004327
P_y = 1.0 lb.	0.010993
P_z = 1.0 lb.	−0.022000
M_x = 1.0 in.−lb.	0.000715
M_y = 1.0 in.−lb.	0.000080
M_z = 1.0 in.−lb.	−0.000040



Warner Robins Air Logistics Center
Technology and Industrial Support Directorate

The C-141 Weep Hole Problem Revisited

A WR-ALC / TI Perspective

Dan Register
Aerospace Engineer
WR-ALC/TIEDD
420 Second St., Suite 100
Robins AFB, GA 31098-1640
(912) 926-4228, FAX: (912) 926-1743

Warner Robins Air Logistics Center
Technology and Industrial Support Directorate

OVERVIEW

- **Introduction**
- Background
- The Problem
- The Solution
- WR-ALC/TI Technical Challenges
- Summary

Warner Robins Air Logistics Center
Technology and Industrial Support Directorate

Introduction

- Technology & Industrial Support Directorate (WR-ALC/TI)
  - Manufacturing/Engineering Support for the Aircraft Directorates (C-141, C-130, F-15, H-53)
- Damage Tolerance Analysis
  - Only One of Many Issues Concerning the C-141 Weep Hole Problem
  - Paper Entitled "*Damage Tolerance Analysis of C-141 Weep Hole Cracks with Boron Composite Repairs*" is available

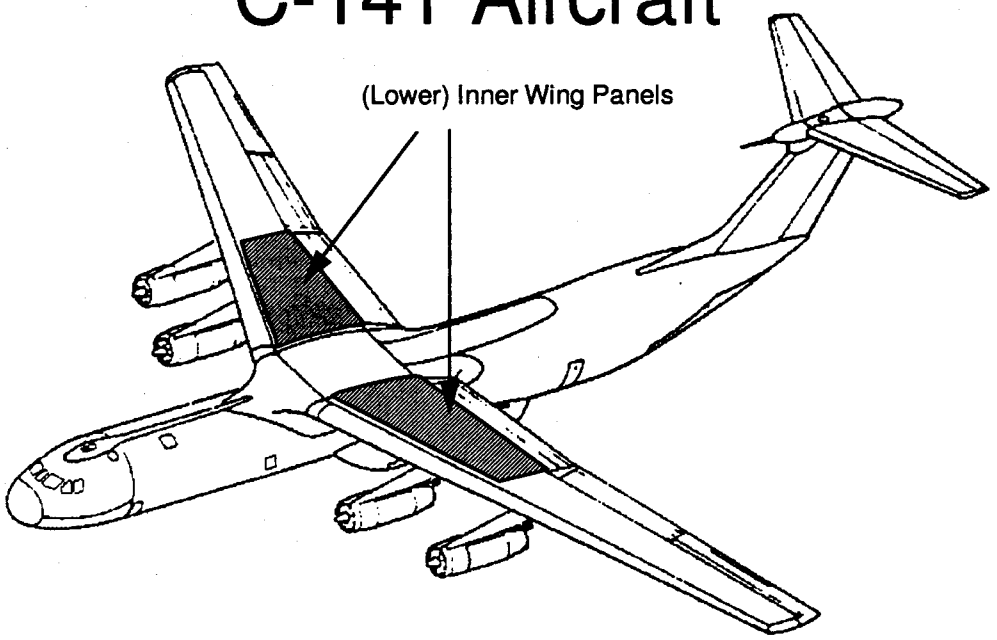
OVERVIEW

- Introduction
- ☞ **Background**
- The Problem
- The Solution
- WR-ALC/TI Technical Challenges
- Summary

Warner Robins Air Logistics Center
Technology and Industrial Support Directorate

Background

C-141 Aircraft



Warner Robins Air Logistics Center
Technology and Industrial Support Directorate

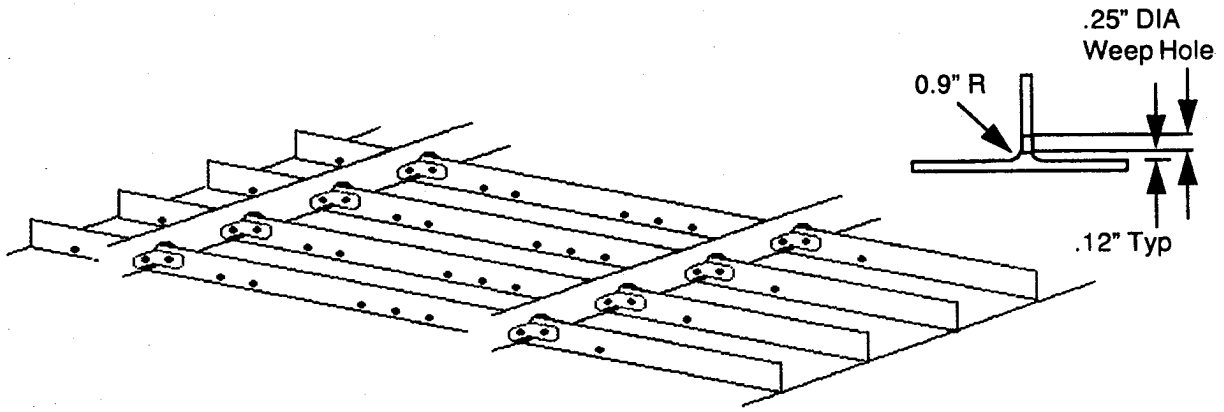
Background

- Prior Condition of C-141B Wings (As of June 1993)
  - Number of Aircraft in the Force: 244
    Average Number of Flight Hours: 35,250
  - WS 405 Multi-Site/Multi-Element Damage
  - Center Wing Box Replacement Program
  - Wing Spanwise Splice Assumed Life Limit - 45,000 Flight Hours

Warner Robins Air Logistics Center
Technology and Industrial Support Directorate

Background

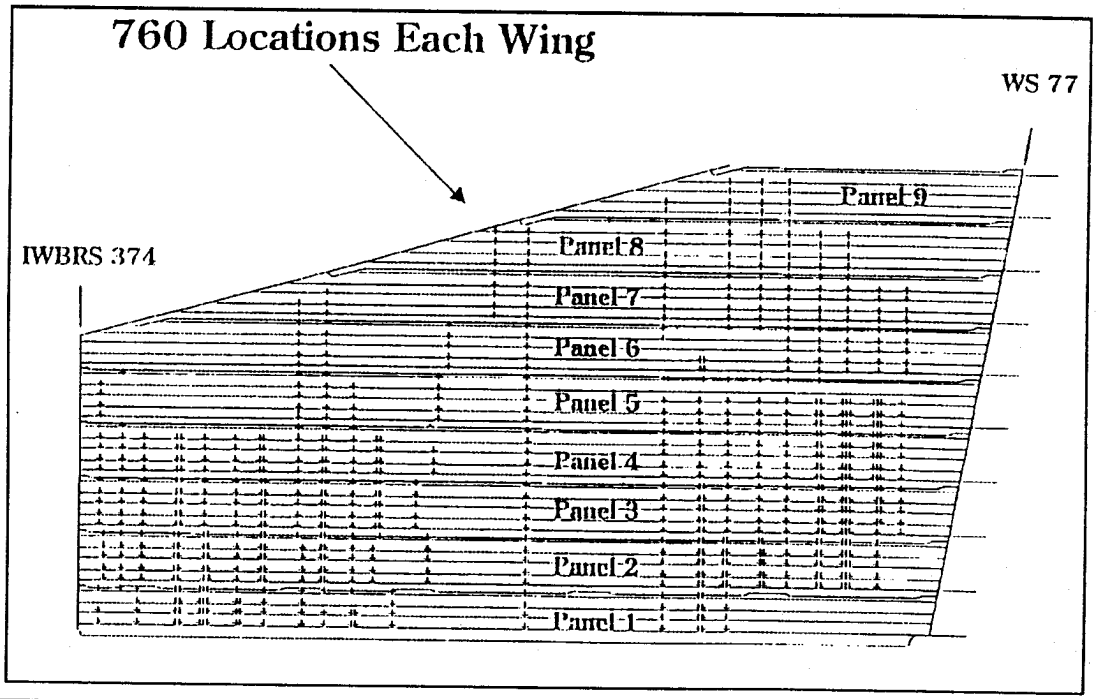
Typical Weep Hole Geometry



Warner Robins Air Logistics Center
Technology and Industrial Support Directorate

Background

Location and Number of Weep Holes





Warner Robins Air Logistics Center
Technology and Industrial Support Directorate

OVERVIEW

- Introduction
- Background
- ☞ **The Problem**
- The Solution
- WR-ALC/TI Technical Challenges
- Summary

Warner Robins Air Logistics Center
Technology and Industrial Support Directorate

The Problem

- How Bad Was It?
  - **Inspection of the Fleet**
    - WR-ALC/TI Development of Reliable Weep Hole NDI Capability / Procedures
    - WR-ALC/TI Training of Depot / Contractor Inspectors
  - **Widespread Fatigue Damage**
    - 45 Aircraft Grounded
    - 116 Aircraft Restricted from Full Operations
  - **Long Lead Time for New Panels**
    - Very Costly to Replace a Whole Wing Panel



Warner Robins Air Logistics Center
Technology and Industrial Support Directorate

OVERVIEW

- Introduction
- Background
- The Problem
- ☞ **The Solution**
- WR-ALC/TI Technical Challenges
- Summary

Warner Robins Air Logistics Center
Technology and Industrial Support Directorate

The Solution

- ***Reaming/Coldworking*** Weep Holes (where possible)
- ***Boron Composite Patches*** (where reaming does not remove crack)
- ***Panel Replacement***
  - When Available (April 1994)
  - Where Number or Extent of Repairs Would Be Excessive → 91 Panels Ordered
- ***Aircraft Retirement*** (if repair impractical)



Warner Robins Air Logistics Center
Technology and Industrial Support Directorate

OVERVIEW

- Introduction
- Background
- The Problem
- The Solution
- ☞ **WR-ALC/TI Technical Challenges**
- Summary



Warner Robins Air Logistics Center
Technology and Industrial Support Directorate

Technical Challenges

- **Weep Hole Inspection Procedure**
- Design of Boron Composite Patch Repairs
- Industrialization of the Wright Lab Patch Installation Procedure
- Quality Assurance of Patch Bonds
- Video Thermography Inspection
- In-Service Durability

Warner Robins Air Logistics Center
Technology and Industrial Support Directorate

Technical Challenges:

Weep Hole Inspection Procedures

- WR-ALC/TI Modified Previous Force-wide Inspection Procedure to Accommodate Weep Hole Reaming/Coldworking Repairs
  - Repairs Required Different Size Reamers to Remove Cracks (up to 0.390 Inch Diameter)
  - WR-ALC/TI Specified the Required Sizes of Bolt Hole Eddy Current NDI Probes
  - WR-ALC/TI Modified Probe Guides to Accommodate Probes of Different Sizes
  - WR-ALC/TI Continued Training Inspectors in the Field and at the Depot

Warner Robins Air Logistics Center
Technology and Industrial Support Directorate

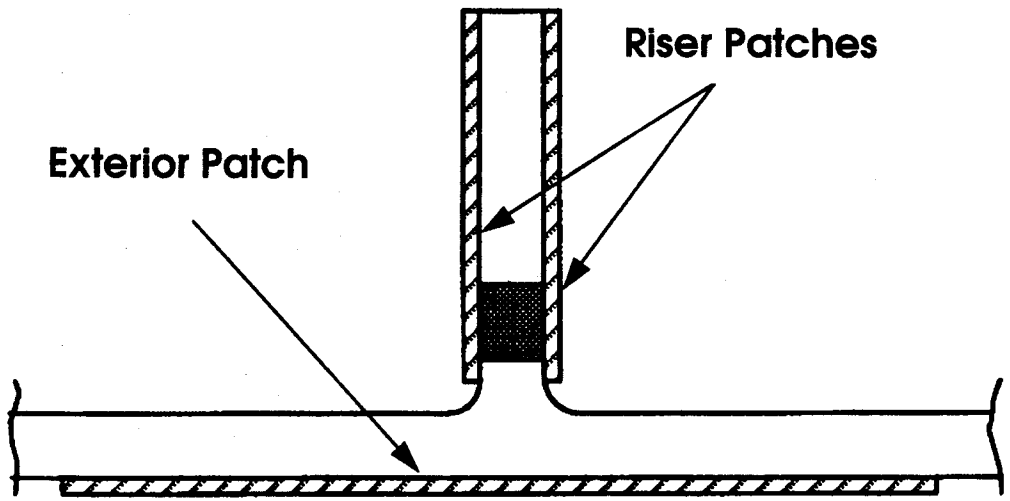
Technical Challenges

- Weep Hole Inspection Procedure
- **Design of Boron Composite Patch Repairs**
- Industrialization of the Wright Lab Patch Installation Procedure
- Quality Assurance of Patch Bonds
- Video Thermography Inspection
- In-Service Durability

Warner Robins Air Logistics Center
Technology and Industrial Support Directorate

Technical Challenges:

Design of Boron Composite Patch Repairs



Warner Robins Air Logistics Center
Technology and Industrial Support Directorate

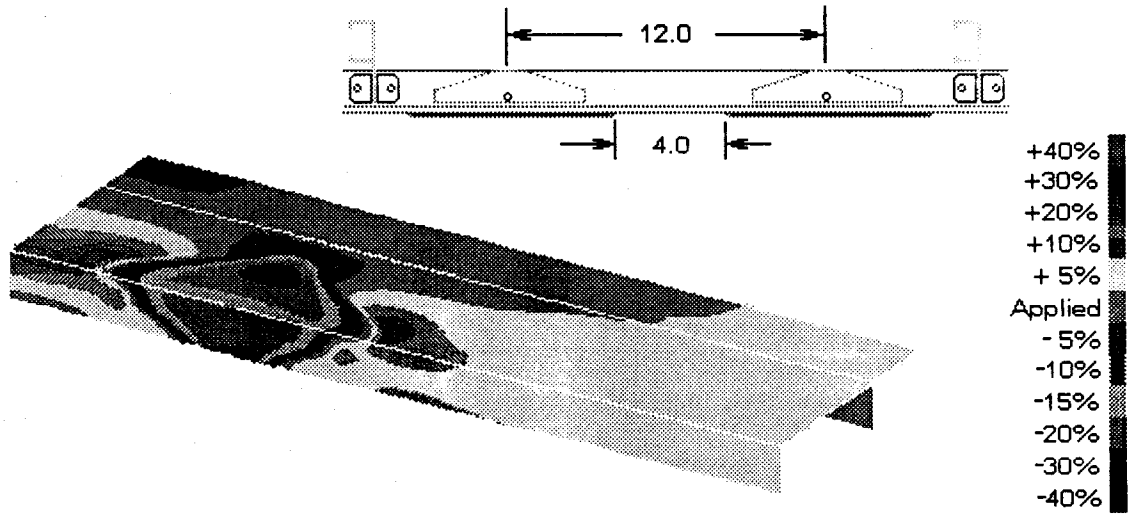
Technical Challenges:

Design of Boron Composite Patch Repairs

- Comparison of Graphite to Boron
- Equivalent Strength & Stiffness
  - ☞ $E_r t_r / E_p t_p$ = 1.2 to 1.5 (Modified Hart-Smith)
    - Assumed Worst Case: Total Fracture
- Lay-Up / Shape Studies
  - Proximity Issues
- Finite Element Analysis - 2D & 3D
- Effect on Surrounding Structure
- Damage Tolerance Analyses

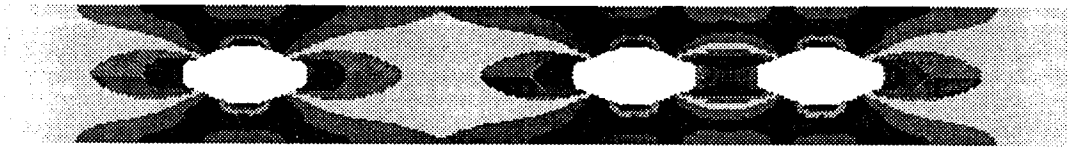
Warner Robins Air Logistics Center
Technology and Industrial Support Directorate

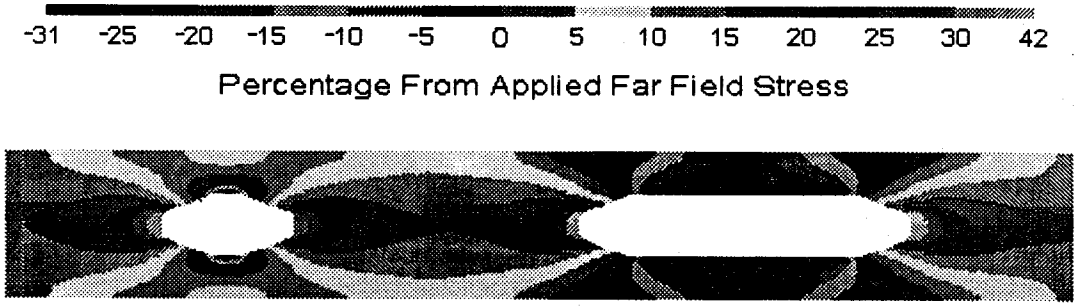
Global Analysis - Proximity



Warner Robins Air Logistics Center
Technology and Industrial Support Directorate

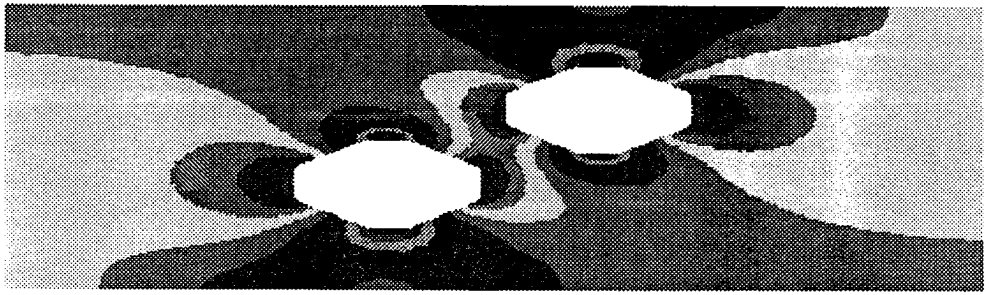
General Stress Analysis





Warner Robins Air Logistics Center
Technology and Industrial Support Directorate

General Stress Analysis





Percentage Above Applied Far Field Stress

Warner Robins Air Logistics Center
Technology and Industrial Support Directorate

Technical Challenges:

Design of Boron Composite Patch Repairs

- Comparison of Graphite to Boron
- Equivalent Strength & Stiffness
  - ☞ $E_r t_r / E_p t_p$ = 1.2 to 1.5 (Modified Hart-Smith)
    - Assumed Worst Case: Total Fracture
- Lay-Up / Shape Studies
  - Proximity Issues
- Finite Element Analysis - 2D & 3D
- Effect on Surrounding Structure
- Damage Tolerance Analyses

Detailed Stress Analysis

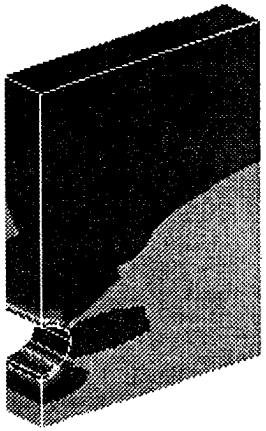
Patched



K_t

2.58
2.25
2.00
1.75
1.50
1.25
1.00
.75
.50
.25
-.08

Unpatched



Warner Robins Air Logistics Center
Technology and Industrial Support Directorate

Technical Challenges:

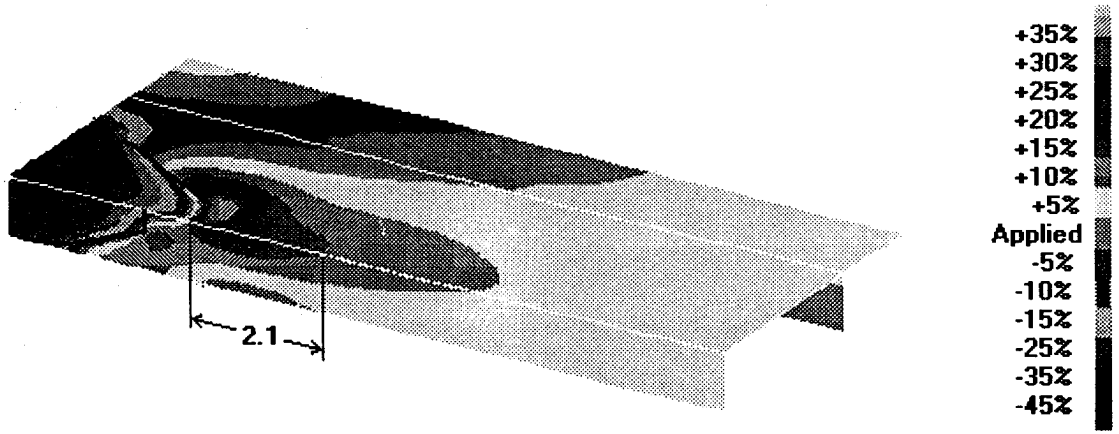
Design of Boron Composite Patch Repairs

- Comparison of Graphite to Boron
- Equivalent Strength & Stiffness
  - ☞ $E_r t_r / E_p t_p$ = 1.2 to 1.5 (Modified Hart-Smith)
    - Assumed Worst Case: Total Fracture
- Lay-Up / Shape Studies
  - Proximity Issues
- Finite Element Analysis - 2D & 3D
- Effect on Surrounding Structure
- Damage Tolerance Analyses

Warner Robins Air Logistics Center
Technology and Industrial Support Directorate

Detailed Stress Analysis

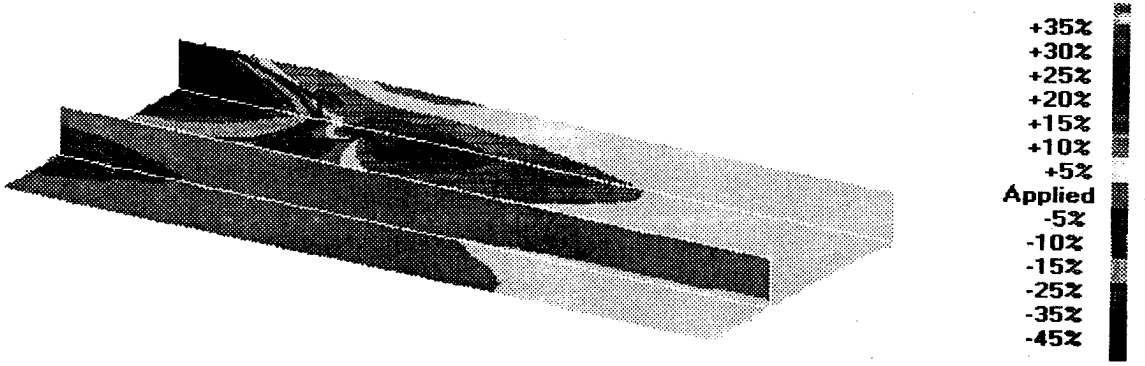
Single Hole Repair - Exterior Surface



Warner Robins Air Logistics Center
Technology and Industrial Support Directorate

Detailed Stress Analysis

Single Hole Repair - Interior Surface

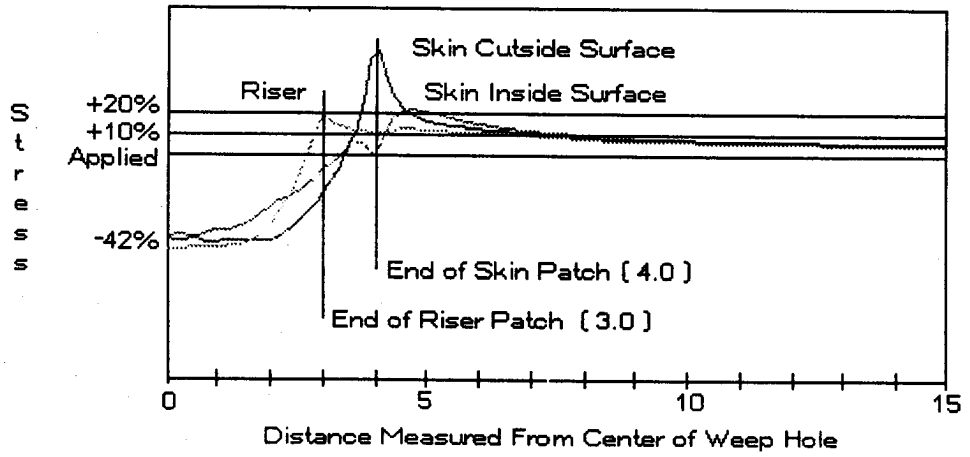


Warner Robins Air Logistics Center
Technology and Industrial Support Directorate

Detailed Stress Analysis



Stress vs. Distance



Warner Robins Air Logistics Center
Technology and Industrial Support Directorate

Technical Challenges

- Weep Hole Inspection Procedure
- Design of Boron Composite Patch Repairs
- **Industrialization of the Wright Lab Patch Installation Procedure**
- Quality Assurance of Patch Bonds
- Video Thermography Inspection
- In-Service Durability

Warner Robins Air Logistics Center
Technology and Industrial Support Directorate

Technical Challenges:

Industrialization of Wright Lab Patch Installation Procedure

- **WR-ALC/TI Aware of Australian Successes on Other Aircraft**
- **WR-ALC/TI Aware of Wright Lab Development of Similar Process**
  - Requested R&D by Wright Lab
  - Demonstrated in Some Applications
  - Very Simple Areas (Geometry and Access)
- **WL/ML and WR-ALC/TI Formed an Integrated Product Team (IPT)**

Warner Robins Air Logistics Center
Technology and Industrial Support Directorate

Technical Challenges:

Industrialization of Wright Lab Patch Installation Procedure

- **Prototype of Industrialized Process**
- **WL/ML Qualification of WR-ALC/TI Mechanics**
- **Procurement of Repair Equipment and Materials**
- **Follow-on Training of Other Mechanics by Previously-qualified Personnel**
- **WR-ALC/TI Process Order**

Warner Robins Air Logistics Center
Technology and Industrial Support Directorate

Technical Challenges:

Industrialization of Wright Lab Patch Installation Procedure

- **Industrialized Process:**
  - Custom Patch Design - Size, Plies, etc.
  - Patch Manufacturing:
    - Precuring with 60 psi Autoclave Pressure
  - Reamed Weep Hole Plugged

Warner Robins Air Logistics Center
Technology and Industrial Support Directorate

Technical Challenges:

Industrialization of Wright Lab Patch Installation Procedure

- **Industrialized Process (Cont'd):**
  - Aluminum Grit Blasting of Aluminum Surfaces
  - Containment of Grit / Cleaning
  - Silane and Primer Application / Curing
  - Hot Bonding of Boron Composite Patches

Warner Robins Air Logistics Center
Technology and Industrial Support Directorate

Technical Challenges:

Industrialization of Wright Lab Patch Installation Procedure

- **Industrialized Process (Cont'd):**
  - Thermographic Inspection of Bonds
  - Removal / Reapplication if Indicated
  - Sealing / Painting of Patches
  - ☞ **Process Cleanliness & Safety for Mechanics**

Warner Robins Air Logistics Center
Technology and Industrial Support Directorate

Technical Challenges:

Industrialization of Wright Lab Patch Installation Procedure

- **Process Improvement - Teamwork!**
  - 16-Hour Average Installation Time Per Repair
    - Down from 40
  - Clean-up Procedure Refinement
    - Saving 64 Manhours per Fuel Tank
  - 87 Aircraft, 312 Repairs
- **The Result: Unrestricted C-141s**

Warner Robins Air Logistics Center
Technology and Industrial Support Directorate

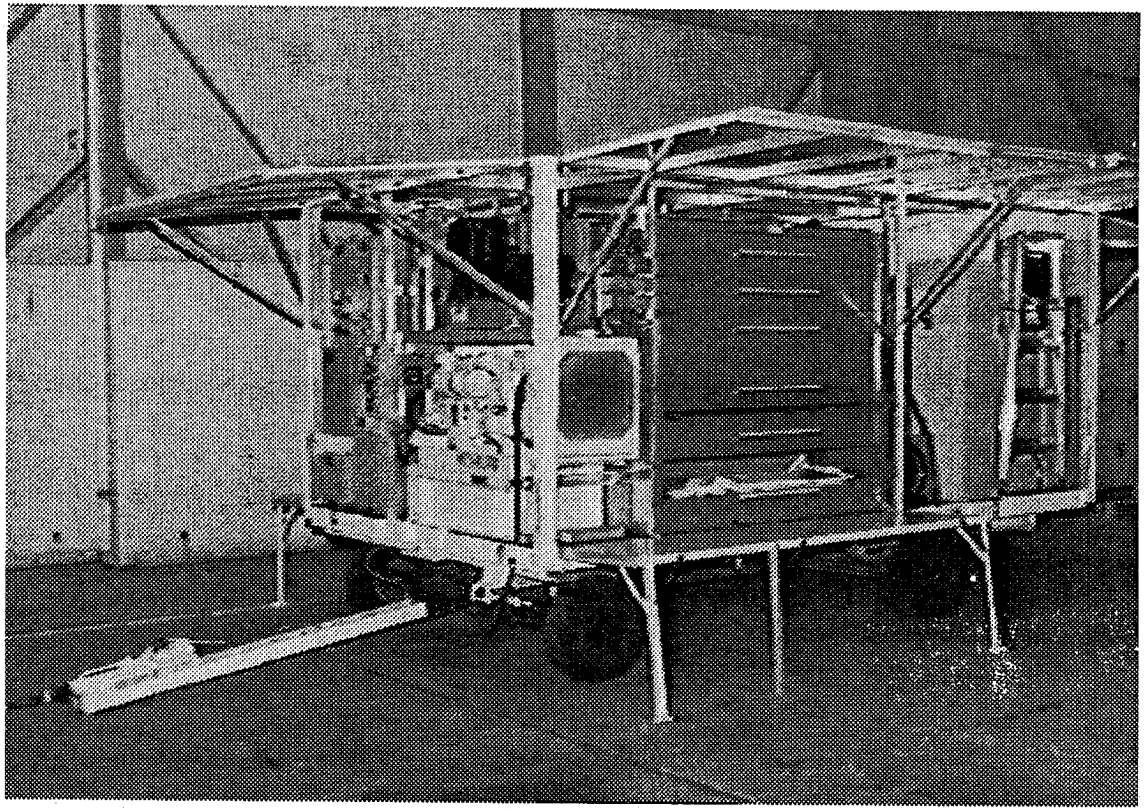
Technical Challenges:

Industrialization of Wright Lab Patch Installation Procedure

- **WR-ALC/TI Using Same Process for Other Repairs on C-141, C-130 and H-53 Aircraft**
- **WR-ALC/TI Working with FAA and Industry to Make the Industrial Installation Process Available for Commercial Aircraft Applications**
- **Unique, Self-Contained, Air-Transportable Composite and Honeycomb Repair Unit Developed to Enable Rapid Field-level Repairs**

Warner Robins Air Logistics Center
Technology and Industrial Support Directorate

Air-Transportable Composite / Honeycomb Repair Unit



Warner Robins Air Logistics Center
Technology and Industrial Support Directorate

Technical Challenges

- Weep Hole Inspection Procedure
- Design of Boron Composite Patch Repairs
- Industrialization of the Wright Lab Patch Installation Procedure
- ☞ **Quality Assurance of Patch Bonds**
- Video Thermography Inspection
- In-Service Durability

Warner Robins Air Logistics Center
Technology and Industrial Support Directorate

Technical Challenges:

Quality Assurance of Patch Bonds

- **Quality is Job 1**
  - 3 Patches per repair, 2 inside fuel tank
  - Location --> Difficult Access --> Process Flexibility
  - Surface Preparation --> Environmental Concerns
  - Continuous Monitoring of Elevated Cure Temperatures / Vacuum
- **Over 900 Patches Installed**
- **WR-ALC/TI Development of Thermographic/ Videographic Inspection Capability**



Warner Robins Air Logistics Center
Technology and Industrial Support Directorate

Technical Challenges

- Weep Hole Inspection Procedure
- Design of Boron Composite Patch Repairs
- Industrialization of the Wright Lab Patch Installation Procedure
- Quality Assurance of Patch Bonds
- ☞ **Video Thermography Inspection**
- In-Service Durability

Warner Robins Air Logistics Center
Technology and Industrial Support Directorate

Technical Challenges:

Video Thermography Inspection

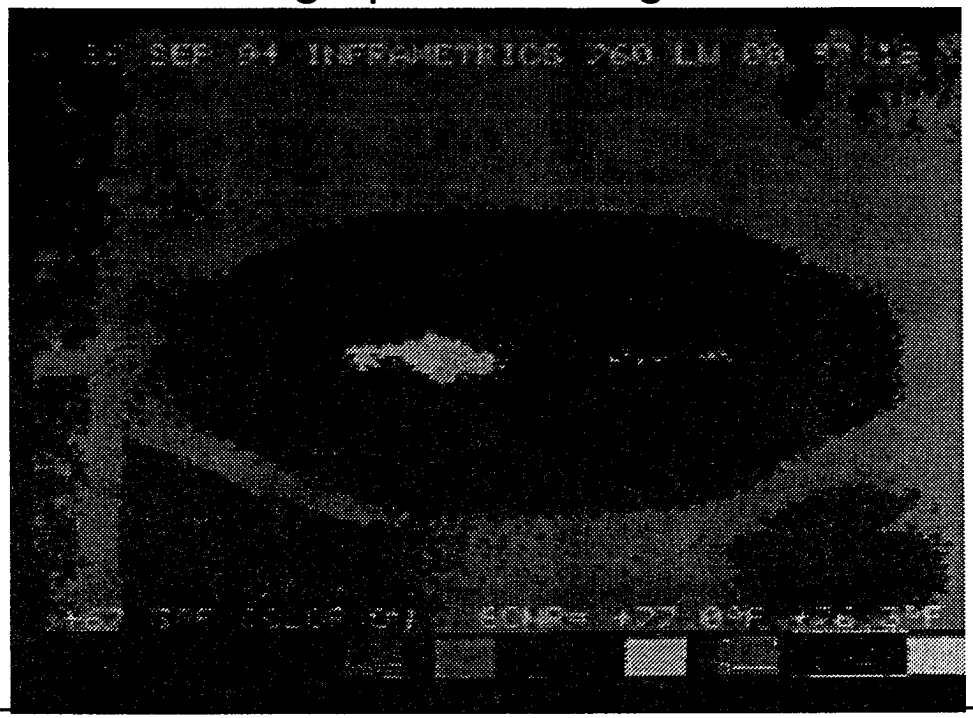
- **Thermal Wave Imaging Combined with Videographic Recording**
  - Off-the-Shelf Technology Extended by Recording Images for Subsequent Processing / Evaluation
  - Patches Checked Before Installation; Bond Line Checked After Installation
  - Accurately Identifies Anomalies as Small as 0.12 Inch Diameter
  - Fast and Easy Inspection of Patches
  - Provides Record of Inspections

Warner Robins Air Logistics Center
Technology and Industrial Support Directorate

Technical Challenges:

Quality Assurance of Patch Bonds

Thermograph Indicating Disbonds



Warner Robins Air Logistics Center
Technology and Industrial Support Directorate

Technical Challenges

- Weep Hole Inspection Procedure
- Design of Boron Composite Patch Repairs
- Industrialization of the Wright Lab Patch Installation Procedure
- Quality Assurance of Patch Bonds
- Video Thermography Inspection
- **In-Service Durability**

Warner Robins Air Logistics Center
Technology and Industrial Support Directorate

Technical Challenges:

In-Service Durability

- **Dependent on Integrity of Bond**
  - Strict Requirements for Allowable Disbond Size
  - Specimen Fatigue Tests
    - Life >>15,000 Flight Hours
- **Environmental Effects**
  - Interior Patches have Protective Fiberglass and Sealant to Protect Against Fuel Degradation
  - Exterior Patches Have Protective Fiberglass, Sealant and Paint
  - Depot Re-inspection of Composite Patches
    - No Degradation of Bonds Evident

Warner Robins Air Logistics Center
Technology and Industrial Support Directorate

Technical Challenges:

In-Service Durability

- **Future Development of Ultrasonic Imaging NDI Capability**
  - **Inspections Without Wing Defueling**
    - Inspections of Both Riser and Panel Patches
    - Evaluation of Patch Bond Integrity
    - Monitoring of Crack Growth at Weep Hole
  - **Technology Exists and the C-141Aircraft Directorate has Provided Prototype Funding**
  - **WR-ALC/TI is Working with a Contractor to Develop Prototype**



Warner Robins Air Logistics Center
Technology and Industrial Support Directorate

OVERVIEW

- Introduction
- Background
- The Problem
- The Solution
- WR-ALC/TI Technical Challenges
- **Summary**



Warner Robins Air Logistics Center
Technology and Industrial Support Directorate

Summary

- The C-141 Weep Hole Problem Required Several Repair Actions.
- WR-ALC/TI Provided a Reliable Weep Hole Inspection Capability.
- The Using Command Mission Provided the Technology Pull to Bring an Emerging Composite Repair Technology to Maturity.



Warner Robins Air Logistics Center
Technology and Industrial Support Directorate

Summary

- The C-141 Weep Hole Problem Demonstrated the Value of the Integrated Product Team Approach to Solving Problems.
- WR-ALC/TI Met the Technical Challenges Associated with Boron Composite Patch Repairs.
- Thermography is a Valuable Tool for Ensuring Quality Repairs.

Warner Robins Air Logistics Center
Technology and Industrial Support Directorate

Summary

- New Technologies Were Required to Ensure the Reliability and Maintainability of Aging C-141s.
- Composite Repairs Require Consideration of Other Factors in Addition to Crack Growth to Establish Inspection Criteria.
- A new Ultrasonic Imaging NDI Capability is Being Prototyped to Minimize Aircraft Downtime.

COMPOSITE REPAIR DURABILITY/DAMAGE TOLERANCE TEST OF C/KC-135 F.S. 880 FLOOR BEAM

Dr. Jaycee Chung *
Albert Arrieta **
Jon Beard ***

The Fuselage Station (F.S.) 880 floor beams of C/KC-135 aircraft are experiencing cracking after over 30 years of service. Composite repair technology was applied to the floor beams for repair and structural life enhancement.

A series of flight tests were conducted to measure the strain magnitudes on the hot spot of the floor beam for each mission segment of C/KC-135 aircraft. Using KC-135R mission profile and mixes, a stress spectrum was developed for a durability/damage tolerance test of a composite repaired F.S. 880 floor beam. A series of static strain surveys on an F.S. 880 floor beam were conducted in a laboratory environment with and without composite doublers installed, prior to the durability/damage tolerance test. A design limit load was applied after 50 years of cyclic fatigue loads application. Then, a through-the-thickness crack was introduced to the hot spot connecting a fastener hole to the triangular cutout of the floor beam for damage tolerance test. Another 50 years of cyclic loads were applied to the beam, and a limit load was applied after the cyclic loads application. Non-Destructive Inspections (NDIs) during and after the test revealed no indication of degradation of composite repair integrity.

* E-Systems, P.O. Box 6056, Greenville, TX 75403
** OC-ALC/TIESM, Tinker AFB, OK 73145
*** OC-ALC/LACRA, Tinker AFB, OK 73145

COMPOSITE REPAIR DURABILITY/DAMAGE TOLERANCE TEST OF C/KC-135 F.S. 880 FLOOR BEAM

USAF ASIP Conf.
7 December 1994

Jaycee Chung E-Systems/GVL
Albert Arrieta OC-ALC/TIESM
Jon Beard OC-ALC/LACRA

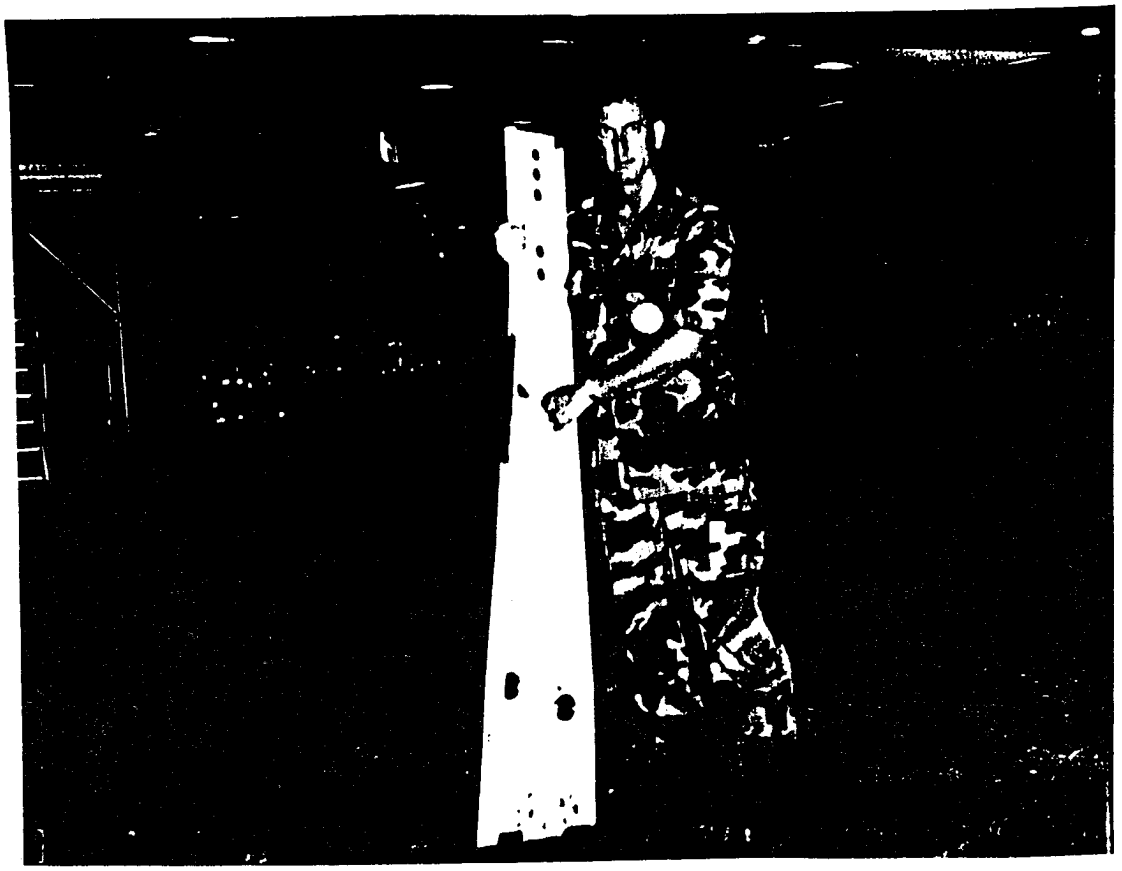
Composite Repair Developmental Task

- Damage Assessment & Structural Eval.
- Repair Design Development
- Repair Process Development
- Validation Test
- Repair Demonstration

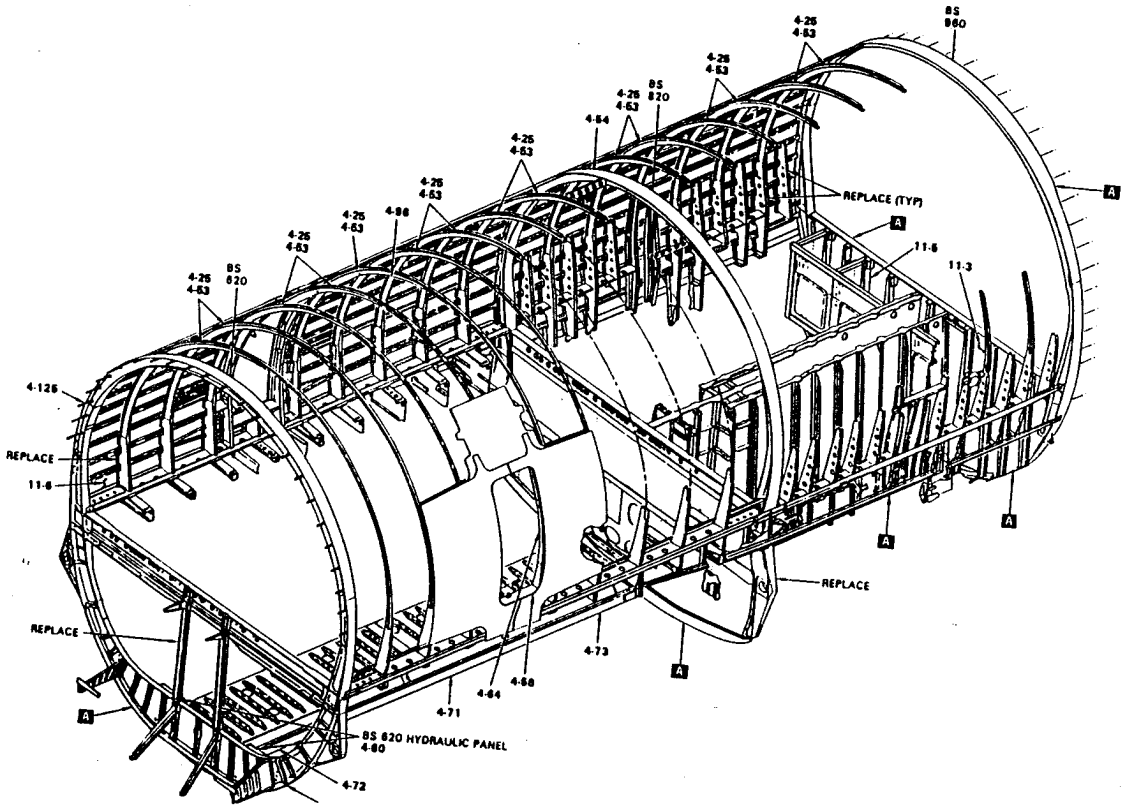
Doubler Installation & Flight Demonstration

- A beam cap doubler was designed and installed on a KC-135 ACFT for bonding integrity monitoring (Tinker AFB, 1990).
- The patch and bondline appeared to be intact when the ACFT's NLG was severely damaged due to a hard impact landing (Edward AFB, 1991).
- The Doubler flew 3.5 years successfully.

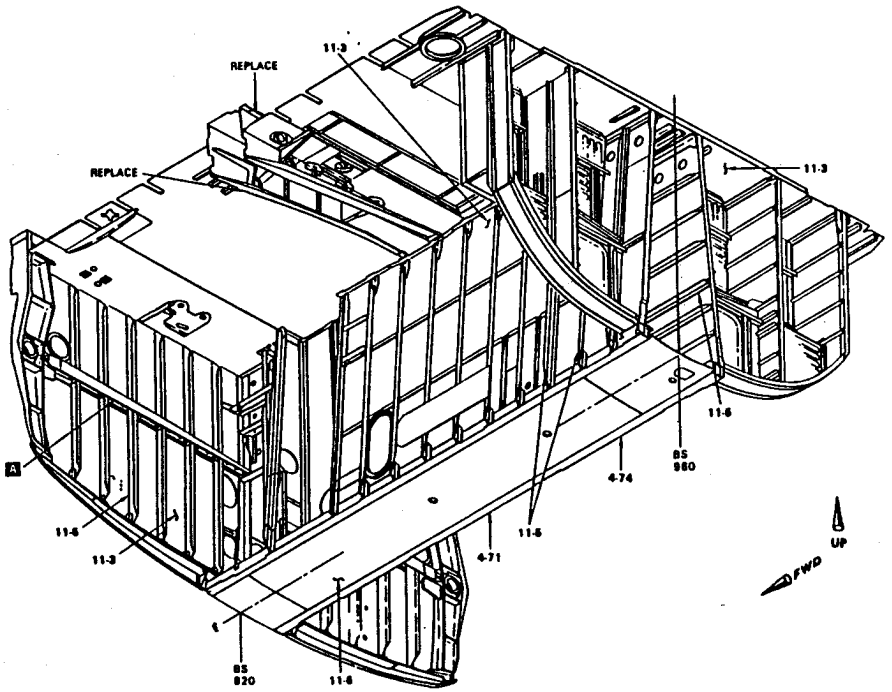
FS 880 Floor Beam Composite Doubler



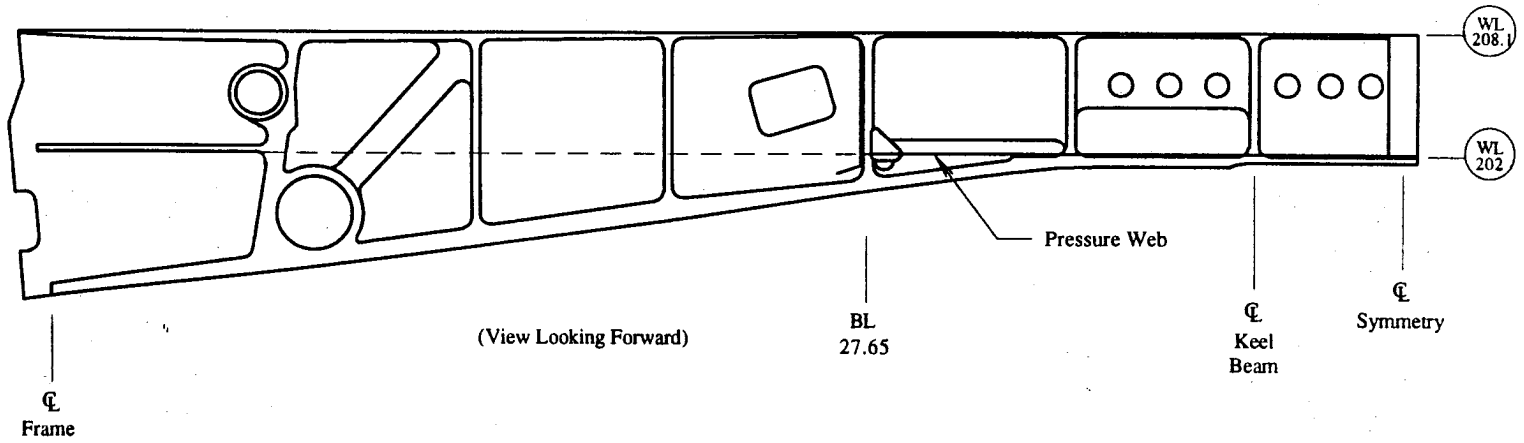
C/KC-135 Section 43 Structural View



FS 880 Floor Beam Location

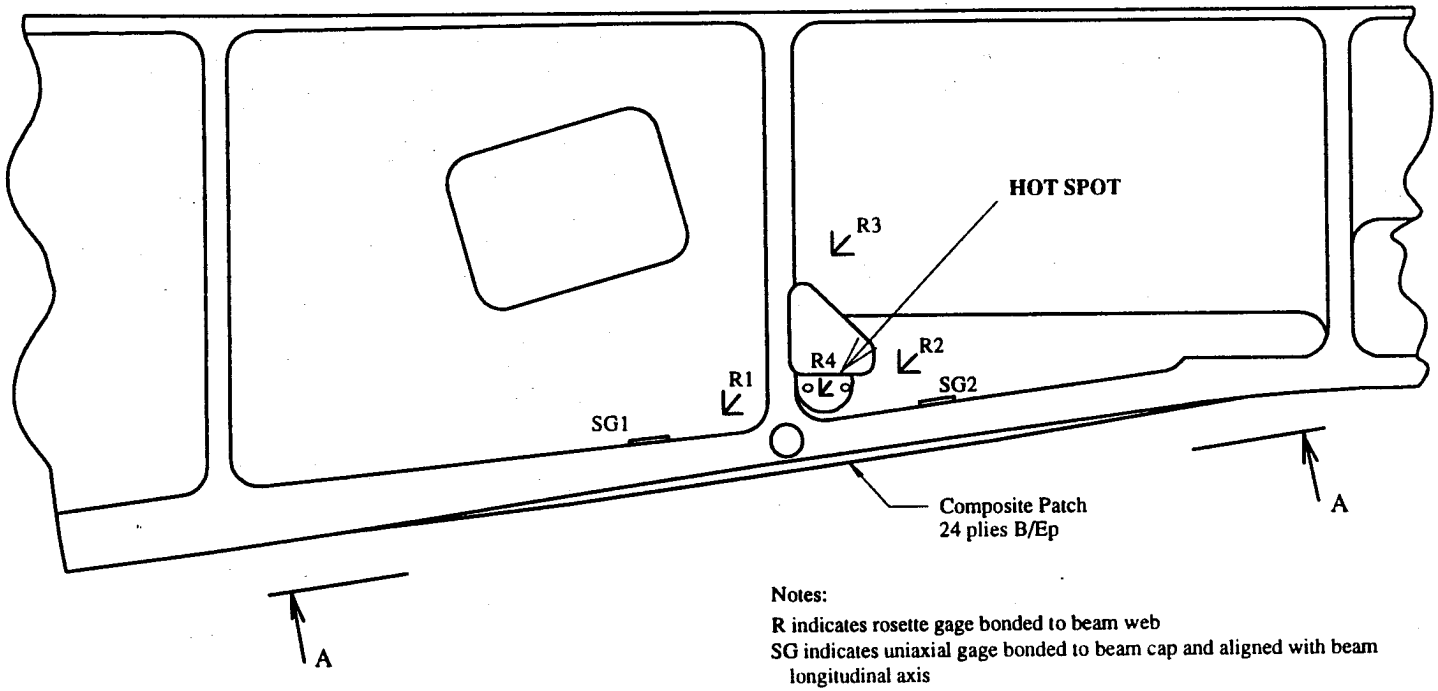


C/KC-135 FS 880 Floor Beam (LHS)



Material : 7075-T6 Forging

FS 880 Floor Beam Patch and S/G Locations

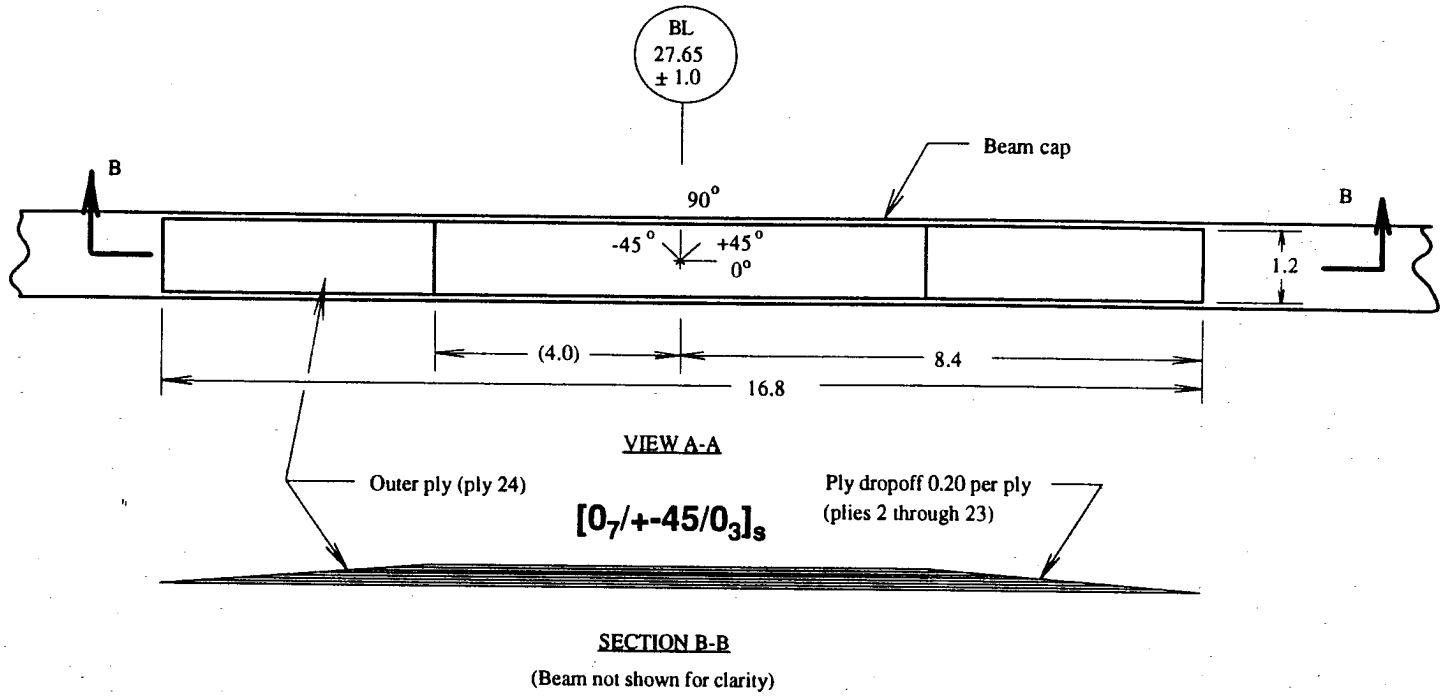


Notes:

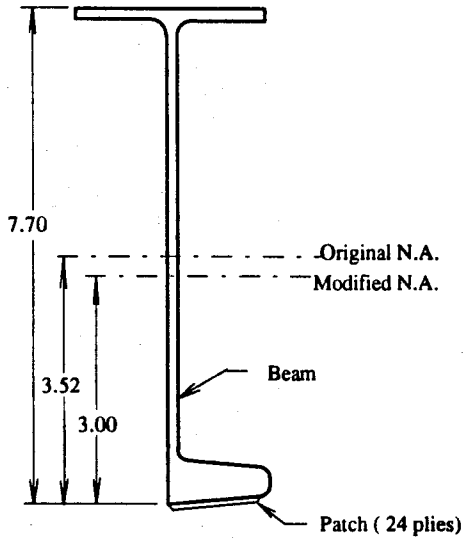
R indicates rosette gage bonded to beam web

SG indicates uniaxial gage bonded to beam cap and aligned with beam longitudinal axis

Beam Cap Composite Patch Configuration



Stress Reduction Assessment



Beam section at B.L. 25

$A = 2.52 \text{ in}^2$

$I = 22.47 \text{ in}^4$

$$A_p = \frac{E_p}{E}(0.12)(1.2)$$

$= 3.0(0.12)(1.2)$

$= 0.432 \text{ in}^2$

$$\bar{I} = I + A d^2 + A_p d_p^2$$

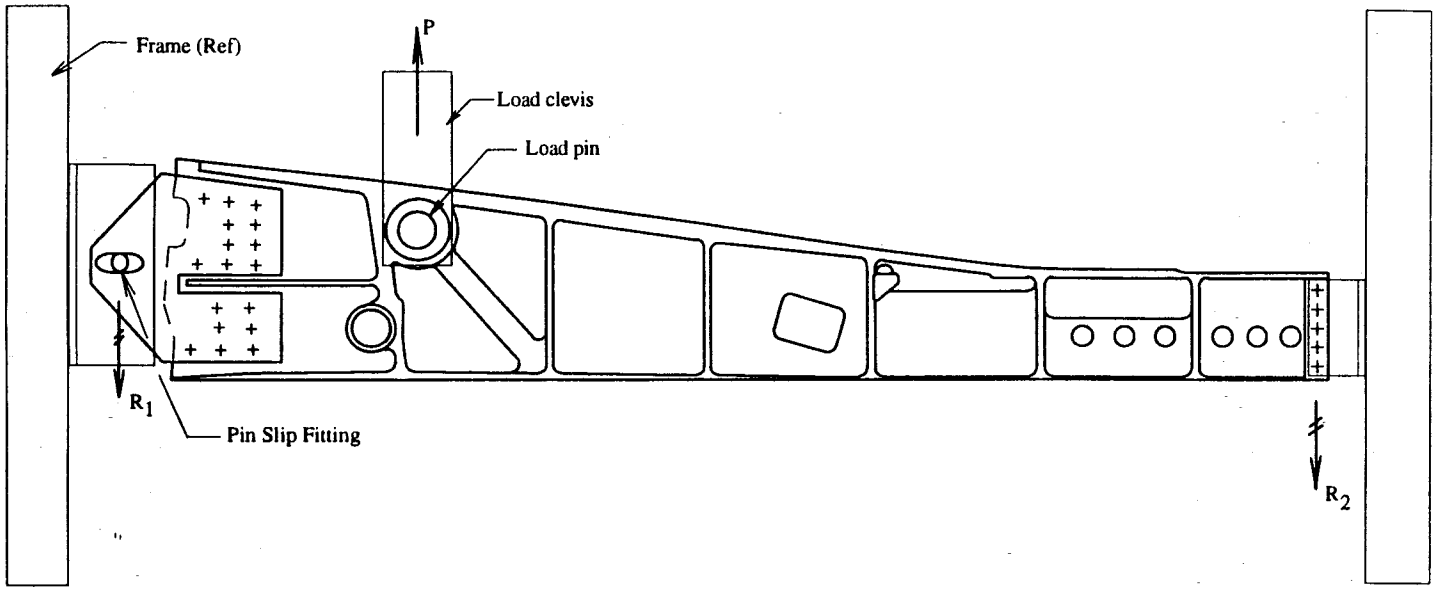
$= 27.0 \text{ in}^4$

Original section: c/I = 3.52/22.47 = 0.157 l/in3

Modified section: c/I = 3.0/27.0 = 0.111 l/in3

Stress Reduction = (0.157 - 0.111)/0.157 = 0.29 or 29%

Preliminary Static Strain Survey



Strain Reduction : 32 % on Beam Cap
10 % on Hot Spot

Instrumented Strain Survey Flight Test

- KC-135E (57-1424) was instrumented, and a flight test was performed on Tinker AFB.
- Twenty two mission segments were flown.
- Strain data were recorded during the flight test.
- The recorded data were down loaded to a PC, and data reduction was performed.

PC software used for Data Reduction

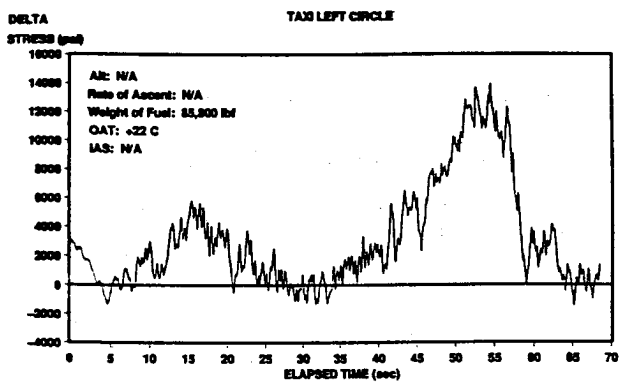
EXCEED [a] ***- To find the max and min strains for each event for each gage.***

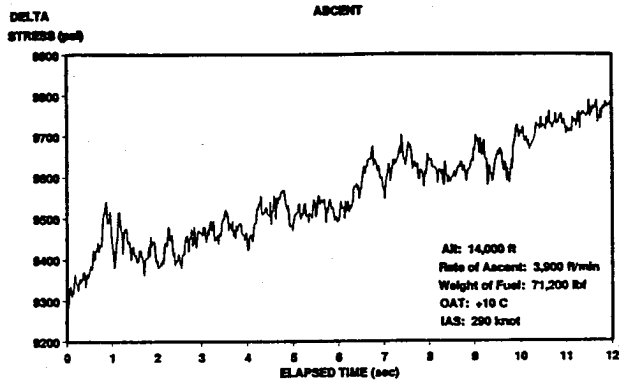
REDUCE [a] ***- To filter and reduce the data files to smaller files with a user input.***

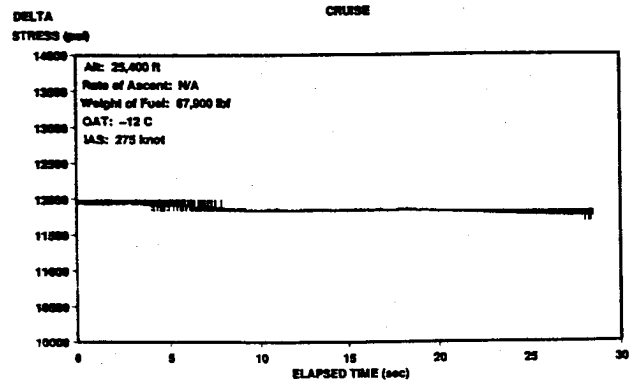
Microsoft® EXCEL - To plot the reduced data.

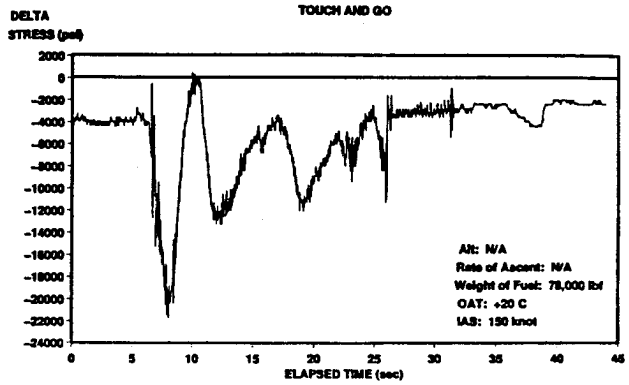
a : PC software developed under this program.

Flight Strain Survey Data Examples









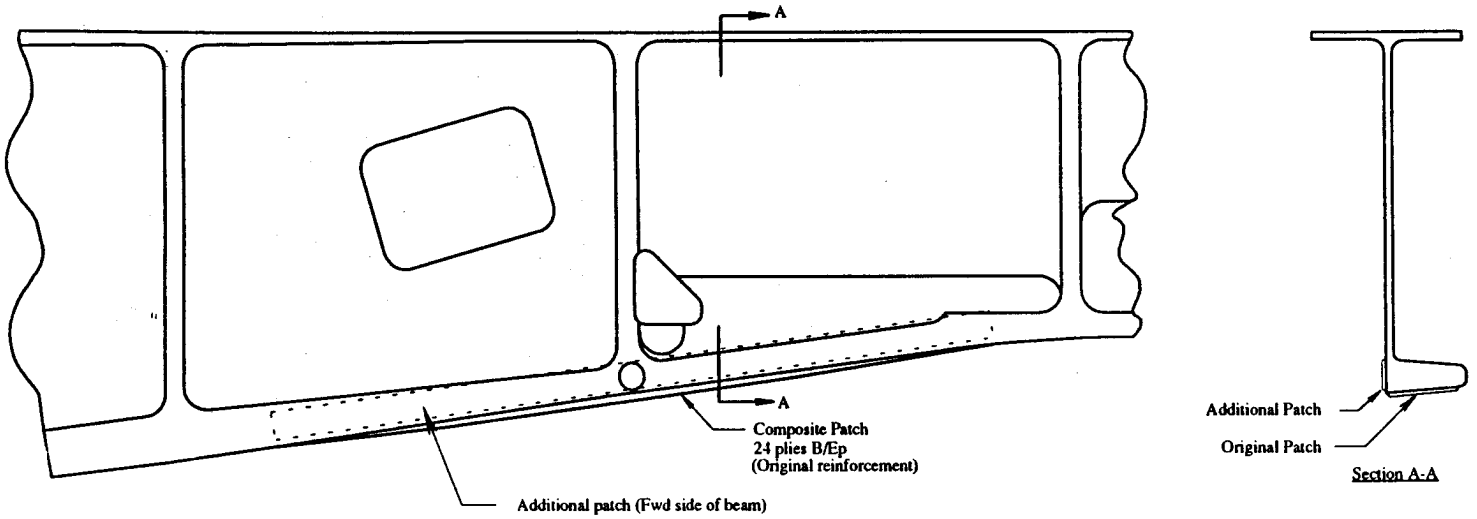
DADT Test Spectrum Development

- KC-135R mission usage was used.
- The usage consists of 404 Flt/Hrs (97 Missions) per year.
- Nine usage missions were combined into 5 test mission profiles.
- A spectrum of 6328 load points was developed for a year equivalent op. loads.

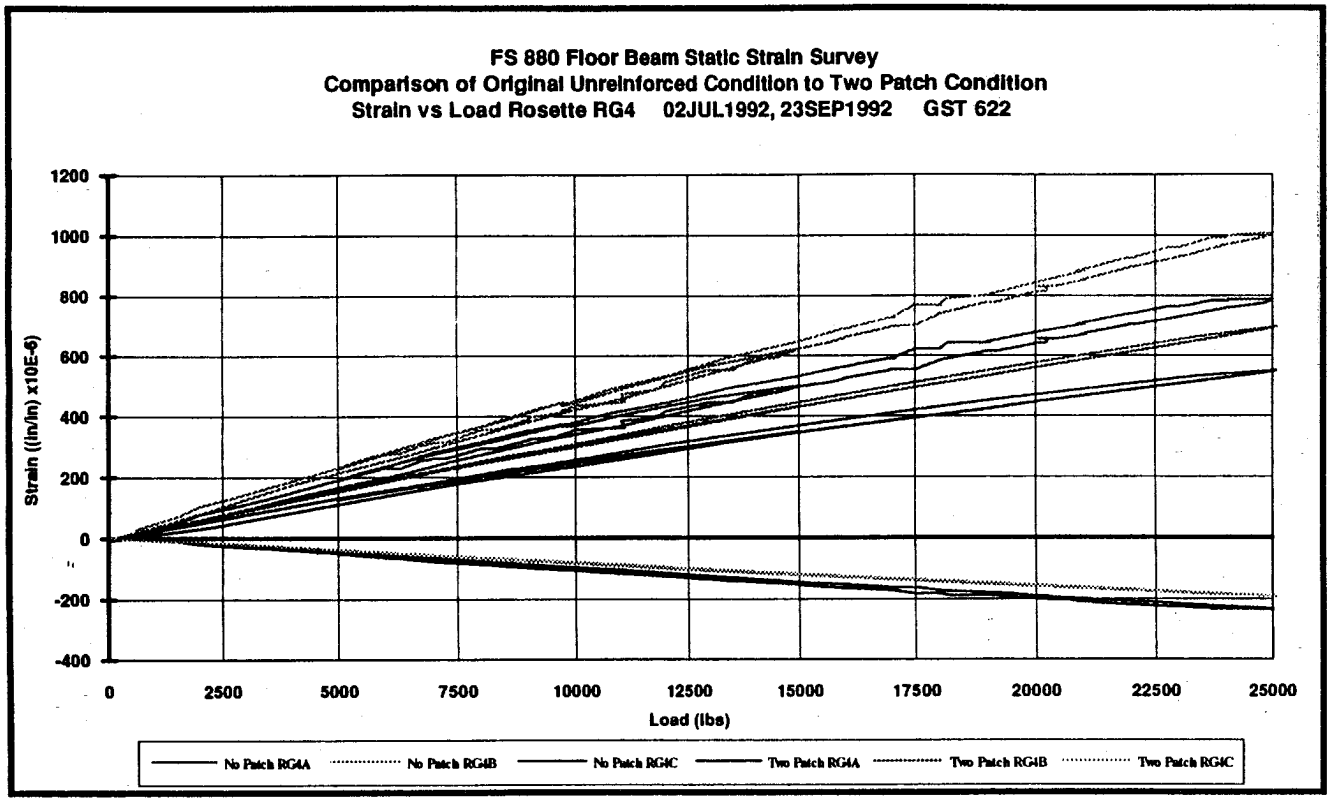
Test Mission	Mission Repetitions	Event Repetition					
		Event 1 Taxi/Turn	Event 2 T-O Roll	Event 3 Cruise	Event 4 T & G	Event 5 Landing	Event 6 Taxi/Turn
Mission 1	14	1	1	1	0	1	1
Mission 2	2	1	1	1	3	1	1
Mission 3	12	1	1	1	5	1	1
Mission 4	14	1	1	1	1	1	1
Mission 5	58	1	1	1	2	1	1

Pre-DADT Test Static Strain Survey

1. Un-reinforced condition
2. A single patch reinforced condition
3. Two patch reinforced condition



Static Starin Survey Results on Hot Spot



Durability/Damage Tolerance Test

- Spectrum loads were repeatedly applied to the test article for 50 times.
  - 2014 goal (2 life times)
  - 2040 goal (1 life time)
- Design limit loads were applied at the 25th and 50th spectrum load applications.
- NDI results : No disbond, delamination, or cracks were detected.

Durability/Damage Tolerance Test (cont'd)

- A connecting slot (saw cut) was made between the triangle cutout and fastener hole to simulate a fully damaged condition.
- Another 50 times of the spectrum loads and design limit loads were applied.
- NDI results : No disbond, delamination, or cracks were detected.

Summary and Lessons Learned

- D/DT Test was successfully conducted for validation of FS 880 Floor Beam composite repair development.
- The test results revealed no indication of degradation of composite repair integrity.
- Flight test should be planned well ahead of other tasks to obtain the necessary data/ information for engineering development.

SESSION III

ENGINE STRUCTURAL INTEGRITY

Chairman: *W. Taylor*, ASC/ENFP

APPLYING PROBABILISTIC CONCEPTS TO GAS TURBINE ENGINE MANAGEMENT

Squadron Leader Chris J Pomfret, Royal Air Force
Wright Laboratory
Wright-Patterson AFB OHIO 45433-7251

INTRODUCTION

The airline industry has an enviable safety record. Actuarial figures show that a male, in the 25-44 age group has a 0.4 in 100,000 chance of dying as a passenger in an civil aircraft accident[1]; this figure is considerably less than risk of death from drowning, poisoning, fire or falling. However, wishing to protect and maintain this safety record should not deter the examination of new methodologies for possible use in the design and management of structurally critical aircraft components. Our increasing knowledge of the behavior of materials and their properties over the last 50 years has helped us to enormously increase the performance and capabilities of civil and military aircraft and it is most laudable that these advances, have not impinged adversely on the currently enjoyed safety and reliability levels .

But, inevitably, new technology is always emerging, enabling researchers and designers to advance further towards more accurate predictions and closer correlation between theory and practice. The concept of probabilistics promises to provide that next step such that a more efficient use could be made of fracture critical aircraft components before their removal for inspection or retirement. Focusing on gas-turbine components alone, thorough inspections of turbine disks for fatigue cracks invariably reveal the disk to be crack-free, suggesting that we inspect too frequently or that the disk is more capable and robust than we expected. Moreover, disks which are crack-free but are deemed to have reached their LCF life are not cyclically spun to failure in a controlled environment to confirm the accuracy of our predictions; unless our TAC cycle is a really accurate representation of life consumption, it could be that there is still appreciable amounts of safe-life remaining in such components. The concept of damage tolerance, a design philosophy which requires that a crack in a fracture critical component will not propagate to failure within an inspection interval, has been successfully employed in the Air Force for almost 20 years and mitigates against catastrophic failure during operation of components such as disks. Retirement for Cause (RFC) is a maintenance policy introduced in the Air Force for some of the more modern fleets of engines in the early 80s but, even within this program, crack-free components are retired because they are deemed to have reached their predicted safe cyclic life. The large preponderance of crack-free disks undergoing inspection suggests that there could be untapped useful life in the disk, either because the disk's life has been conservatively measured or because the disk was conservatively designed for its intended use or a mixture of both. If this is arguable, the fact that costs of both military and civilian aircraft acquisition and operation have risen inexorably in the last decade is indisputable, and, perhaps more than ever before, operators are searching for cost reductions at all levels. In the aircraft industry therefore, it is incumbent on the professional engineer to advance the state-of-the-art not only because it is his fundamental professional purpose but also to reduce costs wherever possible while maintaining safety.

The Air Force currently leads the military and civil field in developing a probabilistic approach for turbine disks in gas-turbine engines. Although probabilistic methods are

already in use in a variety of applications such as civil engineering and the construction industries, there is, for the reasons outlined above, a somewhat understandable reticence to extend the methodology to the aerospace industry. The Air Force's intention is to generate data using probabilistic methods and use the data to design a turbine disk. The design and structural integrity will then be compared with that obtained using deterministically derived data. Only when sufficient evidence is available to show that probabilistic methods can be used in the design of a turbine disk and provide the same reliability as the deterministically designed disk, but with an expected reduction in weight or an increase in life made possible by the more representative input data, will the Air Force propose that probabilistic concepts be accepted as a design standard.

THE MECHANISM OF PROBABILISTIC METHODS

One of the major reasons for people's reticence to entertain probabilistic methods is an insufficient understanding of the methodology. Weibull analysis was greeted with the same reluctance in the early 1950's [2] but, ten years later, engineers were not only using it but also appreciating its particular suitability to the aerospace industry. Now, Weibull methods are in everyday use and accepted as a standard analysis tool. Probabilistics is not a replacement of the well founded deterministic methods but more an extension of them. In the past, and now, a design engineer has used a single value for each of the variables which influence the design of a component. Material properties such as maximum strength and operating parameters such as cycles to failure are typical examples. The single value chosen might be a mean, nominal value or an extreme value such as 3 standard deviations either way from the mean. However, despite the best endeavors of designers, manufacturers and users, we know that two identical looking articles are never the same; in the case of turbine disks, two specimens made from the same batch of material and exposed to the same operational loads will, in practice, fail at different lives. With many supposedly identical components a distribution of actual values could be compiled for the failure; similarly a distribution of values for every variable that influences the design could be compiled if they were known. Sometimes, people mistakenly believe that they apply probabilistics when they look at the statistical variation of a variable and, from the distribution, decide that a new single value for use in the design would be more appropriate. This, however, is not the full application of probabilistic concepts. However, probabilistic methods have already been used within the Engine Structural Integrity Program (ENSIP) to predict lives of components with buried defects. The ENSIP specification assumes that a buried defect will be present and requires that a life be predicted such that there is a 0.0001 chance that the defect will cause fracture of the component within its lifetime. Monte Carlo simulations massage the data for this exercise.

The basis of probabilistics is to take any value from within the statistical range for a variable and map it with any value for each of the other variables being considered. This technique can be achieved using simulation techniques such as Monte Carlo or Importance Sampling, or algebraic methods such as First or Second Order Reliability, Mean-value Methods or Response Surface Methods. Each method has its own strengths and weaknesses and some are more suited to a particular application than others. In the case of a simulation method, repeatedly choosing a different value for each variable and mapping them together will produce a range of output values, which can either be arranged in order of ascendancy or statistically represented with a mean and a standard deviation.

The methodology is shown in Fig. 1. This distribution of values is not possible using deterministic methods because the same single value for each variable is used in a once-

only calculation and all components are then deemed to meet that single output value. With probabilistic methods however, a range of possible values can be scrutinized and with, say, 1000 or more different perturbations a risk level of one in a thousand could be chosen by taking the lowest (or highest) output value and applying it to the fleet of components. The design equations and original data are the same in both the deterministic and probabilistic approach; what is different is the method by which the values, used in the design equations, have been chosen and the interpretation of the results.

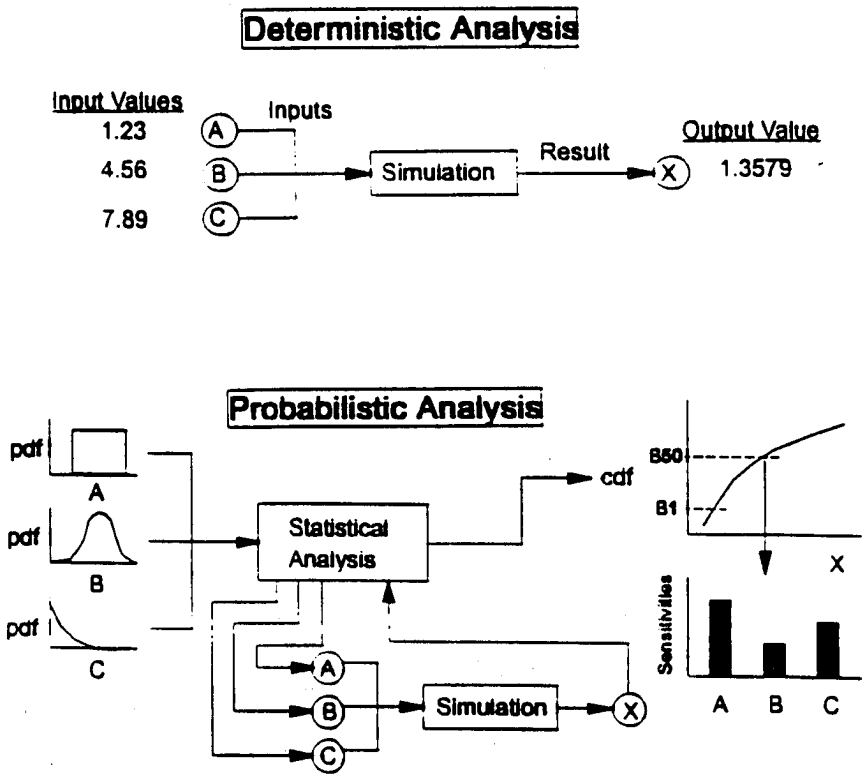


Fig. 1. Probabilistic Methods maps the range of values for each input to produce an output and sensitivity data.

Probabilistics provides sensitivity and a more realistic indication of how the component will last; the assumption that all 1,000 components are a worst case example is replaced by a realistic distribution; it would take a seemingly infinite number of simulations before a component was generated which was deemed to have the worst case of every possible input value in it and this reflects the remote possibility of such a component existing. This is where the pay-off of the probabilistic approach is perceived to be; initial calculations show that as much as 82lbs of the weight of the F119 engine in the F22 aircraft could be saved by designing the disks with probabilistically generated data. This translates into a life cycle cost saving of $490M, yet the risk of disk failure would, because it is now managed in the design, remain the same as a disk designed with deterministic data.

MANAGING RISK

Currently, risk in gas-turbine engine design and operation is not managed; instead a risk level deemed to be acceptable by the public and the legislators exists without anyone really being able to demonstrate a control over it. In the military arena especially, the reason for our lack of control is predicated on a usage which is invariably different from initial design and user definition. In a military context, usage differences occur because of operating in a different environment than originally envisioned (the Persian Gulf with heat and sand is a typical recent example), a declared change in role (the F-4 is a good example) and differences in use by individual Wings and bases as well as individual pilots. At the outset, the designer is told planned usage requirements such as performance expectations of

The Designer Knows	The Designer Computes	The Designer Can't Quantify

- Material Properties
- Material Limitations
- Planned usage requirements, e.g.
  - performance specs
  - roles
  - reliability
  - maintenance/insp. intervals
	Component life to meet requirements (based on HCF, LCF, Thermal Fatigue, Creep)	- Environment in which product operates
		- Variations in mat'ls
		- Pilot use/misuse
		- Change in role
		- Differences in usage by individual bases/ wings.

Fig. 2. The Designer's Dilemma; the unknowns are significant

the engine, the role in which it will fly, the reliability required and the maintenance/inspection intervals desired. Coupled with known specifications of material properties and limitations, the designer will create an engine to meet the needs. He minimizes weight and complexity as much as possible and linked in with the design is an operational life, usually a fatigue life; nonetheless, in the design, he has necessarily catered for excedances of temperature, pressures and speeds, assumed a worst case for usage, and used worst case figures for material properties. Additionally, there are safety factors included in the design to meet the probability of failure laid down by structural integrity programs. All the "layers of fat" are necessary within the current day circumstances, especially as usage of the finished product will, in some undefined way, deviate from the original intention.

If the user has asked for versatility, so as to be able to undertake a wide variety of roles or missions, then the design will, again by necessity, be conservative, more complex and heavier. Robustness is the current day term used to describe "usage tolerance." So as to meet all these uncertainties, yet also satisfy the philosophy that critical components should be designed so that they, in essence, never fail, the declared life of the fracture critical components is set at a very low figure. Typically, under damage tolerance design

criteria, these components are inspected at half-life for cracks of a length which, if left in-service for the second half life, have an unacceptable chance of propagating to failure. Fortunately, very few (for the F110 engine, the figure is around 0.1%) fracture critical components inspected in this way are found to be unacceptably cracked which shows that the design is very safe and is undoubtedly the root of the enviable safety record.

However, we have neither accurate measurement nor prediction of usage deviations nor do we have the quantitative effect of these deviations on life consumption; consequently, we pay more heavily for this level of safety than perhaps we need. Having a better mathematical representation of the uncertainties which go into the design would enable us to manage risk better and therefore be more sure of enjoying the level of risk we care to choose. Because probabilistic methods consider the range of values of a variable, risk can be actively managed by designers and operators but to do so requires data feedback from the field of use. A life usage data acquisition system will be needed to provide this information. Initiatives to translate usage into life consumption have been carried out in the past [3] but, to date, there is no such system in operation in the Air Force. Pilot's throttle excursions, which are translated into cycles (TACs) and then into LCF life is as far as the Air Force currently goes in this arena. With a state-of-the-art data recorder and analyzer fitted to each aircraft, all parameters influencing usage could be tracked and measured. Differences between actual and expected (design) would be detected and quantified. The statistical variation of the parameters will also be different to the distribution originally used. These changes would then be fedback into the probabilistic model but, additionally, the impact that these changes have had on life consumption will be known and the penalty or dividend applied to the life monitoring of the fracture critical components. Retirement for Cause has, so far, saved the Air Force $2B; building on this sturdy foundation with accurate and "personalized" life measurement would make the RFC savings the mere tip of the iceberg.

This idea is the basis of another Air Force initiative which aims to develop on-board life measurement for military engines so that the military commanders have a hands-on view of how life is being consumed in their fleets and the cost/savings associated with changes in role, environment, individual bases etc. Clearly, the operating and maintenance costs of gas-turbine engines would be significantly reduced since more of the useful life than before would be extracted from each component. Finally, the described capability will enable designers and users to manage risk. The probability of failure is not a deterministic figure; in practice, it increases with age (usage), so it is a constantly changing figure. Probabilistics will enable fleet managers to determine the point at which the continued operation of a component is no longer advisable and, at the same time, have a more accurate knowledge of the actual life consumed on each individual component. This would be real and closer management of risk than we have ever been able to exercise. Once probabilistic methods have been proved a safe and worthwhile tool in gas-turbine engine design, then the idea of thorough monitoring of the parameters which influence life will be a necessity rather than an enhancement.

APPLYING PROBABILISTIC METHODS TO GAS TURBINE ENGINES

Design. Taking a nominal or a worst case single value as a input parameter has been discussed earlier. Taking a representative distribution of values of an input parameter is unarguably a more superior approach because it recognizes that the identical looking samples or components are structurally different. The more prominent parameters which contribute to the design of a gas-turbine engine disk are at fig 3.

Often, the distribution of the values of a variable are well known (e.g. dimensions of a manufactured product) and so an accurate mathematical representation of that distribution can be used in the probabilistic code. If the distribution is not so well known or is more uncertain (e.g. pilot mishandling), then it is not necessary to first obtain a wealth of data so as to plot a distribution; however, it is possible to assume a distribution which can be subsequently refined with fedback data. Mapping together the distributions using the probabilistic code enables the designer to see realistic outputs such as cycles to failure or weight for a given risk. Safety factors can then be applied to these realistic figures as a final action rather than in the initial design stages. More importantly, perhaps, the designer can conduct a series of "what ifs" and obtain a realistic appreciation of the impact that a particular parameter has on the overall design model.

The result of the designer's "what ifs" exercises is sensitivity data and this data essentially quantifies the importance and role of each parameter in the design.

LCF
Flaw-Induced Cracking (damage exacerbated by stress concentrating flaws)
Yield
Ultimate Strength
Creep
Part-to-Part Interaction
Operating Temperature
Operating Stress (interacts with dimensional variations and tolerances)
Engine Build (Each engine will perform at slightly different operating parameters)
Basic Properties (Mechanical Properties of basic material)
Material Flaws (Inclusions etc. introduced during processing)
Damage incurred during manufacture (Nicks, gouges etc. from machining, tools)
Handling/Assembly Damage

Fig. 3. Some of the more significant factors affecting engine life [4]; in theory the list is endless but sensitivity analyses highlight the important ones.

The designer can thus assess whether it is essential to have an accurate distribution of a particular parameter's variables or whether a parameter has little or no end-impact on the design. Use of probabilistic methods does not introduce new data nor does it introduce new design algorithms. The deterministic principles are still used; it is purely the analysis of available data and the way in which the data is combined together which is different. Probabilistic methods can therefore be summarized as making better use of known data and statistical relationships to optimize the design of a component. The type and nature of the data relevant to gas-turbine engine component design is no different to that in, for example, the construction of a hotel or bridge, yet probabilistic methods are already in use in the design and inspection of these constructions.

There is uncertainty present in all these applications (e.g. extremes of weather) and so it has to be accepted that absolute reliability is an unattainable goal. What can be attained, however, is a design criteria which ensures that the probability of unfavorable performance is both known and acceptably small.

Application Process. The Air Force is managing two independent programs with Pratt and Whitney and General Electric to develop a probabilistic approach to help compute the design of a turbine disk. The approach has been to re-design, using probabilistically generated input values, a disk previously designed with deterministic inputs, and thus

quantify the differences. Then, a series of model disks, some built with known, seeded faults, will be spun in a rotor spin facility until their LCF life is exhausted. The cycles to failure and type of failure will be compared with the predictions; the degree of correlation will indicate how representative the probabilistically generated inputs were. While earlier, more elementary, tests on static specimens are very encouraging, the rotor tests are just underway and the results are not yet available. Clearly, excellent correlation of the rotor spin results will merely be the first step towards the introduction of probabilistic methods in gas-turbine engine design; anything less than this level of correlation will either necessitate rework or a crystal clear understanding of the differences before the concept can be advanced further. In-field experience studies have also been conducted to determine the differences between perceived usage and actual usage. Two independent programs enables the Air Force to monitor two angles of approach and appraise the relative benefits of each; for instance, the mathematical mapping of the variables is being achieved using a combination of Direct Integration with Monte-Carlo simulation at one company and Response Surface Methods with Monte-Carlo simulation at the other. In the longer term, the application of probabilistics is envisioned for blades, casings, shafts and other structurally significant components.

Composite Materials. With the increasing focus on composite materials to provide some of the higher performance requirements in military gas-turbine engines in the future, consideration must be given to the life prediction of these materials. Despite all the inherent weight and temperature advantages of composites, the variation in their material properties is more scattered than for monolithics. Fiber and void volume ratios, ply misalignment, ply thickness and the basic material properties of fiber and matrix currently have more uncertainty than the equivalent properties in traditional metals and alloys[5] as shown in Fig. 4. Using a single value to try and represent each of these variables is therefore deemed impractical. Moreover, the pay-off from probabilistic methods would probably be quite different from the perceived monolithic application. For example, weight savings would not be as significant but big inroads could be made into optimizing the production process and thus reducing what is currently a large scrap rate. Development of a probabilistic approach for composites is therefore considered not only more plausible but also necessary. The experience gained from first applying probabilistic methods to monolithics will provide an invaluable foundation from which to progress when composite materials are ready for operational use.

USE RELUCTANCE AND LEGAL ASPECT

There is a discernible reluctance in some parts of the aerospace industry, both military and civilian, to pursue probabilistic methods. Reasons for reluctance range from not wishing to interfere with an excellent structural safety record to believing that legislation will not permit its use. Additionally, some misunderstand the mechanisms of probabilistic concepts and therefore their reluctance is founded on misinformation. The SAE G-11 Committee has a 45 strong sub-group which is working to pursue probabilistic methods in a wide variety of applications. Their thrust comes from the fact that probabilistics is in use in everyday life already, and that there is a multitude of other applications in which it could be potentially used with worthwhile benefits. The sub-group includes two attorneys who are actively addressing the legal issues of introducing probabilistics.

VARIATION OF MATERIAL PROPERTIES IN A 20 ft LONG, 2ft DIA COMPOSITE CYLINDRICAL PIPE

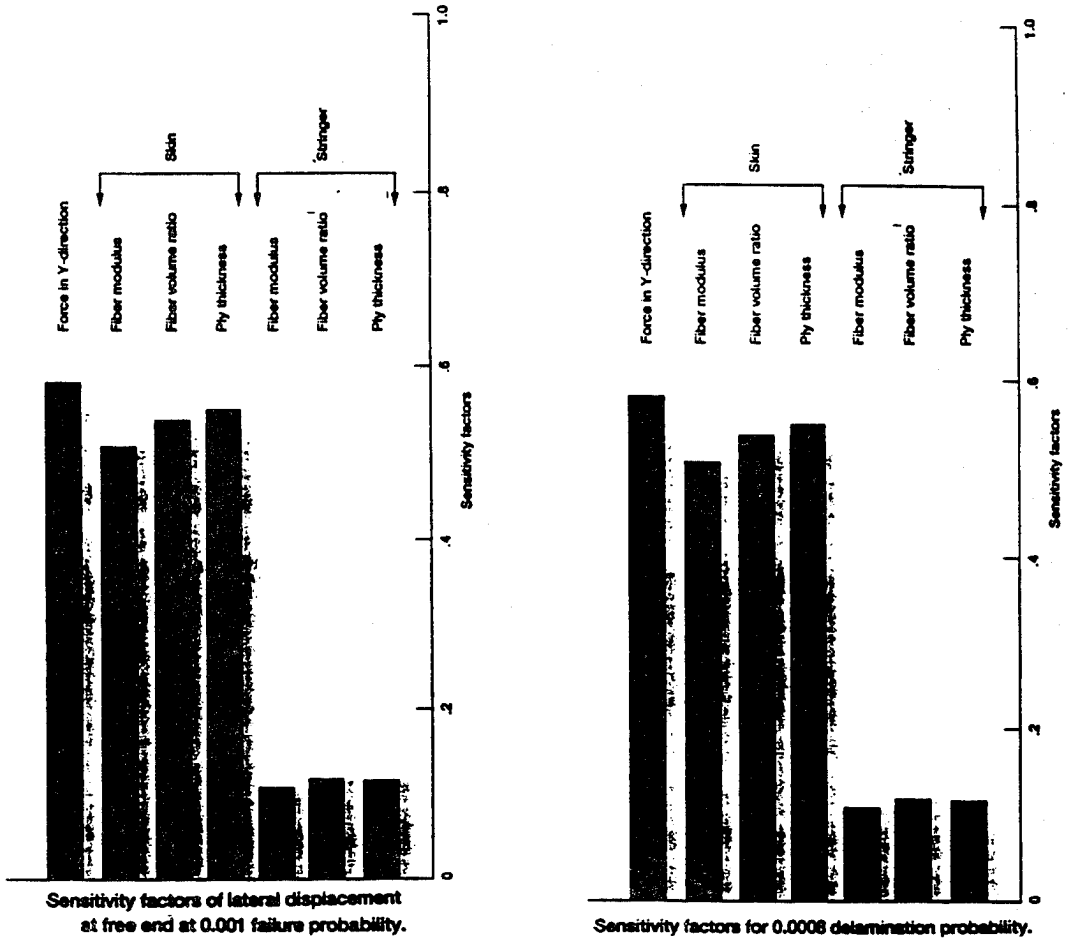


Fig. 4. Sensitivity factors are both large and variable in composite materials.

The tacit assumption is that probabilistics will retain the current safety record of the aerospace industry, and, in particular, gas-turbine engines. The ability to manage risk and safety factors more capably has been explained earlier and so the skeptic reader has hopefully realized that having more control over the uncertain parameters will give designers, maintainers and operators even more confidence in the integrity of their product than hitherto. The philosophy of probabilistics has been explained simply and non-mathematically so that the previously misinformed reader has hopefully a better appreciation of its aims. Finally, the legal worries, while understandable, are neither new nor awesome. Someone, somewhere, deemed that a failure rate of around 0.001 or -3σ was acceptable for deterministic design and this has been collectively accepted as a reasonable

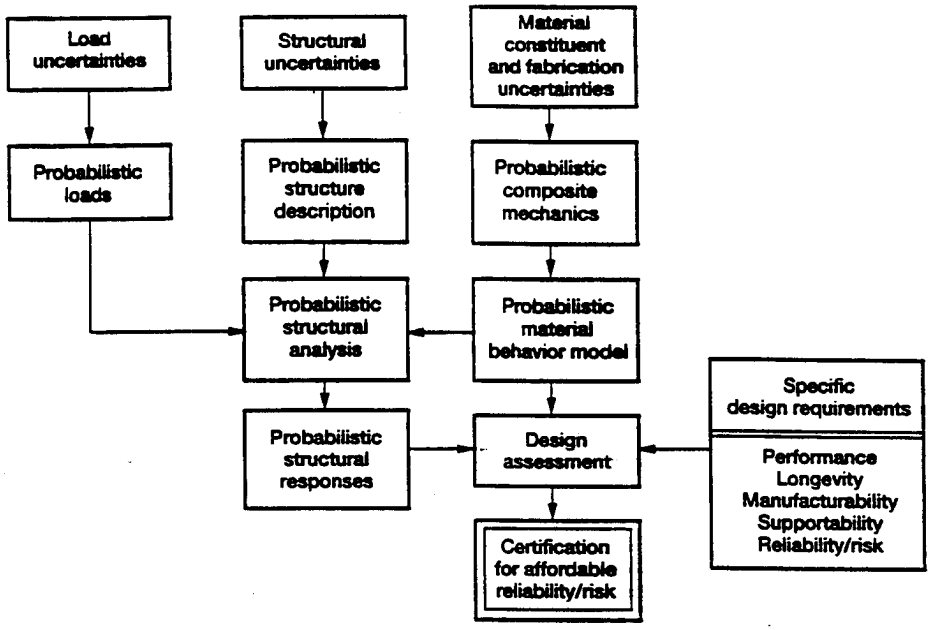


Fig. 5. A Block Diagram approach for applying Probabilistics to Composite Materials; the same Diagram is also relevant to Monolithics.

standard for many years. Worries that a person is going to be required to sign his name to a document saying that, using probabilistics, one engine in one thousand can be allowed to fail, are unfounded because such an action will be neither appropriate nor necessary. There is no logic to the public or designers not accepting the same risk of failure that has been willingly accepted for many years already. The current legal considerations within the SAE G-11 Group are more focused on who is liable for failures of probabilistically designed equipment *before* probabilistics is recognized as a standard. Then, once probabilistics has been accepted as a standard, is a designer who still chooses to use deterministics liable for failures of his deterministically designed equipment? There is a danger of being swallowed up by the legal "what-ifs" of the transition. It would be better therefore to demonstrate that probabilistics has a key role in future gas-turbine engine design and, as it is merely a refinement of deterministic principles, *both* approaches are acceptable. However, if, in time, probabilistics is found to complement the well-founded design methodologies, then it will become widely accepted as a standard and be part of everyday use and teaching. There will always be equipment failures and there is no practical or even possible technology that can guarantee to prevent all failures. Therefore, the premise for suing designers in the event of equipment failures should not, and will not, need to change because of the introduction of probabilistic methods.

CONCLUSIONS

Through the inexorable growth of gas-turbine engine capability in recent years, we have reached a situation where the consequences of failure are increasingly catastrophic yet we cannot accurately monitor the damage accumulation or life usage of the critical components. Moreover, we know that equipment will be used outside the regime for which it was designed, but will not be able to quantify accurately the misuse. Thus, we try to design for no failures in the life of a critical component and to detect the onset of fatigue

(crack propagation) by regular inspection. This laudable approach, by necessity, increases weight and therefore operating costs of engines and creates an enormous maintenance and logistics facility. The challenge is therefore to maintain the first-rate safety record yet reduce the size of the millstone which has subsequently been created. More precise design coupled with accurate monitoring of usage would help achieve the challenge.

Application of probabilistics would assist in the design of components. The science and methodology of probabilistics is already in practice in other manufacturing and construction industries whose design and safety requirements are directly comparable to those of gas-turbine engines. Moreover, probabilistics is not a design system in itself; it is merely a method of selecting and interacting input values of variables which better reflect actuality than a single or worst case value. Probabilistics is thus an additional tool for the well established and understood design equations to utilize. With probabilistics, these equations would not only have more realistic input data, but the design engineer would be able to manage safety because the impact of a small change of a input variable on the output (sensitivity) would be measured. Therefore proper account could be taken of the variations at the outset, giving the engineer and user more confidence that they are in control of the component being designed. Variations in usage of equipment has always been a problem but, with data collection, any changes in the actual statistical distribution and variation of parameters could be fedback to change the original distributions. The ultimate aim is to extract as much of the safe useful life of a fracture-critical component as possible while retaining a tight control on safety. Direct analysis of engine parameter data would more accurately estimate how much LCF, HCF or Creep life has been consumed so that components would be removed for inspection at the optimum frequency.

Weight and life cycle cost savings are not a goal of probabilistics but are a likely fall-out from its introduction. It would be irresponsible of aerospace engineers to ignore the possible application of probabilistics to gas-turbine engine design. The Air Force has sponsored the engine manufacturers to pursue this avenue of investigation and the initiative will continue until either probabilistics is shown to be unsuitable or, like Weibull analysis, a most appropriate tool for managing gas-turbine engine components .

REFERENCES

1. Accident Facts 1991 Edition. National Safety Council, Library of Congress Catalogue, Card # 91-60648.

2. Weibull Analysis Handbook, Abernethy, R.B; Breneman, J.E; Medlin, C.H; and Reinman, G.L. (Pratt and Whitney 1983). Report produced for Aero Propulsion Laboratory, Wright-Patterson AFB, Tech Report AFWAL-TR-83-2079.

3. Engine Component Retirement for Cause, Vol 3, Methodology Demonstration and Validation; Report for Air Force by Mills, M.S; Deluca, D.P; Cawles, B.A; Harris, J.A Jnr; Dec 87. AFWAF-TR-87-4069.

4. Probabilistic Rotor Design System (PRDS) Phase I. Roth P.G, Report for Wright Laboratory, May 1992. WL-TR-2011.

5. A Method for the Probabilistic Design Assessment of Composite Structures, Shiao, M. C, and Singhal, S. N. 24th International SAMPE Technical Conference, Toronto, Canada, October 20-22 1992.



Application of
Probabilistics Concepts
to
Gas Turbine
Engine Management

Sqn Ldr Chris J. Pomfret, RAF



Scope

- BACKGROUND
- WHAT PROBABILISTICS IS
- RISK
- APPLYING PROBABILISTICS TO GAS TURBINE ENGINES
- THE NEXT STEP
- CONCLUSION



Air Force Mechanical Integrity Workshop, Oct 93

- Quotes from Executive Summary Report:
  - Many analytical and experimental tools exist which allow engineers to design mechanical subsystems and components that will meet the Reliability, Maintainability, & Supportability specifications.
  - . . . tools require fully defined operational environments as inputs.
  - . . . problem is that after the design and development have been completed the weapon system or subsystem usage is different than originally identified.
  - . . . often the actual operating environment for a subsystem is significantly different from those used by engineers to make key decisions and tradeoffs during the design phase.
  - The differences are generally not identified until a major problem surfaces.

Air Force Mechanical Integrity Workshop, Oct 93

- **Quotes from Executive Summary Report (Continued):**
  - **. . . the mechanical integrity process does not have an effective, cost efficient procedure for:**
    - *1. Monitoring the operating environment of mechanical subsystems;*
    - *2. Identifying and categorizing variations from original design conditions;*
    - *3. Analyzing the impact of those post-design changes, determined to be critical to reducing the mission capability and/or life of a weapon system;*
    - *4. Conducting sensitivity analyses to develop a coordinated plan for maintaining the mission capability and life of a weapon system;*
    - *5. Providing feedback to Air Force and Industry designers on the performance of and the actual environments experienced by mechanical subsystems.*

Air Force Mechanical Integrity Workshop, Oct 93

- Quotes from Executive Summary Report (Continued):
  - The demands of declining budgets, and defense drawdowns are creating pressures that require a more efficient and effective approach to the engineering of systems.

- A need exists to incorporate systems engineering techniques into the integrity process in order to provide a concurrent engineering approach to the development of more competitive and affordable products.



Gas Turbine Engine Component Design

The Designer Knows

- Material Properties
- Material Limitations
- Planned usage requirements, e.g.
  - performance specs
  - roles
  - reliability
  - maintenance/insp. intervals

The Designer Computes

Component life to meet requirements (based on HCF, LCF, Thermal Fatigue, Creep)

The Designer Can't Quantify

- Environment in which product operates
- Variations in mat'ls
- Pilot use/misuse
- Change in role
- Differences in usage by individual bases/ wings.



Scope

- BACKGROUND
- WHAT PROBABILISTICS IS
- RISK
- APPLYING PROBABILISTICS TO GAS TURBINE ENGINES
- THE NEXT STEP
- CONCLUSION



What is Probabilistics?

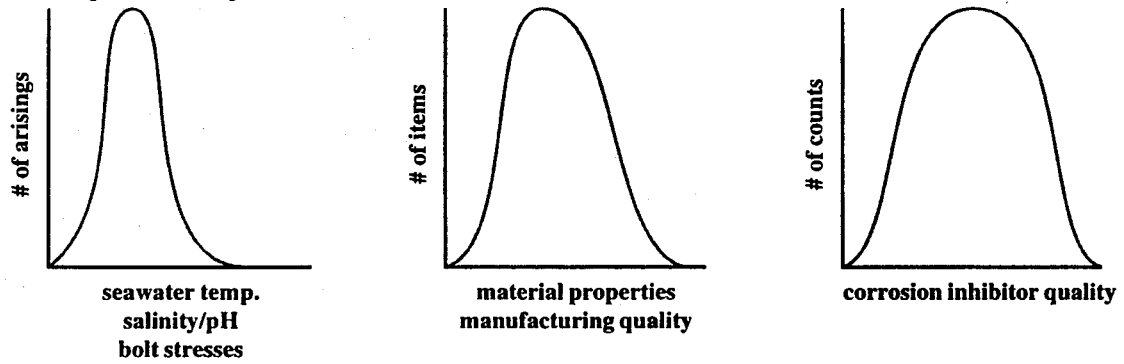
- Statistical Quantification of Previous Unknowns/Variables
- Creating a Distribution Curve for Each Variable
- Understanding Interaction of Variables

QUANTIFICATION BY SAMPLING.

Corrosion of Oil Rig Platform Nuts / Bolts

Rate of corrosion = (chemical reaction rate) fn (Seawater temperature, pH of seawater, quality / effectiveness of corrosion inhibitor, material properties, manufacturing quality, stresses in bolt, . . .)

Probability density function for each:



Output: Accurate prediction of inspection / replacement interval

Scope

- BACKGROUND
- WHAT PROBABILISTICS IS
- RISK
- APPLYING PROBABILISTICS TO GAS TURBINE ENGINES
- THE NEXT STEP
- CONCLUSION

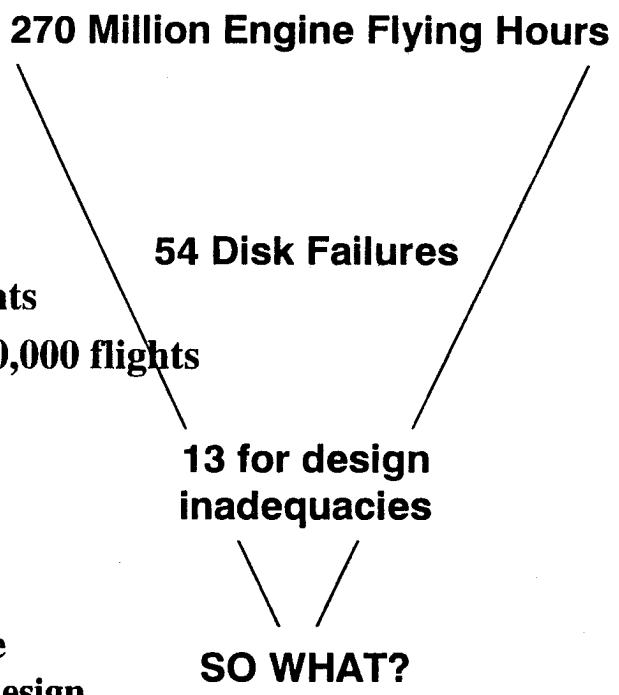
Risk Assessment

- Current Philosophy
  - Accept 1/1000 (-3σ) as a deterministic safety factor
  - What actually happens in practice?
  - When did a disk last fail in commercial or military operation?
  - Who chose - 3σ ?
  - Actual probability of failure/failure rate is 7.2/1000 for an engine so somewhere < 0.72/1000 for an individual disk
- Analysis:
  - Is 'arbitrary' safety factor to cater for unknowns "too safe?"
  - Do lifing algorithms have additional safety built in?

Distilling the Data (FAA/NAWC 1972-1987)

- Assume:
  - 2/engines/airframe
  - 3 hrs/flight
  - = 45 million flights
  - p = 1.2 failures/1,000,000 flights
  - p = 0.289 design failures/1,000,000 flights

- Assume:
  - Engine life is 20,000 cycles
  - 1 cycle/flight
  - p = 0.578% chance of an engine failing through inadequate design in its 20,000 cycle life



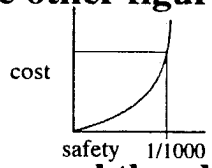


Distilling the Data (Another Angle)

- Mortality Rates (per 100,000 population)
  - All causes 243.1
  - Motor Vehicle 41.6
  - Heart Disease 29.4
  - Cancer 24.1
  - Poisoning 6.7
  - Drowning 3.5
  - Falls 2.3
  - Fires and Burns 1.8
  - Air Transport 0.4
  - Water Transport 0.3
  - Railroads 0.3

Future Philosophy

- Questions:
  1. Do we accept 1/1000 as acceptable risk or some other figure? (e.g., 0.72/1000)
  2. Where is the acceptable compromise between cost and safety?
  3. Do we want the actual probability of failure to equal the planned rate?



- Answers:
  1. Continue with currently experienced failure rates.
  2. The user decides, qualitatively .
  3. Yes, to give everyone increased confidence/control.
- Actions:
  1. Achieve better control/correlation over failure rates set and experienced
  2. Quantify 'nebulous' factors, previously assumed as "-3σ "
  3. Continuously feedback actual statistical data to probabilistic codes.

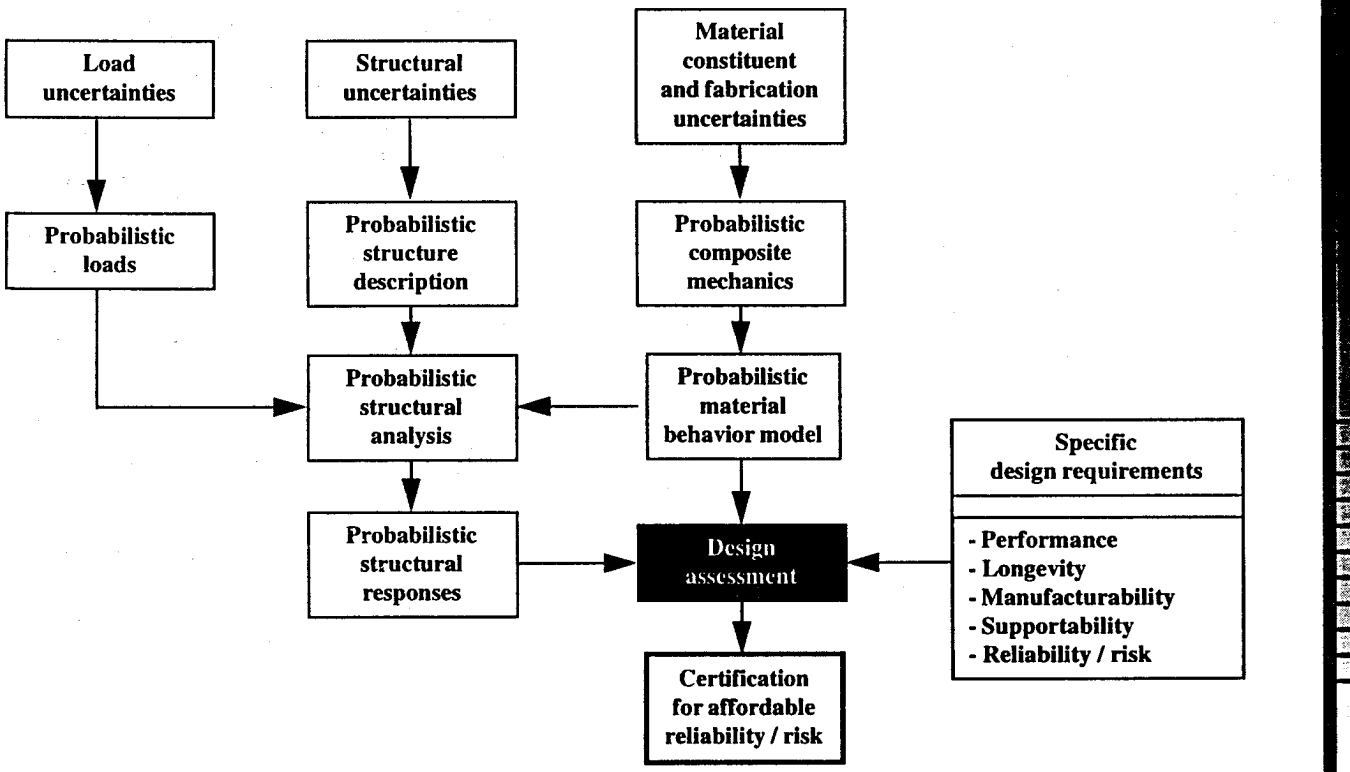
Scope

- BACKGROUND
- WHAT PROBABILISTICS IS
- RISK
- APPLYING PROBABILISTICS TO GAS TURBINE ENGINES
- THE NEXT STEP
- CONCLUSION

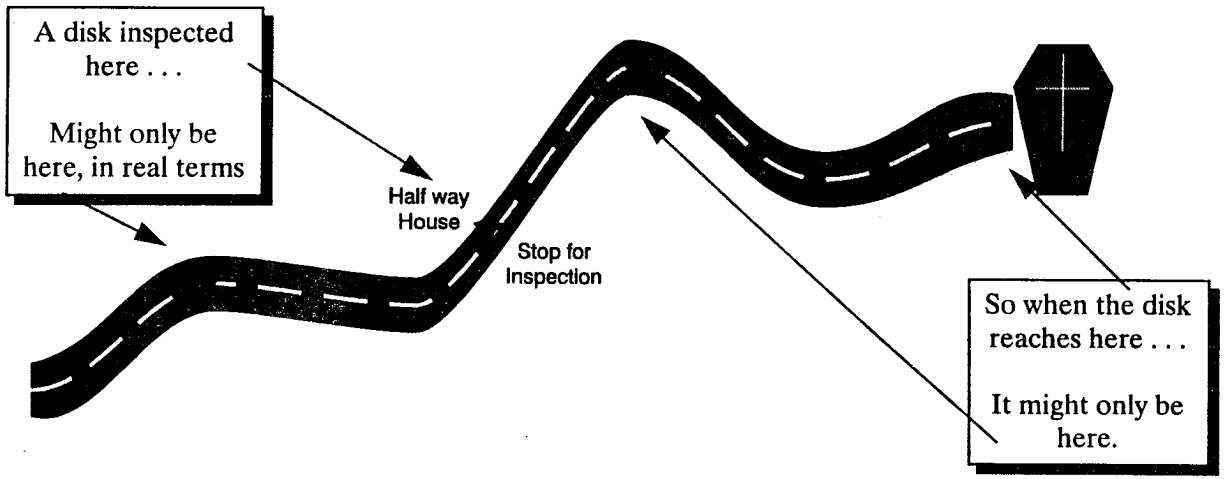
The Probabilistic Recipe

- **Ingredients:**
  - **Variables which influence component life:**
    - *Loads (usage, environment)*
    - *Structure (manufacture, processes, handling)*
    - *Material (physical properties)*
  - **Design codes**
- **Directions:**
  - ***Produce*** **a probability density function (PDF) for each variable based on known data**
  - ***Generate*** **a random value for each variable based on PDF for that variable**
  - ***Blend*** **together outputs from step 2 in the design code**
  - ***Repeat*** **many, many, many times**
  - ***Plot*** **the output statistically or count the number of exceedences**
- **Result: An output (life, probability of failure, weight, etc.) based on known, real data.**

The Probabilistic Approach



The Journey of Life (for a Turbine Disk)



ACCURATE LIFE MONITORING IS ESSENTIAL FOR AFFORDABILITY AND LIFE CYCLE COSTS AND OPERATOR CONFIDENCE

OD-SA\POTC\POMFRET\PROBCON.PPT\ 24 \VP\09094



COMPOSITES
Our Future Material

- A few facts about composites
- Appear good for high performance and reliability but . . .
- Structural behavior widely scattered because of uncertainties
  - Fiber and matrix material properties
  - Fiber and void volume ratios
  - Ply misalignment
  - Ply thickness
  - Environments (loads, temperatures)
- Deterministics cannot computationally simulate scatter in structural behavior

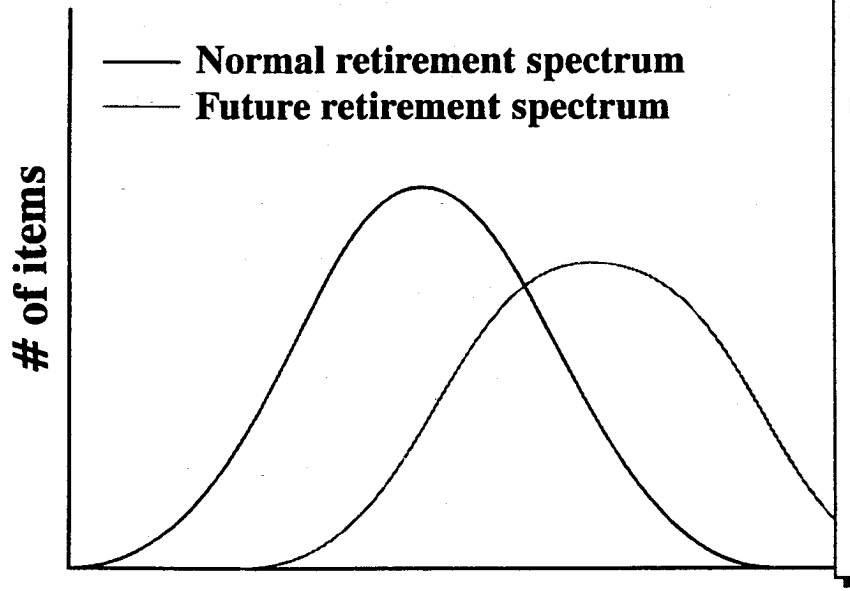
PROBABILISTIC DESIGN METHODOLOGY NEEDED
TO QUANTIFY STRUCTURAL RESPONSE.



Scope

- BACKGROUND
- WHAT PROBABILISTICS IS
- RISK
- APPLYING PROBABILISTICS TO GAS TURBINE ENGINES
- THE NEXT STEP
- CONCLUSION

Fracture Mechanics / Probabilistics and the future



- Monitor components on individual basis
- Inidvidually track life consumption
- Knowledge of crack propagation needs to be extremely good
- Well proven inspection techniques
- Some changes in maintenance
- Feedback to life prediction codes

POTENTIAL TO SIGNIFICANTLY INCREASE DISK LIFE

Legalizing Probabilistics

- Develop the code
- Validate it (static specimens, sub-scale and full-scale spin tests)
- Demonstrate it (demo engines)
- Implement it (partial fleet embodiment)
- Expand it (other alloys, composites)

FEEDBACK

Q: Where does the buck stop?

A: With those who developed deterministics, -3σ, 1/1000, current failure rates. i.e., ALL OF US!

- Bottom Line: The signature of an individual to sanction probabilistics is neither appropriate nor necessary.



Scope

- BACKGROUND
- WHAT PROBABILISTICS IS
- RISK
- APPLYING PROBABILISTICS TO GAS TURBINE ENGINES
- THE NEXT STEP
- CONCLUSION



Conclusions

- Variables associated with gas turbine engine component manufacture and operation can be statistically characterized
- No reasons why probabilistics cannot be applied to engine component design
- Probabilistics will be necessary for composite material usage
- Accurate life monitoring essential for feedback/updating costs
- Probabilistics will enable risk to be quantified
- Skepticism is good! Through scrutiny, validation will occur
- Probabilistics is one step nearer to Theory equating with Practice
- The airline/engine industry should collectively accept probabilistics, when ready for implementation

Effects of Multiple Blade Impact on Aircraft Engine Containment Structures During a Rotor Burst Failure

S. Sarkar[1] and S. N. Atluri[2]
Computational Modeling Center
Georgia Institute of Technology, Atlanta, Ga 30332-0356

Introduction

A major hazard in modern jet powered commercial and military aviation is the failure of a turbine blade or a disc at very high rotational speeds.The consequences of such an event can range from minor to catastrophic, depending upon a number of factors and circumstances. The high energy fragments released during a turbine failure could damage fluid lines, control systems hardware, airframes and such incidents can affect the flying performance in a number of direct and indirect ways and some can even lead to loss of airplane and hundreds of passenger fatalities.

Turbine rotor failure occurs for a number of reasons, the primary one being fatigue due to normal engine operation in a high temperature environment for a sustained period of time. Additionally, they may occur due to overheating, birdstrikes, blade detachment, material defects, etc. A high level of quality control, inspection and maintenance procedures have kept these failures to a minimum, but statistics over the last fifteen years indicate that the reliability approach has reached its limit and a certain number of turbine failures are bound to happen each year. Under such circumstances, it is necessary to develop preventive measures that will contain the high energy fragments in a manner so that all potentially dangerous situations can be averted.

Rotor failure produces both high energy disc fragments and relatively low energy blade fragments. The blade fragments are relatively smaller than the disc fragments and are less destructive, though data collected over a long time indicate that they are more likely to occur during a rotor failure. Under the present guidelines, the engine design requires that the blade fragments are contained within the engine casing structure. It is not practically feasible to contain the disc fragments without incurring high penalty in terms of weight and performance, hence the preventive type approach appears at present the only viable strategy against occurrence of disc failure. The objective of the present study is to develop computational modeling techniques to analyze the impact of blade rotor fragments on containment structures. Rotor fragments, consisting of a single blade and three blades attached together, are released and the deformation response of the ring is computed. The collision of the rotor fragments with the normally operating rotor blades is also modeled in this analysis. A failure criterion based on the effective plastic strain in the region of impact is used to determine the failure of the containment ring due to impact. For each type of fragment, the ring thickness is varied incrementally and the ring response, residual kinetic energy level of fragments, magnitude of impact force and the overall contain-

[1] Postdoctoral Fellow
[2] Institute Professor & Regents' Professor of Engineering

ment or failure is determined. In the first phase, the study is carried out for the case where the other blades are not present on the rotor. Next, the remaining blades are introduced and the effects of the multiple interaction with the other blades on the overall containment process is analyzed. The results obtained in this study are compared with the experimental test results of a T58 rotor performed at the spin chamber facility of Naval Air Propulsion Test Center.

The numerical computation in the present study is performed by using DYNA3D, which is an explicit, nonlinear finite element code developed at Lawrence Livermore National Laboratory for simulation and analysis of large deformation dynamic response of structures. Being an explicit code, a large number of relatively small time steps is used and it is generally applicable to problems where the loading and response are of short duration and contain high frequency components. It has many material models to represent a wide range of material behavior, including elasticity, plasticity, composites and thermal effects. It has a sophisticated contact interface capability to handle impact and mechanical interaction among different bodies. Failure models of materials are also available to simulate fracture and fragmentation of plates or shells that can be used to show the penetration and petalling effects normally associated with high speed impact.

Background

A number of investigators have performed experimental studies and have created analytical models of the rotor burst and containment process. Mangano [1] carried out rotor burst experiments in the rotor test facility at the Naval Air Propulsion Test Center to develop criterion and data for the design of optimum lightweight devices for protection of vital aircraft parts and passengers. In the experiments, turbine rotors were modified to burst into equal pie sector segments and made to impact a freely supported ring made of different materials. McCarthy [2] studied the effects of engine rotor blade fragment size, shape, weight, energy and momentum on U.K. engines. The largest and heaviest fragments were generated when the disc portion of the rotor broke apart and they were the most destructive and were most likely to be uncontained by the casing. Hagg and Sankey [3] conducted a number of tests where slender rods with different length-diameter ratios and velocities were impacted against steel plates with edges clamped in relatively rigid frames. From the experiment, two stages of failure were identified. In stage 1, failure was due to compression and shearing of the material over the perimeter of the impact area, and stage 2 failure was due to the tensile strain exceeding the failure limit over the extended volume of the material. To model the test results, an effective target mass was identified which was the area of the target initially affected due to the impact and was measured from the experiments. A perfectly plastic collision between the impactor and effective target was assumed and conservation of linear momentum was used to determine the final velocities. The net energy loss was computed and if it exceeded the shearing and compression energy at failure of the material, then a stage 1 failure was assumed to have occurred. Otherwise, the residual kinetic energy of the impactor was compared with the tensile energy at failure to determine the stage 2 failure.

Witmer and Wu [4] developed a spatial finite element method to study the response of containment rings that can undergo large elastic, plastic deformation and is

subjected to impact by rotor fragments and compared their findings with the experimental results obtained in a spin chamber facility. The rotor fragment was assumed to be rigid and post impact velocities between the fragment and the nodes of the finite element model were determined from conservation of linear and angular momentum principles. It was assumed that during contact, only the normal forces were generated and frictional forces were ignored and a coefficient of restitution term was used to represent perfectly elastic, perfectly plastic or intermediate behavior during contact. The predicted ring response agreed fairly well but the predicted blade fragment motion was not in satisfactory agreement with the experimental observations. Gerstle [5] developed a large deflection finite element code for the prediction of rotor fragment containment shield test using newly developed ballistic fabrics. For the fragment, an effective target radius was assumed and for the containment shield, an instantaneous equivalent rigid mass and velocity were assumed to exist. Post impact velocities were determined from conservation of linear and angular momentum. Correlation with experimental data showed fair agreement with the initial transients. Mathis et.al. [6] used commercially available software codes ABAQUS and DYTRAN to study the impact response of flat plates and circular rings when they were struck by rigid impactors. The maximum displacement reaction forces and internal energy were determined for different impactor energy levels. No failure criterion was considered in this analysis. Dewhurst [7] studied the case where a single blade was contained but remained in the plane of the rotor that caused the other blades to fail and subsequently large hoop stresses were created which resulted in brittle tensile failure in the containment ring. From experimental and field data, he concluded that during multiple blade failure, the rings were thick enough to prevent shear type of failure but the the thickness was not sufficient to prevent a tensile failure.

Description of the Model

Four different cases are investigated to study the effects of the multiblade interaction on the containment of rotor fragments. The rotor model is based on the T-58 rotor on which a large number of impact and containment tests have been carried out in the past and some data are available in the published literature. In the first case, the rotor consisting of a single blade is released to impact against a ring containment structure. In the second case, the rotor contains the remaining blades and again a single blade is released and its interaction with the ring and with the remaining blades is assessed. In the third case, the rotor fragment consists of three blades that are attached together on a piece of the rim and this impacts against the containment ring. In the fourth case, the effects of multiple interaction among the three bladed rotor fragment, the remaining rotor blades and the containment casing is investigated. The T-58 rotor has a angular speed of 20,000 rpm and the mass of the single blade is 0.084 lbm. The initial kinetic energy of the single blade fragment is 10368.0 lb-in., and the kinetic energy of the three bladed fragment is 34391.1 lb-in. The geometrical and material properties of the rotor fragment and the containment ring are given in Table 1 and Table 2.

The containment ring is assumed to be made of aluminum and is modeled by 1800 four noded shell elements and it is not restrained by any support. The blades are modeled as shell elements and the central hub is taken as rigid and is modeled

by eight noded brick elements. One pair of contact surfaces is defined to model the impact of the released blade with the containment ring. Another pair is defined for the possibility of contact of the blade with itself to model the curling phenomenon of the blade tip when it comes with high speed contact with the ring. When other blades are also present in the rotor, then additional contact surface pairs are needed to model the contact between the released blade and the following blades and also among the existing blades on the rotor with each other. When the three bladed fragment is considered where the blades are attached to the rim of the rotor, it is further necessary to define additional contact surface pairs to model the contact between the rim and other blades and between the rim and the containment ring. Since a large number of contact surface pairs can be computationaly very expensive, it is important to define only those which are important. With this consideration in mind, only nine following blades in a rotor of forty eight blades are modeled with contact surfaces to model the multiblade interactions. For the remaining blades on the rotors, contact surfaces are defined only for the blade tips. This is necessary because when the the ring is hit by the primary fragment, it deforms from its initial circular shape and as a result, comes into contact with the blade tips. The effective plastic strain at failure for the containment ring material is set at 0.1 and if this value is exceeded then the element is assumed to have failed and is deleted. If the entire row of elements along the axial direction of the ring fail, then it signifies non-containment of the fragment.

Results and Discussion

For each type of fragment, the ring thickness is varied incrementally between 0.04 inch and 0.28 inch and its effect on the containment of the fragment is studied. The kinetic energy of the fragment is plotted with respect to time as it is released and impacts the containment ring and other blades on the rotor. The net contact force on the containment ring is also plotted with respect to time to assess the magnitude of the forces.

In Figure 1, the state of deformation of the containment ring and the blade are shown at four different time intervals. The simulation is run for two mili-seconds and the blade fragment is given an initial angular speed of 20,000 rpm. The blade undergoes a curling motion after its impact with the ring. The containment ring also undergoes large plastic deformation though the maximum plastic strain is well below the effective plastic strain at failure. The containment ring of thickness 0.16 inch is able to contain the fragment. In Figure 2, The final deformed shape of the containment ring is compared with the deformed shape of a ring obtained in a spin chamber facility at the Naval Air Propulsion Test Center. In the present study, the blade is initially at the vertically downward position and rotates counterclockwise, while in the experment, the blade is initially at the vertically upward position. While no quantitative data is available for the strains and displacements from the experiments for comparison purposes, a good qualitative agreement can be found for the overall deformed shapes between the computed and the experimental results. In Figure 3, the interactions among a three bladed fragment attached to a rim, containment ring and the other blades are shown at four different time intervals. The unbalanced forces that arise when the rotor fragment is released is neglected in this analysis and the central disc is assumed to be rigid and is modeled by solid elements and a constant

rotational speed is prescribed on it for all times. The remaining rotor blades are attached to the disc at the shell-solid interface and they rotate with the disc. It can be seen that the following blades undergo large deformation after contact with the three bladed fragment and some of the following blades actually break when the plastic strain exceeds the failure strain limit. The rotor fragment causes the containment ring to deform by a significant amount and after some time the fragment is able to nest within the ring without being in any further contact with the remaining blades. The containment ring thickness is 0.24 inch and the fragment is contained.

The kinetic energy variation of a single blade and the resulting contact force on the ring for the case of no multi-blade interaction is shown in Figure 4. The initial tip clearance is 0.2 inch and till the fragment comes into contact with the ring, the kinetic energy remains constant. The kinetic energy subsequently decreases as the blade makes contact and as can be expected, the residual kinetic energy decreases as the ring thickness is increased. The ring fails when its thickness is 0.04 inch, for higher values of thickness, it is able to contain the fragment. The contact forces are plotted for two different values of ring thickness and for the larger thickness, the ring is able to absorb much higher contact forces. In Figure 5, the effect of the remaining blades on the rotor is investigated. The kinetic energy of the fragment receives a boost as it is impacted by the following blade. Due to additional interactions with the remaining blades, the ring fails to contain the fragment when its thickness is less than or equal to 0.16 inch. The peaks of the resultant contact forces are far higher when the multi-blade interactions are considered. In Figure 6 and Figure 7, the kinetic energy and resultant force variation are shown for the three bladed rotor fragment

In Figure 8, the effect of multiblade interaction is contrasted with the case when the other blades are not present on the rotor. For about 0.4 mili-seconds, the kinetic energy variation is the same for the two cases, which signifies the fact that the first following blade has not yet made contact with the released fragment. After contact with the first following blade, the fragment receives a boost in energy. The second peak is due to contact with the second following blade. The residual kinetic energy of the fragment is more when other blades are present on the rotor. When the ring thickness is 0.24 inch, the boost in energy due to impact from the following blade can still be seen in Figure 9, but in terms of magnitude, it is less than the case when ring thickness is equal to 0.04 inch. This is due to the fact that the thicker ring is able to exert a greater force on the rotor fragment and the increase in the retarding force on the fragment causes it to receive a lesser energy boost. When the three bladed fragment is considered for a ring thickness of 0.04 inch, the impact from the following blade causes the kinetic energy of the fragment to go above its initial kinetic energy, as shown in Figure 10. When the thickness is equal to 0.24 inch, there is no increase in the fragment energy level after contact with the first following blade, though the fragment has a slightly higher residual energy level, as shown in Figure 11.

In Figure 12, the residual kinetic energy of a single blade fragment with multiple interaction as determined from analysis is compared with the experimentally observed results. From the experiments, the critical ring thickness to contain the fragment is found to be about 0.13 inch and from the computed values, the critical thickness for containment is determined to be 0.16 inch. The residual kinetic energy level as

predicted by the computed results is in fairly good agreement with the experimentally observed results. In Table 3 and Table 4, the residual kinetic energy levels of a single and three bladed fragment along with the containment results are shown. It can be observed that when the other blades are present, thicker rings are required to contain the fragment. This is partly due to the additional energy the fragment receives due to impact with the following blades. Moreover, the presence of the other blades help to constrain the shape of the deformed ring, as shown in Figure 3, where the remaining blades act as support and try to preserve the original circular shape. In contrast, when the other blades are not present, as in Figure 1, the ring deforms and stretches along the direction of impact. Thus, when the remaining blades act to preserve the original shape, greater tensile loads are generated on the ring as it is pressed upon by the impacting fragment, and as a result, thicker rings are required to contain the fragment.

Conclusions

In this study, a transient, nonlinear finite element method is used to analyze the impact response of high energy rotor fragments on ring type containment structures. The method can model large deformation response and failure of aircraft engine containment structures and a sophisticated contact search interface capability is used to model the mechanical interactions among different bodies. The failure criterion is based on the effective plastic strain exceeding a critical value. The effects of multiple collisions among the remaining blades and the rotor fragment on the containment process are evaluated and compared with the cases where the other blades are absent. The critical ring thickness value and the residual kinetic energy levels of the fragment as determined from spin chamber experiments agree fairly closely with the predicted analytical findings. The methodology as developed here can be used to model and analyze more complicated aspects of rotor failure in aircraft jet engines.

References

1. Mangano, G. J., "Studies of Engine Rotor Fragment Impact on Protective Structures," Agard Conference Proceedings, No. 186, Impact Damage Tolerance of Structures, 41st Meeting of the Structures and Materials Panel, 1975.

2. McCarthy, D., "Types of Rotor Failure and Characteristics of Fragments," A Workshop held at the Massachusetts Institute of Technology, NASA CP-2017, 1977, pp. 65-92.

3. Hagg, A. C. and Sankey, G. O., "The Containment of Disc Burst Fragments by Cylindrical Shells," Journal of Engineering and Power, Transactions of the ASME, Vol. 96, April 1974, pp. 114-123.

4. Wu, R. W. H. and Witmer, E. A., "Approximate Analysis of Containment/Deflection Ring Response to Engine Rotor Fragment Impact," Journal of Aircraft, Vol. 10, Jan. 1973, pp. 28-37

5. Gerstle, J. H., "Analysis of Rotor Fragment Impact on Ballistic Fabric Engine Burst Containment Shields," Journal of Aircraft, Vol. 12, No. 4, April, 1975, pp. 388-393.

6. Mathis, J. A., Parduhn, S. C., Alvarez, P., "Analysis of Turbine Engine Rotor Containment and Shielding Structures," AIAA-93-1817 AIAA/SAE/ASME/ASEE 29'th Joint Propulsion Conference and Exhibit, Monterey, CA, 1993.

7. Dewhurst, T. B., "The Impact Load on Containment Rings During a Multiple Blade Shed in Aircraft Gas Turbine Engines," Presented at the International Gas Turbine and Aeroengine Congress and Exposition, Florida, June, 1991, 91-GT-163

ring radius	7.0 in.
ring axial length	1.5 in.
blade length	3.75 in.
blade axial length	0.9 in.
tip clearance	0.2 in.
angular velocity	2094.4 rad/sec.
blade mass	0.084 lbm
blade moment of inertia	0.0958 lbm-in.^{2}

Table 1: Geometric properties of the blade and the containment ring

	blade(steel)	containment ring(aluminum)
Young's modulus	22.5×10^6 psi	10.5×10^6 psi
Poisson's ratio	0.25	0.33
Yield stress	90,000 psi	44,000 psi
Density	0.283 lbm/in^3	0.1 lbm/in^3
Failure strain	0.3	0.1

Table 2: Material properties of the blade and the containment ring

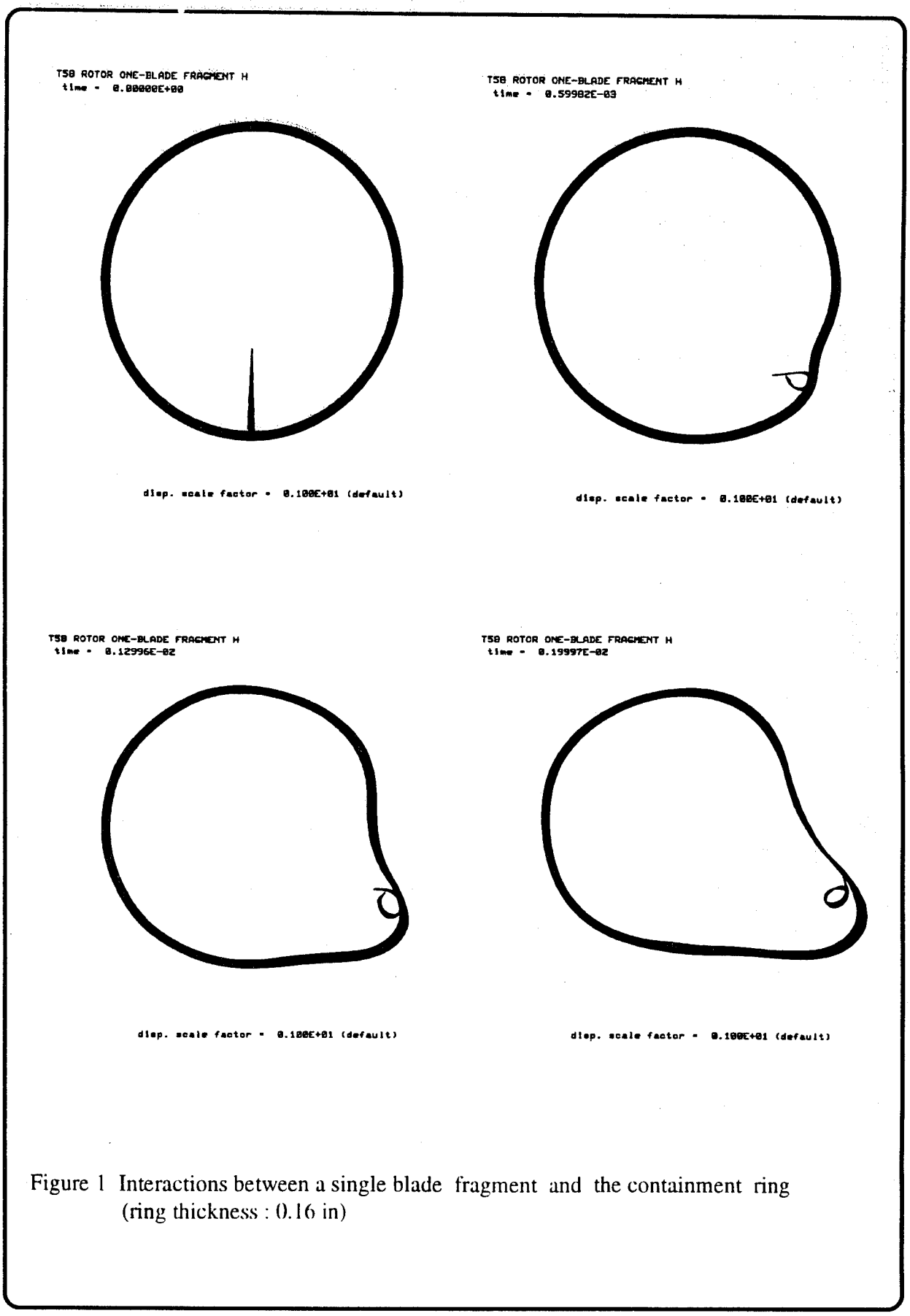
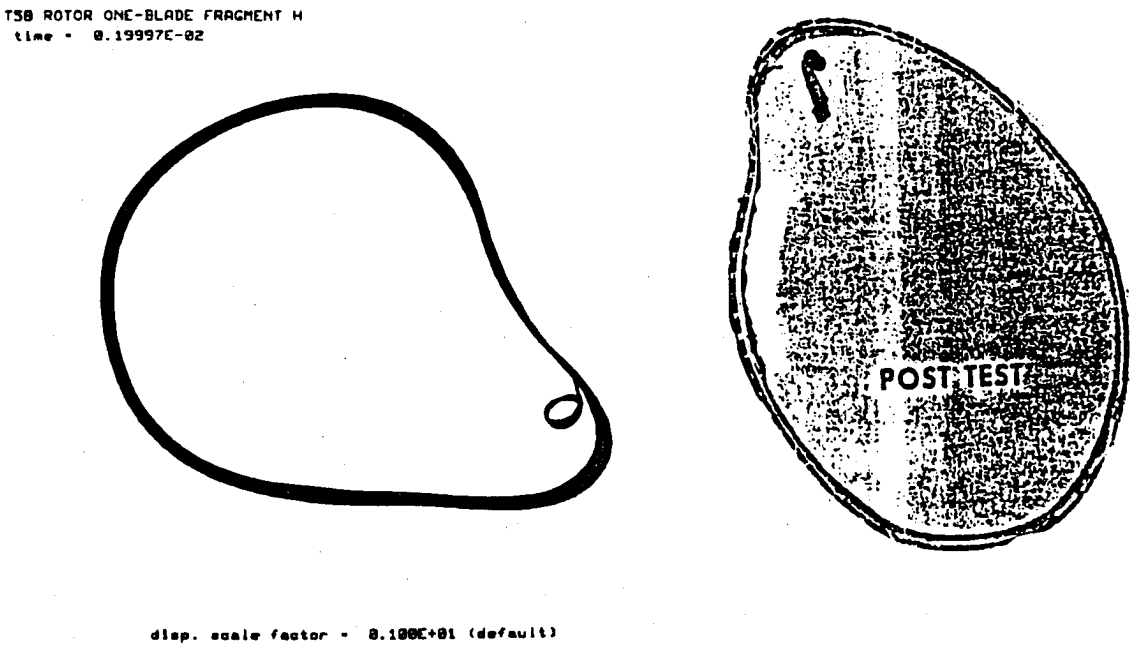


Figure 1 Interactions between a single blade fragment and the containment ring (ring thickness : 0.16 in)



Computation Experiment

Figure 2 Final deformed shape of the containment ring after impact by a single blade fragment

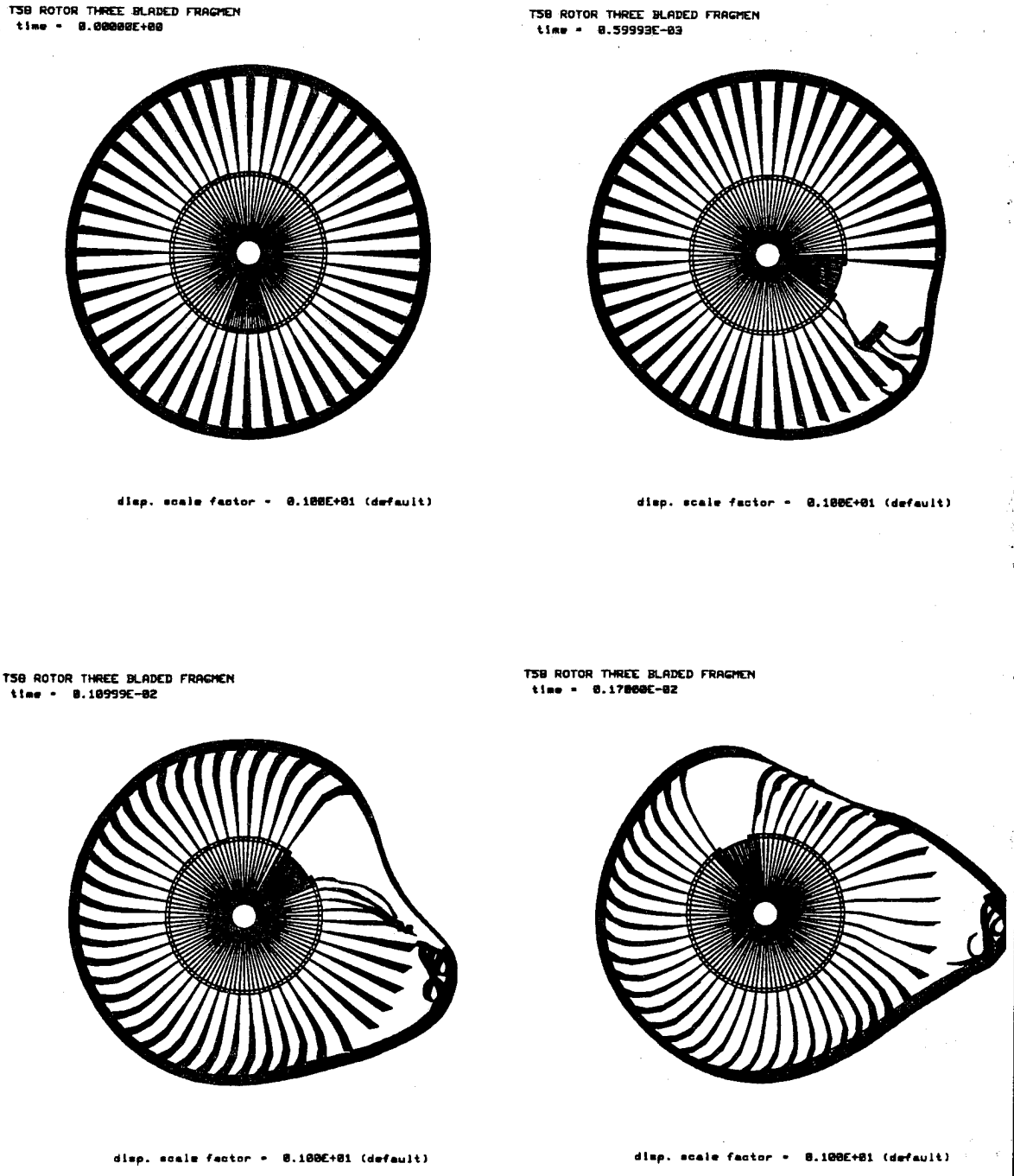


Figure 3 Interactions among a three bladed fragment, containment ring and the other blades (ring thickness : 0.24 in)

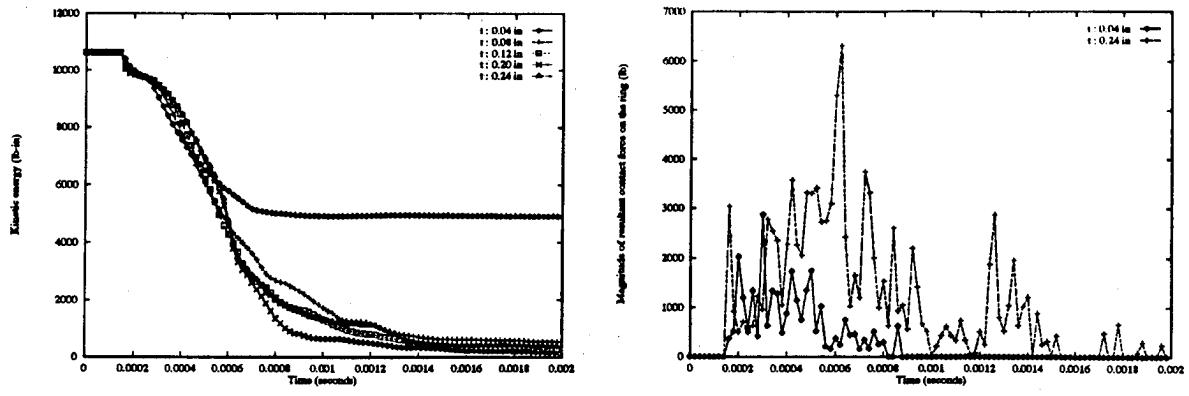


Figure 4 Kinetic energy variation of a single blade fragment and resultant contact force on the ring for different thickness of the ring (no multi-blade interaction)

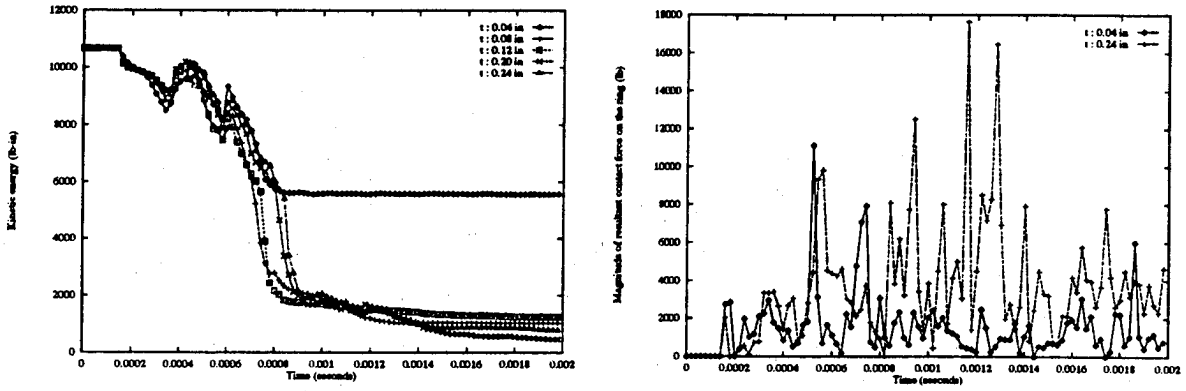


Figure 5 Kinetic energy variation of a single blade fragment and resultant contact force on the ring for different thickness of the ring (multi-blade interaction)

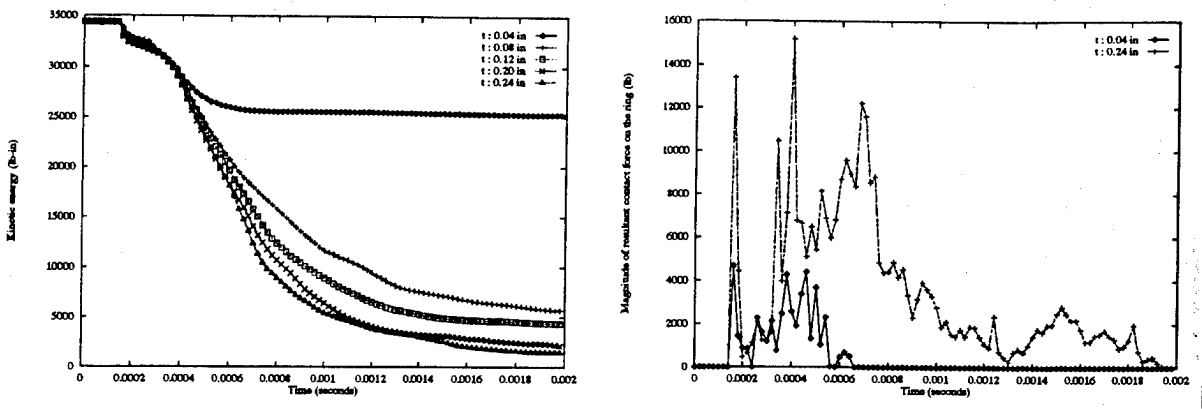


Figure 6 Kinetic energy variation of a three bladed fragment and resultant contact force on the ring for different thickness of the ring (no multi–blade interaction)

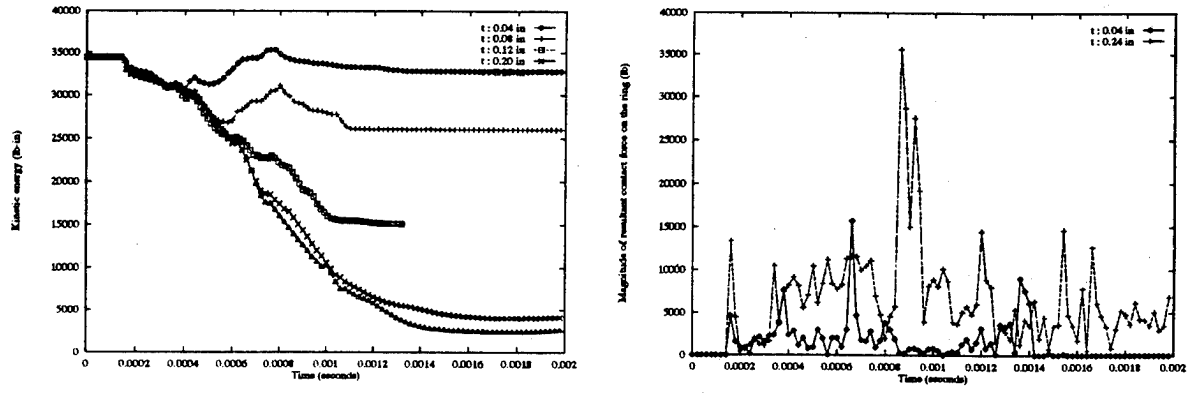


Figure 7 Kinetic energy variation of a three bladed fragment and resultant contact force on the ring for different thickness of the ring (multi–blade interaction)

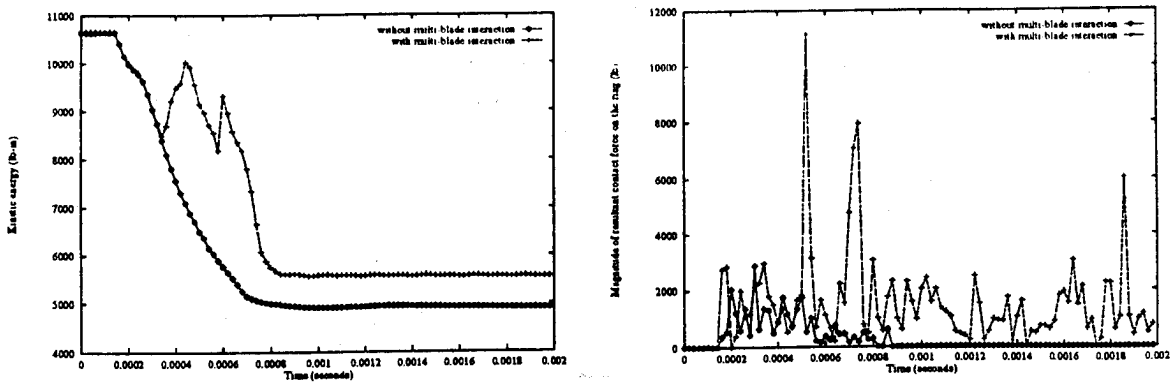


Figure 8 Kinetic energy variiation of a single blade fragment and resultant contact force on a ring of thickness 0.04 in (with and without multi–blade interaction)

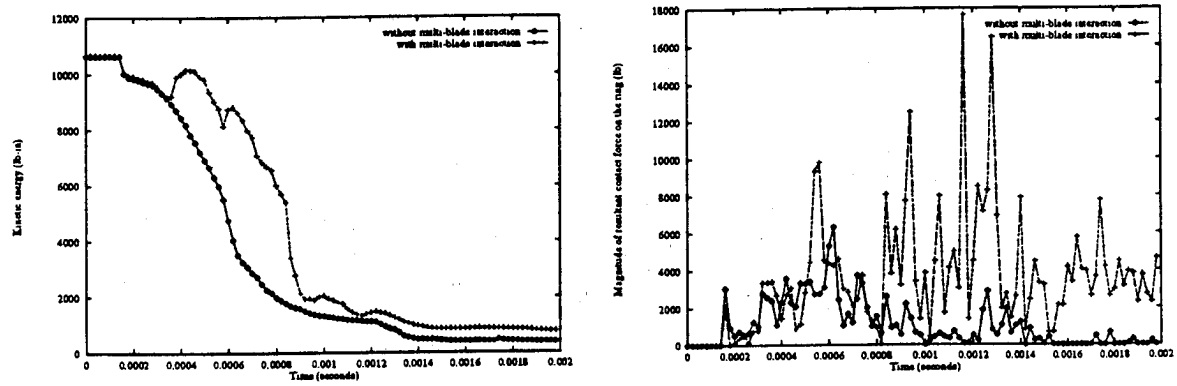


Figure 9 Kinetic energy variiation of a single blade fragment and resultant contact force on a ring of thickness 0.24 in (with and without multi–blade interaction)

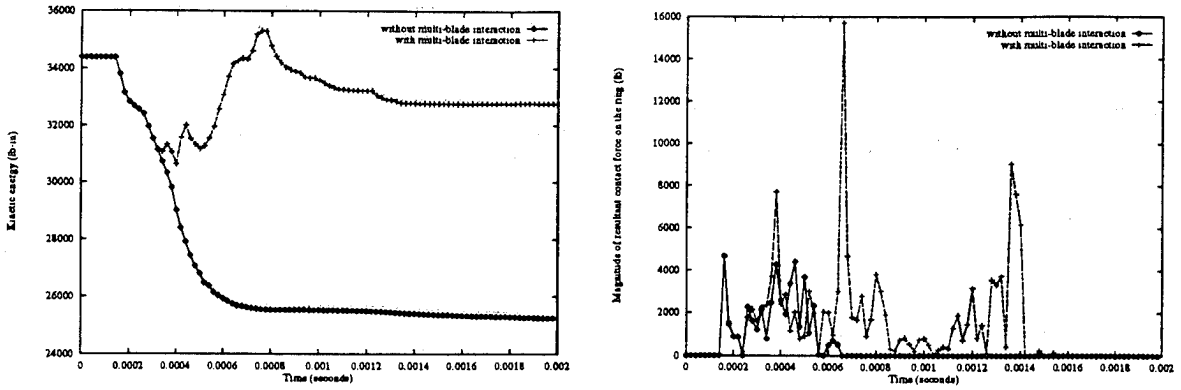


Figure 10 Kinetic energy variiation of a three bladed fragment and resultant contact force on a ring of thickness 0.04 in (with and without multi-blade interaction)

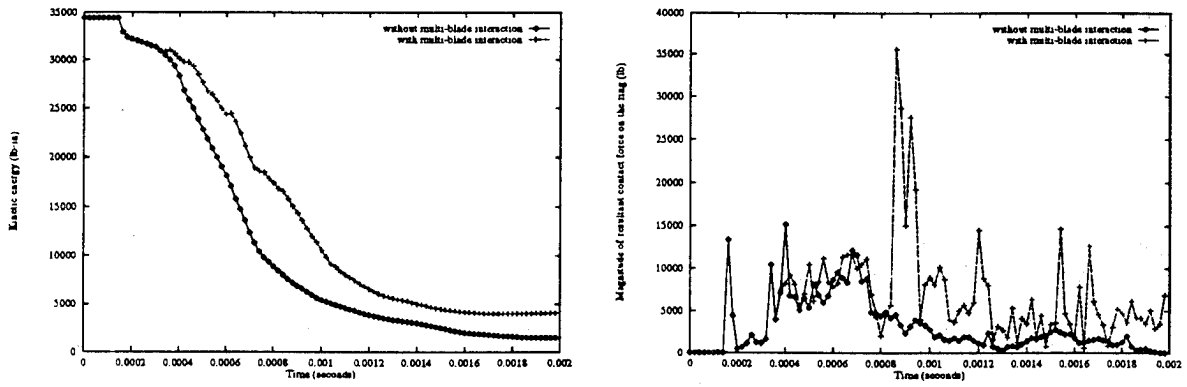


Figure 11 Kinetic energy variiation of a three bladed fragment and resultant contact force on a ring of thickness 0.24 in (with and without multi-blade interaction)

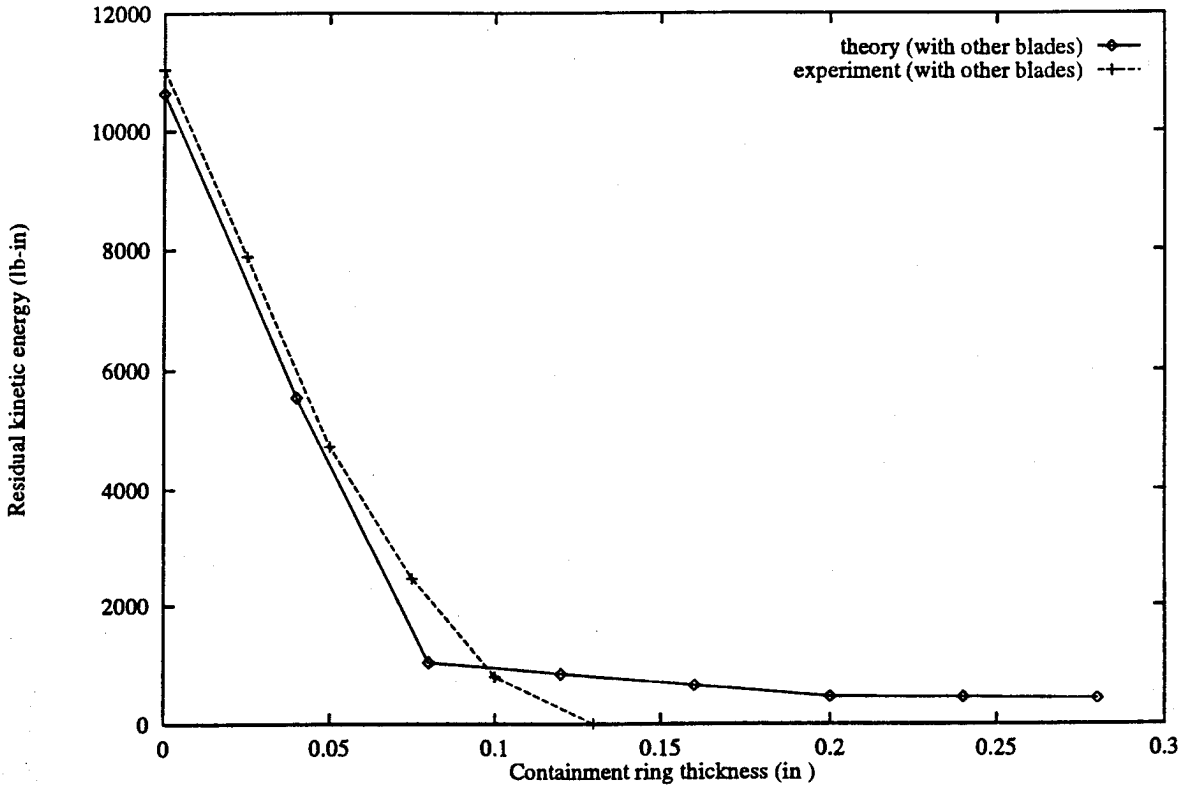


Figure 12 Residual kinetic energy of a single blade vs. containment ring thickness

ring thickness (in)	without other blades		with other blades	
	residual energy (lb-in)	containment	residual energy (lb-in)	containment
0.00	10368.0	-	10638.0	-
0.04	4909.3	no	5553.5	no
0.08	541.2	yes	1030.5	no
0.12	279.3	yes	893.0	no
0.16	251.1	yes	647.5	no
0.20	245.2	yes	456.1	yes
0.24	239.3	yes	450.4	yes
0.28	-	-	425.2	yes

Table 3: Residual kinetic energy of a single blade fragment

ring thickness (in)	without other blades		with other blades	
	residual energy (lb-in)	containment	residual energy (lb-in)	containment
0.00	34391.1	-	34391.1	-
0.04	25236.4	no	32766.9	no
0.08	5662.3	yes	25986.5	no
0.12	4340.0	yes	15087.9	no
0.16	2679.3	yes	6560.8	no
0.20	2136.5	yes	4106.9	no
0.24	1498.5	yes	2998.2	yes
0.28	-	-	2564.2	yes

Table 4: Residual kinetic energy of a three bladed fragment

Validation of a Probabilistic Rotor Design System -- Status of the USAF PRDS Contract

1994 USAF Structural Integrity Program Conference



Dr. P. G. Roth
GE Aircraft Engines
December 7, 1994
(513) 552-4919

PRDS (*P*robabilistic *R*otor *D*esign *S*ystem)

Contract Awarded by WL/POTC - F33615-90-C-2070

USAF Program Monitors:

Sqn Ldr Chris Pomfret (513) 255-2351
Ted Fecke (513) 255-2081

Focusing on advanced gas turbine engine disks

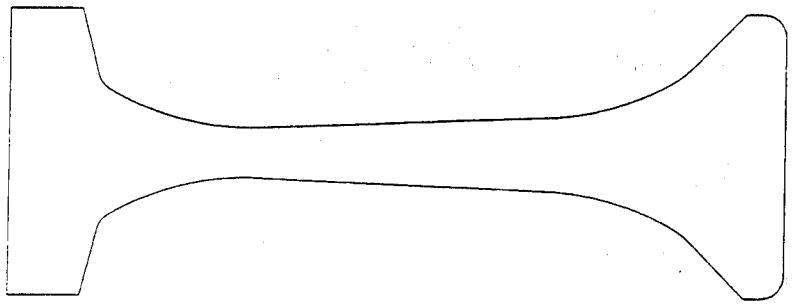
1) Identify limitations of current design practices
2) Develop a probabilistic methodology for basing design limits on calculated risk of failure
3) Validate the methodology
4) Generate proposal for incorporation into an evolving ENSIP

Will Concentrate on the Validation

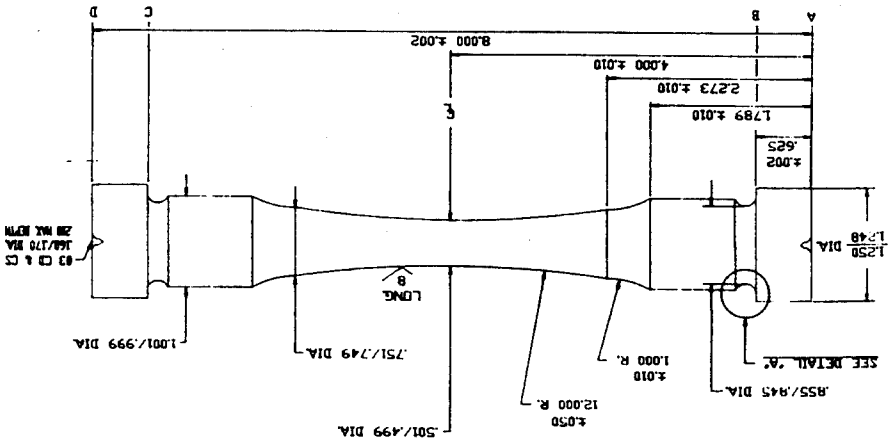
Hourglass Specimens and Model Disks

- Manufactured from Extruded and Isoforged -270 Mesh PM Rene' 88 DT
  - -- Unseeded baseline
  - -- Small seeded material near baseline (-270,+325 mesh and -200,+230 mesh alumina)
  - -- Large seeded material simulating deviation (-140,+170 mesh and -50,+60 mesh alumina)
  - -- If theory works for intentionally dirty material, it should work for clean production quality material

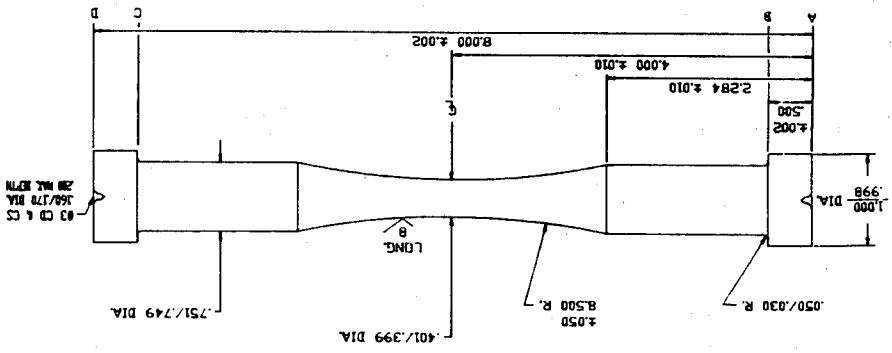
Three Validation Geometries



MD9



HG2



HG1

- Hourglass specimens tested in strain control at elevated temperature ... 115 total
  - -- Simple stress gradients
  - -- Enough testing for statistical comparisons enabled by modest cost

- Model Disks being tested in NAPC spin pits at elevated temperatures ... 20 total
  - -- Surface condition representative of production hardware
  - -- More complex stress gradients
  - -- One step closer to engine application

Hourglass Testing Matrix

	HG1	HG2
Unseeded	**29**	**5**
Small Seeded	**5**	**38**
Large Seeded	**35**	**3**

- All testing and fractography completed
- Will focus on large seeded HG1, small seeded HG2 results and unseeded HG1 results

PDAS (*P*robabilistic *D*esign *A*nalysis *S*ystem)

- Analysis tools and statistical algorithms vary from application to application
  - -- Impossible to hardwire all mixes into any single computer code
- PDAS is more like a language than a program
  - -- Incorporates statistical algorithms and GEAE life methods as high level commands
  - -- Interfaces with other packages (e.g. ANSYS)
- Principal GEAE probabilistic fracture mechanics tool is MISSYDD

MISSYDD (*MIS*sion *SY*nthesis given *D*efect *D*istribution)

- MISSYDD estimates risk of component failure under mission loading given statistically distributed crack initiating flaws
- Statistical combination ... Three steps
  1. Single flaws, specific sizes
     - - *Geometric effect of flaw placement evaluated*
  2. Single flaws, random sizes
     - - *Geometric failure distribution integrated with flaw relative size distribution*
  3. Multiple flaws, random sizes
     - - *Based on Poisson model for flaw occurrence*
- Calculations are sensitive to both size distribution and rate of occurrence

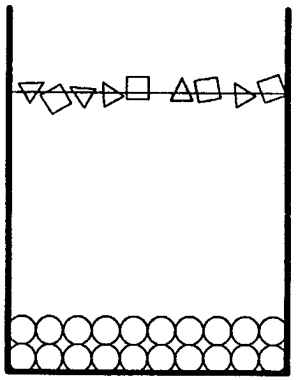
Average Distribution of Natural Inclusions Can Be Determined by Heavy Liquid Separation (HLS) Analysis of Many Powder Lots

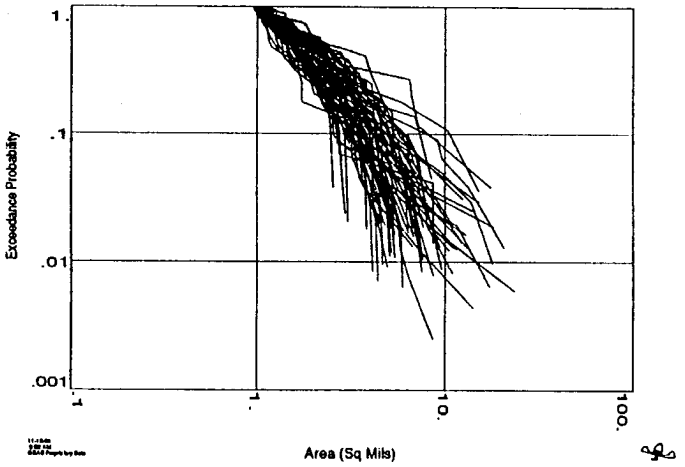
Specific Gravities

BN 2.20
SiO2 2.38
CaO 3.34
MgO 3.58
Al2O3 3.96

TMF 4.05

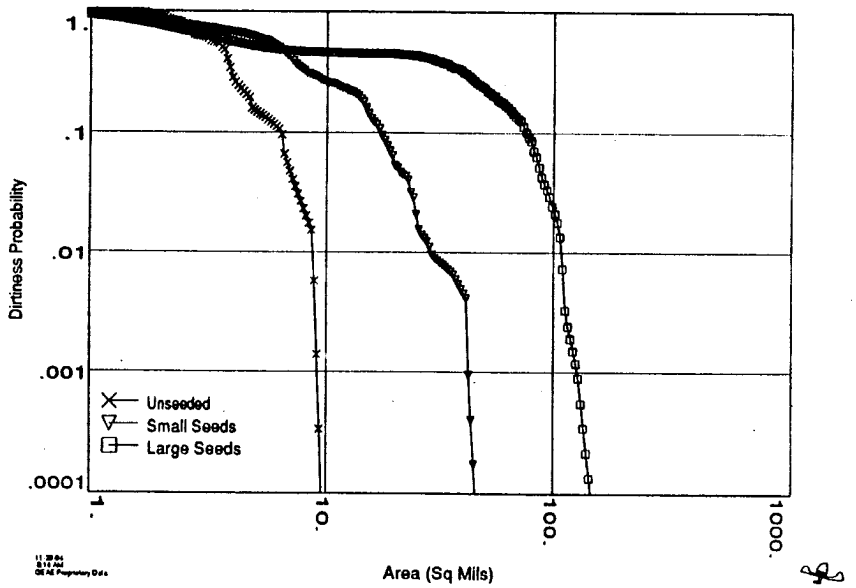
Alloy 8.3





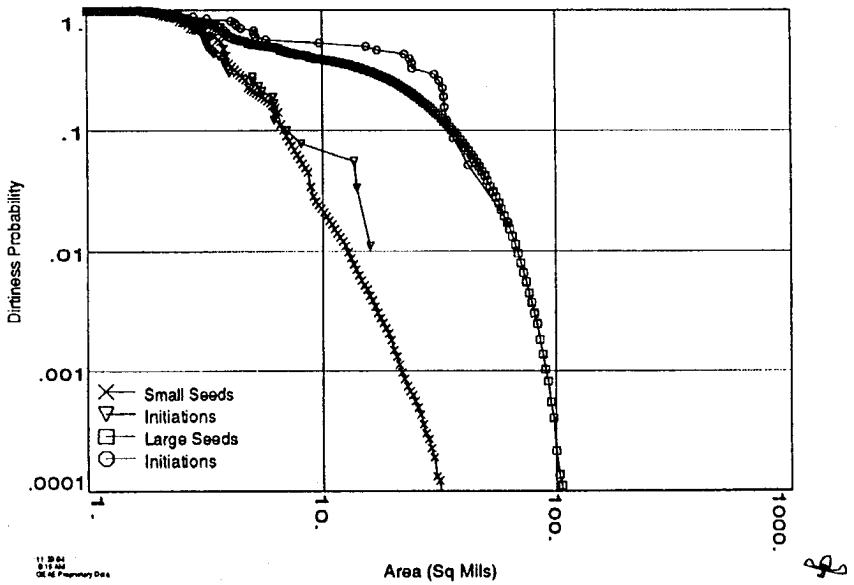
Validation Calculations Employ Much Tighter Distribution of LCF Finds from the Unseeded Specimens

Seeding Distributions Determined by Image Analysis of Mesh Fraction Samples



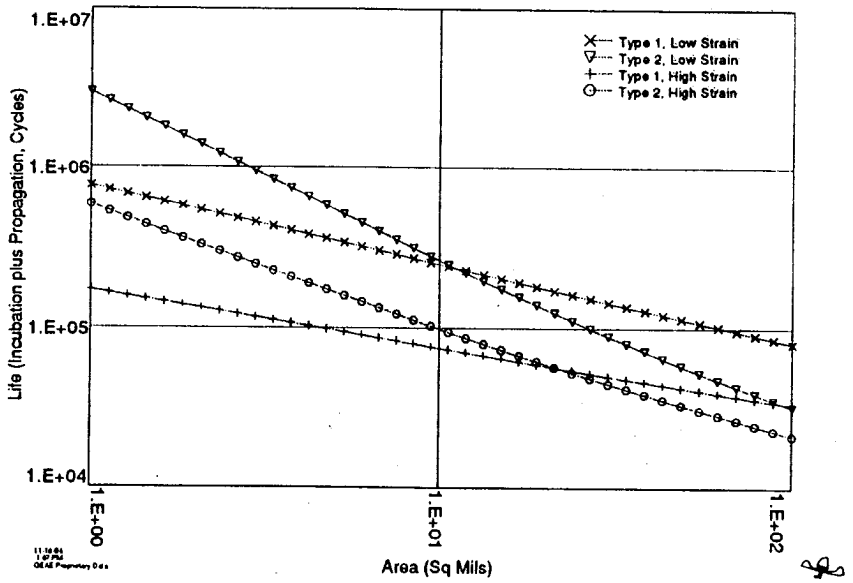
Seeds Added to Powder by Weight

Large and Small Seeding Distributions Modified to Reflect Forging Orientation



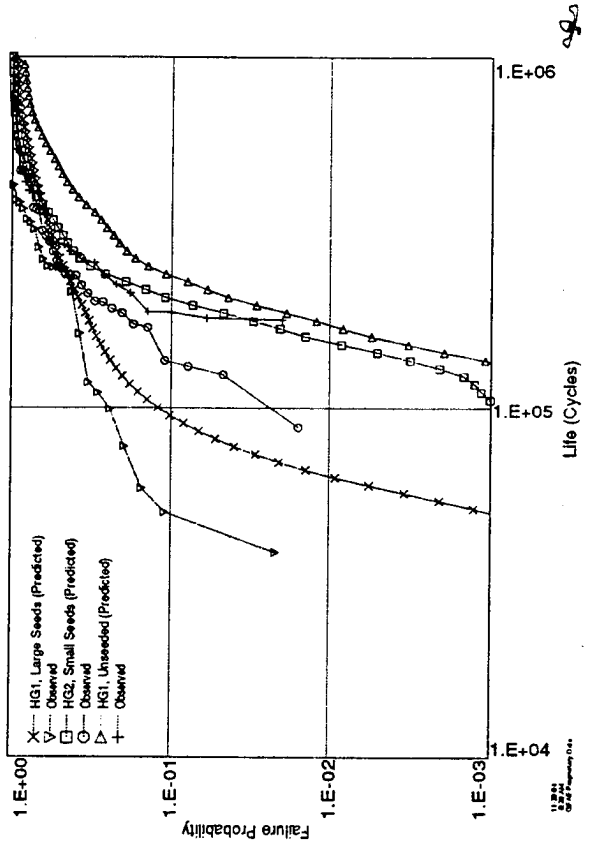
Oriented Distributions Agree with Fractographic Finds -- Little Difference between Small Seeds and Unseeded Baseline

Life Algorithms -- Crack Incubation Followed by Stable Crack Growth

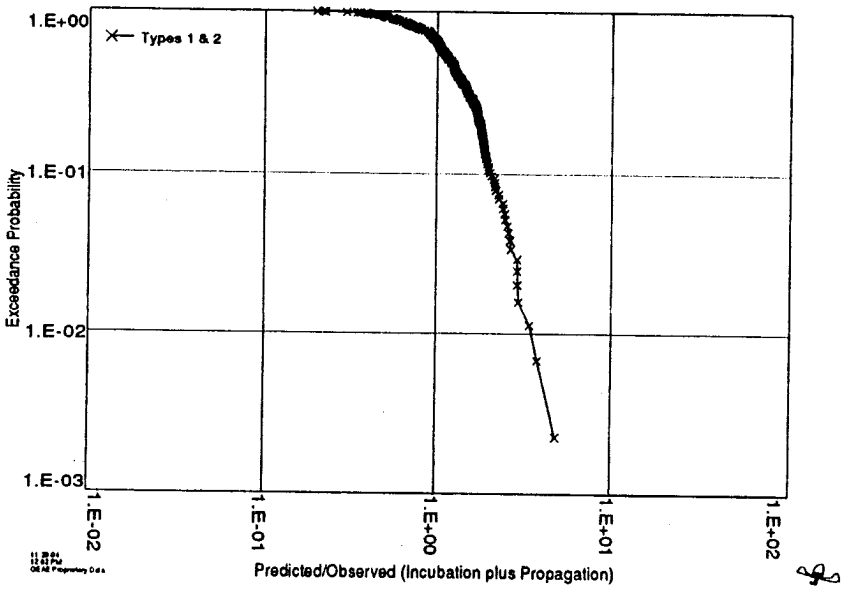


Type 1 Inclusion -- Blocky ... Type 2 Inclusion -- Agglomerated

Predictions -- First Iteration

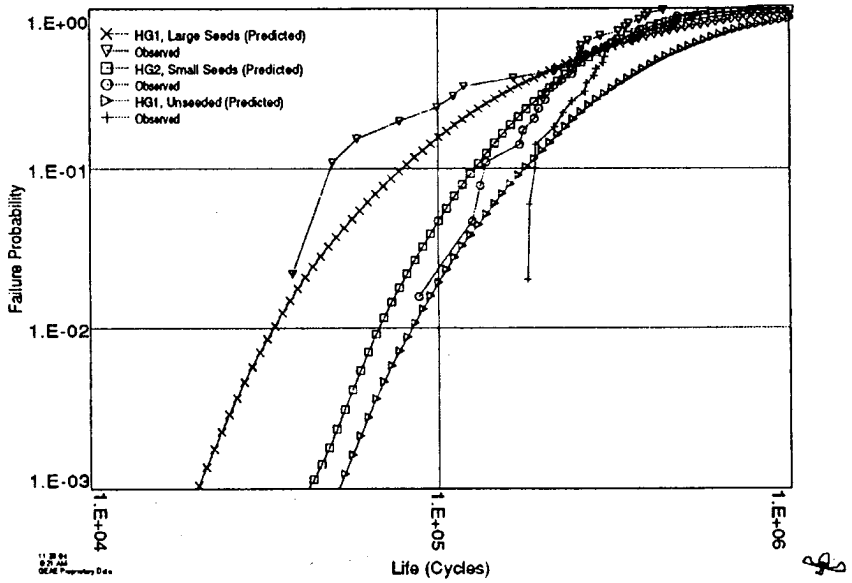


Variability in Inclusion Behavior Recognized



Integrated with First Iteration Predictions

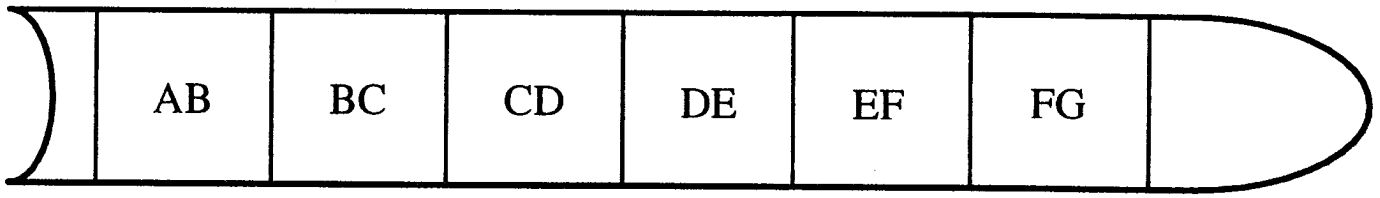
Predictions -- Second Iteration



Comparisons Significantly Improved

Stratification in Inclusion Distribution and Behavior Observed

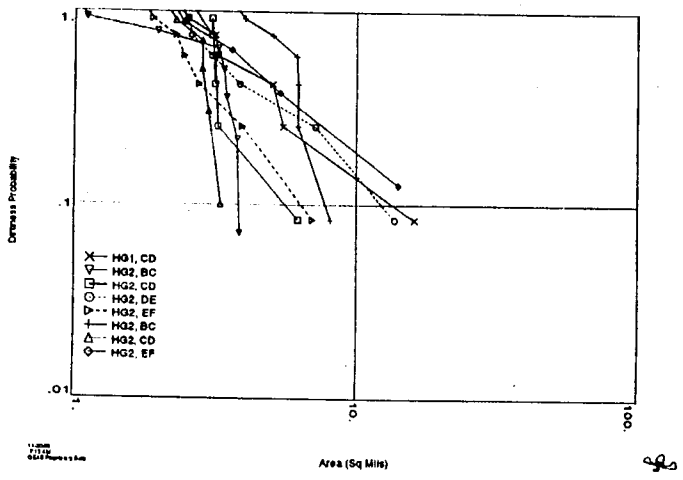
Seeds Blended with -270 Mesh PM Rene' 88 DT and Canned by Cameron Powder Systems in Michigan



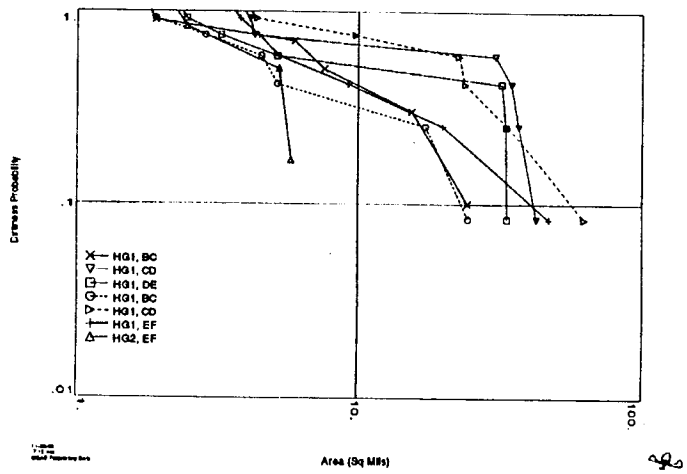
Extruded and Isothermally Forged into Pancakes by Cameron at Texas Facility

Impact on Life Being Evaluated

Stratification in Inclusion Distribution

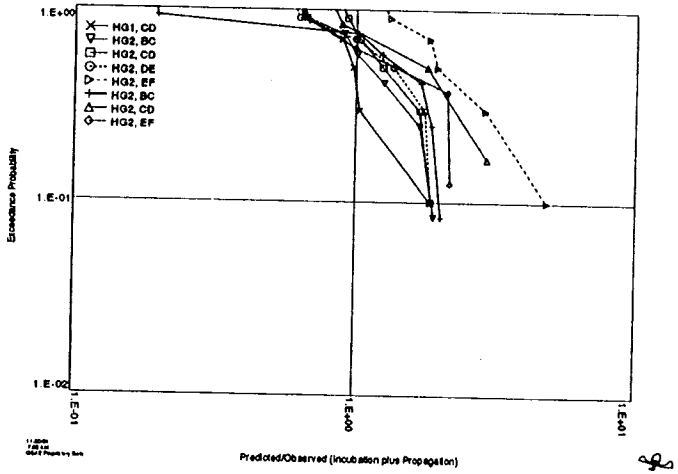


Small Seeds

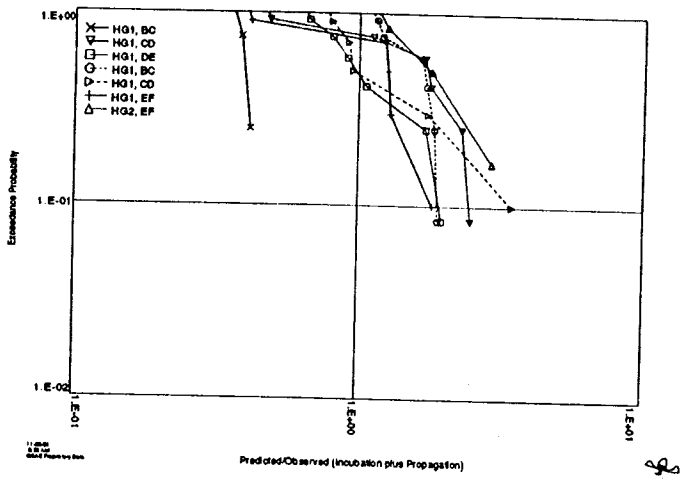


Large Seeds

Stratification in Inclusion Behavior



Small Seeds



Large Seeds

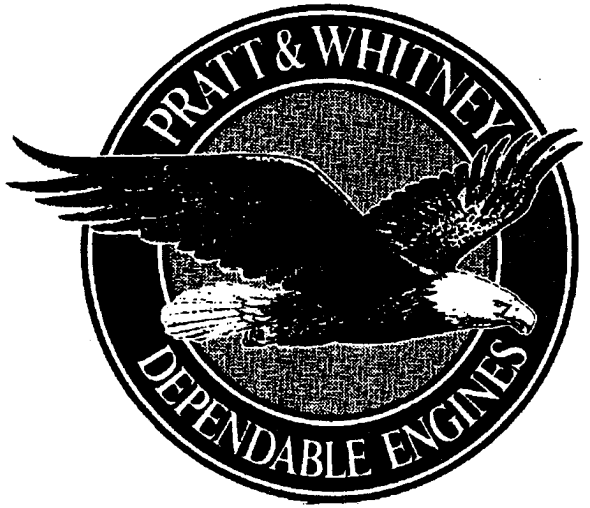
Program Status and Summary

- Hourglass specimen testing and fractography completed
- Comparison of results with predictions good so far
- Stratification interesting
  - -- Reflects real world
  - -- Impacts application and interpretation of probabilistics
- Model disk testing at NAPC experiencing difficulty ... Scheduled to be completed by 9/95

Acknowledgments

John Coomer Norm Austin	Early program managment and specimen design
Greg Bechtel Steve Schrantz Bob Maffeo	Stress analysis support
Tom Daniels Ivan Miller	Fractography
Cameron (Now under Wyman-Gordon)	Material preparation
Metcut	Specimen manufacture and testing

A NEW APPROACH TO TRACKING TURBINE ENGINE LIFE



John P. Hansen ***Michel D. Paquet***

1994 USAF STRUCTURAL INTEGRITY PROGRAM CONFERENCE
San Antonio, Texas
December 7, 1994

A New Approach to Tracking Turbine Engine Life

Slide 1 - Introduction

This presentation describes a new approach to the monitoring and tracking of gas turbine engine life as it pertains to life-critical components. The approach is applicable to the modeling of common failure modes found in turbine engines today including low cycle fatigue (LCF), crack growth, high cycle fatigue (HCF), oxidation/erosion, thermal mechanical fatigue, creep, and overload. The approach utilizing advanced life algorithms can be used for either day-to-day component life tracking or to assist in management of fleet assets in the event of a field problem. Although the technology exists to provide a large amount of life tracking data, current logistics/maintenance data management systems can not effectively manage the multitude of life tracking parameters this approach is capable of providing.

With the advent of electronic controls that employ enhanced engine monitoring using state-of-the-art sensors and high capacity computer memory, modern turbine engine designs have the capability to accurately determine and track the life of critical hardware. This can be accomplished in real-time as life is used up during operational service. New techniques for tracking turbine engine component life have been devised that can render improvements to the current life tracking process thus providing the customer with a more affordable weapon system. The improved affordability will result from several factors including: full utilization of engine life; life management on a module or component basis; improved system safety; and reduced spare parts requirements. The new life tracking techniques employ parametric equations which relate engine and airframe performance to used up increments of life. This new approach utilizes real-time measurable engine performance sensor data which are passed to life algorithms contained within the engine electronic controls. Within the electronic control, calculations are performed to define increments of life used up as the turbine engine is operating in the aircraft or on a ground test stand. The life algorithms can be developed for any critical component or failure mode thus providing greatly improved accuracy as compared to the current method of tracking life based on the simplified Total Accumulated Cycle (TAC) equation. In addition to life tracking, this technology could be used to assist in logistics planning activities and real time damage accumulation whenever field problems arise.

Slide 2 - Outline

The presentation covers a description of the current process utilized to track turbine engine life in today's military or commercial engines. The most commonly used parameters today are hours or total accumulated cycles, referred to as TAC's. These parameters typically track at the engine level, thus no distinction in life is made at the component level. The current approach can be in error since the rate of life usage varies from component to component, dependent upon how the engine is being used.

Next, a description of the new approach to tracking life and the process that is used to employ the life algorithms in the engine electronic control system is given. The advanced life algorithms use engine electronic control sensor data to determine life as the engine is operated. The algorithms reside within the engine control diagnostic unit and the results can be downloaded into the logistic management maintenance information system.

Applications where significant improvements to logistics management could be realized by employing these techniques is discussed next. The advanced life tracking algorithm approach is directly applicable to management of fleet assets whenever a significant field failure is encountered. The life algorithms can be tailored to specific failure modes and component stress states. Engines containing parts that are susceptible to the failure mode would have their electronic controls reprogrammed to incorporate the life algorithm.

Next, the presentation will briefly identify some areas where further work is required prior to full incorporation of the advanced life tracking algorithm process. The biggest obstacle to full introduction of this process is defining appropriate logistics management procedures for handling the potentially large volume of data that this system is capable of generating. Additionally, instead of utilizing only one or two life tracking parameters as currently used, the life algorithms could generate a dozen or more parameters.

Finally, a discussion on some of the benefits of going to the new approach is given. There are benefits to both the customer and engine contractor. The benefits include safer engines, longer usage periods, and more accurate life tracking parameter for use in warranty administration.

Finally, a brief summary to recap the highlights of this presentation is given.

LIFE TRACKING

OUTLINE

- Current Process
- Life Model Development
- Applications
- Issues
- Benefits
- Summary







Slide 3 - Current Process Description

Conventional life tracking methodology utilized in modern fighter aircraft typically track life using simple counters such as hours or on-/off-cycles, or they track life using multiple levels of operation, which are generally a function of severity, such as hot time or rotor speed cycle counts known as TAC's. TAC in the acronym for Total Accumulated Cycles. In conventional life tracking approaches, TAC's are generally the most meaningful parameter in determining life of rotating hardware such as disks or seals while hours are thought to be more meaningful for tracking life of static hardware such as vanes or augmentor liners.

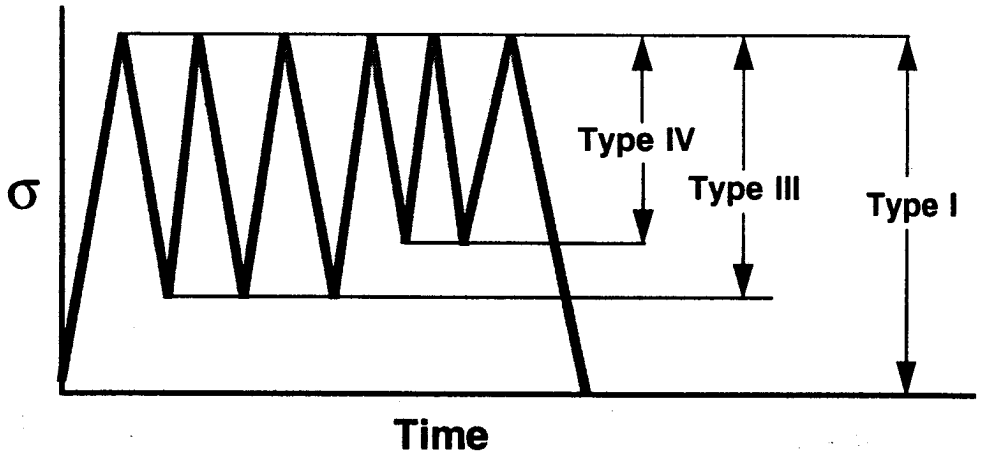
TAC cycles are determined by counting gates which are tripped when certain RPM levels are exceeded. The gates are established at both the high RPM and low RPM range. A TAC cycle is calculated via a fairly simplified equation of the addition of Type I cycle damage, represented by a stress excursion from a shutdown condition to a max stress level, plus 25% of the Type III cycle damage, represented by a stress excursion from an engine idle speed stress condition to a high stress level, usually at an engine power setting at intermediate or above, plus 2.5% of the Type IV cycle damage, represented by a stress excursion from an engine cruise speed stress condition to a high stress level. One major limitation of the conventional TAC cycle approach is that it assumes a fixed level of damage. For example, the TAC equation uses a damage equivalency factor, referred to as a K-factor of .25 for Type III cycles which implies that the accumulation of Type III damage is only 25% as damaging as the damage done by Type I's. Similarly, the equation uses a K-factor of .025 for Type IV's which implies that the accumulation of Type IV damage is only 2.5% as damaging as the damage done by Type I's. This assumption has been shown to be greatly in error for some rotating components such as disks when a significant amount of throttle excursions are exercised. Often the Type III cycle can approach a similar level of damage as a Type I cycle, consequently, the K-factor assumption can be anti-conservative. When using a TAC cycle approach, the K-factors can be adjusted to better represent the damage relationships.

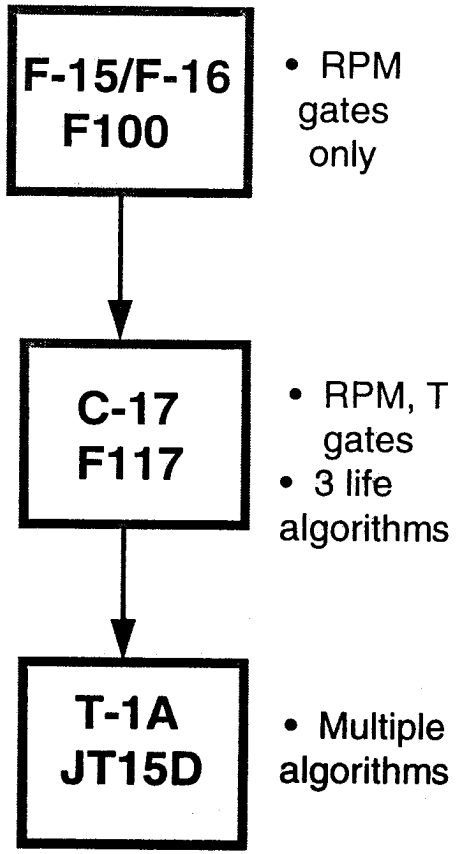
Evolution of life tracking methodology can be examined in several military aircraft operating today. The TF30 engine in the F-14 and F111 aircraft applications track life of critical rotating hardware solely using operating hours. Operating hours, as a tracking parameter, has historically been the basic parameter used for gas turbine engines since their initial introduction in aviation. The F100 engine, as used in the F-15 and F-16 fighter aircraft, in addition to utilizing hours, utilizes the cycle gate counter approach. The F117 engine in the C-17 transport aircraft has taken the gate counter approach one step further and in addition to hours and cycle gate counters, utilizes 3 relatively simplified life algorithms to monitor and track engine life. The JT15D in the T-1A trainer uses multiple (12), full-up life algorithms to track life.

LIFE TRACKING

CURRENT PROCESS IS HIGHLY SIMPLIFIED

- **Hours: Accumulated Engine Operating Hours**
- **Total Accumulated Cycles's (TAC)**
  TAC = Type I + K_3 Type III + K_4 Type IV
  Typically, K_3 = .25 K_4 = .025
- **Misc.: A/B Lights, On/Off Cycles**





Slide 4 - Deficiencies of Gate Counters

The TAC gate counting approach is based on rotor speed. Thus, non-rotating hardware such as cases and engine mounts are not adequately represented by the TAC equation. Stresses in these types of hardware are a function of pressures, temperatures, and aircraft maneuvers.

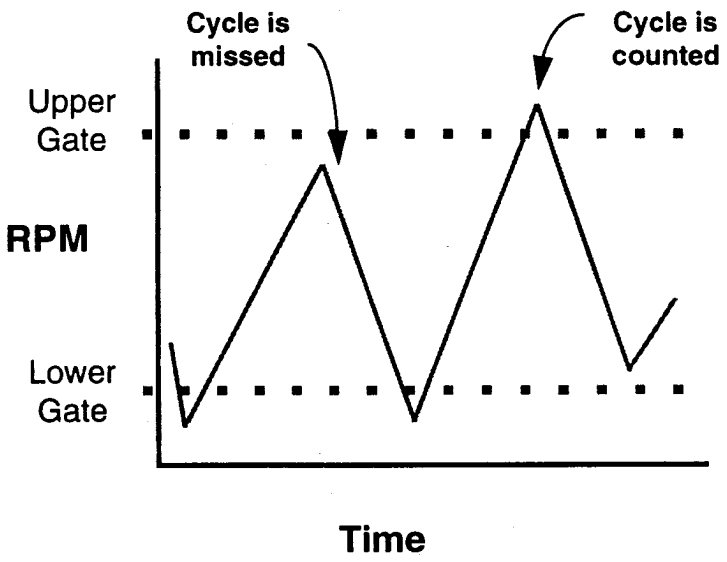
Gate counters have several deficiencies which can lead to significant errors in the determination of the amount of damage done during operation. As shown in this simplified figure, the gates are established at fixed RPM levels. Turbine rotor RPM's will trip the gate if they exceed these levels. They will not trip the gate if they don't exceed the level, thus, one cycle shown on this figure would be counted and one would not. The gate levels are typically set so that most cycles are counted, however, pilots know where these gates are and will at times avoid tripping them in the hopes that they are not using up life in so doing. In reality they are expending a certain level of life even though the gate wasn't tripped. Gate levels are set for Type I's, III's and IV's separately. Gate levels are also a function of engine model performance characteristics and will vary from engine model to engine model. This effect is accounted for in setting the gate level.

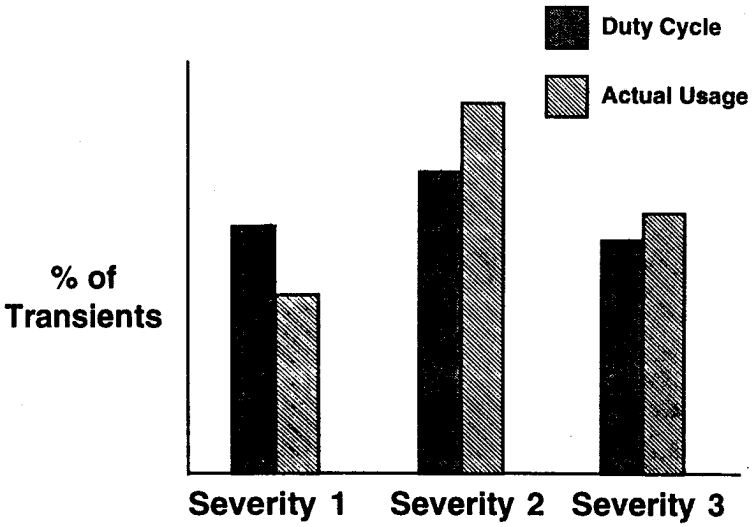
One other deficiency of the gate approach is that all cycles tripped for a given gate level are assumed to produce an equivalent amount of damage. There usually is a significant difference in the amount of damage done by equivalently counted cycles. For instance, the top gate for a Type III cycle is established at 12,500 RPM in the example shown, however, the maximum RPM can reach 13,500 RPM. Stress in rotating parts is a function of the RPM squared, thus the stress could vary by as much as 17% within this 1000 RPM range. Couple the potential errors at the maximum stress condition with similarly potential errors at the minimum stress conditions, and large errors in representation of actual stress can result. Failure modes such as low cycle fatigue and crack growth are very sensitive to changes in stress. A 5% or 10% difference in stress can result in a 50% difference in damage (life).

In addition to missing gates and counting all gates tripped as equivalent, the severity of a given RPM excursion can vary dependent upon flight condition (altitude, mach number) and the nature of the transient (thermal) response. When setting the gate level, a survey of the intended usage is usually undertaken. The gate level is then programmed into the engine electronic control prior to release for operational usage. Additional errors can arise when the actual usage is different than the assumed usage. This is often the case as we will see later.

LIFE TRACKING

DEFICIENCIES OF GATE-TYPE COUNTERS





RPM	Gate Trip
12,500	Top of Type I, III, and IV
11,500	Bottom of Type IV
10,250	Bottom of Type III's

- Max RPM = 13,500
- Idle RPM = 9,500

Slide 5 - What Life Assessments Require

What's required to accurately determine the amount of life used up for a critical component? Stress is generated in a part while operating the engine due to forces such as centrifugal loads, pressure loads, aircraft maneuvers, vibratory environment, and thermal effects. For failure modes such as low cycle fatigue and crack growth, an accurate determination of these loads at appropriate flight conditions is crucial in calculating stress in a part. A time history of stress, as it varies throughout the mission, is required to identify maximum and minimum conditions. Local temperature at critical locations of a part is also important as material properties are a function of both stress and temperature. As with stress, a knowledge of local temperature, as it varies through the mission is necessary. For some failure modes such as creep, oxidation, or erosion, the amount of time spent at different levels of stress and/or temperature is required.

Once the stress and temperature time history is known, life input parameters can be determined. These input parameters are a function of failure mode and include items such as strain range, mean stress, time at stress/temperature, stress ratio, frequency, and maximum and minimum stress/temperature. For failure modes such as low cycle fatigue and crack growth, the maximum and minimum stress levels must be identified and paired 'peaks and valleys' determined. This can be done using procedures such as the 'rainflow' or 'range paring' process.

For LCF, material life properties represented most often by S-N curves (stress versus cycles to failure) are accessed for each stress excursion. Stress/temperature time dependent failure modes must determine incremental damage for each level of stress/temperature. For crack growth failure modes, information on local geometry and material da/dN characteristics are required. The summation of the incremental damage cycles for any failure mode must then be added together to obtain a cumulative life (or representative damage amount) at any given point in time.

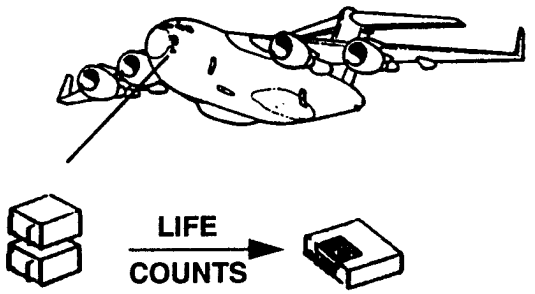
All of these factors must be included in a life algorithm if the algorithm is to be accurate. To avoid excessive engine electronic control storage requirements, it is desirable to perform as many of these functions as possible in real-time and thus on-board the aircraft. With this approach, only the damage parameter accumulated up to that point in time needs to be transferred to the maintenance/logistics data management system.

LCF LIFE ASSESSMENT

LIFE ASSESSMENT REQUIRES THE FOLLOWING

- ➨ Component Environment (Gas Path Performance Plus Localized Component Temperature)
- ➨ Localized Stress Time History
- ➨ Pair "Peaks-Valleys", Determine Strain Range for Each Cycle Pair, and Resulting Cyclic/Mission Life Capability
- ➨ Sum Up the Life Increments to Obtain a Mission Life Capability

- On-board Life Tracking Algorithms Must Retrace These Steps



Slide 6 - Life Algorithm Description

How is the life algorithm developed and what does it represents? As discussed earlier, the life of a part can be determined if the stress, temperature, and material properties are known, thus, life can be expressed as a function of stress, temperature, and material properties. Because stress and temperature are produced by engine operation, they in turn are a function of performance characteristics such as mach number, altitude, gas path pressures and temperatures, airflow rates, and rotor speeds. Substituting this functional relationship into the first equation then yields an equation where life can be expressed as a function of mach number, altitude, gas path pressures and temperatures, airflow rates, and rotor speeds. This principle, along with a life module, are programmed into the engine electronic control system or diagnostic unit. Where required for thermal response predictions, a time function is also employed.

The advanced life algorithm approach utilizes this concept. Statistical regression analysis is used to establish equations which define influence parameters and coefficients for the influence parameters. The influence parameter set used in the regression analysis is made up of all the measured performance parameters available from the engine and airframe. When performing the statistical regression analysis, only influence parameters which are measured or monitored for normal engine control purposes are considered as variables in the analysis. A time function is often employed to model the transient nature of stress and temperature which is especially important for critical rotating hardware such as disks, airseals, and hubs.

The regression analysis is performed to define influence parameters and their coefficients for the local stress and temperature. From the list of influence parameters, a subset is selected based on the degree of correlation to the regressed variable (stress or temperature). Available influence parameters typically include such items as RPM; pressures and temperatures at fan inlet, compressor exit, burner, turbine exit, nozzle; case vibration levels; oil and fuel pressures and temperatures; mach number; altitude; and g-loads. Once the regression equation is defined, checks are made based on the original design analysis to verify the accuracy of the equation.

The evolution of gas turbine engines has been in a direction which has increased the number of measured or monitored parameters as well as increasing the electronic control system capacity, all of which are favorable attributes for advanced algorithm development. The accuracy of the life algorithm is increased when the number of sensors (potential influence parameters) is increased.

ADVANCED LIFE ALGORITHM

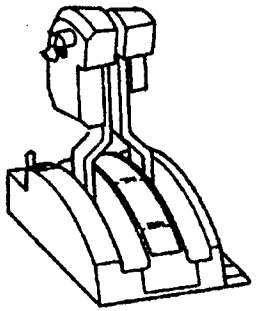
PROCESS UTILIZES MEASURED SENSOR DATA

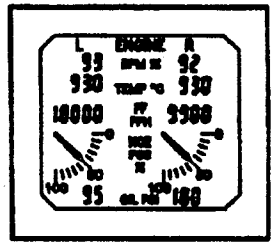
- Life = f (σ_{Local}, T_{Local} Materials Properties)

  Where: σ_{Local}, T_{Local} = f (MN, Alt, Temp Pressure, RPM, Air Flow)

  – Thus: Life = f (MN, Alt, Temp, Pressure, RPM, Air Flow, Material Properties)

- Life = C_1 RPM^2 + C_2 TT_N + C_3 PT_N + C_4 & "Life Module"





Slide 7 - Material Property Requirements

A few words on the life module element of the life tracking algorithm. Contained within the life module element are programmed subroutines to perform the stress and temperature pairing, determine incremental cycle damage, and combine the incremental cycle damage with the damage accumulated up to that point in time. A simplified stress or strain profile for a single flight (mission) is illustrated in the figure shown. Only the maximum and minimum stress conditions are plotted to simplify the figure. Additionally, the time scale has been plotted as a sequence of events instead of an actual time scale. As shown, the max and min stress level varies for each event. The minimum stress condition usually occurs after engine shutdown. The maximum stress seen in the flight can occur anywhere throughout the flight dependent upon conditions such as RPM, temperature and pressure.

There are several cycle pairings (a pair consists of one max stress and one min stress point) that occur in the mission and each significant stress range pair will have some incremental level of damage. Generally with fighter aircraft, there will be several maximum stress conditions in any given flight while transport aircraft may have only one major stress point. Similarly, fighter aircraft engines will experience many large changes in stress while transport aircraft will have only a few significant changes in stress. Life for each of these cycle pairs (max and min points) is determined independently and uniquely and thus avoids some of the inaccuracies characteristic of the TAC gate counting approach as discussed earlier.

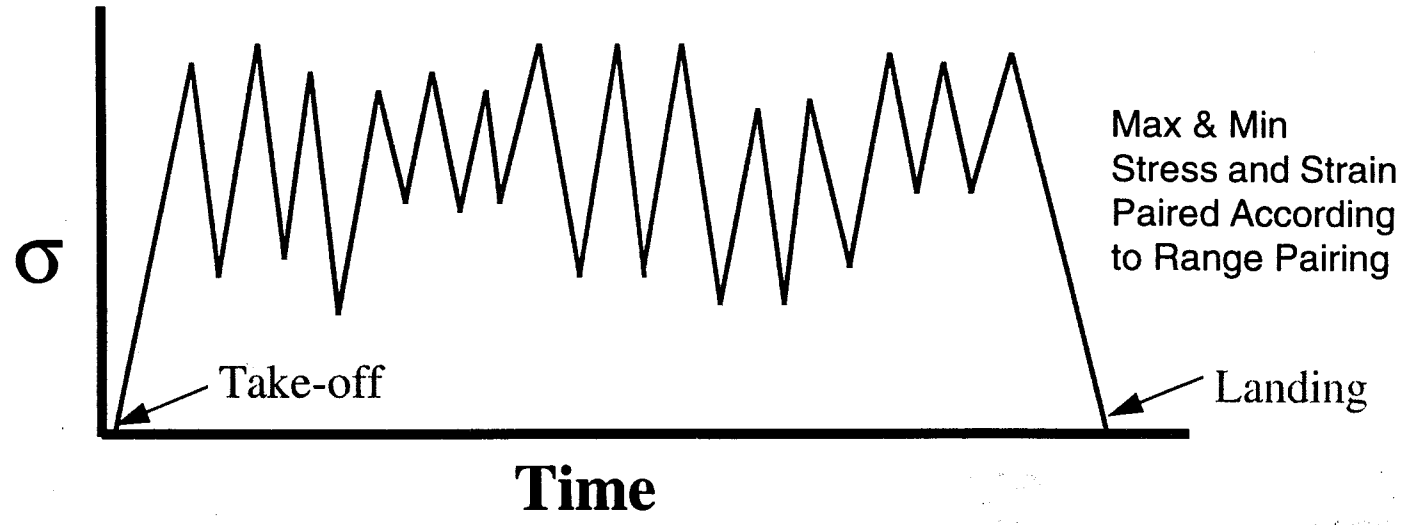
Stress pairings, as pointed out earlier, can be done by several different methods (rainflow, range-pairing, etc.). For failure modes such as LCF and crack growth where the sequence of events is important to the amount of damage accumulated, the pairing procedure must be programmed into the life algorithm. Other failure modes such as creep, oxidation, and erosion are not a function of event sequence and thus do not require that the cycle paring procedure be a part of the life algorithm.

The life property curves for the failure mode and component must be modeled in the life algorithm. Generally, this is relatively simple and in most cases the life property curves are tailored to suit the specifics of the life algorithm (in terms of temperature and stress level). Finally, a damage accumulation calculation is required. For failure modes such as LCF or crack growth, Miners rule for damage accumulation is most often used. The accumulation equation is programmed into the life algorithm as well as a procedure for adding the last flights' damage to the damage accumulated up to the start of that flight.

ADVANCED LIFE ALGORITHM

INCLUDES INTEGRATED MATERIAL DATA

- **Life Module Element**
  - **Stress/Temperature Cycle Pairing**
  - **S/N Curves Programmed**
  - **Damage Accumulation Calculation**



Slide 8 - Operational Schematic

A system schematic is provided to illustrate the previously discussed points. Engine sensor data, along with aircraft data, is measured and/or monitored for engine control purposes. Older aircraft/engine designs tend to have less available sensor data while the newer electronically controlled engine designs utilize more sensor data. As the number of sensors are increased, the advanced life tracking algorithm accuracy, and its relationship with actual mission utilization, is improved. Looking to the future, further improvements could be realized with the introduction of strain sensing devices such as high temperature/long life strain gages, thermal couples, and non-contacting stress measurement systems. The severe environment encountered in gas turbine engines prevent the long term use of these devices today.

The type and number of sensors from which to obtain data from is a function of the engine and aircraft design. Available engine sensor data typically includes: rotor speeds; engine throttle position; augmentation status; gas path temperatures and pressures; and fuel and oil temperatures, pressures, and flow rates. Additional available engine data may include vibration sensor data and nozzle position data. Aircraft sensor data is also used and includes: inlet pressure and temperature; mach number; altitude; maneuver loading (g's, N_z, etc.).

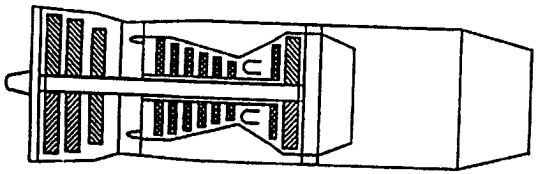
Typically, the engine and aircraft sensor data are processed within the engine electronic control and sent to the on-board engine diagnostic unit where the life algorithms reside. In some engine applications, the engine electronic control may contain the engine diagnostic processor while in other applications, the diagnostics may be a separate unit. In addition to the sensor data, clocks or timers are also employed, where appropriate, to model stress and temperature transient effects (for failure modes such as LCF and crack growth) or to sum time spent at damaging conditions (for failure modes such as oxidation, creep, or TMF).

Following flight operations, the engine diagnostic unit is downloaded using a data transfer unit. Often, a tape cartridge is used to transport the data from the aircraft to a logistics maintenance data management system for appropriate follow-on maintenance, as required. The logistics management system is typically accessible to various user groups including the engine manufacturer, systems program office, and the logistics command.

ADVANCED LIFE TRACKING

OPERATIONAL SYSTEM SCHEMATIC

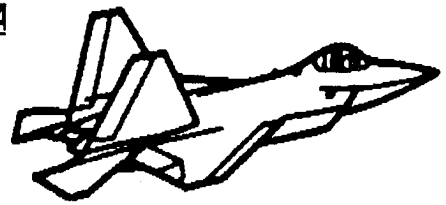
ENGINE SENSOR DATA
- Rotor Speeds (N1, N2)
- Gas Path Temp's (Tt3, Tt4)
- Gas Path Pressure's (Pt3, Pt4)
- Fuel/Oil Temp's, Pressure's
- Vibration Sensor Data



ENGINE ELECTRONIC CONTROLS
- Data Processing
- Clock

ENGINE DIAGNOSTIC UNIT
- Life Algorithms
- Life Limits Output

AIRCRAFT SENSOR DATA
- Mach No.
- Altitude
- Tt2, Pt2, etc.
- g-Loads, Nx, Ny, Nz



DATA TRANSFER UNIT

ALC LOGISTIC DATA SYSTEM

Slide 9 - Algorithm Accuracy

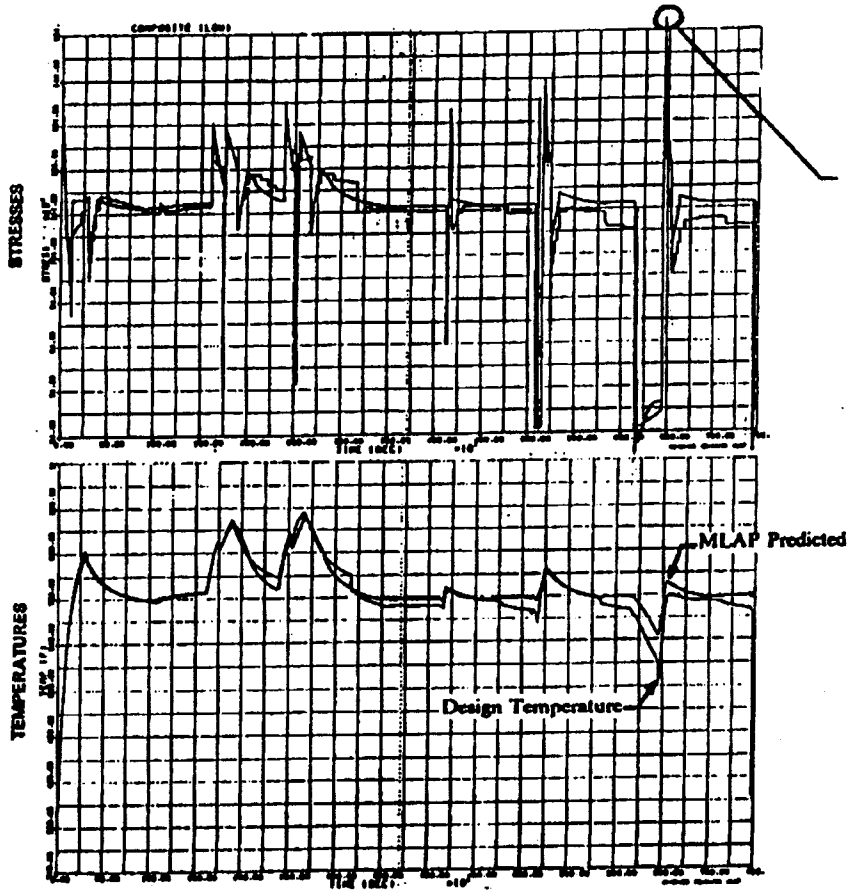
The advanced life algorithm approach discussed here is much more accurate than current life determination processes that track life with hours or TAC cycles. Typically, this advanced algorithm process yields a life accuracy within 10% of the actual life. The plot illustrates a comparison of actual versus predicted stress and local temperature, as calculated by the life algorithm. A typical mission for a transport aircraft is shown. Note the variations in max and min stress and temperature throughout the mission. Since this mission profile was for a transport aircraft, the number of significant stress pairings is small. Fighter aircraft would typically have a significantly greater number of damaging stress pairings. One thing that's very important to note is that the transient response, both in terms of stress and temperature, is accurately modeled and predicted. In this case a time function was employed to determine the transient characteristics of the stress and temperature profile.

A table of cycle pairings is shown off to the side. This mission had 11 cycle pairings with various levels of damage. Some of these cycle pairs contributed to the damage accumulation while others had no impact on cumulative life since the stress range was very small. The time shown in the table is from engine start up and the unit is in seconds. Excluding the transient characteristic, the actual time is not important to the damage calculation since the plot represents an LCF failure mode, however, the sequence of events is important.

As discussed earlier, modern engine designs are moving in a direction to increase the number of control sensors. This will have beneficial effects on the accuracy of the life algorithms. Additionally, there are industry efforts underway to improve sensor technology. Perhaps eventually, accurate, long life, high temperature strain sensors (for both steady and dynamic strains) will be available to measure local stress. Optical sensors also offer some potential for application in engine life tracking.

ADVANCED LIFE ALGORITHM

ACCURATELY CALCULATES STRESS AND TEMPERATURE



Composite A - Cycle Pairing

No.	Values at Max Strain Time	Stress	Temp	Kt	Time	Stress	Temp	Kt
1	6462.00	154217	640	1.000	7472.00	-700	70	1.000
2	6539.00	125203	743	1.000	6485.00	123160	675	1.000
3	6626.00	116537	736	1.000	6550.00	106115	675	1.000
4	7464.00	115047	714	1.000	7463.00	64838	717	1.000
5	10.00	141519	247	1.000	119.00	91475	674	1.000
6	195.00	117574	754	1.000	310.00	105374	740	1.000
7	384.00	117472	747	1.000	720.00	115454	710	1.000
8	1613.00	134352	731	1.000	1741.00	76184	817	1.000
9	1743.00	129775	804	1.000	1892.00	111080	848	1.000
10	1988.00	123542	831	1.000	2344.00	116724	717	1.000
11	2393.00	135193	737	1.000	2881.00	64838	717	1.000

LCF Life

Slide 10 - Failure Modes

So far, most of the discussion referring to life algorithms have pertained to low cycle fatigue or crack growth failure modes. Similar processes are employed to model other failure modes such as high cycle fatigue, creep, or oxidation/erosion. The life parameter used for a given failure mode varies dependent upon the consequence of failure and required follow-on maintenance actions to correct the problem.

Three life parameters typically modeled include: durability/economic life; inspection intervals; and maintenance intervals. Durability/economic life is synonymous with the design service life. This is the period of time that the component is expected to be fully operational, does not inhibit safety, reduce mission effectiveness, or present a durability limitation. Typically, parts are retired from service once the durability/economic life limit is reached. Thus, an advanced life tracking algorithm can be established which tracks the amount of usable life left prior to retirement of the component. In some applications, parts are used past their life limit (Retirement-For-Cause). In these cases, more frequent inspections are performed and the need for a more accurate life tracking methodology is crucial to assuring fleet safety.

Inspection intervals are the period of time between scheduled maintenance events. For fracture critical hardware, the inspection interval will indicate when the parts need to be returned to the depot for non-destructive inspections (typically using zyglo, eddy current, or visual inspection processes). An advanced life tracking algorithm can be set up for crack growth failure modes to indicate the amount of time before the next inspection is required.

The third category of life parameter, maintenance interval, is utilized to track failure modes which are difficult to determine based on projected usage. As a result, forecasting a scheduled inspection period will result in an overly conservative estimate, however, it is desirable to allow the part to remain operational as long as usable life remains in the part. The maintenance interval parameter is especially useful for application in a flexible life algorithm as discussed later.

Functional parameters important to each failure mode are also shown, for example as described earlier, stress, temperature, and material properties are important to the determination of low cycle fatigue. Similarly, parameters important to high cycle fatigue are the number of vibratory stress cycles which occur at resonant conditions. Resonant conditions typically occur over a fairly narrow frequency range, thus a knowledge of the resonant frequency, as it pertains to operating conditions such as RPM for rotating parts, is also required.

ADVANCED LIFE TRACKING

CAPABLE OF MODELING ALL FAILURE MODES

Failure Model	*Life Parameter*	*Functional Parameter*
Low Cycle Fatigue	Durability/Economic Service Life	σ, Temp, Mat'l Properties, Cycles
Oxidation/Erosion	Durability/Economic Service Life, Maintenance Interval	Time, Temp, Mat'l Properties
High Cycle Fatigue	Inspection Interval	# of Cycles/RPM Band
Fracture Mechanics	Inspection Interval	σ, Temp, Mat'l Properties, Cycles
Creep/Stress Rupture	Durability/Economic Service	Time, σ, Temp, Mat'l Properties
Wear, Bearing Life	Durability/Economic Service Life, Maintenance Interval	Time, Load, Temp, Mat'l Properties

Slide 11 - Life Tracking Options

There are three different options that could be pursued using the advanced life algorithm approach. Each option increases the complexity of the algorithm and the difficulty in the logistics management of the engine maintenance data. The first option would be to simply improve the basic TAC equation. This would be accomplished by developing a single advanced life algorithm for the most limiting component and failure mode in the engine. When the life for this one component is used up, the engine would be pulled for maintenance or inspection. This is essentially what is done currently for most engines, however, the generic TAC equation is used instead of an advanced life algorithm.

A second option would be to provide a single life tracking parameter for each major module of the engine, thus you would have one for the fan, one for the compressor, one for the turbine, etc. The module tracking parameter could be based on a composite of the most limiting parts/locations in the module or just the one single most limiting part in the module. In either of these cases, when a life limit is reached the engine would be removed from the aircraft and either the life limited module or complete engine would be refurbished, retired, or inspected based on the failure mode and remaining life left on the other modules.

The third option would be to develop multiple life tracking algorithms for all critical components and failure modes. All tracking parameters would be monitored and maintenance driven by the component with the lowest amount of remaining life. This option, although preferred from an engineering perspective, could be a significant logistics burden if not automated and computerized.

One thing that needs to be tied into the logistics maintenance system is component serial number. Parts or modules are often interchanged between engines during intermediate or depot repair/inspections and thus traceability of part life by component serial number and not engine number is required. The individual part serial number must be associated with the life of the part and this information must be accessible and transferable within the logistics maintenance date system whenever the part is removed for maintenance purposes, since the part may be reinstalled in another engine with a different usage history.

ADVANCED LIFE TRACKING

PROVIDES MULTIPLE TRACKING OPTIONS

1. Improved Accuracy in TAC's, Hours, Etc.

2. Module Tracking Parameter
   - Multiple Locations/Parts Algorithm)
   - Limit Based on Lowest Life Component in Module

3. Multiple Component Tracking
   - Design Service Life (LCF, Buried Flaw)
   - Inspection Interval (Fracture Mech.)
   - On-Condition Service Indicator (TMF, Wear, Erosion)

Slide 12 - Field Problem Resolution

The advanced life tracking algorithm approach can be a valuable tool in the resolution of field problems. The field problem resolution process can be very complex in modern gas turbine engines. The engine development approach utilized in today's engine designs generally account for most of the failure scenario's common to the product. A lessons learned design approach generally prevents repetition of previously experienced failure modes, however, not all operational flight conditions can be evaluated during engine ground testing and some problems inevitably slip through. As a result, the failures most likely to be encountered will be highly complex and multi-dimensional requiring considerable expenditures of manpower and funding to resolve and manage in the field. Because of the complex nature of the failures encountered, understanding the cause of the failure and then redesigning to correct the problem can be extremely challenging.

Resolution of the more critical field problems can be a very lengthily process and is initiated with identification of the problem and driving mechanism. Once an understanding of the problem is achieved, redesign and qualification of the hardware is undertaken. In the mean time, logistics plans are developed to manage engines with the problem hardware. Once an effective redesign is verified, production of field retrofit hardware is initiated. It is not uncommon for this portion of the process to take 14 to 16 months, and sometimes, much longer. The field retrofit may take years depending upon the approach taken, whether it is opportunistic or forced and if its a very serious failure mode. The size and distribution of the fleet can also impact the time required to completely retrofit all engines.

ADVANCED LIFE TRACKING APPLICATIONS

ASSISTANCE IN FIELD PROBLEM RESOLUTION

- **Field Problem Resolution Is Lengthy:**
  - **Identify Problem/Driving Mechanism**
  - **Redesign/Re-Qualify to Eradicate Problem**
  - **Fabricate Revised Parts, Then Retrofit in the Field**

- **Typical Field Resolution Takes a Minimum of 14-16 Months to the Point Where Retrofit Can Start**

- **Retrofit May Take Years Depending On Option Selected (I.E., Forced or Opportunistic), and On Fleet Size**

Slide 13 - Risk Level

Much of the risk associated during a long retrofit process is driven by variations in aircraft usage. To obtain a zero risk level would require grounding the fleet. This option, whether for fighter or transport aircraft, is usually not acceptable to the customer so some level of risk must be assumed. The level of risk will vary from base to base and even aircraft to aircraft depending upon how the airplanes are being used.

Shown in the figure are two mission profiles of altitude versus time for a fighter aircraft. The mission profiles are taken from two different bases. Both missions are the same - Surface Attack, however, the way the aircraft is flown varies drastically between the two bases. Interestingly enough, several pilots having flown at both air bases clearly stated that both locations fulfill the same role and fly identical sorties, i.e., predominantly surface attack, in a similar fashion. Further analysis showed significant variations, due to base location, geographical/local restrictions and proximity to the practice ranges. In one case the aircraft cruised at 15,000 to 20,000 feet, while in the other case the aircraft had to cruise above 30,000 feet to reach far away ranges. Additionally, one base typically practiced 6 bomb deliveries while the other typically had 12 bomb deliveries, the difference being driven by range availability, a function of how many squadrons use the same training range. Correspondingly, the number of rotor speed excursions for these two bomb delivery missions are different by a factor of 2 and thus the amount of damage accumulated during in each of these missions could vary significantly. These mission differences can significantly affect life. Other changes, some very subtle, can also have a significant impact on engine operating conditions. For instance, higher cruise segments require longer climb times and longer descents, and also result in different cruise regimes. Longer low-level operations at one base (due to higher availability of low-level routes) can also have significant life impacts. Internal engine pressures, temperatures, and rotor speeds, therefore, exhibit significant differences due to these different flight operations.

These mission differences can have a tremendous impact on life and setting a maintenance interval or scheduling a retrofit based on an assumed usage could have serious consequences on risk.

ADVANCED LIFE TRACKING APPLICATIONS

RISK LEVEL DRIVEN BY MISSION DIFFERENCES

- "Zero Risk" Would Require Grounding Fleet as soon as Problem is Identified... Not Acceptable!
- Risk Level Driven by Base to Base, Aircraft to Aircraft Mission Variations...

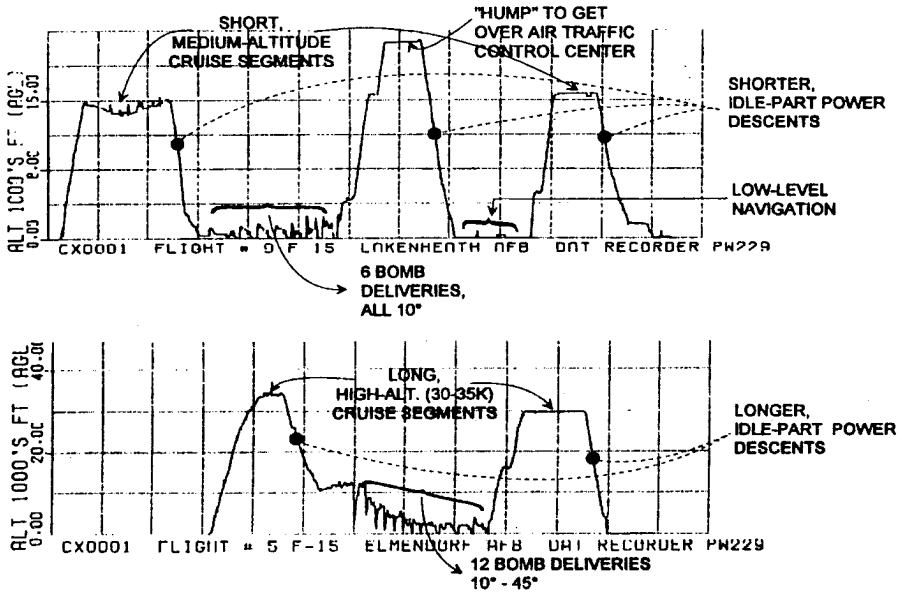


Illustration shows a typical Surface Attack mission as executed at two different bases.

Slide 14 - Flexible Life Tracking

At this point we would like to introduce the concept of "flexible" life algorithm. The term "flexible" implies an algorithm similar to the ones described previously, but of a temporary nature. Its primary use is to address a specific, short-term hardware deficiency after identification of a durability problem, but prior to completion of a field retrofit program to resolve the durability issue.

How could a flexible life tracking approach benefit the field problem resolution application? A flexible life tracking algorithm could be established to model the field failure mode and track damage as a function of actual engine usage. Thus a part due for retrofit could be flown longer, or removed earlier, based on individual aircraft usage, as opposed to depending on an anticipated fleet average or 'worst case' usage projection to force a retrofit. The benefit of this approach is a significant risk reduction while flying defective parts awaiting retrofit as well as improved asset management by allowing parts to stay in the field until their life is used up.

The life as determined by the algorithm would only be used on a temporary basis until the engines with the defective parts were retrofitted. The algorithm would be similar to those discussed earlier for use in tracking life limited parts and determining inspection intervals. To achieve this capability requires that the engine electronic control be capable of being reprogrammed on-wing as well as in the existing engine maintenance database. On-wing reprogramming (or at lease at the intermediate level) of engine electronic control or diagnostic units is now a reality on recently deployed USAF engines (as an example, Pratt & Whitney's PW-229 engine, powering F-15's/F-16's), and has proven to be relatively easy. The ground based maintenance system also has to have the flexibility to incorporate these "temporary" life algorithms, a condition which is currently not the case. This will probably prove to be a bigger (though certainly not insurmountable) problem. The main ground data base containing cycle/time history for all serialized engine parts is by its nature large and unwieldy, and has been in evolution over decades of jet engine operations. Modifications, even simple ones, to an existing engine data base are lengthy, thus significant changes to the database will be required to accommodate our proposed flexible life tracking approach.

ADVANCED LIFE TRACKING APPLICATIONS

INTRODUCING "FLEXIBLE" LIFE TRACKING

➡ **What It Is:**

- **Set of Temporary Life Tracking Algorithms Designed to Track Damage.**
- **Algorithms Similar to Advanced Algorithms Used to Track Life Limited Components.**
- **Requires Capability to Re-Program Logic Unit "On-Wing", As Well As Pre-Structured Ground Data Base.**

Slide 15 - Application Scenario

How could this concept be utilized in a fairly simple failure scenario? Suppose there were some changes made to an existing weapons system application. Further suppose that the changes were made to an aircraft inlet which generated a vibratory excitation source coincident with the resonant frequency of a fan airfoil. The coincidence of the excitation source with the airfoil resonant frequency is illustrated in a Campbell diagram, as shown here. The Campbell diagram is commonly used to illustrate potential vibratory characteristics of engine hardware. The diagram plots frequency versus engine rotor speed. Natural frequencies of the component are plotted as a function of rotor speed. In this example, the horizontal dashed line is shown to illustrate the natural frequency of the 1st bending mode of the part. Note the 100 RPM band surrounding the max RPM condition. Typically, resonant conditions with high vibratory stress occur over a narrow frequency range. High vibratory stresses, and consequently fatigue damage, are only encountered while operating within this band.

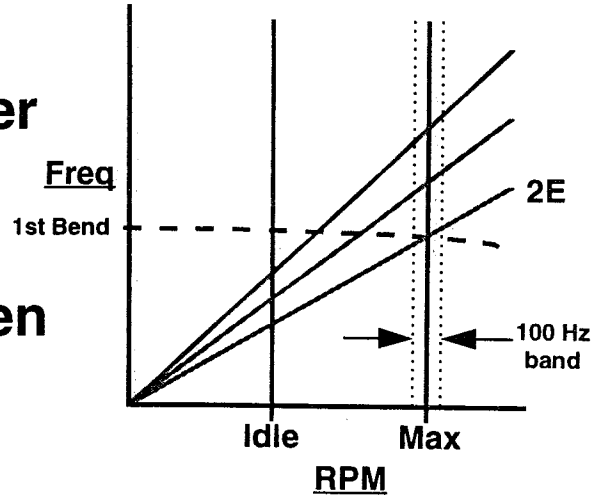
The dashed line represents the airfoil resonant frequency and the lower diagonal line represents the excitation source. The lines cross at max power which usually means that a significant level of energy is available to drive the resonance. In this case lets assume that airfoil cracking is occurring due to high cycle fatigue. A need exists to replace the blades with new blades having a higher natural frequency thus avoiding coincidence with the excitation source at high power settings. In the mean time, advanced life algorithms are used to count the number of stress cycles occurring while operating at the resonant condition. The algorithms are set up to assure that the total number of cycles accumulated, with appropriate safety margin, does not exceed the vibratory endurance limit of the airfoil.

ADVANCED LIFE TRACKING APPLICATIONS

APPLICATION SCENARIO

- **Manage Field Failure eg.: Fan Blade Cracking Due To 2E Driver Introduced By Redesigned Airframe Inlet**
  - **Need to Set Safe Time Between Inspections**

Campbell Diagram



- **Solution: Model Developed to Calculate Accumulated Cycles at Resonant Conditions: Cycles = Σ (Freq X Time in Frequency Band).**
  - **When Cycles = $\frac{10^9 \text{ cycles}}{\text{Safety Factor}}$, Perform Borescope Inspection**

Slide 16 - How Could a Flexible Life Tracking Algorithm Have Helped

How could a flexible life tracking algorithm have helped? HCF failures like this typically occur after enough time is spent operating at a band of rotor speed where the excitation crossing is coincident with the resonant frequency. This band is usually narrow and may span only 50 to 100 RPM. Forecasting how much operation will be spent in this frequency band, and then setting maintenance accordingly, usually results in overly conservative scheduling of maintenance or inspections.

A flexible life tracking approach would solve this problem. The algorithm would be based on only the actual time spent in the RPM band of concern. The algorithm logic would be programmed such that rotor speed, which would be monitored by speed sensors, would sum the cycles accumulated at resonance. Since the failure occurs only after an significant number of stress cycles were accumulated on the airfoil and the resonant frequency of the airfoil occurs over a narrow RPM band, the life algorithm is structured to count cycles only within the RPM band. Once the number of cycles is reached, the airfoils could be inspected or replaced. In so doing, each engine would be pulled for maintenance at the correct time thus avoiding costly and conservative assumptions on usage. The average engine would no longer be penalized by the worst case utilization assumptions which would normally be required to provide overall fleet protection.

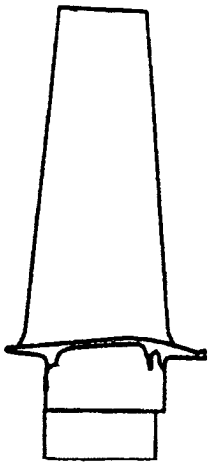
Use of an advanced life tracking algorithm minimizes the impact on flight operation, lowers the logistic management burden, and reduces maintenance costs, all of which are beneficial to the customer and the manufacturer.

And last but not least, this approach provides a significant risk reduction, by forcing hardware retirement based on individual aircraft usage, rather than fleet statistical averages.

ADVANCED LIFE TRACKING APPLICATIONS

HOW COULD "FLEXIBLE" LIFE TRACKING HAVE HELPED?

- Failure Due to Resonance Occurs After Excessive Time in Given Rotor Speed Range (Typically Less Than 100 RPM), Making It Hard to Forecast Time Spent in Range, Leading to Conservatism
- "Flexible" Life Tracking Simplifies Process:
  - Inspection/Replacement Based on Actual Time Spent in Resonance Range
  - "Average" Engine Is No Longer Penalized by "Worst Case" Utilization Factors Which Would Otherwise Be Required to Protect the Fleet.
- Minimizes Impact on Flight Operations, and Reduces Maintenance Costs



Slide 17 - Application Scenario - LCF

As another example, suppose a limited number of rotor disks are manufactured from a batch of defective material which exhibited LCF property degradation. Also assume that from post-production laboratory testing, it was determined that the debit resulted in a 2:1 decrease in LCF capability over the normal condition. In this failure scenario, the batch of defective material has a LCF life debit when compared to material normally used to manufacture other disks prior to the defective batch production. Also assume that only a limited number of parts were manufactured from this defective batch of material and that the parts are serialized. Disks are fracture critical components, consequently, the parts are serialized and tracked, thus their distribution and location among the fleet is known. Thus the aircraft fleet has disks with good material and disks with defective material and part location can be traced by serial number.

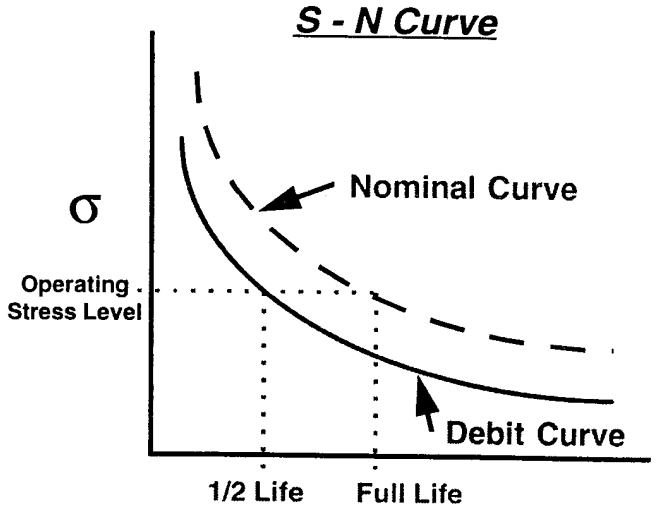
Illustrated in the figure is an S-N curve which shows both the nominal and debit curve. Operating stress levels were not influenced by the material fatigue debit thus the original stress analysis is still suitable to develop a life algorithm from, if one didn't already exist. To assist in the field management of the debited disks, an advanced life tracking algorithm is developed which employs the reduced material property curve. The life algorithm is programmed into the engine controls/diagnostic unit of those engines which have the debited disks. The engines with these disks are then managed to account for the debited material properties and would be pulled at the appropriate point in time.

Without the advanced life tracking algorithm approach, a conservative assumption of usage would have to be made to protect the fleet usage extremes. With an advanced life tracking algorithm, confidence in the ability to track actual component life would allow better management of assets with reduced risk. If the engines with these debited life disks were being used at an accelerated usage rate, the risk would be lowered by employing the life tracking algorithm. If life was not being used up as fast, the engines could stay in the field longer and the necessity to obtain spare parts and retrofit the field would be lowered.

ADVANCED LIFE TRACKING APPLICATIONS

Potential Scenario

- **Manage Fleet Assets eg. LCF Life Debits Found To Exist Due To Material Processing Problems**
  - **Batch Limited**
  - **Need To Reduce Individual Disk Service Life To 1/2 Original Calculated Value**



→ **Solution: Life Tracking Algorithm Developed, Accounting for Material Debit for Affected Disks Only.**
- **Disk's With Debits Pulled at Correct Time Thus Affording Safe Operation and Full Disk Usage to 1/2 Life Period.**

Slide 18 - Concerns

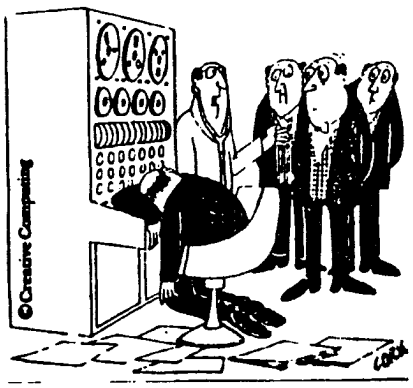
The technology exists today to provide as much data as necessary to safely track life of gas turbine engines. There is one problem and that is, can the logistics/maintenance community integrate the larger amount of data that could be delivered by advanced, multiple life tracking algorithms, some of which may be of a temporary nature (i.e., "flexible" algorithms). The answer currently is no. Besides the engineering interest to generate data, there are requirements to maintain some level of simplicity in the tracking parameters. Certainly using only one or two numbers to track the life of an entire gas turbine engine is enticing from a maintenance management perspective but some penalty in terms of life cycle cost or risk is paid for the simplicity. To employ the full capability of the advanced life tracking algorithm approach will require a different mind set from the maintenance community. The jump from the current way of doing business to this advanced approach is similar to that taken a number of years ago when the switch was made from hours to TAC's. Some logistics difficulties were encountered however, everyone is now happier and accustomed to the TAC cycle approach.

Specific areas of concern to the logistics community include whether the current ground based data systems are capable of handling the advanced approaches discussed here and whether frequent on-wing reprogramming is both practical and desirable. Additionally, whatever approach is taken, life tracking procedures must maintain a clear, fool-proof tracking system for day-to-day utilization at the base level.

Designing a new, complex (but easy to use) life tracking system as proposed here requires a long term, multi-organization effort that must be well thought through, to ensure that work from all disciplines is well integrated thus maximizing benefits for the end user.

ADVANCED LIFE TRACKING

Concerns



"He died from an overdose of data..."

- **Higher Complexity Requires Different Mind-Set From Maintenance Community**
  - **Jump Is Similar to What Was Required When Life Tracking Went From "Hours of Operation" to Today's "Type I, III, IV, and TAC" Cycles in Fighter Community**

- **Logistics Concerns:**
  - **Modify Ground-Based Data System to Handle Flexible Life Tracking**
  - **"On -Wing" Re-Programming Capability Desirable**
  - **Clear, Fool-Proof Tracking for Day-To-Day Utilization at the Base Level.**

Slide 19 - Benefits/Uses

This presentation has alluded to some of the benefits which could be realized by the advanced life tracking algorithm approach. Potential benefits include:

Less Spare Parts: Less spare parts requirements since parts will be replaced or inspected at the correct time, not at some forecasted time based on assumptions regarding usage or fleet worst case conditions. Each aircraft is used differently, just as each car is driven different. Now this usage variation can be accounted for correctly. Even within an engine, the life utilization rates vary from part to part. If the aircraft is being used for high speed, low level flight with minimal throttle cycling, parts such as turbine airfoils and combustor liners will experience life utilization rates much higher than fan or compressor disks. Similarly, if the aircraft is being used for air-to-air combat exercises which have multiple throttle cycling, then parts driven by rotor speed excursions such as disks would have utilization rates much greater than turbine airfoils.

Safer Engine Operation: Another benefit realized by the advanced life tracking algorithm approach is a safer engine operation. The increased safety is achievable due to the improved accuracy of the life algorithm and their ability to distinguish between life utilization rates from part to part. Parts would be pulled at a rate determined by specific usage rather than assumptions based on projected (worst case) usage and cyclic variability. Safer engines would also result through the use of the advanced life tracking algorithm approach as applied to field failure management.

Warranty Benefits: Potential warranty benefits to both the customer and the contractor could be realized by defining the engine warranty based on multiple, module-specific advanced life tracking algorithms instead of the conventional hours or TAC's tracking parameters. Currently, if a part failure occurs prior to the hour or TAC limit, then a warranty claim can be filed by the using command. There may be good reason for the part failing earlier than anticipated (prior to the life as tracked by hours or TAC's is reached). These reasons could include higher hot time or a greater number of rotor speed excursions. Similarly, if the part failed at two-thirds its expected life, then the life algorithm could be pointing out some deficiency such as a bad batch of material or a design problem. With more life tracking parameters available, a better understanding of the actual usage is achieved and determining the responsible party as it pertains to warranty claims is improved.

ADVANCED METHODOLOGY

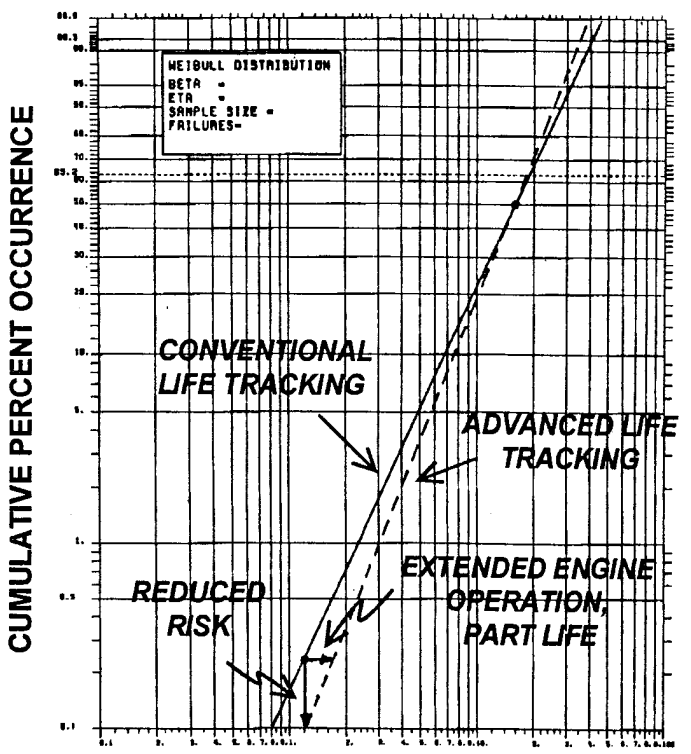
BENEFITS/USES

Benefits:

- **Less Spares - Full Life Usage**
- **Safer - Parts Pulled at Actual Limit**
- **Warranty Paid Based On Contractor Shortfalls**
- **Prevents "Tricking" System**

Uses:

- **Track Service Life**
- **Define Maintenance Interval**
  - **Scheduled Inspections**
  - **Manage Field Problems**



Slide 20 - Summary

The advanced life tracking algorithms offer a sophisticated tracking technology which couples measured sensor data with analytical techniques to improve life management of engine components. The sensor data is available from both the engine and aircraft and included rotor speeds, temperatures, pressures, and aircraft speed, altitude, and maneuver data. The improved life management capability is achieved through the use of advanced life algorithms which have much better accuracy than previous life tracking systems. These advanced life algorithms can also greatly expand the component coverage and applicability of failure modes than possible with the previous systems. The life algorithms are programmed into the engine electronic control or diagnostic unit. Life is calculated in real-time and can be downloaded to the logistics maintenance database for further processing and decision on follow-on maintenance actions, as required. Additionally, the technology provides an opportunity to improve management of fleet assets in the event of unanticipated field problems which inevitably arise once the engine is deployed. This capability will require the flexibility to reprogram the electronic control, preferably with the engine installed in the aircraft. The flexible life tracking approach will provide enhanced risk management of field failures in addition to allowing parts to remain in the field until their actual life is used up, as based on the actual individual aircraft utilization rate.

Because the advanced tracking techniques described here out weigh the capacity of the current ground-based data tracking, there are concerns as to whether the current logistics management institution can effectively utilize the amount of data that this technology can provide. At the very least, re-vamping of the logistics ground-based data system will be required. Our experience in this field has shown that simplicity is a must to ensure fool-proof operations. This certainly does not preclude the use of massive amounts of data (such as can be generated by our proposed approach to support multiple life limits either at the module or part level.) But this more sophisticated system will have to be well engineered from the ground up to ensure that every end-user organization can maximize benefits without being overwhelmed by its complexity.

If this technology is effectively utilized, there will be benefits to both the customer and the contractor. These benefits arise from improved safety and full life utilization of tracked components, and will result in substantial dollar savings.

TURBINE ENGINE LIFE TRACKING

SUMMARY

- Algorithms Offer Sophisticated Tracking Technology Coupling Measured Sensor Data with Analytical Techniques
  - Life Management
  - Field Problems
- Technique Can Be Adapted to Minimize Risk While Resolving Field Problems
- Technology Exists Today, However, Additional Steps Are Required to Allow Logistics Management of This Capability
- Benefits Contractor and Customer
- Improved Safety, Full-Life Usage

SESSION IV

STRUCTURAL MATERIALS/INSPECTION

Chairman: ***T. Cooper*****, WL/MLS**

EFFECT OF TEST PARAMETERS ON THE CORROSION FATIGUE CRACK GROWTH OF AIRCRAFT STRUCTURAL MATERIALS

D. W. Hoeppner and T. Goswami
Quality and Integrity Design Engineering Center
Department of Mechanical Engineering
University of Utah
Salt Lake City, UT 84112.

ABSTRACT

This paper examines the effects of test parameters on the corrosion fatigue crack growth behavior in aircraft structural materials. Test parameters such as stress ratio, frequency, hold time, temperature, pH level of the media, and other parameters are known to alter the corrosion fatigue crack growth rates in aircraft structural materials. It is shown in this paper that there are numerous laboratory test variables which affect the crack growth rates, which in an operating environment of an aircraft are not characterized. Therefore, additional compilation of such data will help establish inspection intervals and assure reliability of safety procedures by assuring availability of appropriate data.

INTRODUCTION

Study of corrosion and corrosion fatigue in aircraft structural materials is very important since corrosion and corrosion fatigue have emerged as one of the potential failure mechanisms in military and commercial fleets. Aircraft usage parameters such as stress and spectrum types, time in each flight segment, environment, corrosivity of the media, temperature and material parameters such as joint characteristics and presence of corrosion in the joints are known only to a limited extent. Component life assessment and damage growth rate prediction is very difficult.

A schematic diagram shows various parameters of fleet operating conditions in Fig. 1. It is evident that quantitative discretization of these parameters is a complex issue since operating conditions change with respect to the individual aircraft. Therefore, research in corrosion fatigue crack growth behavior in aircraft structural materials within the extremity of test parameters and failure mechanisms are very important to simulate and correlate the service failure with laboratory tests. Since the crack or corrosion detection depends upon the crack size or percentage material loss respectively, selection of inspection intervals must be made with extreme care. Individual joint characteristics, fretting induced microscopic cracks aided by corrosion, linking by multiple site fatigue damage (MSFD) and growth of such cracks are known to a limited extent (1) that they will grow at a faster rate than "long" cracks, crack growth equations under such situations are unknown. In addition, effects of prior corrosion on crack growth characteristics also are very important.

Local dissolution in a material causes corrosion. Local dissolution, passivation and repassivation characteristics of the material determines the rate of corrosion. The corrosion rate can be enhanced by the pH level of the media (2) and chloride ion concentrations (3). Test parameters such as load, temperature, strain rate or frequency, presence of hydrogen and other parameters that interact with localized dissolution and passivation characteristics in a material may accelerate the corrosion rates. Interactions among the electrochemical parameters, mechanical parameters, material parameters, time and favorable texture may cause either embrittlement or cracking, growth of which is determined by localized conditions by either corrosion, or when mechanical parameters interact by corrosion fatigue. The synergisms of various processes in the corrosion

fatigue crack growth behavior in aircraft structural materials is not very well understood as there are several potential mechanisms.

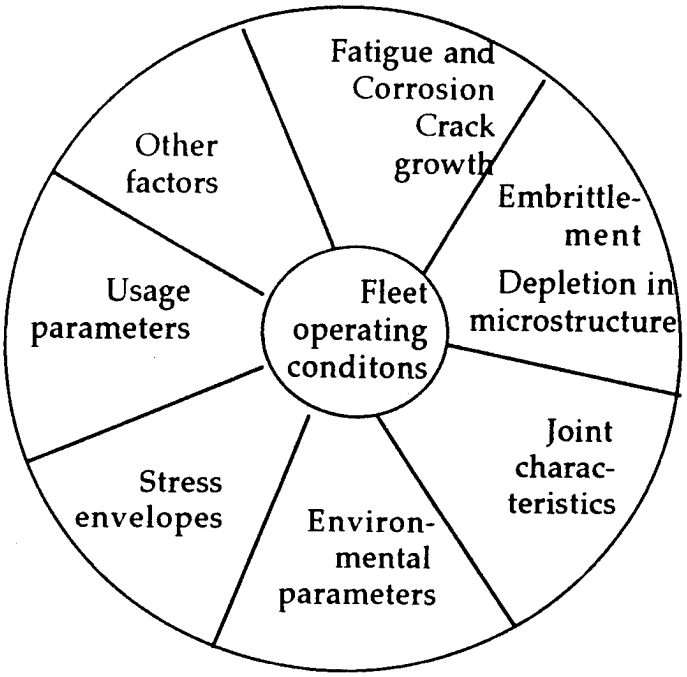


Fig. 1. Schematic operating envelopes of aircraft or fleets.

Fatigue crack growth rates vary in the presence of water in the environment or water vapor pressure, under which a sigmoidal trend in the crack growth rate data is exhibited (4). The environmental sensitivity of a material can be altered by proper selection of test parameters such as crack size, frequency, stress ratio and material parameters such as microstructure and composition. However, in an aircraft the growth of "small" cracks from the joints and the parameters that alleviate environmental sensitivity cannot be altered. Early work reported by Hoeppner and Hyler (5) show that fatigue life in 2024-T351 and 7075-T6 aluminum alloys improved with exposure in vacuum of nominally 10^{-6} mm Hg. With the increase in the exposure time in vacuum the fatigue life improved further.

The effort presented herein this paper was directed toward the study of crack growth behavior in aircraft structural materials as influenced by material/environmental/load/time interactions. Sustained load conditions were evaluated as they affect the corrosion fatigue crack growth behavior in materials which experience sustained loading; for example, that result from an aircraft on the ground with the weight resting on the landing gear for an extended period of time. Therefore, materials studied in this paper were based on the following considerations:

1. the materials are representative of those used in applications such as aircraft wings, fittings, attachment and landing gear components,
2. materials selected represent the major three aerospace materials namely; aluminum, titanium and steel, and

3. materials selected represent those that are used and exist on the fleets at the present time.

MATERIALS AND TESTING:

The materials studied together with the test matrix employed are summarized in Table 1:

Table 1. Summary of materials, alloy types and test conditions examined.

Materials	**Alloy types**	**Test conditions**	**Environment**	**Applications**
Aluminum alloys	2024 T-351	Trapezoidal and conjoint cycles	air and 3.5% NaCl.	wing and skin applications
	2324- T39	same	same	
	7075-T651 7150-T651 2024-T851 2124-T851	same same sustained load CG and FCG Fretting corrosion	same same high humidity and 3.5% NaCl air and 3.5% NaCl	
Titanium alloys	Ti-6Al-4V (RA)	sustained load CG and FCG	high humidity, 3.5% NaCl and sump water	used as fittings attachments doublers etc.
	Ti-6Al-4V (βA)	Sustained load CG and FCG	high humidity, 3.5% NaCl and sump water.	
	Ti-6Al-6V-2Sn (STOA)	fatigue crack growth	humid air and 3.5% NaCl	
Steel	18Ni-Mar-aging Steel	Sustained load crack growth and FCG	high humidity and 3.5% NaCl	landing gear applications

Due mainly to the volume of data that are associated with the above materials it may not be possible to present data, but, this paper will discuss critically the crack growth

behavior under different test conditions. Interested readers are recommended references for more details (6-9).

Load Sequence Parameters for Test Matrix:

The crack growth tests were conducted in air and other environments for the following three major conditions discussed below:

1. Continuous fatigue crack growth tests:

Crack growth tests were conducted under continuous fatigue conditions. Table 2 describes the materials and other details investigated.

Table 2: Summary of continuous fatigue test conditions.

Material	Test type	specim-en type	Stress ratio	freque-ncy	dry air	high hu-midity	3.5% NaCl	sump water
2024-T851	FCG	3/4" WOL[1]	0.1	0.1, 1, 2, 10, 20 Hz		most tests	13 tests	
		PTC[2]						
		CCT						
18 Ni Maraging steel	FCG	WOL	0.1	0.1, 1 and 10 Hz		one test	3 tests	
Ti-6Al-6V-2Sn (STOA)	FCG	WOL and CCT	0.1 and 0.5	0.1, 1 and 10 Hz	2 tests	9 tests	12 tests	
Ti-6Al-4V (RA)	FCG	WOL, PCT and CCT	0.1 and 0.5	0.1, 1 and 10 Hz	1 test	11 tests	12 tests	6 tests
Ti-6Al-4V beta annealed	FCG	WOL and PCT	0.1 and 0.9	0.1, 1 and 10 Hz	4 tests		6 tests	4 tests

2. Sustained load fatigue crack growth tests:

A limited number of sustained load crack growth (SLCG) tests were conducted. A summary of which is provided in Table 3.

Table 3: Summary of sustained load test parameters employed.

Material	Test type	specim-en type	Stress ratio	freque-ncy	dry air	high hu-midity	3.5% NaCl	sump water
2024-T851	SLCG	CT				one test	one test	

[1] WOL: wedge opening load specimen configuration.

[2] PTC: Part through cracked specimen geometry.

18Ni Maraging steel	SLCG					2 tests	3 tests	
Ti-6Al-6V-2Sn (STOA)	SLCG	CT				2 tests	2 tests	2 tests
Ti-6Al-4V (RA)	SLCG	CT				2 tests	2 tests	2 tests
Ti-6Al-4V Beta annealed	SLCG	WOL					one test	one test

3. Ripple fatigue crack growth tests:

Conjoint major-minor waveforms were used to investigate the ripple fatigue crack growth (RFCG) behavior in fatigue and corrosion fatigue conditions in a number of aluminum alloys. A summary of test parameters utilized are tabulated in Table 4.

Table 4: Summary of ripple fatigue crack growth test parameters employed.

Material	Test type	specim-en type	Major Stress ratio	Minor stress ratio	Freque-ncy major	Freque-ncy minor	ampl-itude ratio	cycle ratio
	RFCG	CT	0.1	0.5, 0.9	0.2Hz	20 Hz	0.56-0.11	100
	RFCG	CT	0.1	0.5-0.9	0.2 Hz	20 Hz	0.56-0.11	25

Tests were conducted on 2024-T351, 2324-T39, 7075-T651 and 7150-T651 aluminum alloys. The CT specimens were machined such that crack growth occurred in the T-L orientation.

TEST PROCEDURE:

All the tests outlined in the Tables 2-4 were in accordance with standard procedures described in ASTM E 399-72 and ASTM E 647-91. For the PTC specimens the stress intensity was computed from the following equation:

$$K_I = 1.1\,(P/A)\,\sqrt{\pi}\,.\,a/Q \qquad (1)$$

where P is the load, A is the specimen gross area, a is the crack depth and Q is Irwin plasticity and shape correction factor (10).

The stress intensity for the WOL specimens were calculated by the following equation:

$$K_I = (C_3\,P) / (B\sqrt{a}) \qquad (2)$$

where details of analyzing these specimens are outlined in the paper by Novak and Rolfe (11). For the CCT specimens the stress intensity solution was calculated by the following equation:

$$K_I = P\,\{\sqrt{\pi}\,c\,\sec\,(\pi\,c/w)\} / (WB) \qquad (3)$$

where c is half the total crack length and w is the width of the panel. Other terms have specific meanings described in ASTM E 399 and 647 respectively.

Sustained load crack growth tests were conducted by pre-cracking the specimens in laboratory air at a stress ratio of 0.1 and a frequency of 10 Hz. The specimens then were placed in a static creep frame, the environment added and load applied. The stress intensity solution recommended in ASTM 399 was used. After a specified time specimens were pulled to failure monotonically and fracture surface studied for the crack growth under sustained loading condition.

RESULTS AND DISCUSSION:

The results are discussed for the three groups of crack growth tests conducted in this section.

Continuous fatigue crack growth behavior:

The crack growth rates in the case of 2024-T851 were comparable under test variables such as environment, frequency, orientation, stress ratio and microstructural variables. No significant effect of environment or test frequency in 3.5% NaCl solution was observed. Different specimen sizes produced a slight change in the slope of the crack propagation rate versus stress intensity range data. The samples tested at very high gross stresses showed delamination in the plane parallel to the plate surface at the higher nominal stresses and mode I ΔK values resulting in slight retardation in the crack growth rates. This behavior was expected due mainly to the surface conditions which usually are overworked and constituent particles are often broken as a result of rolling. The stress ratio (0.1 and 0.5) influenced the CGR within the extreme condition of mode I ΔK values in that at the higher values the maximum stress intensity in the load cycle became a significant percentage of the fracture toughness and at the values of the mode I ΔK where the crack growth rate was below 10^{-6} in. per cycle. However, in a 3.5% NaCl solution and 20 Hz frequency the R=0.5 produced faster crack growth rates at lower mode I ΔK ranges than other environments tabulated in Table 2. A general trend of shifting the data upward with the increase in R from 0.1 to 0.5 was by a factor of one to five. The scatter in the data ranged within this envelope with a change in the environment and frequency.

The environmental effects seen in Fig. 2 also found in the literature which was more pronounced at the lower levels of cyclic amplitudes of mode I ΔK. In 2024-T3 tested in a 3.5% NaCl within the range of mode I ΔK from 3.5 to 9 ksiv$\sqrt{\text{in}}$ the CGR varied from 20 to one. In other alloys namely; 7075-T6 and 7178-T6 the environmental effect is not as prominent (4, 12). This behavior was argued due to lower cyclic rates where time dependent corrosion interacted with fatigue. On the contrary, with the increase in the frequency, time for the corrosion attack is reduced substantially, thereby lowering the crack growth rates. An empirical equation for the environmental adsorption effects in fatigue crack propagation was proposed by Achter (13) as follows:

$$(da/dn)_c = 4.87 \times 10\, P/\nu \qquad (4)$$

where the left hand side of the equation denotes the cyclic crack growth rates in inch per cycle, P is the water vapor pressure and ν the frequency. This equation separates the regimes where a cross-over in the CG behavior under the dry air and other environments should occur. The values obtained by this equation for the transition in the environmental CGR and mode I ΔK curve within the frequency range from 0.1 to 20 Hz appeared to be

at the range of 10 ksi$\sqrt{in}$ and 10^{-6} in per cycle, this also conforms to the materials investigated and that found in the literature (4, 12).

The fracture surface appeared to be a mixture of ductile striations, limited cleavage and faceted fracture. However, striations were detected only above a critical value of mode I ΔK range. In (12) striations were found in mild environments (dry air, wet air, and distilled water) beyond the mode I ΔK range of 5 ksi$\sqrt{in}$, in that fine ductile striation networks were observed. Striations were resolved in this study at mode I ΔK of nearly 7.6 ksi$\sqrt{in}$ in both humid and 3.5%NaCl solution, where a limited amount of corrosion found together with secondary cracking, cleavage of second phases and traces of oxides filling the crack. With the increase in the mode I ΔK range, striation spacing increased and more pronounced cleavage with step wise transgranular fracture mode observed.

The maraging steel exhibited a gradual increase in the CGR with the decrease in the frequency from 10Hz to 0.1 Hz in 3.5% NaCl environment. The CGR increased at a particular frequency and environment at a higher mode I ΔK ranges in Fig. 3. In a range of mode I ΔK from 10 to 55 ksi$\sqrt{in}$ the CGR varied in a factor of 2 to 10. A similar trend in the crack growth behavior was observed in the case of 9Ni-4Co-0.3 C steel (14) where at 0.1 Hz frequency the CGR was found faster than that of 1Hz. The fracture surface appearance contained fine striations, however, as the environment changed to 3.5% NaCl secondary cracking associated intergranular failure. These features were more dominant in 3.5% NaCl solution.

In the case of Ti-6Al-6V-2Sn in (STOA) condition exhibited a gradual increase in the CGR in the intermediate range of mode I ΔK in 3.5% NaCl solution when the frequency was 10Hz. With a decrease in the frequency from 10 to 1 and 0.1 Hz the CGR rapidly increased to an order of magnitude than that of CGR in air at 10 Hz. A range in the mode I ΔK, in which the crack growth rates rapidly increased was found to be from 10 to 17 Ksi$\sqrt{in}$ for most Ti-6Al-6V-2Sn in STOA condition. Different specimen thickness produced different crack growth rate in different environments was due mainly to the transition behavior where lower rates were as a result of plane stress fracture. Increasing the humidity from 10% to 90% enhanced the CGR at 0.1Hz observed within the intermediate range of mode I ΔK from 10 to 40 ksi$\sqrt{in}$ in Fig. 4.

The stress ratio has a similar effect on Ti-6Al-6V-2Sn in STOA condition that observed in the case of 2024-T851 aluminum alloy. With the increase in the R from 0.1 to 0.5 under high humidity (90%) the crack growth rates increased either at the higher side of mode I ΔK range or at the lower range of mode I ΔK where CGR increased a factor of three. In other environments and frequency ranges the scatter was not considerable.

Fractographic results indicated secondary cracking at the higher CGR when the frequency was reduced. The extent of cracking in the coarse alpha increased as the growth rates increased to instability. At the region of instability severe sub-surface secondary cracking occurred which were not connected to the main crack. The crack propagation was by means of transgranular cleavage in the fine accicular alpha phase along the interface of the coarse alpha-beta regions. The features observed under corrosion fatigue in this titanium alloy also was reported by Cowgill et al, (15) for stress corrosion of Ti-8Al-1Mo-1V where secondary cracking along alpha-beta interface and in the coarse alpha occurred. Fatigue crack growth and fractographic features in α–β titanium alloys have been extensively researched in references (16-18).

Titanium alloy 6Al-4V in a recrystallized and annealed (RA) condition exhibited a similar trend that observed in the case of Ti-6Al-6V-2Sn under STOA. As the frequency

decreased from 10 to 1 Hz the CGR increased a factor of 4 and 10 respectively in air 3.5% NaCl. At 0.1 Hz the rapid CGR noted in the Ti-6Al-6V-2Sn under STOA was also observed in Ti-6Al-4V under RA condition at mode I ΔK range of 16 ksi$\sqrt{in}$. The sump tank water was less aggressive only at lower frequency (10 and 1Hz) ranges the effects of sump tank water was found equivalent to that of 3.5% NaCl at lower frequency levels of 0.1 Hz or less. Different specimen geometries produced different CGR in different environments where thickness was found causing a transition in plane stress fracture and lower CGR. Under different environments the range of mode I ΔK changed from 10 to 16 ksi$\sqrt{in}$ beyond which the CGR enhanced in Fig. 5.

Effects of stress ratio from 0.1 to 0.5 was found consistent to that observed for 2024-T851 aluminum alloy and Ti-6Al-6V-2Sn (STOA). At R=0.5 the 10 Hz curves in high humidity and 3.5% NaCl solution showed a significant increase in the CGR at high and low mode I ΔK levels when compared to R = 0.1. This effect was found less significant within the intermediate range of the CGR curve. Beyond the range of $9 \geq$ mode I $\Delta K \leq 15$ ksi$\sqrt{in}$ no effect of stress ratio occurred. In other environments namely, high humidity and 3.5% NaCl the CGR decelerated at the higher ranges of mode I ΔK.

Fractographic investigations from before the instability region revealed striation, ductile rupture and cleavage. The fatigue striation spacing increased as the CGR increased, with increase in the cleavage and secondary cracking. The increasing amount of cleavage corresponded to the large jump in CGR at a relatively low mode I ΔK.

In a Ti-6Al-4V under beta annealed condition showed a similar behavior related to CGR that in 3.5% NaCl CGR increased with decreasing frequency in Fig. 6, however, the magnitude of the effect was observed to be much smaller than other two titanium alloys. The fracture surface morphology was quite similar to that observed for other two alloys except that fatigue striations associated stepped appearance with fluted dimples between steps, characteristics of trans-alpha fracture in a beta processed material, were observed.

Sustained load fatigue crack growth tests:

Sustained load CGR in aluminum alloy 2024-T851 was found negligible or no effect al all with the time of exposure from 5 hours to 120 hours. No sub-surface and surface crack growth occurred in this alloy in the environments tabulated in Table 2. However, in a sister program (14) with 7075-T651 aluminum alloy the stress corrosion effect was found significant at all environments and orientations, in which no apparent threshold stress intensity factor was found below which the SCC would not occur in Fig. 7. The CGR became very small at mode I ΔK levels approaching the apparent threshold values, at such point, tests were terminated after nine months since specimens became too corroded (14). For 7475-T651 alloy the effect was more pronounced as above mode I ΔK 12.5 ksi$\sqrt{in}$ SCC rates in the 7475-T651 were faster than 7075-T651, below this range the effect was not much different for the two alloys in 3.5% NaCl solution (14).

A limited number of tests were conducted for maraging steel to examine the effect of exposure time in 3.5% NaCl solution to determine the threshold of sustained load crack growth, however, crack growth was observed in the tests conducted. Most specimens exhibited surface and subsurface crack propagation with a small amount of crack front bowing. Exposure to 3.5% NaCl caused a higher CGR than the exposure in humid air. The CGR in 3.5% NaCl solution appear to be a function of stress intensity level, the rate increasing with increasing stress intensity in Fig. 8. Similar to the observation made for 7075-T3 alloy, no threshold value was found for this maraging steel. For the steel, 9Ni-4Co-0.3C the SCC behavior where the crack velocity increased with the time was observed in distilled water and JP-4 fuel (14).

In titanium alloy 6Al-6V-2Sn in STOA condition exhibited SCC in humid air, 3.5% NaCl solution and sump tank water. In all three environments CG occurred below the K levels where failure occurred. In most cases subsurface than on the surface resulting in significant bowing for most specimens. In 3.5% NaCl solution for a specimen 0.001 inch of surface crack accompanied a subsurface crack growth of 0.123 inch. Therefore, subsurface crack growth measurements becomes meaningful for such material where fracture occurred in all the cases above 30 ksi$\sqrt{in}$. The humid air environment was least severe, where sump tank water was next and the 3.5% NaCl solution was found to be most severe shown in Fig. 9. In the case of Ti-6Al-4V beta annealed condition also exhibited subsurface cracking. A CGR of 10^{-6} in per cycle was noticed at K values as low as 10 ksi$\sqrt{in}$. In RA condition, a similar trend that is the crack growth rates increased with the increase in the exposure time. Crack growth was more severe subsurface than on the surface resulting in severe bowing in many cases.

Ripple fatigue crack growth tests:

Two terms have been investigated in the literature (19) to influence the CGR behavior under ripple or conjoint major-minor cycles are cycle ratio, i.e., the number of minor cycles per major cycle and amplitude ratio (Q) which is a ratio of stress intensity range of the minor loading to the stress intensity range of the major loading. The CGR for four materials listed in Table 1 are found to behave in a similar fashion which showed that as the amplitude ratio increased the CGR increased, however, with the increase in amplitude ratio and the cycle ratio the CGR increased for these materials (20, 21).

In 3.5% NaCl solution, at lower amplitude ratio of 0.11 the ripple cycles had little or no effect on the CG behavior of 2024-T351, however, an increase in the CGR was observed only when the amplitude ratio was increased with the increase in the cycle ratio. Alloy 2324-T39 behaved in a similar manner that of 2024-T351. The 7xxx series alloys also exhibited a similar trend, in which the CGR in 7150-T651 as a result of higher amplitude ratio and cycle ratio was found higher than 7075-T651.

The CGR in 3.5% NaCl environment was found accelerated. The CGR enhanced with the increase in amplitude ratio and cycle ratio as shown in Fig. 10. At higher amplitude ratios the corrosive environment causes a larger increase in CGR.

In addition to the test variables discussed in this paper, other factors also have been investigated such as microstructure, specimen thickness, location of the specimen through the thickness, orientation and texture influence the fatigue and corrosion fatigue crack growth rates. The usage parameters of an aircraft and fleet will provide a volume of variables effects of which on the fatigue and corrosion fatigue behavior of aluminum alloys is not known. Therefore, more research needs to undertaken to generate and compile data that can be used in probabilistic data synthesis in order to conduct the repair and determine further usage of an aircraft or fleet. Current research in the QIDEC programs funded by Boeing Commercial Airplane Company and Boeing Defense and Space Group is supporting the development of additional insight into these areas.

CONCLUSION

The effect of test parameters on the corrosion fatigue crack growth behavior of aircraft structural materials has been examined in this paper. It has been shown that the presence of corrosive environment increases the CGR in all the three major alloy groups used in aircraft namely aluminum alloys, titanium alloys and steel. Numerous test parameters that influence the CGR are as follows:

1. an increase in the stress ratio increased the CGR in aluminum alloys, titanium alloys and steel, where the increase in CGR was seen at the lower and higher ranges of mode I ΔK, which enhanced further with the corrosive environment,
2. as the frequency reduced the crack growth rates increased in most materials, the rate of increase in CGR was found more severe in the corrosive environment,
3. at lower frequency ranges mild environments produced similar CGR to that of more aggressive environments,
4. sub-surface cracking was observed as a major failure mechanism in titanium alloys under SCC,
5. all materials examined in this paper showed a level of CGR in SCC tests, thereby, a range of mode I ΔK threshold was not found existing for these materials,
6. specimen thickness, orientation and the location from where the specimen was machined produced a different CGR,
7. with the increase in cycle ratio and amplitude ratio the CGR increased in four aluminum alloys, the CGR increased further as the environment became more aggressive i.e., in 3.5% NaCl solution, and
8. there are several other parameters which are not usually investigated e.g., texture, grain size, percentage of constituent particles and their sizes etc., produce different CGR in the materials examined in this paper.

More work is recommended to generate and compile data that can be synthesized in the probabilistic analysis pertaining to growth rate estimations and next inspection interval determinations for aircraft/fleets. It is becoming clear that kinetic theory may provide a means of aiding in the compilation of data.

ACKNOWLEDGMENT:

The authors wish to acknowledge the following organizations and individuals for support of activities related to the preparation of this paper:
Boeing Commercial Airplanes Company (Dr. Matthew Miller and Dr. Ulf Goranson), Boeing Defense and Space Group (Mr. George Miller and Mr. Joe Luzar) KC-135 Program (Mr. Don Nieser) and ARINC Research Inc. (Mr. Robert Rennel).

REFERENCES:

1. Hartman, A. (1965) Int. J. Fracture Mech. v. 1, pp. 167.
2. Pourbaix, M. (1966) Atlas of electrochemical equilibrium diagrams in aqueous solutions NACE.
3. Ambat, R. and Dwarakadasa, E. S. (1993) British Corrosion Journal, v.38, No. 2, pp 142.
4. Bradshaw, F. J. and Wheeler, C. (1966) Applied Mats. Res. vol. 5, pp. 112.
5. Hoeppner, D. W. and Hyler, W. S. (1966) Materials Res. and Standards v. 6, no. 12, pp. 599.
6. Petit, D. E., Ryder, J. T., Krupp, W. E. and Hoeppner, D. W. (1974) AFML-TR-74-183.
7. Hoeppner, D. W. (1971) Corrosion fatigue : chemistry, mechanics and microstructure, NACE-2. pp. 3.
8. Krupp, W. E., Hoeppner, D. W. and Walker, E. K. (1971) NACE-2 pp. 468.
9. Hoeppner, D. W. (1994) Unpublished work.
10. Irwin, G. R. (1960) Syracuse University Research Institute, pp IV-63.
11. Novak, S. R., and Rolfe, S. T., (1969) J. of Materials, v. 4, pp. 701.
12. Feeney, J. A., McMillan, J. C. and Wei, R. P. (1970) Met. Trans. v.1, pp. 1741.
13. Achter, M. R. (1968) Scripta Met. v.2 pp. 525.

14. Hall, L. R., Finger, R. W. and Spurr, F. W. (1973) AFML-TR-73-204.
15. Cowgill, D. S., Fritzen, J. S., Krystkowiak, S. and Weber, K. E. (1968) ASTM ARPA Symposium on Stress Corrosion and Corrosion Principles, Atlanta.
16. Yoder, G. R., Cooley, L. A. and Crooker, T. W. (1979) Eng. Fracture Mech. v. 11, pp. 805.
17. Kondas, K. R., Crooker, T. W. and Gilmore, C. M. (1975) Eng. Fracture Mech. v.7, pp. 641.
18. Yoder, G. R.,. Cooley, L. A. and Crooker, T. W. (1977) Met. Trans. v. 8A, pp. 1737.
19. Powell, B. E., Duggan, T. V. and Jeal, R. (1982) Int. J. of Fatigue, v. 4, pp. 4.
20. Paulson, A. D. (1993) Ph.D. Dissertation University of Utah, Department of Mechanical Engineering.
21. Paulson, A. D. and Hoeppner, D. W. (1993) Durability and Structural Integrity of Airframes, 17th ICAF Symposium, EAMS, v. 2, pp. 1099.

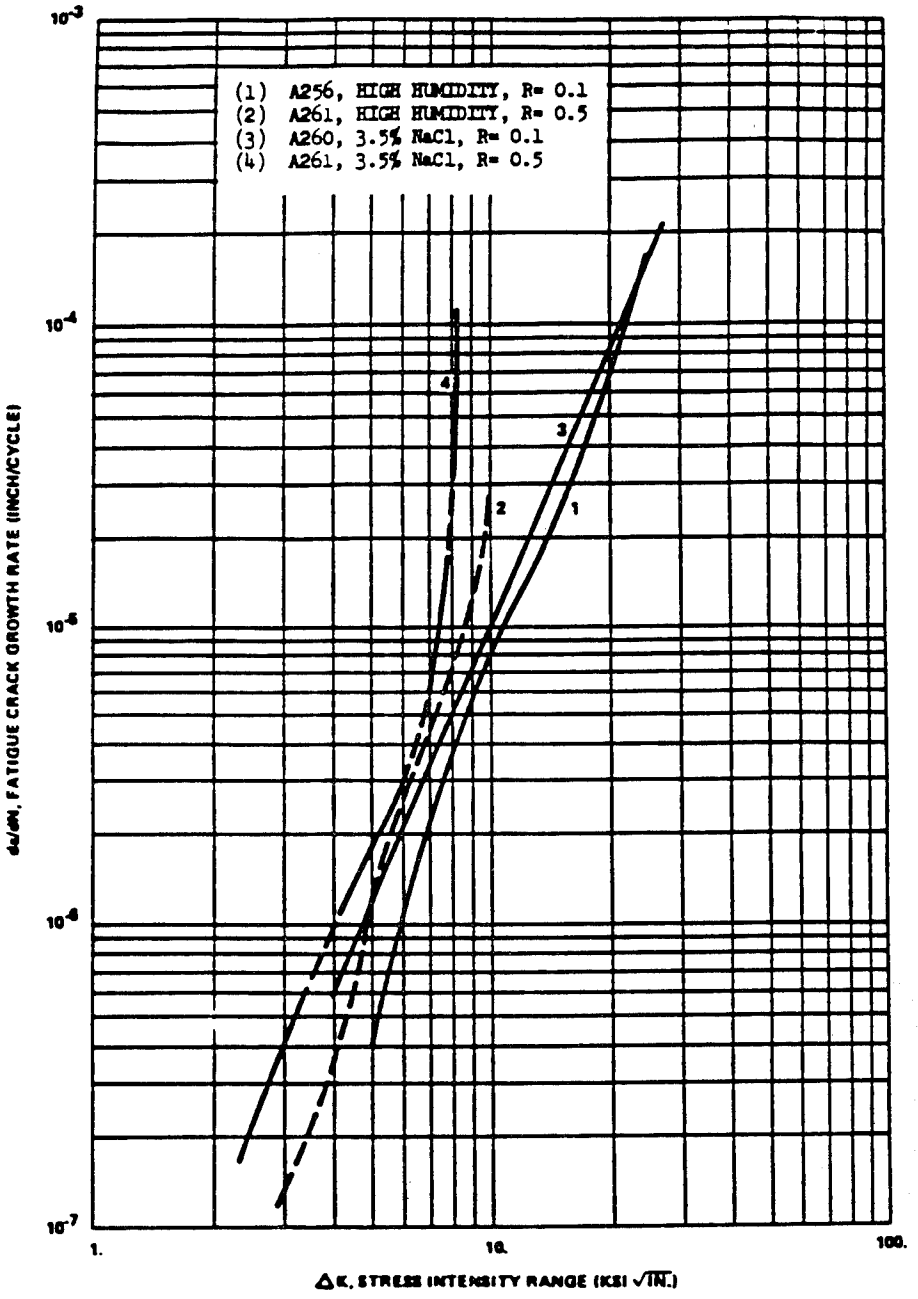


Fig. 2. Effect of stress ratio for 3/8 inch 2024-T851 CCT specimens under 20 Hz, WR orientation.

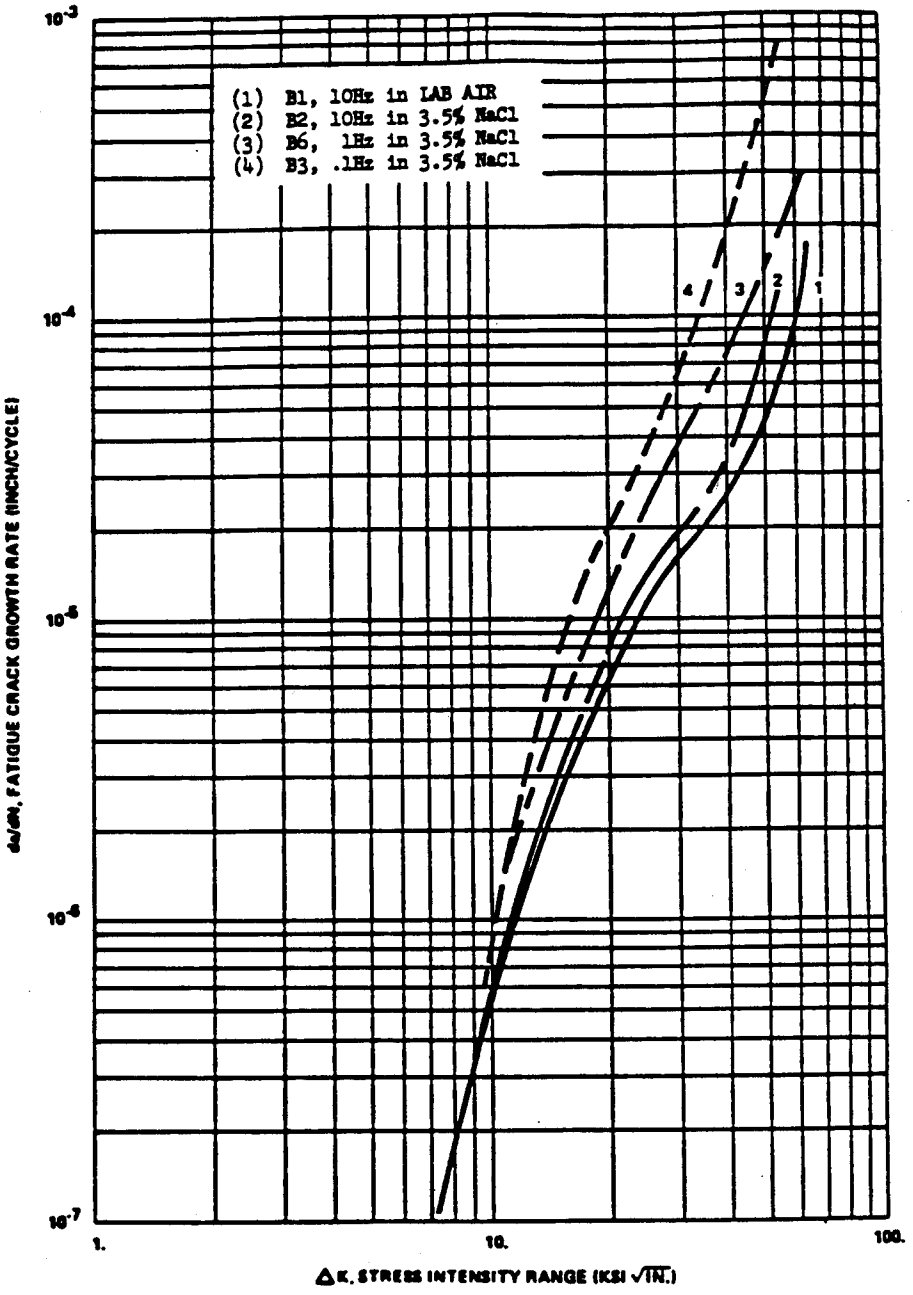


Fig. 3. Effect of frequency for one inch 18Ni- Maraging steel (250 Grade) WOL specimens under R = 0.1, WR orientation.

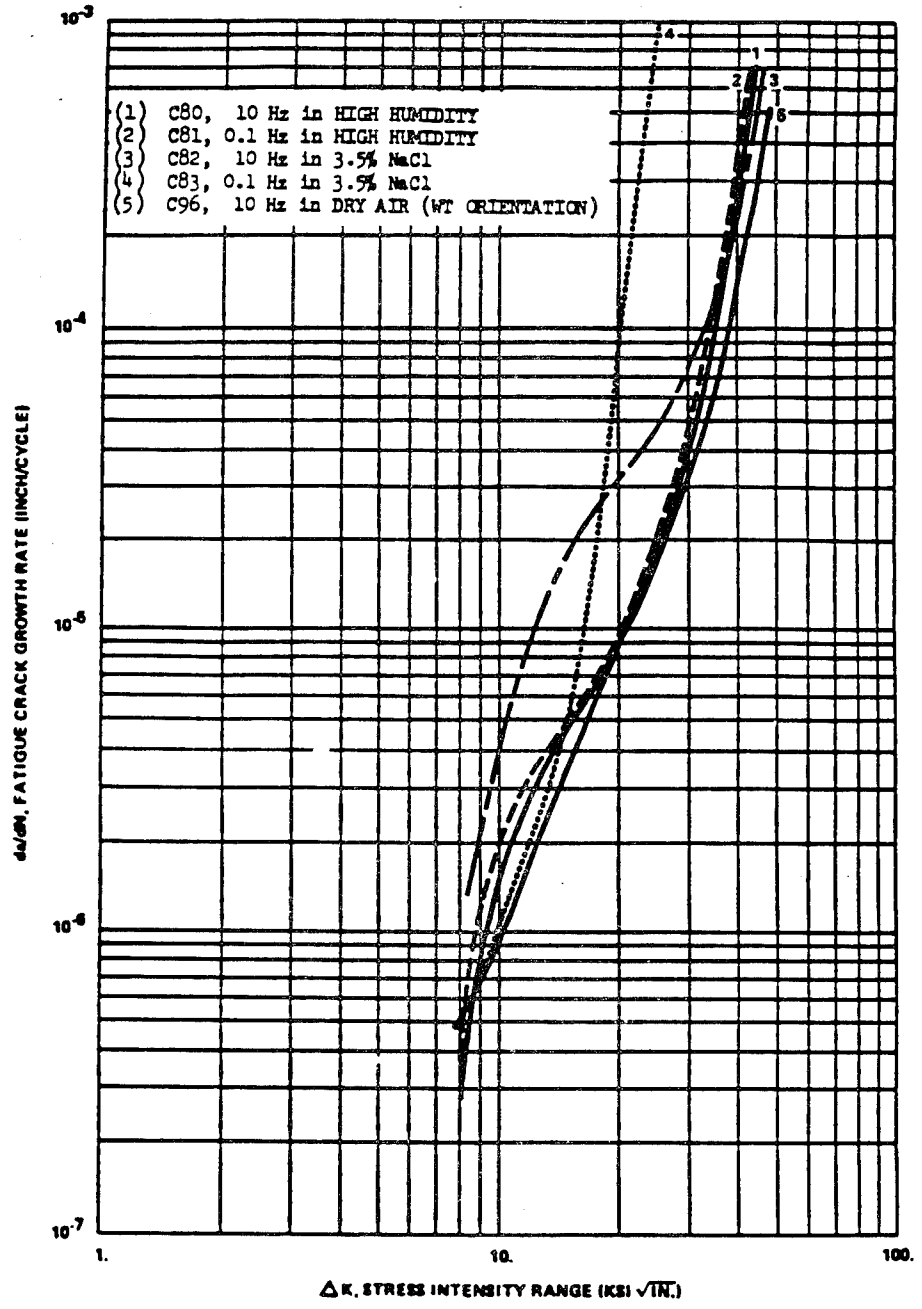


Fig. 4. Fatigue crack propagation results for 3/8 inch Ti-6Al-6V-2Sn (STOA) PTC specimens, R = 0.1, RT orientation.

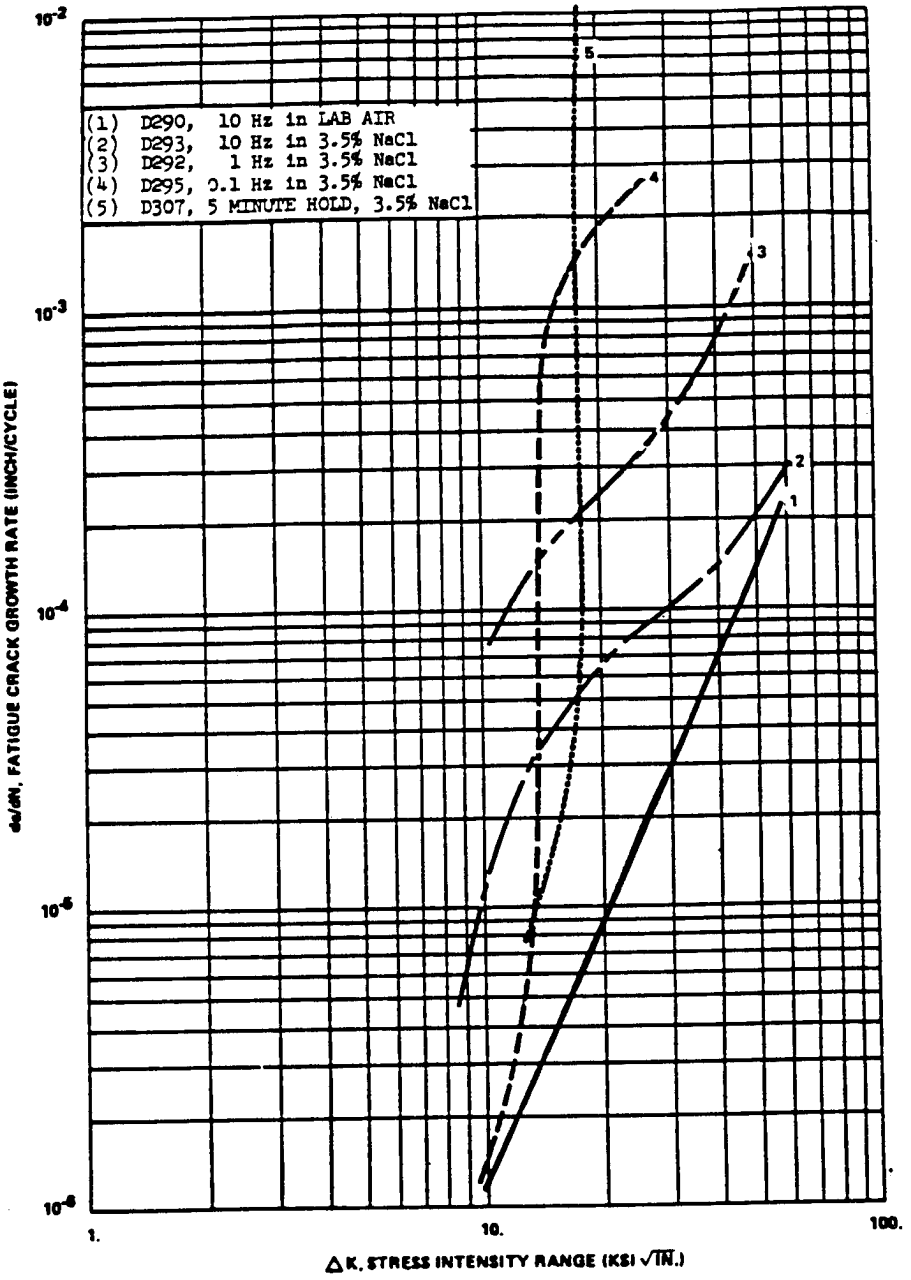


Fig. 5. Effect of frequency for 3/8 inch Ti-6Al-4V (RA) WOL specimens under R = 0.1 in WR orientation.

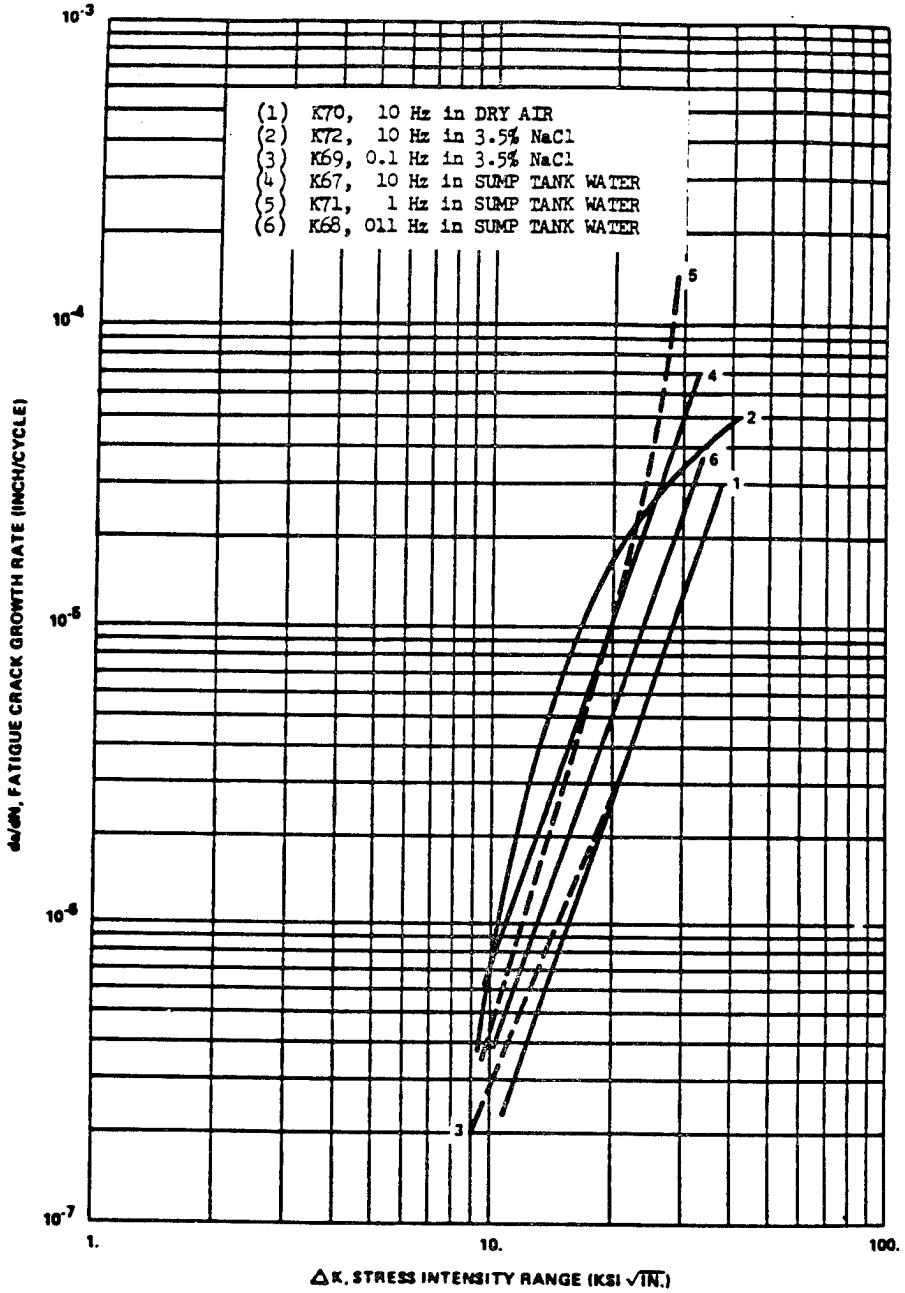


Fig. 6. Comparison of corrosion fatigue results in sump tank water and in 3.5% NaCl solution for 5/8 inch Ti-6Al-4V (Beta) WOL specimens, R = 0.1 in WR orientation.

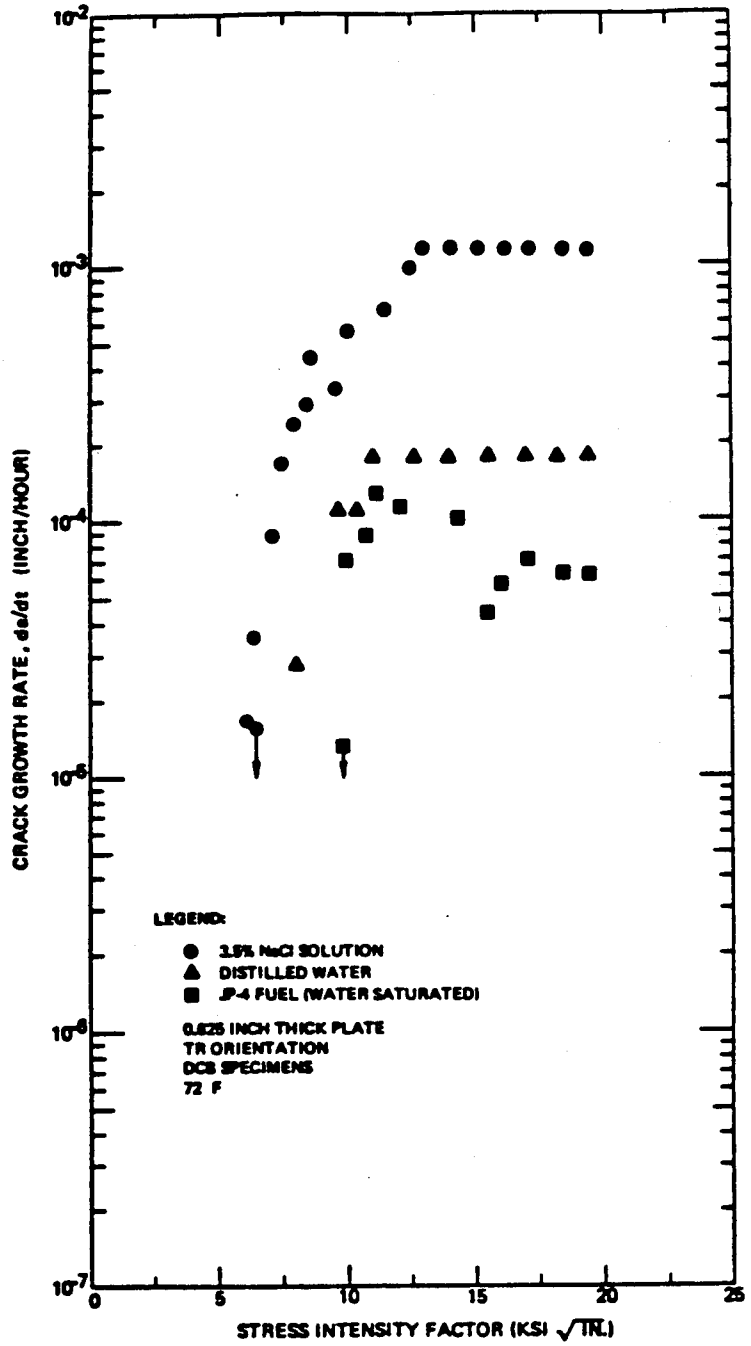


Fig. 7. Stress corrosion cracking velocity data for 7075-T651 aluminum alloy (14).

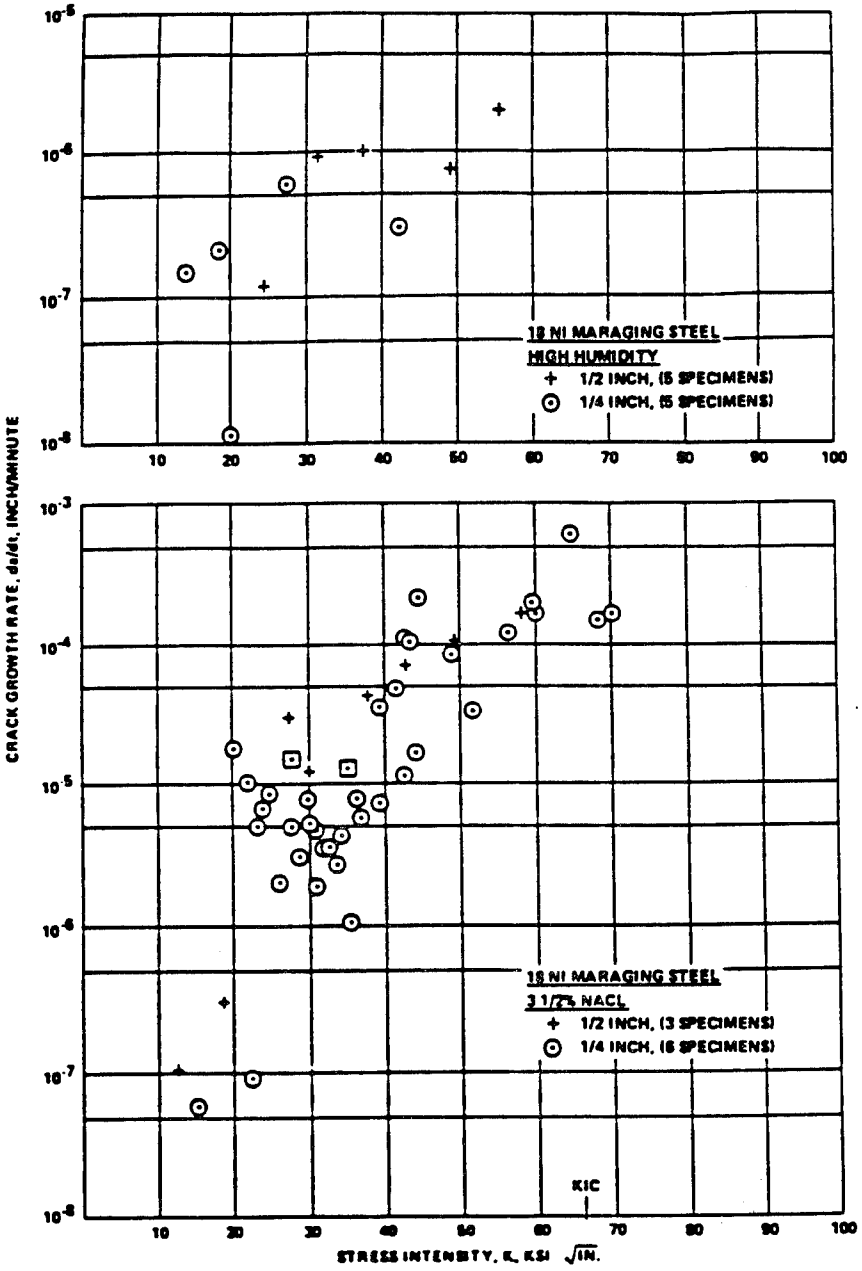


Fig. 8. Stress corrosion crack growth rate behavior of 18Ni Mar-aging steel (250 Grade) CT specimens in WR orientation.

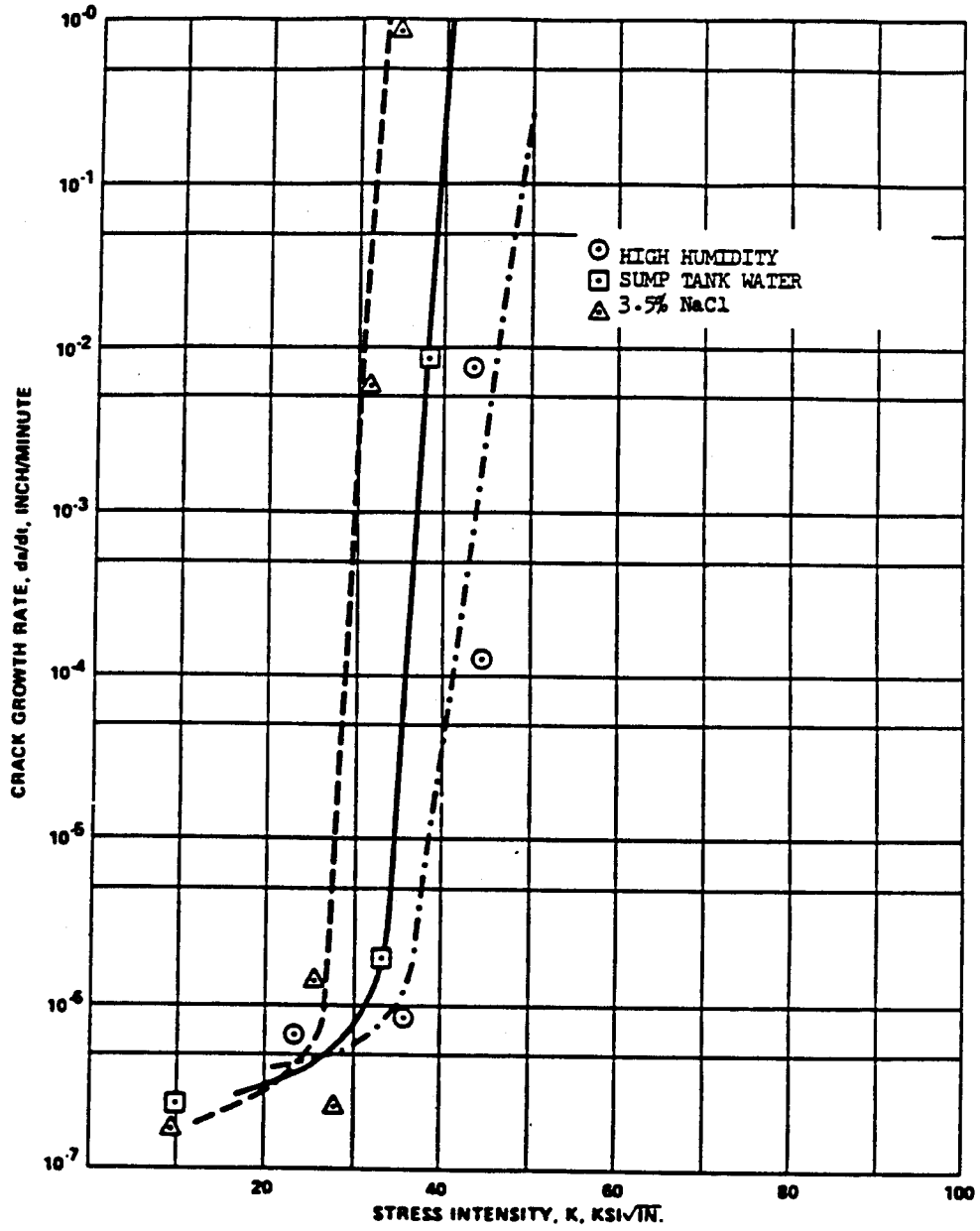
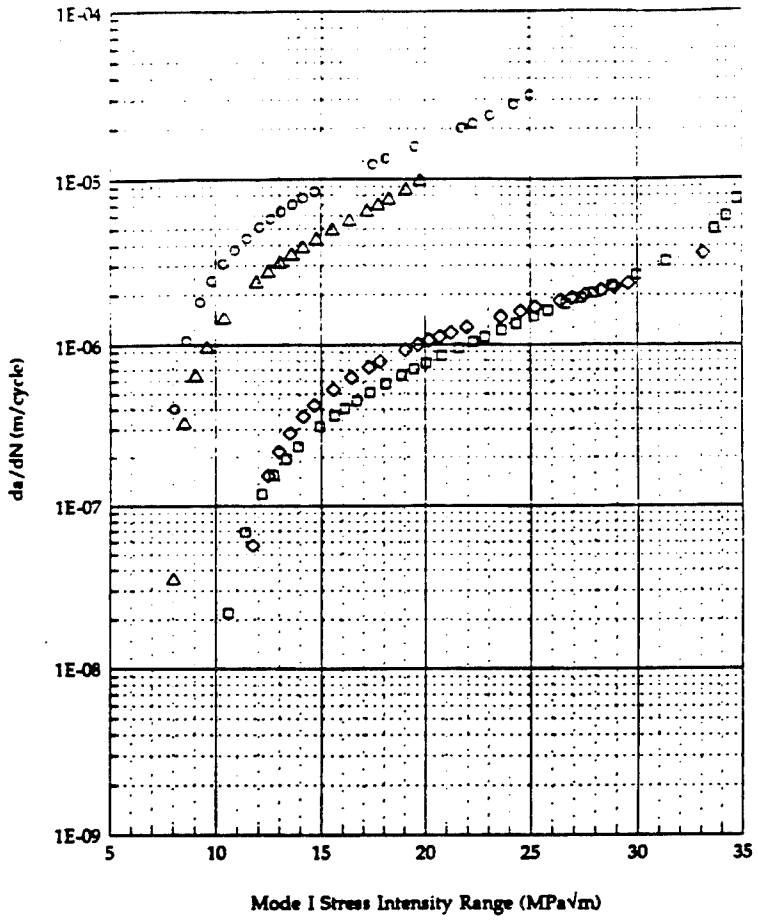


Fig. 9. Stress corrosion crack growth rate for 3/8 inch Ti-6Al-6V-2Sn (STOA) plate material.



Crack growth curves for 2324 in 3.5% NaCl solution.

Fig. 10. Crack growth rate curves for 2324-T39 under ripple fatigue in 3.5%NaCl solution.

The Role of Fretting Corrosion and Fretting Fatigue in Aircraft Rivet Hole Cracking - December 1994 Status Report on an FAA Grant Program

David W. Hoeppner, P. E., Ph. D., Professor and Director of the Quality and Integrity Design Engineering Center (QIDEC) of the University of Utah

Charles B. Elliott III, P. E., Ph. D., Research Assistant Professor in QIDEC

Mark W. Moesser, Graduate Student in QIDEC

Thomas Flournoy, Ph. D., Grant Monitor in the FAA Technical Center

SUMMARY

This is a status report on the FAA Grant No. 93-G-068 program being conducted by the Quality and Integrity Design Engineering Center, an extension of the Department of Mechanical Engineering at the University of Utah, for the Federal Aviation Administration. The purpose of the program is to better understand the role of fretting corrosion and fretting fatigue in aircraft rivet hole cracking. Activities related to basic model and material data development, plans for a sensitivity study of several factors related to fabrication of riveted aircraft joints, and plans for investigation of riveted joints from service aircraft are reported. Accomplishment of the program objectives is expected to occur as planned by October 1995. Results of this program will be reported to the aviation community through the FAA and the open literature.

INTRODUCTION

Fretting describes a state of contact under which two bodies are subjected to oscillatory small amplitude relative motion. In most operational environments, both wear and corrosion are involved in the fretting process. This often results in fretting being referred to as fretting corrosion. The relative motion causes wear. Because the motion is small, most of the resulting debris remains in the interface region where it oxidizes. Often the ratio of normal to tangential load is such that the elastic compliance of the materials results in relative slip occurring over some regions of the interface and no slip in other regions. This complicates analysis of the fretting process because the existence of a slip/no slip boundary causes stress concentrations to occur in the contacting bodies. An example of fretting is shown in Fig. 1.

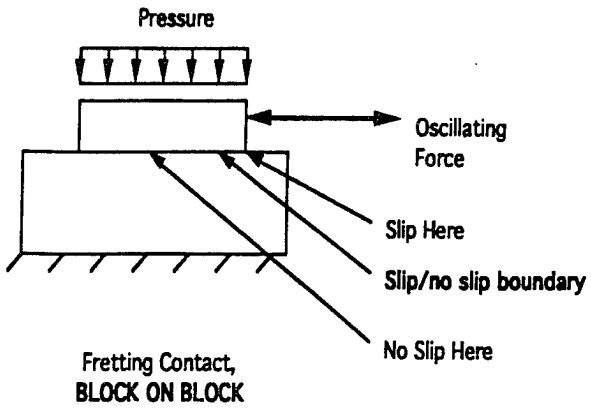


Figure 1. An Example of Fretting

When at least one of the contacting bodies is also subjected to fatigue loading, the process is called fretting fatigue. The presence of fretting can cause more than an order of magnitude reduction in the fatigue life of a component compared to the fatigue life without fretting.

Fretting fatigue is increasingly being recognized in the aircraft industry as a major cause of failure. It is a failure mechanism which frequently leads to high maintenance and inspection costs and could potentially lead to catastrophic failure of aircraft components. Thus, it represents both a durability and a safety problem. Costs associated with fretting fatigue are significant. The 1988 Aloha Airlines disaster focused additional attention on fretting in the aircraft industry as it was thought fretting could have played an important role in that failure.[1]

Fretting can be present in any area of an aircraft structure (e.g. engines, airframe primary and secondary structure, and landing gear components) in which small amplitude cyclic slip between adjacent contacting materials is possible. Rivets and mechanically fastened joints in general are particularly susceptible to fretting and fretting fatigue multiple-site damage. This damage can link up in aircraft structures and create catastrophic results. Thus, it is imperative to understand the role of fretting and fretting fatigue in producing multiple-site damage in riveted aircraft joints.

This paper presents a status report on the grant program being conducted by QIDEC for the Federal Aviation Administration. The purpose of the program is to investigate the role of fretting corrosion and fretting fatigue in aircraft rivet hole cracking. The program has been organized into the following major tasks, which are also shown in Fig. 2:

- Develop and verify basic fretting fatigue models which consider variation in the coefficient of friction with time and location within the fretting interface.

- Determine the coefficient of friction and faying surface sealant materials data necessary as input to the models.
- Plan and conduct a sensitivity study on some of the parameters which affect fretting fatigue in riveted aircraft joints.
- Plan and conduct an examination of riveted joints used in service.
- Develop and verify a fretting fatigue model of a riveted joint which includes the basic fretting fatigue model.
- Use the results of this program to develop fretting fatigue design methods useful to the aviation community.
- Report results of this program to the aviation community through the FAA and the open literature.

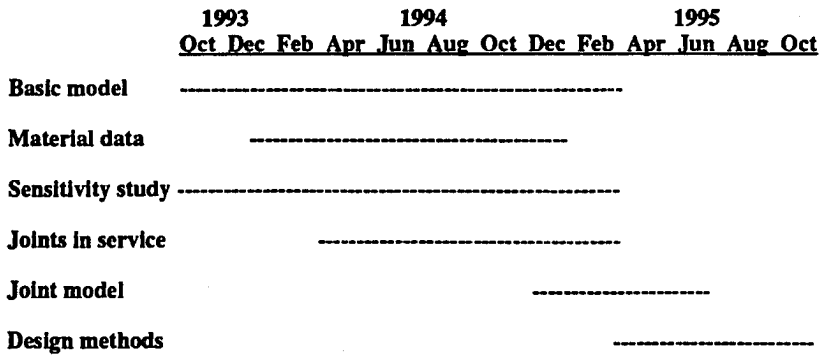


Figure 2. Overview of the FAA Grant Program

As part of a previous grant program, QIDEC conducted a literature review which has been published as DOT/FAA/CT-93/2, *Literature Review and Preliminary Studies of Fretting and Fretting Fatigue Including Special Applications to Aircraft Joints.* [2] Copies are available from QIDEC.

This is one of several research programs being conducted by QIDEC that are leading to improved understanding throughout the aviation community of the adverse synergistic effects of wear, corrosion and fatigue mechanisms on aircraft structural integrity. Related research is being conducted for the Boeing Commercial Airplane Company and the Boeing Defense and Space Group in coordination with the U. S. Air Force.

BASIC MODEL AND MATERIAL DATA DEVELOPMENT

A goal of the program is to develop the capability of predicting the influence that fretting has on the state of stress of a riveted aircraft joint. This requires an understanding of the influence and variation of friction within the interface between the contacting bodies. Friction is recognized as important by the fretting fatigue community, but in the past it has been considered only in terms of the total interface region.[3] Under fretting conditions, however, friction is known to

vary with cycling, as is illustrated in Fig. 3, and also may vary, especially under slip/no slip conditions, with location within the interface.[4] This variation is due to the brief influence of surface films followed by adhesion of the contacting surfaces, plastic deformation, and subsequent metal transfer between the surfaces. The resulting debris also influences the friction state. This influence of the debris changes with cycling as it accumulates, oxidizes and changes with time and cycling.

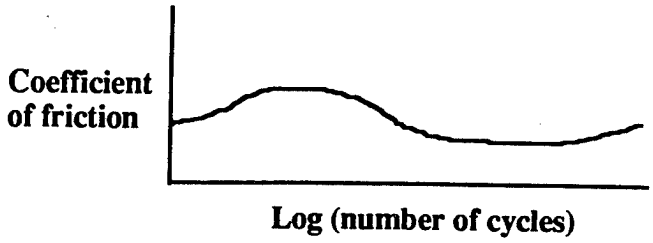


Figure 3. Variation of Coefficient of Friction with Cycling

To be meaningful, the model developed in this program must address this change of friction with cycling and location within the interface. Therefore, an iterative finite element model of a fretting fatigue interface has been developed. The model is solved and verified (The model's assumptions are validated.) at the "base" cycle count. Using material data and the results of the model at the "base" count, how the coefficient of friction will change at the surface finite element nodes after a number of additional cycles is predicted. The model is then updated with the new coefficients of friction and solved. If verified, the new cycle count becomes the new "base" cycle count. If not verified, the original "base" is used but a smaller number of additional cycles is applied. The process repeats until the desired final cycle count is reached. This iterative process is used to control the model. The desired output (the state of stress within the modelled components at a desired number of cycles) also is computed.

The basic finite element model of a fretting fatigue interface has been developed. Current work is focused on obtaining the empirical coefficient of friction data necessary for calibration and experimental verification of the finite element model. This effort also is proving to be significant. Most data collected on the coefficient of friction during fretting are useful only in a qualitative manner. The basic model being developed by QIDEC, however, requires quantitative knowledge of the coefficient of friction and its variability. Therefore, the system that is being developed will obtain accurate coefficient of friction data at values of relative slip less than those previously possible with the material being tested.

Additionally, the design will allow prediction of the uncertainty of the measurements, an important factor that is virtually ignored in the literature.

This work for the first time will allow a reasonably accurate prediction of the stress state within a component subject to fretting. When verified, the basic model will be adapted to a riveted joint configuration. Additionally, faying surface sealant will be considered in a revised model.

SENSITIVITY STUDY

As part of the FAA grant program, QIDEC will conduct a sensitivity study of several factors related to fabrication of riveted aircraft joints. Twenty four riveted joint specimens will be fabricated and tested. Of these, six will be manufactured under each of the following four conditions:

- C-squeeze using 7050 Briles rivets
- C-squeeze using 2017 CE rivets
- Rivet gun with bucking bar using 7050 Briles rivets
- Rivet gun with bucking bar using 2017 CE rivets

The joints have been designed and the plan of test completed. QIDEC is in the process of negotiating to have the joints manufactured.

Results of this investigation will be useful both to aircraft manufacturers and to those concerned with aircraft repair.

JOINTS IN SERVICE

QIDEC also will investigate riveted joints from service aircraft to determine the presence of and effects of fretting on these joints. Requests for riveted joints from service aircraft were sent to several potential sources. The first joint section, accompanied by sufficient documentation as to the location and history of the joint material and the history of the aircraft from which it came, has been received and is being investigated.

CONCLUDING REMARKS

Accomplishment of the program objectives is expected to occur as planned by October 1995. Results of this program will be reported to the aviation community through the FAA and the open literature.

REFERENCES

1. Brewer, J. C., *Fretting Issues for the Aging Aircraft Program,* DOT/FAATC, October 1991.

2. Hoeppner, D., Adibnazari, S. and Moesser, M., *Literature Review and Preliminary Studies of Fretting and Fretting Fatigue Including Special Applications to Aircraft Joints*, DOT/FAA/CT-93/2, April 1994. Copies of this document can be obtained by contacting Dr. Elliott by telephone at (801) 585-6429 or by e-mail at elliott@me.mech.utah.edu .
3. Dobromirski, J. M., "Variables of Fretting Process: Are There 50 of Them?" *Standardization of Fretting Fatigue Test Methods and Equipment, ASTM STP 1159*, M. Helmi Attia and R. B. Waterhouse, Eds., American Society for Testing and Materials, Philadelphia, 1992, pp. 60-66.
4. Berthier, Y., Vincent, L., and Godet, M., "Fretting Fatigue and Fretting Wear," Tribology International, Vol. 22, No. 4, Aug. 1989, pp. 235-242.

An Evaluation of Fatigue Properties of Aging Aircraft Materials

J. N. Scheuring* and A. F. Grandt, Jr.**

Abstract

This paper evaluates changes in the fatigue crack growth and stress-strain properties which result from aging and/or corrosion that occur during aircraft service. Specifically, da/dN-ΔK and tensile stress-strain curves characterizing the "aged aircraft" material are compared with handbook properties for virgin material of the same pedigree. The tested materials were aluminum alloys obtained primarily from fuselage and wing panels from retired KC-135 aircraft. Computer controlled fatigue tests were conducted using compact tension specimens machined from the retired aircraft components. Crack lengths were monitored with an automated compliance measurement in addition to optical crack length measurements. Various levels of corrosion were observed, thus the crack growth rates could be quantified as a function of the level of corrosion present in the material. The resulting da/dN-ΔK curves for the "aged" materials are compared with the fatigue properties for the virgin material. Similar comparisons are performed for the tensile stress-strain properties. The primary objective is to determine whether damage tolerant analyses for older aircraft should employ updated material properties which more accurately represent the current state of the material, or if the virgin material properties properly quantify the crack growth properties of the aged/corroded alloy.

Introduction

Due to various reasons, aircraft fleets are being required to fly beyond their original intended life expectancies. With continued operation of these older aircraft, updated damage tolerant analyses are being performed to determine how much longer the aircraft can be safely flown. One question that arises during these analyses is whether the original material properties are adequate to describe the material or should newly generated material properties that are indicative of the current state of the material be used. Thus the primary question of this project is "Has prior service usage changed the material properties of aging aircraft materials?"

* Graduate Research Assistant, School of Aeronautics and Astronautics, Purdue University.
** Professor, School of Aeronautics and Astronautics, 1282 Grissom Hall, Purdue University, W. Lafayette, IN 47907-1282.

The scope of this project is to characterize the basic fatigue crack growth and tensile properties of materials that have seen prior service usage. Not included in this study are the effects of joints, strengtheners, rivets, etc.; only the basic material properties are characterized. The two major factors that are considered within the scope of this project are the effects of aging and the effect of corrosion on the material properties.

Material and Measurements

The materials considered here are the aluminum alloys 2024-T3, 7075-T6, and 7178-T6. Four panels were obtained from three different aircraft: a retired C/KC-135, a retired Boeing 707-320C which had seen 20 years of service consisting of 19967 flight cycles and 46685 flight hours, and an active C/KC-135. Results for the 2024-T3, 7075-T6, and 7178-T6 aluminum alloys tested to date are presented in this paper. These materials were primarily taken from the fuselage and wing panels of retired aircraft, but other aircraft components were also tested. A brief summary of the panels is shown in Table 1.

The panels were disassembled and specimens were taken primarily from the joint areas. Figure 1 shows a schematic for a typical joint. Specimens were taken from the most visibly corroded areas, primarily the joints . ASTM Standard Compact Tension[1] specimens with a width of W = 1.11 inches were the primary crack growth specimens utilized. This specimen was chosen primarily due to the limited amount of material available in the joints, which were typically joined by several rows of rivet holes. The specimens for tensile testing were ASTM E 8 Standard Subsize Axial Dogbone[2] specimens. For both types of specimens, thickness measurements were obtained using digital calipers to determine a thickness from outside edge to outside edge of each specimen. Table 2 summarizes the specimens used in the tests completed to date.

There were several testing conditions that were used in the fatigue crack growth tests. The stress ratio utilized was R = 0.1 while cycling at a frequency of 10 Hz. The test temperature T = 72±2°F and the relative humidity RH was maintained at 85±2%. These testing conditions were chosen in order to coordinate with other USAF Aging Aircraft Studies. To achieve the aforementioned testing parameters, humid air was pumped into a Plexiglass environmental chamber while the relative humidity was monitored in chamber itself. In additional, control tests were conducted in ambient lab air, RH = 20±10%, to observe the effect of relative humidity on the aged material during testing.

The crack growth was monitored primarily by compliance. The crack length was measured automatically using a PC based materials testing program, MATE (developed by University of Dayton Research Institute). In addition,

optical measurements were taken to check the compliance results during each test. Figure 2 is a representative check of the accuracy of the compliance crack length measurement, as compared to optical measurements taken during a fatigue crack growth test of a Compact Tension specimen with an ASTM width of W =1.11 inches for 5 different specimens. All crack lengths in this study will utilize the compliance crack length for analysis.

Results and Discussion

A comparison of the fatigue crack growth results for the 7178-T6 material is presented in Figure 3. The data were generated from four CT specimens, machined from a retired Boeing 707-320C upper wing skin, with a thickness of 0.192" and showed no signs of visible corrosion on the surface. The data scatter from specimen to specimen was relatively small, as depicted by the narrow scatter band, see Figure 3. Also shown in Figure 3 are crack growth rates for Damage Tolerant Design Handbook[3] data at similarly low R ratios, R= 0.02 and R=0.05. The data generated in this study lie within the scatter of the handbook data, seeming to imply that little, if any, change had occurred to the aged aircraft material in this case.

The stress-strain curve generated for the 7178-T6 is shown in Figure 4 while a summary of the tensile properties is presented in Table 3. The stress-strain curve is a combination of specimens that are tested in one of two ways; 1) as received, with paint and whatever corrosion that is present, and 2) those specimens that have been ground down to apparent bare metal. The Young's Modulus and the Tensile Strength (0.2% Yield Offset, ASTM E 8[2]) agree very well with The Metals Handbook[4] while the Ultimate Strength is comparable to The Metals Handbook Value.

Fatigue crack growth rates for aluminum alloy 7075-T6 are presented in Figure 5. The five CT specimens used to generate this da/dN-ΔK curve were machined from "lightly corroded" material taken from a retired KC-135 fuselage lap joint. The specimen to specimen scatter is larger than that of the tested 7178-T6 material, which had no visible corrosion. When comparing these data to the Damage Tolerant Design Handbook[3], the lightly corroded material shows no appreciable degradation and lies within the handbook data scatter. Additionally, two of the CT specimens were tested in dry lab air, RH=20±10% while the others were tested at RH≥85%, and showed no differing crack growth rates.

Tensile property results, for the same 7075-T6 material, are presented in Table 2 while the stress-strain curves for the specimens used are shown in Figure 6. The stress-strain curves in this study are compared to the MIL-HDBK-5E[5] stress-strain curve in Figure 6. The Young's Modulus, Yield Strength, and Ultimate Strength all agree very well with the MIL-HDBK-5E values with experimental reason; differences of 1%, 2.25% and 4%, respectively.

Crack growth da/dN-ΔK curves for aged and corroded 2024-T3 are shown in Figure 7. These data were produced from 7 CT specimens machined from retired KC-135 tail section panels. Six specimens were machined from a "moderately" corroded access panel while the seventh specimen was machined from a "moderately" corroded doubler panel from the same aircraft. In addition, one of the access panel specimens was tested in lab air conditions, R =20±10%, while the others were tested at high humidity, RH≥85%.

The results from specimen to specimen varied much more than the previously tested materials. Additionally, when compared to DTDH data, the corroded material exhibited slightly faster crack growth rates in all stress intensity factor regimes. There was no apparent effect of testing humidity on the crack growth rates at this testing frequency, 10 Hz.

The tensile properties for the 2024-T3 material are shown in Figure 8 and summarized in Table 3. The stress-strain curves are compared to the MIL-HDBK-5E curve in Figure 8. Six specimens were used, of which three were in their natural state and three were ground to apparent bare metal. The properties all were similar to the MIL-HDBK-5E tensile properties.

Summary and Conclusions

In summary, fatigue crack growth and stress-strain tests were conducted on materials taken from "aged" aircraft. Several conclusions can be drawn from these tests.

1. All three materials tested, 2024-T3, 7075-T6, and 7178-T6, have tensile stress-strain properties that appear unchanged with respect to common handbook data.

2. Minimally corroded materials tested at a stress ratio of R = 0.1 have similar crack growth rates as compared to virgin material properties found in Handbooks. Tests were conducted on a lightly corroded material, 7075-T6, and a material that showed no visible corrosion, 7178-T6.

3. At a stress ratio of R = 0.1, fatigue crack rates for moderately corroded 2024-T3 appear to be slightly faster than handbook values in all crack growth regimes. In addition, the crack growth rates from specimen to specimen showed more variability as the level corrosion increased, with respect to the original thickness.

One possible reason for these phenomena associated with moderately corroded material could be the variability in thickness that arises when a material has appreciable corrosion; the load bearing thickness then becomes a variable though the width of the specimen during testing.

Future work in this project consists of three main areas. The first step is to develop constant amplitude SN data for uncracked specimens obtainable from

the materials tested in this paper. The next step would be to conduct additional fatigue crack growth tests at a high stress ratio level, R = 0.3 or 0.5. The third step considered would be to characterize the corrosion levels of the materials. The two possibilities considered for this phase are surface roughness measurements, by profilometry, and measurement of the load bearing thickness, by eddy-current measurements.

Acknowledgments

Portions of this research were sponsored by Air Force Office of Scientific Research Grant Number F49620-93-1-0377 with Dr. W. F. Jones as program monitor. The authors greatly appreciate the assistance of Mr. D. E. Neiser from the USAF Oklahoma City Air Logistics Center, Mr. J. J. Luzar from The Boeing Company, and Mr. R. R. Rennell from ARINC Research Corporation who provided the test materials from retired aircraft.

References

[1] American Society of Testing and Materials, E647 -93 Standard Test Method for Measurement of Fatigue Crack Growth Rates. *1993 Annual Book of ASTM Standards*, Section 3, Volume 1, pp. 679-706 (1993).

[2] American Society of Testing and Materials, E8 -93 Standard Test Method for Tension Testing of Metallic Materials. *1993 Annual Book of ASTM Standards*, Section 3, Volume 1, pp. 130-149 (1993).

[3] Damage Tolerant Design Handbook, A Compilation of Fracture and Crack Growth Data for High-Strength Alloys, Ch. 8, Vol. 4, University of Dayton Research Institute, Sponsored by Materials Laboratory Air Force Wright Aeronautical Laboratories, 1993, pp. 8.1-15, 8.1-21, 8.1-185, 8.1-186, 8.9-85, 8.9-125.

[4] Metals Handbook, *Properties and Selection: Nonferrous Alloys and Special-Purpose Materials*, Volume 2, pp. 119, 1990.

[5] MIL-HDBK-5E, *Military Standardization Handbook, Metallic Materials and Elements for Aerospace Vehicle Structures*, Sec. 3, Vol. 1, 1987, pp. 3-72, 3-97, 3-309, 3-337.

Panel	Material	Thickness	Aircraft	Corrosion
Fuselage Lap Joint	7075-T6	0.081 in	Retired KC-135 #62-0291	Light
Upper Wing Skin Butt Joint	7178-T6	≈0.20 in	Retired 707-320C	None Visible
Access Panel	2024-T3	≈0.06 in	Active KC-135 xxxx-2618	Moderate
Doubler Structure	2024-T3	≈0.05 in	Active KC-135 xxxx-2618	Moderate

Table 1: Brief summary of the materials in this study tested to data.

Material	da/dN specimens	Tensile specimens
2024-T3	**7 Compact Tension** **W = 1.11 inches** **thickness ≈ 0.08 inches**	**5 Axial Dogbone** **gauge length = 1.5 inches** **thickness ≈ 0.07 inches**
7075-T6	**5 Compact Tension** **W = 1.11 inches** **thickness ≈ 0.075 inches**	**2 Axial Dogbone** **gauge length = 1.5 inches** **thickness ≈ 0.075 inches**
7178-T6	**4 Compact Tension** **W = 3.00 inches** **thickness ≈ 0.192 inches**	**5 Axial Dogbone** **gauge length = 1.5 inches** **thickness ≈ 0.192 inches**

Table 2 : Initial Test Matrix of aluminum alloys tested to date.

Material	Young's Modulus (Msi)	Yield Strength (ksi)	Ultimate Strength (ksi)	Reference
2024-T3	**Exp = 10.86** **Ref = 10.50**	**Exp = 47.0** **Ref = 40.0**	**Exp = 63.4** **Ref = 61.0**	MIL-HDBK-5E, Military Standardization Handbook, Metallic Materials and Elements for Aerospace Structures, 1987.
7075-T6	**Exp = 10.2** **Ref = 10.3**	**Exp = 65.5** **Ref = 67.0**	**Exp = 73.0** **Ref = 76.0**	MIL-HDBK-5E, Military Standardization Handbook, Metallic Materials and Elements for Aerospace Structures, 1987.
7178-T6	**Exp = 10.80** **Ref = 10.40**	**Exp = 78.0** **Ref = 78.0**	**Exp = 84.0** **Ref = 88.0**	Metals Handbook, Volume 2, Properties and Selection: Nonferrous Alloys and Special-Purpose Materials, Tenth Edition, 1990.

Table 3 : Summary of Tensile Properties for aged aircraft materials in this study.

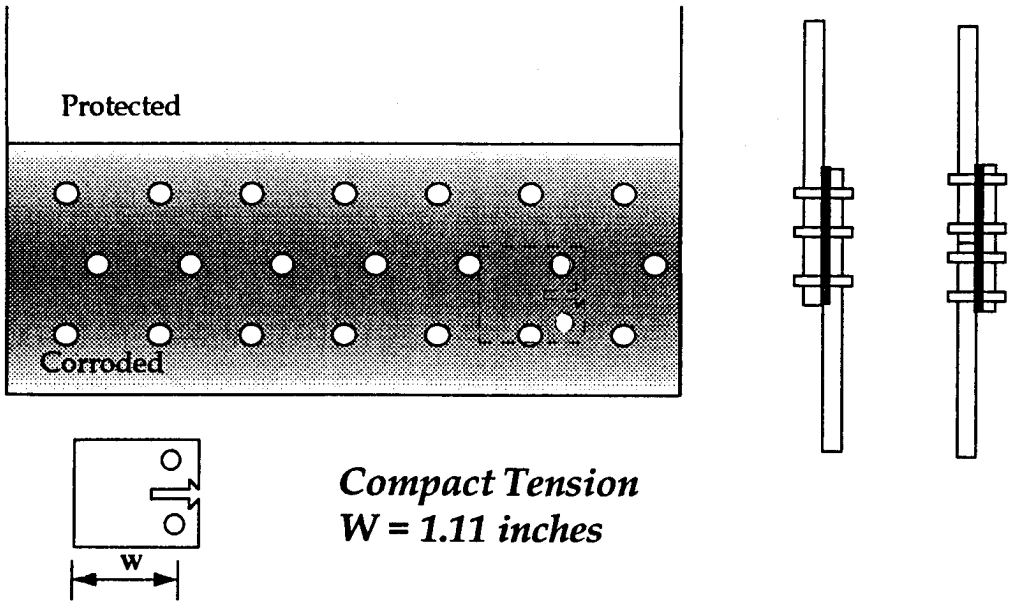


Figure 1 : Schematic of typical joints used in this study. Corrosion typically present in Lap or Butt joints with several rows of rivet holes. Also show is the primary crack growth specimen utilized.

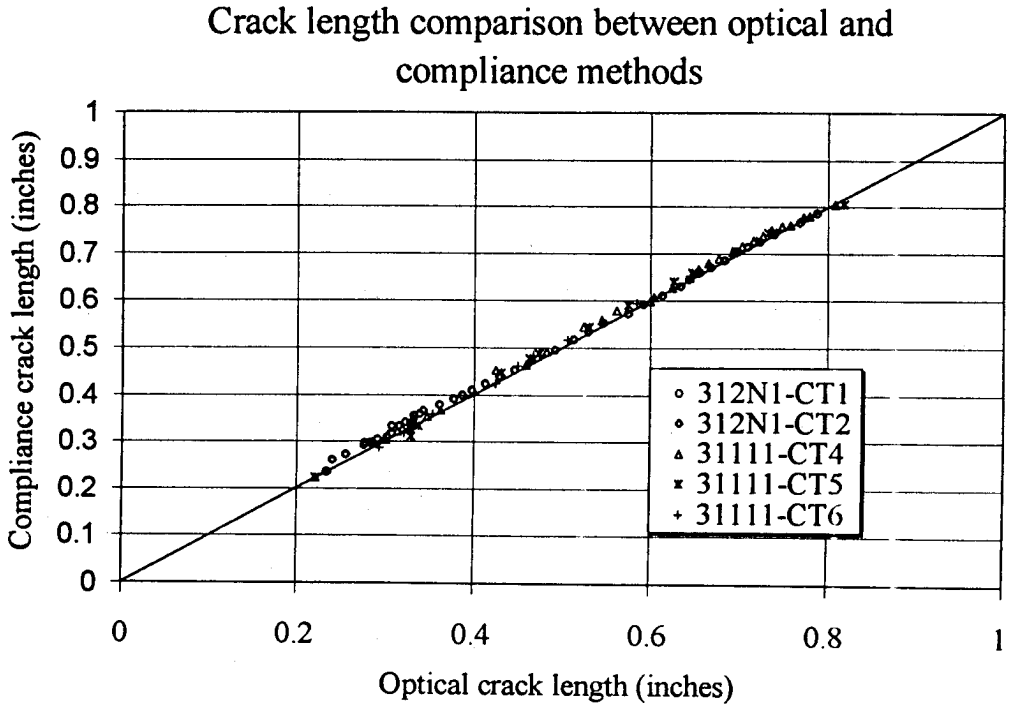


Figure 2 : Compliance measurement comparison with optical crack length measurements on Compact Tension specimens from 7075-T6 alloy.

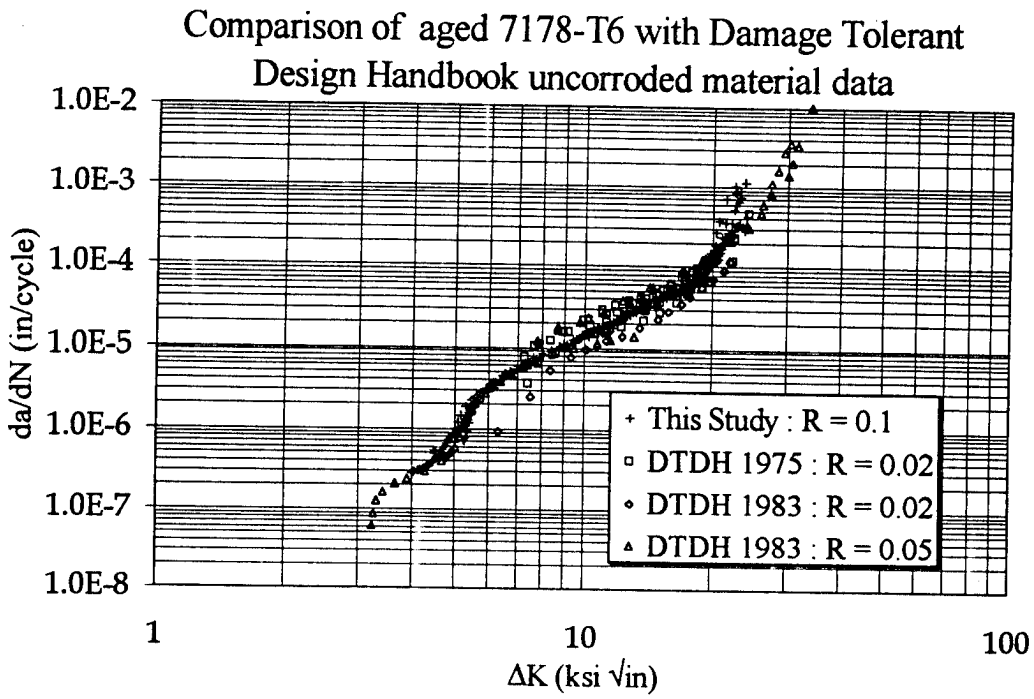


Figure 3 : 7178-T6 crack growth comparison between this study and Damage Tolerant Design Handbook for CT specimens, no visible surface corrosion.

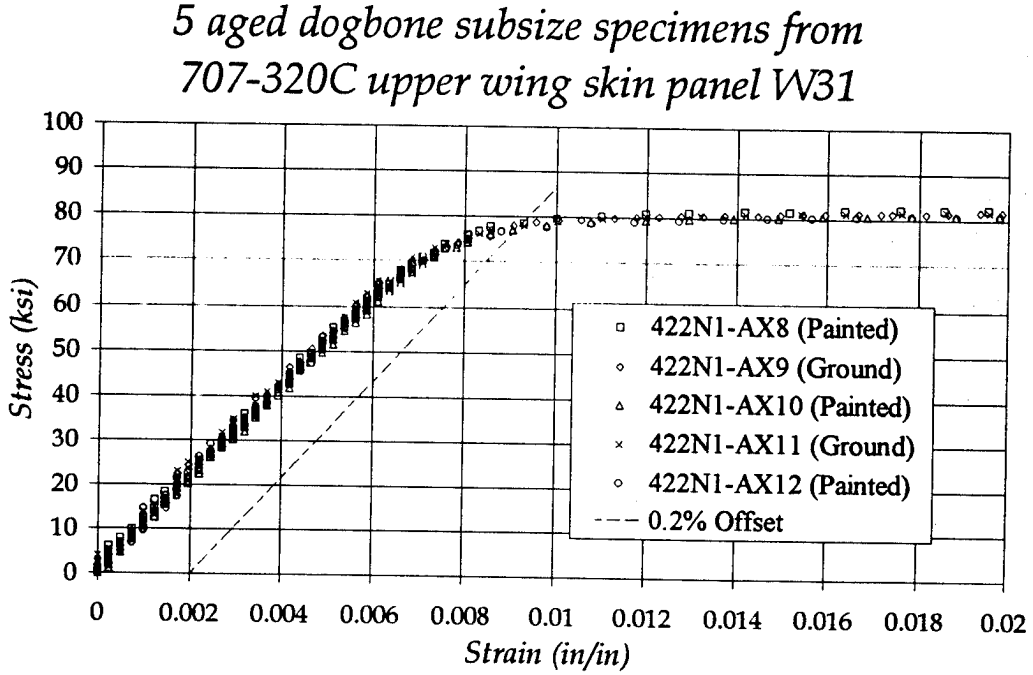


Figure 4 : Stress-strain curve of same 7178-T6 upper wing skin material, with axial specimens that have paint and specimens ground to bare metal.

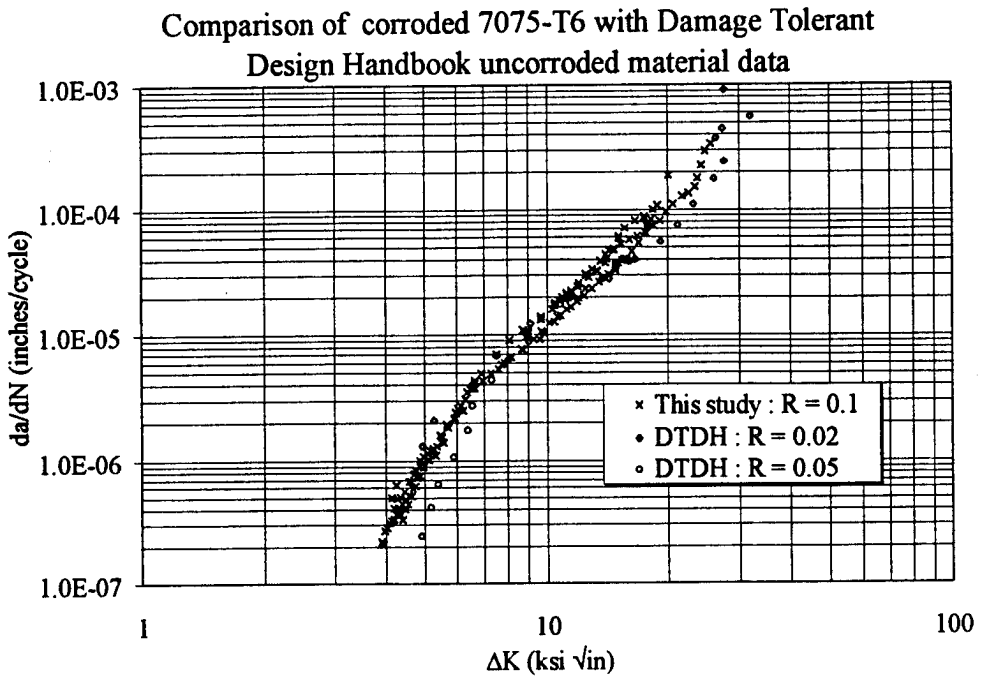


Figure 5 : 7075 -T6 crack growth curve comparison between this study and Damage Tolerant Design Handbook data for CT specimens that are lightly corroded.

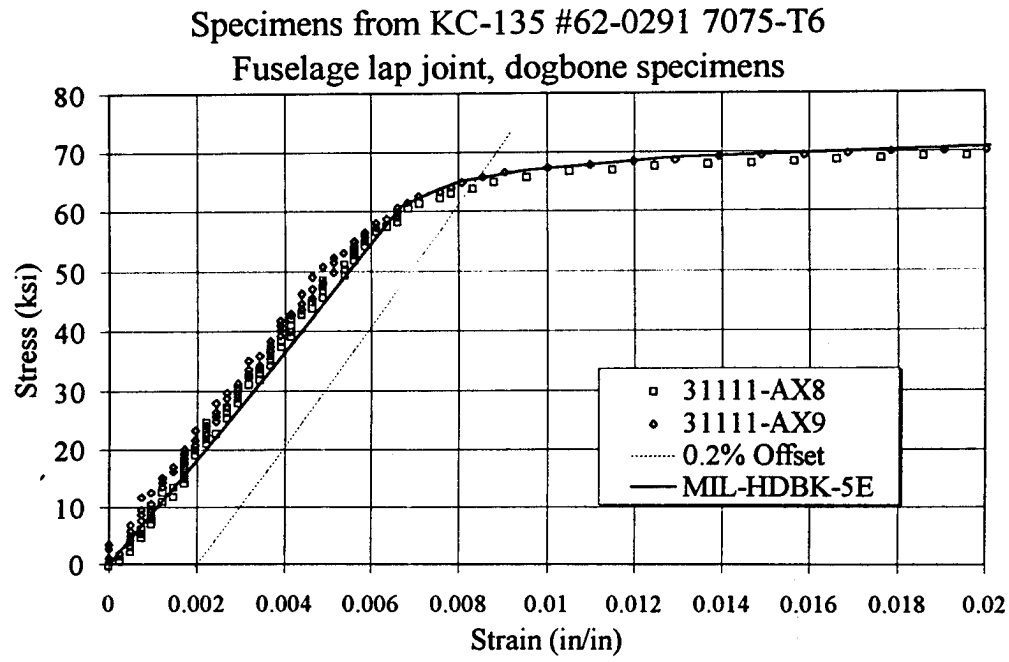


Figure 6 : 7075-T6 Stress-strain curve comparison with MIL-HDBK-5E for lightly corroded specimens from fuselage lap joint.

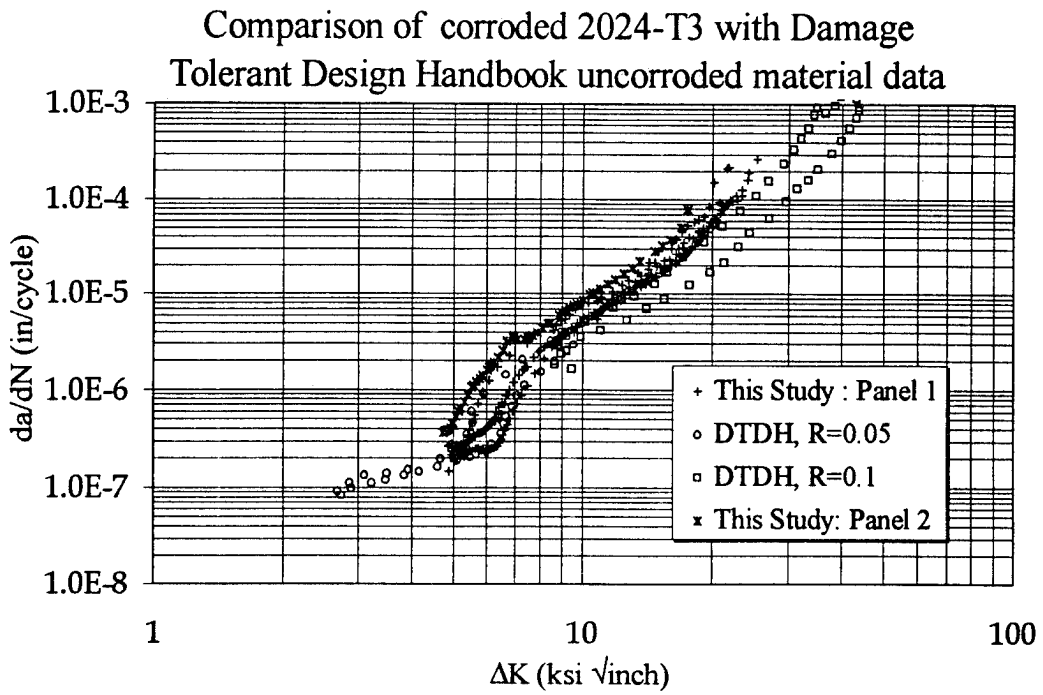


Figure 7 : Crack growth comparison for 2024-T3 Al alloy from two moderately corroded panels to Damage Tolerant Design Handbook.

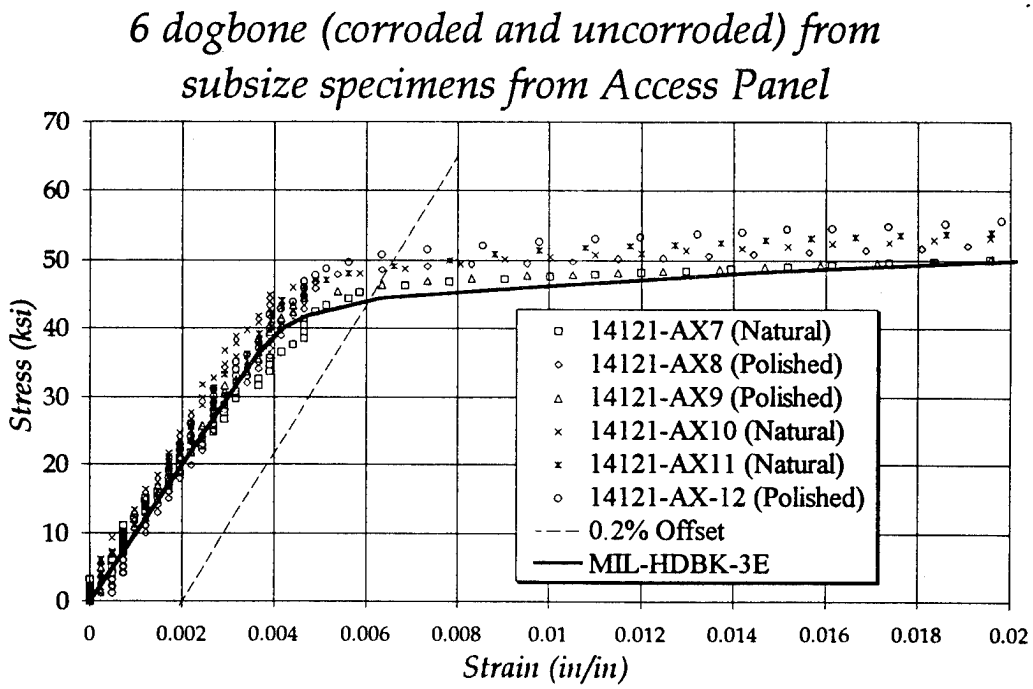


Figure 8 : 2024-T3 Stress-strain comparison for moderately corroded specimens, both corroded surface and ground to pure metal, with MIL-HDBK-5E.

A Fatigue Evaluation of Aging Aircraft Materials

Jason Scheuring &

A. F. Grandt, Jr.

Purdue University
School of Aeronautics and Astronautics

USAF Structural Integrity Program Conference,
San Antonio, Texas
December 6-8, 1994

School of Aeronautics and Astronautics

Acknowledgments

- Air Force Office of Scientific Research
  Grant F49620-93-1-0377
  Dr. W. F. Jones (monitor)

- Aircraft Materials
  - **D. E. Nieser, Oklahoma City Air Logistics Center**
  - **J. J. Luzar, Boeing Wichita**
  - **R. R. Rennell, ARINC Research Corporation**

School of Aeronautics and Astronautics



Outline of Presentation

- Background
- Testing Constraints
- Initial Results
- Future Work
- Summary & Conclusions



Background

- Continued operation of older aircraft requires assessment of remaining life expectancy
- Has prior service changed material properties?
- Use properties that characterize the current state of the material after service usage rather than virgin material properties



Objectives

- Characterize properties of materials that have seen prior service usage
  - **da/dN vs. ΔK**
  - **S-N curves**
  - **Tensile properties**
- Determine if properties have changed with service usage

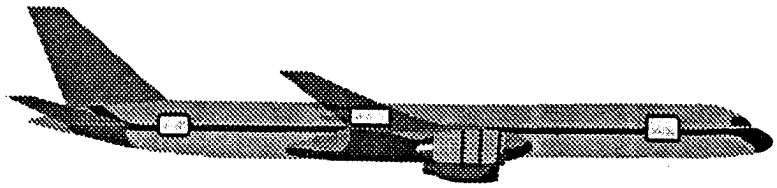


Approach

- Test specimens from aircraft components that have seen prior usage
- Compare with handbook data
- Examine various degrees of corrosion to determine whether corrosion changes the material properties

Test Materials

- Material from retired aircraft or active maintenance programs; C/KC-135's or 707's
  - Primarily Fuselage and Wing panels
- Aluminum Alloys
  - 2024-T3, 2024-T4, 7075-T6, and 7178-T6



Materials Used in this Study

- KC-135 #62-0291, (retired)

⇒ • **7075-T6 clad fuselage lap joint with thickness = 0.081″**

- KC-135, # xxxx-2618, all from tail section, (active maintenance)

⇒ • **2024-T3 Access panel with thickness = 0.06″**

⇒ • **2024-T3 Doubler structure with thickness = 0.05″**

• **2024-T3 Fuselage panel with thickness = 0.04″**

- 707-320C, #20018, 19967 flight cycles and 46685 flight hours, Nov. 1968 to Dec. 1987, (retired)
  - **2024-T3 Clad fuselage joint with thickness = 0.04″ & 0.05″**

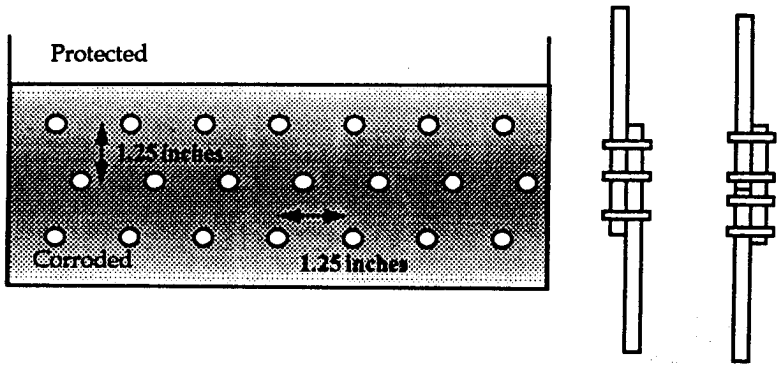
⇒ • **7178-T6 bare upper wing skin with thickness = 0.20″**

Photos of Panels in this Study

- Picture of 7178-T6 Upper Wing Skin from 707-320C
  - Aged only, no corrosion
- Picture of 2024-T3 Doubler Structure from KC-135 tail section
  - Moderately Corroded

Specimen Design Constraints

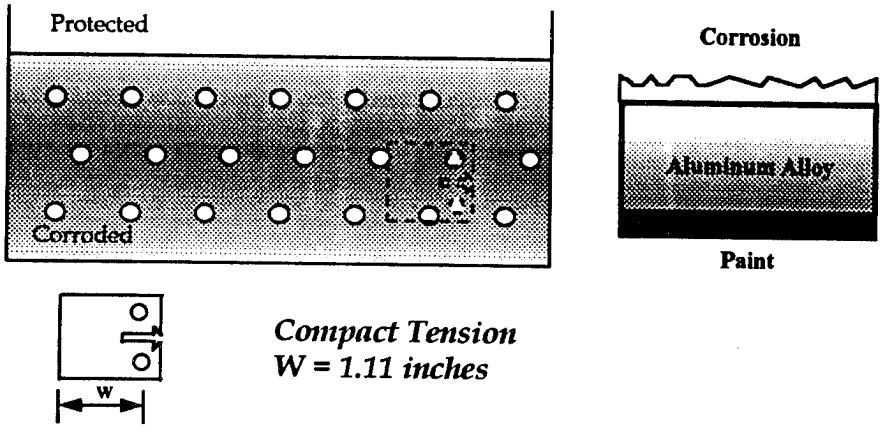
- Schematic of Panels that make Typical Aircraft Joints



Photos of Joints in Various Panels

- 7075-T6 Fuselage Lap Joint from Retired KC-135 #62-0291
  - Lightly corroded
- 2024-T3 Fuselage Lap Joint from Active Maintenance of KC-135 #xxxx-2618
  - Corroded moderately in spotting fashion
- 2024-T3 Doubler Panel from Active Maintenance of KC-135 #xxxx-2618
  - Corroded moderately throughout joint

Specimen Design Constraints



Compact Tension
W = 1.11 inches

Photos of Example Specimen

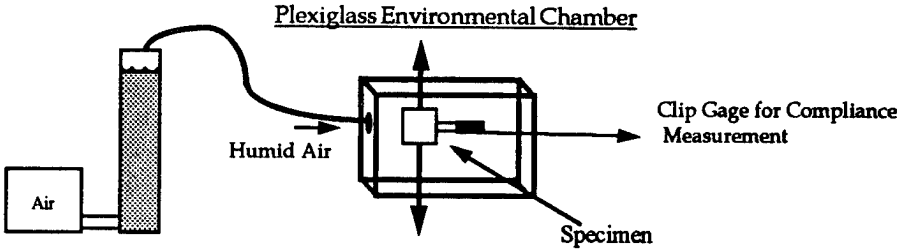
- Photos of specimen 16121-CT3
  - **Front and Back**
  - **Moderately corroded**
  - **From KC-135 Tail Section from active maintenance**

Tests to Date

Material	da/dN specimens	Tensile Specimens
2024-T3	*5 Compact Tension* W = 1.11 inches thickness = 0.068 inches	*5 Dogbone Axial* gauge length = 1.5 inches thickness = 0.070 inches
7075-T6	*7 Compact Tension* W = 1.11 inches thickness = 0.075 inches	*2 Dogbone Axial* gauge length = 1.5 inches thickness = 0.080 inches
7178-T6	*4 Compact Tension* W = 3.00 inches thickness = 0.192 inches	*5 Dogbone Axial* gauge length = 1.5 inches thickness = 0.192 inches

Testing Conditions

- Stress Ratio R = +0.1
- Frequency = 10 Hz
- Temperature = 72°F ± 2°F
- Relative Humidity = 85% ± 2%

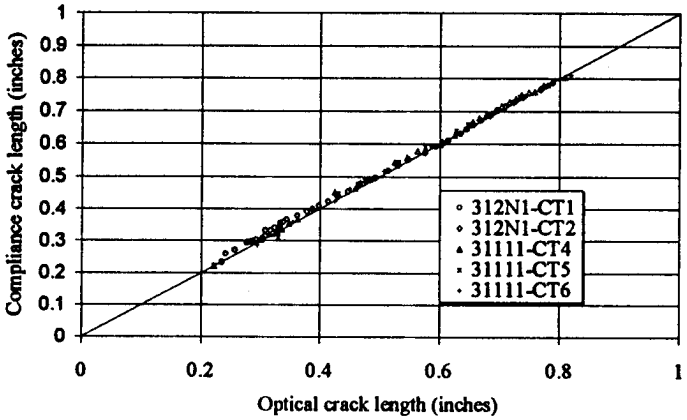


Crack Length Measurements

- Compliance
  - Clip gage and MATE Software run from digital computer
- Optical Measurements
  - 40x traveling microscope and digital scale
  - Polished uncorroded side, both if no corrosion present

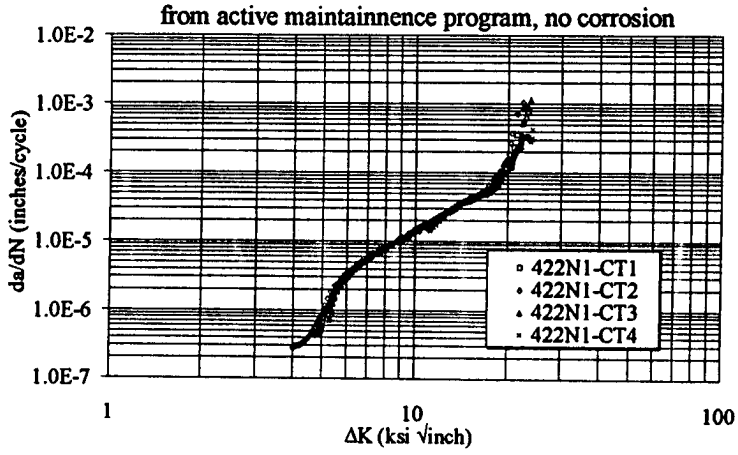
7075-T6 Crack Length Measurements

Crack length comparison between optical and compliance methods



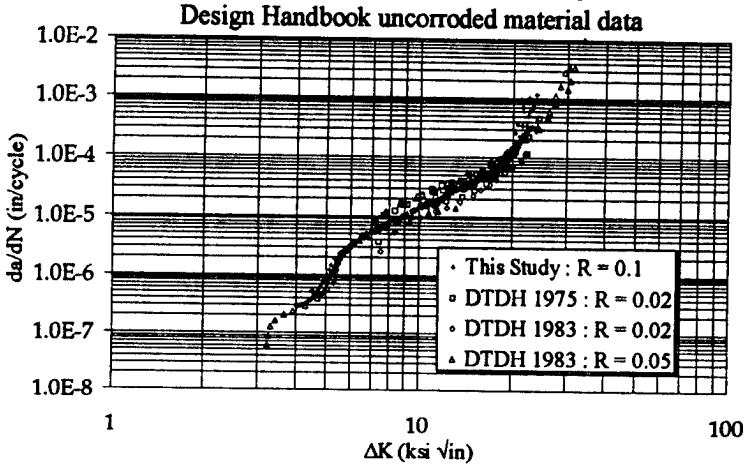
7178-T6 da/dN vs. ΔK

Specimen comparison from 707-320C Upper Wing skin from active maintainnence program, no corrosion



7178-T6 da/dN vs. ΔK Handbook Comparison

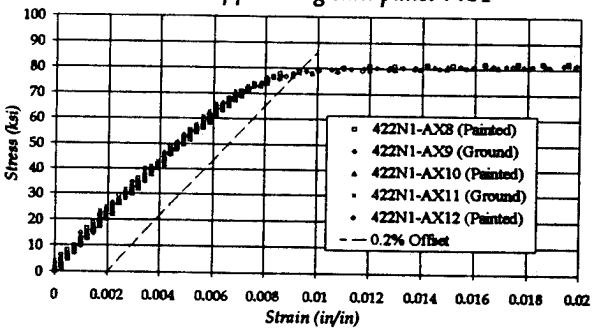
Comparison of aged 7178-T6 with Damage Tolerant Design Handbook uncorroded material data



7178-T6 Stress-Strain Comparison

- Young's Modulus
  - Exp - 10.80 Msi
  - Ref. - 10.40 Msi
- Yield Strength
  - Exp - 78 ksi
  - Ref. - 78.0 ksi
- Ultimate Strength
  - Exp - 84 ksi
  - Ref. - 88 ksi

5 aged dogbone subsize specimens from 707-320C upper wing skin panel W31

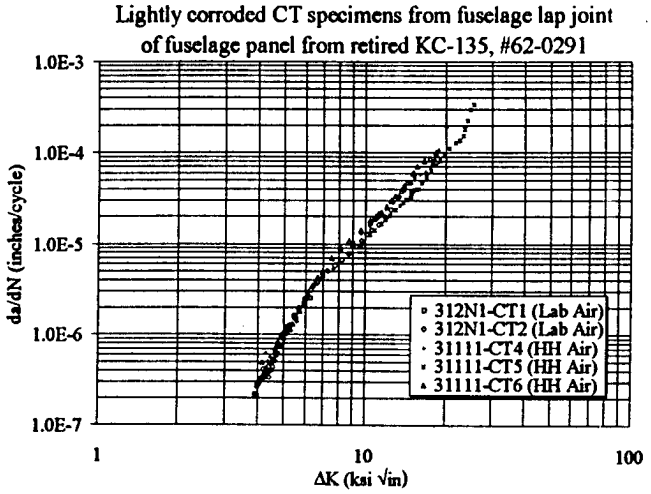


Reference : Metals Handbook, Volume 2, Properties and Selection: Nonferrous Alloys and Special-Purpose Materials, Tenth Edition, 1990.

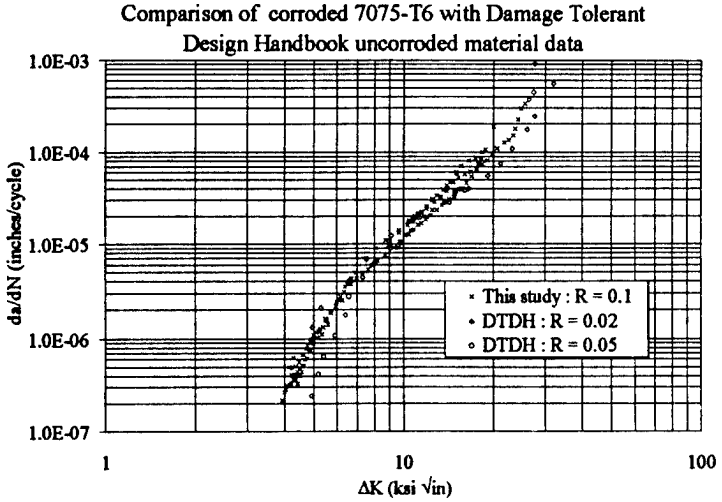
Photo of Specimen 31111-CT6

- 7075-T6 material from KC-135 #62-0291
- Joint - Lightly corroded

7075-T6 da/dN vs. ΔK

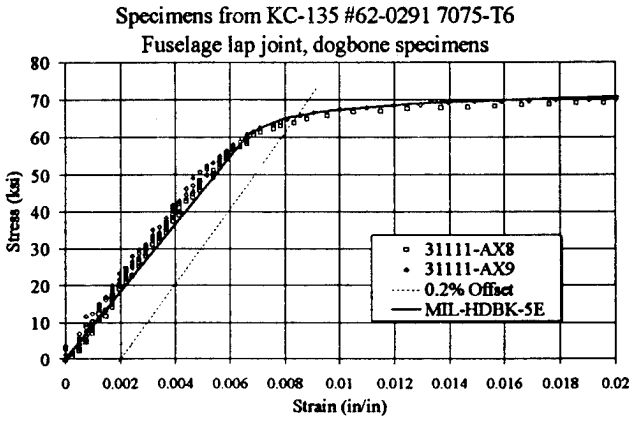


7075-T6 Handbook Comparison



7075-T6 Stress-Strain Handbook Comparison

- Young's Modulus
  - Exp. - 10.2 Msi
  - Ref. - 10.3 Msi
- Yield Strength
  - Exp. - 65.5 ksi
  - Ref. - 67.0 ksi
- Ultimate Strength
  - Exp. - 73.0 ksi
  - Ref. - 76.0 ksi

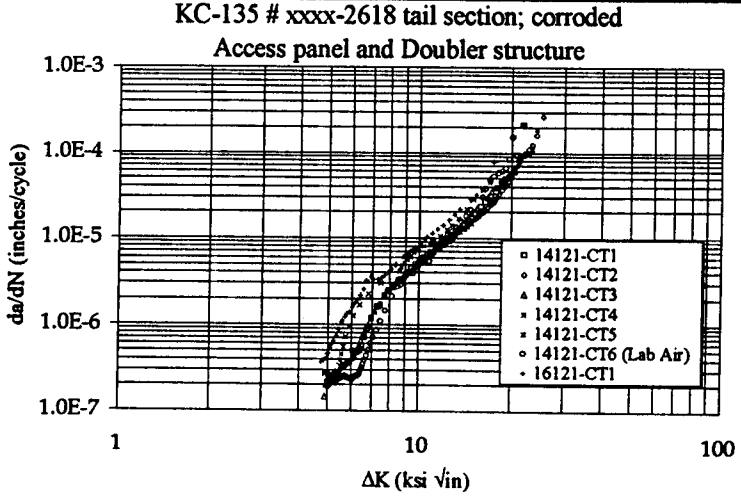


Reference : MIL-HDBK-5E, Military Standardization Handbook, Metallic Materials and Elements for Aerospace Structures, 1987.

Photo of Specimen 14121-CT6

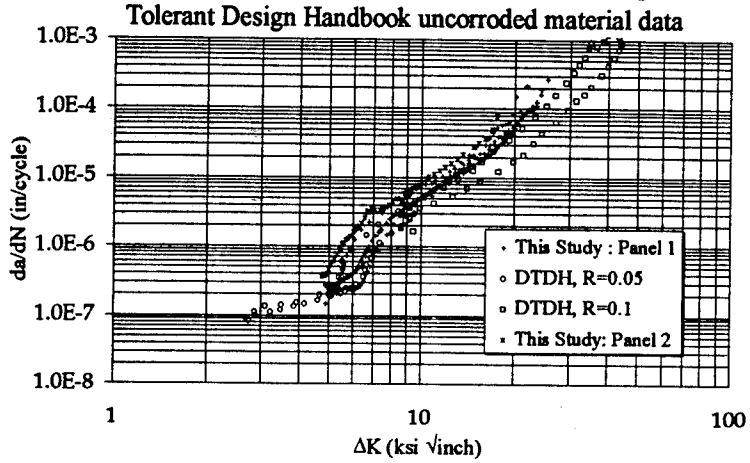
- 2024-T3 material from KC-135 #xxxx-2618
- Joint - moderately corroded

2024-T3 da/dN vs. ΔK



2024-T3 da/dN vs. ΔK Handbook Comparison

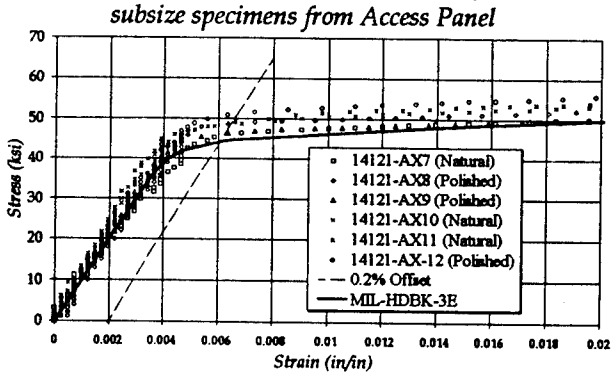
Comparison of corroded 2024-T3 with Damage Tolerant Design Handbook uncorroded material data



2024-T3 Stress-Strain Handbook Comparison

- Young's Modulus
  - Exp. - 10.86 Msi
  - Ref. - 10.50 Msi
- Yield Strength
  - Exp. - 47.0 ksi
  - Ref. - 40.0 ksi
- Ultimate Strength
  - Exp. - 63.4 ksi
  - Ref. - 61.0 ksi

6 dogbone (corroded and uncorroded) from subsize specimens from Access Panel



Reference : MIL-HDBK-5E, Military Standardization Handbook, Metallic Materials and Elements for Aerospace Structures, 1987.

Future work

- Additional da/dN vs ΔK testing
  - Different Load Ratios (R = 0.3 or 0.5)
  - Aged only (no corrosion)
- S-N testing
  - Notched and/or smooth tests
  - Representative Stress Levels
- Corrosion Quantification

Summary and Conclusions

- Fatigue crack growth and stress/strain tests were conducted on retired aircraft components
  - 2024-T3 : KC-135 Access Panel & KC-135 Doubler Structure
  - 7075-T6 : KC-135 Fuselage Lap Joint
  - 7178-T6 : 707-320 Upper Wing Skin Butt Joint
- Tensile properties appear unchanged with respect to Handbook
- Minimally corroded R=0.1 da/dN similar to Handbook Data
  - 7075-T6 ("lightly" corroded)
  - 7178-T6 (no corrosion)
- R=0.1 da/dN-ΔK corroded 2024-T3 differs from Handbook data
  - Slightly faster crack growth rate compared to uncorroded data
  - More variability in the corroded material with respect to the non-corroded Handbook material

HANDBOOK OF NONDESTRUCTIVE EVALUATION (NDE)

CAPABILITY AND RELIABILITY*

Ward D. Rummel
Martin Marietta Astronautics Group
Post Office Box 179, Mail Stop T320
Denver, CO 80201

and

George A. Matzkanin
Nondestructive Testing Information Analysis Center (NTIAC)
TRI-Texas Research Institute
Austin, Inc.
415 Crystal Creek Drive
Austin, TX 78746

INTRODUCTION

Nondestructive inspection (NDI) is often the primary basis for establishing the initial flaw size that is used as the basis safe life analysis of components, structures and systems. It is often desirable to use a small initial flaw size for purposes of fatigue and fracture analysis, thus the capability of applied the nondestructive inspection procedure often becomes a primary design constraint. The introduction of fracture mechanics analysis in design applications has established requirements to quantify the capabilities of applied nondestructive inspection procedures for purposes of determining the "largest flaw that might be missed". That flaw size, in turn, becomes the starting point for fracture mechanics analysis and for crack growth in fatigue life analyses. It is clearly desirable to start with a very small flaw size. In recent years, considerable effort has been expended in both meeting "attainable" flaw requirements and in improving NDI procedures capabilities to detect smaller flaws. Such efforts have identified uncertainties in fracture mechanics analysis procedures in predicting the behavior of small flaws and have greatly increased the complexity and sophistication of NDI procedures being applied.

A large gap exists between the expectations of the capabilities of many NDI procedures and the demonstrated / validated capabilities. One hallmark of maturity of an engineering technology is the ability to quantify the capabilities and reliability of application of the tools that are used in that technology. While methods have been developed and much work has been completed to quantify and document NDE procedure

* This project is sponsored by the Defense Technical Information Center (DTIC), Alexandria, Virginia through the NTIAC program at the Texas Research Institute, Inc.

capabilities, no single baseline reference has been available to integrate this work with user requirements or to provide a baseline reference for NDE engineers and implementers.

Questions of primary engineering interest in the application of NDE are:

- What inspection?
- How small a flaw can it detect?
- What are the relative costs of inspection?
- What special equipment and/or facilities are required?
- What are the special personnel training and skill development requirements?
- What objective evidence of the inspection (out put) is provided?

The answers to those questions are scattered in different reference sources and are not specifically available for many NDE procedures and applications. To this end, the task of documenting demonstrated NDE capabilities in a single reference source is underway and will be published in the form of a handbook.

PURPOSE AND SCOPE

The purpose and goal of the handbook is to provide an initial, single baseline reference source for documented NDE process capabilities and for development, quantification, validation and use of new NDE procedures; more succinctly to provide a common engineering / application knowledge baseline. It is intended to be a general reference and guideline for communicating, documenting and using quantitative nondestructive evaluation capabilities (performance levels) as applied to various material, geometric configurations and systems under various operating / application conditions. Data and reference documentation have been gathered from currently available sources and are being included in the Appendix Volumes to the handbook. Data additions to the Appendix Volumes are anticipated in future work.

HANDBOOK STRUCTURE

The mode of documentation in the handbook is intended to answer many of the primary engineering questions on NDE applications and to present the information and answers in a form that will be most useful to the users of the technology. Primary anticipated use of the information / data provided are in:

- Hardware / system design
- Production / process acceptance
- Field maintenance and life-cycle management
- Hardware / system life extension
- System requalification and acceptance
- Hardware / system retirement for cause

Anticipated individual users of the information / data provided are:

- The designer
- The materials engineer
- The reliability and safety engineer
- The maintenance engineer
- The manufacturing / production process engineer
- The liaison (rework and repair) engineer
- The life-cycle maintenance manager
- The hardware / system operator and customer(s)
- The NDE engineer
- The NDE process manager
- The NDE engineering technology manger

The points of view of the diverse population of anticipated users have been kept in mind in organizing and classifying the information in terms of NDE questions most frequently posed and the applications of the technology. Handbook organization has therefore been approached as a compliance matrix with the intent of rapid access to answer questions of primary engineering interest. This approach combines ideas of a "HELP" module that is familiar to users of modern computer software programs with additional focus on "what I want to know" from the perspective of specific, anticipated users. The general structure of the handbook is shown schematically in FIGURE 1.

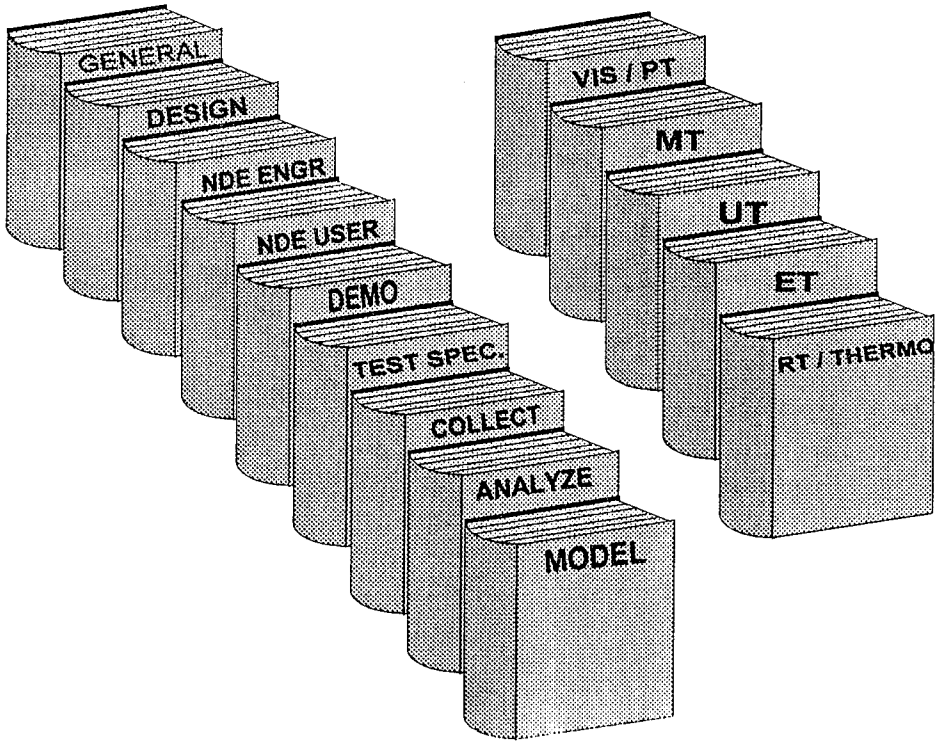


Figure 1. Handbook Structure.

HANDBOOK APPLICATIONS

AS A GENERAL DESIGN REFERENCE - To identify requirements for, and use of, a "minimum detectable flaw size" that may be used in fracture mechanics analyses as a basic design parameter; to identify boundary conditions and operating constraints that may vary the "minimum detectable flaw size" that can be used in design analysis; and to identify requirements and considerations in establishing a "minimum detectable flaw size" for use in life cycle management.

GENERAL NDE ENGINEERING DESIGN REFERENCE - To provide a general reference for selection of candidate NDE procedures; to establish requirements for determining and validating the capabilities of specific NDE procedures applications; and to identify requirements and process control methods for maintaining continuing NDE performance capabilities.

GENERAL REQUIREMENT FOR THE NDE USER - To provide a general reference for materials, equipment, procedure, calibration, and personnel qualification and validation for quantitative NDE processes.
GENERAL REQUIREMENTS FOR DEMONSTRATION OF NDE CAPABILITIES - To provide general requirements and consideration for demonstrating NDE capabilities for small flaws and / or special operating conditions.

GENERAL REQUIREMENTS FOR TEST SPECIMENS - To provide general guidelines for generation, validation, documentation, control and use of test specimens for quantitative NDE demonstration.

GENERAL REQUIREMENTS FOR DATA COLLECTION - To provide general guidelines for data collection in quantitative NDE capabilities demonstrations.

GENERAL REQUIREMENTS FOR DATA ANALYSIS - To provide general guidelines for data analysis and data presentation for purposes of quantitative NDE capabilities validation / demonstration.

PREDICTIVE METHODS FOR QNDE - To provide guidelines for predicting NDE procedure capabilities by experiment and modeling.

CONTENT

APPENDICES - Appendices will be added to provide documentation of demonstrated NDE capabilities as applied to different test objects and problems. These will be organized into separate sections to document the capabilities by NDE method.

RAW DATA - Raw data that supports the capabilities documented in the appendices will be archived in electronic form. Tentatively, the data will be stored in "Microsoft - Excel" spread sheet format. Alternate formats may also be used to assure continuing capabilities for access. It is anticipated that this will be initially in magnetic (floppy disk) media and will be later transferred to compact disk for storage and distribution. An on-line down load capability may be provided depending on demand and resources.

GUIDELINES FOR ADDING TO THE DATABASE - The quantitative NDE process capabilities database is anticipated to continue to grow and the baseline document will include provisions for adding to the database within the resources available.

SUMMARY AND CONCLUSIONS

The is great need for, and interest in, a baseline, general reference source for the generation, control and use of nondestructive evaluation data. Some of the difficulties in building such a reference are in the diverse sources of data and the diverse media on which it is stored. As might be anticipated, strong interest in the handbook has been expressed by the NDE community and useful suggestions have been made for both structure and content. Strong interest has been shown by the user communities in providing a basis for design assumptions and inclusion of initial flaw sizes in flaw growth analysis tools (NASA FLAWGRO*). We anticipate interest in linking this work to analytical tools necessary to build integrated engineering capabilities. It is expected that the handbook will meet a growing need and that continuing support and update will be necessary.

The nature of the work is such that caution in use of data provided must be made and understood by all users. Notably:

This document shall not be used as the primary basis for establishing acceptance criteria. Design acceptance criteria must be established analytically as part of the integrated design process ([i.e. system functional analyses, stress analysis, thermal analysis, fracture mechanics analysis (FAIL SAFE), life-cycle fatigue analysis (SAFE-LIFE), etc.] Users are cautioned that "The guidelines and data presented are specific to the applications and conditions that accompany the data description. Special conditions and/or applications of NDE in the production process must be included in the NDE requirements and process analyses; for example, etching may be required before penetrant inspection and penetrant inspection data on properly prepared test objects are not applicable to inspections performed without preparation".

INFORMATION AND DATA PRESENTED IN THIS HANDBOOK ARE INTENDED FOR TECHNICAL REFERENCE ONLY. THE RESPONSIBILITY FOR DEMONSTRATING NDE CAPABILITIES REMAINS WITH THE USER.

ACKNOWLEDGMENTS

This work is being performed under contract DLA900-90-D-0123 / D.O. No. 5 from the Defense Technical Information Center, Headquarters, Cameron Station, Alexandria, VA,22314.

Eddy Current Inspection Reliability at Airline Inspection Facilities

Floyd W. Spencer
Sandia National Laboratories
Albuquerque, New Mexico 87185-0829

1994 USAF Structural Integrity Program Conference
6-8 December 1994
San Antonio, TX

ABSTRACT

High-frequency eddy current inspections are an integral part of routine maintenance checks and of directed checks for surface fatigue cracks in aircraft fuselage skins. To investigate the achieved reliability in inspections performed in airplane maintenance facilities, an experiment using simulated lap splice joints was designed at the FAA's Aging Aircraft NDI Validation Center. The work was sponsored by the Federal Aviation Administration Technical Center in Atlantic City, New Jersey.

The goal of the experiment was to quantify the reliability of inspections as they are routinely performed in aircraft maintenance facilities. The participants performed the inspections using their own equipment and procedures. The experiment was located in work areas where this type of inspection would normally occur. Included in the experiment design were issues of accessibility, crack orientation, and surface condition (painted or bare).

The experiment was taken to nine (9) maintenance facilities from March to August 1993. At each facility, four (4) inspectors inspected 924 rivet sites. One of the inspectors repeated the inspection. One hundred eighty-four (184) of the 924 rivet sites contained cracks of known length, varying between 0.014 and 0.800 inches. Fifty-seven of the sites contained contained cracks emanating from both sides of the rive. All the cracks were fabricated through load cycle fatigue in aircraft skin material. All inspections were observed and detection data gathered by a team of monitors.

Analyses of the data from the 45 inspections are presented here in the form of probability of detection curves and false call rates. Factors found to affect the probability of detection curves are discussed briefly.

INTRODUCTION

High-frequency eddy current inspections are an integral part of routine maintenance checks and directed checks for surface fatigue cracks in airplane skins. The objective of the Eddy Current Inspection Reliability Experiment (ECIRE) reported on here was to evaluate the capability and reliability of eddy current inspection procedures as they are done routinely at airline maintenance and inspection facilities. Besides data needed to quantify the capability and reliability associated with the inspection process, data were also gathered on the facility environment and on the

training and background of inspectors. Trained monitors traveled with the experiment and recorded, not only the inspection results, but also observations on the maintenance environment and procedures. The intent was not only to be able to quantify the capability and reliability associated with the inspection process, but also to provide some insight into how the process could potentially be improved.

The design considerations for the experiment are given in reference [1]. This paper will focus on summarizing the individual probability of detection curves that were fit to the detect no-detect data gathered in the field experiment. Reference [2] contains additional analysis of the data.

BACKGROUND

The experimental hardware was designed and fabricated to simulate the fuselage of typical narrow body transport aircraft. See Figure 1. Known flaws were engineered into two types of test specimens. Two monitors traveled with the experiment to set up the experimental hardware within each facility visited and to record inspection results. The choice of the lap splice and the curvature of radius that simulates the narrow body transports is one of convenience. The essential inspection characteristic being studied is that of detecting a crack originating from fastener holes in thin aluminum structure.

The experiment was taken to nine (9) different facilities. The facilities were chosen to obtain a cross-section of those where inspections of transport aircraft are performed. At each facility, four inspectors (or inspection teams) completed the inspection task. At each facility, one of the four inspectors (or inspection teams) performed the inspection a second time. The net result was 45 inspections.

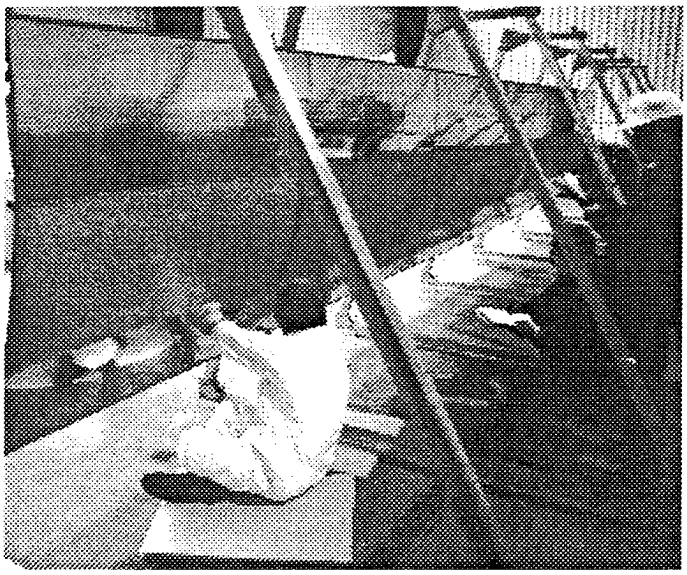


Figure 1. Presentation of lap splice skin specimens. Inspector is shown inspecting bottom row.

The experiment allowed inspections to occur as they normally would in a non-test situation. Therefore, the equipment and the procedures followed were of the inspector's own choosing. This included the use of two person teams to accomplish inspections, if that was normal procedures. The only potential departure from a routine inspection was in the way the inspectors were asked to record the results of their inspection. Crack detections were marked directly on a piece of protective tape put into place before each inspection.

Factors that were accommodated in the overall experimental design are: test specimen type, crack length distribution, off-angle cracks, inspection surface, accessibility, inspection time, shift work, crack density, and within-inspector repeatability. The manner in which each of these factors was addressed is described below.

Test specimen type. Two types of test samples were used in the experiment. One type was 20 inch by 20 inch panels that could be moved and presented differently to each inspector. See Figure 1. This minimized the transference of crack pattern knowledge from one inspector to the next. This was important because of the extended time (approximately one week) that the experiment was located at each participating facility. The 20 inch by 20 inch panels simulated fuselage lap splice joints. The specimens consist of two plates fastened together, using three rows of rivets. These specimens simulated the skins in the lap splice joint without any substructure. They were assembled on a frame and butted against each other to represent a longitudinal lap splice joint.

The second specimen type was large panels produced with all the structural components found on an aircraft fuselage. Figure 2 shows the backside of these specimens. These specimens contained a single lap splice. Cracks were generated in the panels using a custom designed load machine developed for this purpose [3]. The structural test frame provided a bi-axial load (hoop stress and axial stress) that simulated the fuselage loads incurred during aircraft pressurization. The loads were applied in a cyclic manner and the cracks were allowed to initiate as they would in a high cycle aircraft. The aircraft panels were designed to be more realistic than the skin specimens both in size and features. They were included in the experiment to assess any effects in the inspection task that could be attributed to the lack of total realism in the construction and crack placements in the skin specimens.

Crack length distribution. The crack length distributions are reflected in Figure 3. All crack lengths are measured from the rivet shank. The procedures followed by the inspectors call for setting up their equipment on 0.100 inch flaws. It was believed that extending the flaw distribution to include flaws in the 0.2 inch range would be adequate to cover possible detection rate degradations that might occur.

Off-angle cracks Two levels (11° and 22°) of off-angle cracks were included in the lap skin specimens. The top level was chosen to reflect observed characteristics of field detected cracks [4]. Of the 122 lap skin rivet sites containing cracks, 75 were horizontal, 21 were at 11°, and 26 were at 22°. (An additional 62 sites on the large panels contained cracks, but angles were not controlled on these specimens.)

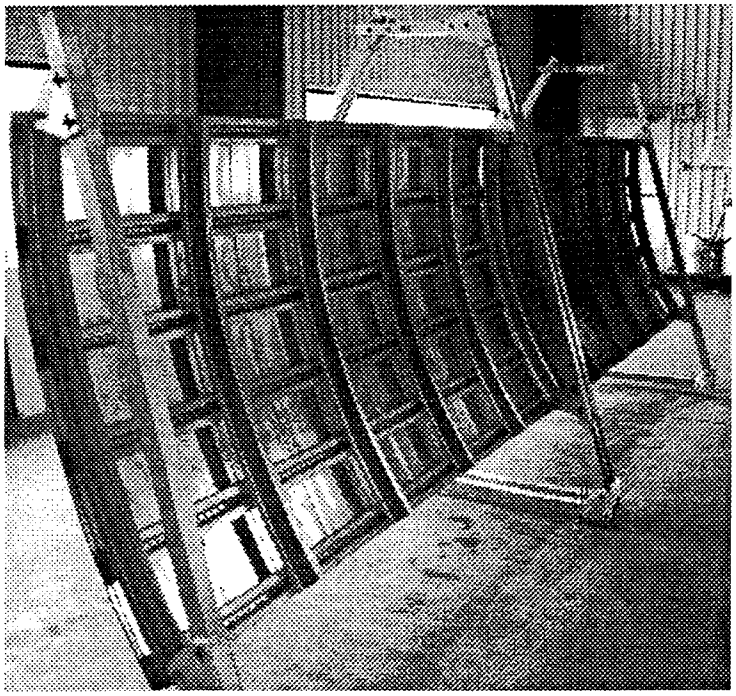


Figure 2. Backside of aircraft panels showing structure.

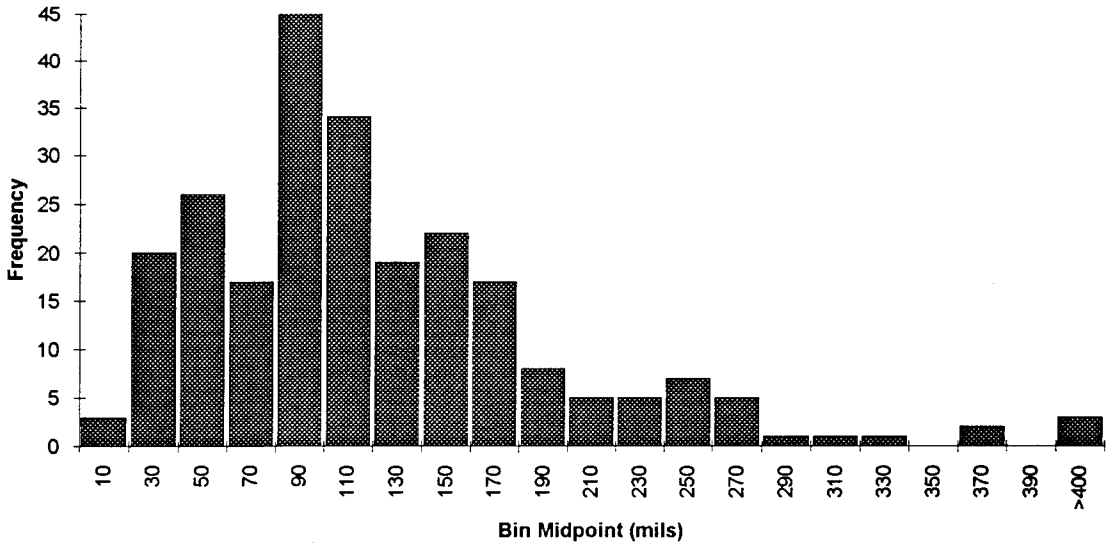


Figure 3. Distribution of crack lengths (241 total cracks).
Some cracks occured in pairs at a single rivet site.

Inspection surface The intent in the design of the experiment was for inspections to be done as they would normally. In a pre-visit questionnaire, the facilities indicated normal surface

conditions, bare or painted, for their inspections. Some indicated that an inspector could be asked to perform a lap splice inspection on either type of surface. On the basis of the questionnaire responses, the surfaces of the 20 inch square skin panels were bare at four (4) of the sites. They were subsequently painted for the final five (5) facilities. To enable a comparison of the effect of the painted condition that would not depend upon the facility choice, one of the full-size aircraft panels (the large panels) was painted and one was not. This condition was maintained at all the facilities.

Accessibility Intuitively, inspection reliability could deteriorate if the inspectors were forced into uncomfortable postures. To address this issue, one half of the skin specimens were presented at approximately knee height (24 inches), while the other half of the specimens were approximately five feet high. See Figure 1. This presentation was done for every one of the inspections. The placement of skin panels was altered between each inspection at a given facility so that each crack was presented in the upper lap splice row twice and in the lower, knee high, row twice.

Inspection time The total amount of inspection included in this experiment was based on estimates of the amount of inspection necessary to take approximately four (4) hours. This amount of time was thought to be enough to allow for the task to become routine, thereby allowing the inspector to "settle into" the inspection.

Shift work Shift work was recognized as a potential variable that could influence inspection results. When possible, inspections were obtained from the various shifts worked within a facility. Many of the facilities did not employ eddy current inspectors during a graveyard shift. Fewer inspectors worked the evening and graveyard shifts, thereby making it harder for the facility to free up inspectors in these shifts. Working with these types of constraints, seventeen (17) of the forty-five (45) inspections occurred on evening and graveyard shifts.

Crack density Does the performance of an inspector change when many cracks are being detected versus when few are being detected? With this question in mind, each of the rows of lap splice was broken into regions of various crack concentrations. Doing this also helped alter the perception of the inspectors to keep them from drawing conclusions concerning the amount of cracks present at any given time in the inspection.

Within inspector repeatability A given inspector using the same equipment and the same procedures may not achieve the same level of performance with every inspection. To estimate how much variation could be expected in individual inspections, one inspector (or team) at each facility was asked to repeat the total inspection task. This was done by asking the inspector doing the first inspection to return after all four of the initial inspections had been completed. The order of the skin test specimens was changed between the two inspections so that the inspector could not rely on his recollection of flaw locations. The inspections also occurred at least three days apart.

The eddy current reliability experiment was taken to nine (9) facilities between April 1, 1993, and August 13, 1993. The facilities visited were: American Airlines in Tulsa, Oklahoma; Dalfort Aviation in Dallas, Texas; Aloha Airlines in Honolulu, Hawaii; Tramco in Everett, Washington; Alaska Airlines in Seattle, Washington; United Airlines in San Francisco, California; Delta Airlines

in Atlanta, Georgia; US Air in Winston-Salem, North Carolina; and Miami NDT in Opa-Locka, Florida. The data that are reported in the next section are not tied to the individual facilities, as confidentiality of results was promised.

ANALYSIS OF DATA

Probability of detection curves have been used extensively to assess the accuracy or reliability of NDI systems and procedures. Background discussion of PoD curves can be found in Berens [5], Annis, et. al. [6], and Hovey and Berens [7]. Here, the results of fitting a probit model are given. Let Y be the random variable that takes on the value of 1 if a crack is detected and the value 0 if the crack is not detected. Then probit model for the probability of detection can be expressed as

$$\mathrm{PoD}(a) = \Pr(Y=1 \mid a) = \Phi(\alpha + \beta \cdot log(a)), \qquad (1)$$

where a is the crack length, α and β are parameters to be fit to the data, Φ is a cumulative distribution function, and $log(\,)$ is the logarithm function. The basic PoD model can be extended to include explanatory factors other than $log(a)$. This is done by expanding $\alpha + \beta \cdot log(a)$ into more parameters that denote the state of other factors present at the time of inspection. This is done in reference 2.

In the probability of detection curves presented here, a modifation of equation (1) was made to model non detections that occured independent of the crack length. The need for such a model was suggested by observing inspectors and noting certain habits that would lead to missed cracks regardless of the length of those cracks.

Specifically, several of the inspectors were observed stopping their inspection to move equipment and then resuming their inspection at a different point, thereby missing several rivet sites. Inspectors also reacted to distractions (e.g., loud noise, conversations with other personnel) and it was not clear that they had maintained their attention through a completed inspection at a given rivet site. One inspector relying on an audible alarm did not immediately respond to hangar ambient noise rising to levels that could effectively mask the instrument alarm. Some of the inspectors experienced intermittent problems with their equipment. All of these conditions lead naturally to considering a PoD model that incorporates a background miss rate independent of crack size.

This extension of the PoD model is accomplished by replacing the model of equation (1) with

$$\mathrm{PoD}(a) = \Pr(Y=1 \mid a) = (1-C) \cdot \Phi(\alpha + \beta \cdot log(a)), \qquad (2)$$

where C is the background miss rate. The parameter C is estimated along with α and β from the data. Note, that the effect of adding this background miss rate is that of having an asymptote other than 1 for the probability of detection, given arbitrarily large cracks.

The Probability of Detection curve fits for the data gathered in this experiment were obtained with the commercially available software SAS®. Specifically, the SAS procedure PROBIT was used.

The PROBIT procedure calculates maximum-likelihood estimates. Details are given in reference [8].

In the pre-inspection briefings, we requested that the inspectors mark the location of cracks around the rivet. The intent was to determine whether all cracks had been detected at a given rivet site. In looking at the data it became clear that many of the rivet sites with cracks from both sides were only being marked once. Sometimes the rivet site marking was up or down and could not be unambiguously attributed to either crack. Conversations with some of the inspectors verified that they usually did not mark crack orientations.

In general, the inspectors were not (and not required to be) accurate in specifying crack orientation. Thus, to reflect fairly the detection capabilities, data were analyzed on a rivet site basis rather than by individual cracks. Thus, at rivet sites containing two cracks, the length of the longest crack was used in the analysis.

Here, we will present the results of the individual fits of model 2 to each inspection. Forty-five inspections were performed at the nine participating facilities. The inspection results are coded in the following manner. The nine facilities are coded A through J (no I). The distinct inspections within a facility are coded 1 through 4 and the repeat inspection at each facility is noted by appending an R to the original code. (Thus, A1R denotes the repeat inspection of A1.) Figures 4 through 12 present the individual inspection fits by facility.

The total number of detections and the number of false calls for each inspector are given in the legend of the graphs of Figures 4 - 12. The "lighter" curves in the figures are for the set of inspections done by the same inspector(s). The equipment and procedures used by the inspectors are given in reference [2].

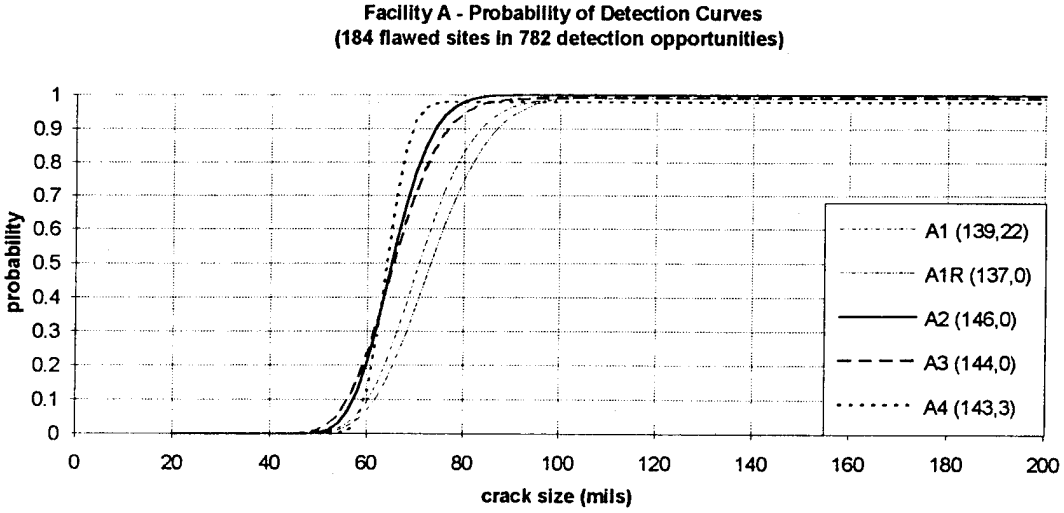


Figure 4 Facility A inspections with (# detects, false calls)

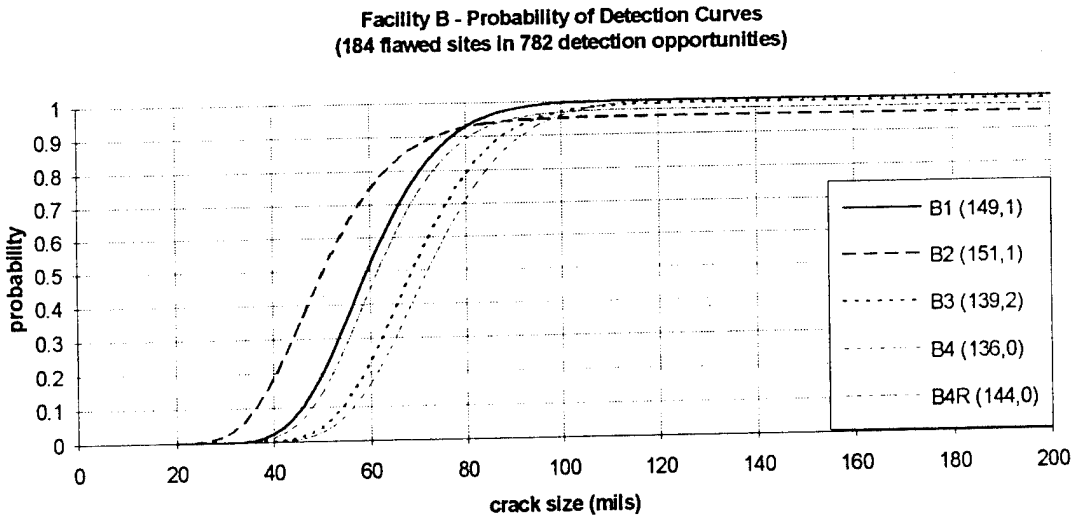


Figure 5 Facility B inspections with (# detects, false calls)

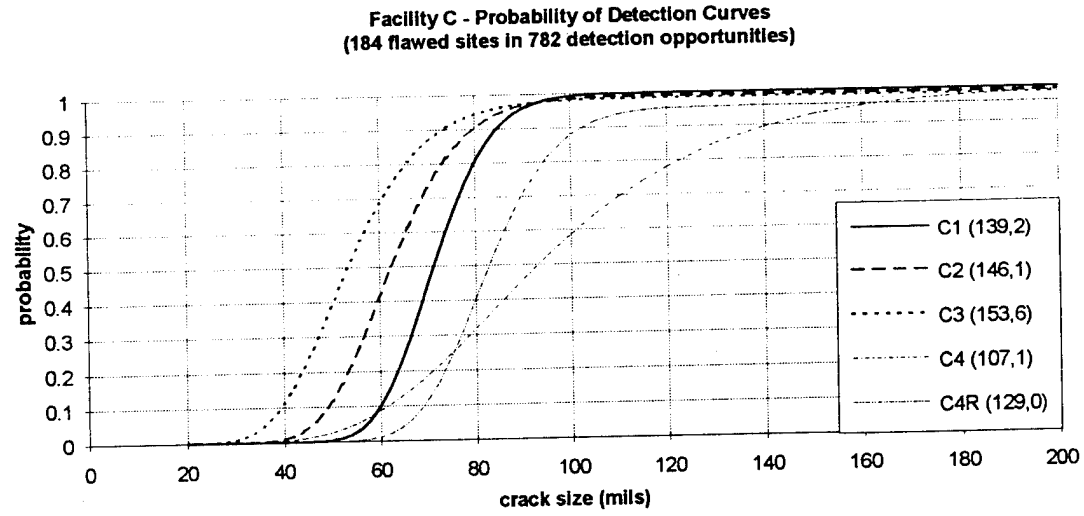


Figure 6 Facility C inspections with (# detects, false calls)

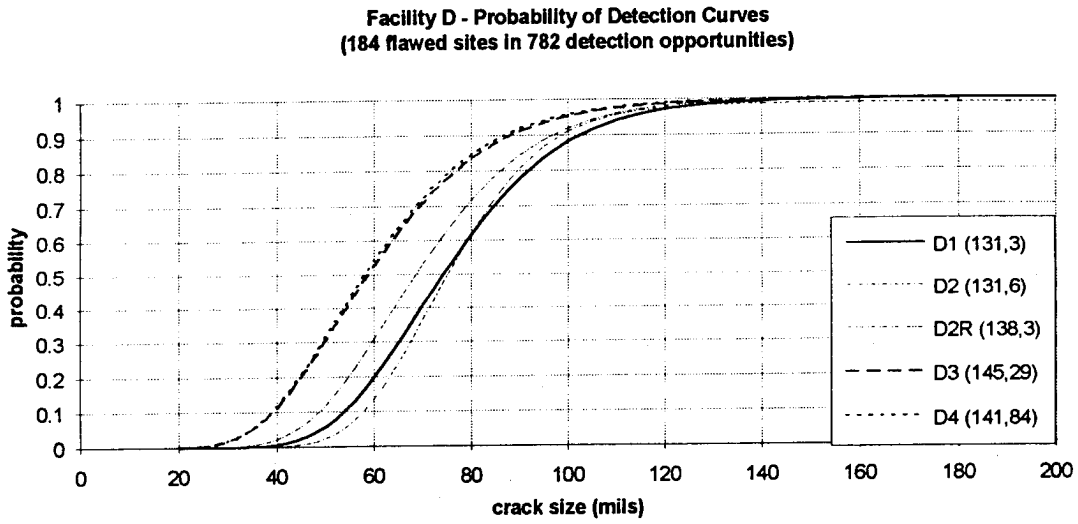


Figure 7 Facility D inspections with (# detects, false calls)

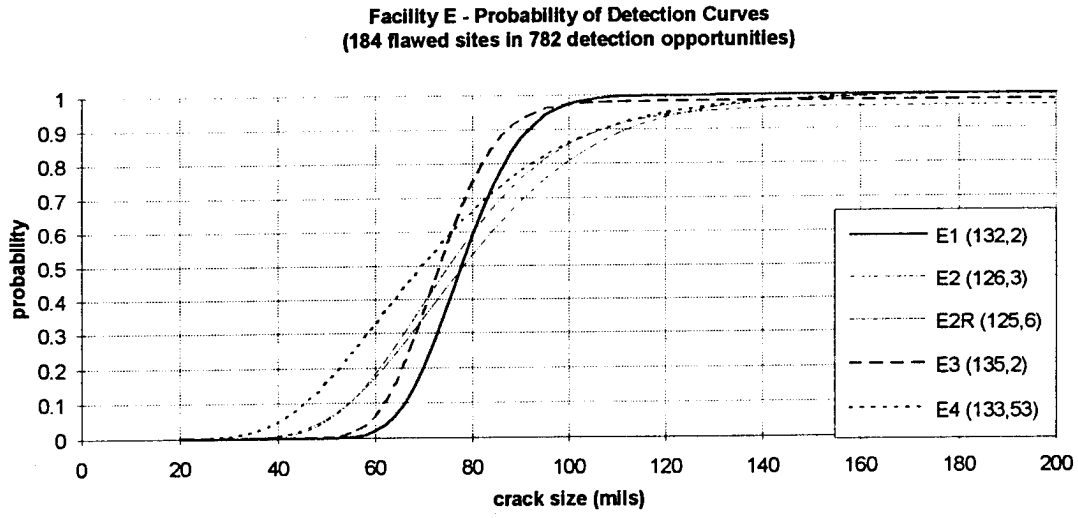


Figure 8 Facility E inspections with (# detects, false calls)

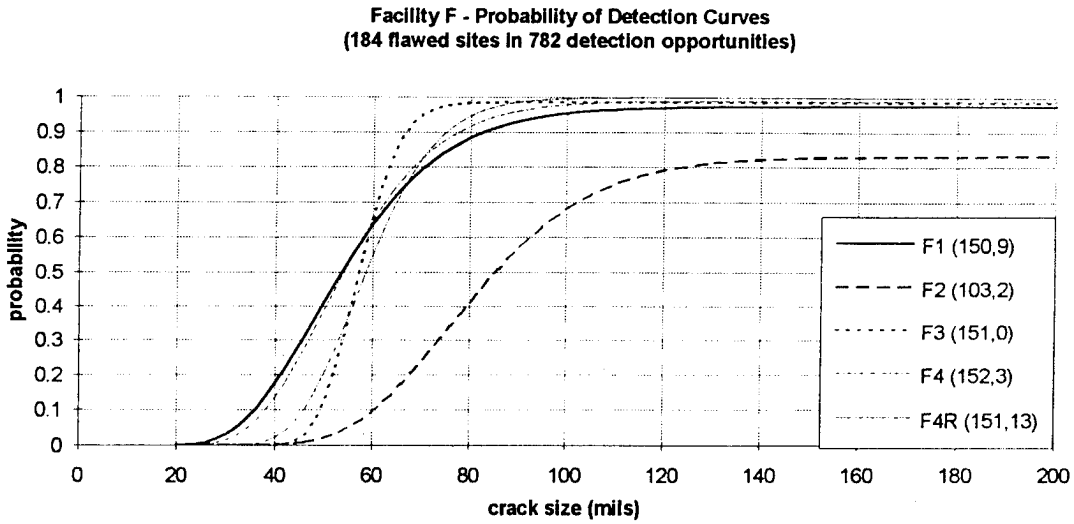


Figure 9 Facility F inspections with (# detects, false calls)

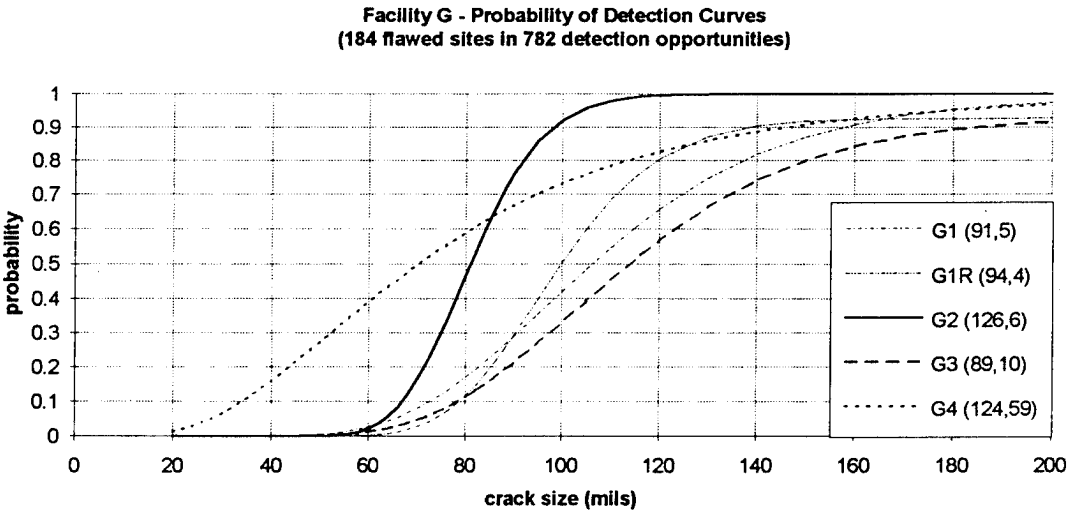


Figure 10 Facility G inspections with (# detects, false calls)

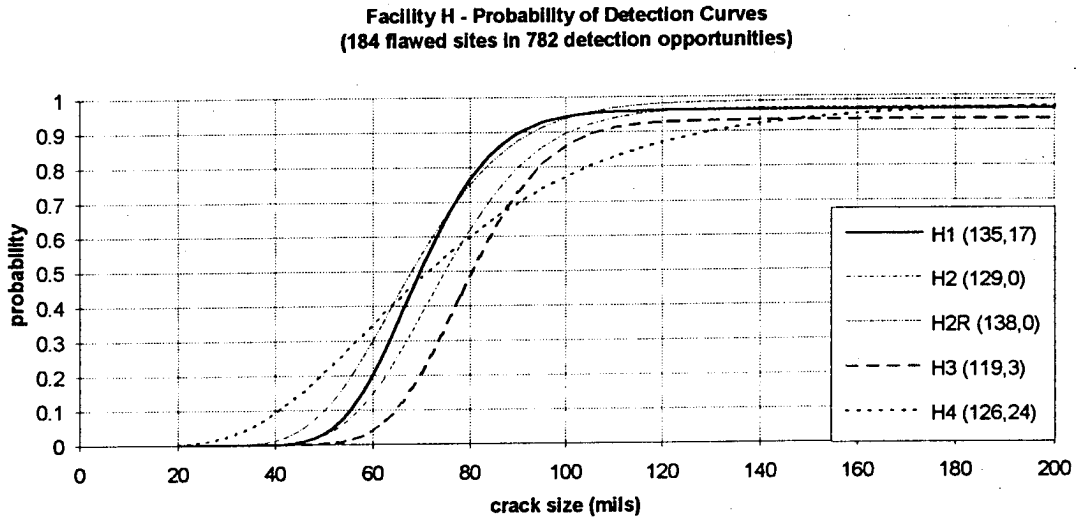


Figure 11 Facility H inspections with (# detects, false calls)

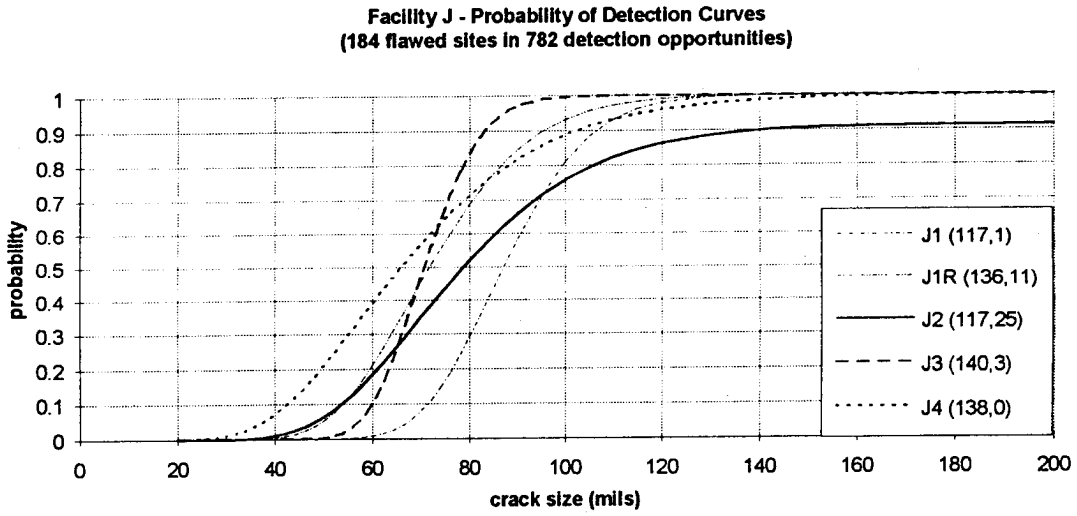


Figure 12 Facility J inspections with (# detects, false calls)

Figure 13 presents single PoD curves fit to the composite data. The proportion of time that each of the 184 flawed sites was detected is shown versus the length of the crack. Also shown are the lognormal curves that are fit to the data with and without the threshold parameter, C. It is stressed that the PoD so represented is an average across inspectors and conditions. It is clear from the curves of Figures 4 through 12 that there was substantial variation amongst the different inspections.

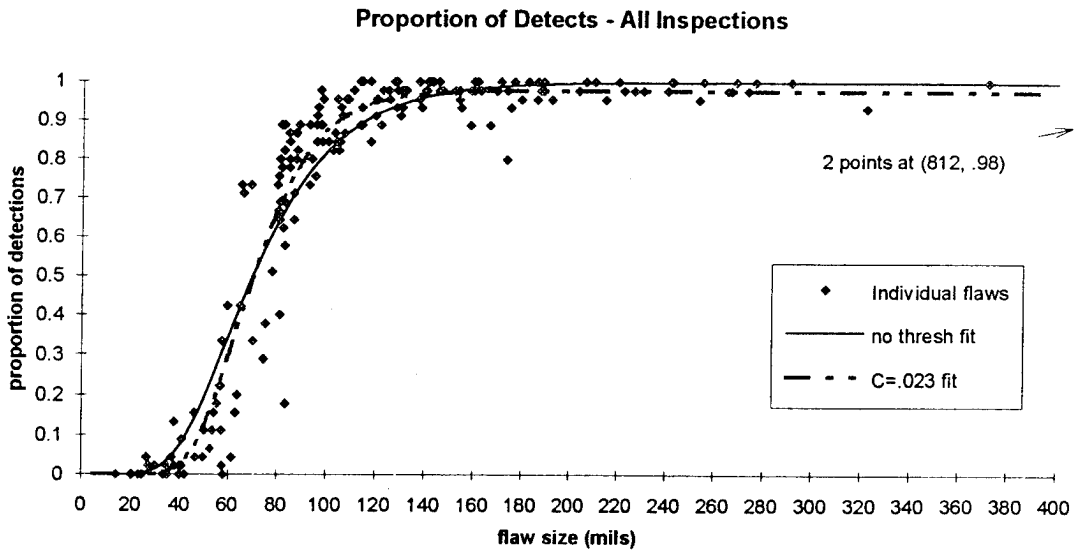


Figure 13 Proportion of detects for all inspections -- with lognormal PoD fits

An analysis for the effects of various factors is given in reference 2. We note here that surface condition at time of inspection (painted or bare), crack orientation, and "accessibility" were factors that influenced the detection rates. The surface condition accounted for shifts of approximately 10 mils in the PoD curves, with the painted surface having a lower probability of detection. There was also a higher background miss rate for the inspections performed on the painted surfaces. The off-angle cracks had lower probability of detection than did the horizontal cracks, with shifts of approximately 13 mils. The more inaccessible the lap splice, the lower the probability of detection, however, the difference was slight.

SUMMARY

Many of the individual inspections were better modeled by introducing a threshold parameter, C, to model a background miss rate. With this parameter in the model, PoD curves increase with larger crack lengths to (1-C) rather than to 1. The estimated background miss rates from the 45 inspections ranged from 0 to 0.168, with an overall average of 0.024.

The incorporation of the threshold, C, into the modeling is consistent with field observation of the inspectors. Some of the conditions contributing to background miss rates, independent of crack length, that were observed are: inadequate procedure to maintain position when moving equipment, lapses of attention, intermittent problems with equipment, and the masking of audible alarms by ambient and intermittent noise in the facility.

Individual Inspection Performance

Procedures called for setting up the eddy current equipment on a calibration standard containing a 0.100 inch crack. Table 1 summarizes how each of the 45 inspections performed about this 0.100 inch level. Shown in the table for each inspection are the largest crack lengths missed, the number of sites missed that contained cracks exceeding 0.100 inches in length, the estimated 90 percentile crack length, and the estimated background miss rate.

***Table 1** Individual Inspection Summary*

Inspection	Largest crack missed (mils)	number missed > 100 mils*	background miss rate (C) estimate	PoD 90th percentile estimate
A1	158	1	.010	83
A1R	87	0	0	87
A2	78	0	0	74
A3	130	1	.010	77
A4	215	3	.021	69
B1	75	0	0	77
B2	322	5	.048	73
B3	154	1	.010	88
B4	88	0	0	92
B4R	174	3	.027	81
C1	87	0	0	84
C2	192	1	.009	80
C3	160	2	.015	73
C4	174	14	0	141
C4R	174	5	.043	102
D1	102	1	0	102
D2	169	2	.013	98
D2R	118	2	0	97
D3	83	0	0	88
D4	85	0	0	87
E1	102	1	0	91
E2	186	5	.034	107
E2R	140	4	0	112
E3	131	2	.018	87
E4	105	1	0	107
F1	175	2	.024	82
F2	812	19	.168	-
F3	118	1	.014	67
F4	222	1	.009	77
F4R	83	0	0	75
G1	188	20	.010	157
G1R	240	17	.073	138
G2	96	0	0	98
G3	322	25	.066	184
G4	158	9	0	146
H1	189	4	.038	90
H2	174	5	.032	101
H2R	812	2	.012	93
H3	322	7	.068	107
H4	265	8	.024	130
J1	105	3	0	106
J1R	98	0	0	95
J2	253	11	.086	141
J3	82	0	0	83
J4	130	2	0	102

* There were a total of 98 rivet sites containing cracks that exceeded .100 inches in length

Eleven of the 45 inspections (24%) were accomplished without missing any cracks exceeding .100 inches in length. An additional 16 of the inspections (36%) detected all but one or two of the .100 inch cracks. On the other extreme, there were six inspections (13%) where eleven or more of the .100 cracks were missed. In all six of the extreme cases, other inspections at the same facility and using the same equipment were performed without any misses of cracks greater than .100 inches. Thus, factors specific to the inspectors and the procedures that they individually follow are implicated as a major source of variation, as opposed to inadequate equipment.

The Eddy Current Inspection Reliability Experiment grew from a basic question about how effective inspections were being done in the aircraft maintenance and inspection facilities. The overall ECIRE field-derived curve is shown in Figure 14 with the curves reported by Boeing in reference [9]. Recall that the ECIRE allowed inspectors to follow their usual procedures. As such the results in Figure 14 are a mixture of template and sliding probe procedures. Also, crack characteristics, such as orientation angles, or other known influential factors have not been accounted for in comparing the ECIRE to the Boeing curves. It is noted however, that inspections occuring in the field are capable of achieving detection rates similar to that obtained in more favorable laboratory settings.

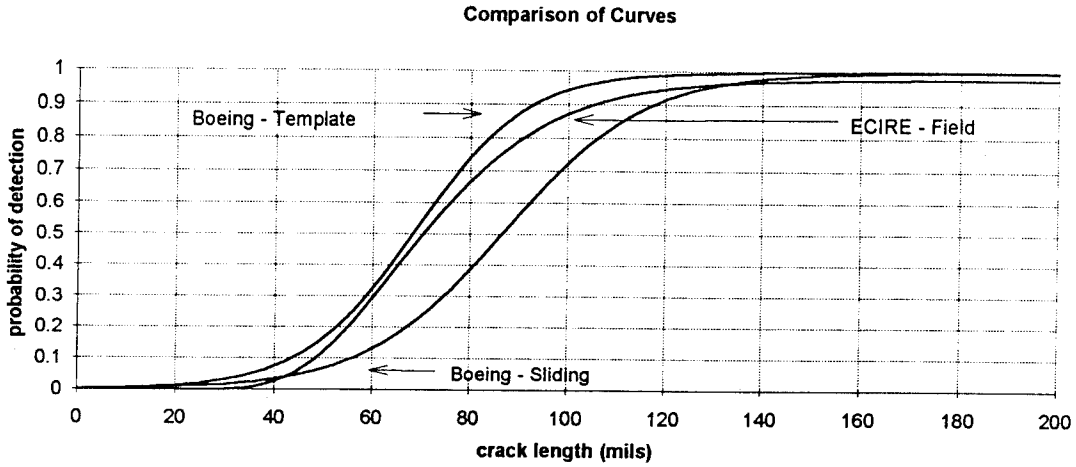


Figure 14 Comparison of PoD curves.
Boeing curves are from Reference [9]. Different test specimens and protocols used in each experiment.

REFERENCES

1. Spencer, Borgonovi, Roach, Schurman, and Smith, "Reliability Assessment at Airline Inspection Facilities, Vol. II.: Protocol for an Eddy Current Inspection Reliability Experiment," DOT/FAA/CT-92/12, II, May 1993.

2. Spencer, F. W. and Schurman, D. L., "Reliability Assessment at Airline Inspection Facilities, Vol. II.: Results of an Eddy Current Inspection Reliability Experiment," DOT/FAA/CT-92/12, III, forthcoming.

3. Samavedam, G. and Hoadley, D. "Fracture and Fatigue Strength Evaluation of Multiple Site Damaged Aircraft Fuselages - Curved Panel Testing and Analysis," Foster-Miller Report No. DTS-9024, May 1991.

4. Swift, T., "Information: Multi-Site Damage," FAA Memorandum from National Resource Specialist, Fracture Mechanics/Metallurgy to Manager, Aircraft Engineering Division AIR-100, January 3, 1991.

5. Berens, Alan P., "NDE Reliability Data Analysis," in *Metals Handbook Volume 17, 9th edition: Nondestructive Evaluation and Quality Control*, ASM International, 1988.

6. Annis, C., Berens, A., Bray, F., Erland, K., Hardy, G., Herron, W., Hoppe, W.. "Proposed MIL-STD for USAF NDE System Reliability Assessment (Draft)," August, 1989.

7. Hovey, P. W. and Berens, A P., "Statistical Evaluation of NDE Reliability in the Aerospace Industry," in *Review of Progress in Quantitative Nondestructive Evaluation*, Vol. 7B, Thompson, D.O. and Chimenti, D.E. editors, pgs 1761-1768, Plenum Press, 1988.

8. SAS Institute Inc., *SAS/STAT® User's Guide, Version 6, Fourth Edition, Volume 2*, Cary, NC: SAS Institute Inc., 1989.

9. Hutchinson, M. C., "Reliability of Eddy Current Lap Splice Inspection Procedures (Interim Report)," Boeing QCR&D document PE373A-1, April 1991.

ACKNOWLEDGMENTS

This work was funded by the Federal Aviation Administration Technical Center (FAATC), Atlantic City International Airport, New Jersey. Dr. Christopher Smith was the FAATC technical monitor. Science Applications International Corporation and AEA Technology also participated in the planning and implementation of the experiment.

Exfoliation Corrosion Located By Search Peening

By James R. Harrison
Manager Technical Services - Wichita,KS
E. Roger Thompson
Manager Technical Services - Newbury, UK

A Presentation for the 1994 U.S.A.F. Structural Integrity Program Conference

Abstract

Search peening can be defined as the use of controlled shot peening as a tool to expose subsurface corrosion. The stretching of the surface coupled with the compressive stress induced by the multiple impacts of the shot help to delaminate hidden layers, as is found in exfolliation corrosion.

Recently, Boeing Airplane Company's Defense and Space Group, in association with the United States Air Force, funded a study to determine the application of using shot peening to identify exfoliation corrosion. Metal Improvement Company and British Airways have also developed a method to determine the extent of corrosion so that the removal of damage can be accomplished with a high degree of accuracy. This certifiable controlled process, "search peening," allows a minimal amount of metal removal, so that engineers have the maximum acceptable material to work with, enabling them to keep tolerances within safe limits.

Introduction

A section of a wing panel taken from a Boeing 707 with existing severe exfoliation corrosion was supplied by Boeing. The purpose was to demonstrate the benefits of sho peening the upper wing skins of KC135 tankers to identify areas of corrosion not visible at the surface. Metal Improvement's intention was to show, on the one panel, all

stages of the process from paint removal through sanding, and search peening, to final shot peening, in accordance with Boeing and military specifications. Later in the paper we will show the use of search peening to repair the horizontal stabilizer center section attachment lugs on older 737s. It should be noted that many of the aircraft designed and manufactured in the 50's and 60's used aluminum alloys, such as 7075-T6, 7079-T6, and 7178-T6, that were more susceptable to corrosion than materials used today. For both commercial and military operations, corrosion has been a major factor in the decision to retire an aircraft.[1]

The Procedure

A line of fasteners was removed by milling off the inner end and driving them out from the inside. The panel was then marked into six areas for progressive treatments. Areas were identified as bands A - F on the edge of the panel. The processing was carried out as follows:

1. Band A was masked and left untreated to show the condition as received.

2. The unmasked area (B - F) was plastic media blasted to remove paint without affecting the material or the corroded areas.

3. Band B was masked and the remainder (C - F) was aluminum oxide blasted to clean the surface and remove products of corrosion.

4. With areas A, B, and C masked, the remainder was sanded, per Boeing Overhaul Manual 20-10-3, to remove all visible corrosion (as viewed with a 10X magnifier.) To remove all visible corrosion it was necessary to remove material to depths varying from .004 inch to .035 inch. (See Appendix 1 for details.)

5. Area D was masked to preserve an area showing the typical standard of sanding.

6. Areas E and F were search peened using MI230R media at an intensity of 5A. Note: At the 5A intensity, or approximately .005 inch depth of compression, no exfoliation became apparent. By raising the energy level to 7A or .007 inch compression depth, exfoliation appeared immediately adjacent to several fasteners and at the joint edge.

7. The more obvious exfoliation appeared in area F and it was decided to leave it for demonstration purposes. Band F was therefore masked and processing continued in area E with corrosion removal and final saturation peening at an intensity of .008A2.

Additional Development Work

The Boeing Overhaul Repair Manual 20-10-03 specifies a final saturation intensity for the section thickness of this skin of between 6A and 12A almen intensity. Based on experience, a small area of bands, E and F, was re-peened at the higher energy level of 11 to 13A, thus increasing the

compression depth and the stretching of the surface. Although slightly higher than that specified by Boeing, this higher intensity level provided evidence of further exfoliation at greater depths.

Summary of Observations

1. There was severe exfoliation at the outset across all bands. (See Photo 1, Appendix 2)

2. Neither plastic media nor aluminum oxide blasting caused more corrosion to become visible but the plastic media blasting focused attention on the corroded areas.

3. At the initial sanding stage, corrosion was found to extend well into the countersink on two holes where fasteners had been removed. No further corrosion was found on search peening these areas. The compressive residual stress left by shot peening these as well as all other areas compensates for the stress raiser effect caused by material removal, therefore increasing overall damage tolerance.

4. Search peening at 5A did not show additional corrosion, but re-peening at 7A brought out exfoliation at fastener locations, panel edges and at a countersink which had been slightly sanded.

5. Peening at full saturation intensity (8A) also showed more exfoliation, but no more was found where fasteners had been removed.

6. Search peening also showed up an area of exfoliation not associated with a hole or edge. This area became visible only as a result of search peening.

7. After re-sanding and re-peening twice at the same intensity in most areas (three times in some), no further exfoliation became evident.

8. Further peening at 11A to 13A, a higher intensity than required by Boeing specification 20-10-3 for the material thickness, did show further evidence of exfoliation at greater depths.

Laboratory Examination of the Wing Panel by Boeing

The panel was examined macro- and micro-scopically to determine the results of the search peening and then sectioned through six fastener holes.

The results of the laboratory examination showed that, "the search peening did reveal surface to slightly sub-surface corrosion." And in the opinion of Boeing's lab, "search peening is effective in detecting surface and slightly sub-surface corrosion, but may not be effective in detecting corrosion that is significantly sub-surface, e.g. exfoliation that originates mid-countersink or in the hole bore."[2] It is interesting to note that no corrosion was found by the lab in the six areas sectioned. The memo went on to say that, "more laboratory testing would be required

to determine the significant depth effectiveness of search peening."

Conclusions

1. Search peening is clearly an aid in identifying exfoliation corrosion. Visual examination alone is inadequate.

2. Search peening at higher intensity has the potential to identify exfoliation at greater depth.

3. Studies should be made to determine at what depths search peening can reliably locate sub-surface corrosion.

4. Controlled shot peening is the only certifiable cold working process that can be used for this process. Often flapper peening is used in small repair areas to induce compressive stresses, but this process is totally operator dependent and not used during manufacturing for many reasons, including the inability to peen areas such as internal radii, holes, and blended areas smaller than ratios of 20 to 1. The depth of compression obtainable by flapper peening generally is less than can be produced by shot peening. Also the time to cover an area such as an entire wing skin can take weeks using flappers versus hours using shot peening. Many engineers responsible for aircraft structures do not consider flapper peening a repeatable, certifiable process, as they do controlled shot peening.

As noted earlier, some aging Boeing 737s have shown corrosion developing on the center section attach lugs of the horizontal stabilizer. Until search-peening was introduced, the only recourse was to machine out the corrosion, often removing more metal than necessary. This process sometimes reduced the lug thickness beyond allowable limits. Since the lugs are part of a large forged spar, the only option was to scrap this very expensive component.

Search peening of these lugs now permits all traces of corrosion to be removed locally, without affecting the overall thickness of the lug, allowing British Airways engineers to keep lugs within safe limits.[3] The repair areas are then shot peened for prevention of fatigue and stress corrosion cracking.

Bibliography

1. Johnson, B.G., and R. Frank, Boeing Aircraft Company, Inter-office memo to G. Miller, September, 1994.

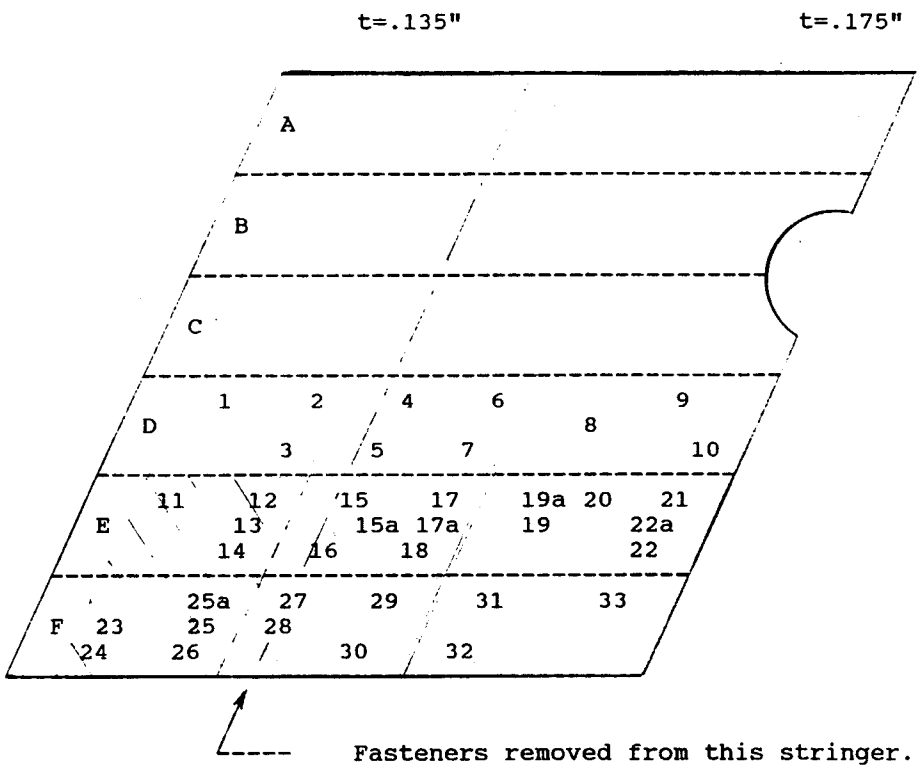
2. Lincoln, John W., and William R. Elliott, "U.S.A.F. Aging Aircraft Program," Aerospace Engineering, October, 1994, p. 11.

3. McGreal, A., British Airways, "Preventative Medicine," World Engineering, September, 1994, pages 12-14.

METAL IMPROVEMENT COMPANY INC.

APPENDIX 1 Sheet 1 of 2

BLEND-OUT DETAILS



Fasteners removed from this stringer.

Band A	=	As received
Bands B-F	=	Plastic media paint stripped
Bands C-F	=	Aluminium oxide blasted
Bands D-F	=	Sanded to remove visual corrosion
Bands E & F	=	Search-peened
Band E	=	Re- sanded & final saturation peened
Shaded area of Bands E & F	=	Re-peened at higher intensity.

Sanded areas are identified by number on the above sketch. Details of depth and width of each blended area are given the Table on Sheet 2 of this appendix.

BLEND OUT DETAILS

No.	BLEND DEPTH		BLEND DEPTH		BLEND RATIO		THICKNESS (MIN)
	1st	FINAL	1st	FINAL	1st	FINAL	
1	0.012		1.2		52/1		
2	0.028		1.35		24/1		.100
3	0.018		0.8		22/1		
4	0.015		0.75		25/1		
5	0.035		1.6		23/1		.100
6	0.030		1.4		23/1		
7	0.033		1.7		26/1		.142
8	0.004		.8		100/1		
9	0.006		.7		58/1		
10	0.006		.8		67/1		
11	0.010		.9		45/1	36/1	
12	0.012	.018	1.2	1.3	50/1	35/1	
13	.004	.022	.7	1.4	87/1	33/1	
14	0.012	.018	1.1	1.2	46/1		
15	0.030		1.7		28/1	83/1	.100
15a	-	.006	-		83/1		
16	0.012		1.25	1.0	52/1	28/1	
17a	-	.025	-	1.3	-		
17	0.012	.015	1.4	1.1	58/1		
18	0.020	.023	1.35	1.3	34/1		
19	0.015		0.9		30/1		.160
19a	-	.008	-	0.7	-	43/1	
20	.006		0.8		67/1		
21	0.010	.022	1.25	1.5	63/1	41/1	
22	.008	.012	1.3	1.3	81/1	54/1	
22a	-	.005	-	0.6	-	60/1	
23	.015		1.3		43/1		
24	.006		1.0		83/1		
25	.019		1.2		32/1		
25a	-		-		-		
26	.006		1.0		83/1		
27	.020		1.1		28/1		
28	.012		0.8		33/1		
29	.015		1.3		43/1		.113
30	.022		1.7		39/1		
31	.008		1.2		75/1		
32	.008		0.9		56/1		
33	.022		1.35		30/1		.153

Areas suffixed 'a' are those where corrosion was not visible prior to peening.

APPENDIX 2 - PHOTOGRAPHS

AS RECEIVED



1. Wing plank section as received. Marked out in bands A-F for progressive treatment.



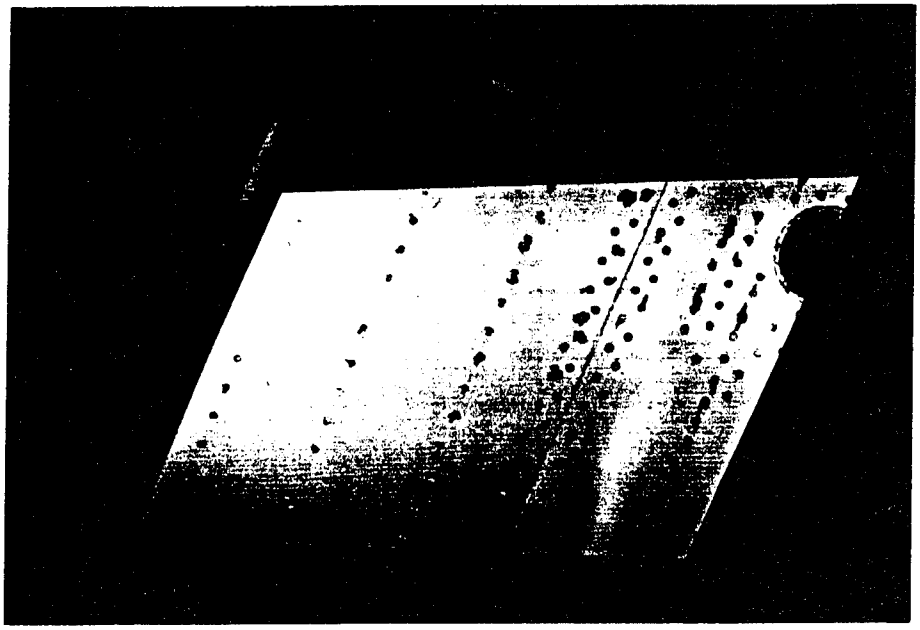
2. Severe exfoliation corrosion at fasteners.



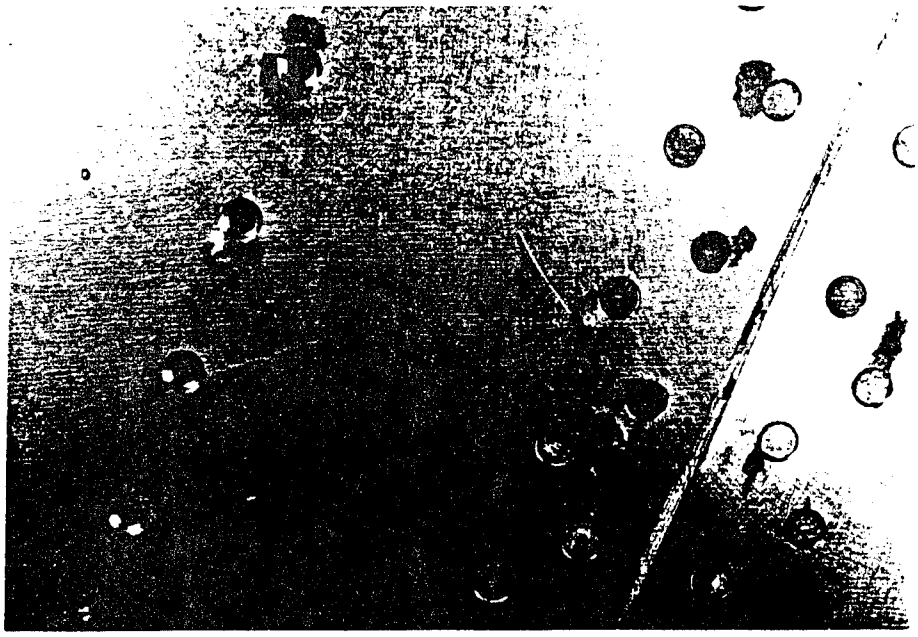
3. One row of fasteners was removed prior to any treatment.

METAL IMPROVEMENT COMPANY INC

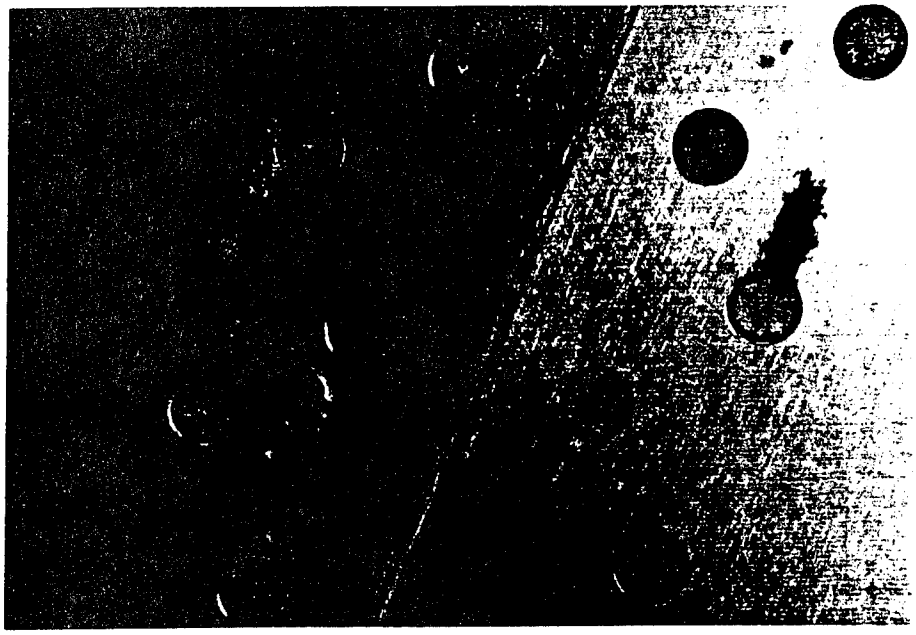
PAINT REMOVED BY PLASTIC MEDIA BLASTING



4. Plastic media paint removal specifically identifies those areas of damage where the substrate is affected as distinct from superficial paint damage. There is little evidence of corrosion away from fasteners.

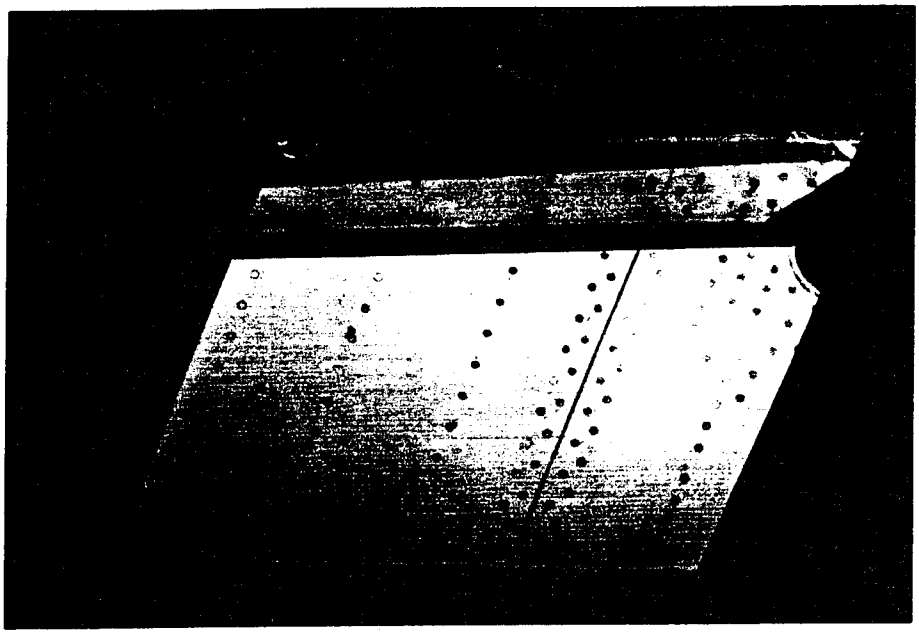


5. Closer view of exfoliation. Also shows one spot of corrosion not associated with a hole or edge.



6. Exfoliation clearly visible around fastener heads.

ALUMINIUM OXIDE BLASTED



7. Aluminium oxide blasting shows no new areas of corrosion.



8. Close up shows severe corrosion around fasteners.

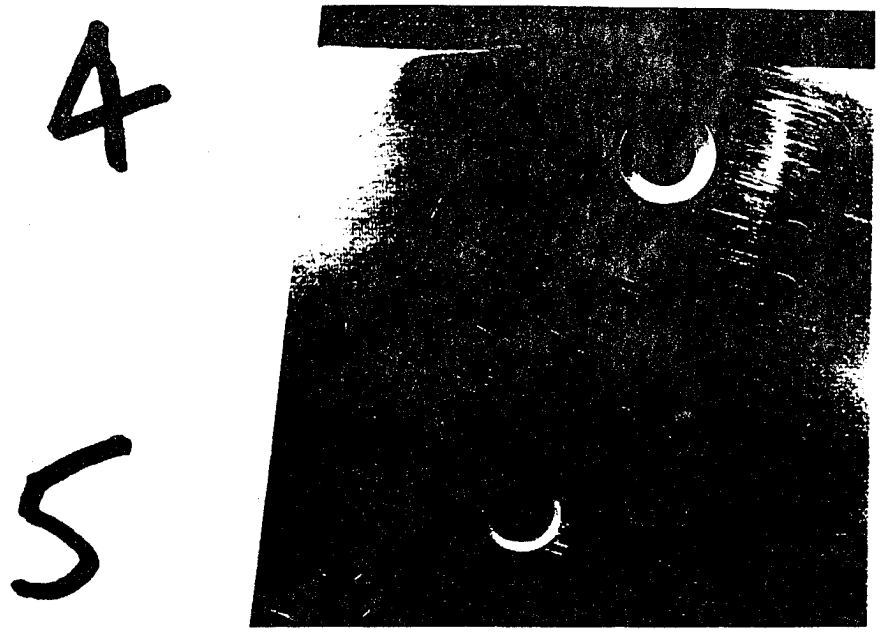


9. Exfoliation corrosion at a countersink. Also shows the spot of corrosion not associated with a hole or edge.

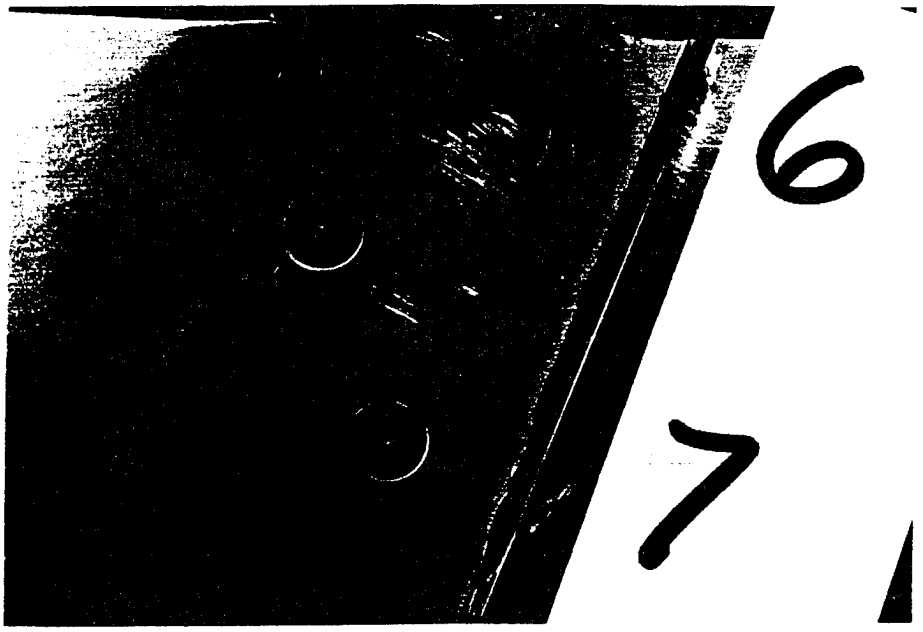
AFTER SANDING TO REMOVE VISUAL CORROSION



10. General view shows areas sanded.
(Numbers in the following photographs relate to the areas mapped out in Appendix 1).

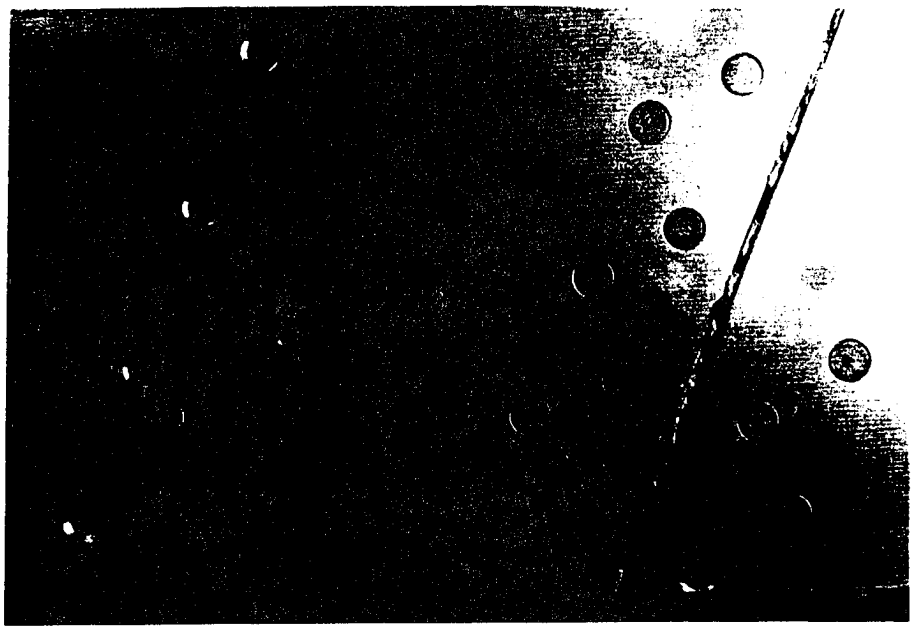


11. Sanding to remove visual corrosion has almost removed the countersink.

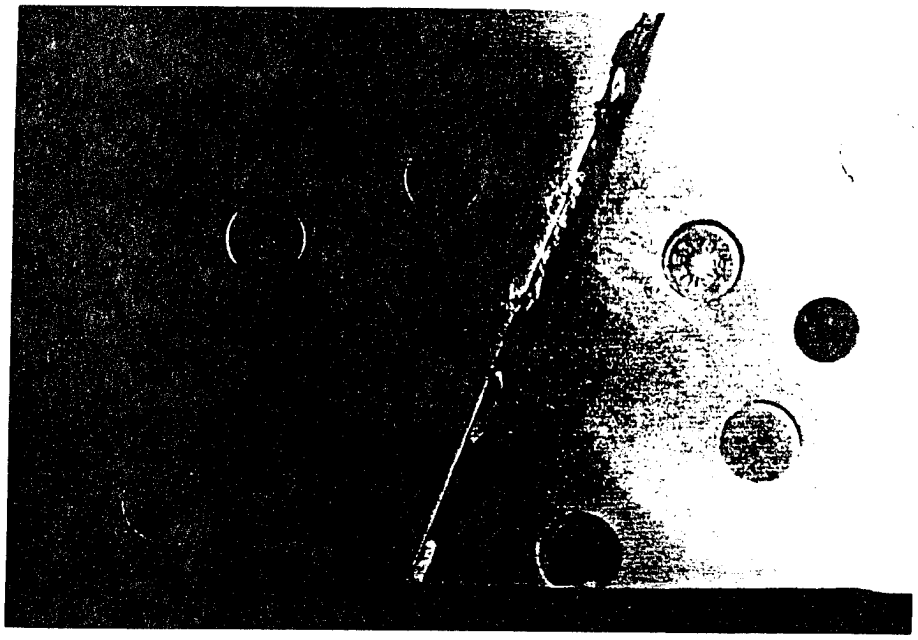


12. Visible corrosion has been removed from around the fasteners.

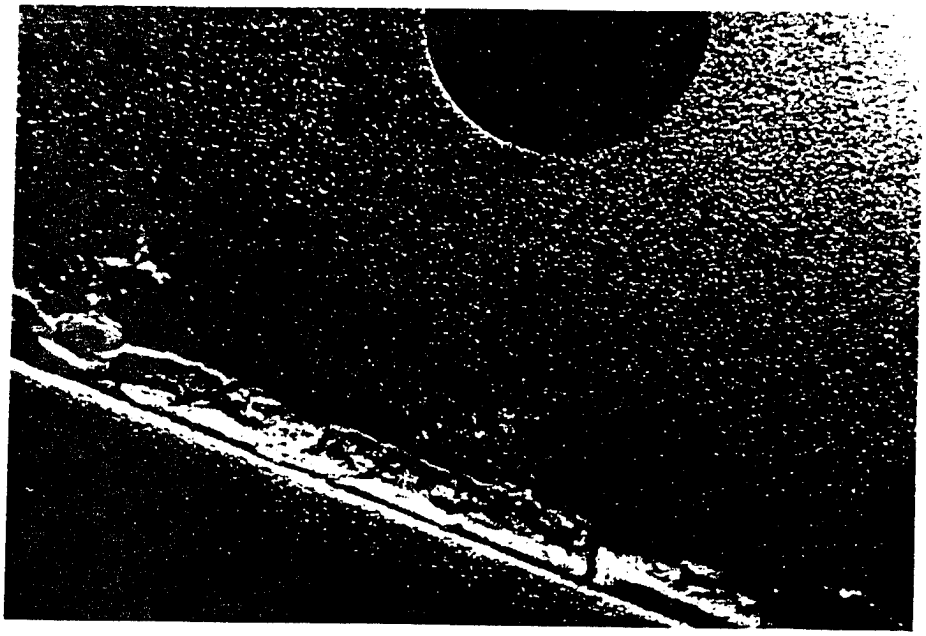
AFTER SEARCH-PEENING



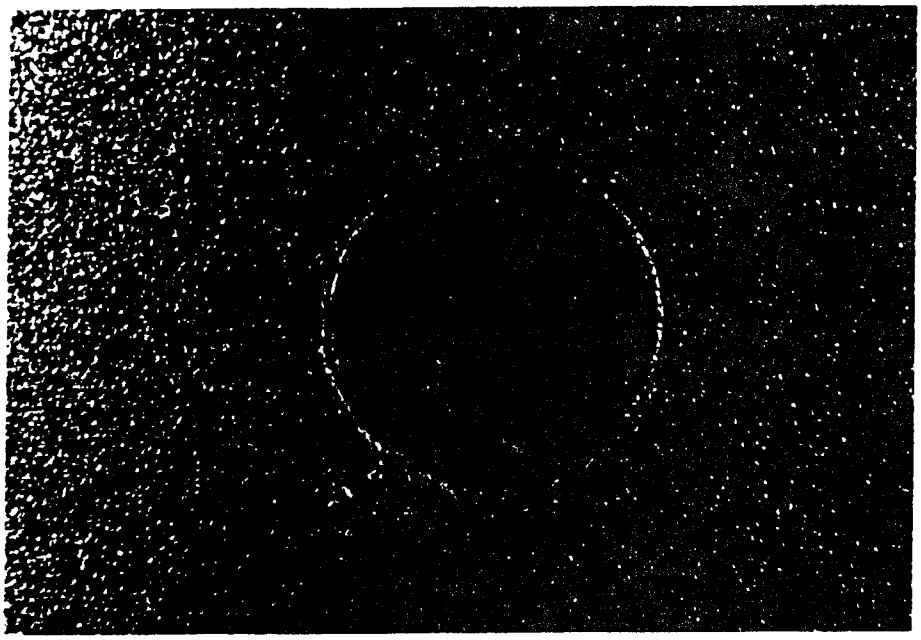
13. Exfoliation becomes apparent at fastener positions and at panel edge where it was not visible before search-peening.



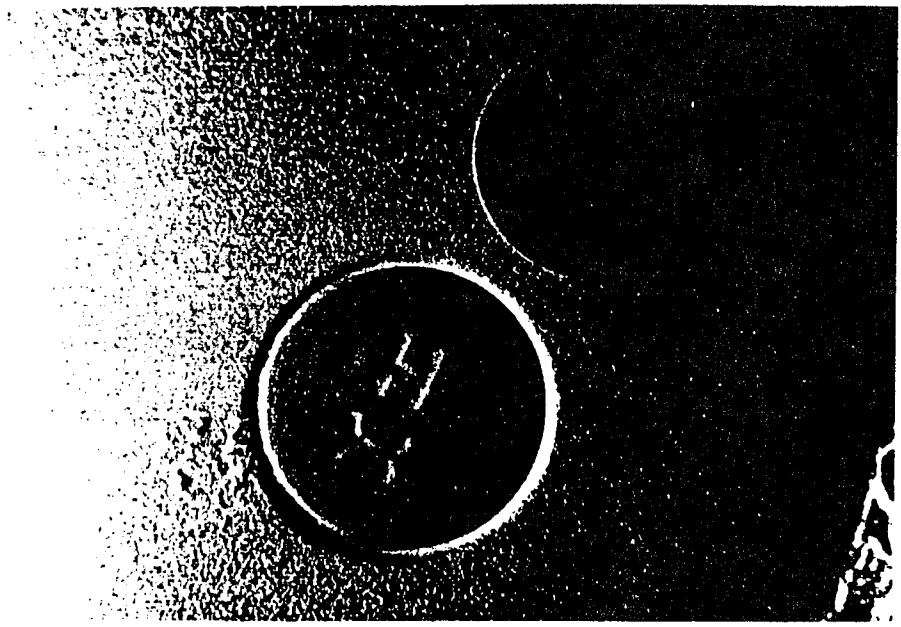
14. After search-peening exfoliation shows as blisters in areas where sanding had removed all visible corrosion.



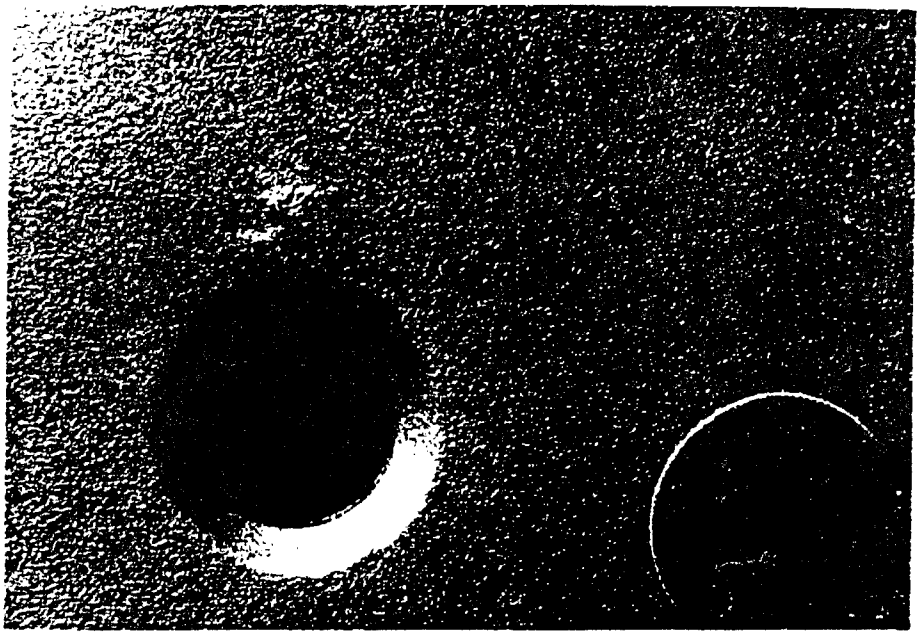
15. Macro view of edge exfoliation.



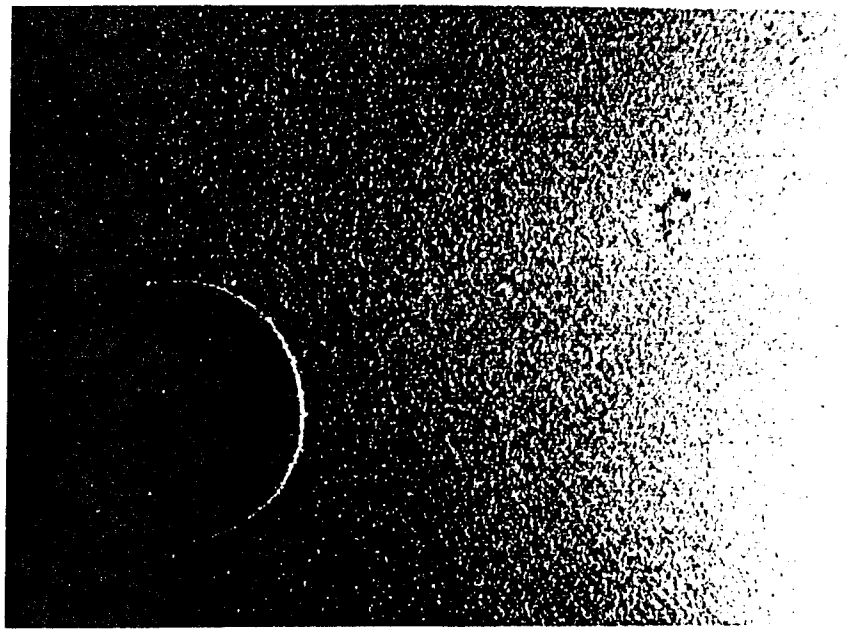
16. This fastener had just a little sanding to remove the visible corrosion. New evidence of exfoliation appeared after search-peening.



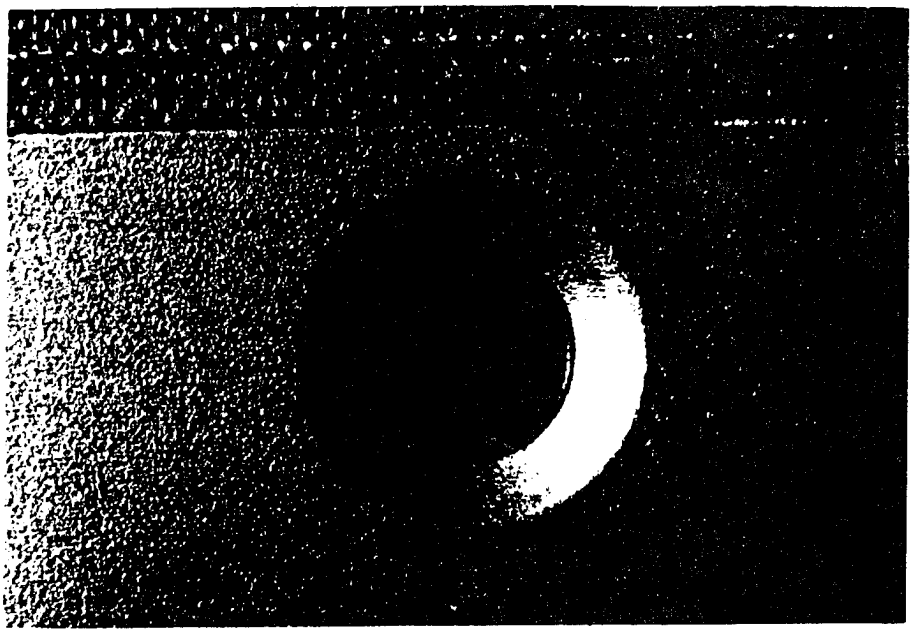
17. There was no visible corrosion at this fastener prior to search-peening.



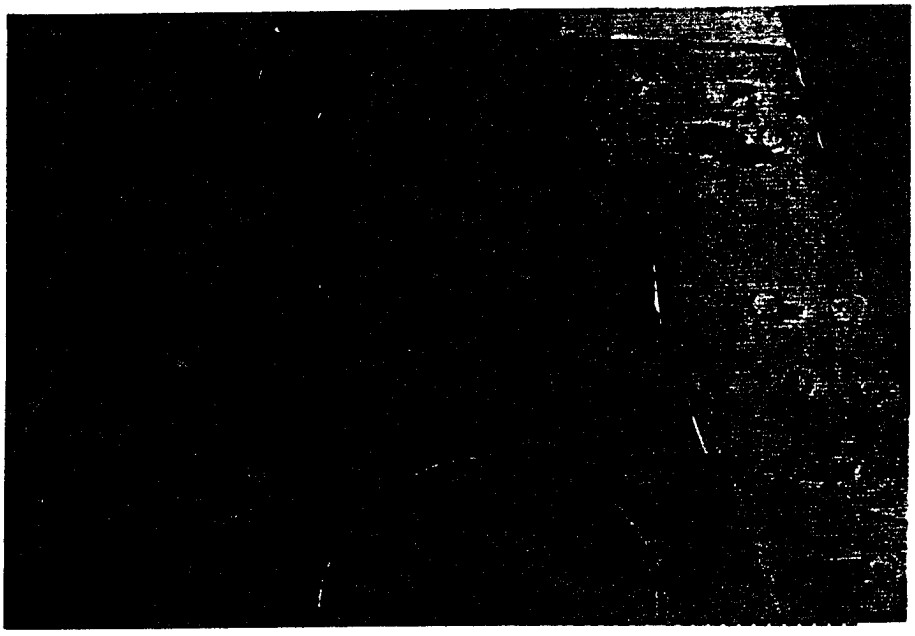
18. Moderate sanding had removed visible corrosion but search-peening identified exfoliation close to the countersink.



19. Peening at saturation intensity also identified an apparently isolated spot of exfoliation away from the fasteners. (Identified as 15a in Appendix 1).



20. There was no visible corrosion at this countersink either before or after search-peening.



21. On the thicker section of the panel the corrosion appears to have tracked between the fasteners in a linear fashion along the panel.

METAL IMPROVEMENT COMPANY INC.

AS SHIPPED FOR FURTHER INVESTIGATION BY BOEING



22. This shows the panel in its final state after the progressive treatments carried out by Metal Improvement Company - Newbury Division.

SESSION V

Structural Repair

Chairman: ***Lt Col J. Rogacki*****, WL/FIB**

Residual Life Analysis and a Novel Repair Method for Cracks in F-16 Center Fuselage Bulkhead

S. Jiny, G. Davidi, E. Makevet, and D. Schur

Israeli Air Force

ABSTRACT

Numerous cracks were detected in a critical panel in the center fuselage bulkhead on IAF F-16 aircraft, at an early stage of their service life. The immediate problem faced by the IAF was to develop an effective repair for cracked panels, and to determine the criteria for the continued safe operation of aircraft exceeding the repair limits.

A residual life analysis was conducted for the most advanced state of damage, in which the crack had severed the ligament between the critical hole and an adjacent cutout in the panel. The results of the analysis served to define an inspection program for the applicable aircraft. For the majority of the fleet, a unique repair method was developed by the IAF. This involved a crescent-shaped cutout removing the crack from the critical hole, followed by cold-working the entire circumference of the resultant geometry. A special tool kit was designed and manufactured to facilitate fleet-wide repair of cracked panels. The effectiveness of the crescent repair method was verified by local finite element analysis and by comparative fatigue testing of coupons. The crescent repair was shown to provide a far superior structural configuration than the original configuration in terms of fatigue life. By implementing this innovative repair method the panel cracking problem was eliminated.

Introduction

In order to maintain the structural integrity of the fleet, the Israeli Air Force (IAF) implements several levels of supporting methodologies under ASIP: DTA and FSMP based on average fleet usage, individual fatigue tracking and finally risk assessment. However, these analytical methods sometimes fail to predict in-service failures. When unexpected failures occur, the IAF addresses the problem by calculating the fatigue life for the critical structural location and by designing an appropriate repair. This is accomplished using stress analysis, DTA analysis and fatigue testing.

An unexpected problem was the detection of numerous cracks in the center fuselage bulkhead panels of IAF F-16 aircraft, at an early stage of their service life. Initially cracks were found at depot level, but as more aircraft were inspected at intermediate maintenance level it transpired that the problem of the bulkhead panel cracking was quite extensive. At the time, existing crack growth analyses and repair methods for the problem area were limited to short cracks, and there were serious concerns about the quality and effectiveness of the available repair. The IAF was therefore faced with the immediate need to develop an adequate repair for cracked panels, and to determine the criteria for the continued safe operation of aircraft exceeding the repair limits. The solution had to be defined, verified and implemented within a short period in order to prevent an escalation of the bulkhead cracking problem.

Statement of Problem

The center fuselage bulkhead is one of the most critical airframe components of the F-16, which reacts the wing bending moment, pitch moment and shear load. The lower bulkhead is a one-piece forging incorporating stiffeners and shear panels, as seen in Figure 1. Also depicted in Figure 1 is the critical panel which developed the cracks.

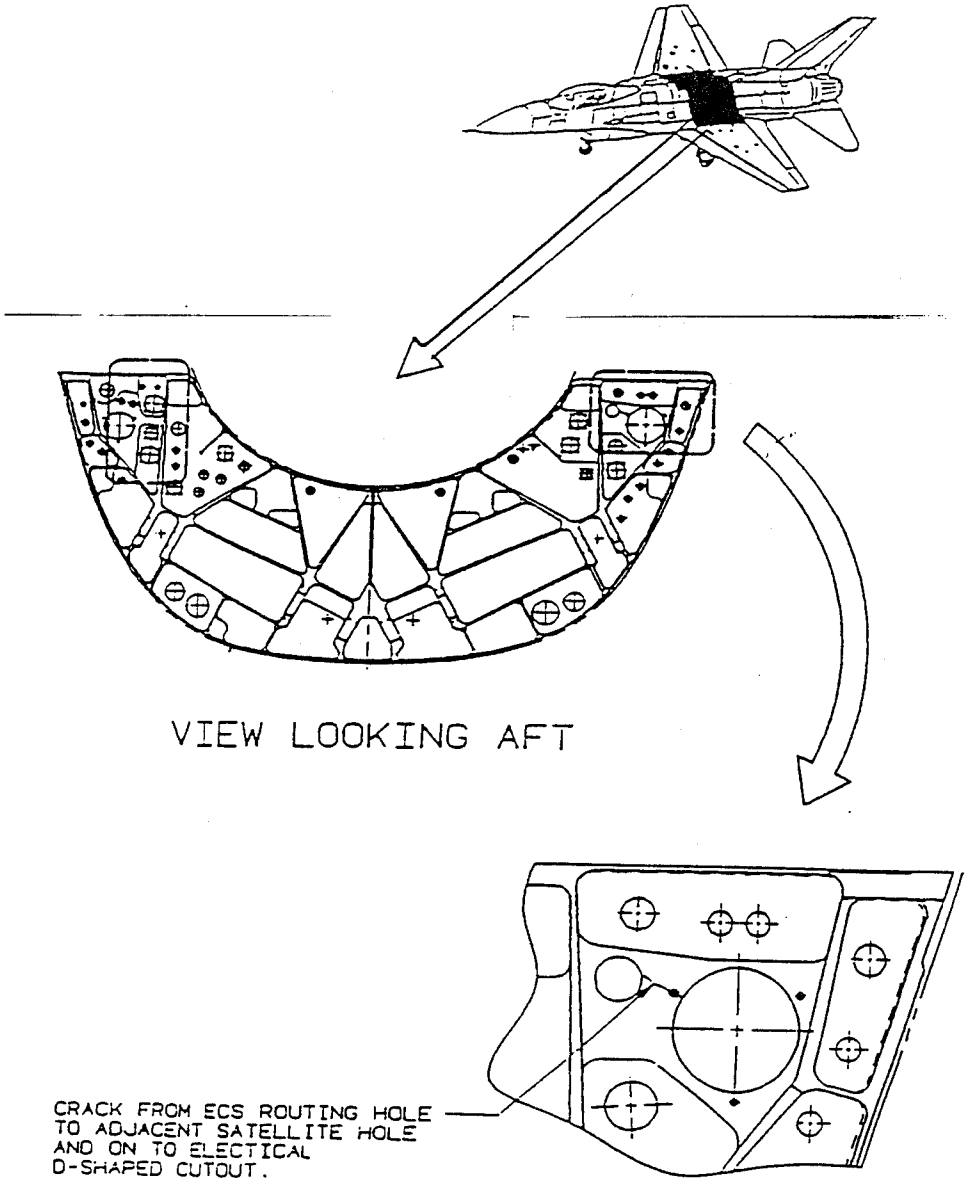


FIG. 1 - General description of the lower bulkhead panel cracking problem.

the F-16 without additional cracking setting in at adjacent locations. Also, the maintenance burden associated with the protective inspections of the bulkhead panel had to be kept down to a minimum. It was therefore decided to concentrate the engineering effort on the following two activities:

(1) A residual fatigue life analysis to determine the remaining safe life of the critical panel in the severed-ligament configuration, and of adjacent critical points in this configuration. This extreme condition already existed in several aircraft. As it was not deemed repairable, the IAF needed the analysis results in conjunction with the planning and scheduling of inspections and major structural modifications at depot level.

(2) Development, verification and implementation of a new repair method for cracks progressing beyond the satellite hole, with the ligament still intact. The repair was required to enhance the fatigue life of the panel sufficiently, to prevent the ligament from severing before the aircraft could undergo depot-level modifications.

Residual Fatigue Life Analysis

The prime consideration in conducting the residual fatigue life analysis by the IAF was to insure maximum consistency with the methodology of previous structural analyses by LFWC. The purpose of the analysis was to identify new "hot spots" in terms of stresses, which are caused by the re-distribution of loads transmitted through the lower bulkhead when the ligament is severed; to verify that the static strength of the structure surrounding the shear panel is not exceeded; and finally, to calculate the crack growth lives of the applicable critical locations for the severed-ligament configuration.

The IAF had acquired the NASTRAN finite element models of the center fuselage bulkhead from LFWC, including a coarse grid model of a symmetrically loaded half-bulkhead and separate fine grid models of the various panels in the bulkhead. Since the cracked (severed-ligament) configuration had to be analyzed and compared to the baseline (non-cracked) configuration, it was decided to incorporate the fine grid panel in the coarse grid bulkhead, rather then conduct coarse grid FEA runs and subsequent fine grid runs for each configuration. The resultant model is depicted in Figure 3. Adjusting the model to accommodate the fine grid panel, and refining the mesh of the adjacent panels for the identification of "hot spots", necessitated extensive modification of the original elment mesh, as can be seen in Figure 4. To validate the "transplant" operation, the unified bulkhead model was run in the baseline configuration, and stress results were found to be in good agreement with results from the fine grid panel run.

In order to model the cracked configuration, the element mesh was "unzipped" between the ECS hole and the D-shaped cutout, thus representing the severed ligament and the fractured satellite hole. Figures 5 and 6 compare the maximum principal stress distribution in the critical panel and the adjacent panel, for the baseline configuration and the cracked configuration respectively. The severed ligament is visible on the deformed geometry of Figure 7. It was found that the severed ligament caused two new "hot spots" in the bulkhead. The first was at the edge of the D-shaped cutout opposite the ligament, where the stress now increased by 80%. The second critical location was identified at the inboard edge of a hole in the side panel, where the stress increased by 13% as compared to the baseline configuration. These two points were denoted CP1 and CP2 respectively (Figure 6). The analysis was conducted for a 9G symmetric maneuver.

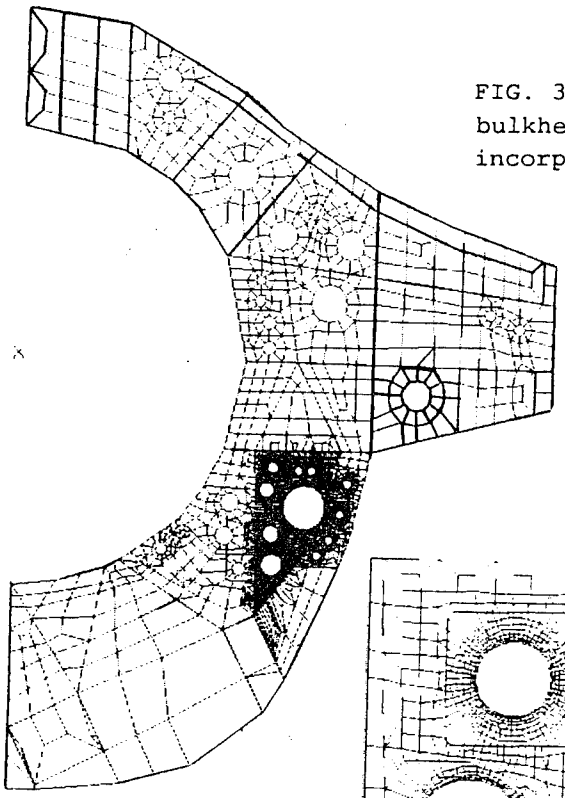


FIG. 3 - Overall view of the lower bulkhead coarse grid model incorporating the fine grid panel.

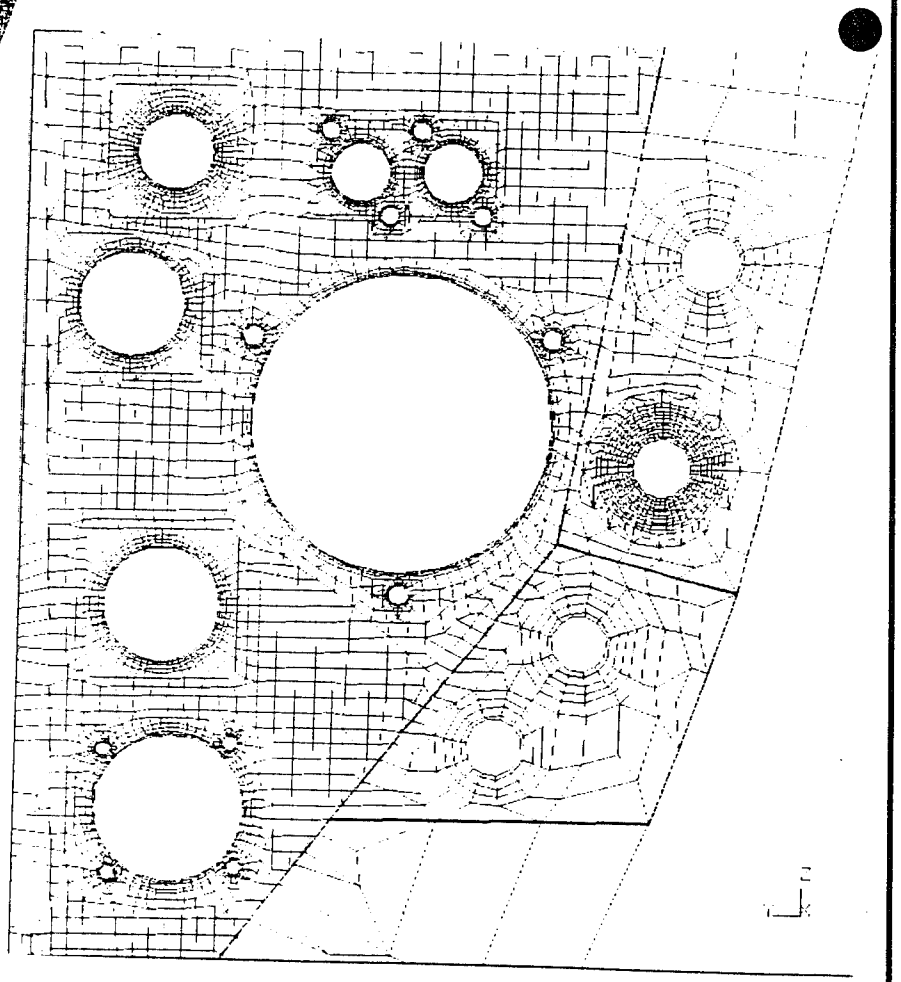


FIG. 4 - Detailed view of the fine grid panel and the interfacing mesh.

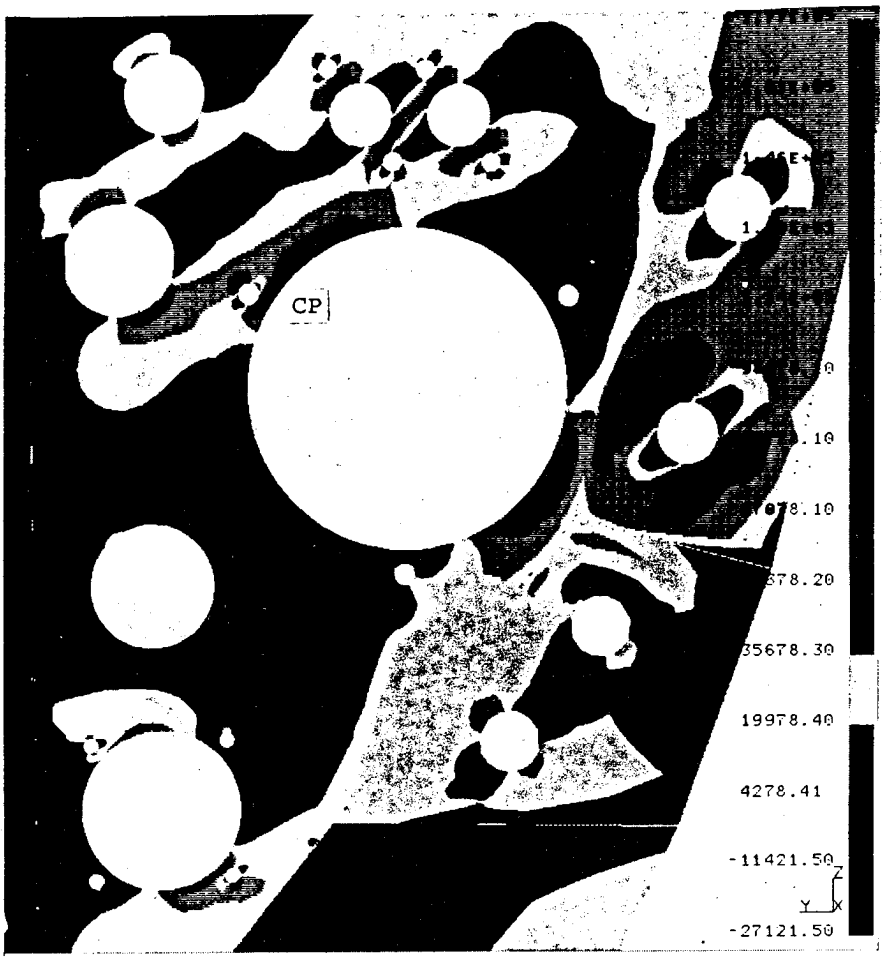


FIG. 5 - Maximum principal stress distribution in the critical panel and the side panel for the baseline configuration.



FIG. 6 - Maximum principal stress distribution for the severed-ligament configuration.

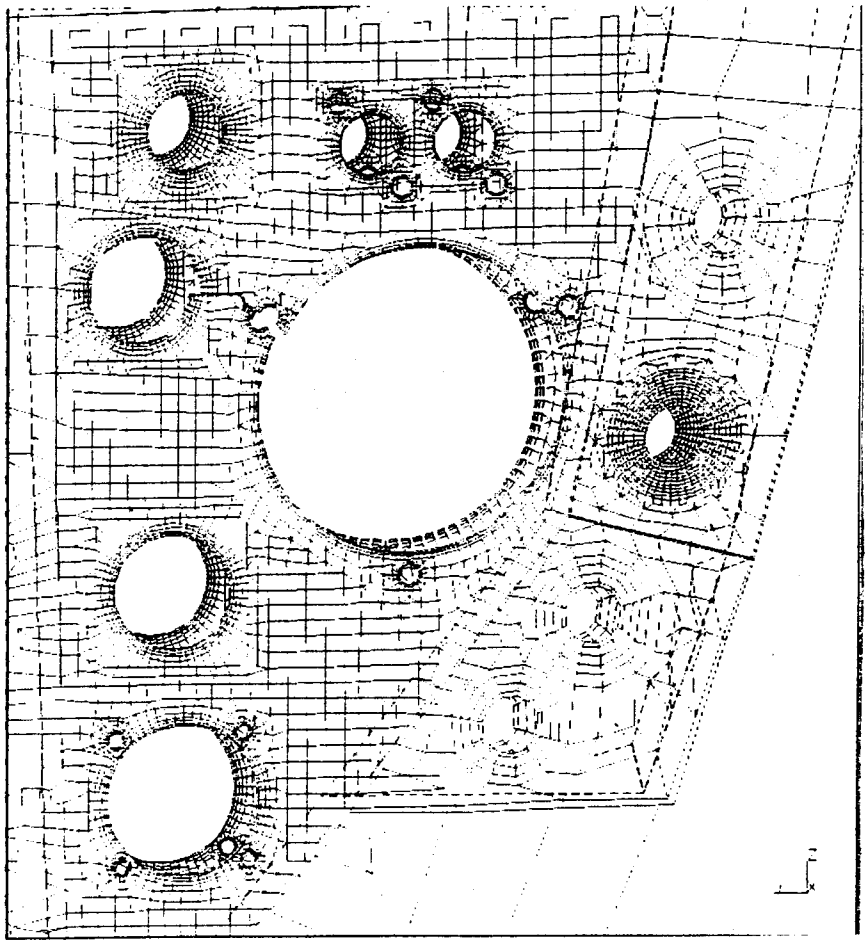


FIG. 7 - Deformed geometry of the critical panel in the severed-ligament configuration.

Next, a stress spectrum for each point was generated from the bulk data of an IAF F-16 usage spectrum tape and from the applicable stress equations [1,2]. The tape contained processed flight parameter data for 500 hours of F-16 operations as measured by FLR (Flight Loads Recorder). The stress equations allowed the calculated wing loads from the tape to be converted to stress at the critical satellite hole, denoted as CP, and to stress at CP2 in the side panel. The final baseline spectra were reduced to nearly 40,000 cycles following some truncation operations. The results of the FEA runs for both configurations were now used to derive stress correction factors for CP1 and CP2 in the cracked configuration. These factors were applied in scaling the baseline stress spectra for use in the "hot spots" of the cracked configuration. The validity of the linear correlation approach for the various flight conditions in the spectrum was demonstrated by previous works pertaining to the bulkhead and will not be discussed here.

To calculate the stress intensity factor K for cracks at the critical locations, the geometric correction factor BETA was derived directly from the gradient of the maximum principal stresses at the applicable locations. This approach was employed in the DTA of the bulkhead shear panels [1], and may be viewed as directly incorporating the stress concentration effect in the expression for K,

$$K = BETA * \sigma\sqrt{\pi a}$$

Where

BETA - The stress gradient along the crack line, normalized by the stress at the critical point (i.e. BETA ≤ 1). The stress is calculated at non-cracked locations in both configurations.

σ - The stress at the critical point as calculated from the stress equation (scaled / unscaled).

a - The crack dimension.

This expression for K constitutes a simplified, one-dimensional representation of the crack instead of a two-dimensional, part-through crack representation.

Finally, crack growth analyses were conducted using a modified Cracks 4 code, with the Closure equation [3] employed for the crack growth model. The analysis method was validated first by reconstructing the original analysis for the satellite hole (CP). The total time for a crack to propagate between the satellite and ECS holes was calculated within 5% of the DTA life [2]. Now the residual fatigue lives at locations CP1 and CP2 could be assessed for the severed-ligament configuration, by implementing the appropriately scaled stress spectra in the crack growth analyses. The results of these analyses are summarized in Table 1. As might be expected, the severed ligament drives the damage at CP1 at a high rate, and consequently the residual life at

TABLE 1-Crack growth analyses summary. The initial crack size is given in the equivalent one-dimensional representation, and is determined by the stress gradient for each configuration.

CRITICAL POINT	CONFIGURATION	INITIAL CRACK SIZE (IN)	CRITICAL CRACK SIZE (IN)	CRACK GROWTH LIFE (HOURS)	REMARKS
CP1	baseline	0.014	0.1	>3000	
CP1	cracked	0.015	0.0333	170	residual life
CP1	cracked, cold-worked	0.002	0.0333	914	residual life
CP2	baseline	0.03	0.783	>3000	
CP2	cracked	0.0128	0.31	526	residual life calculated from approx. 0.16" crack size
CP2	cracked, cold-worked	0.005	0.31	1416	residual life

this location is reduced from a very high baseline value to just 170 flight hours. The same is true for the side panel (CP2), where a residual life of 526 flight hours is calculated for the cracked configuration. However, this is a conservative estimate which is based on the assumption that a crack has propagated simultaneously from CP2 under baseline stress levels. When the ligament is severed, crack growth continues from an 0.16" crack size for more than 500 flight hours, with a 13% increase in the spectrum stresses.

There remained the question of possible fatigue enhancements of these two locations in conjunction with the severed ligament problem. Tools were available to cold-work the D-shaped cutout and the hole in the side panel. The cold-working process was accounted for analytically by a 0.005" x 0.005" initial crack, an assumption practised by the aerospace industry. Crack growth analysis results for the cracked configuration in cold-worked condition indicated a substantial improvement in residual lives, as seen in Table 1.

Lastly, the static strength of the lower bulkhead in the cracked configuration was validated by the application of the Von Mises criterion. Since the FEA of the bulkhead was linear-elastic, a simple screening process took place to identify locations where calculated Von Mises element stresses exceeded the yield stress of the bulkhead material. The screening was limited to the bulkhead stiffeners, because the local yielding of stress concentration locations in the panels is permissible. Only very localized yielding was detected at the stiffeners adjacent to the critical panel, the increase in Von Mises stresses being 6% or less. Based on these results no static strength problem was judged to arise with respect to the presence of the severed ligament in the critical panel.

Repair Design and Analysis

As mentioned earlier, when the extent of the panel cracking problem became evident a repair method was already available to the IAF. This was termed a tangential repair, which routed the material in the cracked location, in an area bounded by tangents of the ECS hole. The geometry of such a repair with respect to the geometry of the cracked location is shown in Figure 8a,b. This type of repair was recommended to the IAF for

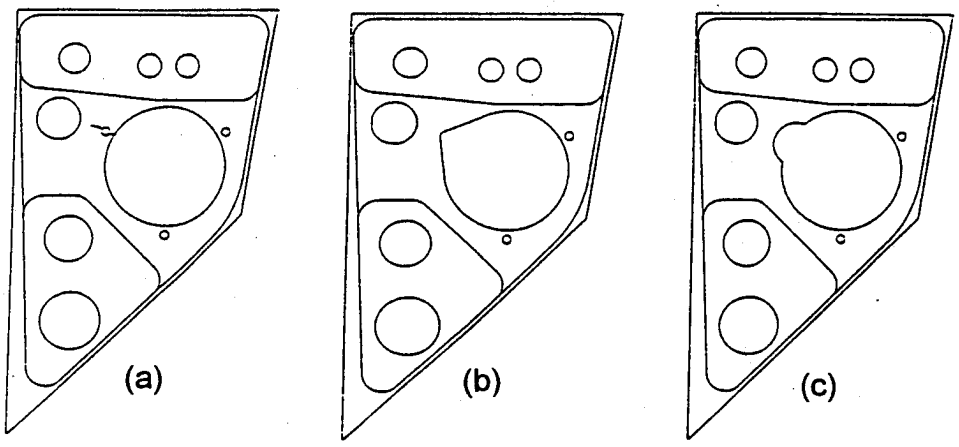


FIG. 8 - Panel geometries (a) baseline (b) tangengetial repair (c) crescent repair.

the removal of cracks up to 0.2" beyond the satellite hole. However, based on some previous experience in the application of this repair method, the IAF was concerned about the quality and effectiveness of the tangential repair. The manual routing proved difficult to control, producing inaccurate geometries and rough surfaces. Furthermore, the repair geometry did not eliminate the high stress concentration in the satellite hole area. The low fatigue initiation resistance of the tangential repair, which is inherent in the design and implementation of this repair method, was verified by coupon fatigue testing as related later in the text. Finally, as there were plans to enhance the ECS and satellite holes by cold-working, the IAF opted for a different repair method that would still allow the repaired ECS hole to be cold-worked.

The evaluation of various alternate repair concepts was guided by the following criteria:

(1) The repair method had to be simple in terms of added tools, controllability and repeatability, and time to perform.
(2) The repair was required to maintain the cold-work capability of the ECS hole and to utilize existing cold-working hardware.
(3) No modifications to mechanical or electrical components in the bulkhead area were allowed in order to facilitate the repair.
(4) The repair method was required to show a substantial improvement in residual fatigue life as compared to the existing tangential repair.
(5) The repair operations had to be within the capability of the intermediate maintenance level.

Only one repair method met all the above criteria by implementing a novel repair principle. This repair method was termed a crescent repair, which is described in essence as follows. First, the cracked material is routed out to form a crescent-shaped cutout emanating from the ECS hole. As can be seen in Figures 8c and 9, the radius of curvature of the

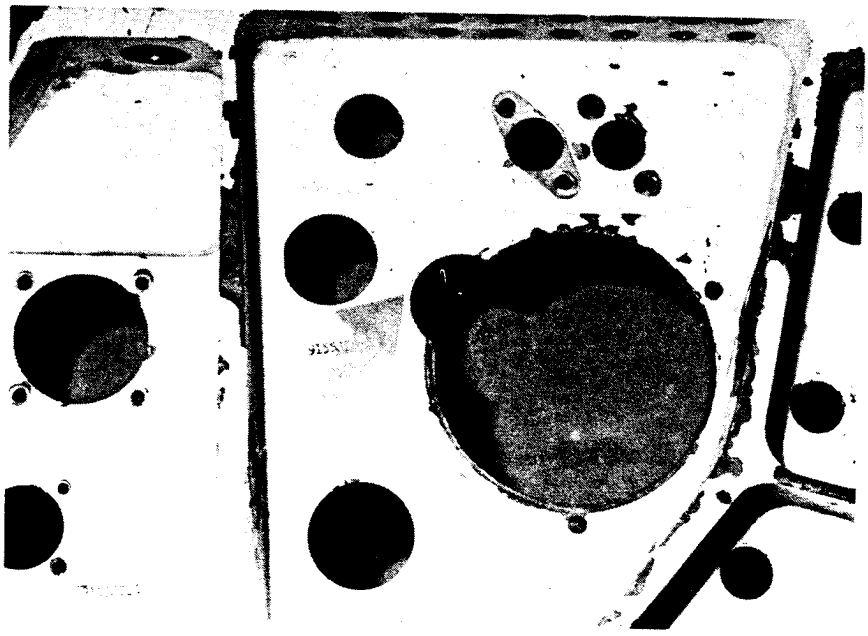


FIG. 9 - Enlarged view of the cresent repair.

cutout is relatively large. Next, a high-tolerance crescent filler is inserted in the cutout to tightly plug the resulting void between the cold-working mandrel and the surrounding panel material. This is clearly depicted in Figure 10. Then the cold-work process is performed using the same procedure and tools as for the cold-working of a round ECS hole. As the mandrel expands the filler acts againts the boundary of the cutout and the entire circumference of the repaired ECS hole is cold-worked.

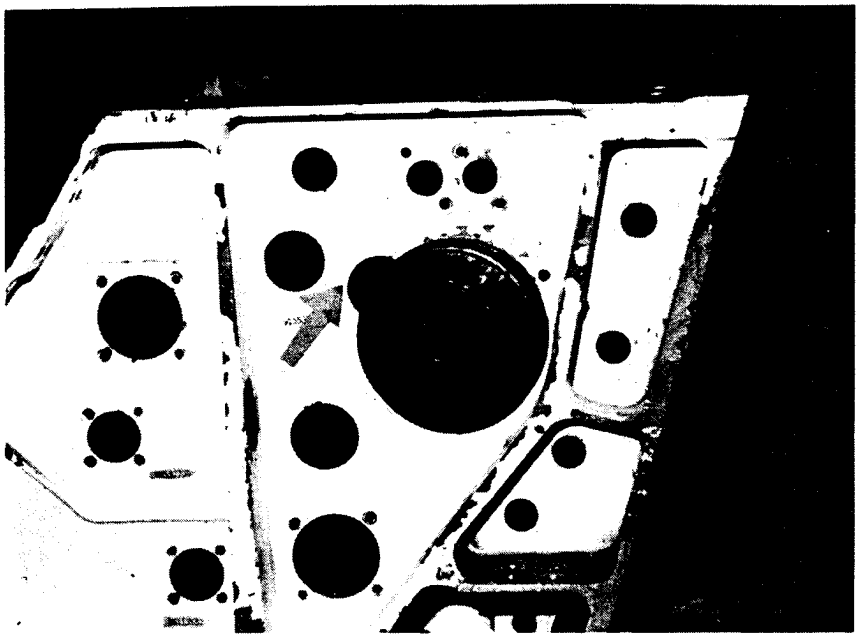


FIG. 10 - View of the mandrel and crescent filler prior to cold-working.

Preliminary design of the crescent repair tool kit concentrated on actual measurements of pertinent geometric dimensions taken from most F-16 aircraft in the fleet. Processing the data allowed the IAF to simplify the design considerably by fixing certain geometric degrees of freedom. The actual tolerances in the manufacture of the ECS hole resulted in the definition of five diametrical increments, each varying the hole diameter by 0.003". Another degree of freedom that had to be retained, naturally, was the distance between the geometric centers of the ECS hole and the cutout. Five 0.04" increments were defined to facilitate the removal of a crack extending up to 0.2" beyond the satellite hole. Accordingly, the main components in the specially designed tool kit were:

(1) A plug manufactured in five different diameters to fit into the ECS hole. The plug is inserted in the hole to facilitate the crack routing process.

(2) A template manufactured to comply with the incremented distances between the ECS and cutout centers. The template is attached to the plug, fixed and accurately orientated by bolts, pins and a counter-plate. The resulting assembly is visible in Figure 11. A press-fit bushing installed in the template guides the reamer accurately to the designated cutout position. A crescent-shaped recess in the plug accomodates the reamer inside the cross-section of the ECS hole. The position of the reamer guide in the template is determined by the required depth of the cutout (up to 0.2" beyond the satellite hole).

(3) A crescent steel filler bounded by a 1.2" outer diameter and a 3.25" (ECS hole) inner diameter. To simplify the design the radii were kept fixed, only the centers distance varying in the final manufacture to match the five different templates used.

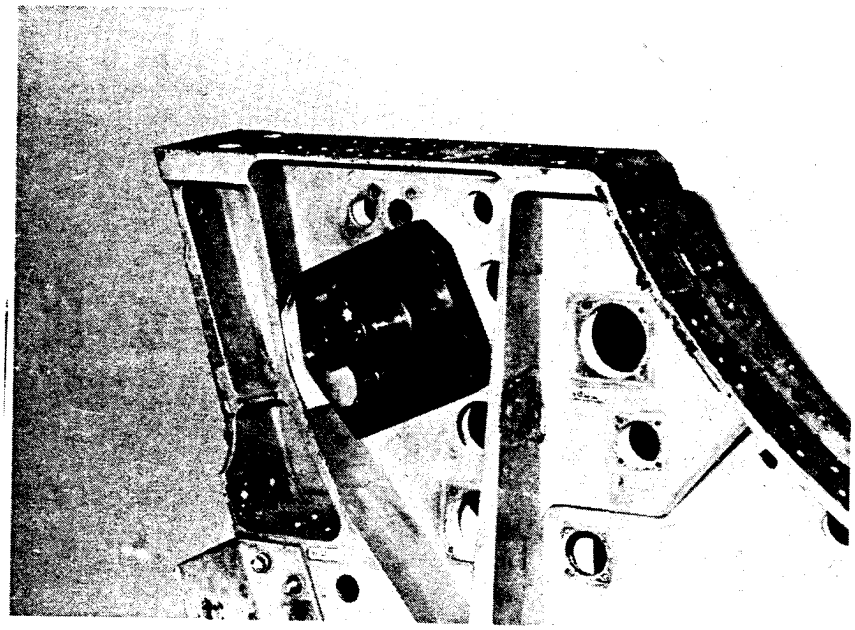


FIG. 11 - View of the template as installed on the panel for routing the crescent cutout.

The complete tool kit manufactured by the IAF depot center consisted of just five plugs, five templates, five crescent fillers and some accessory hardware. To insure the effectiveness of the entire repair process, much empahsis was placed on the high-tolerance design and manufacture of the various components. This requirement was instrumental in accomplishing the high-quality surface finish of the cutout, and the essential tight fit of the filler in the cold-working process. Special care was taken in the simplified design of the filler to make sure that there was no deviation from the out-of-round limits of the cold-working specification for the cutout (when viewed as a round hole).

To complement the design, local FEA of the repair was conducted using ANSYS version 5.0 software. First, a comparative linear-elastic analysis of all three configurations in Figure 8 was run. The ANSYS model for the baseline configuration is seen in Figure 12. Whereas the tangential repair was shown to reduce the local stress at the critical

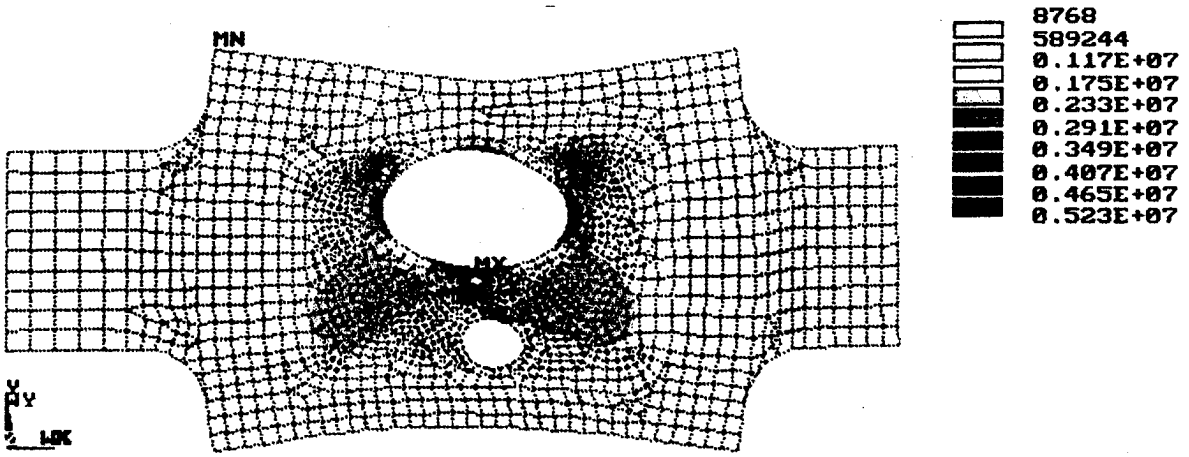


FIG. 12 - Local finite element model of the baseline geometry (deformed).

point by only 4% compared to the baseline configuration, the crescent repair geometry achieved a 12% reduction in stress. Now it was time to analytically assess the compounded effect of the cutout and the cold-working process. This type of non-linear, elastic-plastic FEA is usually an evolved process not without its investigative aspects. As the scope of the design work enabled only limited analytic verification, certain assumptions were employed in the FEA of the crescent repair for simplification. The main assumptions are reflected in the following elastic-plastic analysis stages of the crescent repair model:

(1) The filler is represented as an integral part of the surrounding finite element mesh, differing only in material properties from the bulkhead material (i.e. no contact elements are employed at the interface). This imposes a no-slip condition at the filler interface, signifying a tight fit of the assembly during the cold-working process. The mandrel is not modeled and the mandrel expansion is applied in the first load step as a uniform, radial displacement of the ECS hole. The value of the displacement is calculated as the radial increment required to accomodate the mandrel, assuming an infinitely rigid mandrel material.

(2) liner unloading takes place in small increments, gradually reducing the radial displacement constraint. This procedure is practised in elastic-plastic FEA computations for convergence, and may be viewed as virtual unloading. Since the residual plastic displacement is not known a-priory, the process is terminated at a slightly higher displacement value than that expected for a round hole according to the process specification.

(3) The final unloading is defined in terms of the radial force acting on the circumference of the hole decreasing to zero, simultaneously "killing" the filler. This step represents the release of the mandrel, after which the residual stress field around the repaired ECS hole can be examined. Solution convergence at this stage is verified when the normal stress along the entire circumference of the repaired hole, including the cutout, is found to equal zero.
(4) Uniaxial, tensile forces are applied at the edges of the model to simulate the typical loading condition of the panel with a cold-worked crescent cutout. The load level applied corresponds to the maximum spectrum stress.

The stress results of stage (3) were the most important in the analytic validation of the crescent repair method. The analysis calculated compressive residual tangential stresses along the entire circumference of the hole, as shown in Figure 13. The magnitude of the residual stress is considerably reduced at the tip of the cutout, but the uniform distribution of the tangential stresses around the hole and around the cutout imply that proper cold-working can be accomplished. It should be noted in that context that the residual stress distribution in Figure 13 is somewhat misleading, as the tangential stress $\sigma_{\theta\theta}$ is calculated with respect to the coordinate system of the ECS hole rather than that of the cutout.

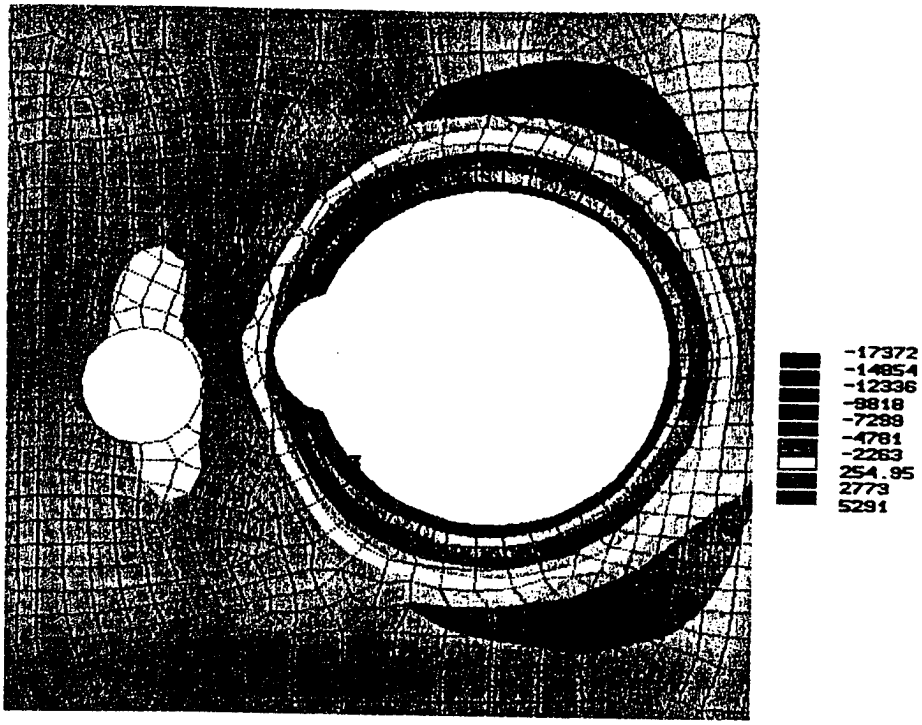


FIG. 13 - Calculated residual tangential stresses along the hole circumference after cold-working.

Finally, the stress results of stage (4) served to assess the overall benefit of the cold-working process with respect to the actual loading spectrum. The calculated stresses were compared with the stresses from an elastic-plastic FEA run of the model without cold-work. The comparison showed that a 16% decrease in the maximum stress at the tip of the cutout, can be obtained by cold-working the cutout. This result, which is significant in itself in terms of fatigue life, refers to the maximum load level. The effect of the cold-working process is even more pronounced at the lower load levels in the spectrum.

In summary, the FEA of the crescent repair provided a qualitative validation of the repair method, indicating a considerable potential for residual life improvement in that configuration. Due to the approximate nature of the stress analysis and various associated uncertainties, and in compliance with general engineering verification practice, fatigue testing was required to complete the substantiation of the crescent repair method.

Fatigue Testing of the Crescent-Shaped Repair

Test coupons were specially designed to simulate the fatigue behaviour of the critical location in the panel under typical loading. The design was supported by the same ANSYS finite elememt model depicted in Figure 12. The baseline geometry of the coupon is illustrated in Figure 14, and is seen to include the ECS hole, statellite holes and

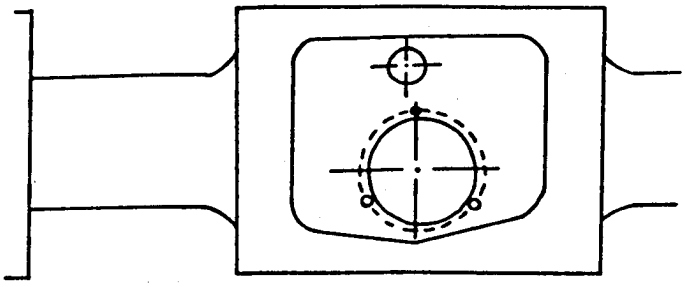


FIG. 14 - Baseline geometry of the test coupon.

D-shaped cutout. The actual coupons were each manufactured with two such bulks as shown in Figure 15, in order to save machine test time. Various repair configurations were implemented in the coupons, but only the baseline, tangential and crescent repair configurations will be referred to in the following text.

The first phase of the fatigue testing program was limited to constant-amplitude loading. However, an effort was made to establish a load level that would correspond to the time-to-failure of actual crack findings in the fleet. This "calibration" was accomplished in an efficient manner by using strain readings from a baseline coupon static test, the measured fleet-average G-spectrum of IAF F-16 aircraft; and the average actual flight hours for a crack to connect the ECS and satellite holes in-service. The load level was set at 12 tons with a load ratio of R=0.1. The coupons were all loaded and cycled by an MTS model 810 machine (Figure 15).

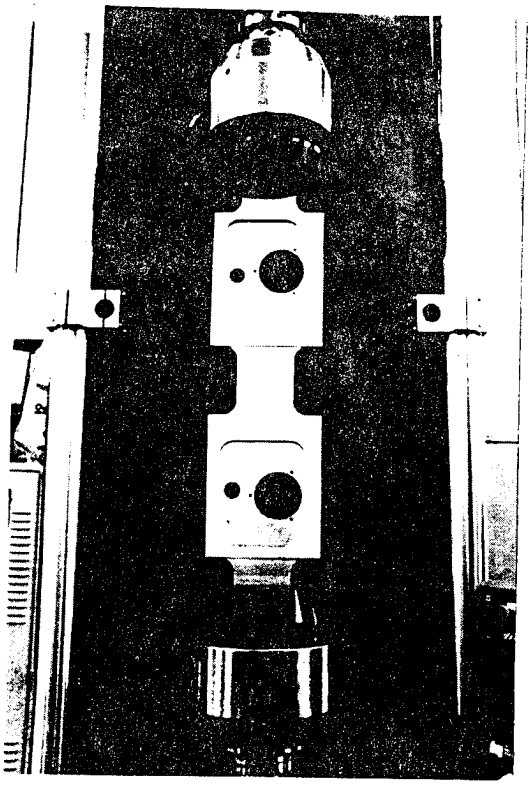


FIG. 15 - Test coupon on the MTS machine.

The results of the constant-amplitude fatigue testing are summarized in Table 2. Although the current sample of test results is quite small, it is sufficient to support the following significant conclusions. It was established than the tangential repair offered no improvement over the baseline configuration in terms of residual life. In fact, the time for a crack to sever the ligament was 30% lower in the tangential repair configuration, even though the cutout surface was polished unlike field repairs. On the other hand, the crescent repair without cold-work was shown to improve the residual life of the panel by an order of magnitude compared to the baseline configuration. When the full crescent repair was implemented in the coupons it was found that cold-working further doubled the residual life of the non cold-worked crescent repair. No cracks were produced in the coupons containing the cold-worked crescent repair.

The panel contains a circular 3.25" (ECS) hole surrounded by three satellite holes, each approximately 0.21" in diameter. These holes are used to attach a connector to the panel, and were drilled at a short distance of about 0.14" from the edge of the ECS hole. The short edge distance, the presence of an adjacent D-shaped cutout in the panel and the direction of the principal stresses under typical loading, all combine to make the inboard satellite hole the most susceptible to fatigue cracking. This was corroborated by the very quick initiation and development of cracks between the ECS and satellite holes. By the time these cracks were detected, they had progressed beyond the satellite hole, in some cases completely severing the ligament between the ECS hole and the D-shaped cutout. This advanced state of cracking is illustrated in Figures 1 and 2.

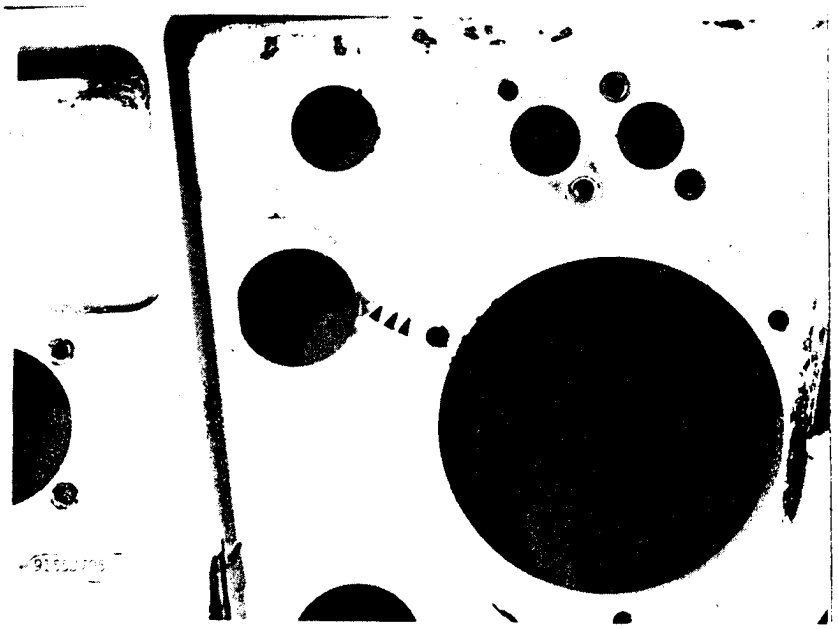


FIG. 2 - Severed ligament in the panel.

Preliminary damage tolerance analysis of the critical satellite hole did not account for continuing damage, i.e. crack propagation towards the D-shaped cutout. Also, the existing repair which allowed a crack up to 0.2" beyond the satellite hole to be removed offered a short-term fix only, and was considered inadequate by the IAF for other reasons as well. These reasons will be discussed later in this paper. It should be noted that a preventive repair, enhancing fatigue life by cold-working the ECS and satellite holes, was already available to the IAF but was not yet implemented at the time of the large-scale panel cracking.

The manufacturer, Lockheed Fort Worth Company (LFWC), had already determined the center fuselage lower bulkhead to be fail-safe in various failure scenarios. Fail-safety of the bulkhead was demonstrated by full airframe finite element analysis (FEA), and was supported by the results of the full-scale airframe fatigue test. However, this added insurance did not alleviate the IAF problem in maintaining the safe operation of

TABLE 2-Coupon fatigue test results summary.

COUPON NO.	CONFIGURATION	NO. OF CYCLES FOR CRACK TO CONNECT ECS AND SAT. HOLES ($X10^3$)	TOTAL NO. OF CYCLES FOR CRACK TO SEVER LIGAMENT ($X10^3$)	REMARKS
1	baseline	155	185	load level changed from 10 to 12 tons
2	baseline	182	211	
3	baseline	84	121	
4	baseline	98	—	testing stopped before the ligament was severed
5	tangential	—	18	
6	tangential	—	18	
7	tangential	—	30	
8	tangential	—	23	
9	crescent, non cold-worked	—	212	
10	crescent, non cold-worked	—	>500	no cracks observed when testing stopped at 0.5M cycles
11	crescent, non cold-worked	—	187	
12	crescent, non cold-worked	—	>500	no cracks observed when testing stopped at 0.5M cycles
13	crescent, cold-worked	—	>1000	no cracks observed when testing stopped at 1M cycles
14	crescent, cold-worked	—	>1000	

Despite the limited scope of testing accomplished under this phase of the program, the IAF concluded by the available results that the crescent repair would provide a very high residual life to the critical panel. It was therefore decided that a full validation of the repair was not required in order to approve this repair method for fleet-wide implementation.

Summary

The immediate problem of severed ligaments in the critical panel in several IAF aircraft could only be addressed analytically by the IAF. Stress analyses and crack growth analyses of the lower bulkhead were conducted, showing the most critical location in this configuration to have a residual life of 170 flight hours. This result allowed the IAF to continue flying these aircraft unrestricted. In parallel, a recurring inspection of the critical panel and the side panel was warranted at a time interval derived from the applicable crack growth curve. It should be emphasized that the IAF gained sufficient confidence in the analysis results by certain correlations with LFWC works and with in-service findings.

Those cracks extending beyond the satellite hole in numerous other aircraft, constituted a problem that required similarly urgent actions. As verified by subsequent testing, the crack propagation life of the ligament was very short once a crack had developed between the ECS and satellite holes (see Table 2). Therefore, all the cracked panels had to be repaired within a short space of time, in order to prevent more panels from severing. Because of the inherent weaknesses of the existing repair method, an expedient design and verification process ensued in order to implement the new crescent repair concept. Following the approval of the crescent repair for fleet-wide implementation, all the aircraft in the fleet except those with severed ligaments, had the critical panel repaired by this method. Since the fatigue testing results indicated that the repair configuration was far superior to the baseline configuration in terms of fatigue life, the crescent repair was implemented as a preventive repair as well. In addition, all the aircraft in the fleet had the D-shaped cutout and the critical hole in the side panel cold-worked. It is recalled that the estimated residual life of the critical hole in the side panel is 1400 flight hours, with the ligament in the adjacent panel already severed at the time of cold-work (see Table 1). As for the D-shaped cutout being cold-worked in the severed-ligament configuration, it was assumed that some amount of cold-work would be incurred in the critical point opposite the ligament. All these operations were carried out at both depot and intermediate levels.

Since the crescent repair is effectively a fix-and-forget solution to the panel cracking problem, the majority of the fleet had actually undergone a fatigue enhancement process as the aircraft were being repaired. The timely implementation of the repair allowed the additional burden of flight-safety inspections to be limited to just a small number of aircraft with severed panel ligaments.

Conclusions

By addressing the various structural integrity aspects of the panel cracking problem, the IAF was able to provide an adequate and timely solution to prevent further deterioration in the structural condition of the F-16 fleet. Those aircraft with severed ligaments in the lower bulkhead still required close monitoring for continuing structural damage. However, the continued safe operation of these aircraft was

substantiated by a conservative residual life analysis. The majority of the fleet had the crescent repair implemented before the ligament in the critical panel was severed, thus eliminating the cracking problem. The effectiveness of this repair method was demonstrated by stress analysis and fatigue testing, at the same time verifying the suspected inadequacy of the recommended repair method.

The engineering effort described in this paper is a characteristic example of the type of engineering capability an air force needs. With limited time, facilities and resources, innovation and engineering judgement are vital in the on-going application of ASIP. In this case, the most critical issues of the problem were addressed in-house, resulting in the independent development of a unique solution. Despite the urgency of the problem, the available solution was ruled out and a novel repair method was validated and implemented instead. To approve the crescent repair for fleet-wide implemention in a short space of time, the repair could not be fully qualified in advance. However, engineering judgement was that there were sufficient data to authorize the repair without further delay.

To complete investigations associated with the crescent repair method, it is planned to conduct the second phase of the fatigue testing program by applying a flight-by-flight loads spectrum to the coupons. This phase is aimed at better quantifying the fatigue enhancement accomplished by the crescent repair. In conjunction with these tests, the effect of cold-working the D-shaped cutout with the ligament already severed will be assessed.

Acknowledgements

The authors wish to thank Dr. Jacob Bortman for his comments, and Mr. Benjamin Prober for his contribution to this paper.

REFERENCES

1. Report 16PR8453, General Dynamics Fort Worth Division, 1989.
2. Report 16PR5973, General Dynamics Fort Worth Division, 1989.
3. Damage Tolerance Manual, Israel Aircraft Industries, 1984.

Structural Durability of Damaged Metallic Panel Repaired with Composite Patches

Christos C. Chamis*
National Aeronautics and Space Administration
Lewis Research Center, Cleveland, Ohio 44135-3191

Levon Minnetyan†
Clarkson University, Potsdam, New York 13699-5710

ABSTRACT

Structural durability/damage tolerance characteristics of an aluminum tension specimen possessing a short crack and repaired by applying a fiber composite surface patch is investigated via computational simulation. The composite patch is made of graphite/epoxy plies with various layups. An integrated computer code that accounts for all possible failure modes is utilized for the simulation of combined fiber-composite/aluminum structural degradation under loading. Damage initiation, growth, accumulation, and propagation to structural fracture are included in the simulation. Results show the structural degradation stages due to tensile loading and illustrate the use of computational simulation for the investigation of a composite patch repaired cracked metallic panel.

INTRODUCTION

In recent years laminated composite patches have been used for the repair of aging aluminum aircraft with potential fatigue cracks. Design considerations regarding the durability of a patch repaired aluminum panel require an a priori evaluation of damage initiation and propagation mechanisms under expected service loading and hygrothermal environments. In general, the controlling design load is tension perpendicular to the orientation of a crack. However, combined shear with tensile loading must also be taken into account when evaluating the performance of a composite patch repair. Concerns for safety and survivability of a patch-repaired aluminum panel require a quantification of the structural fracture resistance under loading.

Discussion in the current paper is focussed on a composite patch repaired aluminum panel subject to tensile loading. Damage initiation, growth, accumulation, and propagation to fracture is simulated. Effect of the length of an existing crack is examined with regard to the damage progression and structural durability under applied loading. The damage initiation load and the structural fracture load are quantified.

Fiber composite patches have tremendous advantages of light weight, high strength, durability, flexibility, and corrosion resistance. Inherent flexibilities in the design of a laminate configuration make composites more capable of fulfilling structural repair patch design requirements. However, for certain designs structural interaction between plies with different fiber orientations and the aluminum panel may adversely affect durability, especially in the presence of combined loading. The computational simulation method presented in this paper is well suited to investigate and identify the effects of structural interactions on damage and fracture propagation under design loads and overloads.

*Senior Aerospace Scientist, Structures Division.
†Associate Professor, Dept Civil and Environmental Engrg., Summer Faculty Fellow, NASA Lewis Research Center.

For the purpose of the present study, the following terminology is used to describe the various stages of degradation in the composite structure: (1) *Initial defect* refers to an existing crack in the aluminum panel that may be due to material/fabrication defect or fatigue loading; (2) *damage initiation* refers to the start of damage induced by loading that the composite patch is helping to carry; (3) *damage growth* is the progression of damage from the location of damage initiation to adjacent regions; (4) *damage accumulation* is the increase in the amount of damage in the damaged region with additional damage modes becoming active; (5) *damage propagation* is the rapid progression of damage to other regions of the specimen; (6) *structural fracture* is the ultimate disintegration or fracture of the specimen into two pieces.

METHODOLOGY

The evaluation of composite structures requires an assessment of their safety and durability under service loads and possible overload conditions. The ability of designing composites with numerous possible fiber orientation patterns, choices of constituent material combinations, tow/ply drops, and hybridizations render a large number of possible design parameters that may be varied for an optimal design. The multiplicity of composite design options presents a logistical problem, prolonging the design and certification process and adding to the cost of the final product. It is difficult to evaluate composite structures due to the complexities in predicting their overall congruity and performance, especially when structural degradation and damage propagation take place. The predictions of damage initiation, damage growth, and propagation to fracture are important in evaluating the load carrying capacity, damage tolerance, safety, and reliability of composite structures. Quantification of the structural fracture resistance is also fundamental for evaluating the durability/life of composite structures. The most effective way to obtain this quantification is through integrated computer codes that couple composite mechanics with structural analysis and damage progression modelling.

An important feature of computational simulation must be the assessment of damage stability or damage tolerance of a structure under loading. At any stage of damage progression, if there is a high level of structural resistance to damage progression under the service loading, the structure is stable with regard to fracture. The corresponding state of structural damage is referred to as *stable damage*. On the other hand, if damage progression does not encounter significant structural resistance, it corresponds to an *unstable damage* state. Unstable damage progression is characterized by very large increases in the amount of damage due to small increases in loading; whereas during stable damage progression the amount of increase in damage is consistent with the increase in loading.

Internal damage in composites is often initiated as cracking due to normal stresses transverse to the fiber orientation. Further degradation is in the form of additional cracking, delaminations, and fiber fractures that usually lead to structural fracture. Because of the numerous possibilities with material combinations, composite geometry, fiber orientations, and loading conditions, it is essential to have an effective computational capability to predict the behavior of composite structures for any loading, geometry, composite material combinations, and boundary conditions. The predictions of damage initiation, growth, accumulation, and propagation to fracture are important in evaluating the load carrying capacity and reliability of composite structures. Quantification of the structural fracture resistance is also required to evaluate the durability/life of composite structures under various loading and environmental conditions, considering also the fabrication process effects.

The CODSTRAN (COmposite Durability STRuctural ANalysis) computer code[1] has been developed for this purpose. CODSTRAN is an integrated, open-ended, stand alone computer code consisting of three modules: composite mechanics, finite element analysis, and damage progression modelling. The overall evaluation of composite structural durability is carried out in the damage progression module[1] that keeps

track of composite degradation for the entire structure. The damage progression module relies on ICAN[2] for composite micromechanics, macromechanics and laminate analysis, and calls a finite element analysis module that uses anisotropic thick shell and three dimensional solid elements, as appropriate, to model laminated composites.[3]

CODSTRAN is able to simulate damage initiation, damage growth, and fracture in composites under various loading and environmental conditions. The simulation of progressive fracture by CODSTRAN has been verified to be in reasonable agreement with experimental data from tensile tests.[4] CODSTRAN has been used to investigate the effects of composite degradation on structural response,[5] composite damage induced by dynamic loading,[6] composite structures global fracture toughness,[7] effect of hygrothermal environment on durability,[8] damage progression in composite thin shells subjected to internal pressure,[9] an overall evaluation of progressive fracture in polymer matrix composite structures,[10] the durability of stiffened composite shell panels under combined loading,[11] and the performances of adhesively bonded[12] as well as bolted[13] composite joints. The purpose of this paper is to describe application of CODSTRAN to simulate damage progression in a cracked aluminum panel with a composite surface patch for an expeditious and efficient design investigation that takes into account damage initiation/propagation mechanisms.

Figure 1 shows a schematic of the computational simulation cycle in CODSTRAN. The ICAN composite mechanics module is called before and after each finite element analysis. Prior to each finite element analysis, the ICAN module computes the composite properties from the fiber and matrix constituent characteristics and the composite layup. The finite element analysis module accepts the composite properties that are computed by the ICAN module at each node and performs the analysis at each load increment. After an incremental finite element analysis, the computed generalized nodal force resultants and deformations are supplied to the ICAN module that evaluates the nature and amount of local damage, if any, in the plies of the composite laminate. Individual ply failure modes are assessed by ICAN using failure criteria associated with the negative and positive limits of the six ply-stress components in the material directions as follows:

$$S_{\ell 11C} < \sigma_{\ell 11} < S_{\ell 11T} \tag{1}$$

$$S_{\ell 22C} < \sigma_{\ell 22} < S_{\ell 22T} \tag{2}$$

$$S_{\ell 33C} < \sigma_{\ell 33} < S_{\ell 33T} \tag{3}$$

$$S_{\ell 12(-)} < \sigma_{\ell 12} < S_{\ell 12(+)} \tag{4}$$

$$S_{\ell 23(-)} < \sigma_{\ell 23} < S_{\ell 23(+)} \tag{5}$$

$$S_{\ell 13(-)} < \sigma_{\ell 13} < S_{\ell 13(+)} \tag{6}$$

In addition to the failure criteria based on the above stress limits, interply delamination due to relative rotation of the plies, and a modified distortion energy (MDE) failure criterion that takes into account combined stresses is considered. The MDE failure criterion is expressed as:

$$F = 1 - \left[\left(\frac{\sigma_{\ell 11\alpha}}{S_{\ell 11\alpha}} \right)^2 + \left(\frac{\sigma_{\ell 22\beta}}{S_{\ell 22\beta}} \right)^2 - K_{\ell 12\alpha\beta} \frac{\sigma_{\ell 11\alpha}}{S_{\ell 11\alpha}} \frac{\sigma_{\ell 22}}{S_{\ell 22}} + \left(\frac{\sigma_{\ell 12S}}{S_{\ell 12S}} \right)^2 \right] \tag{7}$$

where α and β indicate tensile or compressive stress, $S_{\ell 11\alpha}$ is the local longitudinal strength in tension or compression, $S_{\ell 22\alpha}$ is the transverse strength in tension or compression, and

$$K_{\ell 12\alpha\beta} = \frac{(1 + 4\nu_{\ell 12} - \nu_{\ell 13})E_{\ell 22} + \quad (1 - \nu_{\ell 23})E_{\ell 11}}{[E_{\ell 11}E_{\ell 22}(2 + \nu_{\ell 12} + \nu_{\ell 13})(2 + \nu_{\ell 21} + \nu_{\ell 23})]^{1/2}} \tag{8}$$

The type of failure is assessed by comparison of the magnitudes of the squared terms in equation (7). Depending on the dominant term in the MDE failure criterion, fiber failure or matrix failure is assigned. The

generalized stress-strain relationships are revised locally according to the composite damage evaluated after each finite element analysis. The model is automatically updated with a new finite element mesh having reconstituted properties, and the structure is reanalyzed for further deformation and damage. If there is no damage after a load increment, the structure is considered to be in equilibrium and an additional load increment is applied leading to possible damage growth, accumulation, or propagation.

Figure 2 shows a schematic of CODSTRAN damage tracking, expressed in terms of a load-displacement relationship. Point 1 represents the last equilibrium state before initial damage. When the structure is loaded by an additional load increment to point 2, ply failure criteria indicate damage initiation. At this stage CODSTRAN degrades the composite properties affected by the damage, reconstitutes a new computational model with updated finite element mesh and material properties, and reanalizes the structure under the same load increment to reach point 3. However, at point 3, composite ply failure criteria indicate additional damage. Accordingly, structural properties are further degraded and analysis is repeated under the same load increment to reach point 4. There is no further damage at point 4, because the structure is now in equilibrium with the external loads. Subsequently, another load increment is applied leading to point 5 with possible damage growth and progression. Nodal fracture is predicted when major principal failure criteria are met for all composite plies as well as through the thickness of aluminum panel at a node. Fracture zones are created by the fracturing of several adjacent nodes. Typically, an angle-plied composite structure experiences global fracture by the coalescence of multiple fracture zones. In the computational simulation cases presented in this paper analysis is continued through the stage of fracture propagation that breaks the specimen into two pieces.

COMPOSITE PATCH REPAIRED ALUMINUM

An aluminum tensile specimen of L=12 in. long, W=3.0 in wide, and t=0.12 in. thick is considered. The specimen has an initial defect/crack at its center. The central defect is oriented transverse to the tensile load direction. Defects of length 0.1, 0.3, and 0.5 in. are considered. The composite patch measures 2.0 in. wide, 3.0 in. long, and is bonded to the surface of the aluminum specimen, centered at the defect. Figure 3 shows a schematic of the patched aluminum tensile specimen. The patch laminate structure consists of twelve 0.00521 in. thick plies resulting in a composite patch thickness of 0.063 in. The composite system is made of AS-4 graphite fibers in a high-modulus, high strength (HMHS) epoxy matrix. The fiber and matrix constituent properties, as well as properties of the aluminum, are obtained from a databank of material properties resident in CODSTRAN (2). The corresponding properties are as follows:

AS-4 Graphite Fiber Properties:

Number of fibers per end = 10000
Fiber diameter = 0.00762 mm (0.300E-3 in)
Fiber Density = 4.04E-7 Kg/m^3 (0.063 lb/in^3)
Longitudinal normal modulus = 227 GPa (32.90E+6 psi)
Transverse normal modulus = 13.7 GPa (1.99E+6 psi)
Poisson's ratio (ν_{12}) = 0.20
Poisson's ratio (ν_{23}) = 0.25
Shear modulus (G_{12}) = 13.8 GPa (2.00E+6 psi)
Shear modulus (G_{23}) = 6.90 GPa (1.00E+6 psi)
Longitudinal thermal expansion coefficient = 1.0E-6/°C (-0.55E-6 /°F)
Transverse thermal expansion coefficient = 1.0E-6/°C (-0.56E-6 /°F)
Longitudinal heat conductivity = 43.4 J-m/hr/m^2/°C (580 BTU-in/hr/in^2/°F)
Transverse heat conductivity = 4.34 J-m/hr/m^2/°C (58 BTU-in/hr/in^2/°F)

Heat capacity = 712 J/Kg/°C (0.17 BTU/lb/°F)
Tensile strength = 3,723 MPa (540 ksi)
Compressive strength = 3,351 MPa (486 ksi)

HMHS Epoxy Matrix Properties:

Matrix density = 3.40E-7 Kg/m^3 (0.0457 lb/in^3)
Normal modulus = 4.27 GPa (620 ksi)
Poisson's ratio = 0.34
Coefficient of thermal expansion = 0.72/°C (0.4E-4 /°F)
Heat conductivity = 1.25 BTU-in/hr/in^2/°F
Heat capacity = 0.25 BTU/lb/°F
Tensile strength = 84.8 MPa (12.3 ksi)
Compressive strength = 423 MPa (61.3 ksi)
Shear strength = 148 MPa (21.4 ksi)
Allowable tensile strain = 0.02
Allowable compressive strain = 0.05
Allowable shear strain = 0.04
Allowable torsional strain = 0.04
Void conductivity = 16.8 J-m/hr/m^2/°C (0.225 BTU-in/hr/in^2/°F)
Glass transition temperature = 216°C (420°F)

The HMHS matrix properties are representative of the 3501-6 resin. The fiber volume ratio is 0.60 and the void volume ratio is 2 percent. The cure temperature is 96.1°C (205°F) and the loading temperature is 21°C (70°F). The adhesive bond is assumed to have the same properties as the HMHS epoxy matrix.

ALT6 Aluminum Properties:

Density = 0.0443 lb/in^3
Normal modulus = 10000 ksi
Poisson's ratio = 0.33
Coefficient of thermal expansion = 1.29E-5 /°F
Heat conductivity = 104 BTU-in/hr/in^2/°F
Heat capacity = 0.23 BTU/lb/°F
Tensile strength = 52 ksi
Compressive strength = 52 ksi
Shear strength = 26 ksi
Allowable tensile strain = 0.0052
Allowable compressive strain = 0.0052
Allowable shear strain = 0.0905
Allowable torsional strain = 0.00905
Void conductivity = 0.225 BTU-in/hr/in^2/°F
Glass transition temperature = 1080°F

The finite element size at the vicinity of the defect is 0.1 in. Computed results are presented up to global fracture for each case. The defect is simulated by prescribing local failures in the aluminum prior to the application of the load.

In general, overall structural damage may include individual ply damage and also through-the-thickness fracture of the composite laminate. CODSTRAN is able to simulate varied and complex composite damage

mechanisms via evaluation of the individual ply failure modes and associated degradation of laminate properties. In this study, the aluminum panel is subdivided into twelve 0.01 inch layers to enable the simulation of damage progression across the thickness. The type of damage growth and the sequence of damage progression depend on the composite structure, loading, material properties, and hygrothermal conditions. A scalar damage variable, derived from the total volume of the composite material affected by the various damage mechanisms is also evaluated as an indicator of the level of overall damage induced by loading. This scalar damage variable is useful for assessing the overall degradation of a given structure under a prescribed loading condition. The rate of increase in the overall damage during composite degradation may be used as a measure of structural propensity for fracture. Computation of the overall damage variable has no interactive feedback on the detailed simulation of composite degradation. The procedure by which the overall damage variable is computed is given in Reference 7.

Figure 4 shows damage progression for the aluminum specimen, with three different defect sizes and without a patch repair. As expected, the fracture load decreases with increasing defect size. Figure 5 shows damage progression for patch repaired specimens that have 0.1 in. defects. Four different patch laminate configurations are investigated. The best performance is shown by the $[0/90/\pm45/90/0]_S$ or $[\pm45/90_2/0_2]_S$ configuration and the worst performance is shown by $[90/0]_{3S}$ cross-ply laminate. Figure 6 shows the damage progression for $[\pm45/90_2/0_2]_S$ patch with three different defect sizes. Figure 7 indicates the differences among different patch laminates for damage progression from a 0.5 in. defect.

Damage progression characteristics have the following general features:

1. Damage initiation is by matrix failure in the 90° plies of the composite patch adjacent to the defect in aluminum.

2. Damage growth is by further degradation of the patch with fiber fractures as well as new matrix failures in the angle plies.

3. In spite of composite damage growth, the patch is effective as a crack arrestor, inhibiting growth of the initial defect in aluminum.

4. Damage/fracture propagation characteristics depend on the patch laminate configuration.

Figure 8 shows damage energy release rates for $[\pm45/90_2/0_2]_S$ and $[90/0]_{3S}$ patches. The $[90/0]_{3S}$ cross-ply patch shows a very low resistance to initial damage growth from the 0.5 in. aluminum defect. On the other hand, the $[\pm45/90_2/0_2]_S$ patch shows a very high initial resistance to damage growth. The directions of damage growth and progression for the two patches are distinctly different as seen in Figure 9.

Figure 10 shows the effect of combined shear and tension loading on damage progression for a $[\pm45/90_2/0_2]_S$ patch. Very low levels of shear loading do not have a significant effect. However, when the magnitude of the shear loading becomes comparable to the tensile loading, the shear load becomes a very significant factor for damage propagation. Also, ultimate fracture propagation becomes more sudden when the shear load is larger.

Figure 11 shows the strength recovery due to a $[\pm45/90_2/0_2]_S$ patch repair on the original aluminum specimen with 0.5 in. defect. Practically the full strength of defect-free aluminum is regained by the patch repair. Additionally, the composite patch repaired specimen is more damage tolerant compared to the original defect-free aluminum. The demonstrated quantification of defect and damage tolerance for a given patch repair is fundamental in the process of identifying the optimal laminate configuration for each application.

CONCLUSIONS

1. Computational simulation, with the use of established composite mechanics and finite element modules, can be used to predict the influence of an existing defect as well as loading, on the safety and durability of a composite patch repaired aluminum panel.

2. CODSTRAN adequately tracks the damage growth and subsequent propagation to fracture for a patch repaired aluminum specimen with an initial defect.

3. Damage initiation, growth, and accumulation stages involve matrix cracking as well as fiber fractures in the composite patch area that is contiguous to the initial defect in aluminum.

4. The demonstrated procedure is flexible and applicable to all types of constituent materials, structural geometry, and loading. Homogeneous materials as well as composites can be simulated.

5. Fracture toughness parameters such as the structural fracture load and damage progression characteristics are identifiable for any structure with any defect by the demonstrated method.

6. Computational simulation by CODSTRAN represents a new global approach to progressive damage and fracture assessment for any structure.

REFERENCES

1. C. C. Chamis and G. T. Smith, "Composite Durability Structural Analysis," NASA TM-79070, 1978.

2. P. L. N. Murthy and C. C. Chamis, *Integrated Composite Analyzer (ICAN): Users and Programmers Manual*, NASA Technical Paper 2515, March 1986.

3. S. Nakazawa, J. B. Dias, and M. S. Spiegel, *MHOST Users' Manual*, Prepared for NASA Lewis Research Center by MARC Analysis Research Corp., April 1987.

4. T. B. Irvine and C. A. Ginty, "Progressive Fracture of Fiber Composites," *Journal of Composite Materials*, Vol. 20, March 1986, pp. 166-184.

5. L. Minnetyan, C. C. Chamis, and P. L. N. Murthy, "Structural Behavior of Composites with Progressive Fracture," *Journal of Reinforced Plastics and Composites*, Vol. 11, No. 4, April 1992, pp. 413-442

6. L. Minnetyan, P. L. N. Murthy, and C. C. Chamis, "Progression of Damage and Fracture in Composites under Dynamic Loading," NASA TM-103118, April 1990, 16 pp.

7. L. Minnetyan, P. L. N. Murthy, and C. C. Chamis, "Composite Structure Global Fracture Toughness via Computational Simulation," *Computers & Structures*, Vol. 37, No. 2, pp.175-180, 1990

8. L. Minnetyan, P. L. N. Murthy, and C. C. Chamis, "Progressive Fracture in Composites Subjected to Hygrothermal Environment," *International Journal of Damage Mechanics*, Vol. 1, No. 1, January 1992, pp. 60-79

9. L. Minnetyan, C. C. Chamis, and P. L. N. Murthy, "Damage and Fracture in Composite Thin Shells," NASA TM-105289, November 1991

10. C. C. Chamis, P. L. N. Murthy, and L. Minnetyan, "Progressive Fracture of Polymer Matrix Composite Structures: A New Approach," NASA TM-105574, January 1992, 22 pp.

11. L. Minnetyan, J. M. Rivers, P. L. N. Murthy, and C. C. Chamis, "Structural Durability of Stiffened Composite Shells," Proceedings of the 33rd SDM Conference, Dallas, Texas, April 13-15, 1992, Vol. 5, pp. 2879-2886

12. L. Minnetyan, C. C. Chamis, and P. L. N. Murthy, "Effect of Adhesive Thickness on The Durability of a Stiffened Composite Panel," Proceedings of the 39th International SAMPE Symposium and Exhibition, April 11-14, 1994, Anaheim, California, Vol. 39, pp. 2044-2056.

13. L. Minnetyan, C. C. Chamis, and P. L. N. Murthy, "Damage Progression in Mechanically Fastened Composite Structural Joints," Proceedings of the American Society for Composites-Ninth Conference, September 20-22, 1994, University of Delaware, Newark, Delaware, pp. 397-404.

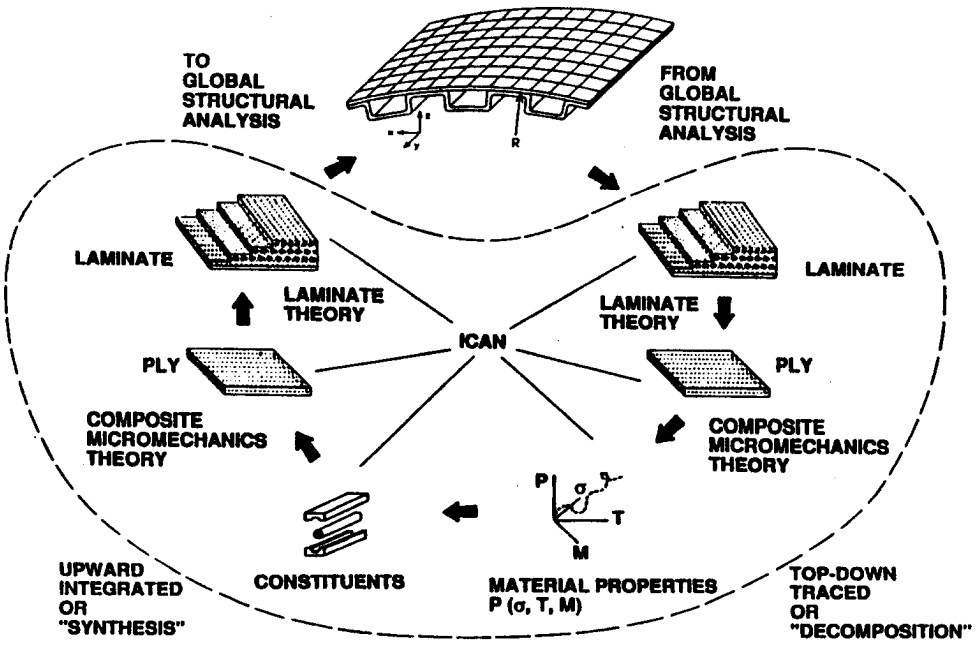


Figure 1 CODSTRAN Simulation Cycle

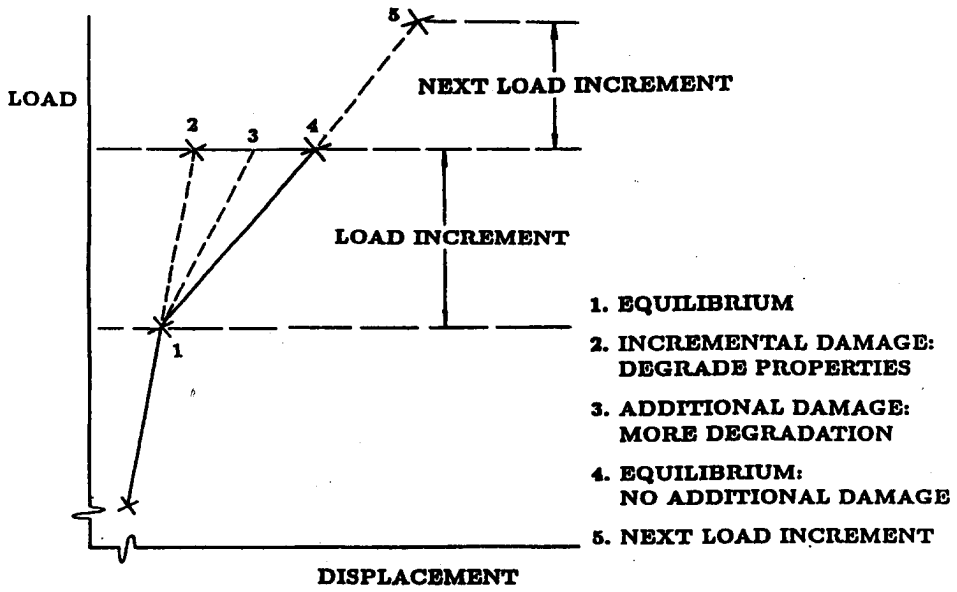
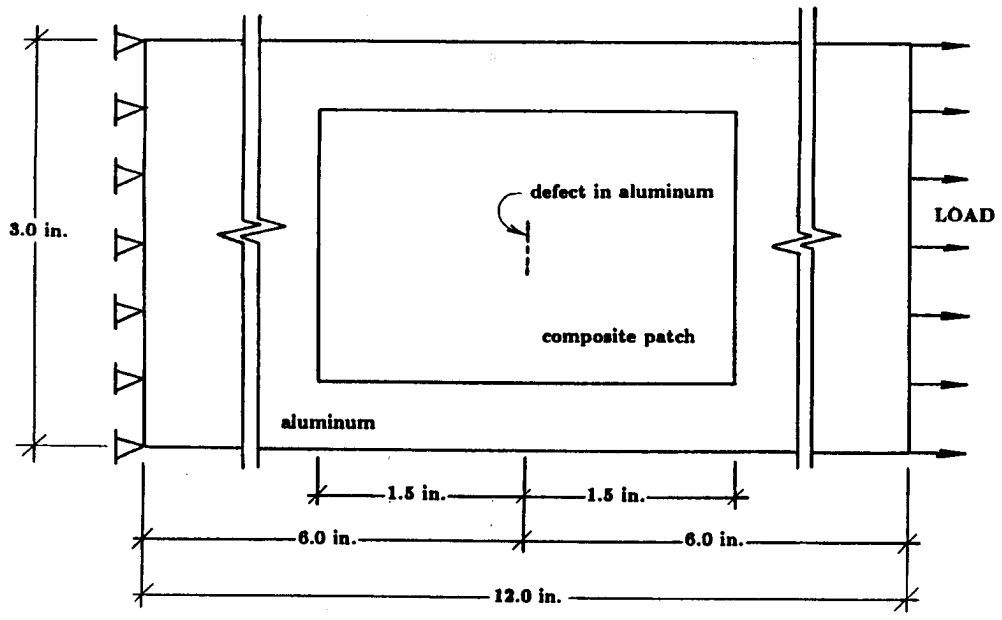


Figure 2 CODSTRAN Damage Tracking



Aluminum thickness = 0.12 in. Composite patch thickness = 0.063 in.
defect in aluminum transverse to tensile load direction
defect lengths considered: 0.1 in., 0.3 in., and 0.5 in.

Figure 3 Composite Patch Repaired Aluminum

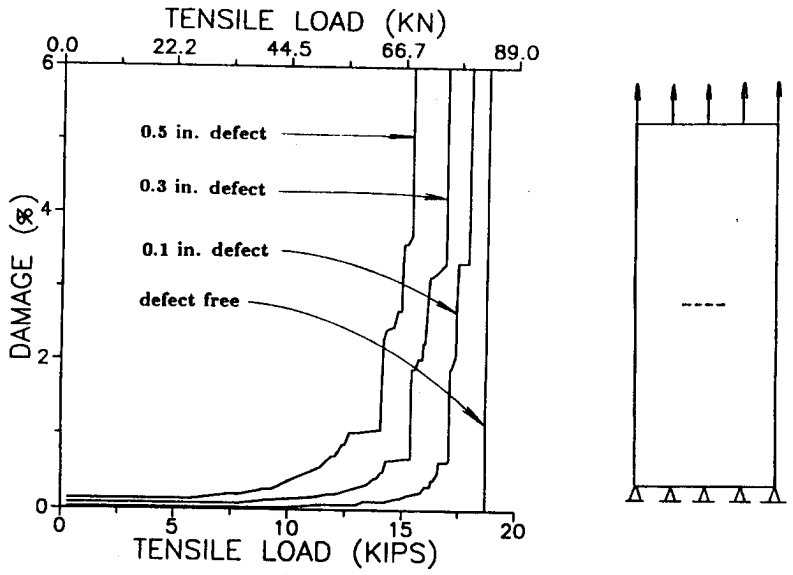


Figure 4 Damage Progression for Aluminum Specimen Without Patch

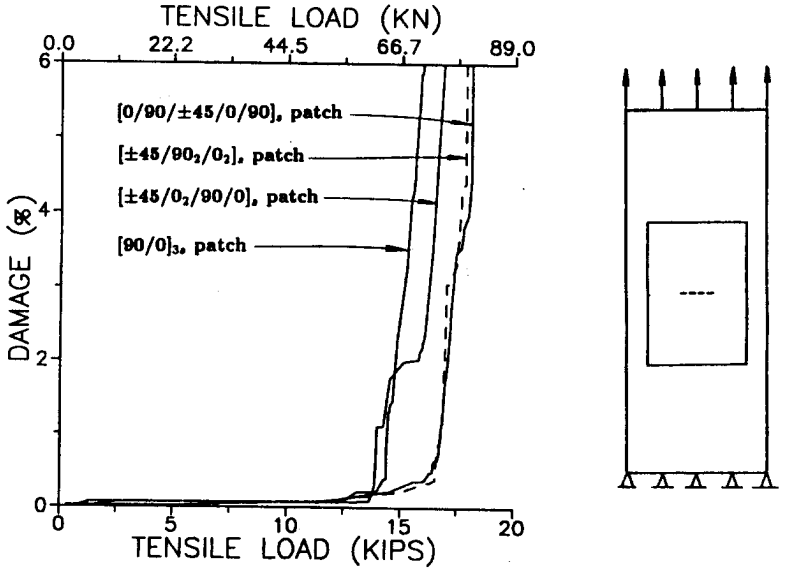
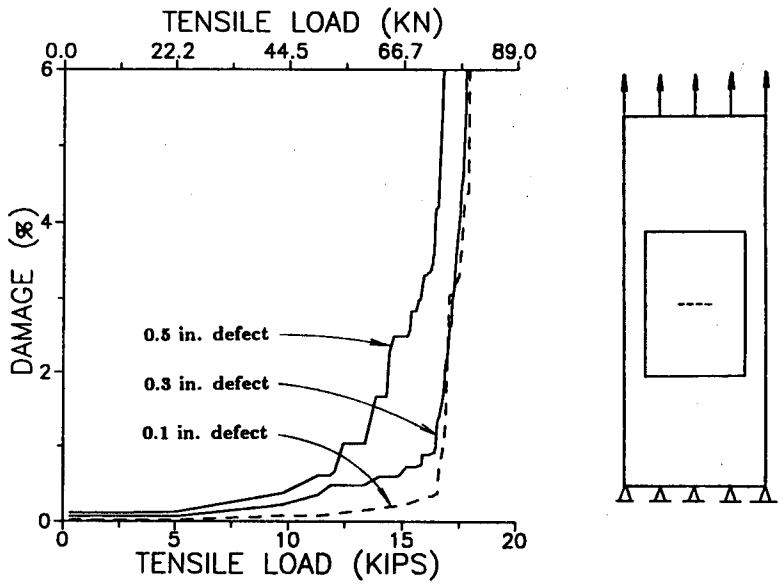


Figure 5 Patch Laminate Configuration Effect On Damage Progression from 0.1 in. long defect



graphite/epoxy $[\pm 45/90_2/0_2]_S$ patch

Figure 6 Defect Size Effect On Damage Progression

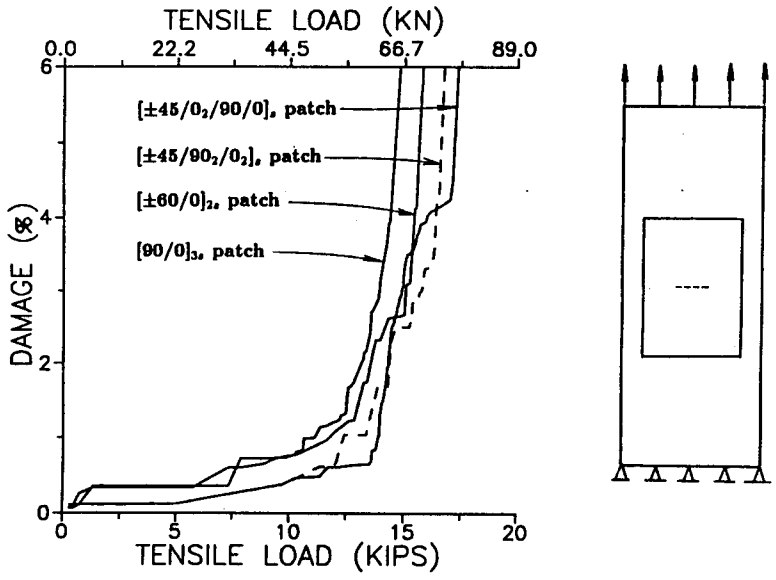
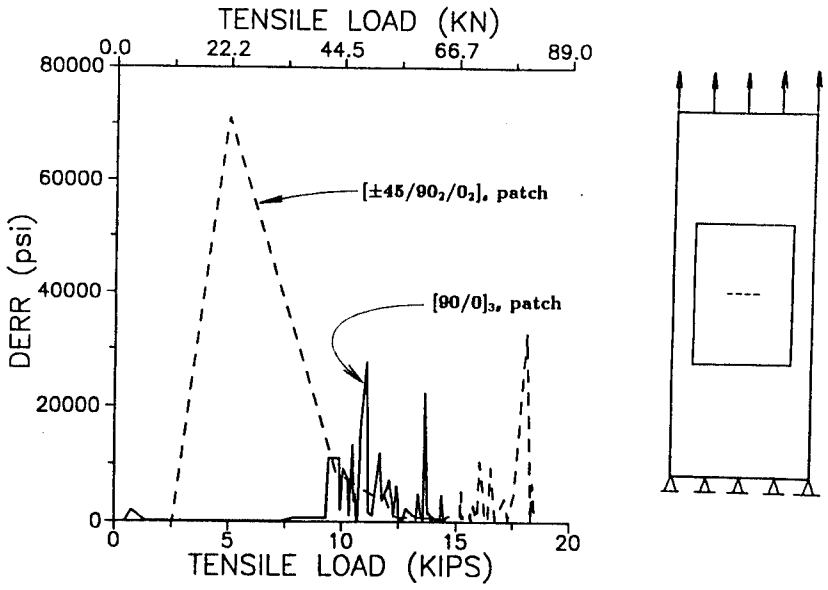
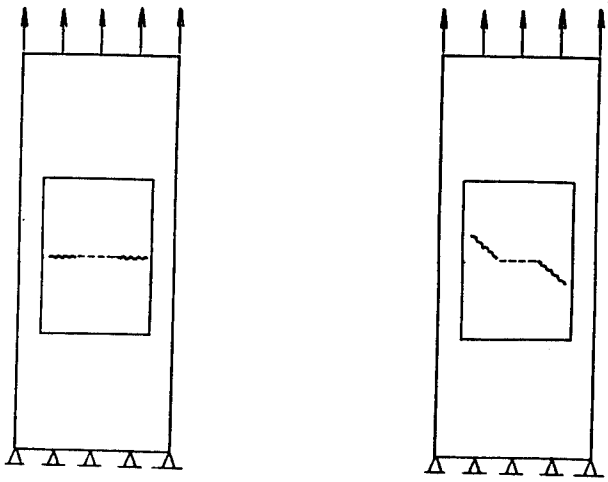


Figure 7 Patch Laminate Configuration Effect On Damage Progression from 0.5 in. long defect



defect length=0.5 in., graphite/epoxy patch

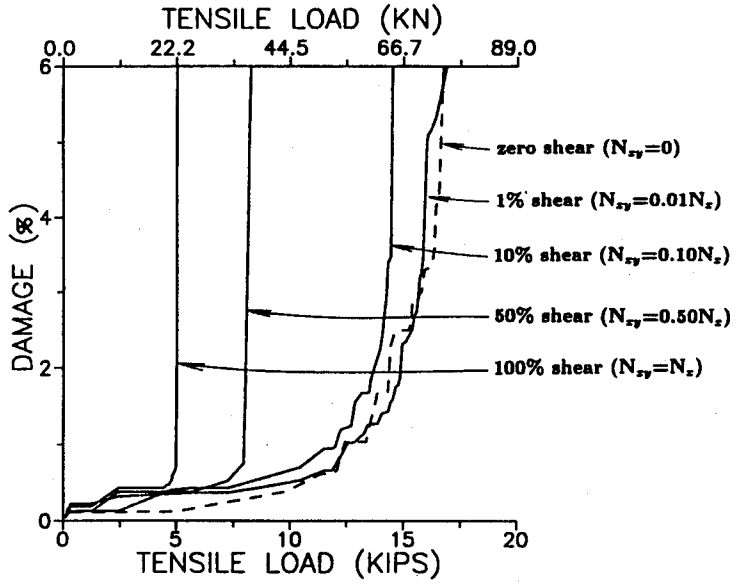
Figure 8 Laminate Configuration Effect On Damage Energy Release Rates



$[\pm 45/90_2/0_2]_S$ patch
self-similar crack growth

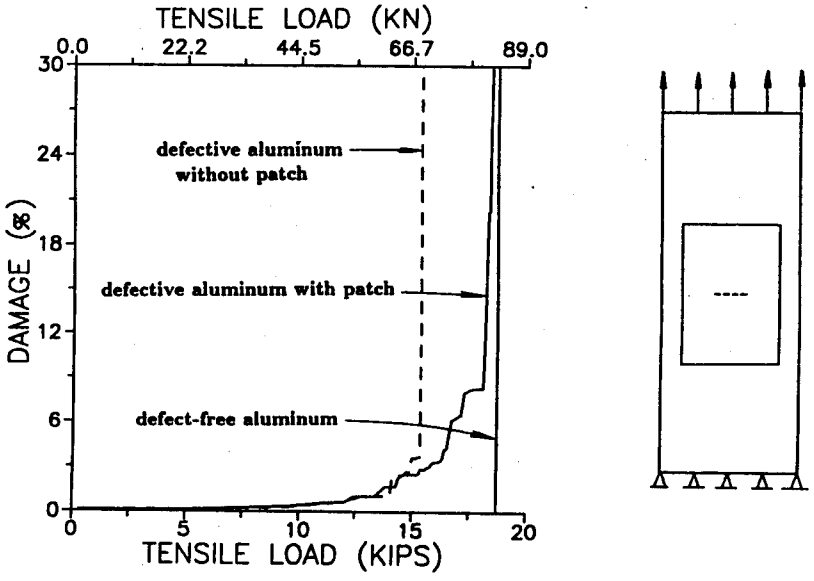
$[90/0]_{3S}$ patch
±45° crack growth

Figure 9 Effect of Patch Laminate On Damage/Fracture Orientation



defect length=0.5 in., graphite/epoxy $[\pm 45/90_2/0_2]_S$ patch

Figure 10 Damage Progression Under Combined Loading



defect length=0.5 in., graphite/epoxy $[\pm 45/90_2/0_2]_S$ patch

Figure 11 Strength Recovery Due To Patch Repair

An Enhanced Method of Stop Drill Repair with Sleeveless Coldworking

Matthew Weigel
West Coast Industries
Seattle, Washington 98133

Anthony Leon
West Coast Industries
Seattle, Washington 98133

Matthew Creager
Structural Integrity Engineering
Chatsworth, California, 91311

Abstract

Coldworking of fastener holes has been used in the aerospace industry for over 25 years to increase the fatigue life of parts. There are two main coldworking processes used in the industry today: split sleeve and split mandrel. These two systems produce comparable results, but the split sleeve process is used in more applications. This test program attempts to provide the data necessary to use the split mandrel process in a new application: stop-drill repair situations.

For this, the first phase of testing, four parameters were investigated: varying applied expansion levels to determine optimum levels for the split mandrel process, the effect of various edge margins (e/D) on life improvement, the effect of different hole types (open, filled) on life improvement, and the comparison of life improvement between the split sleeve and split mandrel processes.

The preliminary test results indicate that split mandrel coldworking provides equivalent results to split sleeve coldworking of stop drilled holes.

Introduction

Fatigue cracking has always been of major concern in the aerospace industry. The industry spends a considerable amount of time and money to locate, replace, or rework components with fatigue cracks. There are some situations when replacement or rework of a fatigued component is not immediately feasible, and an interim repair is used, such as stop drilling. This procedure involves drilling a hole at the crack tip to reduce the stress concentration and, thereby, retard further crack growth until a thorough repair can be done. Unfortunately, stop-drill holes do not always function in this manner. Common problems include cracks quickly initiating at the stop-drilled hole, and stop-drill holes that miss the crack tip, allowing the crack to continue growing. These problems can account for unscheduled repairs, meaning more aircraft downtime, and, thereby, increased maintenance costs.

In the 1980s an enhanced stop-drill procedure was developed [3] that utilized split sleeve coldworking of the stop drilled hole. The coldworking of the holes significantly increased fatigue life, by creating a zone of residual compressive streeses, thereby retarding further crack growth.

The 80's also saw the development of a new coldworking process, utilizing a lubricated collapsible split mandrel and no disposable sleeve. This split mandrel procedure provides equal or better fatigue life improvement than the split sleeve procedure [1,2]. This test program provides the preliminary data necessary to approve the split mandrel process in stop-drill applications.

Test Objective

The objective of this phase of testing is to investigate the feasibility of cold working with split mandrel tooling to increase the lifetime of stop-drill repair holes.

The two main procedures for coldworking holes are through the use of split sleeve or split mandrel tooling. Studies [1,2,4] have shown that split mandrel coldworking provides equal or better results than split sleeve procedures in other applications. It has also been proven [1-2] that the split mandrel process is easier and more cost effective than split sleeve procedures, due to the elimination of the disposable, split sleeve, as well as greater worker productivity.

The researchers hope to prove that coldworking with split mandrel tooling will produce equal, or better, life improvement results as split sleeve tooling to prove its feasibility in this application.

If split mandrel coldworking provides the expected results, then it should be considered the coldworking procedure of choice for this application. This is due to the cost effectiveness and simplicity of the procedure.

The results of this phase of testing are preliminary. A limited number of specimens were available for testing. The results for this phase of testing will be used to plan additional testing in Phase II.

Test Plan

This phase of testing involves two cold working processes, split sleeve and split mandrel. The split

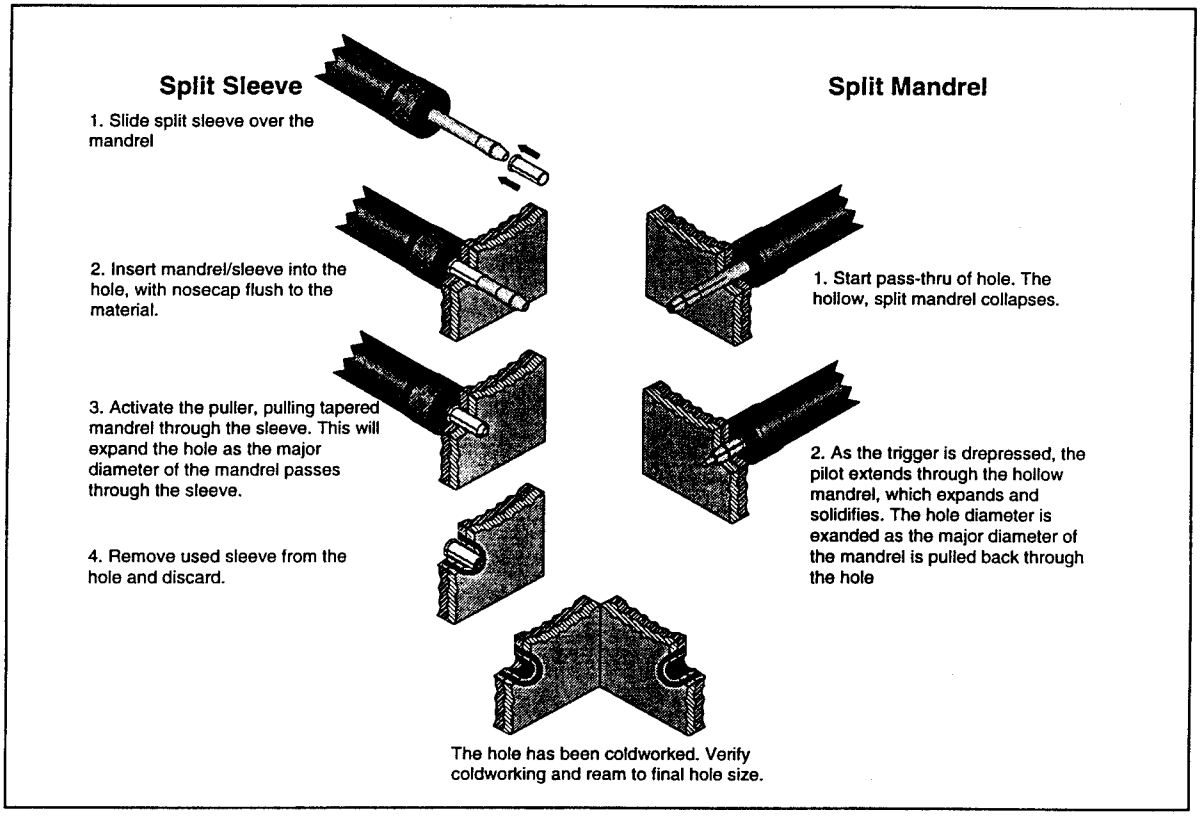


Figure 1–Split Sleeve and Split Mandrel Process Comparison

sleeve process utilizes a solid, tapered mandrel, and an internally lubricated split sleeve. Split sleeve cold working (Ref. Figure 1) is accomplished when the mandrel, with the sleeve placed on its the mandrel minor diameter, is inserted into the hole. The mandrel is then pulled back through the sleeve. The split mandrel process utilizes an axially split, collapsible, tapered mandrel (Ref. Figure 2). The split mandrel coldworking process begins with the mandrel being automatically lubricated with a small amount (one drop) of Boelube lubricant. When the mandrel is pulled through the hole it is supported by the pilot, which expands and solidifies the mandrel (Ref. Figure 1). Each process plastically enlarges the hole leaving a residual compressive zone around the hole. This compressive zone retards crack growth at the hole, thereby increasing the fatigue life of the part.

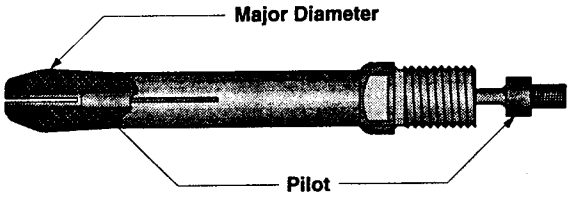


Figure 2–Cutaway View of Split Mandrel Showing Pilot

The main focus of testing will be to determine if split mandrel coldworking provides similar, or better, life improvement than split sleeve coldworking.

To begin establishing a correlation between split mandrel and split sleeve coldworking, the researchers reviewed the literature to locate past testing of split sleeve coldworking in stop-drill applications. A paper [3], authored by Landy, et. al., described experimental and analytical investigation of the effectiveness of an enhanced stop-drill procedure that utilizes split sleeve coldworking. The researchers illustrated, through the use of laboratory experiments and computer finite element analysis, that the fatigue life of a stop-drill repair would be significantly increased by cold working the hole using the split sleeve process.

A decision was made to duplicate portions of the previous test in this test. The researchers decided to duplicate the specimen design, testing conditions, and use of 7075 material. Later 2024 material was added to the test matrix. See Tables 1 and 2 for material information.

The test specimen (Ref. Figure 3) was designed, "to simulate a crack in a structured panel with a stop-drill hole located at the crack tip [3]." The speci-

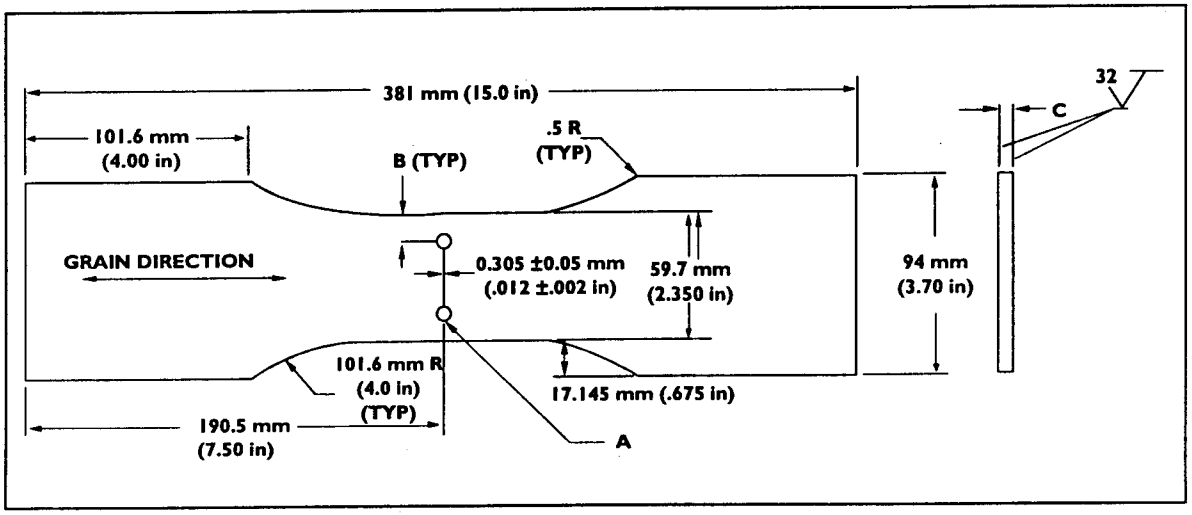


Figure 3–Test Specimen Configuration

men has two 6.35 mm. (0.250 inch) holes representing stop-drill holes. The e/D ratios were either 1.5 to 2.0 (the edge margin ratio is defined as the distance from the center of the hole to the edge of the part.). The specimen has a 0.305 mm wide slot that represents a fatigue crack. The two holes and slot are 90° from the direction of loading.

Specimen preparation was conducted as follows:

- Non-cold worked specimens were reamed to the final hole diameter, 6.35 mm (0.25 inch).
- Split sleeve (Sp. Sl.) cold worked specimens had initial holes drilled and reamed to size. The cold working was performed, using established WCI procedures [5] using standard WCI 8-0-N tooling. The sleeve gap was oriented towards the machined slot. The specimens were then reamed to final hole diameter.
- Split mandrel (Sp. M.) cold worked specimens had initial holes drilled and reamed to size. The cold working was performed using established WCI procedures [6] using standard WCI-CMM-8-0 tooling. The mandrel gaps were oriented at 45° from the machined slot. The specimens were then reamed to the final hole diameter.
- All filled hole specimens were filled with protruding-head, straight-shank, Hi-Lok™ fasteners and secured with Hi-Lok™ collars. A back-up block was used between the back of the specimen and the collars to preclude fretting failures. The fasteners were net clearance fasteners (interference levels of < 0.00 mm.).

The testing conditions used in this test are detailed in Table 3. The test matrix (Ref. Table 4) was developed to determine the effectiveness of split mandrel coldworking in a stop-drill application. The parameters for testing in this phase of testing included:

1. The amount of applied expansion on life improvement.
2. The effect of filling the holes on life improvement.
3. The effect of varying edge margins on life improvement.
4. The difference in life improvement between split mandrel and split sleeve processes.

All specimens were cycled to failure in a closed loop, electro-hydraulic fatigue test machine. Testing was conducted under load control in laboratory air at ambient temperature and humidity. Constant amplitude loads were generated by a digital function generator. The test machines and electronics are calibrated annually with standards traceable to the National Institute of Standards and Technology.

Results

Applied Expansion and Life Improvement

The optimal applied expansion has been determined for the split sleeve process [6], but need to be determined for the split mandrel process for this specific application. In this phase of testing, two applied expansion percentages were tested, 6.1% (similar to the split sleeve enhanced stop-drill repair procedure) and 5.2%. The test results are detailed in Figures 4 & 5.

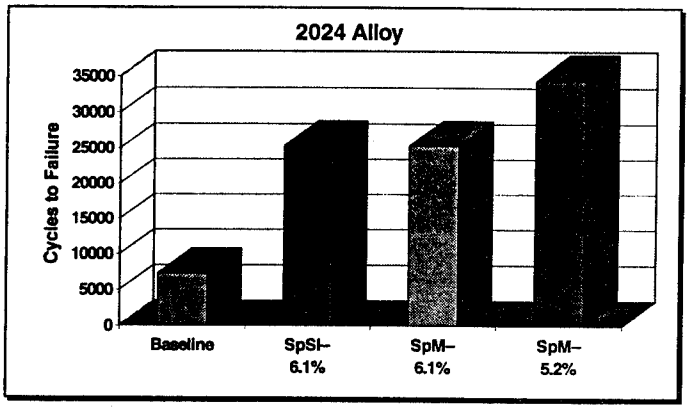


Figure 4–Fatigue Life Results for 2024 Aluminum, Split Mandrel at Various Applied Expansions, Compared to Split Sleeve and Baseline

In both materials, the lower 5.2% applied expansion provided equal or better life improvement results than the higher applied expansion, although both produced significant life improvement. In 2024 specimens, the 6.1% expansion provided a life improvement factor of 3, while the 5.2% expansion provided an improvement factor of 5 (an increase of 27% over the higher applied expansion). In 7075 specimens, both applied expansions provided an order of magnitude life improvement.

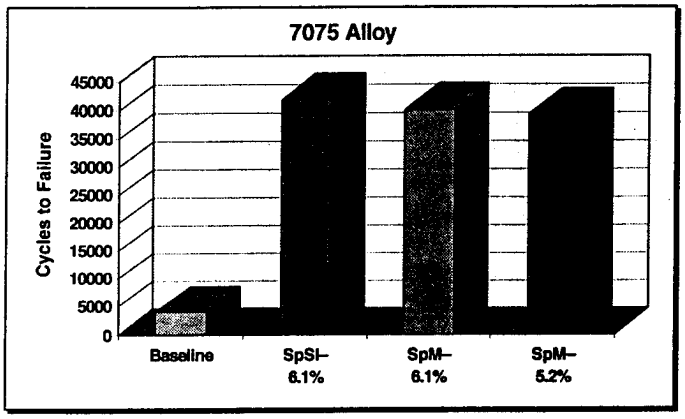


Figure 5–7075 Aluminum Split Mandrel Life Improvement at Different Applied Expansions, Compared to Split Sleeve and Baseline

Split Mandrel vs. Split Sleeve

The data suggests that the test objective will be proven with additional testing. For equal applied expansions of 6.1%, and in both materials tested, the difference in life improvement between the split mandrel and split sleeve processes is statistically insignificant. In 2024 material, both processes produced a life improvement factor of 3, while in 7075 material there was an order of magnitude in life improvement (Ref Fig. 4 & 5).

Edge Margin and Life Improvement

Both cold working processes consider a 2.0 e/D situation as the ideal condition. However, in the real world of repair applications, this is the exception rather than the rule. Reducing the edge-margin results in both a larger stress concentration factor (K_T) and stress intensity factor (K_I), thereby reducing fatigue life. The researchers understand the importance of providing life improvement in less than optimal situations. Thus the split mandrel process was tested with less than the ideal 2.0 e/D.

The researchers were surprised with the results (Ref Figures 5 and 6). In the 2024 specimens, the differences between the results of the 2.0 e/D and 1.5 e/D was approximately 5%, while in 7075 specimens the difference was approximately 5.5%. These results indicate the split mandrel process may provide significant life improvement in short e/D applications.

An important consideration in short e/D situations is the possible expansion of the ligament due to cold working. Precise measurements of the specimen width were taken before and after cold working. There were no visible indications of expansion, and the measured expansion was minimal.

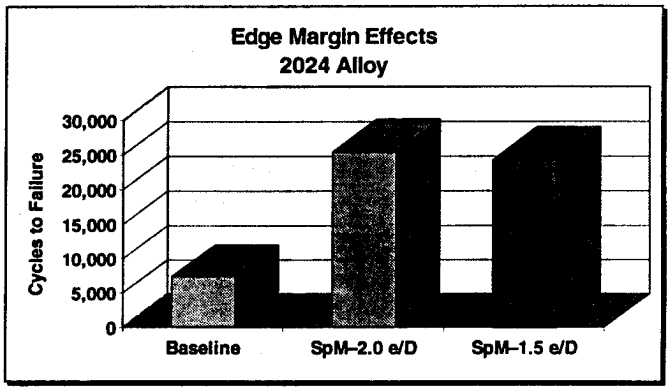


Figure 6–The Effect of Differing Edge Margins in 2024 Aluminum

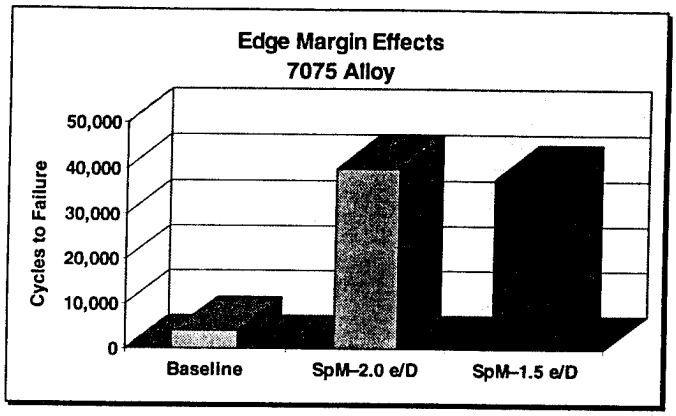


Figure 7–Effect of Differing Edge Margins in 7075 Alloy

The average expansion for all specimens is approximately 0.025 mm. (0.0010 inches), with a maximum expansion of 0.041 mm. (0.0016 inch). The average expansion for 2024 specimens was 0.025 mm. (0.0010 inches) and 0.015 mm. (0.0006 inches) for 7075 specimens with a 2.0 e/D. The maximum measured expansion for 2.0 e/D specimens was 0.0014 inches for 2024 specimens and 0.023 mm.(0.0009 inch) for 7075 specimens. The average expansion in 1.5 e/D specimens is 0.033 mm. (0.0013 inch) for 2024 specimens and 0.020 mm. (0.0008 inch) for 7075. The maximum expansion for 1.5 e/D specimens is 0.041 mm.(0.0016 inch) for 2024 specimens and 0.028 mm. (0.0011 inch) for the 7075 specimens. These measurements reveal that 1.5 e/D specimens had approximately twice the expansion of the 2.0 e/D. However, this expansion is still considered minimal.

Fastener Installation

The preliminary filled hole results are similar to the previous test [3]. It appears that filling the hole improves fatigue life significantly over both the non-coldworked and coldworked, unfilled, holes. The results are plotted in Figures 8 and 9.

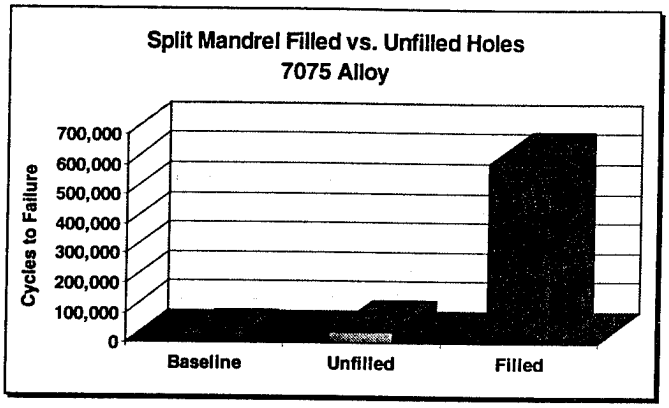


Figure 9–Life Improvement in 7075 Alloy with Non-Interference Fit Fastener Installation

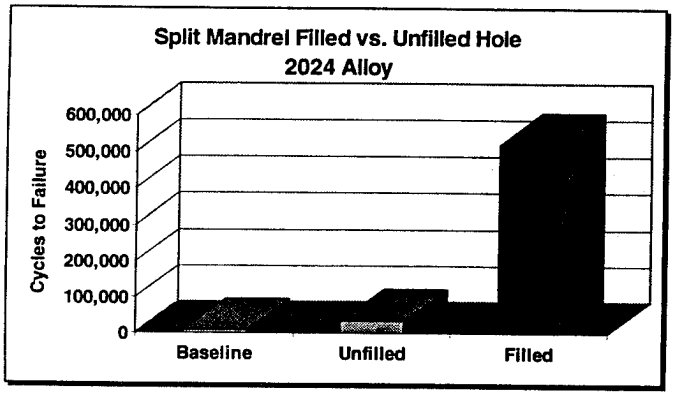


Figure 8–Life Improvement in 2024 Alloy with Non-Interference Fit Fastener Installation

Filling the test holes with non-interference fit steel fasteners considerably increased the fatigue life of specimens. Fatigue lives were increased by a factor of 71 over baseline results and by a factor of 15 over split mandrel cold worked (5.2% applied expansion) results in unfilled 2024 specimens. The fatigue lives increased by a factor of 148 over baseline results and by a factor of 15.5 over split mandrel cold worked (5.2% applied expansion) results in unfilled 7075 specimens.

The researchers believe that additional testing will reveal better life improvement with the use of interference fasteners.

Analysis

The test data can be used to produce preliminary results. The researchers have begun analysis in the following two areas:

1. Filled vs unfilled holes.
2. Optimum applied expansion for split mandrel process

Filled vs. Unfilled Holes

A thorough analysis of the fatigue life improvement achieved by filling fastener holes is non-linear in nature, and more complex than the scope of this report. The basic components of this analysis are known, and are detailed below.

Fastener holes are the sites of high stress concentrations. Cold working a hole reduces the tensile stress concentration at the hole by creating a residual compressive stress zone immediately around the hole. For a given applied stress, the mean stress at the hole is reduced [7]. This reduction in applied stress at the hole retards crack growth [8], thereby increasing fatigue life.

When a remote external force is applied to a coldworked hole, it stretches both the hole and its surrounding compressive zone. This stretching of the compressive zone may cause relaxation of the compressive zone, reducing the effectiveness of the coldworking. Filling the hole with a non-interference, clearance fastener eliminates possible stretching of both the hole and stress zone [9]. Since the compressive zone does not relax, the coldworking is more effective.

Optimal Applied Expansion for Split Mandrel Process

An optimal applied expansion for the split mandrel process was not concluded in the limited testing completed to date. The present results point toward an applied expansion level of 6.1% in 7075 aluminum and 5.2% in 2024, as the optimal levels. More testing is needed to come to a definitive conclusion regarding applied expansion levels for the split mandrel process.

Conclusions

No definite conclusions can be made with the limited data available. Additional testing will be needed (and will be conducted in early 1995) to provide definite conclusions.

The following preliminary conclusions can be inferred from the test results.

1. There is no significant difference between the use of the split sleeve and split mandrel processes.
2. There is no significant difference in the fatigue lives in the two e/D configurations tested.
3. The greatest fatigue life improvement is seen by filling the coldworked stop-drilled hole.

Reference

1. Geoffrey A. Rodman, Matthew Creager, Ph.D., "Split Mandrel Coldworking: A Manufacturing Solution for Automating a Critical Process," Technical Report–TR9308, West Coast Industries, 1993.

2 Geoffrey A. Rodman, Matthew Creager, Ph.D., "Split Mandrel vs. Split Sleeve Coldworking: Dual Methods for Extending the Fatigue Life of Metal Structures." Paper Presented at the 1993 USAF Structural Integrity Program Conference, 1993.

3. Michael A. Landy, Harry Armen, Jr., Harvey Edinoff, "Enhanced Stop Drill Procedure for Cracked Structures," Fatigue in Mechanically Fastened Composite and Metallic Joints, ASTM STP 927, John M. Potter, ED., American Society for Testing and Materials, Philadelphia, 1986.

4. Unpublished Report Draft, "Expanding Mandrel Cold Working Development 1993 Test Report." British Aerospace Test Report, 1994.

5. "Split Sleeve Coldworking Holes (Aluminum, Steel, and Titanium)," Engineering Handout WCI-9201-3, West Coast Industries, 1993.

6. "Split Mandrel Coldworking Holes (Aluminum)," Engineering Handout WCI-9202-5, West Coast Industries, 1994.

7. D.L. Rich, L.F. Impellizzeri, "Fatigue Analysis of Coldworked and Interference Fit Fastener Holes." Cyclic Stress-Strain and Plastic Deformation Aspects of Fatigue Crack Growth, ASTM 637, American Society for Testing and Materials, Philadelphia, 1977.

8. Nopporn Chandawanich, "An Experimental Study of Fatigue Crack Initiation and Growth from Coldworked Holes," Engineering Fracture Mechanics, Vol 11, 1979.

9. H. Armen, Alvin Levy, H.L. Eidinoff, "Elastic-Plastic Behavior of Coldworked Holes," AIAA Paper 83-0865, American Institute of Aeronautics and Astronautics, 1983.

Appendix

Material	Si	Fe	Cu	Mn	Mg	Cr	Zn	Ti	Other, Ea.	Other,Total	Al
2024-T351	0.50	0.50	3.80-4.90	0.30-0.90	1.20-1.80	0.10	0.25	0.15	0.05	0.15	Balance
7075-T651	0.06	0.30	1.63	0.03	2.57	0.19	5.67	0.03	0.05	0.15	Balance

Table 1–Chemical Composition of Specimen Material

Material		Ultimate (ksi.)	Yield (ksi.)	Elongation (%)
2024-T351	max.	70.5	51	15.9
	min.	70.2	50.8	15.3
7075-T651	max.	84.2	74.3	12.0
	min.	83.8	73.6	12.0

Table 2–Physical Properties of Specimen Material

Parameter	Value
Loading	Constant Amplitude Sine Wave
Frequency	5 Hz.
Max. Net Test Stress	262 MPa (38.0 ksi.)
R-ratio	0.05
Test Temperature	Ambient
Test Humidity	Ambient

Table 3–Test Parameters

Material	Description	Cw/NCw	App. Expansion (%)	Edge Margin (e/D)	Filled/Unfilled Hole	# Specimens Group
2024	Baseline	NCw	N/A	2.0	Unfilled	3
	Split Sleeve	Cw	6.1	2.0	Unfilled	3
	Split Mandrel	Cw	6.1	2.0	Unfilled	3
	Split Mandrel	Cw	5.2	2.0	Unfilled	3
	Split Mandrel	Cw	6.1	1.5	Unfilled	3
	Split Mandrel	Cw	5.2	2.0	Filled	3
7075	Baseline	NCw	N/A	2.0	Unfilled	3
	Split Sleeve	Cw	6.1	2.0	Unfilled	3
	Split Mandrel	Cw	6.1	2.0	Unfilled	3
	Split Mandrel	Cw	5.2	2.0	Unfilled	3
	Split Mandrel	Cw	6.1	1.5	Unfilled	3
	Split Mandrel	Cw	5.2	2.0	Filled	3

Table 4–Test Matrix

Bonded Repair of Multiple Site Damage with GLARE™ Fiber Metal Laminate Patches

Major Robert Fredell, USAF
Department of Engineering Mechanics
US Air Force Academy, Colorado

Mr. Richard Müller
Mr. Cees Borsboom
Faculty of Aerospace Engineering
Delft University of Technology
Delft, The Netherlands

Captain Lawrence Butkus, USAF
School of Mechanical Engineering
Georgia Institute of Technology
Atlanta, Georgia

ABSTRACT

Bonded composite "crack patching" has been used successfully to extend the life of numerous cracked or corroded aircraft structures. Most crack patching has been accomplished on small areas of thick structures using relatively expensive boron/epoxy composites. Extending the lives of aging transport fuselage structures, however, may involve repairs to large areas of thin fuselage skins and lap joints. Hence, affordable materials and processes are required.

The hybrid materials known as GLARE™, which consist of bonded alternating thin aluminum alloy sheets and glass/epoxy prepregs, present a relatively low-cost alternative to boron/epoxy. Furthermore, recently published analyses have predicted that GLARE™ 2 can out-perform boron/epoxy in crack patching of thin structures subjected to the low service temperatures experienced in a fuselage skin at cruise altitude.

This paper presents the results of constant amplitude fatigue tests performed at room temperature on large flat stiffened panels and a pressurized unstiffened fuselage "barrel." These specimens simulate pressurized transport fuselage structures with multiple site fatigue damage. Bonded GLARE™ 2 patches successfully halted the growth of multiple fuselage fatigue cracks beneath the patch. Furthermore, the presence of unrepaired fatigue damage adjacent to the bonded patch does not compromise the damage-tolerant nature of the repair. The results confirm GLARE™ 2 to be an effective, damage-tolerant fuselage repair material.

KEY WORDS: adhesive bonding, coefficient of thermal expansion (CTE), crack patching, damage tolerance, durability, fatigue, GLARE™.

1. INTRODUCTION

"Crack patching" refers to the practice of applying adhesively bonded advanced composite repair patches to cracked metal structures. Crack patching was first successfully applied to the wing pivot fitting of the General Dynamics F-111 around 1969 [1]. The concept, first applied to cracked thick structures, has extended the useful lives of flawed airframes for many years when no other cost-effective alternative existed. More recently, the crack patching concept has been extended to the repair of cracked thin fuselage structures. Extensive analysis has shown the fiber metal laminate GLARE™ 2 to be a viable alternative to the five to ten times more expensive composite materials, boron- and carbon-epoxy, for pressurized fuselage skin repairs. (GLARE™ 2 is a hybrid laminate of 2024-T3 aluminum and unidirectional S-glass/epoxy composite [2, 3]). Furthermore, GLARE™ 2 is predicted to give significantly lower adhesive shear strains due to its better thermal expansion compatibility with aluminum [4, 5]. This is an important factor in both the crack closing effectiveness and the long-term durability of the adhesive bond.

The successful implementation of crack patching as a pressurized fuselage repair method requires a "building block" approach of patch designs before a flight test program can be initiated. An earlier paper [6] described laboratory testing of small coupons and larger stiffened panels with saw cuts to simulate bonded repairs made to a single large crack.

These previously reported tests showed crack patching with GLARE™ 2 patches to be durable: that is, the patches remained intact for a reasonable number of aircraft fatigue lifetimes without allowing cracks to grow. However, before crack patching can be accepted by the airworthiness authorities, its damage tolerance must be shown by documenting its

beneficial effect on (or at least its insensitivity to) damage that exists in the structure outside of the repair.

The following sections discuss engineering design guidelines for bonded fuselage repairs. They further describe how a large, repaired stiffened panel with artificial multiple site-damage (MSD) performed under constant amplitude fatigue loading. These results, along with testing of repairs to naturally occurring multiple site fatigue damage in a curved riveted lap joint, validate the damage-tolerant nature of bonded GLARE™ 2 patches in crack patching of fuselage structures.

2. ANALYSIS OF BONDED FUSELAGE REPAIRS

Two recent papers [5, 7] presented general guidelines for the design of bonded patch repairs and are summarized in section 2.3. When one concentrates solely on pressurized fuselage skin repairs, the following special conditions must be considered:

- The structure being repaired is quite thin; thus, extremely stiff patches are not required for effective repairs,
- The adhesive is cured at a temperature ranging from 80 to 120°C (180 to 250°F). The fuselage sees service temperatures ranging from perhaps 60°C (140°F) (unloaded, hot day on the ground) to -54°C (-65°F) (maximum internal pressure at cruise altitude). Because the transport fuselage experiences its greatest internal pressure loads at its minimum service temperature, thermally-induced stresses in a fuselage bonded repair can be a more significant consideration than in, say, a fighter lower wing skin repair.

2.1 Influence of Patch Stiffness Because of the relatively thin structure being repaired, the use of high elastic modulus composites to keep the patch thickness low is not necessary. Any fatigue-resistant, high-strength patch material that satisfies the design criteria for good patching discussed in section 2.3 is suitable.

2.2 Influence of Thermal Effects Most crack patching is performed on the aircraft by locally heating the repair area. During the bonding process, the surrounding (unheated) structure restrains the heated area from free expansion, but the patch expands freely. In stiffened structures, *the effective thermal expansion* of the constrained structure is much less than the unconstrained thermal expansion coefficient. The use of patch materials with relatively low coefficients of thermal expansion (CTE) like boron- or carbon-fiber composites means the bond line is relatively stress free after cooling to room temperature. Moderate- to high-CTE patches actually place the crack in compression at room temperature.

When a transport aircraft climbs to cruising altitude, its fuselage is cooled uniformly to the outside air temperature (-54°C at 10,000 meters). The structure cools and contracts uniformly, but the low thermal expansion composite patch doesn't contract nearly as much. For example, a boron patch shrinks only about 1/6 as much as the now-unconstrained aluminum fuselage. This induces an additional cyclic tensile load on the crack tip at a time when the pressure-induced stress is highest. Further, the adhesive that was ductile and relatively flexible at room temperature is substantially stiffer and more brittle at -54°C. This additional tensile load occurs every flight.

Figure 1 compares the patching efficiency (stress intensity factor or "K" reduction) of two potential fuselage patch materials: boron-epoxy and the

unidirectionally reinforced glass/epoxy/aluminum hybrid GLARE™ 2. While boron's CTE is about 1/6 that of aluminum, GLARE™ 2 has a CTE approximately 2/3 of aluminum.

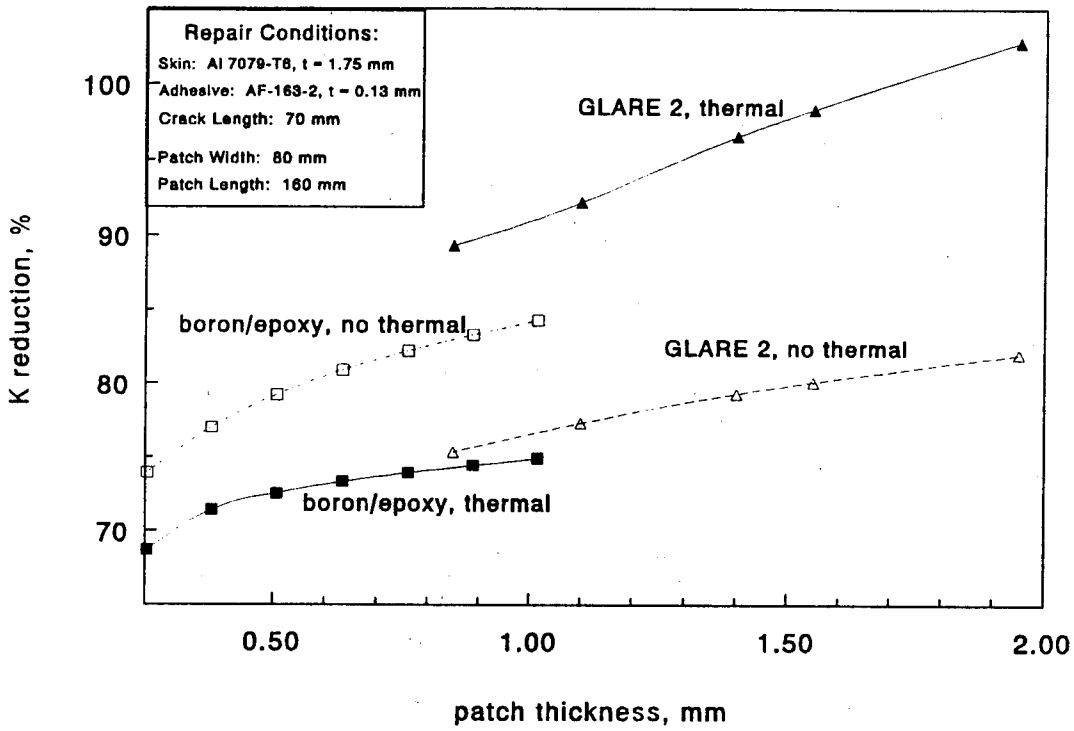


Figure 1. Comparison of reduction in stress intensity factor for bonded GLARE™ 2 and boron patches, with and without considering thermal effects [5].

When thermal effects are ignored, the much stiffer boron patch seems to do a better job closing the crack. (100% K reduction means no crack opening occurs.) However, when the complexities of constraint during bonding and free thermal contraction during cruise flight are considered, the GLARE™ 2 patch comes out as the more effective patch. Consequently, patch extensional stiffness can be relaxed somewhat when the CTE of the patch material and the cracked skin are closely matched [5].

2.3 Design Guidelines for Fuselage Crack Patching Reduction in stress intensity factor is not the only design criterion for effective crack patching. The significant variables to be considered in a crack patching design include:

- sufficient reduction in K to slow or stop crack growth,
- acceptably low normal stresses in the patch to avoid patch failure,
- avoidance of excessively high tensile stresses in the skin adjacent to the repair to preclude new fatigue problems in the skin,
- prevention of widespread adhesive bond line shear yielding, and
- tolerably low peel stresses in the bond line.

3. STIFFENED PANEL TESTING

Detailed design studies and a series of coupon tests indicated the potential utility of GLARE™ 2 as a transport fuselage patch material [4]. Large panel tests were undertaken to scale up the concept and prove the durability and damage tolerance of the concept.

3.1 Test Panel Description Figure 2 shows a sketch of the panel test section, built to represent a fuselage cracking problem on a large USAF transport aircraft. The overall length of the panel was 1.2 meters (3.9 feet); the width was 0.80 meters (2.6 feet). The panel consisted of a continuous 7075-T6 aluminum skin of 1.6 mm (0.063 inch) thickness, to which were bonded two 0.60 mm (0.024 inch) thick 7075-T6 tear straps. Cold-formed 2.0 mm (0.080 inch) thick 7075-T6 frames were then riveted into place over the tear straps. Additional rivets were placed transverse to the loading direction to simulate the stress concentration of a fairing panel attachment on the actual structure. (The rivet line is the location of the fatigue cracking problem in service.) An 80 mm (3.2 inch) saw cut was placed in the center of this rivet line to simulate a fatigue crack.

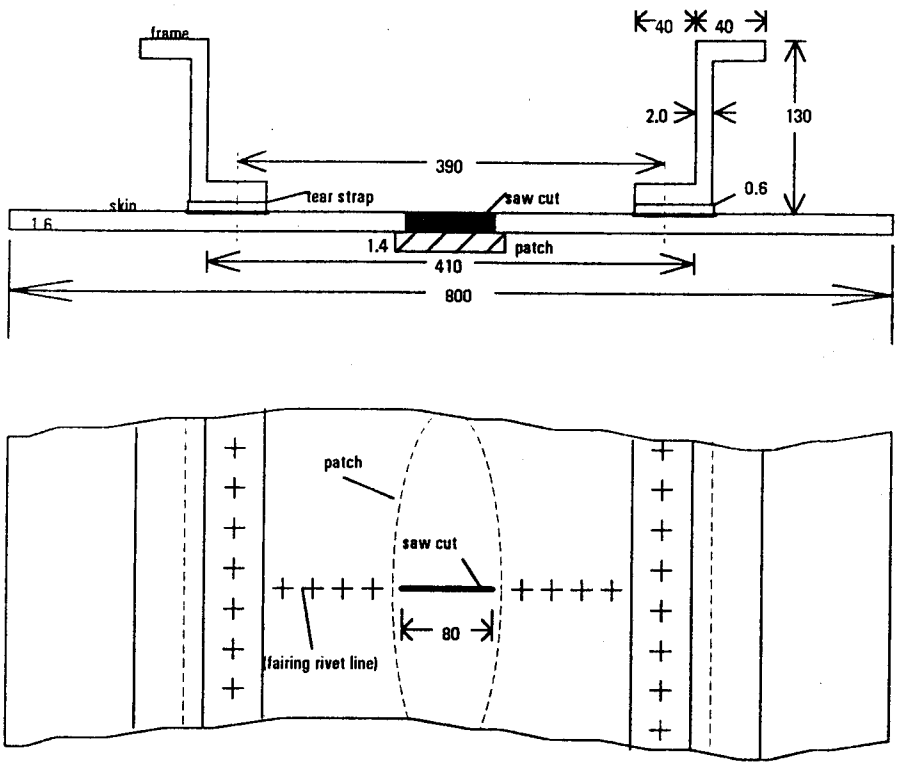


Figure 2. Sketch of large 7075-T6 stiffened test panel. (All dimensions mm).

3.2 Patch Design and Installation A single-sided GLARE™ 2 patch was designed according to the guidelines given in section 2.3. The patch was autoclave-bonded over the saw cut using AF-163-2M adhesive. The total thickness of the patch was 1.4 mm (0.055 inch), giving it an extensional stiffness roughly 80 percent of the skin being repaired. To test the worst case for peel stresses, the patch thickness was *not* tapered at its edges. The patch was 224 mm (8.8 inches) long. The patch overlapped both saw cut tips by 10 mm (0.4 inch), giving a total width of 100 mm (4 inches).

3.3 Test Results The repaired panel was cycled in constant amplitude fatigue (f = 3 Hz, σ_{max} = 86 MPa (12.5 ksi), R = 0.05) at room temperature. After 100,000 cycles (representing about 10 lifetimes at 110% of the limit load situation), no cracking could be found in the test section. Eddy current inspection beneath the patch indicated no extension of the original saw cut underneath the patch.

To test the damage tolerance of the panel, the five rivets in the fairing line on either side of patch were removed, and small saw cuts (1 to 3 mm long) were made with a jeweler's saw in the four rivet holes nearest the patch on both sides. This was done to simulate a condition where a large crack was repaired, but small (presumably undetected) adjacent multiple cracks went unrepaired. The rivets were not re-installed, to aid in crack growth monitoring. Fatigue cycling was resumed under the same conditions as before.

Figure 3 shows the crack growth performance after the multiple saw cuts were added to simulate undetected MSD. Three traces are presented:

- the crack propagation behavior of the "lead crack," which started out as the largest saw cut (nearest the patch) and grew outward from the center, enveloping the other smaller cracks,
- the summation of the length of all cracks,
- the predicted performance of an unrepaired central crack in an unstiffened 800 mm wide panel of 7075-T6 (based on da/dN data [8]).

Fatigue testing was terminated when the lead crack ran under the bonded tear straps, after more than 137,000 cycles. The length of the tip-to-tip crack (including the intact patch) exceeded 360 mm (14 inches).

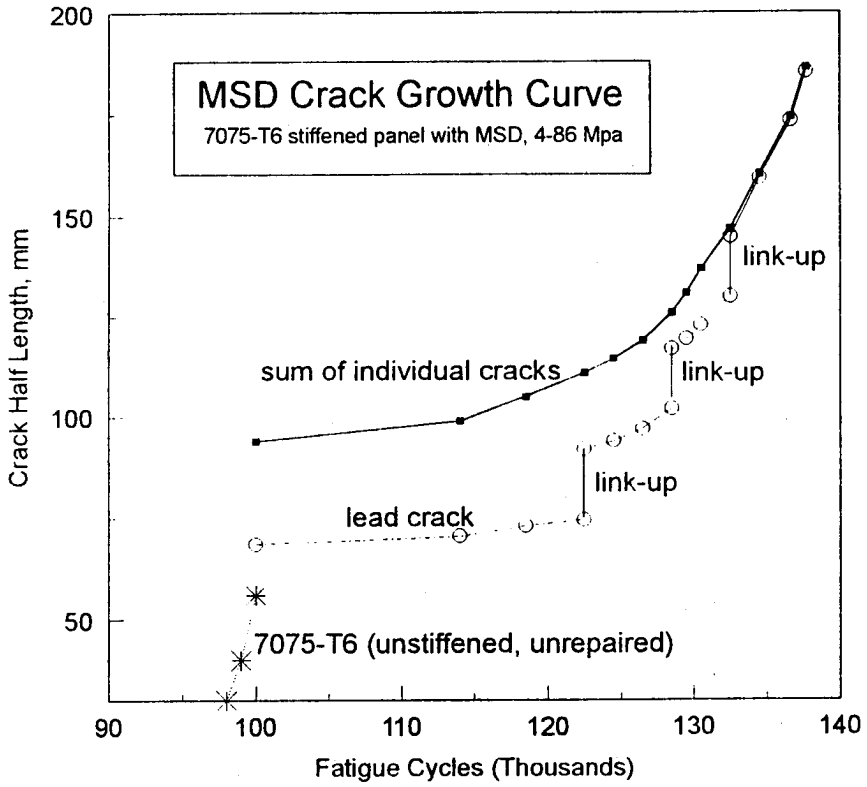


Figure 3. Crack growth performance of repaired panel with artificial MSD. (Saw cuts were added after 100,000 cycles of crack-free testing.)

3.4 Discussion Figure 3 clearly shows the strong influence of the intact patch on the behavior of adjacent multiple fatigue cracks. At crack lengths that would cause fast fracture in an unstiffened panel, the crack hardly grew in 20,000 cycles. This allows continued safe operation of a properly repaired structure, even in the presence of undetected small cracks. Inspection requirements need not be so stringent as to impose an undue workload on maintenance personnel, further increasing the cost-effectiveness of GLARE™ 2.

When crack link-up occurred (shown as vertical lines on the lead crack trace), the crack continued to grow in a slow, stable manner. The propagation rate of the repaired crack can be predicted adequately by the so-called "Erdogan solution," which considers the patch as an unfailed

ligament between two cracks, as discussed in [4]. This proven fracture mechanics approach gives maintainers a relatively simple means by which to set inspection intervals.

4. SCALED PRESSURE BARREL TESTING

4.1 Pressurized Barrel Description The pressurized barrel used for the crack patching described in this section is detailed in another paper in these proceedings [9]. The 2024-T3 aluminum barrel was an unstiffened circular cross-section of 1.2 meters (4.0 feet) diameter, with a skin thickness of 1.0 mm. The barrel was filled with wood blocks to reduce the internal air volume, then pressurized with shop air to produce a hoop stress of 97 MPa (14 ksi) at a frequency of about 0.06 Hz. Tests were performed at room temperature.

The barrel contained three riveted lap joints. The lap joints were riveted with various controlled squeeze forces to produce multiple site damage at significantly different numbers of cycles. When MSD was discovered on 16 of the 20 rivets in the third rivet row after 85,000 cycles, the decision was made to repair the lap joint so testing of the remaining two (uncracked) joints could be continued.

Because of the relatively high flexibility of the unstiffened lap joint, cracking occurred on the inner surface of the joint, as shown in figure 4. This presented two challenges:

- eddy current inspection was required, supplemented by

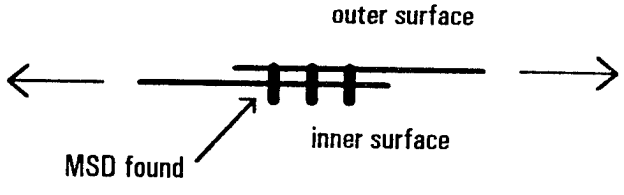


Figure 4. Crack locations on lap joint.

occasional visual inspections when the barrel was unpacked, and

- the external bonded repair would be less effective, because the patch was separated from the crack by a 1.0 mm thick aluminum sheet, causing the patch to behave more as an external doubler.

4.2 Patch Design and Installation A GLARE™ 2 patch was designed according to the previously stated guidelines, cut to final dimensions on a band saw, and cold-rolled to match the curvature of the barrel. Thickness tapering of the patch edges was done manually on a belt sander. The location of the crack meant the patch had to bridge a step-change in the outer mold line. This required the bonding of an additional shim, as shown in figure 5.

The aluminum skin was pre-treated for in-field bonding. The patch was bonded into place using AF-163-2M adhesive and an electric "heat blanket" under vacuum pressure.

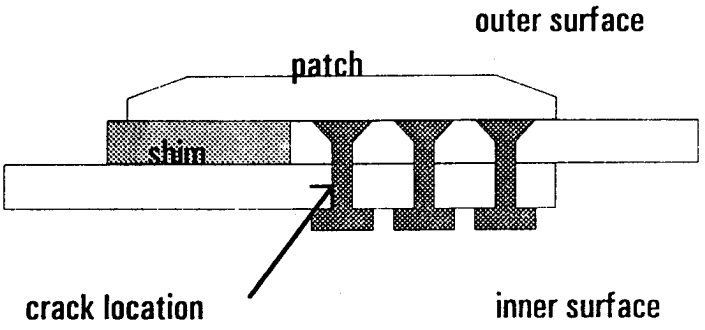


Figure 5. Bonded patch layout with shim shown.

During the bonding process at 100°C, localized heating of the barrel caused a noticeable amount of skin deflection inward (toward the center of the barrel). In a real fuselage situation, the presence of frames and longitudinal stiffeners would probably prevent this. However, due to differences in effective coefficients of thermal expansion, the lap joint experienced some residual compression at room temperature, while the GLARE™ 2 patch was in residual tension.

4.3 Test Results Pressure cycling was resumed after the repair was completed. Recall that at this point, with 85,000 cycles on the lap joint, 16 of 20 rivet holes in the critical row were cracked. The average crack length was 5.25 mm. Cycling was continued with periodic pauses for inspection of all three lap joints. No significant crack growth was noted in the repaired joint during the following 87,000 cycles, at which time MSD was found in a second lap joint. No additional repairs were made at that time, and the second joint ruptured after another 17,000 cycles, or a total of 189,000 cycles. The ruptured joint was replaced, and cycling continued until a total of 193,000 pressure cycles had been placed on the barrel.

Upon tear-down inspection, no new cracks were found in the repaired joint. In the 108,000 cycles following the bonded repair, the 16 original cracks in the repaired joint grew by an average of 0.4 mm (0.02 inches) each.

4.4 Discussion Although the repair was made under less than ideal conditions due to the inner surface location of the cracks, it was clearly quite effective. Almost no crack growth occurred in 108,000 cycles. A similarly cracked, yet unrepaired joint failed in approximately 1/6 the amount of cycling after MSD was discovered.

Because of the less than optimal location of the patch with respect to the crack, the superior fatigue performance of the multiply cracked repaired lap joint must be attributed to the residual thermal stress contribution from the hot bonding process.

5. SUMMARY AND CONCLUSIONS

The results of constant amplitude fatigue tests performed on bonded repairs to a large flat stiffened panel and a pressurized unstiffened fuselage "barrel" were presented. These specimens simulated pressurized transport fuselage structures with multiple site fatigue damage. Bonded GLARE™ 2 fiber metal laminate patches successfully halted the growth of multiple fuselage fatigue cracks beneath the patch. Furthermore, the presence of unrepaired fatigue damage adjacent to the bonded patch did not compromise the damage-tolerant nature of the repair. In other words, multiple unrepaired small cracks near the repair grew slowly in a manner that can be predicted with fracture mechanics.

In the tests described in this paper, GLARE™ 2 patches adhesively bonded to specific representative aluminum fuselage panel geometries successfully:

- reduced the stress intensity factor of existing cracks,
- prevented or greatly reduced further crack growth,
- demonstrated the damage tolerance of the concept by reducing the growth of nearby MSD, and
- suggested a possible relaxation of aging aircraft inspection schedules.

Previous analysis predicted a substantial beneficial influence in GLARE™ 2 versus boron patches due to the much better thermal expansion compatibility between GLARE™ 2 and aluminum. The pressurized barrel section repair confirmed this prediction. The results show GLARE™ 2 to be an effective, damage-tolerant fuselage repair material.

References

1. Baker, A.A. and R. Jones (editors), Bonded Repair of Aircraft Structures, Boston: Martinus Nijhoff Publishers, 1988.

2. Fredell, R. and J. Gunnink, "Fiber Metal Laminates for Improved Structural Integrity," *Proceedings of the International Workshop on Structural Integrity of Aging Aircraft*, Atlanta, Georgia, April, 1992, pp. 362-375.

3. Fredell, R., A. Vlot and G. Roebroeks, "Fiber Metal Laminates: New Frontiers in Damage Tolerance," *Proceedings of the 15th International European Conference of the Society for the Adavancement of Material and Process Engineering*, Toulouse, France, June 1994, pp. 319-328.

4. Fredell, R., "Damage Tolerant Repair Techniques for Pressurized Aircraft Fuselages," WL-TR-94-3134, Wright-Patterson Air Force Base Ohio, June, 1994.

5. Fredell, R., W. van Barneveld and A. Vlot, "Analysis of Composite Crack Patching of Fuselage Structures: High Patch Elastic Modulus Isn't the Whole Story," *Proceedings of the 39th International SAMPE Symposium and Exhibition*, Anaheim, California, April 1994, pp. 610-623.

6. Fredell, R., W. van Barneveld and L.B. Vogelesang, "Design and Testing of Bonded GLARE™ Patches in the Repair of Fuselage Fatigue Cracks in Large Transport Aircraft," *Proceedings of the 39th International SAMPE Symposium and Exhibition*, Anaheim, California, April 1994, pp. 624-638.

7. Davis, M., "The Development of an Engineering Standard for Composite Repairs," to be published in *Proceedings of the 1994 AGARD Specialists' Meeting on Composite Repair of Military Aircraft Structures*, Seville, Spain, October 1994.

8. Hertzberg, R.W., Deformation and Fracture Mechanics of Engineering Materials, 3rd edition, New York: John Wiley & Sons, 1989, p. 523.

9. Müller, R.P.G., J. Schijve, and M. Heerschap, "Fatigue Crack Growth and Residual Strength Characteristics of Riveted Fiber Metal Laminate Lap Joints," to be published in *Proceedings of the 1994 USAF Aircraft Structural Integrity Program Conference*, San Antonio, Texas, December 1994.

FATIGUE TECHNOLOGY INC.

100 Andover Park West • Seattle, WA 98188

Interference Fit Bushing Installation and Hole Repair/Resizing Using an Expanded Bushing

By Len Reid, Vice President of Engineering

Paper presented at:
1994 USAF Aircraft Structural Integrity Program Conference
San Antonio, TX, USA
December 6-8, 1994

Interference Fit Bushing Installation and Hole Repair/Resizing Using an Expanded Bushing

Len Reid
Vice President, Engineering
Fatigue Technology Inc., Seattle, WA USA

Paper presented at:
1994 USAF Aircraft Structural Integrity Program Conference
San Antonio, TX, USA
December 6-8, 1994

INTRODUCTION

Holes are typically the origin of in-service fatigue cracks and also the source of manufacturing defects in production and structural repairs. When fatigue or discrepant hole damage exceeds limits correctable by oversize fasteners, installation of close tolerance interference fit plugs or bushings is generally required. Thermal or freeze fitting techniques are normally used to shrink the bushing prior to installation. The whole process can be expensive and labor-intensive, and can result in a poor quality or structurally deficient repair. Further, there are safety implications associated with the cryogenic fluids used for these shrink-fit installations which preclude its use in many closed locations. In these circumstances, more complex recovery repairs are required.

Fatigue Technology Inc. (FTI) has adapted and combined two of its cold expansion processes; Split Sleeve Cold Expansion$_{TM}$ (SsCx$_{TM}$) and the ForceMate$_{®}$ (FmCx$_{TM}$) bushing installation process, and applied them to provide a convenient method of expanding typical repair or standard bushings into holes. This new patented process, known as BushLoc$_{®}$ (BlCx$_{TM}$) generates a high interference fit bushing installation resulting in an enhanced fatigue resistant repair.

Besides being used to repair holes damaged in production or to resize holes which were oversized to remove fatigue cracks, the BushLoc method can also be used to install typical interference fit bushings. This paper will present the BushLoc process, the system parameters, current applications, and some results from qualification testing.

THE BUSHLOC SYSTEM

The FTI BushLoc system provides solutions to problems associated with shrink-fit bushing installation methods. Thermal or shrink-fit interference fit bushings must be manufactured with tight tolerances, immersed in cryogenic fluids to reduce the outside diameter, and pressed or driven into the hole. This process generally results in only 0.0005 to 0.0025 inches of bushing to hole interference. As an alternative, BushLoc provides a reliable, quick and consistent installation. Bushings are initially clearance fit and are expanded into the hole at equivalent interferences ranging from 0.002 to 0.006 inches, depending on bushing size and material combinations. The basic BushLoc installation is shown in Figure 1.

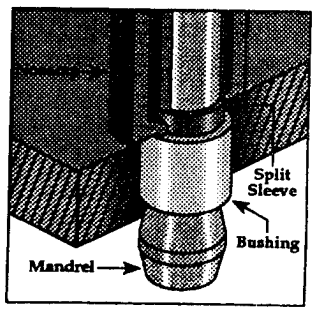


Figure 1: Schematic of BushLoc Bushing Installation

Allowing the bushing to be initially clearance fit in the hole protects the hole from damage and maintains the integrity of any protective coatings on the bushing. Avoiding cryogenics also precludes condensation and later corrosion problems.

In addition to installation consistency, high interference, and ease of installation, the BushLoc method of radially expanding the bushing also generally cold expands the parent material surrounding the bushing. Cold expansion has been shown, through testing and in-service experience, to provide significant fatigue and crack growth life improvement of holes by the formation of beneficial residual compressive stresses around the hole.

PROCESS OVERVIEW

The installation of a bushing using the BushLoc system is accomplished using specially designed FTI Split Sleeve Cold Expansion (SsCx) tooling, similar to that which is used to cold expand a conventional fastener hole although at a much higher expansion level. An internally pre-lubricated stainless steel split sleeve is placed over a tapered expansion mandrel, which is in turn attached to a hydraulically operated puller unit. The bushing, sized to specific BushLoc dimensions, is placed over the sleeve on the mandrel. The sleeve provides a convenient lubrication medium for the high interference mandrel, protects the bushing wall, and allows the bushing installation to be a one-sided operation. The sleeve also ensures that the bushing is expanded radially into the hole. The mandrel, sleeve and bushing combination is placed into the workpiece (see Figure 2) and the puller unit is activated. (Note: Access is only required on one side of the workpiece.) The nosecap on the puller unit holds the split sleeve in place within the bushing while the mandrel is retracted. As the major diameter of the mandrel passes through the split sleeve, the bushing and the parent material are subjected to radial expansion forces. These forces simultaneously install the bushing with high interference and create residual compressive stresses around the hole. The split sleeve, now distorted and with its lubricant coating used up, is removed and discarded after the installation.

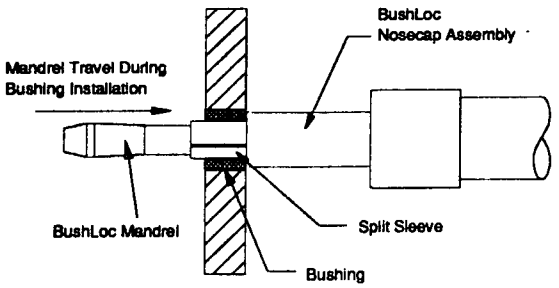


Figure 2: Components of BushLoc Installation Tooling

The bushing may be reamed after installation to the size required for the appropriate fastener or pin. In addition to final sizing the bushing inside diameter, a reaming operation removes the small discontinuity, called the sleeve ridge, from the bushing. While most applications will require this reaming operation to size the hole properly, it may not be necessary in all cases.

ADVANTAGES OF THE SPLIT SLEEVE

The BushLoc process differs from the FTI ForceMate process through the use of the lubricated split sleeve. The ForceMate process utilizes a pre-lubricated bushing whereas with BushLoc, the sleeve provides the lubrication medium and therefore facilitates a one-sided process. Having the dry film lubricant on a disposable sleeve makes for a cleaner installation which does not foul the bushing surfaces or other faying surfaces during expansion. The convenience of the lubricated sleeve permits local manufacture of the bushing to meet the required repair configuration or a typical bushing installation.

In addition to facilitating field repairs, the sleeve enables the higher applied expansion levels required by the process. It promotes an even distribution of expansion forces during installation and therefore uniform residual stresses in both the bushing and surrounding material. Since the sleeve ensures radial expansion without local shearing stresses normally associated with other sleeveless or mandrelizing processes, the BushLoc method accommodates expansion of different bushing materials or parent material combinations with the same tooling. Overall, the sleeve ensures a repeatable, consistent, clean bushing installation.

SYSTEM PARAMETERS

The standard BushLoc system is designed to install bushings with inside diameters ranging from 3/16 to 1 1/4 inches. Bushing wall thicknesses range from around 0.050 inches up to one third (1/3) of the final fastener diameter with a maximum limit of 3/16 (0.1875) inches for the larger sizes. Within this range a high interference fit, accompanied by a degree of cold expansion in the surrounding material, will be achieved. Thicker walled bushings can be installed with levels of interference greater than can be achieved with similar thickness bushings using shrink-fit methods.

BushLoc is compatible with most common aerospace bushing designs; straight, flanged, countersunk, etc., and is intended for installations in aluminum, steel, and titanium structure. Compatible bushing materials of aluminium, steel, aluminum nickel bronze, beryllium copper and stainless steel can be installed. All common coatings and platings may be used on the bushing for corrosion protection. Table 1 shows the material combinations tested.

Table 1: Bushing and Parent Material Combinations Tested with BushLoc

Parent Materials	Bushing Materials
Aluminum (2024-T3)	Aluminum (2124-T851) (1)
Aluminum (7075-T6)	Aluminum (7075-T6) (2)
Aluminum (7050-T651)	Aluminum (7150-T7651) (2)
Aluminum (7475-T7651)	Steel (4130)
Steel (4340)	Steel (4340)
Titanium (Ti-6Al-4V)	Aluminum Nickel Bronze
	Beryllium Copper
	Stainless Steel (17-4)
	Stainless Steel (15-5)
(1) 2124-T851 bushing material was found to be incompatible with BushLoc	
(2) Form and grain orientation must be controlled	

Due to the nature of the installation process, several guidelines concerning bushing length have been established to ensure an adequate installation. For example, single bushings up to two (2) inches long or segmented bushings up to this length can be installed. Longer bushings will require special tooling. The minimum material thickness (bushing length) must be between 0.100 inches (3/16 inch diameter) and 0.250 inches (7/16 inch diameter and greater), depending on the bushing size. Also, the length of the bushing must be at least 85% of the parent material thickness to be effective. Special configurations can also be designed; however, major deviations from basic system parameters and dimensional limits may degrade the performance of the BushLoc system.

Bushing dimensional tolerances are generally less restrictive than the requirements for shrink-fit or press-fit bushings. The starting hole is nominally 0.002 inches larger than the nominal bushing outside diameter for 3/16 to 5/16 inch inside diameters and .0025 inches for large diameters. The bushing has a +/- 0.001 inch tolerance for 3/16 to 5/16 inch inside diameters, and +/- 0.0015 inch for larger diameters. Similarly, the starting hole tolerance for 3/16 to 5/16 inch sizes is +/- 0.001 inches and +/- 0.0015 inches for all other sizes.

BushLoc parameters and specifications are comprehensively defined in an FTI BushLoc process handbook (EH-8) which can be used to design bushings for a range of applications and repair configurations.

BUSHLOC PERFORMANCE

The biggest problem associated with bushing installation is migration. If bushings are not installed with high enough interference, they will migrate or rotate. Under repeated load cycles, bushings which cannot resist migration will induce fretting and increase susceptibility to moisture ingress. Inevitable corrosion pits will exacerbate the situation resulting in fatigue cracks or inadequate bushing retention.

RESISTANCE TO PUSH-OUT

BushLoc achieves a much higher level of interference due to the radial applied expansion of the process. A comparison of the removal forces for BushLoc and shrink-fit installed steel bushings in aluminum alloys is shown in Figure 3. BushLoc has superior resistance to removal forces and therefore will be less susceptible to migration and rotation.

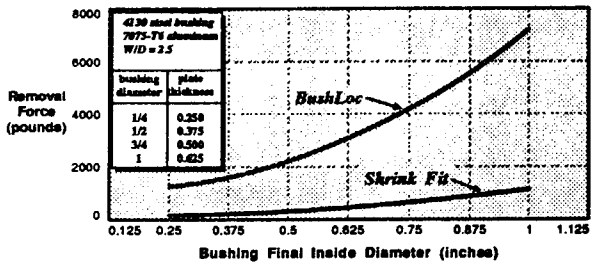


Figure 3: Comparison of Bushing Removal Force for BushLoc and Shrink-Fit Installed Bushings

Several variables, including bushing material and bushing wall thickness, affect the retention and fatigue life of a bushing installed using BushLoc. Bushings made from high strength (high modulus) material, such as stainless steel, will retain more expansion when installed into aluminum than bushings made from low strength material, such as aluminum nickel bronze. The greater retained expansion will produce higher installed interference. Higher interference means more expansion in the parent material and increased fatigue performance.

Bushing wall thickness has a similar effect on bushing performance characteristics. A thick walled bushing will resist collapse after expansion and can maintain a higher interference than a thinner walled bushing. In many cases, however, the expansion that the parent material experiences will be greater than with the thin walled bushing even though they both tend to collapse back again. The greater parent material expansion produces maximum fatigue life enhancement for installations with thinner walled bushings.

Figure 4 shows the variation in resulting interference with increasing bushing wall thickness. During installation of thin walled bushings, most of the expansion is transferred to the parent material. The differences in plastic deformation of the hole and bushing, in combination with the inherent "springback" characteristics after expansion, result in somewhat less interference with very think walled bushings. At large thicknesses, around 50 percent of the fastener diameter, very little expansion was transferred to the parent material which again produced minimum interferences. The optimum was around 25 percent of the fastener diameter. In most repair cases, this would be considered a very thick bushing wall.

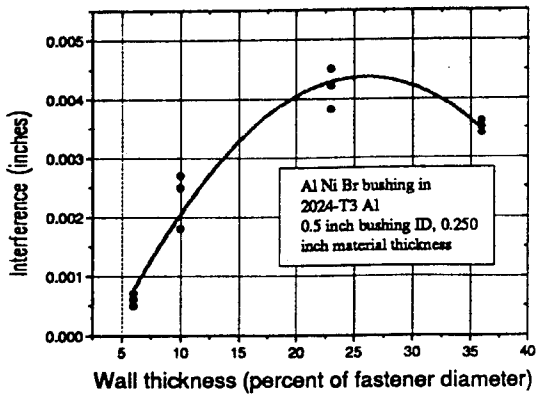


Figure 4: Change in Bushing Interference with Wall Thickness

IMPROVED FATIGUE RESISTANCE

Comparative fatigue life performance for similar bushings installed using BushLoc and shrink-fit methods is shown in Figure 5. Significant fatigue life improvement has been demonstrated through bushing installations using BushLoc. This is due to the synergistic high interference fit and residual compressive stresses resulting from the high applied expansion installation. In an actual repair configuration described later, a BushLoc-repaired joint proved to be better than the original fastener installation.

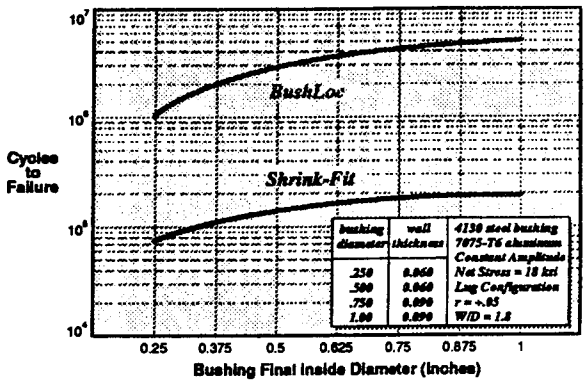


Figure 5 Comparison of Fatigue Life Performance for BushLoc and Shrink-Fit Methods

REPAIR CONFIGURATIONS

Several different BushLoc repair configurations have been evaluated. The following examples demonstrate the versatility of the process to either install multiple bushings or

repair multi-layered stack-up joints containing fatigue cracks or damage.

Figure 6 shows a multi-layered stack-up with individual segmented bushings. All three bushings were installed simultaneously. In this type of installation, the combinations of bushings and parent materials may be different. Final line reaming of the installed bushings would be required if different combinations were used because the final inside diameters would vary due to the different amounts of "springback" after bushing expansion.

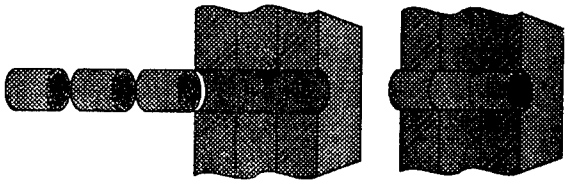


Figure 6: Schematic of Multiple Bushing Installation

In Figure 7, different outside diameter bushings were simultaneously installed allowing minimum material removal to correct hole discrepancies or to remove corrosion damage or fatigue cracks. This "Christmas tree" arrangement can be done without necessarily breaking down the structure to install the BushLoc bushings.

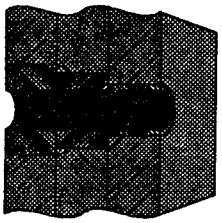


Figure 7: Multiple Variable Wall Thickness Installed Bushings

REPAIR OF COUNTERSUNK HOLES

BushLoc can also be used to repair previously oversized countersunk holes. In this case, a matching countersunk bushing is made to fit the residual countersink in the hole. Figure 8 shows a typical repair situation where two repair bushings are installed in a skin to a sub-structure fastener hole. Either a protruding head or nominal countersunk fastener can be installed. A washer of larger diameter than the outside diameter of the bushing is required under the retaining nut or collar of the installed fastener to secure the bushing and fastener to the structure.

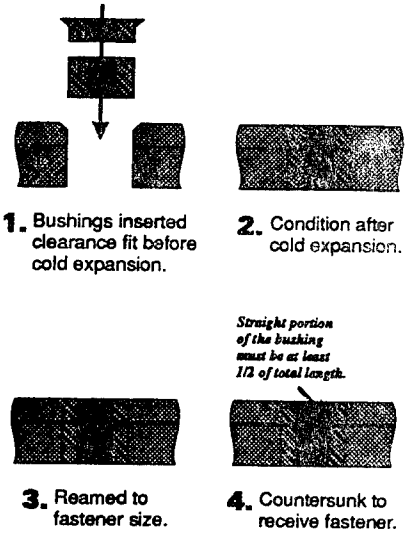


Figure 8: Repair Scenario for Repaired Countersunk Hole

TESTED BUSHLOC REPAIR

Extensive testing was performed to simulate the repair of a spar cap to wing skin fastener hole on a commercial aircraft. The repair was to remove a large crack from the spar cap without removing the skin or oversizing the original 3/8 inch fastener hole in the wing skin. Several bushing repairs were examined. In one case, a 1/8 inch wall thickness BushLoc bushing was installed. The load transfer test coupon configuration is shown in Figure 9.

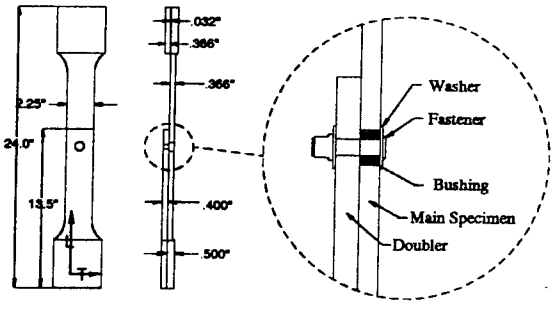


Figure 9: Load Transfer Test Specimen

A typical commercial aircraft wing spectrum load was applied to the specimen and results for various repair scenarios were compared

to baseline (fastener only) configured specimens. Test results in Figure 10 show that specimens repaired using either aluminum or steel BushLoc bushings performed better than the baseline configuration and were substantially better than shrink-fit repaired specimens. Results of this BushLoc test were accepted by the FAA as terminating repair actions for this location.

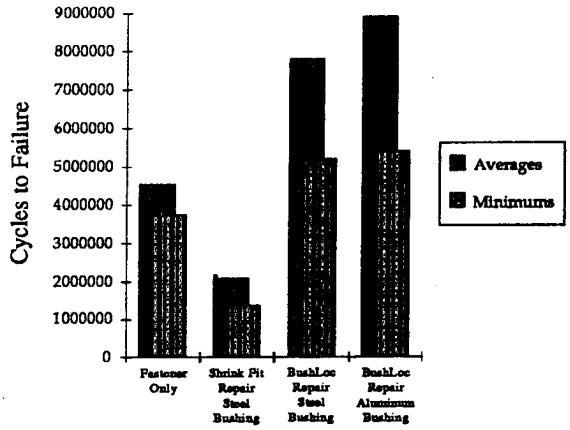


Figure 10: Comparison of Fatigue Life for BushLoc Repaired Specimens

OTHER EVALUATIONS

Douglas Aircraft Company conducted extensive evaluation of BushLoc for use in repairing discrepant production holes on C-17 aircraft. Typical repairs included oversizing holes to remove discrepancies and either press or shrink-fitting aluminium plugs or bushings into the holes. In many non-structural locations, very thick walled bushings or plugs were used to "fill" the hole.

The test program conclusively showed that BushLoc produced a superior repair to other methods used. Push-out or removal forces were superior to similar shrink-fit repairs, even when bushing wall thicknesses exceeded the BushLoc specification (e.g., 1/4 inch fastener holes with 0.200 inch thick bushings). The limits of all BushLoc specified configurations were tested and found to exceed projected values. BushLoc has been specified for use on C-17 aircraft production as an approved repair method.

BushLoc has been, or is currently being, evaluated and approved by most aircraft manufacturers. Some airlines and repair facilities are already using BushLoc to repair damaged holes because of the ease of installation and superior repair quality.

Examples of BushLoc applications are:

a. Repair of worn out-of-round holes in flight control actuator rods on ATR-42/72 aircraft.

b. Replacement of bushing that had migrated on USAF F-15 AMAD (aircraft mounted auxiliary drive).

c. Damaged production holes on C-17 aircraft.

CONVENIENCE OF BUSHLOC REPAIR

FTI has configured the BushLoc tooling in convenient tooling kits containing the complete system of tools sized to install nominal fastener diameter bushings. Installed bushings have adequate ream allowance for post-sizing. All tooling is designed to operate with standard FTI capital cold working tooling.

BushLoc tooling is sized to provide a much higher applied expansion than typical hole cold expansion. This increased expansion is necessary to accommodate the wide range of common bushing materials and to achieve the required interference fit. Testing has shown that nominal hole cold expansion tooling (FTI CB system), when used to install bushings, produced reduced retention and minimal, if any, fatigue life benefit compared to shrink-fit installations.

The BushLoc Engineering Handbook gives all the bushing design parameters to manufacture the bushings for a variety of repair scenarios. Tooling selection is simplified by the convenience of nominal kits based on the required inside diameter of the bushing. Tool sizes are in 1/16 inch increments from 3/16 to 3/4 inches nominal fastener sizes and in 1/8 inch increments from 7/8 to 1 1/4 inches. Larger diameter bushing tooling is also available for special applications.

BUSHING REMOVAL

FTI has configured a range of specially designed bushing removal tools to facilitate removal of bushings. These tools utilize a pull mandrel which attaches to FTI's puller units. A receptacle type nosecap is used to catch the removed bushing. This tooling makes bushing

removal fast and simple and minimizes the possibility of secondary structural damage during removal.

SUMMARY

BushLoc has made repair of damaged or discrepant holes a simple process which can result in a repaired configuration that exceeds the original design fatigue life of basic fastened structure. The convenience of the process simplifies repairs and gives repeatable results which are quantifiable. Because the repair bushing is installed initially clearance fit then radially expanded using a sleeve and mandrel, the hole is protected from damage and has a uniform residual stress zone surrounding it.

The process is faster and safer to use than typical shrink fit methods because no cryogenic fluids are required. Repair time is decreased and the nature of the process facilitates its use in very confined and restricted access locations. A convenient handbook provides step-by-step instructions on how to design and install BushLoc bushings.

BushLoc has been tested, qualified and approved for use on both commercial and military aircraft for production or field repair. The systematic design of the tooling produces a high interference fit bushing installation resulting in an enhanced fatigue resistant repair in a range of bushing and structural materials.

ULTRASONIC TECHNIQUES FOR REPAIR OF AIRCRAFT STRUCTURES WITH BONDED COMPOSITE PATCHES

S.H. Smith
N. Senapati
R.B. Francini

Battelle
505 King Avenue
Columbus, Ohio

SUMMARY

This is a paper on a research and development project to demonstrate a novel ultrasonic process for the field application of boron/epoxy (B/E_p) patches for repair of aircraft structures. The first phase of the project was on process optimization and testing to develop the most practical ultrasonic processing techniques. Accelerated testing and aging behavior of precured B/E_p patches, which were ultrasonically bonded to simulated B-52 wing panel assemblies, were performed by conducting flight-by-flight spectrum loading fatigue tests. The spectrum represented 2340 missions/flights or 30 years of service. The effects of steady-state applied temperature and prior exposure of the B/E_p composite patches were evaluated. Representative experimental results of this phase of the project are presented.

INTRODUCTION

One of the major technical thrust areas in the U.S. Air Force aging aircraft program is the development of structural repair techniques. Primary emphasis is on the development of efficient, durable, inexpensive, and easily implemented repair technology. Previous repair technology has involved the use of metallic structural repair patches and techniques using mechanical and/or bonding techniques [1]. There is an adequate structural material database and design guidelines for designing and installing these aircraft structure repairs. In the past several years, B/E_p composite patches have been used to repair several U.S. Air Force aircraft [2-9]. The thermal blanket curing process was used to install B/E_p composite precured patches. This process takes several hours to cure the adhesive at the required curing temperature not to exceed 250°F.

With U.S. Air Force support, the authors have developed an ultrasonic curing process for the field application of B/E_p composite patches to B-52 aircraft upper wing structures [10]. A summary of the results of this development project is presented in this paper. The project consisted of an initial phase for determining the desirable ultrasonic curing conditions and parameters. Double lap

shear specimens with B/E_p composite strips bonded to 7075-T6 and T651 adherents were tested to determine shear strength and preferred curing conditions. The verification testing of the composite patch design and the ultrasonic curing process consisted of conducting accelerated fatigue and prior exposure tests on repaired structural panel assemblies that simulated the B-52 wing at wing station 402, S-21. Special instrumentation was used to monitor the strain levels in the composite patches and aluminum substrates and to measure the fatigue crack growth behavior during spectrum load testing.

EXPERIMENTAL METHODS AND RESULTS

The experimental techniques and procedures used in this project are described in two parts. The first part is on approaches used in identifying the desired parameters for the ultrasonic bonding process for precured composite patches. The second part involves the experimental techniques and procedures used in the panel assembly testing.

Fabrication of Boron/Epoxy Patches and Test Specimens

The B/E_p patches were precured in an autoclave using a vacuum bag process. All plies in the patches were unidirectional and cured in accordance with the material supplier procedures at a pressure of 50 psi and a temperature of 350°F for 90 minutes. The adhesive selected for bonding the B/E_p patches to the 7075-T6 and T651 aluminum substrates was FM-73 grade 10 and had a polyester mat. The adhesive was stored at 0°F. During room temperature assembly of the specimens any adhesive left over seven days was discarded. The ultrasonic bonding of the B/E_p patches is very sensitive to the surface preparations of the aluminum substrates. Therefore, the surfaces were phosphoric acid anodize and BR127 primed according to procedures defined by the Air Force for field application to B-52 wing structures.

Identification of Process Parameters

The ultrasonic process has several advantages over the thermal blanket technique of curing adhesively bonded composite patches. The advantages are: (1) a better wetting of the substrate surface with the adhesive due to shear thinning with the high intensity ultrasonics, (2) accelerated chemical reactions, (3) less time needed to reach the required curing temperature, (4) a more consistent bond strength, and (5) lower and more uniform residual stresses after cool-down.

The laboratory scale ultrasonic bonding fixture is shown schematically in Figure 1. A series of parametric screening tests were conducted to gain insight into the primary variables and their sensitivity in ultrasonic curing of the B/E_p patches with FM-73 adhesive. It was these variables that were investigated during the parametric screening tests described below. The variables and their ranges investigated were:

Coupling Material—Its purpose was to transfer the ultrasonic energy into the patch. Without a coupling material, very little ultrasonic energy can be transferred to the adhesive via the patch. More than ten types of coupling materials were investigated under this program. The top two were a polymer compound (polyisobutadiene) and a red rubber (styrene butadiene) that was 0.060-inch thick.

Ultrasonic Power—A watt meter was used to measure the power delivered to the ultrasonic converter. The range of powers investigated was 50 to 105 watts. Power levels as high as 400 watts were investigated with the larger size validation test panels.

Duration of the Ultrasonic Energy—During the parametric screening tests the length of time the ultrasonic energy applied to the patch varied from 5 to 120 minutes.

Coupling Pressure—This is the pressure or force that was applied to the patch and test coupon during the application of ultrasonic energy. The force was applied using the hydraulic jack shown in Figure 1. The pressures investigated ranged from 5 to 15 psi.

Several screening tests were conducted to evaluate the thermal cure cycle produced by the ultrasonic bonding technique. Figure 2 shows a plot of temperature versus time for three variable combinations of power, time, and pressure. These are results for five plies of B/E_p bonded to aluminum strips. An embedded thermocouple in the FM-73 adhesive was used to measure temperature with time. As can be seen by the data, a stable temperature is reached after about 15 minutes. Several additional tests were performed with five plies and different combinations of power, time, and pressure. Some screening tests were also conducted with 15 and 40 ply samples. These data were used to select the desired conditions for ultrasonic bonding.

The results of the screening tests were used to develop a master baseline indexed sample for evaluating the degree of cure produced by the ultrasonic process. Figure 3 shows the baseline sample that was developed for undercured, cured, and overcured samples. All subsequent testing and failure mode identification of samples were correlated to this master baseline sample.

The second part of the project involved conducting mechanical tests to quantify the process. In adhesive bonding characterization testing either wedge or lap shear tests are performed to evaluate the integrity of the bondline and process. Double lap shear tests were conducted on ultrasonically cured samples that were bonded according to the desired conditions established in the screening phase. The testing procedures defined in reference 11 were followed. Table 1 shows some of the results for the lap shear strengths developed using the process.

Flight-by-Flight Spectrum Loading Fatigue Tests

Several iterations were performed on the geometry and configuration for the fatigue test specimens. The requirements for the configuration were: (1) that the panel thickness had to be 0.25-inch thick, (2) B/E_p patches were to be bonded to both sides of a single edge crack of 0.30-inch length, (3) grip ends of the specimen had to be designed such that failure would occur in the

cracked section of the panel and not in the grips, and (4) panel configuration and geometry had to be such that monitoring crack growth and load transfer during fatigue could be accommodated.

Initially a single 0.250-inch-thick 7075-T651 aluminum rectangular panel configuration with the B/E_p patches bonded to each surface of the panel with the edge crack was selected. However this configuration was not accepted because of the difficulty and unassured reliability of being able to bond two patches ultrasonically on both sides of the panel at the same time. The second idea of a configuration was to split the thickness of the panel into two 0.125-inch-thick 7075-T6 sheets and ultrasonically bond the two patches on the panels separately and then adhesively bond the two together to form the equivalent 0.250-inch thickness. This configuration had the drawback that Krak gages could not be used on the back side of the crack surface to measure and monitor fatigue crack growth rates. The final idea was to use a honeycomb core or other separator between the two skins/sheets and cut out the core around the crack area for the Krak gages. The honeycomb core or other separator would be adhesively bonded to the aluminum face sheets/skins. This configuration had the added built-in bucking stability required for spectrum loading fatigue testing with compression loading in the spectrum. This concept was retained and the honeycomb core was replaced with Teflon sheets and not bonded to the aluminum face skins/sheets. Solid aluminum inserts were selected as spacers for the grip areas. Figure 4 shows the final specimen configuration selected for the simulated repair. The B/E_p repair patches were eight layers thick with 0.30 and 0.10 inch/ply ramp ups for the vertical and horizontal directions, respectively.

In the grip area, the two repaired sheets were separated by a 7075-T 0.190-inch-thick spacer sheet. The overall geometry of the panel was 8 x 32.5 inches and 6 x 20 inches in the test section. Three 1-inch-radii fillets were machined at the end of the test section. The panel grip ends were designed to accommodate the 50 kip machine grips and bolts with four 17/32-inch- and one 1.00-inch-diameter holes at each end. The panel grip ends and the grips were grit blasted for friction gripping in the grip area. All bolts were torqued to 110 in-lbs.

Instrumentation and Equipment

The flight-by-flight spectrum loading tests conducted on the panel assemblies consisted of four series of tests. These were room temperature, -65°F (-53.9°C), 180°F (82.2°C), and room temperature with prior exposure at 95 percent relative humidity and 180°F (82.2°C) for 60 days. Three fatigue tests were conducted per testing series. The following describes the instrumentation and equipment used for the series of tests.

Figure 5 shows a photograph of the 50 Kip INSTRON electohydraulic system setup with gripping fixtures and load-control console equipment that was used in the fatigue and residual strength testing of the panels. In addition, this system consisted of the primary data taking equipment, which included a 486 PC computer, Labtech software, and signal conditioning equipment. This system was used to measure and monitor the output of the strain gages, Krak gages, and thermocouples. The output of the Krak gages was read by a FRACTOMAT instrument, consisting of two channels for readout. A strip chart recorder was used to continuously measure the spectrum loading applied to the panel assemblies in each test series.

The spectrum loading fatigue testing of the panels for test series 2 and 3 at -65 F(-53.9 C) and 180°F (82.2°C), respectively, required an environmental chamber around the test panel and the repaired area of the final assembled panel. Figure 5 also shows the environmental chamber and the antibuckling guides used in the fatigue testing. A Lexanl (polycarbonate) chamber was constructed and used for -65°F (-53.9°C) and 180°F (82.2°C) steady-state testing temperature environments. This chamber was designed to serve as an external out-of-plane buckling guide and used in all tests. The chamber was nominally 9 x 9 x 2 inches in volume and contained four longitudinal stiffeners, which were bonded to the Lexanl chamber walls. The stiffeners acted as buckling guides, and Teflon pads were bonded to the bottom surface to ride against the aluminum. The stiffeners were grooved to allow for environmental media circulation. The chamber was sealed with insulation material. The experimental setup for the -65°F (-53.9°C) steady-state temperature testing used liquid nitrogen as the cooling media. The temperature in the environmental chamber was controlled within $\pm$ 5°F and monitored with two probe-type thermocouples. The type of probe thermocouple that was selected was the OMEGA Type K with an exposed junction and 304SS material [12]. The temperatures were applied at a rate of 20°F per minute until the steady-state temperature was reached. The experimental setup for the 180°F (82.2°C) steady-state temperature used hot air and was circulated using a hot air blower. The temperature control and applied rates were the same as for the -65°F (-53.9°C) testing.

The series 1, 2, and 3 were preconditioned according to ASTM D 618 Procedure which was 50 percent R.H. and 73.4°F (23.0°C) for 40 hours [13]. This was performed in an ambient laboratory room. A final series of panels, series 4, were environmentally preconditioned. The composite patches which were bonded to aluminum sheets were preconditioned at 95 percent R.H. and 180°F for 60 days in an environmental preconditioning chamber. The environment was circulating hot and humid air and was monitored and controlled using thermocouples for the dry and wet bulb temperatures. The temperatures were read with a digital readout instrument.

Each of the fatigue panels in the test series was instrumented with Krak gages, strain-gage rosettes, and thermocouples as shown in Figure 4. The criteria in the selection of all of the types of instrumentation were based on the post testing environments of the spectrum loading fatigue combined with the applied steady-state environments of -65°F (-53.9°C) and 180°F (82.2°C).

Type KG-B30 with 30 mm or 1.18-inch effective crack length measurement range was selected for use with an initial edge notch of 0.30 inch or 7.62 mm. [14]. This Krak gage is a foil made of constantan alloy (5 micron or 0.0002-inch thickness) with an epoxy-phenolic glass-fiber-reinforced backing (50 microns or 0.002-inch thickness). The gages were mounted with the crack gage backing exactly flush with the longitudinal edge of the aluminum sheet. The apex of the V-groove of the gage was coincident with the tip of the machined notch. The gages were adhesively bonded to the aluminum surface using TTI 353-ND single-part epoxy adhesive. The procedures of reference 18 were followed. Figure 4 shows the edge view of the mounted Krak gages. The installation of the gages was performed in the laboratory under ambient conditions.

Strain-gage rosettes were used to measure the strain levels in the B/E_p patches and the aluminum sheets. The strain gage data taken from these rosettes was used in monitoring the load transfer behavior from the cracked skin of the aluminum to the B/E_p repair patch. This data was used as a measure of the effectiveness of the patch in retarding or stopping fatigue crack growth.

Figure 4 shows the locations of the strain gage rosettes on the B/E_p patches and the aluminum sheets.

The type of strain-gage rosette selected for the B/E_p composite patches was based on (a) thermally activated coefficient of thermal-expansion compatibility of the gage with the substrate, (b) the post-temperature steady-state temperature environments of -65°F (-53.9°C) to 180°F (82.2°C), and (c) the spectrum loading cyclic fatigue life requirement. Micromeasurements WK-06-062RB-350 (unstacked/uniplanar) 45-degree delta strain-gage rosette and bonded with M Bond 610 adhesive satisfied these criteria. All strain gages were self-temperature-compensating gages and were mounted according to the recommended guidelines of strain-gage applications to composites [15 and 16].

Each of the aluminum skins of the repaired panels was precracked under constant amplitude tension-tension loading with P_{max} = 22.5 kips (S_{max} = 15.0 ksi), P_{min} = 0.0 kips (S_{min} = 0.0 ksi), and R = 0.0. The cyclic frequency of the loading was 5 Hz. The constant amplitude fatigue loading was applied until the cracks were detected by each of the Krak gages of the panel. The results showed that all of the skin panels were precracked in 1260 to 1272 cycles.

The spectrum loading block was made up of Missions A, B, C, D, E, and F for blocks 1 and 2 and the repeat mix as shown in Table 2 test spectrum. Additional missions as defined for the 10th application of a given mission were incorporated into the building blocks of the total spectrum. The total application of the spectrum simulated 2340 missions of taxi, take-off, gust, maneuver, and ground-air-ground cycles. The loading frequency was 5 Hz. The total cyclic content of the spectrum consisted of 65,932 cycles.

Data Reduction and Analysis

The data taken included Krak gage output, strain gage rosette output, temperature and humidity, fatigue-crack-growth behavior, and residual strength. Various computer algorithms were used for data analysis. The outputs of the Krak gages, strain-gage rosettes, and thermocouples were analog, and continuous recordings were taken with the computer and data-storage software. Data plots of the Krak gages and thermocouples were generated every 10 seconds and correlated with applied cycles. The output of the load cells for applied loadings were continuously recorded on a strip chart recorder to show the cyclic loading as applied to each specimen. The fatigue-crack-growth behavior is presented as crack length, a, versus cycles. The strain-gage data was taken as continuous recordings of each of the legs of the strain gage rosettes. All data were stored for analysis. The axial/longitudinal strains of each rosette was used to monitor the behavior of the panel assembly during spectrum loading fatigue crack growth testing. The strain gage data plots were generated by sampling the output every 2 seconds at 50 Hz every 10 minutes. Further reduction of the strain gage data involved determining the transverse sensitivity of the strains in the composite patches and calculation of the maximum and minimum principal strains and stresses and the maximum shear strains and stresses.

Fatigue Results and Discussion

Room Temperature Results—Series 1: The spectrum loading fatigue crack growth results of one of the panel assemblies tested at room temperature and laboratory humidity is shown in Figure 6. The fatigue cracks in all of these skins (panels) of the panel assemblies were contained under the repair patches. That is, the total fatigue loading spectrum was applied without these panels failing during fatigue cycling (see Table 3). In addition, these results showed that the fatigue crack growth rate of the cracks in these panels were slow and almost constant. This indicated that the ultrasonically bonded composite patches were effective in slowing down the fatigue crack growth rate. Load transfer from the cracked skin into the composite patches was also effective as shown in the axial or longitudinal strain gage data and the reduced maximum principal stresses and maximum shear stresses. The axial strains, reduced maximum principal stresses, and maximum shear stresses in the patches show that some patches on one side of the panel assemblies were loaded higher than others (see Figures 7 and 8). In addition, the results showed that as the fatigue cracks propagated the strain and stress levels in the patches increased. This was the expected behavior since at longer crack lengths more load is transferred from the cracked skins into the patches.

180°F Steady-State Temperature Results—Series 2: The fatigue crack growth results for one of the panel assemblies tested at a steady-state temperature of 180°F (82.2°C) and laboratory humidity is shown in Figure 9. All of these panel assemblies failed during the spectrum loading fatigue cycling. Table 3 shows the summary of the fatigue results and the longest fatigue life was series panel 3-2B which survived the entire application of the spectrum, but the cracks in the skin sheets were 1.15 and 5.40 inches, respectively. The fatigue crack growth rates of the cracks in the skins of these panels showed that the rates were steadily increasing with applied cycles. At this high applied steady-state temperature of 180°F, ultrasonically bonded repair patches were effective in picking up load transferred from the cracked skins. The axial strains, the reduced maximum principal stresses, and maximum shear stresses in the patches show that some of the patches on one side of the panel assemblies were loaded higher than others.

-65°F Steady-State Temperature Results—Series 3: The spectrum loading fatigue crack growth results of one of the panel assemblies tested at -65°F and laboratory humidity is shown in Figure 10. The fatigue cracks in the skins of these panel assemblies showed a steadily increasing fatigue crack growth rate with the exception of skin sheet no. 31 which did not show much growth. The spectrum loading cyclic fatigue lives of these panel assemblies are also summarized in Table 3 and show much lower fatigue lives than the panel assemblies tested at room temperature or 180°F. The general trend of the effects of lower temperatures on structural adhesives is that the adhesive becomes more brittle at the reduced temperature of -65 F. Likewise at elevated temperatures the adhesive becomes more ductile. In both temperature cases, the ability of the composite patches to pick up load transferred from the cracked skins will be different due to the temperature effects on shear strength of the adhesive.

Prior Exposure and Room Temperature Results—Series 4: The spectrum loading fatigue crack growth results of one of the panel assemblies that were exposed for 60 days at 180°F and 95 percent RH and then room temperature tested is shown in Figure 11. The fatigue cracks in all of these skins (panels) showed a steadily increasing rate of crack growth. The fatigue cracks in skins

4, 9, and 10 were contained more than the others. The results of these panel tests summarized in Table 3 show that the spectrum loading fatigue lives were about the same as the -65°F fatigue lives, but not nearly as long as the 180°F fatigue lives. The 60-day exposure of the panels to the high temperature and humidity produced some degradation of the ultrasonically bonded patches. The mechanism is believed to be moisture diffusion into the bond lines between the patches and the aluminum skins. Degradation of the patches also occurred, since the color on some of the patches changed from black to light brown during exposure.

CONCLUSIONS

Based on the results of this experimental investigation, the following conclusions are made:

(1) It has been successfully demonstrated that ultrasonic energy can be used to cure FM-73 structural adhesive to bond a B/E_p patch to 7075-T and T651 aluminum. The bonding time is about an hour to achieve optimum cure of the adhesive.

(2) The ultrasonic intensity (i.e., energy per unit time per unit area) required to fully cure FM-73 in one hour is only 25 watts/square inch, and the bond strength is comparable to and often better than thermally cured specimens.

(3) At room temperature, none of the test panels with pre-cracks failed when subjected to ground-air-ground flight spectrum loading simulating 2340 missions. At extreme conditions of temperature (-65°F and 180°F) and humidity (95 percent RH), the adhesive appears to be adversely effected and some of the test panels failed before completing 2340 missions.

(4) Other structural adhesive systems under slightly different ultrasonic cure conditions may have the potential to be an effective adhesive for extreme conditions.

ACKNOWLEDGEMENTS

The authors would like to acknowledge Mr. Leonard Wright and his staff at The Boeing Company, Defense and Space Group, Wichita, Kansas, and Mr. Al Clark of Oklahoma Air Logistics Center, Tinker Air Force Base, Oklahoma, for supporting this project.

REFERENCES

1. Rice, R., Smith, S., Rahman, S., Broek, D., et al, "Effects of Repair on Structural Integrity", Final Report to FAA Tech Center, DOT/FAA/AM-DOT-VNTSC-FAA-93-11, July 1993.

2. Baker, A.A., and Jones, R., (Editors), Bonded Repair of Aircraft Structures, Martinus Nijhoff Publishers, 1988.

3. Jones, R., Molent, L., Baker, A.A., and Davis, M.J., Bonded Repair of Metallic Components: Thick Sections", Aeronautical Research Laboratories (ARL), Melbourne, Australia, Elsevier Science Publishers, 1988.

4. Sandow, F.A., and Cannon, R.K., "Composite Repair of Cracked Aluminum Alloy Aircraft Structure", Report Number AFWAL-TR-87-3072, AFWAL/FIB, 1987.

5. Kelly, L.G., "Composite Repair of Cracked Aluminum Structure", U. S. Air Force/Wright Aeronautical Laboratories, AGARD Conference, 1986.

6. Lincoln, J.D., 1987 ASIP/ENSIP Proceedings, AFWAL-TR88-4128, Cochran, J.B., (Lockheed/Georgia), Christian, T., and Hammond, D.O., "C-141 Repair of Metal Structures by use of Composites", 1988.

7. U. S. Air Force Logistics Command, "Composite Patches for Metallic Structures", TT-89034, August 1989.

8. Baker, A.A., "Fibre Composite Repair of Cracked Metallic Aircraft Components -- Practical and Basic Aspects", Aeronautical Research Laboratories; Butterworth & Company, Composites, Volume 18, No. 4, 1987.

9. Caruso, R.P., "Boron/Epoxy Composites for Aircraft Structural Repair", Textron Specialty Materials Report, 1991.

10. Senapati, N., Smith, S.H., and Moulder, R., "Ultrasonic Technique for Repair of Aircraft Structures with Bonded Composite Patches - Phase I - Proof of Concept", Final Report to Boeing Defense and Space Group, October 1993.

11. ASTM Standard D3164, Determining Strength of Adhesively Bonded Plastic Lap-Shear Sandwich Joints in Shear by Tension Loading, 1993.

12. "OMEGA Complete Temperature Measurement Handbook and Encyclopedia," Volume 26, 1988.

13. ASTM D-618, "Method for Conditioning Plastics and Electrical Insulating Materials for Testing," ASTM Vol.8.01, 1993.

14. Instruction Manual, "Fractomat and Krak-Gage," Technical Bulletin KG-581 R, TTI Division, Hartrun Corporation, Chaska, Minnesota, 1982.

16. General Structural Testing of Composites, Applications Note, "Strain Gage Applications on Composites," Measurements Group, Inc., January 1988.

17. "Manual on Experimental Methods for Mechanical Testing of Composites," Edited by R. L. Pendelton and M. E. Tuttle, Society for Experimental Mechanics Inc., 1989.

Table 1. The Lap Shear Strength of Ultrasonically Cured Specimens with 0.25-Inch-Thick 7075-T651 Aluminum Substrate

Cure Condition			Shear Strength
Power, watts	Time, minutes	B/E, plies	psi
75	60	5	257
85	60	5	1,304
95	60	5	1,275
85	60	15	808
95	60	15	1,168
105	60	15	1,439

Table 2. Flight-by-Flight and Mission Mix Spectrum

MISSION A

f_{MAX} (KSI)	f_{MIN} (KSI)	CYCLES
22.55	19.05	23
12.078	-17.83	1
12.078	9.58	4

1/10 FLTS f_{MAX} = 22.99

MISSION B

f_{MAX} (KSI)	f_{MIN} (KSI)	CYCLES
22.55	19.05	23
17.88	-17.86	1
17.88	13.38	9

1/10 FLTS f_{MAX} = 22.99

MISSION C

f_{MAX} (KSI)	f_{MIN} (KSI)	CYCLES
18.90	16.47	9
9.15	-15.25	1
9.15	6.65	1

1/10 FLTS f_{MAX} = 19.29

MISSION D

f_{MAX} (KSI)	f_{MIN} (KSI)	CYCLES
18.97	16.47	10
9.15	-11.47	1
9.15	6.65	1

1/10 FLTS f_{MAX} = 19.29

MISSION E

f_{MAX} (KSI)	f_{MIN} (KSI)	CYCLES
22.55	19.05	23
10.14	-18.59	1
10.14	7.64	1

1/10 FLTS f_{MAX} = 22.99

MISSION F*

f_{MAX} (KSI)	f_{MIN} (KSI)	CYCLES
23.80	14.30	50

TEST MISSION MIX

BLOCK 1 = ABCABDEFABCAB
BLOCK 2 = BEFBECBEFBECA

REPEAT MIX = 5(BLOCK 1) + (BLOCK 2)

NOTE: SPECTRA FOR B-52G/H WING UPPER SURFACE AT W.S. 402, S-21
MISSION MIX FOR B-52G/H BASELINE II
AIR CREW CONTINUATION TRAINING USAGE

Table 3. Summary of Fatigue Life Results for All Panel Assemblies Tested

Panel Assembly Test Series	Testing Environment	Total Applied Fatigue Cycles of Spectrum	Comments
3-1A	Room temperature	65,932	Did not fail
3-1B	Room temperature	63,373	Did not fail
3-1C	Room temperature	65,932	Did not fail
3-2A	180°F	40,937	Failure
3-2B	180°F	65,931	Failure
3-2C	180°F	47,778	Failure
3-3A	-65°F	17,463	Failure
3-3B	-65°F	20,747	Failure
3-3C	-65°F	24,024	Failure
3-4A	Room temperature	19,231	Failure
3-4B	following exposure at	25,563	Failure
3-4C	180°F and 96% RH	20,313	Failure

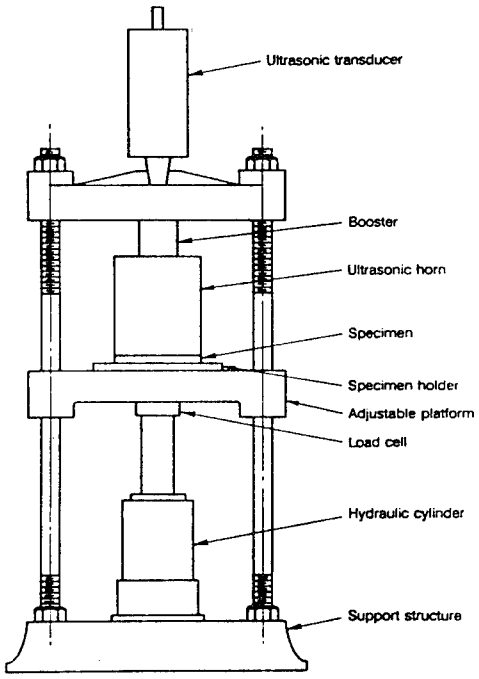


Figure 1. Schematic experimental setup for ultrasonic activation of adhesives.

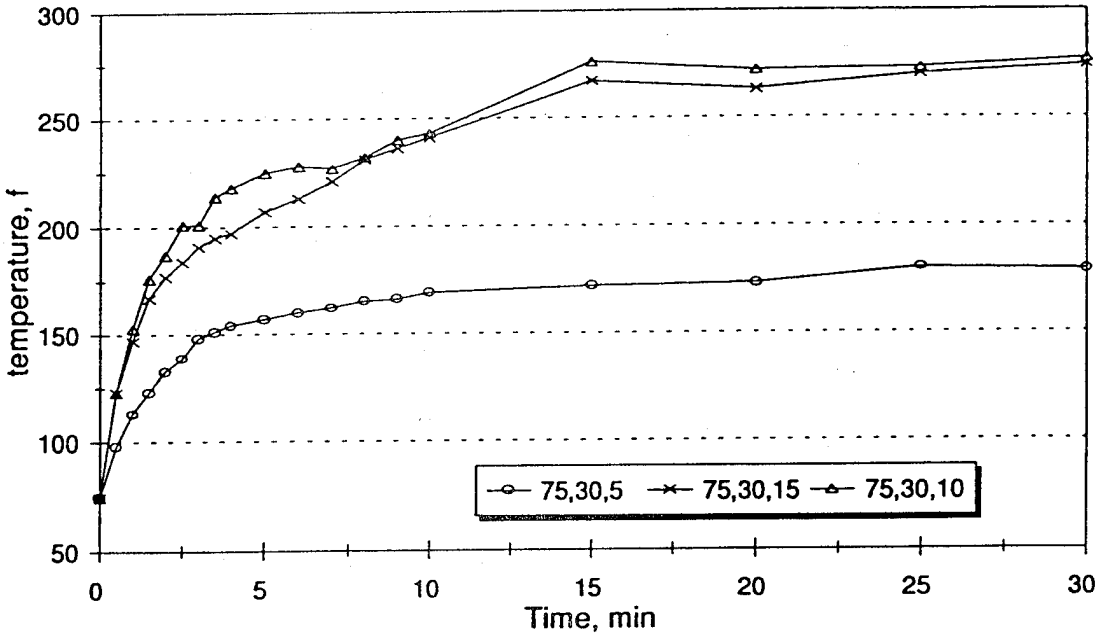


Figure 2. Plot of temperature versus time for three variable combinations.

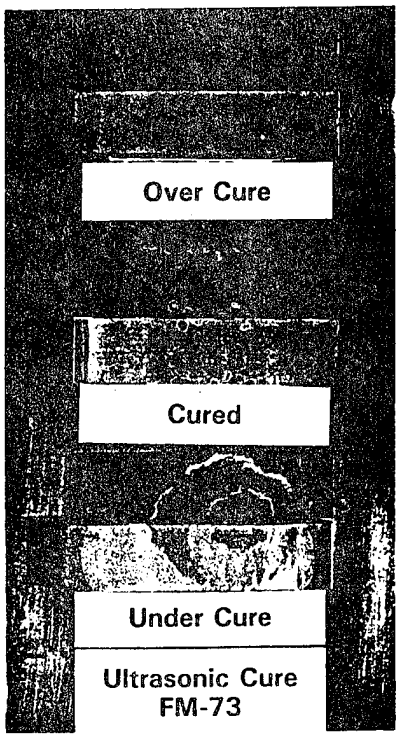


Figure 3. Baseline specimens for degree of cure evaluation.

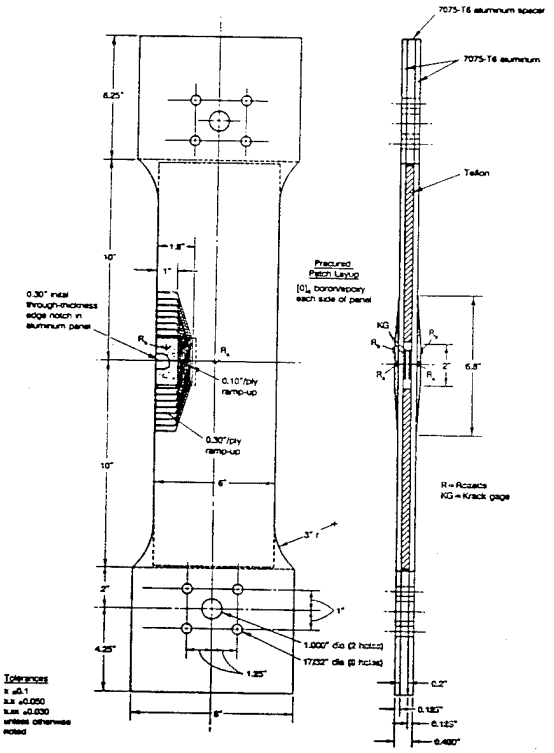
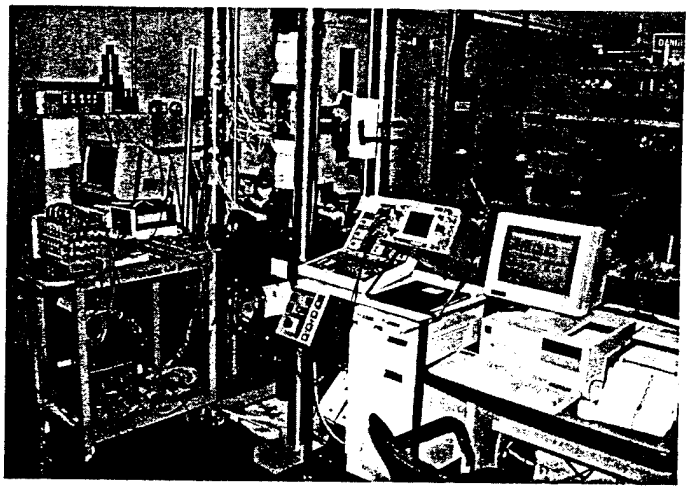
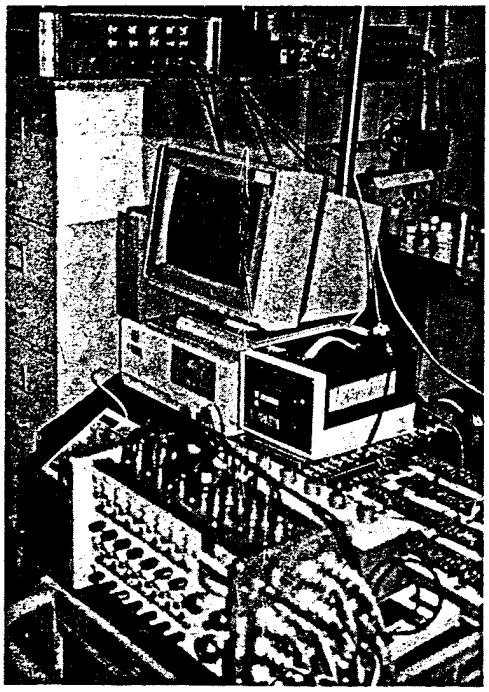


Figure 4. Simulated repair specimen with edge crack - instrumentation. (R = Rosette, KG = KRAK-GAGE).



(a) Testing setup and instrumentation.



(b) Strain and Krak gage instrumentation.

Figure 5. Instron 50 Kip electrohydraulic testing machine for fatigue and residual strength testing of repaired panels.

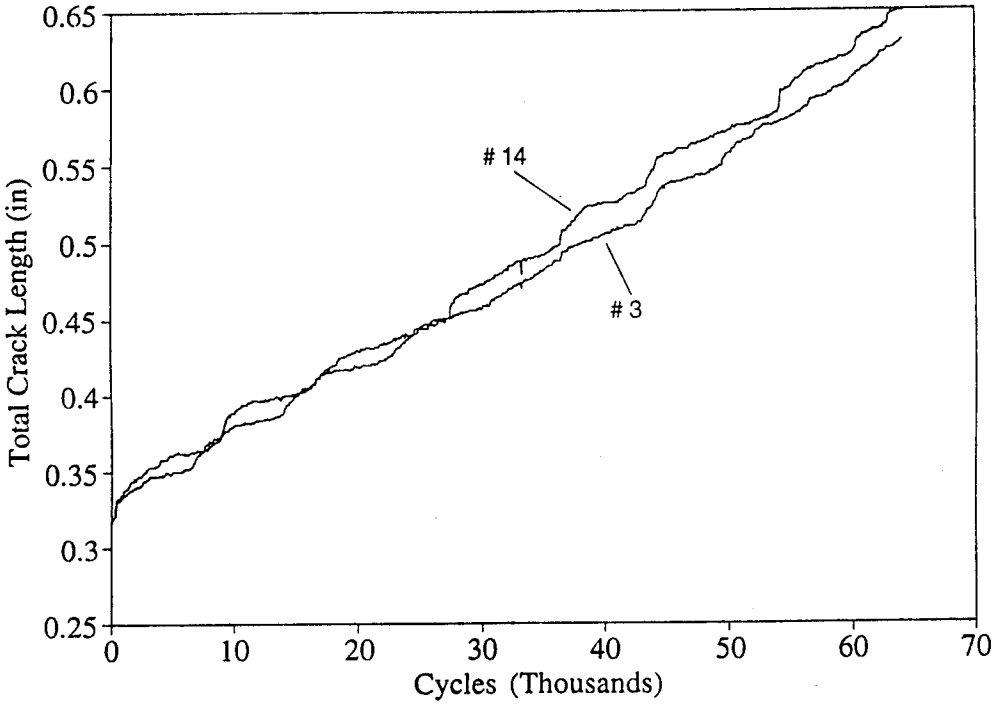


Figure 6. Spectrum loading fatigue crack growth results for skins (panels) 3 and 14, panel assembly 3-1A, room temperature.

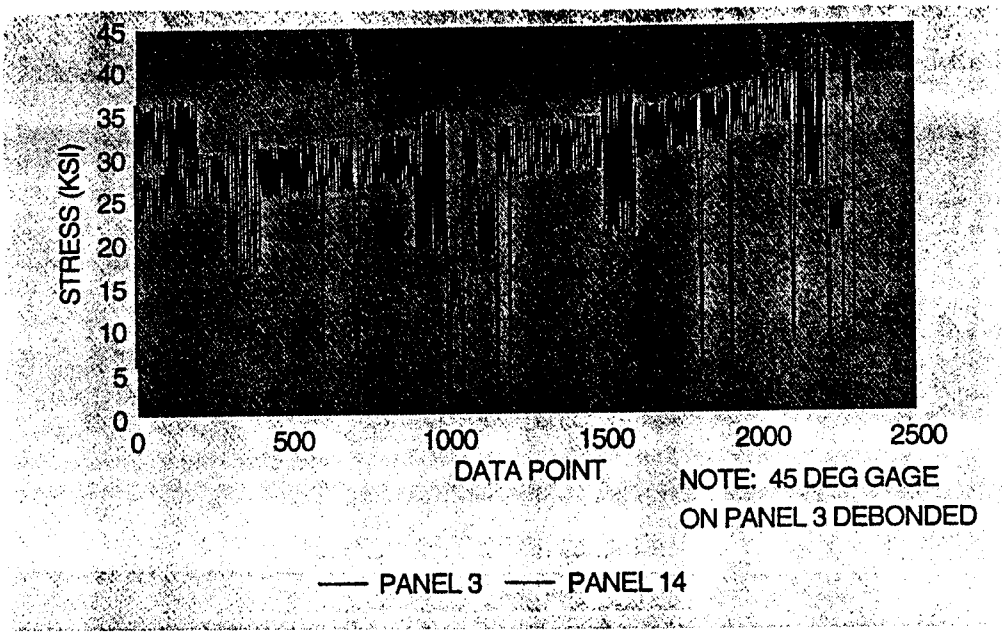


Figure 7. Maximum principal stresses in aluminum skins (panels) 3 and 14, panel assembly 3-1A, room temperature.

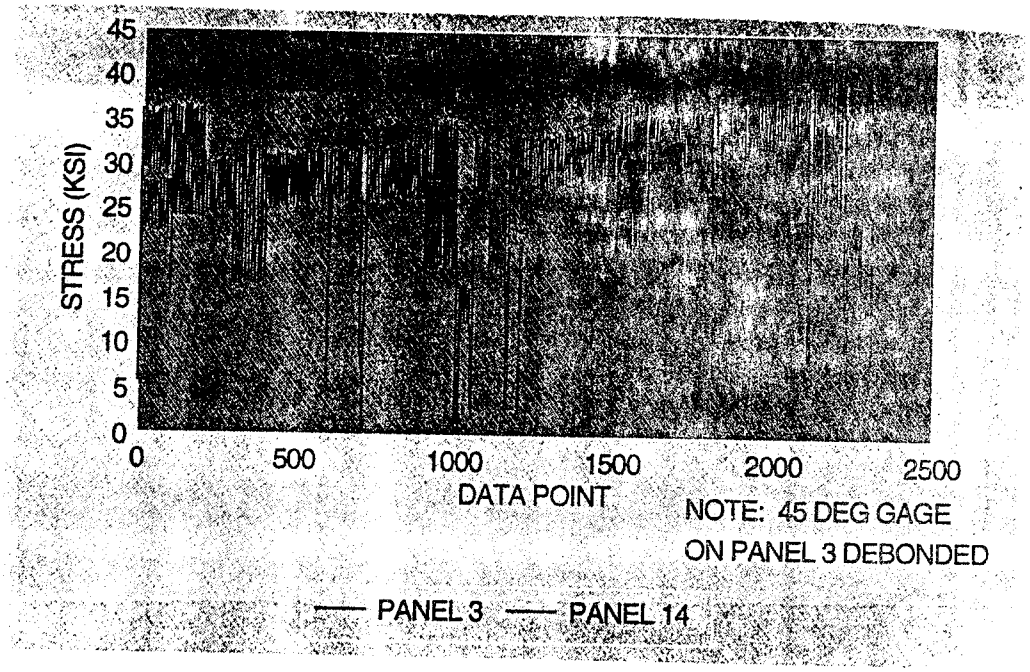


Figure 8. Maximum principal stresses in boron/epoxy patches on skins (panels) 3 and 14, panel assembly 3-1A, room temperature.

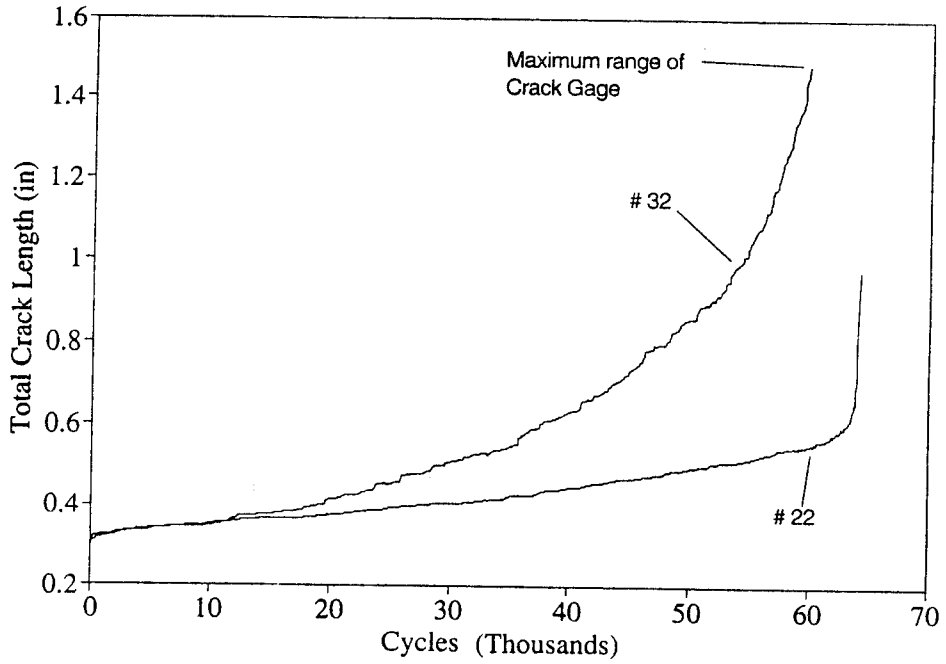


Figure 9. Spectrum loading fatigue crack growth results for skins (panels) 22 and 32, panel assembly 3-2B, 180°F temperature.

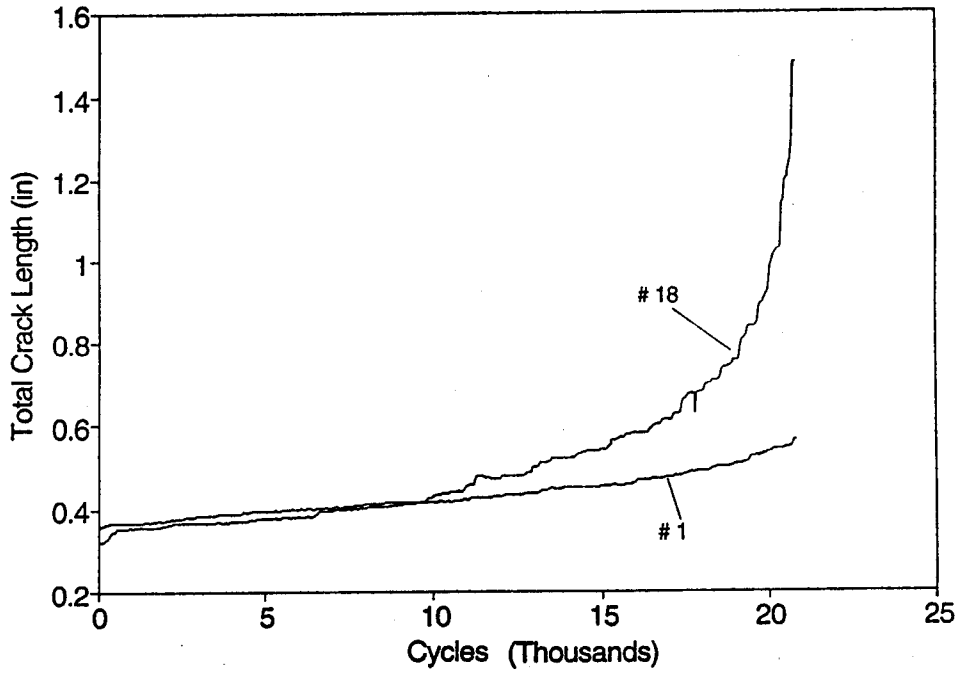


Figure 10. Spectrum loading fatigue crack growth results for skins (panels) 1 and 18, panel assembly 3-3B, -65°F temperature.

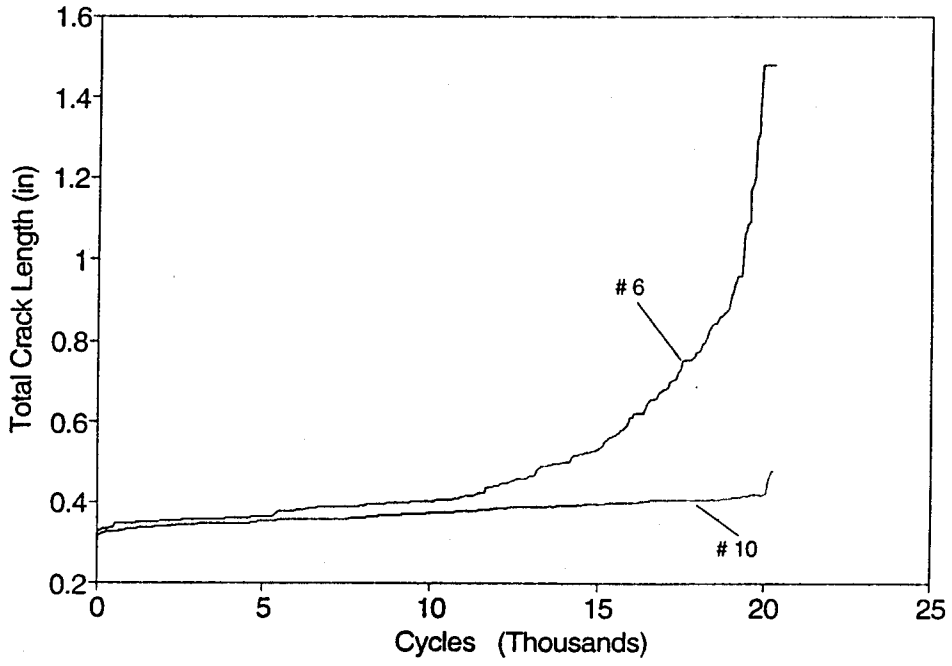


Figure 11. Spectrum loading fatigue crack growth results for skins (panels) 6 and 10, panel assembly 3-4C, prior exposure and room temperature.

AIRCRAFT STRUCTURAL INTEGRITY MANAGEMENT

IN THE ROYAL AUSTRALIAN AIR FORCE

Squadron Leader Terry Saunder
Aircraft Structural Integrity Section
Directorate of Technical Airworthiness - Logistics Systems Agency
Royal Australian Air Force
December 1994

INTRODUCTION

The effective and efficient application of air power is the primary objective of a military Air Force, including the Royal Australian Air Force (RAAF). In reality, the attainment of this objective can be constrained by diminished operational capability through logistics and airworthiness factors. Airworthiness in its simplest terms, is fitness for flight. In the military, aircraft which lack airworthiness are unsafe and also result in a reduction, if not decimation, of operational capability. It is within this context that management and control of both facets of airworthiness - technical and operational - are important functions to the military. Control of airworthiness requires an overarching approach that considers all stages in an aircraft's life cycle from inception to disposal. For example, technical airworthiness begins with good design, as without this no aircraft can succeed, and only concludes at completion of the last flight. Within an aircraft's life cycle, ignoring any dimension that contributes to the maintenance of technical airworthiness can have ramifications upon the RAAF's ability to meet its objectives. The ultimate consequence of a diminished airworthiness is the loss of life and aircraft.

Aircraft structural integrity (ASI) is the ability of all structural elements of an aircraft to withstand normal operating loads within approved flight limitations, without collapse or unacceptable deformation[1] and, hence, ASI is an important dimension of technical airworthiness. The emphasis which major international military airworthiness authorities place on the management of aircraft structure demonstrates the importance of ASI. The RAAF has a history of maintaining aircraft in service long beyond expectations and also in a unique operational environment. As a consequence, technical airworthiness is paramount. Recently there has been the motivation for all airworthiness authorities to review their structural integrity management practices in light of aging aircraft issues. Although the RAAF has been working on the entirety of its technical airworthiness code, a consequence of two RAAF aircraft accidents in 1990 has been the review and re-focusing of RAAF ASI management.

In the last four years, RAAF structural integrity management has developed. It now reflects an entrenched RAAF ASI Program (ASIP), well-defined procedures, and the intention to prepare an overarching doctrinal basis for RAAF structural integrity management. Before the formalisation of a RAAF ASIP, although many elements of an ASIP were performed to some extent, it was not in a rigorous fashion. This was unacceptable. The intent of the RAAF ASIP is not significantly different to the ASIPs of the United States Air Force (USAF) and Canadian Forces (CF) in the fostering of co-ordination of activities required to maintain ASI. However, the RAAF ASIP acknowledges that Australia generally purchases aircraft certified by major international

---

1 Defence Instruction (Air Force) Engineering (DI(AF) ENG) 5-2, para 6.

airworthiness authorities outside the RAAF.[2] Both the context in which this change to RAAF ASI management took place and experiences during this period of change have emphasised the need for the ASIP's holistic approach. This paper provides an overview of the catalysts for the RAAF's re-vitalisation of ASI management and some recent experiences that support the holistic approach.

STRUCTURAL FAILURES

In 1990, the RAAF had two fatal accidents from in-flight structural failures. An Australian designed and built Nomad aircraft suffered the failure of its tailplane. The other was the failure of a wing of a RAAF basic jet trainer. The lessons for the RAAF from these accidents went far beyond their direct cause, these accidents provided valuable insight into structural integrity management requirements. These accidents had a consequential influence on the formulation of the RAAF's new structural integrity management. Thus, a review of the accidents and their lessons is appropriate.

Nomad

The Nomad is a high wing utility aircraft designed for operation from short unprepared airfields and is certified against FAR23. Longitudinal control is effected by an all moving tailplane of constant chord. The tailplane structure is a single spar with torque carried as shear in a two cell torsion box. Across the centre section, where pivot fittings are located, torque is carried by a single cell centre-section box. This box also reacts asymmetric loading on the tailplane and redistributes asymmetric shear between the pivot fittings. The spar web in this box is penetrated by a flanged lightening hole from manufacture.[3]

Nomad A18-401[4] was manufactured in 1982. The aircraft was acquired by the RAAF as a used aircraft and ferried from the previous owner, the original equipment manufacturer, to a RAAF unit in South Australia in 1989. On the 12 March 1990, with less than 10 flying hours since delivery, the aircraft crashed as a consequence of the tailplane failing in flight.

The primary cause of the accident was the aircraft commencing a flight with extensive cracking in the horizontal stabiliser centre section. The cracks had originated from the flanged lightening hole and propagated into the spar cap. This cracking had weakened the structure such that it could not sustain normal flight loads.

Cracking in the centre section of the horizontal tailplane had been known for some time prior to the accident; however, experience suggested that it was associated with extensive flying operations. Periodic inspections were thought to have been sufficient to detect such cracking before it affected tailplane structural integrity. The tailplane fitted to A18-401 had only completed 433 flight hours since new; however, it apparently also endured an additional 182 ground run hours. Subsequent investigation revealed that strain levels from ground running can be up to ten times higher than in flight strains. This demonstrated that there was not a proper appreciation of the structural load distributions in the tailplane, and for this tailplane, the prior operating load

---

2 The RAAF certification process in its entirety addresses this consideration.

3 Australian Government Aircraft Factory (now Aerospace Technologies of Australia, ASTA) Report N22-6000, N22 Design Summary.

4 RAAF tail number in which A18 designates Nomad and -401 is the individual aircraft number with the 400 series representing Nomad N24 models.

spectra. Notably, since this accident, a modification to the tailplane spar has been incorporated. Test has shown this modification to have significantly improved durability in comparison to the pre-modification configuration. This test is continuing to determine critical sites in the new configuration. Furthermore, the RAAF has instituted a flight loads program, in collaboration with the manufacturer, to consolidate our understanding.

Following the Nomad accident, investigation into the history of the aircraft and its introduction to the RAAF indicated that, notwithstanding the involvement of many people in various capacities, the overall engineering management system failed in its responsibility to provide an airworthy aircraft for operations. This failure was of concern to the RAAF. Despite a plethora of instructions and the employment of well trained and highly qualified people, the overall result was one of professional failure.[5]

While in the Nomad case it was the engineering management that failed, the fact that the failure was human rather than systemic suggests that the warning signs are there for all of us to review our performance; to ensure that each of us understands the basic purpose and responsibilities of our particular organisation and our own appointment; that we do not lose sight of that purpose; and that we carry out our functions effectively, especially in communicating our intentions and following them through to conclusion.

Beyond the systemic problems, there were also some engineering lessons. The lack of appreciation of the loads acting on the aircraft structure can be a severe deficiency in the capability to successfully manage an aircraft. In the Nomad's case, limited validation work had been performed on Nomad tailplane loads. Furthermore, there had been no tailplane fatigue test during development. Without such activities and the information they yield, the in-service management did not adequately address all critical areas. A further lesson was in requirements for used aircraft. The prior usage of A18-401 was not well assessed. The requirement to appreciate and understand prior usage and its impact on the structure when acquiring used aircraft is now entrenched in RAAF policy. This lesson prepared the RAAF well for the acquisition of 15 used F-111Gs and for the inevitable future acquisitions of used aircraft.

Macchi

The second accident involved the RAAF's basic jet trainer, the single engine Aermacchi MB326H, a tandem seat aircraft. The primary structural elements of the MB326H are the single spar wing and carry-through structure. Wing spars are built from 7075 U-shaped spar caps joined by two webs to form a box section. Steel wing attachment fittings are fastened to spar caps and transfer load to the steel centre-section. The centre-section is built up from upper and lower booms joined by a web which is penetrated by engine air intake ducts.

Until 1990, the safe-life approach was the means of assuring Macchi structural integrity. This was based on a 1974-75 fatigue test of the MB326H configuration under a RAAF spectrum. In this test the centre-section failed first followed by, at almost twice the life, the lower wing spar cap.

In the early 1980s, the RAAF conducted a Macchi Life of Type Extension (LOTEX) program that included replacement of the wing spar and centre section. The centre section was an improved configuration with an improved fatigue life, although this was not substantiated by test.

---

5 RAAF Letter, Air Headquarters 704/182/P1 Pt 4(48) dated 23 Oct 90.

No fatigue test was undertaken in support of LOTEX and, hence, some fatigue critical sites in the post LOTEX configuration were unknown.

On 19 Nov 1990, during an air combat manoeuvre, the port wing of Macchi A7-076, separated. The pilot was killed and the fleet temporarily grounded. Failure occurred from a fatigue crack in the lower spar boom adjacent to the end of the wing attachment fitting. Fleet management post the accident is beyond the scope of this paper; however, a reduced safe-life was introduced which decimated the fleet and necessitated the purchase of several sets of new wings. There were three pertinent lessons from this accident.

A7-076 had only consumed 70 per cent of its promulgated safe life when the wing failed. Investigation revealed that a fatigue crack had initiated at the base of what should have been a flat bottomed reamed blind web-attachment hole in the lower spar cap. During LOTEX, the drill used had penetrated the inside face and stalled. On withdrawal, the hole was left with two sharp marks from the drill flutes. These marks were orientated normal to maximum stress in the spars at which fatigue cracks initiated. Post assembly, there was no inspection available to determine build quality of individual wings. The only inspection technique available required wing removal to detect cracked ligaments. Additional investigation (ten wings were torn down) revealed a general poor build quality. The apparent poor build standard, in part, was contributed to by the LOTEX program being managed remotely from the then structural integrity managers. This is evidenced in the little attempt given to the phrase 'fatigue enhancement' when providing reasons for conducting the LOTEX program. The lesson is the need for build quality to be controlled during all structural repair and modification programs.

Secondly, the RAAF experience confirms the need to maintain testing which is pertinent to the configuration and operations of the day. This testing is to re-affirm knowledge of critical locations and also the expected life of representative structure tested under a representative spectrum.

Thirdly, review of the algorithms on which Macchi safe life was determined found them to contain an error in methodology. When corrected, the wing on A7-076 had exceeded its fatigue life. This fostered a lack of confidence about all fatigue algorithms the RAAF were utilising to manage aircraft fatigue and a directive was issued for their review. This experience reaffirms the need to regularly asses the basis of algorithms used to monitor fatigue for their appropriateness and accuracy.

REVIEW OF MANAGEMENT

These accidents generated significant concern about the adequacy of RAAF ASI Management to the degree that an external review was commissioned.

External Review

The RAAF commissioned the Australian Civil Aviation Authority (CAA) to review the management of the structural integrity of aircraft within the RAAF. The review was commissioned due to the coincidence of several sets of circumstances including:

a. accidents (A7-076 and A18-401) where structural fatigue was a primary cause;

b. extensive organisational changes and apparent consequent erosion of the RAAF's technology base; and

c. possible inadequacy of structural integrity policy.[6]

The purpose of this external review was to establish the quality of the RAAF aircraft structural integrity management system.[7]

The review was performed in June 1992 with a formal report delivered in August of that year. This review revealed no more with respect to Macchi and Nomad accidents than detailed above. However, the review made extensive comment on the organisation, technology base and structural integrity policy.

Until 1988, RAAF structural integrity management, which had a strong fatigue focus, resided in Air Force Office, the most central element of the RAAF organisation. This function was then devolved to Headquarters Logistic Command (HQLC). At that time, all systems engineering for in-service RAAF aircraft was performed at HQLC. The review noted that the devolution had diminished technological skills. Establishment of experience relies on ensuring there is sufficient organisational depth to provide continuity and educate less experienced personnel in the ways of the organisation. Although theories of structural analysis are taught in university courses, there is little opportunity to gain knowledge of airworthiness standards and application of these standards to individual problems from courses. The reorganisation had separated some layers of the organisation making the RAAF ASI management more fragile. A recommendation of the review was to improve management of ASI specialists within the RAAF.

The review noted the need for greater awareness of ASI issues by Systems Engineers to ensure that they could identify the situations in which specialist ASI assistance is required. In essence, this is ensuring that non ASI specialist engineers have sufficient ASI knowledge on which to asses their competency.[8]

In short, the review identified that the organisation, although being filled with competent individuals, was failing to achieve the objective of ASI management. Compounding this was, as the review noted, that ASI functions had been forced into a mould rather than organised to suit a role. This was attributed to there not being a solid basis for ASI management documented in policy and procedures.

In respect to policy, the review confirmed that RAAF Structural Airworthiness policy (Defence Instruction (Air Force) Technical 12-2) was outdated and relied solely on specifying organisational responsibilities for structural fatigue management. The policy had no consideration of modes of structural degradation beyond fatigue, that is, mechanical damage, battle damage, modifications, repairs and environmental action, such as corrosion. The review concluded that there were serious deficiencies in the RAAF policies and procedures primarily because they did not establish a detailed standard for structural integrity management. Further, that new policies require development at the highest priority. Deficiencies in application of structural integrity philosophies identified by the team required remedial action, including a review of major airworthiness standards to develop a comprehensive structural integrity policy.

---

6 RAAF Air Force Office letter, AF 93/5720 PT 1 (3) para 2.

7 RAAF Air Force Office Letter, AF91/29952 PT 1 (35) of Jun 92.

8 'A test of competence is whether one understands what one is doing. If one does, and calls upon specialist expertise when it is necessary to supplement one's own skills, that is sufficient.' Engineers Australia, 11 Dec 92, p 30.

The common thread of the recommendations was that the RAAF had lost the why of ASI management. The RAAF had become very good at processes, but failed to integrate these into an effective program. The organisation had become too focused on problem solving to the detriment of other functions essential to ASI management; the significance of not performing these functions had been overlooked. The first response to the review was the direction of effort toward formulation of new policy.

Policy

Historically, as the review had identified, management of ASI in the RAAF had concentrated on fatigue as opposed to other forms of structural degradation. Post the external review, the policy was reviewed and a more integrated and holistic approach taken. The lessons from the Macchi and Nomad accidents are well entrenched into the new policy, Defence Instruction (Air Force) Engineering 5-2 (DI(AF) ENG 5-2), issued in Dec 93.

The policy recognises the many forms of structural deterioration that contribute to degradation from the as manufactured condition, and the need to manage these throughout the aircraft's life cycle to constrain both the risk of failure and the costs of continuing operations are to acceptable levels. Central to the policy is the objective of ASI management being:

> *'to enable air operations to be conducted within an acceptable level of risk of structural failure and to preserve the asset to its planned life of type'* [9]

DI(AF) ENG 5-2 identifies outcomes that must be achieved for attainment of the objective, and strategies that must be adopted for achievement of the outcomes. These strategies, which reflect a life cycle approach, are:

a. assessment of aircraft structural design and manufacturing criteria against RAAF standards so that initial aircraft structural integrity management plans (ASIMPs) may be established prior to aircraft acquisition;

b. quality assurance during initial production, routine maintenance, repair or modification;

c. identification of critical components and their detailed through life management;

d. regular re-assessment of certified life limit and/or inspection requirements for structural components based on their actual RAAF usage;

e. ongoing assessment of the physical condition of aircraft for deterioration of the structural integrity;

f. collection, analysis and application of environmental and usage data to support on-going assessment of aircraft structural integrity, the resolution of aircraft structural integrity problems, and the basis of advice for future aircraft acquisition; and

g. provision of timely, germane, structured information to engineering and operational decision makers on aircraft structural integrity management matters.[10]

---

9 DI(AF) ENG 5-2, para 10.
10 DI(AF) ENG 5-2, para 12.

The preferred basis for establishing individual aircraft strategy is a full scale fatigue test using a RAAF representative spectrum and a test article representative of RAAF production standard. Aircraft not tested will have a strategy which provides for a greater degree of conservatism in the management approach.

Although the policy does not segregate the ASI Management into five tasks as the USAF[11] ASIP does, most elements are common. The main differences result from the RAAF's recognition of its inability to specify a unique range of design standards. This reflects the reality that RAAF and Army[12] aircraft are purchased from a number of countries and manufacturers with design already well established and, hence, there is limited opportunity for the RAAF to specify a unique range of design standards. Thus, the RAAF recognises the airworthiness codes and standards from major international airworthiness authorities. Nevertheless, the RAAF has adopted the British Ministry of Defence, Defence Standard 00-970 'Design and Airworthiness Requirements for Service Aircraft' (referred to as DEFSTAN 00-970) as a baseline for aircraft design and through life airworthiness management. This is called the RAAF Structural Design Standard (RAAFSDSTD) and is used to evaluate the alternate standards and design philosophies. This does not mean each aircraft will be managed against the RAAFSDSTD.

Once an aircraft enters RAAF Service and has Type Certification, the airworthiness standard to which the aircraft was designed, the certification structural design standard (CSDSTD), is the standard on which the aircraft's structural integrity is to be based. The CSDSTD is not necessarily the RAAFSDSTD. Re-assessment of the validity of the CSDSTD considering developments in airworthiness practices, and changes in operating role and environment is to be made regularly. This reassessment is to include tear down on an opportunity basis, and monitoring of aircraft condition for deterioration; for example, Aeronautical and Maritime Research Laboratory (AMRL) has torn down many Macchi wings, and is preparing to tear down a MB339 wing from the Royal New Zealand Air Force. Discussion has been initiated with USAF on F-111 wing tear down.

Two further aspects that are central to the RAAF ASI management requirements for every aircraft are:

a. usage monitoring appropriate to the management of the aircraft from when aircraft enter service; and

b. operational loads measurement program for each aircraft to validate aircraft loads in RAAF roles and, hence, the usage monitoring program.

The many facets necessary to achieve such far reaching requirements are documented in Aircraft Structural Integrity Management Plans (ASIMPs). These are similar to USAF ASIP Master Plans, but require consideration of at least the next ten years. A key outcome of the ASIMP is the accumulation of sufficient data to confirm the continuing basis of certification which is reviewed annually. Thus, there is annual re-assessment of the CSDSTD.

Aircraft acquisition also is considered in the policy. Abridged ASIMPs are required for any aircraft being considered. Additionally, assessment of design airworthiness code, against DEFSTAN 970, must be made, particularly in relation to intended role. This may lead to re-validation of the fatigue substantiation. The Nomad accident is reflected in the stringent requirements for acquisition of used aircraft including:

---

11 MIL-STD-1530

12 Aircraft operated by the Australian Regular Army (ARA) have their technical airworthiness maintained under RAAF policies and procedures.

a. assessment of previous service (usage, repairs, etc);

b. physical examination; and

c. assessment of accrued damage, allowing for un-monitored service.

In short, the new policy reflects a cradle to grave approach. This is facilitated by the requirements for a programmed approach so that threats to aircraft structure should not go undetected or worse, unresolved. Procedural guidance for the implementation of the policy has been written over the last twelve months and recently issued within the RAAF's new engineering regulatory system.

Process

The RAAF's Technical Airworthiness Management Manual[13] includes a chapter on ASI Management. This document provides the framework within which efficient management of ASI can take place and the requirements of the policy be met. Although the chapter details organisational relationships and responsibilities it also:

a. describes the RAAF ASIP;

b. defines standards and procedural guidance necessary to achieve, maintain and assure structural integrity of RAAF and Army aircraft;

c. establish a standard to which individual ASIPs shall conform; and

d. specify an acceptable method of compliance with the ASIP requirements.

The procedures specify the requirement for an ASIP as the means to fulfil the policy objectives. The objectives of the RAAF ASIP are identical to that of the USAF, as are the ASIP task elements. Hence, these will be elaborated no further. Furthermore, the major content of the procedures is RAAF organisation specific; and thus beyond the intent of this paper. The procedures detail all requirements and represents the starting point from which to determine specific weapon system requirements. This is a fundamental change to previous guidance which provided the minimum requirements and these were often not satisfied. However, there are some aspects, which go beyond the traditional ASIP.

The 'holistic' view, although the RAAF cannot control design standards, is the consideration of ASIP functional elements from concept phase to disposal. Some dimension of these elements include the training of personnel for Aircraft Structural Integrity Managers (ASIMs), continuation training of ASIMs and formal recognition of the need to educate logistic engineers and operators on structural integrity matters. This responsibility of organisations is often overlooked. Work has already commenced to stream people for structural integrity specialists and on in-house courses for engineers. The RAAF personnel system is establishing streaming for all positions in the RAAF ASI Section. This shall contribute to minimisation of problem with maintaining the required experience level of structural integrity managers when performed by uniformed personnel. Furthermore, operations beyond acceptable level of risk (that is, the risk implicitly embedded in the

13 Australian Air Publication(AAP) 7001.053

CSDSTD), contingency operations, and aging aircraft issues are considered. Included is the requirement for Aging Aircraft Audits at the mid-life point, but no greater than 15 years into service.

Repairs represent a problem, particularly for aging aircraft. The RAAF is initiating the recording of repairs. The information recorded will depend on the reason for recording the repair. For example, repair tracking can be for surveillance of aircraft condition and or because the repair is structurally significant and requires more intensive management. The intent is to provide repair history on a database for ease of management and visibility of aircraft condition in the annual review.

Thus both the policy and procedures represent a significant step forward for the RAAF's structural integrity management. The framework acknowledges the unique influence which structural integrity has over other engineering organisations and the need for absolute rigour. However, the framework also recognises that a balance is required among the three competing facets of the RAAF, that of an independent airworthiness authority under which safety is paramount, an owner for which economics is important and lastly that of an operator for which availability is of concern. The procedures reflect the desired solution and thus represent a point from which each weapon system is assessed against and their individual ASIP formulated. To aid the RAAF in maintaining a world class standard of ASI management, regular external reviews are intended. However, the basic foundation for structural integrity management is not yet entrenched into a suitable document.

Doctrine

From the many reviews of RAAF ASI management, the policy and procedural framework for ASI management has been developed as discussed above. However, the need has been identified for a manual that documents the philosophical basis for, and the principles governing the conduct of structural integrity management in the RAAF. This is an activity which shall start in 1995 with the development of a manual titled 'The RAAF Manual of Aircraft Structural Life Management'.

The main function of this document is to assist in maintaining the organisation's corporate knowledge in light of the impact of postings on retention of expertise in the ASI specialisation.

Organisation

Part of the RAAF's significant reorganisations in recent years has included dispersal of RAAF engineers from a centralised hierarchical organisation to smaller weapon-system focused Logistics Management Squadrons (LMSQNs). However, among this significant change, ASI Management has remained centralised.

The CAA review identified potential exacerbation of structural integrity management deficiencies by instability in the organisation. They advocated a centralised ASI management along with other function which have:

a. fleet-wide application,

b. more cost effectively practiced by experts,

c. independence from operational pressure,

d. require speed of response or flexibility, and

e. need to support regulatory functions which are centralised.

Consequently, there is an ASI Section, within the Directorate of Technical Airworthiness located in the Logistics Systems Agency (LSA) in Melbourne. The ASI Section is manned by up to 10 engineers with at minimum professional qualifications in aeronautical engineering of which usually half have post-graduate training in related fields. ASI Section is very much a pool of people, each having responsibility for management of certain aircraft; however, there is emphasis on teamwork and utilisation of resources to best meet section goals.

The maintenance of this degree of speciality and their effectiveness is through continuation training and specialisation streaming discussed above. Although centralisation of expertise on ASI is accepted, this does not mean we centralise all aspects of the ASIP. Many of the implementation functions of the ASIP are fulfilled by LMSQNs.

Furthermore, there is heavy reliance on Defence Science and Technology Organisation (DSTO). Support is primarily provided by the AMRL located in Melbourne.

The remaining part of the paper focuses on recent experiences of the RAAF which support the re-vitalisation of structural integrity management under the concept of an ASIP.

OPERATIONS

Most aspects of structural degradation are linked back to the operations which are demanded of an aircraft. That is, the type of operations, the frequency, and the environment in which operations occur. Therefore, it can not be denied that a central dimension of an any effort to manage ASI requires the monitoring of operations, or usage monitoring. From the engineers' perspective, the prime objective of this task to monitor loads which the aircraft is experiencing. This is generally achieved by mission monitoring and limited flight parameter collection, often vertical acceleration exceedences. In limited applications, strain based systems are used. This data collection allows the RAAF:

a. to assess if the aircraft is being operated within its defined usage spectrum and hence assess if the basis of certification remains valid,

b. enable structural life assessment to be based on actual individual aircraft usage, and

c. provide historical data on which to base predicted usage spectrums for future acquisitions.[14]

Without effective usage monitoring, a major portion of an ASIP would be founded on data which cannot have its accuracy assessed. A possible outcome of ignoring of the need for usage monitoring is clearly demonstrated by the RAAF experience with the Black Hawk helicopter.

---

[14] DI(AF) ENG5-2, para 26.

Australian Black Hawk Helicopter

The RAAF purchased 39 Sikorsky S-70A-9 aircraft which is a derivative of the US Army's UH-60 helicopter, as are the USAF's HH-60 and MH-60G. The operational control, and airworthiness of these aircraft, resides with the Australian Regular Army (ARA). However, technical airworthiness and logistics are controlled within the RAAF system.

Historically, RAAF policy has been to follow OEM recommendation on helicopter lifing. Consequently, usage assessment of helicopters in the RAAF is not normally performed. Neither is any form of individual aircraft (usage) tracking. At acquisition it was assumed that S-70A-9 aircraft would operate in a similar role to the UH-60. However, there was motivation for a usage assessment of the S-70A-9 from a realisation that the S-70A-9 could be used differently to the UH-60. For example, the ARA planned to use external stores support system (ESSS) to provide additional fuel capacity and, hence, range. Additionally, other recently purchased aircraft had been found to be operating in a significantly different spectrum to that assumed at certification.

During the acquisition phase, the initial intent was to quantify S-70A-9 usage and provide adequate data for fatigue life calculation. In 1990, this approach was terminated primarily due to unavailability of suitable technology. An alternative was chosen in performing a pilot survey, that is to use qualitative information to determine the S-70A-9 spectrum. Even at the time of selecting this course of action, there was the perception that ARA operations would not significantly affect component retirement times.

Sikorsky was contracted to perform a usage survey and dynamic component retirement time assessment. This task was divided into three phases. The first covered collection of data through a pilot survey and an impact study on the calculated retirement times (CRTs) using five components. Phase Two updates the data on which CRTs are based and subsequently determine revised CRTs for 12 low life dynamic components. Phase Three provides the results for remaining components.

Phase One is complete. Indications are that the ARA is one of the most severe H-60 operators in the world. The impact study provided an average 48 per cent reduction in CRTs, this is considered to be indicative of CRT reduction for all S-70A-9 dynamic components. The cost of this, in parts alone, is estimated to be 65 million (Australian) dollars across the life cycle. One objective of Phase Two was the refinement of the data on which CRTs are based, and this is anticipated to result in an average life reduction less than 48 per cent.

However, the S-70A-9 fleet had exceeded two of the Phase One revised lives. To provide an approved management basis pending the receipt of Phase Two results (expected in mid 1995), RAAF ASI Section, co-ordinated a risk assessment of overflying these two safe-lives. This assessment calculated that for an approximate 50 per cent increase in the revised safe-lives, there was a three-fold increase in the risk of losing an aircraft due to component failure. This strategy was put forward as an interim solution. The operational airworthiness authority, the ARA, accepted operations at an increased risk pending Phase Two results.

The severity of operations as indicated in the usage assessment is now also showing up as airframe structural cracking. There are concerns that other problems will manifest in the structure also.

The lesson here is straight forward, monitor usage against a baseline and perform the necessary structural life assessment. In this case the ARA and RAAF are intending to pursue a quantitative program in the medium term, hopefully to remove conservatism from the qualitative

approach. In the near term, regular usage monitoring based on end of mission data collection from aircrew is to be initiated in 1995. The data collected is aimed at factors which affect both dynamic components and airframe structural elements. ASI Managers now appreciate that regardless of the philosophical basis of maintaining structural airworthiness, usage monitoring and assessment are essential elements of the ASIP. Thus, although helicopters are predominantly managed on a safe-life basis, the lessons learnt are equally applicable to safety-by-inspection managed aircraft.

To illustrate the RAAF's commitment to usage monitoring and the need for representative testing, consider the turbo-prop Pilatus PC-9 in use as the RAAF's advanced trainer. It was purchased about eight years ago with a 8000 hour life. RAAF identified early in its service that usage was severe and there was no fatigue test basis to the life, hence, the RAAF reduced the estimated structural life of type to 6000 hours. This has lead to an intensive management program, and the commencement of a full scale fatigue test. Pending results from the fatigue test, usage monitoring is permitting effective fleet management. The usage monitoring is allowing fatigue damage accrual to be managed, on an individual aircraft basis, such that the test article leads the fleet at the 6000 hour point. Likewise for the F/A-18.

The F/A-18 Hornet was designed for a 6000 hour life under a US Navy spectrum. This was based on a series of full scale and component tests. However, the RAAF increased the scatter factor applied to the test results due to concerns about their validity to RAAF operations and structural configuration. Usage monitoring identified that the RAAF operations were more severe compared to structural certification. The extensive usage monitoring system has provided sufficiently detailed information on which to refine operations and reduce fatigue accrual, without constraining aircraft capability. Long term management will be based on a fatigue test being addressed under the International Follow-On Structural Test Program between Australia and Canada. This test is to provide a basis for certification under a RAAF/Canadian Forces (CF) spectrum, validate structural changes not reflected in the production test and determine the economic life potential of the airframe. The RAAF goal is to pursue economic life of the aircraft such that operation beyond 6000 hours can be considered. Such goals can only be achieved through the RAAF's continued commitment to effective usage monitoring.

ASSESSMENT

Although usage monitoring is an essential component to an effective ASIP, its main contribution is to the on-going assessment of an aircraft's structural integrity. The initial step in assessment is setting baseline against which to compare: the RAAF baseline for each aircraft type is its CSDSTD. Assessment activities requires information on materials, identification of structural parts and components which contribute significantly to carrying loads. Furthermore, information on structural degradation of each aircraft is required. Repairs must be considered for their contribution to structural degradation and as an indicator that aspects of the structure require closer examination. Corrosion assessment is becoming important, and in some airframes more important, than fatigue, the traditional focus of ASIPs. Assessment of aging aircraft issues is particularly relevant as the RAAF is an operator which uses aircraft far beyond the life anticipated at design. For example, the RAAF will operate the F-111 until 2020 and the Lockheed P3 is likely to be used for one and half times its safe-life.

In the last year, the need for a holistic approach to assessing ASI has been reinforced by several experiences. Three of these experiences shall be reviewed.

F-111 Lower Wing Skin

In February 1994, a chordwise fatigue crack was discovered in the lower wing skin of a RAAF F-111. The skin is a one piece 2024-T851 aluminium supported by five spars; the second from the leading edge is the forward auxiliary spar. For minimisation of fuel entrapment, two drains are provided under the forward auxiliary spar, one being at two thirds of the semi-span. This drain is effected by locally reducing the spar attachment land and stiffeners are provided either side of the drain to restore bending stiffness.

The cracking resulted from the local stress concentration of the drain hole and secondary bending effects. USAF aircraft were also inspected, and one F-111G which the RAAF was purchasing, had a crack in the same location. This crack was removed from the wing and fractographic analysis performed. Both cracks initiated on the inner surface within the drain. The crack in the RAAF F-111 was 48 mm in length and was discovered when fuel leaked. Preliminary residual strength calculations indicate failure below the Design Limit Load of 6.5g. (Design case is 6.5g pull out at Mach 1.4 and 26,000 feet.) However, in the period immediately before discovery, the aircraft had recorded 4.0g on numerous occasions.

The asset being of significant value to the RAAF, repair was desirable. Consideration was given to a metallic repair, but this was considered undesirable from a fatigue viewpoint. Consequently, a bonded repair using boron-epoxy was chosen. The material's high stiffness is compatible with the RAAF's bonded repair design process and present minimum aerodynamic or galvanic issues. Although the RAAF has had significant experience with bonded repairs, this experience is not with significantly cracked primary structure.

Until this patch, the technique had only been used in applications where structural airworthiness did not rely on patch durability. For example, stress corrosion cracking in C130 (approx 1,000 patches) reduction of stress in F-111 WPF, now a fleet fit. Incidentally, this has taken the calculated interval from less than 500 hours with a confidence factor (CF) of 1.0 to a minimum 1,400 hours and a CF of 2.0.

The repair technique required consideration beyond that at aircraft design, due to temperature effect on the integrity of the repair. Hence, the repair was designed to meet a number of conditions, including cold proof load test. Integrity of the repair depends on:

a. integrity of the adhesive,

b. patch strength, and

c. strength of the repaired structure.

Structural assessment of the repair addressed each of these and during this process some deficiencies were highlighted with the engineering standard.[15] In conjunction with the lack of experience in assessing repair durability (RAAF F-111s are expected to remain in service for another 25 years), interim approval was given in May 1994. This included the application of the following operational limits:

$N_2 < 4g$ for AUW < 75,000 lb

$N_2 < 300{,}000$ lb for AUW > 75,000 lb

---

15 RAAF Engineering Standard C5033 Composite Materials and Adhesive Bonded Repair (Draft).

These restrictions were based on the minimum demonstrated residual strength of 4.0g. This implies that the patch adds a 0.5 increase in residual strength of the crack structure (ie, the difference between limit and ultimate strength). Full certification is under way.

This certification process includes the validation of the formulae used in Engineering Standard C5033. This task will increase the availability of bonded repairs for RAAF applications and reduce down time by improving repair approval process. Analysis and testing will be used to extend the scope of C5033 to more complex damage and repair configurations. In particular, aging aircraft, including P3C, C130 and F-111, are anticipated to benefit from this activity.

This experience has made the RAAF ASIMs far more aware that regardless of the effort to develop an ASIP, we are not immune to surprises. To minimise unforseen problems, mid-life tear-downs, as the RAAF is now pursuing on F-111, are necessary.

C130 Wing Repair

During Jun 1994, it was realised that a Lockheed Service Bulletin (LSB 82-607) initially issued in 1987 and revised in 1993 may not have been fully actioned. The Service Bulletin required the end configuration of all C-130E lower wing riser repairs to be inspected for cracking. This had resulted from the then authorised structural repair manual repairs to be inspected for cracking. This had resulted from the authorised structural repair manual repairs to be of poor durability.

Inspection. The RAAF maintains wing repair maps for C130 aircraft; however, there were some concerns about their accuracy. The aircraft with the largest number of repairs was inspected. This revealed a chordwise crack of 22 millimetres which appeared to be between the last two fasteners of a riser repair. Further investigation revealed a repair with a poor end configuration. A fleet wide inspection program commenced and flight restrictions were enforced pending inspection to confirm no further defects. No more cracking was found.

The experience is now encompassed in the regulatory authority, having responsibility to monitor compliance with service bulletins and the like. However, the more significant lesson here, is the need to demonstrate damage tolerance capability of repairs and surrounding structure.

The RAAF is in the evolutionary stage of repair tracking, and durability considerations are generally left to OEM advice. However, aircraft are commonly repaired on the basis of design requirements applicable when the aircraft was first certificated. For the RAAF fleet, this results in repairs usually being designed on an equivalent static strength basis with little regard to crack growth, residual strength, or the need for subsequent non-destructive inspections of the repair. The effective design and management of repairs are challenges yet to be fully addressed by the RAAF.

C-130 Floor to Ring Fitting

In 1992, a 'bang' was heard during the flight of a C-130H. A cursory inspection was performed post flight which revealed nothing. The next flight a 'thump' was heard. Subsequent inspection revealed a failed chine angle and Fuselage Station (FS) 737 floor to ring fitting. Investigation revealed that the fitting had failed from bolt hole corner flaw with an approximate crack length of 8.0 millimetres. The chine angle cracking was considered to be due to load

shedding consequent to the fitting failure. The aircraft at the time of failure had accrued 10730 airframe hours and 9892 landings.

During the course of RAAF investigations, it was found that the RAF had identified the fitting as a fatigue susceptible location, and an Omani aircraft had suffered a similar failure, which was not discovered until the aircraft was in routine servicing.

From this, the component could be considered fail-safe, provided the load shedding does not normally cause failure of other structural elements pending inspection.

A fleet inspection program was undertaken. Initially it appeared that the problem was not a fleet concern. However, upon rectification of problems with the non-destructive inspection (NDI) technique, subsequent inspection in 1994 revealed most RAAF aircraft fittings had cracks. On the basis of fractographic data, an inspection program was developed to manage cracked fittings until logistically, they could be changed. A replacement life of 2,235 hours has been applied to uncracked and new fittings. This was interim until an improved appreciation of the loads upon which to base a component replacement life.

Inspection of removed fittings have revealed that corrosion, stress corrosion cracking and fatigue all contribute to the fittings cracking. Whilst to inspect the fitting is not relatively resource intense (approximately of one half day), the damage incurred in removing the fastener is of concern. This makes management of the fitting complex and, hence, the current RAAF preferred option to replace fittings at a nominated life.

This example serves to remind us that effective structural integrity management requires the monitoring of all aspects of the structure, not just that identified through a durability and damage tolerance assessment (DADTA) program. This aspect of an ASIP, monitoring in-service defects, becomes increasingly important as fail-safe designed structure may well become flight critical as the aircraft ages and multiple site or multiple element damage occurs.

The resolution of this demonstrates the application of equal energy toward safety and economics. This balance, which is reflected in RAAF procedures, results from the premise that although we may be in a period of extended peace, there are still demands placed on aircraft with equal priority that would be expected in a conflict. Examples of this are disaster relief and peace keeping and the like. Thus timeliness of response must be high and the solution both effective and efficient.

Without the appreciation of load mechanisms (noting that there has been difficulty in locating original design data) it was not plausible to implement flight restrictions. The fitting was not subject to a safety-by-inspection management. The paucity of information lead to an inspection program based on fractographic analysis of one fitting.

Regardless of the fleet size, communication with other operators of similar aircraft can avert disaster. The RAAF being a small operator and also remotely located, we have an emphasis on the need for communication.

CONCLUSION

The RAAF has reorientated its concept of structural integrity management to an ASIP. Although it is well appreciated that an ASIP is multi-faceted, the enormity of the activities required

is now only being fully appreciated by the RAAF. This new awareness has grown from two accidents which caused the realisation that the RAAF had lost the appreciation of the interdependency of the many elements which contribute to an ASIP. Performance of each task in itself is not sufficient to ensure that an adequate level of structural integrity is maintained.

Recent experiences have confirmed the need for an ASIP. The F-111 wing skin cracking highlights that regardless of previous assessments of an aircraft's structural integrity, on-going assessment is required to maintain an effective ASIP. This is even though there may have been significant resources directed to prior assessments. One dimension of this on-going activity is usage monitoring. The risk of structural failure when operations are not well appreciated cannot be assessed. Thus increased margins of conservatism must be added or as usually occurs, the ASIP fails to meet its goal. The Black Hawk demonstrates that perceptions and reality must be continually reviewed, and usage monitoring significantly contributes to the success of an ASIP.

The maintenance of an effective ASIP requires the diligence of the people involved. They must understand the subtleties of the program, particularly the relationships of ASIP activities, and also be competent. Processes must be well documented. This contributes to maintaining awareness and ensuring that best known practices of ASI assessment are used. What must not be forgotten is the data. All too often this aspect is not fully addressed which only leads to compromise of the ASIP. Thus with people, data and processes in mind, the RAAF will maintain an effective ASIP for each aircraft for which we have technical airworthiness responsibility.

Fatigue Crack Initiation, Growth and Residual Strength Characteristics of Riveted Fibre Metal Laminate Lap joints

Authors: R. P. G. Müller
C. Borsboom

Summary

Longitudinal riveted aluminium lap joints are sensitive for fatigue cracking. The internal pressurization is the crack driving force. After the onset of fatigue cracking in aluminium failure occurs soon. The squeeze force is important to extend the fatigue life. Finite element calculations showed that residual stresses occur near the hole edge, which are related to the rivet squeeze force. Tangential compressive stresses occur with large squeeze forces as well as large mating sheet clamping. Also the interference will become larger. As a consequence of larger squeeze force tangential tensile stresses occur away from the hole edge. These stresses in combination with secondary bending and fretting cause a shift in crack initiation location away from the hole edge. Also crack initiation might occur in the bottom row due to bending imperfections with higher squeeze forces. Besides the residual stresses load transfer and secondary bending determine the fatigue behaviour. Fatigue behaviour of a joint is often investigated with small coupons. This is a simplification of the fuselage loading conditions. Finite element calculations revealed a small difference in load transfer for the area not disturbed by the frames for a flat uni-axially loaded riveted lap joint coupon and a lap joint in a pressurized barrel test set-up. This is also true for secondary bending. However, the calculations cannot reveal the consequences of bi-axial stresses for fatigue crack initiation and growth.

For a typical lap joint a comparison study was performed on both monolithic aluminium (2.2 mm) lap joints and Glare (1.4 mm) lap joints. For aluminium lap joints, it was possible to increase the fatigue life with a factor five, whereas for Glare this factor was more then ten. At intermediate squeeze forces and higher, fatigue lives of Glare lap joints are larger than the aluminium joints. However, Glare joints initiate earlier than the aluminium joints due to the higher stress level, but the fatigue crack growth life is substantially larger due to the fibres that bridge the crack and prevent through-the-thickness crack growth. A larger rivet squeeze force contributes to this last mentioned phenomenon. This results in low crack growth rates and unstable crack growth was not seen.

In Glare lap joints, Multiple Site Damage is always present due to the slow crack growth, but it does not lead to hazardous situations. This is in strong contradiction with monolithic aluminium lap joints.

The fatigue life of a Glare lap joint tested in the reduced scale barrel test set-up is half the fatigue life of a riveted joint coupon. A 10% higher stress level for the coupon probably results in a comparable fatigue life for the barrel and the coupon. Residual strength tests indicated that with 60% of all aluminium in the Glare laminate failed the residual strength is still twice the applied fatigue stress. The residual strength is linearly related to the number of cycles and crack length. It is possible to predict the residual strength with a satisfying accuracy.

1. Introduction

Fibre metal laminates grant their excellent fatigue performance to: (1) The crack bridging of intact fibres which reduces the stress intensity at the crack tip and gives crack growth retardation (see figure 1), and (2) Crack initiation through the thickness is postponed, the bending stress gradient in combination with

the residual stresses due to squeezing prevent simultaneous initiation of the mating aluminium layers. For monolithic aluminium the maximum stress at the mating surface determines crack initiation for the total cross section, because of rapid through the thickness growth. Failure will occur soon in those materials after the onset of cracking, due to this rapid reduction of the net section area. In a Glare riveted lap joint the discussed phenomena result in increased fatigue lives compared to monolithic aluminium joints. To predict the fatigue life, parameters that control the fatigue life have to be studied. Calculations will give instructive information about the fatigue behaviour. However, due to its complexity, fatigue tests are inevitable and have to be performed. These experiments have to resemble the reality as close as possible, which includes investigation of the rivet installation conditions and study the performance of joints in curved internally pressurized bi-axially loaded panels.

To understand the fatigue behaviour of riveted lap joints the important observations that are required start with manufacturing and ends with fractographical analysis after fatigue testing or residual strength testing. Simultaneous, calculations have to be made to verify the experimental results or to explain the phenomena. This paper describes the fatigue life of a Glare riveted joint. Only the experimental investigation will be discussed, related finite element calculations are reported in [1].

2. Experiments for the Effect of the Rivet Squeeze Force on the Fatigue Behaviour

2.1 Test Configurations

To study the effect of the rivet squeeze force in a longitudinal lap joint, flat coupons and a barrel test sample were used (see figure 2) [2,3]. The reduced scale barrel test set-up was used to investigate the effect of a more realistic load condition (differential pressure). In this test set-up a bi-axial stress situation is present. As discussed, the radius of the barrel has no significant effect on the stresses in the test sample. However, in conjunction with roll-forming the sheets, a conservative behaviour of the critical end rows is expected.

The Airbus A340 configuration of the longitudinal lap joint was used (figure 3). The lap joint has three rivet rows with a row pitch and rivet pitch of 24 mm. The rivet type used was NAS1097DD6-6. The thickness of the aluminium 2024-T3 skin is 1.6 mm. However, in the lap joint a doubler is used, resulting in a skin thickness of 2.2 mm. In this investigation the aluminium 2024-T3 was replaced by a Glare 3 3/2 0.3 skin with a thickness of 1.4 mm. The Glare 3 3/2 0.3 lap joint has no doublers. This results in significantly higher stresses in the Glare lap joint than in the 2024-T3 lap joint. The fatigue stress used in the 2024-T3 lap joint was 80 MPa (R=0.05, f=10 Hz, sine wave). The reduction in skin thickness from 2.2 mm to 1.4 mm results in a stress in the Glare lap joint of 124 MPa (R=0.05, f=10 Hz, sine wave). In the barrel the frequency was 1/15 Hz (R=0.02).

Because the fatigue cracks in a Glare 3 3/2 0.3 lap joint initiate and grow sub-surface, the eddy current non-destructive inspection technique was used to get initiation and crack length data. The equipment used consisted of the Nortec 19e, Nortec sliding probe SPO 3806 and a Nortec high frequency pencil probe [2,4]. The definition of the aluminium layers in the Glare laminate is as follows (see also figure 4). Layer 1 is the faying layer in the lap joint (at the mating surface); layer 2 is the middle layer in the Glare 3 3/2 0.3 sheet, and layer 3 is the outer layer of the sheet (the visible aluminium layer). The crack length is measured from the hole diameter (the shank of the rivet, figure 5).

2.2 *The Effect of the Rivet Squeeze Force on the Fatigue Behaviour of Monolithic 2024-T3 and Glare 3 3/2 0.3 Lap Joints*

2.2.1 Monolithic Aluminium Lap Joints

The relation between the driven head size and the squeeze force for this typical configuration is given in figure 6. The effect of the rivet squeeze force on the fatigue life of monolithic aluminium lap joints is shown in figure 7. A higher squeeze force led to a higher fatigue life. However, it did not increase the fatigue crack growth life after fatigue crack initiation. At a rivet squeeze force of 22 kN and using a fatigue stress of 80 MPa, the fatigue life was 600 kcycles. At higher squeeze forces, such as 36 kN, the fatigue life was about one million cycles. A higher fatigue life could not be obtained with the monolithic aluminium sheets.

The fatigue crack growth life in monolithic 2024-T3 sheets was 5-10% of the total fatigue life. This gives information about the crack free life and the residual strength of the aluminium lap joint. However, this does not apply to Glare riveted lap joints. The initiation lives of the separate aluminium layers in the laminate is unknown: the crack free life of the Glare lap joint could be only 5-10% of the total fatigue life. This would mean that the residual strength decreases with an increasing number of fatigue cycles. Therefore, inspections must assess the damage in the Glare lap joint and the relation between the damage and the residual strength must be established, as well as the effect of the rivet squeeze force on the fatigue behaviour.

2.2.2 Glare 3 3/2 0.3 Lap Joints

Fatigue life

The effect of the rivet squeeze force on the fatigue life of a Glare 3 3/2 0.3 lap joint (without doublers) is shown in figure 8. At the lowest squeeze force used (13.5 kN), the fatigue was just over 200 kcycles. When a higher squeeze force was used, the fatigue life of the lap joint increased. At an average squeeze force of 20 - 22 kN, the average fatigue life is approximately 850 kcycles. At 26 kN, the lap joint fails after 1800 kcycles.

Initiation

From the fatigue life data it is evident that the rivet squeeze force has a significant effect on the fatigue life of the lap joint. This can be explained by the fatigue behaviour of the different aluminium layers in the Glare sheet. When the initiation lives of the three aluminium layers in Glare 3 3/2 0.3 are compared for each rivet squeeze force (figure 9), it appears that the initiation lives of especially layers 2 and 3 in the top row (figure 10) increased significantly with an increasing rivet squeeze force. The squeeze force did not alter the initiation behaviour of layer 1 considerably, which is in contradiction with layers 2 and 3. However, the initiation in the faying aluminium layers is, besides the squeeze force, affected by bending imperfections due to squeezing [1], which oppose the beneficial effect of the rivet squeeze force. In the top row, at the lowest squeeze force, initiation in layers 2 and 3 occurred simultaneously, while at higher squeeze forces initiation in these layers occurred sequentially. In the bottom row, the increase in initiation life of layer 2 is not as large as in the top row, however, initiation in layer 3 was not detected before failure of the top row.

The Glare 3 3/2 0.3 lap joint riveted with a squeeze force of 36 kN outlives the aluminium lap joint riveted with the same squeeze force. The aluminium lap joint failed after approximately one million cycles (80 MPa), whereas the Glare lap joint sustained 1.5 million cycles (124 MPa) without failure. Inspections showed that layer 1 (in both the top and the bottom row) was broken, and some small indications of fatigue cracks were found in layer 2 of the bottom row.

Fatigue Crack Growth

The crack growth in the top row of the Glare sheet is shown in figure 10 for two different squeeze forces. The crack growth in the sheet with the 15.6 kN rivet squeeze force was higher than in the sheet with the 22 kN rivet squeeze force. The early initiation in layers 2 and 3 caused a higher crack growth rate in all layers, when compared to the 22 kN squeeze force, where the initiation lives were further apart. In the 15.6 kN lap joint, the cracks in the different layers affected each other causing a higher crack growth rate, and a relatively early failure was the result. In the bottom row simultaneous crack growth did not occur for the 22 kN squeeze force, causing a lower average crack growth rate when compared to the 15.6 kN squeeze force. A higher squeeze force not only has a positive effect on initiation, but also on crack growth in the separate layers: simultaneous crack growth in the aluminium layers is prevented. In both samples the crack growth did not become unstable.

In the barrel, where the differential pressure causes a more realistic load condition, a lap joint riveted with a squeeze force of 22 kN was investigated. 22 kN is believed to be a minimum for acceptable fatigue and residual strength capabilities of Glare 3 3/2 0.3 lap joints. The crack growth rates in the lap joint in the barrel were higher than those in the flat panel. In the top row, initiation in layer 2 and 3 occurred earlier than in the flat coupon (figure 11). This can be explained by the lower squeeze force in combination with the hole quality. With lower squeeze forces large radial and tangential compressive stresses and large clamping forces do not occur. This can result in earlier fatigue crack initiation at the hole edge. If the rivet hole diameter or the hole quality fluctuates along the rivet row, the crack initiation life can be different for different holes. For larger squeeze forces (not performed with the barrel because it was desired to investigate a lower threshold) the peak stress in the vicinity of the rivet has a larger effect on crack initiation than the quality of the hole. Nonetheless, the crack growth rate in the lap joint in the barrel remained low: unstable crack growth did not occur. In the bottom row of the barrel initiation in layer 2 also occurred earlier than in the flat coupon (22 kN rivet squeeze force), and the crack growth rate in layer 1 was higher than in the flat coupon. At the time that the residual strength test of the sample in the barrel was performed, cracks in layer 3 of the bottom row were not found.

Failure of the glass fibres did not occur immediately after all aluminium layers were broken. Failure of the fibres occurred several thousands of cycles later during which the fibres were able to transfer the load through the lap joint. Apparently, the glass fibres in the prepreg layer remain intact during fatigue loading.

Assuming that crack initiation occurs at the first fatigue cycle, e.g., as a result of poor rivet installation conditions, the Glare lap joint outperforms the aluminium lap joint for the used configurations and fatigue stresses. This will have significant consequences for the inspection intervals.

2.3 MSD in Monolithic Aluminium and Glare Lap Joints

Multiple Site Damage (MSD), which causes tremendous problems in ageing aircraft, was seen in each sample of the 2024-T3 lap joint. The rivet squeeze force did not have an effect on MSD or the fatigue crack growth life, it only changed the initiation life. MSD in aluminium lap joints leads to hazardous situations if remained undetected (Aloha accident), however, it is difficult to detect the many small cracks that cause a rapid decrease of the residual strength and unstable crack extension.

Also in a Glare lap joint MSD occurs, however, it is by far not as dangerous as in monolithic aluminium lap joints. An important difference between the two materials: in monolithic aluminium the cracks grow through the thickness, whereas the cracks in Glare need to re-initiate in the remaining layers after they have initiated in the faying aluminium layer. The rivet installation conditions are important for aluminium 2024, but for Glare it cannot only increase the crack free life, but also the crack growth life (i.e. fail safe performance) by postponing the re-initiation. As a result the fatigue damage in Glare stays in

one layer only for a substantial amount of cycles. Furthermore, the non-critical cracks in layer 1 are as well detectable and inspectable with the eddy current NDI techniques as the through the thickness cracks in monolithic aluminium, and crack growth remains controlled.

In figure 12, the development of MSD in the Glare lap joint that was tested in the barrel is shown for the bottom row. The first fatigue cracks were detected after 33 kcycles. At 90 kcycles all critical locations showed fatigue cracks. At that moment the crack lengths ranged from 2 mm to 4 mm. At 210 kcycles the first link up was detected, and at 230 kcycles cracks in layer 2 had initiated. After 370 thousand fatigue cycles two layers broken and fatigue cracks in layer 3 could not be found.

In the top row of the lap joint in the barrel (figure 13), initiation took place in the faying layer after 70 kcycles. This increased number of cycles is related to bending imperfections when identical residual stresses due to squeezing are assumed in the mating aluminium layers. After 290 kcycles the first link ups were detected, after which the numbers of link ups steadily grew until the faying aluminium layer was almost completely broken after 310 kcycles. The middle aluminium layer of the top Glare sheet showed small fatigue cracks at a fatigue life of 170 kcycles, which is relatively early. Additional fatigue cracks were detected at 250 kcycles. At a fatigue life of 370 kcycles four link ups were present, and long cracks existed at several other locations. Layer 3 also initiated after 170 thousand pressurization cycles. After 310 kcycles, cracks at other locations were found. Four link ups were present in the outer aluminium layer at the exact same locations as the link ups in layer 2 were found. This "serious" damage was easily detectable and it did not cause unstable crack growth.

3. Residual Strength of the Glare 3 3/2 0.3 Lap Joint

3.1 Test Data

The residual strength of the lap joint showed an almost linear decrease with an increasing damage (detected with the eddy current inspection method), as shown in figure 14. The decrease of the residual strength with the fatigue life is shown in figure 15 for both the 22 kN and the 36 kN rivet squeeze force. The static strength of the investigated lap joint is about 2.9 times the fatigue limit. It is assumed that small cracks (< 4 mm) in layer 1 do not affect the residual strength very much. When two of the three aluminium layers are cracked, the residual strength just drops below twice the fatigue stress. This damage is easily detectable, but difficult to obtain during a normal aircraft design life when a high enough rivet squeeze force is used.

At a rivet squeeze force of 22 kN, a situation where two layers are broken occurs after roughly 700 kcycles (figure 15), however, in the barrel this situation was obtained after already 370 kcycles. The residual strength of the bottom row at this point was higher than 2.07 times the fatigue load, when the top row failed (see also figure 14). Based on 3,000 flights per year, it takes more than a 100 years to obtain such a damage size. The serious fatigue damage in the top row (see previous section) was successfully contained at more than twice the fatigue load.

3.2 Residual Strength Calculation

In addition to the test data, it is desirable to have a model that predicts the residual strength at different stress levels and other configurations. However, a tool obtained by analysis predicting the residual strength is not available yet. The prediction model is based on the blunt notch strength or, as an alternative, the lap joint's static strength.

Glare is a complex material. The combination of monolithic aluminium and unidirectional glass fibres causes problems in the analysis: the glass fibres (which stay intact during fatigue loading) remain elastic

until failure, whereas the aluminium layers are yielding at a given stress. Furthermore, the rivet holes result in a severe stress concentration due to by-pass and pin loading, which make the elastic behaviour of the fibres complex. The stresses in the aluminium layers do not increase very much after the onset of yielding, and as a result the glass fibres take over a considerable part of the load. The glass fibres break at a strain of approximately 5%. When the fibres break, the stresses in the aluminium layer (which were below the failure stress of the aluminium so far) suddenly increase, causing failure of the sheet.

With the residual strength data from the previous section, it should be possible to obtain an empirical equation estimating the residual strength at a given fatigue damage in the lap joint. The first step is that the forces carried by the fibre and the aluminium layer equals the applied force:

$$F_{fi} + F_{al} = F_{tot} \qquad 3\text{-}1$$

where

F_{fi} is the force transferred by the fibre layers,
F_{al} is the force transferred by the aluminium layers, and
F_{tot} is the total applied force on the sheet.

This equation can be rewritten:

$$\sigma_{fi} \left(\frac{t_{fi}}{t_{tot}}\right) + \sigma_{al} \left(\frac{t_{al}}{t_{tot}}\right) = \sigma_{tot} \qquad 3\text{-}2$$

where

s_{fi} is the stress in the fibre layers,
t_{fi} is the total thickness of the load carrying fibre layers ('one fibre layer', 0.25 mm for Glare 3 3/2 0.3 because it is a cross-ply)
s_{al} is the stress in the aluminium layers
t_{al} is the total thickness of the aluminium layers ('one aluminium layer', 0.9 mm for Glare 3 3/2 0.3)
s_{tot} is the average stress in the laminate and
t_{tot} is the total thickness of the laminate (1.4 mm for Glare 3 3/2 0.3).

This equation cannot be solved without estimating the stresses in the fibre and the aluminium layer at the time of failure. Therefore, it is assumed that the strain in both the aluminium layer and the fibre layer are equal at the time of failure (5%). At a strain of 5% the stress in the aluminium is approximately 425 MPa (*net* stress). For s_{tot} the gross blunt notch strength with the same W/d as the lap joint (W/d = 5) can be used, which is 400 MPa gross stress. The 5% strain net stress in the aluminium must be converted to gross stress: 425/1.25 MPa (W/d = 5: W/(W-d) = 1.25). These numbers result in a gross failure stress in the glass fibre layer of 1020 MPa. This can also be done using the static strength of the lap joint, which is 355 MPa (gross stress). This gives a gross failure stress of the glass fibre layer of 760 MPa.
With these data equation (2) for a Glare 3 3/2 0.3 sheet looks like:

$$\sigma_{res} = \left(\sigma_{fi,u} \left(\frac{0.25}{1.4}\right) + \sigma_{al2024,\ 5\%\ strain} \left(\frac{t'}{1.4}\right)\right) \qquad 3\text{-}3$$

where

$s_{fi,u}$ is the net failure stress in the prepreg and depends on the method used (blunt notch strength or lap joint static strength),
$s_{al2024,\ 5\%\ strain}$ is 425/1.25 = 340 MPa, and
t' is the virtual thickness, calculated by:

$$t' = \frac{(t_{\text{aluminium layer}} * (N_L * (W - N_H * d) - l_{\text{total detected crack length}}))}{(W - N_H * d)} \qquad 3\text{-}4$$

where

$t_{\text{aluminium layer}}$	is the thickness of one aluminium layer in the Glare sheet,
N_L	is the number of aluminium layers in the Glare sheet (three in Glare 3 3/2 0.3)
W	is the width of the coupon or area of interest,
N_H	is the number of holes across the width of the coupon,
d	is the hole diameter (4.8 mm) and
$l_{\text{total detected crack length}}$	is the total crack length detected in all aluminium layers in the Glare sheet (rivet holes excluded).

After comparing the calculated data with the test data, it appeared that the blunt notch based calculation predicted the strength 7% too high (on average), and that the lap joint static strength based calculation was 9% too low (on average). Therefore, the blunt notch based model was divided by 1.07, whereas the lap joint static strength based model was multiplied by 1.09. After these modifications the model based on the blunt notch strength, calculating the gross residual strength, looks like:

$$\sigma_{\text{res., blunt notch}} = (170 + 227 * t') \text{ MPa} \qquad 3\text{-}5$$

The modified model based on the lap joint's static strength, also calculating the gross residual strength, is as follows:

$$\sigma_{\text{res., lap joint}} = (148 + 265 * t') \text{ MPa} \qquad 3\text{-}6.$$

Previously obtained residual strength data of the same lap joint were used to verify both models. These samples were fatigue tested at several different fatigue stresses. It showed that the blunt notch based model gave more accurate predictions than the lap joint static strength based model (figure 16).

Apparently, the fatigue does not significantly influence the residual strength. Furthermore, the different squeeze forces do not have an effect on the residual strength of the damaged lap joint. This means that additional correction factors are not necessary. The model works independently from those variables. When the crack growth rate is known, the residual strength as a function of cycles can be calculated.

Scatter can occur due to delaminations, wrong crack length measurements or the residual strength calculation itself. At quite large or very small damage sizes the prediction is expected not to be very accurate.

4. Conclusions

1. Crack initiation is postponed with higher rivet squeeze forces for monolithic aluminium riveted lap joint up to a factor of five within allowable driven head dimensions. For Glare, not only fatigue crack initiation in each individual layer is postponed by a higher squeeze force, but also the crack growth life.

2. When MSD is present in monolithic aluminium lap joint, crack growth becomes unstable at small crack lengths (2 - 5 mm). In contrast to aluminium the crack growth rate in Glare is low and remains stable until failure, despite the presence of MSD. The need for finding small cracks in aluminium lap

joints can be relaxed for Glare lap joints. Cracks in Glare are easily detectable. Substantial damage sizes do not cause a hazardous situation because the fibres can carry the load and do not fail during fatigue loading.

3. The fatigue life of the lap joint in the reduced scale barrel is half the fatigue life of a flat coupon. A 10% higher stress level for the coupon probably results in a comparable fatigue life for the barrel and the coupon.

4. For Glare, the residual strength is linearly related to crack length. Therefore, a sudden drop in strength will not occur during the fatigue life. Higher squeeze forces give a smaller decrease in residual strength with an equal amount of cycles. The residual strength test in the barrel showed that when two layers of the Glare 3 3/2 0.3 are broken, the residual strength is still higher than twice the fatigue load.

5. The residual strength of Glare riveted lap joints can be estimated. Despite linear assumptions the accuracy is within 10%.

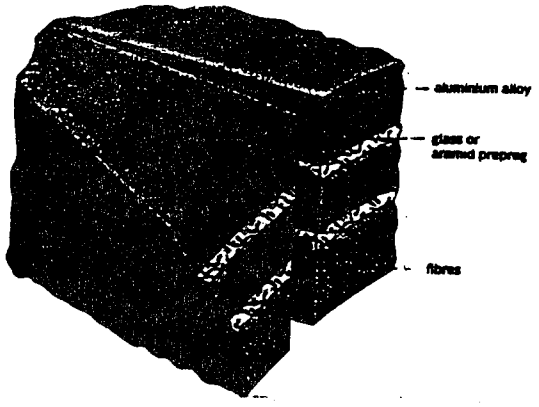
References

[1] Müller, R.P.G., Borsboom, C. Heerschap, M.E., Mahardika, M. " Fatigue Crack Initiation, Growth and Residual Strength Characteristics of Riveted Fibre Metal Laminate Lap Joints", to be published, Delft University of Technology, Delft

[2] Borsboom, C., "Damage Tolerance of Glare Lap Joints in Pressurized Fuselage Structures -- The Effect of the Rivet Squeeze Force on the Fatigue Behaviour", Master Thesis, Structures and Materials Laboratory, Faculty of Aerospace Engineering, Delft University of Technology, Delft, August 1994

[3] Müller, R.P.G., "Secondary Bending Analysis of Glare Riveted Lap Joints - An analytical and experimental comparison of lap joint deformation in flat coupons, a reduced scale barrel test set-up and a full scale barrel test set-up", Delft University of Technology, Faculty of Aerospace Engineering, Delft, The Netherlands

[4] Borsboom, C, "Eddy Current Testing of Fibre-Metal Laminates", Structural Laminates Company, Technical Report TD-R-93008, Delft, The Netherlands, June 1993



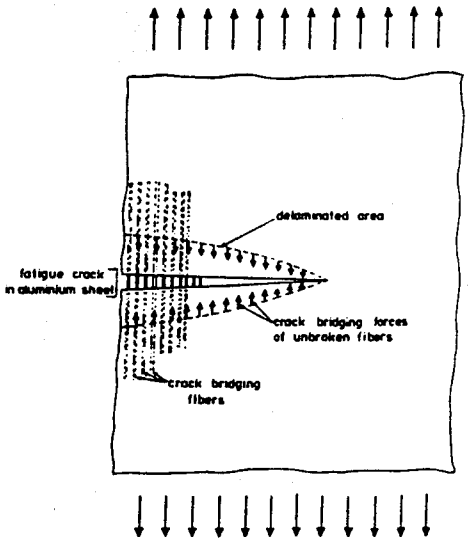


Figure 1 Crack bridging in Glare 3 3/2-0.3

(3-D view & plane view)

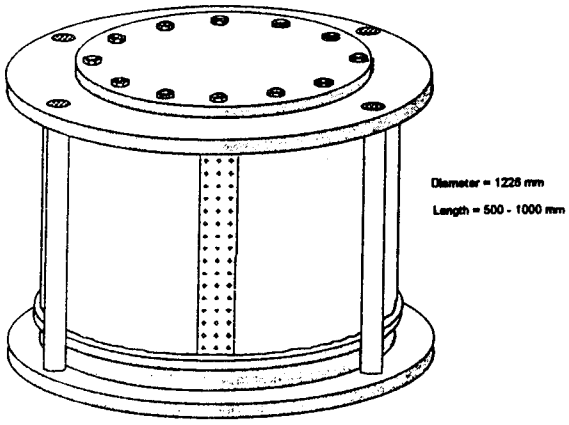


Figure 2 Picture of the barrel test set-up with a lap joint

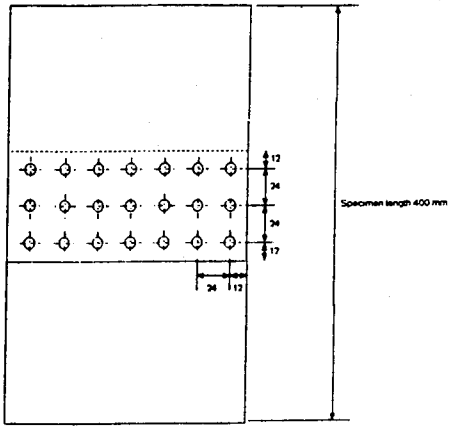


Figure 3 Geometry of a flat coupon containing a lap joint

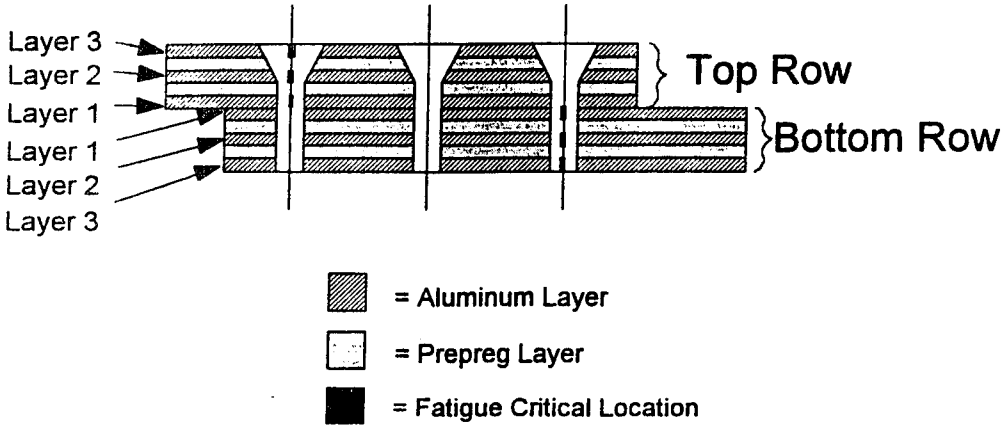


Figure 4 The layer definition for the fibre metal laminate Glare 3 3/2-0.3 with a lap joint

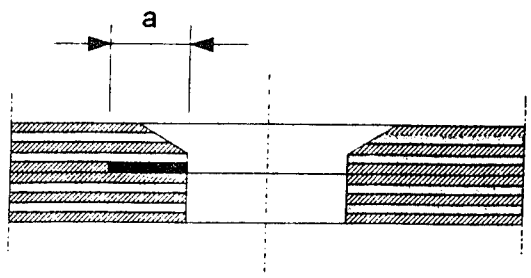


Figure 5 Crack length definition in Glare riveted joints

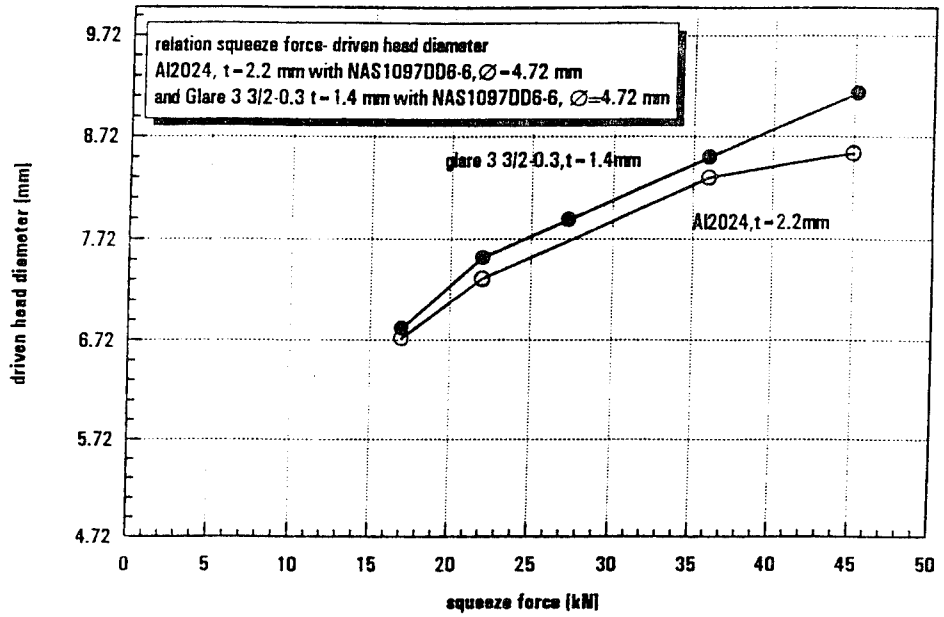


Figure 6 Relation between squeeze force and driven head diameter

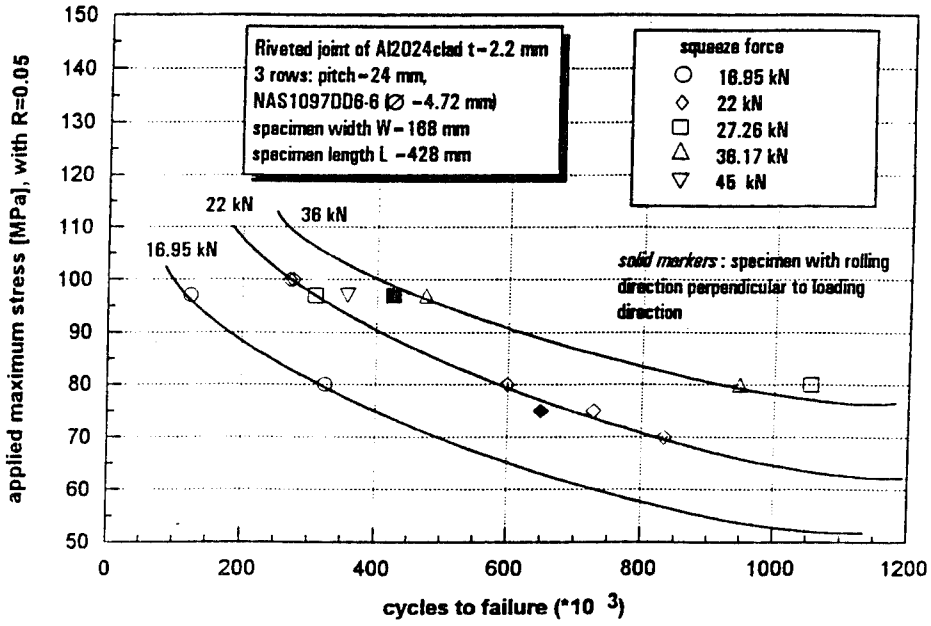


Figure 7 S-n curves for Al2024 lap joint couponsfor different squeeze forces

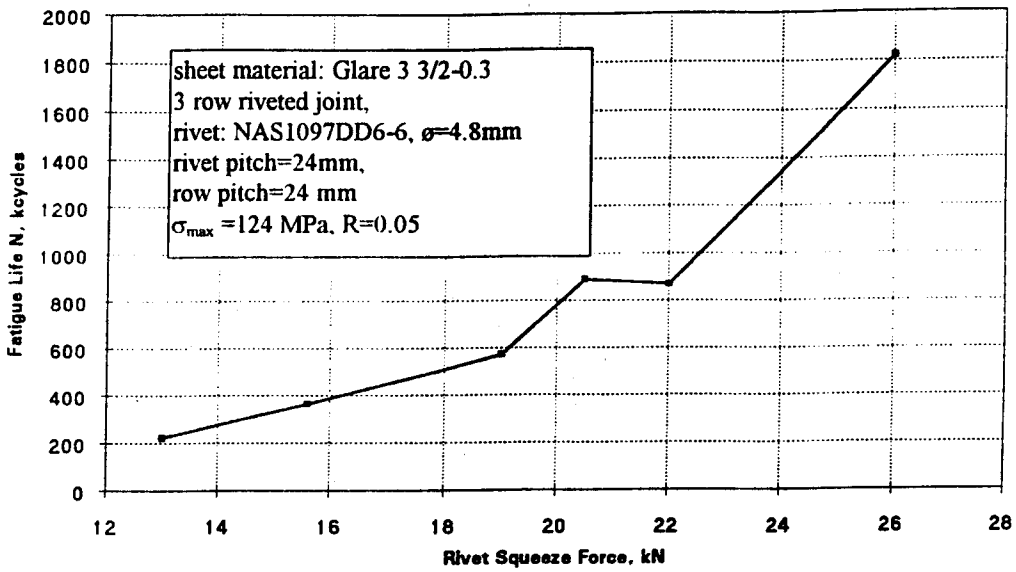


Figure 8 The effect of the rivet squeeze force on the fatigue life of Glare 3 3/2-0.3 riveted lap joints

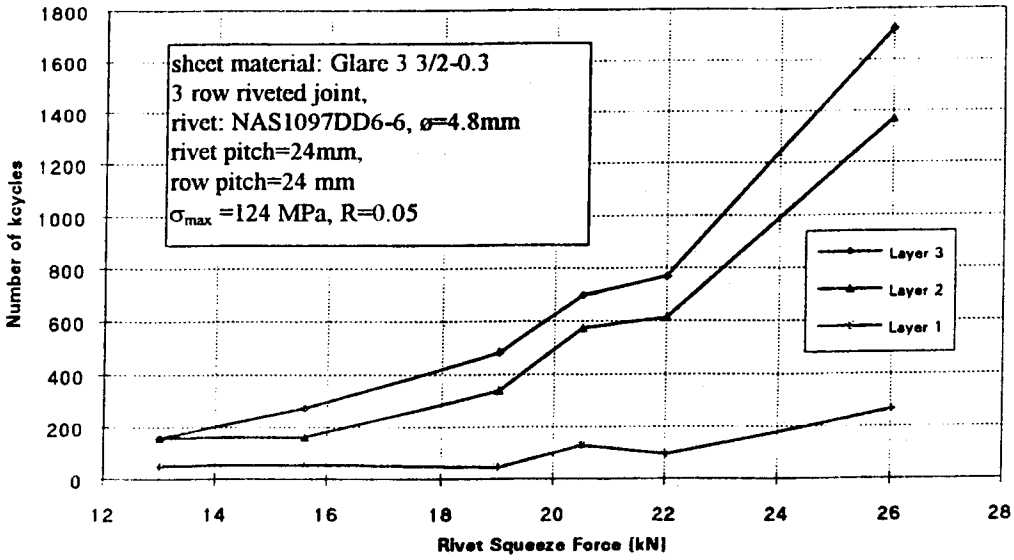


Figure 9 The effect of the rivet squeeze force on the fatigue crack initiation in the individual aluminium layers of the top row

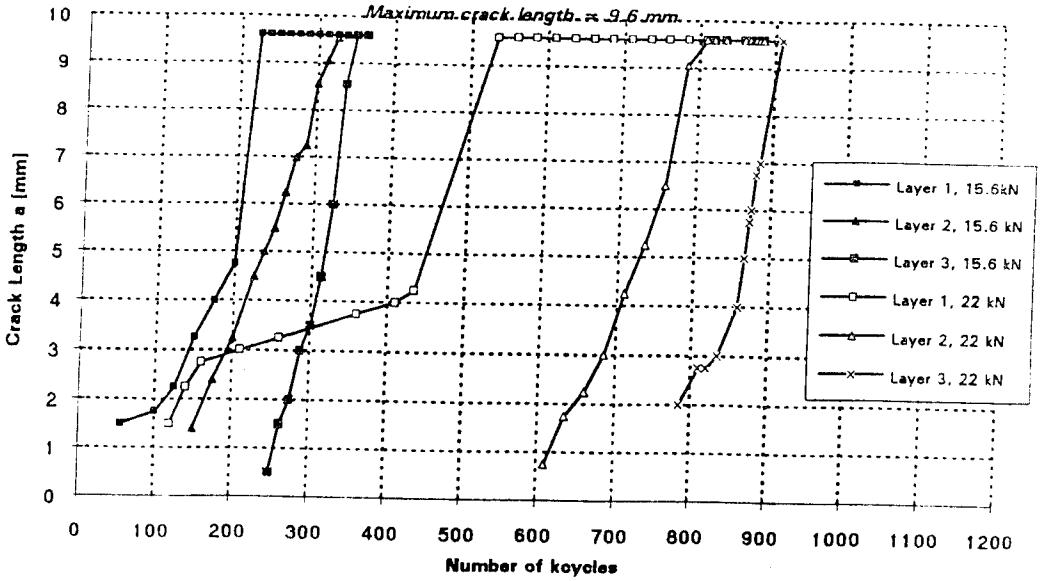


Figure 10 The effect of the rivet squeeze force on the crack growth behaviour in the top row of Glare riveted joints (for dimensions see fig. 31)

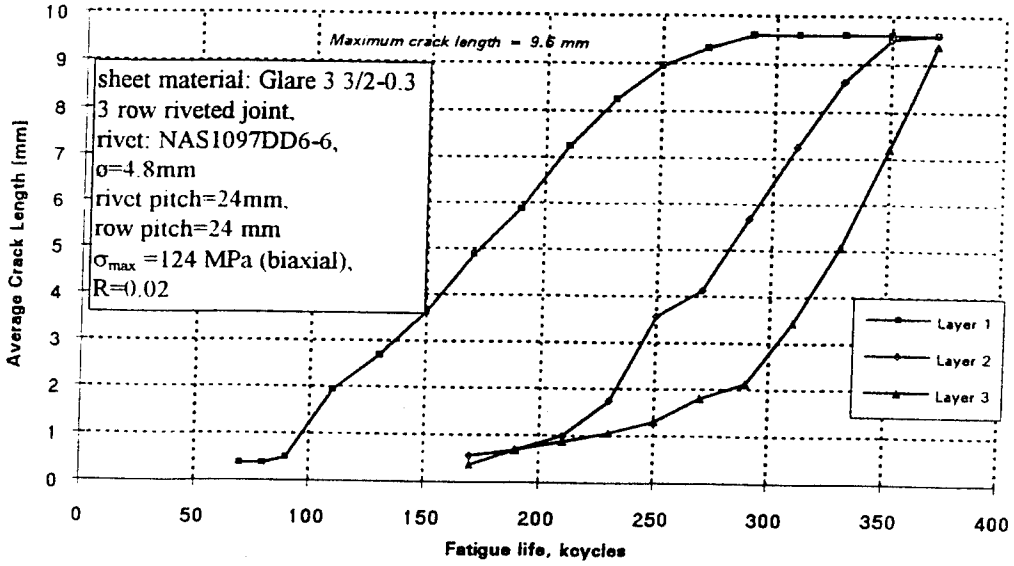


Figure 11 Crack growth in the top row of the lap joint in the reduced scale barrel test set-up

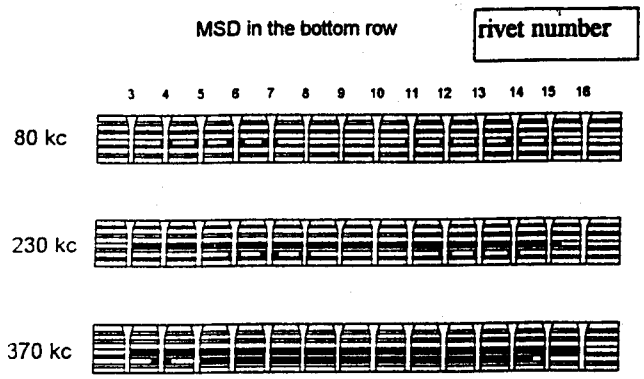


Figure 12 Crack lengths in the bottom row of the riveted joint at different number of cycles

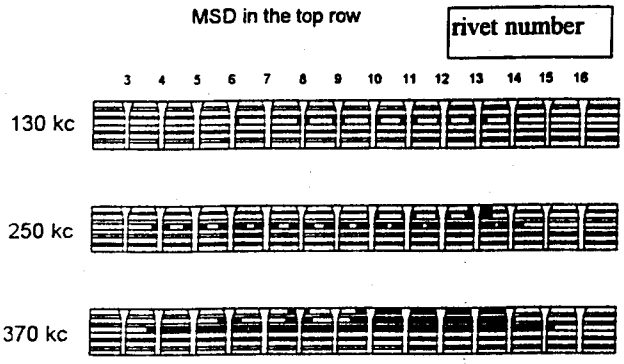


Figure 13 Crack lengths in the top row of the riveted joint at different number of cycles

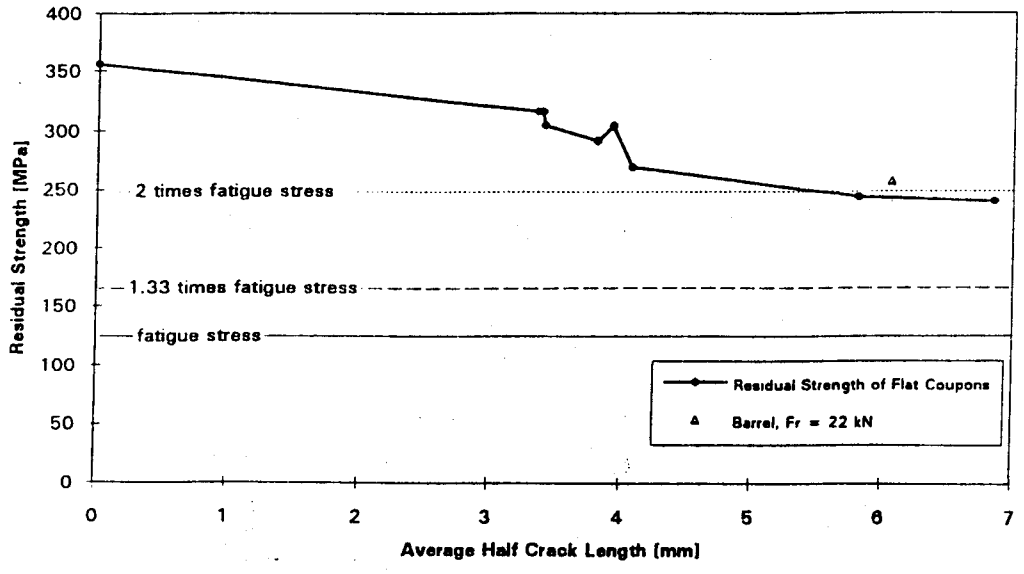


Figure 14 Residual strength of a Glare 3 3/2-0.3 riveted lap joint as function of detected fatigue damage (for dimensions see figure 35)

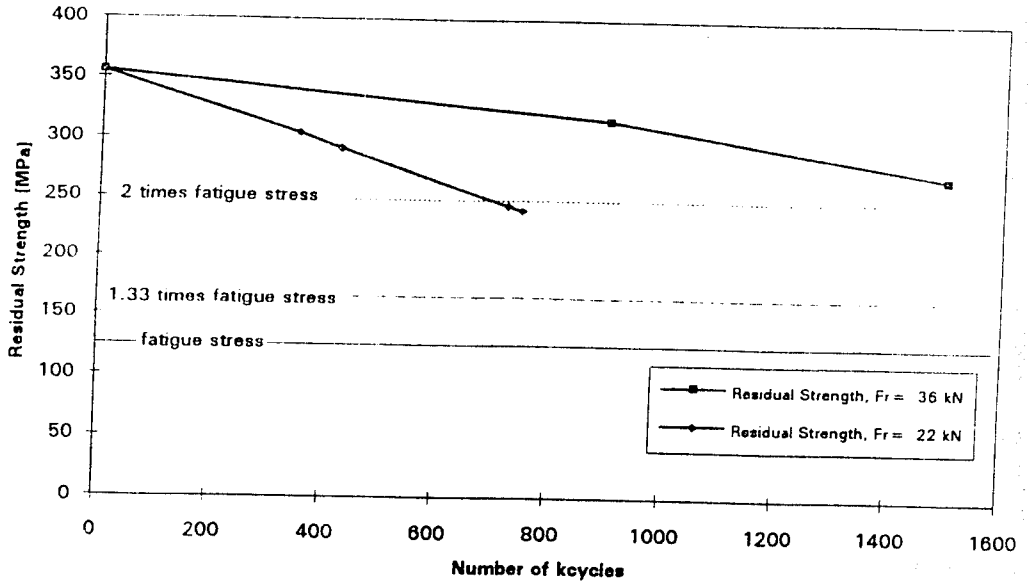


Figure 15 Residual strength as a function of the fatigue life and rivet squeeze force of a Glare riveted joint (for dimensions see figure 35)

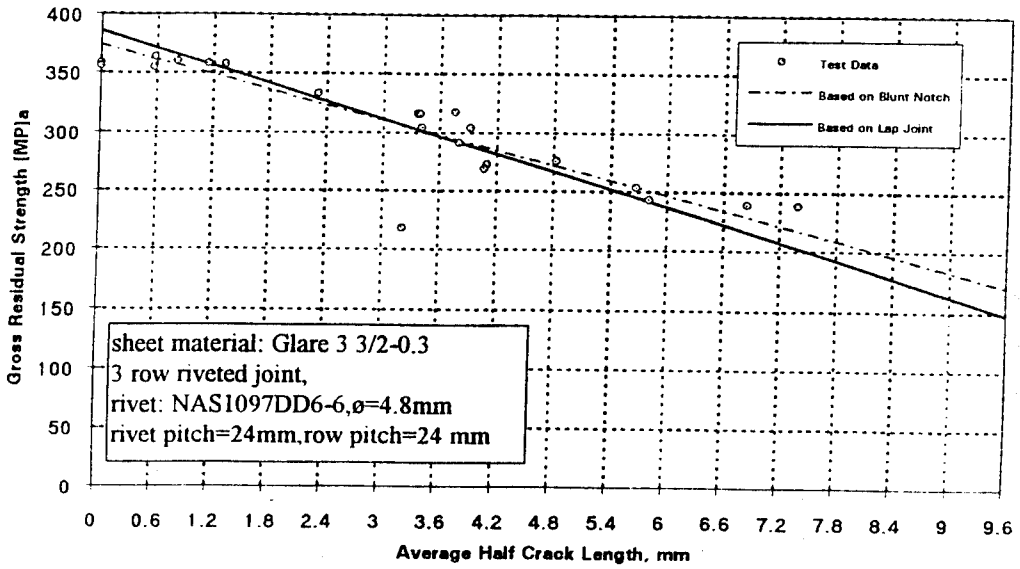


Figure 16 Residual strength calculations compared to test data

SESSION VI

FORCE MANAGEMENT

Chairman: *J. Turner*, SA-ALC/LADD

"Embedded Optical Fiber Sensors for Airframe Repair Health Monitoring"

Research and Development to Ensure Composite Repair Integrity

W. Sproat and D. Szalwinski, Lockheed Aeronautical Systems Co.
J. Sirkis and C. Chang, University of Maryland

A Project Associated With:
Lockheed Independent Research and Development
USAF C-141 Aircraft Structural Integrity Program
The University of Maryland Department of Mechanical Engineering



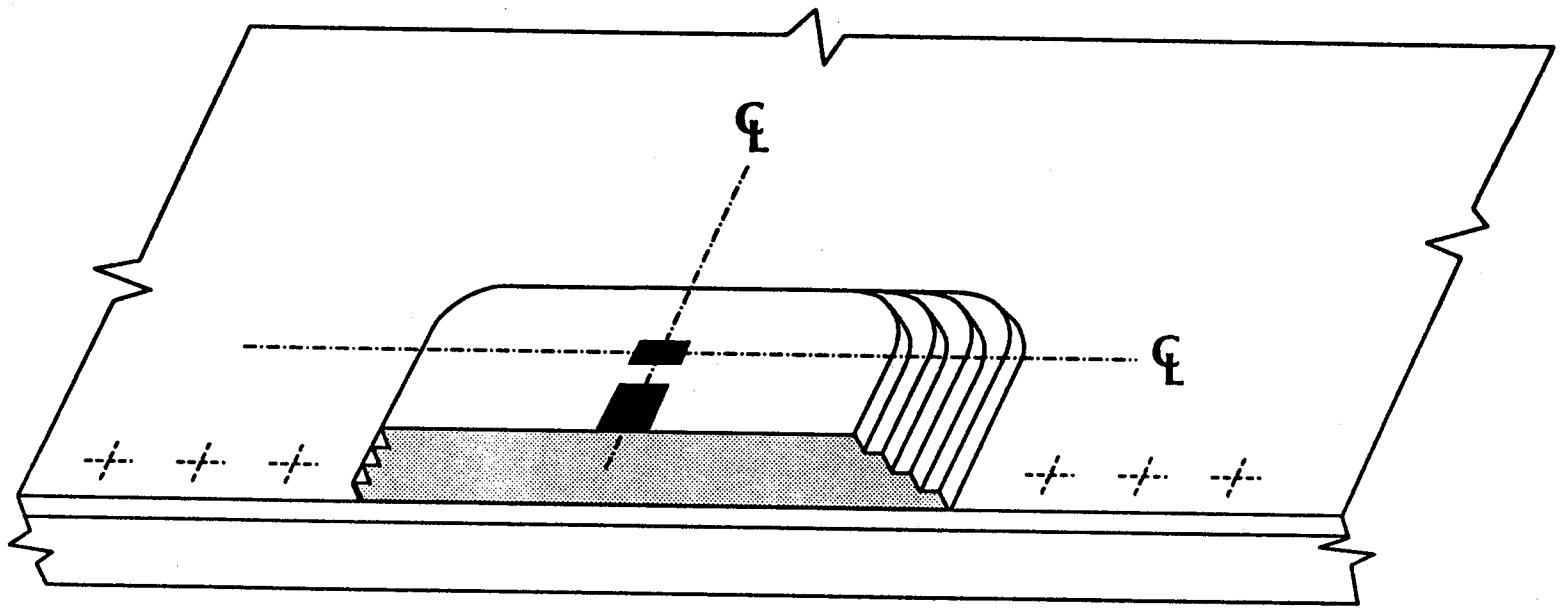
Lockheed Aeronautical Systems Company

A015-01
10-27-94

Overview

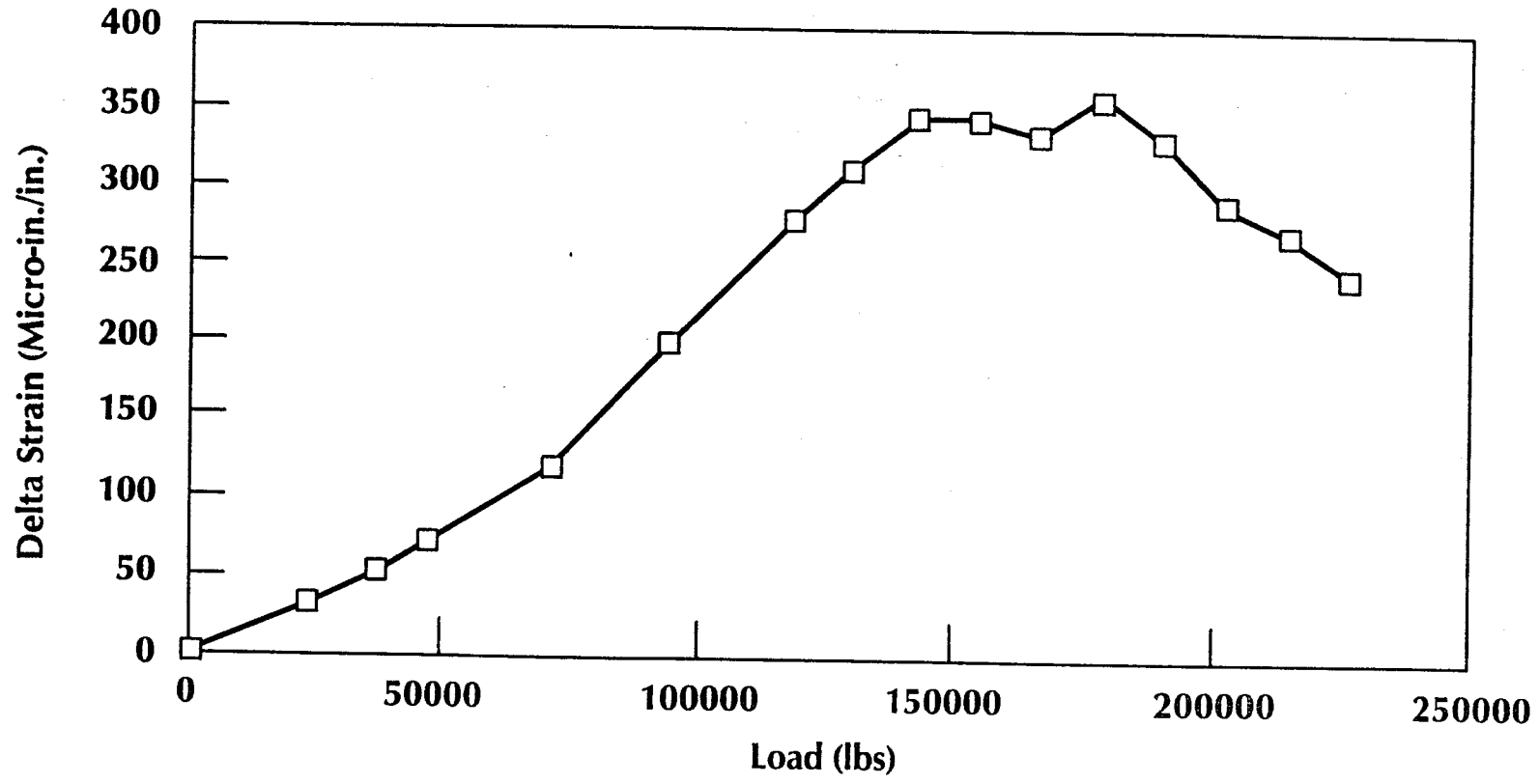
- Boron/Epoxy Repairs to Damaged Structure
- Repair Integrity and Strain Behavior
- Optical Fiber Design Features and Characteristics
- Optical Fiber Strain Sensor Advantages
- Sensor Instrumentation and Theory
- Test Results
- Application Concepts
- Conclusions and Development Status

Boron/Epoxy Repaired Wing Splice Element With Surface Mounted Resistance Strain Gages to Monitor Load Transfer



A015-03
10-27-94

Plot of Boron/Epoxy Doubler Edge and Center Strain Difference As a Function of Static Load



A015-04
10-28-94

Illustrations of Sensor Design and Behavior

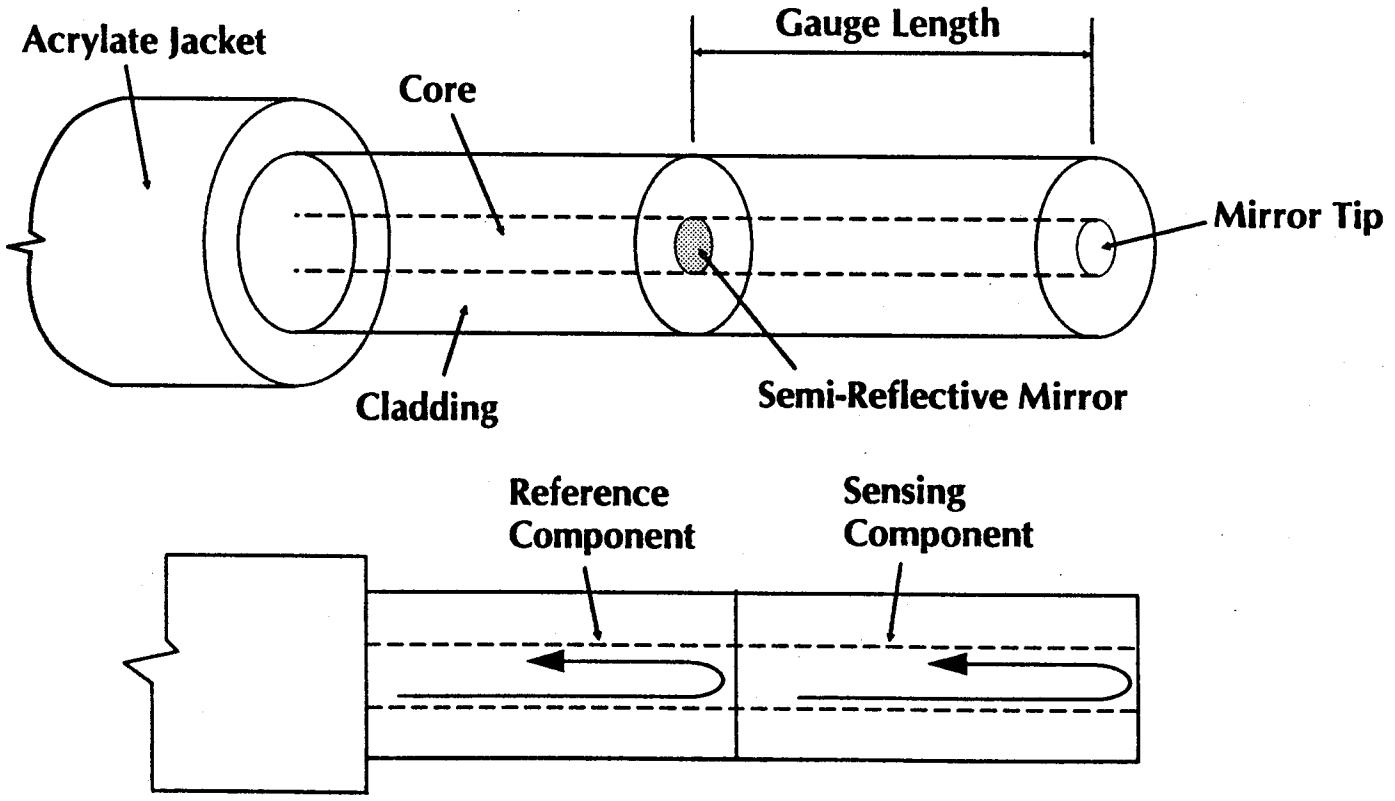


Figure 1. Intrinsic Fabry-Perot Sensor [Valis et al. (1989)]

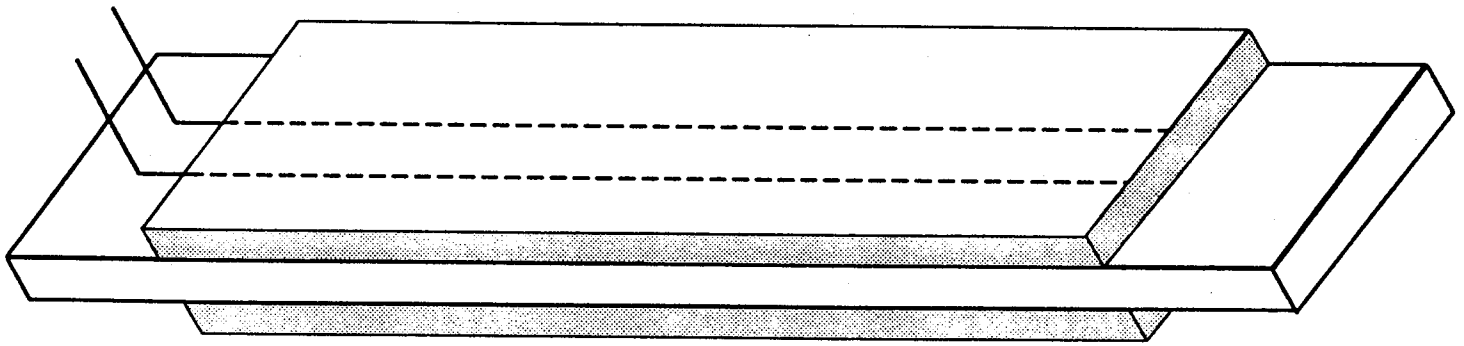
A015-05
10-28-94

Optical Fiber Strain Sensor Advantages

- Embedded Without Altering Material Properties
- Memory Feature "Records" Peak Values
- No Electrical Hazard in Fuel Environment
- Numerous Sensitivity, Gage Length, and Configuration Options
- Remains Calibrated, No Drift
- Building Blocks of "Smart Structures"

A015-06
10-27-94

Concept Trial Specimen, Single Edge Notch "Repaired" Aluminum Fatigue Coupon With Sensors Embedded in the Bondline



A015-07
10-27-94

Sensor Instrumentation Diagram

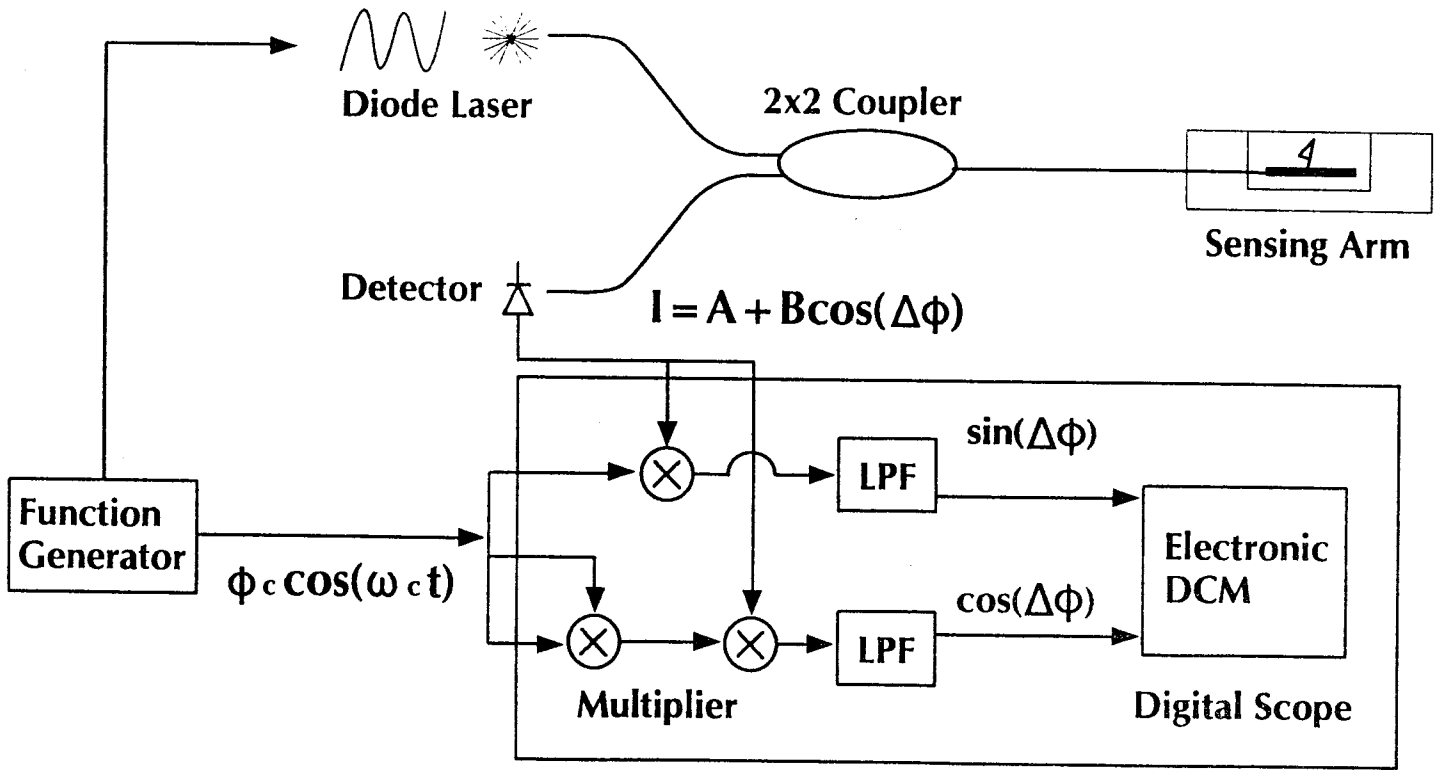


Figure 3. Synthetic Heterodyne Technique and Electronic DCM by Using an Intrinsic Fabry-Perot Sensor

A015-08
10-31-94

Transducer Scheme

- An Optical Fiber Interferometer Converts Displacement of a Fiber End Into Phase Information
- The Intrinsic Fabry-Perot Configuration Offers Single Fiber Interferometer Reference and Sensor Arm
- Elongation of the Sensor Arm Induces Optical Phase Changes
- Demodulation Uses a Differential Cross-Multiplier Technique To Attain a High Dynamic Range
- Instrumentation Provides Voltage Output Proportional to Strain

A015-09
10-27-94

Communication Theory Math Model

$$\phi = \frac{2\pi nL}{\lambda} = \frac{2\pi n\nu}{c} \tag{1}$$

$$\Delta\phi = 2\pi\left(\frac{n}{\lambda}\Delta L + \frac{L}{\lambda}\Delta n + \frac{nL}{c}\Delta\nu\right) \tag{2}$$

$$I = A + B\cos\left(\phi_c \cos(\omega_c t) + \phi(t)\right); \tag{3}$$

$$I = A + B\{[J_0(\phi_c) + 2\sum_{k=1}^{\infty}(-1)^k J_{2k}(\phi_c)\cos(2k\omega_c t)]\cos(\phi(t)) - [2\sum_{k=0}^{\infty}(-1)^k J_{2k+1}(\phi_c)\cos((2k+1)\omega_c t)]\sin(\phi(t))\} \tag{4}$$

A015-10
10-31-94

Communication Theory Math Model

$$I_{\omega_c} = BJ_1(\phi_c)\sin(\phi(t));$$ (5)

$$I_{2\omega_c} = -BJ_2(\phi_c)\cos(\phi(t)).$$ (6)

$$I_3 = -I_{\omega_c}\frac{dI_{2\omega_c}}{dt} + I_{2\omega_c}\frac{dI_{\omega_c}}{dt} = BJ_1(\phi_c)(\cos^2\Delta\phi + \sin^2\Delta\phi\ \frac{d\Delta\phi}{dt} = BJ_1(\phi_c)\frac{d\Delta\phi}{dt}.$$ (7)

$$\Delta\phi = \frac{1}{I_0 A}\int I_3\,dt;$$ (8)

A015-11
10-31-94

Test Results

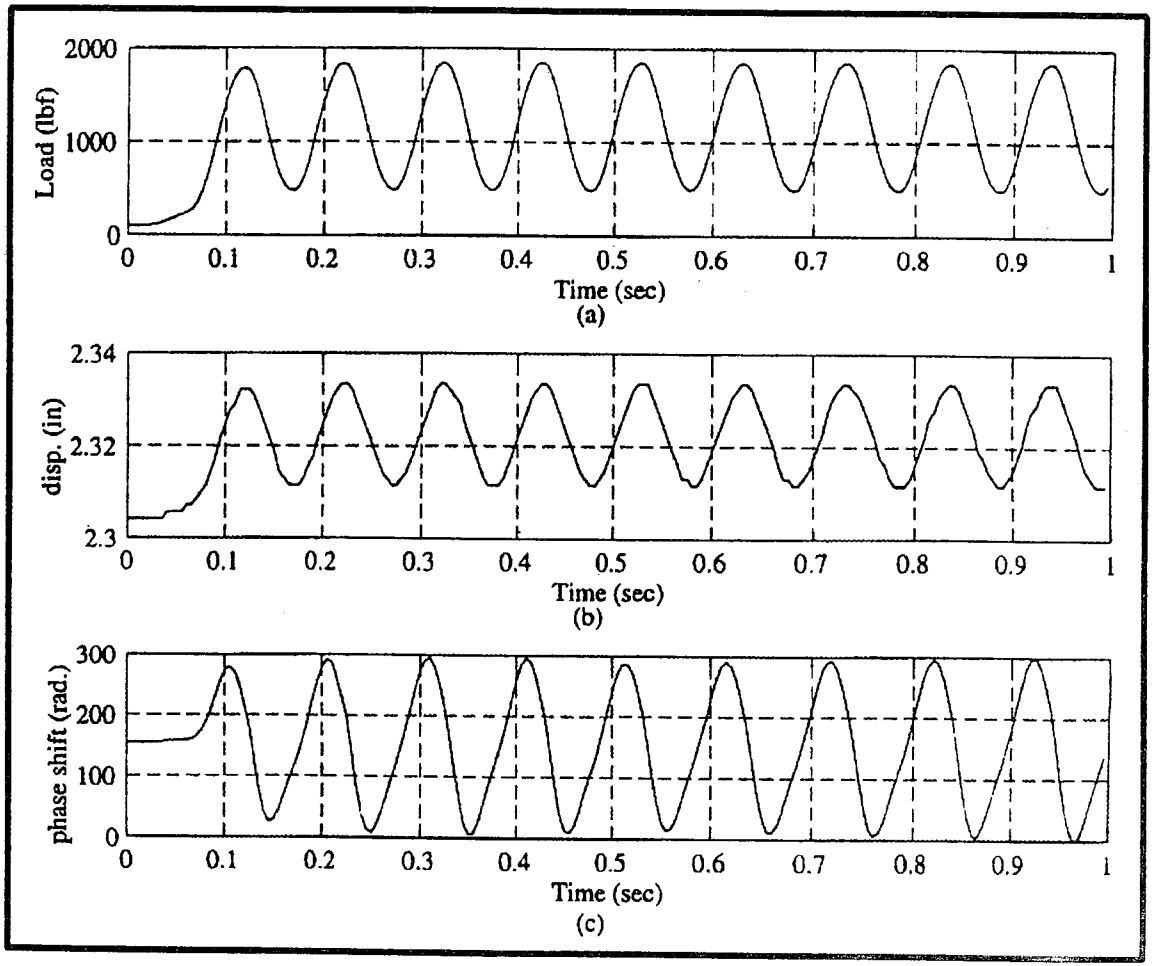
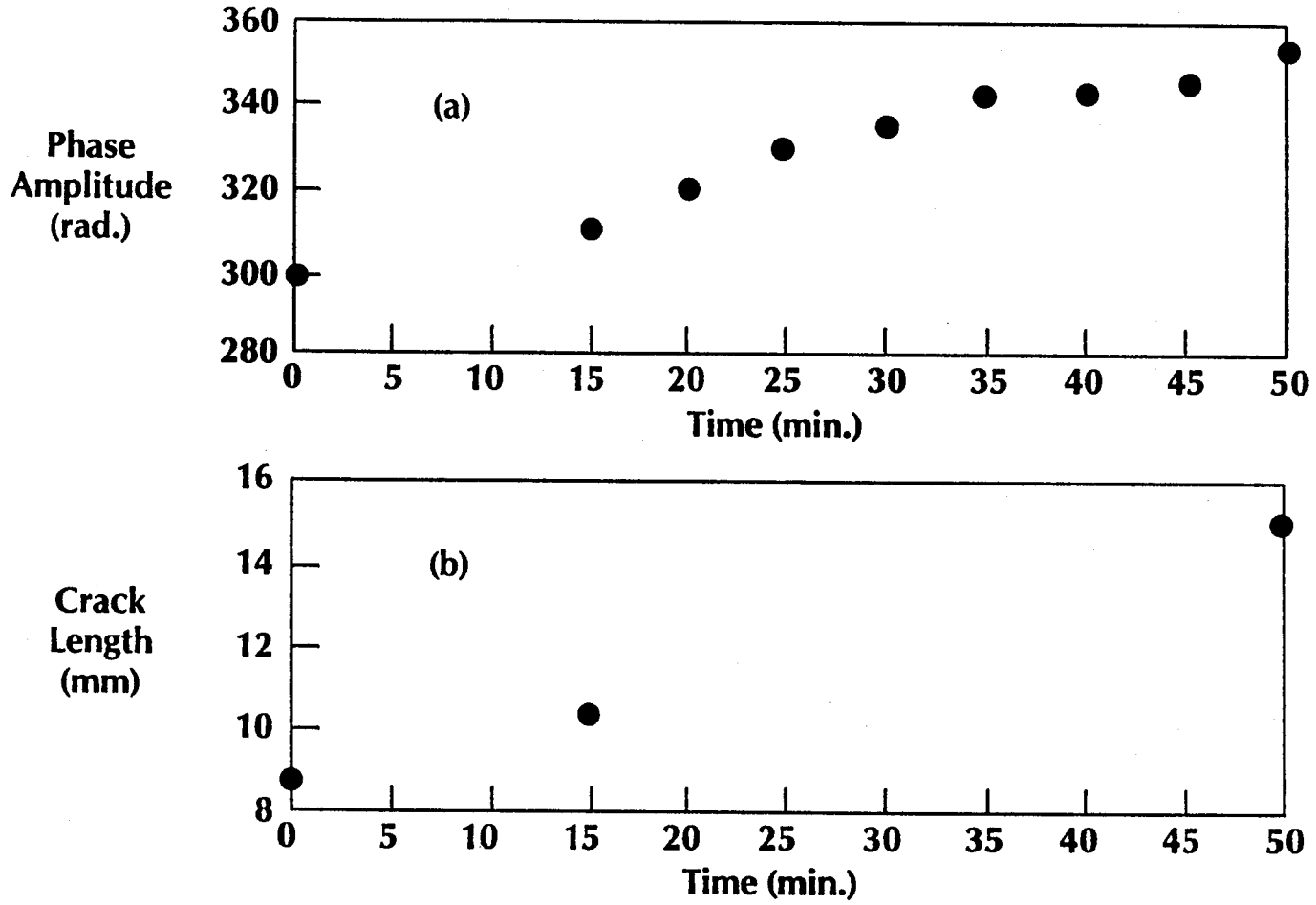


Figure 4. Load, Displacement, and Phase Shift vs Time Traces

A015-12
10-27-94
Opt 6-4B

Test Results



A015-13
10-31-94

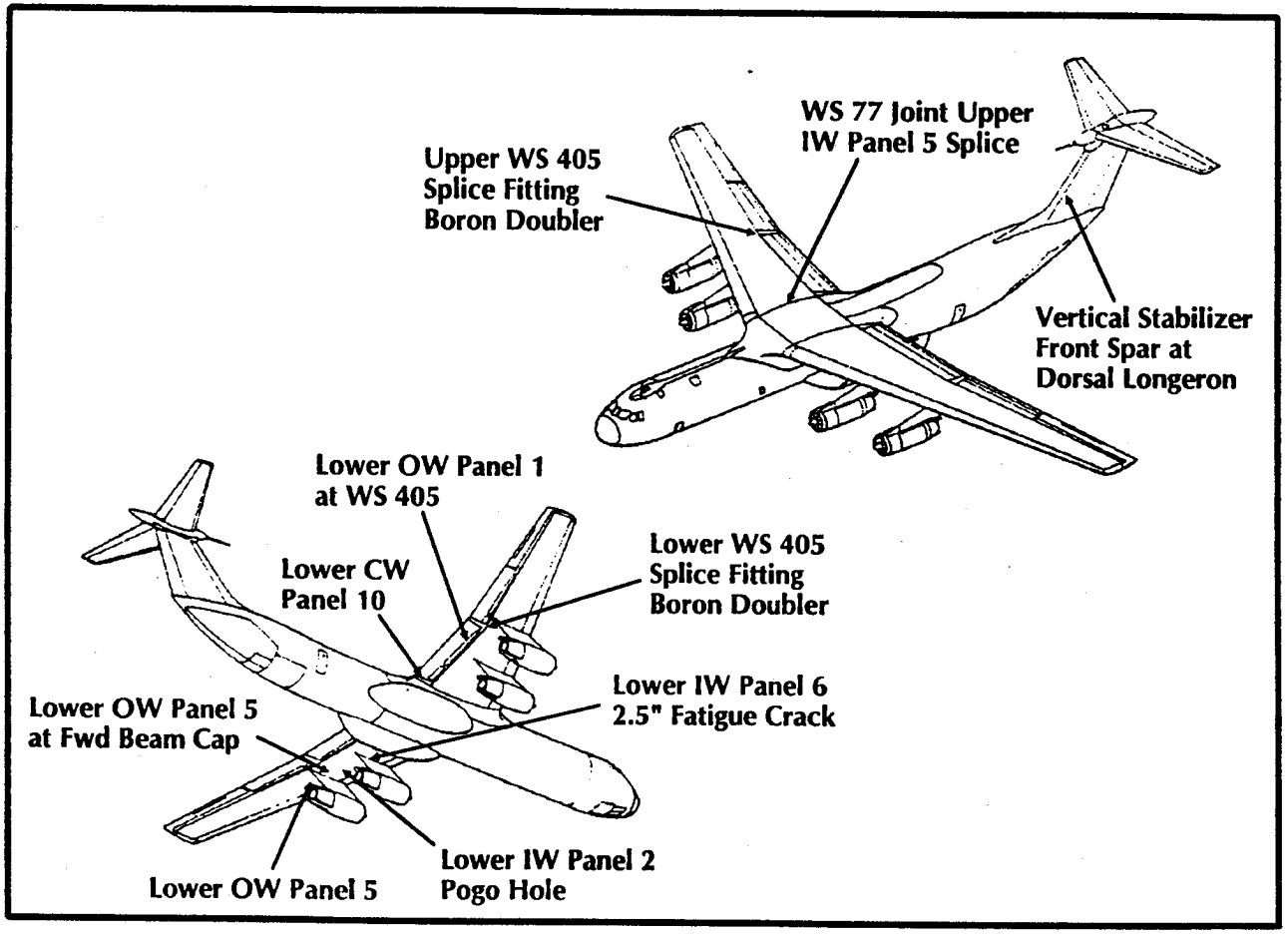
Figure 5. Phase Amplitude and Crack Length vs Time

Summary of Results

- Targeted Sensitivity of 10 Microstrain and Dynamic Range Extending to 3,000 Microstrain Is Feasible
- Optical Fiber Sensors Remained Operable to Specimen Fatigue Failure
- Strain Trends at Adhesive Bondline Provided Early Indication of Impending Failure

A015-15
10-27-94

Installations to Monitor Critical Repairs On High-time Airframes Can Effectively Augment Structural Integrity Efforts



A015-16
10-27-94
Opt 64B

Conclusions and Development Status

- A 60 Radian Optical Sensor Phase Shift Was Observed for a 6 mm Crack Extension
- Optically Measured Strain Hysteresis During Cyclic Loading Exhibited a Distinct Upward Trend With Damage Progression
- Current Development Has Used Non-Metal Coated Fibers -- the Metal Coated Memory Feature for Fatigue Damage Remains to Be Explored
- Instrumentation for Static Loads Being Developed
- Challenge to the NDT Community -- Built-In Systems Will Be Commonplace in Five Years

AIRCRAFT USAGE MONITORING: THE STRUCTURAL DATA RECORDING SET, ASH-37, SOLUTION FOR OPTIMIZATION OF FLIGHT DATA PROCESSING

by:

Jamshid Mohammadi
Systems & Electronics, Inc.
190 Gordon Street
Elk Grove, Illinois 60007
USA

David H. Crocker
Aerostats
1752 Russell Road South
Russell, Ontario K4R IE5
Canada

1994 USAF Structural Integrity
Program Conference

6-8 December 1994
San Antonio, Texas

AIRCRAFT USAGE MONITORING: THE STRUCTURAL DATA RECORDING SET, ASH-37, SOLUTION FOR OPTIMIZATION OF FLIGHT DATA PROCESSING

1.0 INTRODUCTION

Recent developments in advanced monitoring systems provide the structural engineer with the ability to collect a massive amount of data pertaining to an aircraft's loading, strains and flight parameters. Current systems are capable of providing, in various degrees and quality, in-flight and post-flight analyses of this data. In-flight and post-flight approaches to data analysis have their own set of pros and cons; and the concern is to develop a system that maximizes the benefits of both in a cost effective manner. While the in-flight real-time analysis provides a maximum level of data compression, it compromises data visibility. On the other hand, the post-flight analysis essentially provides maximum data visibility but limits timely data error detection and flexibility for making recording criteria adjustments. An ideal system provides the user with adequate data visibility and an on-line and convenient format. An on-line format is useful for timely verification of the system and data integrity; whereas, a convenient format is needed to ensure speedy feedback brought about by rapid data access.

One system that attempted to optimize the benefits of both the in-flight and post-flight methods is the ASH-37 - a system currently used aboard U.S. Navy and Canadian Forces aircraft. This system conducts on-board data compression providing the user with an efficient database for further evaluation. It offers a versatile low-cost monitoring system that can readily be configured to suit the aircraft's specific data acquisition requirements.

Two requirements need to be satisfied with respect to the data processing and data analysis. The first is a format to compress and present the data so that only relevant data is recorded and brought back to the ground for post-flight estimates of (i) the remaining fatigue life of a structural component; and (ii) the aircraft's flight history and loading regimes; and (iii) the aircraft's future inspection requirements. Secondly, a mechanism is needed via which the data can be validated on a timely basis so that problem areas can be identified and remedied before a significant amount of usage data is lost.

An advantage of the data analysis scheme reported in this paper is that it provides for an efficient data acquisition process with only a limited in-flight data compression/analysis, but with a versatile post-flight data analysis, processing and display capability. The post-flight data analysis provides for: (i) a rigorous validation based on the observation of statistical trends and norms in various key flight parameters; and (ii) development of flight data frequency distributions needed for structural fatigue life expectancy analysis.

These capabilities are incorporated in the overall monitoring using ASH-37 and a powerful post-flight data analysis/processing software (FACTS). The software offers an option to process the data and present it in a format which is suitable for a desired application. At the same time, the software can integrate statistical analyses as well as a desired method for fatigue life estimation. Quick graphical display of the data is also possible for the visual observation of trends and examination of various flight parameters.

This paper presents an overview of the ASH-37 monitoring system and its application aboard U.S. Navy aircraft. The paper also reports on the data processing software (FACTS) that affords speedy feedback and data analyses with examples of on-line interactive flight effects using graphs, operational statistics and baseline data.

2.0 AIRCRAFT USAGE MONITORING

Ideally an advanced data analysis and processing system should be capable of providing for an efficient real-time processing of the data; displaying the flight parameters statistics and an intelligent warning system that can be used as a means for early damage detection and troubleshooting. A comprehensive system that can compile the data and perform an efficient in-flight analysis and processing, along with a smart warning system, is not currently available. Although the technologies to construct such a system may be available, the cost of production is expected to be prohibitive. Short of development of such a comprehensive system, the following two concepts are currently considered:

- Systems that conduct most of the data analysis/processing during the flight operations.

- Systems that conduct most of the data analysis/processing following the data compilation on a post-flight basis.

There are advantages and disadvantages to both. Systems with in-flight data compression/analysis/processing provide for a very convenient means for flight data acquisition. However, they lack the data visibility and permit very little user interaction. Systems that rely primarily on post-flight data compression/analysis/processing, on the other hand, provide for data visibility and more active user interaction. They, however, lack the convenience of the in-flight data processing and limit the capability for "on-the-spot" error detection. Moreover, because of their fixed-type of format for data acquisition, they lack the capability to automatically modify the data acquisition parameters during a flight operation, should such a need arise. With current available technologies, a suitable system is one that is a compromise between the two systems and that can provide for some levels of in-flight data compression and processing and a limited in-flight self-check and data verification

capability. In such a system, a versatile, yet user-friendly post-flight data processing scheme is then used, that allows for an adequate data visibility and an on-line convenient format for data presentation. A menu-driven software directs the user to selecting the type of processed data needed for a specific application. For example, the peak/valley frequencies can be developed for use in fatigue analysis; or a data-time history plot can be developed for observing the general trends in the data and verifying the triggering parameters in various flight load regimes and flight missions.

The ASH-37 was designed by Systems & Electronics, Inc. (SEI) to optimize the benefits of both the in-flight and post-flight data compression/analysis/processing concepts with a low initial and operation cost. With the development of an integrated data processing software (FACTS), the ASH-37 offers a unique opportunity to compile and use the flight parameter data in a variety of formats tailored to specific applications.

An overview of the ASH-37 data monitoring system and the description of the integrated software FACTS are provided next.

3.0 ASH-37 SYSTEM OVERVIEW

3.1 System Description

Most current data acquisition and monitoring systems offer versatility in compiling, reducing and analyzing data for a wide variety of flight parameters. SEI has developed and employed data acquisition/processing systems in a variety of airframe applications. The SEI system used aboard Navy aircraft allows for a multi-parameter data collection and, to a limited extend, an on-board data reduction and analysis. The system can easily be configured to suit the data acquisition requirements of a specific aircraft. SEI's Structural Data Recording Set (see Fig. 1), AN/ASH-37 (SDRS) used aboard Navy and

C.F. aircraft has airborne and ground support equipment. The airborne equipment consists of a microcontroller-based 20 channel Recorder-Convertor, RO-601/ASH-37 (RC), a removable Memory Unit, MU-983/ASH-37 (MU), and a multi-axis acceleration Motional Pickup Transducer, TR-354/ASH-37 (MPT). The Recorder-Reproducer, RD-608/ASH-37 (RR) is the ground support equipment portion of the ASH-37. This low-cost versatile system is designed for direct replacement of the MS-25447/25448 or ABU-20/TRU-162 electromechanical Counting Accelerometer Group (CAG). Using advanced inertial sensors and the latest in solid state digital processing technology, the SDRS accommodates a total of 20 flight parameter input channels. The input capability of the recorder includes: pressure pitot-static data, four strain gage data channels, three high-level analog data channels, eight discrete even data channels, and a digital interface port.

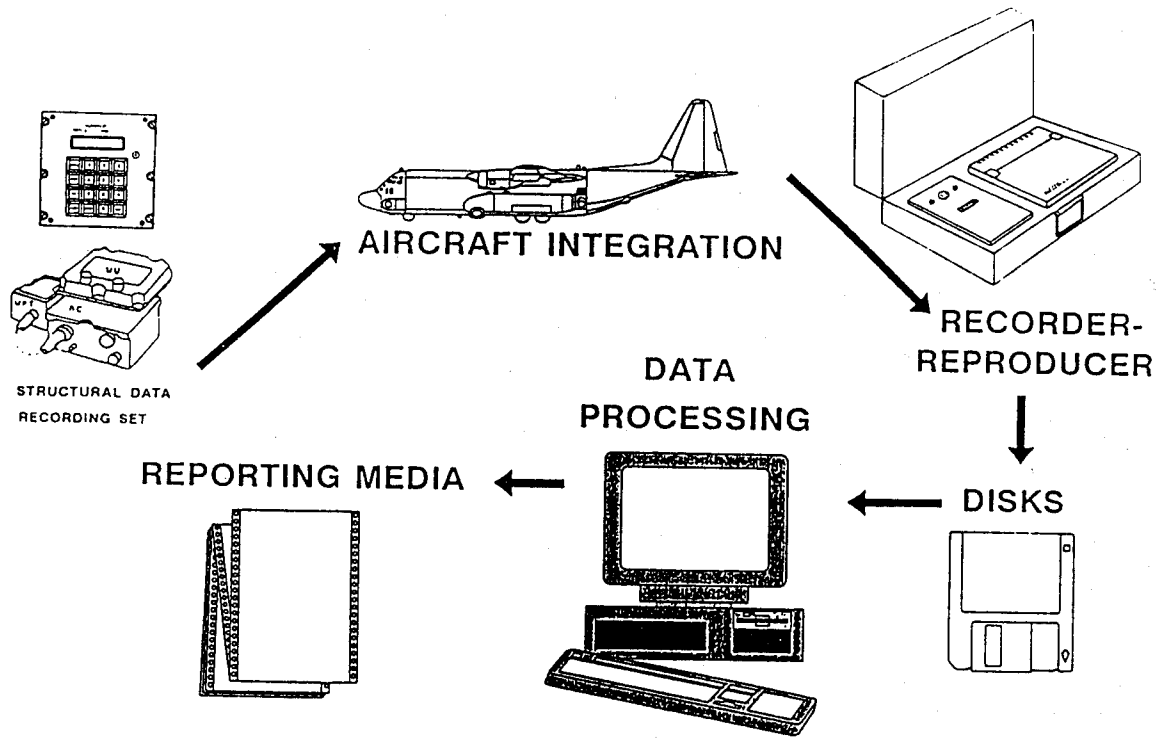


Fig. 1 ASH-37 Flight Data Recording System

The remote Motional Pickup Transducer (MPT) provides normal and longitudinal acceleration data (N_Z and N_X) and roll angular acceleration (β). The accelerometers obtain their operating power and Built-in-Test (BIT) commands from the Recorder-Convertor. The additional inputs typically include strain measurement of structural members, airspeed, altitude, control surface positions, stores release events, mission time from an internal clock, etc.

The system can easily be configured to suit the specific data acquisition needs of a given aircraft. For example, the system can be programmed so that it can change its data compression algorithm to optimize memory usage, if the frequency of a specific parameter increases.

The ground-based Recorder-Reproducer is designed to interpret the BIT messages for required maintenance actions from the recorded flight data and to configure the RC for particular algorithms. The RR reads out the data in the Memory Unit for further processing.

The ASH-37 system has been used aboard the U.S. Navy A-6E and E-2C and the Canadian Forces CP-140A aircraft. The system was modified and configured for application in rotary-wing aircraft (CH-46 and AH-1W). The rotary-wing system records the flight

maneuver sequence of events (Refs. 1 and 2). Depending on the recording algorithm used and the aircraft flight time, the Memory Unit typically stores 30 days of mission data.

3.2 Data Acquisition

The data acquisition process is application-specific and is tailored to the host aircraft's needs. Various control parameters such as the calibration and slope values used in initial recording of the data, peak and valley criteria, etc., are introduced to the system for in-flight data compression. Certain key parameters can be changed and the system re-configured by the recorder. These capabilities increase the efficiency of the system in terms of operation and data storage. A more rigorous analysis of the data is then conducted upon downloading.

3.3 Quality Assurance and Verification of Validity of Data

To assure the quality of the incoming data on a continuous basis, a rigorous program of data inspection and analysis will be needed. As it is expected, flight data are subject to variations. The purpose of the quality assurance (QA) procedure adopted for the aircraft flight parameters is to limit data variations that arise from such factors as:

a. Uncertainty associated with data acquisition process;

b. Errors associated with various sensors' sensitivities; and,

c. Errors introduced during system installation.

The QA procedures are intended to provide a safeguard against recording erroneous data that generally do not fall within the expected norms. Although a total elimination of errors is not feasible, certain measures can be taken to minimize their occurrence and recurrence during the data acquisition process. The QA procedure adopted in the flight survey of aircraft is a three-step procedure. The first step is conducted by the system as a self-test type of approach. The second step consists of a rigorous statistical analysis of the data to establish data trends and to identify any discrepancies in the data that may be an indication of a potential deviation from the norms. The third step involves the identification of the source of the problem and development of an appropriate corrective measure to remedy the potential problem areas. Figure 2 presents a schematic diagram of the QA procedure activities. A brief description of the three steps involved in the QA procedure is provided below.

The ASH-37 system is initially introduced with several pre-identified flight conditions. As the data compilation continues, the system recognizes the occurrence of these pre-defined

flight conditions. The values of the flight parameters within each flight condition are regularly checked against the expected limits. Any discrepancies are flagged for further investigations. If the system does not recognize a flight condition, with all parameters being within their respective acceptable ranges, a new flight condition will be added provided that the unrecognized condition is repeated. This constitutes Step 1 in the QA procedure.

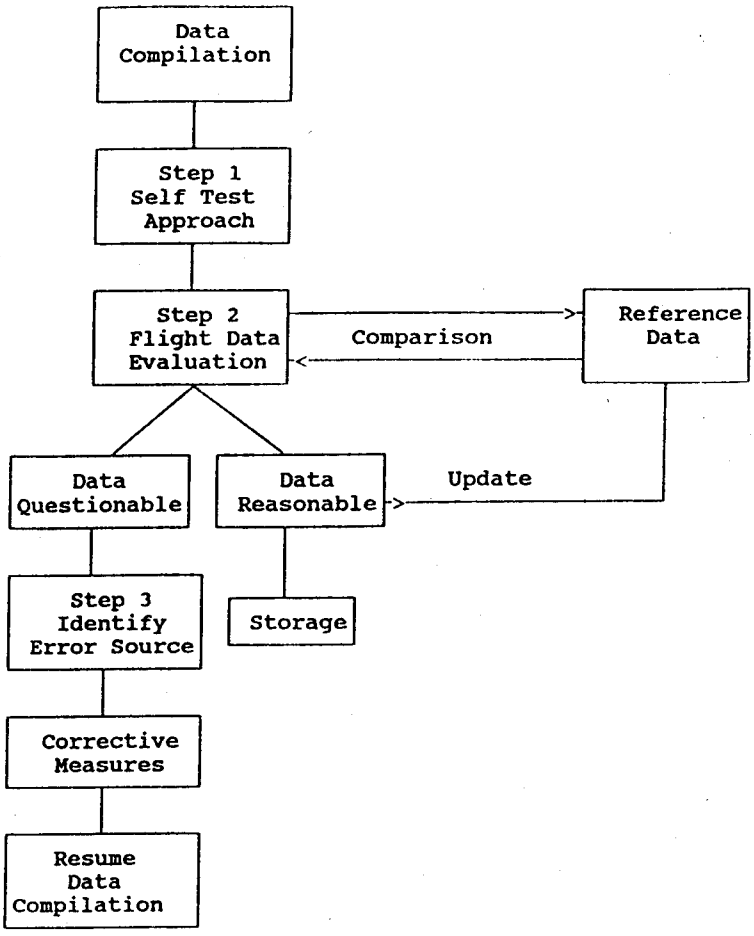


Fig. 2 Flight Data QA Procedure

As flight data are compiled, batches of data are selected for detailed statistical analyses. The purpose of such analyses is to investigate:

- Any statistical correlation that is expected between two or more parameters.
- A trend or pattern in the distribution of a parameter or groups of parameters.
- Consistency among blocks of data compiled for a given flight parameter for the same aircraft or for several identical aircraft.
- Consistency of the data when compared with published results, design values and norms indicated in the aircraft's manual.

An inventory of qualified data or published results is maintained for a reference. The reference data is periodically updated and revised, if necessary, as new data becomes available. Dramatic changes occurring in the data are carefully investigated to identify any

potential problem area associated with the data acquisition process. This constitutes Step 2 in the QA procedure.

Corrective measures are taken only if a problem area has been identified and proven to be the source of error or dramatic change in the data. Appropriate measures could consist only of a few adjustments in the previously-selected expected thresholds for a parameter; a re-calibration of sensors; an added feature to the previously-identified flight conditions; a replacement of a faulty sensor; a reconfiguration of the system; or replacement of the data acquisition system. In most applications the replacement of a sensor or the entire data acquisition system is rarely needed. Most often the problem area can be corrected with a few changes in the system configuration. This constitutes Step 3 in the QA procedure.

4.0 POST-FLIGHT DATA PROCESSING SCHEME

A comprehensive post-flight data analysis scheme is an essential part of any successful aircraft flight data monitoring system. Various types of analyses can be conducted and many forms of processed data generated. However, a successful post-flight data processing scheme is the one that maximizes the benefit of the aircraft data by providing only a manageable volume of processed data and in a format that can readily be used by an outside application.

In most applications, as a minimum, the results generated from the post-flight data processing should meet the following objectives:

- Provide a means for verifying the validity of the compiled data.
- Provide frequency distributions for any desired flight parameter in a format specified by the user.
- Provide statistical trends and/or time history results for visual observations.

The frequency distribution of peak and valley of the normal load factor and/or strains at fatigue critical locations are needed for estimating the percentage fatigue life expended or the remaining fatigue life of a critical structural component. The statistical trends are useful in a quick review of the data and in identifying overstressed components, comparing the results with the norms and obtaining an overall idea on the loading regime in a flight condition or mission.

The FACTS program is an integrated software system made up of several modules. The program was developed to meet the aforementioned post-flight data validation/analysis/processing objectives.

The system has been successfully tested in several aircraft data applications, most notably the CP-140A application where the system is used to enhance data visibility and to provide a second level data QA function by computing statistical trends for various parameters on a flight-by-flight basis.

The program optimizes the data processing effort by utilizing existing software and building a system that takes advantage of the advances in package software development, thereby assuring system currency.

There are three modules which make up the system. The modules are accessible through MS Windows. The current version contains the following modules: (i) data visualization; (ii) statistical analysis; and (iii) damage tolerance analysis. Future versions will incorporate the ability to address the ever present structural corrosion problem by adding a corrosion prediction module.

The data visualization module provides options for displaying time-history and frequency-of-occurrence graphs for a desired flight parameter. Flight severity evaluation and damage source analysis capabilities are also provided. These capabilities are particularly useful in assuming a pro-active stance, by recognizing potentially damaging operational techniques, developing and verifying effective modifications to these operational practices to improve aircraft fatigue life consumption.

The statistical analysis module provides capabilities for conducting multi-variable analyses, including computation of correlation coefficients among parameters that are theoretically related. Data manipulations, transfer function development and report generation are some of the additional features of this module.

The damage tolerance analysis module utilizes crack growth analysis based on the stress loading magnitude and frequency data generated by the previous modules. The software is capable of accepting loading data as a spectrum, or in a sequential peak and valley format. The module output includes critical location crack growth curves and zonal airworthiness inspection requirements. The data output is fed to a data base program and is managed through standard Structural Query Language (SQL) commands.

5.0 APPLICATIONS

The combination of the ASH-37 recorder and the FACTS post-flight software offers a unique solution to data acquisition/visibility/analysis. Such a system meets the needs of all aircraft data users as described below:

a. Operators:

(1) Provides feedback on air operations which has the potential to affect fatigue life, such that corrective action can be taken to modify operational practices to improve fatigue life consumption. Some examples of these practices are:

- heavy landings at high gross weight;
- excessive maneuvering in turbulence;
- excessive Stop-And-Go (SAGs) landings when Touch-And-Go (TAGs) landings would suffice;
- flap developments at higher than necessary airspeed.

b. Maintainers:

(1) Provides maintainers with usage statistics such as frequencies of TAGs/SAGs, flap cycles with airspeed, pressurization cycles and airborne engine shut downs or start-ups; and,

(2) Provides means for the investigations of overstress conditions to aid in assessing severity of a given flight mission.

c. Aircraft Life Cycle Managers:

(1) Provides fatigue damage indices for life cycle management purposes;

(2) Provides usage data for establishing maintenance and inspection actions; and,

(3) Provides a method of verification for analysis assumptions used on other aircraft fleets where fatigue cracking is performed in the traditional manner via crew reporting forme, etc.

6.0 SUMMARY AND CONCLUSIONS

In summary, the ASH Structural Data Recording System when combined with the FACTS system provides for an efficient method for data validation, compression, analysis

and processing. The system meets the needs of all groups of aircraft data users. Its capabilities are particularly useful in assuming a pro-active stance in combating aircraft fatigue. This is accomplished by allowing the user to recognize potentially damaging operational techniques, to develop and verifying effective modifications to these operational practices and, thereby, improve fatigue life consumption.

The systems provides for a cost-effective method of flight data acquisition and processing. It offers a limited in-flight data processing with a comprehensive post-flight data visibility and application-oriented flight parameters summary. The system is designed to operate with an optimum in-flight data acquisition and storage capability. This reduces the need for frequent downloads. The post-flight processing of data is an effective method to optimize handling of large volumes of flight data and provide a feedback mechanism to improve the data acquisition process as the monitoring continues.

7.0 REFERENCES

1. Mohammadi, J. and Olkiewicz C., "Flight parameter monitoring system for tracking structural integrity of rotary-wing aircraft," *FAA/NASA International Symposium on Advanced Structural Integrity Methods for Airframe Durability and Damage Tolerance,* May 4-6, 1994, Hampton, VA, Proceedings published by NASA Langley Research Center, Hampton, VA.

2. Barndt, G.L. and Moon, S., "Development of a fatigue tracking program for Navy rotary wing aircraft," *American Helicopter Society 50th Annual Forum*, Washington DC, May 11-13, 1994.

A FIBER-OPTIC LOADS MONITORING SYSTEM FOR THE CL-600 CHALLENGER AIRCRAFT

F.A. Blaha, Canadian Marconi Company, Montreal, Quebec, Canada
Capt. L. Grenier, National Defence Headquarters, Ottawa, Ontario, Canada

ABSTRACT

The Challenger aircraft fleet of the Canadian Forces flies demanding missions requiring the implementation of a fatigue management program, based on monitoring of in-flight aircraft load conditions. Conventional sensing techniques impose a limit on the number of sensors which can be realistically employed, and experience problems arising from severe electromagnetic interference (EMI). This paper describes the development of an EMI-insensitive loads monitoring system. Fiber-optic (FO) strain gauges are incorporated at critical structural locations in the aircraft wing , fuselage, and empennage. Concept and features of FO sensors and system are presented, together with a long-term plan for the development of a smart structure concept which can support the continuous monitoring of fatigue-prone components, and provide the aircraft with near real-time damage location and assessment.

1. INTRODUCTION

The Canadian Forces operate a fleet of 15 Challenger aircraft, of which eleven are flying in an environment which differs from the original mission profile. Six of the aircraft will be configured for electronic surveillance, in which EMI is a major concern. Antenna locations for this aircraft configuration (which may not be final) are shown in Figure 1.

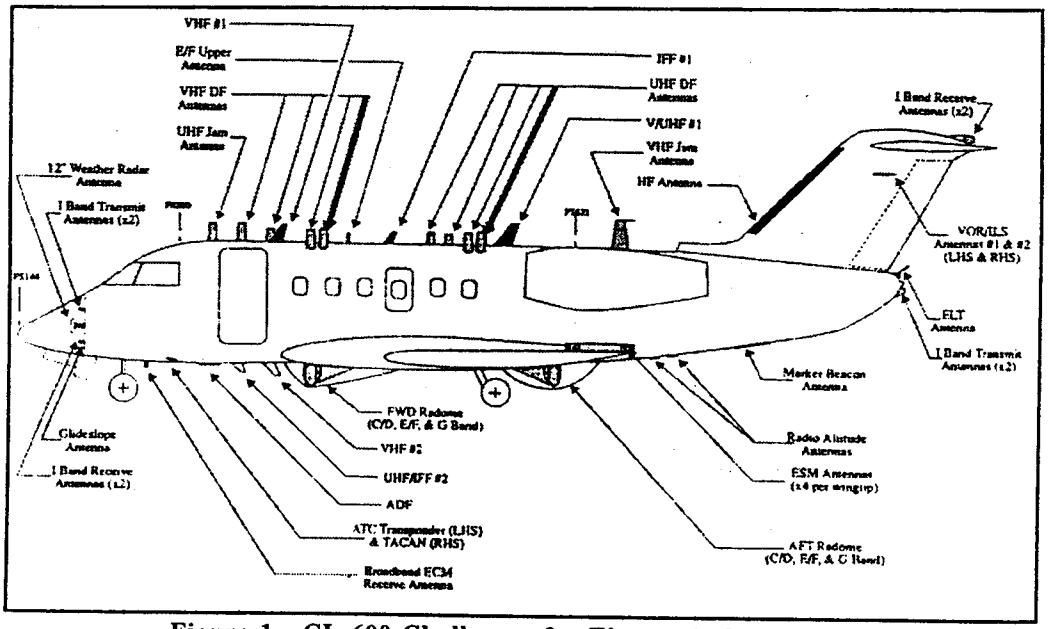


Figure 1 - CL-600 Challenger for Electronic Surveillance

As part of the Aircraft Structural Integrity Program (ASIP), DND is tracking operational loads conditions of individual Challenger aircraft[1]. Continued airworthiness of this aircraft fleet is assured through scheduled inspections of all structurally significant locations. To compensate for uncertainties in the analytical models, conservative assumptions are used in the calculation of the inspection intervals; this has a correspondingly heavy impact on life-cycle costs. A preliminary investigation has focused on the feasibility of reducing the inspection frequencies at some locations.

In this application, sensor technologies currently used by ASIP face two major challenges:

- The electronic sensors have performance and reliability limitations, are difficult to install, and may not meet the EMI requirements. Large-scale electronic sensor networks are not viable, and their EMI/EMC qualification tests are lengthy and costly.

- Many months typically elapse between the acquisition of in-flight data and subsequent data processing/interpretation, which means that fatigue consumption levels in structurally critical parts are not predicted in a timely manner.

FO sensing and real-time on-board health monitoring techniques based on smart-structure technology[2, 3] are expected to eliminate these problems. DND is considering the incremental introduction of these critical technologies in the CL-600 Challenger fleet.

2. BACKGROUND

The Challenger CL-600 is a twin-engine, low-winged monoplane with pressurized fuselage and T-tail arrangement. This damage-tolerant aircraft is designed for an economic life of 30,000 flight-hours. The basic loads monitoring system (LMS) requirements include flight parameter measurements (airspeed, pressure altitude, roll rate, and vertical acceleration), strain measurements at six control points on the aircraft's primary structure, and discrete parameter detection (flap settings, main landing gear retractions). In view of the low number of representative structural test points, extensive fatigue computations must be performed in order to derive fatigue indices for all structurally significant elements away from the control points.

3. NEAR-TERM IMPLEMENTATION OF AN FO SENSOR CONCEPT

3.1 Loads Monitoring System with Conventional Strain Gauges

The first aircraft of the CL-600 Challenger fleet will carry a conventional LMS to support the minimum requirements. The LMS strain sensor complement is shown in Table 1. This system will serve as a benchmark for the subsequent phased introduction of new technologies.

Table 1 - Phased LMS Implementation

Sensor Type	Location	NUMBER OF SENSOR LOCATIONS: Phase 1 LMS with Electronic Sensor System	Phase 2 LMS with FO Sensor System	Phase 3 Smart Structure Concept Validation System
Strain Sensors	Left wing	0	0	2
	Right wing	2	2	18
	Forward fuselage	1	1	4
	Center fuselage	0	0	4
	Rear fuselage	1	1	6
	Empennage	2	2	2
	Subtotal	6	6	36
AE sensors	Right wing	0	0	3
Vert. Acceleration		1	1	1
Rate of Roll		1	1	1
Airspeed		1	1	1
Barometric Altitude		1	1	1

3.2 Loads Monitoring System with FO Strain Gauges

In the second aircraft of the CL-600 Challenger fleet, FO strain gauges will replace the resistive strain gauges. The number of strain gauges will remain the same. The expected benefits are improved performance and reliability, and elimination of any EMI problems.

4. LONG-TERM SMART STRUCTURE DEVELOPMENT

4.1 System and Smart-Structure Requirements

A preliminary cost of inspection analysis (Figure 2) indicates that significant benefits can already be realized with the introduction of a modest FO sensor network. Safety margins adopted for the calculation of inspection intervals can be reduced, by means of using actual (rather than predicted) load data for critical components.

The realization of real-time on-board health monitoring will provide further improvements. Structural maintenance and repair will be performed only as required, not as dictated by scheduled non-destructive inspections and damage accumulation models based on individual aircraft tracking. Apart from providing near-real-time assessment of the airworthiness of the aircraft structure, on-board signal processing can warn the pilot and recommend restrictions to the flight regime. Indications of accumulated damage at all critical locations, and required repair actions, are immediately available to ground and maintenance personnel.

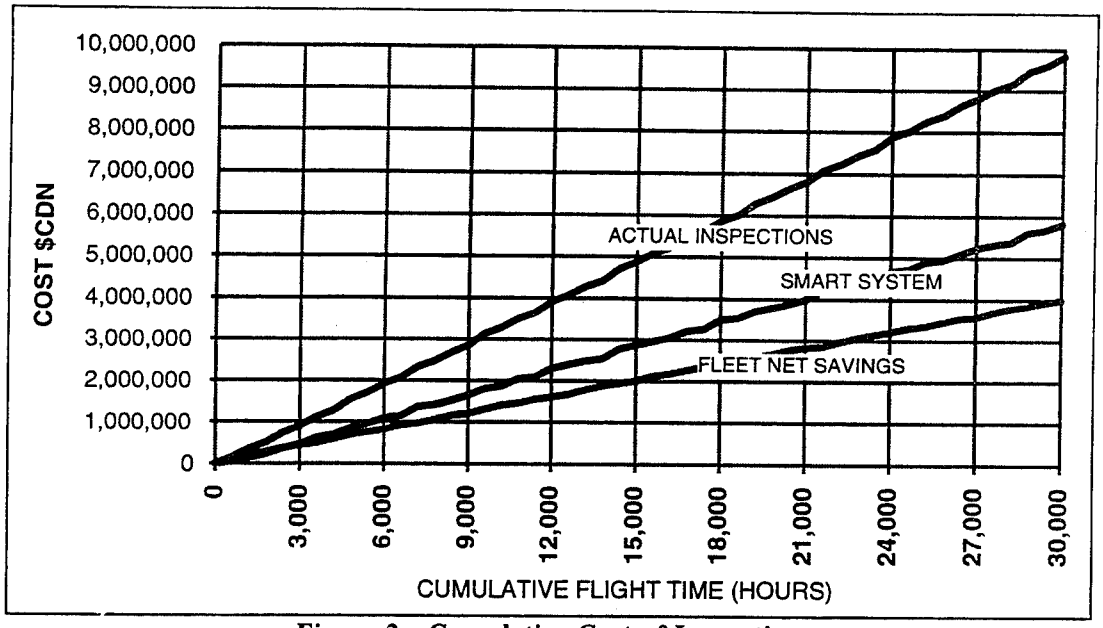


Figure 2 - Cumulative Cost of Inspection

For the realization of the real-time structural health monitoring concept, critical strain-sensor locations are classified on the basis of damage tolerance analysis[4] (DTA) and natural crack growth observed during full-scale fatigue testing[5]. Two hundred and forty-three such sensor locations can be selected: 211 on the basis of DTA, and 32 based on natural crack growth. To facilitate data management and interpretation, the airframe's structural components are grouped in a hierarchical fashion in which the top level comprises the six primary structures of the complete airframe: fuselage, wing, empennage, control surfaces, landing gear, and engine structure (Table 2).

Table 2 - Strain Test Point Requirements

Description	# of groups	# of zones	# of DTA points	# of fatigue test points	# of test points, smart structure system	# of test points, smart structure concept validation system
Fuselage	4	21	58	14	72	14
Wing	6	31	77	18	95	20
Empennage	2	7	21	0	21	2
Control Surfaces	9	8	18	0	8	0
Landing Gear	2	5	3	0	13	0
Engine Structure	3	12	34	0	34	0
Complete Airframe	26	84	211	32	243	36

4.2 Smart Structure Concept Validation

To validate this new maintenance concept, DND is planning the development of a reduced-scale FO sensor network incorporating 36 strain sensors, three acoustic emission (AE) sensors and a high-performance digital signal processor (DSP). The 36 strain signals are monitored at once, when triggered by limit signals of vertical acceleration and airspeed. Unlike current operational loads monitoring systems, the FO system computes in-flight stress and vertical acceleration exceedances, generates crack growth curves and compares them to baseline curves, and stores damage indices (or inspection interval factors) on the aircraft for each component. Table 3 lists the guidelines adopted for selecting FO strain and acceleration sensors and their system.

Table 3. Sensor and System Target Specifications

Strain Sensors	Acceleration Sensor	Sensor System
Local and uniaxial strain measurement Temperature-compensated to host Maximum strain level ±10,000 με Sensitivity 25 με Bandwidth 15 Hz MTBF 30,000 hours (economic life) Operating temperature -50 to +125°C	Range -1.5 to 3 g Accuracy 0.1 g Bandwidth 5 Hz	- Standard multi- or single-mode connectors and fibers - Performance undegraded by fibers up to 100 m long - Costs comparable to conventional sensors and systems

Acoustic emission monitoring will be implemented[6] in one selective area (Table 1) in order to assess its ability to detect unanticipated structural damage.

The DSP, with its associated memory system, is expected to collect raw data and perform the real-time evaluation of structural health. ASIP post-data processing and real-time structural health monitoring are maintained in parallel to perform the concept validation. Today's high-performance and compact DSPs can readily meet the requirements of this smart-structure concept validation system.

4.2 Smart Structures Development Plan

In order to reduce technological risk, satisfy immediate needs, and meet the long-term objective of on-line structural health monitoring, an incremental development plan has been proposed which incorporates the following critical steps and milestones:

- qualification of the FO sensors and systems (in progress)
- installation of the benchmark LMS
- assessment of the analytical model limitations, using at least six months of loads monitoring data
- installation of an FO LMS
- preliminary cost/benefit analysis
- installation of the smart structure concept validation system
- verification of costs/benefits, taking into account factors such as fewer inspections, timely repairs, acquisition cost and reliability.
- installation of an optimal (cost-effective) smart structure system.

5. FO STRAIN SENSORS AND SYSTEMS

5.1 FO Strain Sensor

An external-cavity fiber-optic sensor (EFOS) has been chosen as the best candidate for meeting the requirements of Table 3. The EFOS's intensity-modulated concept is illustrated in Figure 3. The single-mode fiber of the sensor has a bandpass filter deposited at its end surface to form one side of the sensing cavity. The other side is formed by a mirror on a short auxiliary fiber. The return light of the sensor is thus divided into two parts: I_r is the light reflected by the bandpass filter, and I_t is the light transmitted through the filter and reflected by the end mirror. I_t is a near-linear function of cavity length, D, and I_r provides self-referencing. Length, L_T, and the temperature coefficient of the mirrored end fiber can be selected to match the temperature coefficient of the host material. Key features of this EFOS include relatively modest system requirements, temperature compensation and polarization-independence.

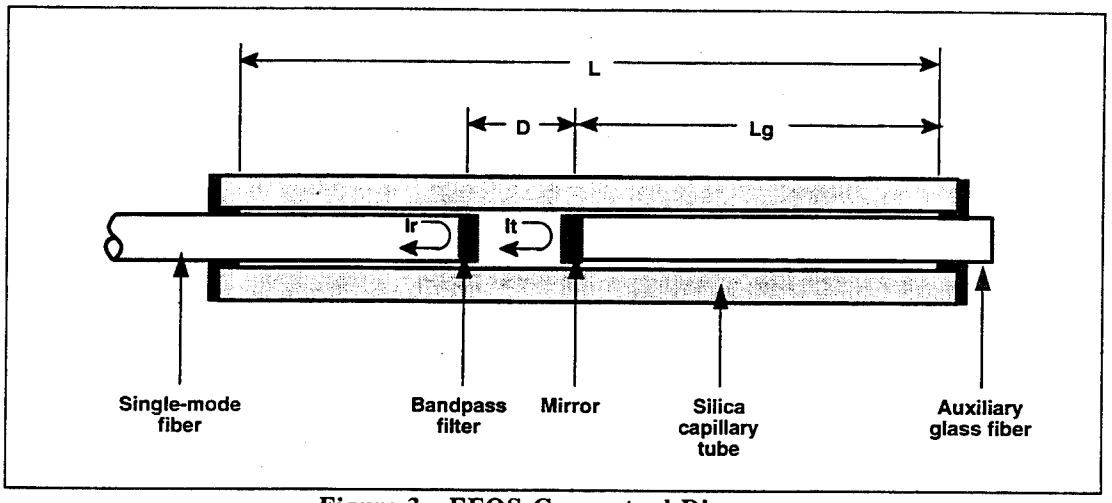
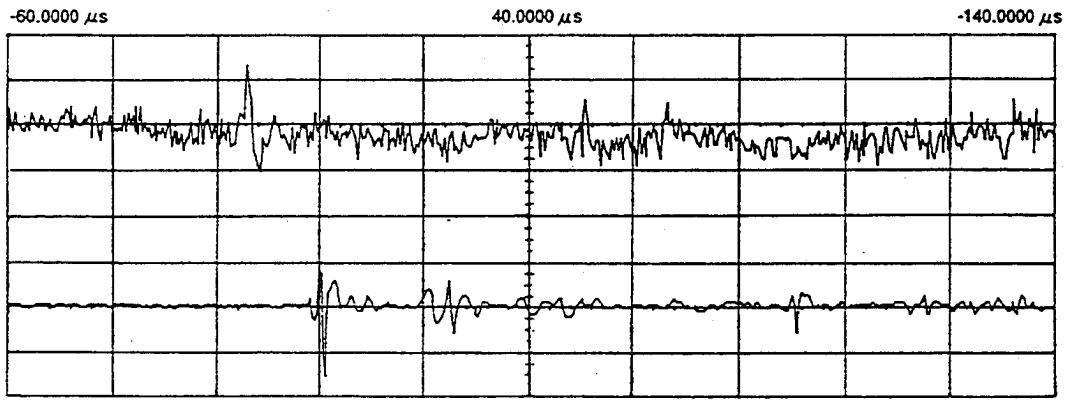


Figure 3 - EFOS Conceptual Diagram

5.2 FO Acoustic Emission Sensing

Over the past fifteen years, the feasibility of applying acoustic emission (AE) sensing to aircraft structural health monitoring has been successfully demonstrated[6]. AE sensing's reliability and cost must be determined before it will be accepted in the ASIP. As part of its smart-structure validation, DND is planning to investigate its reliability by incorporating AE sensing in one critical area of the airframe, and evaluating AE and LMS data over an extended period of time.

FO sensing appears to be the most promising candidate technology for the cost-effective implementation of this highly sensitive sensor network.. Figure 4 illustrates the sensitivity of an FO interferometric and a piezoelectric sensor which, at this time, is exclusively employed for AE sensing. Sensitivities are comparable, with the FO sensor having the crucial advantage of not being affected by EMI.



	TIMEBASE	DELAY	REFERENCE	MODE
MAIN	20.0 μs/div	-60.0000 μs	LEFT	REALTIME (Normal)
	SENSITIVITY	OFFSET	PROBE	COUPLING
Channel 1	10.0 mV/div	0.000000 V	1.000 : 1	ac LF rej (1M ohm)
Channel 2	10.0 mV/div	0.000000 V	1.000 : 1	ac LF rej (1M ohm)

Trigger Mode: Edge on Positive Edge of Chan 2

Trigger Level: Chan 2 = 2.500 mV (noise reject OFF)
Holdoff = 40.000 ns

Figure 4 - AE Signals Detected with FO and Piezoelectric Sensors

5.3 Integrated-Optic Accelerometer

A glass integrated-optic (IO) accelerometer employing a Mach-Zehnder interferometer as the sensing element (Figure 4) has been developed and is being evaluated for this application.

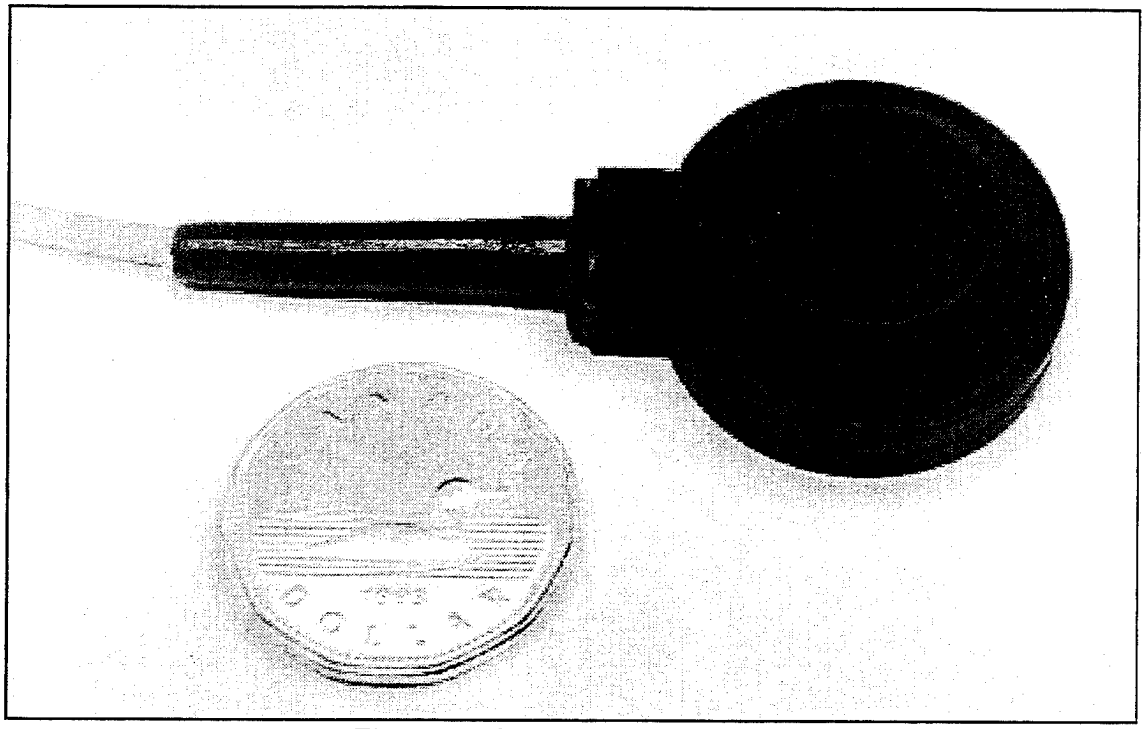


Figure 5 - Glass IO Accelerometer

5.4 FO Strain Sensor System

The light source employed in the system is an LED with a relatively broad emission spectrum (typically 50 nm, centered at 1300 nm). The return signal from a sensor is split to meet two detectors, one of them via a bandpass filter identical to the one in the sensor. The optical power ratio of the two detectors is a function of the sensor air-gap length, D, and is independent of losses in the transmission line, splices or connectors.

An eight -channel system (four FO and four electronic analog channels), which includes a signal processing capability, is currently available on a single printed circuit board. Figure 5 shows this system packaged with a 28-VDC aircraft power supply in a single enclosure. A block diagram of the system is provided in Figure 6. A board which can accommodate sixteen FO channels is being developed.

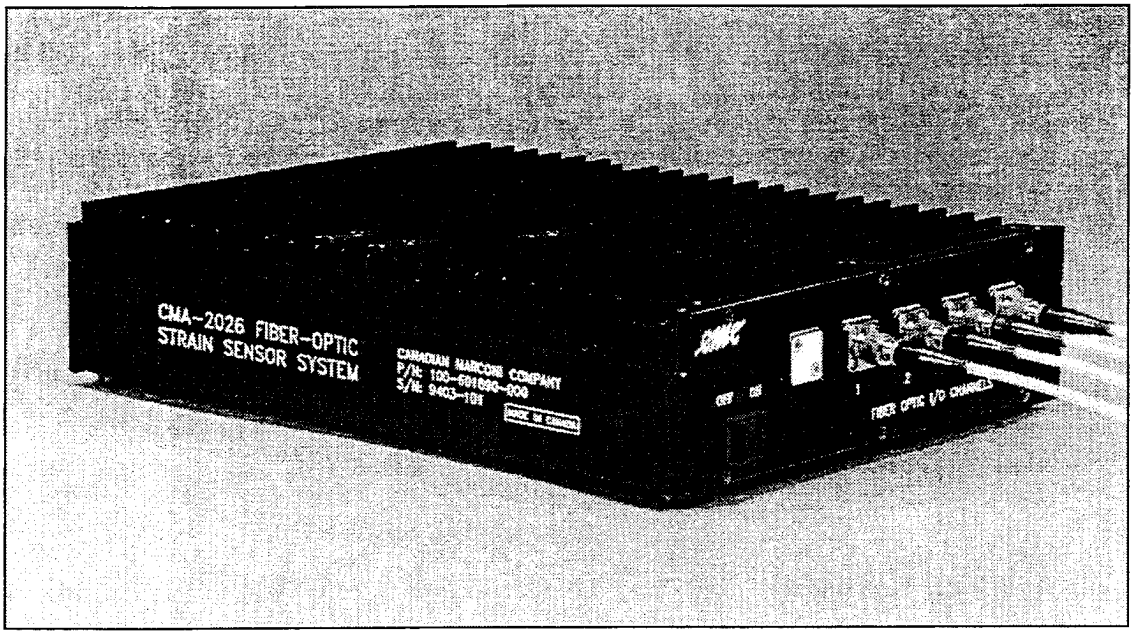


Figure 6 - FO Strain Sensor System

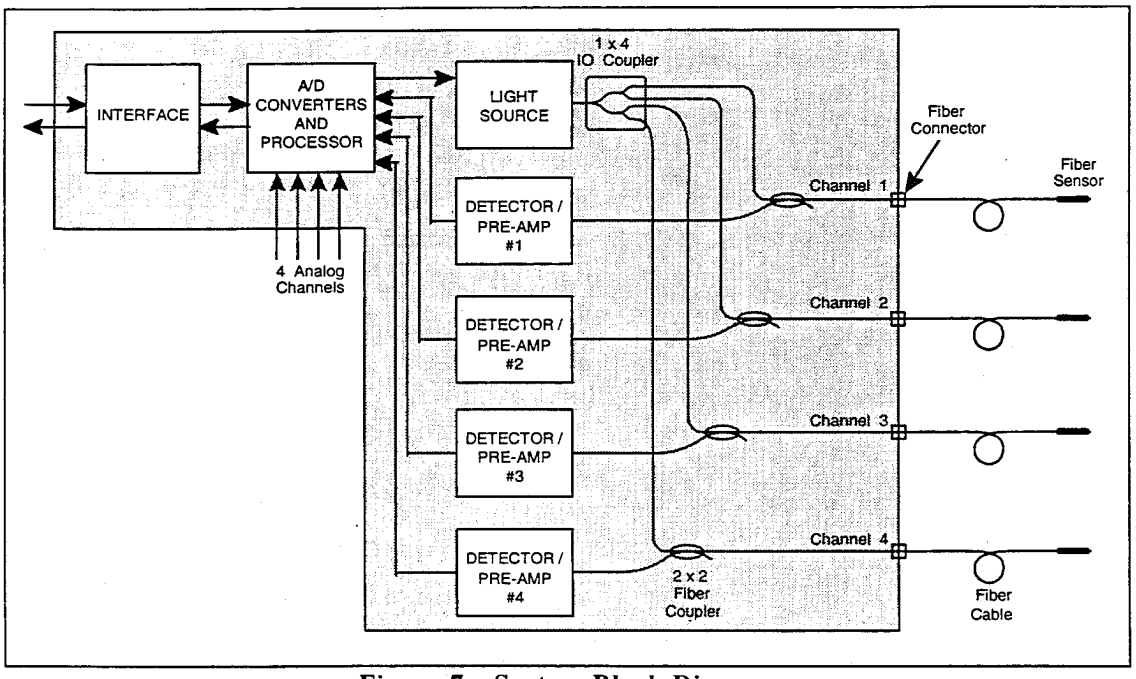


Figure 7 - System Block Diagram

6. CONCLUSIONS

Fatigue management currently relies on extensive post-data analysis; this will change radically with the introduction of smart structures. Structural maintenance and repair will be performed on an as-required basis, not as dictated by life-expectancy models. The timeframe for the implementation of these new fatigue management concepts will depend on the availability of proven, cost-effective, large-scale sensor networks and associated data processing systems.

7. ACKNOWLEDGEMENTS

This work was supported by the Canadian Department of National Defence. The authors wish to express their gratitude to Maj. D. Lamanque and Mr. R.R. Hastings for their assistance and support. The editorial assistance of Andrew Solkin of Canadian Marconi Company is also gratefully acknowledged.

8. REFERENCES

1. Agnes, G.S. and Silva, K., "Aircraft Smart Structures Research in the USAF Wright Laboratory", *75th Meeting of the AGARD Structures and Materials Panel*, Lindau, Germany, October 1992.

2. Blaha, F.A. and McBride, S.L, "Fiber-Optic Sensor Systems for Measuring Strain and the Detection of Acoustic Emissions in Smart Structures", *75th Meeting of the AGARD Structures and Materials Panel*, Lindau, Germany, October 1992.

3. Schmidt, W. and Boller, C., "Smart Structures - a Technology for Next Generation Aircraft", *75th Meeting of the AGARD Structures and Materials Panel*, Lindau, Germany, October 1992.

4. *CC-144 Strength Summary - CL-600 Model*, Canadair Report RAS-600-802, October 1990.

5. *CC-144 Force Structural Maintenance Plan*, Canadair Report RAS-601-910, March 1993.

6. McBride, S.L. et al, "Acoustic Emission Monitoring of Aging Aircraft Structures", *Review of Progress in Quantitative Non-Destructive Evaluation*, Vol. 11, pp. 2275-82, 1992.



Improving Predictions for Helicopter Usage Monitoring

M. E. Hoffman
Naval Air Warfare Center
Warminster, PA

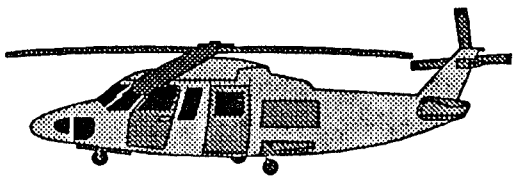
ABSTRACT

The goal of Navy helicopter usage monitoring research is to predict the rotor system and fixed system loads suitable for fatigue calculations. It is not practical to measure helicopter loads on main rotor components during typical flight operations so methods are being developed that predict loads from information gained through instrumented flight tests. Emphasis has been placed on developing regression, neural network, and holometric models for predicting blade bending and lag damping loads [e.g.1-4]. To date, the best results have been obtained using regression models to predict the maximum load that occurs during a maneuver. Neural networks and holometrics have been used successfully in some cases to predict peak and valley loads that occur during specific maneuvers or in specified regimes. All three models can be improved by carefully preparing the data prior to using them to calibrate the model. This paper presents the effect of training data selection on the load predictions for neural network models using a sample of CH-46 data.

Presented at the 1994 USAF Structural Integrity Program Conference, 6-8 December 1994, San Antonio, TX. Approved for Public Release, Distribution Unlimited. NAWCAD, MS08, Warminster, PA, 18974.

Objective

- Show Challenges of CH-46 Data
- Provide Strategy for Preparing Data



NAWCADWAR

The objective of this paper is to illustrate the difficulty in predicting rotating loads on helicopters, and suggest some ways to improve the predictions. Navy Flight test data from the CH-46 aircraft was used to illustrate the difficulties in predicting dynamic rotor system loads. A criteria for filtering data prior to neural network model development is presented, initially. Examples are given for predicting rotating loads during level flight using a neural network model.

The paper emphasizes how to select data for calibrating the neural network models. Some examples are presented that highlight the difficulties.

Background

- Navy Approaches to Usage Monitoring
  - » Hours Based
  - » Regime Based
  - » Loads Based

NAWCADWAR

Helicopter usage monitoring systems have evolved in the Navy. The objective has always been to predict fatigue life and retire the components before they fail in service. Fatigue monitoring of helicopter components has traditionally been based on flight hour usage. When a component reaches its specified retriement life it is removed, reworked or disgarded. The state of the art system currently being installed on Navy Aircraft is the Structural Data Recording Set (SDRS), a regime-based system that records the time spent in a regime. The optimal system would be a loads-based system where a load history would be recorded for each fatigue critical component in the rotating system. Unfortunately, as fatigue monitoring methodology becomes more complex from *hours based* to *regime based* to *loads based*, the difficulty to implement a fleet based fatigue component monitoring system increases. A loads-based system would provide the best method to determine lives accurately on fatigue critical components. This paper explores a loads-based approach using neural networks to predict CH-46 rotating loads.

Predict Actual Loads

- Fatigue-significant ranges
- Ultimate goal- Universal model
  - » Milestones- by Maneuver
  - » Milestones- by Regime

NAWCADWAR

Predicting actual rotor system loads is very difficult. One of the biggest problems is that the amount of data obtained from a flight test is overwhelming. In its current form, loads-based monitoring attempts to predict every load fluctuation in the dynamic component. There are thousands of fluctuations in every maneuver. Much of the load events provide conflicting information. It may be difficult to distinguish significant information. Selecting data records for calibrating or training the model is a difficult task. I wish to propose some guidelines for making this task more rational.

I need to add at this point that a major project which is part of the Navy AVDS program is continuing at NSWC and NAVAIR with SH-60 data using neural networks to predict the maximum and minimum loads occuring per revolution. They have achieved high correlations with regression and neural network prediction versus measurements [4].

Ideally, we would like to invent the universal model that can be used to predict loads independent of the maneuver or regime. For the moment, we are struggling to create a model that can be used for an individual maneuver or regime.

Data Selection Strategy

- Delete Redundancies
  - » Identical information
  - » Highly correlated variables
- Represent region of interest- **INPUT**
- Represent region of interest- **OUTPUT**

NAWCADWAR

When the goal is to predict fatigue significant events, the task is to eliminate all the data that detract from the goal. Since the neural network coefficients are determined from minimizing the least square error, we don't want them overly weighted by the results of many small cycles. The first task is then to delete the redundant data. A second task is to delete the prospective variables that are highly correlated with each other. For example, if a variable is linearly dependent on another, it is not only not useful to the model, but it makes the input matrix singular.

Next I will address the concept of regions of interest for the input and output. These are records that should be included in the model to aid generalization.

A last item that I did not list is to remove the contradictions in the data set. This is an iterative task that involves removing a data record and noting the effect on the prediction of the loads in the calibration and blind test results. A danger in this activity is that you may improve the predictions for the calibration data, but blind predictions may deteriorate.

"Original" Data Set

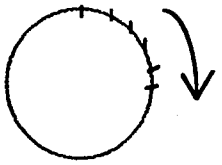
- CH-46 Extended Stub Wing Flight Test
- 9 Input Variables
  - » Nz, coll. lever, long stick, lateral stick, dir. pedal pos., pitch, roll, yaw rates, air speed.
- 3 Loads
  - » Fwd lag damper, fwd & aft blade flap bend

NAWCADWAR

The data set was provided from a flight test of the CH-46 aircraft conducted at PAX River [4]. These data consisted of 99 variables. Nine were selected by my colleague, Dr. Tsai, to be used as independent variables for an in-house holometric analysis [3]. Three were selected for the dependent variables. The gross weight was essentially constant for all tests. My task was to take his variables and use them for a neural network model.

"Original" Data Set

- Data Prepared for Holometric Study
  - » 50 data points per revolution
- 81,900 Data Points
- 19 Maneuvers
- 10 Maneuvers for calibration



NAWCADWAR

Dr. Tsai prepared the data, taking out the extraneous spikes, and interpolating the data so that there were exactly 50 evenly-spaced data points per revolution of the main rotor blade. The data were presented as ten maneuvers available for calibration and nine maneuvers for verification. The original concept called for one model to work for all maneuvers. We quickly found that a universal model was not going to be adequate for either the neural network or the holometric approaches. In particular, for both the least squares methods and the sum squared error methods, small variations about the steady state loads were captured rather than the extreme peaks and valleys.

The approach was then altered to develop predictive models for specific maneuvers.

Redundancies

- Level Flight Data Set-
  - » 450 records
  - » 104 were exact duplicates
    - – based on 9 input variables

NAWCADWAR

After the forward lag damper loads from the level flight data at 30 Kts were selected for modeling, the redundant data records were deleted. One hundred- four records contained information that was exactly duplicated in other records of the independent variables. I might note that these data were need for the holometric analysis because 50 points were needed for each revolution. All data that were deleted immediately proceeded the entry that it duplicated. This task also ensured that strictly contradictory data were deleted. That is, data with the same input was associated with different outputs.

Additional data could have been deleted if tolerances on the data values were considered. All data within a specified tolerance of the subject data could be eliminated without impairing the performance of the neural network. This issue is mentioned later when we talk about sampling regions of interest.

Data Statistics- Level Flight

		Max	Min	Median
	Nz	**1.04**	**0.96**	**1.0**
	Coll Lev	53.69	53.58	53.69
	Long Stk	**52.68**	**50.53**	**50.91**
	Lat. Stk	**45.66**	**42.84**	**43.36**
	Dir Pedal	51.50	51.39	51.50
	Pitch	**4.53**	**3.71**	**4.18**
	Roll	**0.05**	**-6.22**	**-2.61**
	Yaw	**0.07**	**-3.12**	**-1.48**
	Air Spd	31.21	26.74	26.74
Fwd Lag Damper	**Load**	**1909.00**	**-2702.00**	**-387.00**

NAWCADWAR

We looked at some basic statistics of the variables as the first step to deciding if they would be useful for our neural network model. The six independent variables shown in bold print were determined to have enough variation to be of interest. The other three did not vary enough to make any difference to a neural network. Obviously, if we had a choice we would prefer more variation in all of them. At any rate we chose these six to predict the forward lag damper load, whose statistics are shown on the bottom row.

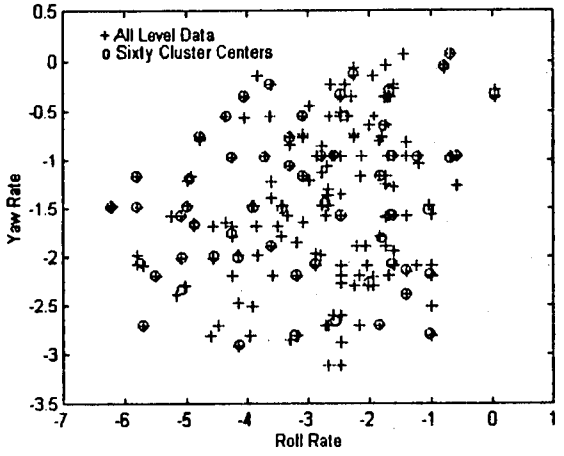
Pearson Correlation Matrix

	Nz	stick	pitch	roll	yaw	load
Nz	1.00	0.02	0.15	-.107	0.04	-.01
stick		1.00	-.14	0.05	0.04	0.10
pitch			1.00	0.04	0.38	0.07
roll				1.00	0.25	-.04
yaw					1.00	0.12
load						1.00

NAWCADWAR

Next, we looked at the correlation coefficients of the six variables in relation to each other and the dependent variable, the forward lag damper load. I show five of the variables here for the sake of space. The other stick variable was also uncorrelated to the others. As can be seen from this table, we were in no danger of including redundant information with these variables. There is no correlation between any of them or with the load, either. We will have no variable in the model that is even remotely linearly related to the dependent variable. It would be helpful if there was some correlation between one of the variables and the load. If this was a simple linear problem, we would not have to look at neural networks for a solution.

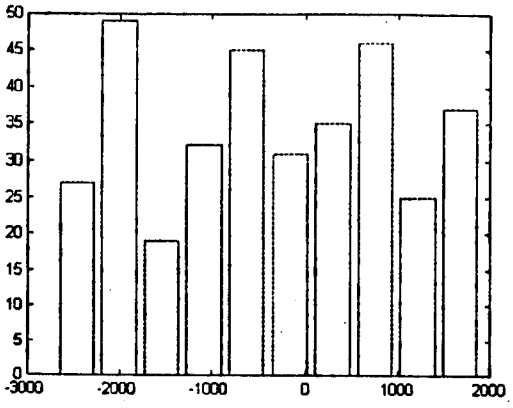
Region of Interest- Input



NAWCADWAR

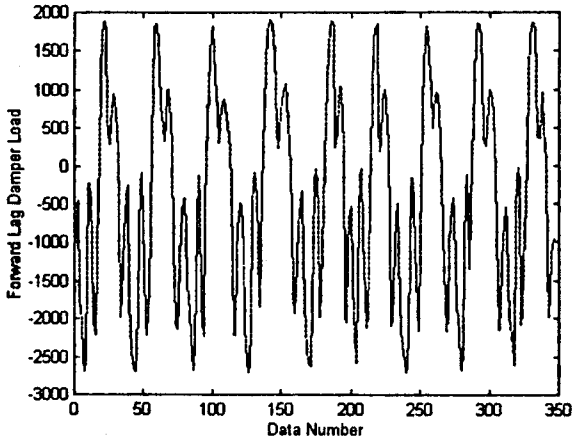
Now we will look at the region of interest. What do I mean by region of interest? It's the location of the space the data occupy in a dimension. Let's take the two dimensional case, which we can graphically represent. In this Vu-graph we have shown Yaw Rate versus Roll Rate. In selecting a sample to work with, we want to ensure that data from all regions of the sample space are included. One way we did this was to perform a cluster analysis. The results shown here resulted from using the Fuzzy C-Means method. This method selects prototypical data that represent the minimum distance between them an a neighborhood of points. The cluster centers were found for the data in 9-space. I show a 2-D portion of the result for sixty cluster centers. Results varied because the method uses random vectors as the initial conditions. After several iterations I concluded that the cluster analysis was extremely computationally intensive, and the results were no better than those achieved from a simple random sample approach. Also the predictions did not capture the extreme peaks and valleys at all, so the cluster analysis was not pursued further.

Region of Interest- Output



The region of interest for the output is easier to visualize. We always recommend developing a neural network with one output. Although multiple outputs are possible, the performance is much better if the coefficients are optimized for one output. The region of interest can be investigated by looking at the maximum and minimum values and the histogram. The ideal calibration set has a uniform distribution over the region of interest. This can usually be achieved with random sampling, provided the sample is large enough. The resulting set can be augmented by manually adding some values where the population is weak.

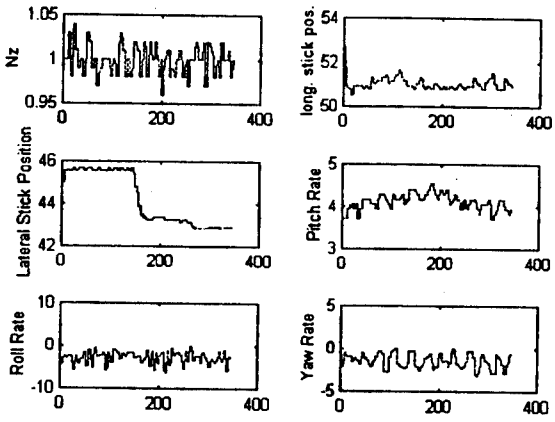
Level Flight Data
Forward Lag Damper Load



NAWCADWAR

This is a graph of the forward lag damper load in the order the loads appeared, after the redundant data had been deleted. It appears to be very consistent and you would think the loads would be very easy to predict. I suppose they are if we could assume that the peaks and valleys do not vary much from one mission to the next, but unfortunately we know they do. We proceed to investigate approaches to designing a neural network to predict the loads, with the intent that the model will be useful for a wide range of pilot techniques and missions.

Neural Network Input- Level Flight

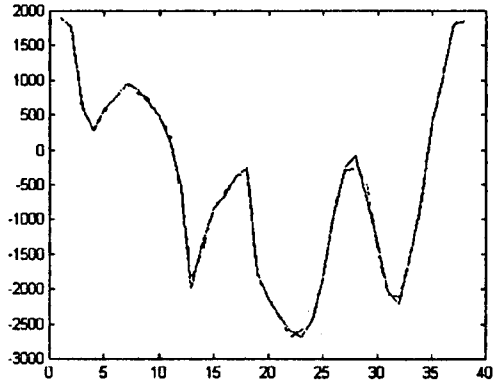


NAWCADWAR

We saw how stationary the loads data were. This is in great contrast to the six inputs that we had to use to predict the loads. They are clearly non-stationary and non-Gaussian. Notice how the values shift as a function of time.

Single Cycle Training Set- Level Flight- 30 KTS

Forward Lag Damper Load

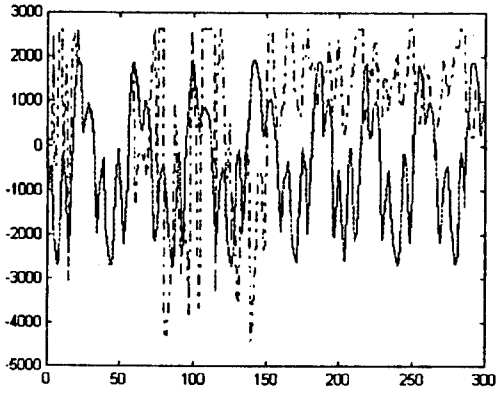


NAWCADWAR

As a first attempt at predicting the load, I selected a data set that represented a single cycle of the output, without consideration to the input. It is desirable to minimize the number of training records and the number of computing neurons. The data set consisted of 38 training records. The neural network with 6 input variables and 5 hidden neurons on one hidden layer trained in 66 epochs to a sum-squared error of 0.009962. The transfer function from the input to the hidden layer was a log-sigmoid, and from the hidden layer to the output layer was a linear function.

Single Cycle Results- Level Flight- 30 KTS

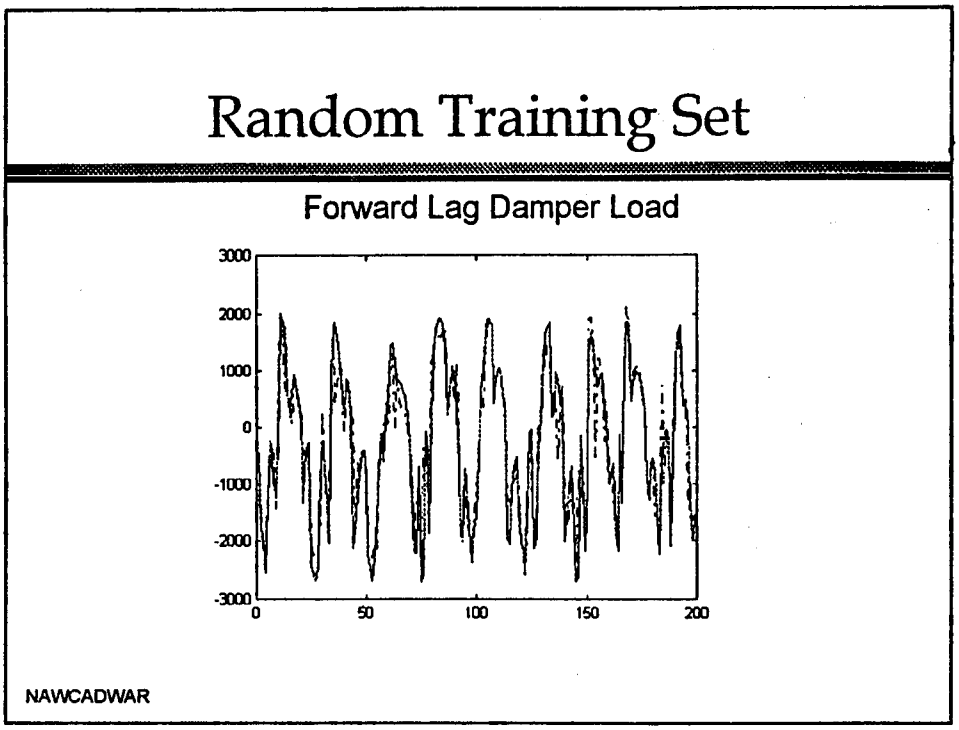
Forward Lag Damper Load



NAWCADWAR

Here are the results from the single cycle training set. Obviously the independent drifting that occurs in the input variables affects the output. Also, because I used a purely linear transfer function to calculate the output, some of the peaks were way out of range. I truncated the peaks at 2620 for this example, but I left the valleys untouched. This approach will not be acceptable in production, especially since it is important to the fatigue prediction to know the maximum ranges. I recommend using log-sigmoid transfer functions in both the hidden layer and the output layer. They will ensure that the values do not swing widely from the anticipated range.

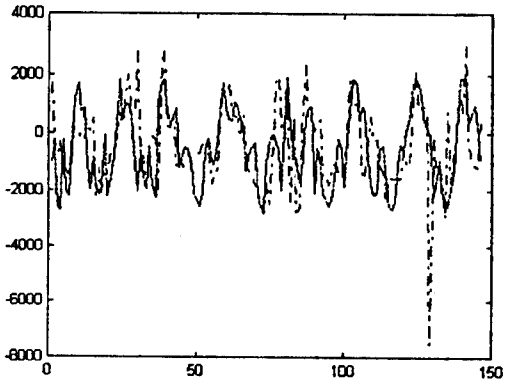
Random Training Set



Next, I tried a larger training set. We randomly selected 200 records out of 346 to be used for calibrating the neural network coefficients. The neural network used six inputs, with ten hidden neurons. It reached a sum-squared error of 2.657 in 100 epochs. The log-sigmoid and pure linear transfer functions were used here also.

Blind Test Results

Forward Lag Damper Load

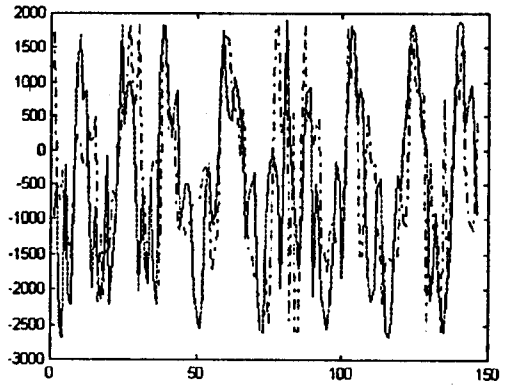


NAWCADWAR

Here are the results from the blind data. The trends were generally captured, but the extreme ranges cannot be taken literally. You can see some spikes that resulted because of the linear transfer function present at the output layer.

Blind Test Results- Truncated Peaks

Forward Lag Damper Load

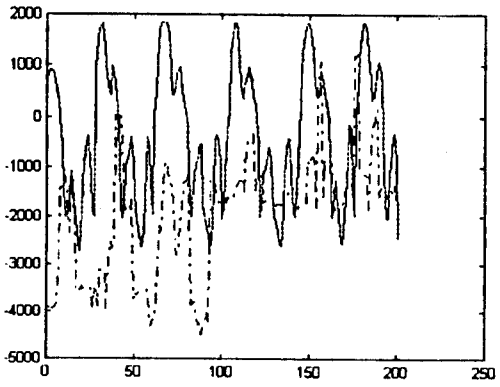


NAWCADWAR

If we truncate the spikes to the maximum values of +1860 and -2590, you can see that the majority of fluctuations are followed. The results are not great, but they seem to be conservative.

Blind Test-
Level Flight, 40 KTS

Forward Lag Damper Load

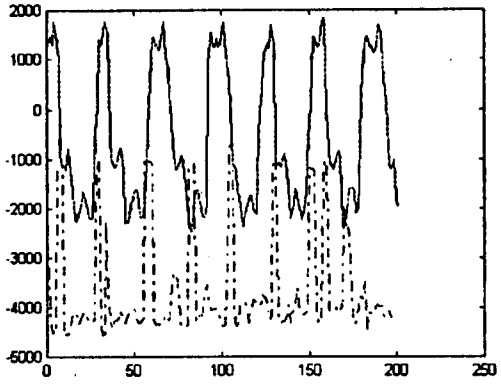


NAWCADWAR

Next we tried the network on two different sets of level flight data. The first set was from the set of maneuvers identified by Dr. Tsai as the blind data. The level flight maneuver was available at 40 knots. It was very similar to the calibration data, as were the results.

Blind Test- Level Flight, 105 KTS

Forward Lag Damper Load



NAWCADWAR

The second was a set of data records from level flight at 105 knots. I show you this to emphasize the difficulties in predicting rotating loads. It looks like the objective to predict raw peaks and valleys is hopeless with these sets of input data and variable selection. The same conclusions have been drawn by Berens who used regression on this data and Tsai who used the holometric approach [1,3]. I suggest counting the data before using it to develop models, and to concentrate on the largest ranges. The coefficients should be optimized for the important events, not the majority of events.

Future Plans

- Obtain better data.
- Count it first- Rainflow
- Explore further relationships between input variables- Fuzzy Logic Operators.

NAWCADWAR

When the traditional methods didn't work, we tried neural networks. This method is the best one available for handling non-linearity and finding patterns in the data. The feed-forward network could not adapt to the ever changing values of the input. I thought the results were amazing, given the task to find some relationships between the uncorrelated input and output. That does not mean that they are useful.

Counting the data first should improve the usefulness of the model. The most important ranges will be used to optimize the values of the coefficients. Rainflow counting the raw data will be the first step in the future work. Then measures can be taken to reduce the redundancies and inconsistencies in the data and to select good data sets that well represent the regions of interest for the input and output.

Finally, I have a modest in-house research project to explore the use of fuzzy-logic operators on the data. The coefficients of the neural network can be used as adaptive ordered weight aggregators. Fuzzy logic operators will consider the maximums and minimums of the input variables in relation to each other, rather than the discrete values.

References

NAWCADWAR

1. Berens, A.P., "Regression Analsysis Prediction of CH-46 Dynamic Loads", UDR-TM-94-102, Aug 1994.

2. Haas, D.J., Flitter, L., and Milano, J. "Helicopter Flight Data Feature Extraction for Component Load Monitoring", AIAA/ASME/ASCE/AHS/ASC 35th Structures, Structural Dynamics, and Materials Conference, April 18-20, 1994, Hilton Head, SC.

3. Tsai, H.C., "Holometric Flight Load Determination for the CH-46 Helicopter", NAWCADWAR Technical Report, to be published, 1994.

4. Gunsallus, C.T. and Robeson, E., "AH-64A Rotating Load Usage Monitoring from Fixed System Information", Proceedings of the American Helicopter Society Rotorcraft Structures Specialists' Meeting, Williamsburg, VA, Oct 29-31, 1991.

5. Raley, Paul. CH-46 Flight Test Program Report. Naval Air Warfare Center, Aircraft Division, Patuxent River, MD, 1992.

DEVELOPMENT OF AN AUTOMATED PROCEDURE FOR CORRELATION OF TWO SETS OF RANGE MEAN PAIR FATIGUE SENSOR DATA

by
K. Walker and L. Molent
(Senior Professional Officers)

DSTO, AERONAUTICAL AND MARITIME RESEARCH LABORATORY
Airframes and Engines Division
506 Lorimer St, Fishermens Bend, Victoria, Australia, 3207.
Ph: (61 3) 626 7653 Fax: (61 3) 626 7089

1. INTRODUCTION

The safe and economical operation of the RAAF's aircraft fleet throughout its life cycle is an essential requirement for the Australian Defence Force as it is for all defence fleet managers. To assist the fleet manager in attaining these goals a number of fatigue life monitoring tools and systems have been established by the RAAF. Most RAAF aircraft contain on-board fatigue monitoring devices ranging from the relatively simple "counting accelerometers" through to near real-time flight parameter recorders.

One fatigue monitoring tool common to a large number of aircraft types in the RAAF inventory (F/A-18, F-111C, Macchi and PC-9) is the DSTO pioneered Aircraft Fatigue Data Analysis System (AFDAS). AFDAS is an electronic device which pairs turning points (ie maxima and minima) in time histories of strain or acceleration according to a range-mean-pair (RMP) counting algorithm, and stores the counts in an array. The RMP method is generally deemed one of the most appropriate means of presenting fatigue usage data (see Reference 1). As the AFDAS compresses usage data in this form, little post-processing is required to obtain useful usage data.

Although there exists within the AFDAS a self-check capability, this is limited to hardware faults and gross errors of the recorded RMP structure. This capability is very useful, but it is not sufficient to guarantee the integrity of the accumulated data. For this reason additional interrogation, using a suitable criterion, is required before data integrity is assured and mature AFDAS utilisation can proceed.

This report presents the details of a technique developed to correlate two individual AFDAS data channels, as a method of data screening or validation. Although the technique is here-in demonstrated by using operational Mirage, F-111 and F/A-18 AFDAS data, the approach is not aircraft type dependent, and is intended for general AFDAS data screening purposes.

AFDAS has the potential to be a powerful fatigue life management tool. Once data integrity can be routinely assured, fatigue damage assessment may be possible, even at the individual aircraft squadron level.

2. AFDAS

AFDAS was invented by Australia's DSTO Aeronautical Research Laboratory (ARL[1]) and was developed and is currently marketed by British Aerospace Australia Limited. AFDAS directly monitors and counts relevant fatigue strain cycles occurring at selected locations on the aircraft structure. In the case of the RAAF F-111 and F/A-18 aircraft these locations, which were chosen for their fatigue criticality, are listed in Tables 1 and 2 below.

TABLE 1 : F/A-18 AFDAS STRAIN SENSOR LOCATIONS

Number (AMRL)	Channel No.	Descriptor (RAAF)	Location
1	4	RHWR	Right Hand (RH) Wing Root (WR) Lower Lug at Y470.5
2	10	WTEF	RH Wing Trailing Edge Flap Actuator
3	3	RHWF	RH Outer Mould Line (OML) Skin at the Wing Fold (WF)
4	5	FF	RH Forward Fuselage (FF) Canopy Sill at Y213
5	6	FS645HT	RH Horizontal Tail (HT) Spindle Support Frame at Y645
6	7	FS657HT	RH HT Spindle Support Frame at Y657
7	9	FS598VT	RH Vertical Tail (VT) Attachment Stub at Y598
8	8	FS566VT	RH VT Attachment Stub at Y566
9	0	FS453	Y453 Bulkhead (inboard of LH wing attachment)
10	1	FS470	Y470 Bulkhead (inboard of LH wing attachment)
11	2	FS488	Y488 Bulkhead (inboard of LH wing attachment)
12	11	N_Z	Normal Acceleration

TABLE 2 : F-111 AFDAS STRAIN SENSOR LOCATIONS

Number (AMRL)	Channel No.	Descriptor (RAAF)	Location
1	0	W1	Wing Pivot Fitting Lower Plate Fuel Flow Hole 58
2	1	W3	Wing Pivot Fitting Lower Splice Joint
3	2	W5	Wing Rear Spar Access Hole Near RSS 190
4	3	C1	Wing Carry Through Box Lower Forward Corner Radius
5	4	C2	Nacelle Tie Link Support Lug at FS 496
6	5	FF1	Wing Fuselage Intersection Longeron at FS 448
7	6	W6	Wing Pivot Fitting Upper Plate Fuel Flow Vent Hole 13
8	7	VT4	Vertical Fin Pedestal Splice
9	8	CF3	Overwing Longeron at FS 568
10	9	CF5	Bolt Hole Number 253 at FS 496
11	10	AF2	Bulkhead 770.25 Horizontal Tail Pivot Shaft
12	11	N_Z	Normal Acceleration

[1] Now the Aeronautical and Maritime Research Laboratory (AMRL)

Central to the AFDAS is an airborne unit referred to as the Strain Range Pair Counter (SRPC), which automatically processes and stores the information from the sensors, thereby building up a database. Fresh data is added to the data base each time the aircraft flies. This data can then be transferred to a usable medium (eg. *floppy disc*) by means of a portable data readout computer. Software is available to interrogate this data to provide additional fleet management capability. The SRPC monitors the output of the sensors during the flight load-time waveform, and pairs and extracts, the maxima and minima, which are known as "Range Pairs", which then form the basis of subsequent analyses. The assumption that fatigue damage is independent of the rate of change of stress and of the time sequencing of cycles is thus inherent in AFDAS. Time sequence effects which are known to influence fatigue crack growth behaviour are accounted for to a limited extent depending on the amount of flying contained within a range pair table. Each range pair table would normally span one flight only and this may give sufficient resolution within a sequence of many flights to account for load sequence effects.

2.1 Range Pairs

This method of load cycle counting states that fatigue damage produced by a sequence of loads is dependent upon the magnitude of stress at turning points regardless of where they occur in a sequence, and is widely accepted as suitable in identifying cycles for the purpose of cumulative damage analyses. In effect, maxima and minima are paired to form cycles in such a way that each cycle produces the same damage as would a cycle of the same amplitude and mean value in a constant amplitude fatigue test. Thus constant amplitude fatigue data along with an appropriate damage theory, can be used to assess damage due to a random load history.

The process of converting a load-time history to range pair can be regarded as a successive extraction and smoothing process, see Reference 1. Here, the smallest perturbation is found first, the values of the two turning points are noted as the first range pair, and the perturbation replaced by a smooth curve. This process is repeated until all turning points are accounted for. A range pair cycle is deemed to have occurred when its maximum and minimum are contained within other maxima and minima of at least the same magnitude. Only those turning points which are greater than a specified quantisation level are kept and recorded in terms of counts of maxima and minima. In AFDAS, the magnitude of the ranges are quantised into a number of bands. The number of bands is currently set at 16. The resolution of the bands is effectively determined by the strain (or acceleration) range which is pre-set in the SRPC hardware. The process of detecting and counting range pair cycles is performed continuously in real time. This significantly reduces the amount of subsequent processing required. Further range pair and AFDAS details are given in References 1 and 2.

2.2 Channel Ranges

The F/A-18 AFDAS (currently Mark 3 - Mk3) strain ranges have been pre-set based on the expected maximum and minimum strain at each AFDAS location as derived analytically by the aircraft's manufacturer McDonnell Douglas Aircraft Company (McAIR), see Table 3 on the following page.

TABLE 3 : RAAF F/A-18 ESTIMATED AFDAS STRAIN RANGES

No	MATERIAL	PREDICTED STRAIN RANGE			
		MAXIMUM		MINIMUM	
		με	CONDITION**	με	CONDITION
			Case, Mach, Alt (kft), g		Case, Mach, Alt (kft), g
1	6AL-4V Titanium	2100	SSPU,0.8,SL,9.25	-650	SSPD,0.9,SL,-3.0
2	6AL-4V Titanium	2650	360°,0.95, 20, 1.0	-3300	SSPU,0.54,SL,7.5
3	Carbon/Epoxy Comp.	1200	SSPU,0.8,SL,7.5	-700	SSPD,0.9,SL,-3.0
4	7050-T7351 Al. Plate	1600	SSPU,V_L*,SL,7.5	-550	OFF CENT. CAT'
5	♣6AL-4V Titanium	1550	360°,V_L, SL, 1.0	-1200	RPO,0.93,5,6.0
6	♣6AL-4V Titanium	1400	360°,V_L, SL, 1.0	-1900	RPO,0.93,5,6.0
7	7050-T73652 Al. Forg.	1700	RPO,0.7,5,6.0	-1700	SSPD,V_H♦,SL,-3.
8	7050-T73652 Al. Forg.	2200	RPO,0.7,5,6.0	-2200	SSPD,V_H,SL,-3.0
9	7050-T73651 Al. Plate	1250	SSPD,0.8,SL,-2.25	-3300	SSPU,0.8,SL,9.25
10	7050-T73651 Al. Plate	600	SSPD,0.8,SL,-2.25	-1600	SSPU,0.8,SL,9.25
11	7050-T73651 Al. Plate	900	SSPD,0.8,SL,-2.25	-2250	SSPU,0.8,SL,9.25
12	N_Z (g)	10	-	-10	-

V_L* = V_H♦ = limit speed = 1.1 M

** Condition leading to predicted strain

♣ = some aircraft only, refer to Reference 3.

The F-111 AFDAS (currently Mark 3 - Mk3) strain ranges have been pre-set based on the expected maximum and minimum strain at each AFDAS location determined following a series of flight trials performed in 1986 and 1987, see Table 4 below.

TABLE 4 : RAAF F-111 ESTIMATED AFDAS STRAIN RANGES

Channel No	Descriptor	Material	Predicted Strain Range με	
			Maximum	Minimum
0	W1	D6AC Seel	3000	-1000
1	W3	2024-T851 Al	1500	-500
2	W5	2024-T851 Al	2000	-1000
3	C1	D6AC Seel	2000	-1000
4	C2	D6AC Seel	4000	-1000
5	FF1	D6AC Seel	1500	-1000
6	W6	D6AC Seel	600	-1200
7	VT4	2024-T851 Al	1000	-1000
8	CF3	D6AC Seel	2000	-1000
9	CF5	D6AC Seel	1500	-1000
10	AF2	D6AC Seel	1000	-2000
11	N_Z	N_Z (g)	7.33	-2.4

In both cases the strain ranges have been found to be inappropriate for some channels. The F/A-18 ranges have been reviewed and new ranges recommended, Reference 3. The F-111 ranges are being reviewed. Changing the ranges requires hardware changes in the SRPC.

The N_Z channel (channel 11) on the F/A-18 has exhibited particular problems (see Reference 4 for further details). The problems are such that the correct range to be used when analysing the output is not known, and the operation of the sensor itself is not fully understood. The interpretation of N_Z data obtained so far is therefore unresolved.

3. AFDAS TRANSFER FUNCTIONS

Before a meaningful correlation procedure can be developed, it must be determined which combinations of AFDAS channels will produce a linear transfer function, and the (theoretical) value must be determined.

Transfer functions for the F/A-18 were developed using flight data obtained from the International Follow On Structural Test Project (IFOSTP) RAAF Aircraft Research and Development Unit (ARDU) flight trials conducted on F/A-18 A21-032 (see References 5 to 7 inclusive). The flights, manoeuvres and configuration of the aircraft used in developing these transfer functions are detailed in Reference 8.

From this analysis it was found that twelve (12) combinations of AFDAS channels produced linear transfer functions. The results are summarised in Table 5 below. The transfer functions were derived to represent average values, and represent the flight configurations and regimes described in Reference 8. The relationships between some channels exhibit a bi-linear trend (eg. different slope for positive and negative *g*), the transfer functions in Table 5 represent the quadrant containing the bulk of the data (ie. positive *g*).

TABLE 5 : AFDAS TRANSFER FUNCTIONS

No	Combination X versus Y		Description	Transfer Function με Y = aX + C		R^2	σ (με)
	X	Y		a	C		
1	Ch1	Ch0	Y470.5 vs Y453 b'lhd	1.04	-8	0.994	48
2	Ch2	Ch0	Y488 vs Y453 b'lhd	1.39	70	0.983	73
3	Ch2	Ch1	Y488 vs Y470.5 b'lhd	1.33	76	0.996	34
4	Ch11	Ch0	N_Z vs Y453	-283	72	0.966	103
5	Ch11	Ch1	N_Z vs Y470.5	-271	74	0.969	96
6	Ch11	Ch2	N_Z vs Y488	-202	-4	0.964	75
7	Ch11	Ch3	N_Z vs RHWF	130	-66	0.776	128
8	Ch11	Ch4	N_Z vs RHWR	230	-174	0.968	78
9	Ch11	Ch5	N_Z vs FF	105	-	0.712	232
10	Ch3	Ch4	RHWF VS RHWR	1.38	73	0.755	203
11	Ch6	Ch7	Y645 vs Y657	1.1	-61	0.976	41
12	Ch9	Ch8	Y598 vs Y566	1.15	-43	0.971	74

The detailed work of developing similar transfer functions for the F-111 is still in progress. The work performed so far has revealed that the response of the gauges is expected to change markedly during the course of a flight. This is due to the significant All Up Weight (AUW) reduction due to fuel burn. Configuration variables such as stores and role equipment will also have an effect. These comments apply particularly to relating the strain gauge responses to the normal acceleration, N_Z. The relationships between strains measured at different locations are not expected to vary to the same extent.

Preliminary F-111 work has included examining the relationship between Channel 0 (W1) and N_Z. Based on static strain survey results (Reference 9), and allowing for typical fuel burn, a response of between 400 and 600 $\mu\varepsilon$ per g is anticipated.

4. DEVELOPMENT OF A CORRELATION PROCEDURE

AFDAS processing software has been developed by Hawker de Havilland Victoria Limited (Reference 10). The software interrogates data extracted from the SRPC and includes routines to screen for potential errors including the following:

a. Documentary data discrepancies including invalid tail number and dates/times.

b. Errors in the hardware including amplifier errors, low battery voltage level and strain gauge errors.

c. Checking the range pair data outputs providing warnings if there are counts in the extreme windows, if there is an invalid range pair data structure (trough higher than a peak), or if the counts in any window exceed a certain predetermined value.

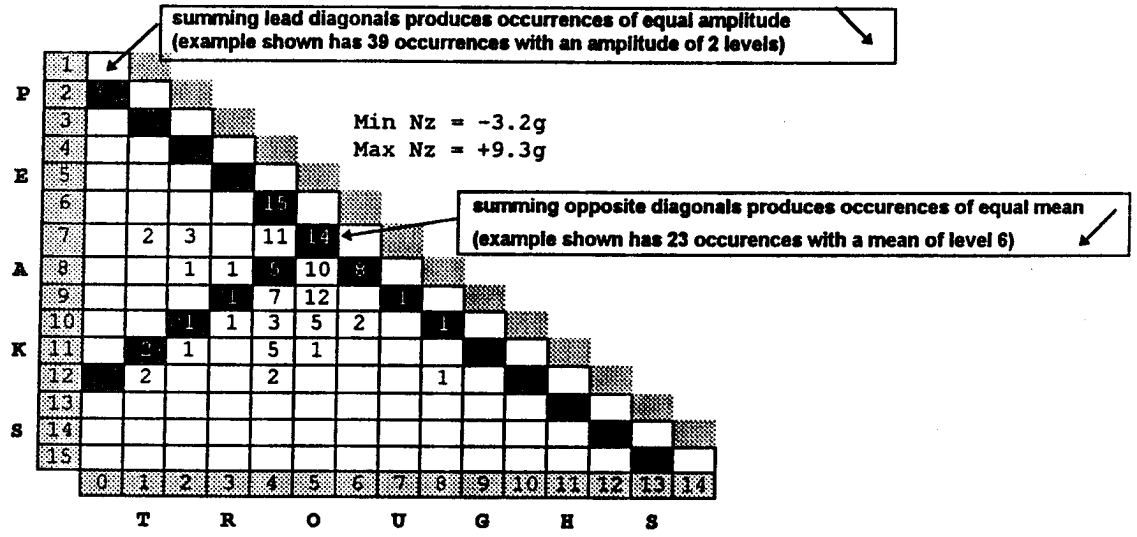
The data screening as described above is useful and necessary, but is very limited. The checks described in sub paragraph (c) above are defined based on expected theoretical outputs for a particular channel. For example, if the strain ranges have been properly set, counts would not be expected in the extreme windows. However, a method of checking the correlation of separate channels on the system both internally and against some expected value was identified as being required. A method which could be readily incorporated into a computer program would be the most practical solution.

Reference 11 details several potential methods of correlating two channels from AFDAS when the data is presented in the form of two range pair tables. The primary method is based on comparing the frequency distributions from two different sources to check for correlation. For example, one would expect to obtain good correlation between the vertical acceleration channel (N_Z) and a strain channel which is primarily driven by N_Z (See Section 3). In the Reference 11 report, data from the Mirage aircraft is used, and a comparison is made between the N_Z channel and a strain gauge located on the wing main spar tension flange. Very good correlation results were obtained.

The Reference 11 correlations were performed by comparing four distributions obtained from the RMP tables: amplitudes, means, peaks and troughs. Summing the occurrences along the diagonals parallel to the leading diagonal produces the amplitude distribution, summing along the opposite diagonals produces the mean distribution, summing vertically produces the peak

distribution and summing horizontally produces the trough distribution. A slight modification of the method was applied to the individual distributions. The range mean pair tables for the N_z and strain data from Reference 11 and a demonstration of the summing procedure is shown in Figure 1 below.

Nz RANGE MEAN PAIR TABLE



STRAIN RANGE MEAN PAIR TABLE

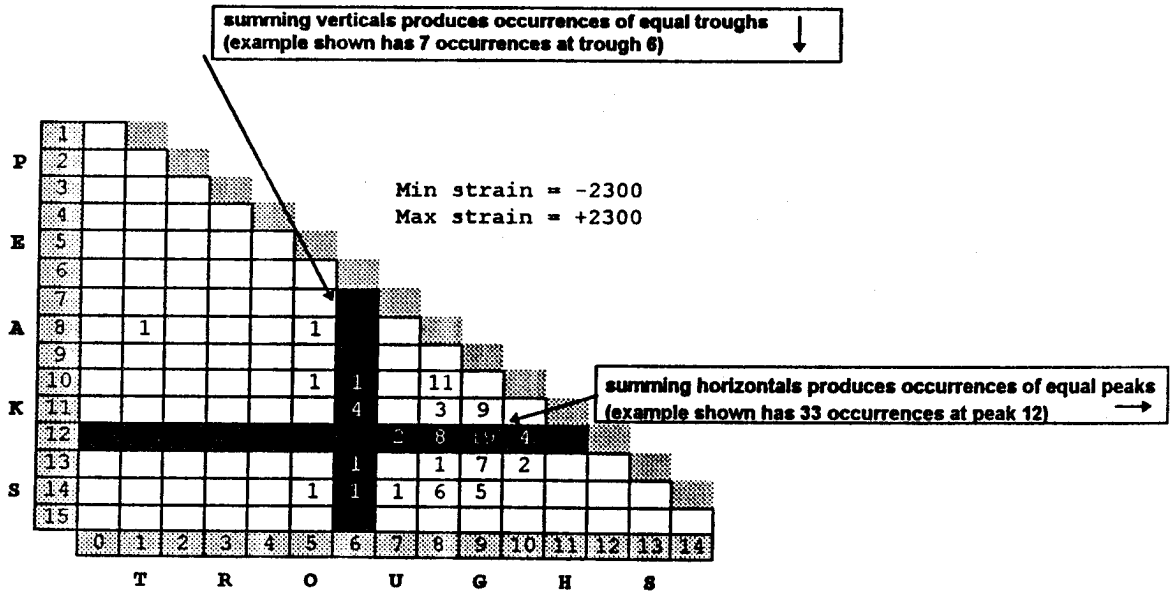


FIGURE 1 : MIRAGE RANGE MEAN PAIR TABLES

The Reference 11 correlation technique is based on the notion that even though a one to one relationship between the load (N_z) and strain ($\mu\varepsilon$) events cannot be extracted from the AFDAS strain range pair tables, the exceedence distributions of the two parameters should be

similar. By comparing the two distributions, it is possible to determine if a linear relationship (as expected) exists between the two.

The Reference 11 procedures involved manual plotting and correlating to produce a final strain per *g* value. A modification of these concepts have been used in a simplified procedure as described in the following section. This procedure was designed to be automated so that it could be incorporated in a computer based screening system.

[A check of the N_Z range pair table against the fatigue meter data is also possible by running the range pair data through a fatigue meter logic algorithm, but this is not pursued here.]

4.1 Simplified Correlation Procedure

Details of a simplified correlation procedure which has been developed are as follows:

a. Sum the lead diagonals, opposite diagonals, horizontals and verticals of the two range mean pair tables of interest, thus producing occurrence distributions based on amplitudes, means, peaks and troughs.

b. Express each occurrence as a percentage of the total.

c. Working in order of increasing load/strain, determine the mid point of the current occurrence percentage at each load/strain level, cumulative with the previous occurrence percentages. For each load/strain level there is therefore one unique cumulative occurrence mid point percentage.

d. Construct a table linking the cumulative mid point percentages with the load/strain levels from the two range pair tables, performing linear interpolation as necessary to obtain one or other of the quantities.

e. Plot the load/strain values obtained from (d) against each other on a linear scale and fit a straight line to the result. The slope of this line is the quantity of interest, for example strain per *g* (same as strain per N_Z).

A complicating factor in the above procedure relates to the way the two channels to be correlated are expected to behave. Where they are expected to act in the same sense, ie an increase in one is expected to correlate with an increase in the other, the procedure is performed exactly as discussed. If the converse is true, then the RMP table must first be transposed before performing the comparison. The transposition effectively swaps the peaks and troughs. Where the channels operate in the same sense a peak in one relates to a peak in the other, and a trough relates to a trough. Where the two channels operate in opposite senses a peak in one relates to a trough on the other, so a transposition is required to one channel to allow a valid comparison to be performed.

This procedure has been applied to the Reference 11 data set. The results for the amplitude distribution are shown in the Table 6 and Figure 2 on the following page. A similar exercise was performed for the other three distributions and the results are presented in Reference 12.

TABLE 6 : STRAIN VS LOAD RESULTS BASED ON AMPLITUDE DISTRIBUTIONS FROM REF 11 DATA

Load Amplitude "g"	Occurrences	Cumulative Occurrences Mid-point %	Strain Amplitude "με"	Occurrences	Cumulative Occurrences Mid -point %
0.391	39	16.53	143.75	24	13.48
0.781	21	41.95	287.5	25	41.01
1.172	20	59.32	431.25	16	64.04
1.563	16	74.58	575	13	80.30
1.953	8	84.75	718.75	6	91.01
2.344	6	90.68	862.5	3	96.07
2.734	3	94.49	1006.25	1	98.31
3.125	1	96.19	1150	1	99.44
3.516	2	97.46			
3.906	2	99.15			

%	Load (g)	Strain (με)	%	Load (g)	Strain (με)
16.53	0.391	159.7	90.68	2.344	714.3
41.01	0.767	287.5	91.01	2.378	718.8
41.95	0.781	293.4	94.49	2.734	817.6
59.32	1.172	401.8	96.07	3.097	862.5
64.04	1.293	431.3	96.19	3.125	870.2
80.30	1.782	575	97.46	3.516	951.7
74.58	1.563	524.4	98.31	3.672	1006.3
84.75	1.953	634.7	99.15	3.906	1113.1

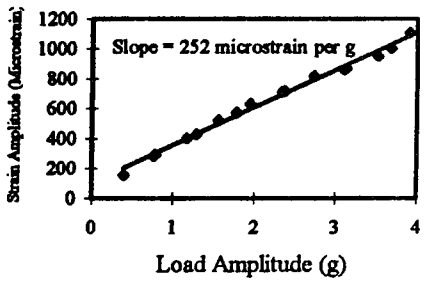


Fig 2: LOAD VERSUS STRAIN

The simplified procedure has been implemented on a PC based computer program called "Corrtest". Full details of the program are given in Reference 4. The program was written in the "C" computer language. Features of the program include the following:

a. A parameter file is used to specify the strain/load ranges, expected correlation[2] values, channels for comparison, error band and whether transposition of a channel is required. The file is customised as necessary to suit the particular aircraft type. The program is applicable to any AFDAS aircraft. Tables 7 and 8 on the following page present the parameter file data for the F/A-18 and F-111 respectively.

b. The program computes the slope (either strain per *g* or strain per strain) relating to the four distributions (amplitudes, means, peaks and troughs) and provides this, plus the average of the four, as the output. The results are compared to an expected range of correlation values (a

[2] Based on theory and/or separate testing and regression analysis, such as Table 3

user input). The program also produces the regression coefficient of the fit between the two channels, and informs the user if this value is less than a predefined value, currently set at 0.90.

TABLE 7 : F/A-18 PARAMETER FILE DATA

CORRELATION X vs Y		Expected Value (slope)*	Specified Error Band	Transpose ?
Channel No. X	Channel No. Y			
3	4	1.58	0.2	N
11	4	230	50	N
2	1	1.3	0.3	N
1	0	1.04	0.2	N
2	0	1.36	0.3	N
11	0	-286	50	Y
11	1	-276	50	Y
11	2	-208	50	Y
6	7	1.1	0.2	N
11	5	110	50	N
11	3	130	26	N

* See Table 5

TABLE 8: F-111 PARAMETER FILE DATA

CORRELATION X vs Y		Expected Value (slope)	Specified Error Band	Transpose?
Channel No. X	Channel No. Y			
11	0	500	100	N

The program has been tested against the Reference 11 data and the results are shown in Table 9 below. This shows that the program gives results identical to the manual process. The program was then checked against a series of F/A-18 flights as described in Section 5 and F-111 flights as described in Section 6.

TABLE 9: COMPARISON OF STRAIN PER g RESULTS

	Amplitudes	Means	Peaks	Troughs	Average
Ref 9 Results	347	346	359	381	358
Simplified Correlation Procedure (Manual)	252	350	314	313	307
Simplified Correlation Procedure (Computer Program)	252	350	314	313	307

Note: These figures were obtained by using the positive section only of the load/strain data

It should be noted that the program uses only data from one quadrant of the *g*/strain or strain/strain curve in conducting the regression. The reasons for this are:

a) bi-linearity of the gauges' response (ie different slope between the positive and negative quadrants).

b) The tendency of fighter aircraft to have many more positive *g* exceedences than negative. Thus the result is biased towards the bulk of the data.

Therefore the program uses only data from the negative quadrant for transposed cases; otherwise, only data from the positive quadrant is used.

Corrtest was designed to run in "batch" mode, that is, it searches for the end-of-flight (EOF) marker within each AFDAS output file (eg. M93354155.**FDS**) and produces outputs for each flight.

5. F/A-18 AFDAS CORRELATION

Also, for the purposes of validating the Corrtest program a number of F/A-18 AFDAS .FDS for a sample of aircraft was used. This data covered a period from July 1992 to Feb 1994. A typical output from the program is presented in Table 10 below.

TABLE 10 : TYPICAL CORRTEST OUTPUT

FLIGHT1

Channel X Y	AMP	MEAN	PEAK	TROUGH	MIN	MAX	AVGE
3 4	1.63/0.95φ	2.10 *Fϕ/0.95	1.99 *F/0.99	2.17*F/0.93	1.38	1.78	1.97
11 4	297.42/0.99	1063.78*F/0.96	442.65*F/0.95	926.81*F/0.94	180	280	682.66
2 1	1.05 /1.00	1.01 /1.00	0.96 *F/1.00	0.97 *F/1.00	1.0	1.6	1.00
1 0	1.16 /1.00	1.02 /0.99	0.94 /0.97	1.19 /0.99	.84	1.24	1.08
2 0	1.22 /1.00	1.02 *F/0.99	0.89 *F/0.98	1.20 /1.00	1.06	1.66	1.08
11 12	-350.34*F/0.98	-872.82*F/0.97	-603.67*F/1.00	-790.46*F/0.94	-336	-236	-654.3
11 13	-288.30/0.98	-715.06*F/0.96	-518.93*F/0.99	-459.85*F/0.89*Fβ	-326	-226	-507.4
11 14	-279.73*F/0.97	-821.39*F/0.97	-365.80*F/0.94	-662.14*F/0.95	-258	-158	-532.3
6 7	0.84 *F/0.99	0.75 *F/0.95	0.92 /0.96	1.33 *F/1.00	0.9	1.3	0.96
11 5	74.15/0.99	162.53*F/0.99	101.39/0.98	196.17*F/0.98	60	160	133.56
11 3	151.38/0.97	481.37*F/0.99	197.38*F/0.95	457.43*F/0.98	104	156	321.9
9 8	0.63*F/0.97	0.68*F/0.98	0.79*F/0.96	0.78*F/0.99	0.95	1.35	0.72

where: min, max = predefined allowable range of slope.
average = average of amplitude, mean, peak and valley results
φ = regression coefficient of linear fit R^2
ϕ = "F" proceeding "*" implies slope outside error band.
β = "F" proceeding "/" implies regression values outside predefined limit. Note these values are excluded from the calculation of the average value.

A summary of the "amplitude" test output for the sample aircraft is presented in Table 11 below.

TABLE 11 : AMPLITUDE TEST FOR SAMPLE AIRCRAFT

Aircraft :	A21-17	A21-17	A21-26	A21-38	A21-38	A21-44	A21-44	A21-107	A21-117
File :	M93354155	M93362141	M93342099	M93334236	M93346211	M93335159	M93352132	M93343091	M93342091
TOF* :	300	300	600	300	300	300	300	500/900	600
FLT hrs :	5.4	27.7	20.9	27	10	18.4	12	16.1	33.1

CH : X Y	ACTUAL	SLOPE	SLOPE	SLOPE	SLOPE	SLOPE	SLOPE	SLOPE	SLOPE	SLOPE
3 - 4	1.38	1.63	1.63	1.18	1.86	1.71	1.5	1.78	2.33	2.05
11 - 4	230	297	318	201	290	314	320	328	212	231
2 - 1	1.33	1.05	0.95	1.23	1.12	1.31	1.03	0.99	0.91	1.05
1 - 0	1.04	1.16	1.39	0.73	1.42	1.3	1.35	1.32	0.97	1.23
2 - 0	1.39	1.22	1.3	0.92	1.59	1.71	1.43	1.33	0.92	1.44
11 - 0	-283	350	399	154	375	392	418	398	223	274
11 - 1	-271	288	285	196	276	304	301	293	224	204
11 - 2	-202	279	305	170	239	229	301	293	248	194
6 - 7	1.1	0.84	1.23	1.3	1.13	1.04	1.16	1.1	1.42	1.61
11 - 5	105	74	87	89	96	87	66	62	45	37
11 - 3	130	151	149	123	121	120	149	140	83	91
9 - 8	1.15	0.78	0.68	0.7	0.78	0.65	0.61	0.72	0.59	0.54

* TOF = type-of-flight code, see Ref 3.

The statistics from this analysis are presented in Table 12 below. The data used consisted of the 9 AFDAS files [6 aircraft], totalling approximately 170 flying hours.

TABLE 12 : SAMPLE AIRCRAFT CORRELATION STATISTICS

(a)		AMPLITUDE		MEAN		PEAK		TROUGH	
CH X : Y	ACTUAL	μ	σ	μ	σ	μ	σ	μ	σ
3 - 4	1.38	1.74	0.33	2.23	0.28	2.08	0.19	2.21	0.26
11 - 4	230	279	50	623	174	433	37	559	145
2 - 1	1.33	1.07	0.13	1.09	0.17	1.05	0.15	1.02	0.09
1 - 0	1.04	1.21	0.22	1.07	0.24	1.08	0.26	1.21	0.24
2 - 0	1.39	1.31	0.27	1.2	0.39	1.2	0.38	1.28	0.3
11 - 0	-283	331	93	-557	164	-481	115	-524	160
11 - 1	-271	263	43	-448	117	-419	59	-392	70
11 - 2	-202	251	48	-487	165	-382	68	-387	167
6 - 7	1.1	1.2	0.22	1.3	0.33	1.23	0.3	1.33	0.23
11 - 5	105	71	21	176	73	147	45	186	59
11 - 3	130	125	25	273	86	204	24	267	94
9 - 8	1.15	0.67	0.08	0.79	0.29	0.75	0.07	0.65	0.11

b) *COMBINED (average of all) METHODS :*

CH X : Y	ACTUAL	μ	σ	% σ
3 - 4	1.38	2.1	0.32	15
11 - 4	230	479	173	36
2 - 1	1.33	1.06	0.14	13
1 - 0	1.04	1.18	0.23	19
2 - 0	1.39	1.3	0.32	25
11 - 0	-283	-477	191	40
11 - 1	-271	-377	139	37
11 - 2	-202	-382	166	43
6 - 7	1.1	1.25	0.28	22
11 - 5	105	124	63	51
11 - 3	130	216	87	40
9 - 8	1.15	0.72	0.16	22

Where : μ - Mean Slope
σ - Standard Deviation Slope

From these results it can be seen that consistent correlations were achieved for all four methods. The values of standard deviations were reasonable, and were used in defining the expected range of the correlations, against which each method is tested. From these results it was concluded that the AFDAS data used in this investigation was free of irregularities, and were true representations of the usage of the aircraft during the periods considered.

Of the four methods, the amplitude test gave the most consistent values and these were closest to the theoretical transfer function (see Section 3 and References 5 to 8 inclusive). Of the combinations of channels tested, Ch 2-0 and Ch 6-7 produced the smallest standard deviations, and this was attributed to the fact that the specified range of these channels were close to the values determined when the ranges were reviewed. It should also be noted that although the results of the correlation containing the N_z channel appear good, solution of the problems discussed in Section 2.2 may affect the results. If these channels are ignored, then the standard deviation of the average value of all four methods is within 25% of the theoretical transfer function. It is therefore considered feasible to use the expected correlation range for particular channel combination comparisons and thus check on the quality and consistency of the AFDAS data.

As the aircraft configuration and missions vary with time, it can be expected that the correlation values will also vary. Theoretically, the correlation (or transfer function) will vary during a particular flight. As an example of this, as the aircraft consumes fuel from the wing internal/external tanks, the wing inertia will change thus affecting the strain response to g at the wing root sensor etc. Thus the correlation results must be considered as "period" averages. In order to ascertain this variability, approximately one year of AFDAS .FDS files from aircraft A21-117 and A21-017 were obtained and were "run" through Corrtest. The results for this analysis are presented in Figures 3 and 4 on the following page.

The AFDAS.AFS files used in deriving these results span approximately 20 months for aircraft A21-117 and 12 months for A21-17.

From these results it can be seen that consistent correlations were achieved for all four methods. The values of standard deviations were reasonable, and ignoring again the N_z channel, were within 25% of the theoretical transfer function.

It can be seen that the results for each aircraft were consistent over the period considered. Again, it is considered feasible to use the expected correlation range for particular channel comparisons and thus check on the quality and consistency of the AFDAS data. The form in which Figures 3 and 4 are presented is considered the most useful, as trends over a period of time can be readily deduced, and thus an irregular flight (or data) easily detected.

From these results it was concluded that the AFDAS data used in this investigation were free of irregularities, and were true representations of the usage of the aircraft during the periods considered.

When comparing results from different aircraft, apart from the mission and configuration differences already mentioned, variations between individual gauge response should also be considered. Due to varying gauge factors, structural component build differences and sensor positioning errors, gauges at nominally similar position on different aircraft may produce different results for nominally identical manoeuvres. All these factors need to be considered when comparing inter-aircraft correlations.

6. F-111 AFDAS CORRELATION

Pending the availability of good quality operational data, a test was performed using F-111 AFDAS information from a series of flight trials performed in 1987. Nine flights of information were available from Reference 13. The data was judged at the time to indicate that the AFDAS system was functioning correctly

For test purposes it was decided to run the program using the N_z channel and a strain channel expected to be highly N_z sensitive. Channel 0 relates to AFDAS gauge W1 which is located on the wing pivot fitting lower plate adjacent to fuel flow hole 58 in the centre web stiffener. This channel was compared with the C.G. acceleration (N_z, Channel 11). From static strain survey results, an expected strain per *g* value could be calculated. This will vary with fuel burn, and for the F-111 on a typical mission, a range of 400 to 600 microstrain per *g* was expected (ie: a "band" of 200 microstrain per *g*). This is based on strain survey results (Reference 9).

The strain per *g* results for the 10 flights from Reference 13 are presented in Figure 5 on the following page. A 200 microstrain per *g* "band" is plotted between 250 and 450 microstrain per *g*. The band was placed there to demonstrate that, neglecting any offset error which may be present, the variation between flights in strain per g is generally less than the 200 microstrain per g "band" expected due to fuel burn. In particular the average of the strain per g calculated by the four different techniques is always within the 250 to 450 microstrain per g range. Flight three also stands out as being significantly different to the others, certainly in terms of the amplitude distribution, which may warrant further investigation to determine if there was anything unusual about that flight or a data acquisition error had occurred. These

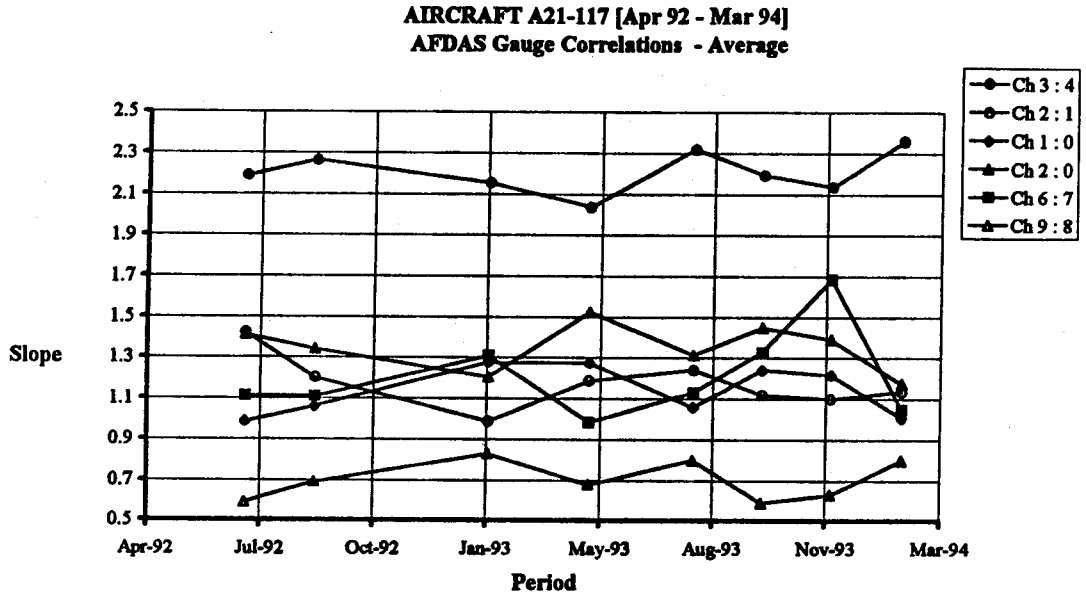


FIGURE 3 : AIRCRAFT A21-117 GAUGE CORRELATIONS

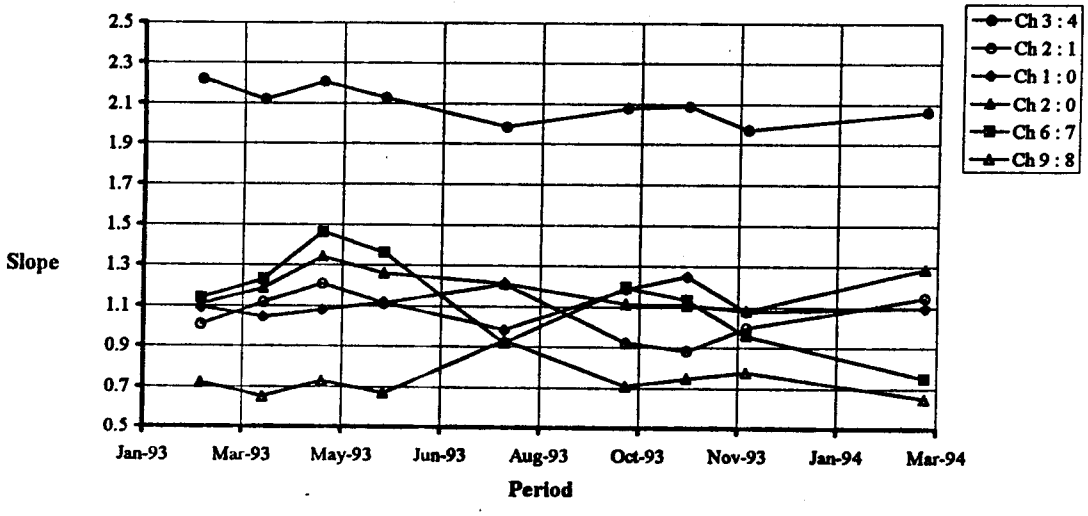


FIGURE 4 : AIRCRAFT A21-017 GAUGE CORRELATIONS

results indicate that it is feasible to set up an expected correlation range for particular channel comparisons and use this as a check on the quality and consistency of the data.

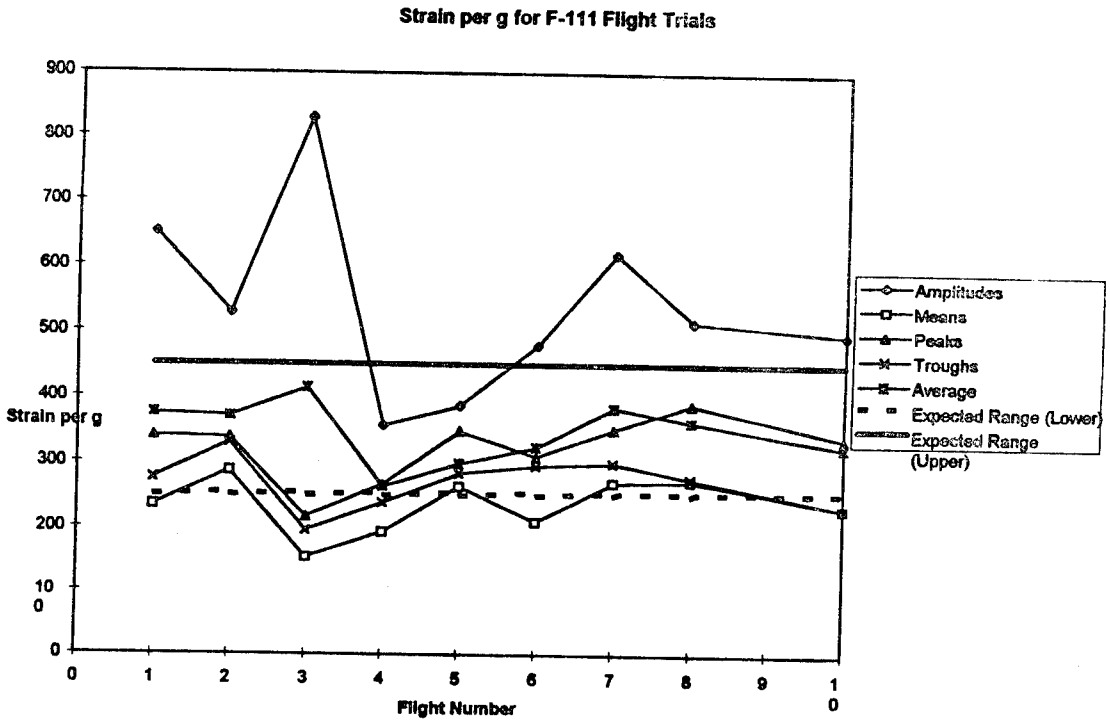


FIGURE 5: STRAIN PER G RESULTS F-111 1987 FLIGHT TRIALS

7. DISCUSSIONS AND RECOMMENDATIONS

The method described in this report, along with the program developed, shows good potential as a means of screening AFDAS usage data. It is recommended that operational AFDAS data be periodically "screened" using this method, and the average result for each aircraft and period be monitored over time. If an irregularity is noted, that individual data set leading to the observation, should be interrogated. If the cause (eg spurious large count in a cell) can be determined then the data file can be "salvaged", otherwise the file should be omitted from subsequent aircraft usage analyses. It should be noted that the data should first be screened through the Hawker de Havilland program to determine the existence of gross errors.

The expected range of the correlation between channels, will need to re-assessed once the AFDAS SRPC's are modified to incorporate the optimum channel ranges.

8. CONCLUSIONS

This report presents the details of a technique developed to correlate two individual AFDAS data channels, as a method of data screening or validation. A PC based program developed to implement the technique routinely for operational AFDAS flight data is also described.

Although the technique was here-in demonstrated by using operational, Mirage, F-111 and F/A-18 AFDAS data, the approach is not aircraft type dependent, and is intended for general AFDAS (or range mean pair) data screening purposes.

This method can now be used to routinely assure AFDAS data integrity, from which fatigue damage assessment can be subsequently conducted, even possibly at the individual aircraft squadron level. The data screening capability will enhance the potential of AFDAS as a powerful fatigue life management tool.

9. ACKNOWLEDGMENTS

The authors wishes to acknowledge the assistance and support from Ms A. Houston who developed the PC based software. Also to Messrs B. Aktepe, R. Ogden and G. Swanton of Airframes and Engines Division AMRL, for assistance and input.

10. REFERENCES

1. Finney, J.M. and Denton, A.D., "Cycle Counting and Reconstitution, with Application to the Aircraft Fatigue Data Analysis System", Int Conf on Fatigue of Engineering Materials and Structures, Univ of Sheffield, Proc of Inst Mech Eng, Vol 1, Sept 1986, pp 231-240.

2. Fraser, R.C., "A One-Pass Method for Counting Range Mean Pair Cycles for Fatigue Analysis", DSTO, ARL-Struc-Note-454, Australia, June 1979.

3. Molent, L., Aktepe, B. and Polanco, F., "F/A-18 Airframe Fatigue Data Analysis System Validation", DSTO, ARL-TR-54, Australia, Jan 1994.

4. Molent, L., Walker, K. and Ogden, R., "A Data Screening Technique for AFDAS", DSTO-TR (in press).

5. "Aircraft Configuration and Flight Summary", RAAF ARDU Task 0021 (IFOSTP Phase 2), report to be issued.

6. "Hornet Flight test Programme to Obtain Flight Loads Data", RAAF ARDU Task 0021 Formal Report, to be issued.

7. A.J.Dietz and C.K.Rider, "RAAF Hornet Flight test Programme to Obtain Flight Loads Data", Proc Fifth Australian Aeronautical Conference, Melbourne, 13-15 September 1993, IEAust No. 93/6, pp49-355, 1993.

8. L. Molent, F. Polanco, R. Ogden, and Y. Guan Ooi, "Development Of Parametric Strain Equations For Fatigue Sensors On The RAAF F/A-18, DSTO-TR (in press).

9. Molent, L., "Ambient Proof Load Test of a Boron/Epoxy Reinforced F-111C Wing Pivot Fitting", ARL Structures Technical Memorandum 486, Melbourne, June 1988.

10. Floratos, A., Garrick, P., "F-111 Aircraft Software Users Guide", Hawker de Havilland Victoria Limited Report No AA-AIR-5.

11. Howard, P.J. "Correlation Between Two Sets of Data Presented as Range-Mean-Pair Counts", ARL Structures Note 477, Melbourne, July 1981.

12. Walker, K., "F-111 Aircraft Fatigue Data Analysis System (AFDAS) In Service Development - Progress Report Number One", DSTO-TR (in press).

13. Denton, A., Reintals, V., "F-111 AFDAS Flight Trials report", British Aerospace Ltd, Salisbury SA, March 1987.

Aircraft Structural Integrity Program for the Aero Vodochody L 139 Jet Trainer

Jiří Fidranský
Aero Vodochody a.s.
Czech Republic

Mark Trabert and Ali Ghannadan
MOOG Esprit Inc.
U.S.A.

SUMMARY

Sufficient service life and service reliability are important features of both military and commercial aircraft. There is a number of tasks necessary to accomplished to ensure successful development and operational service.

The Czech Republic company, Aero Vodochody , has a long background as a manufacturer of military aircraft, having been the primary supplier of advanced trainers to the most of the former Warsaw Pact and some other countries. Aero produced more than 6 000 jet trainers over the past thirty (30) years, including more than 2 800 of L 39. The L 139, which is the latest version of Aero's family of trainers, incorporates "western" engine and avionics into the L 39's proven airframe. The L 139 is designed to meet the requirements of the USAF/USN JPATS aircraft.

Aero plans to implement Loads Environment Spectrum Survey (LESS) and Individual Aircraft Tracing (IAT) Programs for the lot of L 139 production. An ESPRIT Technology Flight Data Recording System is installed to process and record desired flight data. Analysis of these flight data and their affect on the fatigue life of the aircraft's structure will be accomplished by Aero using a self-designed software program.

Aero's basic philosophy is to assess most structural components using a Safe Life approach, however, some fatigue critical components are evaluated using damage tolerance methodology. Flight data expressing the loading sequence of individual aircraft enables Aero to estimate crack initiation/crack growth. In some cases, strain gauges are used to directly monitor loads in certain fatigue critical locations.

Current results show that implementing this program will enable at least to double the aircraft's service life without structural modifications.

INTRODUCTION

Aircraft design and production in the Czech Republic has a long and successful tradition. Aero had been established in 1919 as a private aircraft producer. Before the WW II about 55 types of indigenous design were produced both for military and commercial purposes.

During the WW II and German occupation the company was constraint to produce German-designed military trainers.

At the beginning of the jet age, since 1953, licence-built MiG-15 in three variants were leaving the factory during the succeeding decade, followed by more advanced twin engined MiG-19s, as well as famous MiG-21s.

Gained experience with jet fighter technology, as well as own well qualified and

skilled research and development staff was a basic platform for indigenous jet trainer introduction. In the early sixties the development and tests of L 29 Delfin, the first military jet trainer of Czech design was successfully completed. The aircraft had been delivered to former Warsaw Pact and some other countries in large quantities. More than 3,500 units had been built up to mid-seventies and lot of them are still in service. Expanding jet trainer success resulted in the L 39 Albatros basic/advanced turbofan trainer, with the deliveries to 18 customers all over the world since the seventies. More than 2800 these aircraft of different versions were produced. Of course, there is also a new Ae-270 turboprop utility/transport aircraft under development. A complete history of Aero company can be found in reference 1.

There are new versions of the jet trainer with sophisticated equipment being delivered today. The jet trainer family consists of three basic members, the L 39 Albatros with well proven airframe and excellent training characteristics, the L 59 as a more powerful version with strengthened airframe and the latest L 139 Albatros 2000, which incorporates "western" engine and avionics into the L 39's proven airframe. The main differences, as compared with previous models, is Allied Signal TFE731-4 engine and upgraded aircraft systems, including e.g. OBOGS, advanced weapon delivery and navigation systems and combat training system and Individual Aircraft Tracing system. The aircraft is designed to meet basic requirements of the USAF/USN JPATS aircraft (reference 2). As a prototype, the L 139 is used also as a test bed for advanced aircraft systems. It is possible to offer such systems as midlife upgrade kits for L39 already in use.

Sufficient durability of airframe is a basic requirement for current jet trainers. Durability analyses, tests, as well as service experience have showed the possibility of significant service life extension. To be able to reach this goal Aircraft Structural Integrity Program was initiated.

DESIGN AND QUALIFICATION PHILOSOPHY

Military jet trainers currently in use all over the world were originally designed under safe life concept. Such feature is similar to both "western" and "eastern" producers.

Jet trainers originally designed for former Warsaw Pact countries have been qualified according to Soviet military airworthiness requirements. Requirements for airframe durability qualification approach, valid for trainer class, were the same as for other aircraft categories for commercial purposes, see reference 3. Technical Specifications under Contract required moderate service life, due to relative low annual training intensity life figures which were far below 10,000 flight hours. Adopted design philosophy depends on producer's decision, but safe life approach was considered as less demanding. Up to the late eighties the crack growth analyses, based on analytical models were expected to be inaccurate and therefore not widely used in military programs. The major interest was focused on full scale and in some cases on component fatigue tests.

Initial experience in fatigue testing within the aerospace industry in former Czechoslovakia dates back to late fifties. The first fatigue test was performed on the Ae-45 utility aircraft, followed by the L 29 jet trainer test. Evaluation of the tests was conservative to fulfill the motto "safety first". More than thirty year's service of the fleet confirms such premise, no aircraft has been lost due to structural failure.

The first durability tests of the L 39 jet trainer were performed in the '70s. The theoretical durability analysis based on Miner's rule, was verified by three fatigue full-scale

structure tests - the prototype and two production versions of the aircraft. Both production versions featured design changes and enhanced service life.

The program for increasing of the L 39 durability was completed in the 80's. Technical changes on structure were analyzed and supported by an extensive program of fatigue tests on fatigue specimens and airframe components. The "flight by flight" method was applied with a quasi-random loading using service spectra. The program was based on feasibility study and lot of data sources, including flight measurement, strain surveys on full scale tests, fatigue crack measurement during the tests, fractography analysis, residual test results. Of course, an important source was also the database of about 4.5 million flight hours accumulated by the L 39 fleet during customer service, without any serious structural failure. Detail description of the program is summarized in reference 4 and 5.

When the former Soviet approach was followed the significant margin was hidden in the factor of safety (scatter factor) value, to provide safety in the presence of uncertainties and statistical variability in the information, because it is ranging from 5.2 to 13.5, e.g. much higher than similar values in "western" practice (reference 6).

The durability tests have been carried out by the Prague based Aeronautical Research and Test Institute (ARTI). The test facility is equipped with MTS TSC 872 40-channel electrohydraulic test system. The software is tailored to quasi-random loading. Indigenous software for random loading generation was developed (reference 7). Durability test is expected to be finished when near the critical crack length is reached. After completion of residual static testing, teardown inspection and detailed metallurgical and fractographic evaluation is performed. The SYSTEM 4000 Vishay multichannel data acquisition system is used for measurement.

Tests in our case are performed up to serious damage of primary structure and initial defects are repaired after their significant length is reached. Repair is designed not to significantly influence the remaining structure. This approach enables to achieve more than first defect. It is necessary to emphasize, that our scatter factor is still slightly above the value of four (4.2) because it is based on statistic evaluation of possible influence in variability of loads and evaluation of a number of test results (reference 4).

General approach, which may be slightly different when compared with "western" practice, is to gain as many data as possible and not to finish the tests immediately when expected life multiplied by the factor of two or four is reached. This approach is time consuming and therefore costly, but it has a significant advantage for future life extension programs and in the case when actual service spectrum is more severe than expected. It is also very important when it is necessary to redesign some component and thereafter evaluate the influence of such change.

Great part of the structure is still assessed, in our practice, according to safe life concept, but some critical areas are evaluated according to limited damage tolerance practice. Loading sequence of individual aircraft, when such aircraft is equipped by IAT, enables to estimate crack initiation and crack growth. This approach is not used for aircraft in customer use, mainly because there has not been any reason for it yet. For research purposes such theoretical models like PREFFAS and ONERA were analyzed and verified by measurement on the test. Results of such program are described in reference 8. We have the WILLENBORG model in use involved in P3/FATIGUE program package of PDA company at present.

AERO AIRCRAFT STRUCTURAL INTEGRITY PROGRAM APPLICATION

Aero Aircraft Structural Integrity program concentrates on service life extension and all questions concerning static strength are omitted, because there is no significant reason to enhance current status. Core of the program is based on information described in reference 9.

Initial service life of the L 39 aircraft in early seventies was established at 3,000 flight hours. The value was valid for early series of the aircraft and it was based on conservative estimates of service spectra as well as preliminary evaluation of constant amplitude full scale fatigue test of early prototype.

Improved variant of the L 39 production version since early eighties had 4,500 flight hours of service life, with further extension up to 6,000 flight hours, but analyses were still conservative because there was no demand to extend the life. The potential for service life extension was tremendous. Theoretical analyses and component testing started in late eighties with the main goal to introduce "flight by flight" testing, gain some data concerning crack growth on primary structure and last but not least significantly enhance durability of the structure. The goals were broadened in the early nineties when the necessity to convert qualification process into "western" similar standards was obvious. The Structural Integrity Program started and has been aimed at the whole family of indigenous jet trainers. Final goal is to reach the value of service life approaching JPATS requirements. It is evident that the strengthened L 59 airframe will be closer to that value, but L 39 or L 139 will follow.

Former analyses always expected an average service spectrum, based on customer usage. During the seventies and eighties extensive Loads Environment Spectrum Survey totaling more than one thousand service hours was made, for several Air Forces (reference 10 and 11). Such feedback gave us important data on average loading spectrum, but also discovered significant scatter among individual aircraft. The only way how to overcome such obstacle is to implement continuous Individual Aircraft Tracing.

The program has been boosted by several factors:

Many former Warsaw Pact operators had several times more military aircraft of corresponding categories in service, compare with NATO counterparts. It resulted in a very low annual usage.

From our experience is obvious, that airframe designed to follow static strength requirements only is able to reach at least 3,000 flight hours of safe life, when the aircraft is used for training purposes. Such value, proven by full scale fatigue test, was desirable in case of the above mentioned low usage and when military budgets enables to replace the aircraft after 20-30 years of service.

Initial impulse for jet trainer life extension was initiated by Aero company, because of necessity to enhance our ability to compete in the third world market. Results of company funded research program showed the great potential for life extension. Progress has been concentrated in two areas, design changes and changes in qualification methodology. In some cases incorporation of more sophisticated approach also improves service safety and reliability.

The shift from Safe Life concept to Damage Tolerance concept has been caused not only by economical pressure, but also by implementation of a piece of knowledge concerning the behavior of structures under cyclic loading. The Safe Life concept in its early stages reminds "black box" philosophy and there is no technical reason to follow it if more details about crack initiation and propagation were discovered. Research work in that field has been done in both "western" and "eastern" laboratories simultaneously.

Political and economical changes in East European "new democracies" resulted in their

Air Forces transformation as well as in budgetary problems for many operators. That was the reason for acceleration of life extension programs as well as great challenge for midlife upgrade programs.

LESS & IAT SYSTEM DESCRIPTION

The L 139 prototype is also used as a test bed for advanced aircraft systems. Although another jet trainer family member the L 59, is equipped with a Czech made on board complex diagnostic system, L 139 has been equipped since 1993 by ESPRIT with an eight channel ESPRIT Flight Load Data Recorder.

ESPRIT system has been chosen due to its significant advantage. The system can be set for common long-term data acquisition using triggers, as well as for flight measurement using adjustable values of gates, rates and triggers for a continued fast sampling of shorter sequences. The system features independent triggers on five channels (Nz and strain gauges in fatigue sensitive areas) which enables to analyze and correlate the events with additional parameters of airspeed, altitude and fuel flow at the rest three channels.

Strain gauges (full bridge compensated Columbia modules) are located near the critical part of the wing spar and near the maximal bending moment on the main fuselage longeron. Strain gauges have been calibrated by means of full scale static and durability tests on practically the same airframes as well as during flight tests on the L 139.

Basic software output, delivered by ESPRIT gathers and preprocesses data in the form of time sequences of local extremes (reference 12). Such approach keeps the data order, which is important for crack propagation assessment.

Further part of the software, developed in Aero and VZLU-SPEEL Company is used for data evaluation and life assessment. The software has been certified by The Czech Air Force Authority to be used for military purposes and it is an improved variant of similar software already in use in the L 59 service. Basic methods implemented in the software are Rainflow counting method and cumulative damage method with experimentally proven S-N curves. The data are based on full scale test results. The software enables a full access to the raw data for a supervisor and a limited access without any possibility to enter for maintainance Air Force staff.

It is evident that only a few aircraft of the fleet can be equipped with a relatively expensive eight channel Load Monitoring System (LMS). That is why ESPRIT and AERO are preparing a four channel LMS for the L 139 fleet, including vertical accelerometer and three strain gauge channels.

There will be no other data describing flight parameters. Naturally, technical capability will be a compromise, but price will be cut down. But for the production aircraft in service, it is much more important to have valuable data from fatigue sensitive areas for life assessment before having the possibility to analyze a flight profile. Actually we know WHAT happened, not HOW it happened. However, there are some problems concerning reliability and durability of sensors, but because strain gauges modules can be replaced at a certain period, such problems concentrate on the necessity to replace and recalibrate the system in service.

Besides ESPRIT system, the L 139 jet trainer is also equipped with a FDR 139 crash recorder. It is a Czech made, 64 channel digital system with a solid memory. Some data acquired by the system are suitable as additional data for life assessment in conjunction with the ESPRIT data (airspeed, altitude, the data from the attitude and heading reference system).

The data from both systems can be synchronized.

The shortcoming of our "paperless" approach with no requirements on maintainance staff of the LMS is that we do not know actual TOW and store configuration of the aircraft. That is why we prefer strain gauges without any necessity to know a variation of stress per G relation. There are areas on the structure for which we have the data with certain error. In spite of the fact that we prefer this approach because of a huge fleet of Aero's jet trainers being in service in underdeveloped countries with different level of the maintenance. It is easier to download the data within certain period of service than to cope with the necessity to fill in some form before each flight. The system is fully independent with low requirements on staff skill.

Proposed solution depends on possible maintenance level and environmental conditions in the country of destination. Under very harsh climatic conditions and in case of extremely poor maintenance, strain gauge installation seems to be unreliable. In such case gathering of flight parameters is probably the only acceptable way for the LMS from the service point of view. It is necessary to emphasize that even only Nz tracing is the great achievement, compare with untraced aircraft. Further improvement is beneficial, but not inevitable for a basic reliable system. Essential knowledge of Nz history enables to get a lot of LMS benefits.

The data taken from LMS are inevitable for a fleet management system. An example can be given concerning the load severity of the prototype aircraft, which is used namely for flight tests, presentations, air shows etc. The service spectrum is approximately eight times more severe, compare to average spectra of the whole fleet. Such example emphasizes importance of the LMS for every tail number.

Current experience shows, that ESPRIT system seems to be powerful, reliable and flexible means for Individual Aircraft Tracing and expected benefits will be achieved.

DISCUSSION OF THE BENEFITS

Aircraft Structural Integrity program requires successful solution of a number of tasks and collaboration between producer and customer. It is necessary to have a "closed loop" of information covering analyses, tests and service experience.

The main tasks of the program are expected to be finalized in 1996, but significant results seem to be already evident. Majority of results are transferable on all versions of airframe family. It enables also significant mid life upgrade of the L 39 fleet already in service.

Adoption of "western" similar approach in durability tests and its evaluation enables to extend the basic safe service life to more than 10,000 hours.

When inspection intervals, based on full scale test results, including crack growth rate, and IAT are implemented, the value far above 15,000 service hours seems to be realistic.

Both values mentioned above expect a service loading spectrum corresponding to advanced trainer role.

Because all analyses and tests have been performed for the average spectrum, it is a common approach to reduce such value by some additional factor, usually 1.5, to be sure that no scatter in severity among individual aircraft has exceeded the average spectrum. There is an additional benefit if every individual aircraft is traced. In such case there is additional 30% life extension without degradation of assessment reliability, compared with a case when no aircraft is traced. Naturally a usual scatter factor of about 4.0 still remains. It enables us to reach service life value near to JPATS requirements for advanced trainer role in the near

future. Details are described in reference 13.

Current results enable service life extension without any major structural changes. Some minor changes may be necessary due to the necessity to increase the inspectability of the primary structure. Several minor components may be replaced or repaired during service.

The proposed Individual Aircraft Tracing system has been designed as a fully independent system with no pre-flight check requirements. Such philosophy is preferred, because it significantly reduces demands on Air Force staff qualification and skills and eliminates possible mistakes made by the staff. Continuous data evaluation and sophisticated fleet management significantly reduce risk of too optimistic life assessment.

CONCLUSIONS

The Aircraft Structural Integrity Program performed at Aero Vodochody facility concentrates on a number of tasks, but a needful effort is to optimize gaining maximum benefits at moderate costs. First of all is necessary to improve service life parameters, but only if the risk is reasonable low.

The important advantage is a well proven robust structure which was extensively tested up to its durability limits. In conjunction with a more sophisticated and realistic approach to life assessment such activity resulted in tremendous life extension. It is possible to apply the gained results to new aircraft variants as well as, even if with some restrictions, to in-service aircraft.

The main data source is, in the applied method based on test results, both full scale durability tests and flight loads data survey. Life assessment based especially on analyses seems to be, from our point of view, excessively unreliable. It is inevitable to have actual service data of load history available for every tail number. Significant life extension is impossible without data feedback from aircraft operation. The data have to be gathered as simply as possible, with minimum demands on maintainance staff skills and activity. From our point of view it is better to gain less data and consequently less benefits, but to keep the system reliable and simple.

It is also necessary to have in mind that durability of the airframe structure is influenced by a lot of damage sources, like accidental damage, corrosion in conjunction with fatigue damage, or by widespread fatigue. Such threats are not traceable or observable by current load monitoring systems.

REFERENCES

1. Nemecek, V.,"Czechoslovak aircraft",vol.1 and 2,Nase Vojsko Publ.,1983 (in Czech)

2. Department of the Air Force, "Aircraft System Requirements Document (SDR) for the Joint Primary Aircraft Training System, Draft", 1993

3. Committee for Aeronautics, "Joint Airworthiness Requirements (JeNLGS)",Chapter 4, Airframe Structural Integrity, Moscow, 1983 (in Russian)

4. Fidransky,J.,Fiala,J.,Vrhel,J., "Durability Test of L 39 Wing Spar Booms under Flight by Flight Loading," Report No. V 1641/89, ARTI, 1989 (in Czech)

5. Fidransky,J.,Fiala,J.,"Full Scale Flight by Flight Wing Spar Fatigue Test", Proccedings of the 8th Biennial Conference on Fracture, Torino, Italy, 1990

6. Department of the Air Force, " Airplane Strength and Rigidity, Ground Tests", Military Specification MIL-A-8867B (USAF),1975

7. Fidransky,J.," A Brief Description of Random Loading Algorithm for Airframe Test", Report No. PP.1-152.86, Aero Vodochody, 1986 (in Czech)

8. Ruzek, R., "Software Guide for Crack Growth Models of Airframe Structures under Service Spectrum," Report No. R 2739/94, ARTI,1994 (in Czech)

9. Department of the Air Force,"Aircraft Structural Integrity Program, Airplane Requirements," Military Standard MIL-STD- 1530 A, 1975

10. Budil,F.,"In Flight Load Spectrum of L39 Jet Trainer", Air Force Research Institute,VZS 031,1975 (in Czech)

11. Budil,F.,"In Flight Load Spectrum of L39ZÂ Jet Trainer", Report No. 22/2-272,Air Force Research Institute,1983 (in Czech)

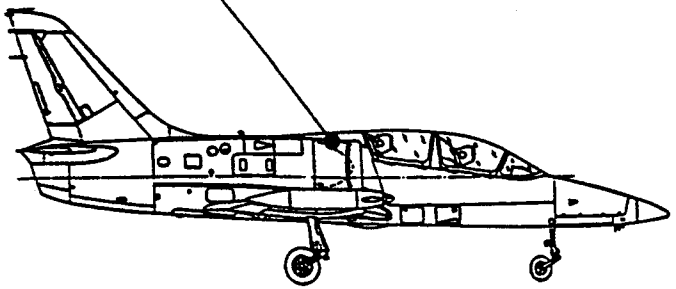
12. ESPRIT Technology Inc. system description

13. Aero Company Internal Data of L59/139 Life Assessment (in Czech)

Aero VODOCHODY

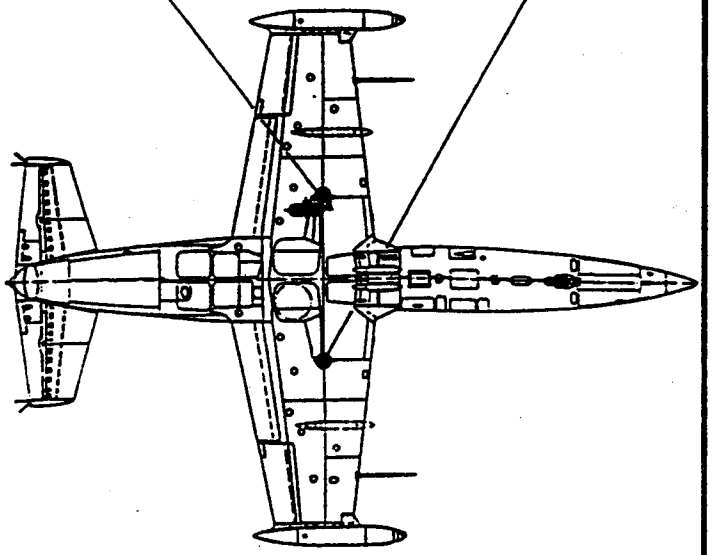
Strain Gauges Locations

Left & Right longeron



Right wing spar

Left wing spar



CHRYSLER TECHNOLOGIES
AIRBORNE SYSTEMS, INC.

A SIMPLIFIED APPROACH TO REPEATED LOADS DEVELOPMENT

1994 USAF Structural Integrity Conference
6 – 8 December, 1994

Chris Manders
Specialist
Chrysler Technologies Airborne Sytems, Inc.

Thanks to:

James Abel, Section Head
Chrysler Technologies Airborne Sytems, Inc.
Test supervision

Joy Ransom, Senior Lab Engineer
Fatigue Technology Inc.
Testing

TABLE OF CONTENTS

Paragraph	Title	Page
1.0	INTRODUCTION	1
1.1	Background	1
1.2	Purpose	1
2.0	TECHNICAL DISCUSSION	2
2.1	Discussion of Approach	2
2.1.2	Simplified Approach	2
2.2	Generation of Spectra for a Center Fuselage	3
2.2.1	Analysis Methodology	3
2.2.2	Spectra Analyzed and Tested	4
2.2.3	Flight Profiles	4
2.2.4	Exceedance Data	4
2.2.5	Design External Loads	4
2.2.6	Segmental External Loads	7
2.2.7	Spectrum Generation	7
2.3	Validation Testing	23
2.3.1	Introduction	23
2.3.2	Technical Discussion	24
3.0	RESULTS AND CONCLUSIONS	31
3.1	Results	31
3.1.1	Analyses	31
3.1.2	Test Results	32
3.1.3	Discussion and Correlation	33
3.2	Conclusions and Recommendations	34
3.2.1	Recommendations	34

CHRYSLER TECHNOLOGIES
AIRBORNE SYSTEMS, INC.

A SIMPLIFIED APPROACH TO REPEATED LOADS DEVELOPMENT

1994 USAF Structural Integrity Conference
6 – 8 December, 1994

Chris Manders
Specialist
Chrysler Technologies Airborne Sytems, Inc.

Thanks to:

James Abel, Section Head
Chrysler Technologies Airborne Sytems, Inc.
For test supervision and support

LIST OF ILLUSTRATIONS

Figure	Title	Page
2.2.3-1	Altitude and Mach Number Profiles	5
2.2.3-2	Equivalent Airspeed and Gross Weight Profiles	6
2.2.7.1.2-1	Conventional Spectrum, No Negative Loads, 1 Flight	10
2.2.7.1.2-2	Conventional Spectrum, No Negative Loads, 100 Flights	11
2.2.7.1.3-1	Conventional Spectrum, With Negative Loads, 1 Flight	13
2.2.7.1.3-2	Conventional Spectrum, With Negative Loads, 100 Flights	14
2.2.7.2.2-1	Simplified Spectrum, No Negative Loads, 100 Flight Block	17
2.2.7.2.2-2	Simplified Spectrum, No Negative Loads, 100 Flight Block, Randomized	18
2.2.7.2.3-1	Simplified Spectrum, With Negative Loads, 100 Flight Block	20
2.2.7.2.3-2	Simplified Spectrum, With Negative Loads, 100 Flight Block, Randomized	21
2.2.7.3-1	Reversed Simplified Block Test Spectrum	25
2.3.2-1	Fatigue Test Specimen	26
3.2.1-1	Typical Test Setup for a Non-reversed Spectrum Test	27
3.2.1-2	Typical Test Setup for a Reversed Spectrum Test	28
3.1.3.1-1	Test and Analysis Results, Spectra Without Negative Loads	37
3.1.3.1-2	Test and Analysis Results, Spectra With Negative Loads	38
3.1.3.2-1	Test Results, Spectra Without Negative Loads, Secondary Objective	39

LIST OF TABLES

Table	Title	Page
2.3.2-1	Basic Test Matrix	25
2.3.2-2	Extended Test Matrix	25
3.1.2.2-1	Basic Test Results	35
3.1.2.2-2	Extended Test Program Results	36

1.0 INTRODUCTION

This paper outlines the development of simplified load spectra for use in preliminary fatigue assessments. The simplified generation approach utilizes a limited amount of external load information with a potentially large reduction in the number of external load cases required, when compared to conventionally generated spectra. It presents analytical and test fatigue life data for the conventional, multiple load case spectra and the simplified spectra.

1.1 Background

Fatigue and Damage Tolerance evaluations require the development of Repeated Load Spectra. Conventionally, the development of these load spectra require the generation of numerous external load cases that are completed late in the project. This often results in the Fatigue and Damage Tolerance analyses occurring after designs are complete, making design changes expensive and time consuming.

It would be advantageous to have spectra available that would make use of the limited external load information that is available at the design phase of a project. This would facilitate a reliable preliminary assessment of the fatigue characteristics of the aircraft modifications.

1.2 Purpose

The primary purpose of this study is to generate Repeated Load Spectra by conventional and simplified methods, to compare the analytical fatigue life results from the spectra generated, and to verify these analytical results by testing the spectrum generated by the conventional approach.

A secondary purpose was to make a preliminary assessment of the sequencing effects on fatigue life; this by including the testing of the spectra at different overall load levels and in various sequences.

2.0 TECHNICAL DISCUSSION

2.1 Discussion of Approach

Paragraphs 2.1.1 and 2.1.2 contain brief descriptions of the conventional and simplified approaches to the load spectrum generation.

2.1.1 Conventional Approach

The conventional approach is summarized as follows:

a. Define basic aircraft configuration and performance.

b. Establish projected or actual usage.

c. Develop detailed mission profiles in terms of flight segments, allowing for variations in flight parameters such as segment time, gross weight, altitude, airspeed, mach number, attitudes and center of gravity (cg).

d. Determine load environment for each Mission Segment, including maneuvers, gusts and ground loads.

e. Establish exceedance data for each event and mission segment.

f. Develop inertial, dynamic and external load cases for each segment.

g. Combine load cases with exceedance data to create a sequenced load spectrum for each mission.

h. Combine individual mission spectra in accordance with the usage data to form a complete Repeated Load Spectrum.

2.1.2 Simplified Approach

The simplified approach is summarized as follows:

a. Define basic aircraft configuration and performance.

b. Establish projected or actual usage.

c. Develop simplified mission profiles in terms of flight segments, allowing for variations in primary flight parameters such as segment time, gross weight, altitude and airspeed.

d. Determine primary flight events, maneuvers, touchdowns, gusts, ground maneuvers for each mission type.

e. Establish exceedance data for each selected event and mission.

f. Select design load cases for each selected event.

g. Create 'Primary Pairs', 'Secondary Pairs' and 'Significant Other' pairs by examination.

h. Combine selected pairs with exceedance data to form block mission spectra.

i. Combine mission spectra to form a lifetime Repeated Loads Spectrum.

2.2 Generation of Spectra for a Center Fuselage

Two center fuselage spectra are generated. The cases chosen are for two locations on a typical transport aircraft center fuselage crown skin/stringer structure. The two locations are chosen to result in one spectra containing, and one not containing significant negative loads.

2.2.1 Analysis Methodology

Fatigue analysis was performed with a linear S-N damage accumulation routine that utilizes the equivalent stress coefficients from Reference [1]. This method does not allow for the effect on fatigue life of load sequencing interaction. The analysis was performed using data for 2024 T3 aluminum sheet, assuming a K_t of 3.0. The cycle counting required to convert the simplified test spectra into analytic spectra was executed on a two parameter cycle counting routine in accordance with the procedures outlined in Reference [2].

2.2.2 Spectra Analyzed and Tested

The following spectra were analyzed and tested:

a. Conventional generation, negative loads included.
b. Simplified generation, negative loads included.
c. Conventional generation, negative loads not included.
d. Simplified generation, negative loads not included.

2.2.3 Flight Profiles

Figures 2.2.3-1 and 2.2.3-2 show the flight profiles utilized for the development of both spectra. They are representative of a single occurrence of a single mission type for a military transport and contain details of altitude, mach number, equivalent airspeed and gross weight.

2.2.4 Exceedance Data

The exceedance data used was primarily derived from the exceedance data given in References [3] and [4].

2.2.5 Design External Loads

Design external loads and inertial loads used in the simplified spectrum development were derived from load cases contained in Reference [5]. These loads were used as generic loads for a typical transport type aircraft; not as loads for the specific aircraft referenced. The loads are extracted in the form of longitudinal bending moments, M_y.

In the discussion of load cases and environments, fuselage internal pressurization is referred to as an external load case. This is for convenience of reporting total cases only, in this particular case, the effects of pressurization are evaluated as internal stresses superimposed, where appropriate, on the stress levels generated from the true external loads conditions.

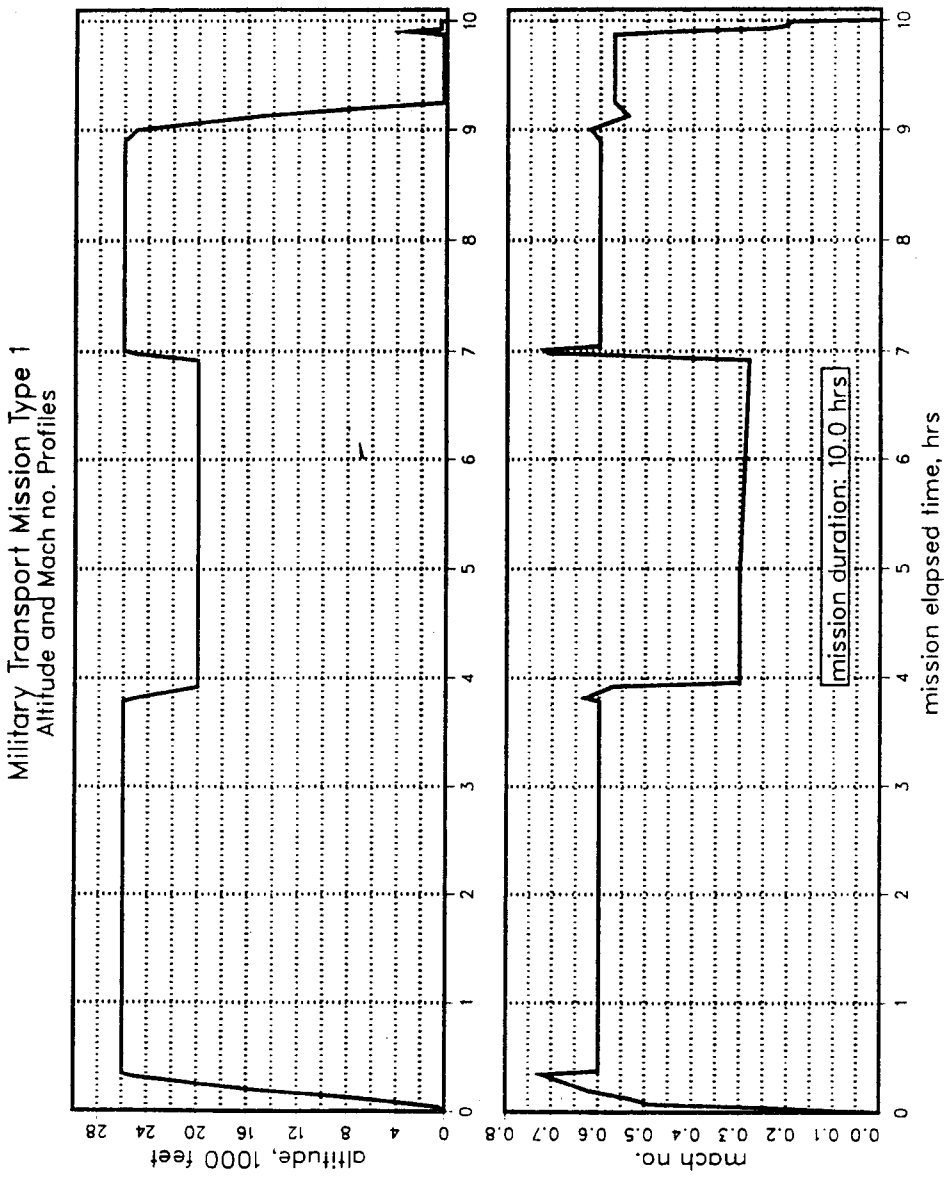


Figure 2.2.3-1 Altitude and Mach Number Profiles

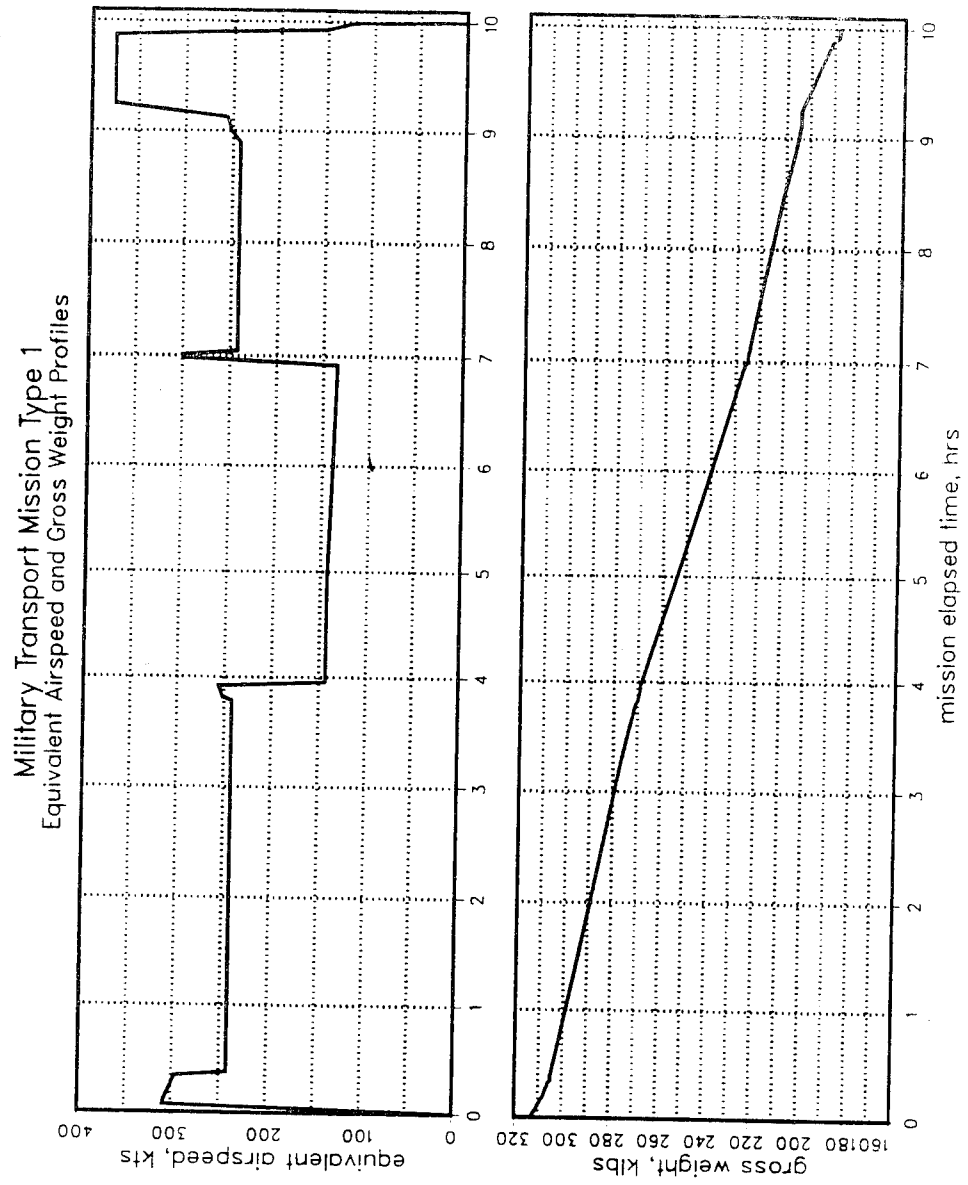


Figure 2.2.3-2 Equivalent Airspeed and Gross Weight Profiles

2.2.6 Segmental External Loads

Segmental external loads and inertial loads used in the development of the conventional, flight by flight spectrum were derived from load cases contained in Reference [6]. These loads were used as generic loads for a typical transport type aircraft; not as loads for the specific aircraft referenced. The load cases required for each flight segment were obtained for this study by the use of a regression technique applied to specific flight parameters. This approach was outlined in Reference [7], and ensures that the loads used are generic in nature.

2.2.7 Spectrum Generation

Paragraphs 2.2.7.1 and 2.2.7.2 contain details of the spectrum development process for the conventional approach and the simplified approach.

2.2.7.1 Conventional Spectrum Generation

This spectrum is a true flight by flight type, with flight segments in real time order, and external and inertial loads within each segment applied in random order.

2.2.7.1.1 Load Cases/Load Environment

For the conventional approach, 40 flight segment conditions were evaluated for the single selected mission, of which 22 formed the primary data points for load evaluation. They are summarized as follows, together with the relevant load environment(s) considered:

1.	Taxi-out[1,2]	Ground maneuver
2.	Take-off[1]	Ground maneuver
3.	Climb 1[1]	Balanced maneuvers, gusts, flaps down, gear down
4.	Climb 2	Balanced maneuvers, gusts, fuselage internal pressure
5.	Climb 3	Balanced maneuvers, gusts, fuselage internal pressure
6.	Climb 4	Balanced maneuvers, gusts, fuselage internal pressure
7.	Climb 5[1]	Balanced maneuvers, gusts, fuselage internal pressure
8.	Loiter 1[1]	Balanced maneuvers, gusts, fuselage internal pressure

9.	Loiter 2	Balanced maneuvers, gusts, fuselage internal pressure
10.	Loiter 3	Balanced maneuvers, gusts, fuselage internal pressure
11.	Loiter 4[1]	Balanced maneuvers, gusts, fuselage internal pressure
12.	Descent 1[1]	Balanced maneuvers, gusts, fuselage internal pressure
13.	Descent 2[1]	Balanced maneuvers, gusts, fuselage internal pressure
14.	Cruise 1[1]	Balanced maneuvers, gusts, fuselage internal pressure
15.	Cruise 2	Balanced maneuvers, gusts, fuselage internal pressure
16.	Cruise 3	Balanced maneuvers, gusts, fuselage internal pressure
17.	Cruise 4[1]	Balanced maneuvers, gusts, fuselage internal pressure
18.	Climb 6[1]	Balanced maneuvers, gusts, fuselage internal pressure
19.	Climb 7[1]	Balanced maneuvers, gusts, fuselage internal pressure
20.	Loiter 5[1]	Balanced maneuvers, gusts, fuselage internal pressure
21.	Loiter 6	Balanced maneuvers, gusts, fuselage internal pressure
22.	Loiter 7[1]	Balanced maneuvers, gusts, fuselage internal pressure
23.	Descent 3[1]	Balanced maneuvers, gusts, fuselage internal pressure
24.	Descent 4	Balanced maneuvers, gusts, fuselage internal pressure
25.	Descent 5[1]	Balanced maneuvers, gusts
26.	Sea level operations 1[1]	Balanced maneuvers, gusts
27.	Sea level operations 2[1]	Balanced maneuvers, gusts
28.	Climb 8	Balanced maneuvers, gusts
29.	Descent 6	Balanced maneuvers, gusts
30.	Approach 1[1]	Balanced maneuvers, gusts, flaps down, gear down
31.	Approach 2	Balanced maneuvers, gusts, flaps down, gear down
32.	Approach 3	Balanced maneuvers, gusts, flaps down, gear down
33.	Approach 4[1]	Balanced maneuvers, gusts, flaps down, gear down
34.	Two-point-landing[1,2]	Dynamic ground condition
35.	Three point roll[1,2]	Ground maneuver
36.	Taxi-in[1,2]	Ground maneuver

The combination of ± gusts (2 per case), +/1g balanced maneuvers for each condition and ± Nz taxi maneuvers resulted in a total of 87 load cases being evaluated for this study.

[1]Primary data point.

[2]Two Load cases required.

2.2.7.1.2 Conventional Spectrum, No Negative Loads

The load cases and exceedance data are combined to create a 100 flight (1000 equivalent flight hour) complex load spectrum presented in unit load form in Figures 2.2.7.1.2-1,2.

Figure 2.2.7.1.2-1 shows one typical flight taken from the 100 flight repeatable block used for the test and analysis.

Figure 2.2.7.1.2-2 shows the complete 100 flight block.

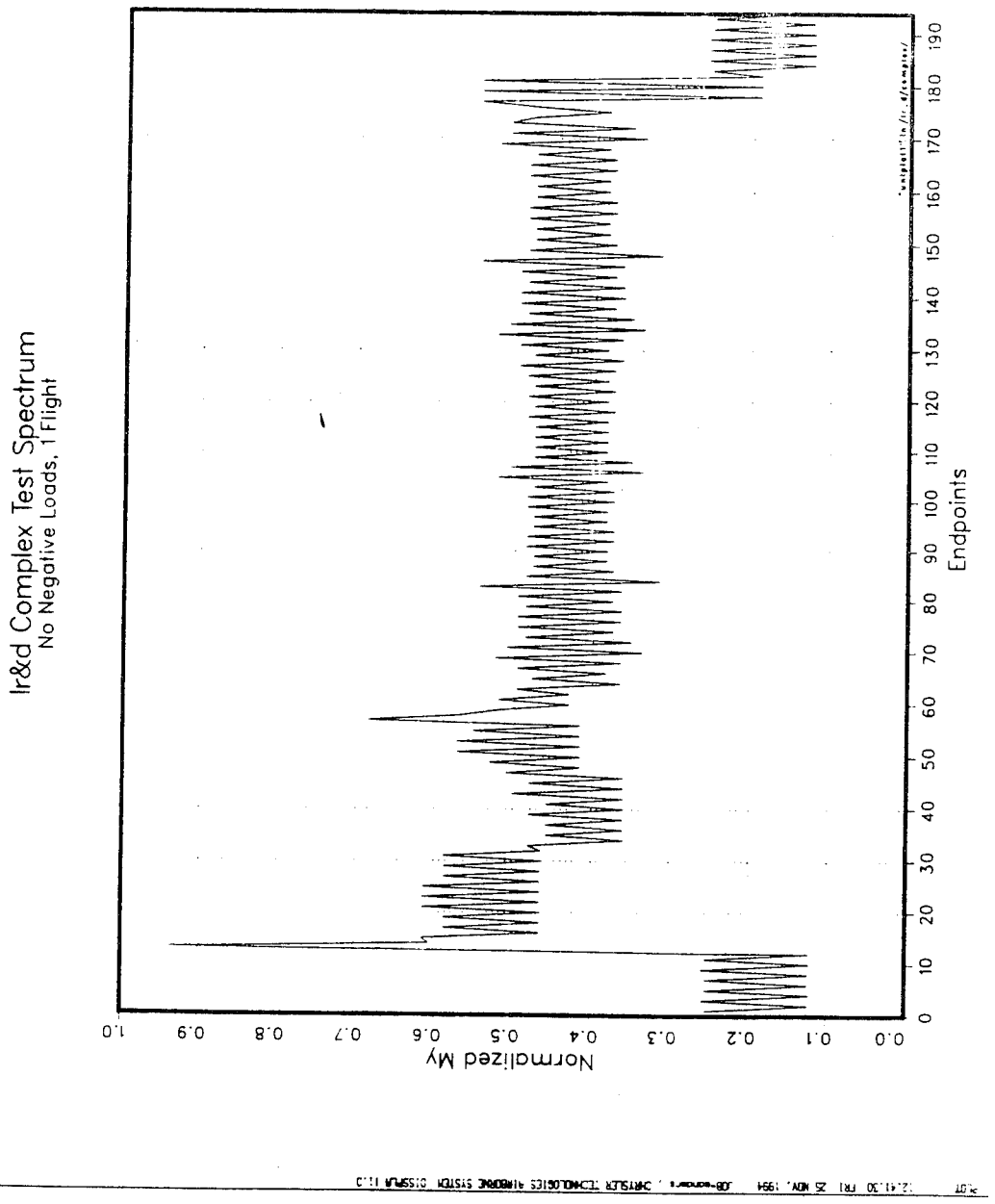


Figure 2.2.7.1.2-1 **Conventional Spectrum, No Negative Loads, 1 Flight**

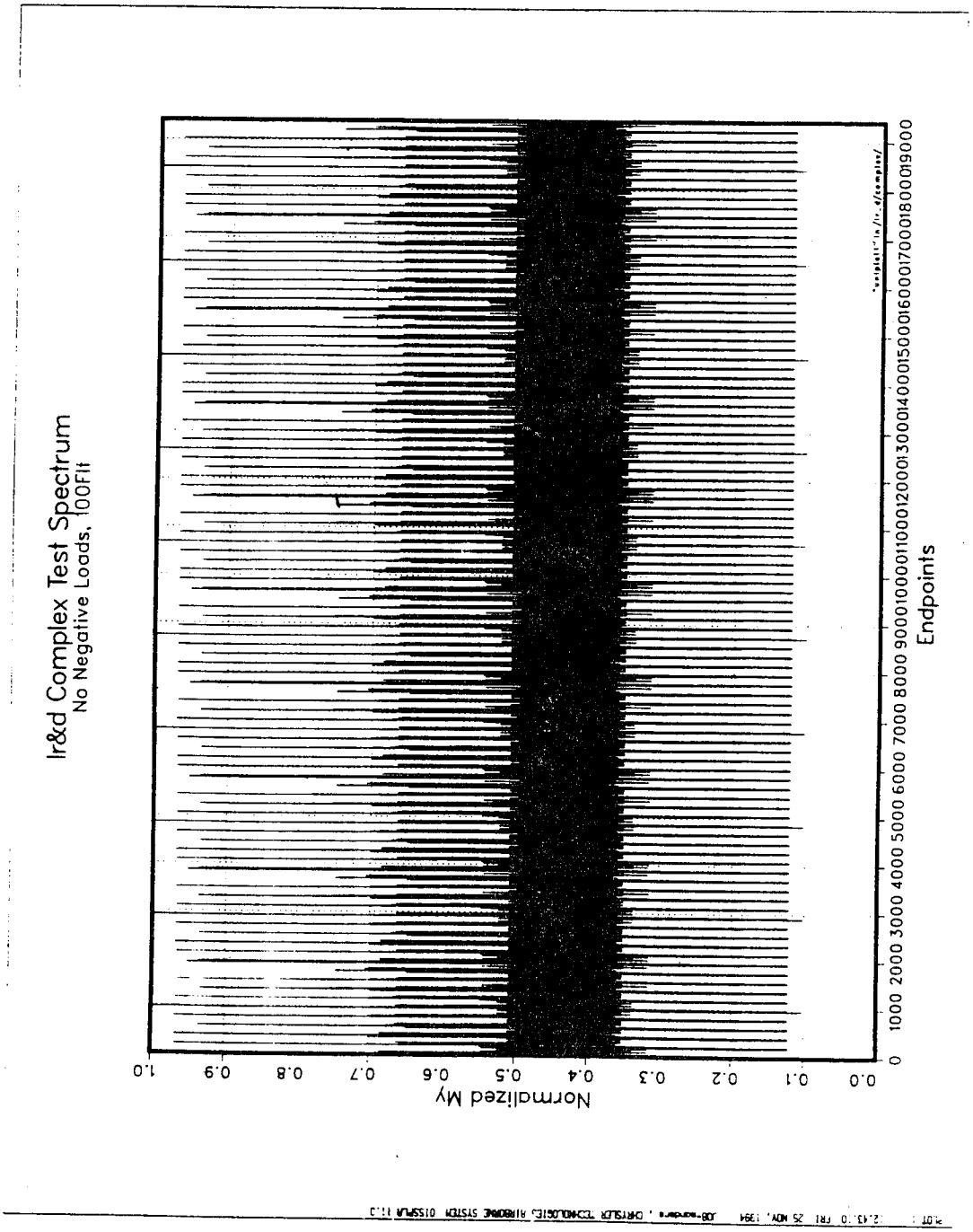


Figure 2.2.7.1.2-2 Conventional Spectrum, No Negative Loads, 100 Flights

2.2.7.1.3 Conventional Spectrum, with Negative Loads

As for the spectrum without negative loads, the load cases and exceedance data are combined to create a 100 flight (1000 equivalent flight hour) complex load spectrum presented in unit load form in Figures 2.2.7.1.3-1/2.

Figure 2.2.7.1.3-1 shows one typical flight taken from the 100 flight repeatable block used for the test and analysis.

Figure 2.2.7.1.3-2 shows the complete 100 flight block.

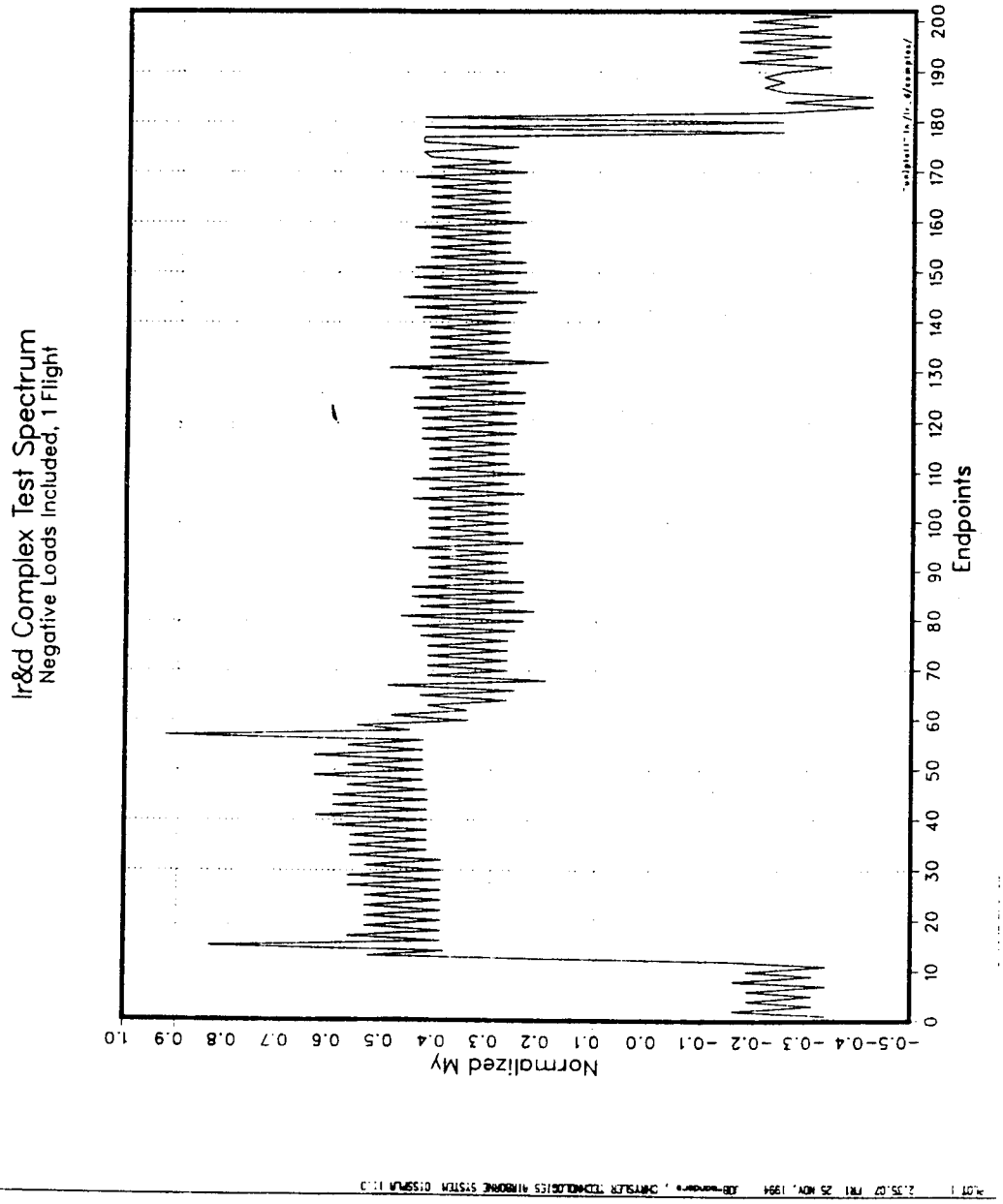


Figure 2.2.7.1.3-1 Conventional Spectrum, With Negative Loads, 1 Flight

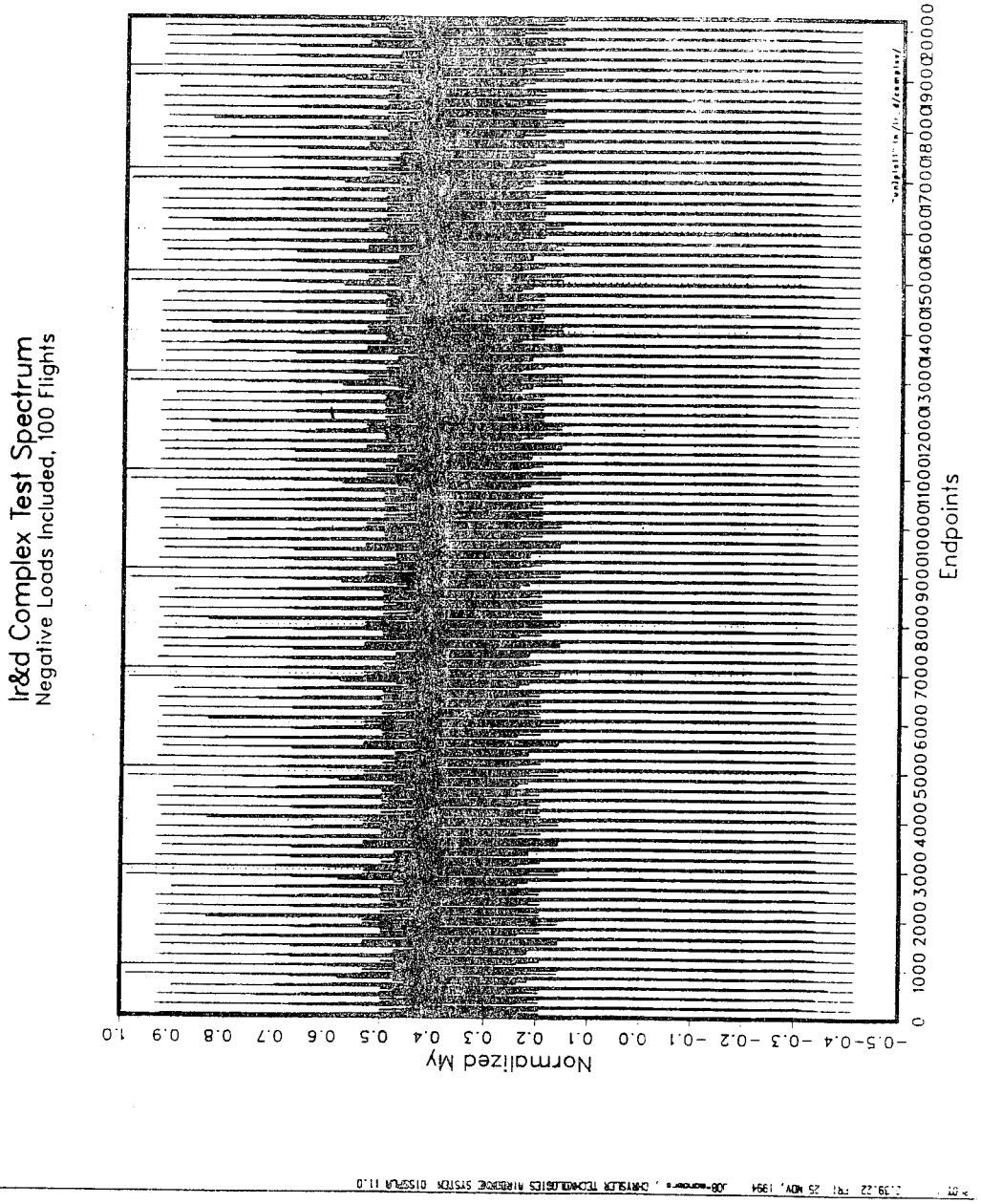


Figure 2.2.7.1.3-2 Conventional Spectrum, With Negative Loads, 100 Flights

2.2.7.2 Simplified Spectrum Generation

This spectrum is a block type, where the occurrences of each event are derived from a lifetime total. Design loads are used throughout the spectrum. The sequence of events is in the order of selection of the load case events.

The spectrum shown is that used for the analyses and for the tests. As the loads are generated as pairs, and the analysis technique used does not allow effects of load sequence, the spectrum is not cycle counted for the analysis.

2.2.7.2.1 Load Cases/Load Environment

For the simplified approach, five event pairs were selected and evaluated for the single mission. They are summarized as follows, together with the relevant load environment(s) considered:

The events are selected on the basis of maximum or minimum load levels occurring once or more in a flight at the location under review. The appropriate cases include the effect of fuselage pressurization.

a. The Primary event pair is formed from the design positive flight maneuver and negative taxi maneuvers (or the three point braked roll). This occurs once per flight, and represents the main GAG cycle.
b. The Secondary major pair is formed from the design two point landing and secondary negative taxi. This also occurs once per flight, and represents a secondary GAG cycle.
c. Remaining maneuvers paired with 1g flight
d. Positive/Negative gusts paired as equal velocities
e. Taxi ± maneuvers

As a direct comparison with the conventional approach, a total of 10 load cases were required for this approach (as against 87).

Taxi maneuvers: 2
Braked roll: 1
Two point landing: 2
Design gusts: 2
Balanced maneuvers: 2
Fuselage internal pressurization : 1

2.2.7.2.2 Simplified Spectrum, No Negative Loads.

The load events are combined to make a 100 flight (1000 equivalent flight hour) block spectrum presented in unit load form in Figures 2.2.7.2.2-1/2.

Figure 2.2.7.2.2-1 shows the 100 flight repeatable block used for the analysis.

Figure 2.2.7.2.2-2 shows the randomized 100 flight block.

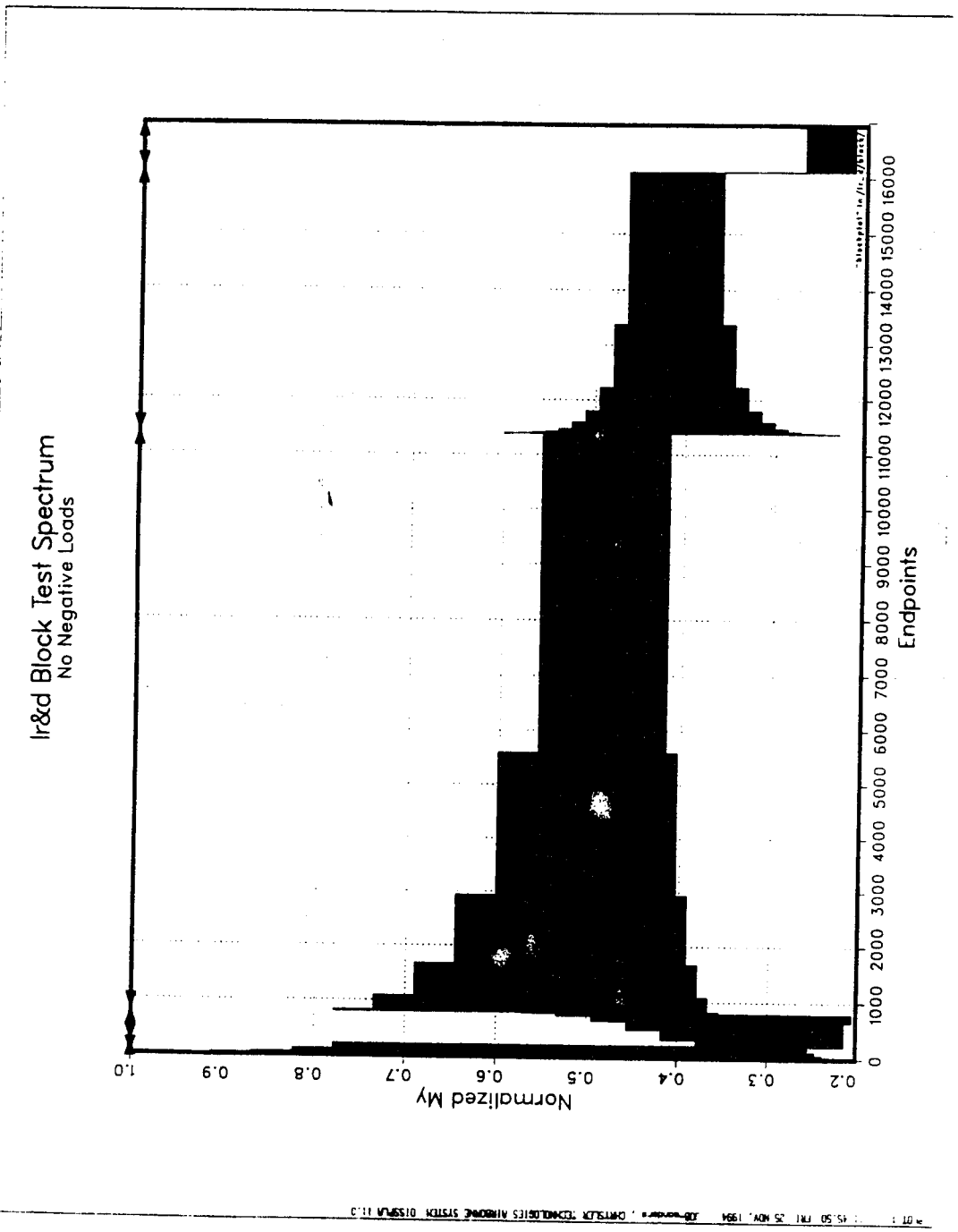


Figure 2.2.7.2.2-1 Simplified Spectrum, No Negative Loads, 100 Flight Block

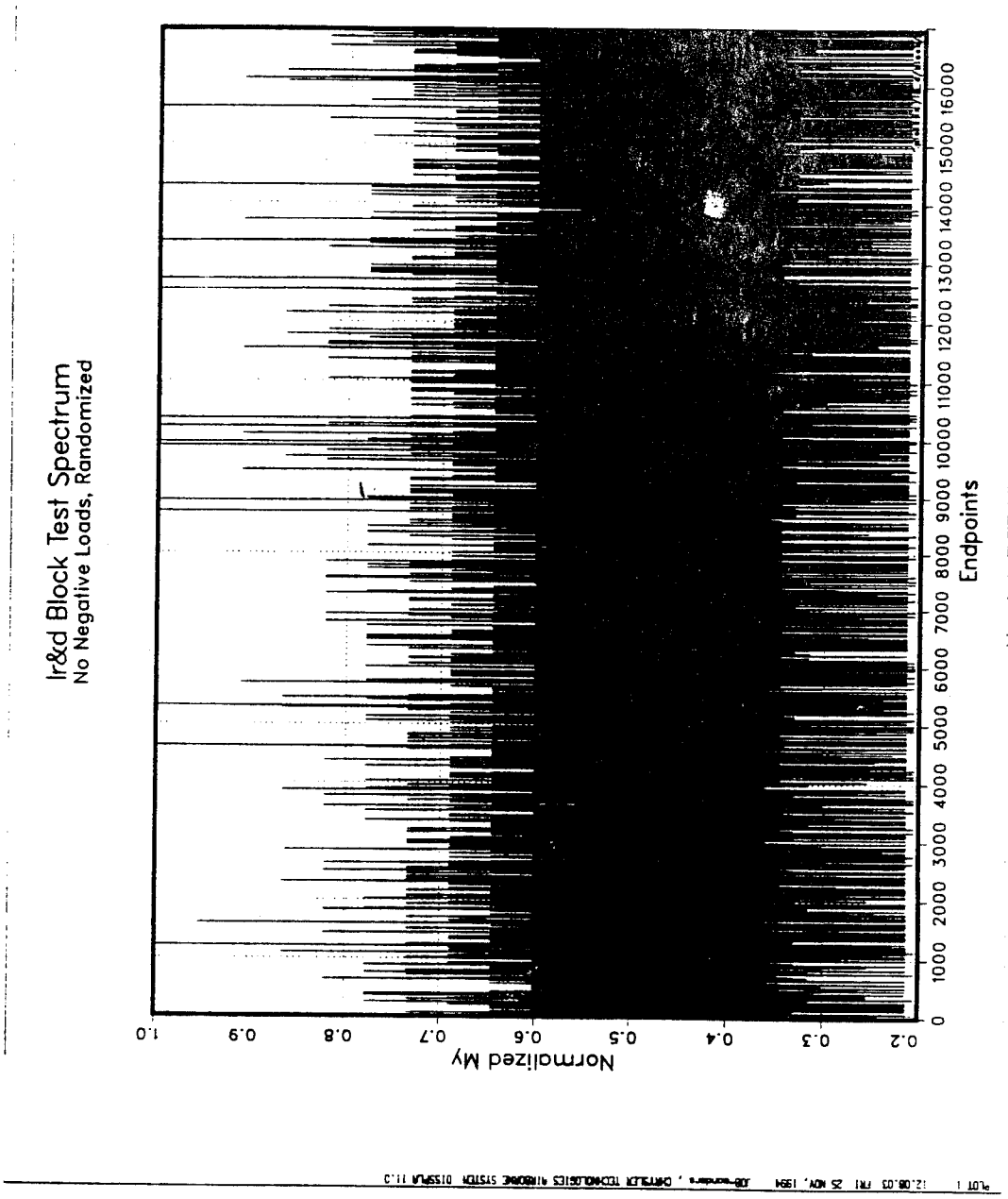


Figure 2.2.7.2.2-2 Simplified Spectrum, No Negative Loads, 100 Flight Block, Randomized

2.2.7.2.3 Simplified Spectrum, with Negative Loads

The load events are combined to make a 100 flight (1000 equivalent flight hour) block spectrum presented in unit load form in Figures 2.2.7.2.3-1/2.

Figure 2.2.7.2.3-1 shows the 100 flight repeatable block used for the analysis.

Figure 2.2.7.2.3-2 shows the randomized 100 flight block.

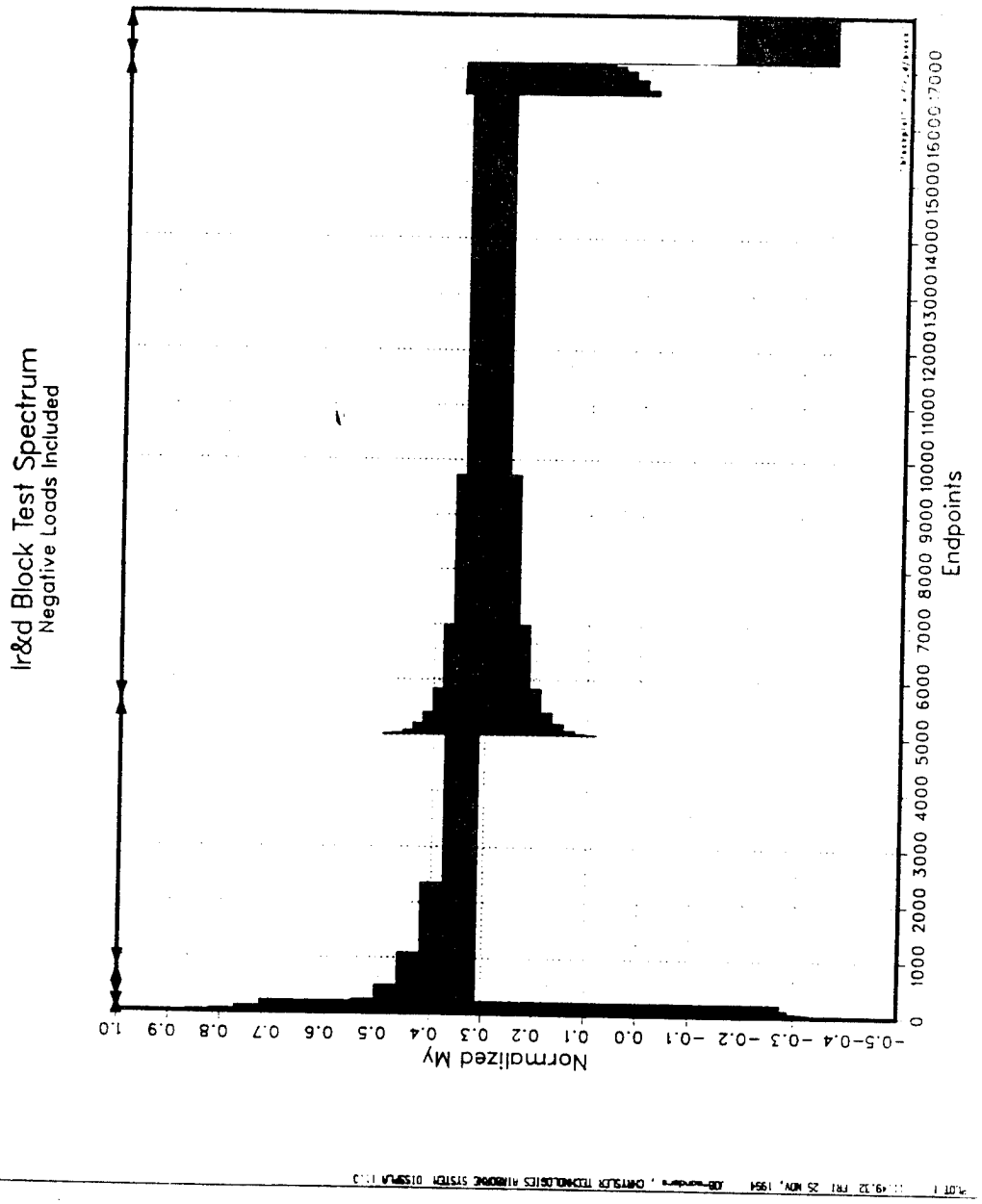


Figure 2.2.7.2.3-1 Simplified Spectrum, With Negative Loads, 100 Flight Block

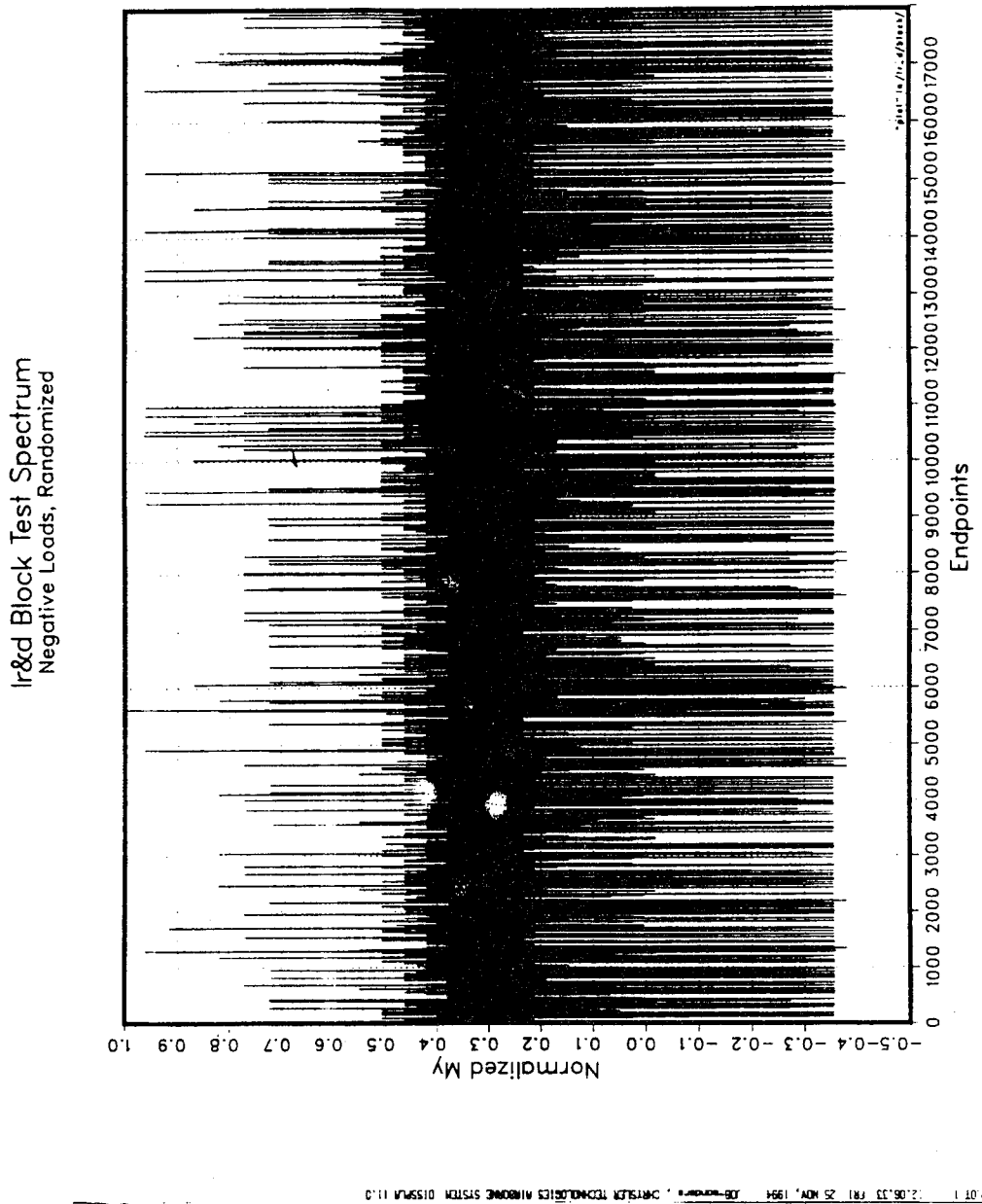


Figure 2.2.7.2.3-2 Simplified Spectrum, With Negative Loads, 100 Flight Block, Randomized

2.2.7.3 Spectra for Additional Testing

The test procedures are discussed in detail in Section 2.3 of this report; the first set of tests were performed at an elevated load level to achieve reasonable test durations. In addition, the test of the simplified spectra, which were not required for achievement of the primary objective, was performed using a randomized sequence. (This was chosen to reduce the load sequencing effects.) The results of these tests are presented in Paragraph 3.1.1. The indicated that the primary objective had been met, but there was a significant anomaly in the test results for the simplified spectrum including negative loads. This indicated a need for further testing of that simplified spectra to evaluate the effects of load sequencing and overall load levels. The conventionally generated spectrum (with negative loads) was also re-tested at lower overall load level.

Four test spectra were generated as follows:

a. Conventional sequenced spectrum, as in Figure 2.2.7.1.3-2, at a reduced overall load level.
b. Simplified, randomized spectrum, as in Figure 2.2.7.2.3-2, at a reduced overall load level.
c. Simplified, block spectrum, as in Figure 2.2.7.2.3-1, at the same overall load level as (b.) above.
d. Simplified, block spectrum, shown in Figure 2.2.7.3-1, at the same load level as (b.). This is the same spectrum as used in (c.) above, applied in the reverse direction.

2.3 Validation Testing

2.3.1 Introduction

This section of the document contains the final test data used to validate the fatigue spectrum generation procedures defined in the previous sections of this report. The cyclic fatigue testing was conducted in accordance with two subcontract statements of work, 94-01916-SM-FT-001 and 94-01916-SM-FT-002, for the basic and extended testing, respectively. After a competitive request for proposal was issued, the test vendors (3) technical and cost proposals were reviewed, and a test subcontract was awarded to Fatigue Technologies, Inc. based on past contract performance, technical approach, schedule, and cost.

2.3.1.1 Scope

The original scope of the test program was to provide fatigue test data for two spectra containing non-reversed loads and two spectra containing reversed loads. This scope was expanded upon the completion of the initial test effort to include four additional test spectra each containing modified versions of the original test spectra.

2.3.1.2 Objective

The objective of the test program was to generate empirical data for four spectra to validate the fatigue spectrum generation procedures developed in the previously documented sections of this report. This test program was performed by CTAS as an internal research and development program and was not related to any specific airframe program.

2.3.1.3 Methodology

The test program was comprised of comparative testing of one modified ASTM E468 specimen configuration using four varying amplitude spectra. Two of the spectra were generated utilizing conventional repeated loads generations techniques, one containing only tensile endpoints and the second containing tensile and compressive endpoints. Two additional spectra were produced utilizing a simplified approach for comparison with the two conventionally generated spectra. An extended

and overall loads level as compared to the first four spectra tested. A total of five repetitions of each test spectrum was performed.

2.3.2 Technical Discussion

The test validation program was performed in two separate efforts, a basic and an extended test program. A test matrix for the basic test program is shown in Table 2.3.2-1 and for the extended test program in Table 2.3.2-2. The test specimen configuration for the total test program is shown in Figure 2.3.2-1.

2.3.2.1 Test Apparatus

The spectrum fatigue testing was accomplished on four closed-loop servohydraulic universal test frames. The specimens were centered and mounted in 2-inch wide hydraulic grips. Frame alignment was verified prior to starting the tests. To preclude frame effects in the spectrum comparison, the spectrum sets without compressive loading were performed in one frame and the sets with compressive loads were run in the other frames. Buckling restraints were utilized on all specimens tested with spectrum containing compressive loads. Typical test setups can be found in Figures 2.3.2.1-1 and 2.3.2.1-2.

The spectrum waveform was generated by a Digital Equipment Corporation (DEC) PDP 11/23+ computer equipped with MTS 486 test processor. Overload protection was provided by a limit detector module in the frame which was preset to prevent the induction of loads outside the test spectrum envelope. After an initial spectrum loads verification, the spectra were periodically checked using a load verification routine built into the test vendor's spectrum software. The routine is designed to compare feedback and control signals and to shut down the program if various error conditions occur. Real time monitoring of the control and feedback signals in all the tests performed using a Tektronix 2213A oscilloscope. In some cases a X-Y plotter was connected to the system and spectrum verification was manually recorded periodically during the testing.

Table 2.3.2-1 Basic Test Matrix

Set	Spectrum Definition	Number of Repetitions
1	Complex, non-reversed	5
2	Complex, reversed	5
3	Simplified, non-reversed	5
4	Simplified, reversed	5
Tensile	None	2
Total		20
Number of Specimens		22

Table 2.3.2-2 Extended Test Matrix

Set	Spectrum Definition	Number of Repetitions
1	Complex, reversed	5
2	Simplified, reversed	5
3	Simplified, reversed modification 1	5
4	Simplified, reversed modification 2	5
Total		20
Spares		4
Number of Specimens		24

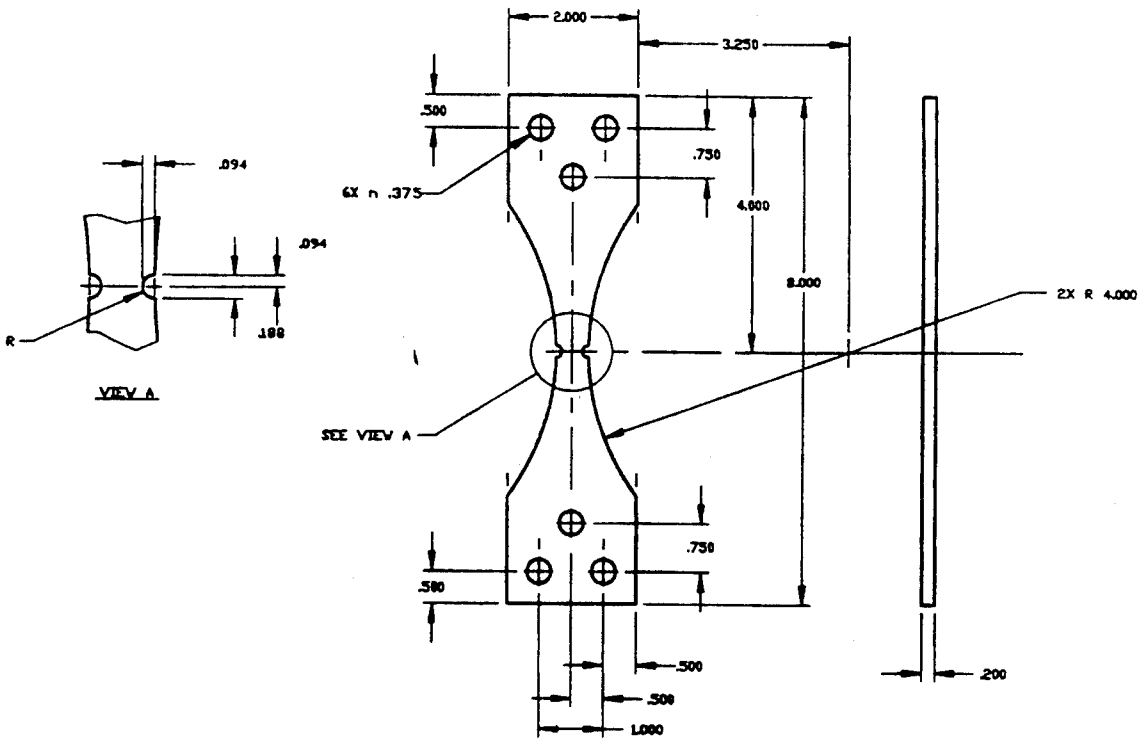


Figure 2.3.2-1 Fatigue Test Specimen

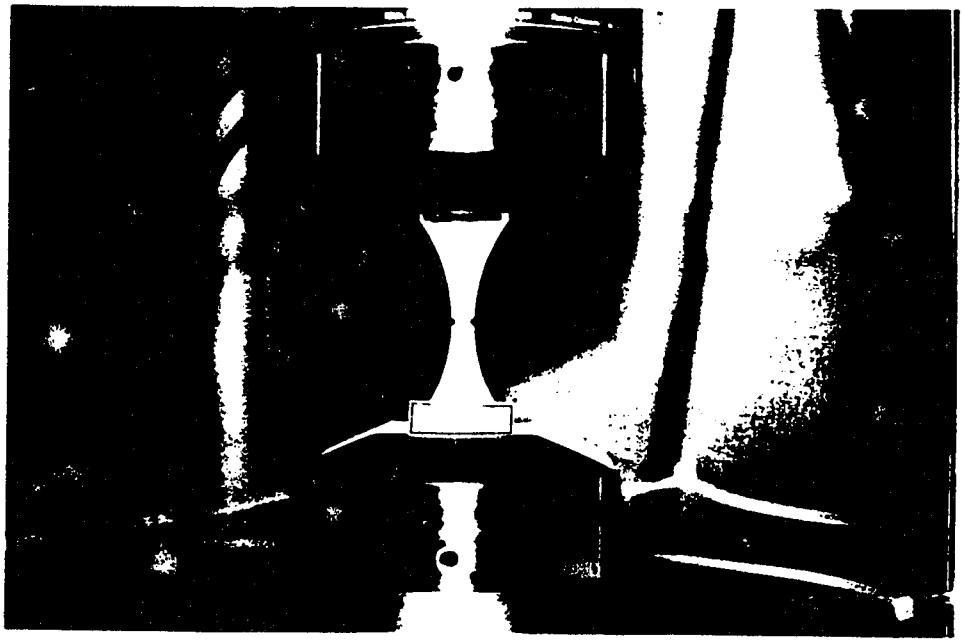


Figure 2.3.2.1-1 Typical Test Setup for a Non-reversed Spectrum Test

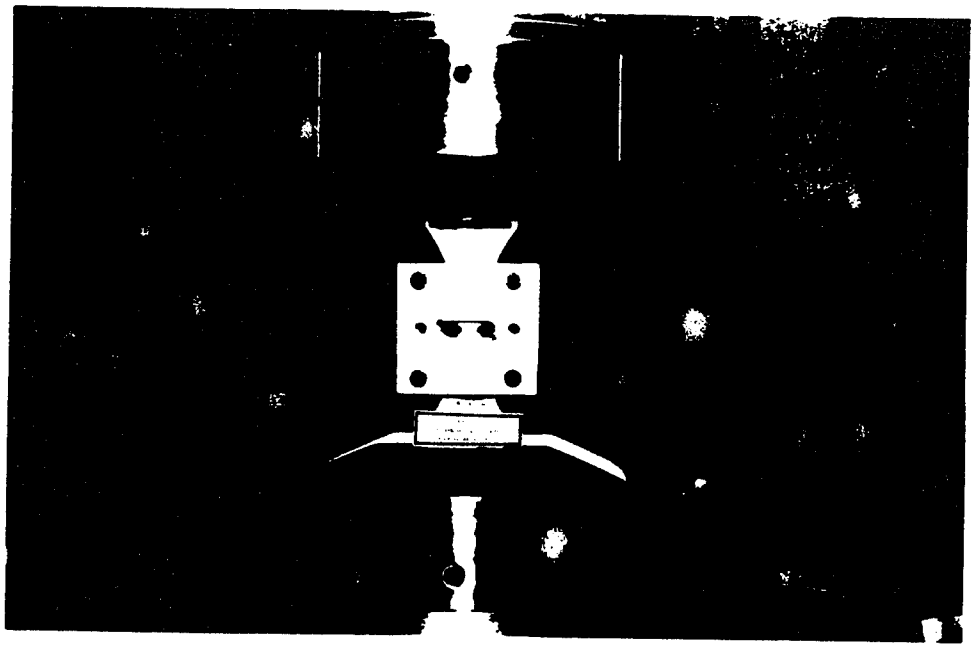


Figure 2.3.2.1-2 Typical Test Setup for a Reversed Spectrum Test

The instrumentation used by the testing laboratory complies with MIL-STD-45662A. The test frames and controlling computers are calibrated as a system in accordance with the guidelines of ASTM E-4. All test equipment is periodically calibrated using standards traceable to the National Institute of Standards and Technologies.

2.3.2.2 Environmental Requirements

All tests were performed in ambient temperature and humidity conditions. Specific environmental conditions are recorded on test logs for each test.

2.3.2.3 Specimen Preparation

The test vendor purchased 2024-T3 QQA-A-250/4 bare sheet aluminum to manufacture to total number of specimens required to the basic and extended test programs. All materials were inspected and suppliers material certifications were reviewed and forwarded to CTAS for approval and included in the final test reports prepared by the test vendor (References 8 and 9). The specimens were manufactured in accordance with the subcontract statement of work (Ref Figure 2.3.2-1). Material for each test set was manufactured from the same manufactures lot to preclude test variables.

2.3.2.4 Tensile Tests

Two tensile test were performed using the spare specimens from the basic fatigue test effort for the purpose of material characterization. These tests were conducted using a MTS Test Link® system with software designed to ASTM E8 specifications. A calibrated extensometer was used to record strain, elogation was also recorded. The test results were consistent with the manufactures material certification and within the material properties defined in MIL-STD-5. The test results were documented in the final Test vendor test report (Ref 8). Rockwell hardness was also checked and documented (Ref 8).

2.3.2.5 Strain Surveys

A strain survey was performed prior to testing on each frame. One specimen had two gages bonded on the front and back surface adjacent to the notch. The strain gages were installed in accordance with guideline specified in ASTM E1237-93 and the manufactures specifications. The strain measurements were recorded at four equal load steps to eighty percent of the maximum spectrum, returned to zero, then if the spectrum contained compressive loads the survey was continued in steps to sixty percent of the maximum compressive spectrum load. The survey was repeated twice to ensure that there were no hysteresis effects. The results of the strain surveys were reviewed and approved by CTAS prior to the start of testing. Results of the strain surveys can be found in references 8 and 9.

3.0 RESULTS AND CONCLUSIONS

This section contains the results of the analyses and tests. It also contains a discussion of the results, and some conclusions.

3.1 Results

3.1.1 Analyses Results

3.1.1.1 Primary Objective

The results of the fatigue analyses for comparison with the initial set of tests are as follows:

a. Conventional Spectrum, no negative loads:
   117 spectrum block passes.
b. Conventional Spectrum, with negative loads:
   156 spectrum block passes.
c. Simplified Spectrum, no negative loads:
   112.2 spectrum block passes.
d. Simplified Spectrum, with negative loads:
   91.8 spectrum block passes.

3.1.1.2 Secondary Objective

The results of the fatigue analyses for comparison with the second set of tests are as follows:

a. Conventional spectrum, with negative loads, reduced overall load level:
b. Simplified spectrum, reduced overall load level, randomized sequence:
c. Simplified spectrum, reduced overall load level, block sequence:
d. Simplified spectrum, reduced overall load level, reversed block sequence:

NOTE

The load pairs and their respective levels remain unaltered between these three simplified spectra; only the order of their appearance within the spectrum changes. This means that for an analytic process that ignores sequence, as in this case, all three will give identical answers.

3.1.2 Test Results

3.1.2.1 Discussion

A minimum of five specimens per set were successfully tested to failure or maximum spectrum runout (twelve million segments) as required by the subcontract statement of work. The following paragraphs provides relevant discussion for each phase of the test program.

3.1.2.1.1 Basic Test Program

Initially, for the basic test program, the maximum stress level for Set 2 specimens with IRDREV spectrum was 40.95 ksi. The remaining specimens of this set were tested using a maximum stress level of 36.04 ksi. A spare specimen was tested at a lower stress level to complete the repetitions for the spectrum set.

3.1.2.1.2 Extended Test Program

After testing specimen CTR135, maintenance was performed on the test frame. The high pressure accumulator was found to be empty and recharged. This may have effected the test results for specimens tested on that frame. Test Set 3 specimens were replaced with spare specimens (CTR130 - CTR136) and retested. Specimen CTR130 was tested on an independent frame to ensure additional frame effects were not present and could be accounted for. Additionally, a spare specimen was tested for spectrum Set 2. The fracture surface for specimen CTSR22 appeared to contain a manufacturing/accidental flaw or material defect and was replaced with CTSR26.

3.1.2.2 Summary

The test results for the basic test program are summarized in Table 3.1.2.2-1. The results of the tests performed with the two non-reversed spectrums produced similar fatigue lives. The simplified reversed spectrum had significantly higher test lives than specimens with the complex reversed spectrum. Individual specimen test results including specimen dimensions, test conditions, physical crack size vs. segment or cycle count can be found in reference 8.

The test results for the extended test program are summarized in Table 3.1.2.2-2. All specimens were tested to failure or to spectrum run out (twelve million segments). It should be noted that a number of the specimens did not experience failure (two part separation) as with the basic test program, however, the specimens did experience crack initiation or crack growth (Ref Table 3.1.2.2-2). Individual specimen test results including specimen dimensions, test conditions, physical crack size vs. segment or cycle count can be found in reference 9. All test specimens have been returned to CTAS and will be retained by the Life Assurance Section for one year.

3.1.3 Discussion and Correlation

3.1.3.1 Results Related to the Primary Objective

Figure 3.1.3.1-1 shows the test and analysis results for the non-reversed spectra. The analysis for the simplified spectrum is 156 passes, the conventional; 117, and the conventional test log mean; 154.61. The simplified test log mean is 135.32.

Figure 3.1.3.1-2 shows the test and analysis results for the reversed spectra. The analysis for the simplified spectrum is 91.8, the conventional: 112.2, and the conventional test log mean: 94.84. The simplified test log mean is 215.64.

In both cases, the simplified analysis matches the conventional test results extremely closely, which fulfills the prime objective, and is acceptably close to the conventional analysis.

For the simplified test results, the reversed set shows considerable discrepancy. As stated before, this is not a requirement for the main objective, but it does raise a question as to the analytical capabilities. This result led to the second set of tests, reported in paragraph 3.1.3.2, with the intention of assessing any quantitive effect of load overall levels or sequencing.

3.1.3.2 Results Related to the Second Objective

The test results are shown in Figure 3.1.3.2-1. At this time, the analysis has not been completed, so a complete correlation cannot be performed.

The preliminary indications from the test results are that the difference between the conventional and simplified reversed spectra is maintained at reduced overall load levels, and that the sequencing does not result in a large change in the tested lives.

3.2 Conclusions and Recommendations

3.2.1 Conclusions

The primary objective of the program was to show that a simplified spectrum generation technique would give acceptable analytic fatigue life results when compared with the analytic and test results for a conventionally generated spectrum.

The results for both spectrum types (with and without negative loads) show that this objective has been met.

Only 10 external/inertial load cases were required for the simplified generation, as against 87 for the conventional approach which would result in a significant "up-front" capability.

3.2.2 Recomendations

a. Extend the spectrum generation methodology to include the generation of spectra for use in damage tolerance analysis; assess the results by crack growth tests.
b. Examine the effect on predicted fatigue lives by refining the curve fitting procedures in the software accessing the S-N material database.
c. Put in place an alternative fatigue life evaluation method and examine the effects of using this methodology on the calculated fatigue lives.

Table 3.1.2.2-1 Basic Test Results

SET	SPECIMEN	SPECTRUM	WIDTH (in)	THICKNESS (in)	CRACK LENGTH		SEGMENTS TO FAILURE	PASSES TO FAILURE
					LEFT (in)	RIGHT (in)		
1	CTCN11	IRDNOR	0.3166	0.1997	0.107	0.034	2,886,710	148.80
	CTCN12	IRDNOR	0.3146	0.1992	0.041	0.118	2,507,460	129.25
	CTCN13	IRDNOR	0.3154	0.1995	0.121	0.027	2,709,230	139.65
	CTCN14	IRDNOR	0.3165	0.2004	0.021	0.116	4,500,260	231.97
	CTCN15	IRDNOR	0.3159	0.2000	(1)	0.121	2,750,540	141.78
Minimum			0.3146	0.1992			2,507,460	129.25
Log Avg.			0.3158	0.1998			2,999,354	154.61
Std. Dev.			0.0008	0.0005			310,539	41.78
2	CTCR21	IRDREV	0.3158	0.2002	0.089	0.110	1,029,050(2)	0.00
	CTCR22	IRDREV	0.3156	0.1998	0.157	0.090	1,715,850	84.94
	CTCR23	IRDREV	0.3149	0.1995	(1)	0.173	1,790,770	88.65
	CTCR24	IRDREV	0.3144	0.2008	0.165	(1)	1,806,750	89.44
	CTCR25	IRDREV	0.3140	0.2003	(1)	0.169	2,190,550	108.44
	CTCR26	IRDREV	0.3151	0.2000	0.161	(1)	2,122,060	105.05
Minimum			0.3140	0.1995			1,715,850	84.94
Log Avg			0.3148	0.2001			1,915,780	94.84
Std. Dev.			0.0006	0.0005			215,113	10.65
3	CTSN31	SIMNOR	0.3160	0.1995	0.064	0.102	2,417,740	142.74
	CTSN32	SIMNOR	0.3161	0.2002	(1)	0.122	2,071,060	122.27
	CTSN33	SIMNOR	0.3157	0.1997	(1)	0.122	2,287,850	135.07
	CTSN34	SIMNOR	0.3164	0.1999	(1)	0.127	2,367,110	139.75
	CTSN35	SIMNOR	0.3153	0.2000	(1)	0.112	2,333,060	137.74
Minimum			0.3153	0.1995			2,071,060	122.27
			0.3159	0.1999			Log Avg.	
Std. Dev.			0.0004	0.0003			134,083	7.92
4	CTSR41	SIMREV	0.3167	0.2003	(1)	0.180	4,205,680	234.27
	CTSR42	SIMREV	0.3158	0.1995	0.072	0.150	4,008,210	223.27
	CTSR43	SIMREV	0.3166	0.2000	0.083	0.137	3,931,490	219.00
	CTSR44	SIMREV	0.3170	0.1997	0.066	0.145	3,769,920	210.00
	CTSR45	SIMREV	0.3149	0.1998	0.063	0.149	3,479,880	193.84
Minimum			0.3149	0.1995			3,479,880	193.84
Log Avg.			0.3162	0.1999			3,871,222	215.64
Std. Dev.			0.0009	0.0003			272,656	15.19

Notes:

(1) Crack initiations were noticed along the thickness of the specimen. These sites were smaller than 0.005 inches.

2. The initial stress level for Set 2 specimens with spectrum IRDREV was 40.95 ksi. This stress level did not provide the predicted life from the analysis. The remaining specimens of this set were tested using a maximum stress level of 36.04 ksi. The data from CTCR21 is not included in the statistical calculations.

3. The maximum spectrum stress for the non-reversed spectrums was 44.22 ksi, and for the reversed spectrums 36.04 ksi. All tests were run at an average frequency of 15 Hz.

Table 3.1.2.2-2 Extended Test Program Results

SET	SPECIMEN	SPECTRUM	WIDTH (in)	THICKNESS (in)	CRACK LENGTH		SEGMENTS TO FAILURE	PASSES TO FAILURE (1)
					LEFT	RIGHT		
1	CTIR11	IRDREV	0.1998	0.3100	0.010	0.217	8,658,780	428.65
	CTIR12	IRDREV	0.2000	0.3100	0.201	0.020	5,990,170	296.54
	CTIR13	IRDREV	0.2000	0.3087	0.187	0.049	5,554,050	274.95
	CTIR14	IRDREV	0.2002	0.3098	0.112	0.118	4,501,620	222.85
	CTIR15	IRDREV	0.2003	0.3104	0.016	0.201	5,137,720	254.34
Minimum			0.1998	0.3087			5,501,620	222.85
Log Avg.			0.2001	0.3098			5,817,401	287.99
Std. Dev.			0.0002	0.0006			1,800,920	79.25
2	CTSR21	SIMREV	0.2004	0.3083	None	0.087 (2)	12,000,000	668.45
	CTSR22	SIMREV	0.1999	0.3097	0.041	0.204	10,030,500	558.74
	CTSR23	SIMREV	0.2002	0.3122	0.019	0.214	9,423,400	524.92
	CTSR24	SIMREV	0.2005	0.3095	0.170	0.201	10,591,700	590.00
	CTSR25	SIMREV	0.2003	0.3094	0.004	0.195	7,981,170	444.58
	CTSR26	SIMREV	0.2002	0.3096	0.0009	0.204	10,462,200	582.79
Minimum			0.1999	0.3083			7,981,170	444.58
Log Avg			0.2002	0.3098			10,005,246	557.33
Std. Dev			0.0002	0.0013			1,336,635	74.46
3	CTR131	SIMRV1	0.1989	0.3138	0.03	0.14	4,493,690 (5)	250.23
	CTR132	SIMRV1	0.2002	0.3163	MI (3)	MI (3)	12,000,000	668.23
	CTR133	SIMRV1	0.2003	0.3160	0.140	0.030	972,706 (5)	54.17
	CTR134	SIMRV1	0.2004	0.3164	0.141	0.056	1,171,280 (5)	65.22
	CTR135	SIMRV1	0.2007	0.3156	0.156	0.025	1,709,060 (5)	95.17
	CTR136	SIMRV1	0.1990	0.3175	0.051	0.192	7,255,030	404.00
	CTR137	SIMRV1	0.2003	0.3153	None	None	12,000,000	668.23
	CTR138	SIMRV1	0.2001	0.3156	None	None	12,000,000	668.23
	CTR139	SIMRV1	0.2002	0.3155				
	CTR130	SIMRV1	0.2004	0.3096	None	None	12,000,000	668.23
Minimum			0.1989	0.3096			7,255,030	404.00
Log Avg.			0.2000	0.3152			10,851,077	604.25
Std. Dev.			0.0006	0.0022			2,122,015	118.17
4	CTR241	SIMRV2	0.1988	0.3182	MI (3)	MI (3)	12,000,000	668.45
	CTR242	SIMRV2	0.1996	0.3161	None	None	12,000,000	668.45
	CTR243	SIMRV2	0.2006	0.3163	None	None	12,000,000	668.45
	CTR244	SIMRV2	0.2003	0.3159	MI (3)	0.044 (2)	12,000,000	668.45
	CTR245	SIMRV2	0.2000	0.3169	None	None	12,000,000	668.45
Minimum			0.1988	0.3159			12,000,000	668.45
Log Avg			0.1999	0.3167			12,000,000	668.45

Notes:

1. The passes to failure are calculated from the segments to failure divided by the number of end points in the spectrum. Each spectrum had a different number of end points (See Appendix A).
2. The specimens did not fail. Corner cracks were noticed and measured along the surface of the specimen.
3. The specimens did not fail. Crack initiations were noticed along the thickness of the specimen. These cracks did not progress to the front or back surface.
4. On the crack surface, there appeared to be a material flow. One additional test, CTSR26, was performed to replace specimen CTSR22. Specimen STSR22 data was not used in any analysis.
5. A possible frame problem was noticed after testing the 5 specimens of Set 3. These tests were replaced with specimens CTR136 through CTR130. Specimen CTR130 was tested on a different frame than the other specimens in this set to complete the 5 repetitions and to cross check the frame results. Results from specimens CTR131 through CTR135 were not used in any analysis.

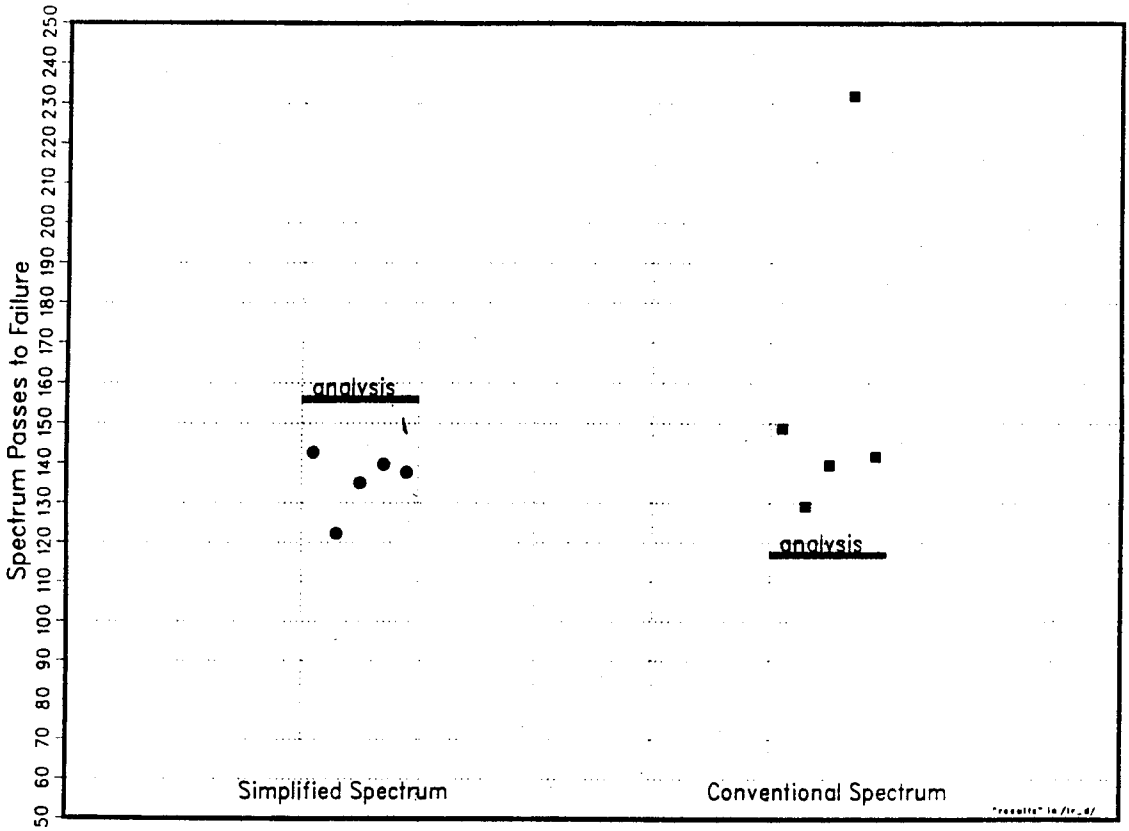


Figure 3.1.3.1-1 Test and Analysis Results, Spectra Without Negative Loads

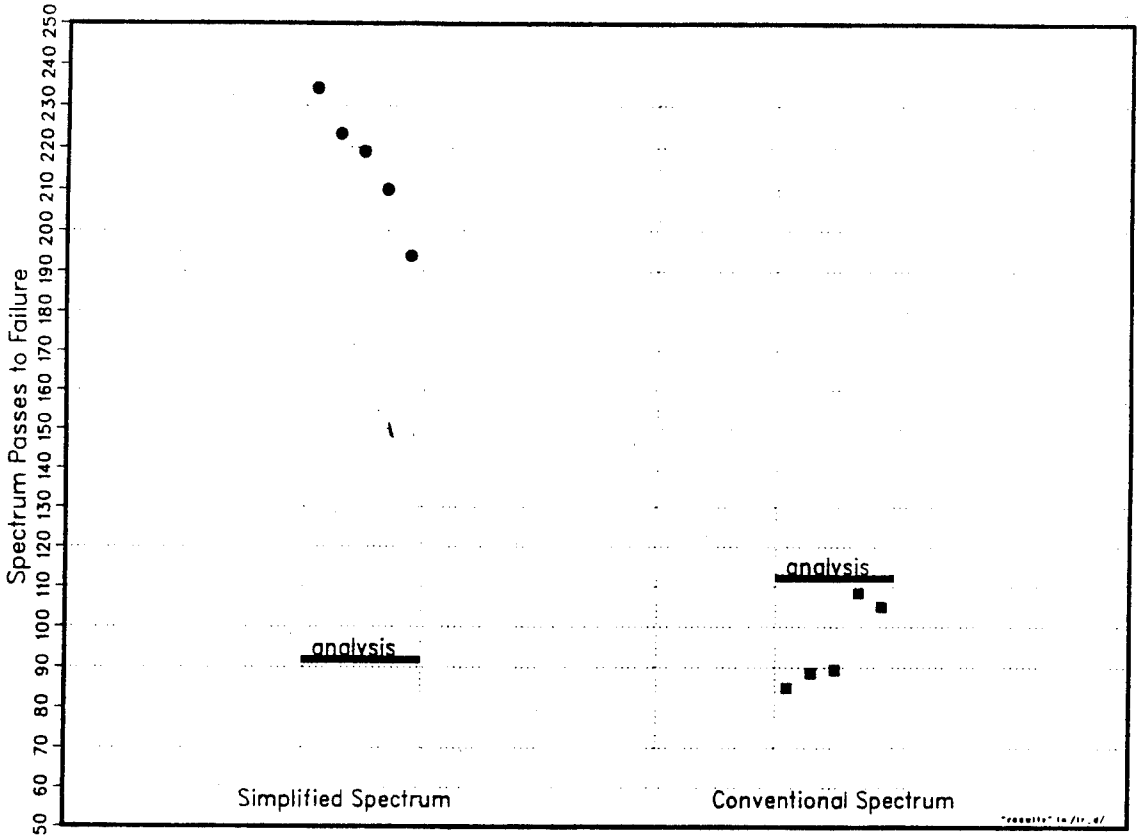


Figure 3.1.3.1-2 Test and Analysis Results, Spectra With Negative Loads

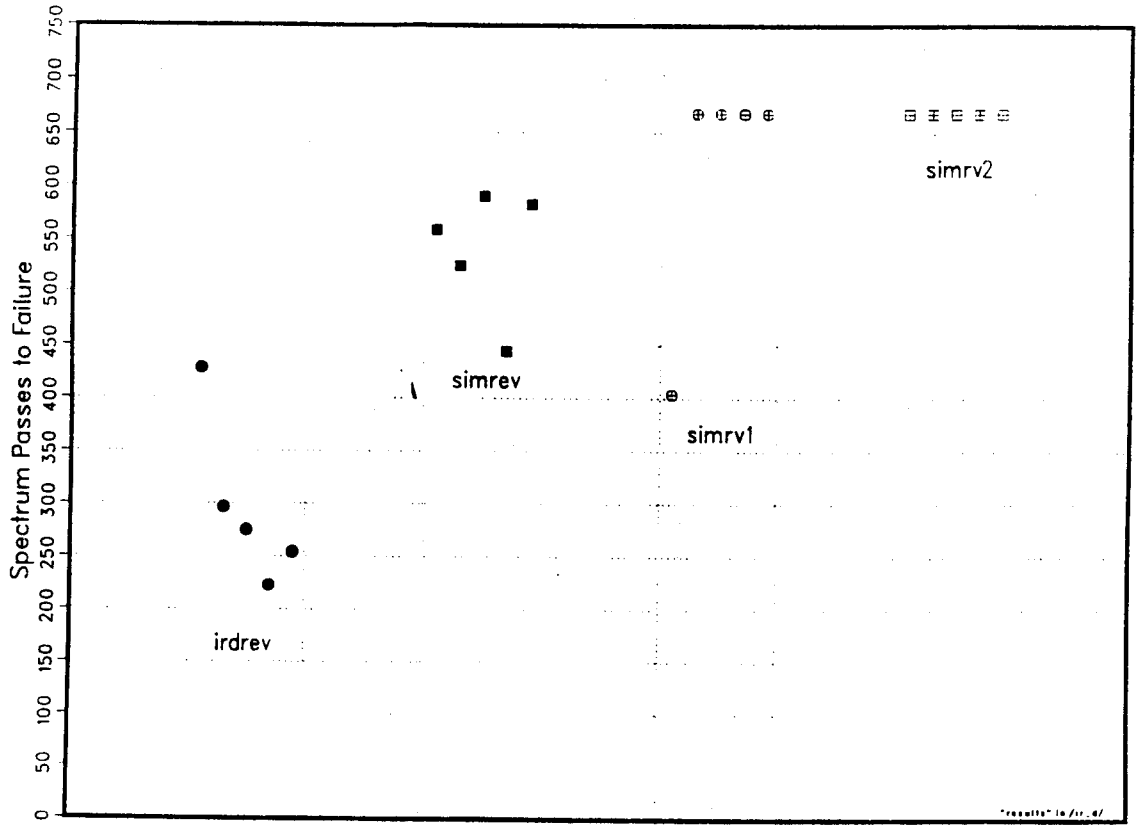


Figure 3.1.3.2-1 Test Results, Spectra With Negative Loads, Secondary Objective

REFERENCES

1. MIL-HDBK-5F. Military Handbook, Metallic Materials and Elements for Aerospace Vehicle Structures. Department of Defense. June 1987.
2. ASTME 1049. Standard Practices for Cycle Counting in Fatigue Analysis. American Society for Testing and Materials. June 1985.
3. MIL-A-8866C(AS). Military Specification, Airplane Strength and Rigidity Requirements, Repeated Loads, Fatigue and Damage Tolerance. Naval Air Systems Command. May 1987.
4. ASD-TR-82-5012. Handbook of Military Aircraft Design Normal Load Factor Exceedance Data,
5. Boeing Document Nos. D409-12200-1, 2 & 3. E-6A External Loads and Inertial Loads Report. July and August 1986.
6. CTAS Document No. 92022114-001. Loads Analysis Report, External Loads and Inertial Loads Report for E-6 ABU Program.
7. USN Specification No. NADC-77194-60. Improved Fatigue Life Tracking Procedures. November 1981.
8. Fatigue Technologies, Inc., Technical Report No. 45267, Fatigue and Damage Tolerance (FDT) Enhancement: Fatigue Spectrum Development, Fatigue Spectrum Validation Testing, Final Report, 8 September 1994.
9. Fatigue Technologies, Inc., Technical Report No. 47002, Fatigue and Damage Tolerance (FDT) Enhancement: Fatigue Spectrum Development, Fatigue Spectrum Validation Extended Testing, Final Report, 18 January 1995.

ATTENDEES LIST

MR JAMES J ABEL
FLIGHT SCIENCES DEPT
CHRYSLER TECH AIRBORNE SYS
7500 MAEHR M/S 1135
PO BOX 154580
WACO TX 76715-4580
(817)-867-4116
FAX: (817)-867-4597

DR RICARDO ACTIS
SR RES ENGR
ESRD INC
7750 CLAYTON RD
STE 204
ST LOUIS MO 63117-1342
(314)-645-1423
FAX: (314)-645-1649

MR JOHNNY D ADAMSON
PROJ ENGR
PRATT & WHITNEY
M/S 714-03
PO BOX 109600
W PALM BEACH FL 33418-9600
(407)-796-2402
FAX: (407)-796-8993

MAJ PIERRE ALEXANDRE
US AIR FORCE
OC-ALCLAKI
3001 STAFF DR/STE 2AH110
TINKER AFB OK 73145-3022
(405)-736-5183
FAX: (405)-736-4360

MR RUSSELL E ALFORD
US AIR FORCE
WR-ALC/LJLEA
270 OCMULGEE CT
ROBINS AFB GA 31098-1646
(912)-926-9146
FAX: (912)-926-9142

MR ROBERT D ALLEN JR
LOCKHEED AERO SYS CO
M/S 0484 DEPT 73-51
86 S COBB DR
MARIETTA GA 30063-0484
(404)-494-5991
FAX: (404)-494-2028

MR ROBERT ALLERSTON
ROYAL AIR FORCE
NON DESTRUCTIVE TEST SQUAD
RAF ST ATHANMORLEY
BARRY S GLASMORGAN S WALES UK-0001

MR JOHN W ALTIZER
LOCKHEED ADV DEV CO
M & P ENGINEERING
1011 LOCKHEED WAY
BLDG 636/D 27-24
PALMDALE CA 93599-2720
(805)-572-7940

MR ROBERT H ANDERSEN
STRESS ANALYST
MENASCO AEROSYSTEMS
4000 HWY 157
EULESS TX 76040-7012
(817)-267-3551

MR CHARLES ANNIS
PRATT & WHITNEY
M/S 707-22
PO BOX 109600
W PALM BEACH FL 33410-9600
(407)-796-6565
FAX: (407)-795-7454

MR HANS R ANSELL
SAAB MILITARY AIRCRAFT
SAAB SCANIA AB
MS TUDLB
LINKIPING SWEDEN S 58188-0001
(461)-318-1698
FAX: (461)-318-3363

DR KEMAL ARIN
US/DOT
VOLPE NATL TRANSP SYS CTR
M/S DTS-74
55 BROADWAY
CAMBRIDGE MA 02142-1093
(617)-494-2066
FAX: (617)-494-3066

MR BERT ARISPE
US AIR FORCE
SA-ALC/TIESM
450 QUENTIN ROOSEVELT RD
BLDG 183
KELLY AFB TX 78241-5000
(210)-925-8745
FAX: (210)-925-4916

MR ALBERT J ARRIETA
AEROSPACE ENGR
US AIR FORCE
OC-ALC/TIESM
4750 STAFF DR
TINKER AFB OK 73145-3317
(405)-736-5008
FAX: (405)-737-8628

MR CHARLES A BABISH
AEROSPACE ENGR
US AIR FORCE
ASC/YCEF
WRIGHT-PATTERSON AFB OH 45440-0001
(513)-255-5427
FAX: (513)-255-3207

MR ROBERT M BADER
1613 KINGSWAY DR
XENIA OH 45385-9589
(513)-426-4871

MR H J BADERSCHNEIDER
DEUTSCHE AERO AG MIL AIR
LME22 STREEE
81663 MUENCHEN
GERMANY

MR BRAD M BAKER
US AIR FORCE
SA-ALC/LFES
KELLY AFB TX 78241-5443
(210)-925-4284
FAX: (210)-925-0097

DR KARL O BALL
GROUP DIRECTOR
SRL
M/S 10
2800 INDIAN RIPPLE RD
DAYTON OH 45440-3696
(513)-426-6000
FAX: (513)-427-7875

MR RAYMOND BANISTER
BOMBARDIER INC
400 COTEVERTU WEST
DORVAL
MONTREAL QUEBEC CANADA H4S-1Y9
(514)-855-7549
FAX: (514)-855-8201

DR MEHMET I BASCI
DIRECTOR
SWALES & ASSOC INC
5050 POWDERMILL RD
BELTSVILLE MD 20705-0001
(301)-572-1445
FAX: (301)-595-5518

MR PRESTON R BATES
RES ENGR
GEORGIA TECH RES INST
AERO LAB CCRF 2-111
225 N AVE NW
ATLANTA GA 30332-0844
(404)-528-7887
FAX: (404)-528-3271

MR GREGORY L BAUGHMAN
US AIR FORCE
LJLEA
6236 COURTSIDE DR
NORCROSS GA 30092-2359
(404)-368-0233

MR SCOTT D BAYS
SPEC ENGINEER
BOEING
PO BOX 7730
MS K83-14
WICHITA KS 67277-7730
(316)-523-1311
FAX: (316)-526-4214

MR MICHEL BEAULIEU
STRUCT ENGR
BOMBARDIER INC
CANADAIR
INTL AIRPORT
10,000 CARGO A-4 ST
MIRABEL QUEBEC CANADA J7N-1H3
(514)-476-4201
FAX: (514)-476-4207

MR E BRUCE BELASON
DIR ADV PROD
TEXTRON SPECIALTY MATLS
M/S 8
TWO INDUSTRIAL AVE
LOWELL MA 01851-0001
(508)-454-5234
FAX: (508)-934-7593

DR ALAN P BERENS
UNIV OF DAYTON RES INST
300 COLLEGE PARK DR
DAYTON OH 45469-0120
(513)-229-4475
FAX: (513)-229-3712

LTC KARL-ROMAN BERLINGHOF
NATO LIAISON
NATO EARLY WARNING FORCE CMD
OC-ALC/LAKI-NATO
3001 STAFF DR STE 2AH110
TINKER AFB OK 73145-3022
(405)-736-3108
FAX: (405)-736-4360

MS JUDITH BHANSALI
US ARMY AVIATION & TROOP CMD
AMSAT-R-NST
4300 GOODFELLOW BLVD
ST LOUIS MO 63120-1798
(314)-263-1470
FAX: (314)-263-1397

MR ROBERT L BISHOP JR
E-SYSTEMS GREENVILLE DIV
CBN 151
POB BOX 6056
GREENVILLE TX 75403-6056
(903)-457-7609
FAX: (903)-457-5611

MR WILLIAM C BECKER
MTS SYS CORP
M/S STE 202
26500 W AGOURA RD
CALABASAS CA 91302-0001
(818)-878-9512
FAX: (818)-878-9515

MR TERRY C BELL
STRUCT ENGR
LOCKHEED AERO SYS CO
M/S 0160
86 S COBB DR
MARIETTA GA 30132-0160
(404)-494-4902
FAX: (404)-494-9610

MR STANLEY G BERKLEY
TECH DIRECTOR
FATIGUE MGMT ASSO
1000 N US HWY
MS #615
JUPITER FL 33477-4481
(407)-743-0600
FAX: (407)-743-6777

MR CLAUDE BERRON
BOMBARDIER INC
CANADAIR
10,000 CARGO RD A-4 ST
MIRABEL QUEBEC CANADA J7N-1H3
(514)-476-4385
FAX: (514)-476-4451

2LT MICHAEL BISHOP
US AIR FORCE
SA-ALC/LFES
KELLY AFB TX 78241-5443
(210)-925-4284
FAX: (210)-925-0097

MR EDWARD BITTEL
SQUADRON LEADER
ROYAL AIR FORCE
ENG 17A RAF
RM 421/LACON HOUSE
LONDON UK WCIX 8RY-0001
(071)-305-6688
FAX: (071)-305-6653

MR FRANZ BLAHA
CANADIAN MARCONI CO
600 DR FREDERIK PHILIPS BLVD
VILLE SAINT-LAURENT
QUEBEC CANADA H4M-2S9
(514)-748-3075
FAX: (514)-748-3136

MR PHIL R BOGERT
NASA HQ
CODE RS
300 E ST SW
WASHINGTON DC 20546-0001
(202)-258-4608
FAX: (202)-358-3750

MR GUSTAV R BOLFING
STRUC ENGR
SWISS FED AIRCRAFT FACTORY
STRUCTURE & SYSTEMS
6032 EMMEN
SWITZERLAND 6032-0001

DR DAVID E BOWLES
DEPUTY PROG MGR
NASA
LANGLEY RESEARCH CTR
MAIL STOP 265
HAMPTON VA 23681-0001
(804)-864-2936
FAX: (804)-864-8093

MR KEVIN L BOYD
US AIR FORCE
FATIGUE & FRACTURE TEST FAC
BLDG 65/AREA B
WRIGHT-PATTERSON AFB OH 45433-0001
(513)-255-0434
FAX: (513)-476-7379

MR BRADLEY J BRAUN
PRESIDENT
SYS & ELECTRONICS INC
190 GORDON ST
ELK GROVE VILLAGE IL 60193-0001
(708)-228-0985
FAX: (708)-228-1164

MAJ JOHN W BRIDGE
ASST PROF
US AIR FORCE ACADEMY
HQ/USAFA/DFEM
2345 FAIRCHILD DR/STE6H2
USAF ACADEMY CO 80840-6240
(719)-472-2531
FAX: (719)-472-2944

MS VICKI O BRITT
AERO ENGR
NASA LANGLEY RES CTR
M/S 190
HAMPTON VA 23681-0001
(804)-864-8030
FAX: (804)-864-7791

MR JOHN R BROCKENBROUGH
ENGR ASSO
ALCOA
PREDUCT DESIGN & MECH
100 TECHNICAL DR/MS D
ALCOA CENTER PA 15069-0001
(412)-337-5924
FAX: (412)-337-5436

MR CRAIG L BROOKS
MCDONNELL AIRCRAFT CO
FATIGUE & FRACTURES METHODS
M/C 0012741
PO BOX 516
ST LOUIS MO 63166-0516
(314)-232-9391
FAX: (314)-232-6934

MR ABRAHAM BROT
FATIGUE DEPT MGR
ISRAEL AIRCRAFT INDUSTRIES
DEPT 2444
BEN-GURION INTL AIRPORT
ISRAEL --

MR AL G BRUETSCH
US AIR FORCE
SM-ALC
5020 DUDLEY BLVD STE 3
MCCLELLAN AFB CA 95652-1391
(916)-643-5300
FAX: (916)-643-1405

DR ROBERT J BUCCI
SR TECH CONSULTANT
ALCOA
PRODUCT DESIGN & MECH
100 TECHNICAL DR
ALCOA CTR PA 15069-0001
(412)-337-2671
FAX: (412)-337-5436

MR WILLIAM F BUCKEY
PROJ ENGR
US AIR FORCE
ASC/ENFSL
WRIGHT-PATTERSON AFB OH 45433-6533
(513)-255-7076
FAX: (513)-255-8516

MR JAMES S BURD
STRUCTURAL ANALYST
CHRYSLER TECH AIRBORNE SYS
M/S 1135
7500 MAEHR
WACO TX 76715-4580
(817)-867-4115
FAX: (817)-867-4597

COL STANLEY D BURMAN
US AIR FORCE
C-141 PROG
1910 RIVERVIEW DR
ALC/LJ
MARIETTA GA 30067-4842
(404)-494-2564
FAX: (404)-494-7883

DR O HAL BURNSIDE
MGR/ENGR MECH
SOUTHWEST RES INST
PO DRAWER 28510
SAN ANTONIO TX 78238-5166
(210)-522-2332
FAX: (210)-522-3042

MR CHARLES F BUYNAK
MATLS ENGR
US AIR FORCE
WL/MLLP BLDG 655 RM 173
2230 TENTH ST STE 1
WRIGHT-PATTERSON AFB OH 45433-7817
(513)-255-9807
FAX: (513)-255-9804

MR PETE COCCHIOLA
NE REGIONAL SALES MGR
FATIGUE TECH INC
EIGHT FOUNTAIN RD
ROCKY PT NY 11778-0001
(516)-744-6730
FAX: (516)-744-6731

MR DAVE J CALLIGAN
MENASCO AEROSYSTEMS INC
PO BOX 500
4000 S HWY 157
EULESS TX 76040-0500
(817)-685-3568
FAX: (817)-283-4591

MR JOE CARDINAL
ENGR
SOUTHWEST RES INST
6220 culebra rd
PO DRAWER 28510
SAN ANTONIO TX 78228-0510
(210)-522-3323
FAX: (210)-522-3042

MR DOUGLAS P CARMODY
3C FATIGUE ENGRG INC
13 SHADOW LN
ST PETERS MO 63376-0001
(314)-926-3157
FAX: (314)-928-8196

MR PETE J CARUSO
SR ENGR
LASC
F-22 STRUCTURAL INTEGRITY
DEPT 73-HE
M/S 0987
MARIETTA GA 30063-0062
(404)-793-0131
FAX: (404)-793-0149

MR DONALD W CHAFFEE
LOCKHEED AERO SYS
M/S 0199 D/73-05 CC34
86 S COBB DR
MARIETTA GA 30063-0199
(404)-494-3074
FAX: (404)-494-5207

MR GARY CHAMBERLAIN
AERO ENGR
US AIR FORCE
WR-ALC/TIEDD
420 SECOND ST/STE 100
ROBINS AFB GA 31098-1640
(912)-926-4228
FAX: (912)-926-1743

DR CHRISTOS C CHAMIS
AEROSPACE ENGR
NASA LEWIS RES CTR
M/S 49-6
21000 BROOKPARK RD
CLEVELAND OH 44135-3191
(216)-433-3252
FAX: (216)-433-5649

MR BRIAN C CHISHOLM
SR ANALYTICAL ENGR
PRATT & WHITNEY
M/S 163-09
400 MAIN ST
E HARTFORD CT 06108-0001
(203)-565-1451
FAX: (203)-565-1560

MR JOHN CHRISTIANSEN
APPLI ENGR
MTS SYS CORP
14000 TECHNOLOGY DR
EDEN PRAIRIE MN 55344-2290
(612)-937-4000
FAX: (612)-937-4515

DR JAYCEE H CHUNG
SEC MGR
E-SYS INC
CBN 204
PO BOX 6056
GREENVILLE TX 75403-6056
(903)-457-5096
FAX: (903)-457-7609

MR JOSEPH B COCHRAN
STAFF ENGR
LOCKHEED AERO SYS CO
DEPT 73-25 ZONE 0160
86 S COBB DR
MARIETTA GA 30063-0160
(404)-494-2166
FAX: (404)-494-9610

MR THOMAS J CONQUEST
SYS ENGR
SMITHS INDUSTRIES
M/S 119
4141 EASTERN AVE SE
GRAND RAPIDS MI 49518-8727
(616)-241-7900
FAX: (616)-241-7965

MS SHARON COOPER
AERO ENGR
NASA/GODDARD SPACE FLT CTR
MECH ENGR BR
CODE 722.2
GREENBELT MD 20771-0001
(301)-286-9939
FAX: (301)-286-1658

MR THOMAS D COOPER
CHF SYS SUPPORT DIV
US AIR FORCE
WL/MLS BLDG 652
2179 TWELFTH ST STE 1
WRIGHT-PATTERSON AFB OH 45433-7718
(513)-255-2282
FAX: (513)-476-4419

MR TOBEY M CORDELL
BR CHF
US AIR FORCE
WL/MLLP BLDG 655
2230 TENTH ST STE 1
WRIGHT-PATTERSON AFB OH 45433-7817
(513)-255-9807
FAX: (513)-255-9804

MR DOUGLAS O CORNOG
STRUCTURES ENGR
US AIR FORCE
ASC/ENFS
2335 7TH ST STE 6
WRIGHT-PATTERSON AFB OH 45433-7809
(513)-255-3330
FAX: (513)-476-4546

MR MICHAEL B COVINGTON
AERO ENGR
HQ AIR FORCE SAFETY AGY
9700 AVE G SE
STE 251 F
KIRTLAND AFB NM 87117-5670
(505)-846-0990
FAX: (505)-846-2721

DR JOSEPH J COX JR
DYNCORP
ONE RIDGMAR
6500 W FREEWAY
FT WORTH TX 76116-0001

MS DARLA Y CRAIN
VICE PRESIDENT
3C FATIGUE ENGINEERING INC
13 SHADOW LANE
ST PETERS MO 63376-0001
(314)-928-3157
FAX: (314)-928-8196

MR CHARLES C CRAWFORD
CHF ENGR
GEORGIA TECH RES INST
AEROSPACE LAB BLDG 2 RM 150
ATLANTA GA 30332-0001
(404)-528-7052
FAX: (404)-528-3271

DR JON T CUTSHALL
SOUTHWEST RES INST
6220 CULEBRA RD
PO DRAWER 28510
SAN ANTONIO TX 78228-0510
(210)-522-3016
FAX: (210)-522-3042

MR LOUIS G DARBY
STRUC MGR
LOCKHEED AERO SYS CO
DEPT 73-78 ZONE 0199
86 S COBB DR
MARIETTA GA 30063-0199
(404)-494-5714
FAX: (404)-494-9617

MR JEAN-MARCEL DAUPHANT
MINISTRY OF DEFENSE
STPA
4 AVE DE LA PORTE D'ISSY
75015 PARIS FRANCE-0001
(33)-1-45525349

CMSGT JAMES F DEAN II
COMMAND MGR
US AIR FORCE
HQ AFSOC/LGMW
100 BARTLEY ST
BLDG 1 STE 309
HURLBURT FLD FL 32544-5000
(904)-884-2092
FAX: (904)-579-5776

MR PIERRE J DEBRUGE
ENGR MGR
CHRYSLER TECH AIRBORNE SYS
7500 MAEHR RD
MS 1900 E-6 PROGRAMS
WACO TX 76705-0001
(817)-867-4137
FAX: (817)-867-2560

MR MARK S DEFAZIO
AERO ENGR
US AIR FORCE
ASC/YPVF
WRIGHT-PATTERSON AFB OH 45433-7205
(513)-255-4236
FAX: (513)-476-4896

MR ARY U DEKONING
NLR
PO BOX 153
EMMELOORD NETHERLAND 8300 AD-0001

MR ANTHONY G DENYER
TECH STAFF
ROCKWELL INTL
2800 WESTMINSTER BLVD
PO BOX 3644AS ST
SEAL BEACH CA 90740-7644
(310)-797-2825
FAX: (310)-797-3756

MR CLAUDE G DESROCHERS
SR ENGR
MARTEC LIMITED
1888 BRUNSWICK ST
HALIFAX NOVA SCOTIA CANADA B3J-3J8
(902)-425-5101
FAX: (902)-421-1923

MR GERALD DEZIEL
CANADA NATIONAL DEFENCE
NATL DEF HQ/DAS ENG 6-3-5
MGEN G R PEARKES BLDG
OTTAWA ONTARIO CANADA K1A-OK2
(613)-991-9541
FAX: (613)-998-6922

MR CLAUDE P DIEPART
DIR MKT
METAL IMPROVEMENT CO
10 FOREST AVENUE
PARAMUS NJ 07652-0001
(201)-843-7800
FAX: (201)-843-3460

MS SANDRA W DIXON
GULFSTREAM AERO CORPANCE
M/S D-04
PO BOX 2206
SAVANNAH GA 31402-2206
(912)-965-4345
FAX: (912)-965-4812

MR JONATHAN P DUBKE
AEROSPACE ENGR
US AIR FORCE
SA-ALC/LADD
485 QUENTIN ROOSEVELT STE 1
KELLY AFB TX 78241-6420
(512)-925-4525
FAX: (512)-925-9940

MR ERIC T EASTERBROOK
ENGRG MGR
FATIGUE TECH INC
100 ANDOVER PARK W
SEATTLE WA 98188-2868
(206)-246-2010
FAX: (206)-244-9886

MR ROBERT G EASTIN
BR MGR
MCDONNELL DOUGLAS AERO
M/S TA-EEO 159-59
1510 HUGHES WAY
LONG BEACH CA 90810-1864
(310)-982-5423
FAX: (310)-496-9112

MR MATTHEW S EDGHILL
ENGR SENIOR
LOCKHEED FT WORTH CO
PO BOX 748
FT WORTH TX 76101-0001
(817)-763-4421
FAX: (817)-777-2115

MR CHARLES ELLIOTT III
RES ASST PROF
UNIV OF UTAH
MECH ENGR
MEB ROOM 3209
SALT LAKE CITY UT 84112-0001
(801)-585-6429
FAX: (801)-581-8692

MR WILLIAM R ELLIOTT
SUPR AEROSPACE ENGR
US AIR FORCE
WR-ALC/TIED
255 2ND ST STE 122
ROBINS AFB GA 31098-1637
(912)-926-9835
FAX: (912)-926-1743

MS ANN M EMBREY
FEDERAL AVIATION ADMIN
AVIATION SYS STDS
M/S AVN-347
6500 S MCARTHUR
OKLAHOMA CITY OK 73125-4932
(405)-954-8713
FAX: (405)-954-4740

MR RICHARD A EVERETT JR
US ARMY VEHICLE STRUCTURES DIR
NASA LANGLEY RES CTR
M/S 188E
ANSRL-VS-S
HAMPTON VA 23681-0001
(804)-864-3459
FAX: (804)-864-3459

MR ALBERT G EWELL
LOG MGMT SPECIALIST
US AIR FORCE
WR-ALC/LFIT
296 COCHRAN ST
ROBINS AFB GA 31098-0001
(912)-926-3016
FAX: (912)-328-2206

MR JOAO FI FALCAO
STRUC SCIENCES GRP LDR
GRUMMAN MELBOURNE SYS
M/S H09-223
2000 NASA BLVD
MELBOURNE FL 32904-2322
(407)-951-6467
FAX: (407)-951-6218

MR PHILLIP T FARLEY
AEROSPACE ENGR
US AIR FORCE
SA-ALC/LFES
KELLY AFB TX 78241-5443
(210)-925-4284
FAX: (210)-925-0097

MR SCOTT FAWAZ
US AIR FORCE
KLUYVERWEG 1
2629 HS DELFT
NETHERLANDS

MR ROBERT W FERGUSON
DESIGN ENGR
BRISTOL AEROSPACE LTD
660 BERRY ST
PO BOX 874
WINNIPEG MANITOBA CANADA R3C-2S4
(204)-775-8331
FAX: (204)-783-2168

DR JIRI FIDRANSKY
AERO VODOCHODY
250 70 ODOLENA VODA
PRAGUE
CZECH REPUBLIC
42-2-6858047-9

MR LUPE FLORES
US AIR FORCE
SA-ALC/LADD
485 QUENTIN ROOSEVELT RD STE 1
KELLY AFB TX 78241-6420
(210)-925-4525

DR THOMAS H FLOURNOY
CORROSION TECH MGR
FEDERAL AVIATION ADMIN
FAA TECHNICAL CTR
AGING AIRCRAFT GR/ACD-220
ATLANTIC CITY NJ 08405-0001
(609)-485-5327
FAX: (609)-485-4569

MR ROYCE G FORMAN
NASA JOHNSON SPACE CTR
MATERIALS BRANCH (EM2)
HOUSTON TX 77058-0001
(713)-483-8926
FAX: (713)-483-2162

MR DONALD M FORNEY JR
SR PROG MGR
UNIVERSAL TECH CORP
4031 COL GLENN HWY
DAYTON OH 45431-1600
(513)-426-8530
FAX: (513)-426-7753

MR MIKE L FORTSON
US AIR FORCE
WR-ALC
LJLE
ROBINS AFB GA 30063-0986

MR MICHAEL C FOSTER
SR PROJ ENGR
MCDONNELL DOUGLAS
DEPT 352D MS 1069050
PO BOX 516
ST LOUIS MO 63166-0516

FAX: (314)-233-2232

MR JEFFREY A FRADY
SR ENGR
LEARJET
FATIGUE DEPT
PO BOX 7707
M/S 29
WICHITA KS 67277-7707
(316)-946-2522
FAX: (316)-946-2809

MR JOBST F FRANK
GERMAN MOD
AMC PO BOX 33668
WRIGHT-PATTERSON AFB OH 45433-0668
(513)-255-6660
FAX: (513)-255-1970

CAPT ROBERT S FREDELL
US AIR FORCE
ACADEMY
2354 FAIRCHILD DR STE 6H2
USAF ACADEMY CO 80840-6240
(719)-472-2196
FAX: (719)-472-2944

DR JOSEPH P GALLAGHER
HEAD STRUC INTEG
UNIV OF DAYTON
RES INST
300 COLLEGE PARK DR
DAYTON OH 45469-0120
(513)-229-4417
FAX: (513)-229-3712

MR JESUS GARCIA
SPANISH AIR FORCE
LOGISTIC SUPPORT
EG AIRE
MADRID SPAIN-0001
(341)-549-0700

MR KEVIN D GARDNER
ALLIEDSIGNAL AERO
1300 W WARNER RD
PO BOX 22200
TEMPE AZ 85285-2200
(602)-893-4439
FAX: (602)-893-5123

MR WILLIAM GARDNER
ROLLS-ROYCE INC
2849 PACES FERRY RD
STE 450
ATLANTA GA 30339-3769
(404)-436-7900
FAX: (404)-436-8570

MR MICHAEL GASPERT
ROYAL AUSTRALIAN AF
RAAF F-111 LIAISON OFF
5111 ROBERTS AVE/STE 4
MCCLELLAN AFB CA 95652-1325

MR ROBERT P GERAMI
US AIR FORCE
ASC/ENFS
2335 7TH ST STE 6
WRIGHT-PATTERSON AFB OH 45433-7809
(513)-255-3330
FAX: (513)-476-4546

MR FRANCIS E GERBER
VP ENGR
DAYTON T BROWN INC
DEPT 17
CHURCH ST
BOHEMIA NY 11716-0001
(516)-589-6300
FAX: (516)-567-9045

MR ALI GHANNADAN
MOOG ESPRIT TECHNOLOGY
140 MAYHEW WAY
BLDG E
PLEASANT HILL CA 94523-4337
(510)-947-0400
FAX: (510)-947-0900

MR LIONEL C GIDNEY
STRESS ENGR
DE HAVILLAND INC
GARRATT BLVD
MS N18-10
DOWNSVIEW ONTARIO M3K 1Y5-0001
(416)-375-3876
FAX: (416)-375-4537

MR GREG GLINKA
PROFESSOR
UNIVERSITY OF WATERLOO
MECHANICAL ENGR
WATERLOO ONTARIO N2L 3G1-0001
(519)-742-6363
FAX: (519)-888-6197

DR MATTHEW J GOLIS
PRES
ADV QUALITY CONCEPTS
264 FAIRLAWN
PO BOX 141388
COLUMBUS OH 43214-0001
(614)-268-0518
FAX: (614)-267-6288

MR TARUN GOSWAMI
UNIV OF UTAH
DEPT OF MECH ENGRG
3209 MERRILL ENGRG BLDG
SALT LAKE CITY UT 84112-0001
(801)-585-3228
FAX: (801)-581-8692

MR MARKUS GOTTIER
AEROSPACE ENGR
MCDONNELL DOUGLAS
DPRO M/S 2704406
PO BOX 516
ST LOUIS MO 63166-0516
(314)-232-4932
FAX: (314)-232-1672

MR STEPHEN C GOULD
US AIR FORCE
LADD
485 QUENTIN ROOSEVELT RD
KELLY AFB TX 78241-6420
(210)-925-4525
FAX: (210)-925-9940

DR ALTEN F GRANDT JR
PURDUE UNIV
AERO & ASTRO
1282 GRISSOM HALL
W LAFAYETTE IN 47907-1282
(317)-494-5141
FAX: (317)-494-0307

MR STEPHEN C GRESLEY
PROG MGR
SMITHS INDUSTRIES
M/S 231
4141 EASTERN SE
GRAND RAPIDS MI 49505-8727
(616)-241-7517
FAX: (616)-241-7858

LTC KENNETH E GRIFFIN
SOUTHWEST RESEARCH
6220 CULEBRA RD
PO DRAWER 28510
SAN ANTONIO TX 78228-0510
(210)-522-6873
FAX: (210)-522-3042

MR FRANK M GRIMSLEY
AEROSPACE ENGR
US AIR FORCE
ASC/YS
WRIGHT-PATTERSON AFB OH 45440-0001
(513)-255-9518

MR ALLAN W GUNDERSON
TECH AREA MGR
US AIR FORCE
WL/MLLN BLDG 655
2230 TENTH ST STE 1
WRIGHT-PATTERSON AFB OH 45433-7817
(513)-255-1351
FAX: (513)-476-4840

MR CORNELIS B GUYT
USAFA/DELFT UNIV
2354 FAIRCHILD DR
STE 6H2
COLORADO SPRINGS CO 80840-6240
(719)-472-3041
FAX: (719)-472-2944

MR KEVIN B HALL
LOCKHEED
DEPT 73-25/ZONE 0160
86 S COBB DR
MARIETTA GA 30063-0001
(404)-494-4712
FAX: (404)-494-9610

MR STEPHEN R HALL
CELERIS AERO CANADA INC
PO BOX 51001
ORLEANS
ONTARIO CANADA K1E-3W4
(613)-837-1161
FAX: (613)-834-6420

MR DEVARD O HAMMOND
C-141 ASIP MGR
US AIR FORCE
WR-ALC/LJLEA
270 OCMULGEE CT
ROBINS AFB GA 31098-1646
(912)-926-9141
FAX: (912)-926-9142

MR ROY W HAMPTON
NASA AMES RES CTR
M/S 213-4
MOFFET FIELD CA 94035-1000
(415)-604-6223
FAX: (415)-604-1000

MR JOHN P HANSEN
ENGR
PRATT & WHITNEY
M/S 713-55
PO BOX 109600
W PALM BEACH FL 33410-9600
(407)-796-4827
FAX: (407)-796-3637

MR ODED HARARI
SECTION MGR
VITRO CORP
400 VA AVE
STE 825
WASHINGTON DC 20024-2730
(202)-646-6391
FAX: (202)-646-6398

MR DAVID W HARPER
AEROSPACE ENGR
US AIR FORCE
HQ AFSA/SES
9700 AVE G SE
KIRTLAND AFB NM 87117-5670
(505)-846-0996
FAX: (505)-846-2721

MR JAMES G HARPER
US AIR FORCE
WR-ALC/LBI
265 OCMULGEE CT
ROBINS AFB GA 31098-1647
(912)-926-9167
FAX: (912)-926-9142

MR JIM HARRISON
METAL IMPROVEMENT CO
1618 S IDA
WICHITA KS 67211-0001
(316)-267-8201

CAPT KARL A HART
US AIR FORCE
WL/FIBEC STE 1
2130 8TH ST
WRIGHT-PATTERSON AFB OH 45433-7542
(513)-255-6104

MR PETER F HEDGES
AERO ENGR
US AIR FORCE
SM-ALC/YFLB
4234 59TH ST
STE 2
MCCLELLAN AFB CA 95652-1530
(916)-643-0372
FAX: (916)-643-0361

MR JUERGEN HEILIG
NATO AIRBORNE FORCE CMD
FCLE
HQ NAENFC LISBONNE
B 7010 SHAPE
BELGIUM
32 65 44 4647

MR MICHAEL HEINER
US AIR FORCE
OO-ALC/LAIT
6089 WARDLEIGH RD
HILL AFB UT 84056-5838
(801)-777-6086
FAX: (801)-773-9782

MR MARKUS B HEINIMANN
PURDUE UNIVERSITY
1282 GRISSOM HALL
W LAFAYETTE IN 47907-0001

MR LAWRENCE R HEITZMANN
DAYTON T BROWN
CHURCH ST
BOHEMIA NY 11716-0001
(516)-589-6300
FAX: (516)-567-9045

MR CHARLES R HENDERSON
STRUC ENGR
US AIR FORCE
ASC/LPGH
1895 FIFTH ST
WRIGHT-PATTERSON AFB OH 45440-0001
(513)-255-9740
FAX: (513)-476-7503

MR TORBEN HENRIKSEN
EUROPEAN SPACE AGY
PO BOX 299
2200AG
NOORDWICK NETHERLAND

DR PAUL HEULER
IABG
DEPT TAB
EINSTEINSTR
OTTOBRUNN GERMANY 85521-0001

MR THOMAS B HEWTON
MGR STRUC INTEGRITY
GE AIRCRAFT ENGINES
M/S Q8
ONE NEUMANN WAY
CINCINNATI OH 45215-6301
(513)-552-4756
FAX: (513)-552-4857

MR ROBERT W HEYGR
VEDA INC
1800 N BEAUREGARD ST
ALEXANDRIA VA 22311-1708
(703)-413-4784
FAX: (703)-413-8031

MR JAMES M HILL
US AIR FORCE
OC-ALC/TILO
TINKER AFB OK 73145-0001
(405)-736-2663
FAX: (405)-736-3086

MR KURT W M HILL
SQUADRON LEADER
ROYAL AIR FORCE
AIRFRAME SQUADRON
HQ LOGISTICS CMDEY
WYTON HUNTINGDON
CAMBRIDGESHIRE NR20 4LJ-0001

PROF BEN M HILLBERRY
PURDUE UNIV
SCHOOL OF MECH ENGRG
1228 MECH ENGR BLDG
W LAFAYETTE IN 47907-1288
(317)-494-5721
FAX: (317)-494-0539

PROF DAVID W HOEPPNER
UNIV OF UTAH
3209 MERRILL ENGRG BLDG
SALT LAKE CITY UT 84112-0001
(801)-581-3851
FAX: (801)-585-5889

DR MARGERY E HOFFMAN
AEROSPACE ENGR
NAVAL AIR WARFARE CTR
CODE 4333
PO BOX 5152
WARMINSTER PA 18974-0591
(215)-441-1695

DR RENE HOLLIGER
SWISS FED AIRCRAFT FACTORY
DEPT TA
EMMEN
CH SWITZERLAND
41 41 594359

MR ROGER D HOWELL
AERO ENGR
US AIR FORCE
7278 4TH STREET
OGDEN UT 84056-0001

MR TROY S HULLANDER
NAVAL AVIATION DEPOT
PSC 8021 BLDG 4224
PSD 310
CHERRY POINT NC 28533-0021
(919)-466-8120

MR LEX C HUTCHESON
PROG MGR
SVERDRUP TECH INC
ADV SYS GROUP
4538 CENTERVIEW DR
SUITE 130
SAN ANTONIO TX 78228-0001
(210)-733-3383
FAX: (210)-733-3389

MR TETSUJI ITOH
ASST SR ENGR
NASDA
SPACE STAT DEPT
2-1-1 SENGEN
TSUKUBA-SHI IBARAKI

LTC COR J JANSEN
US AIR FORCE
RNLAF OO-ALC/LAA-NE
6061 GUM LANE
HILL UT 84056-5826
(801)-777-4930
FAX: (801)-773-7250

MR DANIEL A JANSEN
US AIR FORCE
FATIGUE & FRACTURE TEST FAC
BLDG 65/AREA B
WRIGHT-PATTERSON AFB OH 45433-0001
(513)-255-0434
FAX: (513)-476-7379

MR DAVID Y JEONS
US DOT/VOLPE CTR
M/S DT5-74
KENDELL SQ
CAMBRIDGE MA 02142-1093
(617)-494-3654
FAX: (617)-494-3066

MR JAMES K JOBSON JR
ENGR SPEC
LOCKHEED AERO SYS CO
DEPT 73-25/MS 0160
86 S COBB DR
MARIETTA GA 30063-0001
(404)-494-2981
FAX: (404)-494-9610

MR FRANK R JOHNSON JR
LEAD STRUC ANALYST
CHRYSLER TECH AIRBORNE
7500 MAEHR RD
MS 1135
WACO TX 76705-0001
(817)-867-2536
FAX: (817)-867-4597

MR HERMAN E JOHNSON
FRACTURE MECHANICS
PRATT & WHITNEY
M/S 714-03
PO BOX 109600
W PALM BEACH FL 33410-9600
(407)-796-5151
FAX: (407)-796-8993

MR WILLIAM JOHNSON
TECH EXPERT
US AIR FORCE
ASC/ENF
WRIGHT-PATTERSON AFB OH 45433-0001
(513)-255-3330
FAX: (000)-000-0001

LTC CRAIG R JONES
C-141 STRUC TEAM
US AIR FORCE
WR-ALC/LJLEA
PO BOX 11424
ALBUQUERQUE NM 87192-0424
(505)-845-9063
FAX: (505)-844-8711

DR WALTER F JONES
PROG MGR
US AIR FORCE
AFOSR/NA STE B-115
110 DUNCAN AVE
BOLLING AFB DC 20332-0001
(202)-767-0470
FAX: (202)-767-4988

LTCOL JOHN R JOOSTEN
ROYAL NETHERLANDS AF
MOD FIGHTER DIV
BINCKHORSTLAAN 135
PO BOX 20703
THE HAGUE NETHERLAND 2500ES-0001

MR DIAZALOND JOSE
SAF
MATERIAL GRP/ALA 12
TORREJON AFB
MADRID SPAIN-0001
(341)-675-5066
FAX: (341)-677-1675

MR VICTOR JUAREZ
SR ENGRG SPEC
LOCKHEED FT WORTH CO
M/Z 2846
PO BOX 748
FT WORTH TX 76101-0001
(817)-763-2926
FAX: (817)-777-2115

MR DANIEL KALAL
CESSNA AIRCRAFT CO
DEPT 178 ENGR
PO BOX 7704/MS 09
WICHITA KS 67277-0001
(316)-941-6227
FAX: (316)-941-7258

MR SAM KANTIMATHI
PRESIDENT
FATIGUE CONCEPTS
300 SALAMON FALLS RD
EL DONADO HILLS CA 95762-9734
(916)-933-3360
FAX: (916)-933-3361

MAJ HEIKKI K KARPPINEN
FINNISH AIR FORCE
PO BOX 516
MS 270-4396
ST LOUIS MO 63166-0516
(314)-234-6227
FAX: (314)-234-1672

LTC ROLF KEIMER
LIAISON OFFICER
GERMAN AIR FORCE
AIR LOGISTICS CNTR OGDEN
OO-ALC / LAI-GY
6089 WARDLEIGH RD
HILL AFB UT 84056-5838
(801)-777-5743
FAX: (801)-773-7620

MR TIMOTHY C KELLEY
E-SYSTEMS
M/S 101
PO BOX 6056
GREENVILLE TX 75403-6056
(903)-457-4719
FAX: (903)-457-4413

MR LARRY G KELLY
GROUP LEADER
UDRI
STRUCTURAL INTEGRITY DIV
300 COLLEGE PK
DAYTON OH 45469-0120
(513)-229-4479
FAX: (513)-229-3712

MR ALAN P KERR
DYNCORP
ONE RIDGMAR CTR
6500 W FREEWAY
FT WORTH TX 76116-0001

MR ROBERT J KERR
US AIR FORCE
OC-ALC/TILO
7851 2ND ST RM 105
TINKER AFB OK 73145-9145
(405)-736-2054
FAX: (405)-736-3206

1ST LT GERNOT KESSLER
GERMAN AIR FORCE-MATL OFC
3 B 3 C
PO BOX 902500-503
COLOGNE GERMANY 51140-0001
011 49 2203 6022431

MR JON C KIMMEL
US AIR FORCE
OC-ALC/LAKRA
TINKER AFB OK 73071-0001
(405)-736-3343
FAX: (405)-734-2179

MR WILLIAM G KING
US AIR FORCE
WR-ALC/LKSA
460 2ND ST STE 221
ROBINS AFB GA 31098-1640
(912)-926-1808
FAX: (912)-926-1646

MR JAMES E KNUTSON
SYS & ELECTRONICS INC
190 GORDON ST
ELK GROVE VILLAGE IL 60007-1120
(708)-228-0985
FAX: (708)-228-1120

DR GERHARDUS M KOCH
CC TECHNOLOGIES
2704 SAWBURY BLVD
COLUMBUS OH 43235-0001
(614)-761-1214
FAX: (614)-761-1633

MR JAMES KOKORIS
NORTHROP GRUMMAN CORP
M/S A13-115
1111 STEWART AVE
BETHPAGE NY 11714-0001
(516)-346-8814
FAX: (516)-346-3290

LT DERIC V KRAXBERGER
US AIR FORCE
OC-ALC/TIETR STE 2AF66A
3001 STAFF DR
TINKER AFB OK 73145-3040
(405)-736-5015
FAX: (405)-736-5431

MAJ DENIS LAMANQUE
NATIONAL DEFENCE
DAS ENG 6-5
NAT DEF HQ
OTTAWA ONTARIO K1A 0K2-0001
(613)-993-0663
FAX: (613)-998-6921

MR ROGER H LARSEN
ARINC RES CORP
STE 210
4335 PIEDRAS DR W
SAN ANTONIO TX 78228-0001
(210)-733-7559
FAX: (210)-733-9406

KALMEN I LEIKACH
NAVAL AIR SYS CMD
1421 JEFFERSON DAVIS HWY
ARLINGTON VA 22243-5120
(703)-604-3400
FAX: (703)-604-4396

MAJ PATRICK LEMMERS
US AIR FORCE HQ AMC
UNIT 2A2
402 SCOTT DR
SCOTT AFB IL 62225-5308
(618)-256-2059
FAX: (618)-256-5544

MR THOMAS G LILJA
SAAB MILITARY AIRCRAFT
SMA TUDH
SAAB SCANIA AB
LINKOPING SWEDEN 5-58188-0001
46 13 181522

POH G LIM
SINGAPORE AERO LTD
ENGRG & DEF CTR
540 AIRPORT RD
SINGAPORE 1648-0001

DR JOHN W LINCOLN
TECH EXPERT
US AIR FORCE
ASC/ENFS
BLDG 125 RM 1248
WRIGHT-PATTERSON AFB OH 45433-6553
(513)-255-6879
FAX: (513)-255-4789

MR GEORGE R LINDBERG
GENERAL ELECTRODYNAMICS
8000 CALENDAR RD
PO BOX 150089
ARLINGTON TX 76017-0001
(817)-572-0366
FAX: (817)-572-0373

MR KO-WEI LIU
MCDONNELL DOUGLAS AERO
M/S TA-EEX 159-59
1510 HUGHES WAY
LONG BEACH CA 90810-1864
(310)-982-5422
FAX: (310)-982-5164

MR ANTHONY S LIZZA
US AIR FORCE
WL/FIBEC
2130 8TH ST STE 1
WRIGHT-PATTERSON AFB OH 45433-7542
(513)-255-6104
FAX: (513)-476-4999

MR CHARLES P LOGAN
DIR BUS DEV
BP CHEMICALS (HITCO) INC
1600 W 135TH ST
GARDENA CA 90249-2506
(310)-527-0700
FAX: (310)-516-5786

CAPT ANTHONY M LOGUE
US AIR FORCE
ESC/JSEP
3 EGLIN ST
HANSCOM AFB MA 01731-0001
(617)-377-6838
FAX: (617)-275-9631

Y CHEN LONG
LOCKHEED ADV DEV CO
M/S 25-42
1011 LOCKHEED WAY
PALMDALE CA 93599-0001
(805)-572-7807

DR M C LOU
NASA
JET PROPULSION LAB
4800 OAK GROVE RD
PASADENA CA 91109-0001
(818)-354-3034
FAX: (818)-393-5169

MR JOSEPH LUDWIG
AIR INC/AERO-IND REPS INC
2500 RADCLIFFE DR
ARLINGTON TX 76012-0001
(817)-543-1564
FAX: (817)-277-4561

MR AUDGEIR LUNDE
ROYAL NORWEGIAN AF MATL CMD
M/S DFIS
PO BOX 10
KJELLER NORWAY
47 63808311

DR BERNARD E LUTZ
PRESIDENT
MEYER ANALYTICS INC
STRUC RESEARCH
6738 BRIDLE PATH
WARRENTON VA 22186-9212
(703)-349-4560
FAX: (703)-349-1207

MR JOSEPH J LUZAR JR
BOEING DEF & SPACE GRP
M/S K86-81
PO BOX 7730
WICHITA KS 67277-7730
(316)-523-5408
FAX: (316)-523-5705

MR ROBERT MACH
AEROSPACE ENGR
US AIR FORCE
ASC/LPCH BLDG 46
1895 FIFTH ST
WRIGHT-PATTERSON AFB OH 45433-7200
(513)-255-2300
FAX: (513)-255-0987

MR PAUL E MAGNUSEN
ALCOA LABS
100 TECHNICAL DR
ALCOA CENTER PA 15069-0001
(412)-337-5915
FAX: (412)-337-5436

MR ELIMOR MAKEVET
ISRAELI AIR FORCE
PO BOX 799
BEER-SHEVA ISRAEL 84-106
(972)-396-8444

MR CHRIS MANDERS
CHRYSLER TECH AIRBORNE SYS
M/S 1135
7500 MAEHR
WACO TX 76715-4580
(817)-867-4051
FAX: (817)-867-4597

DR SHERRELL D MANNING
LOCKHEED FT WORTH CO
M/Z 4267
PO BOX 748
FT WORTH TX 76101-0001
(817)-935-2913
FAX: (817)-935-3800

MR EDWARD L MARTIN
CHRYSLER TECH AIRBORNE SYS
7500 MAEHR RD
M/S 1135
WACO TX 76715-4586
(817)-867-4285
FAX: (817)-867-4597

MR JAMES MARTIN
SR ENGR SPEC
BELL HELICOPTER TEXTRON INC
FATIGUE ANALYSIS
PO BOX 482
FT WORTH TX 76101-0001
(817)-280-3517
FAX: (817)-280-8772

MR SCOTT K MASTERS
BOEING
M/S 4A-14
PO BOX 3707
SEATTLE WA 98124-0001
(206)-655-6475
FAX: (206)-655-0315

DR GEORGE A MATZKANIN
DIR
NTIAC TRI
415 CRYSTAL CREEK DR
AUSTIN TX 78746-4725
(512)-263-2106
FAX: (512)-263-3530

DR STUART L MCBRIDE
AEMS INC
PHYSICS DEPT
STE 306
KINGSTON ONTARIO CANADA K2K-127
(613)-544-6192

MR JAMES E MCCALL
LOCKHEED AERO SYS CO
M/S 0160
86 S COBB DR
MARIETTA GA 20062-0001
(404)-494-8420
FAX: (404)-494-5610

MR ROBERT C MCCLUNG
SOUTHWEST RES INST
6220 CULEBRA
PO DRAWER 28510
SAN ANTONIO TX 78228-0510
(210)-522-2422
FAX: (210)-522-5122

MR BRIAN MCCOUBREY
SHORTS BROTHERS PLC
PO BOX 241
AIRPORT RD
BELFAST N IRELAND BT-3902

MR JOHN MCCOURY
CHRYSLER TECH AIRBORNE SYS
M/S 1135
7500 MAEHR
WACO TX 76715-4580
(817)-867-4116
FAX: (817)-867-4597

MR JAMES M MCGINN
NAVAL AIR SYS CMD
AIR 05H2
1421 JEFFERSON DAVIS HWY
ARLINGTON VA 22243-0001
(703)-604-2265
FAX: (703)-604-2976

DR PETER C MCKEIGHAN
SR RESEARCH ENGR
SOUTHWEST RESEARCH INST
6220 CULEBRA RD
PO DRAWER 28510
SAN ANTONIO TX 78228-0510
(210)-522-3617
FAX: (210)-522-5122

MR ROBERT L McKINLEY
LEAD STRUC ENGR
US AIR FORCE
ASC/ENFS
WRIGHT-PATTERSON AFB OH 45433-6503
(513)-255-7076
FAX: (513)-255-8516

MR MIKE MCMAHON
NAVAL AIR SYS CMD
1421 JEFFERSON DAVIS HWY
WASHINGTON DC 22243-5120
(703)-604-3400
FAX: (703)-604-4396

MR ROBERT D MEADOWS
FEDERAL AVIATION ADMIN
M/S AVN-347
PO BOX 25082
OKLAHOMA CITY OK 73125-4932
(405)-954-4700
FAX: (405)-954-4740

MR JESSE MEDINA
US AIR FORCE
SA-ALC/LPFE BLDG 171
485 QUENTIN ROOSEVELT RD
KELLY AFB TX 78241-6420
(210)-925-6474
FAX: (210)-925-1328

MR ROBERT J MELLYN
NEW BUSINESS DEV DIR
ELECTRODYNAMICS INC
1200 HICKS RD
ROLLING MEADOWS IL 60008-0001
(708)-259-0740
FAX: (708)-255-3827

MR DANIEL MERENVIELLE
AIRFRAME ENGR
AIR FRANCE
AIRFRAME ENGR
FR AWACS DLM PROG
AEROPORT DU BOORGET
FRANCE 93350-0001

MR SAMBI R METTU
ADV SYS ENGR SPEC
LOCKHEED
DEPT 23-22
2400 NASA RD 1/MS C 62
HOUSTON TX 77258]-8561
(713)-483-3960
FAX: (713)-483-2162

MR RICHARD P MICKLOS
NAVAL AIR WARFARE CENTER
CODE 4333
MS 08
WARMINSTER PA 18974-0591
(215)-441-2893
FAX: (215)-956-4005

LTCMDR JOSEPH E MIHELIC
US COAST GUARD
ARSC ENGINEERING
ELIZABETH CITY NC 27909-0001
(919)-335-6837
FAX: (919)-335-6463

MR MICHAEL A MIKE
ENSIP TECH MGR
PRATT & WHITNEY
400 MAIN ST
MS 163-09
E HARTFORD CT 06108-0001
(203)-565-7865
FAX: (203)-565-1560

MAJ JAMES B MILLER
MGR STRUC INTEG
NATIONAL DEFENCE
DAS ENG 6-3
NAT DEF HQ
OTTAWA ONTARIO K1A 0K2-0001
(613)-993-2320
FAX: (613)-998-6922

MR GERALD H MINTZ
TECH STAFF
ROCKWELL INTL
VEHICLE & SYS ANALYSIS
M/S AB94
12214 LAKEWOOD BLVD
DOWNEY CA 90241-0001
(310)-922-3358
FAX: (310)-922-1214

MR W CRAIG MITCHELL
US AIR FORCE
OO-ALC/LAIA F-4 TCG
6089 WARDLEIGH RD
HILL AFB UT 84056-5838
(801)-777-5891
FAX: (801)-773-7620

MR ROBERT L MOORE
US AIR FORCE
HQ AFMC/ENSP
4375 CHIDLAW RD/STE 6
WRIGHT-PATTERSON AFB OH 45433-5006
(513)-257-5561
FAX: (513)-257-0841

MR ROBERT L MOORE
US AIR FORCE
2335 SEVENTH ST/STE 6
AREA B BLDG 125
WRIGHT-PATTERSON AFB OH 45433-7809
(513)-255-3330
FAX: (513)-476-4546

MR STEVEN MOORE
CHIEF TECH
ROYAL AIR FORCE
STRUCTURES FLIGHT
HQ LOGISTICS CMDT
WYTON HUNTINGDON
CAMBERIDGESHIRE ENGLAND-0001

MR JOHN E MORGAN
US AIR FORCE
OC-ALC/LABEF STE 2AB
3001 STAFF DR
TINKER AFB OK 73145-3006
(405)-736-5194
FAX: (405)-736-5598

MR ROBERT J MORRIS
PRATT & WHITNEY
M/S 714-03
PO BOX 109600
W PALM BEACH FL 33410-9600
(407)-796-5981
FAX: (407)-796-8993

MR TERRY MORRIS
ALLIEDSIGNAL AEROSPACE CO
AIRESEARCH
M/S TOR-36-2-93080
2525 W 190TH ST
TORRANCE CA 90504-6099
(310)-512-3614
FAX: (310)-512-2477

MR RICHARD MULLER
DELFT UNIV OF TECH
STRUC MATLS LAB
PO BOX 5058
NETHERLANDS

MR EDWIN G MULLIN
NAVAL AVIATION DEPOT
S-3 ENGINEERING
CODE O5113
ALAMEDA CA 94501-5021
(510)-263-8014
FAX: (510)-263-6949

MR GEORGE W NEAT
US DOT/VOLPE CTR
KENDALL SQUARE
M/S DTS-74
CAMBRIDGE MA 02142-1093
(617)-494-2679
FAX: (617)-494-3096

MR ROGER NESJE
ROYAL NORWEGIAN AF
MATERIAL COMMAND
PO BOX 10
KJELLER NORWAY N2007-0001

MR DOUGLAS H NETHAWAY
MGR EXP MECH
PRATT & WHITNEY
M/S 707-22
PO BOX 109600
W PALM BEACH FL 33410-9600
(407)-796-6551
FAX: (407)-796-7454

MR JAMES C NEWMAN
SR SCIENTIST
NASA LANGLEY RES CTR
MECHANICS OF MATLS
M/S 188E
HAMPTON VA 23681-0001
(804)-864-3487
FAX: (804)-864-7729

MR CHI-TECK T NG
HQ-RSAF
ALD
GOMBAK DR
SINGAPORE S(1646)-0001
65 7682710

LT ANDREW H NICHOLS
US AIR FORCE
ASC/YCEF
2600 PARAMOUNT PIKE
WRIGHT-PATTERSON AFB OH 45324-6766
(513)-255-5427
FAX: (513)-255-3207

MR DONALD E NIESER
US AIR FORCE
STE 2AC489D
OC-ALC-LACRA
3001 STAFF DR
TINKER AFB OK 73145-3019
(405)-736-3834
FAX: (405)-736-5604

MR WILLIAM R NOBLE
C-17 LOADS & SFDR
US AIR FORCE
2600 PARAMOUNT PLC
ASC/YCEF
WRIGHT-PATTERSON AFB OH 45324-6766
(513)-255-5427
FAX: (513)-255-3207

MR MARVIN R NUSS
SMALL AIR POLICY
FEDERAL AVIATION ADM
601 EAST 12TH ST
M/S ACE-111
KANSAS CITY MO 64106-0001
(816)-426-6941
FAX: (816)-426-2169

MR THOMAS R O'CONNOR
DYNCORP
ONE RIDGMAR CTR
6500 W FREEWAY
FT WORTH TX 76116-0001
(817)-737-1680
FAX: (817)-737-1605

MR HARARI ODED
SECTION MGR
VITRO CORP
SPACE OPS
400 VA AVE
SUITE 825
WASHINGTON DC 20024-2730
(202)-646-6391
FAX: (202)-646-6398

MR MATS-OLOF OLSSON
DEFENCE MATL ADM
S-115 88
STOCKHOLM SWEDEN
46-8-7824884

MR WILLIAM E OVERACKER
DYNCORP
ONE RDGMAR CTR
6500 W FREEWAY
FT WORTH TX 76116-0001
(817)-737-1535
FAX: (817)-737-1605

MR DANNY E OWENS
ARINC RES CORP
STE 500A
5600 LIBERTY PKWY
MIDWEST CITY OK 73110-2835
(405)-739-0939
FAX: (405)-739-0003

MR TIM PADFIELD
BRISTOL AEROSPACE
DEPT 712
PO BOX 874
WINNIPEG CANADA R3C-254
(204)-775-8331
FAX: (204)-783-2168

MR CARLOS PAIRAZAMAN
SYS RES LABS
2800 INDIAN RIPPLE
DAYTON OH 45440-3696
(513)-427-7850
FAX: (513)-427-7745

MR MIKE PAQUET
PRATT & WHITNEY
M/S 731-82
PO BOX 109600
W PALM BEACH FL 33410-0001
(407)-796-2515
FAX: (407)-796-5362

MR ARMAND PAQUIN
BOMBARDIER INC
INTL AIRPORT
10,000 CARGO A-4 ST
MIRABEL QUEBEC CANADA J7N-1H3
(514)-476-4350
FAX: (514)-476-4451

MR RAYMOND M PATIN
MATLS ENGINEER
NASA JOHNSON SPACE CTR
2101 NASA RD 1
MS AH3
HOUSTON TX 77058-0001
(713)-483-3073
FAX: (713)-483-3789

MR CLARE A PAUL
US AIR FORCE
WL/FIBEC
2130 8TH/STE 1
WRIGHT-PATTERSON AFB OH 45433-7542
(513)-255-6104
FAX: (513)-476-4999

MR PAUL R PEACOCK
STRUC MGR
US AIR FORCE
HQ/AFSOC
DEPT LGMW
100 BARTLEY ST/STE 309
HURLBURT FIELD FL 32544-0001
(904)-884-2091
FAX: (904)-884-5776

MR CHARLES J PELLERIN
MATLS ENGR
US AIR FORCE
WL/MLSE-3
2179 TWELFTH ST/STE 1
WRIGHT-PATTERSON AFB OH 45433-7718
(513)-255-3953
FAX: (513)-476-4378

MR RAYMOND PEPE
LOCKHEED AERO SYS CO
D/73-40 M/S 0943
86 S COBB DR
MARIETTA GA 30063-0943
(404)-793-0939
FAX: (404)-793-1012

MR NICHOLAS B PETRI
PRODUCT MGR
DEVICE TECH INC
3 BRIGHAM ST
MARLBOROUGH MA 01752-1340
(508)-229-2000
FAX: (508)-229-2622

MR PAUL R PIPER
AEROSPACE ENGR
US AIR FORCE
SA-ALC/LFES
KELLY AFB TX 78241-5443
(512)-925-4284
FAX: (210)-925-0097

MR DANIEL S PIPKINS
GEORGIA TECH
RM 225 FRENCH BLDG
MS 0356
ATLANTA GA 30332-0356
(404)-894-9519
FAX: (404)-894-2299

MR CHRISTOPHER J POMFRET
US AIR FORCE
WL/POTC/BLDG 18D
1950 FIFTH ST
WRIGHT-PATTERSON AFB OH 45433-7251
(513)-255-2351

MR ALFRED L PRIESTLEY
PROJ STRUC ENGR
LOCKHEED ADV DEV CO
1011 LOCKHEED WAY
PALMDALE CA 93599-2540
(805)-572-4431
FAX: (805)-572-4398

LTC BERND J PROELSZ
MINISTRY OF DEFENSE
AIRSTAFF 5-3
PO BOX 1328
BONN GERMANY 53003-0001
011 49 228 124633

DR MOHAN M RATWANI
DIR AGING AIRCRAFT
NORTHROP GRUMMAN CORP
AIRCRAFT DIV
M/S 3850/63 NORTHROP AVE
HAWTHORNE CA 90250-3277
(310)-332-9742
FAX: (310)-332-0583

MR DAVID L RATZER
AEROSPACE ENGR
US AIR FORCE
SA-ALC/LADD
485 QUENTIN ROOSEVELT RD STE 1
KELLY AFB TX 78241-6420
(210)-925-4525
FAX: (210)-925-3854

MR JOHN R REAGAN
CHIEF-AEO
NASA LERC
OSMA
21000 BROOKPARK RD
MS 601-4
CLEVELAND OH 44135-0001
(216)-433-2357
FAX: (216)-433-5270

MR RICK REAMS
US AIR FORCE
ASC/YSDF
2275 D ST/STE 4/BLDG 16
WRIGHT-PATTERSON AFB OH 45433-7221
(513)-255-9518

MR RICHARD P RECKERT
NAVAL AVIATION DEPOT
CODE 331
JAX FL 32212-0016
(904)-772-3714
FAX: (904)-772-3713

MR DANIEL C REGISTER
US AIR FORCE
WR-ALC/TIEDD
255 2NDST STE 122
ROBINS AFB GA 31098-1637
(912)-926-9892
FAX: (912)-926-2592

MR KEVIN A REID
US AIR FORCE
WR-ALC/LKSE
460 2ND ST STE 221
ROBINS AFB GA 31098-1640
(912)-926-0620
FAX: (912)-926-1646

MR LEONARD F REID
VP ENGRG PROG
FATIGUE TECH INC
100 ANDOVER PARK W
SEATTLE WA 98188-2868
(206)-246-2010
FAX: (206)-244-9886

MR THEODORE J REINHART
CHF MATLS ENGRG
US AIR FORCE
WL/MLSE BLDG 652
2179 TWELFTH ST STE 1
WRIGHT-PATTERSON AFB OH 45433-7718
(513)-255-4643
FAX: (513)-476-4706

MR BURKHART REITER
GERMAN AIR FORCE
AIR MAT OFFICE IIIB
POSTFACH G02500/502 1-13
COLOGNE GERMANY 51140-0001
2203-602-2423

MR ROBERT R RENNELL
ARINC
STE 500A
5600 LIBERTY PKWY
MIDWEST CITY OK 73110-2833
(405)-739-0939
FAX: (405)-739-0003

MR JOHN R RENTMEESTERS
SR ENGINEER
DYNCORP
ONE RIDGMAR CTR
6500 W FREEWAY
FT WORTH TX 76116-2187
(817)-737-1554
FAX: (817)-737-1605

MR DANNY J REYNOLDS
VOUGHT AIRCRAFT CO
M/S 220-J5
PO BOX 655907
DALLAS TX 75265-5907
(214)-266-2749
FAX: (214)-266-2407

MR YVES RICHARD
BOMBARDIER INC
CANADAIR DIV
INTL AIRPORT
10,000 CARGO A-4 ST
MIRABEL QUEBEC CANADA J7N-1H3
(514)-476-4357
FAX: (514)-476-4451

MR GARRY RICHMOND
SHORTS BROTHERS PLC
PO BOX 241
AIRPORT RD
BELFAST N IRELAND BT-3900

MR LARRY G RIEGERT
PROG MGR
BOMBARDIER INC
10000CARGO A-4 ST
MIRABEL QUEBEC J7N 1H3-0001
(514)-476-4424
FAX: (514)-476-4460

MR MATTHEW C ROBBINS
US AIR FORCE
ASC/LDAC(EN)
BLDG 28 RM 224
WRIGHT-PATTERSON AFB OH 45433-7200
(513)-255-2308
FAX: (513)-255-6803

MR THOMAS A ROBERTS
PRIN STAFF ENGR
LOCKHEED AIRCRAFT
1800 E AIRPORT DR
PO BOX 33
ONTARIO CA 91761-0033
(909)-395-6690
FAX: (909)-395-6500

MR GERALD W ROBERTSON
SR SPEC ENGR
BOEING CO
M/S 3E-JA
PO BOX 3999
SEATTLE WA 98124-2499
(206)-657-3824
FAX: (206)-657-3736

MR WILLIAM D ROBINSON
US AIR FORCE
ASC/VF BLDG 32
2300 D ST
WRIGHT-PATTERSON AFB OH 45433-7249
(513)-255-1404
FAX: (513)-476-7169

DR JOHN R ROGACKI
US AIR FORCE
WL/FIB
2130 EIGHTH ST STE 11
WRIGHT PATTERSON AFB OH 45433-0001
(513)-255-3031

DR PAUL G ROTH
STRUC TECH STAFF ENGR
GE AIRCRAFT ENGINES
M/D A333
ONE NEUMANN WAY
CINCINNATI OH 45215-6301
(513)-583-5014
FAX: (513)-552-4921

MR JEAN ROUSSEL
BOMBARDIER INC
MONTREAL INTL AIRPORT
10,000 CARGO ST A-4 ST
MIRABEL QUEBEC CANADA J7N-1H3
(514)-476-4056
FAX: (514)-476-4451

MR JAMES L RUDD
CHF STRUC INTEGRITY BR
US AIR FORCE
2130 EIGHTH ST/STE 1
WL/FIB/BLDG 45
WRIGHT-PATTERSON AFB OH 45433-6553
(513)-255-3031
FAX: (513)-255-3740

MR WARD D RUMMEL
MARTIN MARIETTA ASTRO
8776 W MOUNTAIN VIEW LN
LITTLETON CO 80125-9406
(303)-977-1751
FAX: (303)-977-1145

MR STEPHAN M RUSS
MATLS ENGR
US AIR FORCE
WL/MLLN BLDG 655
2230 TENTH ST STE 1
WRIGHT-PATTERSON AFB OH 45433-7817
(513)-255-1356
FAX: (513)-476-4840

MR DENNIS P RYAN
ENGINEER
NORTHROP-GRUMMAN
ONE NORTHROP AVE
M/S W-6
HAWTHORNE CA 90250-0001
(310)-332-3753

MR JOHN M SAENZ
US AIR FORCE
OC-ALC/LIINT
TINKER AFB OK 73145-0001
(405)-736-2400
FAX: (405)-736-7262

MR SUBHASIS SARKAR
GEORGIA TECH
COMP MODELING CTR
M/S 30332-0356
ATLANTA GA 30332-0001
(404)-894-9334
FAX: (404)-894-2299

MR TERRY J SAUNDER
ROYAL AUSTRALIAN AF
HQ LOGISTICS CMD
M/SDRVI-T-6
350 ST KILDA RD
MELBORNE AUSTRALIA 3034-0001
032826829

CAPT FELIX SCHAFBERG
GAF
PO BOX 902500/502/09
COLOGNE GERMANY 51140-0001

MR JASON N SCHEURING
PURDUE UNIV
M/S 1282
GRISSOM HALL
W LAFAYETTE IN 47907-1282
(317)-494-1378

MR GEORGE J SCHNEIDER
CHF STRUC RES
SIKORSKY AIRCRAFT
M/S 314A2
6900 MAIN ST
STRATFORD CT 06497-0001
(203)-386-3784
FAX: (203)-386-3717

MR ROBERT L SCHNEIDER
TECH ADVISOR
US AIR FORCE
WL/FIBT
WRIGHT-PATTERSON AFB OH 45433-6533
(513)-255-5059
FAX: (513)-255-6210

MR KURT H SCHRADER
SR RES ENGR
SOUTHWEST RES INST
6220 CULEBRA RD
PO DRAWER 28510
SAN ANTONIO TX 78228-0510
(210)-522-3322
FAX: (210)-522-3042

MR PAUL SCREEN
CHIEF TECHNICIAN
ROYAL AIR FORCE
AWAC E3 PROGRAM
SEN TRM AEDIT
RAF WADDINGTON LN5 9N3-0001

MR MITCHELL E SIMMONS
STRUC ENGR
US AIR FORCE
ASC/YF BLDG 50
2130 5TH ST
WRIGHT-PATTERSON AFB OH 45433-7809
(513)-255-8697
FAX: (513)-255-7635

DR PAVEL SINDELAR
FFA AERO RES INST OF SWEDEN
BOX 11021
S-161-11
BROMMA SWEDEN
46-8-634-1134

MR DONALD E SKOUMAL
STRUCTURES ENGRG MGR
BOEING CO
M/S 82-96
PO BOX 3999
SEATTLE WA 98124-2499
(206)-773-1362
FAX: (206)-773-4946

DR R LOWELL SMITH
SR SCIENTIST
TEXAS RESEARCH INST INC
9063 BEE CAVES RD
AUSTIN TX 78733-6201
(512)-263-2101

MR SAMUEL H SMITH
BATTELLE
505 KING AVE
COLUMBUS OH 43201-2693
(614)-424-4447
FAX: (614)-424-3315

MR JAMES Y SONG
STRUC ENGR
US AIR FORCE
SM-ALC/TIEC
5201 BAILEY LP/BLDG 243E
MCCLELLAN AFB CA 95652-0001
(916)-643-3810
FAX: (916)-643-0487

NAJ CHUA CHOY SOON
HQ-RSAF
MINDEL BLDG
GOMBAK DR
SINGAPORE 2300-0001
7606188

MR TIMOTHY J SORENSEN
US AIR FORCE
OO-ALC/LAAS
6080 GUM LANE
HILL AFB UT 84056-5825
(801)-777-5195
FAX: (801)-777-3928

MR WILLIAM A SPARKS
ENGINEERING CONSULTANT
31220 POST OAK TRAIL
FAIR OAKS RANCH TX 78006-0510
(210)-981-8725

MR FLOYD W SPENCER
SANDIA NATL LABS
DEPT 323/MS 0829
PO BOX 5800
ALBUQUERQUE NM 87185-0829
(505)-844-5647
FAX: (505)-844-9037

MR KERRY L SPRINGER
SR ENGR
LOCKHEED FT WORTH CO
PO BOX 748
M/S 2849
FT WORTH TX 76101-0748
(817)-763-2485
FAX: (817)-777-2115

MR WILLIAM H SPROAT
PROJ ENGR
LOCKHEED AERO SYS CO
STRUC TEST LAB
86 S COBB DR
M/S 0484
MARIETTA GA 30063-0484
(404)-494-5313
FAX: (404)-494-2028

HUGO H STEIN
US AIR FORCE
SA-ALC/LFE
KELLY AFB TX 78241-5443
(210)-925-6311
FAX: (210)-925-0097

PROF C T SUN
PURDUE UNIV
SCHOOL OF AERO & ASTRO
GRISSOM HALL 325
W LAFAYETTE IN 47907-1282
(317)-494-5130
FAX: (317)-494-0309

MR BILL SUTHERLAND
CHIEF F111/A-10 STRUC ENGR
SACRAMENTO ALC
SM-ALC/LAFFE
5020 DUDLEY BLVD
MCCLELLAN AFB CA 95652-1391
(916)-643-4224
FAX: (916)-643-1405

MR JAMES J SUZEL
US AIR FORCE
WL/FIBEC STE 1
2130 8TH ST
WRIGHT-PATTERSON AFB OH 45433-7542
(513)-255-6104
FAX: (513)-476-4999

DR REDA TADROS
BMW ROLLS RR
ESCHWENWEG II
DAHLEWITS GERMANY D-15827-0001
011 49 33 70861103

MR FRANK G TALOMIE JR
DIR-MENTOR PROTEGE PROG
PAR
8383 SENECA TURNPIKE
NEW HARTFORD NY 13413-4991
(315)-792-0037
FAX: (315)-792-1989

MR ARCHIE TANNOCK
PROJ ENGR
PRATT & WHITNEY CANADA
M/S 2EJ1
1801 COURTNEY PK DR
MISSISSAGUA ONTARIO CANADA L5T-1J3
(905)-564-3718
FAX: (905)-564-3884

MR LARRY E TARRANT
AEROSPACE ENGR
US AIR FORCE
OC-ALC/TILOF
TINKER AFB OK 73145-9145
(405)-736-5424
FAX: (405)-736-3086

MR WILSON R TAYLOR
US AIR FORCE
ASC/ENFP BLDG 125
2335 SEVENTH ST STE 6
WRIGHT-PATTERSON AFB OH 45433-7809
(513)-255-9595
FAX: (513)-255-5677

MR JAMES A TELINDA
MTS SYSTEMS CORP
AERO STRUCT & MATLS GRP
STE 199
800 E CAMPBELL RD
RICHARDSON TX 75081-0001
(214)-437-3288
FAX: (214)-437-4015

MR HAROLD O THOMAS
PRESIDENT
GEC
8000 CALEDAR RD
ARLINGTON TX 76017-0001
(817)-572-0366
FAX: (817)-572-0373

DR PIN TONG
DIV CHF
HONG KONG UNIVERSITY
MECH ENGR DEPT
CLEAR WATER BAY
KOWLOON HONG KONG-0001
(852)-358-7202
FAX: (852)-358-1543

MR WILLIAM A TOWNSEND
FRAC CONTROL ANALYST
TELEDYNE BROWN ENGR
PO BOX 070007
M/S 172
HUNTSVILLE AL 35807-7007
(205)-726-5143
FAX: (205)-726-5280

MR MARK TRABERT
ESPRIT TECHNOLOGY INC
SALES & ADMN
144-A MAYHEW WAY
WALNUT CREEK CA 94596-2031
(510)-947-0400
FAX: (510)-947-0900

MR BILLY R TRUSSELL
F-15 ASIP MGR
US AIR FORCE
WR-ALC/LFEFS
296 COCHRAN ST
ROBINS AFB GA 31098-1622
(912)-926-5482
FAX: (912)-926-5463

MR JIMMY A TURNER
BR CHF
US AIR FORCE
SA-ALC/LADD
KELLY AFB TX 78241-5000
(512)-925-4525

MR R L TYNER
US AIR FORCE
WR-ALC/LJLB
ROBINS AFB GA 31098-0001
(912)-926-9100
FAX: (912)-926-9142

NARESH P VAGHELA
CURTISS-WRIGHT FLIGHT SYS
DEPT 500
300 FAIRFILA RD
FAIRFIELD NJ 07004-0001
(201)-808-2394
FAX: (201)-575-2591

MR BRADLEY D VAN PEURSEM
VICE PRES
WEST COAST IND
14900 WHITMAN AVE N
SEATTLE WA 98133-0001
(206)-365-7513
FAX: (206)-365-7483

DR A K VASUDEVAN
PROG MGR
OFC OF NAVAL RES
800 N QUINCY ST
CODE 332
ARLINGTON VA 22217-5660
(703)-696-8181
FAX: (703)-696-0934

MR STAMATIS F VLASSIS
HELLENIC AIR FORCE
RESEARCH CTR
TERPSIHEA
ATHENS GREECE 16501--

MS SHARON I VUKELICH
ENSIP TECH SPECIALIST
US AIR FORCE
ASC/ENFP
2335 SEVENTH ST STE 6
WRIGHT-PATTERSON AFB OH 45433-7809
(513)-255-9594
FAX: (513)-255-5677

MR JOHN H WAFFORD
CHF LOAD & DYNAMICS
US AIR FORCE
2335 SEVENTH ST
ASC/ENFS B-125
WRIGHT-PATTERSON AFB OH 45433-7809
(513)-255-3330
FAX: (513)-476-4546

MR RAY A WALDBUSSER
C-130 ASIP MGR
US AIR FORCE
WR-ALC/LBLRS
265 OCMULGEE CT
ROBINS AFB GA 31098-1647
(912)-926-6012
FAX: (912)-926-3167

MR KEVIN F WALKER
AERO MARITIME RES LAB
506 LORIMER ST
PO BOX 4331
MELBOURNE VICTORIA AUSTRALIA-3001

MR DOUGLAS C WALLING
AEROSPACE ENGR
NAVAL AVIATION DEPOT
PSD BOX 310
BLDG 4224
CHERRY POINT NC 28533-0021
(919)-466-8042
FAX: (919)-466-7574

DR PATRICK L WALTER
MGR AGING AIRCRAFT PROJ
SANDIA NATL LABS
DEPT 2757
ALBUQUERQUE NM 87185-5800
(505)-844-5226
FAX: (505)-844-8711

MR JOHN L WARD
US AIR FORCE
OC-ALC/LIINM
3001 STAFF DR/MS 1AG194B
TINKER AFB OK 73145-3029
(405)-736-2230
FAX: (405)-736-7262

HAFIZULLAH WARDAK
BOEING
M/S JR-34
PO BOX 240002
HUNTSVILLE AL 35824-0001
(205)-461-5932
FAX: (205)-461-5600

DR ALLISON S WARREN
ALCOA
100 TECHNICAL DR
ALCOA CTR PA 15069-0001
(412)-337-4774
FAX: (412)-337-4075

MR MATTHEW J WEIGEL
ENGR MGR
WEST COAST IND
14900 WHITMAN AVE N
SEATTLE WA 98133-0001
(206)-365-7513
FAX: (206)-365-7483

MR MARK R WEISS
LEAD PROJ ENGR
FATIGUE TECH INC
100 ANDOVER PARK WEST
SEATTLE WA 98188-2868
(206)-246-2010
FAX: (206)-244-9886

MR DAVID H WIELAND
RES ENGR
SOUTHWEST RES INST
6220 CULEBRA RD
SAN ANTONIO TX 78228-0510
(512)-522-3864
FAX: (512)-522-3042

MR BILL WILKINSON
SR PROJ ENGR
PRATT & WHITNEY CANADA
1000 MARIE VICTORIA
M/S O1KCH
LONGUEUIL QUEBEC O1K-CH
(514)-647-2244
FAX: (514)-647-7461

MR MICHAEL R WILLIAMS
AERO ENGINEER
US AIR FORCE
SM-ALC/LAFFE
5020 DUDLEY BLVD
MCCLELLAN AFB CA 95652-1391
(916)-643-0253
FAX: (916)-643-1405

SQN LDR JOHN WILTSHIRE
US AIR FORCE
OC-ALC/LAKI-UK
3001 STAFF DR/STE 2AH110
TINKER AFB OK 73145-0001
(405)-736-5170
FAX: (405)-736-4360

MR RICHARD A WOLF SR
BOEING DEF & SPACE GRP
M/S K86-92
3801 S OLIVER
WICHITA KS 67277-7730
(316)-526-8220
FAX: (316)-523-2972

DR SPENCER T WU
PROG MGR
AF OFC OF SCI RES
NA STE B-115
110 DUNCAN AVE
WASHINGTON DC 20332-0001
(202)-767-6962
FAX: (202)-767-4988

MR RICHARD WURM
US AIR FORCE
OO-ALC/LAIA F-4 TC5
6089 WARDLEIGH RD
HILL AFB UT 84056-5838
(801)-777-6175
FAX: (801)-773-7620

FUTOSHI YAMAGUCHI
JAPANESE AIR SELF DEF FORCE
WR-ALC/FM-JA
ROBINS AFB GA 31098-0001
(912)-926-2102
FAX: (912)-923-9484

MR MARKO YANISHEVSKY
DEPT OF NATIONAL DEF
QUALITY ENGR TEST EST
OTTAWA ONTARIO K1AOK2-0001
(819)-997-1539
FAX: (819)-997-2523

DR HSING C YEH
PROJ ENGR
US AIR FORCE
ASC/ENFS BLDG 125
2335 SEVENTH ST STE 6
WRIGHT-PATTERSON AFB OH 45433-7809
(513)-255-3330
FAX: (513)-476-4546

MR MICHAEL YENTZEN
AERO ENGR
NASA
TEST & ENGR DIV
MS KA50/BLDG 1100
SSC MS 39529-0001
(601)-688-7252
FAX: (601)-688-1925

MR RYUJI YOSHINAGA
SR ENGR
MITSUBISHI HEAVY IND LTD
10 OYE-CHO
MINATO-KU
NAGOYA 455 JAPAN-0001

DR ZOHAR YOSIBASH
VISITING ASST PROF
WASHINGTON UNIV
CAMPUS BOX 1129
ST LOUIS MO 63130-4899
(314)-935-6360
FAX: (314)-935-4014

MR JIN C YU
MGR DUR/TOLERANCE GRP
MCDONNELL DOUGLAS AERO
1510 HUGHES WAY
M/S 71-34
LONG BEACH CA 90810-1870
(310)-593-2072
FAX: (310)-982-7787

MR MASOOD A ZAIDI
SR PRINCIPAL ANALYST
MCDONNELL DOUGLAS AERO
M/S 71-11
1510 HUGHES WAY
LONG BEACH CA 90810-1870
(310)-593-9569
FAX: (310)-593-0648

MAJ MIRKO ZGELA
SR AIRCRAFT STRUCTURES
MARTER LTD
79 PERE BERIAULT
GATINEAU QUEBEC CANADA J8V-1N3
(819)-246-8105
FAX: (819)-246-8215